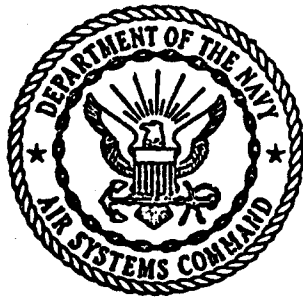


UNCLASSIFIED

AD NUMBER
AD859330
NEW LIMITATION CHANGE
TO Approved for public release, distribution unlimited
FROM Distribution authorized to U.S. Gov't. agencies and their contractors; Critical Technology; AUG 1968. Other requests shall be referred to Naval Air Systems Command, Washington, DC 20362.
AUTHORITY
USNASC ltr dtd 19 Nov 1971

THIS PAGE IS UNCLASSIFIED

AD 859330



Technical Report No. 129-1

AIRCRAFT DYNAMICS AND AUTOMATIC CONTROL

Duane McRuer
Irving Ashkenas
Dunstan Graham

SYSTEMS TECHNOLOGY, INC.®
Hawthorne, California

August 1968

THIS DOCUMENT IS LOANED TO
SPECIAL EMPLOYEES OF EACH
TO FORMULATE RECOMMENDATIONS
ON FORMS AND PROCEDURES MADE
ONLY WHEN REQUIRED BY THE
COMMANDER, NAVAL AIR SYSTEMS COMMAND

AIR 6072

Contract No. N0w 62-0781-c
NAVAL AIR SYSTEMS COMMAND
DEPARTMENT OF THE NAVY
WASHINGTON, D. C.

PREFACE

A preface is written last, placed first, and most likely, not read at all. Nevertheless, authors have a certain fondness for prefaces. Here they are permitted to say why and how the book came to be written, as well as to point out, as best they can, the advantage which they hopefully expect it may bring to the reader.

Flight control is a systems discipline which brings together the component dynamic characteristics of aircraft and flight controllers to form the system dynamic characteristics of the vehicle under the action of feedback control. Unfortunately, it has seemed to us that, by and large, the texts, monographs, and courses of instruction which treat these topics have tended to emphasize their disparities. There is certainly no lack of books on aircraft stability and control nor on feedback control systems. Our conviction, however, is that there is a field which comprises both of these subjects, and, indeed, that an understanding of either one can help to illuminate the other.

The purpose of this book is to present an integrated, analytical treatment of the dynamics of the vehicle (the controlled element), and of its flight control systems. The book has been written by and for engineers concerned with the analysis of aircraft dynamics and with the synthesis of aircraft flight controls. Such studies are at least as old as powered flight itself and they seem likely to remain pertinent as long as there are new and more advanced aeronautical vehicles.

Not long ago the intellectual mathematical equipment of skilled stability and flight control analysts generally exceeded their physical ability to perform all the design and tradeoff calculations which might be needed or desired. Nowadays quite the opposite situation exists because advances in both analog and digital computation allow the consideration of problems which at one time would have been rejected as being too time consuming. As a consequence, the analyst's physical means now often exceed his mental grasp, and what he can compute may, possibly, far exceed his understanding or appreciation. This can lead to an excessively empirical approach to design which is similar to the one used by "practical" designers thirty or more years ago. Then airplane stability and control properties were evaluated only in flight test, and flight control equipment was also "designed" with the aid of extensive full scale testing. A difference, of course, lies in the abstractions involved, for regardless of the detail and complexity of our mathematical models they remain just that, whereas the physical equipment and the aircraft are the objects of our abstractions. Viewed in these terms, too great a reliance on a numerical-empirical approach to design is no better and may be even worse than the physical empiricism of earlier days. Inundated by computer printouts and strip chart recordings, the analyst is confronted with a crucial problem—what is the essence, what does it all mean?

For this reason we have strongly emphasized an analytical approach to flight control system design and have summarized an eclectic collection of efficient, neatly interconnected techniques which inherently and readily display the essential aspect of complex system problems. When skillfully applied, either with pencil and paper or using computer aids, these techniques enable one to attain a high level of insight and physical understanding with a minimum of effort. They are suitable for the establishment of nominal system designs, for the forecast of off-nominal problems, and for the diagnosis of the root causes of the pathological syndromes which almost inevitably occur in the course of the design process.

While we have tried to be as definitive as possible on the subject of aircraft and flight control system dynamics and the procedures which are employed to accomplish automatic flight control system designs, the scope of our work has had to be limited to keep within the Procrustean confines of one volume (albeit a large volume). The necessary limitation has been accomplished primarily by considering the aircraft only as a rigid body, and by, almost exclusively, emphasizing the theory of linear constant coefficient systems. The decisions on both these limitations were made somewhat reluctantly, since the flexible airframe and nonlinear features of flight control are always fascinating academically and are often important practically. We should hasten to remark, however, that regardless of the number of modes or nonlinearity of a problem, linearized solutions to comparatively low order problems almost always give reasonable approximate answers. They provide, as it were, a most useful species of limiting case solution, and limiting cases are, in general, the basis for much of our physical understanding of complex phenomena. With a solid grounding in linear theory, the extension of the results to nonlinear problems, especially of stability, is ordinarily rewarding and effective. Thus, linear theory is, very generally, a theory of a first approximation which has the great virtue that it can be conceptually assimilated in its entirety. Further, as a practical matter, it is our observation that the great majority of the physical problems of aircraft flight control which are susceptible to mathematical treatment are, in fact, handled to a very good first approximation by linear treatments.

This book has a genealogy. Its immediate predecessors are the series of BuAcr volumes prepared in the early 1950's at Northrop Aircraft, Inc. The considerable success and the reputation of these volumes in industrial design departments, government laboratories, and in engineering schools prompted the original intent of the Naval Air Systems Command in sponsoring a large portion of the present work (Contract N0w 62-0781-c), so as to provide revisions and an updating for two of those volumes:

"Dynamics of the Airframe," BuAcr Report AE-61-4111,
September 1952

"Automatic Flight Control Systems for Piloted Aircraft,"
BuAcr Report AE-61-4116, April 1956

Although some of the numerical data and examples from these earlier volumes have been used here, we present an essentially new effort rather than a revision. Furthermore, in order to provide an integrated treatment, we have included material which partially revises the first of the BuAer volumes:

"Methods of Analysis and Synthesis of Piloted Aircraft
Flight Control Systems," BuAer Report AE-61-4I, March
1952

Consequently, this book will, in the main, supersede the above three volumes of the BuAer series.

We are indebted to many people and organizations for their assistance in the preparation of this book. First and foremost is the Naval Air Systems Command, which sponsored the preparation of much of the manuscript. The NASC project monitor, Mr. Jack Crowder, was an ideal supporter, continually interested and anxious to get the job done, yet patient and understanding in spite of the inevitable delays that projects of this sort seem to incur. We also owe major debts to our colleagues, at Systems Technology, Inc., and elsewhere, who have critically reviewed various versions and portions of the manuscript and have offered constructive criticisms and suggestions for its improvement. First in this group is Mr. Robert L. Stapleford of STI, who has been through the book several times exercising his penchant for clarity and his keen eye for error. He may have missed some things, but the very many mistakes which he caught and corrected make his role in the book important indeed—to the authors and readers alike. Mr. Robert J. Woodcock of the Air Force Flight Dynamics Laboratory, who thoroughly reviewed several chapters, was also a great help in getting and keeping things straight. Mr. H. R. Hopkins of the Royal Aircraft Establishment, Farnborough, U. K., reviewed Chapter 1, making many helpful suggestions, and very graciously offered us the use of his own extensive material on the history of flight control. Dr. Malcolm J. Abzug of TRW also made a number of correcting and clarifying remarks related to the history presented in Chapter 1 for which we are very grateful, and Mr. Ronald O. Anderson of the Air Force Flight Dynamics Laboratory made available to us his bibliography on the history of feedback controls. Mr. Gary Teper of STI was responsible for the collection and presentation of the data contained in Appendix A. Particular acknowledgment is further due to STI's publication staff, who labored long and hard to prepare the manuscript for publication, and especially to Mr. Junichi Taira, STI's Publications Manager, whose meticulous attention to every detail is revealed on each page of the book.

Besides those who helped directly there are others in the background. Most important, of course, are our many colleagues in the flight control and automatic control community whose original work is reflected here. We have tried to acknowledge them throughout the book with pertinent references to the published literature. As is evident from these

footnotes, a great deal of the work summarized here was originally accomplished for the Control Criteria Branch of the Air Force Flight Dynamics Laboratory. In fact, some of the material appearing here for the first time is based on unpublished notes prepared in the course of USAF-sponsored work. We must also acknowledge our former colleagues at Northrop Aircraft, Inc., Messrs. Warren Koerner and Robert E. Trudel, who were among the authors of the old BuAer "Dynamics of the Airframe" volume on which parts of Chapters 4, 5, and 6 is based. Finally, we wish to acknowledge our present or past STI co-workers, J. J. Best, T. S. Durand, D. E. Johnston, H. R. Jex, W. A. Johnson, L. G. Hofmann, J. D. McDonnell, R. A. Peters, R. J. Wasicko, D. H. Weir, and J. Wolkovitch, for their several original contributions to portions of the material which are presented in the following pages.

The merits which this book may possess can, in large part, be attributed to all these people. Its faults are not likely to be charged to them. The authors cannot expect to have produced a work without blemish, but they have the right to hope that it may prove both instructive and useful to others, like themselves, who may wish to help to solve the flight control system design problems of future generations of aircraft.

Duane McRuer
Irving Ashkenas
Dunstan Graham

Hawthorne, California
August, 1968

CONTENTS

	<u>Page</u>
Chapter 1 Introduction and Antecedents.	1-1
1.1 Outline of the Volume: A Guide for the Reader.	1-8
1.2 A Definition of Flight Control	1-13
1.3 Why Feedback?	1-19
1.4 Early History of the Subject of Aircraft Dynamics	1-23
1.5 Early History of Automatic Flight Control	1-28
1.6 The Joining of Control Technology and Dynamic Analysis	1-49
Chapter 2 Mathematical Models of Linear System Elements	2-1
2.1 Introduction	2-1
2.2 Laplace Transformation.	2-2
2.3 Response Determination.	2-7
2.4 Simplified Methods to Obtain an Approximate $f(t)$ from its Unfactored Transform $F(s)$	2-16
2.5 Partial Fraction Coefficient Ratios	2-25
2.6 Weighting Function and Modal Response Coefficients	2-30
2.7 Time Vector Representations for the Weighting Function	2-36
2.8 Transfer Function Models	2-45
2.9 Representations of Transfer Functions.	2-50
2.10 Combining Transfer Functions.	2-63
Chapter 3 Feedback System Analysis	3-1
3.1 Introduction	3-1
3.2 Conventional and Three-Dimensional Root Locus	3-5
3.3 Bode Root Locus and Generalized Bode Diagram	3-28
3.4 Simplified System Characteristics and Literal Approximate Factors.	3-47
3.5 Analysis of Multiloop Vehicular Control Systems.	3-60
3.6 Sensitivity of Closed-Loop Roots to System Parameter Variations	3-77
Chapter 4 Vehicle Equations of Motion	4-1
4.1 Introduction	4-1

	<u>Page</u>
4.2 Newton's Second Law and Reference Frames. . .	4-3
4.3 Expansion of the Inertial Forces and Moments . .	4-8
4.4 Expansion of the Gravity Force	4-21
4.5 Linearization of the Inertial and Gravitational Components.	4-35
4.6 Expansion of the Aerodynamic Forces and Moments	4-43
4.7 Expansion of the Direct Thrust Force	4-57
4.8 Complete Linearized Equations of Motion . . .	4-60
4.9 Description of the Dimensional and Nondimensional Stability Axis Derivatives . .	4-68
Chapter 5 Longitudinal Dynamics	5-1
5.1 Introduction	5-1
5.2 Recapitulation and Further Simplification of the Longitudinal Equations of Motion	5-3
5.3 Control-Input Transfer Functions	5-4
5.4 Example Transfer Functions, Bode Forms, and Time Responses for a Conventional Airplane . .	5-6
5.5 Two-Degree-of-Freedom Short-Period Approximations	5-14
5.6 Three-Degree-of-Freedom Phugoid Approximations.	5-15
5.7 Hovering Equations of Motion, Control-Input Transfer Functions, and Modal Responses . . .	5-19
5.8 Example Transfer Functions, Bode Forms, and Time Responses for a Hovering Vehicle. . . .	5-25
5.9 Gust-Input Transfer Functions	5-27
5.10 Coupling Numerators.	5-34
5.11 Approximate Factors.	5-36
5.12 Approximate Modal Response Ratios	5-47
Chapter 6 Lateral Dynamics.	6-1
6.1 Introduction	6-1
6.2 Recapitulation and Further Simplification of the Lateral Equations of Motion.	6-1
6.3 Control-Input Transfer Functions	6-3
6.4 Example Transfer Functions, Bode Forms, and Time Responses for a Conventional Airplane . .	6-6

	<u>Page</u>
6.5 Two-Degree-of-Freedom Dutch Roll Approximations.	6-16
6.6 Three-Degree-of-Freedom Dutch Roll Approximations.	6-17
6.7 Three-Degree-of-Freedom Spiral and Roll Subsidence Approximations	6-20
6.8 Commentary on Approximate Equations of Motion .	6-23
6.9 Hovering Equations, Control-Input Transfer Functions, and Time Responses.	6-28
6.10 Gust-Input Transfer Functions.	6-35
6.11 Coupling Numerators	6-42
6.12 Approximate Factors	6-42
6.13 Approximate Modal Response Ratios	6-54
Chapter 7 Elementary Longitudinal Feedback Control	7-1
7.1 Feedback of Pitch Angle and Pitch Rate to the Elevator.	7-1
7.2 Feedback of Speed Error to the Elevator . . .	7-23
7.3 Feedback of Angle of Attack to the Elevator . .	7-28
7.4 Feedback of Normal Acceleration to the Elevator.	7-32
7.5 Feedback of Altitude to the Elevator	7-41
Chapter 8 Elementary Lateral Feedback Control.	8-1
8.1 Feedback of Bank Angle and Rolling Velocity to the Ailerons	8-1
8.2 Feedback of Other Quantities to the Ailerons. .	8-17
8.3 Feedback of Heading Angle to the Rudder . . .	8-21
8.4 Feedback of Yawing Velocity to the Rudder. . .	8-23
8.5 Feedback of Sideslip to the Rudder	8-30
8.6 Feedback of Lateral Acceleration to the Rudder .	8-31
Chapter 9 Requirements, Specifications, and Testing.	9-1
9.1 Introduction: The System Design Process . . .	9-1
9.2 Mission Phases and Operational Requirements . .	9-4
9.3 An Approach to Implied Requirements for System Design	9-9
9.4 General Feedback Control System Considerations in Flight Control.	9-13

	<u>Page</u>
9.5 Bases for Compromise in Selecting Crossover Region.	9-33
9.6 Specifications and Testing	9-43
Chapter 10 Inputs and System Performance Assessment	10-1
10.1 Introduction.	10-1
10.2 Response to Deterministic Inputs	10-6
10.3 The Description of Random Processes	10-15
10.4 Analytical Description and Catalog of Special Random Processes	10-32
10.5 Properties of Random Processes with Gaussian Amplitude Distributions	10-39
10.6 Response of Linear Systems to Random Inputs	10-42
10.7 Computer Methods	10-57
Supplement Bibliography to Supplement Aircraft Dynamics and Automatic Control.	S-1
Appendix A. Stability Derivatives and Transfer Function Factors for Representative Aircraft.	A-1
Appendix B. Elements of Probability	B-1

CHAPTER 1

INTRODUCTION AND ANTECEDENTS

"We now know a method of mounting into the air, and, I think, are not likely to know more. The vehicles can serve no use till we can guide them; and they can gratify no curiosity till we mount with them to greater heights than we can reach without; till we rise above the tops of the highest mountains."*

The economic or military value of any vehicle depends fundamentally on its ability to traverse a controllable path between its point of departure and its destination or "target." Abstractly, the vehicle is a velocity vector in space. It has a direction in which it is going and a speed with which it is going there. The time integral of the velocity vector is the path. Each type of vehicle, however, is made to move and carry in a certain medium and its motions may be subject to constraints. Means for control of the path vary widely and depend on the constraints. Thus a train, for example, is constrained to move along a track and the control which is provided is merely a speed control. The train is not steered. An automobile or a ship, on the other hand, while constrained to move on the surface of the land or the sea, must be steered as well. Aircraft share with submarines and torpedos an unusual freedom from constraints, and the problems of the control of aircraft are of unusual complexity. We do indeed "know a method of mounting into the air," but the solution of the problems of control still requires both sensibility and diligence.

An aeronautical vehicle or weapon system contains spatial sensors, and guidance and control devices (possibly all subsumed in the human pilot) whose purpose it is to develop three-dimensional flight path

*Samuel Johnson, "A Dissertation on the Art of Flying," Chapt. VI in History of Rasselas, originally published in 1759, republished by Clarendon Press, Oxford, 1931.

commands appropriate to steering so as to reach a destination or target, and then to execute those commands by maintaining or modifying the forces on the vehicle so as to maintain or modify the velocity vector. This allows an intended purpose or "mission" to be accomplished.

Qualities of an aircraft which tend to make it resist changes in the direction or magnitude of its velocity vector are referred to as stability, while the ease and expedition with which the vector may be altered are referred to as the qualities of control. Stability makes a steady unaccelerated flight path possible; maneuvers are made with control. The path of an aircraft, however, is never stable of itself, and whether through the intervention of the human pilot or by means of automatic control, stability is actually secured with the mechanism of feedback, a principle by which cause-and-effect systems are modified to secure certain desirable properties. Information about the effect (or output) is fed back (or returned) to the input and is used to modify the cause. Typical of feedback control is its speed of response and its accuracy in following commands and in suppressing the effects of disturbances. Also typical, however, is its tendency to "hunt" or oscillate. The particular advantages of feedback are enhanced by high gain, but this is inimical to dynamic stability, and high gain also increases the susceptibility of the system to spurious signals or "noise." Therefore a designer intending to exploit the potential advantages of feedback is compelled to strike a fine balance between the desirable properties which might be secured and the pressing danger of disastrous performance.

The earliest aeronautical experimenters had hoped to achieve "inherent" stability (i.e., without feedback), and while many, such as Cayley, Penaud, Lilienthal, Chanute, and Langley, pursued this goal and discovered how to set the incidence of the tailplane so as to achieve longitudinal stability with respect to the relative wind, and to use wing dihedral so as to achieve "lateral stability," it gradually became clear that configurations with a large amount of such inherent stability were particularly, and distressingly, susceptible to being upset by gusts.

Speaking before the Western Society of Engineers in 1901, Wilbur Wright said: "Men already know how to construct wings or aeroplanes,

which when driven through the air at sufficient speed, will not only sustain the weight of the wings themselves, but also that of the engine, and of the engineer as well. Men also know how to build lines and screws of sufficient lightness and power to drive these planes at sustaining speed.... Inability to balance and steer still confronts students of the flying problem.... When this one feature has been worked out, the age of flying machines will have arrived, for all other difficulties are of minor importance."*

While this statement was somewhat optimistic with respect to the state of knowledge concerning airfoils and propellers, as the Wright Brothers themselves soon discovered, it was correct in its essentials, and there is no doubt at all that suitable stability and control characteristics were the very last features of the first successful airplane to be developed. It is now generally agreed that the principal contribution of Wilbur and Orville Wright was their recognition that the frustrating search for inherent stability might well be abandoned if only the operator were provided with sufficiently powerful controls with which to balance and steer, i.e., that the human pilot, operating on feedback signals, could use the controls to stabilize a neutrally stable or an inherently unstable aircraft.[†] Of course the Wright Brothers did not use this language, and indeed the recognition of the essential character of the airplane as an element in a feedback control loop came comparatively recently.

While the first automatic feedback control system for an airplane actually antedated the first successful flight by more than a decade, and the demonstration of completely automatic control of an airplane in full flight took place more than 50 years ago in 1914, the means employed to secure satisfactory flying qualities of the aircraft themselves, and to develop artificial stabilizers and automatic pilots were, at first,

*M. W. McFarland, ed., The Papers of Wilbur and Orville Wright, Vol. I, McGraw-Hill Book Co., New York, 1953, pp. 99-100.

†C. S. Draper, "Flight Control," J. Roy. Aeron. Soc., Vol. 59, July 1955, pp. 451-477.

largely empirical arts. They seem to have made progress with a minimum amount of mathematics until after the end of the 1939-45 war.

The modern view of the dynamics of aircraft and their control systems in terms of the stability and response of the entire closed-loop (feedback) system can be traced from its sources, by way of three separate branches of technical knowledge, to their confluence, and the recent advance and augmentation of the subject (see Fig. 1-1). During roughly the first 50 years of aviation's history, the study of the dynamics of aircraft and their control systems was of negligible interest to designers, who learned to get by with rules of thumb for proportioning the stabilizing and control surfaces and to develop automatic feedback controls by cut-and-try methods. This was in spite of the fact that a mathematical theory for the stability of the unattended motion and of the aircraft's response to control was developed at an early date. On the other hand, design trends since World War II, which have greatly extended the flight envelope of fixed-wing airplanes and introduced new types of vehicles, such as helicopters, VTOL airplanes, ground effect machines, hydrofoil boats, winged missiles, and space launchers, have so enormously multiplied the number and type of problems that the techniques formerly employed in practice would have been totally inadequate. Very fortunately wartime pressures produced two developments which fundamentally altered techniques for the design of automatic flight control systems. The first of these was the theory of servomechanisms, and the second was the electronic computer. Analysis and simulation are today the twin pillars on which the entablature of aircraft flight control system design stands.

There has been an explosive growth in the practice of "experimenting" with mathematical models. It has been urged by both the expanding complexity of the problems and the increasing availability of appropriate methods and techniques. Further, the mathematical theory has served for the classification, interpretation, and extrapolation of the growing number of results of physical experiments.

It is to the development, exposition, and demonstration of methods of analysis and synthesis for aircraft automatic flight control systems

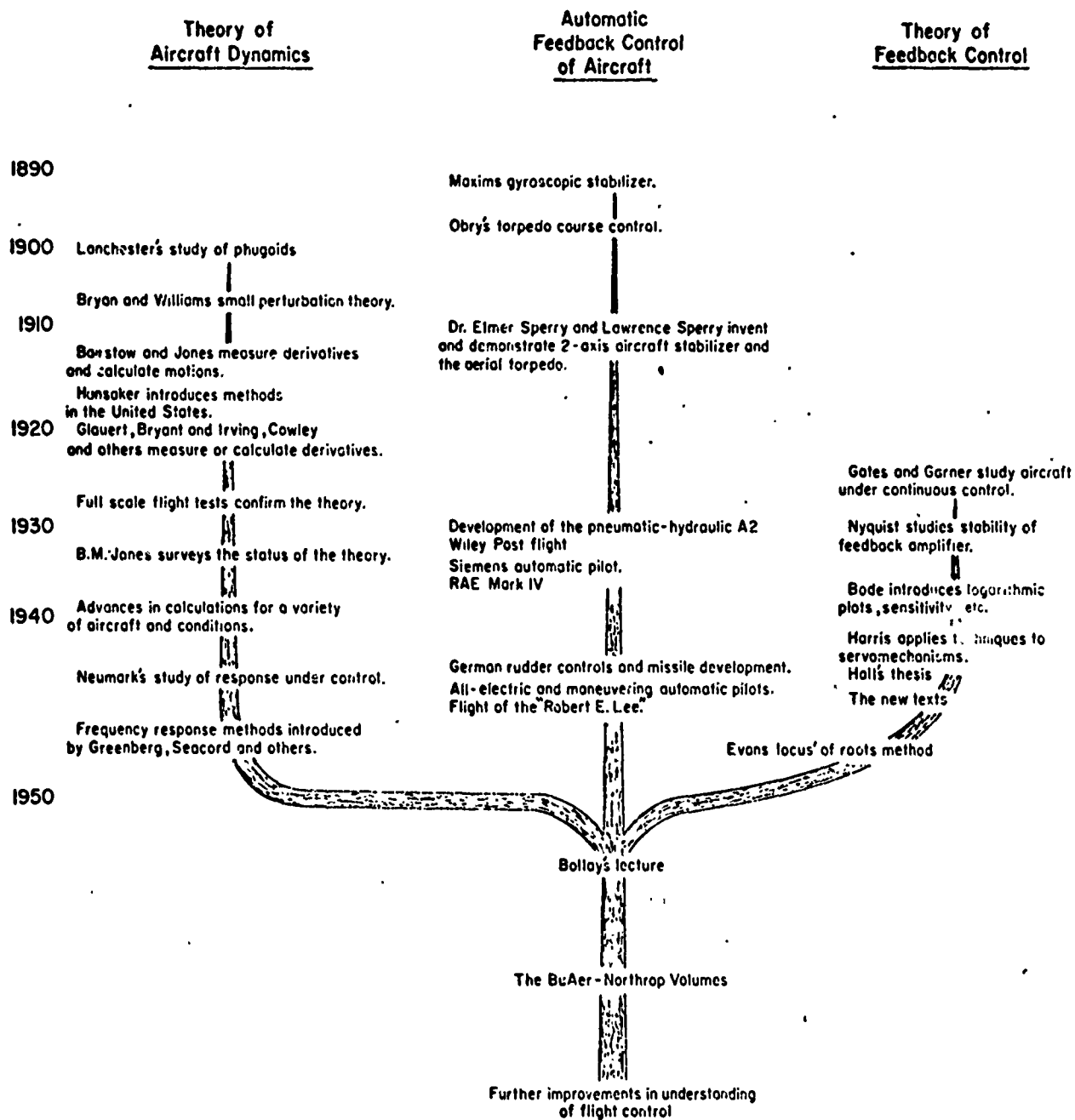


Fig. 1-1. Confluence and Augmentation of the Theory and Practice of Automatic Feedback Control of Aircraft

that this monograph is addressed. It is not a text on design, but is rather a guide to the consideration of the effects of vehicle and equipment features on the dynamic performance of the system. Where possible the emphasis in treating the elements of the system is on the largest entities. Thus, attention is directed to the response of the airplane to elevator motion rather than to the change in airflow over the tail, and to the input/output characteristics of a rate gyro rather than to detailed consideration of the torques acting on the gimbal. The vehicles considered are the ones which are heavier than the fluid in which they operate, but which are acted on by significant fluid dynamical forces. This class includes at least the following types of vehicles:

- Airplanes
- Helicopters
- Vertical takeoff and landing aircraft
- Ground effect machines
- Hydrofoil boats

Control, as somewhat distinct from guidance, is taken to be the subject of interest. For this reason it will ordinarily be possible to consider the motions in moving coordinate systems fixed in the vehicle, and to avoid the coordinate axis transformations required to obtain the vehicle motion in, for example, a coordinate system fixed in the earth. When the origin of the moving coordinate system is in an "equilibrium" state of motion along a nominal trajectory, the equations of motion of the vehicle can be linearized for small perturbations, and the linearized equations will have constant coefficients. Then it is possible to use the convenient transfer function models for the dynamics of the vehicle, and all the analytical techniques for the study of linear feedback systems can be brought to bear on the problem.

Although there are a number of modern treatments of the stability and control of aircraft,* all of which emphasize the same approach to the linearized dynamics which is to be adopted here, and there is a very wide selection of both introductory texts and more advanced treatises on

*See footnote at the beginning of Chapter 4.

automatic feedback control,* there has been a conspicuous lack of any significant treatment of these subjects in concert and therefore no proper introduction to the area between these fields. It is a fact that the methods of servomechanism analysis can be used as a powerful tool in the study of aircraft dynamics, and, additionally, that the characteristics of aircraft and their control systems provide a series of both subtle and complex problems which are likely to carry the student of feedback systems beyond what he may have learned in connection with the customary examples of remote position control, speed regulation, process control, and instrumentation. The discussion which follows will serve to bridge a gap between existing technical disciplines and to make more readily available some of the results contained in a scattered engineering report literature which is now familiar only to a small group of specialists.

The authors have adopted an eclectic view, taking from several fields what best appeals and suits, but attempting, at the same time, to provide a unified treatment. Where a completely unified view is not feasible the dominant theme is stated and the minor theme is contraposed.

It is the conviction of the authors that only the most thorough understanding of the dynamics of each element is a suitable basis for system synthesis. While digital and analog computers are now generally available to produce "solutions," even a sheaf of solutions may not clearly show the designer how to obtain the most satisfactory behavior and to avoid unpleasant surprises when the machinery is built. It is for this reason that the mathematical analysis of aircraft feedback control systems is emphasized throughout the treatment here. Of course simulation and flight testing are valuable tools in the development of aircraft control systems, but, to an extent, a good theory is a summary of and substitute for experience, and the understanding which is conferred by analysis is a short-cut to the best results. It may seem, however, that a linearized theory is unrealistic because practical aircraft feedback control systems inevitably include nonlinear elements.

*See footnote at the beginning of Chapter 3.

The results which are achieved justify its use. Restrictions which are implicit in the use of linear theory are nowhere near as severe as might be imagined. In part this is because linear approximations often have a substantial validity, and in part it is so because feedback, in itself, tends to "linearize" the system.

Finally, it may or may not be true, as George Santayana said, that "those who cannot remember the past are condemned to repeat it," but there is enough truth there so that the history of the present subject can be studied with considerable profit. It is evident upon knowledgeable consideration that some costly mistakes might have been avoided with a better appreciation for the difficulties which confronted previous investigators of the problems of flight control.

1.1 OUTLINE OF THE VOLUME: A GUIDE FOR THE READER

The subject of the feedback control of flight has a considerable scope and variety, and there is no canonical approach to its understanding. Its students will typically have acquired a considerable knowledge of the theory of linear feedback systems, and of the dynamic stability of aircraft and their response to control, as substantially independent subjects. The background of the typical reader will probably include some knowledge of operational or Laplace transform techniques for the solution of ordinary linear differential equations with constant coefficients, conventional servoanalysis techniques such as the root locus and frequency response methods, response calculations with either deterministic or random inputs, and the describing function method for the treatment of common control system nonlinearities. While many of these matters are reviewed here before they are applied, the pace is brisk and the treatment is not intended as an introduction to the elements of the theory. The reader is further presumed to have some acquaintance with the dynamics of rigid bodies, although it is not, strictly speaking, necessary to have studied the dynamics of aircraft. Again the latter subject is treated here ab initio, but with a purpose not shared with the conventional texts cited on p. 4-2.

Fig. 1-2 is a graphical representation of the outline for this volume.

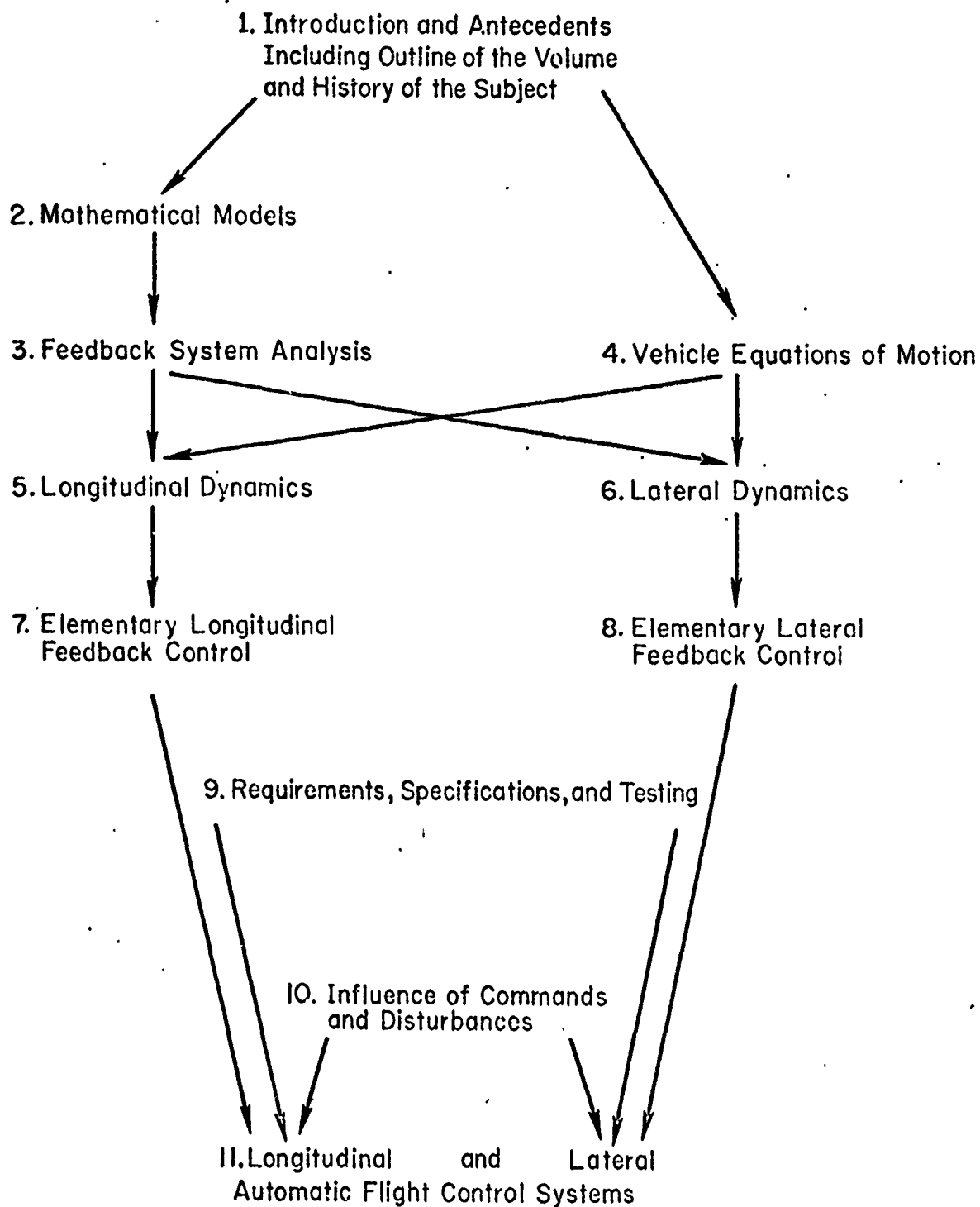


Fig. 1-2. Graphical Outline of the Volume
Showing Interrelationship Between Topics

The book begins, in this first chapter, with a definition of control appropriate to aeronautical vehicles and a distinction between control and guidance. This is followed by a brief summary of the advantages of feedback for control and an introduction to some of the earliest examples of feedback control. Historical sketches of the development of aircraft dynamic stability and control, practical automatic flight control systems, and feedback system analysis complete the introduction.

Chapter 2 comprises a review of those aspects of applied mathematics pertinent to the construction and use of linear mathematical models of aircraft and their control systems. The Laplace transform method and the transfer function model, which play such a prominent part later, are discussed in detail and considerable emphasis is placed on graphical representations and graphical constructions. While the typical reader is assumed to already have a considerable familiarity with this material so that he should be able to move ahead rapidly, he is likely to find that certain matters, such as time vectors and the steady-state response to polynomial inputs, are treated here in a unique way which provides a background for subsequent developments.

The material of Chapter 3 is a condensed account of the particular topics in feedback system analysis on which the remainder of the monograph strongly depends. Here the reader will find not only a review of the root locus method and the conventional open-loop/closed-loop logarithmic "frequency response" methods, but also their presentation as elements of a unified servoanalysis method which is a complete generalization of the semigraphical analytical techniques. The reader will also find here an exposition of multiloop analysis procedures particularly appropriate to the study of vehicular control systems, and, finally, a discussion of sensitivity including the connection between gain sensitivity and the modal response coefficients (time vectors or eigenvectors) of the system response. This chapter is one of the most unusual features of the volume because many of the techniques, and especially their highly organized connections, are not explained in the conventional textbooks on linear feedback system analysis.

The main issue is joined in Chapter 4 where the equations of motion of aeronautical vehicles are developed from first principles. It is shown there that these equations can be linearized about a nominal flight path, and that when this flight path lies in the plane of symmetry of the unperturbed vehicle the equations can normally be separated into two independent sets, the longitudinal equations and the lateral equations. This simplification is the basis for the division of the greater part of the balance of the discussion.

Still with the intention of studying the aircraft under active control, the longitudinal dynamics of the aircraft-alone are explored in Chapter 5. The transfer functions for the aircraft's response to control are evolved from the equations of motion, and approximate factors for the numerators and denominators are presented in terms of coefficients in the equations. While approximate factors for parts of the characteristic functions (denominators) of airplanes have been known for some 40 years, it was only a few years ago that a similar understanding of the numerators was developed, and a similar approach to VTOL aircraft has only been successful even more recently. Here again, the presentation in Chapter 5 departs considerably from the conventional practice because little or no attention is paid to transfer function factors in the existing texts, and the developments summarized there represent a part of the novel approach which is a feature of this volume.

Chapter 6 does for the lateral motions what Chapter 5 does for the longitudinal motions. The treatment is exactly parallel although the results are different because of the distinction between the typical motions in the several degrees of freedom.

In Chapters 7 and 8 the discussion finally turns to the feedback control of airplanes and helicopters. The stability and response of vehicles under continuously active control are considered with the assumption of ideal proportional control, i.e., no account is yet taken of the practical imperfections, such as lags, which inevitably are associated with real sensors, amplifiers, and actuators. The possible ideal feedback systems for control of the longitudinal motions are canvassed in Chapter 7, while a similar presentation on ideal feedback systems for control of the lateral motions is made in Chapter 8.

Chapter 9 is on the subject of general requirements, specifications, and testing. These subjects are presented in the context of a design process outline. Emphasis is placed on the sources of operational requirements, and the logical evolution of the requirements from these origins. The requirements which derive from a consideration of flight control systems as feedback devices are also treated at length.

In Chapter 10 the effects of inputs and disturbances are treated as a performance consideration. Up to that point, the inputs to the system are considered to be relatively simple test signals, such as an impulse or a sine wave. Now the influence on design of considering the structure of the inputs and disturbances is introduced for the first time. Actually the inputs and disturbances are approximated by either deterministic signals more complicated than the ones previously considered, or, where their nature demands it, in probabilistic terms. The first probability density function and the second probability distribution function are reviewed, and their use in system performance calculations is explained in some detail for the cases in which the signals have a Gaussian distribution and are stationary. In that case convenient calculations of the performance of linear systems can be carried out in the frequency domain by making use of the power and cross-spectral density functions. The "transient analog" and adjoint technique, which underlie the computer approach to more complex problems, are also introduced.

Finally, much of the material of all the previous chapters is used in discussions of longitudinal and lateral automatic flight control systems in Chapter 11. The influence of requirements and of imperfections in the components is particularly pointed out. Multiloop flight control systems of several types are treated as illustrative examples.

At the end of the book there are two appendices and a bibliography. The bibliography supplements this book by providing references to those aspects of aircraft dynamics and automatic control which are not extensively treated here. It covers vehicle flexibility and other higher-order dynamic effects, components, and descriptions of flight control systems. The first appendix presents tabulations of dynamic characteristics for some representative aircraft, and the second serves as a brief introduction to probability theory.

1.2 A DEFINITION OF FLIGHT CONTROL

It is not surprising that, when considered in detail, the abstract or physical attributes of an aeronautical vehicle or weapon system and its elements are so interrelated as to almost preclude discussion of any one aspect of the system without simultaneously treating most of the others. Still, it ultimately becomes necessary to stake out definite domains which can be treated more or less individually. This can be accomplished with some generality if other factors and entities in the system can be considered either precursory or by definition separated from the subject of special attention.

As a first step in separating the automatic flight control area from other aspects of the over-all aeronautical vehicle or weapon system it is necessary to distinguish control from guidance. Unfortunately the boundary between these two areas is seldom inherently sharp because of basic functional, operational, and equipment interactions which they may share. As a practical matter, however, the following definitions can ordinarily be used:

Guidance.... The action of determining the course and speed relative to some reference system, to be followed by a vehicle

Control..... The development and application to a vehicle of appropriate forces and moments which

Establish some equilibrium state of vehicle motion (operating point control)

Restore a disturbed vehicle to its equilibrium (operating point) state and/or regulate, within desired limits, its departure from operating point conditions (stabilization)

To apply these definitions to a specific example, consider the air-to-surface missile system shown in Fig. 1-3. In this figure the blocks inscribed with capital letters in square brackets are not simple transfer functions relating outputs to inputs, but instead are matrix operations. It is readily apparent that the complete system, when viewed in the large, is complicated and analytically intractable. However, two major types of "loops" are seen to be present: one a series of "inner"

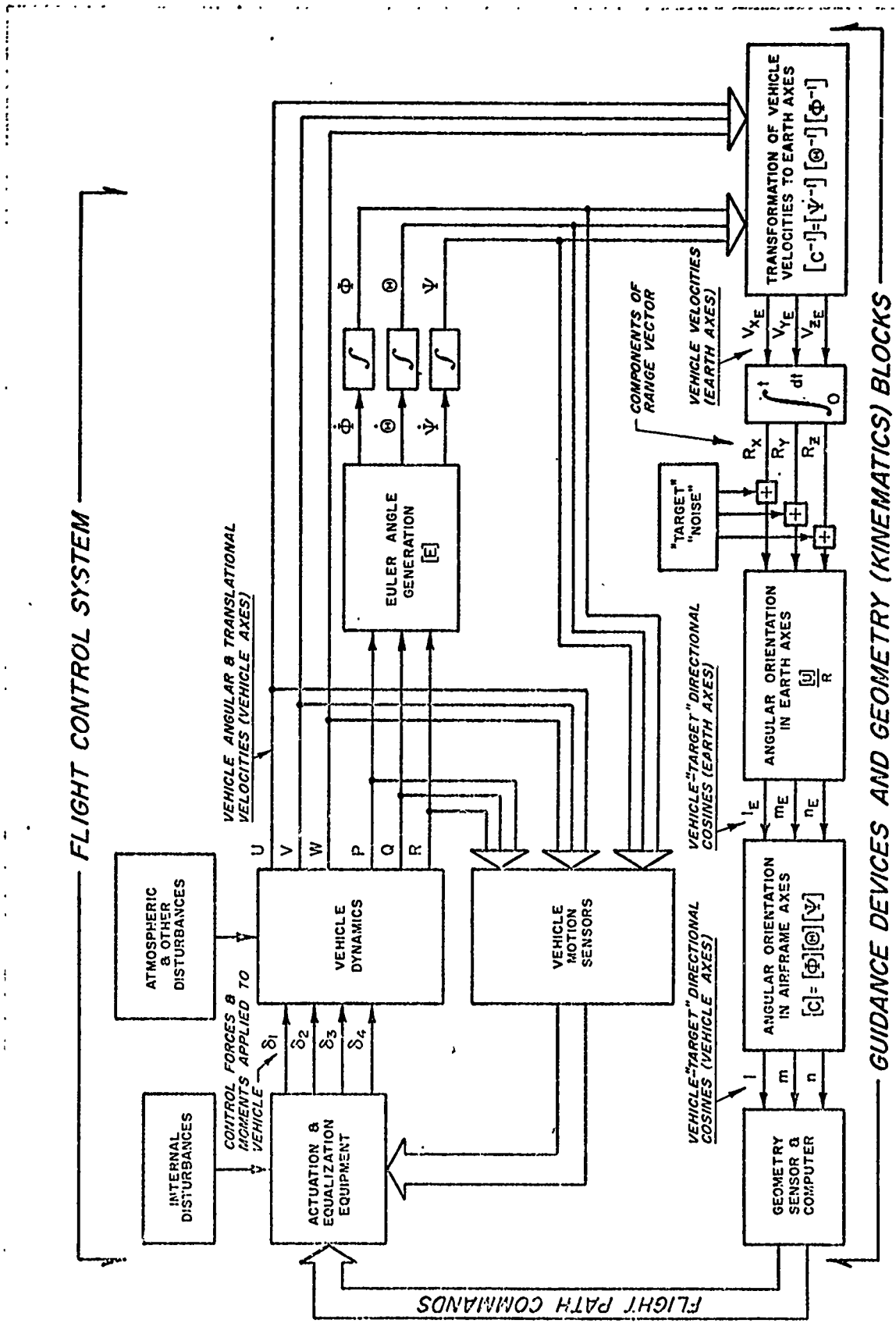


Fig. 1-3. Air-to-Surface Missile System Block Diagram

loops involving the feedback of airframe motion quantities; the other an outer loop containing the kinematic transformations required to generate the relative orientation between target and vehicle, and closed through a geometry sensor and computer which generates flight path commands. Using the definitions given above it is now possible to separate the guidance and the control areas, at least in terms of the matrix operators shown in the block diagram.

Note, parenthetically, that an abstract or functional picture, rather than one drawn in terms of physical equipment, is preferred at this stage. If, for example, in Fig. 1-3 the Euler angles, Φ , Θ , and Ψ , used as measures of vehicle motion, were obtained from a stable platform, this equipment would have to be considered a part of the flight control system; yet to many people the very words "stable platform" imply an item of guidance equipment.

On a physical basis Fig. 1-3 makes apparent an important distinction between the two types of loops. The flight control loop is concerned only with vehicle motion quantities measured in the aircraft (although two reference axis systems are necessary), while the guidance loop involves axis system transformations which put the vehicle and target on comparable terms. For many systems this distinction is quite helpful in separating guidance from control. There is little doubt that the control of aircraft attitude angles is one of the functions of flight control, while the control of the path is, strictly speaking, a guidance function. Later it will become clear, however, that there are pseudo path variables, such as pressure altitude and heading, which are measured in the aircraft, and whose control, therefore, is logically considered to be a part of the domain of flight control. Further, it is often possible to formulate guidance problems, such as terrain avoidance and approach to a runway on a localizer beam, without involving more than linear approximations to the kinematic transformations in the guidance loop, and then, with a single notable exception, guidance problems can be considered as minor extensions to the problem of flight control.

The exception is in those cases where there are important dynamic interactions between the control and guidance loops. The complex diagram

of Fig. 1-3 can be simplified by specifying the general type of guidance to be used and defining ideal steady-state "trajectories." The desired steady-state conditions can then be used as "operating points," and all of the equations indicated by the block diagram of Fig. 1-3 can be linearized about these operating points. A simplified block diagram, emphasizing the system dynamics in a form suitable for dynamic analysis, can finally be drawn. Figure 1-4 shows "linearized" block diagrams (derived from Fig. 1-3) which relate perturbed quantities when the vehicle is on a straight line collision course with the target and is operating about straight and level flight conditions.* Figure 1-5(a) results when the longitudinal control system block diagram is redrawn so as to use flight path angle, γ , instead of pitching velocity, q , and plunging velocity, w , as the motion variables. Here the geometry relationships are shown in a single block, while the flight control system portion of the diagram is separated into functional divisions. Figure 1-5(b) goes one step further and shows a single closed-loop flight control system block with the geometry block broken into two parallel channels. Both diagrams in Fig. 1-5 assume unity dynamics for the geometry sensor and computer.

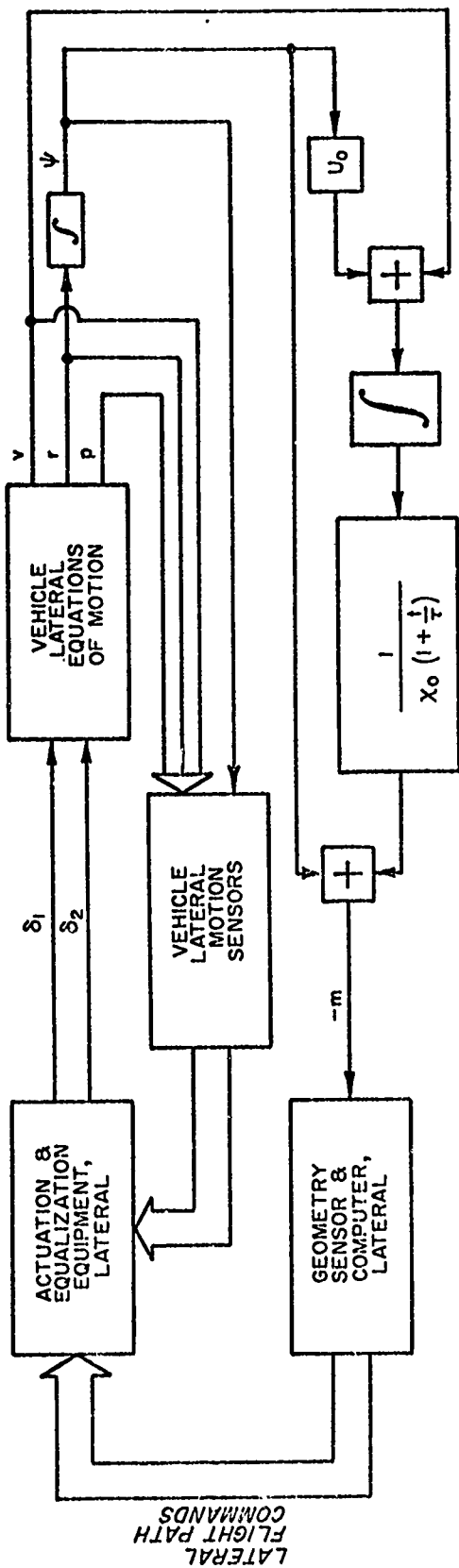
Figure 1-5 emphasizes the fact that the geometry block contains a time-varying parameter $(1 - t/\tau)$ where the time variable, t , appears explicitly. The magnitude of the parameter defines the relative degree of dynamic interaction between the flight control and the guidance. When the ratio time:time-to-go, t/τ , is very small the sole dynamic effect of the guidance elements is to add a unity feedback path to the closed-loop flight control system. In most cases this effect, while certainly worthy of consideration, does not complicate the problem. It can easily be taken into account as just another loop in the flight control system. On the other hand, as t/τ approaches unity the geometry block gain

*While the implied assumption is surely a tremendously simplifying one, aeronautical vehicles do, in fact, spend most of their time in the air in straight and level flight, and the control system must be made to work for that flight condition first. The choice of operating point, however, is illustrative and is not necessary to the argument.

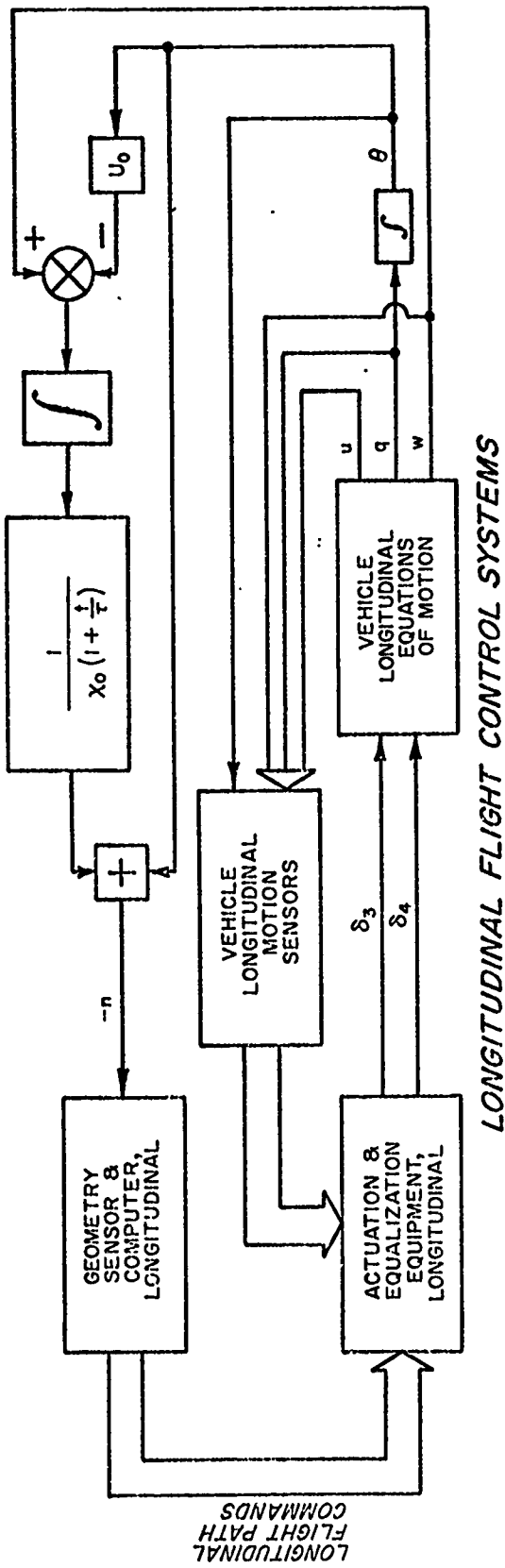
$$P_0 = Q_0 = R_0 = V_0 = W_0 = \dot{\psi}_0 = R_{\dot{\psi}_0} = \dot{\phi}_0 = 0$$

NO LATERAL-LONGITUDINAL CONTROL CROSSFEEDS

LATERAL FLIGHT CONTROL SYSTEM



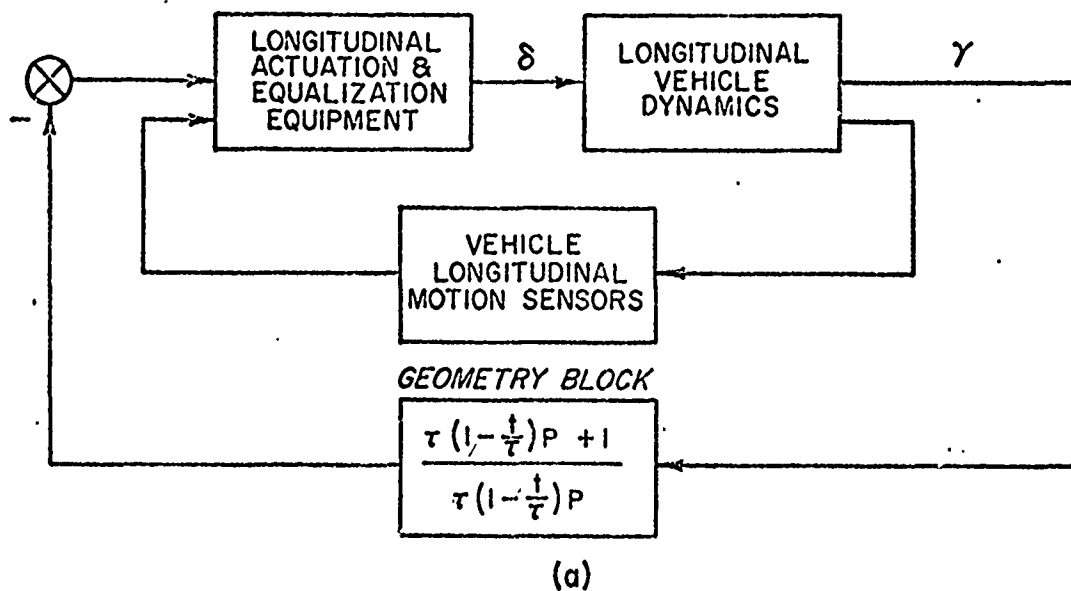
GUIDANCE DEVICES & GEOMETRY BLOCKS



LONGITUDINAL FLIGHT CONTROL SYSTEMS

Fig. 1-4. Air-to-Surface Missile System Linearized Block Diagram

FLIGHT CONTROL SYSTEM



Note: P is the operator, $\frac{d}{dt}$

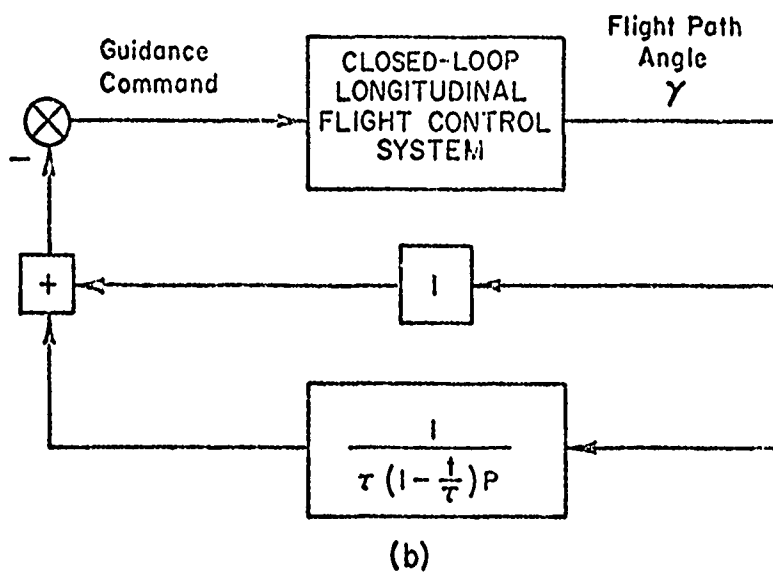


Fig. 1-5. Simplified Longitudinal Collision Course Guidance and Control System

approaches infinity and the dynamic interactions between guidance and flight control may become the most prominent feature of system performance.

If the considerations exemplified in the discussions above are generalized for a variety of guidance system types, it is found that guidance and control can interact in only three ways. These are illustrated in Fig. 1-6 as connections between the two parts of a guidance and control dichotomy. The interaction with operating point control, as illustrated in the example above, is the starting point in the development of diagrams, such as the ones shown, which emphasize the dynamics. Guidance system effects on limiting involve the characteristics of particular physical mechanizations and, in any event, relate only to conditions outside the realm of linear theory. Finally, dynamic interaction between guidance and control occurs only in homing guidance, and even then the interaction is slight until the target is "close." On these bases it should be clear that linear constant approximations to flight control and guidance systems can be treated completely separately, as far as their dynamics are concerned, for all guidance modes except final "homing" maneuvers. Assuming, therefore, a particular operating point—straight and level flight—and neglecting a possible interest in homing maneuvers, the subject of control can be separated from guidance, and the synthesis of automatic flight control systems can be studied in their own right.

1.3 WHY FEEDBACK?

The flight control systems in Figs. 1-3 to 1-5 are, quite apparently, shown as feedback systems in which a portion of each output is fed back so as to modify the input. Effective flight control systems invariably are feedback systems for a number of important reasons.

Even if invention had ultimately produced a satisfactory "inherently" stable aircraft, the disadvantage of open-loop, i.e. nonfeedback, control would probably still preclude its use for the control of flight. Open-loop controls are programmed and calibrated. Their proper operation depends on the computation of an appropriate program and on maintaining the calibration of the controlled element or object of control. In flight

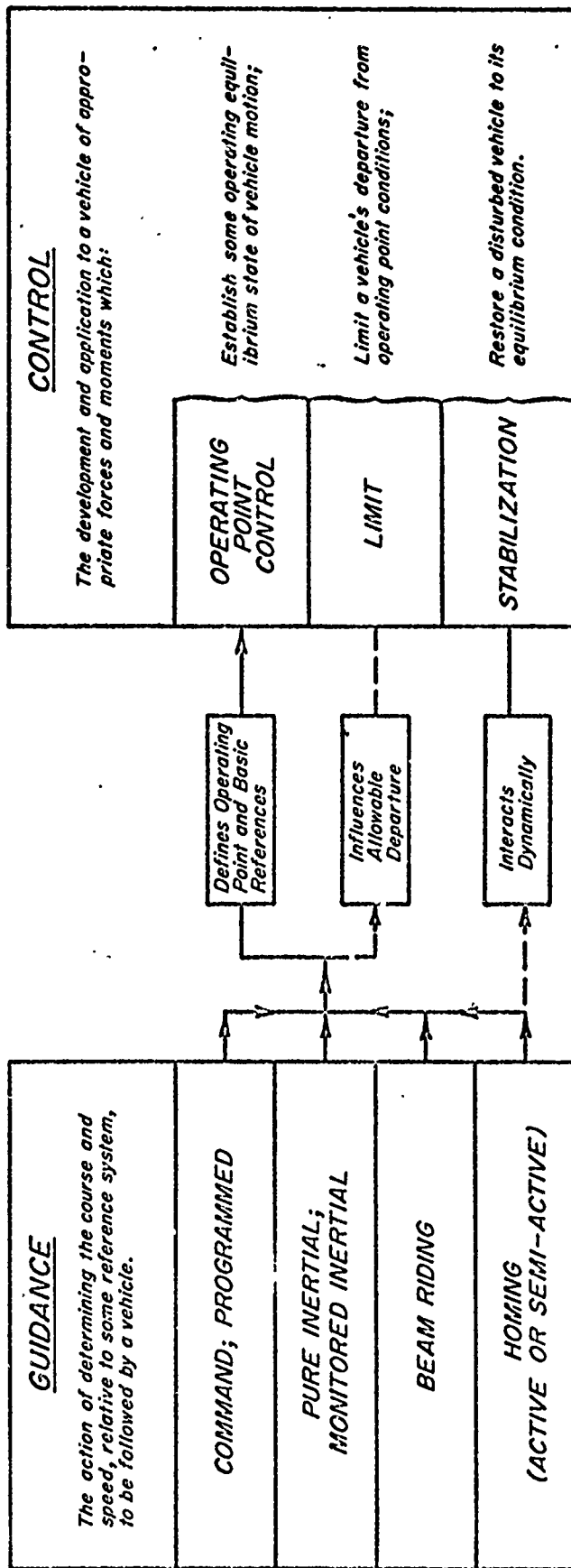


Fig. 1-6. Guidance/Control Dichotomy

control applications the appropriate program is often of considerable complexity, and a most notable feature of the aircraft's response to control is that it changes markedly with speed, altitude, and loading.

The advantages of feedback control are:

- The provision of stability
- The adjustment of dynamic response, including
 - Reduction of lags
 - Provision of desired or specified command/
response relationships, especially as regards
the improvement of linearity and the reduction of the effect of vehicle cross-coupling forces
- The suppression of unwanted inputs and disturbances
- The suppression of the effects of variations and uncertainties in the characteristics of the controlled element

Feedback can make an unstable system stable. (It can, of course, also make a stable system unstable, and that is a subject to which we shall have frequent occasion to return later.) Unfortunately, aircraft are never stable by themselves. At the very best they are neutrally stable in heading and altitude, and continuous corrections must be made in order to fly a straight and level course. Otherwise, and this is especially true of modern configurations, a disturbance may start an aperiodically divergent motion, such as the one pilots sometimes call the "graveyard spiral," or a similar disturbance may initiate weakly damped or perhaps divergent oscillations in the rolling, yawing, and pitching degrees of freedom. It is for the repair of any such deficiencies in stability that the classes of automatic flight control systems known as stability augmenters and automatic pilots are principally useful.

Feedback can improve the speed of response and may be used so as to enforce some desired correspondence between the input and output of the system. The series of figures which have been presented have served to emphasize the fact that one of the purposes of the flight control system is to follow the commands generated by the guidance system. Rapid and accurate response to commands, so that the commanded flight path is matched by the actual flight path, for example, is made possible or is

largely enhanced by the feedback of aircraft motion quantities. These feedbacks have been illustrated and are defined in the figures to comprise the flight control system.

It is not only the case that the (feedback) flight control system will improve the speed of response and accuracy in following commands, but it will also tend to suppress the effect of disturbances, such as the atmospheric (gust) disturbances illustrated in Fig. 1-3, as well as the effects of changes in the characteristics of the vehicle's response to control. These are not the least reasons for employing feedback. The aircraft must typically fly in atmospheric turbulence which tends to upset it and to alter its flight path, and the response to control may very well be substantially changed by the consumption of fuel, the release of stores, and changes in the flight speed or altitude.

Some of the earliest inanimate feedback controls, aside from water level controls which were known in antiquity, were speed regulators for prime movers.* These were primarily designed to regulate against changes in speed because of disturbances, such as changes in the load, or changes in the response of the machine to control, such as a change in speed at the same throttle setting because of an increase in steam pressure. The early governors secured some of the very practical advantages of feedback, but they also tended to display the largest disadvantage—a tendency to hunt or oscillate. The phenomenon of hunting of engine governors motivated a number of authors to study the stability of feedback control systems and to lay the foundations of a mathematical theory of the subject. Among the earliest of these investigators was the physicist J. C. Maxwell,[†] who in his own paper on the subject conceded his inability to discover the criteria for the stability of higher order systems. Later he was one of the examiners who set the subject "The Criterion of Dynamical Stability" for the Adams Prize Essay Contest in

*James Watt is commonly credited with the invention of the flyball governor, about 1784, but it seems likely that these were in use on wind-mills before his time. (See A. Wolf, A History of Science, Technology, and Philosophy in the XVIIIth Century, The Macmillan Co., New York, 1939.)

[†]J. C. Maxwell, "On Governors," Proc. Roy. Soc., (London), Vol. 16, 1869, pp. 270-283.

1877. The prize was won by E. J. Routh,* who considered not only governors but the stability of general motion of rigid bodies. His studies in that field became the basis for the investigation of the dynamic stability of aircraft and for many years provided the principal tool for the study of feedback control systems.

1.4 EARLY HISTORY OF THE SUBJECT OF AIRCRAFT DYNAMICS

F. W. Lanchester was the first to investigate analytically the dynamic stability of aircraft. Before the turn of the century, he experimented with glider models and studied the properties of the solutions to a simplified set of equations for motion in the plane of symmetry.† He called the resulting flight paths "phugoids," a name which persists to this day.

In the year of the first powered flight, 1903, Bryan and Williams, using more conventional mathematical methods, introduced the linearized equations of motion which have been the foundation of studies of dynamic stability and response to control ever since.‡ Later the theory of both the longitudinal and lateral motions was presented by Bryan.§ The six Euler equations for the general motion of a rigid body were considered for "small" departures from steady, straight flight of an airplane with a plane of symmetry. Under these assumptions, the equations were shown to be separable into two groups of three each. One group related the motion variables in the plane of symmetry, while the other group related

*E. J. Routh, Stability of a Given State of Motion, Macmillan and Co., London, 1877.

†F. W. Lanchester, Aerodonetics, Archibald Constable and Co., London, 1903. See also B. Melvill Jones, "Dynamics of the Aeroplane," in W. F. Durand, ed., Aerodynamic Theory, Vol. V, Durand Reprinting Committee, Pasadena, Calif., 1943; republished (Vols. V and VI bound in one volume) by Dover Publications, New York, 1963; pp. 2-3, 169.

‡G. H. Bryan and W. E. Williams, "The Longitudinal Stability of Aerial Gliders," Proc. Roy. Soc., Vol. 73, No. 489, 1904, pp. 100-116.

§G. H. Bryan, Stability in Aviation, Macmillan and Co., London, 1911.

the motion variables out of the plane of symmetry. Neither group contained any variable which occurred in the other, so that they could be treated entirely separately. The separate groups of equations were called the "symmetric" or longitudinal and the "asymmetric" or lateral equations. A further consequence of the assumption of small perturbations was that the air forces on the airplane could be shown to depend on certain constants or "stability derivatives" as they were called, and Bryan suggested that these might be determined experimentally.

As early as 1912, Bairstow and Melvill Jones, at the National Physical Laboratory in Great Britain, had taken up Bryan's suggestion and had developed some of the wind tunnel techniques for measuring the stability derivatives of models. They reported the results of their initial effort the following year, showing how features of the motion could be recognized in the mathematical solutions for the free response of a hypothetical airplane for which they had measured or calculated all the derivatives.* In both language and notation this report is thoroughly "modern"; it might be used as a text on the dynamic stability of airplanes today.

The theory and the experimental practice were subsequently extended by the original investigators and others. Bairstow considered the stability of more complicated motions such as circling flight, and treated the motion of dirigible airships. He provided a comprehensive account of the subject in 1920.[†] Hunsaker, who had visited the National Physical Laboratory in 1914, introduced Bairstow's wind tunnel techniques and the method of Bryan and Bairstow for the calculation of dynamic stability in the United States. He collaborated on the first report of the United States National Advisory Committee for Aeronautics which was concerned with the response of aircraft to gusts.[‡] Glauert calculated the stability

*L. Bairstow, B. Melvill Jones, and B. A. Thompson, Investigation Into the Stability of an Airplane, A.R.C. R&M 77, 1913.

†L. Bairstow, Applied Aerodynamics, Longmans Green and Co., London, 1st ed., 1920, 2nd ed., 1959.

‡J. C. Hunsaker, Experimental Analysis of Inherent Longitudinal Stability for a Typical Biplane, NACA TR 1, Pt. I, 1915. See also "Dynamic Stability of Aeroplanes," Smithsonian Misc. Collection, 1916.

derivatives of a running propeller and the motions of an airplane with the elevator free.* The model measurement[†] or calculation[‡] of particular stability derivatives continued to attract attention, and a considerable effort was made to measure derivatives, free motions, and the response to controls[§] in full scale flight tests. The references given in the footnotes are only typical, not comprehensive. More details are given in the historical sketch appended to the 1947 paper by Milliken,^{||} and anecdotal accounts of the work of the British pioneers are presented in several contributions to the "Centenary Journal" of the Royal Aeronautical Society,[#] particularly the ones by A. V. Stevens, Sir Harry Garner, J. L. Mayler, and R. W. McKinnon Wood.

Certainly by 1935, when the survey by B. Melvill Jones appeared in Durand's Aerodynamic Theory, the classical approach of Bryan and Bairstow was well established, but was very little used. Results of the full scale experiments had led to the conviction that the theory of infinitesimal

*H. Glauert, The Stability Derivatives of an Airscrew, A.R.C. R&M 642, Oct. 1919. See also The Longitudinal Stability of an Airplane, A.R.C. R&M 638, 1919.

†L. W. Bryant and H. B. Irving, Apparatus for the Measurement of M_Q on a Complete Model Airplane, A.R.C. R&M 616, 1919.

‡W. L. Cowley, The Effect of the Lag of Downwash on the Longitudinal Stability of an Aeroplane..., A.R.C. R&M 718, Feb. 1918.

§H. Glauert, Analysis of Phugoids Obtained by a Recording Airspeed Indicator, A.R.C. R&M 576, Jan. 1919.

E. P. Warner and F. H. Norton, Preliminary Report on Free Flight Tests, NACA TR 70, 1919.

F. H. Norton, Practical Stability and Controllability of Airplanes, NACA TR 120, 1921. (See also NACA TR 112, TR 167, and TR 170.)

M. A. Gerner and S. B. Gates, The Full-Scale Determination of the Lateral Resistance Derivatives of a Bristol Fighter, A.R.C. R&M 987, Aug. 1925. (See also A.R.C. R&M 1068 and R&M 1070.)

H. A. Soule, and J. B. Wheatley, A Comparison Between the Theoretical and Measured Longitudinal Stability Characteristics of an Airplane, NACA TR 442, 1933.

||W. F. Milliken, Jr., "Progress in Dynamic Stability and Control Research," J. Aeron. Sci., Vol. 14, No. 9, Sept. 1947, pp. 493-519.

#"Centenary Journal, Royal Aeronautical Society 1866-1966," J. Roy. Aeron. Sci., Vol. 70, No. 661, Jan. 1966.

motions was practical for the prediction of the stability of motion, the time history of the motion following a disturbance, and the response to the application of control. The effect of variations in the configuration of a typical airplane had been traced, via their influence on the derivatives, to the result in terms of stability of motion. Furthermore, these results were appreciated not only in terms of the solutions to specific numerical examples, but more generally, at least in part, as approximate solutions given in terms of the dominant literal stability derivatives.

Melvill Jones himself, speaking of complete solutions to the equations of motion and of approximate solutions to the stability quartic equations, evaluated the state of affairs in the following words:

"In spite...of the completeness of the experimental and theoretical structure...it is undoubtedly true that, at the time of writing, calculations of this kind are very little used by any but a few research workers. It is in fact rare for anyone actually engaged upon the design and construction of aeroplanes to make direct use of [such] computations..., or even to be familiar with the methods by which they are made.... In my own opinion it is the difficulty of computation...which has prevented designers of aeroplanes from making use of the methods....

"Though the process...will, if worked correctly, give the final answer required, it is so involved that it is not easy to trace the connection between the final answer and the separate characteristics of the airplane which are represented by the various derivatives included in the equation of motion.

"With regard to the response to specific disturbances no convenient means of tracing this connection has yet been devised; but when...the form of the solution of the quartic for λ [i.e., the frequencies and damping factors of the free modes] in normal flight is all that is required, the omission of certain terms, which are then relatively unimportant, allows such drastic simplifications to be made that the relation between cause and effect can be displayed with comparative ease."*

*B. Melvill Jones, "Dynamics of the Aeroplane," in W. F. Durand, ed., Aerodynamic Theory, Vol. V, Durand Reprinting Committee, Pasadena, Calif., 1943; republished (Vols. V and VI bound in one volume) by Dover Publications, New York, 1963; pp. 2-3, 169.

The situation was hardly altered during the next ten years. In spite of the introduction of the method of operators,^{*} which did reduce the labor of computation, and in spite of earnest efforts to make the techniques as simple and general as possible by introducing a non-dimensional notation,[†] and by summarizing information on the stability factors in convenient charts,[‡] and, further, in spite of hortatory expositions of the theory,[§] designers of airplanes continued to disdain dynamic stability analysis.

Nevertheless, research continued at a pace which was accelerated by the advent of the war, and some improvements were made in the understanding of, for example, the importance of wing/fuselage interference and power effects on the stability derivatives, the effect of closely balanced free controls on the motion, the response to particular motions of particular controls, such as spoilers, and the influence of changes in design on the character of the motions.

^{*}L. W. Bryant and D. H. Williams, The Application of the Method of Operators to the Calculation of the Disturbed Motion of an Airplane, A.R.C. R&M 1346, July 1930.

R..T. Jones, A Simplified Application of the Method of Operators to the Calculation of the Disturbed Motion of an Airplane, NACA TR-560, 1936. See also "Calculation of the Motion of an Airplane Under the Influence of Irregular Disturbances," J. Aeron. Sci., Vol. 3, No. 12, Oct. 1936, pp. 419-425.

A. Klemin and B. F. Ruffner, "Operator Solutions in Airplane Dynamics," J. Aeron. Sci., Vol. 3, No. 7, May 1936, pp. 252-255.

[†]H. Glauert, A Non-Dimensional Form of the Stability Equations of an Aeroplane, A.R.C. R&M 1095, 1927.

[‡]S. B. Gates, A Survey of Longitudinal Stability Below the Stall, With an Abstract for Designers' Use, A.R.C. R&M 1118, July 1927.

C. H. Zimmerman, An Analysis of Longitudinal Stability in Power-Off Flight with Charts for Use in Design, NACA TR-521, 1935; also An Analysis of Lateral Stability in Power-Off Flight with Charts for Use in Design, NACA TR 589, 1937.

[§]O. C. Koppen, "Happier Landings," Aviation, Sept. 1934; "Control Sensitivity," Aviation, Oct. 1935; "Smart Airplanes for Dumb Pilots," paper presented to the SAE, Detroit, Mich., Jan. 1936; "Airplane Stability and Control from the Designer's Point of View," J. Aeron. Sci., Vol. 7, No. 4, Feb. 1940, pp. 135-140.

The point of view then current, however, did not permit one (with very rare and soon forgotten exceptions) to consider the response of the airplane under the continuous action of the controls, i.e., as a feedback system. The controls were, almost invariably, considered as:

- Fixed, as in the earliest studies
- Free, i.e., restrained only by aerodynamic hinge moments (or later by friction as well)*
- Programmed, i.e., moved as a simple function of time, such as a step or ramp function or a smooth pulse†

It may have been not only the fact that the calculations were laborious, but also that the assumptions of the analysis appeared unrealistic, which discouraged their use in design. The stability of unattended motion with the controls fixed or free and the response to programmed control motions were and are, indeed, of some interest in connection with the dynamics of an airplane, but it is evident that the human or an automatic pilot flies by operating the controls more or less continuously. The airplane plainly is an element in a system which includes a human or an automatic pilot. This view did not come to be generally accepted until after the war, and the understanding of convenient means of tracing the connection between the response to specific disturbances, such as the operation of the controls, and the characteristics of the airplane which are represented by the various derivatives was of an even later date.

1.5 EARLY HISTORY OF AUTOMATIC FLIGHT CONTROL

The development of automatic flight, like the development of airplanes themselves, proceeded for a long time without the benefit of very little theoretical knowledge.

*H. Glauert, The Longitudinal Stability of an Aeroplane, A.R.C. R&M 638, 1919.

R. T. Jones and D. Cohen, Analysis of the Stability of an Airplane with Free Controls, NACA TR 709, 1940.

†R. T. Jones, A Simplified Application of the Method of Operators to the Calculation of the Disturbed Motion of an Airplane, NACA TR 560, 1936.

K. Mitchell, Lateral Response Theory, R.A.E. Rept. Aero. 1952, Mar. 1944.

Sir Hiram Maxim (1840-1916) was a prodigious inventor and when, in 1891, he turned his attention to the design and construction of a heavier-than-air flying machine, he proposed to secure its longitudinal stability by means of a servo drive and automatic feedback. The devices which are described in Maxim's book* and are illustrated there by a photograph of the installation in an airplane are surprisingly modern in concept and in execution.

A steam-driven pendulous vertical gyroscope was made to operate a valve which ported steam to a servo cylinder.[†] Motion of the piston drove the elevators, and the feedback link from the piston repositioned the gyro-operated valve body so as to close the valve. In principle, this "gyroscopic apparatus for automatically steering [the] machine in a vertical direction" is indistinguishable from the elevator control portion of automatic pilots of much more recent date. Easily recognizable are the elements of any automatic flight control system: the sensor (gyroscope), the amplifier (valve), and the control surface positioning servo. Unluckily, tests of the flying machine for which the gyroscopic control was designed ended in disaster when the aircraft lifted off the tracks designed to restrain it, turned over, and was destroyed. Maxim, who felt that his special contribution was to be the development of lifting surfaces and power plants, thought that the point about lift and power had been proven, and the inventor turned his energies in other directions.

Still in the nineteenth century, however, successful gyroscopic feedback control of the "flight" path was demonstrated by Ludwig Obry, an Austrian, who in 1894 introduced a course-keeping gyro as an improvement for the naval torpedo invented by Robert Whitehead in 1866.

*H. S. Maxim, Artificial and Natural Flight, Whittaker and Co., London, 1908, pp. 92-94.

[†]The principles of steam and hydraulic servomotors had already been known for some time. See A. B. Brown, British Patent No. 2253, 1871, and J. Farcot, Le Servo Moteur ou Moteur Asservi. Gouvernails a Vapeur Farcot, Description Theoretique et Pratique, J. Baudry, Paris, 1873. Among early applications to vehicle control were steering engines for steamships.

(Whitehead's torpedo had an automatic depth control.) Only a little later the principle of gyroscopic stabilization of ships was introduced, and, although depending on a completely different principle, was the model for the next attempt at gyroscopic control of an aircraft. In 1909-1910 Dr. Elmer Sperry attempted to make a gyroscopic "stabilizer" for an airplane. This was a rigidly mounted engine-driven wheel with its spin axis vertical. It would have opposed rolling motions with a pitching torque and vice versa. It was apparently never brought to a test because of the lack of success of the airplane in which it was installed, but it served as the inspiration for further trials.*

Between 1910 and 1912 Dr. Sperry and his son Lawrence developed and installed, in an airplane belonging to Glenn H. Curtiss, an all-electric two-axis automatic pilot. Roller contacts on a gyro platform, measuring the bank and pitch angles, actuated solenoid clutches which connected the ailerons and elevator to a propeller-driven "air turbine," and motion of the surfaces repositioned the contactor segments[†] (e.g., see Fig. 1-7).

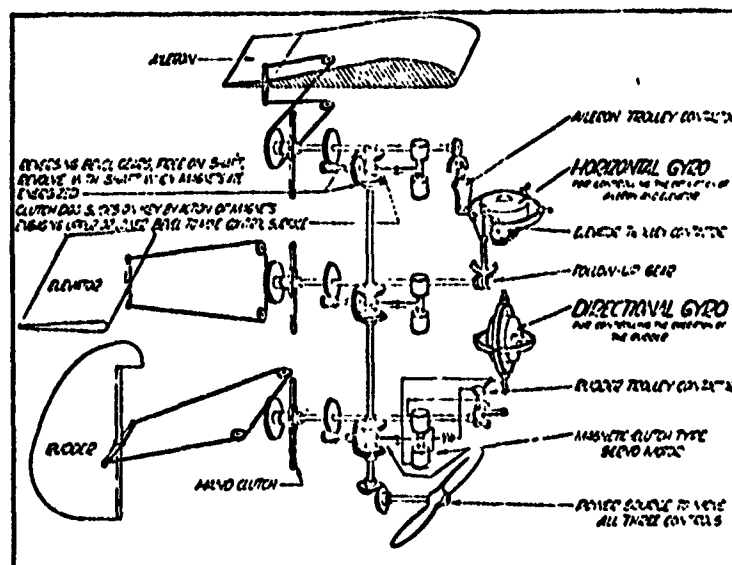


Fig. 1-7. Diagrammatic Plan of Sperry Automatic Pilot

*C. S. Draper, "Flight Control," J. Roy. Aeron. Soc., Vol. 59, July 1955, pp. 451-477.

[†]One observer vividly recalls the loud groaning noise which this type of automatic pilot made. Presumably, the noise came from the grinding of the toothed clutch faces. See the "Discussion" by Dr. A. L. Rawlings of article by F. W. Meredith and P. A. Cooke, "Aeroplane Stability and Automatic Control," in J. Roy. Aeron. Soc., Vol. 61, No. 318, June 1937, pp. 415-436.

The machine was announced to the public in October 1912. In 1914 the aircraft and its automatic pilot were entered in a safety contest sponsored by the Aero Club of France. Lawrence Sperry made a dramatic demonstration of automatic flight as he flew at low altitude along the Seine in the vicinity of Paris, standing upright in the cockpit of the Curtiss flying boat, holding his hands over his head, while his mechanic walked out along the wing. The quaint photograph of this event has been reproduced by Bollay and by Richardson among others.* A similar demonstration was planned for early the next year in New York, but there the aircraft was overturned and extensively damaged by wind before the demonstration of its performance could be satisfactorily completed.†

This first automatic pilot was intended as an aircraft "stabilizer." In other words, it was intended to supply stability, as we now say, "artificially," to aircraft which were often painfully deficient in this regard. Other inventors were pursuing the same goals by the same and other means. Feedback of angle of attack and angle of sideslip, speed, longitudinal, side, and normal acceleration, lift, and body axis rates, as well as attitude angles were all tried singly and sometimes in combination. Clarke‡ in an early paper described some of his own experiments in Great Britain, while Haus§ has sketched some of the history of early developments on the continent of Europe (see Table 1-1). However, none of these original inventors were successful enough so that his device passed immediately into common use.

The design of aircraft made giant strides during the 1914-1918 war and it was found that sufficient "stability" for the human pilot's use

*W. Bollay, "Aerodynamic Stability and Automatic Control," J. Aeron. Sci., Vol. 18, No. 9, Sept. 1951, pp. 569-624.

K. I. T. Richardson, The Gyroscope Applied, The Philosophical Library, New York, 1954.

†"The Sperry Gyroscopic Stabilizer," Flight, No. 318 (Vol. XII, No. 5) Jan. 29, 1915, pp. 74-76.

‡T. W. K. Clarke, "Auto-mechanical Stability," Aeron. J., Apr. 1912, pp. 101-115.

§Fr. Haus, Automatic Stability of Airplanes, NACA TM 695, Dec. 1932; Automatic Stabilization, NACA TM 802, Aug. 1936, and TM 815, Dec. 1936.

TABLE 1-1

SELECTED EARLY INVENTIONS IN THE FEEDBACK CONTROL OF AIRCRAFT

(Adapted from F. Haus, "Automatic Stabilization," NACA TM 802, Aug. 1936)

FEEDBACK VARIABLE	CONTROL	INVENTOR AND DATE	ACTUATING MEANS
Speed, U	Elevator deflection, δ_e	Buig.....1912 Etévé.....1914	Mechanical connection to sensor
"Incidence," α	" " "	Etévé.....1910	" " "
"Inclination," θ	" " "	Regnard.....1910 Sperry.....1912 R.A.E.....1927	Electric type of servo Air-turbine-driven clutch servo Pneumatic servo
Angular velocity, $\dot{\theta}$	" " "	Lucas.....1929 Girardville.....1910	Mechanical connection to sensor
Direction of apparent gravity, $g \sin \theta + dU/dt$...	" " "	Moreau.....1912	Electric-motor-driven clutch servo
Speed, U , and "incidence," α	" " "	Etévé.....1914	Mechanical connection to sensor
Speed, U , and direction of apparent gravity, $g \sin \theta + dU/dt$	" " "	Doutre.....1911	Pneumatic servo
Speed, U , and magnitude of apparent gravity, a_z	" " "	Doutre.....1913	Pneumatic servo
Speed, U , and "inclina- tion," θ	" " "	Harmonier.....1909	Unknown type of servo
Speed, U , and angular velocity, $\dot{\theta}$	" " "	Boykov.....1928	Hydraulic servo
Sideslip, β	Aileron deflection, δ_a	Constantin.....1920	Mechanical connection to sensor
Bank angle, ϕ	" " "	Sperry.....1912	Air-turbine-driven clutch servo
Heading, ψ	Rudder deflection, δ_r	R.A.E.....1927	Pneumatic servo
Yawing velocity, r , and side acceleration, a_y	Rudder deflection, δ_r } Aileron deflection, δ_a }	Masade & Aveline..1922	Pneumatic servos
Side acceleration, a_y , and yawing velocity, r			
Bank angle, ϕ	Aileron deflection, δ_a } Rudder deflection, δ_r }	Sperry.....1922	Air-turbine-driven clutch servos
Heading, ψ			

could be supplied by suitable choice of the size and shape of the aerodynamic surfaces. Actually many aircraft were still unstable, but not dangerously so, and, with reference to the ground, the human pilot performed the stabilizing and control functions of the (feedback) control and guidance systems. Neither artificial stabilizers nor automatic pilots were found to be particularly useful on the manned warplanes. They, in effect, disappeared from view. Under the cover of military secrecy, however, the development of the automatic pilot was continued for possible application to pilotless aircraft, and indeed in 1917-1918 Lawrence Sperry completed the construction and test of an "aerial torpedo" for the U. S. Navy.* In an advanced version the aerial torpedo was even remotely controlled by radio. The success of the project, however, came too late for the use of a "flying bomb" in the First World War. Following the war, and turning to more prosaic applications, the Sperry Gyroscope Company had, by 1932, developed an automatic pilot for possible commercial transport use† (see Fig. 1-7). Except for the gyroscopic references which comprised the then new directional and vertical gyroscopes and the fact that it provided for control about all three aircraft axes, this automatic pilot retained many of the features of the original one of 1910-1915. Better things, however, were just around the corner.

In 1933 the prototype of the A2 automatic pilot was under construction. It featured panel-mounted gyroscopes with pneumatic pickoffs and three-axis control with proportional hydraulic servos. When Wiley Post, visiting the Sperry factory, saw it, he insisted that it be installed in his Lockheed Vega 5-C.‡ During the period 15-22 July 1933 Post, flying alone, set a round-the-world record of 7 days, 18 hours. The performance and reliability of the automatic pilot, which allowed the human pilot to perform the navigator's function and even to nap in flight, played a considerable

*P. R. Bassett, "Instruments and Control of Flight," Aeron. Eng. Rev., Vol. 12, No. 12, Dec. 1953, pp. 118-123, 133.

†E. A. Sperry, Jr., "Description of the Sperry Automatic Pilot," Aviation Eng., Jan. 1932, pp. 16-17. See also E. S. Ferry, Applied Gyrodynamics, John Wiley and Sons, New York, 1932, pp. 123-125.

‡Bassett, loc. cit.

role in this feat. The prototype automatic pilot used by Wiley Post, together with his airplane, the "Winnie Mae," are in the National Aeronautical Collection of the Smithsonian Institute in Washington.

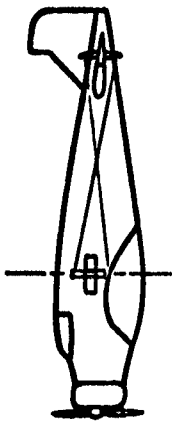
The A2 automatic pilot came into widespread use among the airlines during the 1930's. This was due partly to its demonstrated reliability, partly because the panel-mounted instruments then coming into extensive use for routine operations under low visibility conditions supplied its gyroscopic references (an obvious economy in cost and weight), and partly because airplanes had achieved a range performance which made pilot relief attractive. The A2 was first introduced to airline service on the Boeing Model 247 in 1934. Its defects, if any, were its virtues; it flew straight and level. It was not designed for maneuvering.

In effect, this automatic pilot provided for control surface deflections in three axes which were proportional to the departures from the reference attitude. (A description of its operation is given by Richardson,* among others.) It was as if the surfaces were "geared" to the instrument (see Fig. 1-8). This concept of "gearing" was frequently employed in some of the early mathematical studies of automatic control of aircraft, but it lacks the generality offered by the concept of feedback.

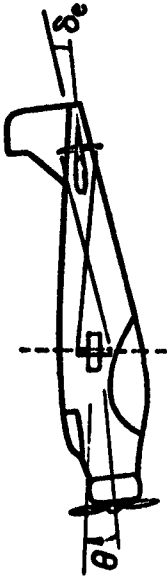
During roughly the same period of time (1922-1937), somewhat similar automatic pilot developments were under way in Great Britain, although the aim there was the satisfaction of military requirements and the work was, at first, carried out in secrecy.[†] Interestingly, in both the earlier

*Richardson, loc. cit. See also: P. R. Bassett, "Development and Principles of the Gyropilot," Instruments, Vol. 9, No. 9, Sept. 1936, pp. 251-254; The Sperry Aircraft Gyropilot, Sperry Gyroscope Co. Publication 15-665, July 1940.

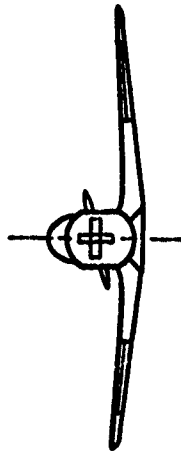
[†]A comprehensive bibliography of British and foreign work on automatic flight control, both theoretical and experimental, from 1903 to 1957 has been prepared by the Royal Aircraft Establishment. See R. C. Wright, A. T. E. Bray, and H. R. Hopkin, List of Published and Unpublished References on the Remote and Automatic Control of Aircraft and Missiles, Pilotless Target Aircraft, Autopilots and Gyroscopic Flight Instruments, Inertial Guidance and Automatic Landing of Aircraft, R. A. E. Library Bibliography No. 224, Ministry of Aviation, Sept. 1960 (RESTRICTED DISCREET)



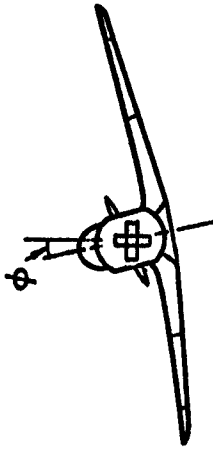
Airplane in level flight
Gyro axis vertical
Elevator in trim position



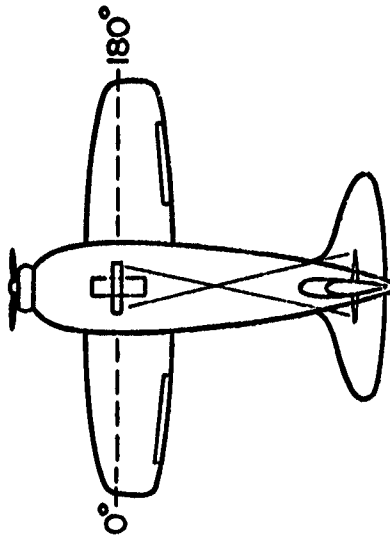
Airplane dives
Gyro axis vertical
Elevator deflected trailing edge up



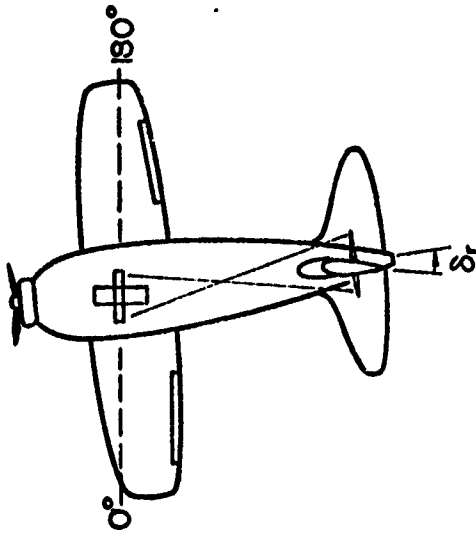
Airplane level
Gyro axis vertical
Ailerons in trim position



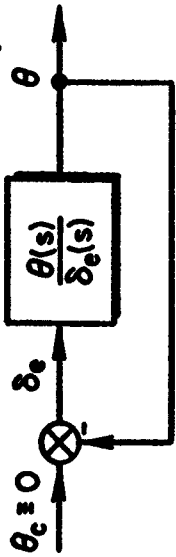
Airplane banked left
Gyro axis vertical
Ailerons deflected so as to roll right



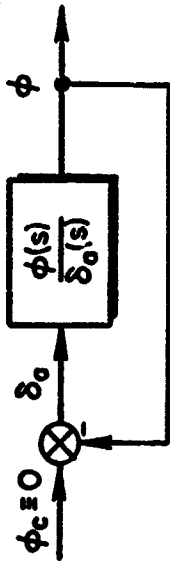
Airplane flying on 90° heading
Gyro axis aligned N - S
Rudder trailing



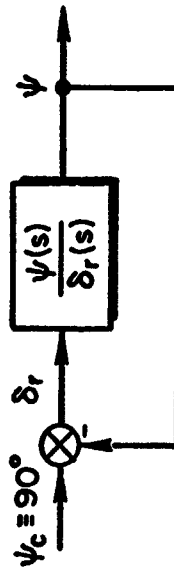
Airplane swings left
Gyro axis aligned N - S
Rudder deflected



Pitch control illustrated as a feedback system



Bank angle (roll) control illustrated as a feedback system



Heading (Azimuth) control illustrated as a feedback system

Figure 1-8. Simple Three-Axis Attitude Control Illustrating the Concept of Gearing

(Mark I) and later (Mark VII and Mark VIII) versions the British pursued the design of two-axis controls with great diligence. The Mark I used a single free gyroscope measuring heading and pitch to control the rudder and elevators by means of low pressure pneumatic servos. An account of the results of the early efforts was presented by the pioneers Meredith and Cook of the Royal Aircraft Establishment in 1937.* This account describes the use of the automatic pilot in aerial map-making and suggests its superiority over the Sperry three-axis design for applications requiring maneuvers. It also shows the considerable acquaintance of the authors with the theory, methods, and conclusions of their colleagues at the Royal Aircraft Establishment who had been engaged in the study of the dynamic stability of airplanes. The action of the automatic pilot was clearly explained in those terms. In fact the methods of dynamic stability analysis had been applied in the design of the R.A.E. flight control equipment from 1924 on, but very few results were ever published in the open literature.

Following in the footsteps of Bairstow[†] and Glauert[‡] and using a method developed by S. B. Gates,[§] who employed it in the obscure R.A.E. Reports BA 487 and BA 494, Garner,^{||} in 1926, made an analysis of the lateral/directional motion of an airplane under the influence of feedback control. Gates assumed that the controls were moved according to certain "laws," e.g., in proportion to certain output variables and their derivatives. He also stressed that good stability was not enough,

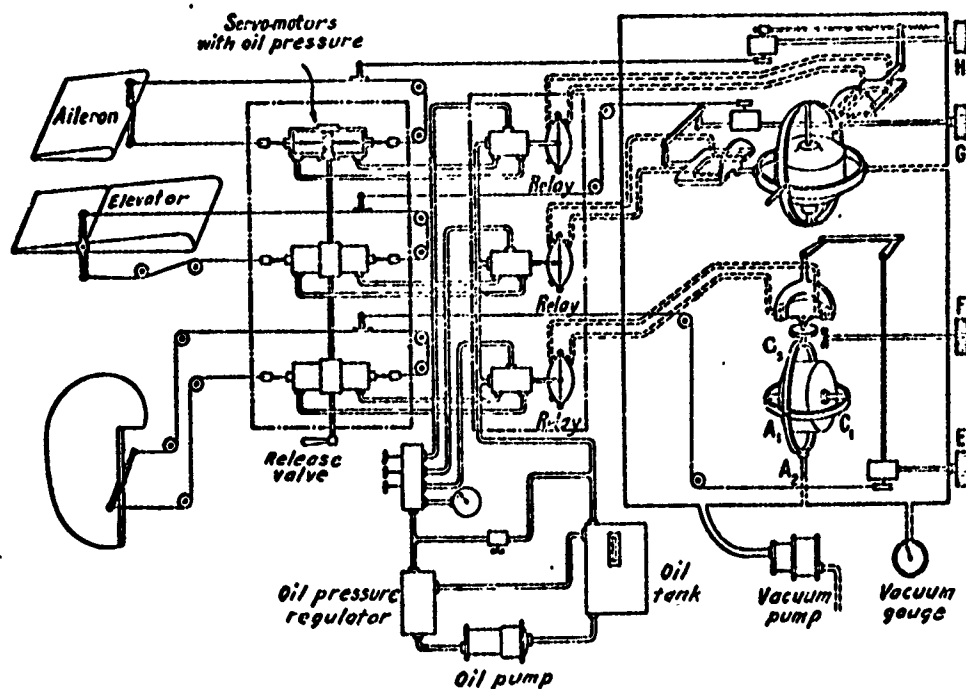
*F. W. Meredith and P. A. Cooke, "Aeroplane Stability and the Automatic Pilot," J. Roy. Aeron. Soc., Vol. 61, No. 318, June 1937, pp. 415-436.

†L. Bairstow, Applied Aerodynamics, 1st ed., Longmans Green and Co., London, 1920.

‡H. Glauert, Summary of the Present State of Knowledge with Regard to Stability and Control of Aeroplanes, A.R.C. R&M 710, Dec. 1920.

§S. B. Gates, Notes on the Aerodynamics of Automatic Directional Control, R.A.E. Rept. No. BA 487, 19 Feb. 1924, and Notes on the Aerodynamics of an Altitude Elevator Control, R.A.E. No. BA 494, 19 Mar. 1924. (The latter report discusses the instability of altitude control with elevator at speeds below the speed for minimum power required.)

||H. M. Garner, Lateral Stability with Special Reference to Controlled Motion, A.R.C. R&M 1077, Oct. 1926.



(H, climbing knob; G, banking knob; for other references, see text)

Fig. 1-9. Assembly Sketch of Sperry Stabilizer

it being essential also to consider the amplitudes of the several modes of motion. With similar assumptions, Garner calculated the stability of the undisturbed motion and the transient motion, following an initial disturbance, under the influence of the feedback control system. It was specifically pointed out that the movements of the controls might be regarded as made either by the (human) pilot or by some mechanical means. Garner then further had the wit and vision to make provision in the theoretical treatment for "lag" in the application of controls, and was able to point to a qualitative correspondence between his analytical results and flight tests of an R.A.E. (automatic) rudder control which had appreciable "reaction lag." Only shortly after Garner's report there appeared a further contribution by Cowley* which proposed more elaborate methods of taking into account the time lag in the application of control. Both a pure time delay and a second-order lag were successfully treated.

*W. L. Cowley, On the Stability of Controlled Motion, A.R.C. R&M 1235, Dec. 1928.

It now seems surprising that these papers are not given more prominence in accounts of the development of the theory of automatic control systems. Perhaps they were simply too far ahead of their time. Perhaps, on the other hand, it was only in Great Britain where automatic flight control system development was the responsibility of a government research establishment that it was thought to be desirable to make response calculations in connection with the design of "practical" systems. In spite of an apparently adequate theory, however, stability difficulties attended the early flight trials of the R.A.E. Mark IV automatic pilot circa 1934.* A solution to the problem was apparently not found by analysis or simulation. The problem went away when the autopilots were installed in the larger aircraft for which they were intended, no doubt because of the larger inertia and slower response of the multiengined bombers.

Comprehensive details of subsequent British Automatic pilot development (1937-1947) as well as comments on American and German efforts are set forth in the report by Hopkin and Dunn.[†] Included there is the story of the uniquely conceived Mark VII autopilot. In this device the elevator was moved in response to airspeed error and error rate, while the ailerons were actuated by a combination of yaw and roll signals detected by a free gyroscope. The rudder was left free. Calculations showed that the stability properties of this arrangement should have been satisfactory, as indeed they were. Unfortunately, although the performance in average weather was good, in very rough air and in some aircraft at low speed, the elevator, responding to detected changes in the airspeed and airspeed rate, caused violent changes in pitch attitude. These were large enough in some cases so that the acceleration on the fuel system caused the engines to stop momentarily. Later the matter was investigated

*H. R. Hopkin and R. W. Dunn, Theory and Development of Automatic Pilots, 1937-1947, Royal Air. Estab. Rept. T.A.P. 1459, Monograph 2.5.03, Aug. 1947.

[†]Hopkin and Dunn, however, omit any mention of the Pollock/Brown all hydraulic automatic pilot. This again was a two-axis unit driving the elevators and rudder. It is described in the article "A New Automatic Pilot," Flight, Vol. 27, No. 1360, 14 Mar. 1935.

theoretically by Neumark* and by Sudworth and Hopkin.[†] They were quite able to identify the source of the difficulty and to show that the calculation of damping factors alone was not sufficient to insure satisfactory performance. At the R.A.E. similar calculations were made both by hand and with a mechanical differential analyzer. Very few of the results, however, were published. The understanding of response to specific disturbances which Gates had stressed and for which B. Melvill Jones had predicted was thus only modestly enhanced.

Interestingly, by 1935 the German firm of Siemens had developed an elevator control which successfully used an airspeed reference, and a rudder control with one of the earliest magnetic compass tie-ins.[‡] Hydraulic positioning servos were employed to move the surfaces, but the key feature in both cases was the use of a rate gyro feedback. The rudder "course control" was an independent unit. In Germany it was argued that only the largest and heaviest airplanes would require a complete automatic pilot, but that practically all small and medium machines could make good use of a course control.[§]

The firms of Siemens and Askania both developed three-axis automatic pilots which included an independent course control,^{||} but during the war they concentrated on the production of the single-axis units. Eventually more than 80 percent of the aircraft in the German Air Force were equipped

*S. Neumark, The Disturbed Longitudinal Motion of an Uncontrolled Aeroplane and of an Aeroplane with Automatic Control, A.R.C. R&M 2078, Jan. 1943.

[†]J. Sudworth and H. R. Hopkin, Influence of Automatic Pilots in Stabilization and Dynamic Stability in Pitch, R.A.E. Tech. Note No. Instn. 775, July 1943.

[‡]Fr. Haus, Automatic Stabilization, NACA TM 802, Aug. 1936. See also "Siemens Autopilot," Flight, Vol. 27, No. 1359, 10 Jan. 1935, pp. 41-42.

[§]G. Klein, "Bedeutung automatischer Flugzeugsteuerungen für den Flugzeugbau," Jahrbuch 1938 der Deutschen Luftfahrtforschung, Ergänzungsband, R. Oldenbourg, Munich and Berlin, 1938, pp. 237-242.

^{||}E. Fischel, "Verfahren und Bauglieder automatischer Flugzeugsteuerungen," Jahrbuch 1938 der Deutschen Luftfahrtforschung, Ergänzungsband, R. Oldenbourg, Munich and Berlin, 1938, pp. 231-236.

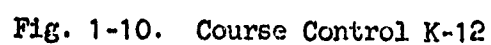
with similar automatic stabilizers. A schematic diagram of the Siemens K-12 unit is shown in Fig. 1-10. It was recognized at an early date that such a control could be used to supplement any deficiency in the aerodynamic damping about the yaw axis,* and that the course-holding feature, providing the airplane with a heading sense, would permit unattended operation, to a degree, so that even a pilot inexperienced in instrument flying could conduct operations in instrument weather in comparative safety. It may be noted that the methods of mathematical analysis which were introduced by Oppelt† for the study of automatic course-holding were rather sophisticated for their time. While he used much simplified linear equations to represent the aircraft in the 1937 paper, he also used phasor diagrams and approximate describing functions for friction and hysteresis to explore the deleterious effects on the action of the automatic control of these and other imperfections in the system, such as quantized signals, and he pointed to the use of a rudimentary simulator as a means for exploring the effect of nonideal equipment characteristics in practice.

Later, during the war, the Germans introduced the rate-rate principle in the Siemens K-23 and Askania PKS-12 "fighter" course controls, and also in the experimental Patin three-axis automatic pilot. (Here the surfaces were made to move at a rate proportional to the rate of body axis rotation measured by a rate gyro, but damping was insured by electrical differentiation of the signal in the case of the Siemens and Askania units and by special design of the gyros to pick up a component of angular acceleration in the case of the Patin design. No feedback units measured the output of the servos.) All three of these control systems were all-electric.

It can be appreciated, even from this abbreviated account, that airplane automatic pilot development proceeded quite independently in

*K. Wilde, "Über neuere Arbeiten auf dem Gebiet der automatischer Steuerungen," Jahrbuch 1938 der Deutscher Luftfahrtforschung, Ergänzungsband, R. Oldenbourg, Munich and Berlin, 1938, pp. 243-247.

†W. Oppelt, "Die Flugzeugkursteuerung im Geradeausflug," Jahrbuch 1937 der Deutscher Luftfahrtforschung, R. Oldenbourg, Munich and Berlin, 1937, pp. III-22-III-34; also Comparison of Automatic Control Systems, NACA TM 966, Feb. 1941.



Germany from its course in the United States and in Great Britain. Some idea of how it might have evolved can be obtained from Dudenhausen's* description of a three-axis rate-rate automatic flight control system actually built in 1955 but based to a large extent on developments carried out just before the final collapse of Hitler's armies. (It is further amusing to note in the same issue of Luftfahrttechnik in which the Dudenhausen article appears that a speaker from an American company, tracing the history of automatic pilot development, says that course control was easily added after the more difficult problem of stabilizing the aircraft in pitch and roll was accomplished. His German translator felt constrained to correct him. From the German point of view the course control came first.†)

The Germans were also, of course, very active in the development of pilotless aircraft and missiles.‡ The V-1 flying bomb had a conventional two-axis (elevator and rudder) automatic pilot with altitude and compass tie-ins (see Fig. 1-11). An air mileage counter determined when the final dive should begin. And in spite of its, in many ways, very advanced technology the V-2 (A-4) simply used two free gyros—the master control gyro to control yaw and roll, and the "verticant" to control pitch by means of hydraulic servo-driven vanes in the exhaust blast of the rocket engine (see Fig. 1-12). A pitch maneuver was preprogrammed and thrust was cut off by an integrating accelerometer. Provision was made for monitoring and correcting the course with a radio beam. The gyro and vane arrangement was somewhat similar to the one evolved some time

*H. J. Dudenhausen, "Dreiaachsen-Flugregelung für Hochleistungsflugzeuge mit Integrations-Wendekreiseln als Haupttrichtgeber," Luftfahrttechnik, Band 4, Nr. 3, 18 Mar. 1958, pp. 49-58.

†J. F. Wiren, "Geschichtliches zur Entwicklung der Flugregelungen," Luftfahrttechnik, Band 4, Nr. 3, 18 Mar. 1958, pp. 46-68, and notes by the translator, Dpl. Ing. Manteufel.

‡T. H. Benecke and A. W. Quick, eds., History of German Guided Missiles, Verlag E. Appelhans and Co., Brunswick, Germany, 1959.

J. N. Thiry, Control Projects in the German Army, Air Force, and Navy, unpublished translation of a German report with the same title written in Aug. 1944, 10 Sept. 1958.

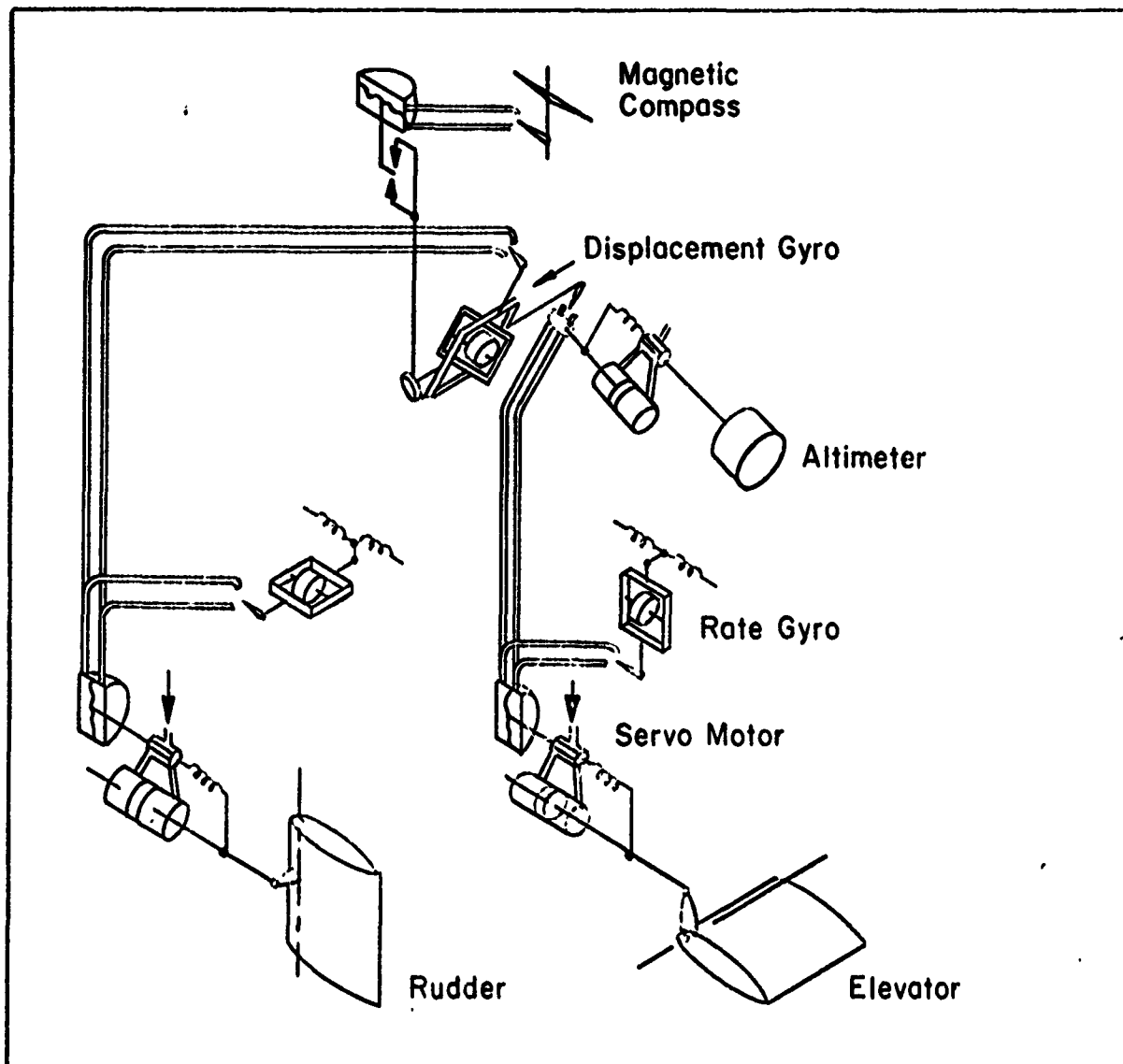


Fig. 1-11. V-1

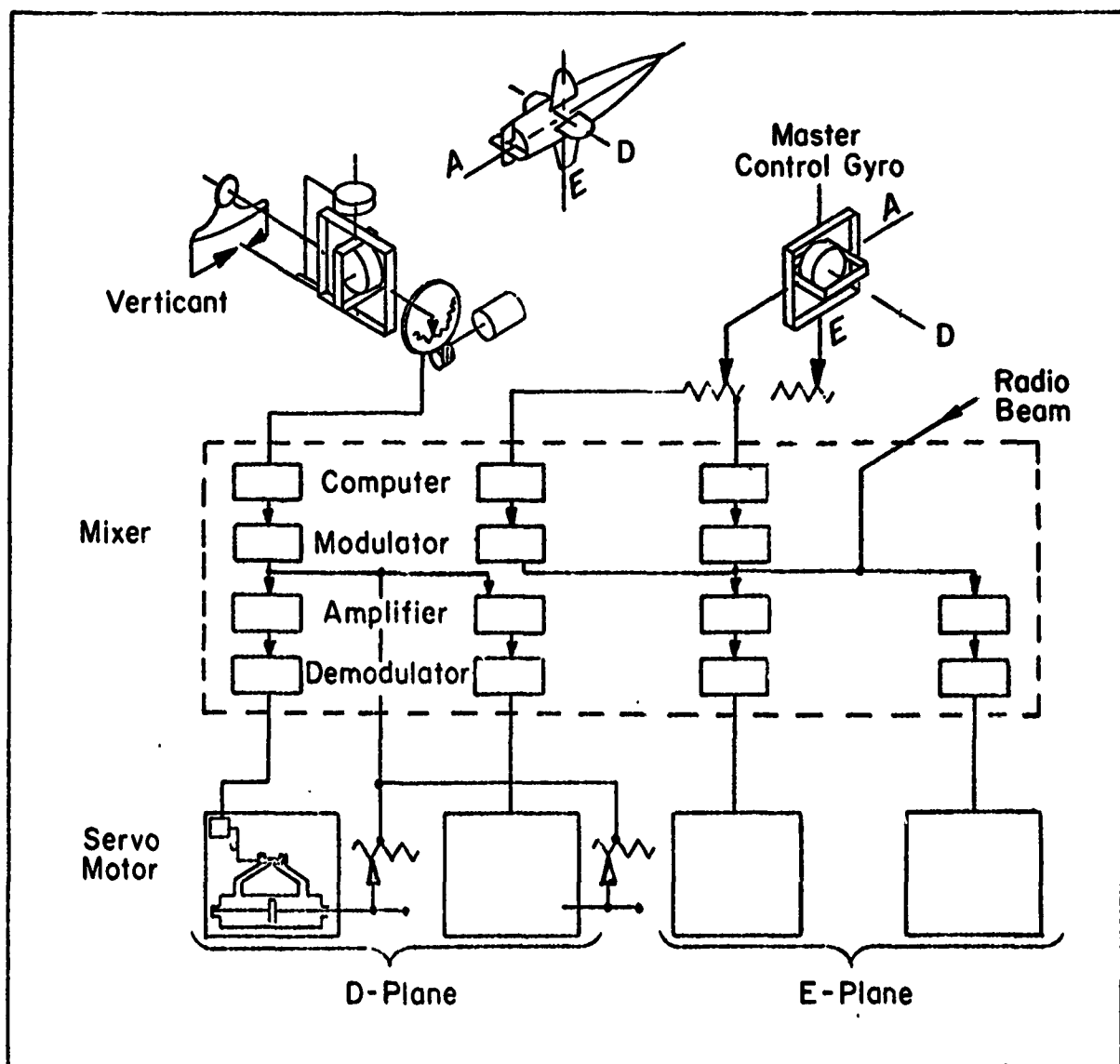


Fig. 1-12. V-2

earlier (1932) by the pioneer R. H. Goddard for the control of his rockets.*

Beginning in 1941 there was a considerable amount of activity in the United States aimed at the development of electric automatic pilots ultimately capable of accepting maneuvering commands either from the human pilot or from some other source of guidance information, such as a bombsight. The first of these "all-electric" automatic pilots was the C-1 built by the Minneapolis-Honeywell Regulator Company.[†] It was installed in all the American four-engined bombers, such as the B-17, B-24, and B-29. In the C-1 deviations from the reference attitude in pitch, roll, and yaw were measured with vertical and directional gyroscopes, as in the Sperry A2 design, but the amplified signals were applied to electrical positioning servomotors driving the elevators, ailerons, and rudders. The automatic pilot unit was specifically designed to slave the aircraft to commands originating in the bombardier's operation of the bombsight, but a single-knob turn control, and later a "formation stick," was also provided for the pilot. Erection cutout in turns was one of the novel features of this automatic pilot. The electrically driven gyroscopes were not intended to be used as flight instruments. Later, in the C-1A (1945), a number of improvements were introduced including the addition of a yaw rate gyro signal to the rudder.

This unit was closely followed in time by the General Electric design,[‡] which was similar to the Sperry pneumatic/hydraulic A2 unit in its functions, and which differed from the C-1 in its design mainly in that the electrically driven gyroscopes were also the panel-mounted flight instruments, and in that electrohydraulic positioning servomotors provided the

*M. Lehman, This High Man: The Life of Robert H. Goddard, Farrar Straus and Co., New York, 1963, pp. 202 et seq.

[†]W. H. Gille and R. J. Kutzler, "Application of Electronics to Aircraft Flight Control," Trans. AIEE, Vol. 63, Nov. 1944, pp. 849-853. See also W. H. Gille and H. T. Sparrow, "Electronic Autopilot Circuits," Electronics, Oct. 1944, pp. 110-117.

[‡]C. M. Young, E. E. Lynch, and E. R. Boynton, "Electrical Control in Automatic Pilots," Trans. AIEE, Vol. 63, Nov. 1944, pp. 939-943.

final stage of power amplification. At first the controls were merely trim knobs, one for each axis, but later a single-knob turn control was introduced.* This automatic pilot was notable for its light weight (74.5 lb) so that it was suitable for installation in fighters and light attack aircraft.

The Sperry Gyroscope Company also developed an electric automatic pilot during the war, the A5. It had a number of novel features such as altitude control, automatic elevator trim by means of an additional trim tab servo, and, notably, equalizing circuits which provided for phase advance of the servo actuating signals. The servos were electrohydraulic units with force feedback. This was thought to be a desirable feature in that, since control surface effectiveness and aerodynamic hinge moment vary in much the same way with speed and altitude, the closed-loop response with force feedback should tend to be invariant with flight condition.† Early flight tests in a Fairchild 22 were encouraging. Unfortunately, as it turned out in practice, the deleterious effect of control cable friction made it extremely difficult to secure satisfactory operation in the large aircraft,‡ such as the B-24E "Liberator," for which this automatic pilot was intended.

The Eclipse-Pioneer Division of the Bendix Corporation began work on the "flux-gate" compass in 1939 and, about 1943, introduced automatic heading control from the "flux-gate" compass in the all-electric P-1 (A-10) autopilot. This equipment obviated the very tiresome necessity of frequently resetting the directional gyro by reference to the magnetic compass. The P-1 also featured a yaw rate gyro signal fed to the rudder, automatic synchronization so that it could be engaged in any attitude, and a computed up-elevator signal in turns.

*H. R. Hopkin and R. W. Dunn, Theory and Development of Automatic Pilots, 1937-1947, Royal Airc. Estab. Rept. I.A.P. 1459, Monograph 2.5.03, Aug. 1947.

†P. Halpert and O.E. Esval, "Electric Automatic Pilots for Aircraft," Trans. AIEE, Vol. 63, Nov. 1944, pp. 861-866.

‡B. Levine, "Discussion" of paper by P. Halpert and O. E. Esval, Trans. AIEE, Vol. 63, Nov. 1944, p. 1501.

Somewhat later considerable effort was expended in designing automatic pilots specifically for fighter aircraft, and Lear, Incorporated, introduced the F-5 automatic pilot about 1950.* In the F-5 the problem of supplying power amplification for the control surface positioning servos was solved with magnetic powder clutches. The use of these units eliminated much relatively heavy equipment, such as electronic or rotating power amplifiers, and provided for high performance servomechanisms in a compact and lightweight package. The gyroscopic references, however, were the conventional vertical and directional gyroscopes, and the maneuvers which could be made under automatic control were limited by the phenomenon of "gimbal lock." This problem was attacked by Westinghouse† and the Instrumentation Laboratory at the Massachusetts Institute of Technology,‡ both of whom constructed laboratory models of fighter airplane all-attitude sensors using different kinds of single-degree-of-freedom gyroscopes.

Improvements were also made in providing for guidance tie-ins. Immediately after the war the Sperry Gyroscope Company brought out the A-12 automatic pilot§ and Bendix introduced the PB-10.|| Both of these were equipped with approach couplers and the Bendix system had automatic throttle controls for the control of airspeed on the approach to the runway. In England the Smith's firm brought out the all-electric rate-rate SEP-2 automatic pilot and approach coupler.¶

*J. Harper, "George Turns Tiger," Flying Safety, Jan. 1956.

†C. R. Hanna, K. A. Oplinger, and G. R. Douglas, "Automatic Flight Control System Using Rate Gyros for Unlimited Maneuvering," Electrical Engineering, Vol. 73, No. 5, May 1954, pp. 443-448.

‡H. P. Whitaker, J. A. Gautraud, and S. A. Wingate, Flight Test Evaluation of the MIT Automatic Control System for Aircraft, MIT Instrumentation Lab. Rept. R-55, 1953.

§P. Halpert, The A-12 Gyropilot, paper presented to the SAE, New York, 13-15 Apr. 1948.

||J. C. Owen, "Automatic Pilots," Electrical Engineering, Vol. 67, No. 6, June 1948, pp. 551-561.

P. A. Noxon, "Flight Path Control," Aeron. Eng. Rev., Vol. 7, No. 8, Aug. 1948, pp. 36-45.

¶F. W. Meredith, "The Modern Autopilot," J. Roy. Aeron. Soc., May 1949, pp. 409-428. See also W. H. Coulthard, Aircraft Instrument Design, Pitman, 1952.

All the elements of a modern automatic pilot were now at hand, and in 1947 the U. S. Air Force All-Weather Flying Division's C-54 "Robert E. Lee," equipped with a Sperry automatic pilot and approach coupler and Bendix throttle controls, made a dramatic demonstration of completely automatic flight. Taking off from Stephenville, Newfoundland, on the evening of 21 September, it flew through the night across the Atlantic and landed the next day at Brize-Norton in England. From the time the brakes were released for the takeoff roll until the landing roll was complete, no human hand touched the controls. Selection of course, radio station, speed, flap setting, landing gear position, and the final application of wheel brakes were all accomplished automatically from a program stored on punched cards. The complete automation of aircraft flight seemed to be at hand. Anast* described the performance and the prospects early in 1948.

While the development of automatic pilots up to 1950 had, in general, been responsive to the needs of potential users, and while such features as single-knob turn control, erection cutout, automatic trim, altitude control, synchronizers, rate gyro feedbacks, compass tie-in, and approach coupling served useful purposes in some applications, in many cases they were introduced only as the technology became readily available and certainly not because they were required for any particular airplane. The automatic pilot was almost universally regarded as a useful but hardly an essential item of equipment, and the day had not yet arrived when an automatic pilot would be designed for a specific airplane by taking into account, right from the beginning, particular and peculiar features of the mission of the airplane and of the design of its control system.

Perhaps because of the obvious necessity for a special design of the flight control system in a missile and the successes which were achieved with that approach, and certainly further, in part, because the postwar generation of jet airplanes almost invariably needed some form of stability augmentation whose particular nature was often dictated by the unique configuration or mission of the vehicle, the most common design practice later came to be based on a careful enumeration of requirements to be met

*J. L. Anast, "Automatic Aircraft Control," Aeron. Eng. Rev., Vol. 7, No. 7, July 1948.

and functions to be performed by each system. This alteration in the methods of design was only one of several which, together, radically changed the nature of work in automatic flight control.

1.6 THE JOINING OF CONTROL TECHNOLOGY AND DYNAMIC ANALYSIS

While the mathematical tools for performing analyses of automatic flight control systems for aircraft had existed in at least a rudimentary form before the war of 1939-1945, there has been occasion to remark that they did not seem to be much used. The work of Gates, Garner, and Cowley* seems to have been nearly forgotten. Oppelt,[†] even though translated into English, does not seem to have attracted much attention, while Minorsky's paper[‡] on the steering of ships was fairly widely known but did not seem to inspire other workers to follow similar lines. There had appeared, here and there, papers or monographs on the theory of servomechanisms,[§] the regulation of prime movers,^{||} process control,[#] the dynamics of

*See footnotes, pp. 1-36-1-37.

[†]W. Oppelt, Comparison of Automatic Control Systems, NACA TM 966, Feb. 1941.

[‡]N. Minorsky, "Directional Stability of Automatically Steered Bodies," J. Amer. Soc. of Naval Eng., Vol. 34, 1922, pp. 280-309.

[§]H. L. Hazen, "Theory of Servomechanisms," J. Franklin Inst., Vol. 218, No. 3, Sept. 1934, pp. 279-331; also "Design and Test of a High Perform- and Servomechanisms," J. Franklin Inst., Vol. 218, No. 5, Nov. 1934, pp. 543-580.

^{||}A. Stodola, Steam and Gas Turbines, translated from German 6th ed. by C. L. Loewenstein, Vol. I, McGraw-Hill Book Co., New York, 1927.

W. Trinks, Governors and the Governing of Prime Movers, Van Nostrand Co., New York, 1919.

H. K. Weiss, "Constant Speed Control Theory," J. Aeron. Sci., Vol. 6, No. 4, Feb. 1939, pp. 147-152.

[#]G. Wunsch, Regler für Druck und Menge, R. Oldenbourg, Munich, 1930.

A. Ivanoff, "Theoretical Foundations of the Automatic Regulation of Temperature," J. Inst. of Fuel (London), Feb. 1934.

S. D. Mitereff, "Principles Underlying the Rational Solution of Automatic Control Problems," Trans. ASME, Vol. 57, No. 4, May 1935, pp. 159-163.

E. S. Smith, Jr., "Automatic Regulators, Their Theory and Application," Trans. ASME, Vol. 9, No. 4, May 1936, pp. 159-163; also Automatic Control Engineering, McGraw-Hill Book Co., New York, 1944.

A. Callender, D. R. Hartree, and A. Porter, "Time Lag in a Control System," Phil. Trans. Roy. Soc. London, Vol. 235A, 1936, pp. 415-444.

C. E. Mason and G. A. Philbrick, "Automatic Control in the Presence of Process Lags," Trans. ASME, Vol. 62, 1940, pp. 295-308.

instruments,* and the Cauchy/Heaviside operational calculus applied to the dynamic response of aircraft,[†] but apparently the need to study the feedback control of aircraft for practical reasons was not yet felt.

The subject of the theory of automatic control of aircraft did receive some attention in the universities, technical institutes, and research laboratories, however. Longitudinal stability of an airplane under the action of a control system of the Sperry A2 or A3 automatic pilot type was investigated by Klemin, Pepper, and Wittner[‡] at New York University, and H. K. Weiss[§] at MIT performed a comprehensive study of the stability of an automatically controlled airplane, including both the free longitudinal and lateral motions and the response to gusts, as his thesis research for the Master's degree. There was also a very original contribution from Imlay^{||} who explored the problem of selecting "optimum" gearings, but all this barely carried the matter further than the state in which it had been left by the British authors nearly 15 years before. The difficulty, as Weiss pointed out, lay in the necessity for

*C. S. Draper and G. V. Schliestett, "General Principles of Instrument Analysis," Instruments, Vol. 12, No. 5, May 1939, pp. 137-142.

C. S. Draper and G. P. Bentley, "Design Factors Controlling the Dynamic Performance of Instruments," Trans. ASME, Vol. 62, No. 5, July 1940, pp. 421-432.

[†]L. W. Bryant and D. H. Williams, The Application of the Method of Operators to the Calculation of the Disturbed Motion of an Airplane, A.R.C. R&M 1346, July 1930.

R. T. Jones, A Simplified Application of the Method of Operators to the Calculation of the Disturbed Motion of an Airplane, NACA TR 560, 1936; see also "Calculation of the Motion of an Airplane Under the Influence of Irregular Disturbances," J. Aeron. Sci., Vol. 3, No. 12, Oct. 1936, pp. 419-425.

A. Klemin and B. F. Ruffner, "Operator Solutions in Airplane Dynamics," J. Aeron. Sci., Vol. 3, No. 7, May 1936, pp. 252-255.

[‡]A. Klemin, P. A. Pepper, and H. A. Wittner, Longitudinal Stability in Relation to the Use of an Automatic Pilot, NACA TN 666, Sept. 1938.

[§]H. K. Weiss, Theory of Automatic Control of Airplanes, NACA TN 700, Apr. 1939.

^{||}F. H. Imlay, A Theoretical Study of Lateral Stability with an Automatic Pilot, NACA TR 693, 1940.

factoring characteristic functions of the fifth, sixth, and seventh degree. The same problem, of course, plagued students of other feedback control devices, and a considerable effort was made to find convenient methods for accomplishing the tedious algebra.*

In 1944, discussing the subject of automatic flight and airplane stability (which he treated separately), Zand[†] still found the situation very unsatisfactory. He wrote, "...a thorough knowledge of the stability of the airplane is a prerequisite toward the successful solution of the problem of automatic flight. We have sketched the difficult path which led airplane designers toward the understanding of fundamentals of dynamic stability. An equally thorny road full of obstacles has been conquered by the instrument engineer who succeeded against such odds as space and weight limitations, lack of power, etc. In many instances the airplane engineering field and the instrument engineering fraternity have worked independently on the problem which concerns both branches directly. Pooling the knowledge of dynamic stability with the knowledge of instrument design for the general betterment of aeronautics is essential.... Experience has shown that if the matching is performed theoretically first the number of experimental flying hours will be reduced to a minimum and the results obtained superior." Indeed, the theoretical matching of the two subjects was shortly to become not merely a desideratum but an absolute necessity.

The war had seen the advent, on both sides, of the turbojet engine, so that suddenly the limits of the flight envelope were enormously

*Y. J. Liu, Servomechanisms, Charts for Finding Their Stability and for Finding the Roots of Their Third and Fourth Degree Characteristic Equations, Dept. of Electrical Eng., MIT, Oct. 1941.

Shi-Nge Lin, "Method of Successive Approximations of Evaluating the Real and Complex Roots of Cubic and Higher Order Equations," J. Math. and Phys., Vol. 20, Aug. 1941, pp. 231-242.

A. Porter and C. Mack, "New Methods for the Numerical Solution of Algebraic Equations," Phil. Mag., Vol. 40, No. 304, May 1949, pp. 578-585.

H. R. Hopkin, Routine Computing Methods for Stability and Response Investigations on Linear Systems, A.R.C. R&M 2392, Aug. 1946.

[†]S. J. Zand, "Automatic Flight and Airplane Stability," Aviation, Vol. 43, No. 6, June 1944, pp. 140-141, 290-296.

extended in both speed and altitude, with concomitant configuration changes involving increased wing loadings, mass distributions concentrated in long thin fuselages, and the aerodynamic benefits of short span, swept wings. These things, taken together, led to a marked defect in the damping of the longitudinal short-period and dutch roll oscillations in the airplanes of the immediate postwar period. However, it was not only the "classical" modes which were deficient in stability, previously unknown coupled modes made their appearance. Among these were fuel slosh* and the rolling instability.[†] Furthermore, thinner wings and finer fuselages combined with advances in materials and manufacturing processes made for increased structural flexibility. Power-boosted controls[‡] had also come into use to handle the large hinge moments of the control surfaces. Early hydraulic power units had stability difficulties of their own,[§] and the inevitable lag was inimical to the stability of automatic flight control systems. All these trends were bad news for the automatic flight control system designer, who now desperately wanted analytical help.

The intimate joining of control technology and vehicle dynamic analysis which would, no doubt, have come about in any event, was forced,

*A. Schy, A Theoretical Analysis of the Effects of Fuel Motion on Airplane Dynamics, NACA Rept. 1080, 1952.

H. Luskin and E. Lapin, "An Analytical Approach to the Fuel Sloshing and Buffeting Problems of Aircraft," J. Aero. Sci., Vol. 19, No. 4, Apr. 1952, pp. 217-228.

[†]F. D. Graham and R. C. Uddenberg, The Dynamic Stability and Control Problem of a Pivoted-Wing Supersonic Pilotless Aircraft, Boeing Airplane Co., Document D-8810, Feb. 1948.

W. H. Phillips, Effect of Steady Rolling on Longitudinal and Directional Stability, NACA TN 1627, June 1948.

[‡]D. J. Lyons, "Present Thoughts on the Use of Powered Flying Controls in Aircraft," J. Roy. Aeron. Soc., Mar. 1949, pp. 253-277.

T. A. Feeney, "Powered Control System Design Practice at Northrop Aircraft," Proc. of the BuAer Symposium on Analysis and Design of Power Boosted and Power Operated Surface Control Systems, 6-7 Oct. 1949.

[§]D. T. McRuer, "An Analysis of Northrop Aircraft Powered Flight Controls," ibid.

by the marked deficiencies in stability of the new jet aircraft and also by the advent of the guided missile where it was obviously essential to match the dynamics of the airframe and the control system from the first flight on.* One of the first children of the marriage was the "stability augmenter," a feedback control designed to modify the inherent aerodynamic stability of the airframe, "augmenting" one or more of the stability derivatives by imposing forces or moments through actuation of the controls in response to motion variables. Thus, in short order, there were invented or reinvented the:

- Yaw damper
- Sideslip stability augmenter
- Pitch damper
- Roll damper
- Transonic trim shifter
- Autothrottle

and other devices. Since both the problem and the solution were inevitably connected with a particular aircraft and its control system, the old methods of designing general purpose equipment were totally inadequate. Extensive analysis and simulation for each application to a piloted aircraft or missile was found to be required.

In the interim, wartime pressures for very high performance servo-mechanisms and regulators for such uses as servo-controlled aircraft wing spar milling machines,[†] process controls in the manufacture of fissionable material,[‡] and particularly for fire control and navigation

*While it seems surprising that the developers of the V-2 were able to make do with stability diagrams and a rudimentary simulator, they did not entirely neglect analysis in the design of the control and guidance equipment. The frequency response method and Nyquist stability criterion were known but were not "popular." See O. Müller, "The Control System of the V-2," in T. Benecke and A. W. Quick, eds., History of German Guided Missile Development, Verlag E. Appelhans and Co., Brunswick, Germany, 1959.

[†]Electronics, Oct. 1944.

[‡]H. Smyth, Atomic Energy for Military Purposes, Sections 7 and 27 and Appendix 4, Princeton University Press, 1945.

computers,* as well as antenna drives for tracking radars,[†] had led to the widespread adoption of analytical design techniques originally developed for long distance telephone amplifiers.[‡] While James, Nichols, and Phillips credit John F. Taplin, at MIT, with working with frequency response techniques for servomechanisms as early as 1937, substantially nothing concerning the matter appeared in public print until after the war was over. It seems clear that the same or very similar ideas were shared by widely separated investigators. At both the Bell Telephone Laboratories and MIT classified memoranda were prepared on the eve of the United States' involvement.[§] As far as the present authors know, these historic documents have still not been seen in the light of day.

*I. A. Greenwood, Jr., J. V. Holdam, Jr., and D. MacRae, Jr., Electronic Instruments, McGraw-Hill Book Co., New York, 1948.

†H. M. James, N. B. Nichols, and R. S. Phillips, Theory of Servomechanisms, McGraw-Hill Book Co., New York, 1947.

‡H. Nyquist, "Regeneration Theory," Bell Systems Tech. J., Vol. 11, No. 1, Jan. 1932, pp. 126-147; see also "The Regeneration Theory," Trans. ASME, Vol. 76, No. 8, Nov. 1954, p. 1151.

H. S. Black, "Stabilized Feedback Amplifiers," Bell System Tech. J., Vol. 13, No. 1, Jan. 1934, pp. 1-18; see also U.S. Patent No. 2,102,671, Dec. 1937.

E. Peterson, J. G. Kreer, and L. A. Ware, "Regeneration Theory and Experiment," Bell System Tech. J., Vol. 13, No. 10, Oct. 1934, pp. 680-700.

H. W. Bode, Amplifiers, U.S. Patent No. 2,123,17, 12 July 1938; see also "Relations Between Attenuation and Phase in Feedback Amplifier Design," Bell System Tech. J., Vol. 19, No. 3, July 1940, pp. 421-454; Network Analysis and Feedback Amplifier Design, Van Nostrand Co., New York, 1945; and "Feedback—The History of an Idea," in Active Networks and Feedback Systems, Polytechnic Press, Brooklyn, New York, 1961.

§D. C. Bomberger and B. T. Weber, Stabilization of Servomechanisms, Bell Telephone Laboratories Restricted Publication M.M.-41-110152, Dec. 10, 1941.

H. Harris, Jr., The Analysis and Design of Servomechanisms, OSRD, NDRC (Sec. D-2), Rept. 454, Jan. 1942. (Brown and Campbell give the date of this report as Dec. 1941, but other authorities agree on the one given here.)

later, at MIT, Hall* prepared a dissertation which was initially classified but which was released in 1947. The effort to keep all this information classified probably did more harm than good. Certainly it did not prevent the duplicate development and use of the ideas on several sides. Almost simultaneously with Hall's dissertation, Profos† contributed his own at Zurich, while only a little later the book which we know in translation as The Dynamics of Automatic Control‡ was published in Munich. The system wasn't even airtight on our own side. The earliest published work in English which makes reference to the frequency response method in control seems to have been the 1941 paper by Prinz.§

Immediately upon the cessation of hostilities there appeared a rash of papers by the original contributors, and others, who had been kept silent for more than five years.¶ Almost simultaneously with the papers

*A. C. Hall, The Analysis and Synthesis of Linear Servomechanisms, Technology Press, Cambridge, Mass., 1943.

†P. Profos, Die Behandlungen von Regel Problemen vermittels des Frequenzganges des Regelkreises, Ph.D. Dissertation, A. G. Gebr. Leeman and Co., Zurich, 1943; also "A New Method of Regulating System Design," Sulzer Tech. Rev., No. 2, 1945.

‡R. C. Oldenbourg, and H. Sartorius, Dynamik Selbsttätiger Regelung, R. Oldenbourg, Munich, 1944; see also The Dynamics of Automatic Control, ASME, New York, 1948.

§D. G. Prinz, "Contributions to the Theory of Automatic Controllers and Followers," J. Sci. Instr. (London), Vol. 21, No. 4, Apr. 1944, pp. 53-64.

¶D. P. Campbell, "Theory of Automatic Control Systems," Industrial Aviation, Sept. 1945, pp. 62-64, 94, 95.

E. P. Ferrell, "The Servo Problem as a Transmission Problem," Proc. IRE, Vol. 33, No. 11, Nov. 1945, pp. 763-767.

G. S. Brown and A. C. Hall, "Dynamic Behavior and Design of Servomechanisms," Trans. ASME, Vol. 68, 1946, pp. 503-524.

A. C. Hall, "Application of Circuit Theory to Design of Servomechanisms," J. Franklin Inst., Vol. 242, No. 4, Oct. 1946, pp. 279-307; see also "Early History of the Frequency Response Field," Trans. ASME, Vol. 76, No. 8, Nov. 1954, pp. 1153-1154.

H. Harris, Jr., "Frequency Response of Automatic Control Systems," Trans. AIEE, Vol. 65, 1946, pp. 539-545.

R. E. Graham, "Linear Servo Theory," Bell System Tech. J., Vol. 25, No. 4, Oct. 1946, pp. 616-651.

H. T. Marcy, "Parallel Circuits in Servomechanisms," Trans. AIEE, Vol. 65, 1946, pp. 521-529.

there also began to appear a growing number of books, many of which are almost as valuable today as when they were first published.* Typically, these books not only expounded the new theory of the frequency response of automatic control systems, but further connected it to the performance in the time domain via the correspondence between the transfer function and the transient response as revealed by the Laplace transform method. Operational techniques were not new, but their rigorous and respectable foundation in the Laplace transformation was, at that time, a comparatively recent development.[†]

There also appeared, immediately after the war, accounts of the improved mechanical analog computer developed at MIT[‡] and of the digital

*L. A. McColl, Fundamental Theory of Servomechanisms, Van Nostrand Co., New York, 1945.

H. Iauer, R. Lesnick, and L. E. Matson, Servomechanism Fundamentals, McGraw-Hill Book Co., New York, 1947.

H. M. James, N. B. Nichols, and R. S. Phillips, Theory of Servomechanisms, McGraw-Hill Book Co., New York, 1947.

W. R. Ahrendt and J. F. Taplin, Automatic Regulation, Vol. I, Ahrendt and Taplin, P.O. Box 4673, Wash., D. C., 1947.

I. A. Greenwood, Jr., J. V. Holdam, Jr., and D. MacRae, Jr., Electronic Instruments, McGraw-Hill Book Co., New York, 1948.

G. S. Brown and D. P. Campbell, Principles of Servomechanisms, John Wiley and Sons, New York, 1948.

[†]G. Doetsch, Theorie und Anwendung der Laplace Transformation, Springer-Verlag, Berlin, 1937.

N. W. MacLachlan, Complex Variable and Operational Calculus, Cambridge University Press, London, 1939.

H. S. Carslaw and J. C. Jaeger, Operational Methods in Applied Mathematics, Clarendon Press, Oxford, 1941.

M. F. Gardner and J. L. Barnes, Transients in Linear Systems, Vol. I, John Wiley and Sons, New York, 1942.

R. V. Churchill, Modern Operational Mathematics in Engineering, McGraw-Hill Book Co., New York, 1944.

[‡]V. Bush and S. H. Caldwell, "A New Type of Differential Analyzer," J. Franklin Inst., Vol. 240, No. 4, Oct. 1945, pp. 255-326.

scientific calculators developed at Harvard University,* at the Bell Telephone Laboratories,[†] and at the University of Pennsylvania.[‡] These machines had originally been employed primarily to compute ballistic tables, but their potentialities for the solution of other problems, including the design of feedback control systems for aircraft, was quite plain. Furthermore, requirements for fire control computers had led to the development of a variety of new or improved components. Among these was the d-c or operational amplifier. In a prophetic paper published in 1947, Ragazzini, Randall, and Russell[§] pointed out that these might be used in a general-purpose machine for solving differential equations, an electronic analog computer. A number of firms almost immediately developed such machines for sale or their own use, and by 1950 they were fairly common. Several universities also developed their own machines. Among the first was the University of Michigan. In an early report^{||} on the feasibility of electronic analog computation, autopilot control of the longitudinal motion of an airplane was given as one of the illustrative examples.

Knowledge of the development of the new methods of analysis and of the newly available computers spread very rapidly, and one could almost

*H. H. Aiken and G. M. Hopper, "The Automatic Sequence Controlled Calculator - I," Elec. Eng., Vol. 65, No. 8-9, Aug.-Sept. 1946, pp. 384-391; "The Automatic Sequence Controlled Calculator - II," Elec. Eng., Vol. 65, No. 10, Oct. 1946, pp. 449-454; "The Automatic Sequence Controlled Calculator - III," Elec. Eng., Vol. 65, No. 11, Nov. 1946, pp. 522-528.

[†]F. L. Alt, "A Bell Telephone Laboratories Computing Machine - I," Math. Tables and Other Aids to Computation, Vol. 3, No. 21, Jan. 1948, pp. 1-13; "A Bell Telephone Laboratories Computing Machine - II," Math. Tables and Other Aids to Computation, Vol. 3, No. 22, Apr. 1948, pp. 69-84.

[‡]H. H. Goldstine and A. Goldstine, "The Electronic Numerical Integrator and Computer (ENIAC)," Math. Tables and Other Aids to Computation, Vol. 2, No. 15, July 1946, pp. 97-110.

[§]J. R. Ragazzini, R. H. Randall, and F. A. Russell, "Analysis of Problems in Dynamics by Electronic Circuits," Proc. IRE, Vol. 35, No. 5, May 1947, pp. 442-452.

^{||}D. W. Hagelbarger, C. E. Howe, and R. M. Howe, Investigation of the Utility of an Electronic Analog Computer in Engineering Problems, External Memo. 28, Eng. Res. Inst., Univ. of Mich., Ann Arbor, Mich., 1 Apr. 1949.

say that a new branch of the engineering profession came suddenly into being. Men were proud to call themselves a feedback systems engineer, or "systems engineer" for short, and not a few of these became aircraft control system engineers. Application of the frequency response (or transfer function) technique to the design of aircraft and their control systems was pointed out early,* and it quickly became a part of the design process for actual aircraft (or missile) control systems.†

Further improvements and extensions to the analytical techniques were also discovered. By no means the least of these, Evans' locus of roots method‡ was inspired by consideration of the problems of aircraft and missile flight control. In the classic Fourteenth Wright Brothers Lecture for the year 1950, Bollay summarized the then existing state of the art and pointed to the use of the Laplace transformation, frequency response techniques, the Nyquist stability criterion, the root locus

*W. F. Milliken, Jr., "Progress in Dynamic Stability and Control Research," J. Aeron. Sci., Vol. 14, No. 9, Sept. 1947, pp. 493-519.

J. B. Rea, Automatic Tracking Control of Aircraft, Sc.D. Thesis, Mass. Institute of Technology, 1947.

H. Greenberg, Frequency-Response Method for Determination of Dynamic Stability Characteristics of Airplanes with Automatic Controls, NACA TN 1229, Mar. 1947.

R. C. Seamans, Jr., B. G. Bromberg, and L. E. Payne, "Application of the Performance Operator to Aircraft Automatic Control," J. Aeron. Sci., Vol. 15, No. 9, Sept. 1948, pp. 535-555.

J. R. Moore, "Application of Servo Systems to Aircraft," Aeron. Eng. Rev., Vol. 8, No. 1, Jan. 1949, pp. 32-43, 71.

C. L. Seacord, "Application of Frequency Response Analysis to Aircraft Autopilot Stability," J. Aeron. Sci., Vol. 17, No. 8, Aug. 1950, pp. 481-498.

†P. A. Noxon, "Flight Path Control," Aeron. Eng. Rev., Vol. 17, No. 8, Aug. 1948, pp. 38-45.

R. J. White, "Investigation of Lateral Dynamic Stability in the XB-47," Airplane, "J. Aeron. Sci.", Vol. 17, No. 3, Mar. 1950, pp. 133-148.

‡W. R. Evans, Servo Analysis by Locus of Roots Method, North Amer. Aviation, Inc., Rept. AL-787, Nov. 1, 1948; "Graphical Analysis of Control Systems," Trans. AIEE, Vol. 67, 1948, pp. 547-551; "Control System Synthesis by the Root Locus Method," Trans. AIEE, Vol. 69, 1950, pp. 66-69; "The Use of Zeros and Poles for Frequency Response or Transient Response," Trans. ASME, Vol. 76, No. 8, Nov. 1954, pp. 1335-1342; Control System Dynamics, McGraw-Hill Book Co., New York, 1954.

method, analog computers, and other tools of the systems engineer in the design departments of the major aircraft manufacturers.*

At Northrop Aircraft, Inc., based in part on the experiences gained with the power controls and stability augmentation system developments needed for tailless† and other advanced designs, and in a comprehensive study of the F-5 automatic pilot for the F-89A aircraft,‡ an attempt was made to summarize the most useful aspects of the new knowledge of aircraft control system engineering in a series of seven volumes, prepared for the U. S. Navy Bureau of Aeronautics.§ These volumes began to appear in March 1952. The genealogy of the present work can be traced directly to several of the "Northrop Volumes." In fact, it began, some ten years after the initial summary, as an effort to revise and update Volumes II and VI and to provide between a single pair of covers a comprehensive account of the theory and application of analytical techniques in the design of automatic flight control systems.

*W. Bollay, "Aerodynamic Stability and Automatic Control," J. Aeron. Sci., Vol. 18, No. 9, Sept. 1951, pp. 569-624.

†D. T. McRuer, "An Electronic Tail for the Flying Wing," Flight Lines, Nov. 1950.

‡Analysis Final Report: Analysis of Type F-5 Automatic Pilot Applied to the Type F-89 Aircraft and Control System, Northrop Aircraft, Inc., Servomechanisms and Dynamics Section, Rept. SMD-3, 13 Sept. 1950.

§Fundamentals of Design of Pilot Aircraft Flight Control Systems, BuAer Rept. AE-61-4; Vol. I, Methods of Analysis and Synthesis of Piloted Aircraft Flight Control Systems, Mar. 1952; Vol. II, Dynamics of the Airframe, Sept. 1952; Vol. III, The Human Pilot, Aug. 1954; Vol. IV, The Hydraulic System, Mar. 1953; Vol. V, The Artificial Feel System, May 1953; Vol. VI, Automatic Flight Control Systems for Piloted Aircraft, Apr. 1956; Vol. VII, Methods of Design and Evaluation of Interceptor Fire Control Systems, Oct. 1959.

Available at cost from Northrop Corporation, Specifications and Data Department, 1001 East Broadway, Hawthorne, California.

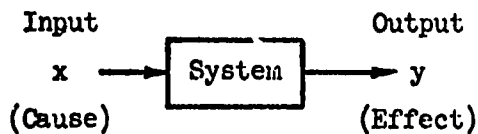
CHAPTER 2

MATHEMATICAL MODELS OF LINEAR SYSTEM ELEMENTS

2.1 INTRODUCTION

A major task in systems analysis is the estimation of system response to commands or disturbances. The most concrete way to determine behavior is to test the actual system. This direct experimental approach is precluded in the early phases of design, when the "system" may be but one of a number of competing possibilities, or when the physical system may be unavailable. Fortunately, many of the potential results of actual physical measurements can be foreseen by performing "experiments" utilizing various models of the system.

As the underlying basis for system models, consider the block diagram representation of Fig. 2-1. The input, stimulus, command, disturbance, or



forcing function elicits an output or response from the "system." The "system" might be one of a very large number of things including a human being, an airplane, or a society, and the words

Fig. 2-1. A Pattern

appropriate to the several portions of the diagram of Fig. 2-1 are quite different in these different contexts. Nevertheless, it is assumed here that we are dealing with cause and effect elements, perhaps combined into larger systems; and that an input and output of a particular element can always be identified. It is further assumed that the relationship between the input and output can be represented by one or more ordinary differential equations. These equations become the mathematical attorneys for the physical elements or systems, and it is through them as intermediaries that the transactions in which we are to engage will ordinarily be conducted.

Many physical elements and systems are practically linear and time-invariant; that is, they can be described adequately over a limited range by linear differential equations with constant coefficients.

Examples of linearization abound in the literature,* and Chapter 4 presents an example of the assumptions and techniques which are employed, in this case, to linearize the equations of motion of an aircraft. It can be demonstrated that feedback control itself has the property of linearizing the performance of the systems or elements to which it is applied,[†] so that while all systems and elements are in fact nonlinear, the assumptions of our analyses are often not so restrictive as they may at first appear.

Proceeding on the assumption, for the moment, that we need only be concerned with systems which are linear with constant coefficients, or which may legitimately be linearized, we shall introduce in this chapter the powerful and convenient concepts of the Laplace transformation. The rudiments of response calculations are first reviewed, including approximate calculations and modal response ratios. Following this is a discussion of the system descriptors—the weighting function or impulse response and its transform, and the transfer function. Graphical representations for both these functions are emphasized: time vectors for the weighting function, and pole-zero plots, $j\omega$ -Bode diagrams, and σ -Bode diagrams for the transfer function.

2.2 LAPLACE TRANSFORMATION

The system of Fig. 2-1 is, according to our assumptions, described by the equation

$$\left(\frac{d^{m+n}}{dt^{m+n}} + b_1 \frac{d^{m+n-1}}{dt^{m+n-1}} + \cdots + b_{m+n-1} \frac{d}{dt} + b_{m+n} \right) y(t) = k \left(\frac{d^n}{dt^n} + a_1 \frac{d^{n-1}}{dt^{n-1}} + \cdots + a_{n-1} \frac{d}{dt} + a_n \right) x(t) \quad (2-1)$$

*D. Graham and D. McRuer, Analysis of Nonlinear Control Systems, John Wiley and Sons, Inc., New York, 1961, pp. 9-12, 445-454.

R. W. Jones, "Stability Criteria for Certain Non-linear Systems," in A. Tustin, ed., Automatic and Manual Control, Butterworths Scientific Publications, London, 1952, pp. 319-324.

[†]J. C. West, Analytical Techniques for Non-linear Control Systems, English Universities Press, Ltd., London, 1960, pp. 16-23.

For any physical system, $m \geq 1$. We are interested in discovering certain aspects of the performance of the system, such as the stability, accuracy, and speed of response of the output for certain inputs. The analysis problem is defined as follows: Given the input and the differential equation, find the output. If the analysis problem were solved for all the inputs to which the system might be subjected and these solutions were tabulated as input-response pairs, the analyst would have a complete description of the performance of the system. Very luckily this turns out to be unnecessary for linear systems.

In modern engineering analysis an equation such as Eq. 2-1 is most often solved, if it has to be, by a digital or an analog computer. On the other hand, a great deal of information concerning the nature of the solutions for a variety of inputs can be found without solving the equation itself. The techniques which are commonly employed, however, are intimately related to the method of solving Eq. 2-1 by means of the Laplace transformation.

The Laplace transformation of a function of time is defined as

$$\mathcal{L}[f(t)] = F(s) = \lim_{\substack{T_2 \rightarrow \infty \\ T_1 \rightarrow 0}} \int_{T_1}^{T_2} f(t)e^{-st} dt \quad (2-2)$$

where s is the complex variable $s = \sigma + j\omega$. Application of the definition allows the construction of tables of the transforms of operations, such as differentiation and integration, and tables of the transforms of functions, such as an impulse or a sine wave. The inverse transformation [i.e., $f(t)$, given $F(s)$] is usually carried out by finding the appropriate pair in a table so arranged that $f(t)$ can be associated with a particular $F(s)$.

The most interesting and useful properties of the Laplace transformation are summarized (without proof) in Table 2-1.*

*For more details on the properties of the transformation and its uses, see for example: M. F. Gardner and J. L. Barnes, Transients in Linear Systems, John Wiley, N. Y., 1942; J. A. Aseltine, Transform Method in Linear System Analysis, McGraw-Hill, N. Y., 1958; R. V. Churchill, Operational Mathematics, 2nd ed., McGraw-Hill Book Co., N. Y., 1958; W. Kaplan, Operational Methods for Linear Systems, Addison-Wesley, Reading, Mass., 1962; G. Doetsch, Guide to the Applications of Laplace Transforms, Van Nostrand, London, 1961.

TABLE 2-1

FUNDAMENTAL PROPERTIES OF THE LAPLACE TRANSFORMATION

ITEM	$F(s)$	$f(t)$	SPECIAL RESTRICTIONS AND REMARKS
Laplace transformation	$F(s)$	$f(t)$	<p>"t" is a real variable $f(t)$ is known and single valued almost everywhere for $0 \leq t$</p> $\lim_{\substack{t_2 \rightarrow \infty \\ t_1 \rightarrow 0}} \int_{t_1}^{t_2} f(t) e^{-\sigma t} dt < \infty$ <p>for some real number σ</p>
Differentiation	$sF(s) - f(0+)$ $s^2F(s) - sf(0+) - \frac{df}{dt}(0+)$ $s^nF(s) - \sum_{k=1}^n s^{n-k} \frac{d^{k-1}f}{dt^{k-1}}(0+)$	$\frac{df(t)}{dt}$ $\frac{d^2f(t)}{dt^2}$ $\frac{d^nf(t)}{dt^n}$	<p>$f(t)$ and $df(t)/dt$ are Laplace transformable</p> <p>$f(t)$, $df(t)/dt$ and $d^2f(t)/dt^2$ are Laplace transformable</p> <p>$f(t)$, $df(t)/dt$, \dots, $d^nf(t)/dt^n$ are Laplace transformable</p>
Integration	$\frac{F(s)}{s} + \int \frac{f(t)}{s} \frac{dt}{s} \Big _{t=0+}$ $\frac{F(s)}{s^k} + \sum_{n=1}^k \frac{f^{(n)}(0+)}{s^{k-n+1}}$	$\int f(t) dt$ $\int \dots \int f(t) (dt)^k$	<p>$f(t)$ is Laplace transformable</p> <p>$f(t)$ is Laplace transformable</p>
Linearity	$aF(s)$ $F_1(s) + F_2(s)$	$af(t)$ $f_1(t) + f_2(t)$	<p>"a" is a constant or a variable which is independent of "t" and "s"</p> <p>$f(t)$ is Laplace transformable</p> <p>$f_1(t)$ and $f_2(t)$ are Laplace transformable</p>

Table 2-1 (Continued)

ITEM	$F(s)$	$f(t)$	SPECIAL RESTRICTIONS AND REMARKS
Scale change	$aF(as)$	$f(t/a)$	$f(t)$ is Laplace transformable "a" is positive, and is a constant or variable independent of "t" or "s"
Convolution or complex multiplication	$F_1(s)F_2(s)$	$\int_0^t f_1(t-\tau)f_2(\tau) d\tau$ or $f_1(t) * f_2(t)$	$f_1(t)$ and $f_2(t)$ are Laplace transformable
Real multiplication	$\frac{1}{2\pi j} \int_{C_2-j\infty}^{C_2+j\infty} F_1(s-\lambda)F_2(\lambda) d\lambda$ or $F_1(s) \odot F_2(s)$ $\sum_{i=1}^n \frac{N_i(s_i)}{\left[\frac{dD_1(s)}{ds} \right]_{s=s_i}} F_2(s-s_i)$	$f_1(t)f_2(t)$	$f_1(t)$ and $f_2(t)$ are Laplace transformable $\sigma_{a1} + \sigma_{a2} < \sigma$ $\sigma_{a1} < C_2 < \sigma - \sigma_{a2}$ In the special case where $F_1(s) = N_1(s)/D_1(s)$, a rational fraction having no higher order and "k" first-order poles, s_1, s_2, \dots, s_n
Real translation	$e^{-\tau s}F(s)$ $e^{\tau s}F(s)$	$f(t-\tau)$ $f(t+\tau)$	$f(t)$ is Laplace transformable, τ is non-negative real number, and $f(t-\tau) = 0 ; 0 < t < \tau$ $f(t+\tau) = 0 ; -\tau < t < 0$
Complex translation	$F(s+1/T)$ $F(s-1/T)$ $F(Ts-b)$	$e^{-t/T}f(t)$ $e^{t/T}f(t)$ $(1/T)e^{bt/T}f(t/T)$	$f(t)$ is Laplace transformable T has a non-negative real part

Table 2-1 (Concluded)

ITEM	$F(s)$	$f(t)$	SPECIAL RESTRICTIONS AND REMARKS
Final value	$\lim_{s \rightarrow 0} sF(s)$	$\lim_{t \rightarrow \infty} f(t)$	$f(t)$ and $df(t)/dt$ are Laplace transformable $sF(s)$ is analytic in the right half plane and on axis of imaginaries
Initial value	$\lim_{s \rightarrow \infty} sF(s)$	$\lim_{t \rightarrow 0} f(t)$	$f(t)$ and $df(t)/dt$ are Laplace transformable $\lim_{s \rightarrow \infty} sF(s)$ exists
Complex differentiation	$-\frac{d}{ds} F(s)$ $(-1)^n \frac{d^n F(s)}{ds^n}$	$tf(t)$ $t^n f(t)$	$f(t)$ is Laplace transformable
Complex integration	$\int_s^\infty F(s) ds$	$(1/t) f(t)$	$F(t)$ and $f(t)/t$ are Laplace transformable $\int_s^\infty F(s) ds$ exists
Periodic functions	$\frac{\int_0^T e^{-st} f(t) dt}{1 - e^{-Ts}}$	$f(t)$	$f(t)$ is Laplace transformable $f(t) = f(t + T)$
Antiperiodic functions	$\frac{\int_0^T e^{-st} f(t) dt}{1 + e^{-Ts}} = F(s)$ $\frac{F(s)}{1 - e^{-Ts}}$ $F(s) \coth (Ts/2)$	$f(t)$ Half-wave rectification of $f(t)$ Full-wave rectification of $f(t)$	$f(t)$ is Laplace transformable $f(t) = -f(t + T)$

Common transform pairs for the time functions which occur in the analysis and testing of feedback control systems are cataloged in the short illustrated table of transform pairs presented in Table 2-2.* It may be noted that in many cases two alternative forms are given for the transform. In some problems one form is more suitable than the other, so they are used interchangeably as convenience may dictate. To emphasize the physical interpretations of the $f(t)$ - $F(s)$ dichotomy, graphical representations of $f(t)$ are given as an integral part of the table. A knowledge of the details of these time histories enables the analyst to picture, either mentally or by a sketch, the behavior of a system element characterized by a given $F(s)$ or $f(t)$.

It is also necessary to point out that the integral which defines the Laplace transformation may fail to converge. For transformable functions this situation is avoided by defining an abscissa of absolute convergence, σ_a , which is set just large enough to assure the convergence of the transform integral. This is the minimum value which the real part of the complex variable $s = \sigma + j\omega$ may take. In the case of a function, such as $f(t) = t^t$, no value of σ_a can be found which will assure convergence of the integral. The function is then said to be not Laplace transformable.

2.3 RESPONSE DETERMINATION

When the definition of the transform for the operation of differentiation is applied to Eq. 2-1, if it is assumed that all initial conditions

*A table of transform pairs of particular value for vehicular control problems is S. Neumark's Operational Formulae for Response Calculations, ARC Tech. Rept. R & M 3075, Her Majesty's Stationary Office, London, 1958. This report comprehensively treats operational fractions of the first, second, third, and fourth order and has additional tables on the reduction of every fraction of fifth or sixth order to a combination of fractions of lower order. Other useful tables of transform pairs are the references on the Laplace transformation and its uses cited previously and:

F. E. Nixon, Principles of Automatic Controls, Prentice-Hall, Inc., New York, 1953. The same table has also been published separately as Handbook of Laplace Transformations, Prentice-Hall, Inc., New York, 1960.

A. Erdélyi, F. Oberhettinger, and F. G. Tricomi, Tables of Integral Transforms, Vol. I, McGraw-Hill Book Co., Inc., New York, 1954.

TABLE 2-2

COMMON TRANSFORMATION PAIRS AND PROPERTIES OF THEIR TIME RESPONSE

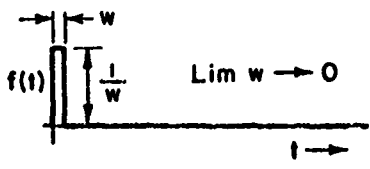
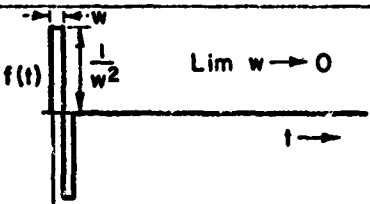
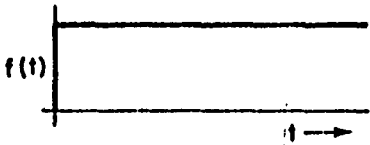
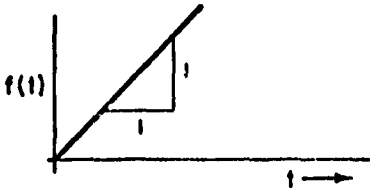
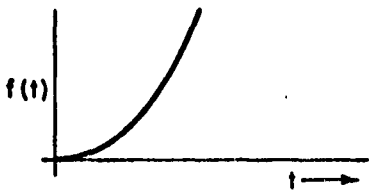
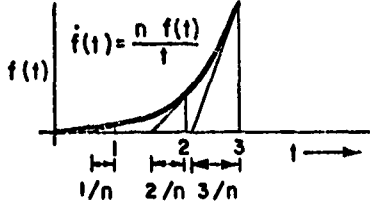

	$F(s)$	$f(t)$	TIME RESPONSE PROPERTIES
UNIT IMPULSE	1	$\delta(t)$	
UNIT DOUBLET	s	$\dot{\delta}(t)$	
STEP FUNCTION POSITION	$\frac{1}{s}$	1 or $u(t)$	
STEP FUNCTION VELOCITY	$\frac{1}{s^2}$	t	
STEP FUNCTION ACCELERATION	$\frac{1}{s^3}$	$\frac{1}{2} t^2$	
n^{th} ORDER STEP FUNCTION	$\frac{n!}{s^{n+1}}$	t^n	
PURE TIME DELAY	$e^{-\tau s} F(s)$	$f(t-\tau)$ Where: $f(t-\tau) = 0, t < \tau$	

Table 2-2 (Continued)

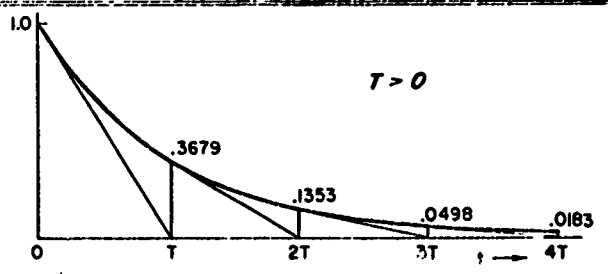
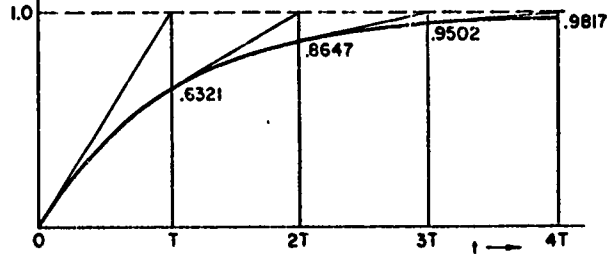
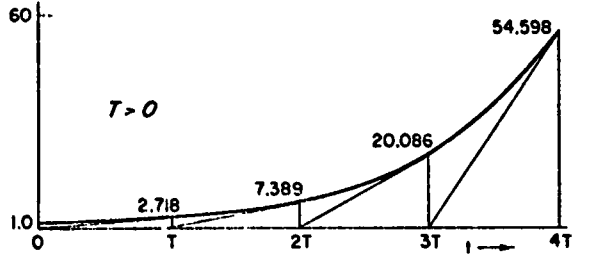
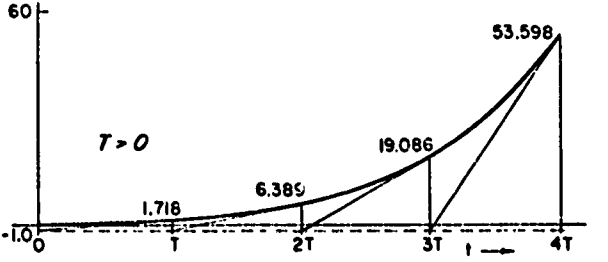
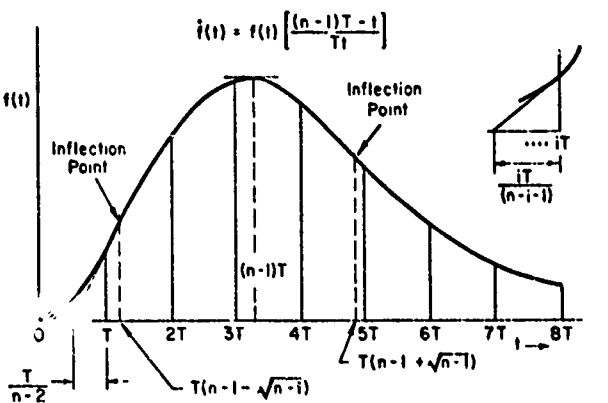
	$F(s)$	$f(t)$	TIME RESPONSE PROPERTIES
FIRST ORDER LAG CONVERGING	$\frac{T}{Ts+1}$ or $\frac{1}{s+a}$ $0 < a = \frac{1}{T}$	$e^{-t/T}$ e^{-at}	
FIRST ORDER LAG CONVERGING and FIRST ORDER POLE AT ORIGIN	$\frac{1}{s(Ts+1)}$ or $\frac{a}{s(s+a)}$ $0 < a = \frac{1}{T}$	$1 - e^{-t/T}$ $1 - e^{-at}$	
FIRST ORDER LAG DIVERGING	$\frac{-T}{-Ts+1}$ or $\frac{1}{s-a}$ $a = \frac{1}{T}$	$e^{t/T}$ e^{at}	
FIRST ORDER LAG DIVERGING and FIRST ORDER POLE AT ORIGIN	$\frac{1}{s(-Ts+1)}$ or $\frac{-a}{s(s-a)}$ $a = \frac{1}{T}$	$-1 + e^{t/T}$ $-1 + e^{at}$	
MULTIPLE FIRST ORDER	$\frac{T^n}{(Ts+1)^n}$ or $\frac{1}{(s+a)^n}$ $a = \frac{1}{T}$	$\frac{1}{(n-1)!} t^{n-1} e^{-t/T}$ $\frac{1}{(n-1)!} t^{n-1} e^{-at}$	

Table 2-2 (Continued)

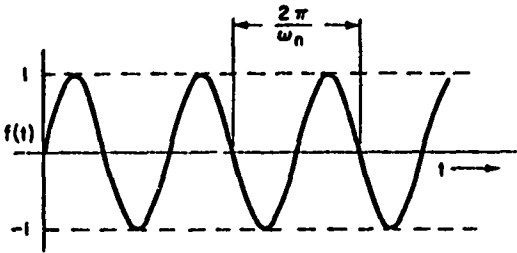
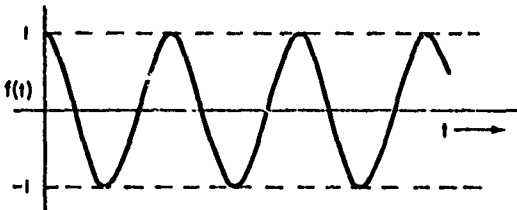
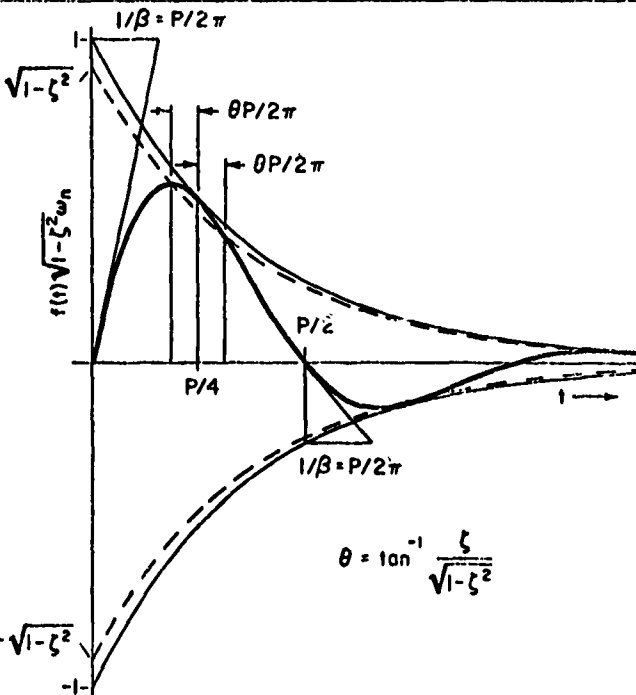
	$F(s)$	$f(t)$	TIME RESPONSE PROPERTIES
UNDAMPED SECOND ORDER	$\frac{\frac{1}{\omega_n}}{\frac{s^2}{\omega_n^2} + 1}$ <p>or</p> $\frac{\omega_n}{s^2 + \omega_n^2}$	$\sin \omega_n t$	
	$\frac{\frac{s}{\omega_n^2}}{\frac{s^2}{\omega_n^2} + 1}$ <p>or</p> $\frac{s}{s^2 + \omega_n^2}$	$\cos \omega_n t$	
CONVERGING SECOND ORDER	$\frac{1}{s^2 + 2\zeta\omega_n s + \omega_n^2}$ <p>or</p> $\frac{1}{(s+a)^2 + \beta^2}$	$\frac{1}{\omega_n \sqrt{1-\zeta^2}} e^{-\zeta\omega_n t} \sin \omega_n \sqrt{1-\zeta^2} t$ <p>or</p> $\frac{1}{\beta} e^{-\alpha t} \sin \beta t$ <p>Where: $\alpha = \zeta\omega_n$ $\beta = \omega_n \sqrt{1-\zeta^2}$ </p>	

Table 2-2 (Concluded)

	$F(s)$	$f(t)$	TIME RESPONSE PROPERTIES
CONVERGING SECOND ORDER	$\frac{s}{s^2 + 2\zeta\omega_n s + \omega_n^2}$ <p>or</p> $\frac{s}{(s+a)^2 + \beta^2}$ <p> $a = \zeta\omega_n$ $\beta = \omega_n\sqrt{1-\zeta^2}$ </p>	$\frac{e^{-\zeta\omega_n t}}{\sqrt{1-\zeta^2}} \cos[\omega_n\sqrt{1-\zeta^2} t + \theta]$ <p>where:</p> $\theta = \tan^{-1} \frac{a}{\beta} = \tan^{-1} \frac{\zeta}{\sqrt{1-\zeta^2}}$	
CONVERGING SECOND ORDER	$\frac{\omega_n^2}{s(s^2 + 2\zeta\omega_n s + \omega_n^2)}$ <p>or</p> $\frac{a^2 + \beta^2}{s[(s+a)^2 + \beta^2]}$ <p> $a = \zeta\omega_n$ $\beta = \omega_n\sqrt{1-\zeta^2}$ </p>	$1 - \frac{e^{-\zeta\omega_n t}}{\sqrt{1-\zeta^2}} \cos[\omega_n\sqrt{1-\zeta^2} t + \theta]$ <p>where:</p> $\theta = \tan^{-1} \frac{\zeta}{\sqrt{1-\zeta^2}}$	
DIVERGING SECOND ORDER	$\frac{1}{s^2 - 2\zeta'\omega_n s + \omega_n^2}$ <p>or</p> $\frac{1}{(s-a')^2 + \beta^2}$ <p> $a' = \zeta'\omega_n$ $\beta = \omega_n\sqrt{1-\zeta'^2}$ </p>	$\frac{e^{\zeta'\omega_n t}}{\omega_n\sqrt{1-\zeta'^2}} \sin \omega_n\sqrt{1-\zeta'^2} t$ <p>or</p> $\frac{1}{\beta} e^{a't} \sin \beta t$	

are zero, the transformed equation is:

$$\begin{aligned} (s^{m+n} + b_1 s^{m+n-1} + \dots + b_{m+n-1} s + b_{m+n}) Y(s) \\ = K (s^n + a_1 s^{n-1} + \dots + a_{n-1} s + a_n) X(s) \end{aligned} \quad (2-3)$$

The Laplace transformation has reduced the linear differential equation with constant coefficients to an algebraic equation in the transform variable, s . For any transformable input $x(t)$, which has the transform $X(s)$, Eq. 2-3 may be solved for $Y(s)$.

$$Y(s) = K \frac{(s^n + a_1 s^{n-1} + \dots + a_{n-1} s + a_n)}{(s^{m+n} + b_1 s^{m+n-1} + \dots + b_{m+n-1} s + b_{m+n})} X(s) \quad (2-4)$$

In principle, then, the inverse transformation yields $y(t) = \mathcal{L}^{-1}[Y(s)]$.

Example: The procedure can be illustrated with an elementary example. Consider the (rotary) spring-mass-damper system of Fig. 2-2. This device is the all-mechanical analog of a simple servomechanism. The equation of motion, obtained by

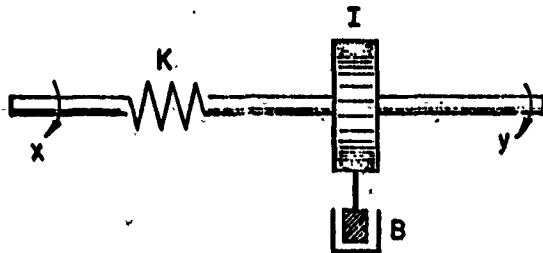


Fig. 2-2. Spring-Mass-Damper System

summing torques on the wheel, is:

$$I\ddot{y} + B\dot{y} + Ky = Kx \quad (2-5)$$

If this ordinary differential equation with constant coefficients is Laplace transformed, it may be written as:

$$[Is^2 + Bs + K]Y(s) = KX(s) + [Isy(0+) + I\dot{y}(0+) + By(0+)] \quad (2-6)$$

where $y(0+)$ and $\dot{y}(0+)$ are the initial conditions. Note that the action of the initial conditions is equivalent to that

of an input made up of delta functions and higher order delta functions. That is, $Iy(0+)$ amounts to a doublet of weight $Iy(0+)$, while $I\dot{y}(0+)$ and $By(0+)$ are equivalent to a delta function input with weight $[I\dot{y}(0+) + By(0+)]$. Solving for $Y(s)$,

$$Y(s) = \frac{\left(\frac{K}{I}\right)X(s)}{s^2 + \frac{B}{I}s + \frac{K}{I}} + \frac{sy(0+) + \left[\dot{y}(0+) + \frac{B}{I}y(0+)\right]}{s^2 + \frac{B}{I}s + \frac{K}{I}} \quad (2-7)$$

Letting $x(t) = \delta(t)$, the unit impulse, so that $X(s) = 1$, setting the initial conditions to zero, and defining an "undamped" natural frequency, $\omega_n = \sqrt{K/I}$, and a "damping ratio," $\zeta = B/(2\sqrt{KI})$,

$$Y(s) = \frac{\omega_n^2}{s^2 + 2\zeta\omega_n s + \omega_n^2} \quad (2-8a)$$

or

$$Y(s) = \frac{1}{\frac{s^2}{\omega_n^2} + \frac{2\zeta s}{\omega_n} + 1} \quad (2-8b)$$

Inverse transformation of this function can be carried out by recognizing that the right side of Eq. 2-8 is a pair in Table 2-2 and that:

$$y(t) = \frac{\omega_n}{\sqrt{1 - \zeta^2}} e^{-\zeta\omega_n t} \sin \omega_n \sqrt{1 - \zeta^2} t ; \zeta < 1 \quad (2-9)$$

When the response transform has a more complex denominator, the transform can be broken down into a sum of partial fractions before inverse transforming. Suppose that the algebraic solution for the transform of the response is given in the form

$$Y(s) = K \frac{(s^n + a_1 s^{n-1} + \dots + a_{n-1} s + a_n)}{(s^{m+n} + b_1 s^{m+n-1} + \dots + b_{m+n-1} s + b_{m+n})} \quad (2-10)$$

where $m \geq 1$. The polynomials can be factored. Then,

$$Y(s) = \frac{N(s)}{D(s)} = K \frac{\prod_{j=1}^n (s + z_j)}{\prod_{i=1}^{m+n} (s + q_i)} = K \frac{\alpha(s)}{\beta(s)} \quad (2-11)$$

or

$$Y(s) = \frac{N_1(s)}{D_1(s)} = \frac{K \prod_{j=1}^n \left(\frac{s}{z_j} + 1 \right)}{s^k \prod_{i=1}^{m+n-k} \left(\frac{s}{q_i} + 1 \right)} = K \frac{A(s)}{B(s)} \quad (2-12)$$

and the numerator and denominator roots, $-z_j$ and $-q_i$, are respectively called zeros and poles. For reasons which will appear later, the first style of the transform factors is called the root locus form and the second style is called the Bode form. Both are used extensively.

In principle, the right side of Eq. 2-11 or 2-12 can be reformulated in a partial fraction expansion and elementary inverse Laplace transformations can then be carried out on each term. This yields the time response, $y(t)$.

$$Y(s) = \sum_{i=1}^{m+n} \frac{C_i}{s + q_i} \quad (2-13)$$

$$y(t) = \mathcal{L}^{-1} [Y(s)] = \sum_{i=1}^{m+n} C_i e^{-q_i t} \quad (2-14)$$

Thus, any response transform which is a ratio of rational polynomials with real coefficients results in a time domain response which is a sum of real or complex conjugate exponentials. The amount or magnitude of each mode which is present in the total response is indicated by the partial fraction coefficient, C_i .

When the response transforms have either of the equivalent rational proper fraction forms

$$Y(s) = \frac{N(s)}{D(s)} = K \frac{(s+z_1)(s+z_2) \dots}{(s+q_1)(s+q_2) \dots} = \frac{C_1}{s+q_1} + \frac{C_2}{s+q_2} + \dots \quad (2-15)$$

or

$$Y(s) = \frac{N_1(s)}{D_1(s)} = K \frac{(T_a s + 1)(T_b s + 1) \dots}{(T_1 s + 1)(T_2 s + 1) \dots} = \frac{C'_1}{T_1 s + 1} + \frac{C'_2}{T_2 s + 1} + \dots \quad (2-16)$$

the coefficients C_i or C'_i may be evaluated as shown in Table 2-3.

TABLE 2-3

PARTIAL FRACTION COEFFICIENTS

FIRST-ORDER POLES

General: The coefficient of the component involving $1/(s+q_1)$ or $1/(T_1s+1)$ will be

$$C_1 = \left[\frac{N(s)(s+q_1)}{D(s)} \right]_{s=-q_1} ; \quad C'_1 = \left[\frac{N_1(s)(T_1s+1)}{D_1(s)} \right]_{s=-1/T_1}$$

First-Order Pole at the Origin: For this case,

$$X(s) = \frac{N(s)}{sD(s)} \quad \text{or} \quad \frac{N_1(s)}{sD_1(s)} ; \quad C_0 = \frac{N(0)}{D(0)} = \frac{N_1(0)}{D_1(0)}$$

First-Order Poles on the Imaginary Axis (at $s = \pm j\omega_1$): The inverse transform of this component of $X(s)$ will be

$$\text{Re} \left[\frac{(s^2 + \omega_1^2)}{s} \frac{N(s)}{D(s)} e^{st} \right]_{s=j\omega_1} = \text{Re} \left[\frac{-s[(s^2/\omega_1^2) + 1] N_1(s)}{D_1(s)} e^{st} \right]_{s=j\omega_1}$$

One Conjugate-Complex Pair with N Real First-Order Poles:

$$\frac{N(s)}{D(s)} = \frac{a_{N+1}s^{N+1} + a_N s^N + \dots + a_1 s + a_0}{\left[\prod_{i=1}^N (s+q_i) \right] (s^2 + bs + c)} = \sum_{i=1}^N \frac{C_i}{s+q_i} + \frac{As+B}{s^2+bs+c}$$

$$A = a_{N+1} - \sum_{i=1}^N C_i ; \quad B = \frac{a_0}{\prod_{i=1}^N q_i} - c \sum_{i=1}^N \frac{C_i}{q_i}$$

HIGHER ORDER POLES

$D(s)$ will contain terms such as $(s+q_1)^m$, and $D_1(s)$ will contain terms such as $(T_1s+1)^m$. The coefficients C_{m-k} and C'_{m-k} , for the components $1/(s+q_1)^{m-k}$ and $1/(T_1s+1)^{m-k}$ of the $X(s)$ expansion, will be:

$$C_{m-k} = \frac{1}{k!} \left[\frac{d^k}{ds^k} \frac{(s+q_1)^m N(s)}{D(s)} \right]_{s=-q_1} ; \quad C'_{m-k} = \frac{1}{k! T_1^k} \left[\frac{d^k}{ds^k} \frac{(T_1s+1)^m N_1(s)}{D_1(s)} \right]_{s=-1/T_1}$$

where $m-k \geq 1$.

If the explicit differential equation which describes the system is of low order, the polynomials in the system transfer function are of the same low degree. Then the task of factoring the polynomials and of finding the partial fraction coefficients can be carried out without difficulty.* On the other hand, if the characteristic (denominator) polynomial is of the fourth degree or higher, the algebraic factoring of the polynomial and the determination of the partial fraction coefficients may be excessively tedious. It was partly to avoid most of the tedious labor involved in the solution of the equations of motion of linear systems that the semigraphical methods of linear feedback system analysis discussed in Chapter 3 were developed.

2.4 SIMPLIFIED METHODS TO OBTAIN AN APPROXIMATE $f(t)$ FROM ITS UNFACTORED TRANSFORM $F(s)$

A major source of practical difficulty in solving linear constant-coefficient differential equations arises in finding the time response, $f(t)$, after its transform, $F(s)$, is known. This occurs because the poles of $F(s)$ must usually be found as a necessary preliminary to the partial fraction expansion or to entry into a transform table. Factoring the polynomials of $F(s)$ to find its poles and zeros may be more time consuming than warranted. Therefore, schemes which avoid this operation, yet still allow the extraction of some information about the time response, $f(t)$, directly from its transform, $F(s)$, are valuable techniques for many applications.

In this section three ways are described to find information about a time function, $f(t)$, from its transform, $F(s)$, in unfactored form. The first two are fundamental properties of the Laplace transformation, the initial and final value theorems. Application of these properties gives the values of $f(t)$ at $t=0$ and as $t \rightarrow \infty$. In essence, these theorems state an equality between two particular values of $f(t)$ and two particular

*Concise summaries of preferred methods appear in:

J. J. D'Azzo and C. H. Houpis, Feedback Control System Analysis and Synthesis, McGraw-Hill Book Co., Inc., New York, 1960 (Appendix B)

Y. H. Ku, Analysis and Control of Linear Systems, International Textbook Co., Scranton, Pa., 1962, pp. 171-181.

values of its transform, $F(s)$. The initial value theorem can also be used to obtain the derivatives of the initial time response, thereby permitting its expansion in a Maclaurin series. The third method involves the expansion of the response transform in a Maclaurin series, which has a degree of validity in the steady state after transients have become insignificant, or in cases where the input can be approximated as a power series. This series is the basis of the error coefficients so valuable in some phases of servo design.

The Initial Value Theorem. The initial value theorem is a basic property of the Laplace transformation which allows the value of $f(t)$ and its derivatives at $t=0$ to be found from its transform, $F(s)$. Specifically, if $f(t)$ and its first derivative have Laplace transforms and the limit as $s \rightarrow \infty$ of $sF(s)$ exists, where $F(s)$ is the transform of $f(t)$, then

$$\lim_{s \rightarrow \infty} sF(s) = \lim_{t \rightarrow 0} f(t) \quad (2-17)$$

For example, if $F(s) = K/(s^3 + as^2 + bs + c)$, then

$$\lim_{t \rightarrow 0} f(t) = \lim_{s \rightarrow \infty} \frac{Ks}{s^3 + as^2 + bs + c} \quad (2-18)$$

and

$$f(0) = 0$$

If the derivatives of $f(t)$ are Laplace transformable, they have Laplace transforms given by

$$\mathcal{L}[\dot{f}(t)] = sF(s) - f(0+) \quad (2-19)$$

$$\mathcal{L}[\ddot{f}(t)] = s^2F(s) - sf(0+) - \dot{f}(0+) \quad (2-20)$$

$$\mathcal{L}[\ddot{\ddot{f}}] = s^3F(s) - s^2f(0+) - s\dot{f}(0+) - \ddot{f}(0+) \quad (2-21)$$

$$\mathcal{L}[\ddot{\ddot{\ddot{f}}}] = s^4F(s) - s^3f(0+) - s^2\dot{f}(0+) - s\ddot{f}(0+) - \ddot{\ddot{f}}(0+) \quad (2-22)$$

and so forth. Use of the initial value theorem to evaluate the derivatives for the example proceeds as follows.

Since $f(0+) = 0$,

$$\lim_{t \rightarrow 0} \dot{f}(t) = \lim_{s \rightarrow \infty} s[sF(s)] = \lim_{s \rightarrow \infty} s \frac{Ks}{s^3 + as^2 + bs + c} = 0 \quad (2-23)$$

and similarly, since $f(0+)$ and $\dot{f}(0+)$ are zero,

$$\lim_{t \rightarrow 0} \ddot{f}(t) = \lim_{s \rightarrow \infty} s[s^2 F(s)] = \lim_{s \rightarrow \infty} s \frac{Ks^2}{s^3 + as^2 + bs + c} = K \quad (2-24)$$

Because $\ddot{f}(0) = K$, the initial value of the third derivative will be

$$\begin{aligned} \lim_{t \rightarrow 0} \dddot{f}(t) &= \lim_{s \rightarrow \infty} s[s^3 F(s) - \ddot{f}(0+)] \\ &= \lim_{s \rightarrow \infty} s \left[\frac{Ks^3}{s^3 + as^2 + bs + c} - K \right] \\ &= \lim_{s \rightarrow \infty} \left[-\frac{Ks(as^2 + bs + c)}{s^3 + as^2 + bs + c} \right] = -Ka \quad (2-25) \end{aligned}$$

For the initial value of the fourth derivative,

$$\begin{aligned} \lim_{t \rightarrow 0} \ddddot{f}(t) &= \lim_{s \rightarrow \infty} s[s^4 F(s) - s\ddot{f}(0+) - \ddot{f}(0+)] \\ &= \lim_{s \rightarrow \infty} s \left[\frac{Ks^4}{s^3 + as^2 + bs + c} - sK + Ka \right] \\ &= \lim_{s \rightarrow \infty} K \left[\frac{(a^2 - b)s^3 + (ab - c)s^2 + acs}{s^3 + as^2 + bs + c} \right] = K(a^2 - b) \quad (2-26) \end{aligned}$$

and so forth.

The derivatives evaluated in the fashion illustrated above are valuable as check points and to enhance one's physical grasp of the initial character of a response. Also, several derivatives can be combined into a Maclaurin series to give an approximation to the initial response. The Maclaurin series, in general, is

$$f(t) = f(0) + t\dot{f}(0) + \frac{t^2}{2!}\ddot{f}(0) + \frac{t^3}{3!}\ddot{\ddot{f}}(0) + \dots \quad (2-27)$$

For the example above this series would be

$$\begin{aligned} f(t) &= K\left[\frac{t^2}{2} - a\frac{t^3}{6} + (a^2-b)\frac{t^4}{24} + \dots\right] \\ &= \frac{Kt^2}{2}\left[1 - \frac{at}{3} + \frac{(a^2-b)t^2}{12} + \dots\right] \end{aligned} \quad (2-28)$$

This initial response version of the Maclaurin series supplements the Maclaurin series developed later for the steady-state response.

The Final Value Theorem. The final value theorem equates the value of a time function, $f(t)$, as t approaches infinity to that of the function $sF(s)$ as s approaches zero. Obviously, there must be more restrictions on the application of this theorem than there were on that for the initial value. For example, an $F(s)$ which has poles in the right half plane, or on the axis of imaginaries (both allowed in the initial value theorem), gives rise to an $f(t)$ which has no final value. So in addition to the requirement shared with the initial value theorem, i.e., that the function $f(t)$ being evaluated at $t=0$ and its derivative are Laplace transformable, it is also necessary to specify that the function $sF(s)$ is analytic on the axis of imaginaries and in the right half plane. Then, with these restrictions,

$$\lim_{s \rightarrow 0} sF(s) = \lim_{t \rightarrow \infty} f(t) \quad (2-29)$$

Using the previous example and assuming that $F(s)$ has no poles in the right half plane or on the imaginary axis,

$$\lim_{t \rightarrow \infty} f(t) = \lim_{s \rightarrow 0} s \frac{K}{s^3 + as^2 + bs + c} = 0 \quad (2-30)$$

Similarly, all higher derivatives also have zero final values.

As another example, consider

$$F(s) = \frac{K}{s^2(s + \alpha)} \quad (2-31)$$

The initial value theorem gives $f(0) = 0$, but the application of the final value theorem to find $f(t)]_{t \rightarrow \infty}$ is not possible because $sF(s)$ has a pole at the origin (on the imaginary axis). However, if α is positive, the derivative $\dot{f}(t)$ does have a final value, i.e.,

$$\lim_{t \rightarrow \infty} \dot{f}(t) = \lim_{s \rightarrow 0} s \frac{Ks}{s^2(s + \alpha)} = \frac{K}{\alpha} \quad (2-32)$$

Further, since the theorem would show that $\ddot{f}(t)$, $\ddot{\ddot{f}}(t)$, and all the higher derivatives are zero as t goes to infinity, it is apparent that $f(t)$ can be approximated for large values of t by

$$f(t) \doteq \frac{K}{\alpha} t \quad (2-33)$$

In addition to giving the type of particular answers illustrated above, the initial and final value theorems may be regarded as a basis for establishing the intuitive feeling that the steady-state time response is determined largely by the behavior of $F(s)$ at small values of the complex frequency, s , and that the time response at small values of time depends largely on $F(s)$ at large values of s . This is often a helpful concept (although the restrictions of the two underlying theorems should be kept thoroughly in mind whenever it is used).

As a case in point consider a distinction between the so-called Bode and root locus gains. A response transform, or some one of its derivatives or integrals if more than one power of free s is present, may be written either as

$$Y(s) = K \frac{(s^n + a_1 s^{n-1} + \dots + a_{n-1} s + a_n)}{s(s^{m+n} + b_1 s^{m+n-1} + \dots + b_{m+n-1} s + b_{m+n})} \quad (2-34)$$

or as

$$Y(s) = K \frac{\left(\frac{s^n}{a_n} + \frac{a_1}{a_n} s^{n-1} + \dots + \frac{a_{n-1}}{a_n} s + 1 \right)}{s \left(\frac{s^{m+n}}{b_{m+n}} + \frac{b_1}{b_{m+n}} s^{m+n-1} + \dots + \frac{b_{m+n-1}}{b_{m+n}} s + 1 \right)} \quad (2-35)$$

As introduced by Eq. 2-10, et seq., the first style (Eq. 2-34) is in the root-locus form, with a root locus gain, κ ; the second (Eq. 2-35) is in Bode form, with a Bode gain, K . Assuming that the final value theorem is applicable, it is easy to see that the Bode gain is the final value, i.e.,

$$\lim_{t \rightarrow \infty} y(t) = \lim_{s \rightarrow 0} [sY(s)] = K \quad (2-36)$$

The root locus gain, on the other hand, is connected with the initial response. It is, in fact, the first nonzero derivative at $t=0$, i.e.,

$$\left. \frac{d^m y(t)}{dt^m} \right|_{t=0} = \lim_{s \rightarrow \infty} s [s^m Y(s)] = \kappa \quad (2-37)$$

Steady-State Response Calculations by a Maclaurin Series. In the first article of this section a Maclaurin series having time as the variable was used to develop an expression for the initial response of a system. In this article a Maclaurin series will again be used, but in the transform domain and to evolve an approximation to the steady-state response. As a result of the two developments, approximate expressions for both the initial and final phases of response can be obtained directly from the polynomial ratio form of $F(s)$ without factoring.

As shown in previous parts of this chapter, the output of an element when excited by some input is given by

$$\begin{aligned} Y(s) &= \frac{N(s)}{D(s)} X(s) \\ &= W(s)X(s) \end{aligned} \quad (2-38)$$

where $Y(s)$ is the transform of the output response, $X(s)$ that of the input, and $W(s) = N(s)/D(s)$ is a ratio of polynomials in s containing all the system characteristics. If $W(s)$ is expanded in a Maclaurin series in s , the series will converge for small values of s .

$$\begin{aligned}
W(s) &= W(0) + s \left. \frac{dW(s)}{ds} \right|_{s=0} + \frac{s^2}{2!} \left. \frac{d^2W(s)}{ds^2} \right|_{s=0} + \dots + \frac{s^n}{n!} \left. \frac{d^nW(s)}{ds^n} \right|_{s=0} + \dots \\
&= C_0 + C_1 s + C_2 s^2 + \dots + C_n s^n + \dots
\end{aligned}
\tag{2-39}$$

where

$$C_n = \frac{1}{n!} \left. \frac{d^nW(s)}{ds^n} \right|_{s=0} = W^{(n)}(0)$$

Multiplying the series by $X(s)$ to give the output transform, $Y(s)$, one obtains

$$Y(s) = C_0 X(s) + C_1 s X(s) + C_2 s^2 X(s) + \dots + C_n s^n X(s) + \dots \tag{2-40}$$

This expression is valid in the region near $s=0$, where the series is convergent. Recognizing that

$$\mathcal{L} \left[\frac{d^n x(t)}{dt^n} \right] = s^n X(s) - s^{n-1} x(0+) - s^{n-2} \dot{x}(0+) - \dots - \frac{d^{n-1} x}{dt^{n-1}}(0+)$$

the series for the output transform reduces to

$$\begin{aligned}
Y(s) &= C_0 \mathcal{L}[x(t)] + C_1 \mathcal{L}[\dot{x}(t)] + C_2 \mathcal{L}[\ddot{x}(t)] + \dots + C_n \mathcal{L} \left[\frac{d^n x}{dt^n} \right] \\
&\quad + \dots + \left\{ x(0+) [C_1 + C_2 s + \dots] \right\} \\
&\quad + \left\{ \dot{x}(0+) [C_2 + C_3 s + \dots] \right\} + \dots
\end{aligned}
\tag{2-41}$$

If an infinity of higher order impulse functions (which occur at $t=0$ and hence have no effect on large t) are ignored, the inverse transform is given by

$$\begin{aligned}
y(t) &= W(0)x(t) + W'(0)\dot{x}(t) + \frac{1}{2!}W''(0)\ddot{x}(t) + \dots + \frac{1}{n!}W^{(n)}(0)\frac{d^n x}{dt^n} + \dots \\
&= C_0 x(t) + C_1 \dot{x}(t) + C_2 \ddot{x}(t) + \dots + C_n \frac{d^n x}{dt^n} + \dots
\end{aligned}
\tag{2-42}$$

where the primes denote differentiation with respect to s . This series is valid only at those times corresponding to $s \rightarrow 0$, i.e., in the

neighborhood governed by the final value theorem, and all of the restrictions of the theorem apply. As a practical matter the series is suitable to define the steady-state components of a system response, presuming either that the transients have died away or that they have been otherwise removed.

The C_n 's shall be called general output response coefficients. In the special case where $x(t)$ is the system command input and $y(t)$ is the system error, these coefficients are the well-known error coefficients of conventional servo analysis.

As might be expected, the result given by Eq. 2-42 is the forced solution for a system subjected to a power series input. The transient component of the solution is not obtained, although all the output terms having time variations identical with those of the power series input are given by the relation. Because power series are handy devices to describe such things as idealized command signals derived from empirical data, average effects of random functions which have stationary characteristics about a time-varying mean, etc., the response series has many uses.

To complete the discussion of the response series the first few output response coefficients will be developed for a general system. For this purpose let $W(s)$ have the form

$$\begin{aligned} W(s) &= \frac{b_0 + b_1 s + b_2 s^2 + \dots + b_n s^n}{a_0 + a_1 s + a_2 s^2 + \dots + a_n s^n} \\ &= \frac{b_0 + b_1 s + b_2 s^2 + \dots + b_n s^n}{a_0 \left[1 + \frac{s}{a_0} (a_1 + a_2 s + a_3 s^2 + \dots + a_n s^{n-1}) \right]} \end{aligned} \quad (2-43)$$

For most input-output combinations the order of the numerator will be less than that of the denominator, so b_n and perhaps other b_i 's will be zero. In Eq. 2-43 the numerator is allowed to be the same order as the denominator to include such important cases as input-error closed-loop response functions.

Perhaps the simplest way to generate the required Maclaurin series for functions like those of Eq. 2-43 is to simply divide the denominator

into the numerator. Because the denominator is of the form $[1 + z(s)]$, this can be readily accomplished by expanding $[1 + z(s)]^{-1}$ as $1 - z(s) + z^2(s) - \dots$, and then multiplying by the numerator polynomial. Proceeding in this way,

$$\begin{aligned}
 W(s) &= \frac{1}{a_0} (b_0 + b_1 s + b_2 s^2 + \dots + b_n s^n) \left\{ 1 - \frac{s}{a_0} (a_1 + a_2 s + \dots + a_n s^{n-1}) \right. \\
 &\quad \left. + \left(\frac{s}{a_0} \right)^2 (a_1 + a_2 s + \dots + a_n s^{n-1})^2 - \left(\frac{s}{a_0} \right)^3 (a_1 + a_2 s + \dots + a_n s^{n-1})^3 + \dots \right\} \\
 &= \frac{1}{a_0} (b_0 + b_1 s + b_2 s^2 + \dots + b_n s^n) \left\{ 1 - \frac{a_1}{a_0} s + \left[\left(\frac{a_1}{a_0} \right)^2 - \frac{a_2}{a_0} \right] s^2 \right. \\
 &\quad \left. - \left[\left(\frac{a_1}{a_0} \right)^3 - \frac{2a_1 a_2}{a_0^2} + \frac{a_3}{a_0} \right] s^3 + \dots \right\} \\
 &= \frac{1}{a_0} \left[b_0 - \left(\frac{a_1}{a_0} b_0 - b_1 \right) s + \left\{ \left[\left(\frac{a_1}{a_0} \right)^2 - \frac{a_2}{a_0} \right] b_0 - \frac{a_1}{a_0} b_1 + b_2 \right\} s^2 \right. \\
 &\quad \left. - \left\{ \left[\left(\frac{a_1}{a_0} \right)^3 - \frac{2a_1 a_2}{a_0^2} + \frac{a_3}{a_0} \right] b_0 - \left[\left(\frac{a_1}{a_0} \right)^2 - \frac{a_2}{a_0} \right] b_1 + \frac{a_1}{a_0} b_2 - b_3 \right\} s^3 + \dots \right] \\
 &\hspace{25em} (2-44)
 \end{aligned}$$

Putting this result in a somewhat different form, which is often easier to work with,

$$\begin{aligned}
 W(s) &= \frac{b_0}{a_0} + \frac{a_0 b_1 - a_1 b_0}{a_0^2} s + \left[\frac{a_0 b_2 - a_2 b_0}{a_0^2} - \left(\frac{a_0 b_1 - a_1 b_0}{a_0^2} \right) \frac{a_1}{a_0} \right] s^2 \\
 &\quad + \left\{ \frac{a_0 b_3 - a_3 b_0}{a_0^2} + \frac{a_0 b_1 - a_1 b_0}{a_0^2} \left[\left(\frac{a_1}{a_0} \right)^2 - \frac{a_2}{a_0} \right] - \frac{a_0 b_2 - a_2 b_0}{a_0^2} \frac{a_1}{a_0} \right\} s^3 + \dots \\
 &= c_0 + c_1 s + c_2 s^2 + c_3 s^3 + \dots \hspace{10em} (2-45)
 \end{aligned}$$

The dependence of successive output response coefficients upon preceding coefficients can be deduced by properly associating various combinations of terms in Eq. 2-45, viz:

$$c_0 = \frac{b_0}{a_0}$$

$$c_1 = \frac{b_1}{a_0} - \frac{a_1}{a_0} c_0$$

(2-46)

$$c_2 = \frac{b_2}{a_0} - \frac{a_2}{a_0} c_0 - \frac{a_1}{a_0} c_1$$

$$c_3 = \frac{b_3}{a_0} - \frac{a_3}{a_0} c_0 - \frac{a_2}{a_0} c_1 - \frac{a_1}{a_0} c_2$$

This form, which is readily extended by inspection, provides a convenient algorithm for the computation of output response coefficients in a sequential fashion.

2.5 PARTIAL FRACTION COEFFICIENT RATIOS

Higher order equations come about through multidegree-of-freedom systems. In many cases the responses of more than one degree of freedom are desired. These can be found using the technique already described, i.e., decompose the response transforms for each degree of freedom into partial fraction expansions, then inverse transform term by term. With this procedure the labor is increased in proportion to the number of degrees of freedom for which information is desired.

A far more efficient way to determine responses for the several degrees of freedom starts with the original equations of motion for the system. In these the degrees of freedom are dependent variables in a set of simultaneous constant-coefficient differential equations. Transformation of the simultaneous differential equations simplifies them to a set of linear algebraic equations. At this point, determinants or any equivalent method such as the elimination of variables between equations can be applied to find the transform of each dependent variable. In the technique to be described the partial fraction coefficients are determined for one degree of freedom. For all the other degrees of freedom, ratios of partial fraction coefficients are obtained from the transformed equations of motion. The partial fraction coefficient ratios can then be used with the partial fraction coefficients for the first degree of

freedom to determine the coefficients appropriate to the other degrees of freedom.

The procedure outlined above is best understood with the aid of an illustration. Consider the following set of three simultaneous equations:

$$a_{11}(s)X(s) + a_{12}(s)Y(s) + a_{13}(s)Z(s) = b_1(s)\delta_1(s) \quad (2-47)$$

$$a_{21}(s)X(s) + a_{22}(s)Y(s) + a_{23}(s)Z(s) = b_2(s)\delta_2(s) \quad (2-48)$$

$$a_{31}(s)X(s) + a_{32}(s)Y(s) + a_{33}(s)Z(s) = b_3(s)\delta_3(s) \quad (2-49)$$

Here, $x(t)$, $y(t)$, and $z(t)$ are the dependent variables, the δ 's are the input forcing functions, and the equations are in the transformed state so that the coefficients $a_{ij}(s)$ are polynomials in s . Equations 2-47 and 2-49 are simple linear equations and can be solved by determinants or an equivalent procedure. $X(s)$ becomes:

$$X(s) = \frac{\begin{vmatrix} b_1\delta_1 & a_{12} & a_{13} \\ b_2\delta_2 & a_{22} & a_{23} \\ b_3\delta_3 & a_{32} & a_{33} \end{vmatrix}}{\Delta(s)} = \frac{N_x(s)}{\Delta(s)} \quad (2-50)$$

and similarly, $Y(s)$ and $Z(s)$ are given by:

$$Y(s) = \frac{\begin{vmatrix} a_{11} & b_1\delta_1 & a_{13} \\ a_{21} & b_2\delta_2 & a_{23} \\ a_{31} & b_3\delta_3 & a_{33} \end{vmatrix}}{\Delta(s)} = \frac{N_y(s)}{\Delta(s)} \quad (2-51)$$

and

$$Z(s) = \frac{\begin{vmatrix} a_{11} & a_{12} & b_1\delta_1 \\ a_{21} & a_{22} & b_2\delta_2 \\ a_{31} & a_{32} & b_3\delta_3 \end{vmatrix}}{\Delta(s)} = \frac{N_z(s)}{\Delta(s)} \quad (2-52)$$

where

$$\Delta(s) = \begin{vmatrix} a_{11} & a_{12} & a_{13} \\ a_{21} & a_{22} & a_{23} \\ a_{31} & a_{32} & a_{33} \end{vmatrix}$$

The denominator, $\Delta(s)$, is the characteristic function of the system. When it is equated to zero to make the characteristic equation $\Delta(s) = 0$, the separate factors yield the roots, $s = -q_1$, which determine the nature of the individual exponential motions or modes of motion. These equations can be solved for $x(t)$, $y(t)$, and $z(t)$ by performing the following conventional steps:

Expand the determinant, $\Delta(s)$ and find its roots. These roots, and the poles introduced by $\delta_1(s)$, are the poles shared by $X(s)$, $Y(s)$, and $Z(s)$. In the illustrative case the poles will be denoted by subscripts 1,2,3,...n.

$$\begin{aligned} \kappa_{\Delta}(s + q_1)(s + q_2)(s + q_3) \cdots (s + q_n) &= \Delta(s) = 0 \\ \text{or} \quad \Delta(-q_1) &= \Delta(-q_2) = \Delta(-q_3) = \Delta(-q_n) = 0 \end{aligned}$$

Expand $X(s)$, $Y(s)$, and $Z(s)$ as partial fractions, and find the partial fraction coefficients as shown in the last section. Examples of this for $X(s)$ and $Y(s)$ are given below. The expressions for $X(s)$ and $Y(s)$ are continued to allow for poles of $\delta_1(s)$, $\delta_2(s)$, and $\delta_3(s)$, which are left as arbitrary functions.

$$\begin{aligned} X(s) &= \frac{x_1}{s + q_1} + \frac{x_2}{s + q_2} + \cdots + \frac{x_n}{s + q_n} + \cdots \\ Y(s) &= \frac{y_1}{s + q_1} + \frac{y_2}{s + q_2} + \cdots + \frac{y_n}{s + q_n} + \cdots \end{aligned}$$

As the final step, perform the inverse transformation term by term by utilizing Table 2-2.

$$\begin{aligned} x(t) &= x_1 e^{-q_1 t} + x_2 e^{-q_2 t} + \cdots + x_n e^{-q_n t} + \cdots \\ y(t) &= y_1 e^{-q_1 t} + y_2 e^{-q_2 t} + \cdots + y_n e^{-q_n t} + \cdots \end{aligned}$$

In the above procedure the partial fraction coefficients x_k , y_k , z_k for each dependent variable are found separately. These coefficients

will, of course, be partially determined by the particular type of input, requiring some recalculation if the forms of the inputs are changed.

The simplification promised at the outset of this section is made by finding the ratios of the partial fraction coefficients which describe a particular mode, i.e., the component of each dependent variable characterized by a particular root of $\Delta(s) = 0$. These ratios, say y_1/x_1 or z_k/x_k , are independent of the input δ 's, and can therefore be found in general terms.

To illustrate the lack of dependence on input, consider the ratio of x_k to y_k . For the mode characterized by the roots s_k ,

$$x_k = \left[\frac{N_x(s)}{\Delta(s)} (s + q_k) \right]_{s = -q_k} ; y_k = \left[\frac{N_y(s)}{\Delta(s)} (s + q_k) \right]_{s = -q_k} \quad (2-53)$$

Dividing x_k by y_k ,

$$\frac{x_k}{y_k} = \left[\frac{N_x(s)}{\Delta(s)} (s + q_k) \right]_{s = -q_k} \left[\frac{\Delta(s)}{N_y(s) (s + q_k)} \right]_{s = -q_k} = \left[\frac{N_x(s)}{N_y(s)} \right]_{s = -q_k} \quad (2-54)$$

For a set of arbitrary input δ 's, say δ_1 , δ_2 , and δ_3 , the $N_x(s)/N_y(s)$ ratio becomes

$$\frac{N_x(s)}{N_y(s)} = \frac{b_1 \delta_1 \Delta_{11} - b_2 \delta_2 \Delta_{21} + b_3 \delta_3 \Delta_{31}}{-b_1 \delta_1 \Delta_{12} + b_2 \delta_2 \Delta_{22} - b_3 \delta_3 \Delta_{32}} \quad (2-55)$$

where the Δ_{ij} are the minors of the determinant $\Delta(s)$. Δ_{11} , for example, is obtained from $\Delta(s)$ by crossing out the row and the column in which a_{11} appears. For another set of arbitrary inputs, δ_a , δ_b , and δ_c , the ratio becomes

$$\frac{N_x(s)}{N_y(s)} = \frac{b_1 \delta_a \Delta_{11} - b_2 \delta_b \Delta_{21} + b_3 \delta_c \Delta_{31}}{-b_1 \delta_a \Delta_{12} + b_2 \delta_b \Delta_{22} - b_3 \delta_c \Delta_{32}} \quad (2-56)$$

The various δ 's are arbitrary, so $[N_x(s)/N_y(s)]_{1,2,3}$ is not equal to $[N_x(s)/N_y(s)]_{a,b,c}$ in general. However, the ratio may conceivably be equal for some values of s . to find these particular values, the two equations are set equal to one another. Then,

$$\frac{b_1 \delta_a \Delta_{11} - b_2 \delta_b \Delta_{21} + b_3 \delta_c \Delta_{31}}{-b_1 \delta_a \Delta_{12} + b_2 \delta_b \Delta_{22} - b_3 \delta_c \Delta_{32}} = \frac{b_1 \delta_1 \Delta_{11} - b_2 \delta_2 \Delta_{21} + b_3 \delta_3 \Delta_{31}}{-b_1 \delta_1 \Delta_{12} + b_2 \delta_2 \Delta_{22} - b_3 \delta_3 \Delta_{32}} \quad (2-57)$$

Multiplying the means by the extremes, and combining some terms,

$$\begin{aligned} & b_1 b_2 (\Delta_{11} \Delta_{22} - \Delta_{12} \Delta_{21}) (\delta_2 \delta_a - \delta_1 \delta_b) \\ & + b_1 b_3 (\Delta_{11} \Delta_{32} - \Delta_{12} \Delta_{31}) (\delta_1 \delta_c - \delta_3 \delta_a) \\ & + b_2 b_3 (\Delta_{31} \Delta_{22} - \Delta_{21} \Delta_{32}) (\delta_2 \delta_c - \delta_3 \delta_b) = 0 \end{aligned} \quad (2-58)$$

Now the difference in products of the minors can be identified as

$$\begin{aligned} \Delta_{11} \Delta_{22} - \Delta_{12} \Delta_{21} &= a_{33} \Delta(s) \\ \Delta_{11} \Delta_{32} - \Delta_{12} \Delta_{31} &= -a_{23} \Delta(s) \\ \Delta_{22} \Delta_{31} - \Delta_{21} \Delta_{32} &= a_{13} \Delta(s) \end{aligned}$$

so that equation (2-58) becomes

$$\begin{aligned} \Delta(s) [a_{33} b_1 b_2 (\delta_2 \delta_a - \delta_1 \delta_b) - a_{23} b_1 b_3 (\delta_1 \delta_c - \delta_3 \delta_a) \\ + a_{13} b_2 b_3 (\delta_2 \delta_c - \delta_3 \delta_b)] = 0 \end{aligned} \quad (2-59)$$

$$\text{or} \quad \Delta(s) = 0$$

Since $\Delta(s)$ is and can be zero only at the roots $s = -q_1, -q_2, -q_3, \dots, -q_n$, the ratio $x_k/y_k = [N_x(s)/N_y(s)]_{s=-q_k}$ is independent of the input δ 's.

Because of this lack of dependence on inputs, the various ratios y_k/x_k and z_k/x_k can be computed for any input. Ordinarily the simplest results are obtained when all the δ 's but one are set equal to zero. Thus, the modal response ratio y_k/x_k can be found from any of the ratios of minors given below evaluated at $s = -q_k$:

$$\frac{y_k}{x_k} = - \left. \frac{\Delta_{12}}{\Delta_{11}} \right|_{s=-q_k} = - \left. \frac{\Delta_{22}}{\Delta_{21}} \right|_{s=-q_k} = - \left. \frac{\Delta_{32}}{\Delta_{31}} \right|_{s=-q_k} \quad (2-60)$$

The mode of motion corresponding to q_k will be represented in the several degrees of freedom by the terms

$$\begin{array}{lll} x_k e^{-q_k t} & \text{in} & x(t) \\ (y_k/x_k) x_k e^{-q_k t} & \text{in} & y(t) \\ (z_k/x_k) x_k e^{-q_k t} & \text{in} & z(t) \end{array} \quad (2-61)$$

where x_k is presumed to be the partial fraction coefficient which is individually computed for the particular input of interest. The total responses are obtained by summing the responses for the several modes, e.g., for $y(t)$

$$y(t) = \left(\frac{y_1}{x_1}\right)x_1 e^{-q_1 t} + \left(\frac{y_2}{x_2}\right)x_2 e^{-q_2 t} + \dots + \left(\frac{y_n}{x_n}\right)x_n e^{-q_n t} + \dots \quad (2-62)$$

Modal response ratios are, in general, complex quantities and can be considered as plane vectors. When the components for any one mode are inserted into the equations of motion, each term in the equations becomes, in general, complex and can also be treated as a plane vector. Thus, when the components from Eq. 2-61 are inserted into the homogeneous form of Eq. 2-47 there results

$$\left[a_{11}(s) + \left(\frac{y_k}{x_k}\right)a_{12}(s) + \left(\frac{z_k}{x_k}\right)a_{13}(s) \right]_{s=-q_k} = 0 \quad (2-63)$$

Interpreted graphically as a vector diagram, Eq. 2-63 amounts in general to a closed polygon. This provides a convenient check on the calculation of modal response ratios. As will appear later, both the modal response ratios and the vector polygons play a central role in the description and physical interpretation of vehicle motion characteristics.

2.6 WEIGHTING FUNCTION AND MODAL RESPONSE COEFFICIENTS

The preceding sections have reviewed techniques for finding the transient response of an element when it is subjected to general types of analytical input functions. Definition of such transient responses for all system-dependent variables, together with the input functions which cause them, is one reasonable way to characterize the system. It has great virtue as a direct prediction of expected system behavior when the inputs used are representative of those to which the system will be subjected in practice.

On the other hand, the calculation of a catalog of input-response pairs can be a lot of trouble, and can sometimes tend to overcomplicate the physical picture. For instance, when the input is complex the part

of the response dominated by the system characteristics is usually difficult to separate from that part which depends primarily on the input. To alleviate the labor and to circumvent potential confusion, another way is needed to characterize the transient response. Two special transient responses to simple input forms are commonly used for this purpose. One is the weighting function, or system response to a unit impulse; and the other is its integral, the indicial response or indicial admittance, which is the system response to a unit step function. Because the inputs in both cases are simple, these standard responses exhibit the characteristic modes of the system in the simplest ways possible without contamination due to complex input shapes. Also, with the weighting function or indicial response known, the time response, $y(t)$, of the system to any input, $x(t)$, is readily found by the use of superposition. For the weighting function the convolution integral is used, i.e.,

$$y(t) = \int_0^t w(t-\tau)x(\tau) d\tau, \quad t \geq 0$$

A modified form of this integral, called Duhamel's integral, is appropriate when the indicial response, $I(t)$, is available,

$$y(t) = x(0+)I(t) + \int_0^t I(t-\tau) \frac{dx}{d\tau}(\tau) d\tau \quad (2-64)$$

As a consequence of these equations, all response calculations can be carried out directly in the time domain if desired.*

More often than not the weighting functions or indicial responses are used as ends in themselves to exhibit in a standard way the transient characteristics of the system, and not as intermediaries in response calculations using the convolution or Duhamel integral. The latter

*There are convenient algorithms for numerical convolution when this may be required. See, for example,

J. G. Truxal, Automatic Feedback Control System Synthesis, McGraw-Hill Book Co., Inc., New York, 1955, pp. 63-71.

A. Tustin, "A Method of Analyzing the Behavior of Linear Systems in Terms of Time Series," J. IEEE, Pt. IIA, Vol. 94, 1947, pp. 152-160.

procedure is seldom followed because transient responses will usually be more easily obtained by working in the transform domain, i.e., by transforming the convolution to the algebraic equation

$$Y(s) = W(s)X(s) \quad (2-65)$$

expanding into partial fractions, and inverting to the time domain. There are cases, too, where one finds a convolution integral itself of value.

These applications include situations where:

- It is easier to integrate directly than to go through the other transformation processes
- The input function or weighting function does not possess a rational Laplace transform
- The input function or weighting function is so complex that taking its Laplace transform is impractical
- The input function or weighting function is known only graphically or experimentally

Thus the use of the convolution approach is often a practical necessity.

Like other transient responses, the impulse response or weighting function will have a transform which can be resolved into partial fractions. In this case the partial-fraction coefficients are called modal response coefficients and are accorded a special symbol, Q_1 . Thus the transformed weighting function will be

$$W(s) = \sum_{i=1}^{m+n} \frac{Q_1}{s + q_1}$$

where the roots $-q_1$ are those of the system's characteristic equation $\Delta(s) = 0$. Upon inverse transforming, the weighting function becomes

$$w(t) = \sum_{i=1}^{m+n} Q_1 e^{-q_1 t}$$

Splitting $W(s)$ into partial fractions is equivalent to replacing the $(m+n)$ th-order differential equation for $w(t)$ by $m+n$ first-order differential equations of the form

$$\dot{w}_1(t) + q_1 w_1(t) = Q_1 \delta(t) \quad , \quad 1 = 1, 2, \dots, m+n$$

where $w_1(0) = 0$ and the total weighting function is

$$w(t) = w_1(t) + w_2(t) + \dots + w_1(t) + \dots + w_{m+n}(t)$$

Thus the total weighting function is equivalent to the summed responses of $m+n$ first-order systems excited by an impulse input, as shown in Fig. 2-3. The modal response coefficients can also be thought of as initial conditions on unity-gain elemental systems (the Q_1 's in Fig. 2-3 replaced by 1's) which, with no other excitation (no impulse input to the system), results in a system output equal to the weighting function. For this interpretation the elemental differential equations would be

$$\dot{w}_1(t) + q_1 w_1(t) = 0 \quad , \quad 1 = 1, 2, \dots, m+n \quad (2-66)$$

where

$$w_1(0) = Q_1$$

The output response coefficients developed in Section 2.4 can be interpreted as time-weighted moments of the weighting function. The Laplace transform of the n th time moment, $t^n y(t)$, of the output $y(t)$ is

$$\mathcal{L}[t^n y(t)] = (-1)^n \frac{d^n Y(s)}{ds^n} \quad (2-67)$$

so the transform of the integral of $t^n y(t)$ will be

$$\mathcal{L}\left[\int_0^t \tau^n y(\tau) d\tau\right] = \frac{(-1)^n}{s} \frac{d^n Y(s)}{ds^n} \quad (2-68)$$

Under conditions where the final value theorem will apply, i.e., where

$\lim_{t \rightarrow \infty} \int_0^t \tau^n y(\tau) d\tau$ exists,

$$\begin{aligned} \lim_{t \rightarrow \infty} \int_0^t \tau^n y(\tau) d\tau &= \lim_{s \rightarrow 0} s \frac{(-1)^n}{s} \frac{d^n Y(s)}{ds^n} = (-1)^n \frac{d^n Y(s)}{ds^n} \Big|_{s \rightarrow 0} \\ &= (-1)^n \left[\frac{d^n}{ds^n} W(s)X(s) \right]_{s \rightarrow 0} \end{aligned} \quad (2-69)$$

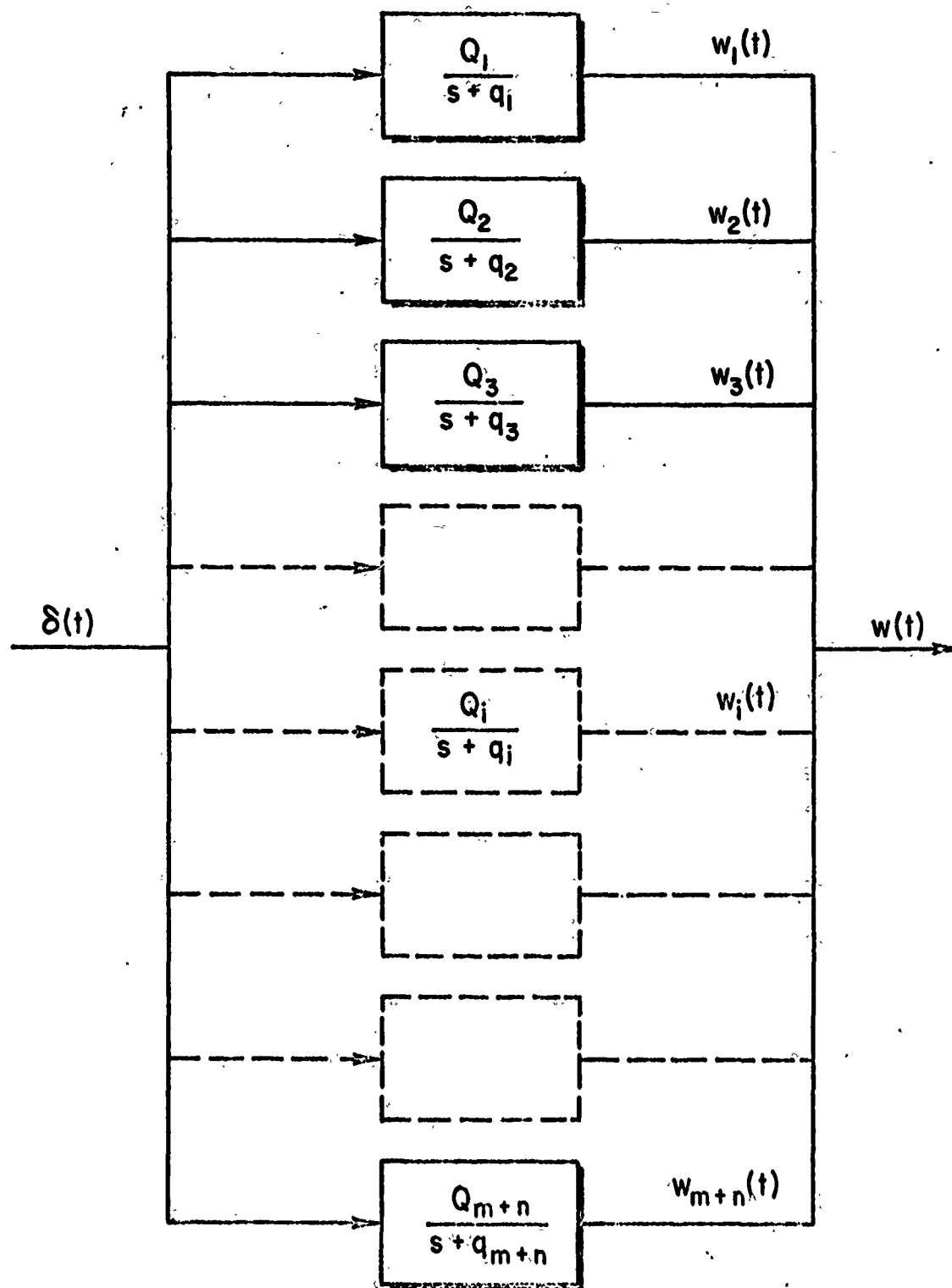


Fig. 2-3. Elemental First-Order Systems
Corresponding to Components of the Weighting Function

If the input, $x(t)$, is taken to be a unit impulse, then $X(s) = 1$ and the output, $y(t)$, will be the system weighting function. When these conditions are inserted into Eq. 2-69, the result becomes

$$\int_0^{\infty} \tau^n w(\tau) d\tau = (-1)^n \left[\frac{d^n W(s)}{ds^n} \right]_{s \rightarrow 0} \quad (2-70)$$

Using Eq. 2-39, the output response coefficients C_n can be identified as

$$C_n = \frac{1}{n!} \left. \frac{d^n W(s)}{ds^n} \right|_{s \rightarrow 0} = \frac{(-1)^n}{n!} \int_0^{\infty} \tau^n w(\tau) d\tau \quad (2-71)$$

This relationship between output response coefficients and the time moments of the weighting function is helpful for physical interpretation and also provides the basis for simple measurement of the response coefficients using computer techniques.

Other useful connections between the output response coefficients and weighting function parameters are relationships involving the modal response coefficients, Q_i . It can be shown* that

$$\begin{aligned} C_0 &= \sum_{i=1}^{m+n} \frac{Q_i}{q_i} \\ C_1 &= - \sum_{i=1}^{m+n} \frac{Q_i}{q_i^2} \\ C_2 &= \sum_{i=1}^{m+n} \frac{Q_i}{q_i^3} \\ &\vdots \\ C_k &= - \sum_{i=1}^{m+n} \frac{Q_i}{(-q_i)^{1+k}} \end{aligned} \quad (2-72)$$

*D. T. McRuer and R. L. Stapleford, Sensitivity and Modal Response for Single-Loop and Multiloop Systems, ASD-TDR-62-812, Jan. 1963, pp. 19-21.

2.7 TIME VECTOR REPRESENTATIONS FOR THE WEIGHTING FUNCTION

The weighting function is most conventionally shown as a time history. This gives a general view of system response characteristics and is often all that is required on low order systems. For higher order systems, however, many modes make up the composite motions, some more dominant than others. Also, a given mode is, in general, reflected with different scales into each of the several degrees of freedom. For these reasons attention must be focused on the modal components of the system weighting functions if a complete physical picture is to be obtained. This is accomplished by application of the principles already described in the discussion of modal response ratios as enhanced by the use of a graphical interpretation using the time vectors.

The method of time vectors is based on the concept of rotating vectors to represent component or total motion quantities. It is particularly useful in representing the amplitude and phasing relationships between such quantities in oscillatory motion. The concepts of time vectors stem from harmonic motion analysis and alternating current theory, with minor modifications to handle time-variable amplitudes.* The basic ideas are readily grasped with the aid of simple examples, so this procedure will be adopted here.

Consider the second-order system described by the differential equation

$$\frac{d^2x}{dt^2} + 2\zeta\omega_n \frac{dx}{dt} + \omega_n^2 x = \omega_n \sqrt{1 - \zeta^2} f(t) \quad (2-73)$$

If the desired response, x , is to be the weighting function, $w(t)$, then the forcing function, $f(t)$, is replaced by the unit impulse, $\delta(t)$, and Eq. 2-73

*R. K. Mueller, "A Graphical Solution of Stability Problems," Jour. Aeron. Sc., June 1937.

M. F. Gardner and J. L. Barnes, Transients in Linear Systems, John Wiley and Sons, Inc., New York, 1942 pp. 174 ff.

K. H. Doetsch, The Time Vector Method for Stability Investigations, ARC R and M 2945, 1957.

W. O. Breuhaus, Résumé of the Time Vector Method as a Means for Analyzing Aircraft Stability, WADC-TR-52-299, Nov. 1952.

becomes

$$\frac{d^2 w}{dt^2} + 2\zeta\omega_n \frac{dw}{dt} + \omega_n^2 w = \omega_n \sqrt{1 - \zeta^2} \delta(t) \quad (2-74)$$

The right side of this equation is zero for $t > 0$, and most of our interest will be centered on the solutions in this region. When Laplace transformed, Eq. 2-74 becomes

$$\begin{aligned} W(s) &= \frac{\omega_n \sqrt{1 - \zeta^2}}{s^2 + 2\zeta\omega_n s + \omega_n^2} \\ &= \frac{x_1}{s + (\zeta\omega_n - j\omega_n \sqrt{1 - \zeta^2})} + \frac{x_2}{s + (\zeta\omega_n + j\omega_n \sqrt{1 - \zeta^2})} \end{aligned} \quad (2-75)$$

where $x_1 = 1/2j$ and $x_2 = -1/2j$. The inverse transform can be written either as a real function or as a sum of the two modes involved represented as complex numbers. Both forms are useful for time vector considerations; each one is given below.

$$w(t) = e^{-\zeta\omega_n t} \sin \omega_n \sqrt{1 - \zeta^2} t, \quad t \geq 0 \quad (2-76)$$

or

$$\begin{aligned} w(t) &= w_1(t) + w_2(t) \\ &= x_1 e^{-\zeta\omega_n t} e^{j\omega_n \sqrt{1 - \zeta^2} t} + x_2 e^{-\zeta\omega_n t} e^{-j\omega_n \sqrt{1 - \zeta^2} t}, \quad t \geq 0 \end{aligned} \quad (2-77)$$

The two complex modes in Eq. 2-77 when combined become the damped real oscillation of Eq. 2-76. Either mode can be used to represent the real weighting function by considering only their real parts, i.e.,

$$w(t) = 2 \operatorname{Re} w_1(t) = 2 \operatorname{Re} w_2(t) \quad (2-78)$$

To remove the $t \geq 0$ restriction on the weighting function given as Eq. 2-76, the form there can be multiplied by the unit step function, $u(t)$. This makes $w(t)$ zero for $t < 0$ and equal to the damped oscillation

thereafter. This will be of no consequence for the time vector representation, although it is required in order that $w(t)$ satisfy Eq. 2-74. Using this form, the weighting function and its first and second derivatives become

$$w(t) = \left[e^{-\zeta\omega_n t} \sin(\omega_n \sqrt{1-\zeta^2} t) \right] u(t) \quad (2-79)$$

$$\dot{w}(t) = \left[\omega_n e^{-\zeta\omega_n t} \sin\left(\omega_n \sqrt{1-\zeta^2} t + \frac{\pi}{2} + \theta\right) \right] u(t) \quad (2-80)$$

$$\ddot{w}(t) = \left[\omega_n^2 e^{-\zeta\omega_n t} \sin\left(\omega_n \sqrt{1-\zeta^2} t + \pi + 2\theta\right) \right] u(t) + \omega_n \sqrt{1-\zeta^2} \delta(t) \quad (2-81)$$

where θ , the so-called damping angle, is given by the equivalent expressions

$$\begin{aligned} \theta &= \sin^{-1} \zeta \\ &= \cos^{-1} \sqrt{1-\zeta^2} \\ &= \tan^{-1} \frac{\zeta}{\sqrt{1-\zeta^2}} \end{aligned} \quad (2-82)$$

Insertion of Eqs. 2-79 through 2-81 into the differential equation for the weighting function identically satisfies the latter. Without the unit step function multiplier, the δ function term in $\ddot{w}(t)$ (Eq. 2-81) would not have arisen and Eq. 2-74 would then be satisfied only for $t > 0$. Now that this point has been made, we will drop the awkward $u(t)$ multipliers and the δ function in \ddot{w} and consider only those times greater than zero.

The first mode of Eq. 2-77 and its derivatives are

$$w_1(t) = x_1 e^{-\zeta\omega_n t} e^{j\omega_n \sqrt{1-\zeta^2} t}, \quad t \geq 0 \quad (2-83)$$

$$\dot{w}_1(t) = \omega_n x_1 e^{-\zeta\omega_n t} e^{j\left[\omega_n \sqrt{1-\zeta^2} t + \pi/2 + \theta\right]}, \quad t \geq 0 \quad (2-84)$$

$$\ddot{w}_1(t) = \omega_n^2 x_1 e^{-\zeta\omega_n t} e^{j\left[\omega_n \sqrt{1-\zeta^2} t + \pi + 2\theta\right]}, \quad t \geq 0 \quad (2-85)$$

Comparing these three equations with their equivalents for the real oscillation provides the basis for a very useful and simple rule, to wit: When any derivative of a component of motion is differentiated, the amplitude is multiplied by ω_n and the phase angle is increased by $\pi/2 + \theta$ (when applying the rule to the second mode, the phase angle would be considered as all of the exponent multiplied by $-j$; thus, $\pi/2 + \theta$ is added to $\omega_n \sqrt{1 - \zeta^2} t$).

The fundamental concept of time vectors is that either periodic or aperiodic motions can be considered as generated by a time vector rotating with constant angular velocity about a fixed point. When the motion is a constant-amplitude oscillation the time vector is of fixed length, whereas its length varies with time for subsiding or diverging oscillations and aperiodic motions. The generating motion of the time vector for the damped sinusoidal weighting function is illustrated in Fig. 2-4 for a damping ratio of 0.3. As the time vector rotates at a constant velocity, $\omega_n \sqrt{1 - \zeta^2}$, its amplitude decreases exponentially, so that the trace of the tip is a logarithmic spiral. At any time, the angle between the tangent and the normal to the radius vector of the spiral is just the damping angle, θ .

The connection between the generating vector and the weighting function can be appreciated by considering the projection of the vector onto the vertical axis. At each instant the projection is equal to the value of the weighting function at that time. The derivatives of the weighting function can be considered in a similar fashion.

As illustrated in Fig. 2-4, \dot{w} is displaced by $\pi/2$ plus the damping angle from w , and \ddot{w} is further displaced by this same increment from \dot{w} . Also, the generating vectors are longer than that for the weighting function by the factors ω_n and ω_n^2 , respectively. If there were no damping, θ would be zero and the system would be a simple harmonic oscillator wherein the velocity and acceleration are, respectively, 90° and 180° out of phase with the displacement.

Figure 2-5 reproduces the time vectors for the weighting function and its derivatives, and also indicates the scaling of quantities in the differential equation proportional to these terms. When these individual

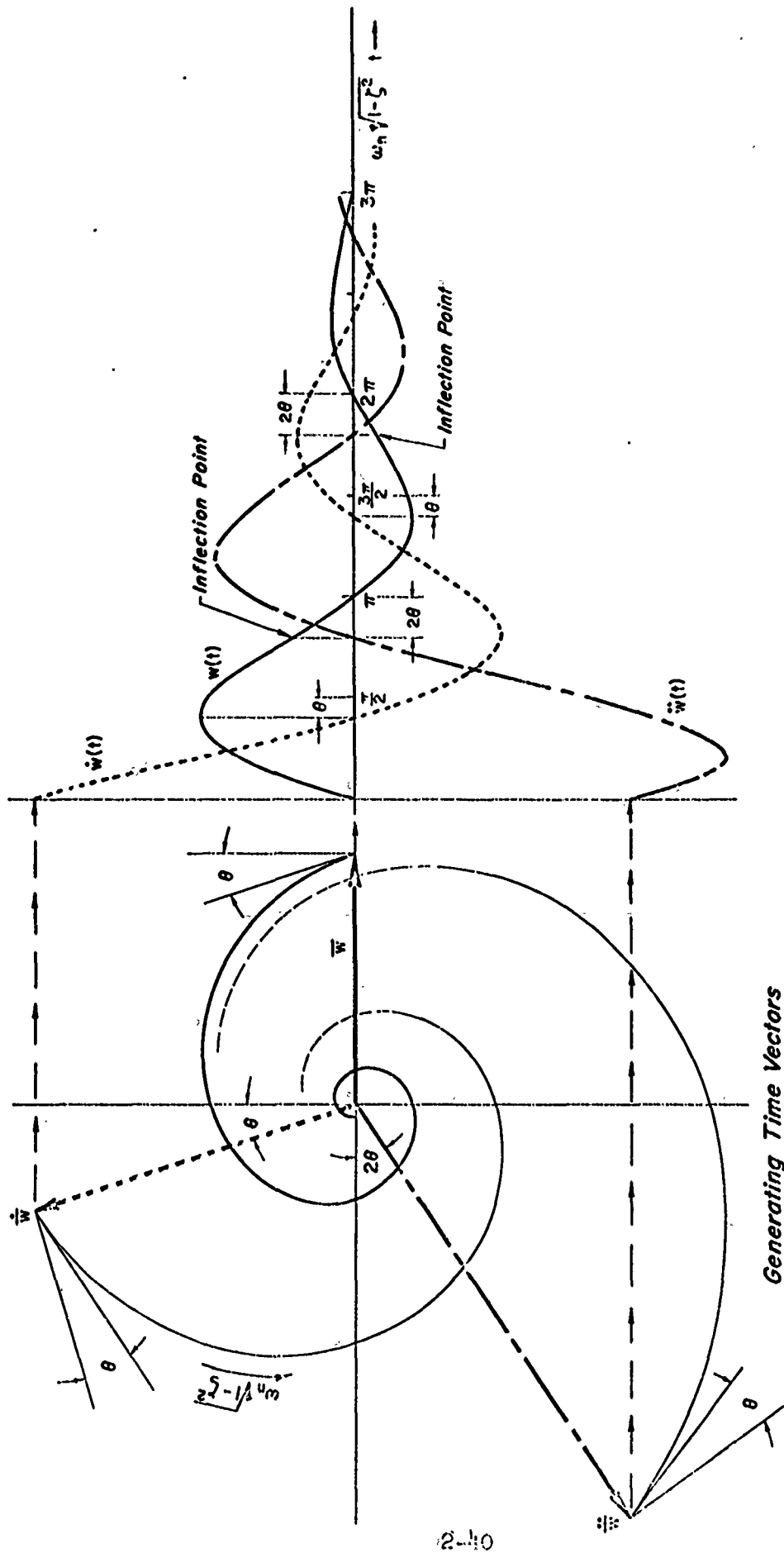


Figure 2-4. Time Histories and Their Generating Time Vectors for a Second - Order System

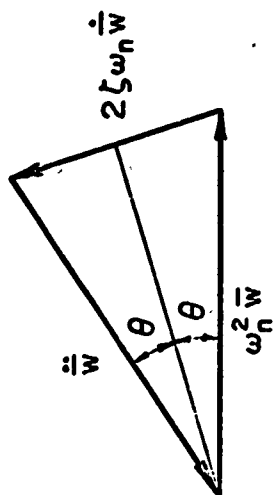
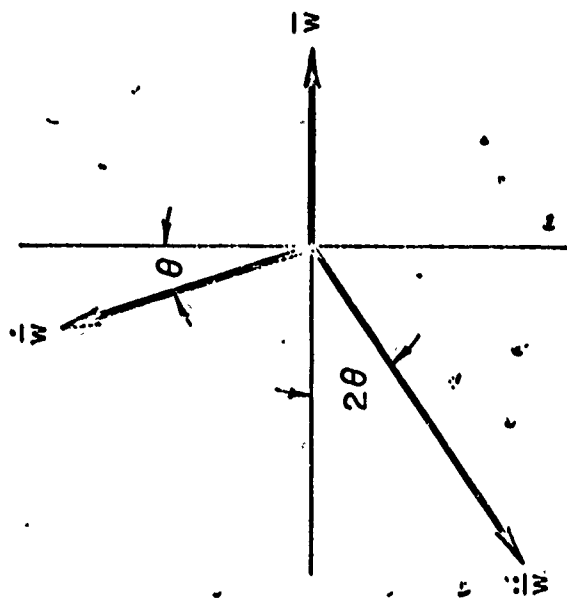


Figure 2-5. Time Vectors and a Polygon of Forces for Second-Order Systems

components of the differential equation are added together, they form a time vector diagram which represents in graphical fashion the equation and its components. For the second-order system this is always an isosceles triangle. The vertex angle is equal to 2θ , which indicates the degree of damping in the system. The ratio of the altitude of the triangle to an isosceles side is equal to the cosine of θ and is therefore a measure of the frequency of the damped motion, $\omega_n \sqrt{1-\zeta^2}$, as compared with that of the undamped motion, ω_n . The length of each time vector in the triangle, and thus the entire triangle, shrinks at the same rate as the parameters of motion. The relative relationships, however, are unmodified so it is usual to consider the time vector triangle to be frozen at a particular instant.

These explanations have been carried out using the real form of the weighting function, although the w_1 complex component could have been used just as well. For that matter, the w_2 component can also serve, although conventions would have to be changed because its direction of rotation is opposite that assumed in the figures.

The illustrative problem has thus far been treated as a one-degree-of-freedom system. Since it is second-order, however, it can as well be considered a two-degree-of-freedom system and thus serve as the simplest example of the use of modal response ratios in construction of time vector diagrams. A two-degree-of-freedom system having the weighting function already described is given by

$$\begin{aligned} (s + \zeta\omega_n) X(s) - \omega_n \sqrt{1-\zeta^2} Y(s) &= 0 \\ \omega_n \sqrt{1-\zeta^2} X(s) + (s + \zeta\omega_n) Y(s) &= F(s) \end{aligned} \quad (2-86)$$

The characteristic function is, of course, $\Delta = s^2 + 2\zeta\omega_n s + \omega_n^2$ and the numerators of the X and Y response transforms are

$$\begin{aligned} N_X(s) &= F(s) \omega_n \sqrt{1-\zeta^2} \\ N_Y(s) &= F(s) (s + \zeta\omega_n) \end{aligned} \quad (2-87)$$

The modal response ratios are given by

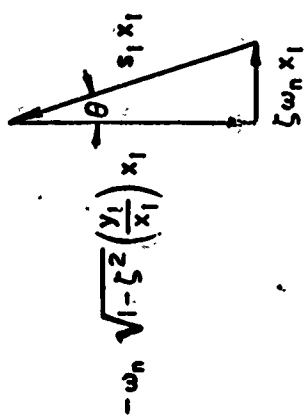
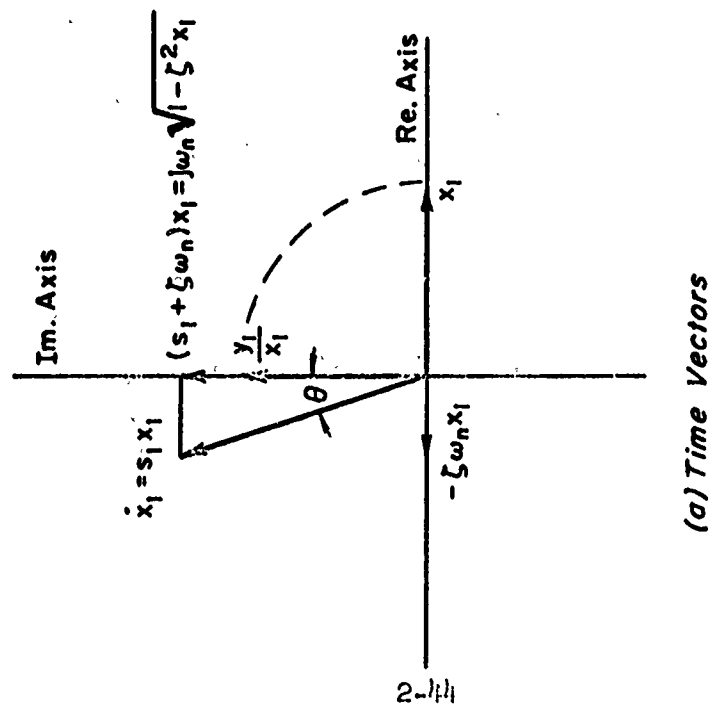
$$\begin{aligned} \frac{y_1}{x_1} &= \frac{s + \zeta\omega_n}{\omega_n\sqrt{1-\zeta^2}} \Big|_s = -\zeta\omega_n + j\omega_n\sqrt{1-\zeta^2} = j \\ \frac{y_2}{x_2} &= \frac{s + \zeta\omega_n}{\omega_n\sqrt{1-\zeta^2}} \Big|_s = -\zeta\omega_n - j\omega_n\sqrt{1-\zeta^2} = -j \end{aligned} \quad (2-88)$$

Considering the first mode only, the time vectors for \dot{x}_1 and \ddot{x}_1 and the modal response ratio, y_1/x_1 , are shown in Fig. 2-6a. Also given there are scaled quantities involved in the two equations of motion. The two vector triangles shown in Figs. 2-6b and 2-6c illustrate the time vector diagram for the two equations of motion. The point illustrated here over and above those described previously is that the terms involving y are derived from x_1 or \dot{x}_1 by using the modal response ratio y_1/x_1 . Because all variables have the same phase angle ($\pi/2 + \theta$) and the same multiplying factor (ω_n) between successive derivatives, the ratio of two derivatives of different components is not affected by increasing or lowering the order of differentiation simultaneously for both components; that is,

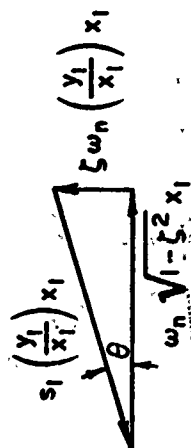
$$\frac{y_1}{x_1} = \frac{\dot{y}_1}{\dot{x}_1} = \frac{\ddot{y}_1}{\ddot{x}_1} \quad \text{or} \quad \frac{\dot{y}_1}{x_1} = \frac{\ddot{y}_1}{\dot{x}_1} \quad \text{etc.}$$

Thus, the modal response ratio y_1/x_1 can be used to obtain either y_1 or \dot{y}_1 by multiplying by x_1 and \dot{x}_1 , respectively.

While the above developments have used the simplest possible example to provide clarity of explanation, the greatest benefits of the time vector method appear for higher order systems with several degrees of freedom. The vector diagrams in these cases become polygons of forces or moments, with, for each mode, one polygon per equation of motion. Because of cross-coupling forces or moments linking the different degrees of freedom, these polygons are generally more complicated than simple triangles. The graphical nature



$$(s_1 + zeta\omega_n)x_1 - \omega_n\sqrt{1-zeta^2}y_1 = 0$$



$$\omega_n \sqrt{1-zeta^2} x_1 + (s_1 + zeta\omega_n) y_1 = 0$$

Figure 2-6. Time Vectors and Vector Polygons for Second-Order Systems Considered as a Two-Degree-of-Freedom System

of the polygons, however, still allows the ready visualization of key physical relationships. Thus, the diagrams show the relative amplitudes and phasings between the different variables of oscillatory motion modes and provide a direct physical appreciation for the effects of individual parameters on the motion.

2.8 TRANSFER FUNCTION MODELS

The discussion of mathematical models to this point has emphasized the transient response performance of an element when subjected to various inputs. This has been done because the usual end result of a system study is a prediction of the physical performance of a system, and transient responses are as physical a result as can be attained. However, analytical models should not be restricted to those of the transient response variety alone because transient response models have several defects. First, the transient response to a particular input is usually dominated by one or two modes, even though the system may be of higher order, because of differences in time and amplitude scale factors among the several modes. Modes that might be important in responses to different inputs, or that might have pronounced effects on performance if system parameters were slightly changed, may be suppressed to a large extent. Second, it is seldom easy to combine directly the transient response models of several complex elements into a single one describing the combination of the elements in a system. Even to combine two or more series elements having known weighting functions into an over-all weighting function using repeated convolution is an irksome computational task. Third, and finally, it is sometimes troublesome, using the convolution integral, to modify the transient response model obtained for simple inputs to one consistent with other more complex inputs. To overcome these difficulties a different form of mathematical model is desired which

- Defines the element as an entity by exhibiting with equal emphasis all of the element characteristic parameters and/or modes
- Allows the models of individual elements to be combined simply into those of the combination
- Can be directly applied in the transform domain for the intermediate stages of transient response calculations

The transform of the weighting function, which is the transform of the output (with all initial conditions zero) divided by the transform of the input, is a model which fulfills these requirements. This function has a supreme theoretical and practical importance, and again a special name. It is called a transfer function of the system. For the general system of Eqs. 2-1 through 2-4 the transfer function will be

$$\frac{Y(s)}{X(s)} = W(s) = \frac{\kappa(s^n + a_1 s^{n-1} + \dots + a_{n-1} s + a_n)}{(s^{m+n} + b_1 s^{m+n-1} + \dots + b_{m+n-1} s + b_{m+n})} \quad (2-89a)$$

$$= \kappa \frac{\prod_{j=1}^n (s + z_j)}{\prod_{i=1}^{m+n} (s + q_i)} \quad (2-89b)$$

$$= \sum_{i=1}^{m+n} \frac{Q_i}{s + q_i} \quad (2-89c)$$

Although the transfer function is one step removed from a transient response model, it still has a direct interpretation in transient response terms. All the information necessary for the construction of weighting function time responses or time vector diagrams is implicitly contained in the transfer function in all its forms. This information is explicit in only the third form given above (Eq. 2-89c). The factored form (Eq. 2-89b) provides all the time history information, i.e., the system characteristic roots, $-q_i$, but the modal response coefficients are one step away. Finally, the first form (Eq. 2-89a) cannot, in general, be interpreted in time response terms without additional operations. Of particular interest in this connection is the application of tests which can describe the general position of the poles without factoring the polynomial. These tests will be covered later under the subject of stability.

The transfer function contains only parameters which stem from the system; it does not depend on the inputs. In this sense the system as an independent entity is equivalent to the $(m+n)r$ transfer functions

corresponding to its $m+n$ independent degrees of freedom when subjected to r independent inputs. Alternatively, it can be stated that the gains (κ), zeros ($-z_j$), and poles ($-q_i$) of the transfer functions completely define the system.

Because input transforms are converted to output transforms by multiplication with the appropriate transfer functions, it is convenient to characterize the input and output of the "pattern" of Fig. 2-1 by their Laplace transforms, and to represent the system by its transfer functions. The "pattern" of Fig. 2-1 in the case of the example system of Fig. 2-2 then becomes the block diagram of Fig. 2-7.

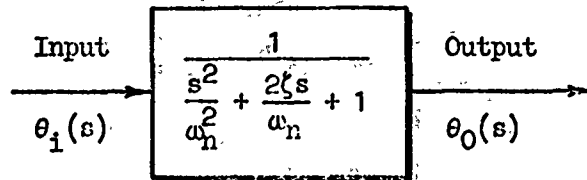


Fig. 2-7. Block Diagram of the Spring-Mass-Damper System

The ease of combining element transfer functions to form the transfer function of the combination can be illustrated by considering two elements in series. If the first has a transfer function

$$W_1(s) = \frac{Y(s)}{X(s)} \quad (2-90)$$

and the second a transfer function

$$W_2(s) = \frac{Z(s)}{Y(s)} \quad (2-91)$$

then the combination has a transfer function which is the product of the individual transfer functions

$$W(s) = \frac{Z(s)}{X(s)} = \frac{Y(s)Z(s)}{X(s)Y(s)} = W_1(s)W_2(s) \quad (2-92)$$

Contrast this with the same operation using the time domain models. Since the weighting function is the inverse transform of the transfer function

$$\mathcal{L}^{-1}[W(s)] = w(t)$$

and

$$\mathcal{L}^{-1}[W_1(s)] = w_1(t)$$

$$\mathcal{L}^{-1}[W_2(s)] = w_2(t)$$

then, by the convolution theorem of the Laplace transform,

$$\begin{aligned} w(t) &= w_1(t) * w_2(t) = \int_0^t w_1(\tau) w_2(t-\tau) d\tau \\ &= \int_0^t w_2(\tau) w_1(t-\tau) d\tau \end{aligned} \quad (2-93)$$

Because convolution is ordinarily much more difficult to perform than simple multiplication, the transfer function is generally the most convenient form of mathematical model to use for manipulations of this type.

Although the transfer function is fundamentally a system descriptor, it does have a physical interpretation as response components in the output response to the hypothetical signal $e^{s_1 t}$. When such an input is applied, the differential equation of the system takes the form

$$\begin{aligned} \frac{d^{m+n} x}{dt^{m+n}} + b_1 \frac{d^{m+n-1} x}{dt^{m+n-1}} + \dots + b_{m+n-1} \frac{dx}{dt} + b_{m+n} x \\ = \kappa \left(\frac{d^n}{dt^n} + a_1 \frac{d^{n-1}}{dt^{n-1}} + \dots + a_{n-1} \frac{d}{dt} + a_n \right) e^{s_1 t} \end{aligned} \quad (2-94)$$

Transforming with initial conditions zero, this becomes

$$\begin{aligned} X(s) &= \frac{\kappa (s^n + a_1 s^{n-1} + \dots + a_{n-1} s + a_n)}{(s^{m+n} + b_1 s^{m+n-1} + \dots + b_{m+n-1} s + b_{m+n}) (s - s_1)} \\ &= \sum_{i=1}^{m+n} \frac{C_i}{s + q_i} + \left[\frac{\kappa (s^n + a_1 s^{n-1} + \dots + a_{n-1} s + a_n)}{(s^{m+n} + b_1 s^{m+n-1} + \dots + b_{m+n-1} s + b_{m+n})} \right]_{s=s_1} \left(\frac{1}{s - s_1} \right) \\ &= \sum_{i=1}^{m+n} \frac{C_i}{s + q_i} + \frac{W(s_1)}{s - s_1} \quad \text{for } s_1 \neq -q_i \end{aligned} \quad (2-95)$$

or, in the time domain,

$$x(t) = \sum_{i=1}^{m+n} C_i e^{-q_i t} + W(s_1) e^{s_1 t} \quad (2-96)$$

The term in brackets in Eq. 2-95 is seen to be the transfer function evaluated at $s = s_1$. In essence, this is the partial fraction coefficient for the forced mode of the system, i.e., that mode having a time history identical to the input $e^{s_1 t}$. The summation represents the effect on the output of the system's natural modes as excited by the forcing function.

It is instructive to consider Eq. 2-96 for several special values of s_1 . First, if s_1 is a real number, either $+\sigma$ or $-\sigma$, then the forced component in the time response is either $W(+\sigma)e^{+\sigma t}$ or $W(-\sigma)e^{-\sigma t}$. Here, the amplitude of the forced component is the transfer function for the particular values of s represented by $+\sigma$ or $-\sigma$.

More generally, s_1 will be complex, as will $W(s_1)$. In this event, $e^{s_1 t}$ is one of the two complex conjugate components of a damped sinusoidal or damped cosinusoidal wave. Alternatively, $e^{s_1 t}$ may be considered as a generating vector resulting in a damped sinusoidal or cosinusoidal time history. In either event, the real response to, say, a damped sinusoidal input, $e^{-\sigma_1 t} \sin \omega_1 t$, can be seen to be

$$x(t) = \sum_{i=1}^{m+n} C_i e^{-q_i t} + |W(s_1)| e^{-\sigma_1 t} \sin [\omega_1 t + \angle W(s_1)]$$

where

$$s_1 = -\sigma_1 + j\omega_1$$

Here, the transfer function $W(s_1)$ appears as a magnitude and phase angle in the forced component of the response.

In all of the cases examined above the transfer function could, in principle, be measured from the responses to various $e^{s_1 t}$ input forms to the extent that the forced response can be separated from the transients represented by the summation. Ordinarily this is frustratingly difficult or practically impossible. However, for stable or just slightly unstable

systems the separation is readily accomplished for the special case $s = j\omega$. Then the forced response is a sinusoid which is separated from the total response by the simple expedient of waiting for the transients to become insignificant for the stable case, or by subtracting out the slightly divergent mode(s) in the unstable case. The motion component remaining consists of a sinusoidal oscillation at frequency ω characterized by an amplitude equal to the magnitude of the transfer function evaluated at $j\omega$, and a phase angle relative to the input given by the angle of $W(j\omega)$. The special transfer function form, $W(j\omega)$, obtained in this manner is called the frequency response because of its connection with the system response to oscillatory inputs.

2.9 REPRESENTATIONS OF TRANSFER FUNCTIONS

The transfer functions of systems or elements can be represented in several useful ways. Among the more prominent of these are the algebraic representation, the pole-zero plot, and several varieties of the Bode diagram.* These all explicitly reflect part or all of the system's pole and zero characteristics. Other possible representations, such as the polar plot of the frequency response function, implicitly contain the same information, but pole and zero data are more difficult to dissect from the total representation. Because our emphasis is on transfer function representations which maximize the easily extractable information, such forms will not be considered here.

The transfer functions of concern are, as we have seen, ordinarily ratios of rational polynomials in which the denominator is of a higher degree than the numerator. When the polynomials are factored, they may be written in the alternative forms:

*H. W. Bode, Network Analysis and Feedback Amplifier Design, D. Van Nostrand Co., Inc., New York, 1945.

N. L. Kusters and W. J. M. Moore, "A Generalization of the Frequency Response Method for the Study of Feedback Control Systems," Automatic and Manual Control, Butterworths Scientific Publications, London, 1952.

D. T. McRuer, Unified Analysis of Linear Feedback Systems, ASD-TR-61-118, Wright-Patterson Air Force Base, Ohio, July 1961.

F. P. De Mello, "Evaluation of Transient System Response," AIEE Trans., Pt. II, Vol. 78, Sept. 1959, pp. 177-186.

$$G(s) = K \frac{\alpha(s)}{\beta(s)} = K \frac{\prod_{j=1}^n (s + z_j)}{\prod_{i=1}^{m+n} (s + q_i)} = K \frac{\prod_{j=1}^n (s + z_j)}{s^k \prod_{i=1}^{m+n-k} (s + q_i)} \quad (2-97)$$

$$G(s) = K \frac{A(s)}{s^k B(s)} = K \frac{\prod_{j=1}^n \left(\frac{s}{z_j} + 1\right)}{s^k \prod_{i=1}^{m+n-k} \left(\frac{s}{q_i} + 1\right)} \quad (2-98)$$

Equations 2-97 and 2-98 display the algebraic representation of the transfer functions. The s^k style is appropriate when some (k) of the poles are zero. The s^k style can also serve for zeros if the k in the denominator product superscript is shifted to the numerator.

The function $G(s)$ is a function of a complex variable, which can be characterized by its poles and zeros. $G(s)$ itself then can be represented by plotting its poles and zeros on the complex s-plane. This would constitute a pole-zero plot. The pole-zero plots of the most common transfer functions or transfer function factors are shown in Table 2-5, where an open circle represents a zero and a cross represents a pole.

Because $G(s)$ for a particular value of s is a complex number, $A + jB$, it can be represented by a modulus or magnitude, $|G| = \sqrt{A^2 + B^2}$, and an argument or phase angle, $\angle G = \tan^{-1} (B/A)$. It is particularly convenient for the purpose of graphical constructions to plot $20 \log_{10} |G|$ and $\angle G$ against $\log_{10} |s|$ while letting the complex variable, $s = \sigma + j\omega$, take on special values in the s-plane. The simplest special values of s are obtained by letting s vary along a straight line in the s-plane. When this is done the transfer function plot comprising $20 \log_{10} |G|$ and $\angle G$ versus $\log_{10} |s|$ is called a generalized Bode diagram. The term $20 \log_{10} |G|$ has the dimensions of decibels (dB) and is abbreviated as $|G|_{dB}$. A chart for converting magnitudes to dB and vice versa is given as Fig. 2-8.

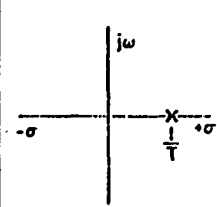
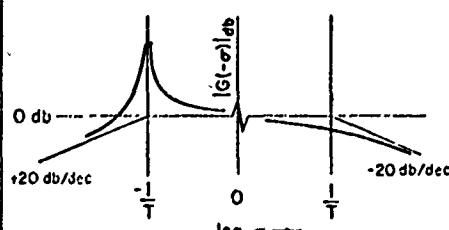
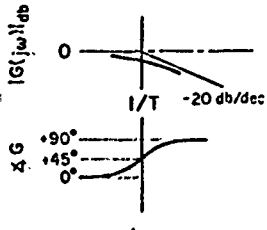
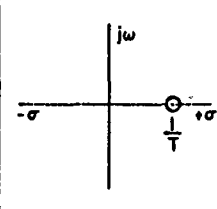
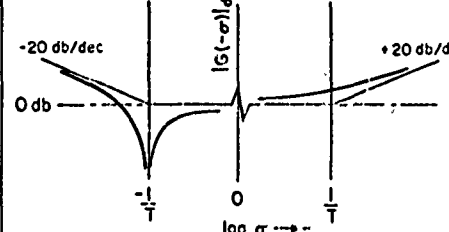
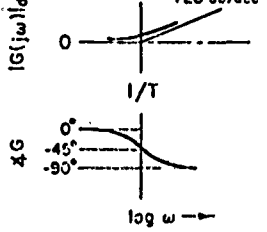
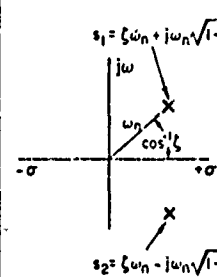
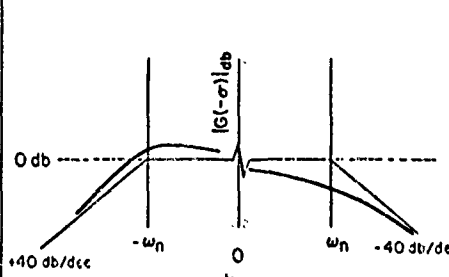
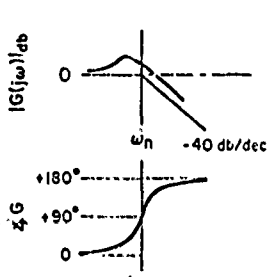
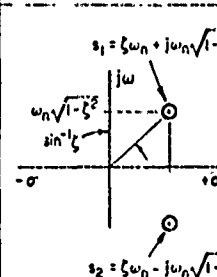
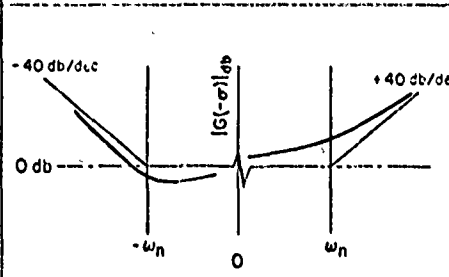
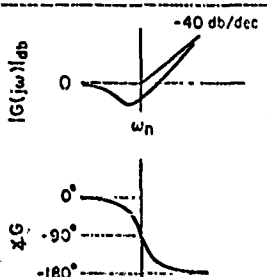
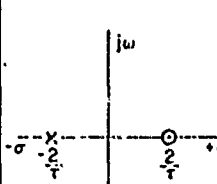
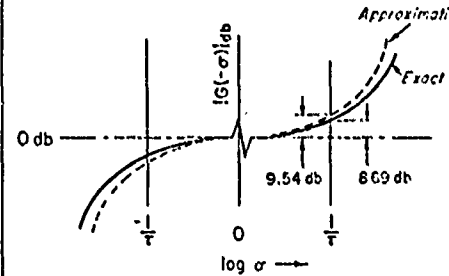
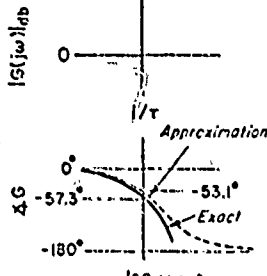
There are four types of generalized Bode diagrams which are often used, corresponding to four different s-plane pathways along which s is compelled to vary. First is the one in which $s = 0 + j\omega$, called the

TABLE 2-5

SUMMARY OF THE REPRESENTATIONS OF SIMPLE TRANSFER FUNCTIONS

Transfer Function $G(s)$	s - Plane Representation	σ - Bode Representation	$j\omega$ - Bode Representation
① K			
② $\frac{K}{s}$			
③ $\frac{K}{s^2}$			
④ Ks			
⑤ Ks^2			
⑥ $\frac{1}{Ts+1}$			
⑦ $Ts+1$			
⑧ $\frac{1}{(\frac{s}{\omega_n})^2 + \frac{2\zeta s}{\omega_n} + 1}$			
⑨ $(\frac{s}{\omega_n})^2 + \frac{2\zeta s}{\omega_n} + 1$			

Table 2-5 (Concluded)

Transfer Function $G(s)$	s-Plane Representation	σ -Bode Representation	$j\omega$ -Bode Representation
⑩ $\frac{1}{-Ts + 1}$			
⑪ $-Ts + 1$			
⑫ $\frac{1}{(\frac{s}{\omega_n})^2 - \frac{2\zeta s}{\omega_n} + 1}$			
⑬ $(\frac{s}{\omega_n})^2 + \frac{2\zeta s}{\omega_n} + 1$			
⑭ $e^{-\tau s} \frac{(\tau/2)s + 1}{(\tau/2)s + 1}$ First Order Padé Approximation			

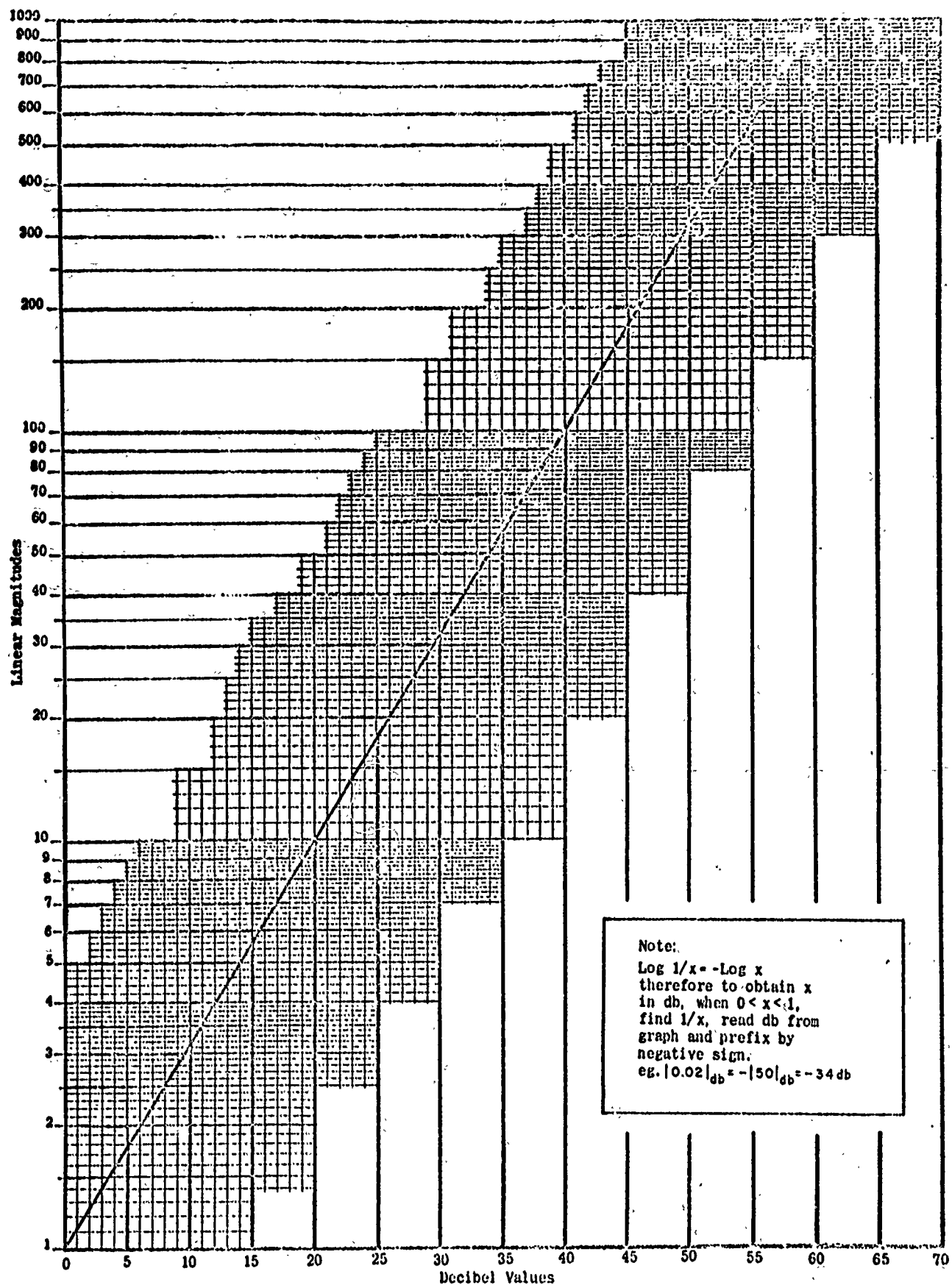


Fig. 2-8. Linear Magnitudes Versus Decibel Values

$j\omega$ -Bode diagram, or simply Bode diagram. This is the classical plot introduced by Bode. Second is the diagram for which $s = +\sigma$ or $s = -\sigma$. These are called σ -Bode diagrams, or "siggy" diagrams for short. For the $j\omega$ -Bode and $\pm\sigma$ -Bode diagrams, s takes on its simplest values as either an imaginary or a real number, and the s -plane pathways are along the imaginary or real axes (Fig. 2-9). These are both special cases of general radial pathways along which $s = |s|(-\xi + j\sqrt{1-\xi^2})$, i.e., for $s = j\omega$, $\xi = 0$, whereas for $s = \pm\sigma$, $\xi = \mp 1$. Third are the type of Bode diagrams based on these general radials, called ξ -Bodes. These are useful in concept and principle, but practical constructions require a very large number of ξ -templates as graphical aids. Because most of the information obtainable using ξ -Bodes can be found just as well with other types of conventional templates, we shall not consider ξ -Bode plots further here.* Fourth, and finally, is the diagram in which the complex

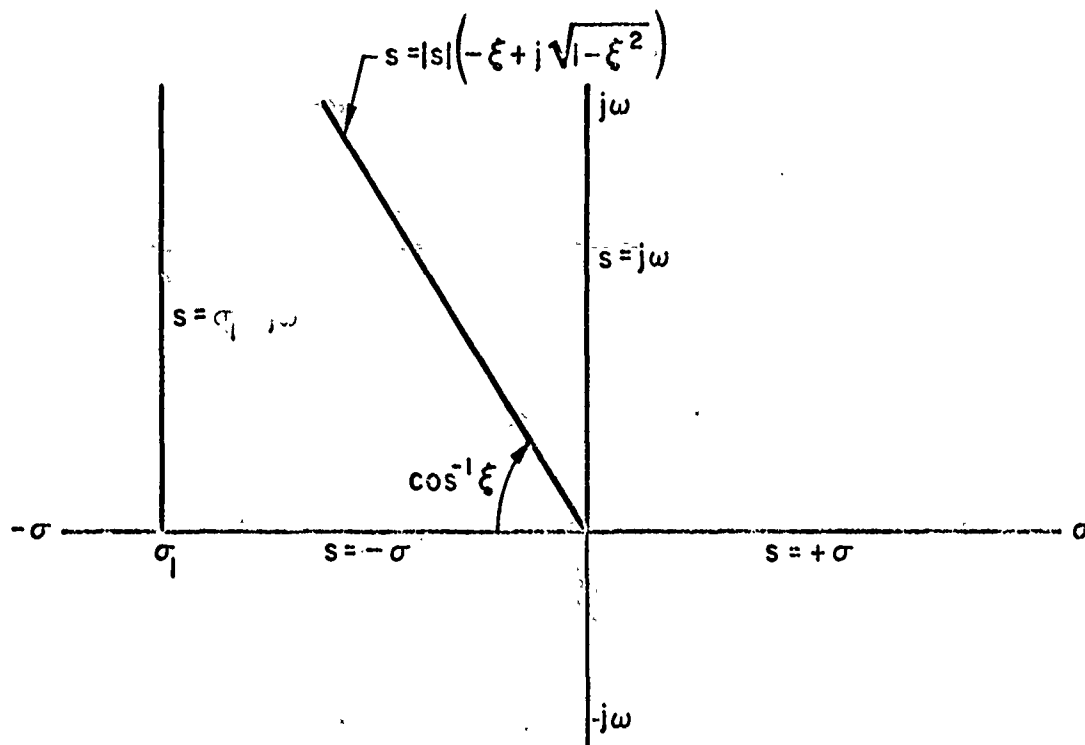


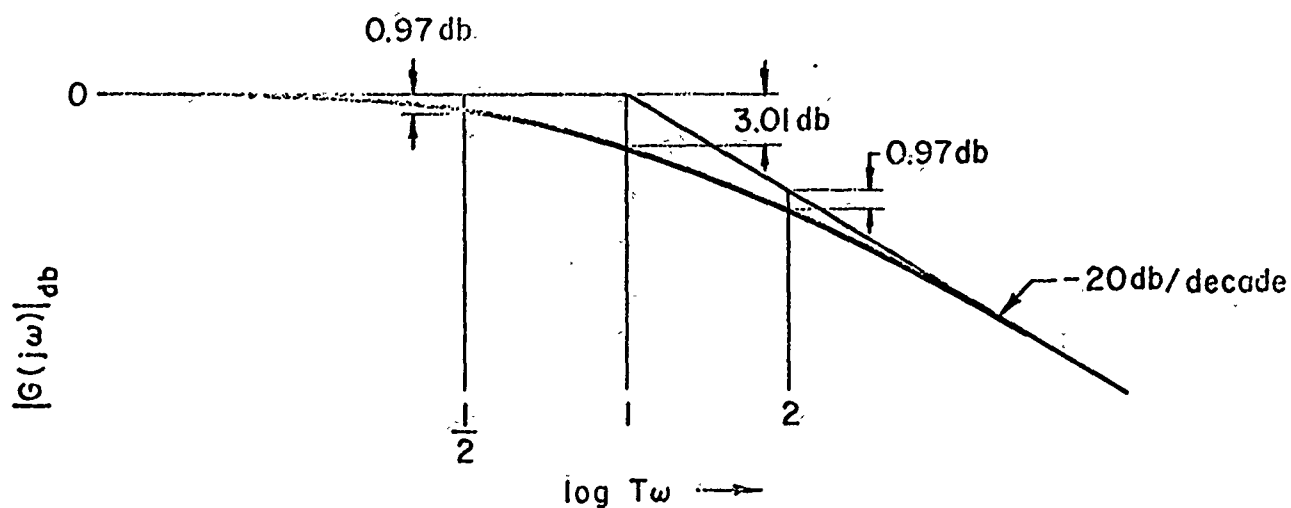
Fig. 2-9. s -Plane Pathways for Generalized Bode Diagram

*A comprehensive set of ξ -Bode diagrams for first- and second-order elements appears in McRuer, *loc. cit.*

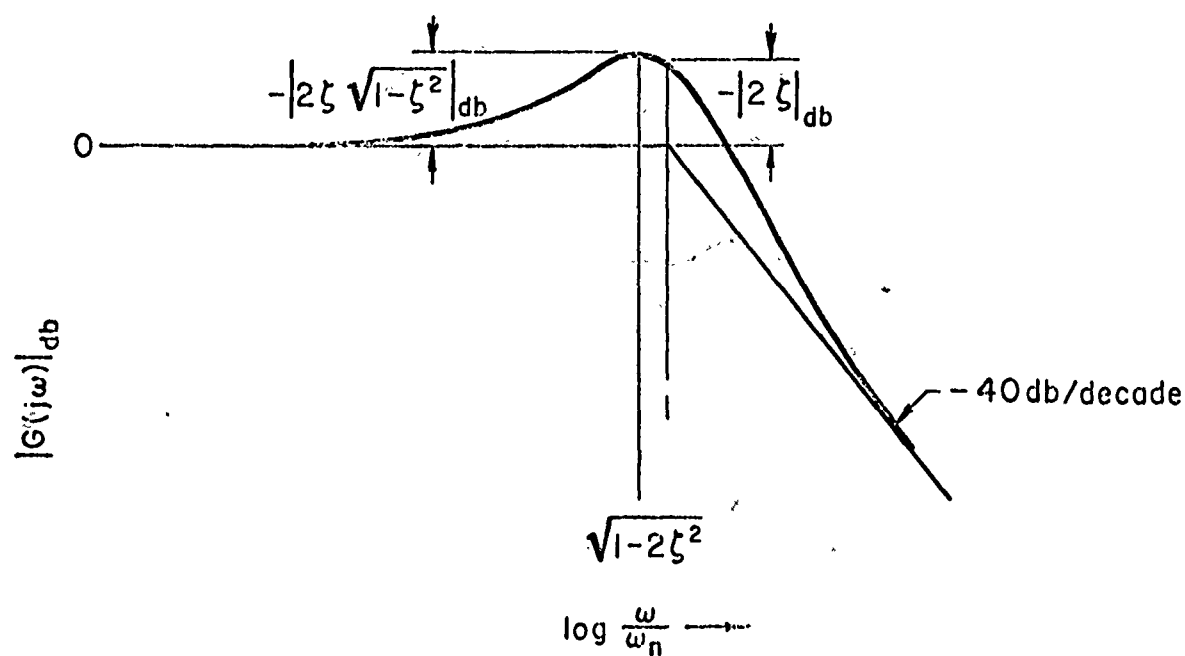
variable has a constant real part, σ_1 , and a variable imaginary part, $s = \sigma_1 + j\omega$. Such diagrams are called shifted Bode diagrams. The $j\omega$ -Bode diagrams and the sigma diagrams for the common transfer function factors are also summarized in Table 2-4.

As is apparent in Table 2-5, the Bode magnitude diagrams are closely approximated for wide ranges of the independent variable by straight-line segments with slopes which are integral multiples of ± 20 db/decade. This fact, a simple consequence of the way in which the diagrams are defined, represents one of the principal practical advantages of the Bode diagram. The actual functions "depart" from the straight-line "asymptotes" only in the vicinity of changes in the slope of the asymptotic approximation. The breakpoint in slope occurs at the magnitude of the pole or zero, e.g., $1/T$ or ω_n . For the second-order $j\omega$ -Bodes the departure of the amplitude ratio at the breakpoint is $-|2\xi|_{db}$ for a pole or $|2\xi|_{db}$ for a zero. These and other properties of the first- and second-order amplitude ratio components are shown in Fig. 2-10. Also at the breakpoint (ω_n), the phase slope, $d \angle G/d(\ln \omega/\omega_n)$, is equal to $-1/\xi$ ($-131.92/\xi$ deg/decade) for a second-order pole and $+1/\xi$ for a second-order zero. This provides the basis for phase asymptotes, as illustrated in Fig. 2-11, which are almost as convenient as the amplitude ratio asymptotes. As indicated by the slope formula above, and the $j\omega$ -Bode summaries in Table 2-5, the direction of the phase shift depends on the sign of ξ . In both the table and the figures described here the abscissa is a log scale but, since semilog graph paper is customarily used, the quantities called out along the scale are expressed in linear units.

For σ -Bodes, illustrations similar to those of Figs. 2-10 and 2-11 are given in Fig. 2-12. Only the amplitude ratios are shown because the phase is always zero for second-order factors and shifts abruptly from zero to -180° at $\sigma = 1/T$ for first-order factors. Items 10 and 14 in Table 2-5 indicate the lack of symmetry between the siggy plots in the left and right half planes. This has to be taken into account when right half plane poles or zeros are present. In an actual problem the presentation with suppressed zero and both right and left half plane $|G(-\sigma)|$ shown separately is awkward. When the need arises it is usually more

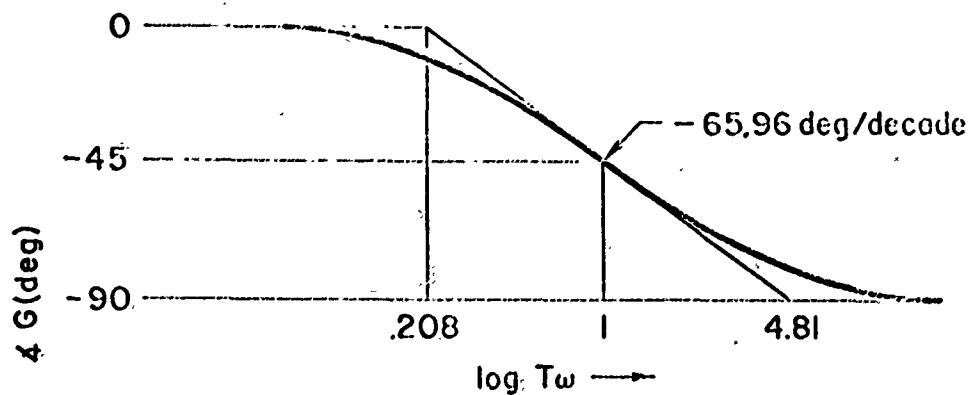


(a) Amplitude Ratio for 1st Order Lag, $G = \frac{1}{Tj\omega + 1}$

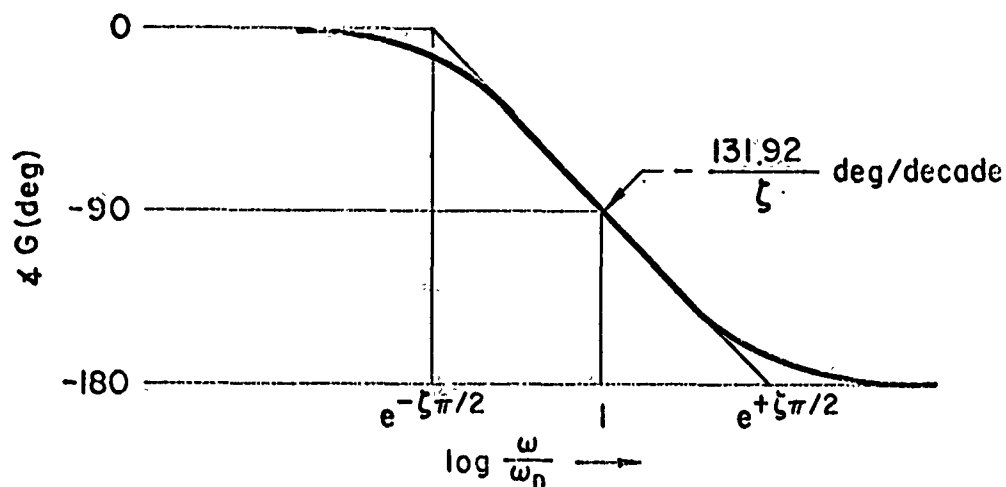


(b) Amplitude Ratio for 2nd Order Lag, $G = \frac{1}{\left(\frac{j\omega}{\omega_n}\right)^2 + 2\zeta \frac{j\omega}{\omega_n} + 1}$

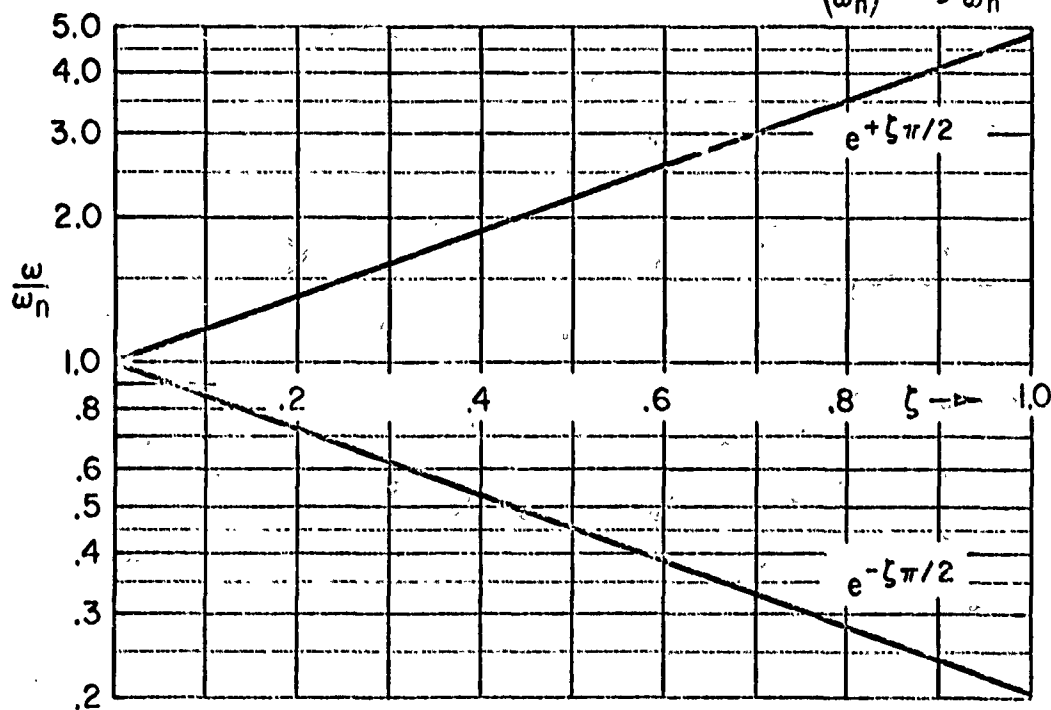
Fig. 2-10. $j\omega$ -Bode Amplitude Ratio Properties for First- and Second-Order Lags



(a) Phase Asymptotes for 1st Order Lag, $G = \frac{1}{Tj\omega + 1}$, $T \geq 0$



(b) Phase Asymptotes for 2nd Order Lag, $G = \frac{1}{\left(\frac{j\omega}{\omega_n}\right)^2 + 2\zeta \frac{j\omega}{\omega_n} + 1}$, $\zeta \geq 0$



(c) Breakpoints for 2nd Order Phase Asymptotes

Fig. 2-11. $j\omega$ -Bode Phase Asymptotes for First- and Second-Order Lags

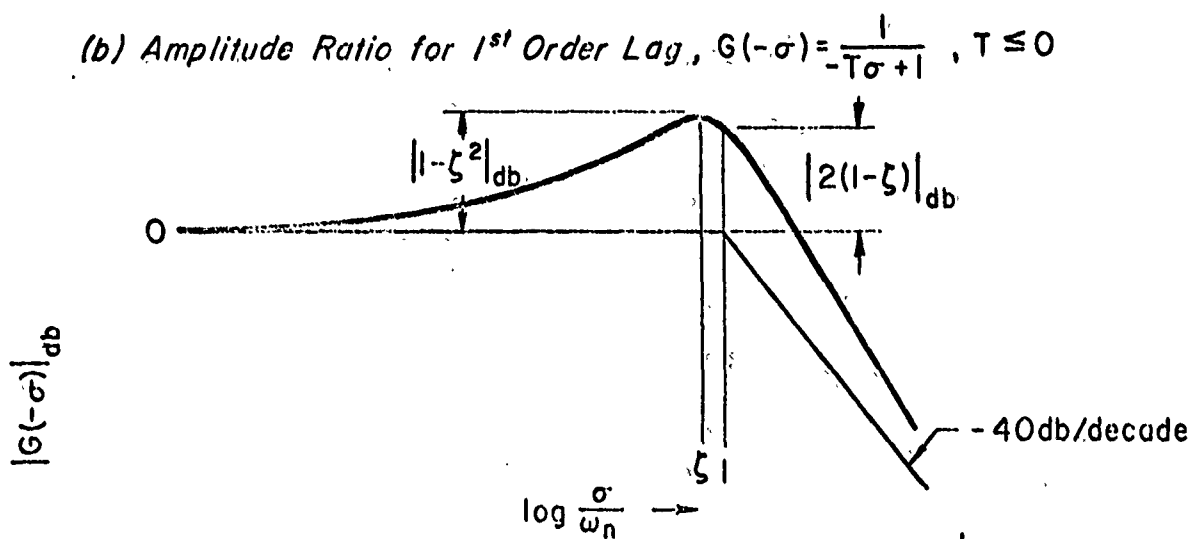
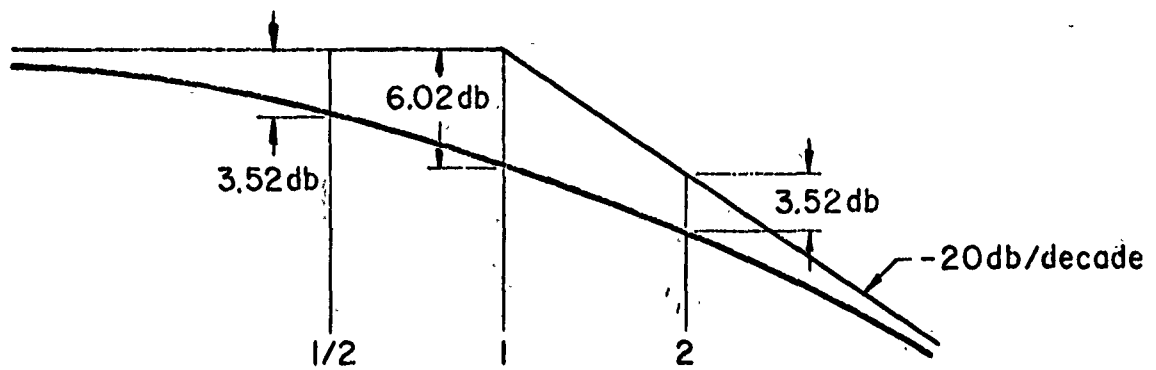
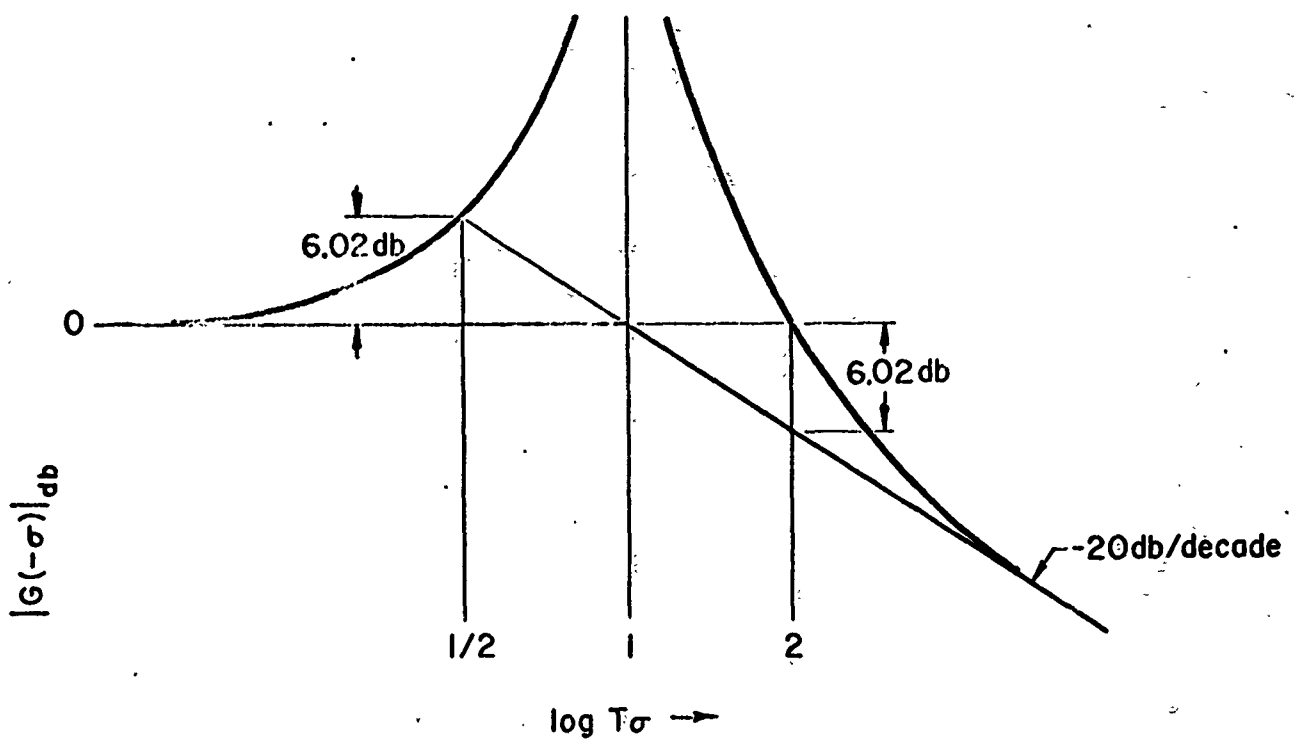


Fig. 2-12. σ -Bode Amplitude Ratio Properties for First- and Second-Order Lags

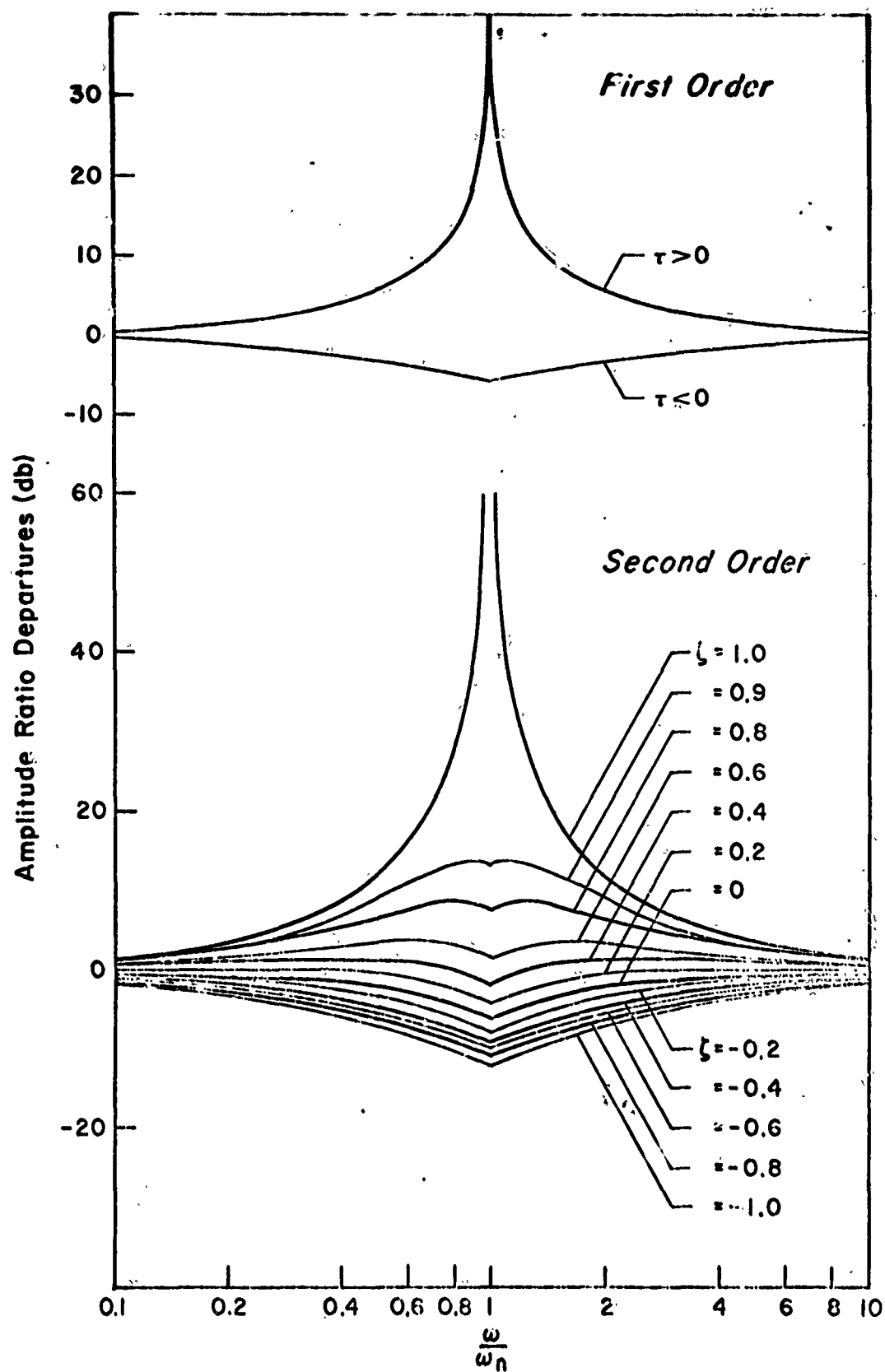


Fig. 2-13. Amplitude Ratio Departures for α -Bode, First- and Second-Order Poles.

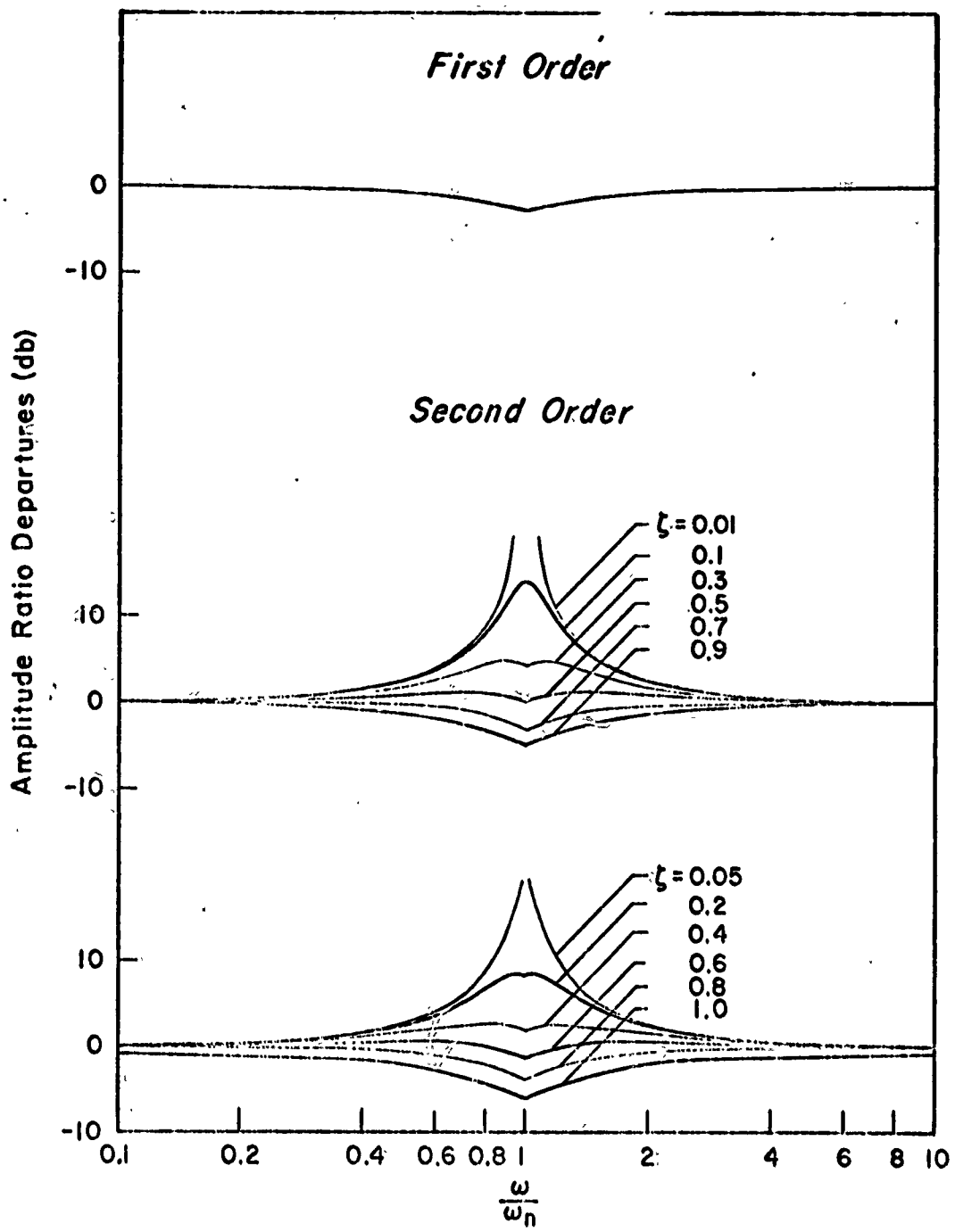


Fig. 2-14. Amplitude Ratio Departures for $j\omega$ -Bode, First- and Second-Order Poles

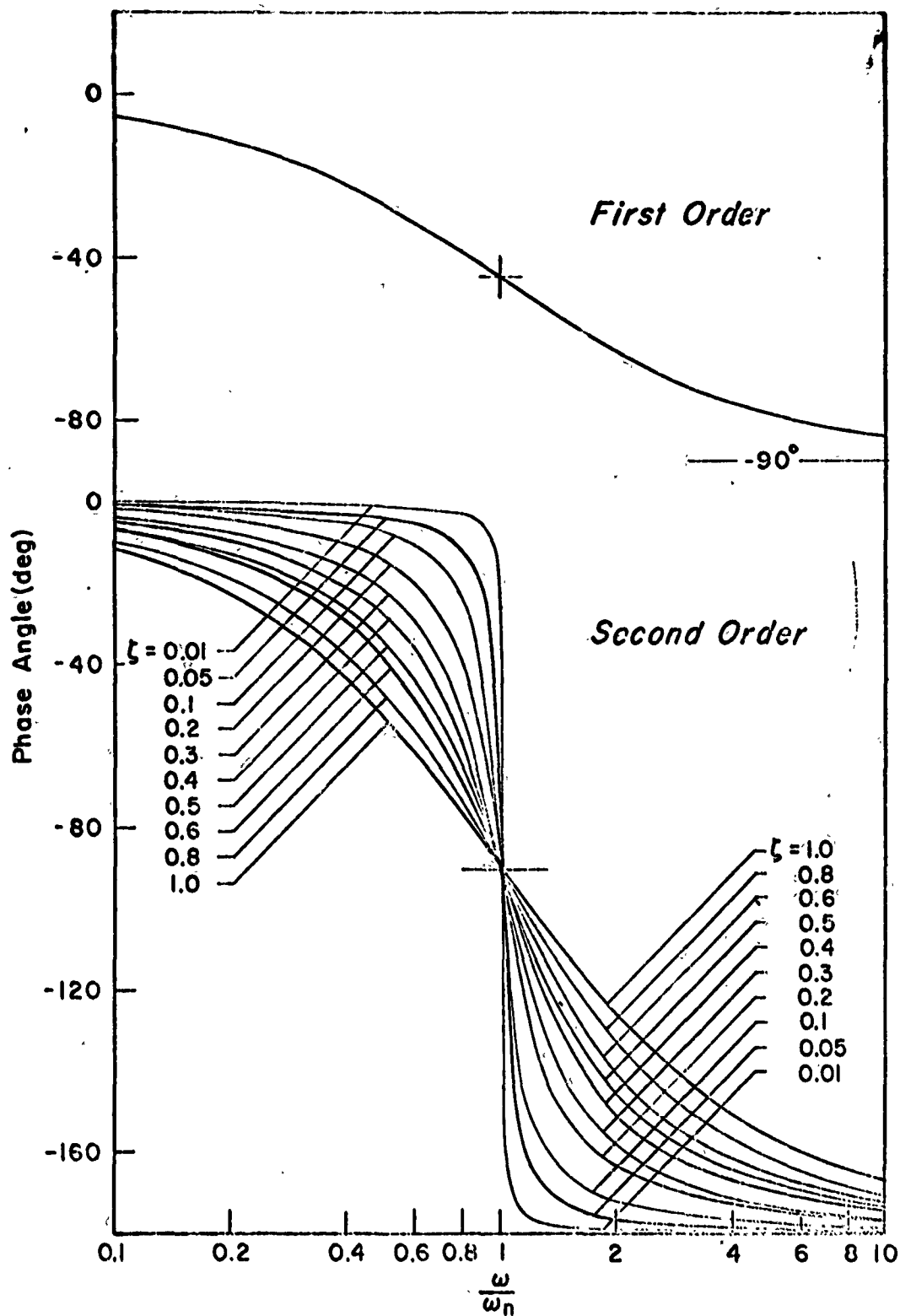


Fig. 2-15. Phase Angles for jw-Bode,
First- and Second-Order Poles

convenient to flip the right half plane $|G(-\sigma)|_{dB}$ plot so that it plots along the same axis as the left half plane siggy and the $j\omega$ -Bode.

Charts which accurately show the "departures" for both the Bode and sigma diagrams as well as the actual $4 G$ curves for the Bode diagrams of first- and second-order factors are given in Figs. 2-13, 2-14, and 2-15.

2.10 COMBINING TRANSFER FUNCTIONS

A great advantage is enjoyed by the transfer function representation when the output of one of the elements or subsystems is the input to another; then the simple subsystem transfer function models are easily combined into the transfer function of the whole system. Thus, as already shown, the transfer function of the cascaded elements is simply the product of the transfer function of the individual elements.

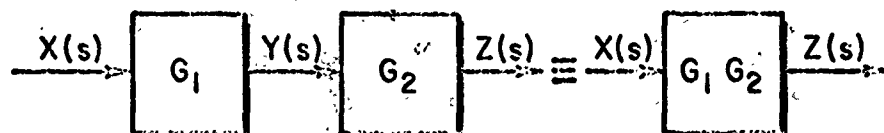


Fig. 2-16. Combining the Transfer Functions of Cascaded Elements

It should be clear that the multiplication of concatenated transfer functions, illustrated in Fig. 2-16, is carried out on the pole-zero diagram by simply superposing the poles and zeros of the component transfer functions. On the $j\omega$ - and σ -Bode diagrams the individual transfer function factors are represented by a quantity proportional to the logarithm of the magnitude and an angle. Recalling that complex numbers are multiplied together by multiplying their magnitudes and adding their angles, it can be appreciated that the multiplication of transfer functions is carried out by addition of the logarithmic magnitude curves together with addition of the phase-angles.

Since the Laplace transformation is a linear operation, we can justify the use of summers and differentials in the block diagram which show how the transfer functions of system elements may be combined. The summer, differential, and takeoff point are graphically illustrated in Fig. 2-17.

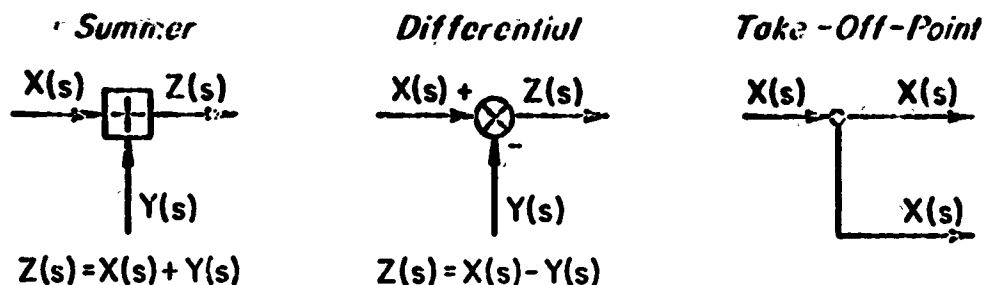


Fig. 2-17. Block Diagram Representations of the Summer, Differential, and Takeoff Point

With the rules for combining the transfer functions of cascaded elements and the use of the symbols for the summer, differential, and takeoff point, it is possible to redraw block diagrams in a variety of ways by means of block diagram algebra.^{*} The algorithms of block diagram algebra are justified by showing that two different configurations represent the same transformed equation. For example, the system of Fig. 2-2 could be represented in block diagram form by the configuration displayed in Fig. 2-18.

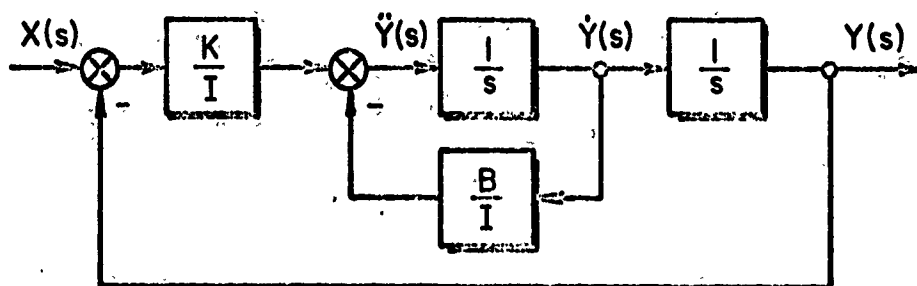


Fig. 2-18. Mathematical Block Diagram of the Spring-Mass-Damper System

The most important algorithm of the block diagram algebra of feedback systems is the series of identities displayed in Figs. 2-19 and 2-20.

^{*}T. D. Graybeal, "Block Diagram Network Transformation," Electrical Engineering, Vol. 70, No. 11, Nov. 1951, pp. 985--990.

D. T. McRuer, ed., Methods of Analysis and Synthesis of Piloted Aircraft Flight Control Systems, BuAer Rept. AE-61-4-1, Bureau of Aeronautics, Wash., D. C., 1952.

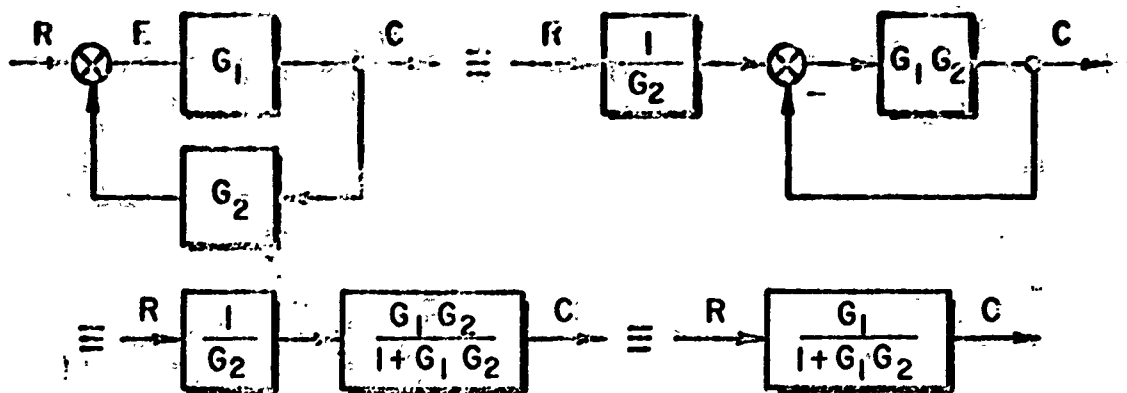


Fig. 2-19. Feedback System Block Diagram Identities

Figure 2-20 shows the special case in which the feedback transfer function, G_2 , is unity. The use of the identities of Figs. 2-19 and 2-20 allows the

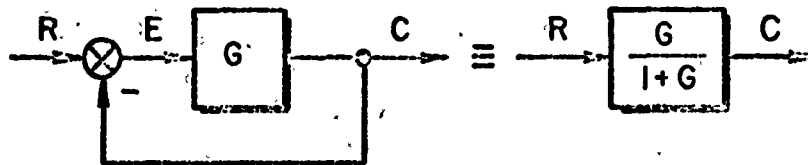
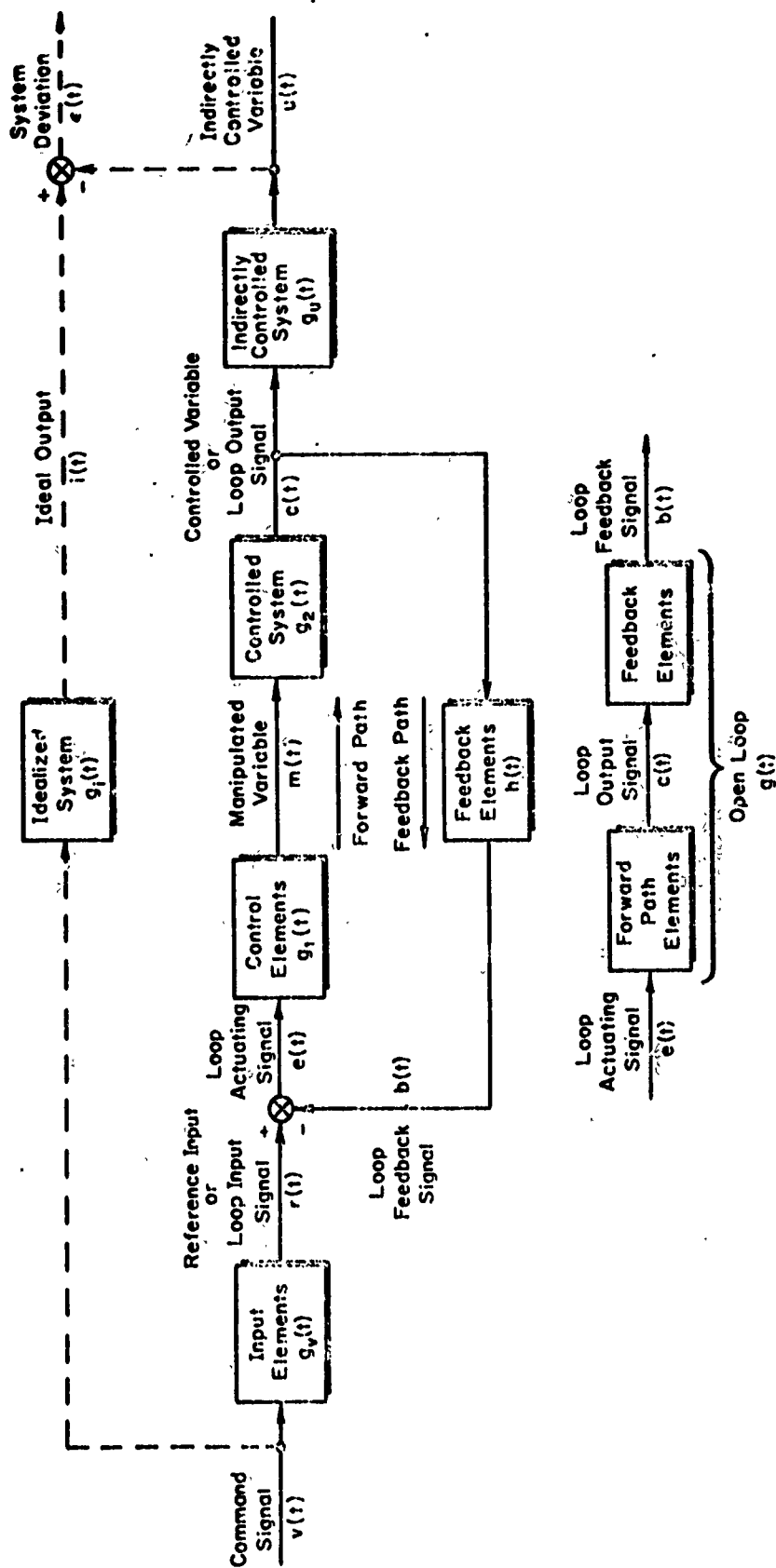


Fig. 2-20. Reduction of the Unity Feedback System Block Diagram

the reduction of the diagram of Fig. 2-18 to the equivalent form shown in Fig. 2-7, for example.

Figure 2-21 shows the general block diagram of a feedback control system and the terms used to describe the several parts and signals. The algebraic derivation of the closed-loop transfer functions is also shown.

The transfer functions of the several blocks in the forward path, G_1 , and the feedback path, G_2 , are often known, or are easily found in factored form, but both the error-input and output-input transfer functions involve a denominator which appears as $1 + G$. Thus the problem inherent in linear feedback system analysis is to find the factors of $1 + G$ and other information about the closed-loop system, such as the modal response coefficients, when given the open-loop characteristics, G . The means to accomplish this are discussed in the next chapter.



Actuating Error Equation:

$$E(s) = R(s) - B(s) = R(s) - H(s)C(s) = G_v(s)V(s) - H(s)C(s)$$

Closed-Loop Equations:

$$\text{Output-Input Ratios: } \frac{C(s)}{R(s)} = \frac{G_1(s)G_2(s)}{1+G_1(s)G_2(s)H(s)} = \frac{1}{H(s)} \left[\frac{G(s)}{1+G(s)} \right]$$

$$\frac{U(s)}{V(s)} = \frac{G_v(s)G_u(s)}{H(s)} \left[\frac{G(s)}{1+G(s)} \right]$$

$$\text{Error-Input Ratios: } \frac{E(s)}{R(s)} = \frac{1}{1+G_1(s)G_2(s)H(s)} = \frac{1}{1+G(s)}$$

Fig. 2-21. Elements in a General Single-Loop System

CHAPTER 3

FEEDBACK SYSTEM ANALYSIS

3.1 INTRODUCTION

The early development of automatic flight controls evolved substantially independently of the use of any mathematics. By 1947, however, it was widely recognized that the dynamic problems of vehicle control could not be mastered by cut-and-try techniques or engineers' rules of thumb. To fill the need, the elaborate and extensive theory of linear feedback systems was further developed and then quickly applied to an increasingly wide range of flight control problems. There was a dramatic interplay between theory and practice where, in many cases, aircraft and missiles provided both the inspiration for the theoretical developments and the examples of practical application.

In the intervening years, there have been a large number of both introductory and advanced texts written on the subject of feedback control systems. Indeed it is assumed that the reader will have already acquainted himself with the contents of one or more of these.* In order, however, to

*See, for example:

H. M. James, N. B. Nichols, and R. S. Phillips, Theory of Servomechanisms, McGraw-Hill Book Co., Inc., New York, 1947.

H. S. Tsien, Engineering Cybernetics, McGraw-Hill Book Co., Inc., New York, 1954.

J. G. Truxal, Automatic Feedback Control System Synthesis, McGraw-Hill Book Co., Inc., New York, 1955.

H. Chestnut and R. W. Mayer, Servomechanisms and Regulating System Design, Vol. I, 2nd ed., McGraw-Hill Book Co., Inc., New York, 1959.

J. J. D'Azzo and C. H. Houpis, Feedback Control System Analysis and Synthesis, McGraw-Hill Book Co., Inc., New York, 1960.

R. N. Clark, Introduction to Automatic Control Systems, John Wiley and Sons, Inc., New York, 1962.

E. C. Barbe, Linear Control Systems, International Textbook Co., Scranton, Pa., 1963.

I. M. Horowitz, Synthesis of Feedback Systems, Academic Press, Inc., New York, 1963.

C. J. Savant, Jr., Control System Design, McGraw-Hill Book Co., Inc., New York, 1964.

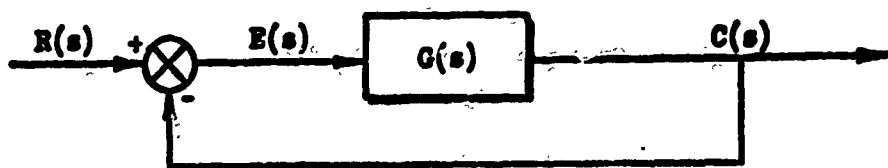
allow a connected account of our subject, it is necessary to review briefly some of the mathematical and physical bases on which it rests. This chapter continues in sequence from the last, which discussed the characterization of physical systems and system elements by means of mathematical models. The sections which follow contain condensed expositions of those elements of linear feedback control system theory needed to understand the later discussions of flight control systems.

All of these topics are involved with system analysis which, for linear constant-coefficient systems typified by the single-loop system shown in Fig. 3-1, consists of five essential steps:

1. Delineation of nominal open-loop system characteristics. This ordinarily starts with the differential equations which describe the nominal controlled element and one or more of the controller possibilities. This stage is concluded when one or more nominal open-loop transfer functions, $G(s)$, are available, in factored form, for further analysis.
2. Determination of nominal closed-loop transfer functions, $G_{cr}(s)$ and $G_{er}(s)$, from the open-loop transfer function, $G(s)$.
3. Calculation of nominal closed-loop system responses for pertinent inputs.
4. Determination of the changes in $G(s)$ resulting from the expected variations in the controller and controlled element characteristics.
5. Consideration of the effects of open-loop system variations on closed-loop behavior

The topics considered in the next two sections are concerned with Step 2 for single-loop systems. The similar analysis of multiloop systems is taken up in Section 3.5. Response calculations (Step 3) have already been treated in Chapter 2, and receive further attention in Chapter 10. Techniques for accomplishing Step 5 are discussed in Section 3.6 for both single-loop and multiloop systems. The discussion of Steps 1 and 4 is for the most part deferred to subsequent chapters.

The first step above—delineation of the open-loop characteristics in terms of a transfer function, $G(s)$ —is relatively easy for linear time-invariant systems because transform methods can be used to convert



Open-Loop Transfer Function:

$$G(s) = \frac{C(s)}{E(s)} = \kappa \frac{s^n + a_1 s^{n-1} + a_2 s^{n-2} + \dots + a_n}{s^{m+n} + b_1 s^{m+n-1} + b_2 s^{m+n-2} + \dots + b_{m+n}} = \kappa \frac{\sum_{j=0}^n a_j s^{n-j}}{\sum_{i=0}^{m+n} b_i s^{m+n-i}} \quad (3-1a)$$

$$= \kappa \frac{\alpha(s)}{\beta(s)} = \kappa \frac{\prod_{j=1}^n (s + z_j)}{\prod_{i=1}^{m+n} (s + p_i)} \quad (3-1b)$$

$$= \frac{KA(s)}{s^k B(s)} = \frac{\kappa \prod_{j=1}^n \left(\frac{s}{z_j} + 1\right)}{s^k \prod_{i=1}^{m+n-k} \left(\frac{s}{p_i} + 1\right)} \quad (3-1c)$$

Output/Input Transfer Function:

$$G_{cr}(s) = \frac{C(s)}{R(s)} = \frac{G(s)}{1 + G(s)} = \frac{\kappa \alpha(s)}{\beta(s) + \kappa \alpha(s)} = \frac{\kappa \prod_{j=1}^n (s + z_j)}{(1 + \kappa \delta_m^0) \prod_{i=1}^{m+n} (s + q_i)} \quad (3-2)$$

$$\delta_j^i = \begin{cases} 0, & i \neq j \\ 1, & i = j \end{cases}$$

Error/Input Transfer Function:

$$G_{er}(s) = \frac{E(s)}{R(s)} = \frac{1}{1 + G(s)} = \frac{\beta(s)}{\beta(s) + \kappa \alpha(s)} = \frac{\prod_{i=1}^{m+n} (s + p_i)}{(1 + \kappa \delta_m^0) \prod_{i=1}^{m+n} (s + q_i)} \quad (3-3)$$

Fig. 3-1. Single-Loop Linear Feedback System and Basic Notation

the system differential equations to algebraic equations. This conversion permits the intermediate steps in an analysis sequence (e.g., reduction of simultaneous equations using Cramer's rule and transfer function development, manipulation, and combination) to be carried out using algebraic forms. Most such forms either are, or can be approximated by, rational polynomials. Thus, the delineation of open-loop transfer functions in the form indicated in Fig. 3-1 is basically elementary, with the possible exception of polynomial factoring (which is also a part of Step 2).

The second step in the analysis sequence—given $G(s)$, find $G_{cr}(s)$ and/or $G_{er}(s)$ —is the central problem of feedback system analysis. This requires only the solution for the roots of

$$1 + G(s) = 0 \quad (3-4)$$

Trivial as it may seem, a great deal of effort has been devoted to finding methods for performing this operation which are effective and at the same time promote insight.

An attack on the linear feedback analysis problem is usually presented in one of two artificially separated ways referred to as the "root locus" and the "frequency response." The intent here is to show the interrelationships between the methods and to present a "unified" technique which is more efficient and flexible than either method used by itself.* Nevertheless, by way of introduction we shall briefly review the features of the root locus method both in two dimensions (wherein gain is a parameter along the plot) and in three dimensions (where gain is a dimension),[†] and then discuss the use of the two principal logarithmic plots. Only then

*The two sections following contain an abbreviated account of only those parts of a more complete report which are required for subsequent developments. See:

D. T. McRuer, Unified Analysis of Linear Feedback Systems, ASD-TR-61-118, Wright-Patterson Air Force Base, Ohio, July 1961.

[†]W. R. Evans, "Graphical Analysis of Control Systems," Trans. AIEE, Pt. I, Vol. 67, 1948, pp. 547-551; "Control System Synthesis by Root-Locus Methods," Trans. AIEE, Pt. I, Vol. 69, 1950, pp. 66-69.

W. R. Evans, Control System Dynamics, McGraw-Hill Book Co., Inc., New York, 1954.

3.2 CONVENTIONAL AND THREE-DIMENSIONAL ROOT LOCUS

$$G(s) = -1 \quad (3-4)$$
$$|G(s)|e^{j\angle G(s)} = e^{j(2k+1)\pi} \quad ; \quad k = 0, \pm 1, \pm 2, \dots \quad (3-5)$$
$$4G(s) = (2k + 1)\pi \quad ; \quad k = 0, \pm 1, \pm 2, \dots \quad (3-6)$$
$$|G(s)| = 1 \quad (3-7)$$

(3-8)

$$G(s) = \kappa \frac{\prod_{h=1}^n (s + z_h)}{\prod_{i=1}^{m+n} (s + p_i)} = \kappa \left[\frac{\prod_{h=1}^n r_{N_h}}{\prod_{i=1}^{m+n} r_{D_i}} \right] \exp \left(j \sum_{h=1}^n \varphi_{N_h} - \sum_{i=1}^{m+n} \varphi_{D_i} \right)$$

$$\text{Criterion angle: } \left(\sum_{h=1}^n \varphi_{N_h} - \sum_{i=1}^{m+n} \varphi_{D_i} \right) = \begin{matrix} (2k+1)\pi & ; & \kappa > 0 \\ 2k\pi & ; & \kappa < 0 \end{matrix} \quad (3-9)$$

$$\text{Magnitude: } \left| \kappa \right| \frac{\prod_{h=1}^n r_{N_h}}{\prod_{i=1}^{m+n} r_{D_i}} = 1 \quad (3-10)$$

or finally, as is often more convenient, Eq. 3-10 can be expressed as:

$$20 \log_{10} \kappa + \sum_{h=1}^n 20 \log_{10} r_{N_h} - \sum_{i=1}^{m+n} 20 \log_{10} r_{D_i} = 20 \log_{10} 1 = 0 \text{ db}$$

which in shorthand form becomes

(3-11)

$$|\kappa|_{\text{db}} + \sum_{h=1}^n (r_{N_h})_{\text{db}} - \sum_{i=1}^{m+n} (r_{D_i})_{\text{db}} = 0$$

Figure 3-2 shows how at any point on the s-plane the individual factors of the open-loop function can be graphically represented as vectors.

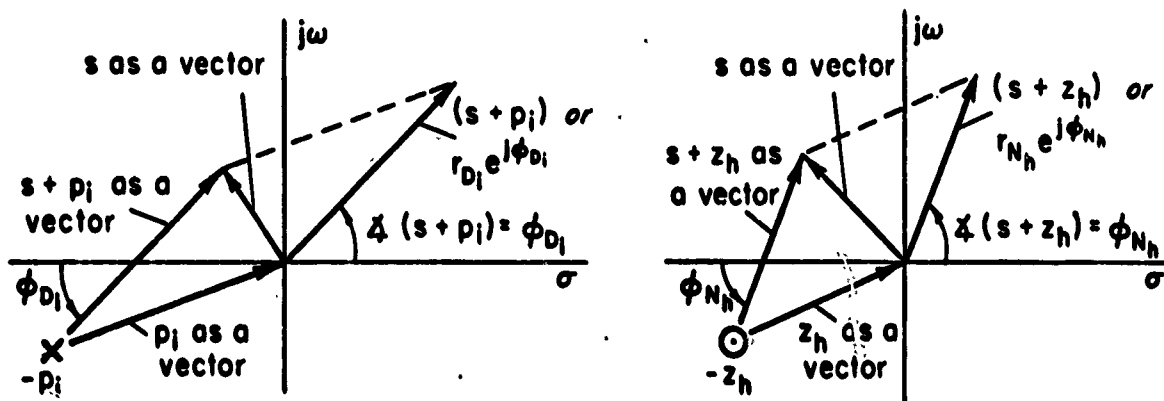


Fig. 3-2. The Graphical Representation of Open-Loop Function Factors

Note from the geometry of the diagrams that when the factors are represented by vectors drawn from the singularities to the test point, their angles may be measured counterclockwise from a horizontal line through the test point.

The vectors from the singularity to all possible points in the s-plane can be represented by isomagnitude and isocargument (phase) curves.*

*Y. Chu, "Synthesis of Feedback Control System by Phase-Angle Loci," Trans. AIEE, Pt. II, Vol. 71, 1952, pp. 330-339.

Isomagnitude curves for first-order factors are constructed as loci in the s -plane for which $|(s+p_1)^{-1}|$ or $|s+z_h|$, or some measures thereof, are constant. If the logarithm is taken as the base for the magnitude measure, the plots for poles and zeros show useful symmetrical forms, and multiplication operations involving more than one singularity become additions. There is also a convenient tie-in later with other analysis techniques. Consequently the isomagnitude plots for first-order factors are constructed for constant values of $20 \log_{10} |1/(s+p_1)| = -(r_{D1})_{db}$ or $20 \log_{10} |s+z_h| = (r_{Nh})_{db}$. The result is a series of concentric circles, as shown in Fig. 3-3. If log magnitude is considered as a dimension measured along an axis perpendicular to the plane of the paper, then the isomagnitude loci shown would occur at heights appropriate to the magnitude dimension. The isomagnitude loci are thus contour maps of a surface which rises to a point for a pole or sinks to a point for a zero.

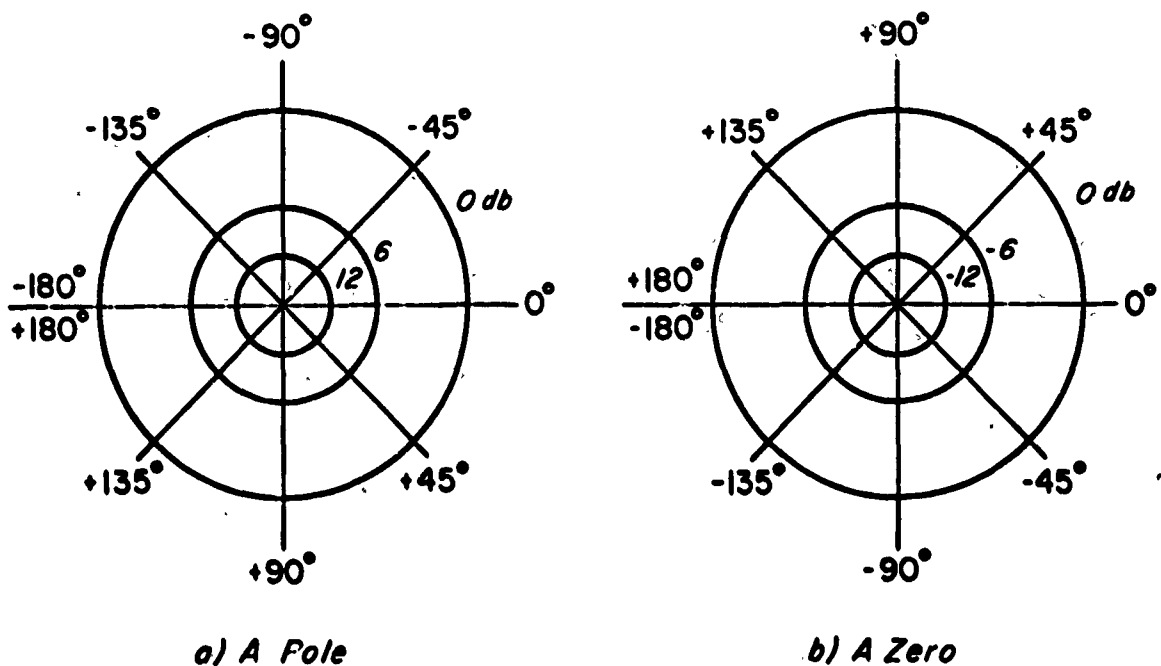


Fig. 3-3. Contour Maps and Isoargument Curves for a Pole and a Zero

The isoargument curves for the first-order factors are simply straight lines, issuing radially from the origin which is located at the pole or zero location in the s -plane. These are also shown in Fig. 3-3.

When more than one pole or zero is present, the open-loop function can be represented as a contour map by adding logarithmic magnitudes of the several poles and zeros so as to represent the left side of Eq. 3-11. Points of equal magnitude throughout the s-plane are then joined to make the contours. The isoargument lines are found similarly by adding the angle contribution of each pole and zero so as to represent the left side of Eq. 3-9 and then joining points for which these are equal. The isoargument lines are always orthogonal to the contour lines, so they are along the gradient. Several examples of such maps are presented later in this section.

In the root locus method the roots of the characteristic equation are found with semigraphical techniques based on the vector representation of the factors in $G(s)$. An attempt to determine a root of $1 + G(s) = 0$ is started by choosing a trial value of s (a point on the s-plane) and imagining the vectors drawn to this point from each of the open-loop poles and zeros. Figure 3-4 illustrates the angle measurement convention in root locus construction. When a trial point is discovered which satisfies the phase condition of Eq. 3-9, a possible root location is identified. In principle, this procedure, repeated a sufficient number of times, delineates the locus of all possible closed-loop roots.

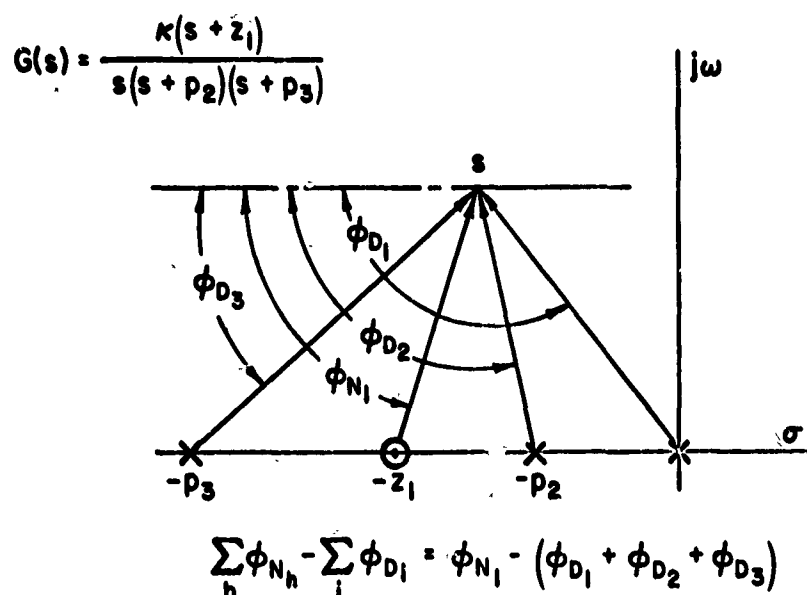


Fig. 3-4. Angle Measurement Convention in Root Locus Construction

The second step in the method is to find the points on the locus corresponding to the satisfaction of the magnitude condition, i.e., Eq. 3-10, for particular values assigned to κ .*

Although the root locus can be found using the repetitive process outlined above, one of the most attractive features of the method is that large segments of the locus can be found by applying root locus construction rules, which do not require the search for satisfactory trial points. The rules which apply when $G(s)$ is a ratio of rational polynomials are recapitulated, without proof, as follows:†

1. The total number of separate branches of the locus is equal to the total number of open-loop poles, $m+n$.
2. The root locus is symmetrical about the real axis ($\omega = 0$).
3. The branches of the locus originate at the open-loop poles.
4. The branches of the locus terminate at the open-loop zeros or at infinity.
 - a. n (the total number of zeros) branches of the locus terminate on the open-loop zeros.
 - b. m branches approach points at infinity and are asymptotic to straight lines which originate at a point on the real axis, commonly called the "center of gravity," given by

$$\sigma_{c.g.} = - \frac{\sum_{i=1}^{m+n} p_i - \sum_{j=1}^n z_j}{m} \quad (3-12)$$

and which make angles with the real axis of

$$\begin{aligned} \frac{(2k+1)\pi}{m} ; \quad \kappa > 0 \\ \varphi_m = \quad \text{or} \quad k = 0, \pm 1, \pm 2, \dots \quad (3-13) \\ \frac{2k\pi}{m} ; \quad \kappa < 0 \end{aligned}$$

*While both of these steps could be carried out with a protractor, dividers, and a slide rule, a device for mechanically adding angles and logarithmic magnitudes has been developed especially for the purpose. This is the "Spirule," copyright 1959 by North American Aviation, Inc., available from The Spirule Company, 9728 El Venado, Whittier, California.

†McRuer, *ibid.* Also: Evans, *ibid.*; W. R. Evans, "Control System Synthesis by Root Locus Methods," *Trans. AIEE*, Pt. I, Vol. 69, 1950, pp. 66-69; F. M. Reza, "Some Mathematical Properties of Root Loci for Control System Design," *Trans. AIEE*, Pt. I, Vol. 75, 1956, pp. 103-108; H. Lass, "A Note on the Root-Locus Method," *Proc. IRE*, Vol. 44, May 1956, p. 693.

5. The root locus on the real axis lies along alternate segments connecting real poles and zeros (or the point at infinity). When κ is positive (negative), the locus exists in the intervals where there is an odd (even) total number of poles and zeros to the right of the interval.

6. The tangents to the locus at departure from a pole or arrival at a zero are given by:

$$\text{Departure angle} = \left(\begin{array}{c} \text{Net angle from} \\ \text{other poles and zeros} \end{array} \right) - (\text{Criterion angle})$$

$$\text{Arrival angle} = - \left(\begin{array}{c} \text{Net angle from} \\ \text{other poles and zeros} \end{array} \right) + (\text{Criterion angle})$$

7. The breakaway of the locus from the real axis (or its rendezvous thereon) is located where the net change in angle caused by a small vertical displacement of the trial point is zero. These points correspond to the real roots of the equation

$$\frac{dG(s)}{ds} = 0 \quad (3-14)$$

8. At junction points (where the roots coalesce) the tangents to the branches of the locus are equally spaced over $2\pi \text{ rad} = 360^\circ$.

9. The direction in which the locus moves for increasing $|\kappa|$, at the point $-q_1$ on the locus, is shown by the orientation of the sensitivity vector:

$$s_k^1 = \frac{1}{\left[\frac{\partial G}{\partial s} \right]_{s=-q_1}} = \left[\sum_{j=1}^{m+n} \frac{1}{p_j - q_1} - \sum_{j=1}^n \frac{1}{z_j - q_1} \right]^{-1} \quad (3-15)$$

Note that this rule does not work to find the direction of the locus at breakaway and rendezvous points. On the other hand, in an algebraic form, it may be effectively employed to find the location of breakaway or rendezvous points when the poles and zeros are on the real axis.

10. When m (the excess of poles over zeros) ≥ 2 , the sum of the roots is a constant equal to the sum of the open-loop poles. Then branches tending to the left must be "balanced" by branches tending to the right. When $m=1$, the sum of the roots is the same constant added to $-\kappa$.

11. The locus crosses the imaginary axis when $1 + G(s) = 0$ has pure imaginary roots. This corresponds to the neutral stability condition indicated by the Routh-Hurwitz criterion or a similar test for stability, and is indicated by the vanishing of the imaginary part of the inverse open-loop function evaluated with $\sigma=0$, i.e.,

$$\text{Im} \left[\frac{\beta(j\omega)}{\alpha(j\omega)} \right]_{\sigma=0} = 0 = \text{Im} [\beta(j\omega)\alpha^*(j\omega)]_{\sigma=0} \quad (3-16)$$

12. When a complete set of closed-loop roots is available for some value of κ , these roots may be used in the same fashion as open-loop poles for the purpose of continuing the plot of the locus. As a consequence, for example, the result of Rule 9 may be obtained by using Rule 6 in connection with any complete set of closed-loop roots.

13. The product of the negatives of the roots is equal to the sum of the product of the negatives of the open-loop poles, b_{m+n} , and κ times the product of the negatives of the open-loop zeros, κa_n , i.e.,

$$\prod_{i=1}^{m+n} q_i = b_{m+n} + \kappa a_n, \quad m \geq 1 \quad (3-17)$$

The application of the rules for the construction of root loci can now be illustrated with the aid of several simple examples. These are chosen so as to clarify the introduction to the "unified" method.

Example 1: First-order system

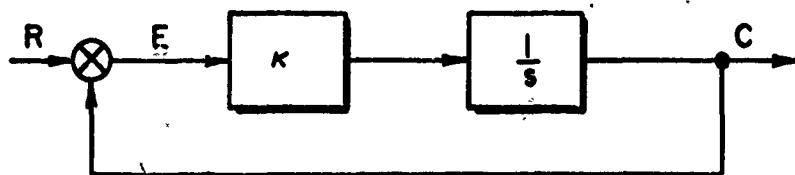


Fig. 3-5. Negative Feedback Around an Integrator

The open-loop function is $G(s) = \kappa/s$ and the only root of $1+G(s) = 0$ is almost trivially found to be $s = -\kappa$. The closed-loop function is

$$\frac{C}{R} = \frac{G(s)}{1+G(s)} = \frac{\kappa}{(s + \kappa)}$$

and, if necessary, the weighting function or indicial response could be found by the inverse Laplace transformation using Table 2-2.

Suppose, however, that the algebra were not so easy, and we wanted to apply the techniques discussed so far. The contour map of the function $1/s$ has already been presented as Fig. 3-3a. The pole-zero plot is simply a pole at the origin, and the use of Rules 1 to 5 tells us that the root locus shown in Fig. 3-6 has only one branch which lies along the negative real axis between the origin and the point at infinity. Rules 6 to 9 might be invoked but are not necessary. Rule 10 indicates the algebraic result already derived, and indeed Eq. 3-10 may be used to obtain the same result. The closed-loop roots are located along the locus at a radial distance from the origin equal to the gain constant κ . The closed-loop roots are marked along the locus for several values of the gain. A comparison of Fig. 3-6 with Fig. 3-3a shows that the locus of roots, marked

with the position of the closed-loop roots for selected values of the gain constant, κ , is the same thing as the criterion angle contour ($-\pi$ in this case) marked with the intersections of the appropriate magnitude contours.

1. There is one branch of the locus
2. The locus is symmetrical about the real axis
3. The locus originates on the open-loop pole
4. The locus terminates on a point at infinity and is asymptotic to a line which originates at $\sigma=0$ and makes an angle with the real axis of π rad
5. The root locus exists in the interval between the pole and the point at infinity where there is one (an odd number) pole to the right

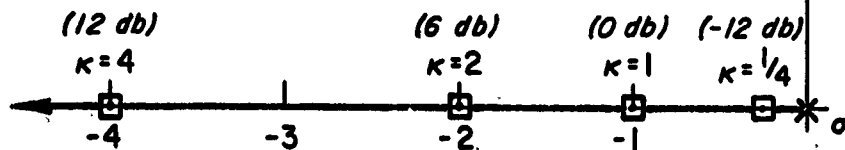


Fig. 3-6. Root Locus for First-Order System, $G(s) = \kappa/s$

In Fig. 3-6 gain is a parameter along the locus. Alternatively, an additional dimension, coming out of the plane of the paper, can be introduced to show the variation of the closed-loop root with gain. This leads to the three-dimensional surface shown in isometric view in Fig. 3-7. The surface is, of course, identical to that represented by the contour map of Fig. 3-3a. When the gain is very small, i.e., $\kappa \rightarrow 0$, the addition of the logarithmic magnitudes would remove the zero db reference plane to an infinite distance, and only the top of the mountain (which stretches up to infinity) would protrude above the waterline. The closed-loop root would be at the location of the open-loop pole, i.e., $s=0$. As the gain is increased, the mountain is shoved up like a volcano emerging from the ocean. The closed-loop root is always found at the intersection of the waterline and the criterion angle contour. For example, with $\kappa=1$, the waterline for the function κ/s would be in the reference plane (zero db). With $\kappa=2$, so that $20 \log_{10} \kappa = +6$ db, the waterline for κ/s would be at the level marked -6 db for the function $1/s$ itself. The various positions of the closed-loop root, as the surface is raised or lowered with respect to the reference plane by raising or lowering the gain, κ , are illustrated for several values of κ in Fig. 3-7. From this figure it can be readily appreciated that an increase in the gain, which raises the surface with respect to the reference plane, is entirely equivalent to lowering the reference plane with respect to the surface. We shall ordinarily take the latter view for convenience.

Example 2. Unit numerator second-order system

Consider now the feedback system illustrated in Fig. 3-8.

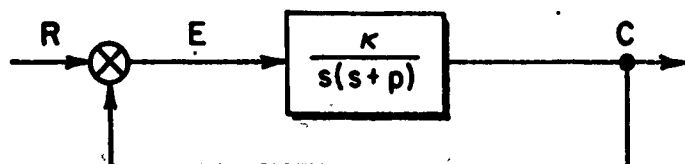


Fig. 3-8. A Second-Order Servomechanism

The closed-loop function is given by the expression

$$\frac{C}{R} = \frac{G(s)}{1 + G(s)} = \frac{\kappa}{(s^2 + ps + \kappa)}$$

and the closed-loop roots may be found from the quadratic formula

$$s_{1,2} = \frac{-p}{2} \left[1 \pm \sqrt{1 - \frac{4\kappa}{p^2}} \right]$$

As long as the gain, κ , is less than $p^2/4$, the roots are real, while, when $\kappa > p^2/4$, the roots are complex conjugates.

The root locus for the function $\kappa/s(s+p)$ is presented in Fig. 3-9 for $\kappa > 0$. The application of Rules 1-3, 5, and 6 is straightforward. The breakaway point coincides with the origin of the high gain asymptotes, which make angles of $+90^\circ$ and -90° with the real axis, so Rules 4 and 7 yield the same result for this particular problem. In fact, the high gain asymptotes are the locus in this case. The breakaway condition is an example of the junction point (Rule 7), and it is seen that the tangents of both the coalescing and the departing locus branches are equally spaced over 360° . It is also easy

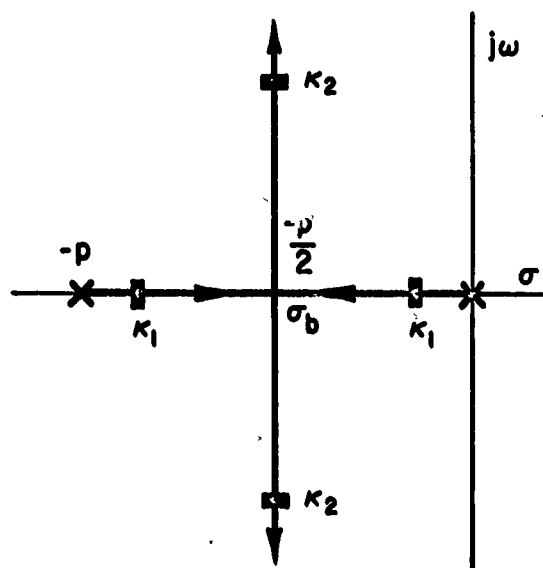


Fig. 3-9. Root Locus for Unit Numerator Second-Order System,
 $G(s) = \kappa/[s(s+p)]$

to see that, at the breakaway point, Rule 9 leads to

$$s_K^b = \frac{1}{\left[\frac{\partial G}{\partial s}\right]_{s=-p/2}} = \left[\frac{1}{p - \frac{p}{2}} + \frac{1}{0 - \frac{p}{2}}\right]^{-1} \rightarrow \infty$$

This is an example of the blowup of the sensitivity vector at multiover poles, a topic which will be discussed more fully later.

Application of Rule 10 (for $m \geq 2$) to find closed-loop roots which are compatible in that they have the same open-loop gain is extremely easy for this example because the sum of the roots is $-p$ and there are only two roots present. Selection of one then immediately specifies the other (e.g., see points labeled κ_1 and κ_2 in Fig. 3-9). Specific values for the gains must be found using Eq. 3-10, although one can, of course, solve the characteristic equation at various values of gain in this elementary example. Also, the gain at breakaway will be $\kappa = p^2/4$, found, as already noted, by the condition for two equal roots.

The contour map for the function $1/s(s+p)$, with $p=1$, is presented in Fig. 3-10. The locus of roots is identified with the -180° angle contour which lies between the poles and leaves the real axis at the breakaway point, $\sigma_b = -1/2$. The locus approaches the points at infinity along the two asymptotes. Points on the locus corresponding to closed-loop roots for particular values of the gain, κ , are indicated by the intersections of the magnitude contours with the locus. The values illustrated (+20 db, +12 db, +6 db, 0 db, -6 db, -12 db) correspond, in decibel measure, to the inverse of the gain, i.e., $\kappa = 1/10, 1/4, 1/2, 1, 2, 4$.

The isometric view of the surface corresponding to the transfer function $1/s(s+1)$ is presented in Fig. 3-11. Several contours of constant angle and constant magnitude are shown on the surface. Remembering that the increase in gain from zero is analogous to starting the reference plane at infinity and moving it down, we can see that the closed-loop roots at the intersection of the $\pm 180^\circ$ angle contour and the waterline move "downhill" from the poles toward each other, coalesce at the saddle point, and then split apart and continue "downhill."

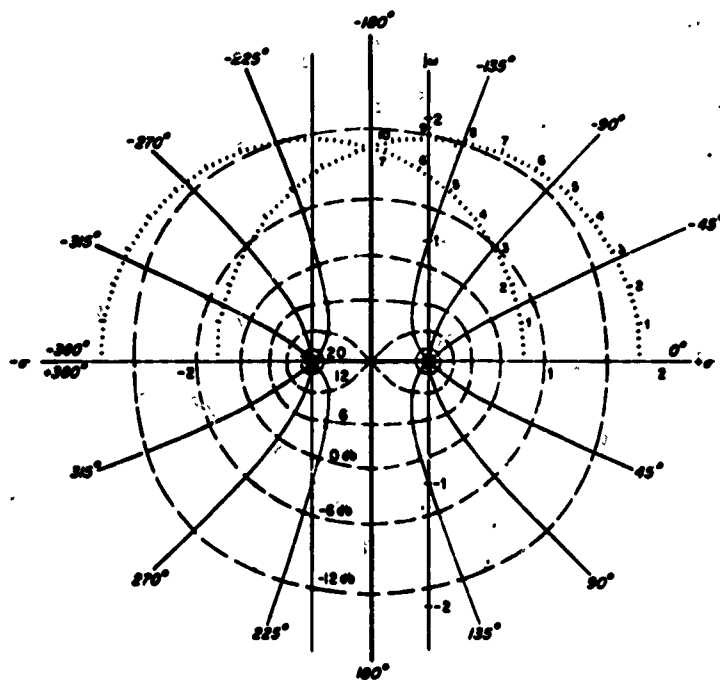


Figure 3-10. Contour Map and Iso-Argument Curves for $G(s) = \frac{1}{s(s+1)}$

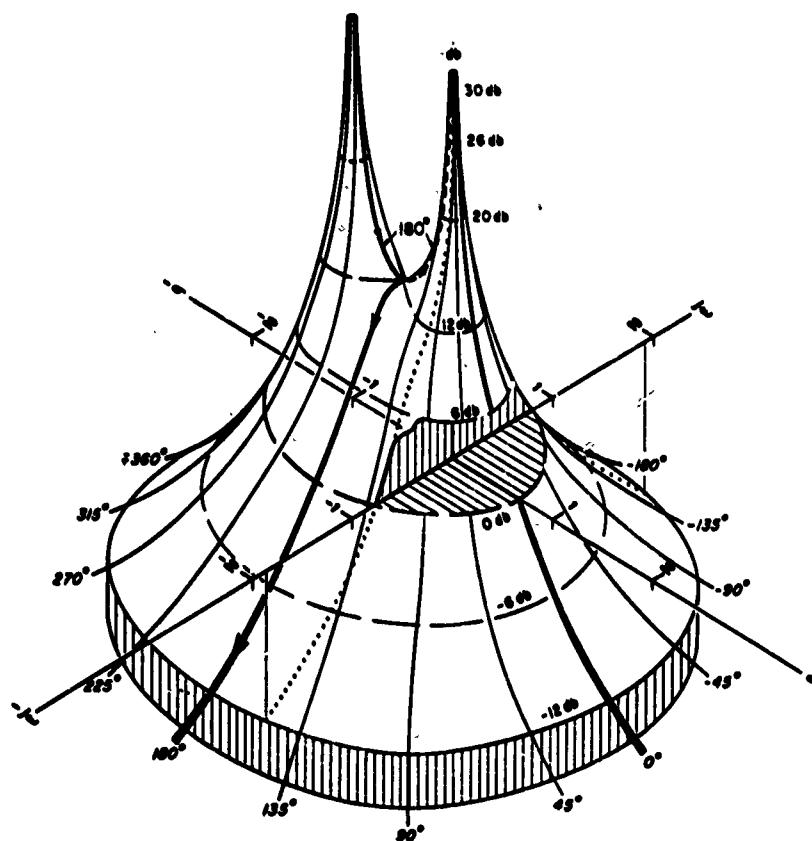


Figure 3-11. Isometric View of the Surface of $G(s) = \frac{1}{s(s+1)}$

Example 3: Second-order system with a zero

Figure 3-12 shows another second-order system feedback controller which, in this case, contains a first-order lead.

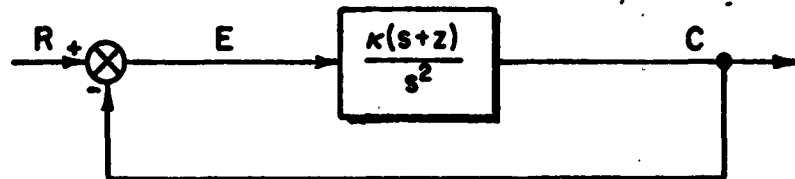


Fig. 3-12. A Second-Order Feedback Control with Lead

The closed-loop characteristic equation is given by

$$s^2 + Ks + Kz = 0$$

which has the roots

$$s_{1,2} = -\frac{K}{2} \left[1 \pm \sqrt{1 - \frac{4z}{K}} \right]$$

These will be complex for $0 < K \leq 4z$ and real for $K > 4z$.

From Rules 4 and 5 the real axis to the left of the zero is seen to be on the root locus, with one of the closed-loop poles terminating on the zero as the other proceeds to infinity along the -180° (negative real axis) high gain asymptote. Rule 7, i.e.,

$$\frac{dG(s)}{ds} = -\frac{K(s+2z)}{s^3} = 0$$

indicates a rendezvous of two complex roots at $s = -2z$. The roots start their journey into the complex plane along pathways tangent to the imaginary axis, per Rule 6 or 8. As shown in Fig. 3-13, the pathway is a circle, centered at the zero $s = -z$. This can be shown analytically by considering the equation for the root locus as developed below.

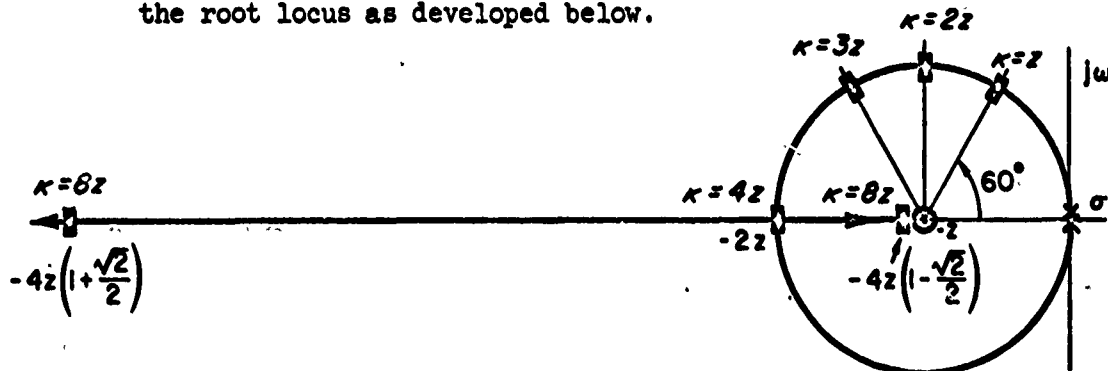


Fig. 3-13. Root Locus for Second-Order System with Lead, $G(s) = K(s+z)/s^2$

The statement $G(s) = -1$ is equivalent to

$$\frac{\beta(s)}{\alpha(s)} = -\kappa \quad (3-18)$$

Because $\beta(s)/\alpha(s)$ is complex, Eq. 3-18 can be rewritten as

$$\operatorname{Re} \left[\frac{\beta(s)}{\alpha(s)} \right] + j \operatorname{Im} \left[\frac{\beta(s)}{\alpha(s)} \right] = -\kappa \quad (3-19)$$

Since κ is real, the imaginary term must vanish on the locus of roots. Consequently the root locus criteria statements then become

$$\operatorname{Im} \left[\frac{\beta(s)}{\alpha(s)} \right] = 0 = \operatorname{Im} [\beta(s)\alpha^*(s)] \quad (3-20)$$

$$\operatorname{Re} \left[\frac{\beta(s)}{\alpha(s)} \right] = -\kappa \quad (3-21)$$

These correspond to Eqs. 3-9 and 3-10. Equation 3-20 in particular can be very useful when equations for the root locus are desired.* Thus, applying Eq. 3-20 to the case at hand,

$$\begin{aligned} \operatorname{Im} [\beta(s)\alpha^*(s)] &= \operatorname{Im} [s^2(s+z)^*] \\ &= \operatorname{Im} [(\sigma+j\omega)^2(\sigma-j\omega+z)] \\ &= \operatorname{Im} [\sigma^2(\sigma+z) + \omega^2(\sigma-z)] + j\omega[\sigma^2 + 2\sigma z + \omega^2] \\ &= \omega[(\sigma+z)^2 + \omega^2 - z^2] = 0 \end{aligned}$$

$$\text{or,} \quad \omega = 0$$

$$\text{and} \quad (\sigma+z)^2 + \omega^2 = z^2$$

*V. C. M. Yeh, "Synthesis of Feedback Control Systems by Gain-Contour and Root-Contour Methods," Trans. AIEE, Pt. II, Vol. 75, 1956, pp. 85-95.

H. Banerjee and T. J. Higgins, "Root Locus Delineations for Higher-Order Servomechanisms," Proc. of the National Electronic Conf., Vol. XIII, 1957, pp. 520-536.

The first equation ($\omega = 0$) is that of the locus along the real axis, while the second is the circle, centered at $\sigma = -z$, with a radius z .

Figure 3-14 is the contour map for the function $G(s) = (s+z)/s^2$, with $z=1$. It represents the addition of the logarithmic magnitudes and the angle contributions of two of the poles of Fig. 3-3a located at the origin and one of the zeros of Fig. 3-3b located at $s=-1$. Again, of course, the locus of roots is traced by the $\pm 180^\circ$ angle contour.

Figure 3-15 is a cutaway isometric view of the surface represented by the contour map of Fig. 3-14. The view shown emphasizes the real axis, the cavity due to the zero and the coincident twin peaks due to the poles at the origin. A conventional root locus is also given in Fig. 3-15 to better show the circular portion of the locus which is largely behind the hill on the isometric view. On these plots the change in sensitivity of the roots to gain changes is apparent. Starting with the open-loop poles at the origin with $\kappa=0$, there is initially very little shift in the roots with gain, i.e., the slope of the peak is very steep and a large vertical movement produces but a small horizontal displacement. By the time a gain of $|\kappa|_{db} = 0$ is reached, the locus has only progressed along an arc of 60° in the plan view (see Fig. 3-15a). From this point a mere factor of four (12 db) moves the roots all the rest of the way to the rendezvous point where they coalesce. Then a very small additional increment in gain separates them very rapidly as the one travels along the asymptote to the point at infinity, while the other closed-loop root is driven toward the location of the zero. The region of high sensitivity is readily recognized in the isometric view because the surface is relatively flat there. Note again how the locus appears to run "downhill" approaching, in this case, the point at infinity and the zero.

Example 4: Unit-Numerator Third-Order System

Figure 3-16 shows the block diagram of a third-order servomechanism:

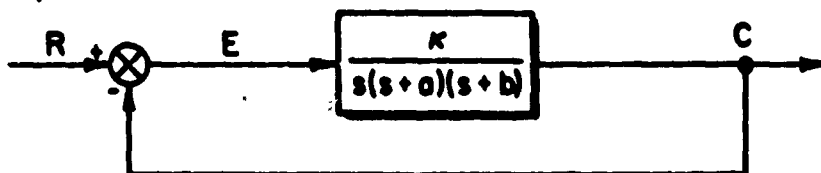


Fig. 3-16. Block Diagram of a Third-Order Servomechanism

The closed-loop function in this case is:

$$\frac{C}{R} = \frac{\kappa}{s^3 + (a+b)s^2 + abs + \kappa}$$

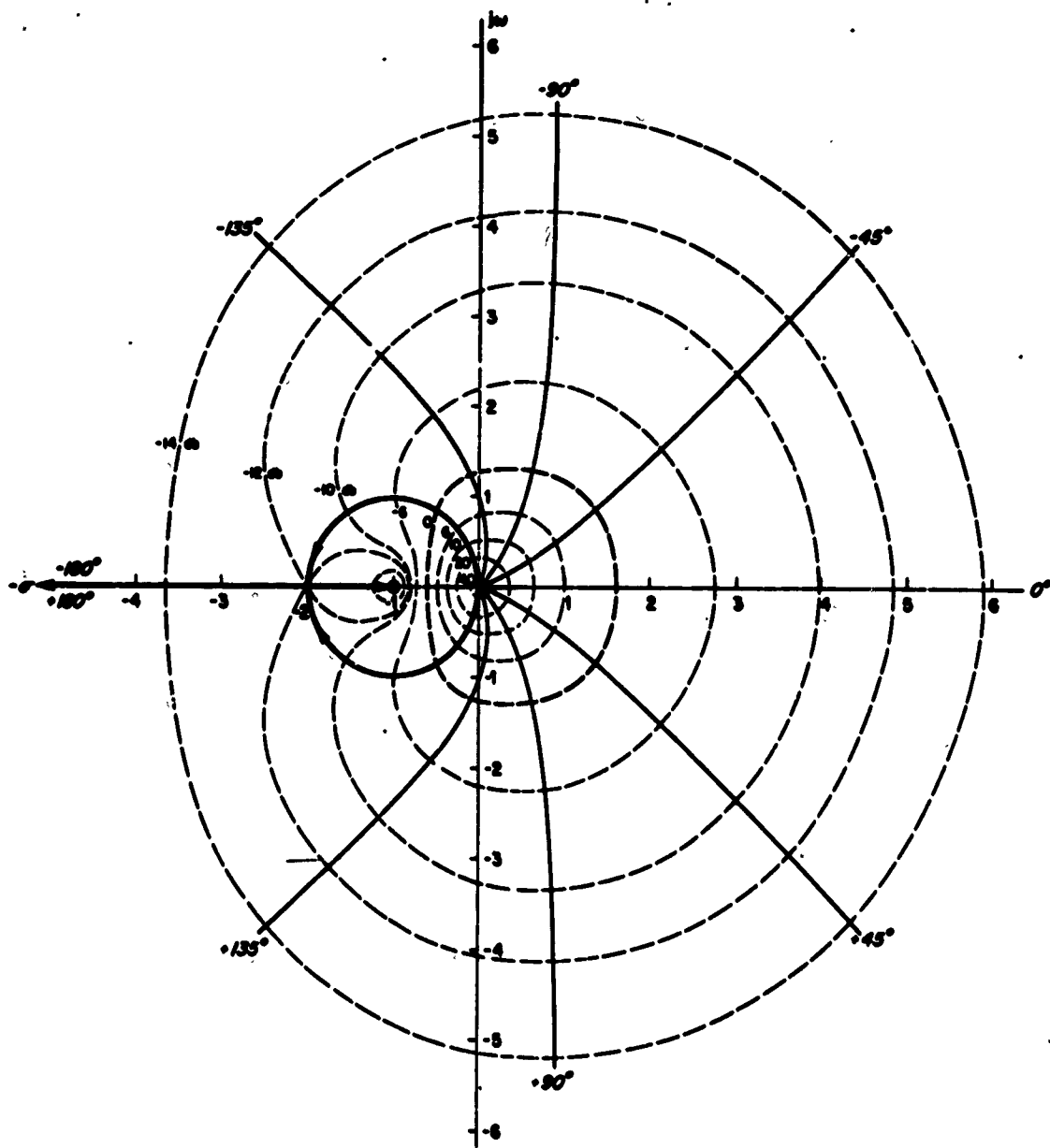
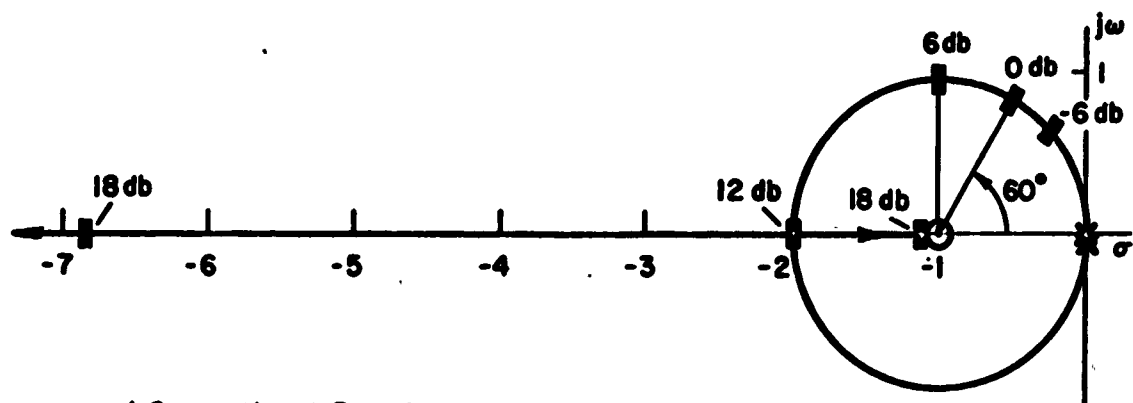
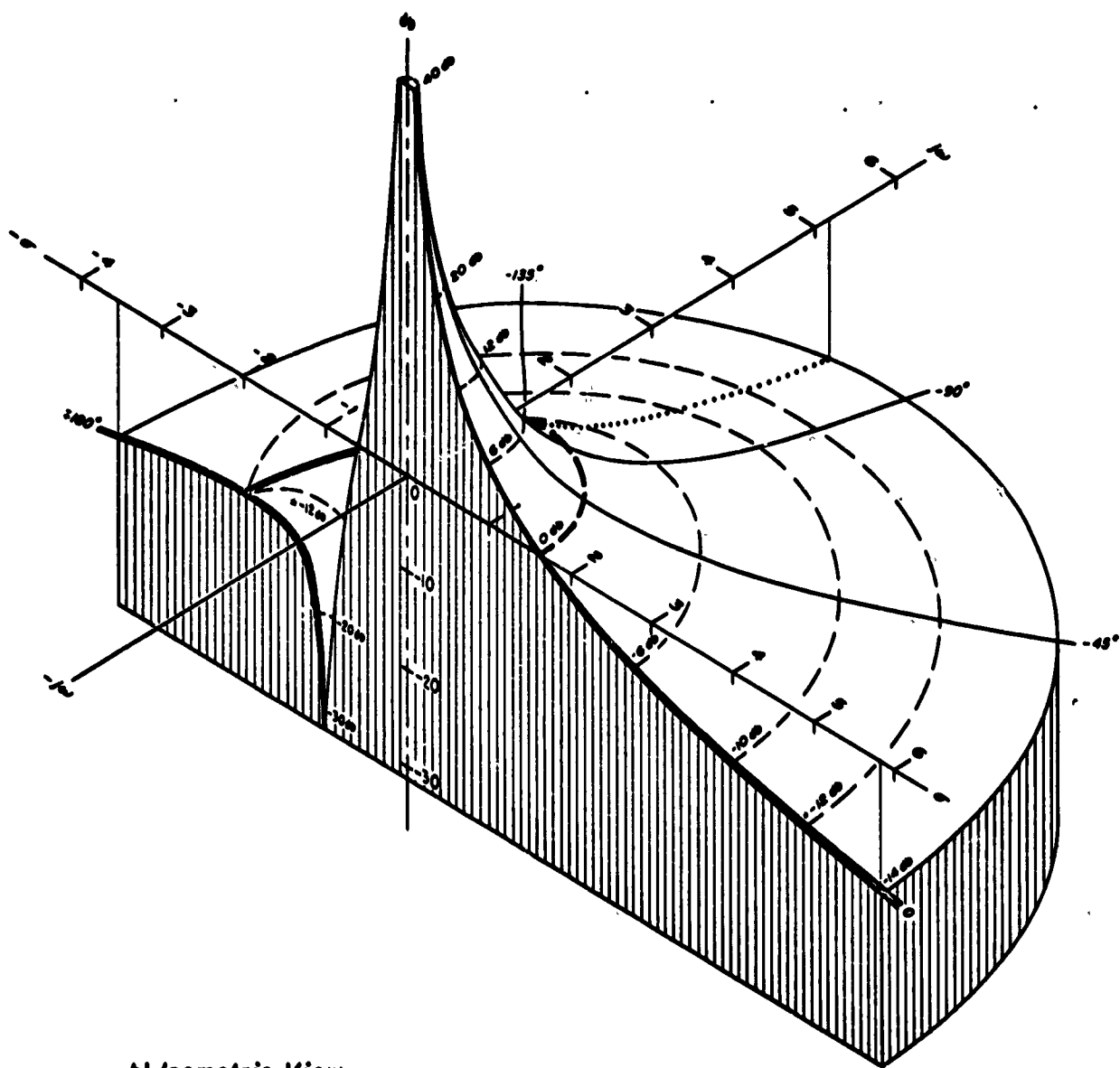


Figure 3-14. Contour Map and Iso-Argument Curves for $G(s) = \frac{s+1}{s^2}$



a) Conventional Root Locus.



b) Isometric View

Figure 3-15. Conventional Root Locus and Isometric View of the Surface $G(s) = \frac{(s+1)}{s^2}$

While, in principle, it is still possible to solve the characteristic equation algebraically, the job is now a little more difficult and, conversely, the advantages of the root locus method are now more prominent. In the case of higher order systems the algebraic factoring of the characteristic function can only be done with repetitive numerical trials, and the semigraphical methods really come into their own.

The root locus for the system of Fig. 3-16 is shown in Fig. 3-17. Rules 1, 3, and 5 are used to find the branches of the locus on the real axis. Rule 4 is invoked to determine the origin of the asymptotes and the angles which they make with the real axis. Either Rule 7 or Rule 9 may be used to determine the breakaway point,

$$\sigma_b = -\frac{1}{3}[(a+b) - \sqrt{a^2 - ab + b^2}] ; \kappa > 0$$

Rule 8 says that here the four branches are at right angles to one another, and Rule 11 shows where the locus crosses the imaginary axis, i.e., $\omega^2 = ab$. [In this case, the Routh-Hurwitz stability criterion requires $ab(a+b) > \kappa$ for stability, so that the value of the gain at this point is also established.] Rule 10 can be used to determine the position of the third root when the gain is just sufficient to produce neutral oscillatory stability, and Rule 12 enables the angle, γ , to be readily found. To obtain the equation for the locus, Eq 3-20 is applied:

$$\begin{aligned} \text{Im} \left[\frac{\beta(s)}{\alpha(s)} \right] &= \text{Im} [(j\omega + \sigma)(j\omega + \sigma + a)(j\omega + \sigma + b)] \\ &= \omega \{-\omega^2 + [3\sigma^2 + 2(a+b)\sigma + ab]\} \\ &= 0 \end{aligned}$$

So the locus is given by

$$\begin{aligned} \omega &= 0 \\ \omega^2 &= 3\sigma^2 + 2(a+b)\sigma + ab \end{aligned}$$

After a few manipulations, the latter equation can be put into the conventional form for a hyperbola:

$$\left[\frac{\sigma + \frac{1}{3}(a+b)}{\frac{1}{3}\sqrt{a^2 - ab + b^2}} \right]^2 - \left[\frac{\omega}{\frac{\sqrt{3}}{3}\sqrt{a^2 - ab + b^2}} \right]^2 = 1$$

For higher order systems the locus equations become exceedingly complex, so they are not too helpful in either the construction process or as an aid to the more analytically inclined.

With the choice $a=1$, $b=5$, the contour map of the open-loop function is shown in Fig. 3-18. The locus of roots, of course, lies along the angle contour lines corresponding to $\pm 180^\circ$ and $\pm 540^\circ$, and crosses the imaginary axis when the gain is just a little less than 30 db. $K = 5(1+5) = 30 \approx 29.5$ db is the actual gain for the onset of instability.

Figure 3-19 is an isometric view of the surface represented by the contour map of Fig. 3-18. It is particularly clear here that as the gain is increased the closed-loop roots do not move evenly along the locus represented in two dimensions. Instead, the closed-loop roots move a large distance along the locus for a small increment in gain where the surface is flat, and where the surface is steep the roots move hardly at all for comparatively big increments in gain. Both this and similar observations for the last example are associated with the concept of "sensitivity," to which we shall return later.

Example 3: Generalization of the Simple Examples 1-3

As a final example of the root locus, the three simple systems described previously will be generalized to systems which have poles at locations other than the origin (for Example 1, a first-order lead is also added). Loci for all these systems are given in Fig. 3-20. For these it is particularly worth remarking that the addition of the same real part to, or subtraction from, all the open-loop poles and zeros does not alter the geometry of the locus; it merely moves the whole locus right or left with respect to the imaginary axis.

As a final comment on the root locus method, it should be noted that the technique is useful not only to find the closed-loop roots of feedback systems, but also to factor any polynomial, $\beta(s) + K\alpha(s)$. $\alpha(s)$ and $\beta(s)$ do not have to represent respectively the numerator and denominator of the transfer function of a physical system, nor does K have to be a "gain." If $\alpha(s)$ and $\beta(s)$ are any polynomials whose factors are known, and K is any parameter (which appears only linearly in the complete polynomials) whose influence we wish to trace, we can put the problem into root locus form, i.e., write:

$$\begin{aligned} \beta(s) + K\alpha(s) &= 0 \\ \frac{K\alpha(s)}{\beta(s)} &= -1 \end{aligned} \tag{3-22}$$

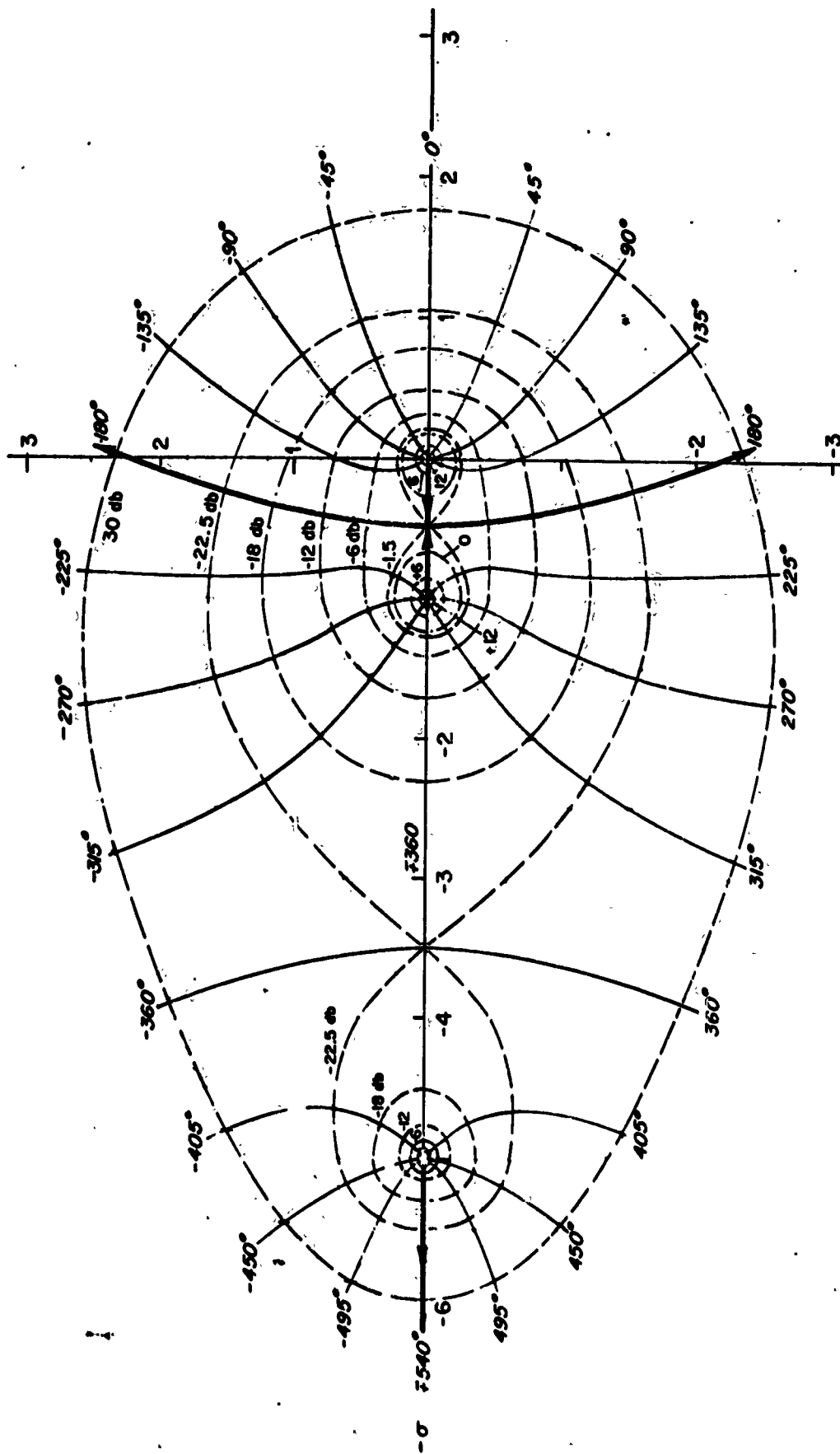


Figure 3-18. Contour Map and Iso - Argument Curves

$$\text{for } G(s) = \frac{K}{s(s+1)(s+5)}$$

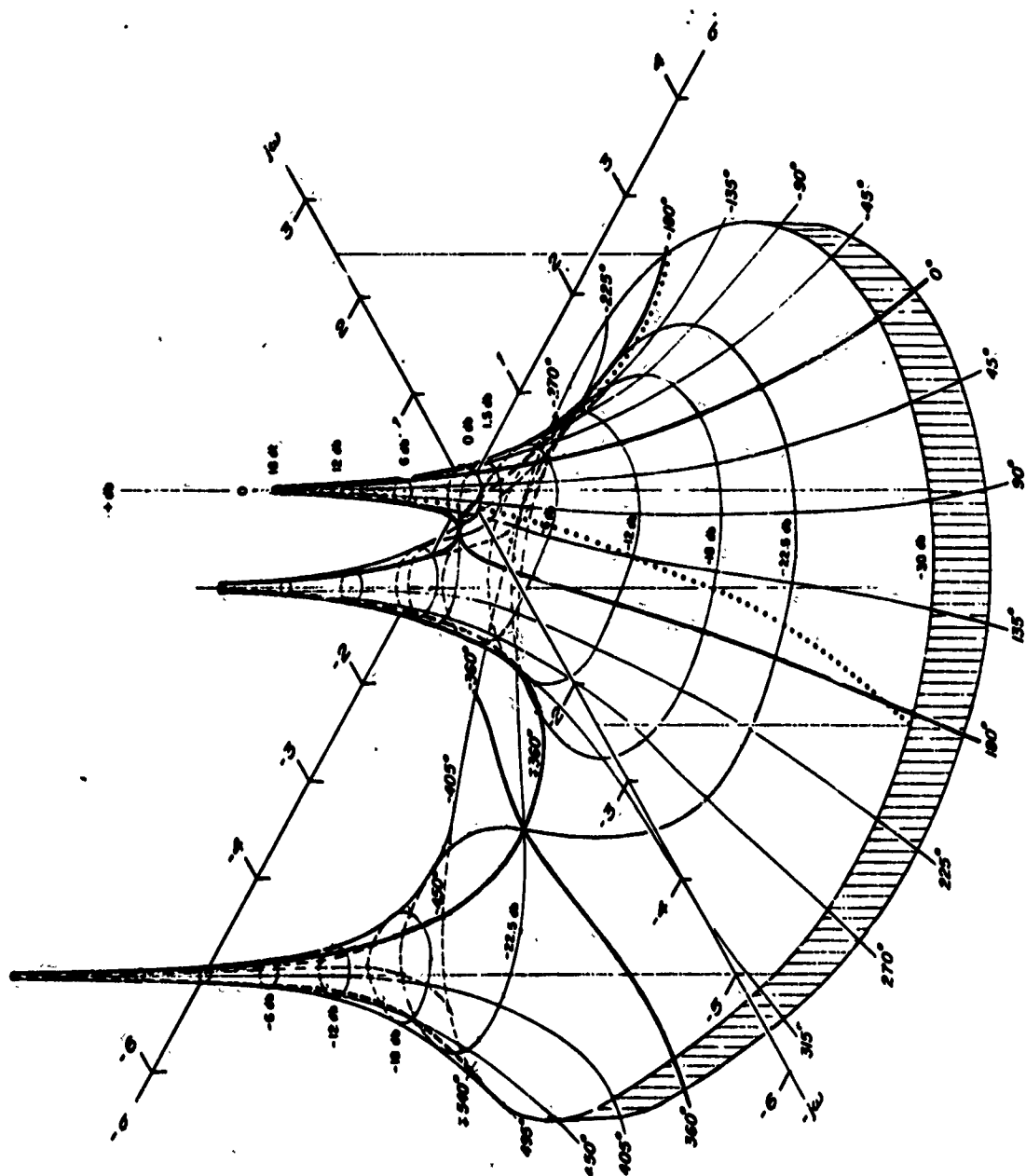
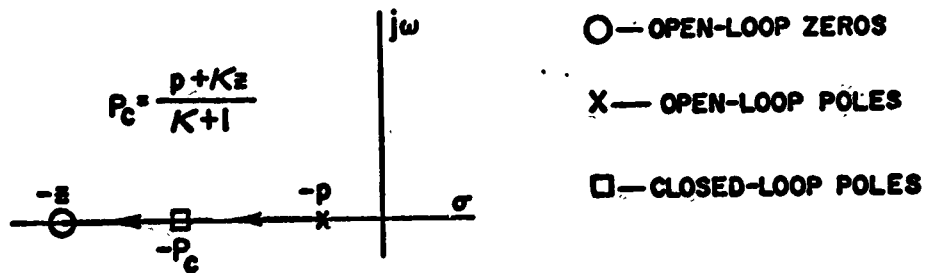
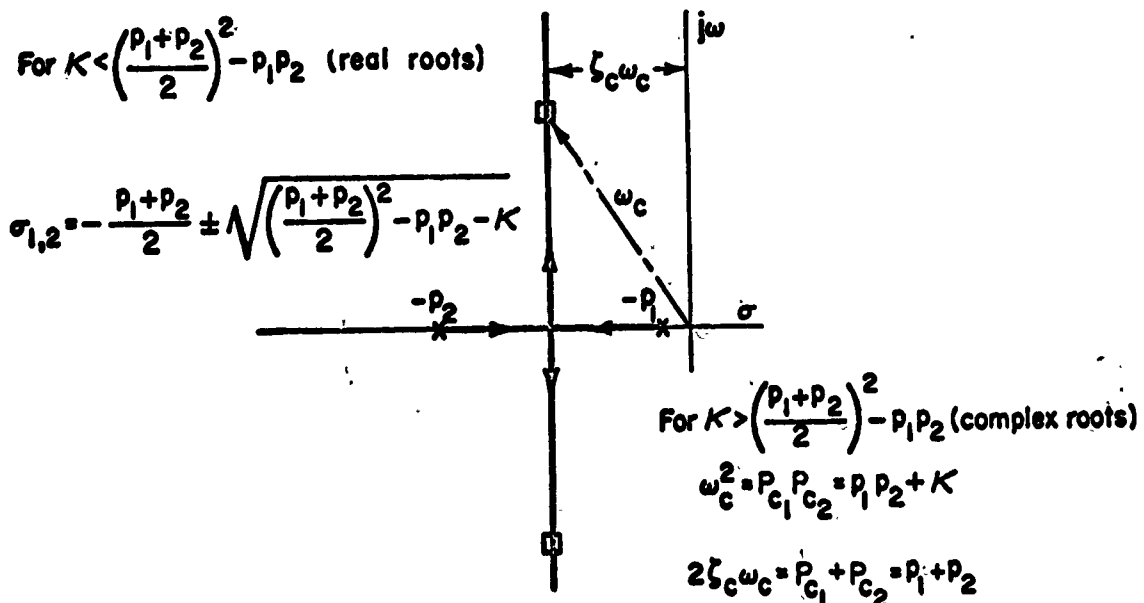


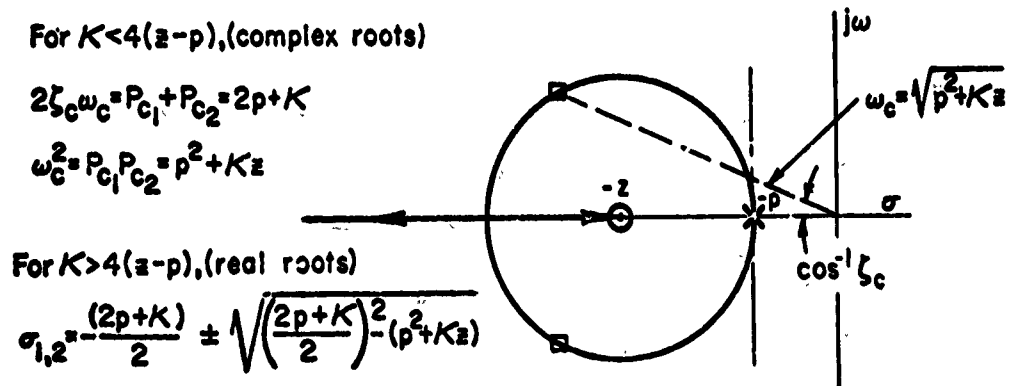
Figure 3-19. Isometric View of the Surface for $G(s) = \frac{K}{s(s+1)(s+5)}$



(a) System with single pole & zero $G(s) = \frac{K(s+z)}{(s+p)}$



(b) System with two poles $G(s) = \frac{K}{(s+p_1)(s+p_2)}$



(c) System with lead & second order pole $G(s) = \frac{K(s+z)}{(s+p)^2}$; $z > p$

Fig. 3-20. Root Loci for Simple Systems

3.5 BODE ROOT LOCUS AND GENERALIZED BODE DIAGRAM

We have had occasion to note that for a given value of s , $G(s)$ is a complex number which can be expressed in terms of a modulus or magnitude and an argument or phase angle. The variable s itself is complex ($\sigma + j\omega$) so that a plot of $G(s)$ as a continuous function of s would, in general, require four dimensions or two plots each of three dimensions, e.g., $|G(s)|$ versus s and $\angle G(s)$ versus s . The contour maps presented in the last section are plan views of such plots, whereas the isometric views directly show $|G(s)|_{db}$ versus s . Unfortunately such constructions are impractically difficult even for moderately uncomplicated cases. Consequently the usual practice is to construct only the root locus plan view with compatible sets of gain contour intersections marked on each branch; and even this construction, which contains only the most essential information, can be tedious without automatic computation.

To obtain more complete information without undue labor, the graphical requirements can be reduced to one plot of three or two plots of two dimensions if the real and imaginary parts of s , σ and ω , are taken to be linearly connected. That is to say, we would find it relatively easy to plot $|G|$ and $\angle G$ versus s , as s takes all values along a straight line in the s -plane. The simplest and most practical forms of such plots correspond to $s = \pm\sigma; \omega = 0$ and $s = \pm j\omega; \sigma = 0$. Sometimes a plot with $s = \sigma_1 \pm j\omega$; $\sigma_1 =$ a nonzero constant is also used and, finally, there is a version where $s = (\xi + j\sqrt{1-\xi^2})u$, $\xi =$ a constant. In Bode plot form these are the σ -Bode, $j\omega$ -Bode, shifted Bode, and ξ -Bode diagrams which have all been described in Section 2.9.

In the analysis of closed-loop systems our objective is to find the roots of $1 + G(s) = 0$. This may be accomplished in either of two ways by means of the logarithmic Bode plots. The first, and more direct, procedure is to find the conditions under which $G(s) = -1$. The second procedure, often combined with the first, involves two steps: (a) Development of a graphical representation of the closed-loop function and (b) decomposition of this closed-loop form into its zeros and poles. The poles of the closed-loop function are the roots of the characteristic

equation. Both operations can be clarified by solving the same set of simple examples used to illustrate the root locus method.

Example 1: First-order system

Consider the system of Fig. 3-5 with the open-loop function $G(s) = K/s$. The surface of Fig. 3-7 is symmetric around the origin. A section in a vertical plane containing the real axis would appear as in Fig. 3-21, as would also a section in a vertical plane containing the axis of imaginaries.

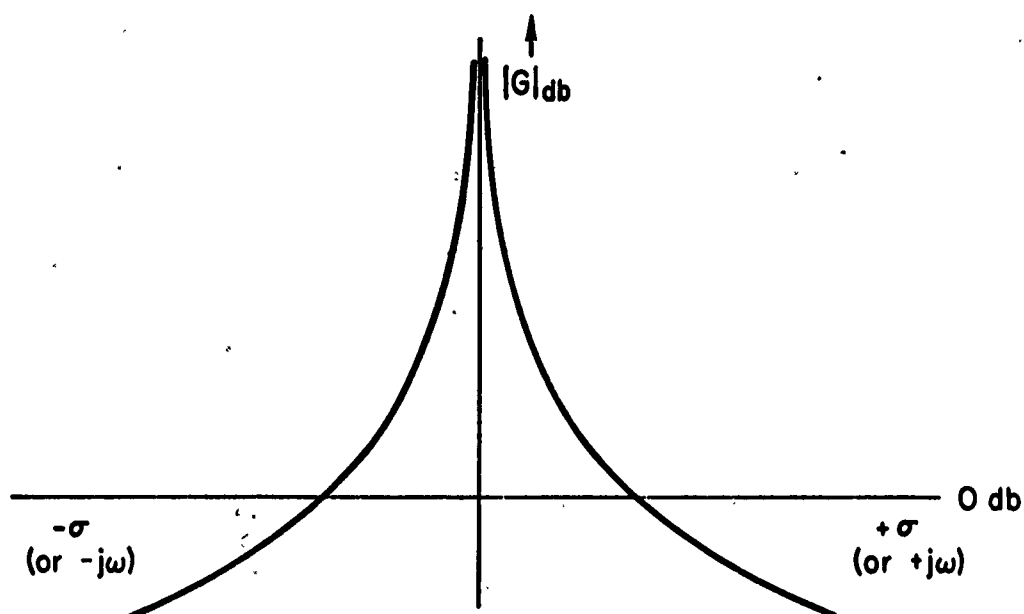


Fig. 3-21. A Section Containing the Real Axis or the Axis of Imaginaries

When the abscissas are distorted so that $20 \log_{10} |G(-\sigma)|$ is plotted against $\log_{10} |\sigma|$, the branch of the sigma diagram illustrated in Table 2-5, Item ②, is the result. It often happens, as is the case here, that only the branch corresponding to the section containing the negative real axis, where $s = -\sigma$ so $G(s) = G(-\sigma)$, is of any interest. Because the poles and zeros of the transfer functions with which we are concerned are always real or occur in complex conjugate pairs, the $j\omega$ -Bode diagram is symmetrical about the origin. The plot for negative frequencies is the reflection of the plot for positive frequencies. Therefore, it is customary to superpose the logarithmic plot of $G(s)$; $s = -\sigma$ on the logarithmic plot of $G(s)$; $s = +j\omega$. This is done in Fig. 3-22, where it is seen that not only do $|G(-\sigma)|$ and $|G(j\omega)|$ have the same asymptotes, but, in this case, are themselves identical. In fact, the more general plot of $|G(s)|_{db}$ versus $\log |s|$ will also coincide with the two special cases for $s = -\sigma$ and $s = j\omega$.

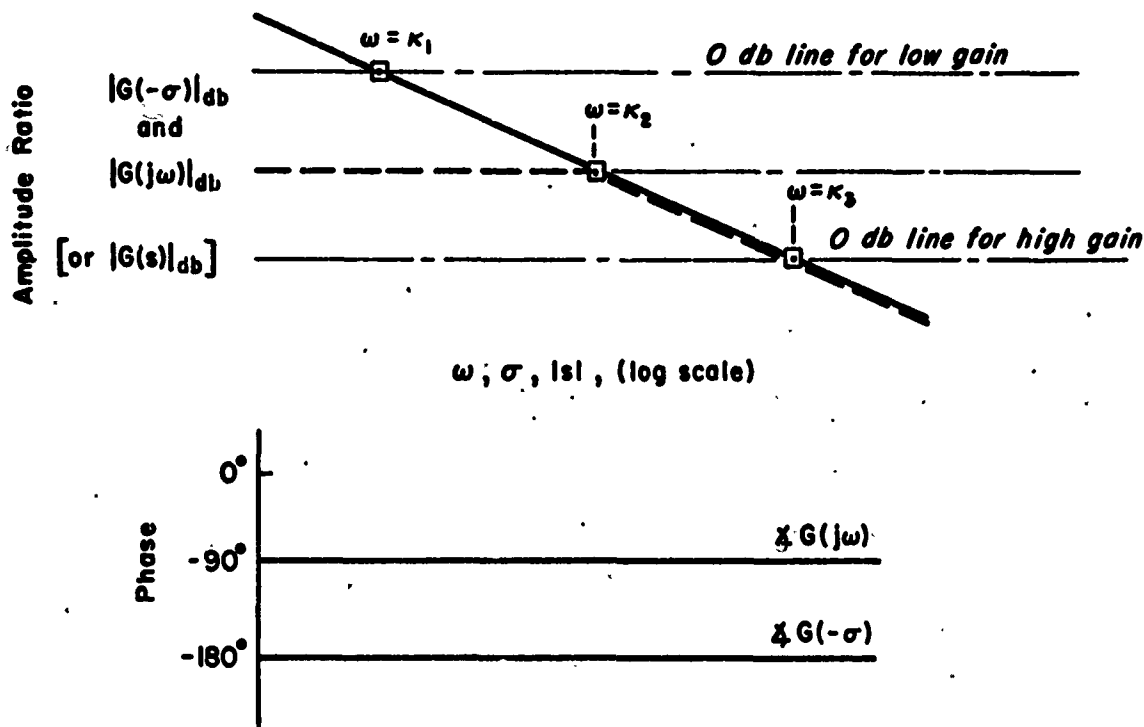


Fig. 3-22. σ -Bode and $j\omega$ -Bode Diagrams; $G(s) = K/s$

In the plot of Fig. 3-22 the effect of adding the σ -Bode or $j\omega$ -Bode representation of the constant, K , would be to shift the whole plot up or down an amount $20 \log_{10} K$ with respect to the reference zero-db line. This, of course, has the same appearance as moving the zero-db line. We can therefore identify positions of the zero-db line with values of the constant. When the line is high the gain constant, K , is small; and when the zero-db line is set low it corresponds to high gain. When the plot is made on semilogarithmic paper, the transfer function, K/s , is plotted by making the line with -20 db/decade slope intersect the zero-db line where the value of the independent variable on the logarithmic scale is numerically equal to the value of K . Note that in this example the phase angle of the $j\omega$ -Bode plot is always -90° , while the phase angle of the $G(-\sigma)$ plot is always -180° . That this should be so has already been made evident in the contour map of Fig. 3-3a and the isometric view of Fig. 3-7.

While it is somewhat like using an elephant gun to kill a flea, we can use the plot of Fig. 3-22 to demonstrate the two methods of determining the closed-loop root(s) from the logarithmic plots. Using the direct method, it is seen that the condition $G(s) = -1$ is satisfied where the zero-db line intersects the $|G(-\sigma)|$ plot and $\angle G(-\sigma) = -180^\circ$. Since, in this case, the angle criterion is satisfied over the whole range of the plot, each

intersection of a zero-db line with the sigma diagram represents a closed-loop factor $(s+K)$ or, alternatively, a closed-loop root, $s = -K$. This result, of course, is precisely the same as the ones already obtained by means of algebra and the root locus method. The σ -Bode is seen, in fact, to be a root locus plot wherein the negative of the root is given as a function of gain. This is the simplest example of the so-called Bode root locus.

The decomposition method of using the logarithmic plot can be illustrated as follows:

$$G_{cr} = \frac{G(s)}{1 + G(s)} \begin{cases} \approx 1 & ; G(s) \gg 1 \\ \approx 1 & ; s = 0 \end{cases}$$

$$G_{cr} = \frac{G(s)}{1 + G(s)} \approx G(s) \quad ; G(s) \ll 1$$

Therefore, the asymptotes of the closed-loop function lie along the zero-db (magnitude = 1) line when $G(s)$ is large, and along the same asymptote as the open-loop function when $G(s)$ is small. Starting from the low frequency end where $G(s) \gg 1$ and the high frequency end where $G(s) \ll 1$, these asymptotes can be projected toward each other. They intersect at $\omega = K$. This, then, is the asymptotic magnitude diagram of the closed-loop function G_{cr} . It is shown by the dashed lines in Fig. 3-22 for the gain K_2 . This closed-loop function may be recognized as a first-order lag, Item ⑥ of Table 2-5, with an inverse time constant $1/T = K$. The pole of the closed-loop function, $s = -1/T = -K$, is the root of the characteristic equation, and we have discovered for the fourth time the dependence of this root on K .

Example 2: Unit-numerator second-order system

Figure 3-23 shows the σ -Bode and $j\omega$ -Bode diagrams for the system of Fig. 3-8 with $p=1$. Several possible positions of the zero-db line corresponding to both low and relatively high values of the gain are marked on the diagram. Closed-loop roots on the real axis are indicated by the intersections of the zero-db line with the sigma diagram where $\angle G(-\sigma) = -180^\circ$. Only the portion of the sigma diagram between $\sigma=0$ and $\sigma=1$ is therefore of any interest. The diagram shows two separate real roots (marked with squares) for a low value of gain. As the gain is increased, the indicated positions of these roots move toward each other and coalesce at the local minimum of the sigma diagram. As the gain is further increased, no real roots are indicated. In fact, as we know, the roots have become complex.

The second procedure is still applicable, however. The low frequency and high frequency asymptotes can be projected so as to meet at a point where there is a local change in the slope of the asymptotic approximation of from zero to -40 db/decade.

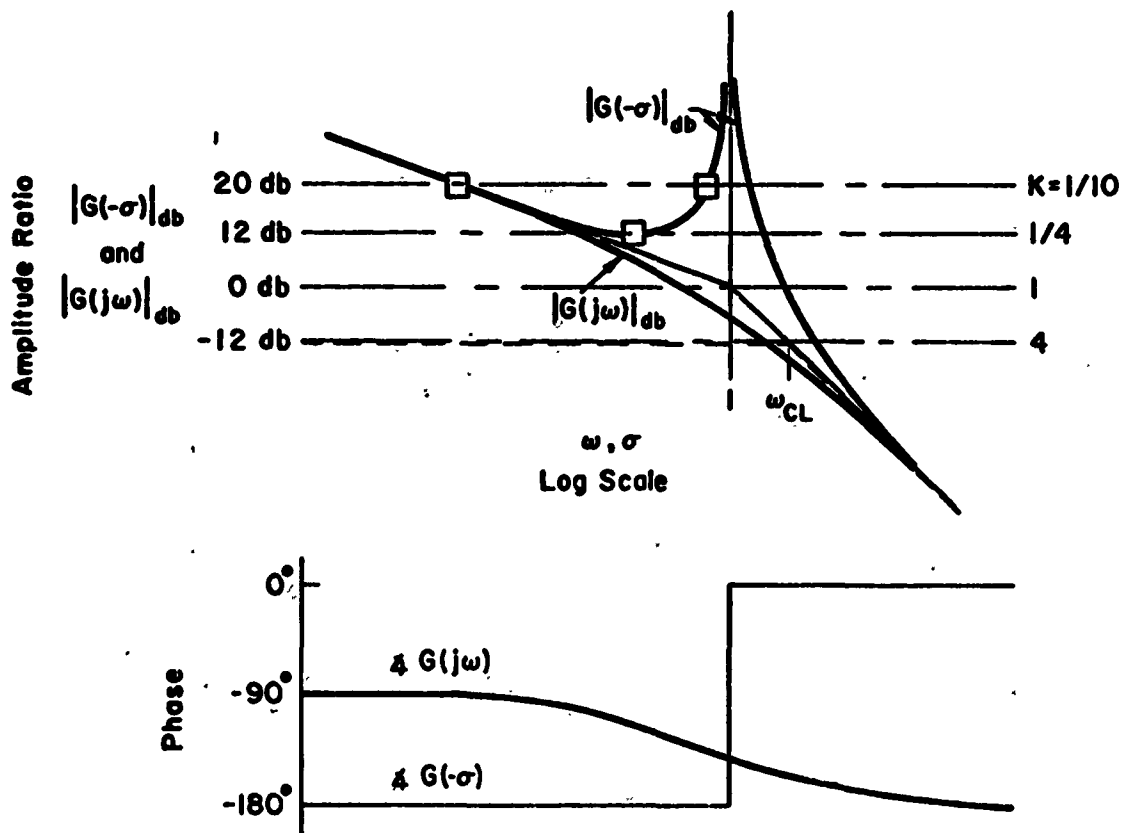
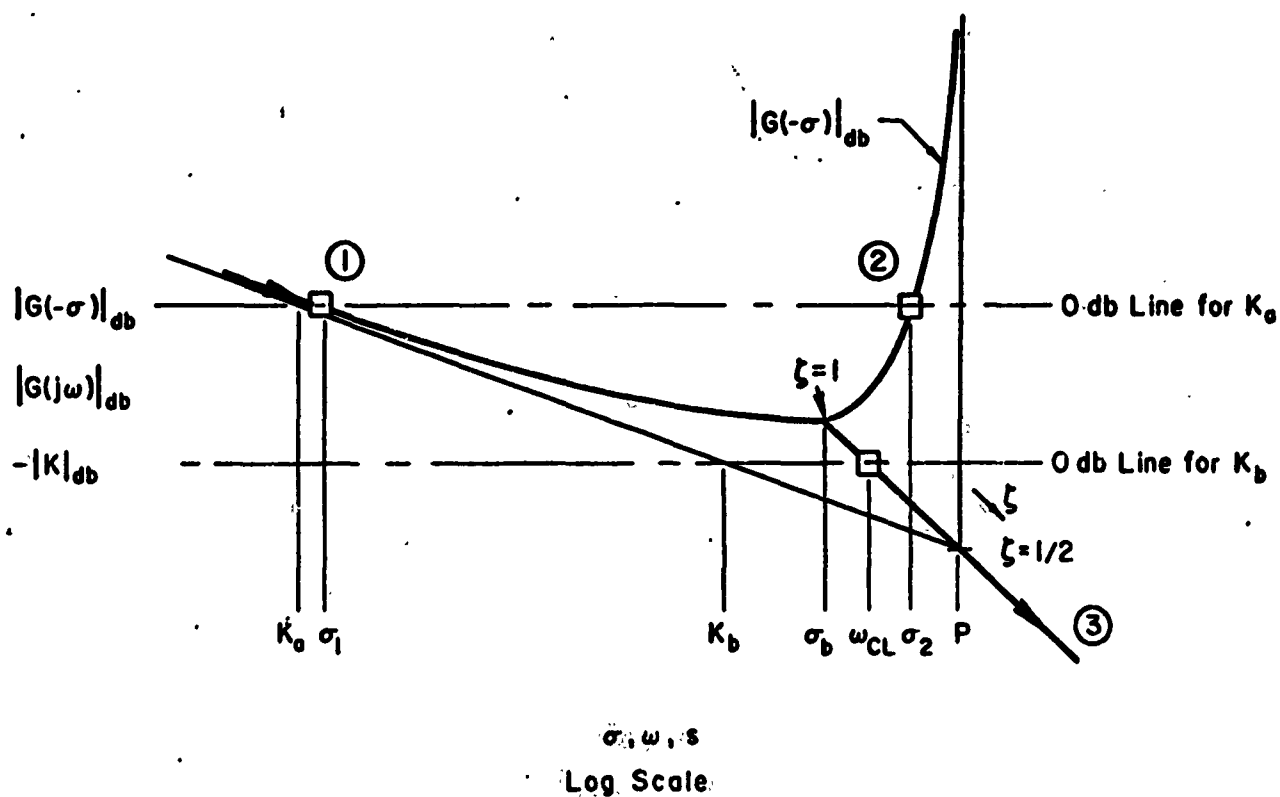


Fig. 3-23. σ -Bode and $j\omega$ -Bode Diagrams; $G(s) = K/s(s+1)$

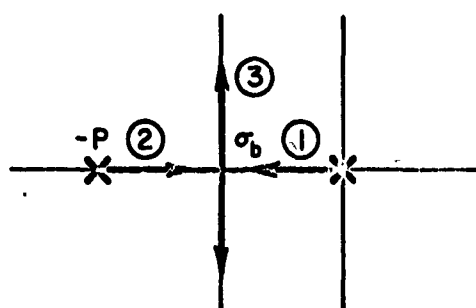
The figure shows this construction in dashed lines. This closed-loop asymptotic approximation is recognized as the representation of a second-order transfer function with damping ratio $\zeta < 1$ and an undamped natural frequency, ω_{CL} , indicated by the break or corner frequency. Then, since the sum of the roots is the sum of the poles, $2\zeta_{\text{CL}}\omega_{\text{CL}} = 1$, and the closed-loop damping ratio will be $\zeta_{\text{CL}} = 1/2\omega_{\text{CL}}$.

A complete root locus, in which the magnitudes of the roots appear versus gain in Bode diagram coordinates, is the result of the combined procedures described above. This is shown in Fig. 3-24, for the case where the pole, $-p$, is kept general. The conventional root locus of Fig. 3-9 is also given for comparison and correlation.

As in the first example, the locus of real roots coincides with that portion of the σ -Bode diagram for which $\angle G(-\sigma) = -180^\circ$. These correspond to the real axis roots on the conventional root locus, with branch ① moving toward branch ② and meeting at the breakaway point, σ_b . On this part of the Bode root locus the abscissa scale used is $\log \sigma$, with the closed-loop characteristics at a particular gain, K_a , being read as the negative of the roots, σ_1 and σ_2 , i.e., as they appear in the closed-loop factors, $(s + \sigma_1)(s + \sigma_2)$.



(a) Bode Root Locus



(b) Conventional Root Locus

Fig. 3-24. Bode and Conventional Root Locus
for $G(s) = K/s[(s/p) + 1]$

For gains larger than that for breakaway there are two complex conjugate roots, which have a damping ratio, ζ_{CL} , and a magnitude, given by the undamped natural frequency, ω_{CL} . In this elementary system the locus of ω_{CL} versus gain coincides with the high frequency asymptote of $|G(j\omega)|_{db}$, and its extrapolation back to the breakaway point. This branch, labeled ③, corresponds to the similarly labeled branch on the conventional root locus. For a given gain, K_b (ordinate), the closed-loop undamped natural frequency, ω_{CL} , is read as the abscissa ($\log |s|$) of branch ③. The damping ratio, on the other hand, cannot be considered as a dimension; instead, it must be treated as a parameter and noted along the plot. At breakaway it is, of course, identically 1, and it decreases as gain increases. For the current example it is just $\zeta_{CL} = p/2\omega_{CL}$, so it is readily obtained.

In more complicated problems than this one, the closed-loop complex roots are seldom obtained as simply as illustrated here. For these recourse to supplementary techniques is often required. One such technique is the shifted Bode diagram, which can be readily illustrated by this example. If, in the numerical version of the example, the variable s is changed to $s' = s + (1/2)$, then the open-loop function becomes

$$G(s') = \frac{K}{\left(s' + \frac{1}{2}\right)\left(s' - \frac{1}{2}\right)} = \frac{-K}{(2s' + 1)(-2s' + 1)} ; K = 4k$$

This shift in s to s' corresponds to a shift in the origin of one-half unit to the left. Addition of the logarithmic representations of the $j\omega$ -Bode magnitude diagrams of the individual factors yields the second-order magnitude characteristic illustrated in Fig. 3-25. The negative sign of the Bode gain, $-K$, is taken into account by making the phase angle -180° at low frequency. The phase angle contributions of the other transfer function factors exactly cancel, so that it is readily appreciated that the angle criterion is satisfied over the whole range of ω . This, of course, is to be expected since Fig. 3-25 is a representation of the section through the transfer function surface of Figs. 3-10 and 3-11 at $\sigma = -1/2$ where the angle is always -180° . As for the magnitude criterion, the figure shows that there is no intersection of the zero-db line and the magnitude plot for $K \leq 1$, but as soon as K exceeds 1, there is an intersection. The intersection moves along the actual magnitude curve (with the departures applied to the asymptotes) toward the right as the gain, K , is increased. A typical intersection is shown by the square. The frequency, $|\omega'|$, at which this intersection occurs is the damped frequency of the closed-loop root. For the case in which $K=4$, the intersection is at $\omega = \sqrt{3}/2$ and the closed-loop factor can be written in terms of the real part, α , and imaginary part, β , as $(s + \alpha)^2 + \beta^2 = [s + (1/2)]^2 + (\sqrt{3}/2)^2 = 0$.

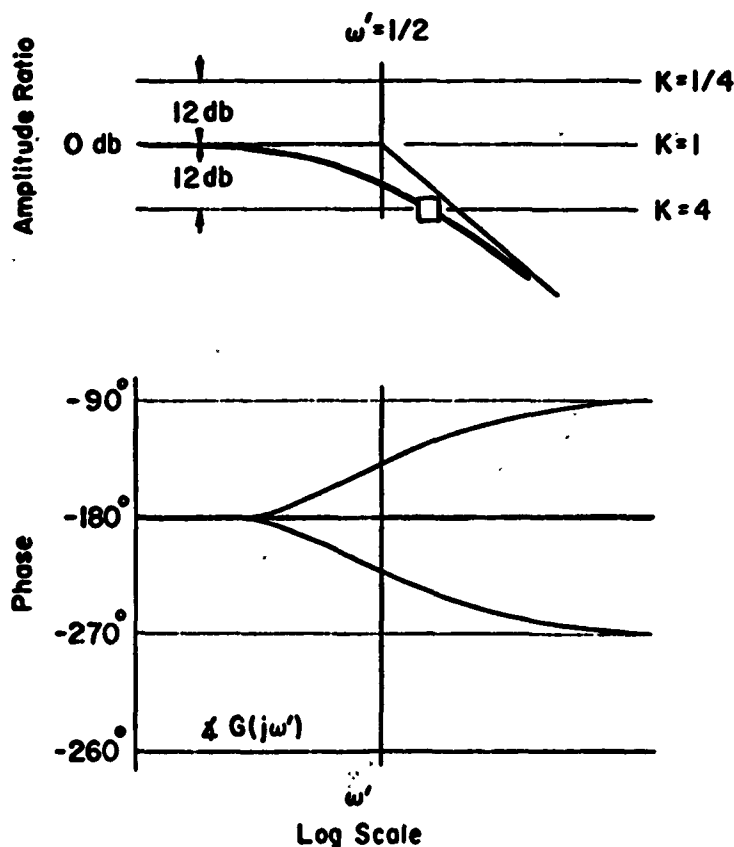


Fig. 3-25. Shifted $j\omega$ -Bode Diagram

Example 3: Second-order system with a zero

σ -Bode and $j\omega$ -Bode diagrams for the system of Fig. 3-12 are presented in Fig. 3-26. The rendezvous point on the real axis is again indicated by the extremum of the $|G(-\sigma)|$ plot where $\angle G(-\sigma) = -180^\circ$. Also, the near cancellation of the zero and the closed-loop pole at high gain is shown by the closed-loop asymptotic plot which is constructed proceeding from both ends. The zero of the open-loop function is also a zero of the closed-loop function, while the roots are poles of the closed-loop function. The asymptotic approximation therefore has appropriate breakpoint corners at each of the magnitudes corresponding to these singularities.

At gains less than that for breakaway the roots are complex (i.e., along the circular part of the locus in Fig. 3-13). The magnitudes of these are readily found by decomposition, as exemplified in Fig. 3-27 for two values of gain, K_1 and K_2 . At very small values of ω the amplitude ratio, $|G(j\omega)|$, is very large compared with unity, so the low frequency closed-loop asymptote coincides with the open-loop zero-db line. This low

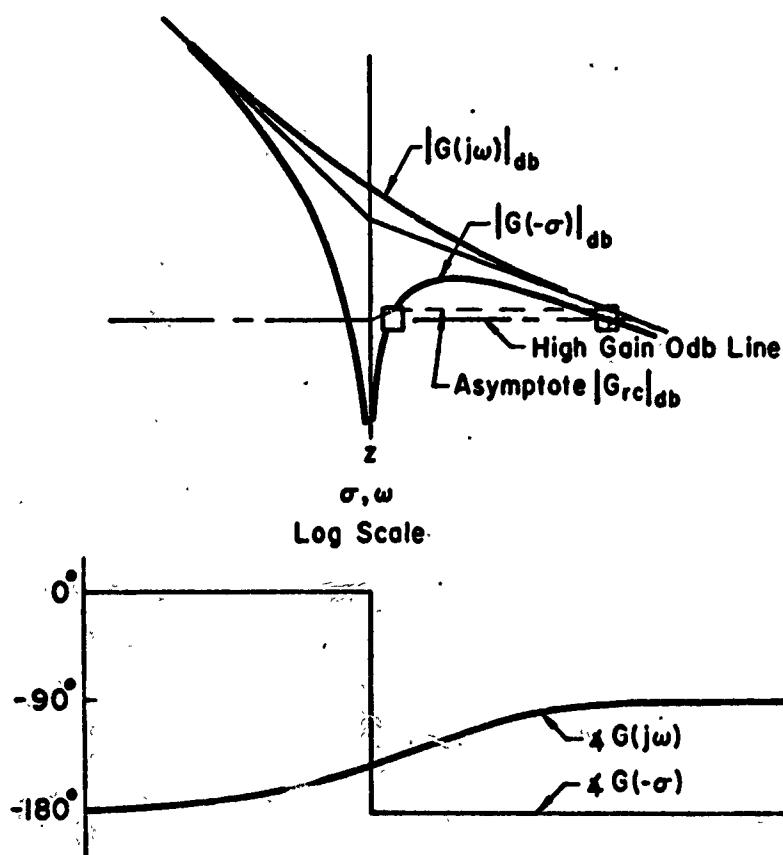


Fig. 3-26. σ -Bode and $j\omega$ -Bode Diagrams for $G(s) = K[(s/z) + 1]/s^2$

frequency asymptote of $|G_{rc}|_{db}$ either runs into the $|G(j\omega)|_{db}$ asymptotes, e.g., at ω_{CL1} for K_1 , or reaches the magnitude of the zero, e.g., at z for K_2 , before intersecting the asymptote $|G(j\omega)|_{db}$ plot. In either event there is a change in slope. This is -40 db/decade for the K_1 case, corresponding to the closed-loop undamped natural frequency ω_{CL1} , and $+20$ db/decade for the K_2 example, associated with the appearance of the zero. The asymptotic $|G_{rc}|_{db}$ plot for the low gain case has its final breakpoint at the zero, whereas the last slope change for the higher gain example occurs at the closed-loop undamped natural frequency ω_{CL2} . Finally, the damping ratio is found from the sum of the roots relationship, which in this case is

$$2\zeta_{CL}\omega_{CL} = \kappa = K/z$$

$$\zeta_{CL} = \kappa/2\omega_{CL} = K/2z\omega_{CL}$$

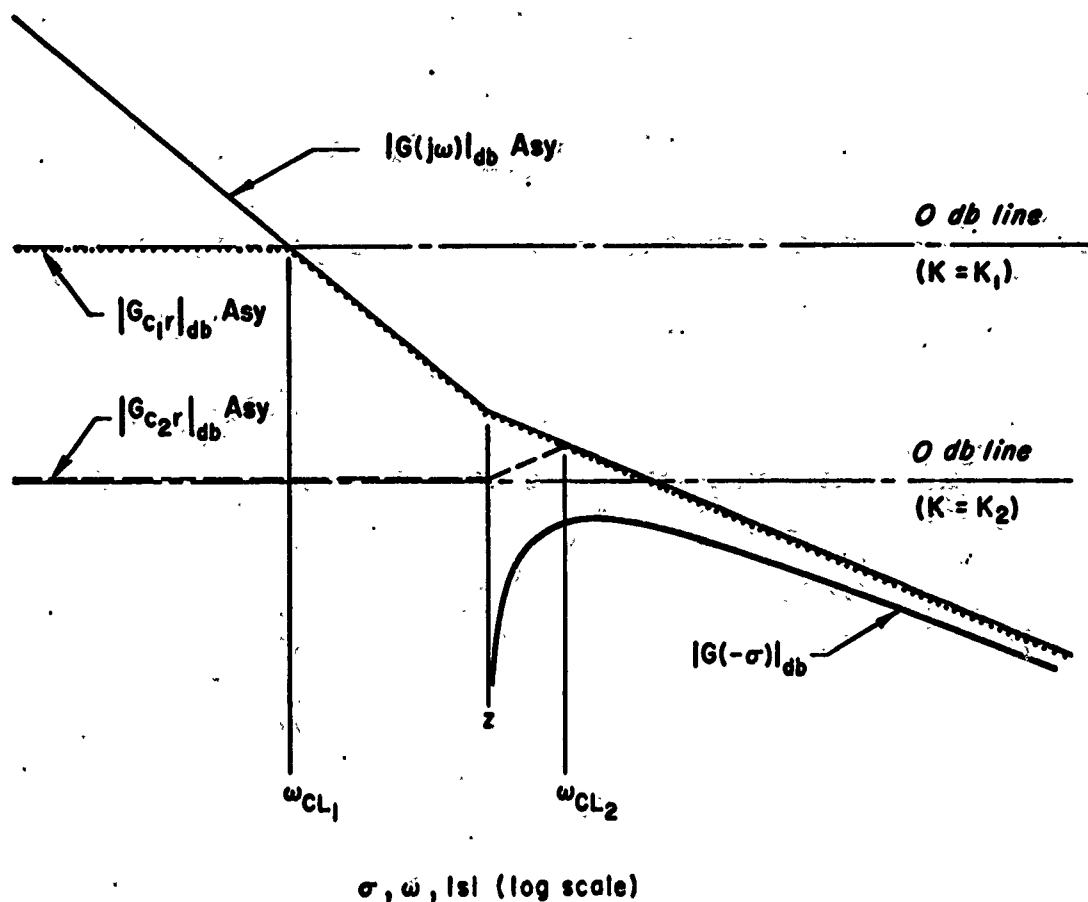
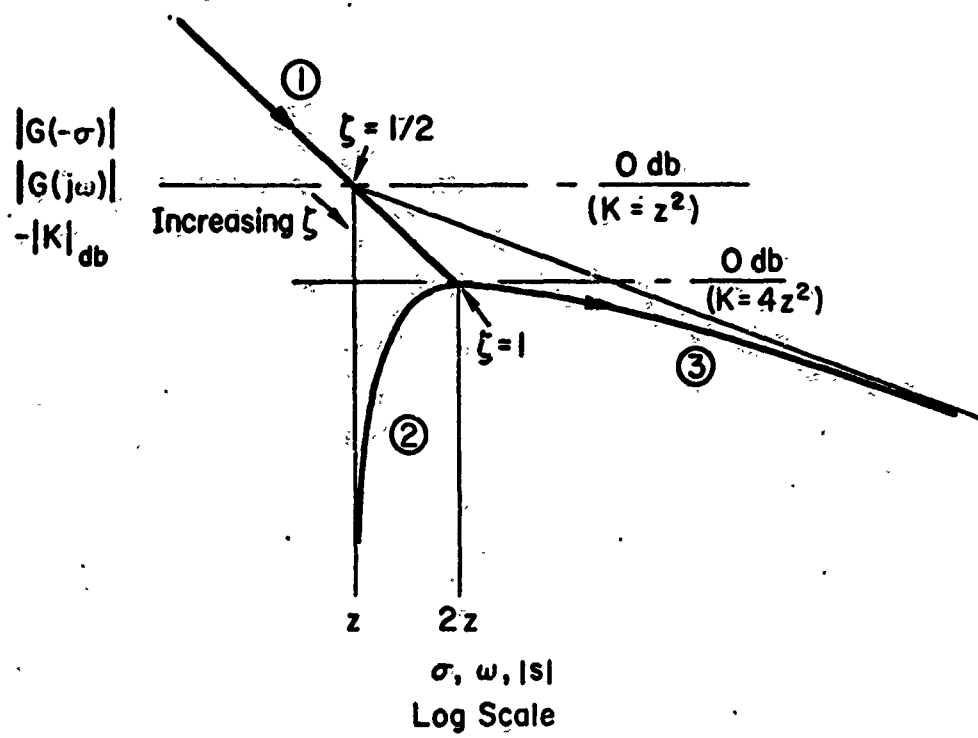
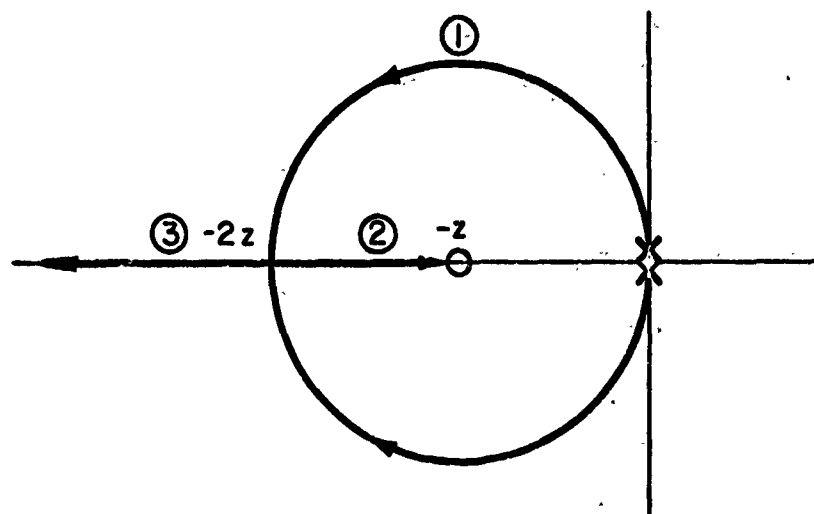


Fig. 3-27. Determination of the Magnitude of Complex Roots by Decomposition

Gathering the above data together into a common presentation results in the Bode root locus of Fig. 3-28. The branches shown thereon correspond with the similarly numbered ones on the conventional root locus also shown. The closed-loop natural frequency is presented along branch ① of the Bode root locus, and is read on the logarithmic abscissa scale as $|s|$. On this branch ξ_{CL} is a parameter. At breakaway, where the gain is $|4z^2|_{db}$, the branch ① rendezvous with its mirror image (with which it coincides on the Bode root locus), and the two branches then depart in opposite directions along the real axis as branches ② and ③.



(a) Bode Root Locus



(b) Conventional Root Locus

Fig. 3-28. Bode and Conventional Root Locus for $G(s) = K[(s/z) + 1]/s^2$

Example 4: Unit-numerator third-order system

When the σ -Bode and $j\omega$ -Bode diagrams for the system of Fig. 3-16 are constructed they appear as in Fig. 3-29. The saddle point where the real roots coalesce and then break away, becoming complex conjugates, is recognized as the local minimum of the $|G(-\sigma)|$ diagram where $\angle G(-\sigma) = -180^\circ$. The diagram also shows that at the value of gain where this occurs, the third real root has hardly moved from the open-loop pole. The point where the locus of roots crosses the axis of imaginaries is recognized as the frequency where $\angle G(j\omega)$ is -180° and the gain required is read off by inspection. (This corresponds to the simultaneous satisfaction of the angle and magnitude criteria in the plane containing the axis of imaginaries.)

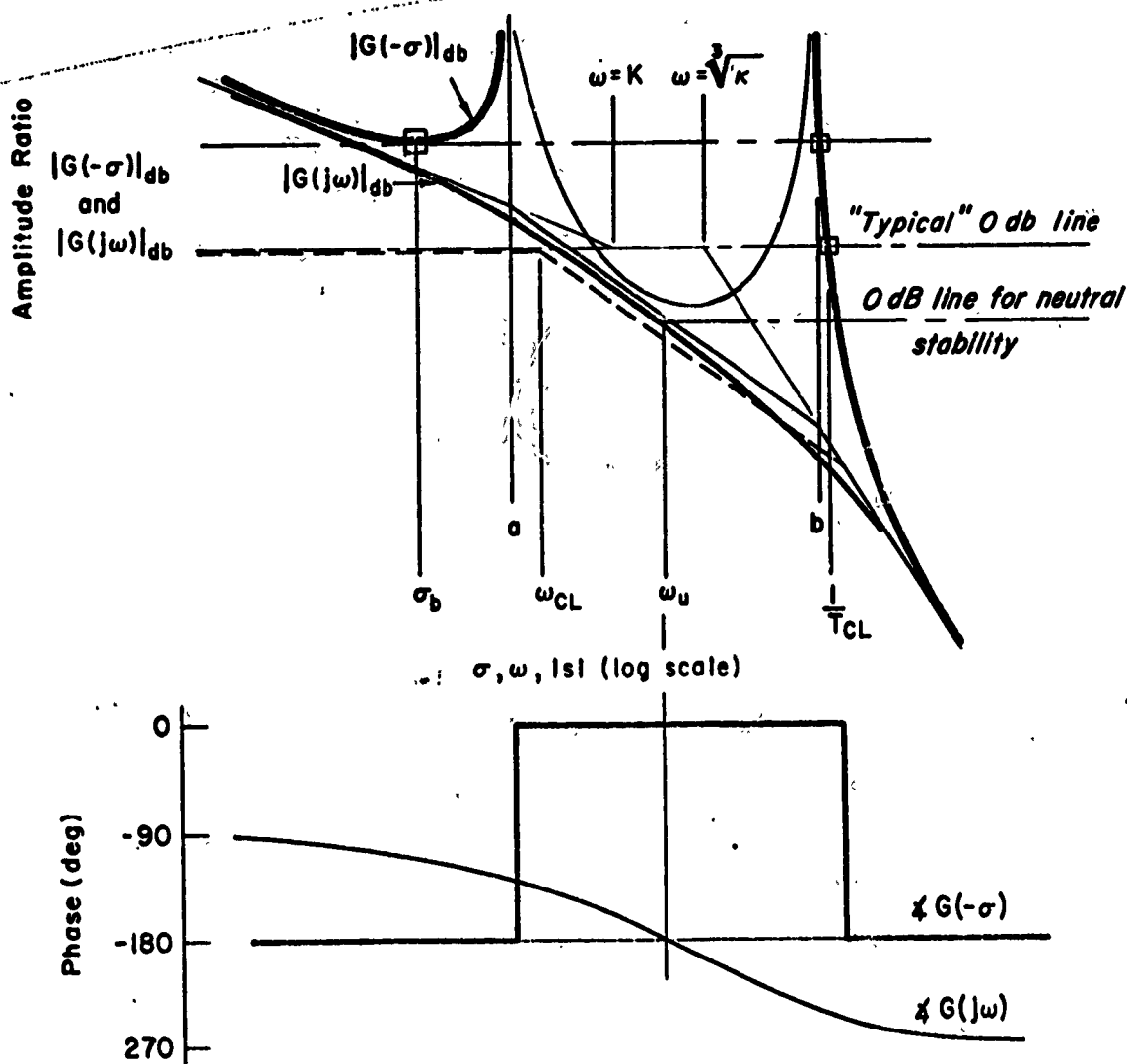


Fig. 3-29. σ -Bode and $j\omega$ -Bode Diagrams;
 $G(s) = K/s[(s/a) + 1][(s/b) + 1]$

The σ -Bode and $j\omega$ -Bode plots show without effort the breakaway points and the condition for marginal stability. These important points are usually only tediously determined by algebraic or root locus methods.

Location of the closed-loop roots for a typical value of the gain may again be determined by decomposition of the closed-loop function. The low frequency asymptote of the closed-loop function lies along the zero-db line and the high frequency asymptote lies along the high frequency asymptote of the open-loop function. At the frequency at which the "typical" zero-db line intersects the $|G(-\sigma)|_{db}$ curve where $\angle G(-\sigma) = -180^\circ$, there is a closed-loop real pole, with magnitude $1/T_{CL}$. The negative slope of the asymptotic approximation therefore changes here by -20 db/decade. Using this change (decrease in slope), the asymptotic approximation can be continued back from the high frequency so as to intersect the low frequency asymptote. This intersection gives the undamped frequency of the closed-loop quadratic factor, ω_{CL} . The damping ratio then may be determined from the sum of the roots formula:

$$\zeta_{CL} = \frac{1}{2\omega_{CL}} \left(a + b - \frac{1}{T_{CL}} \right)$$

Again, the closed-loop roots for a given value of gain are completely determined by simple operations on the logarithmic plots without the necessity of repetitive trial-and-error manipulations. When several such are combined, the Bode root locus of Fig. 3-30 results (here $a=1$ and $b=5$). The branches are again numbered to correspond with the conventional root locus shown in Fig. 3-17.

Now that the several examples have been worked out using both conventional and $G(s)$ logarithmic methods to find root locus plots for the closed-loop system, it should be apparent that, as a practical matter, the feedback analysis problem can be attacked in either way. Each method does, however, present some difficulties when used alone. For instance, the calculation of breakaway points or all the roots compatible with a given gain is tedious in conventional root locus; and the determination of closed-loop quadratic factors using the logarithmic methods can be equally tiresome if decomposition is not completely applicable and auxiliary shifted Bodes must be constructed. Fortunately, the awkward or difficult aspect of one technique is usually a strong point of the other, so the methods tend to be highly supplementary. Consequently, for many practical problems an intermix of techniques often provides the most effective and efficient solution. Since the best combination depends on

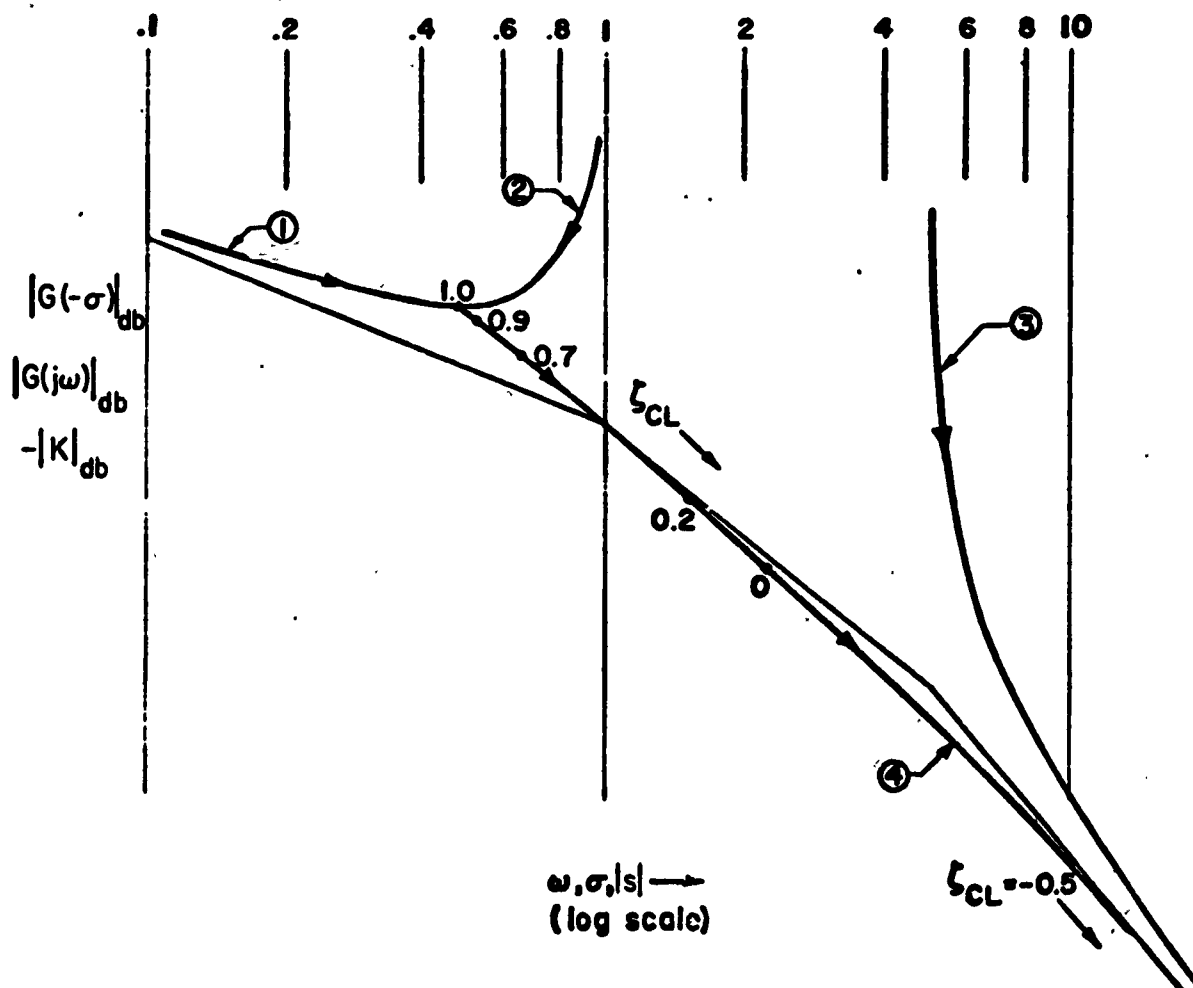


Fig. 3-30. Bode Root Locus for $G(s) = K/s(s+1)((s/5)+1)$

the specifics of a given problem, an example provides the simplest way to illustrate some of the possibilities for joint use.

Example 5:

Consider an an open-loop transfer function given by

$$\begin{aligned}
 G(s) &= \frac{4 \left[\left(\frac{s}{7.5} \right)^2 + \frac{2(0.1)s}{7.5} + 1 \right]}{s \left[\left(\frac{s}{10} \right)^2 + \frac{2(0.1)s}{10} + 1 \right] \left[\left(\frac{s}{15} \right)^2 + \frac{2(0.1)s}{15} + 1 \right]} \\
 &= \frac{1600 [s^2 + 2(0.1)(7.5)s + (7.5)^2]}{s [s^2 + 2(0.1)(10)s + (10)^2] [s^2 + 2(0.1)(15)s + (15)^2]}
 \end{aligned}$$

The first step in the solution for the closed-loop roots is the construction of the asymptotic $|G(s)|_{db}$ plot (Fig. 3-31). The departures from the asymptote of $|G(-\sigma)|_{db}$ are then added, in the immediate region of crossover, to establish the value of the one real root, $\sigma = -4.4$. Portions of the closed-loop asymptotic plot for $|G_{cr}(s)|_{db}$ can then be found. These include:

1. The low frequency asymptote, a—b, which extends from zero to 4.4
2. A mid-frequency asymptote with a -20 db/decade slope, b—c, going from 4.4 to the frequency (7.5) of the complex zeros
3. Another mid-frequency asymptote, starting at c and having a slope of +20 db/decade reflecting the +40 db/decade increment due to the complex zeros
4. The high frequency asymptote, extending back from f with a slope of -60 db/decade

At this stage only one closed-loop factor is known, and only one asymptote (of the two required) is available for each of the two complex pairs remaining to be found. To find the missing intermediate asymptote, by far the simplest procedure is to construct one branch of the root locus, and solve for the root when $\kappa = 1600$ ($K = 4$). This is shown in Fig. 3-32, where the high frequency closed-loop factor is found to be $s^2 - 2(0.123)(16.6)s + (16.6)^2$. The value of 16.6 for the undamped natural frequency establishes the point e on the high frequency asymptote of Fig. 3-31. The final intermediate asymptote is then constructed through e with a slope of -20 db/decade. Its intersection at d with the +20 db/decade asymptote from c determines the value of the final undamped natural frequency, 8.8. This undamped natural frequency can also be found using the product of the roots relationship (Rule 13, Eq. 3-17). The fact that all the roots must sum to -5 per Rule 10 is used to determine a value for the last remaining damping ratio. Thus, the final result for the closed-loop transfer function is

$$G_{cr}(s) = \frac{\left[\left(\frac{s}{7.5} \right)^2 + \frac{2(0.1)s}{7.5} + 1 \right]}{\left(\frac{s}{4.4} + 1 \right) \left[\left(\frac{s}{8.8} \right)^2 + \frac{2(0.267)s}{8.8} + 1 \right] \left[\left(\frac{s}{16.6} \right)^2 - \frac{2(0.123)s}{16.6} + 1 \right]}$$

The closed-loop transfer function obtained using this integrated graphical procedure compares favorably with the more precise version:

$$G_{cr}(s) = \frac{\left[\left(\frac{s}{7.5} \right)^2 + \frac{2(0.1)s}{7.5} + 1 \right]}{\left(\frac{s}{4.32} + 1 \right) \left[\left(\frac{s}{8.81} \right)^2 + \frac{2(0.262)s}{8.81} + 1 \right] \left[\left(\frac{s}{16.39} \right)^2 - \frac{2(0.120)s}{16.39} + 1 \right]}$$

obtained by factoring the characteristic equation. The numerical differences are, of course, due solely to the graphical processes involved and are not fundamental.

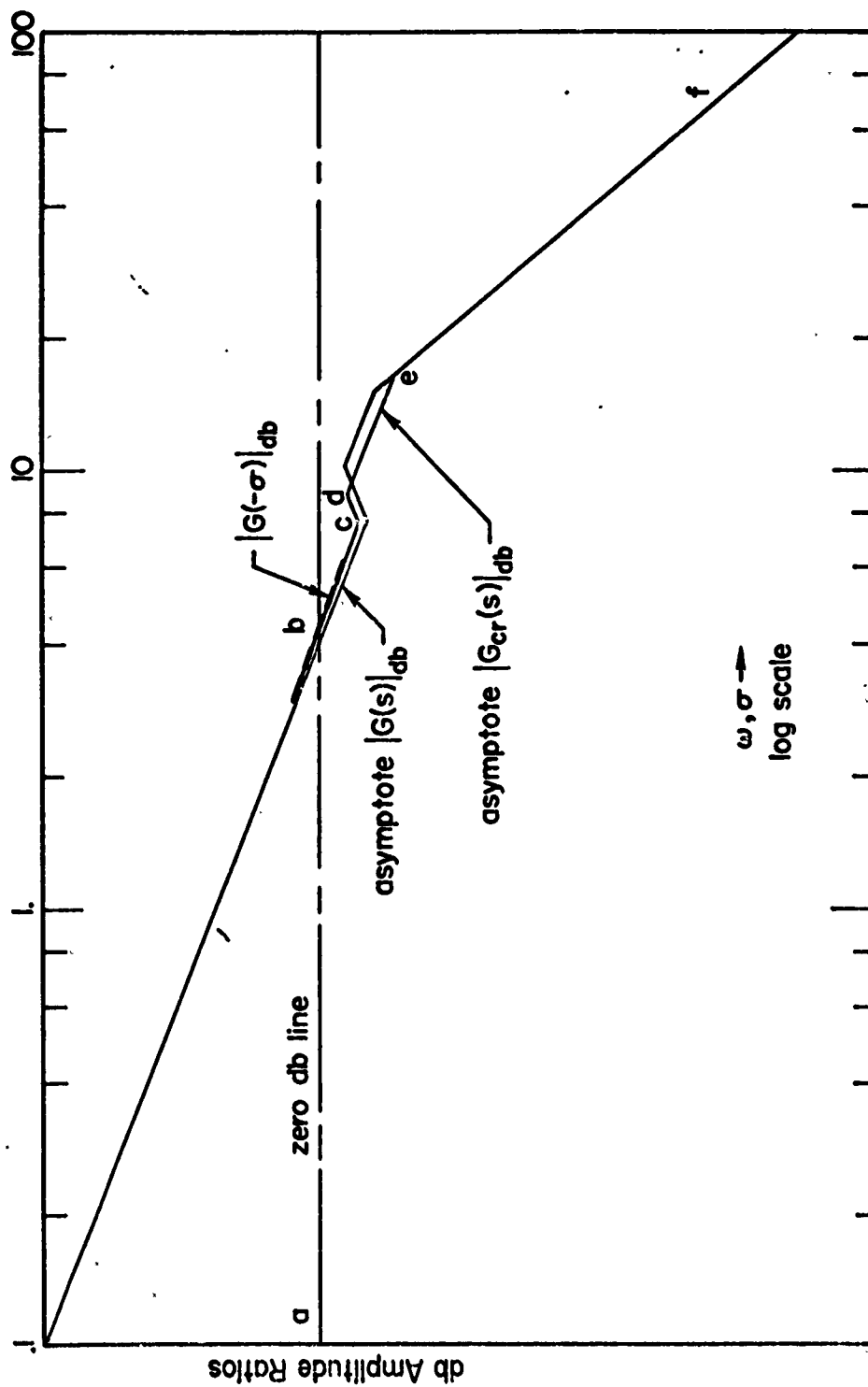


Fig. 3-31. Solution for Closed-Loop Roots for $G(s)$ =
$$\frac{4 \left[\left(\frac{s}{7.5} \right)^2 + \frac{2(0.1)s}{7.5} + 1 \right]}{s \left[\left(\frac{s}{10} \right)^2 + \frac{2(0.1)s}{10} + 1 \right] \left[\left(\frac{s}{15} \right)^2 + \frac{2(0.1)s}{15} + 1 \right]}$$

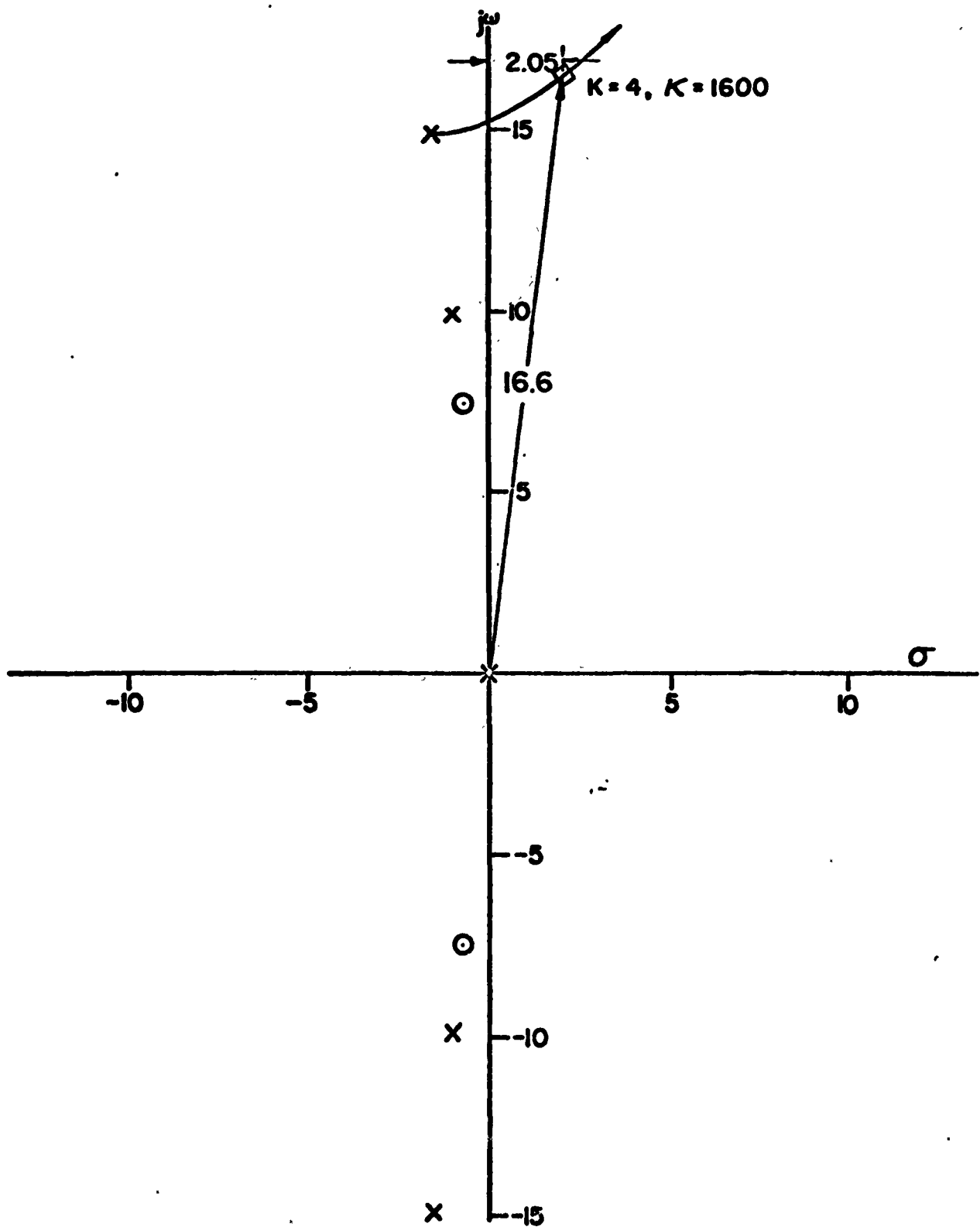


Fig. 3-32. High Frequency Portion of Root Locus for

$$G(s) = \frac{1600[s^2 + 2(0.1)(7.5)s + (7.5)^2]}{s[s^2 + 2(0.1)(10)s + (10)^2][s^2 + 2(0.1)(15)s + (15)^2]}$$

This last example nicely illustrates the efficiency gained by adopting an eclectic viewpoint in which all available feedback system analysis methods are used in concert. It can hardly have escaped the reader that the ties between the conventional root locus and the $G(s)$ logarithmic plots are extremely close. These have been emphasized by the contour maps and the isometric views whose sections would amount to magnitude $G(s)$ logarithmic plots except for the distortions accompanying the use of logarithmic abscissa scales. Such "distortion" is only a matter of convenience to achieve the very valuable asymptotic and symmetric properties exhibited by the $G(s)$ logarithmic plots, and does not constitute anything fundamental.

The common bonds revealed by the various forms of the open-loop transfer function have their origin in potential theory. $G(s)$ may be expressed

$$\begin{aligned} G(s) &= G(\sigma + j\omega) = |G(\sigma, \omega)| e^{j\varphi(\sigma, \omega)} \\ &= U(\sigma, \omega) + jV(\sigma, \omega) \end{aligned} \quad (3-23)$$

where

$$|G(\sigma, \omega)|^2 = U^2(\sigma, \omega) + V^2(\sigma, \omega)$$

$$\varphi(\sigma, \omega) = \tan^{-1} \frac{V(\sigma, \omega)}{U(\sigma, \omega)}$$

and $\ln G(s)$ is given by

$$\ln G(s) = \ln |G(\sigma, \omega)| + j\varphi(\sigma, \omega) \quad (3-24)$$

$G(s)$ is an analytic function for all values of s except those which correspond to poles and zeros. Consequently $G(s)$ and $\ln G(s)$, or their real and imaginary components in Eqs. 3-23 and 3-24, will obey Laplace's equation in the two variables σ and ω in all regions of the s -plane devoid of singularities. Thus,

$$\nabla^2 U(\sigma, \omega) = \frac{\partial^2}{\partial \sigma^2} U(\sigma, \omega) + \frac{\partial^2}{\partial \omega^2} U(\sigma, \omega) = 0$$

$$\nabla^2 V(\sigma, \omega) = 0$$

$$\nabla^2 \ln |G(\sigma, \omega)| = 0$$

$$\nabla^2 \varphi(\sigma, \omega) = 0$$

While $\ln |G(\sigma, \omega)|$ obeys Laplace's equation, $|G(\sigma, \omega)|$ and $e^{j\varphi(\sigma, \omega)}$ do not. This points out the theoretical basis for the use of logarithmic magnitudes in the isometric plots. The fact that Laplace's equation also describes a wide variety of physical phenomena suggests that physical analogies be used to help delineate the connections between the various forms of transfer function representations.*

As one such analogy, consider the s -plane as an infinite sheet of uniformly conducting resistive material. The open-loop poles and zeros can then be represented as point sources and sinks of current, placed at the pole and zero locations, with strength proportional to the order of the pole or zero. At any point s on the sheet the potential $\Phi(s)$, measured with respect to the potential $\Phi(s_0)$ existing at some reference point s_0 , will be

$$\Phi(s) \propto \ln \frac{G(s)}{G(s_0)} \quad (3-25)$$

Similarly, the current, i , flowing across a path between the two points will be

$$i \propto \Phi(s) - \Phi(s_0) \quad (3-26)$$

so that the lines of constant current in the s -plane correspond to lines of constant phase.

*V. C. M. Yeh, "Synthesis of Feedback Control Systems by Gain-Contour and Root-Contour Methods," Trans. AIEE, Pt. II, Vol. 75, 1956, pp. 85-95.

P. J. Daniell, Analogy Between the Interdependence of Phase-Shift and Gain in a Network and the Interdependence of Potential and Current Flow in a Conducting Sheet, Ref. B39, Ministry of Supply Servo Library, 1942.

A. R. Boothroyd and J. H. Westcott, "The Application of the Electrolytic Tank to Servo-mechanism Design," Automatic and Manual Control, ed. A. Tustin, Butterworths Scientific Pub., London, 1952, pp. 87-103.

M. W. Fossier and H. A. Rosen, "A Field-Mapping Method for Analysis and Synthesis of Linear Closed-Loop Systems," J. IAS, Vol. 20, Mar. 1953, pp. 205-209.

H. S. Tsien, Engineering Cybernetics, McGraw-Hill Book Co., Inc., New York, 1954, pp. 46-58.

Applying this analogy to the elementary third-order system, the three poles would be represented as unit sources of current located at $s=0$, $-a$, and $-b$, as shown in Fig. 3-33. This figure also shows the results which would be obtained by measuring the potential along the σ and $j\omega$ axes, and along the line $s = (\xi + j\sqrt{1-\xi^2})\mu$. From Eq. 3-25 it is apparent that these potential functions are proportional to the open-loop logarithmic amplitude ratio plots for $s = \sigma$, $j\omega$, and $(-\xi + j\sqrt{1-\xi^2})|s|$, except that the abscissa is in linear rather than logarithmic units. They correspond directly to sections through the surface of Fig. 3-19. Lines of constant potential form the constant gain lines on the contour map of Fig. 3-18, and the isoargument curves, or lines of constant phase, correspond to constant current flow lines.*

3.4 SIMPLIFIED SYSTEM CHARACTERISTICS AND LITERAL APPROXIMATE FACTORS

In almost all flight control problems the open-loop transfer functions are of very high order, with $m+n$ seldom less than four, more often of the order of ten, and occasionally as large as twenty or thirty. The techniques described in the previous sections still apply and, in fact, are in everyday use in the analytical design of flight control systems. But inevitably the price of complexity in analyses is a reduction in the physical appreciation of the essential nature of a problem, and an accompanying diminished insight into potential solutions. Fortunately there are two counters available. These are the concept of the simplified or equivalent system and that of literal approximate factors. Both concepts can be converted into practical reality by the application of the feedback analysis techniques summarized above.

A simplified system is, in essence, a lower order approximation to a higher order system which is valid for specifiable conditions. Literal approximate factors are approximate expressions for transfer function

*Similar analogies can be made with fluid dynamic, gravitational, magnetostatic, elastic, or electrostatic potential problems. For two-dimensional irrotational flow of an incompressible fluid, for example, the poles and zeros are again sources and sinks, $\ln |G(\sigma, \omega)|$ is the potential function, and $\phi(\sigma, \omega)$ is the stream function. Phase loci become streamlines, and the root locus is the one-half streamline.

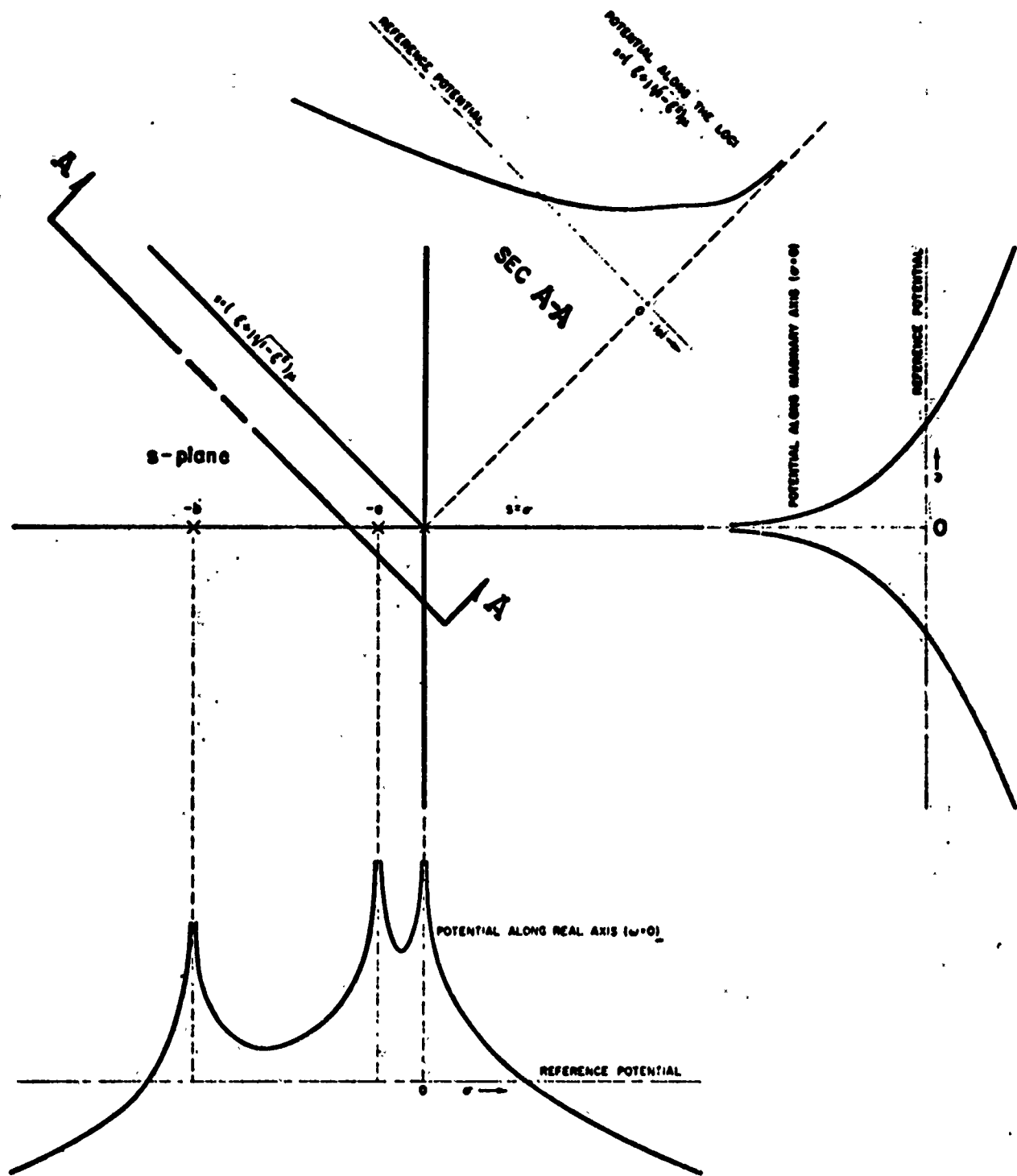


Fig. 3-33. Potential Surveys Along Various Lines in the s -Plane

poles and zeros in terms of the basic parameters of the system, defined only as symbols rather than as numbers. Their most important application in flight control is for aircraft transfer functions, for which the approximate factors are expressions which relate the poles and zeros with the stability derivatives and inertial properties of the vehicle. Typical examples of simplified systems and approximate factors will be described below to introduce the key notions; many other examples will follow throughout this book.

Simplified or Equivalent Systems

As long ago as 1939 the feedback systems analysis pioneer, H. W. Bode, considered two central concepts in his mathematical definition of feedback. The first was the idea of a loop transmission, or return of output to input measured by a "return difference"; and the second was "sensitivity," or effective reduction of open-loop system variations when seen in a closed-loop context. On the surface, these two concepts might be considered as a cause-effect pair, but both are equally fundamental in either an analytical or physical sense. In fact, Bode's "mathematical definition of feedback"* had the two entities the inverse of one another, and subsequent writers have redefined "sensitivity" so that it, as a physical measure, is identical to the "return difference." The point of bringing this up is not to give a history of feedback system definitions, but instead to focus attention on sensitivity as a fundamental concept inseparable from feedback systems. In a gross sense, if there is no reduction in the effects of open-loop system variations on closed-loop behavior, there is no feedback worthy of mention; whereas large feedback can reduce such effects to negligible levels. This limiting case of large feedback leads directly to the equivalent system concept, for if changes in certain open-loop parameters have no appreciable effect on closed-loop behavior, the open-loop system can be replaced by simpler, albeit approximate, descriptions which yield substantially the same closed-loop results.

*H. W. Bode, Network Analysis and Feedback Amplifier Design, D. Van Nostrand Co., Inc., New York, 1945.

To make these remarks more concrete, consider the elementary feedback system shown in Fig. 3-34:

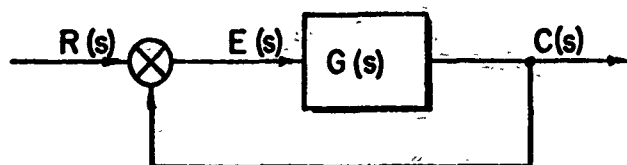


Fig. 3-34. Elementary Feedback System

The closed-loop transfer function, $G_{cr}(s)$, is given in terms of the open-loop transfer function by

$$G_{cr}(s) = \frac{C(s)}{R(s)} = \frac{G(s)}{1 + G(s)} \quad (3-27)$$

The classical "sensitivity" function, $S_G^{G_{cr}}(s)$, which measures the relative effects of open- and closed-loop changes, is (where $G_{cr}(s)$ and $G(s)$ are analytic),

$$S_G^{G_{cr}}(s) = \left[\frac{\frac{dG_{cr}(s)}{G_{cr}(s)}}{\frac{dG}{G}} \right] = \frac{1}{1 + G(s)} \quad (3-28)$$

It provides a comparison between the relative change in closed-loop characteristics and the causative relative change in open-loop characteristics. Now, when feedback is really operable, sensitivity, from the discussion in the paragraph above, must be very small, i.e., the percentage change in closed-loop characteristics must be much less than the percentage change in open-loop characteristics. This implies that $G(s)$ is very large, which also implies that

$$G_{cr}(s) \doteq 1, \quad |G(s)| \gg 1 \quad (3-29)$$

When this condition applies the closed-loop $G_{cr}(s)$ is insensitive to the precise form of $G(s)$ in the region of s where $|G(s)| \gg 1$, so the actual $G(s)$ could conceivably be replaced by a simpler form in this region. On the other

hand, when $|G(s)|$ is not large relative to one, the sensitivity approaches one, $G_{cr}(s)$ approaches $G(s)$, and such a replacement cannot be made. All of these esoteric remarks amount to the obvious, i.e., that

$$G_{cr}(s) \begin{cases} \doteq 1 & \text{when } s \text{ is such that } |G(s)| \gg 1 \\ = \frac{G(s)}{1 + G(s)} & \text{when } s \text{ is such that } |G(s)| = O(1) \\ \doteq G(s) & \text{when } s \text{ is such that } |G(s)| \ll 1 \end{cases} \quad (3-30)$$

Viewed another way, the relationships of Eq. 3-30 essentially partition the s domain into regions where $G(s)$ needs to be specified with little accuracy ($|G(s)| \gg 1$), or fairly good accuracy [$|G(s)| = O(1)$ or less] if the closed-loop $G(s)$ is to be known to a reasonable approximation.

This function of feedback can be used to reduce the analytical complexity of practical problems. The basic idea is to replace the actual controlled-element transfer function (or equation) with a far simpler approximate transfer function (or set of equations) which would yield approximately the same closed-loop results. The simpler—"equivalent" system would then be suitable for use in many calculations.

To illustrate the procedure for equivalent system evolution, consider the concrete example of a high performance pitch attitude autopilot. As will be more thoroughly described in later chapters, the vehicle transfer function and a sensor-controller transfer function might be described by the following open-loop transfer function:

$$G(s) = K \left\{ \underbrace{\frac{(T_{\theta_1}s + 1)(T_{\theta_2}s + 1)}{\left[\left(\frac{s}{\omega_p} \right)^2 + \frac{2\zeta_p s}{\omega_{sp}} + 1 \right]}}_{\text{Phugoid}} \underbrace{\left[\left(\frac{s}{\omega_{sp}} \right)^2 + \frac{2\zeta_{sp}s}{\omega_{sp}} + 1 \right]}_{\text{Short Period}} \right\} \underbrace{\left\{ \frac{\overbrace{(T_E s + 1)}^{\text{Equalization}}}{\underbrace{\left[\left(\frac{s}{\omega_\sigma} \right)^2 + \frac{2\zeta_\sigma s}{\omega_\sigma} + 1 \right]}_{\text{Sensor and Servo Actuator}}} \right\}}_{\text{Controller}} \quad (3-31)$$

Vehicle Dynamics Controller

Open-loop $G(j\omega)$ and $G(-\sigma)$ Bode diagrams of this system are shown in Fig. 3-35, with values for equalization, $1/T_E$, and open-loop gain set within ranges compatible with a "good" system. The complete open-loop system amounts to a controlled element (vehicle plus controller) equation of order six. By the direct decomposition technique of Unified Servo Analysis, the closed-loop transfer function will be

$$G_{cr}(s) = \frac{K}{1+K} \frac{(T_{\theta_1}s + 1)(T_{\theta_2}s + 1)(T_Es + 1)}{(T'_{\theta_1}s + 1)(T'_{\theta_2}s + 1)(T'_Es + 1)(T_cs + 1) \left[\left(\frac{s}{\omega_\sigma} \right)^2 + \frac{2\zeta'_\sigma s}{\omega_\sigma} + 1 \right]} \quad (3-32)$$

For the condition shown, the closed-loop denominator factor $(T'_{\theta_1}s + 1)$ is very close to the numerator factor $(T_{\theta_1}s + 1)$.

If K is much greater than one, the amplitude ratio in the entire frequency region to the left of about $1/T_{\theta_2}$ will be much greater than one (and, in particular, $|G(j\omega_p)| \gg 1$). This suggests that the open-loop system could be approximated by the transfer function

$$G_1(s) = \frac{KT_{\theta_1}\omega_p^2(T_{\theta_2}s + 1)(T_Es + 1)}{s \left[\left(\frac{s}{\omega_{sp}} \right)^2 + \frac{2\zeta_{sp}s}{\omega_{sp}} + 1 \right] \left[\left(\frac{s}{\omega_\sigma} \right)^2 + \frac{2\zeta_\sigma s}{\omega_\sigma} + 1 \right]} \quad (3-33)$$

The closed-loop transfer function formed from this equivalent system, $|G_1/(1 + G_1)|$, will be almost identical to the exact closed-loop transfer function given by Eq. 3-32. The major difference will be that the closed-loop d.c. gain is 1 instead of $K/(1 + K)$, and the nearly canceling dipole pair, $(T_{\theta_1}s + 1)/(T'_{\theta_1}s + 1)$, will not appear at all. When $|K|_{db}$ is 20 db or so these effects are trivial. The equivalent system is of order 5, which is one step in the right direction.

A further step can be taken by noting that the complete closed-loop system denominator factors $(T'_{\theta_2}s + 1)$ and $(T'_Es + 1)$ are not far removed from the numerator factors $(T_{\theta_2}s + 1)$ and $(T_Es + 1)$. Their proximity makes them act as dipole effects in the closed-loop system response, i.e., the modal response

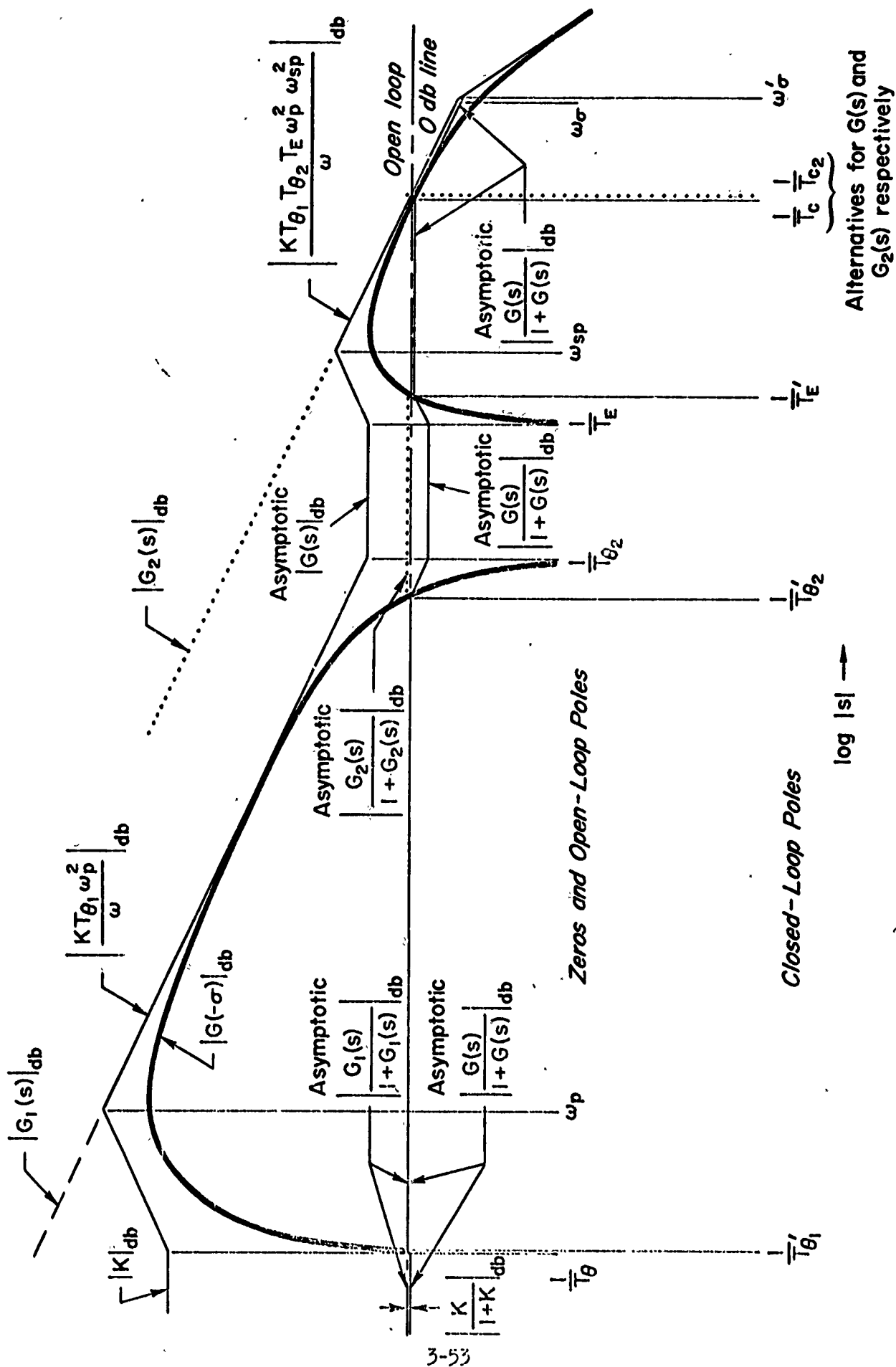


Figure 3-35. Open- and Closed-Loop Asymptotic Plots
Illustrating the Development of Equivalent Systems

coefficients for the modes corresponding to $T_{\theta 2}'$ and T_E' are relatively small because of the proximity of these time constants to $T_{\theta 2}$ and T_E , respectively. Thus these modes in the closed-loop system response will be minor, if not negligible. To the extent that they can be ignored, a further equivalent system can be defined. This will be

$$G_2(s) = \frac{KT_{\theta 1}T_{\theta 2}T_E\omega_p^2\omega_{sp}^2}{s\left[\left(\frac{s}{\omega_\sigma}\right)^2 + \frac{2\zeta_\sigma s}{\omega_\sigma} + 1\right]} \quad (3-34)$$

Equation 3-34 is a striking reduction in dimensions to three. The resulting closed-loop transfer function will be

$$\frac{G_2}{1 + G_2} = \frac{1}{(T_{c1}s + 1)\left[\left(\frac{s}{\omega_{\sigma 1}'}\right)^2 + \frac{2\zeta_{\sigma 1}' s}{\omega_{\sigma 1}'} + 1\right]} \quad (3-35)$$

Except for the absence of the two dipoles and the very low frequency effects, this closed-loop transfer function differs from that of Eq. 3-32 primarily in that T_{c1} will be slightly greater than T_c , and $\omega_{\sigma 1}'$ slightly less than ω_σ' . However, the range of validity based on use of Eq. 3-34 will be considerably narrower than that based on the higher order equivalent system approximation given by Eq. 3-34.

For some problems the equivalent systems given by Eqs. 3-33 and 3-34 can be further simplified. For low-pass inputs the major gross effect of the highest frequency modes, assuming that they are well beyond the crossover frequency, is an initial time delay. This can be approximated by noting that all high frequency leads and lags having break points beyond a given frequency affect the characteristics below that frequency primarily in the phase shift. Thus, if the actual system's high frequency characteristics are

$$G_{hi}(s) = \frac{\prod_{i=1}^n (T_i s + 1)}{\prod_{i=1}^m (\tau_i s + 1)} \quad (3-36)$$

the contributions of these terms to the amplitude ratio and phase at frequencies, ω , much less than $1/T_i$ and $1/\tau_i$ are

$$|G_{hi}(j\omega)| = \frac{\prod_{i=1}^n \sqrt{(T_i\omega)^2 + 1}}{\prod_{i=1}^m \sqrt{(\tau_i\omega)^2 + 1}} \doteq 1$$

$$\angle G_{hi}(j\omega) = \sum_{i=1}^n \tan^{-1} T_i\omega - \sum_{i=1}^m \tan^{-1} \tau_i\omega \quad (3-37)$$

$$\doteq \sum_{i=1}^n T_i\omega - \sum_{i=1}^m \tau_i\omega = \omega \left[\sum_{i=1}^n T_i - \sum_{i=1}^m \tau_i \right]$$

These are the same contributions as those of a pure time delay, $e^{j\omega\tau}$, where $\tau = \sum T_i - \sum \tau_i$. That is, for low frequency equivalence the delay τ is just the sum of the high frequency leads minus the sum of the high frequency lags. For the illustrative case, the servo is the only term for which this type of approximation might apply. In this case τ would be $-2\zeta_\sigma/\omega_\sigma$, so the equivalent systems, for low-pass inputs, could be further reduced to

$$G_1(s) \doteq \frac{(KT\theta_1\omega_p^2)(T\theta_2s + 1)(T_Es + 1)}{s \left[\left(\frac{s}{\omega_{sp}} \right)^2 + \frac{2\zeta_{sp}s}{\omega_{sp}} + 1 \right]} e^{-(2\zeta_\sigma/\omega_\sigma)s} \quad (3-38)$$

and

$$G_2(s) \doteq \frac{(KT\theta_1 T\theta_2 T_E \omega_p^2 \omega_{sp}^2)}{s} e^{-(2\zeta_\sigma/\omega_\sigma)s} \quad (3-39)$$

Having gone to this extreme, one further step is easy to take to obtain an even lower order set of systems formed by neglecting the minor high frequency effects entirely. This will often lead to better approximations than the fairly major shift from the first to the second equivalent systems in the first place. In other words, the $G_1(s)$ shown in Eq. 3-38 without the $e^{-(2\zeta_\sigma s/\omega_\sigma)}$ term will ordinarily be a better approximation to reality (and of no higher

order) then the $G_2(s)$ shown in Eq. 3-34. Indeed, a form

$$G_1(s) = \frac{(KT_{\theta_1} \omega_p^2)(T_{\theta_2}s + 1)(T_Es + 1)}{s \left[\left(\frac{s}{\omega_{sp}} \right)^2 + \frac{2\zeta_{sp}s}{\omega_{sp}} + 1 \right]}$$

is ordinarily a very good approximation for problems of pitch attitude control.

Literal Approximate Factors

Transfer functions are totally specified, with the exception of a multiplying constant, by their poles and zeros. The poles and zeros are functions of the system's constants, and are therefore directly affected by changes in any of the constants. Because of the intimate relationships between poles and zeros and the system constants, an extremely important prerequisite to a rational system design is an understanding of the effects of changes in the physical system configuration (as reflected by the system constants) on the transfer function poles and zeros. Unfortunately, in complex systems the transfer functions are made up of ratios of higher order rational polynomials which are difficult to factor in general and meaningful terms. In airframe transfer functions, for example, the polynomials involved are largely of third or fourth order, having coefficients which are complicated functions of the stability derivatives. The usual approach to determination of the effect on aircraft motions of varying the airframe configuration requires numerical values for the derivatives and is ordinarily a time-consuming and irksome computational task. To alleviate this situation we would like to have some relatively simple, albeit approximate, expressions for the poles and zeros in terms of literal aircraft stability derivatives. But the derivation of approximate factors depends very strongly on the relative magnitudes and signs of the various polynomial coefficients, making approximations difficult to determine and the degree of approximation difficult to assess. One way out of this seeming quandary is the use of servo analysis methods where, in general:

1. An algebraic equation can be manipulated to have the form of a feedback system with:

- a. The open-loop transfer function given by $G(s)$
- b. The closed-loop transfer function given by $G(s)/[1 + G(s)]$
- c. The characteristic equation $1 + G(s) = 0$, identical to the original algebraic equation

Then,

2. All of the servo-type methods for solving for the roots of $1 + G(s) = 0$ from a knowledge of $G(s)$ are applicable to the determination of factors for the algebraic equation.

and, in particular,

3. A Bode plot representation, where wide regions of a graphical representation of $G(s)$ can be approximated by asymptotes having simplified equations, can be invaluable. The asymptotic and other properties of the Bode plot make the regions where simple approximate solutions apply quite clear. Further, since exact solutions are possible using the plot, the degree of error involved in a particular case is readily determined.

Although a quadratic is trivially simple, it will serve to illustrate the details of this "equivalent servo" technique for approximate factoring. Many more complex examples appear elsewhere.*

The second-order equation

$$s^2 + 2\zeta\omega_n s + \omega_n^2 = 0$$

can, of course, be factored exactly, i.e.,

$$(s + \zeta\omega_n + \omega_n\sqrt{\zeta^2 - 1})(s + \zeta\omega_n - \omega_n\sqrt{\zeta^2 - 1}) = 0$$

When dealing with transfer functions containing second-order terms with $\zeta < 1$, the unfactored form is usually suitable as is, while the factored form is called for when $\zeta > 1$. When $\zeta^2 \gg 1$, the factors become

*I. L. Ashkenas and D. T. McRuer, Approximate Airframe Transfer Functions and Application to Single Sensor Control Systems, WADC-TR-58-82, June 1958.

approximately

$$\left[s + \zeta\omega_n + \zeta\omega_n \left(1 - \frac{1}{2\zeta^2} + \dots \right) \right] \left[s + \zeta\omega_n - \zeta\omega_n \left(1 - \frac{1}{2\zeta^2} + \dots \right) \right]$$

$$\doteq \left[s + \left(2\zeta\omega_n - \frac{\omega_n}{2\zeta} \right) \right] \left(s + \frac{\omega_n}{2\zeta} \right)$$

which, as ζ becomes larger still, approaches $(s + 2\zeta\omega_n)s$. The degree of adequacy of these various approximations can be seen readily by considering the second-order equation as the characteristic equation of the closed loop system shown in Fig. 3-36.

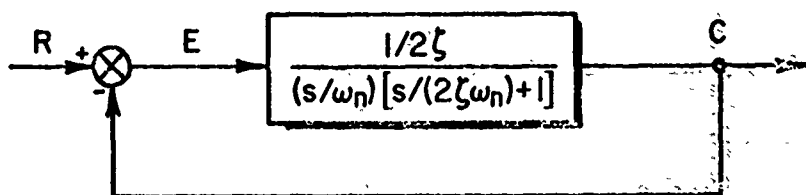


Fig. 3-36. Closed-Loop System with Closed-Loop Transfer Function $\left[(s/\omega_n)^2 + (2\zeta s/\omega_n) + 1 \right]^{-1}$

Because only the real roots will be of interest here, only the σ -Bode need be used. This is shown in Fig. 3-37, with the abscissa normalized to σ/ω_n . For $\zeta > 0$ the phase, although not shown, will be -180° over the range $0 \leq \sigma/\omega_n \leq 2\zeta$. Relating this plot to the previous approximations, one can readily see that any value of the "gain," $1/2\zeta$, which results in an intersection of the zero-db line with the amplitude ratio curve when it is near the low frequency asymptote will give a root magnitude which is approximately

$$\frac{1}{2\zeta} \frac{\omega_n}{\sigma_1} \doteq 1 \quad \text{or} \quad \sigma_1 = \frac{\omega_n}{2\zeta}$$

Also, the magnitude of the larger root can be seen to approach $\sigma_2/\omega_n = 2\zeta$ as ζ becomes very large (gain very small). Since the system total damping, $2\zeta\omega_n$, is constant, the sum of the two real closed-loop roots must always be $-2\zeta\omega_n$; therefore the magnitude of the second root will be given by

$$\sigma_2 \doteq 2\zeta\omega_n - \frac{\omega_n}{2\zeta}$$

as long as an intersection of the zero-db line and the amplitude ratio occurs near the low frequency asymptote. The error involved in the approximate roots becomes increasingly larger as the intersections of the amplitude ratio and the zero-db line depart further from the low frequency asymptote. The error will be a maximum at open-loop gains where $\zeta=1$, i.e., at the breakaway condition. The exact root magnitudes in this case are both ω , while reliance on the approximations would give $\sigma_1 = \omega/2$ and $\sigma_2 = 3\omega/2$. In all cases it should be noted that the errors involved in the use of the approximate roots can always be determined readily by noting the departure of the actual amplitude ratio from the asymptotic plot at the point of intersection.

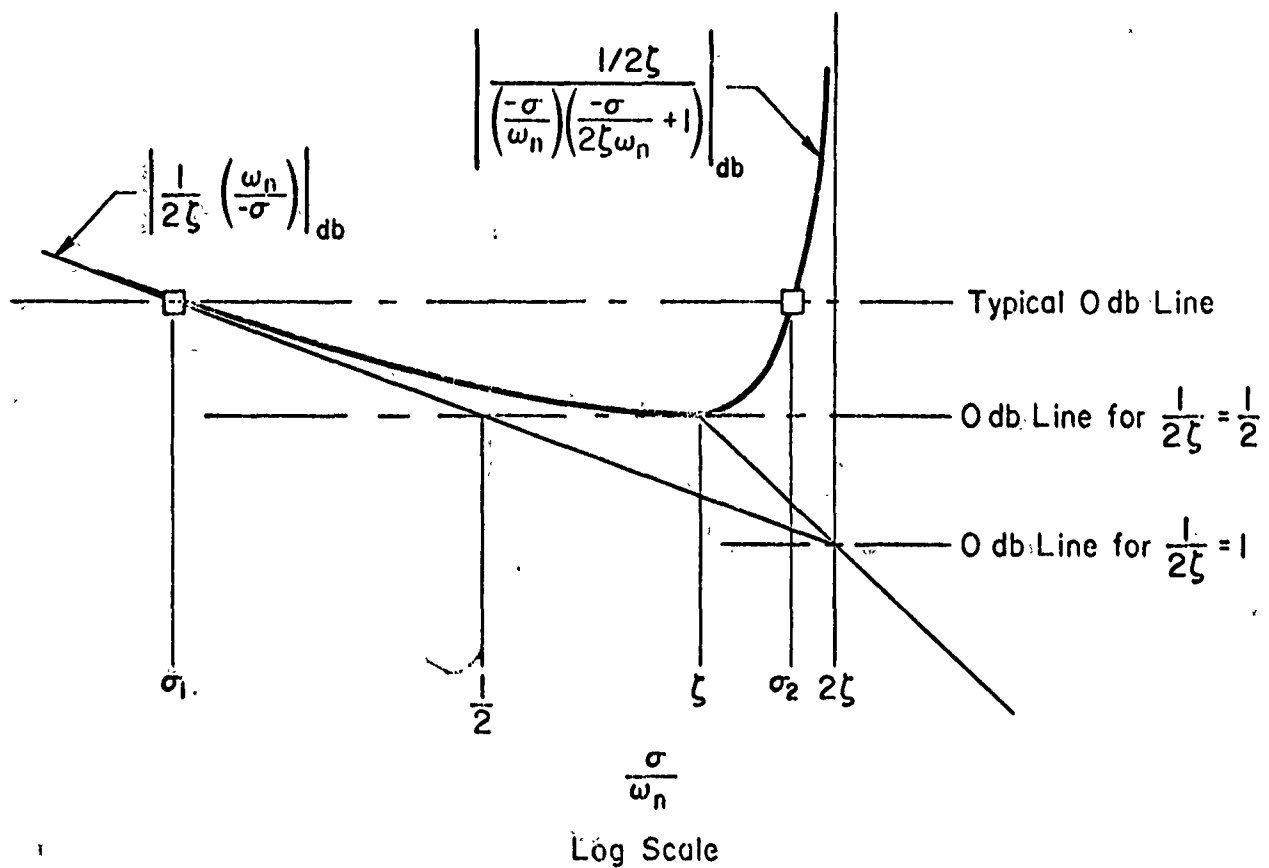


Fig. 3-37. σ -Bode Diagram for $G(s/\omega_n) = \frac{(1/2\zeta)}{(s/\omega_n) [(1/2\zeta)(s/\omega_n) + 1]}$

3.5 ANALYSIS OF MULTILoop VEHICULAR CONTROL SYSTEMS

It often happens in the design of feedback control systems for vehicles that the system cannot be conveniently represented by single-loop block diagrams. Until comparatively recently, this made the pencil-and-paper analysis of vehicular control systems either oversimplified or entirely too difficult, and the most usual approach to the design of multiloop systems was repetitive analysis using the analog computer as a tool. Complete dependence on an analog computer, however, does have deficiencies. First, because of the dominance of only particular modes in the time histories, modes which might be of great importance under slightly changed conditions may be effectively suppressed. Then not only will these modes tend to be overlooked, but their variation with the governing parameters will be difficult to evaluate; accordingly some understanding of the over-all performance of the system is lost. Second, elements described only in frequency response terms, such as subsystem and human pilot describing functions, cannot be used directly in computer operations. Third, and perhaps most important, all problems solved by computer can provide only specific results which, in the absence of a suitable theory, cannot be readily and effectively extrapolated to different conditions or generalized. Thus gross trends and grand simplifications are harder to come by, insight is constricted, and initiative is stifled, as always happens when only a single approach to a problem is used.

To surmount these deficiencies we should like to have a multiloop analysis technique with the following properties:

- A formulation which clearly displays vehicle-alone and controller-alone characteristics in conventional and well-understood terms
- Analytical operations which can be performed using the most efficient graphical techniques of servoanalysis so as to enhance transfer of skill and intuition from the simpler single-loop situations
- Sequences and procedures which are highly responsive to physical insights and intuition so as to lead to "good" systems with a minimum of iteration
- A presentation of results which is supplementary as well as equivalent to the results obtained using an analog computer.

The elements of such an analytical technique are presented below for a fairly simple case. Detailed developments for more complex systems are given elsewhere,* and specific examples which elucidate the use of the method are deferred to later chapters.

A generalized notation for vehicle and controller transfer characteristic quantities is introduced and used throughout this development. A compact matrix formation is appropriate for multiloop problems, and this is employed from the outset; but, to make the developments easier to follow, explicit equations in matrix form are used concurrently with the more compact matrix generalizations. This makes possible an inductive approach wherein the matrix equations are both a shorthand for the equations of relatively simple systems and, viewed more broadly, the appropriate equations for far more complex systems.

Development of Closed-Loop Transfer Functions for Multiloop Systems

A multiloop vehicular control system which is relatively simple, yet complex enough for our present purposes, is shown in the block diagram of Fig. 3-38. It consists of a vehicle and control equipment comprising sensing, equalizing, and actuating elements. The vehicle has three independent degrees of freedom, and is subject to control forces and moments applied by two control deflections and an external disturbance. The control deflections are functions of a command input and feedbacks from two of the three degrees of freedom.

The Laplace-transformed linearized equations of motion of the vehicle can be written in matrix form as

$$\begin{bmatrix} a_{11}(s) & a_{12}(s) & a_{13}(s) \\ a_{21}(s) & a_{22}(s) & a_{23}(s) \\ a_{31}(s) & a_{32}(s) & a_{33}(s) \end{bmatrix} \begin{bmatrix} X_1(s) \\ X_2(s) \\ X_3(s) \end{bmatrix} = \begin{bmatrix} b_{11}(s) & b_{12}(s) \\ b_{21}(s) & b_{22}(s) \\ b_{31}(s) & b_{32}(s) \end{bmatrix} \begin{bmatrix} \delta_1(s) \\ \delta_2(s) \end{bmatrix} + \begin{bmatrix} e_{11}(s) & e_{12}(s) \\ e_{21}(s) & e_{22}(s) \\ e_{31}(s) & e_{32}(s) \end{bmatrix} \begin{bmatrix} \eta_1(s) \\ \eta_2(s) \end{bmatrix} \quad (3-40)$$

*D. T. McRuer, I. L. Ashkenas, and H. R. Pass, Analysis of Multiloop Vehicular Control Systems, ASD-TDR-62-1014, Wright-Patterson Air Force Base, Ohio, Mar. 1964.

or, more compactly,

$$[A(s)][X(s)] = [B(s)][\delta(s)] + [E(s)][\eta(s)] \quad (3-41)$$

The a_{ij} , b_{ij} , and e_{ij} are, in general, functions of s and the vehicle characteristics (stability derivatives), but to go along with the economy of notation of matrix methods, the functional dependence on s of these quantities and the various transfer functions is not indicated in the remainder of this section.

The vehicle transfer functions for control or disturbance inputs are found from Eq. 3-40 by Cramer's rule. Typical examples are:

$$\frac{x_1}{\delta_1} = \frac{N_{\delta_1}^{x_1}}{\Delta} = \frac{\begin{vmatrix} b_{11} & a_{12} & a_{13} \\ b_{21} & a_{22} & a_{23} \\ b_{31} & a_{32} & a_{33} \end{vmatrix}}{\begin{vmatrix} a_{11} & a_{12} & a_{13} \\ a_{21} & a_{22} & a_{23} \\ a_{31} & a_{32} & a_{33} \end{vmatrix}} \quad (3-42)$$

$$\frac{x_2}{\delta_1} = \frac{N_{\delta_1}^{x_2}}{\Delta} = \frac{1}{\Delta} \begin{vmatrix} a_{11} & b_{11} & a_{13} \\ a_{21} & b_{21} & a_{23} \\ a_{31} & b_{31} & a_{33} \end{vmatrix} \quad (3-43)$$

In these transfer functions Δ is the determinant of the coefficients of the left side (characteristic determinant of the vehicle),

$$\Delta = \begin{vmatrix} a_{11} & a_{12} & a_{13} \\ a_{21} & a_{22} & a_{23} \\ a_{31} & a_{32} & a_{33} \end{vmatrix} \quad (3-44)$$

and the numerator, $N_{\delta_j}^{x_i}$, is obtained by replacing the column of x_1 coefficients in Δ by the column of δ_j coefficients from the right side of Eq. 3-40.

From the block diagram the controller characteristics are seen to

be

$$\begin{bmatrix} \delta_1(s) \\ \delta_2(s) \end{bmatrix} = \begin{bmatrix} 0 & 0 \\ G_{21c} & 0 \end{bmatrix} \begin{bmatrix} x_{1c} \\ x_{2c} \end{bmatrix} - \begin{bmatrix} 0 & G_{12} & 0 \\ G_{21} & 0 & 0 \end{bmatrix} \begin{bmatrix} x_1 \\ x_2 \\ x_3 \end{bmatrix} \quad (3-45)$$

or

$$[\delta] = [G_c][X_c] - [G][X] \quad (3-46)$$

where $[G_c]$ will be called the command matrix and $[G]$ the feedback matrix. The subscript convention used to identify the components of G is that the first number identifies the controller output (control surface); the second number the controller input (sensed motion quantity). Equations 3-41 and 3-46 can be depicted as the deceptively simple matrix block diagram shown in Fig. 3-39.

Substituting Eq. 3-46 into Eq. 3-41 gives

$$\begin{aligned} [A][X] &= [B][\delta] + [E][\eta] \\ &= [B]\{[G_c][X_c] - [G][X]\} + [E][\eta] \end{aligned}$$

Collecting like terms,

$$\{[A] + [B][G]\}[X] = [B][G_c][X_c] + [E][\eta] \quad (3-47)$$

and, after premultiplying by the inverse of $\{[A] + [B][G]\}$, the explicit expression for $[X]$ becomes

$$[X] = \{[A] + [B][G]\}^{-1} \{[B][G_c][X_c] + [E][\eta]\} \quad (3-48)$$

Equation 3-48 is the formal matrix solution for the transform of the outputs of the closed-loop system. It is not restricted to the equations of the example, but is, in fact, applicable to systems with larger or smaller matrices.

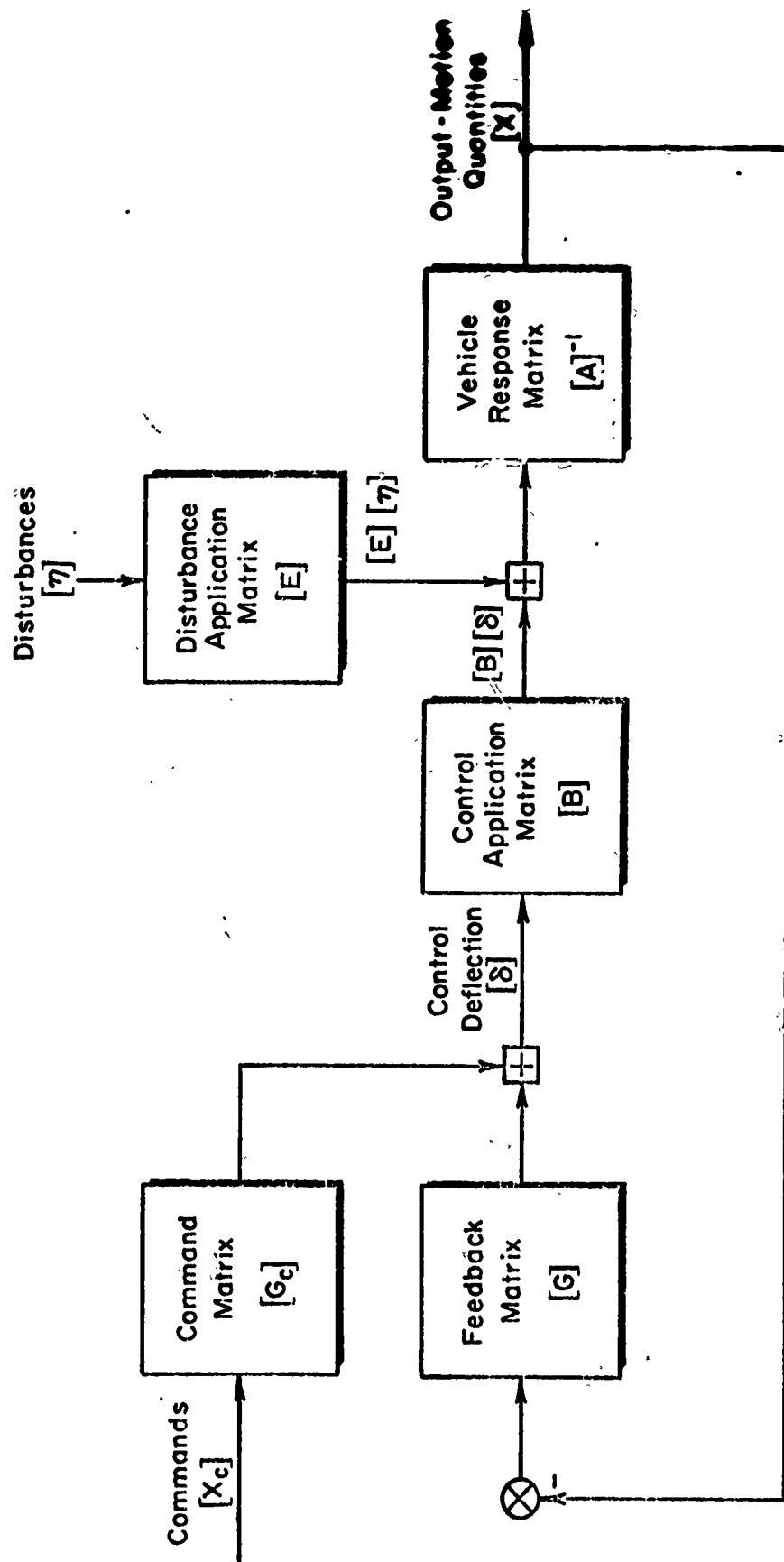


Fig. 3-59. Matrix Block Diagram for General Multiloop Control System

The determinant of the coefficients of the matrix expression $\{[A] + [B][G]\}$ will become the characteristic function of the closed-loop system, i.e.,

$$\Delta_{sys} = \det \{[A] + [B][G]\} \quad (3-49)$$

This determinant can be expanded in such a way as to explicitly retain the vehicle-alone characteristics, which is a powerful advantage. Also, the resulting expressions can be made amenable to the conventional servo-analysis techniques described in the previous section. Thus, in the case of the simplified system of Eqs. 3-40 and 3-45,

$$\begin{aligned} \Delta_{sys} &= \det \{[A] + [B][G]\} \\ &= \begin{vmatrix} a_{11} + b_{12}G_{21} & a_{12} + b_{11}G_{12} & a_{13} \\ a_{21} + b_{22}G_{21} & a_{22} + b_{21}G_{12} & a_{23} \\ a_{31} + b_{32}G_{21} & a_{32} + b_{31}G_{12} & a_{33} \end{vmatrix} \\ &= \Delta + G_{12}N_{\delta_1}^{x_2} + G_{21}N_{\delta_2}^{x_1} + G_{12}G_{21}N_{\delta_1\delta_2}^{x_2x_1} \end{aligned} \quad (3-50)$$

Δ and $N_{\delta_j}^{x_i}$ have the same significance as in Eqs. 3-42, 3-43, and 3-44, while terms of the form $N_{\delta_1\delta_2}^{x_1x_k}$, called coupling numerators, are found by replacing both the i th and k th columns of the determinant of the left-hand coefficients in Eq. 3-40 by the columns of δ_1 and δ_2 coefficients, respectively. The awkward, but descriptive, symbol with two subscripts and two superscripts is intended to suggest this replacement. For example,

$$N_{\delta_1\delta_2}^{x_2x_1} = \begin{vmatrix} b_{12} & b_{11} & a_{13} \\ b_{22} & b_{21} & a_{23} \\ b_{32} & b_{31} & a_{33} \end{vmatrix} \quad (3-51)$$

The coupling numerator $N_{\delta_1\delta_2}^{x_1x_k}$ has no meaning when $i=k$, and is arbitrarily defined to be equal to zero. The properties of determinants can also be

used to show:

$$\frac{x_1 x_k}{N_{\delta_1 \delta_1}} = \frac{x_1 x_k}{N_{\delta_2 \delta_2}} = 0 \quad (3-52)$$

$$\frac{x_1 x_k}{N_{\delta_1 \delta_2}} = -\frac{x_1 x_k}{N_{\delta_2 \delta_1}} = \frac{x_k x_1}{N_{\delta_2 \delta_1}} \quad (3-53)$$

$$\frac{x_1 x_k}{N_{\delta_1 \delta_2}} = \frac{1}{\Delta} \left(\frac{x_1 x_k}{N_{\delta_1} N_{\delta_2}} - \frac{x_1 x_k}{N_{\delta_2} N_{\delta_1}} \right) \quad (3-54)$$

For the most general case of two control deflections fed by each of the three degrees of freedom, the system characteristic determinant can be shown* to have the form

$$\Delta_{\text{sys}} = \Delta + \sum_{i=1}^3 \sum_{j=1}^2 G_{ji} N_{\delta_j}^{x_i} + \sum_{i=1}^3 \sum_{k=1}^3 G_{1i} G_{2k} N_{\delta_1 \delta_2}^{x_i x_k} \quad (3-55)$$

While the system characteristic function, Δ_{sys} , is the denominator for all closed-loop transfer functions, regardless of the command or disturbance input, the numerator of a closed-loop transfer function will depend on the particular command or disturbance.

The inverse matrix, $\{[A] + [B][G]\}^{-1}$, which appears in Eq. 3-48 can be expressed in terms of the basic matrix by the standard form†

$$\{[A] + [B][G]\}^{-1} = \frac{\begin{bmatrix} \Delta_{11} & \Delta_{21} & \Delta_{31} \\ \Delta_{12} & \Delta_{22} & \Delta_{32} \\ \Delta_{13} & \Delta_{23} & \Delta_{33} \end{bmatrix}}{\Delta_{\text{sys}}} \quad (3-56)$$

where the numerator is the transpose of the matrix of the cofactors, and the denominator is the determinant, of the basic matrix, $[A] + [B][G]$.

*Ibid.

†For example, L. A. Pipes, Matrix Methods for Engineering, Prentice-Hall, Inc., Englewood Cliffs, New Jersey, 1963.

Thus, for the example, $\Delta_{\text{sys}} = \det \{ [A] + [B][G] \}$ (Eq. 3-49), and

$$\Delta_{11} = \begin{vmatrix} a_{22} + b_{21}G_{12} & a_{23} \\ a_{32} + b_{31}G_{12} & a_{33} \end{vmatrix} \quad (3-57)$$

is the cofactor of $(a_{11} + b_{12}G_{21})$ in the determinant of Eq. 3-50.

For command inputs the other matrix involved in Eq. 3-48 is $[B][G_c][X_c]$. For the case at hand, the matrix multiplication yields:

$$\begin{aligned} \frac{x_1}{x_{1c}} &= \frac{\Delta_{11}b_{12}G_{21c} + \Delta_{21}b_{22}G_{21c} + \Delta_{31}b_{32}G_{21c}}{\Delta_{\text{sys}}} \\ &= \frac{G_{21c}(b_{12}\Delta_{11} + b_{22}\Delta_{21} + b_{32}\Delta_{31})}{\Delta_{\text{sys}}} \\ &= \frac{\begin{vmatrix} b_{12}G_{21c} & a_{12} + b_{11}G_{12} & a_{13} \\ b_{22}G_{21c} & a_{22} + b_{21}G_{12} & a_{23} \\ b_{32}G_{21c} & a_{32} + b_{31}G_{12} & a_{33} \end{vmatrix}}{\begin{vmatrix} a_{11} + b_{12}G_{21} & a_{12} + b_{11}G_{12} & a_{13} \\ a_{21} + b_{22}G_{21} & a_{22} + b_{21}G_{12} & a_{23} \\ a_{31} + b_{32}G_{21} & a_{32} + b_{31}G_{12} & a_{33} \end{vmatrix}} \quad (3-58) \end{aligned}$$

This same result is obtained, more directly but with less general carry-over to more complex situations, by the application of Cramer's rule to Eq. 3-47 expanded to include the example matrix elements. It is apparent in Eq. 3-58 that the cofactors, such as Δ_{11} , which appear in the numerator are identical to the terms which would appear multiplied by G_{21} in the expansion of the denominator. Thus the expansion of the closed-loop transfer function numerator can be inscribed by analogy, and the complete closed-loop transfer function for a command input, x_{1c} , becomes:

$$\frac{x_1}{x_{1c}} = \frac{G_{21c} \left(\frac{x_1}{N\delta_2} + G_{12} N\delta_1 \delta_2 \frac{x_2 x_1}{\delta_2} \right)}{\Delta + G_{12} N\delta_1 \frac{x_2}{\delta_1} + G_{21} N\delta_2 \frac{x_1}{\delta_2} + G_{12} G_{21} N\delta_1 \delta_2 \frac{x_2 x_1}{\delta_2}} \quad (3-59)$$

A similar development would yield the transfer function relating the response, x_1 , to the disturbance, η_1 :

$$\frac{x_1}{\eta_1} = \frac{\frac{x_1}{N\eta_1} + G_{12} N\eta_1 \delta_1 \frac{x_1 x_2}{\delta_1} + \left[G_{21} N\eta_1 \delta_2 \frac{x_1 x_1}{\delta_2} \right]}{\Delta + G_{12} N\delta_1 \frac{x_2}{\delta_1} + G_{21} N\delta_2 \frac{x_1}{\delta_2} + G_{12} G_{21} N\delta_1 \delta_2 \frac{x_1 x_2}{\delta_2}} \quad (3-60)$$

Here, of course, the disturbance does not go through the block G_{21c} to get into the doubly closed-loop system. Therefore, the leading numerator term is not multiplied by G_{21c} in this case. Note also that the term in square brackets is identically zero.

The pattern which is evident in Eqs. 3-59 and 3-60 can be described by the following rules:*

1. The effective denominator is equal to:
 - a. The open-loop denominator
 - b. Plus the sum of all the feedback transfer functions, each one multiplied by the appropriate numerator
 - c. Plus the sum of all the feedback transfer functions taken two at a time, each pair multiplied by the appropriate coupling numerator
2. The effective numerator is equal to:
 - a. The open-loop numerator
 - b. Plus the sum of all the feedback transfer functions, each one multiplied by the appropriate coupling numerator

*These rules are due to R. L. Stapleford. See Appendix C of ASD-TDR-62-109¹, Analysis of Multiloop Vehicular Control Systems, Mar. 1964.

3. The responses to a command input are obtained from the matrix equation

$$[X] = \left[\begin{array}{c} \text{matrix of effective} \\ \text{transfer functions} \end{array} \right] [G_c] [X_c] \quad (3-61)$$

In the common situation where a command is only fed to one control, Eq. 3-61 reduces to

$$\frac{X_1}{X_{jc}} = \frac{\left(\frac{\delta_k}{x_{jc}} \text{ transfer function} \right) \left(\text{effective } \frac{x_1}{\delta_k} \text{ numerator} \right)}{\left(\text{effective denominator} \right)}$$

In Rule 1-b the "appropriate" numerator is the one with the same output/input pair as the feedback, e.g., the product $G_{21} N_{\delta_2}^{x_1}$ is appropriate to the specific example used earlier, while in Rule 1-c the "appropriate" coupling numerator has the same two output/input pairs as the feedbacks, e.g., $G_{12} G_{21} N_{\delta_2 \delta_1}^{x_1 x_2}$. Recall that $N_{\delta_k \delta_1}^{x_1 x_j}$ is zero (from the properties of determinants) if $i = j$ or $k = 1$. In general cases with many feedbacks, several of the coupling numerators will be zero.

In Rule 2 the "appropriate" coupling numerator is the one for the output/input pair of the original numerator as well as for the feedback output/input pair. For example, the feedback $x_2 \rightarrow \delta_1$ modifies the x_1/δ_j numerator by adding to it the term $G_{12} N_{\delta_j \delta_1}^{x_1 x_2}$, and modifies the x_1/η_j numerator by adding to it the term $G_{12} N_{\eta_j \delta_1}^{x_1 x_2}$.

While the above discussion and the earlier derivations are adequate for determining the command response with feedbacks to two independent controls or the disturbance response with feedbacks to one control, a complete generalization (for a three-degree-of-freedom system) requires the introduction of a second type of coupling numerator. In a type-two coupling numerator, three columns of the open-loop characteristic determinant are replaced by the appropriate control or disturbance coefficients. A type-two coupling numerator is zero if any two of the outputs or any two of the inputs are identical, i.e.,

$$N_{\delta_k \delta_1 \delta_m}^{x_1 x_1 x_j} = 0 \quad (3-62)$$

$$N_{\delta_1 \delta_1 \delta_m}^{x_1 x_j x_k} = 0 \quad (3-63)$$

The rules for forming the effective denominator and numerator are generalized by adding:

- 1-d. Plus the sum of all the feedback transfer functions taken three at a time, each combination multiplied by the appropriate type-two coupling numerator.
- 2-c. Plus the sum of all the feedback transfer functions taken two at a time, each pair multiplied by the appropriate type-two coupling numerator

It often happens that it is necessary or desirable to feed back a quantity which is a linear combination of terms in the variables which appear in the equations of motion. Two alternatives are available. An additional not linearly independent equation can be inscribed together with the equations of motion, and developments similar to the previous ones can be carried out, expanding the determinants which are now larger. On the other hand, all the terms which are required can be developed by adopting a special definition for the word "numerator":

$$\text{Numerator} = \Delta (\text{transfer function})$$

This definition does not, as we shall see later, exclude the possibility that a "numerator" can include a "denominator." For convenience the words will be used from here on as they are defined above, and the use of quotation marks will not be continued. Then, for example, if

$$x_4 = ax_1 + bx_2 + cx_3 \quad (3-64)$$

$$\frac{x_4}{N_{\delta_1}} = a \frac{x_1}{N_{\delta_1}} + b \frac{x_2}{N_{\delta_1}} + c \frac{x_3}{N_{\delta_1}} \quad (3-65)$$

and

$$\frac{x_4 x_1}{N_{\delta_2 \delta_1}} = \left[\frac{x_1 x_1}{a N_{\delta_2 \delta_1}} \right] + b \frac{x_2 x_1}{N_{\delta_2 \delta_1}} + c \frac{x_3 x_1}{N_{\delta_2 \delta_1}} \quad (3-66)$$

etc. The term in square brackets is again identically zero. Otherwise it is worth noting that the replacements indicated by the right column of subscripts and superscripts are the same throughout the equation for the coupling numerator.

Factoring the Transfer Function

Returning now to the case of the simple example, the transfer function of Eq. 3-59 contains terms which are readily recognized as vehicle transfer function numerators and denominators. Dividing the numerator and denominator by Δ , X_1/X_{1c} can be expressed in terms of vehicle-alone transfer functions.

$$\frac{X_1}{X_{1c}} = \frac{G_{21}X_{1\delta_2} \left(1 + G_{12} \frac{N_{\delta_1\delta_2} x_2 x_1}{N_{\delta_2} x_1} \right)}{1 + G_{12}X_{2\delta_1} + \left\{ G_{21}X_{1\delta_2} \left(1 + G_{12} \frac{N_{\delta_1\delta_2} x_2 x_1}{N_{\delta_2} x_1} \right) \right\}} \quad (3-67)$$

where

$$X_{1\delta_2} = \frac{x_1(s)}{\delta_2(s)}$$

$$X_{2\delta_1} = \frac{x_2(s)}{\delta_1(s)}$$

Since the term in braces in the denominator of Eq. 3-67 is identical to the numerator, it makes it easy to recognize that the open-loop function $N(s)/D(s)$ corresponding to the closed-loop function $N(s)/[D(s) + N(s)]$ is:

$$\frac{X_1}{X_{1c}} = \frac{G_{21}X_{1\delta_2} \left(1 + G_{12} \frac{N_{\delta_1\delta_2} x_2 x_1}{N_{\delta_2} x_1} \right)}{1 + G_{12}X_{2\delta_1}} \quad (3-68)$$

$$= G_{21}X_{1\delta_2} \left[\frac{1 + G_{12} \frac{N_{\delta_1\delta_2} x_2 x_1}{N_{\delta_2} x_1}}{1 + G_{12}X_{2\delta_1}} \right]$$

Equation 3-68 can be represented in block diagram form in a particularly instructive way. Figure 3-40 shows that the effect of feeding back $x_2 \rightarrow \delta_1$ is to modify the $X_{1\delta_2}$ transfer function of the vehicle so that when the $x_1 \rightarrow \delta_2$ feedback loop is opened the "effective" vehicle transfer function is $X'_{1\delta_2}$ and the open-loop function for the second loop closure is $G_{21}X'_{1\delta_2}$. In this case, both the poles and zeros of $X_{1\delta_2}$ have been modified.

The primed notation $X'_{1\delta_2}$ is used to indicate merely that one loop has been closed, and, by itself, it is not intended to specify the particular loop closure which is involved. The meaning of the primed notation in terms of which loops have been closed, therefore, depends on the local context. Later, the prime is similarly added to individual transfer function terms to indicate the number of prior loop closures.

Note here that since, typically, s appears raised to higher powers in the denominators of $G_{12}X_{2\delta_1}$ and $G_{12}N_{\delta_1\delta_2}^{x_2x_1}/N_{\delta_2}^{x_1}$ than in the numerators,

$$\lim_{s \rightarrow \infty} (G_{12}X_{2\delta_1}) \doteq 0 \quad (3-69)$$

and

$$\lim_{s \rightarrow \infty} \left(G_{12} \frac{N_{\delta_1\delta_2}^{x_2x_1}}{N_{\delta_1}^{x_1}} \right) \doteq 0 \quad (3-70)$$

so that the so-called root locus or high frequency gain of $X'_{1\delta_2}$ is identical to the one for $X_{1\delta_2}$.

We may also remark, in passing, that Fig. 3-40 shows particularly clearly that the "modification" made by the first loop closure, $x_2 \rightarrow \delta_1$, might be made in such a way as to compensate or "equalize" the open-loop transfer function, $G_{21}X_{1\delta_2}$. This is a thought to which we shall return later.

Now in order to make an analysis of the effects of closing the second loop, $x_1 \rightarrow \delta_2$, it is first necessary to know the factors of $X'_{1\delta_2}$, and finding the factors of $X'_{1\delta_2}$ involves finding the factors of

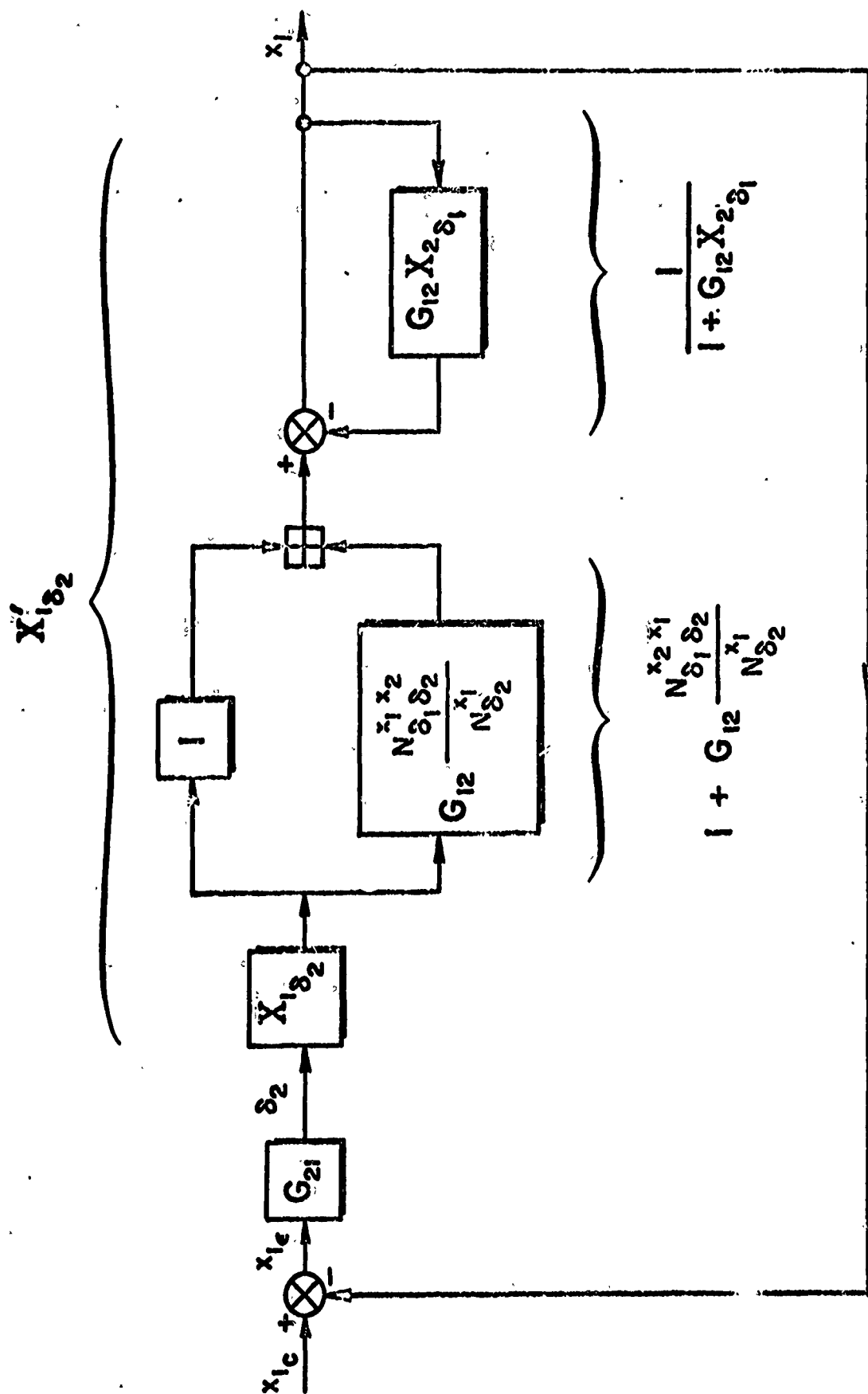


Fig. 3-40. Equivalent Block Diagram for the System

$x_{1c} \rightarrow \delta_2; x_2 \rightarrow \delta_1$

and of

$$1 + G_{12} X_{2\delta_1} \quad \text{given the factors of} \quad G_{12} X_{2\delta_1}$$

$$1 + G_{12} \frac{N_{\delta_1 \delta_2}^{x_2 x_1}}{N_{\delta_2}^{x_1}} \quad \text{given the factors of} \quad G_{12} \frac{N_{\delta_1 \delta_2}^{x_2 x_1}}{N_{\delta_1}^{x_1}}$$

Of course, these operations are relatively easily accomplished by conventional servoanalysis techniques. They correspond to finding the closed-loop roots of the characteristic equations for the feedback systems of Fig. 3-41. Note that the roots of the "system" of Fig. 3-41a are the poles of $X'_{1\delta_2}$, while the roots of the "system" of Fig. 3-41b become the zeros of $X'_{1\delta_2}$.

$$X'_{1\delta_2} = \frac{N_{\delta_2}^{x_1} + G_{12} N_{\delta_1 \delta_2}^{x_2 x_1}}{1 + G_{12} N_{\delta_1}^{x_1}} = \frac{\text{Closed-loop pole factors of } \textcircled{2}}{\text{Closed-loop pole factors of } \textcircled{1}} \quad (3-71)$$

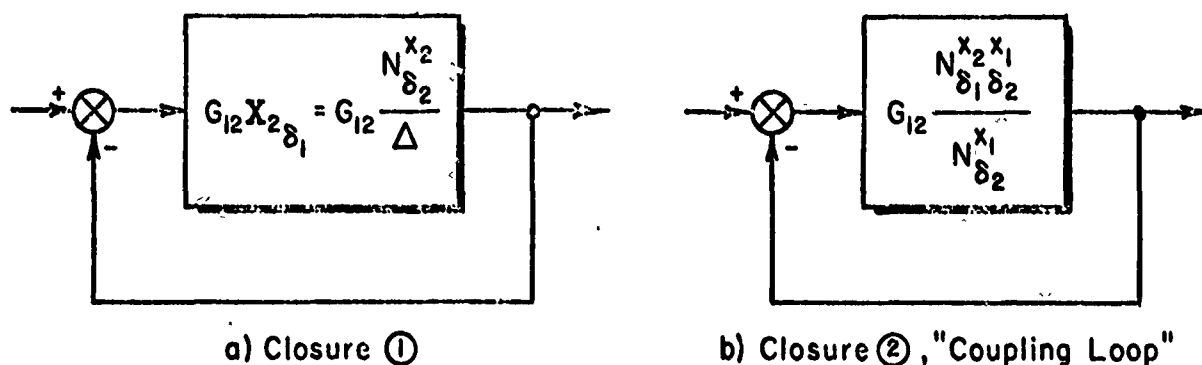


Fig. 3-41. x_2 Loop Closures Involved in the System, $x_{1c} \rightarrow \delta_2: x_2 \rightarrow \delta_1$

If the characteristics of the vehicle are fixed, G_{12} is the only variable in both relationships. Thus, choosing G_{12} appropriate to either closure ① or closure ② completely determines the characteristics of the other closure.

The two loop closures considered here are further related, in typical applications to aircraft, in that the high frequency open- and closed-loop asymptotes of systems ① and ② are often nearly identical, and therefore

the "root locus gains" are nearly the same. This observation is easy to appreciate because typically the terms of highest degree in s in the expansion of Δ come from the product of main diagonal terms ($a_{11}a_{22}a_{33}$), while the control effectiveness terms (b_{1j}) are usually constants. Then at high frequencies, denoted as " $|s|$ large,"

$$\left. \frac{x_1}{N_{\delta_2}} \right|_{|s| \text{ large}} \rightarrow \left. b_{12}a_{22}a_{33} \right|_{|s| \text{ large}} \quad (\text{see Eq. 3-42}) \quad (3-72)$$

$$\left. \frac{x_2 x_1}{N_{\delta_1 \delta_2}} \right|_{|s| \text{ large}} \rightarrow \left. (b_{12}b_{21} - b_{11}b_{22})a_{33} \right|_{|s| \text{ large}} \quad (\text{see Eq. 3-50}) \quad (3-73)$$

and

$$\left. \frac{\frac{x_2 x_1}{N_{\delta_1 \delta_2}}}{\frac{x_1}{N_{\delta_2}}} \right|_{|s| \text{ large}} \rightarrow \left. \frac{b_{21}}{a_{22}} - \frac{b_{11}b_{22}}{b_{12}a_{22}} \right|_{|s| \text{ large}} \quad (3-74)$$

Similarly (Eq. 3-43),

$$\left. X_{2\delta_1} \right|_{|s| \text{ large}} \rightarrow \left. \frac{a_{11}b_{21}a_{33}}{a_{11}a_{22}a_{33}} \right|_{|s| \text{ large}} = \left. \frac{b_{21}}{a_{22}} \right|_{|s| \text{ large}} \quad (3-75)$$

Quite typically for aircraft controls $b_{21} \gg b_{11}b_{22}/b_{12}$, so that in general for large $|s|$:

$$\frac{\frac{x_2 x_1}{N_{\delta_1 \delta_2}}}{\frac{x_1}{N_{\delta_2}}} = \frac{b_{21}}{a_{22}} - \frac{b_{11}b_{22}}{a_{22}b_{12}} \doteq \frac{b_{21}}{a_{22}} \doteq X_{2\delta_1} \quad (3-76)$$

It is helpful to keep this fact in mind while actually making the analysis of the "simultaneous" closures for systems ① and ②.

When $X'_{1\delta_2}$ has been found in factored form, the closed-loop system characteristics can readily be determined by a conventional analysis of the system of Fig. 3-42.

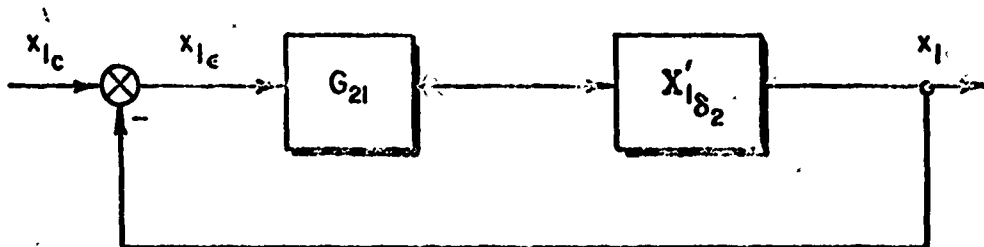


Fig. 3-42. Command Loop Closure

In summary, the steps involved in the analysis of the system in Fig. 3-38 are:

1. The control channels are divided into two categories, "inner" and "outer" loops, reflecting the closure sequence. The x_2 (or δ_1) loop, closed first, is thus the "inner" loop; whereas the x_1 (or δ_2) loop, being closed second, is the "outer" loop.
2. The "inner" loop, $G_{12}X_{2\delta_1}$ (①, Fig. 3-40), is closed with tentatively selected equalization and gains, and the closed inner loop roots are found. These roots become the vehicle's poles for the outer loop closure.
3. Using the same gain and equalization selected above, i.e., the same G_{12} , the coupling loop (②, Fig. 3-40) is closed. The closed-loop roots resulting from this closure become the vehicle's zeros for the outer loop closure.
4. The outer loop is closed in a conventional manner around the modified outer loop vehicle transfer function.
5. Possible repetitions of Steps 2 through 4 with different equalizations and gains may be required if the result of Step 4 is not satisfactory.

3.6 SENSITIVITY OF CLOSED-LOOP ROOTS TO SYSTEM PARAMETER VARIATIONS

We have thus far treated the system analysis problem for nominal characteristics, including the determination of open- and closed-loop transfer functions and time responses. We turn now to consideration of off-nominal behavior resulting from variations in the system parameters from their assigned values. The many ramifications of this subject are commonly encompassed by the name "sensitivity," referring generally to the change of some aspect of system behavior due to some change in the system elements. Because the sensitivity measures developed here are directly related to the modal response coefficients needed in response calculations, sensitivity and response factors become inseparable. Therefore while this section is explicitly on sensitivity, it also implicitly covers the calculation of modal response coefficients.

Sensitivity considerations have long been of dominant interest in vehicle dynamic and control system design activities. As noted in Section 3.4, the "sensitivity" of a feedback system was originally one of the bases for the mathematical definition of feedback. This was natural since feedback systems possess the "fundamental physical property that the effects of variations in the forward loop, whether they are taken as changes in $G(s)$ or as departures from strict linearity, or as freedom from extraneous noise, are reduced by the factor $1/(1+G)$ in comparison with the effects which would be observed in a system without feedback."* The $1/(1+G)$ factor is the classical sensitivity function, $S_G^{G_{cr}}(s)$, which compares the relative change in closed-loop characteristics to the causative relative change in open-loop characteristics, i.e.,

$$S_G^{G_{cr}}(s) = \frac{\left[\frac{dG_{cr}(s)}{G_{cr}(s)} \right]}{\left[\frac{dG(s)}{G(s)} \right]} = \frac{1}{1+G} \quad (3-77)$$

*H. W. Bode, Network Analysis and Feedback Amplifier Design, P. Van Nostrand Co., Inc., New York, 1945, p. 141.

Thus, the measure $1/(1+G)$ indicates directly the reduction in the "sensitivity" of the system to many of the influences which would otherwise tend to corrupt its performance.

Although classical sensitivity has been a popular subject in control topics ever since Bode's original work we shall depart from the classical view to emphasize newer conceptions of sensitivity. These concepts are more pertinent here because they result in measures which are directly related to the pole-zero description of system characteristics.* The basic measures, called here "gain," "(open-loop) pole," "(open-loop) zero," and "(open-loop) parameter" sensitivities, were evolved to determine changes in the position of closed-loop poles due to shifts or changes in open-loop gain, poles, zeros, or other parameters. In the simplest terms these sensitivities connect open-loop differential variations with closed-loop differential shifts.

The sensitivity factors can play a significant role in synthesis as well as analysis activities. In analysis, as already remarked, design calculations are inherently nominal because the system assumed in an analytical study can never precisely match the actual physical.

*K. Mitchell, "Estimation of the Effect of a Parameter Change on the Roots of Stability Equations," Aeron. Quart., Vol. I, May 1949.

Ordway B. Gates, Jr., and C. H. Woodling, A Method for Estimating Variations in the Roots of the Lateral-Stability Quartic Due to Changes in Mass and Aerodynamic Parameters of an Airplane, NACA TN 3134, Jan. 1954.

A. Papoulis, "Displacement of the Zeros of the Impedance $Z(p)$ Due to Incremental Variations in the Network Elements," Proc. IRE, Vol. 43, 1955.

R. Y. Huang, "The Sensitivity of the Poles of Linear Closed Loop Systems," Trans. AIEE, Pt. II, Vol. 77, 1958, pp. 182-186.

F. F. Kuo, Pole-Zero Sensitivity in Network Functions, Ph.D. Dissertation, Univ. of Illinois, 1958.

H. Ur, "Root Locus Properties and Sensitivity Relations in Control Systems," IRE Trans., Vol. AC-5, No. 1, Jan. 1960.

D. T. McRuer, and R. L. Stapleford, Sensitivity and Modal Response for Single-Loop and Multiloop Systems, ASD-TDR-62-812, Jan. 1963.

I. M. Horowitz, Synthesis of Feedback Systems, Academic Press, New York, London, 1963.

system. An assessment of the effects of system uncertainties and/or the implications of parameter tolerances thus becomes a matter of great concern to the designer. Sensitivity concepts provide the direct means to make such assessments. For synthesis the use of sensitivity is more subtle. Practical control systems usually require complex dynamical descriptions and are expected to meet a variety of diverse and often conflicting criteria. Because of this intrinsic complexity, the interrelationships between the system parameters and the diverse system performance measures are always involved and often obscure. Consequently, system synthesis is invariably accomplished by iterative analysis. In such iterations, knowledge of the effects of parameter variations is of great value in determining appropriate modifications. The guidance provided by sensitivity factors can be used to suggest both improvement in nominal system characteristics and the reduction of system sensitivity to parameter variations.

Our development sequence will first consider single-loop systems with first-order closed-loop poles. The notions here are elementary and easily traced, as befits an introduction to the subject. This will be followed by a more general development which subsumes all forms of root sensitivities for open-loop, single-loop, and multiloop systems.

Sensitivities for Single-Loop Systems

The single-loop system open-loop transfer function has the form

$$G(s) = K \frac{\alpha(s)}{\beta(s)} = K \frac{\prod_{j=1}^n (s + z_j)}{\prod_{j=1}^{m+n} (s + p_j)} \quad (3-78)$$

$$= G(s, K, z_j, p_j)$$

The effects of small variations in the parameters of $G(s)$ on the closed-loop roots can be found by starting with the total derivative of the closed-loop characteristic function, $1 + G$,

$$d(1+G) = dG$$

$$= \frac{\partial G}{\partial s} ds + \frac{\partial G}{\partial K} dK + \sum_{j=1}^n \frac{\partial G}{\partial z_j} dz_j + \sum_{j=1}^{m+n} \frac{\partial G}{\partial p_j} dp_j \quad (3-79)$$

Now because the closed-loop poles, λ_i , are defined by the equation

$$[1 + G(s)]_{s=\lambda_i} = 0 \quad (3-80)$$

the total differential of Eq. 3-79 is zero at the position of a closed-loop pole $s = \lambda_i$. Setting $dG = 0$ and $s = \lambda_i$ in Eq. 3-79, and rearranging terms gives

$$d\lambda_i = \left[\frac{-1}{\frac{\partial G}{\partial s}} \right]_{s=\lambda_i} \left\{ \frac{\partial G}{\partial K} dK + \sum_{j=1}^n \frac{\partial G}{\partial z_j} dz_j + \sum_{j=1}^{m+n} \frac{\partial G}{\partial p_j} dp_j \right\}_{s=\lambda_i} \quad (3-81)$$

The variation, $d\lambda_i$, in the closed-loop pole can be expressed in another way by noting that the closed-loop roots depend only on the open-loop gain, poles, and zeros. Functionally,

$$\lambda_i = \lambda_i(K, z_j, p_j) \quad (3-82)$$

The total derivative $d\lambda_i$ is then

$$\begin{aligned} d\lambda_i &= K \frac{\partial \lambda_i}{\partial K} \frac{dK}{K} + \sum_{j=1}^n \frac{\partial \lambda_i}{\partial z_j} dz_j + \sum_{j=1}^{m+n} \frac{\partial \lambda_i}{\partial p_j} dp_j \\ &= s_K^i \frac{dK}{K} + \sum_{j=1}^n s_{z_j}^i dz_j + \sum_{j=1}^{m+n} s_{p_j}^i dp_j \end{aligned} \quad (3-83)$$

As indicated in the last form of Eq. 3-83, the factors $\kappa(\partial\lambda_i/\partial\kappa)$, $\partial\lambda_i/\partial z_j$, and $\partial\lambda_i/\partial p_j$ are accorded a special symbol, S . These are the first order sensitivity factors. The subscript and superscript notation indicates that a differential increment in the open-loop parameter (defined by the subscript) results in a differential increment of the i th closed-loop root (denoted in the superscript) which is equal to the sensitivity factor times the open-loop parametric variation.

By equating like coefficients in Eqs. 3-81 and 3-83

$$\begin{aligned} S_{\kappa}^i &\equiv \frac{\partial\lambda_i}{\partial\kappa/\kappa} = - \left[\frac{\partial G/\partial\kappa}{\partial G/\partial s} \right]_{s=\lambda_i} \\ S_{z_j}^i &\equiv \frac{\partial\lambda_i}{\partial z_j} = - \left[\frac{\partial G/\partial z_j}{\partial G/\partial s} \right]_{s=\lambda_i} \\ S_{p_j}^i &\equiv \frac{\partial\lambda_i}{\partial p_j} = - \left[\frac{\partial G/\partial p_j}{\partial G/\partial s} \right]_{s=\lambda_i} \end{aligned} \quad (3-84)$$

Note that the gain sensitivity is based on a fractional (percentage) change in κ , while the pole and zero sensitivities are based on absolute shifts of p_j and z_j . These definitions were adopted here in order to provide some simplifications in relationships.

In terms of the open-loop transfer function form of Eq. 3-78, the gain sensitivity factor, remembering that $G(\lambda_i) = -1$, is,

$$\begin{aligned} S_{\kappa}^i &= \left[-\frac{1}{\partial G/\partial s} \right]_{s=\lambda_i} \left[\frac{\partial G}{\partial\kappa} \right]_{s=\lambda_i} \\ &= \left[-\frac{1}{\partial G/\partial s} \right]_{s=\lambda_i} [G(s)]_{s=\lambda_i} \\ &= \left[\frac{1}{\partial G/\partial s} \right]_{s=\lambda_i} \end{aligned} \quad (3-85)$$

Using Eq. 3-78,

$$s_K^i = - \left[\frac{\kappa \alpha(s)}{\kappa \frac{d\alpha(s)}{ds} + \frac{d\beta(s)}{ds}} \right]_{s=\lambda_i} \quad (3-86)$$

or, since $\kappa \alpha(\lambda_i) = -\beta(\lambda_i)$,

$$s_K^i = \left[\frac{\beta(s)}{\kappa \frac{d\alpha(s)}{ds} + \frac{d\beta(s)}{ds}} \right]_{s=\lambda_i} \quad (3-87)$$

With the factored form of Eq. 3-78,

$$\begin{aligned} \frac{\partial G}{\partial s} &= G(s) \left[\frac{1}{\alpha(s)} \frac{\partial \alpha}{\partial s} - \frac{1}{\beta(s)} \frac{\partial \beta}{\partial s} \right] \\ &= G(s) \left[\frac{1}{\alpha} \sum_{j=1}^n \prod_{\substack{k=1 \\ k \neq j}}^n (s + z_k) - \frac{1}{\beta} \sum_{j=1}^{m+n} \prod_{\substack{k=1 \\ k \neq j}}^{m+n} (s + p_k) \right] \\ &= G(s) \left[\sum_{j=1}^n \frac{1}{(s + z_j)} - \sum_{j=1}^{m+n} \frac{1}{(s + p_j)} \right] \end{aligned}$$

so

$$s_K^i = \left[\frac{1}{\partial G / \partial s} \right]_{s=\lambda_i} = \left[\sum_{j=1}^{m+n} \frac{1}{\lambda_i + p_j} - \sum_{j=1}^n \frac{1}{\lambda_i + z_j} \right]^{-1} \quad (3-88)$$

Using Eqs. 3-78, 3-81, and 3-85, the zero sensitivity becomes

$$\begin{aligned}
 s_{z_j}^i &= - \left[\frac{\partial G / \partial z_j}{\partial G / \partial s} \right]_{s=\lambda_i} = \left[\frac{1}{\partial G / \partial s} \right]_{s=\lambda_i} \left[- \frac{\partial G}{\partial z_j} \right]_{s=\lambda_i} \\
 &= s_K^i \left[\frac{- \kappa \prod_{\substack{k=1 \\ k \neq j}}^n (s + z_k)}{\prod_{k=1}^{m+n} (s + p_k)} \right]_{s=\lambda_i} \left[\frac{(s + z_j)}{(s + z_j)} \right]_{s=\lambda_i} \\
 &= s_K^i \left[-G(\lambda_i) \right] \left(\frac{1}{s + z_j} \right)_{s=\lambda_i} \\
 &= \frac{s_K^i}{\lambda_i + z_j} \quad (3-89)
 \end{aligned}$$

Developed similarly, the pole sensitivity will be

$$s_{p_j}^i = - \frac{s_K^i}{\lambda_i + p_j} \quad (3-90)$$

Further examination and interpretation reveals six interesting and useful properties of the sensitivity factors:

- a. The gain sensitivity is a measure of the slope along a conventional root locus.
- b. The gain sensitivity is a factor in each of the sensitivity terms. Thus, Eq. 3-83 becomes

$$\Delta \lambda_i = s_K^i \left[\frac{d\kappa}{\kappa} + \sum_{j=1}^n \frac{dz_j}{\lambda_i + z_j} - \sum_{j=1}^{m+n} \frac{dp_j}{\lambda_i + p_j} \right] \quad (3-91)$$

- c. The gain sensitivity is the negative of the modal response coefficient for the root λ_i . This will be shown for the general case of N th order roots in the next article but will be taken for granted here. Thus,

$$s_K^i = -Q_i \quad (3-92)$$

This equality is very useful since all of the properties previously derived for the modal response coefficients are applicable to the gain sensitivity. Using this correspondence, other formulas for the gain sensitivity can be developed.

$$s_K^i = - \left[(s - \lambda_i) G_{cr}(s) \right]_{s=\lambda_i}$$

$$= - \left[\frac{(s - \lambda_i) K \prod_{j=1}^n (s + z_j)}{(1 + K \delta_m^0) \prod_{j=1}^{m+n} (s + q_j)} \right]_{s=\lambda_i}$$

$$\delta_m^0 = \begin{cases} 1, & m=0 \\ 0 & \text{otherwise} \end{cases}$$

Remembering that $\lambda_i = -q_i$, and that $K\alpha(\lambda_i) = -\beta(\lambda_i)$,

$$s_K^i = \frac{-K \prod_{j=1}^n (\lambda_i + z_j)}{(1 + K \delta_m^0) \prod_{\substack{j=1 \\ j \neq i}}^{m+n} (\lambda_i + q_j)} \quad (3-93)$$

$$= \frac{\prod_{j=1}^{m+n} (\lambda_i + p_j)}{(1 + K \delta_m^0) \prod_{\substack{j=1 \\ j \neq i}}^{m+n} (\lambda_i + q_j)}$$

- d. Some combinations of gain sensitivities or modal response ratios are simple functions of the open-loop transfer function polynomial coefficients and gains. These are conveniently developed by matching coefficients in expressions for the closed-loop transfer function and in the partial fraction expansion.* Among the relationships are the following for $m \geq 1$:

$$\sum_{i=1}^{m+n} Q_i = - \sum_{i=1}^{m+n} S_K^i = \kappa \delta_m^1 \quad (3-94)$$

$$\sum_{i=1}^{m+n} Q_i Q_i = - \sum_{i=1}^{m+n} S_K^i Q_i = \kappa [b_1 - a_1 + \kappa] \delta_m^1 - \kappa \delta_m^2 \quad (3-95)$$

$$\sum_{i=1}^{m+n} \frac{Q_i}{Q_i} = - \sum_{i=1}^{m+n} \frac{S_K^i}{Q_i} = \begin{cases} 1 & , k \geq 1 \\ \frac{\kappa}{1+\kappa} & , k = 0 \\ 0 & , k \leq -1 \end{cases} \quad (3-96)$$

- e. The sum of all the zero and pole sensitivities for each closed-loop pole must equal minus one. This follows directly from Eqs. 3-88, 3-89, and 3-90. Thus,

$$\sum_{j=1}^n S_{z_j}^i + \sum_{j=1}^{m+n} S_{p_j}^i = -1 \quad (3-97)$$

This result is easily explained by recalling that on a root-locus plot if all the open-loop zeros and poles are moved the same amount, all the closed-loop poles will also be moved by that amount. The minus sign is because z_j and p_j are the negatives of the open-loop zeros and poles.

*D. T. McKuer, and R. L. Stapleford, Sensitivity and Modal Response for Single-Loop and Multiloop Systems, ASD-TDR-62-842, Jan. 1963.

- f. The gain sensitivities are the residues, evaluated at the closed-loop poles, of the classical sensitivity s_{Gcr}^{Gcr} . This is a direct consequence of the relationship between the modal response coefficients and gain sensitivities.

$$s_{Gcr}^{Gcr} = G_{cr} = 1 - \sum_{i=1}^{m+n} \frac{Q_i}{s + q_i}$$

$$= 1 + \sum_{i=1}^{m+n} \frac{s_K^i}{s + q_i} \quad m \geq 1 \quad (3-98)$$

Evaluation Procedures for Sensitivities

The evaluation of single-loop gain sensitivities, or modal response coefficients, may be accomplished in several ways.* The fundamental bases are the formulas given by Eqs. 3-85, 3-86, 3-87, 3-88, or 3-93. All of these are appropriate for direct computation, which is probably the most common means employed for sensitivity calculation.

Some of the gain sensitivity equations are readily interpreted graphically in terms of vectors in the complex plane. Equation 3-88, for example, instructs us to draw, at any point, λ_i , on the locus of roots, vectors directed toward the zeros and away from the poles of the open-loop function, and inversely proportional in magnitude to the distance from λ_i to the singularity in question. The sum of these vectors shows the direction of the locus with increasing gain. A second graphical method using vectors in the complex plane is based on conventional root locus constructions. The basis is Eq. 3-93, which involves a ratio of vector products. With a complete set of closed-loop roots plotted on the locus this calculation can be quickly evaluated, as exemplified in Fig. 3-43. The operations involved can be accomplished particularly rapidly when the logarithmic spiral features of the "Spirule"[†] are used as an aid. This is the method

*McRuer and Stapleford, Ibid.

[†]See footnote, p. 3-9.

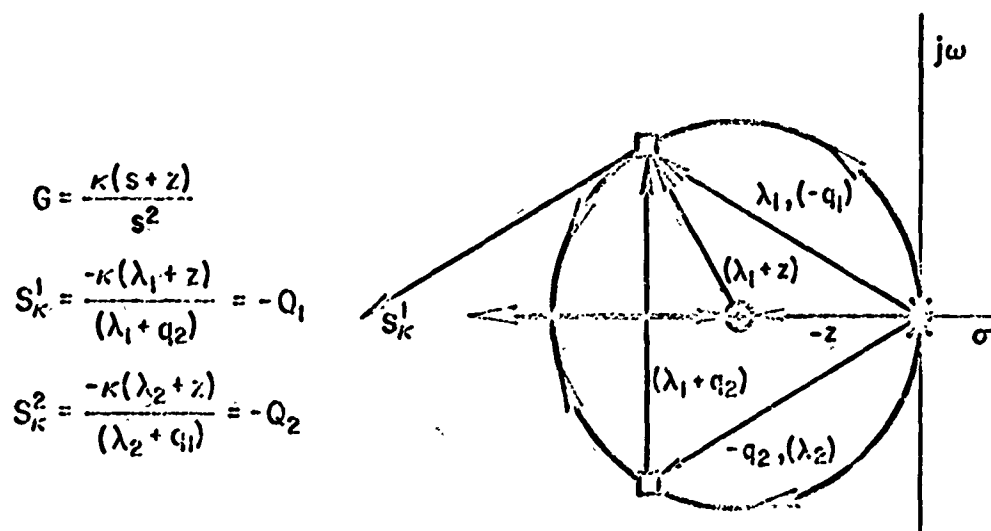


Fig. 3-43. Illustration of Gain Sensitivity and Modal Response Coefficient Calculations Using Vectors from the Complete Root Locus

most often given for the graphical evaluation of the modal response coefficients. Its disadvantage for sensitivity calculations is that it requires a complete set of compatible closed-loop roots plotted on the locus.

Besides these vector forms, sensitivities can be obtained from any of the common plots used in the unified servo analysis techniques treated earlier in this chapter.* Most of the methods depend on the interpretation of Eq. 3-85 in terms of slopes from the particular plot (e.g., $j\omega$ -Bode, conventional root locus, etc.) available.

When the complete set of conventional and Bode root locus plots are available graphical methods using increments in the gain and closed-loop poles offer the simplest way to obtain a rapid appreciation of sensitivity considerations. The direction of the gain sensitivity is most easily determined from the conventional root locus, as it is

*McRuer and Stapleford, Ibid.

simply along the tangent to the locus. A close approximation to the magnitude can be obtained using the location of the closed-loop pole for two slightly different gains, such as the segment of a locus shown in Fig. 3-44. The gain perturbation method requires the locations of the closed-loop pole for two slightly different gains, such

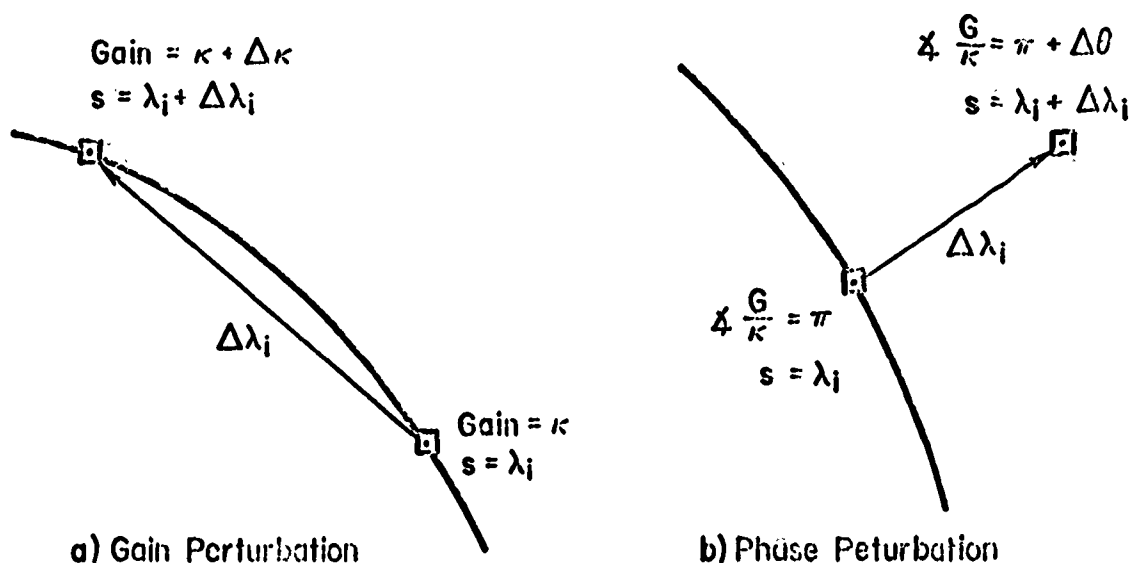


Fig. 3-44. Root-Locus Perturbation Methods for Gain Sensitivity

as the segment of a locus shown in Fig. 3-44a. Using finite increments as approximations to differential changes, Eq. 3-84 gives

$$S_{\kappa}^i = \frac{d\lambda_i}{d\kappa/\kappa} \doteq \frac{\kappa(\Delta\lambda_i)}{\Delta\kappa} \quad (3-99)$$

Equation 3-99 can also be used if the change in the closed-loop pole is obtained by some other technique, such as from root decomposition.

The phase perturbation method is based on considering κ to be a complex quantity. The normal root locus is then a graph of the closed-loop pole locations for κ real. Now consider a small perturbation in the phase of κ . The closed-loop pole must then be perturbed a small distance normal to the conventional root locus, and the phase perturbation of (G/κ) must be minus that of κ (see Fig. 3-44b). Consequently,

for perturbations normal to the root locus, $\Delta k/k = -j\Delta\theta$, and Eq. 3-99 becomes

$$S_K^i = \frac{d\lambda_i}{dk/k} = j \frac{\Delta\lambda_i}{\Delta\theta} \quad (3-100)$$

where

$\Delta\theta$ = phase change, in rad, of G/k

For the Bode root locus a more natural sensitivity factor is the proportional change in the negative of the closed-loop root, i.e., dq_i/q_i instead of $d\lambda_i$. Considering gain sensitivity alone,

$$dq_i = -d\lambda_i = -S_K^i \frac{dk}{k}$$

or

$$\begin{aligned} \frac{dq_i}{q_i} &= -\frac{S_K^i}{q_i} \frac{dk}{k} \\ &= M_K^i \frac{dk}{k} \end{aligned} \quad (3-101)$$

where M_K^i is the sensitivity factor relating proportional changes in the negative of the closed-loop pole, q_i , and the gain. Because $dx/x = d \ln x$, the proportional sensitivity, M_K^i , will be

$$\begin{aligned} M_K^i &= -\frac{S_K^i}{q_i} = \frac{dq_i/q_i}{dk/k} \\ &= \frac{d \ln q_i}{d \ln k} \end{aligned} \quad (3-102)$$

The proportional sensitivity can thus be estimated from the Bode root locus by considering small increments about the nominal gain. For real roots this will simply be the slope of the siggy Bode plot at q_i . As often as not this would be expressed in decades/dB. To convert to a unit-less form of M_K^i we note that

$$\begin{aligned}
 M_K^i \Big|_{\text{decades/db}} &= \frac{d(\log_{10} q_i)}{d(20 \log_{10} \kappa)} = \frac{\log_{10} e (d \ln q_i)}{20 \log_{10} e (d \ln \kappa)} \\
 &= \frac{1}{20} M_K^i
 \end{aligned} \tag{3-103}$$

When the roots are complex the most convenient quantities to measure along the Bode root locus are increments in the closed-loop damping ratio, $\Delta \zeta$, and logarithmic increments in the closed-loop natural frequency, $\Delta \ln \omega_n$, and open-loop gain $\Delta \ln \kappa$. These can readily be related to the proportional sensitivity. The negative of the closed-loop root in the upper half of the s-plane is,

$$q_i = \zeta \omega_n - j \sqrt{1 - \zeta^2} \omega_n$$

so

$$\begin{aligned}
 dq_i &= \frac{\partial q_i}{\partial \zeta} d\zeta + \frac{\partial q_i}{\partial \omega_n} d\omega_n \\
 &= \frac{j[\zeta \omega_n - j \sqrt{1 - \zeta^2} \omega_n]}{\sqrt{1 - \zeta^2}} d\zeta + (\zeta - j \sqrt{1 - \zeta^2}) d\omega_n \\
 &= q_i \left[\frac{j}{\sqrt{1 - \zeta^2}} d\zeta + \frac{d\omega_n}{\omega_n} \right]
 \end{aligned}$$

The proportional sensitivity, M_K^i , will then be

$$\begin{aligned}
 M_K^i &= \frac{d \ln q_i}{d \ln \kappa} = \frac{dq_i/q_i}{d \ln \kappa} \\
 &= \frac{\frac{d\omega_n}{\omega_n} + \frac{j}{\sqrt{1 - \zeta^2}} d\zeta}{d \ln \kappa} \\
 &= \frac{d \ln \omega_n}{d \ln \kappa} + \frac{j}{\sqrt{1 - \zeta^2}} \frac{d\zeta}{d \ln \kappa}
 \end{aligned} \tag{3-104}$$

The first term is converted from decades/dB by multiplying by 20, just as with first-order terms. The imaginary part will usually be measured as

$$\frac{\Delta \zeta}{\Delta(20 \log_{10} \kappa)} = \frac{\Delta \zeta}{20 \log_{10} e (\Delta \ln \kappa)}$$

so

$$\begin{aligned} \frac{d\zeta}{d \ln \kappa} &= 20 \log_{10} e \frac{d\zeta}{d(20 \log_{10} \kappa)} \\ &= 8.6859 \frac{d\zeta}{d(20 \log_{10} \kappa)} \end{aligned} \quad (3-105)$$

The gain sensitivity in these terms will then be

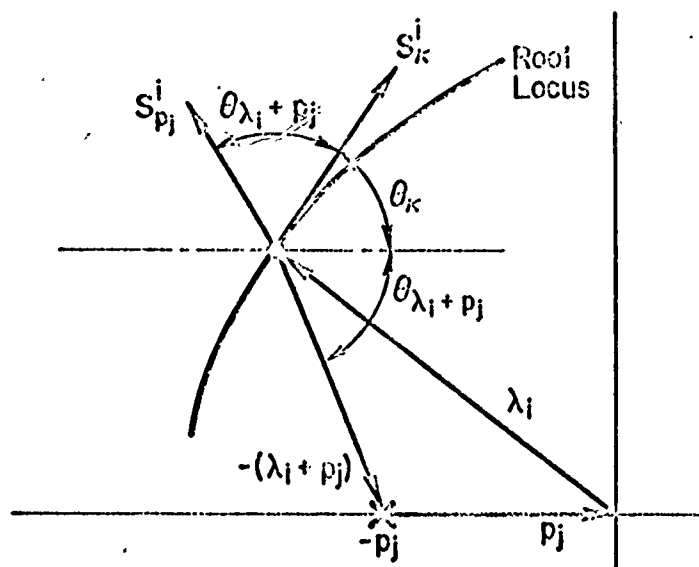
$$S_K^i = \lambda_i M_K^i = \lambda_i \left[\frac{20 d(\log_{10} a_n)}{d(20 \log_{10} \kappa)} + \frac{j 8.6859}{\sqrt{1-\zeta^2}} \frac{d\zeta}{d(20 \log_{10} \kappa)} \right] \quad (3-106)$$

The pole and zero sensitivities are easily obtained once the gain sensitivities have been found. A geometric appreciation is gained by considering these as vectors in the s-plane, as in Fig. 3-45. Note that the zero sensitivity vector is in a direction tending to pull the locus more toward the zero, whereas the pole sensitivity vector would tend to push the locus away from the pole.

Example: Unit-numerator third-order system

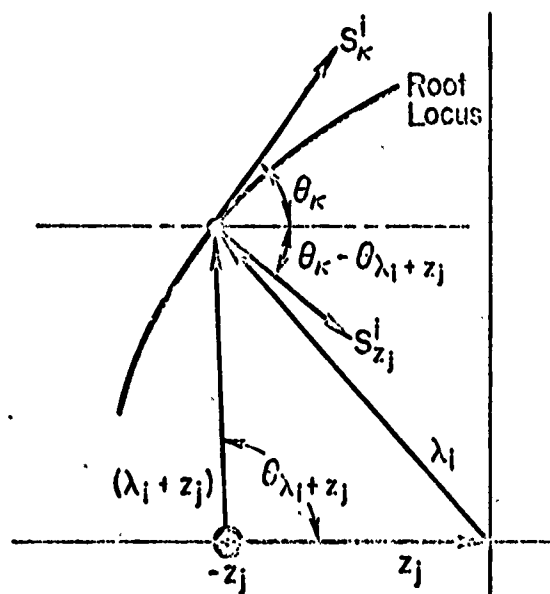
The analysis of the system

$$G(s) = \frac{\kappa}{s(s+1)(s+5)}$$



$$S_{p_j}^i = \frac{-S_K^i}{\lambda_i + p_j} = \frac{|S_K^i| \angle \theta_K}{|\lambda_i + p_j| \angle -(\theta_{\lambda_i + p_j})} = \left| \frac{S_K^i}{\lambda_i + p_j} \right| \angle (\theta_K + \theta_{\lambda_i + p_j})$$

a) Pole Sensitivity



$$S_{z_j}^i = \frac{S_K^i}{\lambda_i + z_j} = \frac{|S_K^i| \angle \theta_K}{|\lambda_i + z_j| \angle \theta_{\lambda_i + z_j}} = \left| \frac{S_K^i}{\lambda_i + z_j} \right| \angle (\theta_K - \theta_{\lambda_i + z_j})$$

b) Zero Sensitivity

Fig. 3-45. Geometric Illustrations of Pole and Zero Sensitivity Vectors

has been extensively treated on pp. 3-19 et seq. and 3-39 et seq. A complete "system survey," comprising block diagram, $G(j\omega)$ and $G(-\sigma)$ Bode plots, and Bode and conventional root locus plots is given in Fig. 3-46. In this example we will compute the gain sensitivities in several ways for illustration and as an indication of relative accuracies.

The gain is set so that a pair of complex closed-loop poles with damping ratio of $\sqrt{2}/2$ exists. For this situation the important parameters are,

$$K = 31\sqrt{26} - 156 = 2.070$$

$$\eta_1 = -\lambda_1 = \sqrt{26} = 5.099$$

$$\eta_2 = -\lambda_2 = \frac{1}{2}(6 - \sqrt{26})(1-j) = 0.450(1-j)$$

$$\eta_3 = -\lambda_3 = \frac{1}{2}(6 - \sqrt{26})(1+j) = 0.450(1+j)$$

1. Direct Calculation

Using Eq. 3-86 for the numerator and denominator derivatives method,

$$S_K^i = \left(\frac{-K\alpha}{K \frac{\partial \alpha}{\partial s} + \frac{\partial \beta}{\partial s}} \right)_{s=\lambda_i}$$

$$\alpha = 1$$

$$\frac{\partial \alpha}{\partial s} = 0$$

$$\beta = s^3 + 6s^2 + 5s$$

$$\frac{\partial \beta}{\partial s} = 3s^2 + 12s + 5$$

Therefore,

$$S_K^i = \frac{-K}{3\lambda_i^2 + 12\lambda_i + 5}$$

Using the value for λ_2 gives

$$S_K^2 = \frac{-3276 + 701\sqrt{26} + j(8112 - 987\sqrt{26})}{6290}$$

$$= 0.0474 + j0.490$$

$$= 0.492 \angle 84.47 \text{ deg}$$

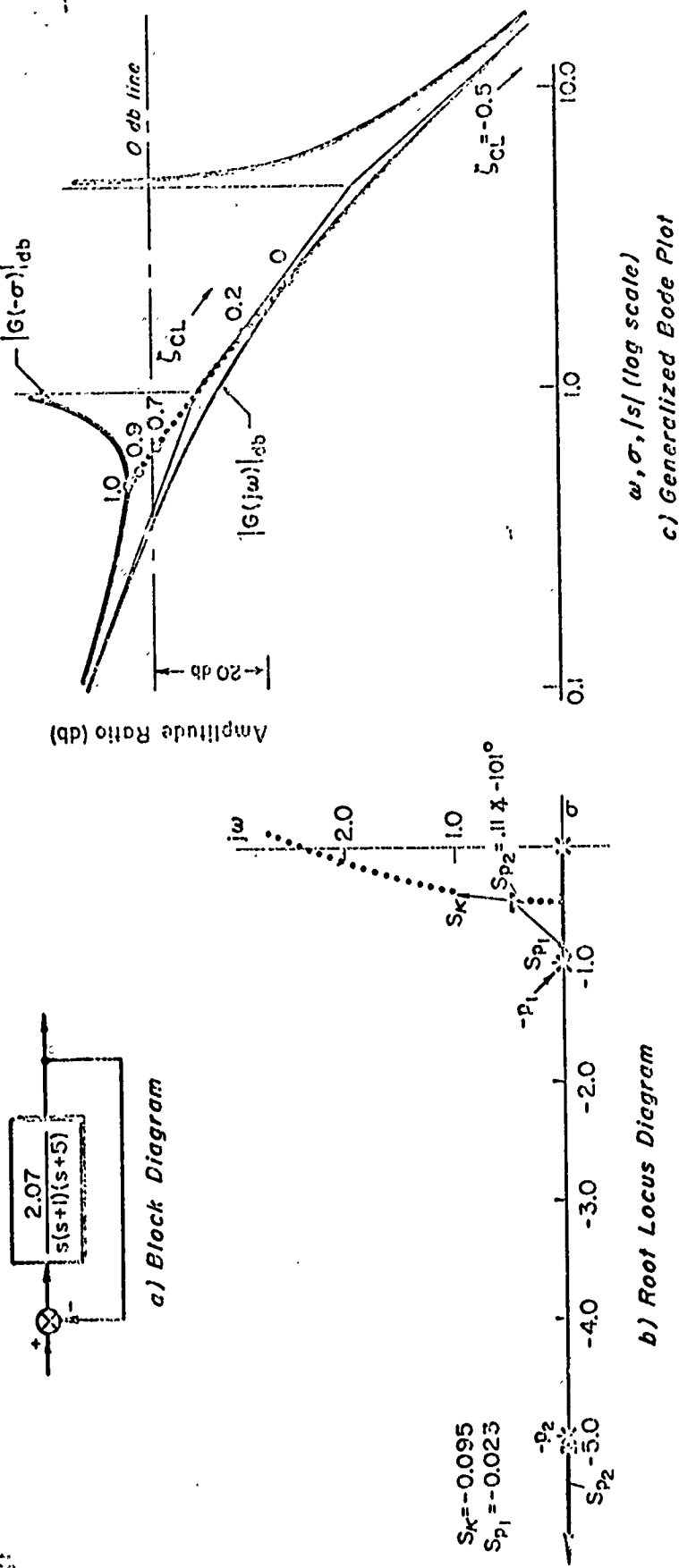


Fig. 3-46. System Survey for Unit-Numerator Third-Order System

Because λ_3 is the complex conjugate of λ_2 , S_K^3 is the complex conjugate of S_K^2 or

$$\begin{aligned} S_K^3 &= \frac{-3276 + 701\sqrt{26} - j(8112 - 987\sqrt{26})}{6290} \\ &= 0.0474 - j0.490 \\ &= 0.492 \angle -84.47 \text{ deg} \end{aligned}$$

Using the value of λ_1 in the equation for S_K^1 ,

$$S_K^1 = \frac{3276 - 701\sqrt{26}}{3145} = -0.0949$$

The modal response coefficients are, of course, the negatives of these sensitivities.

As a check, recall that if the number of system poles is greater than the number of zeros by two or more ($m \geq 2$), then the sum of the modal response coefficients or gain sensitivities is zero. These conditions are met for this example, and we can see that the values do sum to zero.

The second method of direct calculation, called the summation of terms method, uses Eq. 3-88, i.e.,

$$S_K^i = \frac{1}{\sum_{j=1}^{m+n} \frac{1}{\lambda_i + p_j} - \sum_{j=1}^n \frac{1}{\lambda_i + z_j}}$$

These computations may be performed in the following manner:

p_j	$(p_j + \lambda_2)$	$\frac{1}{p_j + \lambda_2}$
0	$-0.45049 + j0.45049$	$-1.1099 - j1.1099$
1	$0.54951 + j0.45049$	$1.0383 - j0.8922$
5	$4.54951 + j0.45049$	$0.2177 - j0.0216$

$$\sum \left(\frac{1}{p_j + \lambda_2} \right) = 0.1961 - j2.0237$$

$$S_K^2 = 0.0474 + j0.490 = 0.492 \angle 84.47 \text{ deg}$$

$$S_K^3 = 0.0474 - j0.490 = 0.492 \angle -84.47 \text{ deg}$$

and

p_j	$(p_j + \lambda_1)$	$\frac{1}{p_j + \lambda_1}$
0	-5.09902	-0.1961
1	-1.09902	-0.2440
5	-0.09902	-10.0990

$$\Sigma \left(\frac{1}{p_j + \lambda_1} \right) = -10.5391$$

$$s_K^1 = -0.0949$$

The results naturally agree with the first method because both methods are exact.

The sensitivities to the poles at -1 and -5 are easily computed from Eq. 3-90. For the pole at -1,

$$s_{p_1}^1 = \frac{-s_K^1}{\lambda_1 + p_1} = \frac{0.0949}{-1.10} = -0.0863$$

$$s_{p_1}^2 = \frac{-(0.0474 + j0.490)}{0.550 + j0.450} = -0.487 - j0.494$$

$$= 0.695 \angle -135 \text{ deg}$$

For the pole at -5,

$$s_{p_2}^1 = \frac{0.0949}{-0.0990} = -0.959$$

$$s_{p_2}^2 = \frac{-(0.0474 + j0.490)}{4.55 + j0.450} = -0.0208 - j0.1058$$

$$= 0.1077 \angle -101 \text{ deg}$$

2. Vector Method

The vector method uses Eq. 3-93. For this example, the equation reduces to

$$s_K^1 = \frac{-K}{(\lambda_1 + q_2)(\lambda_1 + q_3)}$$

$$s_K^2 = \frac{-K}{(\lambda_2 + q_1)(\lambda_2 + q_3)}$$

The following were measured with a Spirule:

$$\frac{1}{(\lambda_1 + q_2)(\lambda_1 + q_3)} = 0.0459$$

$$\frac{1}{(\lambda_2 + q_1)(\lambda_2 + q_3)} = 0.237 \angle -95.5 \text{ deg}$$

which gives

$$s_K^1 \doteq -0.0952$$

$$s_K^2 \doteq 0.490 \angle 84.5 \text{ deg}$$

These values are extremely close to the exact values. Both amplitude errors are less than 1 percent, and the angular error of s_K^2 is less than 1 deg.

3. Root-Locus Perturbation Methods

To estimate the gain sensitivity from Eq. 3-99, a perturbed position on the locus of $-0.41 + j0.76$ was chosen. The measured gain at that point was 3.89. This gives an estimate of

$$\begin{aligned} s_K^2 &\doteq \frac{K\Delta\lambda_2}{\Delta K} = 2.07 \frac{[(-0.41 + j0.76) - (-0.45 + j0.45)]}{3.89 - 2.07} \\ &= 0.045 + j0.353 = 0.356 \angle 82.7 \text{ deg} \end{aligned}$$

which has a magnitude error of 28 percent and an angular error of 2 deg.

For S_K^1 the point -5.42 was selected as the perturbed value of λ , for which the gain was 10.06. Then

$$S_K^1 = \frac{2.07[(-5.42) - (-5.10)]}{10.06 - 2.07} = -0.083$$

Although the gain was increased to nearly 5 times its original value, this estimate is within 13 percent of the exact value.

To obtain estimates from Eq. 3-100, perturbations normal to the locus were considered. For S_K^2 a perturbed λ of $-0.64 + j0.47$ was selected, for which the measured phase change was -24 deg. Then

$$\begin{aligned} S_K^2 &= \frac{j\Delta\lambda_2}{\Delta\theta} = \frac{[(-0.64 + j0.47) - (-0.45 + j0.45)]}{-24/57.3} \\ &= 0.0477 + j0.454 = 0.457 \angle 84 \text{ deg} \end{aligned}$$

For this estimate the amplitude error is 7 percent and the angular error is less than 1 deg.

For S_K^1 a perturbed λ of $-5.10 + j0.10$ was chosen. The phase change was 47.5 deg, so

$$S_K^1 = \frac{j(j0.10)(57.3)}{47.5} = -0.121$$

This estimate is in error by 27 percent.

4. Bode Root Locus Increments

The pertinent slope on the Bode root locus for the complex root was measured as

$$\frac{\Delta 20 \log_{10} K}{\Delta \log \omega_{CL}} = 39 \text{ dB/decade}$$

and a gain decrease of 3.8 dB increases ζ_{cy} to 0.9 over the original 0.7, or 0.0527/dB. The proportional sensitivity (Eq. 3-104) is then

$$\begin{aligned} M_K^2 &= \frac{d \ln \omega_n}{d \ln K} + \frac{j}{\sqrt{1-\zeta^2}} \frac{d \zeta}{d \ln K} \\ &= \frac{20}{39} + \frac{j}{0.707} (8.686) \left(\frac{0.2}{-3.8} \right) \\ &= 0.513 - j0.647 \end{aligned}$$

The conventional gain sensitivity is then

$$\begin{aligned} S_K^2 &= \lambda_2 M_K^2 = (0.513 - j0.647)(-0.450)(1-j) \\ &= 0.0603 + j0.522 \\ &= 0.525 \angle 83.4 \text{ deg} \end{aligned}$$

This is an error of about 7 percent in amplitude and 1 deg in angle.

To obtain S_K^1 the slope of the high frequency branch of the siggy is used. A slope measured from this plot is -830 dB/decade, although the root is too close to the open-loop pole to get an accurate value. Nevertheless,

$$M_K^1 = \frac{20}{830} = 0.0241$$

and

$$S_K^1 = \lambda_1 M_K^1 = (-5.1)(0.0241) = -0.123$$

This estimate is about 29 percent higher than the correct value.

Limiting Behavior and Special Cases

The magnitudes of gain sensitivities can cover the entire range of values from minus to plus infinity. Yet, intuitive notions of "sensitivity" as a general concept in closed-loop systems make part of this range appear unreasonable. One part of the problem is a direct consequence of the sensitivity definition, while another is associated with its nature as a first-order approximation. A better understanding of both facets can be gained by an examination of limiting cases.

In general, closed-loop poles are close to open-loop poles for low values of gain, and proceed to either open-loop zeros or unbounded values as the open-loop gain becomes very large. Throughout this travel the gain sensitivity is (Eq. 3-88 repeated here)

$$s_K^i = \frac{1}{\sum_{j=1}^{m+n} \frac{1}{\lambda_1 + p_j} - \sum_{j=1}^n \frac{1}{\lambda_1 + z_j}} \quad (3-107)$$

As K approaches zero, the closed-loop root, λ_1 , approaches the open-loop pole from which it derives, i.e., $\lambda_1 \rightarrow -p_1$. Then the term $1/(\lambda_1 + p_1)$ in Eq. 3-107 is dominant, so

$$s_K^i \Big|_{K \rightarrow 0} \rightarrow \frac{1}{\frac{1}{\lambda_1 + p_1}} \rightarrow 0 \quad (3-108)$$

Similarly, as K becomes very large, n of the closed-loop poles approach open-loop zeros. If the i th closed-loop pole is one of these, and it approaches the j th open-loop zero so that $\lambda_1 \rightarrow -z_j$, then

$$s_K^i \Big|_{K \rightarrow \infty} \rightarrow \frac{-1}{\frac{1}{\lambda_1 + z_j}} \rightarrow 0 \quad (3-109)$$

Finally, m of the closed-loop poles have no zeros to go to, and hence become very large relative to the $|p_j|$ and $|z_j|$. The sensitivity for these poles is

$$s_K^1]_{\lambda_i \gg |z_j|, |p_j|} \rightarrow \frac{1}{\sum_{j=1}^m \frac{1}{\lambda_j}} = \frac{\lambda_i}{m} \quad (3-110)$$

When the gain is sufficiently large for the open-loop zero dB line to intersect the high frequency asymptote, the open-loop transfer function is approximately

$$G(s) \doteq \frac{\kappa}{s^m}$$

so that λ_i will be

$$\lambda_i \doteq \sqrt[m]{-\kappa} \quad (3-111)$$

Thus, the sensitivity of the unbounded pole will be

$$s_K^1]_{\lambda_i \gg |z_j|, |p_j|} \rightarrow \frac{\sqrt[m]{-\kappa}}{m} \quad (3-112)$$

Equation 3-112 indicates that the sensitivity increases as the mth root of κ as gain is increased, although for finite gains the sensitivity is always finite.

Another circumstance in which the sensitivity can become very large is revealed by Eq. 3-93. Here it is apparent that the gain sensitivity for a closed-loop pole becomes very large as that pole nears another closed-loop pole. Indeed, as λ_i becomes equal to λ_j , indicating a branch point on the root locus, the gain sensitivity goes to infinity. This is to be expected since the sensitivity factors defined thus far have not considered multiple-order, closed-loop roots. As long as the gain is finite, an infinite gain sensitivity always indicates multiple-order, closed-loop poles.

A special situation of considerable interest can occur when a closed-loop root lies between an open-loop pole and zero which are much closer to each other than to all other open-loop poles and zeros. This is the so-called dipole case. The sensitivity for the bounded closed-loop pole will be, approximately,

$$S_K^i \doteq \frac{1}{\frac{1}{\lambda_i + p_i} - \frac{1}{\lambda_i + z_i}}$$

$$\doteq \frac{(\lambda_i + z_i)(\lambda_i + p_i)}{z_i - p_i} \quad (3-113)$$

The maximum value of S_K^i will occur when $\lambda_i = -(z_i + p_i)/2$, for which S_K^i becomes

$$S_K^i \Big|_{\max} \doteq \frac{1}{4} (p_i - z_i) \quad (3-114)$$

First-Order Root Sensitivities for a General Characteristic Equation*

We turn now to the general case where multiple-order closed-loop roots are permitted, and where the open-loop system parameters are not confined to gains, poles, and zeros. To accomplish the generalization we shall repeat many of the steps involved in the special case with first-order roots only.

For linear constant-coefficient systems of n th order the system characteristic equation can be written as

$$F[\lambda_i, \underline{\alpha}] = 0, \quad i = 1, 2, \dots, n \quad (3-115)$$

where λ_i is a root and $\underline{\alpha}$ is a vector with components α_j representing the set of system parameters. Each component, α_j , is nominally constant, but potentially variable. Open-loop poles, zeros, and gains are typical α_j 's, although other system parameters are also included. If λ_i is a first-order root, the total derivative of F will be

$$dF = \frac{\partial F}{\partial \lambda_i} d\lambda_i + \sum_j \frac{\partial F}{\partial \alpha_j} d\alpha_j = 0 \quad (3-116)$$

*This article is a shortened version of the paper: R. I. Stapleford and D. T. McRuer, "Sensitivity of Multiloop Flight Control System Roots to Open-Loop Parameter Variations," AJAA J., Vol. 4, No. 9, Sept. 1966, pp. 1655-1661.

When λ_i is an N th order root, $F(s)$ has the form $(s-\lambda_i)^N F_1(s)$. Then the first $N-1$ derivatives of F with respect to s , when evaluated at $s = \lambda_i$, become zero. In this event the total differential given above must be expanded to incorporate the first nonzero higher order term. Equation 3-116 is then modified to

$$dF = \frac{1}{N!} \left(\frac{\partial^N F}{\partial \lambda_i^N} \right) (d\lambda_i)^N + \sum_j \frac{\partial F}{\partial \alpha_j} d\alpha_j = 0 \quad (3-117)$$

Equation 3-117 can be solved for $d\lambda_i$ to give

$$d\lambda_i = \left[-\frac{N!}{\frac{\partial^N F}{\partial s^N}(s)} \sum_j \frac{\partial F}{\partial \alpha_j}(s) d\alpha_j \right]_{s=\lambda_i}^{1/N} \quad (3-118)$$

This relates differential changes, $d\alpha_j$, in the system parameters to the differential change in a system root. The expression can be written more compactly by defining parameter sensitivities as

$$S_{\alpha_j}^i = -N! \left[\frac{\partial F}{\partial \alpha_j}(s) / \frac{\partial^N F}{\partial s^N}(s) \right]_{s=\lambda_i} \quad (3-119)$$

The parameter sensitivity, S , is made specific to a particular system root by the superscript, i , while the pertinent system parameters, α_j , is indicated by the subscript. While it then has the same form as the previous sensitivities, it is not yet totally equivalent since the differential increment in the i th system root is given by

$$d\lambda_i = \left[\sum_j S_{\alpha_j}^i d\alpha_j \right]^{1/N} \quad (3-120)$$

The parameter sensitivities are partial derivatives, so shifts in system roots predicted using the sensitivities are only exact in the limit as the parameter variations approach zero. The practical extent to which this linear first-order theory will apply cannot be defined generally, although experience and an intimate knowledge of system details usually provides an appreciation for the conditions under which the first-order results should be accurate or suspect. When in doubt, practical restrictions on ranges can be evolved by comparing the first-order results with auxiliary complete solutions, or by developing second-order sensitivities.

The simplest special case using the above results is the single-loop system with the open-loop transfer function $G(s)$. Here $F(s) = 1 + G(s)$ and the components of \underline{a} are the gain, K , the open-loop zeros, $-z_j$, and the open-loop poles, $-p_j$. Using the open-loop transfer function form given by Eq. 3-78, the relation $G(\lambda_1) = -1$ in Eq. 3-118, and the basic formulations of Eqs. 3-81 through 3-88 gives the result

$$\begin{aligned} d\lambda_1 &= \left\{ \frac{N!}{\left[\frac{\partial^N G(s)}{\partial s^N} \right]_{s=\lambda_1}} \left[\frac{dK}{K} + \sum_{j=1}^m \frac{dz_j}{\lambda_1 + z_j} - \sum_{j=1}^{m+n} \frac{dp_j}{\lambda_1 + p_j} \right] \right\}^{1/N} \\ &= \left[S_K^1 \frac{dK}{K} + \sum_{j=1}^m S_{z_j}^1 dz_j + \sum_{j=1}^{m+n} S_{p_j}^1 dp_j \right]^{1/N} \end{aligned} \quad (3-121)$$

Comparison of Eq. 3-121 with its predecessor equivalent for first-order poles, Eq. 3-83, shows that key changes for the multiple-pole case are in the gain sensitivity and in the exponent N on the closed-loop pole shift, $d\lambda_1$ (or, as written in Eq. 3-121, an exponent $1/N$ on the sum of the sensitivities). The pole and zero sensitivities are also changed as the gain sensitivity,

$$S_K^1 = \frac{N!}{\left[\frac{\partial^N G(s)}{\partial s^N} \right]_{s=\lambda_1}} \quad (3-122)$$

is a common factor. Equation 3-121 reflects the well-known characteristics of a branch point on a root locus plot. The incoming branches, which at their junction represent an Nth order closed-loop root, are evenly spaced and separated from each other by $2\pi/N$. The departing branches are also separated from each other by $2\pi/N$ and are midway between the incoming branches.

Except for these isolated multiple-order root points, the root locus consists of branches characterizing the paths of the closed-loop roots as open-loop gain is changed. The gain sensitivity is tangent to these paths, whereas the zero and pole sensitivities will make angles with the tangents given by $\angle(\lambda_i + z_j)^{-1}$ and $-\angle(\lambda_i + p_j)^{-1}$, respectively.

Sensitivity factors for system parameters other than poles and zeros can also be determined. For instance, for the system parameter α_j where $G(s, \alpha_j) = KN(s, \alpha_j)/D(s, \alpha_j)$ the sensitivity factor is

$$S_{\alpha_j}^i = S_K^i \left[\frac{1}{N} \frac{\partial N}{\partial \alpha_j} - \frac{1}{D} \frac{\partial D}{\partial \alpha_j} \right]_{s=\lambda_i} \quad (3-123)$$

Connections Between Sensitivity and Modal Response

As noted previously, without proof, the gain sensitivities are simply related to the transient response characteristics of a unity-feedback system via the modal response coefficients for the closed-loop roots. The partial fraction expansion of the system's weighting function will contain the terms

$$\mathcal{L}^{-1} \left[\frac{Q_{i1}}{s - \lambda_i} + \frac{Q_{i2}}{(s - \lambda_i)^2} + \dots + \frac{Q_{iN}}{(s - \lambda_i)^N} \right] = e^{\lambda_i t} \left[Q_{i1} + Q_{i2}t + \dots + \frac{Q_{iN}t^{N-1}}{(N-1)!} \right] \quad (3-124)$$

as the contribution of an Nth order root. The N modal response coefficients, Q_{ik} , $k = 1, 2, \dots, N$, are evaluated by

$$Q_{ik} = \frac{1}{(N-k)!} \left\{ \frac{d^{N-k}}{ds^{N-k}} \left[\frac{(s - \lambda_i)^N G(s)}{1 + G(s)} \right] \right\}_{s=\lambda_i} \quad (3-125)$$

The gain sensitivity is the negative of the Nth modal response coefficient, i.e.,

$$S_K^i = -Q_{iN} = - \left[\frac{(s - \lambda_i)^N G(s)}{1 + G(s)} \right]_{s=\lambda_i} \quad (3-126)$$

To prove this relationship, it is convenient to introduce the variable $Q_{iN}^*(s)$ which is defined by

$$Q_{iN}^*(s) = \frac{(s - \lambda_i)^N G(s)}{1 + G(s)} \quad (3-127)$$

where $Q_{iN}^*(\lambda_i) = Q_{iN}$. Rewriting Eq. 3-127 as

$$[1 + G(s)] Q_{iN}^*(s) = (s - \lambda_i)^N G(s) \quad (3-128)$$

and differentiating with respect to s gives

$$[1 + G(s)] \frac{dQ_{iN}^*(s)}{ds} + Q_{iN}^*(s) \frac{dG(s)}{ds} = N(s - \lambda_i)^{N-1} G(s) + (s - \lambda_i)^N \frac{dG(s)}{ds} \quad (3-129)$$

Evaluating Eq. 3-129 at $s = \lambda_i$, and noting that $G(\lambda_i) = -1$, gives

$$Q_{iN} \left[\frac{dG(s)}{ds} \right]_{s=\lambda_i} = 0 \quad \text{if } N > 1 \quad (3-130)$$

Therefore,

$$\left[\frac{dG(s)}{ds} \right]_{s=\lambda_i} = 0 \quad \text{if } N > 1 \quad (3-131)$$

Repeated differentiation of Eq. 3-129 shows that the first $N-1$ derivatives of G are zero at $s = \lambda_i$, i.e.,

$$\left[\frac{d^k G(s)}{ds^k} \right]_{s=\lambda_i} = 0, \quad 1 \leq k \leq N-1 \quad (3-132)$$

and that

$$Q_{iN} = \frac{-N!}{\left[\frac{d^N G(s)}{ds^N} \right]_{s=\lambda_i}} \quad (3-133)$$

Finally, comparison with Eq. 3-122 gives

$$Q_{iN} = -S_K^i \quad (3-134)$$

Multiloop Sensitivity Ratios

The multiloop situation and notation are straightforward extensions of those introduced above. Instead of one open-loop transfer function, G , there are L open-loop transfer functions, G_k . Each of these has a gain, κ_k ; n_k zeros, $-z_{kj}$; and m_k+n_k poles, $-p_{kj}$. The closed-loop system characteristic function F is, in general, a summation of terms, each of which may be the product of several transfer functions, e.g., $F = 1 + G_1 + G_1 G_2 + G_2 G_3 G_4 + \dots$. Under these circumstances Eq. 3-118 becomes

$$d\lambda_i = \left[\frac{-N!}{\frac{\partial^N F(s)}{\partial s^N}} \sum_{k=1}^L \frac{\partial F}{\partial G_k} \left(\frac{\partial G_k}{\partial \kappa_k} d\kappa_k + \sum_{j=1}^{n_k} \frac{\partial G_k}{\partial z_{kj}} dz_{kj} + \sum_{j=1}^{m_k+n_k} \frac{\partial G_k}{\partial p_{kj}} dp_{kj} \right) \right]_{s=\lambda_i}^{1/N} \quad (3-135)$$

or in terms of the sensitivity factors

$$d\lambda_i = \left[\sum_{k=1}^L \left(S_{\kappa_k}^i \frac{d\kappa_k}{\kappa_k} + \sum_{j=1}^{n_k} S_{z_{kj}}^i dz_{kj} + \sum_{j=1}^{m_k+n_k} S_{p_{kj}}^i dp_{kj} \right) \right]_{s=\lambda_i}^{1/N} \quad (3-136)$$

Thus the gain sensitivities are

$$S_{K_k}^i = \left[\frac{-N!}{\frac{\partial^N F}{\partial s^N}(s)} \frac{\partial F}{\partial G_k} \frac{\partial G_k}{\partial K_k} K_k \right]_{s=\lambda_i} \quad (3-137)$$

The pole and zero sensitivities are given in terms of ratios involving the gain sensitivities by

$$\frac{S_{z_{kj}}^i}{S_{K_k}^i} = \left[\frac{\partial G_k / \partial z_{kj}}{K_k (\partial G_k / \partial K_k)} \right]_{s=\lambda_i} = \left[\frac{\partial G_k / \partial z_{kj}}{G_k} \right]_{s=\lambda_i} \quad (3-138)$$

$$\frac{S_{p_{kj}}^i}{S_{K_k}^i} = \left[\frac{\partial G_k / \partial p_{kj}}{K_k (\partial G_k / \partial K_k)} \right]_{s=\lambda_i} = \left[\frac{\partial G_k / \partial p_{kj}}{G_k} \right]_{s=\lambda_i} \quad (3-139)$$

These zero and pole sensitivity ratios can be considerably simplified.

For example, for the z_{kj} term

$$\frac{\partial G_k}{\partial z_{kj}} = \frac{G_k}{s + z_{kj}} \quad (3-140)$$

Combining this with the sensitivity ratio, Eq. 3-138, gives

$$\frac{S_{z_{kj}}^i}{S_{K_k}^i} = \left(\frac{1}{s + z_{kj}} \right)_{s=\lambda_i} = \frac{1}{\lambda_i + z_{kj}} \quad (3-141)$$

This and several other sensitivity ratios are summarized in Table 3-1. Besides the ratios of simple pole and zero to gain sensitivities, similar ratios are also provided for quadratic elements which result when complex conjugate pairs of poles or zeros are joined. The basic forms for these quadratics are $s^2 + 2\zeta\omega s + \omega^2$ and $s^2 + 2as + (a^2 + b^2)$.

Table 3-1. Sensitivity Ratios

$\frac{S_{K_j}^i}{S_{K_k}^i}$	$= \left[\frac{G_j(\partial F/\partial G_j)}{G_k(\partial F/\partial G_k)} \right]_{s=\lambda_i}$
$S_{z_{kj}}^i$	$= \frac{S_{K_k}^i}{z_{kj} + \lambda_i}$
$S_{p_{kj}}^i$	$= \frac{-S_{K_k}^i}{p_{kj} + \lambda_i}$
S_{ω}^i	$= \frac{* \pm 2(\omega + \zeta\lambda_i)S_K^i}{\lambda_i^2 + 2\zeta\omega\lambda_i + \omega^2}$
S_{ζ}^i	$= \frac{* \pm 2\omega\lambda_i S_K^i}{\lambda_i^2 + 2\zeta\omega\lambda_i + \omega^2}$
S_a^i	$= \frac{* \pm 2(a + \lambda_i)S_K^i}{\lambda_i^2 + 2a\lambda_i + a^2 + b^2}$
S_b^i	$= \frac{* \pm 2bS_K^i}{\lambda_i^2 + 2a\lambda_i + a^2 + b^2}$

*Use upper sign for zeros, lower sign for poles.

Also included in Table 3-1 is a key relationship between gain sensitivities for different transfer functions but relating to the same closed-loop root. Using Eq. 3-137 for two different gains gives

$$\frac{S_{K_j}^i}{S_{K_k}^i} = \left[\frac{G_j(\partial F/\partial G_j)}{G_k(\partial F/\partial G_k)} \right]_{s=\lambda_i} \quad (3-142)$$

Since F is a linear function of G_k , i.e., each transfer function G_k appears in F only with an exponent of unity, the term $G_k(\partial F/\partial G_k)$ is simply the sum of all the terms of F which include G_k . When evaluating sensitivity factors, Eq. 3-142 is of central importance, for all the gain sensitivities pertinent to a given closed-loop root can be calculated using ratios once a single gain sensitivity is known. Since a multiloop analysis is usually done as a sequence of loop closures the single-loop techniques can be applied to obtain the gain sensitivity for the last or outermost closure, thereby providing a starting point. The pole and zero sensitivity factors follow directly once the gain sensitivities are available.

The evaluation of the ratios of Eq. 3-142 can be quite involved. Considerable simplifications are sometimes possible by recalling that $F=0$ at $s=\lambda_1$. Thus, if F were given by

$$F = G_1 G_2 + G_1 G_3 G_4 + G_1 G_2 G_3 + G_3 G_4 \quad (3-143)$$

then

$$\frac{s_{K_2}^1}{s_{K_1}^1} = \left(\frac{G_1 G_2 + G_1 G_2 G_3}{G_1 G_2 + G_1 G_3 G_4 + G_1 G_2 G_3} \right)_{s=\lambda_1} = - \left[\frac{G_1 G_2 (1 + G_3)}{G_3 G_4} \right]_{s=\lambda_1} \quad (3-144)$$

$$\frac{s_{K_3}^1}{s_{K_1}^1} = \left(\frac{G_1 G_3 G_4 + G_1 G_2 G_3 + G_3 G_4}{G_1 G_2 + G_1 G_3 G_4 + G_1 G_2 G_3} \right)_{s=\lambda_1} = \left(\frac{G_1 G_2}{G_3 G_4} \right)_{s=\lambda_1} \quad (3-145)$$

$$\frac{s_{K_4}^1}{s_{K_1}^1} = \left(\frac{G_1 G_3 G_4 + G_3 G_4}{G_1 G_2 + G_1 G_3 G_4 + G_1 G_2 G_3} \right)_{s=\lambda_1} = -(1 + G_1)_{s=\lambda_1} \quad (3-146)$$

CHAPTER 4

VEHICLE EQUATIONS OF MOTION

4.1 INTRODUCTION

With our background in feedback control and analysis methods established in the preceding chapters, we come now to the object of such control—the vehicle. We want to characterize the vehicle in a way that is especially instructive to the flight control system designer rather than to the stability and control aerodynamicist or dynamic specialist. In order to do this, we deliberately emphasize the vehicle dynamic properties as a whole rather than as the sum of its component parts. For example, we avoid the fine-grain details of stability derivatives, and their dependence on configuration layout, in favor of a rudimentary understanding of the origins of aerodynamic forces and moments. Also, we look for and identify simplifying but generally valid assumptions which eventually lead us to a direct appreciation for the important factors governing the vehicle's response characteristics. Such an understanding of the over-all aspects of the object to be controlled is an implicit requirement for effective and efficient flight control system design activities. It affords a basic appreciation of vehicle/control-system interactions and flight controller possibilities most likely to succeed.

With this object and bias in mind we proceed, in this chapter, to establish the most generally useful (and used) sets of the basic equations of motion. The process is specifically designed to appeal to readers who are not necessarily conversant with formal advanced dynamic methods. Accordingly, we relate the developments to simple physical pictures of the phenomena involved rather than only to compact mathematical formulation. All the assumptions required to get to the final set of equations are specifically identified, as are their simplifying effects. The factors involved in selecting an appropriate axis system, and the process of converting from one set of axes to another, are set forth. The effects of linearizing about an operating point or trim condition and the influences of the selected trim condition on the resulting

linearized perturbed equations of motion are noted. Finally, the general origins of the aerodynamic forces which produce the usually important stability derivatives are discussed and illustrated. The over-all treatment* presents an ensemble of selected descriptions, explanations, and formulations eclectically combined to illuminate, as brightly as possible, an area which is often incompletely understood.

Proceeding from this base, in Chapters 5 and 6 we establish the various transfer functions of interest, in factored form, for longitudinal and lateral control. Here some of the feedback notions and methods exposed in past chapters are used to illustrate the effects of derivative changes and to extract approximate transfer function factors in literal[†] rather than numeric terms. Such literal expressions show the direct connections between the transfer function poles and zeros as a

*For other versions the reader can refer to the early works mentioned in the historical survey of Chapter 1 or to a variety of more recent texts, e.g.,

C. D. Perkins and R. E. Hage, Airplane Performance, Stability and Control, John Wiley and Sons, New York, 1949.

W. J. Duncan, Control and Stability of Aircraft, Cambridge Univ. Press, London and New York, 1952.

B. Etkin, Dynamics of Flight, John Wiley and Sons, New York, 1959.

W. R. Kolk, Modern Flight Dynamics, Prentice-Hall, New York, 1961

A. W. Babister, Aircraft Stability and Control, Pergamon Press, New York, 1961.

R. L. Halfman, Dynamics, Vol. I, Particles, Rigid Bodies, and Systems, Addison-Wesley Publishing Co., Reading, Mass., 1962.

E. Seckel, Stability and Control of Airplanes and Helicopters, Academic Press, New York, 1964.

[†]Such approximations go back to Bairstow, with more modern examples, of varying validity, appearing in:

Dynamics of the Airframe, BuAer Rept. AE-61-4, Vol. II, Sept. 1952.

H. H. B. M. Thomas and S. Neumark, Interim Note on Stability and Response Characteristics of Supersonic Aircraft, RAE TN Aero 2412, 1955.

I. L. Ashkenas and D. T. McRuer, Approximate Airframe Transfer Functions and Application to Single Sensor Control Systems, WADC-TR-58-82, June 1958.

A. J. Ross, The Lateral Oscillation of Slender Aircraft, RAE Rept. Aero 2666, June 1962.

function of the relative values of certain key derivatives, and give valuable insight into the probable nature of the associated control problem. A feature of both Chapters 5 and 6 is the tabulation of all presently known literal approximate factors and the specific conditions under which they are expected to be reasonably valid. The tabulations cover not only conventional single-loop numerators, but also the coupling numerators required for the analysis of conventional multiloop flight control systems; they also cover vehicles ranging from entry gliders to VTOL machines.

With this preview of the ramifications issuing therefrom, we turn now to the formulation of the vehicle equations of motion.

4.2 NEWTON'S SECOND LAW AND REFERENCE FRAMES

In this section we lay the basic groundwork for the developments which follow, starting with some assumptions and definitions.

Assumption 1. The airframe is assumed to be a rigid body.

In a rigid body the distances between any specified points in the body are fixed, so this assumption eliminates consideration of the forces acting between individual elements of mass. Consequently, the airframe motion can be described completely by a translation of the center of mass and by a rotation about this point.

Actual vehicles depart from the rigid-body assumptions in two ways—they are composed of several major elements which are required to move relative to one another, such as engines, rotors, or control devices; and incidental elastic deformations of the structure do occur, as in wing bending caused by air loads. Some of the changes required in the description of the aerodynamic forces due to such static deflection characteristics are illustrated later in this chapter (§4.9). Other changes, involving the dynamics of the structure* which can greatly increase the degrees of freedom to be considered in the equations of motion, are beyond the scope of the present treatment.

*A good basic treatment of such considerations is given in R. L. Bisplinghoff, H. Ashley, and R. L. Halfman, Aeroelasticity, Addison-Wesley Publishing Co., Reading, Mass., 1955.

Example equations of motion and resulting transfer functions for specific aircraft are limited features of this flight control literature; an exemplary cross section is contained in:

B. F. Pearce, W. A. Johnson, and R. K. Siskind, Analytical Study of Approximate Longitudinal Transfer Functions for a Flexible Airframe, ASD-TDR-62,279, June 1962.

Since all motion is relative, a suitable frame of reference must be selected to describe airframe motion. To this end, the following assumption is made:

Assumption 2. The earth is assumed to be fixed in space.

The inertial frame of reference defined by this assumption, i.e., one which is fixed or moves at constant velocity relative to the earth, permits a description of vehicle motion which is accurate for relatively short term guidance and control analysis purposes. It does have practical limitations when very long term navigation or extra-atmospheric operations are of interest.

With the above two assumptions as a basis, we have a reference frame in which Newton's laws are valid, and a rigid body to which these laws may be applied. To proceed, consider that the aircraft has a linear momentum vector, p , and an angular momentum vector, H , each measured in the inertial coordinate frame. By Newton's second law the time rate of change of linear momentum equals the sum of all externally applied forces,

$$\frac{dp}{dt} = F \quad (4-1)$$

and the rate of change of the angular momentum is equal to the sum of all applied torques,

$$\frac{dH}{dt} = M \quad (4-2)$$

These vector differential equations provide the starting point for a complete description of the rigid-body motions of the vehicle.

In almost all aeronautical vehicles some part of the thrust forces are produced by the expenditure of vehicle mass; and the mass variation must be considered in determining the rate of change of linear momentum.* At time t let the linear momentum be

$$p_1 = mV \quad (4-3)$$

where m is the mass and V the velocity of the vehicle. Then, if at time $t + \Delta t$, $-\Delta m$ is the net mass which has left the vehicle with an effective exhaust velocity, v_e , relative to the vehicle, the linear momentum will

*A. Sommerfield, Mechanics, Academic Press, New York, 1952.

J. B. Rosser, R. R. Newton, and G. L. Gross, Mathematical Theory of Rocket Flight, McGraw-Hill Book Co., New York, 1947.

$$p_2 = (m + \Delta m)(V + \Delta V) + (-\Delta m)(V + v_e) \quad (4-4)$$

Here $V + \Delta V$ and $m + \Delta m$ are the velocity and mass of the vehicle at time $t + \Delta t$, and $V + v_e$ is the effective velocity relative to inertial space of the mass increment exhausted. It should be noted in passing that the effective exhaust velocity depends on the exit area, the differential between exit and ambient pressures, and the exit velocity of the mass leaving the vehicle. The incremental change in momentum from time t to time $t + \Delta t$ is then

$$\begin{aligned} \Delta p &= p_2 - p_1 = (m + \Delta m)(V + \Delta V) - \Delta m(V + v_e) - mV \\ &= m\Delta V - v_e\Delta m + \Delta m\Delta V \end{aligned}$$

Dividing by Δt , and taking the limit as $\Delta t \rightarrow 0$, the time rate of change of momentum becomes

$$\frac{dp}{dt} = m \frac{dV}{dt} - v_e \frac{dm}{dt} = F$$

$$\text{or} \quad m \frac{dV}{dt} = F + v_e \frac{dm}{dt} = F + T_e \quad (4-5)$$

In Eq. 4-5 the thrust term, T_e , is defined by $v_e(dm/dt)$, and represents only that component of thrust due directly to the expulsion of vehicle mass. Thus, the rate of change of linear momentum can be computed as if the mass were constant and the product of the change in mass per unit time and the relative velocity between the exhausted mass and the vehicle were an external force. Equation 4-5 directly follows from Eq. 4-1 when the thrust is developed by a momentum exchange other than one directly involving the vehicle mass, as in a propeller (in the present context such a thrust would constitute an external force). Thus, if the thrust force includes exhaust products, Eq. 4-5 is correct in general for vehicles traveling at speeds small relative to the speed of light. Consequently, from this point on we shall consider that the thrust component, T_e , is contained in the general applied force, F .

If inertial space is now represented as a right-hand system of Cartesian axes, x, y, z , and the velocity vector, V , and total applied force,

\mathbf{F} , are resolved into their components \mathcal{U} , \mathcal{V} , and \mathcal{W} and F_x , F_y , and F_z along \mathcal{X} , \mathcal{Y} and \mathcal{Z} , respectively, then the vector equation, Eq. 4-5, can be written as the three scalar equations

$$\begin{aligned} m \frac{d\mathcal{U}}{dt} &= F_x \\ m \frac{d\mathcal{V}}{dt} &= F_y \\ m \frac{d\mathcal{W}}{dt} &= F_z \end{aligned} \quad (4-6)$$

These equations would describe the motion of the airframe center of mass as seen by an observer in the \mathcal{XYZ} frame. So far the definition of \mathcal{XYZ} is still quite arbitrary—it can have any orientation and can move at any constant velocity relative to the earth. We will later present a more specific definition.

The rotary equivalent of the linear momentum equation for the angular momentum, \mathbf{H} , is, unfortunately, far more complicated. The rotary analog of the mass, m , is the moment of inertia, which is a dyad,* \mathbf{I} . The angular momentum is the vector dot product of the inertia dyad with the angular velocity Ω , i.e.,

$$\mathbf{H} = \mathbf{I} \cdot \Omega \quad (4-7)$$

In the simplest case where the applied moment is about (or, as a vector, is along) a principle axis, \hat{i} , of the rigid body, the angular velocity will also be about the same axis. Then the vector equation will reduce to the scalar equation

$$H = I_{\hat{i}\hat{i}} \Omega$$

where $I_{\hat{i}\hat{i}}$ is the moment of inertia about the principal axis considered.

*See, for example, A. P. Wills, Vector Analysis With an Introduction to Tensor Analysis, Dover Publications, New York, 1958.

In the general case there are up to nine angular momentum components which differ in detail, depending on the axis system selected as a reference frame for the equations of motion. Consider the derivatives of Eq. 4-7,

$$\frac{dH}{dt} = I \cdot \frac{d\Omega}{dt} + \frac{dI}{dt} \cdot \Omega = M \quad (4-8)$$

If the inertias and angular velocities are computed in the space-fixed axis system, xyz , the moment of inertia about each axis will, in general, vary continuously as the vehicle moves with respect to the axis origin. Even if the aircraft's motions are restricted to constant velocities so that the xyz axes can be attached to the aircraft center of mass, the inertias will change as the craft rotates about the axes. Such variations in inertia will contribute to the time rate of change of angular momentum via the $(dI/dt) \cdot \Omega$ term in Eq. 4-8. The resulting equations are therefore complicated by time-varying parameters—an extremely undesirable feature.

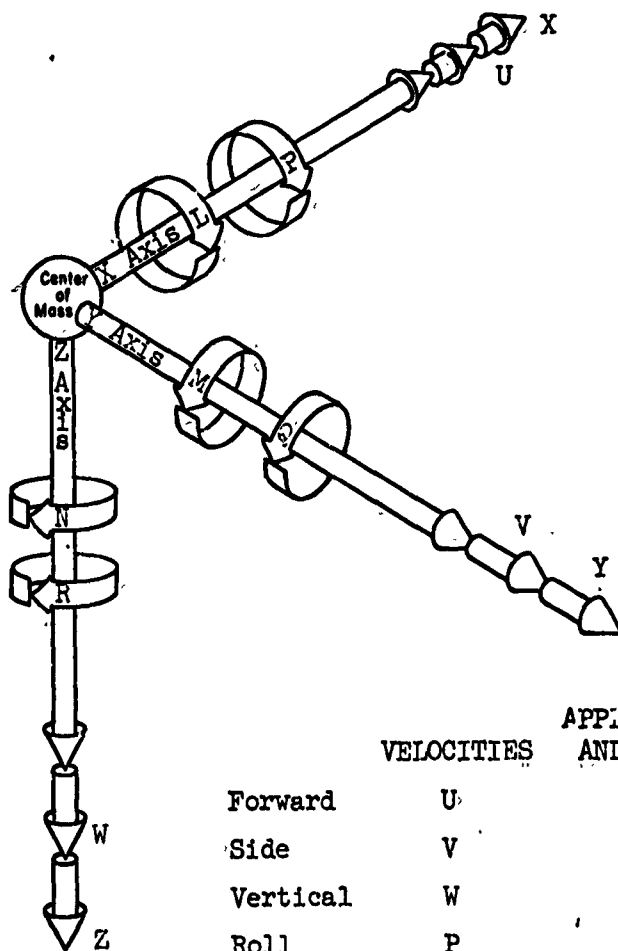
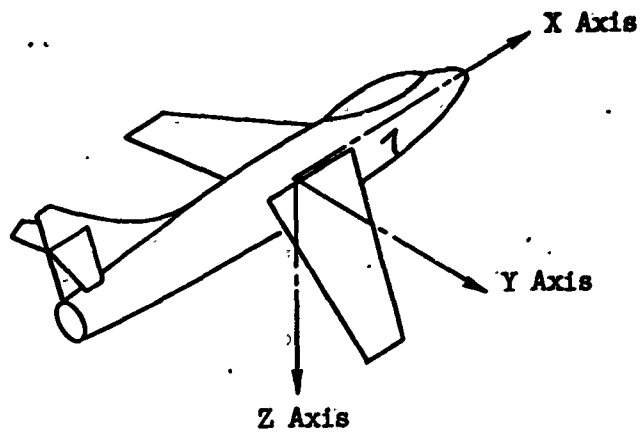
An attractive alternative is to select an axis system which is fixed in the body. In this kind of system the measured rotary inertial properties are constant to the extent that the mass can also be considered constant; and terms containing such quantities as dI_{xx}/dt are always zero. A body-fixed axis system has another virtue—it is the natural frame of reference for most vehicle-borne observations and measurements of the vehicle's motions. For example, a pilot is fundamentally aware of rotary motions about the vehicle's center of gravity rather than about a space-fixed point. He feels accelerating forces with respect to his own alignment with the body-fixed frame rather than with respect to a space-fixed frame. Also, many flight instruments and sensors, especially those used for short term control of the vehicle, are similarly constituted; i.e., in general they measure motions with respect to body-fixed axes.

Unfortunately the above advantages are not obtained without some penalty. For instance, the very simple inertial force forms of Eq. 4-6 are replaced by more complex ones when the linear velocities are measured

in a body-fixed axis system. Some of the applied forces, as well, are more simply and naturally expressed in the inertial reference frame. Also, instrumentation designed for long term navigation and guidance is of necessity aligned to measure linear velocities and distances in space or earth-fixed coordinate systems, and the pilot himself is visually oriented to earth-fixed as well as vehicle-fixed axes. These factors raise the possibility of a desirable intermixing of axis systems; for example, an earth-fixed reference for forces and linear accelerations, and a body-fixed reference for moments and angular motions. Such dual systems are, in fact, needed for a complete treatment of the vehicle's motion. However, for flight-control applications the expansion of the left sides of Eqs. 4-1 and 4-2 is usually made in a manner appropriate to a body-fixed axis system with its origin on the vehicle's center of mass. This axis system is shown in Fig. 4-1a, together with the notation and sign conventions used to identify linear and angular velocities and applied forces and moments. The body-fixed X, Y, and Z axes are oriented in the aircraft with X forward, Y out the right wing, and Z out the bottom as shown.

4.3 EXPANSION OF THE INERTIAL FORCES AND MOMENTS

The left-hand side of Eq. 4-5 and of Eq. 4-2 can readily be expanded formally, especially when vector or matrix algebra is used; however, this process affords little physical insight into the origins of the resulting terms. To better narrow the gap between simple mathematical routine and difficult physical interpretation we will carry out the development of the inertial forces and moments in two different ways. First, the developments will be related as much as possible to simple physical pictures of the phenomena involved, and then it will be repeated as an essentially mathematical exercise.



ARROWS INDICATE
POSITIVE SENSE

	VELOCITIES	APPLIED FORCES AND MOMENTS	DISTANCES
Forward	U	X	x
Side	V	Y	y
Vertical	W	Z	z
Roll	P	L	
Pitch	Q	M	
Yaw	R	N	

Fig. 4-1. Vehicle-Fixed Axis System and Notation

Rectilinear Acceleration Components

The total rectilinear acceleration is dV/dt . The components of V are U , V , and W along the X , Y , and Z body-fixed axes. The translational acceleration components of dV/dt along these axes will contain not only the obvious components dU/dt , dV/dt , and dW/dt , but also centripetal acceleration components due to the rotation of the body-fixed axis system relative to inertial space. A simple two-dimensional example is helpful to develop an intuitive understanding of these statements. Figure 4-2 shows the plan view of an airplane at two slightly separated points along its flight path. At the left the airplane has the velocity components U and V along the X and Y axes, respectively; at the right a small increment of time, Δt , later the aircraft's velocity has changed in both magnitude and direction. The craft has rotated through an incremental angle, $R\Delta t$, and the linear velocity components are now $U + \Delta U$ and $V + \Delta V$.

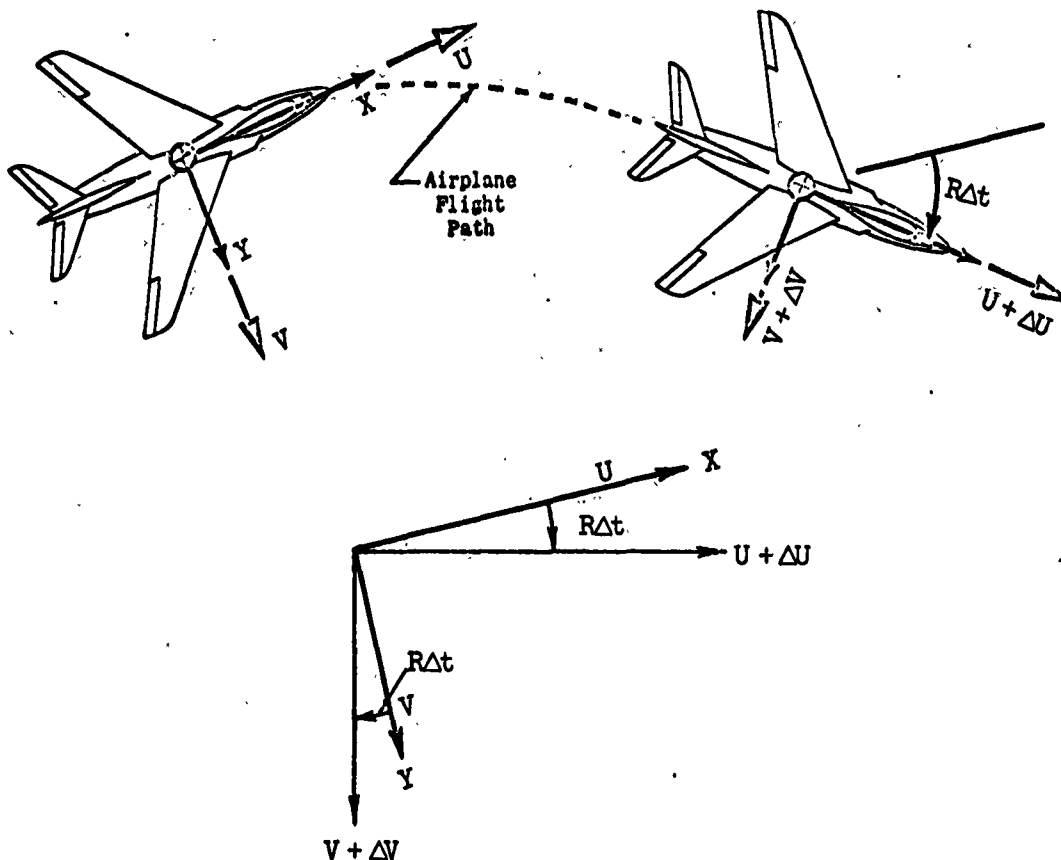


Fig. 4-2. An Airplane in Two-Dimensional Accelerated Flight

When the acceleration is written as a time rate of change of the velocity, the components with respect to the original X and Y axes are:

$$a_x = \lim_{\Delta t \rightarrow 0} \frac{(U + \Delta U) \cos R\Delta t - U - (V + \Delta V) \sin R\Delta t}{\Delta t}$$

$$= \dot{U} - VR \quad (4-9)$$

and

$$a_y = \lim_{\Delta t \rightarrow 0} \frac{(V + \Delta V) \cos R\Delta t - V + (U + \Delta U) \sin R\Delta t}{\Delta t}$$

$$= \dot{V} + UR \quad (4-10)$$

where the dot-superior on U and V indicate the time derivatives of these velocity components measured in body-fixed axes. The vector acceleration, **a**, is the vector sum of the two components given in Eqs. 4-9 and 4-10. With **i**, **j**, and **k** taken as unit vectors along X, Y, and Z, the acceleration vector becomes:

$$\mathbf{a} = a_x \mathbf{i} + a_y \mathbf{j}$$

$$= [\dot{U} \mathbf{i} + \dot{V} \mathbf{j}] + [-VR \mathbf{i} + UR \mathbf{j}] \quad (4-11)$$

The first term is just the time derivative of the velocity measured in the body-fixed coordinates. The second term can be identified, by recalling the rules for vector cross-multiplication,* as the cross-product of the angular and linear velocities; in this case **Rk** and **V = U_i + V_j**, respectively, i.e.,

$$\mathbf{k} \times [\mathbf{U} \mathbf{i} + \mathbf{V} \mathbf{j}] = UR(\mathbf{k} \times \mathbf{i}) + VR(\mathbf{k} \times \mathbf{j})$$

$$= UR \mathbf{j} - VR \mathbf{i} \quad (4-12)$$

since **i × j = k**, **j × k = i**, **k × i = j**, **k × j = -j × k**, etc. If these results are now generalized to the three-dimensional case, the vector acceleration will be:

$$\mathbf{a} = \frac{d\mathbf{V}}{dt} = \dot{\mathbf{V}} + \boldsymbol{\Omega} \times \mathbf{V} \quad (4-13)$$

*Wills, op. cit.

Here dV/dt is used to denote the time derivative of velocity relative to inertial space axes, whereas the dot-superior notation indicates the time derivative of velocity observed in the body-fixed coordinates.

Physically, the cross-product term arises from the centripetal accelerations along any given axis due to angular velocities about the remaining two axes. Thus, for rotations about the Y axis, the pitching velocity, Q , and vertical velocity, W , can both be represented by simple angular motions about some instantaneous center in space defined by $x = W/Q$, as shown in Fig. 4-3. The centripetal acceleration component

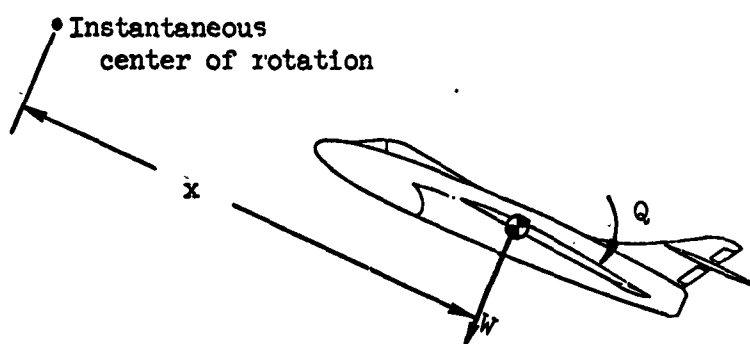


Fig. 4-3. Centripetal Acceleration Along X Due to Pitching and Plunging

is then directed forward (positive) and is equal in magnitude to the product, WQ . The picture about the Z axis is similar except that, following the right-hand rule, the sign of the side velocity is negative and the corresponding acceleration component is $-VR$ (Fig. 4-4).

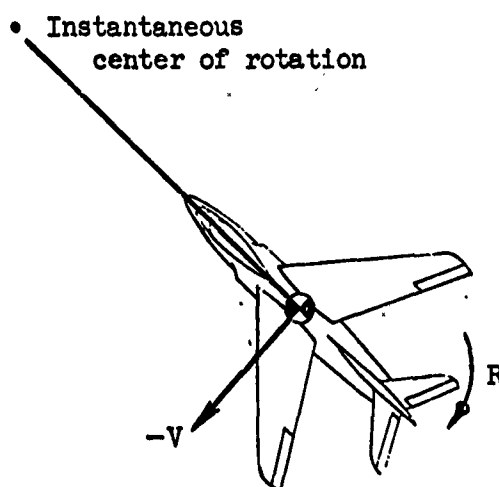


Fig. 4-4. Centripetal Acceleration Along X Due to Yawing and Sideslipping

These constructions can be repeated for each axis in turn with the similar and general result (including linear acceleration) that

$$a_1 = \dot{v}_1 + \omega_2 v_3 - \omega_3 v_2 \quad (4-14)$$

where v and ω are linear and angular velocities, respectively, and the subscripts 1, 2, and 3 represent axes taken in right-hand progression (e.g., if 1 is Y, then 2 and 3 are Z and X, respectively). Accordingly, the complete set of linear accelerations, obtained by specializing Eq. 4-14, is given by

$$\begin{aligned} a_x &= \dot{U} + QW - RV \\ a_y &= \dot{V} + RU - PW \\ a_z &= \dot{W} + PV - QU \end{aligned} \quad (4-15)$$

Precisely this same result can be derived formally using the vector equation, Eq. 4-13, with

$$\mathbf{V} = U\mathbf{i} + V\mathbf{j} + W\mathbf{k} \quad (4-16)$$

$$\boldsymbol{\Omega} = P\mathbf{i} + Q\mathbf{j} + R\mathbf{k} \quad (4-17)$$

Inserting these into Eq. 4-13,

$$\begin{aligned} \mathbf{a} &= \frac{d\mathbf{V}}{dt} = [\dot{U}\mathbf{i} + \dot{V}\mathbf{j} + \dot{W}\mathbf{k}] + \begin{vmatrix} \mathbf{i} & \mathbf{j} & \mathbf{k} \\ P & Q & R \\ U & V & W \end{vmatrix} \\ &= [\dot{U} + QW - RV]\mathbf{i} + [\dot{V} + RU - PW]\mathbf{j} + [\dot{W} + PV - QU]\mathbf{k} \end{aligned} \quad (4-18)$$

Inertial Torque Components

The total inertial torque about a given axis is due to both direct angular acceleration about that axis and to components arising from linear acceleration gradients resulting from combined rotations about all axes. To obtain a physical understanding of how these effects arise, we will first investigate the dynamics of an infinitesimal element of mass, dm , as shown in Fig. 4-5.

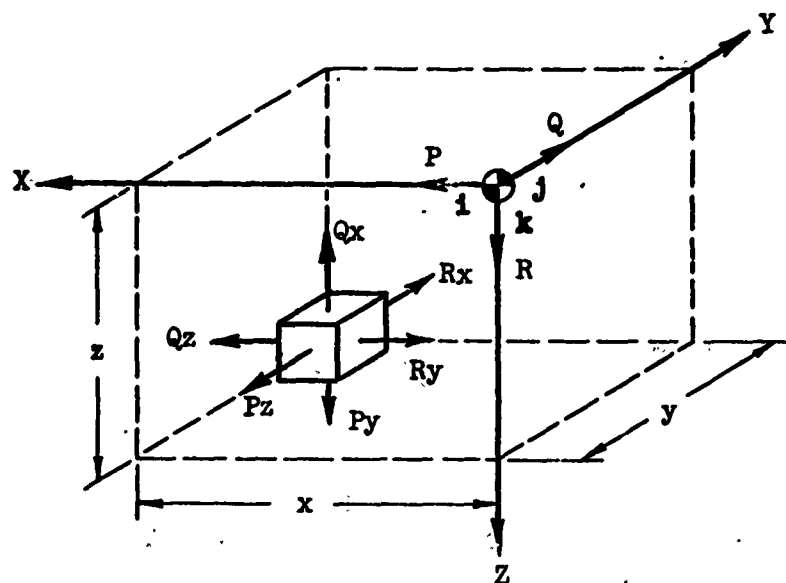


Fig. 4-5. Linear Velocity Components of an Element of Mass Due to an Angular Velocity Ω Having Components P, Q, and R

Figure 4-5 shows the linear velocity components of the elemental mass due to the angular velocity components P, Q, and R. The accuracy of this representation can be verified by inspection, or by multiplying the angular velocity and the radius (distance) from the axis system origin at the vehicle center of mass to the elemental mass. That is,

$$\begin{aligned}
 v_{dm} &= \Omega \times \rho = [P\mathbf{i} + Q\mathbf{j} + R\mathbf{k}] \times [x\mathbf{i} + y\mathbf{j} + z\mathbf{k}] \\
 &= \begin{vmatrix} \mathbf{i} & \mathbf{j} & \mathbf{k} \\ P & Q & R \\ x & y & z \end{vmatrix} \\
 &= \mathbf{i}[Qz - Ry] + \mathbf{j}[Rx - Pz] + \mathbf{k}[Py - Qx] \quad (4-19)
 \end{aligned}$$

Associated with each of these linear velocities is a linear momentum, which is simply the velocities multiplied by dm . The moment of momentum (i.e., angular momentum) is obtained by summing the moments of these linear momenta about each axis. For example, about the X axis the angular momentum component will arise from the j and k components multiplied, respectively by the z and y lever arms (see Fig. 4-5),

$$dH_X = [-z(Rx - Pz) + y(Py - Qx)] dm$$

or, expanding,

(4-20)

$$dH_X = y(yP) dm + z(zP) dm - z(xR) dm - y(xQ) dm$$

The complete set of equations obtained in this way is:

$$\begin{aligned} dH_X &= (y^2 + z^2) P dm - zx R dm - yx Q dm \\ dH_Y &= (z^2 + x^2) Q dm - xy P dm - yz R dm \\ dH_Z &= (x^2 + y^2) R dm - zx P dm - zy Q dm \end{aligned} \quad (4-21)$$

Again, these can be derived by inspection of Fig. 4-5 or by using the vector relationship for the angular momentum, i.e.,

$$\begin{aligned} d\mathbf{H} &= \rho \times d\mathbf{p} = \rho \times \mathbf{v}_{dm}(dm) \\ &= dm \begin{vmatrix} \mathbf{i} & \mathbf{j} & \mathbf{k} \\ x & y & z \\ [Qz - Ry] & [Rx - Pz] & [Py - Qx] \end{vmatrix} \end{aligned} \quad (4-22)$$

For a finite rigid body the components of the moment of momentum will be the integrals of Eq. 4-21 over the entire mass of the vehicle:

$$\begin{aligned} H_X &= P \int (y^2 + z^2) dm - Q \int xy dm - R \int xz dm \\ H_Y &= Q \int (z^2 + x^2) dm - R \int yz dm - P \int yx dm \\ H_Z &= R \int (x^2 + y^2) dm - P \int zx dm - Q \int zy dm \end{aligned} \quad (4-23)$$

Notice now that the integral $\int (y^2 + z^2) dm$ is, by definition, the moment of inertia, I_{XX} , of the entire mass of the airplane about the X axis. Similarly, the integral $\int xy dm$ is defined as the product of inertia, I_{XY} . The remaining integrals in Eq. 4-23 are similarly defined and the equations may be rewritten as

$$\begin{aligned}
H_X &= PI_{xx} - QI_{xy} - RI_{xz} \\
H_Y &= QI_{yy} - RI_{yz} - PI_{xy} \\
H_Z &= RI_{zz} - PI_{xz} - QI_{yz}
\end{aligned}
\tag{4-24}$$

where $I_{yz} = I_{zy}$, from the form of the integrals.

An alternative, still physically satisfying approach to the derivation of Eq. 4-24 is to consider the aircraft at the outset as a rigid body having principal axis moments of inertia, I_{x_0} , I_{y_0} , and I_{z_0} . Because the body-fixed XYZ axes do not necessarily coincide with the principal axes, we require an appreciation for the angular momentum components due to product of inertia terms. This can be obtained by reference to Fig. 4-6 which shows the XZ coordinates rotated with respect to the principal axes of inertia. Resolving the angular velocity, with

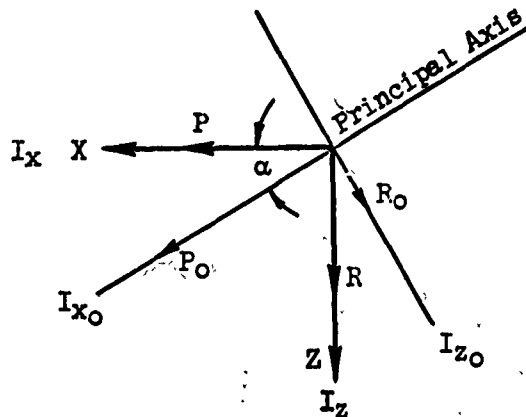


Fig. 4-6. Principal and Body-Fixed Axes

components P and R in body-fixed axes, along the principal axes,

$$\begin{aligned}
P_0 &= P \cos \alpha + R \sin \alpha \\
R_0 &= R \cos \alpha - P \sin \alpha
\end{aligned}
\tag{4-25}$$

Accordingly the total angular momenta about the principal axes become

$$\begin{aligned}
H_{X_0} &= P_0 I_{X_0} = I_{X_0} (P \cos \alpha + R \sin \alpha) \\
H_{Z_0} &= R_0 I_{Z_0} = I_{Z_0} (R \cos \alpha - P \sin \alpha)
\end{aligned}
\tag{4-26}$$

Resolving these back into the X,Z axes,

$$H_X = H_{X_0} \cos \alpha - H_{Z_0} \sin \alpha$$

$$H_Z = H_{Z_0} \cos \alpha + H_{X_0} \sin \alpha$$

and, substituting Eq. 4-26 and collecting terms,

$$H_X = P[I_{X_0} \cos^2 \alpha + I_{Z_0} \sin^2 \alpha] + R\left[\frac{(I_{X_0} - I_{Z_0})}{2} \sin 2\alpha\right]$$

$$H_Z = P\left[\frac{(I_{X_0} - I_{Z_0})}{2} \sin 2\alpha\right] + R[I_{Z_0} \cos^2 \alpha + I_{X_0} \sin^2 \alpha]$$

The bracketed terms are moments and products of inertia in the XZ axis system, i.e.,

$$\begin{aligned} I_{XX} &= I_{X_0} \cos^2 \alpha + I_{Z_0} \sin^2 \alpha \\ I_{ZZ} &= I_{Z_0} \cos^2 \alpha + I_{X_0} \sin^2 \alpha \\ I_{XZ} &= \frac{(I_{Z_0} - I_{X_0})}{2} \sin 2\alpha \end{aligned} \quad (4-27)$$

Consequently,

$$\begin{aligned} H_X &= PI_{XX} - RI_{XZ} \\ H_Z &= RI_{ZZ} - PI_{XZ} \end{aligned} \quad (4-28)$$

Repeating the above process for the other two planes results finally in

$$\begin{aligned} H_X &= PI_{XX} - QI_{XY} - RI_{XZ} \\ H_Y &= QI_{YY} - RI_{YZ} - PI_{YX} \\ H_Z &= RI_{ZZ} - PI_{ZX} - QI_{ZY} \end{aligned} \quad (4-29)$$

which is identical to Eq. 4-24.

Turning now to the calculation of the time rate of change of angular momentum, it is apparent that this will be simplified if the products of inertia do not vary with time. Formally, this requires:

Assumption 3. The mass and mass distribution of the vehicle are assumed to be constant.

Actually there may be considerable differences in mass and its distribution throughout a mission as fuel is burned, stores expended, etc. The assumption is, nonetheless, ordinarily reasonable because the rates of change are relatively small and may be safely neglected for the time periods covered by most analyses.

With this assumption it is easy to see (Eq. 4-29) that angular accelerations \dot{P} , \dot{Q} , and \dot{R} will lead directly to the contributions

$$\begin{aligned}\dot{H}_X &= \dot{P}I_{XX} - \dot{Q}I_{XY} - \dot{R}I_{XZ} \\ \dot{H}_Y &= \dot{Q}I_{YY} - \dot{R}I_{YZ} - \dot{P}I_{XY} \\ \dot{H}_Z &= \dot{R}I_{ZZ} - \dot{P}I_{XZ} - \dot{Q}I_{YZ}\end{aligned}\quad (4-30)$$

These amount to the time derivatives of the angular momentum components as expressed in body-fixed coordinates. They do not constitute the total time rate of change of the angular momentum because, even with zero angular acceleration, steady rotations about a given axis change the direction of the angular momentum vectors about the remaining axes. For instance, from Fig. 4-7 it is clear that a steady angular velocity, Q , about the Y axis produces a change of angular momentum

which is directed along the X axis, i.e.,

$\Delta H_X = H_Z Q \Delta t$. This rotation will add a component of dH_X/dt equal to $H_Z Q$ to the X component and, similarly, a term $-H_X Q$ to the Z component of dH/dt . Analogous constructions in the remaining planes, when added to the above and to the time variation of the angular momentum relative to the body-fixed axes, yield the components of the total time rate of change of angular momentum:

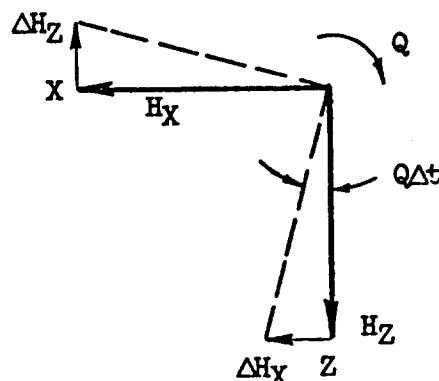


Fig. 4-7. Angular Momentum Change Due to Steady Rotation

$$\begin{aligned}\frac{dH_X}{dt} &= \dot{H}_X + QH_Z - RH_Y \\ \frac{dH_Y}{dt} &= \dot{H}_Y + RH_X - PH_Z \\ \frac{dH_Z}{dt} &= \dot{H}_Z + PH_Y - QH_X\end{aligned}\quad (4-31)$$

Substituting the angular momentum components of Eq. 4-24, the total time rate of change of momentum about a typical axis (X) will be

$$\begin{aligned}
\frac{dH_X}{dt} &= \dot{H}_X + QH_Z - RH_Y \\
&= \underbrace{(\dot{P}I_{XX} - \dot{Q}I_{XY} - \dot{R}I_{XZ})}_{\dot{H}_X} + \underbrace{Q(RI_{ZZ} - PI_{XZ} - QI_{YZ})}_{QH_Z} - \underbrace{R(QI_{YY} - RI_{YZ} - PI_{XZ})}_{RH_Y} \\
&= \dot{P}I_{XX} + QR(I_{ZZ} - I_{YY}) - (PQ + \dot{R})I_{XZ} + (PR - \dot{Q})I_{XY} - (Q^2 - R^2)I_{YZ}
\end{aligned}$$

By considering the simplified picture shown in Fig. 4-7 and such appropriate momentum change components as QH_Z , the physical origin of even such strange and obscure terms as $-Q^2I_{YZ}$ is readily seen. (4-32)

When all of the components are inserted in Eq. 4-31, and the notation on the inertias I_{XX} , I_{YY} , and I_{ZZ} is simplified to I_X , I_Y , and I_Z , the result is

$$\begin{aligned}
\frac{dH_X}{dt} &= \dot{P}I_X + QR(I_Z - I_Y) - (PQ + \dot{R})I_{XZ} + (PR - \dot{Q})I_{XY} - (Q^2 - R^2)I_{YZ} \\
\frac{dH_Y}{dt} &= \dot{Q}I_Y + PR(I_X - I_Z) - (QR + \dot{P})I_{XY} + (PQ - \dot{R})I_{YZ} - (R^2 - P^2)I_{XZ} \\
\frac{dH_Z}{dt} &= \dot{R}I_Z + PQ(I_Y - I_X) - (PR + \dot{Q})I_{YZ} + (QR - \dot{P})I_{XZ} - (P^2 - Q^2)I_{XY}
\end{aligned} \quad (4-33)$$

This completes the simplified development of the inertial torque components.

For a formal development of the inertial moments we note that the form of Eq. 4-13, and the steps leading to it, are actually suitable for any vector whose components are measured in the body-fixed XYZ axis system. Thus, substituting H for V in Eq. 4-13, the time rate of change of the angular momentum will be

$$\frac{dH}{dt} = \dot{H} + \Omega \times H \quad (4-34)$$

This equation can be used directly once a vector expression for the angular momentum is obtained.

The moments and products of inertia in Eq. 4-24 are the rotational analog of the mass in Eq. 4-5. There are, however, nine components or

six magnitudes, since $I_{ij} = I_{ji}$, required to specify the rotary inertia properties. For use in vector algebra operations this inertia is written as the dyad \underline{I} :

$$\begin{aligned}\underline{I} = & I_{xx}\mathbf{i}\mathbf{i} - I_{xy}\mathbf{i}\mathbf{j} - I_{xz}\mathbf{i}\mathbf{k} \\ & - I_{xy}\mathbf{j}\mathbf{i} + I_{yy}\mathbf{j}\mathbf{j} - I_{yz}\mathbf{j}\mathbf{k} \\ & - I_{xz}\mathbf{k}\mathbf{i} - I_{yz}\mathbf{k}\mathbf{j} + I_{zz}\mathbf{k}\mathbf{k}\end{aligned}\quad (4-35)$$

In forming the dot product between a dyad and a vector, the unit vectors in the vector quantity are dotted into the closer of the unit vector pairs shown in the dyad, i.e.,

$$\begin{aligned}(\mathbf{i}\mathbf{j}) \cdot \mathbf{j} &= \mathbf{i} \\ (\mathbf{k}\mathbf{i}) \cdot \mathbf{i} &= \mathbf{k} \\ (\mathbf{i}\mathbf{j}) \cdot \mathbf{i} &= \mathbf{0}, \text{ etc.}\end{aligned}\quad (4-36)$$

With this convention the angular momentum can now be written directly as

$$\begin{aligned}\mathbf{H} &= \underline{I} \cdot \dot{\mathbf{Q}} = H_x\mathbf{i} + H_y\mathbf{j} + H_z\mathbf{k} \\ &= [PI_{xx} - QI_{xy} - RI_{xz}]\mathbf{i} \\ &\quad + [-PI_{xy} + QI_{yy} - RI_{yz}]\mathbf{j} \\ &\quad + [-PI_{xz} - QI_{yz} + RI_{zz}]\mathbf{k}\end{aligned}\quad (4-37)$$

This result is the same as that given in Eq. 4-29 and, when used with Eq. 4-34, produces the Eq. 4-33 values of the components of $d\mathbf{H}/dt$ along X, Y, and Z. There is no instructional advantage to be gained in carrying out the algebraic operation (which is analogous to that of Eq. 4-18 for the rate of change of linear momentum).

Recapitulation of Inertial Forces and Simplification of Inertial Moments

The linear acceleration and moment equations expressed in quantities referred to body-fixed axes are given in Eqs. 4-15 and 4-33, respectively. The linear acceleration set will be recapped here just as is; but the rotary equations are overcomplicated and can be simplified by adopting an additional assumption.

Assumption 4. The XZ plane is assumed to be a plane of symmetry.

Assumption 4 is a very good approximation for most airborne vehicles. When it applies, we see from Fig. 4-8 that there is both a positive and a negative value of y for each value of x and z ; consequently, $I_{yz} = \int yz \, dm = 0$ and $I_{xy} = \int xy \, dm = 0$.

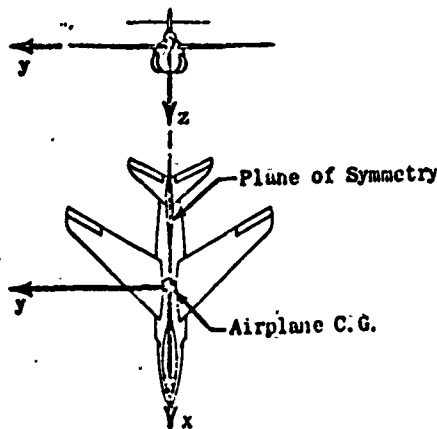


Fig. 4-8. Airframe Plane of Symmetry

The expanded form of the equations of motion referred to body-fixed axes can then be written as

$$\begin{aligned}
 \sum X &= m(\dot{U} + QW - RV) \\
 \sum Y &= m(\dot{V} + RU - PW) \\
 \sum Z &= m(\dot{W} + PV - QU) \\
 \sum L &= \dot{P}I_x - \dot{R}I_{xz} + QR(I_z - I_y) - PQI_{xz} \\
 \sum M &= \dot{Q}I_y + PR(I_x - I_z) - R^2I_{xz} + P^2I_{xz} \\
 \sum N &= \dot{R}I_z - \dot{P}I_{xz} + PQ(I_y - I_x) + QR I_{xz}
 \end{aligned}
 \tag{4-38}$$

4.4 EXPANSION OF THE GRAVITY FORCE

Components of the Gravity Force

Among the forces and moments acting externally on the vehicle, those due to gravity are always present. Neglecting gravity gradient considerations which are only important when all other external forces are essentially nonexistent (e.g., in extra-atmospheric flight), the gravity force can be considered to act at the vehicle's center of gravity. Since the

center of gravity coincides with the center of mass, the gravity force produces no external moments about that point. Thus, for our body-fixed axes, gravity can contribute components only to the summation of the external forces.

To determine these components consider the alignment of the gravity vector with respect to the XYZ axes as shown in Fig. 4-9. Here the problem is essentially that of defining the relative orientation of a line (the g vector direction) with a rectangular coordinate reference frame. Rotations (in azimuth) of the frame about the g vector have no effect on the relative orientation of the g-vector/reference-frame, so only the two angles Θ and Φ are needed to describe the physical situation.

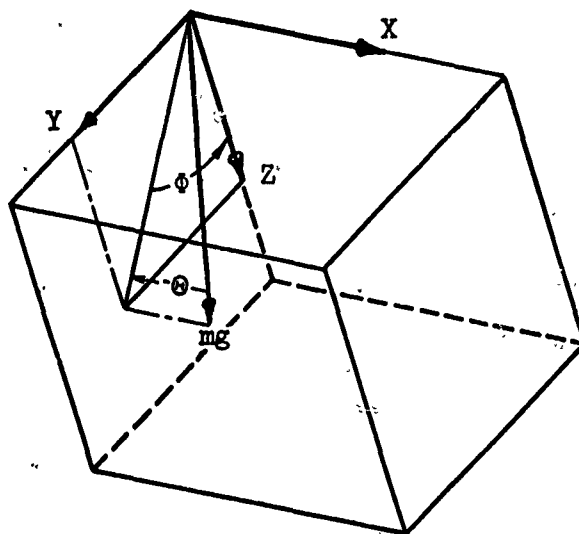


Fig. 4-9. Orientation of Gravity Vector with XYZ Body-Fixed Axis System

Direct resolution of the gravity-induced force, mg , results in

$$\begin{aligned}\Delta X &= mg \sin (-\Theta) = -mg \sin \Theta \\ \Delta Y &= mg \cos (-\Theta) \sin \Phi = mg \cos \Theta \sin \Phi \\ \Delta Z &= mg \cos (-\Theta) \cos \Phi = mg \cos \Theta \cos \Phi\end{aligned}\tag{4-39}$$

Unfortunately the angles Θ and Φ are not in general simply the integrals of Q and P , respectively, so that we have, in effect, introduced

two new motion quantities. We must, therefore, connect the angular velocities P , Q , and R with Θ and Φ and their derivatives. The details of this will depend on whether the gravitational vertical as seen in the vehicle is assumed to be fixed or rotating relative to inertial space. The first situation is generally an excellent approximation whenever the vehicle speed is small relative to orbital velocities, whereas the second is more appropriate for very high speed flight. Both situations will be examined below in separate articles. Interspersed between these two treatments will be a short resume of axis transformation considerations which are needed here for the first time in this book.

Angular Velocity of XYZ Relative to the Gravitational Vertical

To express the angular orientation and velocity of the XYZ system with respect to the gravity vector requires the introduction of the angular velocity of the axes about the g vector. This is the azimuth rate, $\dot{\psi}$. With this angular velocity added to $\dot{\Phi}$ and $\dot{\Theta}$, the resolutions of interest are pictured in Fig. 4-10. Note that the $\dot{\psi}$ vector is not normal to either Θ or Φ , but that its projection in the YZ plane is.

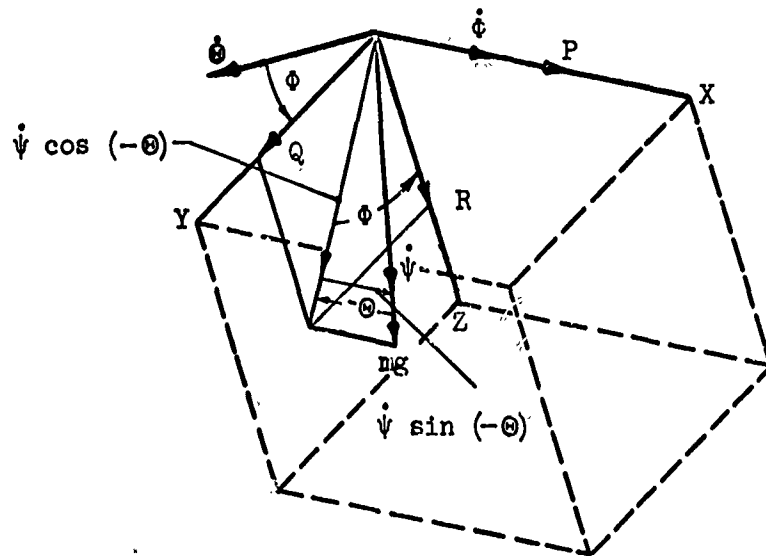


Fig. 4-10. Angular Orientation and Velocities of g Relative to XYZ

Then, recognizing that $\cos(-\Theta) = \cos \Theta$ and $\sin(-\Theta) = -\sin \Theta$, and assuming that the g vector does not rotate relative to inertial space, the following relations are apparent by direct resolution:

$$\begin{aligned} P &= \dot{\Phi} - \dot{\Psi} \sin \Theta \\ Q &= \dot{\Theta} \cos \Phi + \dot{\Psi} \cos \Theta \sin \Phi \\ R &= -\dot{\Theta} \sin \Phi + \dot{\Psi} \cos \Theta \cos \Phi \end{aligned} \quad (4-40)$$

The converse case is also directly apparent from Fig. 4-10, i.e.,

$$\begin{aligned} \dot{\Phi} - \dot{\Psi} \sin \Theta &= P \\ \dot{\Theta} &= Q \cos \Phi - R \sin \Phi \\ \dot{\Psi} \cos \Theta &= R \cos \Phi + Q \sin \Phi \end{aligned}$$

which reduces to

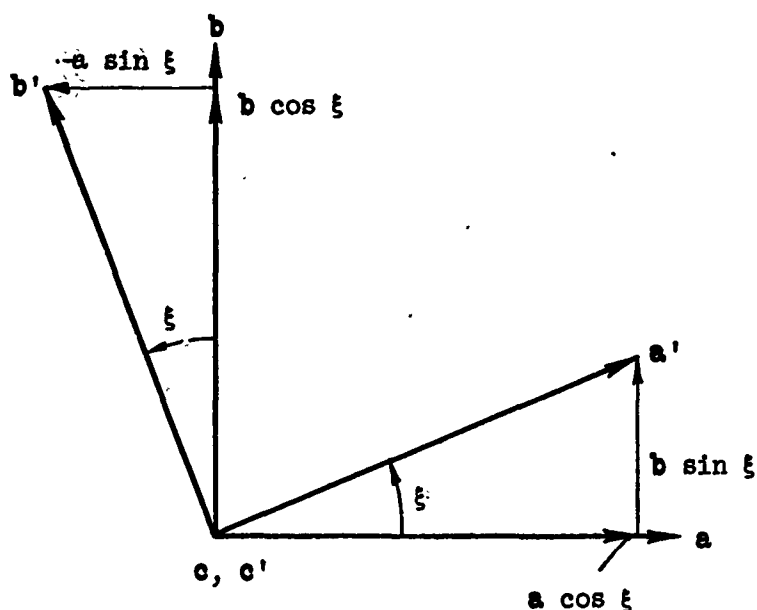
$$\begin{aligned} \dot{\Phi} &= P + Q \tan \Theta \sin \Phi + R \tan \Theta \cos \Phi \\ \dot{\Theta} &= Q \cos \Phi - R \sin \Phi \\ \dot{\Psi} &= R \left(\frac{\cos \Phi}{\cos \Theta} \right) + Q \left(\frac{\sin \Phi}{\cos \Theta} \right) \end{aligned} \quad (4-41)$$

These relationships supply the required connections between Θ and Φ and P , Q , and R .

Vector Resolutions and Axis Transformations

When two or more frames of reference are needed to define physical relationships, it becomes necessary to orient these reference frames one to another and to establish the transformation relations needed to define a given vector quantity in terms of components in the several frames. Perhaps the simplest way to accomplish these requirements is to define a matrix of direction cosines which relates unit vectors in one axis system to those in another. The determination of the elements in such matrices can be accomplished efficiently by a combination of inspection and matrix multiplication procedures. These will be described below.

In Fig. 4-11 the unit vectors a' , b' , and c' of the right-handed orthogonal coordinate system are found in terms of unit vectors a , b , and c of another. The a' , b' , c' system is obtained from a , b , c by a rotation about c through the angle ξ . As a directional cosine array



$$\begin{aligned} a' &= a \cos \xi + b \sin \xi \\ b' &= -a \sin \xi + b \cos \xi \\ c' &= c \end{aligned}$$

Fig. 4-11. Resolution of Vectors

this transformation becomes

	a	b	c
a'	$\cos \xi$	$\sin \xi$	0
b'	$-\sin \xi$	$\cos \xi$	0
c'	0	0	1

(4-42)

This array may be read either left to right or down. For instance, reading down in the a column,

$$a = a' \cos \xi - b' \sin \xi + 0 \cdot c'$$

whereas reading b' from left to right,

$$b' = -a \sin \xi + b \cos \xi + 0 c$$

The array can also be interpreted as a matrix and its inverse; these correspond, respectively, to the array being read left to right and the array being read down.* The matrices will be

$$[\xi] = \begin{bmatrix} \cos \xi & \sin \xi & 0 \\ -\sin \xi & \cos \xi & 0 \\ 0 & 0 & 1 \end{bmatrix} \quad (4-43)$$

which is appropriate when going from a', b', c' to a, b, c , i.e.,

$$\begin{bmatrix} a' \\ b' \\ c' \end{bmatrix} = [\xi] \begin{bmatrix} a \\ b \\ c \end{bmatrix} \quad (4-44)$$

and the inverse,

$$[\xi^{-1}] = \begin{bmatrix} \cos \xi & -\sin \xi & 0 \\ \sin \xi & \cos \xi & 0 \\ 0 & 0 & 1 \end{bmatrix} \quad (4-45)$$

which applies when going from a, b, c to a', b', c' , i.e.,

*Such substitution of rows for columns in a matrix in general produces a transposed matrix. In the present case the product of the matrix and its transpose is a unit matrix which makes the transpose also an inverse. Aside from this, perhaps extraneous, explanation, the gist of the matrix operations needed for axis transformations can be followed directly in this presentation. If additional background is required, the reader may refer to any good text on matrix operations, e.g.,

A. C. Aiken, Determinants and Matrices (Interscience Book), John Wiley and Sons, New York, 1956.

E. A. Guillemin, The Mathematics of Circuit Analysis, John Wiley and Sons, New York, 1949.

L. A. Pipes, Matrix Methods for Engineering, Prentice-Hall, Inc., Englewood Cliffs, New Jersey, 1963.

$$\begin{bmatrix} a \\ b \\ c \end{bmatrix} = \begin{bmatrix} 1 & 0 & 0 \\ 0 & \cos \xi & \sin \xi \\ 0 & -\sin \xi & \cos \xi \end{bmatrix} \begin{bmatrix} a' \\ b' \\ c' \end{bmatrix} \quad (4-46)$$

This rotation and resolution can also be symbolized conveniently by a "transformation" box, as shown in Fig. 4-12.* The interconnections therein indicate the multiplication and additions required in the resolutions. Although the arrows indicate progression from a, b, c to a', b', c' , the transformation works equally well in both directions.

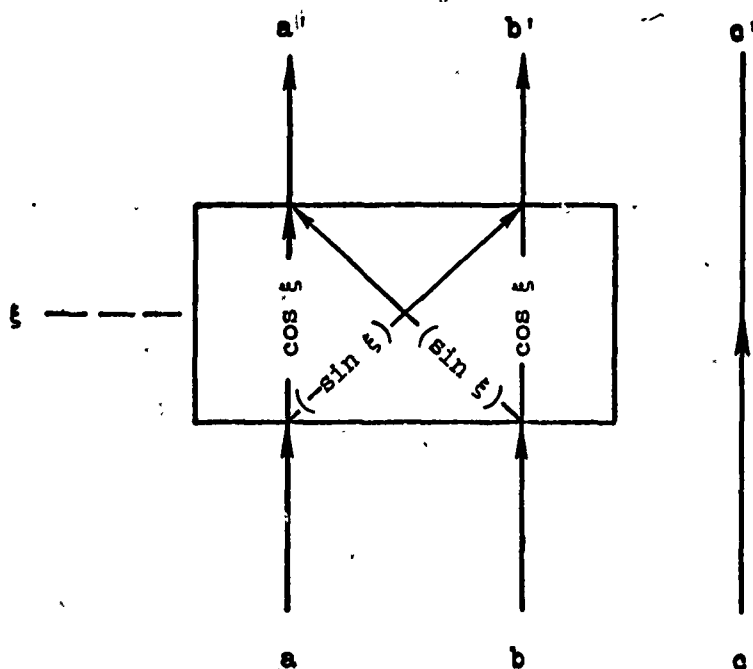


Fig. 4-12. Transformation Box for Single Rotation

The Eq. 4-42 array exhibits certain general properties which, once recognized, make it possible to write out the appropriate array for any single rotation by inspection.

- The main diagonal terms are always either the cosine of the angle of rotation or 1.
- The 1 is always associated with the axis about which rotation occurs.
- The remaining elements in the row and column containing the 1 are all zeros.

*This convenient rubric for vector resolution is due to Robert W. Bond.

- The remaining places in the matrix contain the sine of the angle of rotation and are always symmetrically placed relative to the cosine terms.
- In the direct right-handed rotation the negative sine always appears in the row above the 1 (this is to be interpreted as the third row if the 1 is in the first).

Any set of axes can be obtained from any other by a sequence of three rotations. For each rotation a matrix or transformation box corresponding to the array described above applies. The total array for the three rotations is simply obtained by multiplication of the three matrices representing the individual rotations.*

The most common transformation set in vehicle dynamics is that between an axis system which incorporates the g vector as one axis and the body-fixed X, Y, Z axes. The actual rotations involved, following the usual order, are indicated in Fig. 4-13. This shows the unit vectors **i**, **m**, and **n** in the vehicle-centered, gravity-directed set and **i**, **j**, and **k** in the vehicle body axes. The matrices for each of the three rotations shown can be written by inspection, in terms of the "Euler angle," ψ , θ , ϕ , as

$$\begin{aligned} [\psi] &= \begin{bmatrix} \cos \psi & \sin \psi & 0 \\ -\sin \psi & \cos \psi & 0 \\ 0 & 0 & 1 \end{bmatrix} \\ [\theta] &= \begin{bmatrix} \cos \theta & 0 & -\sin \theta \\ 0 & 1 & 0 \\ \sin \theta & 0 & \cos \theta \end{bmatrix} \\ [\phi] &= \begin{bmatrix} 1 & 0 & 0 \\ 0 & \cos \phi & \sin \phi \\ 0 & -\sin \phi & \cos \phi \end{bmatrix} \end{aligned} \quad (4-47)$$

These rotations are also shown in the transformation boxes of Fig. 4-14.

*A matrix product has the form

$$\begin{bmatrix} a_{11} & a_{12} \\ a_{21} & a_{22} \end{bmatrix} \begin{bmatrix} b_{11} & b_{12} \\ b_{21} & b_{22} \end{bmatrix} = \begin{bmatrix} a_{11}b_{11} + a_{12}b_{21} & a_{11}b_{12} + a_{12}b_{22} \\ a_{21}b_{11} + a_{22}b_{21} & a_{21}b_{12} + a_{22}b_{22} \end{bmatrix}$$

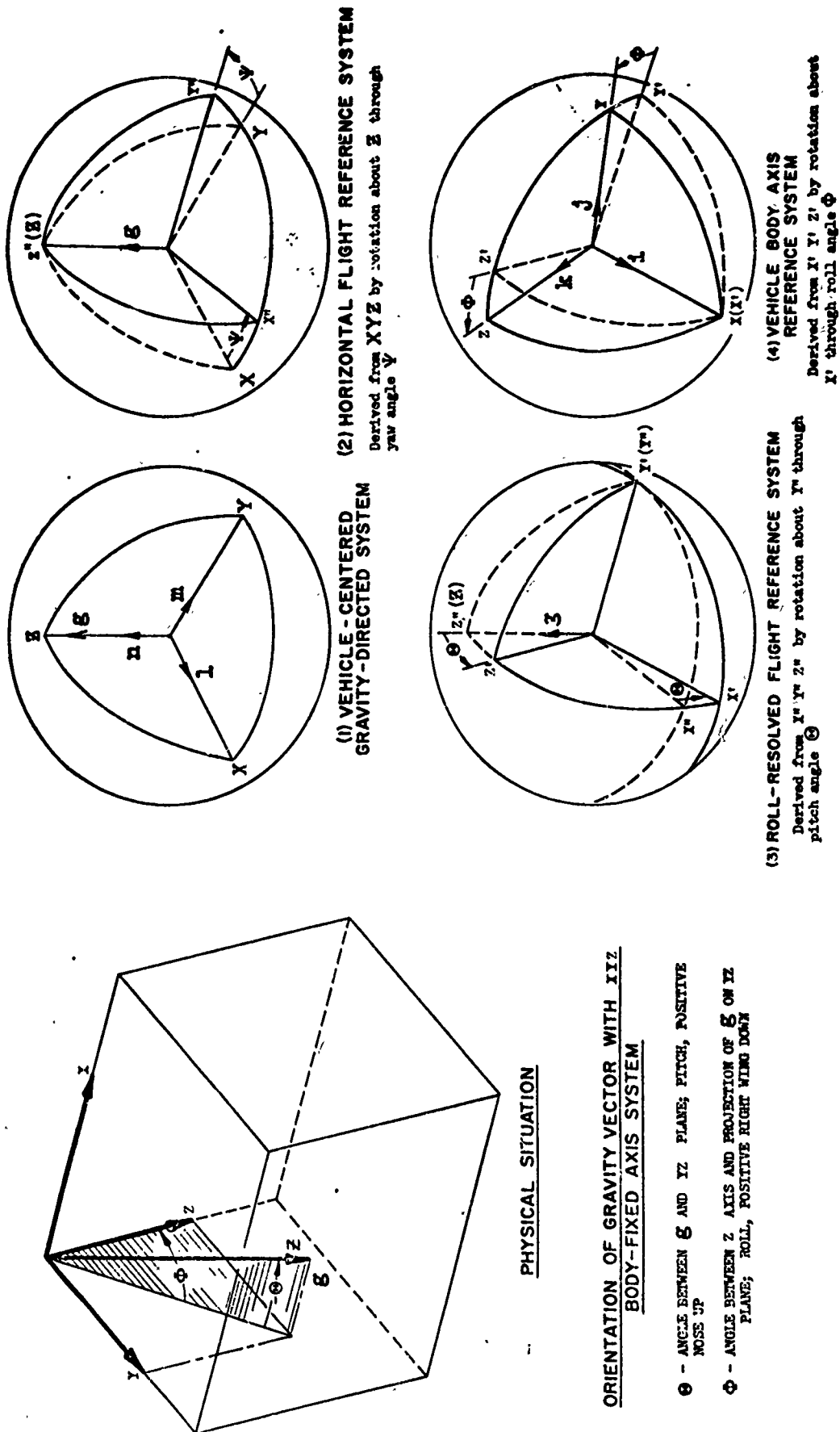


Fig. 4-13. Relationship Between Vehicle-Centered Gravity-Directed and Vehicle-Fixed Axis Systems

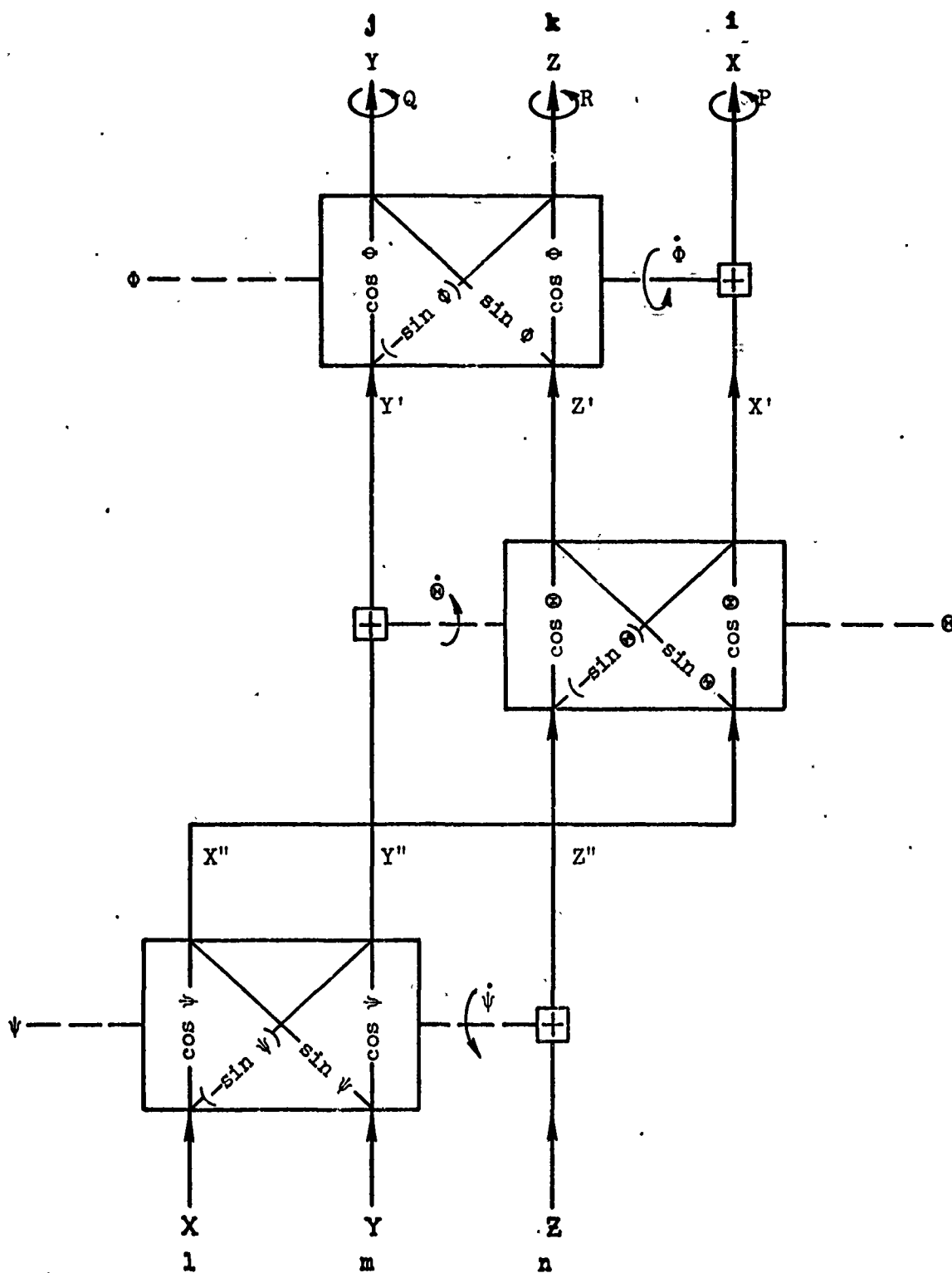


Fig. 4-14. Transformation Boxes for Relationships Between Vehicle-Centered Gravity-Directed and Vehicle-Fixed Axis Systems

Carrying out the matrix multiplications in the order appropriate to the rotations, i.e.,

$$[E] = [\phi][\theta][\psi] \quad (4-48)$$

the complete direction cosine array is found. That is,

	1	m	n
1	$\cos \psi \cos \theta$	$\sin \psi \cos \theta$	$-\sin \theta$
j	$\cos \psi \sin \theta \sin \phi - \sin \psi \cos \phi$	$\sin \psi \sin \theta \sin \phi + \cos \psi \cos \phi$	$\cos \theta \sin \phi$
k	$\cos \psi \sin \theta \cos \phi + \sin \psi \sin \phi$	$\sin \psi \sin \theta \cos \phi - \cos \psi \sin \phi$	$\cos \theta \cos \phi$

(4-49)

Just as in the simple single-rotation example, the array can be read from left to right or down. As matrices these correspond to

$$[E] \begin{bmatrix} 1 \\ m \\ n \end{bmatrix} = \begin{bmatrix} 1 \\ j \\ k \end{bmatrix} \quad (4-50)$$

the array being read left to right, or

$$[E^{-1}] \begin{bmatrix} 1 \\ j \\ k \end{bmatrix} = \begin{bmatrix} 1 \\ m \\ n \end{bmatrix} \quad (4-51)$$

the array being read down.

In general, any pair of coordinate systems can be associated by a sequence of three rotations such as those exemplified above. There are, however, six possible sets of rotation angles corresponding to the six possible ways of getting from one axis system to the other. Each of these results in a different directional cosine array. The forms of all are similar in that, of the nine terms involved, one contains a single angle, four involve two angles, and the remaining four contain all three angles. While in principle any of the possible rotational sequences can be used, there is in practice ordinarily one to be preferred. In

the present case the rotational sequence and angles were defined to result in the least complicated resolution of the g vector into the body-fixed XYZ system. This is given by

$$\mathbf{g} = g\mathbf{n} = g[-\sin \Theta \mathbf{i} + \cos \Theta \sin \Phi \mathbf{j} + \cos \Theta \cos \Phi \mathbf{k}] \quad (4-52)$$

The basic simplicity of the components shown is insured by taking the first rotation about the gravity vector through an azimuth angle, ψ . As already remarked, rotations of the body-fixed axes about the g vector can have no effect on the relative orientation of the g vector and the XYZ frame. The two remaining rotations can conceivably be accomplished in two different ways without complicating the g vector description. The sequence and angles selected are the more natural cyclic sequence, and also have the advantage of being those measured by a typically oriented vertical gyro. (As will be seen in Chapter 9, a two-degree-of-freedom gravity-erected vertical gyro oriented with its outer gimbal bearing axis along X measures Θ and Φ on its inner and outer gimbals, respectively.)

The angular velocities are readily found using the transformation boxes of Fig. 4-14. Thus, the angular velocities P, Q, and R about X, Y, and Z, respectively, can be found by tracking the angular velocities associated with the transformation boxes $\dot{\psi}$, $\dot{\Theta}$, and $\dot{\Phi}$ through the intervening transformations, with the result

$$\begin{aligned} P &= \dot{\Phi} - \dot{\psi} \sin \Theta \\ Q &= \dot{\Theta} \cos \Phi + \dot{\psi} \cos \Theta \sin \Phi \\ R &= \dot{\psi} \cos \Theta \cos \Phi - \dot{\Theta} \sin \Phi \end{aligned} \quad (4-53)$$

This is the same result as that previously derived on a more physical basis in the discussion leading to Eq. 4-40. Although the axis transformations can be run in either direction through the transformation boxes, the angular velocities go only one way. Consequently, the equations (Eq. 4-41) for $\dot{\psi}$, $\dot{\Theta}$, and $\dot{\Phi}$ in terms of P, Q, and R are most conveniently obtained via the physical picture of Fig. 4-10 or by solution of Eq. 4-53.

Angular Velocity of the Gravitational Vertical Relative to Inertial Space

If the aircraft travels at a very high speed, the angular velocity relative to inertial space of the gravitational vertical is no longer approximately zero. Consequently, the right side of Eq. 4-53 must have additional terms added which take into account the rotation of the XYZ axes as the aircraft moves about the earth. To take this effect into account, inertial space will now be defined as an $X_I Y_I Z_I$ axis system, with its origin at the center of the earth and its axes nonrotating relative to the fixed stars. For any given flight path this system is oriented so that the $X_I Z_I$ plane contains the equilibrium flight velocity and gravity vectors. Then, as shown in Fig. 4-15, the vehicle-centered, gravity-directed system, XYZ, is oriented so that its XZ plane also contains the equilibrium flight vector. Then the angular velocity of XYZ relative to inertial space is $\dot{\psi}$, or

$$\dot{v} = \frac{U}{r} \quad (4-54)$$

Thus, the angular velocity of XYZ is

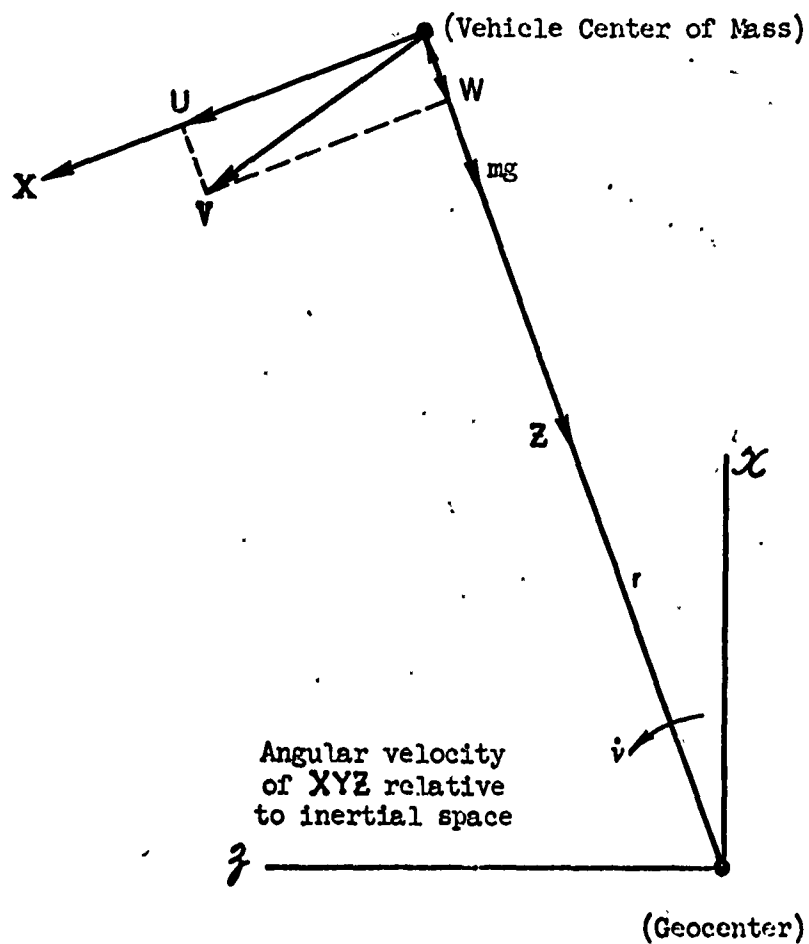
$$\dot{n}_{XYZ} = -im \quad (4-55)$$

or, referenced to measurements in the body-fixed frame via Eq. 4-49,

$$\mathbf{n}_{XYZ} = -\hat{\mathbf{i}}[(\sin \psi \cos \Theta)] + (\sin \psi \sin \Theta \sin \Phi + \cos \psi \cos \Phi)\hat{\mathbf{j}} \\ + (\sin \psi \sin \Theta \cos \Phi - \cos \psi \sin \Phi)\hat{\mathbf{k}}$$

Consequently, the components of the angular velocity relative to inertial space then become

[illegible]



AXES	UNIT VECTORS	DESCRIPTION
$x y z$	$l m n$	Inertial system with origin at geocenter. xz plane coincident with equilibrium flight velocity vector.
XYZ	$l m n$	Rotating system with origin at vehicle center of mass. Z directed toward geocenter. XZ plane coincident with equilibrium flight velocity vector.

Fig. 4-15. Definition of Inertial Space and Radially Directed Rotating Axis System

4.5 LINEARIZATION OF THE INERTIAL AND GRAVITATIONAL COMPONENTS

Both the inertial forces of Eq. 4-38 and the gravitational forces of Eq. 4-39 are proportional to the vehicle mass. It is therefore convenient to combine these terms into components which represent the accelerations which would be sensed by instruments located with their input axes coincident with the body-fixed X, Y, and Z axes. When this is done and the remaining external aerodynamic and propulsive forces and moments are represented by their generalized symbols, the six-degree-of-freedom rigid-body equations of motion become

$$\begin{aligned}
 m a_{x c.g.} &= m [\dot{U} + QW - RV + g \sin \Theta] = X \\
 m a_{y c.g.} &= m [\dot{V} + RU - PW - g \cos \Theta \sin \Phi] = Y \\
 m a_{z c.g.} &= m [\dot{W} + PV - QU - g \cos \Theta \cos \Phi] = Z \\
 \dot{P} I_x - \dot{R} I_{xz} + QR(I_z - I_y) - PQ I_{xz} &= L \\
 \dot{Q} I_y + PR(I_x - I_z) - R^2 I_{xz} + P^2 I_{xz} &= M \\
 \dot{R} I_z - \dot{P} I_{xz} + PQ(I_y - I_x) + QR I_{xz} &= N
 \end{aligned} \tag{4-57}$$

To these must be added the auxiliary relations of Eq. 4-56 which relate Φ , Θ , Ψ to P, Q, and R.

These equations contain products of the dependent variables, some of which appear as transcendental functions; therefore they are in general nonlinear. To reduce them to tractable form the total motion can be considered as composed of two parts—an average or mean motion which is representative of the operating point or trim conditions, and a dynamic motion which accounts for small perturbations about the mean motion.

The operating point equations are obtained by recognizing that zero translational and rotational accelerations are implicit in the concept of a trim condition. Then, denoting such a condition with zero subscript, the trim equations are given directly by

$$\begin{aligned}
m[\dot{W}_0 Q_0 - V_0 R_0 + g \sin \Theta_0] &= \dot{X}_0 \\
m[\dot{U}_0 R_0 - W_0 P_0 - g \cos \Theta_0 \sin \Phi_0] &= \dot{Y}_0 \\
m[\dot{V}_0 P_0 - U_0 Q_0 - g \cos \Theta_0 \cos \Phi_0] &= \dot{Z}_0 \\
Q_0 R_0 (I_z - I_y) - P_0 Q_0 I_{xz} &= L_0 \\
P_0 R_0 (I_x - I_z) - R_0^2 I_{xz} + P_0^2 I_{xz} &= M_0 \\
P_0 Q_0 (I_y - I_x) + Q_0 R_0 I_{xz} &= N_0
\end{aligned} \tag{4-58}$$

Because steady-state rolling, pitching, and yawing are possible as a trim condition, the operating point equations for P_0 , Q_0 , and R_0 will, in general, contain all the terms shown in Eq. 4-56, although each will have a zero subscript.

The perturbed motions are by definition those obtained by subtracting the trim motions from the total motion. Thus, the perturbed equations of motion can be obtained by substituting $U = U_0 + dU$, $P = P_0 + dP$, $\Phi = \Phi_0 + d\Phi$, etc., into Eq. 4-57, expanding, and then subtracting the trim equation. A more straightforward process is to differentiate both sides of Eq. 4-57 to obtain the perturbed equations directly. To simplify the notation, we designate the perturbed motion quantities by their lower case equivalents (e.g., $dU = u$, etc.); also we make another assumption.

Assumption 5

The disturbances from the steady flight conditions are assumed to be small enough so that the sines and cosines of the disturbance angles are approximately the angles themselves and 1, respectively, and so that the products and squares of the disturbance quantities are negligible in comparison with the quantities themselves.

Using this assumption, the perturbed equations of motion for the vehicle become

$$\begin{aligned}
m[\dot{u} + W_0 q + Q_0 w - V_0 r - R_0 v + (g \cos \Theta_0) \theta] &= d\dot{X} \\
m[\dot{v} + U_0 r + R_0 u - W_0 p - P_0 w - (g \cos \Theta_0 \cos \Phi_0) \phi + (g \sin \Theta_0 \sin \Phi_0) \theta] &= d\dot{Y} \\
m[\dot{w} + V_0 p + P_0 v - U_0 q - Q_0 u + (g \cos \Theta_0 \sin \Phi_0) \phi + (g \sin \Theta_0 \cos \Phi_0) \theta] &= d\dot{Z}
\end{aligned}$$

(Eq. 4-59 cont'd next page)

$$\begin{aligned}
\dot{p}I_x - \dot{r}I_{xz} + (Q_0r + R_0q)(I_z - I_y) - (P_0q + Q_0p)I_{xz} &= dL \\
\dot{q}I_y + (P_0r + R_0p)(I_x - I_z) - (2R_0r - 2P_0p)I_{xz} &= dM \quad (4-59) \\
\dot{r}I_z - \dot{p}I_{xz} + (P_0q + Q_0p)(I_y - I_x) + (Q_0r + R_0q)I_{xz} &= dN \quad \text{concl'd}
\end{aligned}$$

Perturbed equations are also required for the auxiliary relations, Eq. 4-56. The portions of these equations which represent the rotation of the vertical relative to inertial space are excessively complicated when presented in general, and are seldom if ever used in their entirety. On the other hand, the angular velocity components which represent the rotation of the body-fixed XYZ axes relative to XYZ are occasionally needed. These are presented below:

$$\begin{aligned}
p &= \dot{\phi} - \dot{\psi} \sin \Theta_0 - \theta(\dot{\psi}_0 \cos \Theta_0) \\
q &= \dot{\theta} \cos \Phi_0 - \theta(\dot{\psi}_0 \sin \Theta_0 \sin \Phi_0) + \phi(\dot{\psi}_0 \cos \Theta_0 \cos \Phi_0 - \dot{\Theta}_0 \sin \Phi_0) \\
&\quad + \dot{\psi} \cos \Theta_0 \sin \Phi_0 \\
r &= \dot{\psi} \cos \Theta_0 \cos \Phi_0 - \phi(\dot{\psi}_0 \cos \Theta_0 \sin \Phi_0 + \dot{\Theta}_0 \cos \Phi_0) \\
&\quad - \dot{\theta} \sin \Phi_0 - \theta(\dot{\psi}_0 \sin \Theta_0 \cos \Phi_0)
\end{aligned} \quad (4-60)$$

Also, in view of Assumption 5, the rotation array of Eq. 4-49 can be written in its most general linearized form as

	1	m	n	
i	$\begin{Bmatrix} [\cos \Psi_0 \cos \Theta_0] \\ -\phi(\sin \Psi_0 \cos \Theta_0) \\ -\theta(\cos \Psi_0 \sin \Theta_0) \end{Bmatrix}$	$\begin{Bmatrix} [\sin \Psi_0 \cos \Theta_0] \\ \phi(\cos \Psi_0 \cos \Theta_0) \\ -\theta(\sin \Psi_0 \sin \Theta_0) \end{Bmatrix}$	$\begin{Bmatrix} [-\sin \Theta_0] \\ -\theta(\cos \Theta_0) \end{Bmatrix}$	
j	$\begin{Bmatrix} [\cos \Psi_0 \sin \Theta_0 \sin \Phi_0 - \sin \Psi_0 \cos \Phi_0] \\ -\phi(\sin \Psi_0 \sin \Theta_0 \sin \Phi_0 + \cos \Psi_0 \cos \Phi_0) \\ +\theta(\cos \Psi_0 \cos \Theta_0 \sin \Phi_0) \\ +\phi(\cos \Psi_0 \sin \Theta_0 \cos \Phi_0 + \sin \Psi_0 \sin \Phi_0) \end{Bmatrix}$	$\begin{Bmatrix} [\sin \Psi_0 \sin \Theta_0 \sin \Phi_0 + \cos \Psi_0 \cos \Phi_0] \\ \phi(\cos \Psi_0 \sin \Theta_0 \sin \Phi_0 - \sin \Psi_0 \cos \Phi_0) \\ +\theta(\sin \Psi_0 \cos \Theta_0 \sin \Phi_0) \\ +\phi(\sin \Psi_0 \sin \Theta_0 \cos \Phi_0 - \cos \Psi_0 \sin \Phi_0) \end{Bmatrix}$	$\begin{Bmatrix} [\cos \Theta_0 \sin \Phi_0] \\ -\theta(\sin \Theta_0 \sin \Phi_0) \\ +\phi(\cos \Theta_0 \cos \Phi_0) \end{Bmatrix}$	$= [E] \cdot [E_0] + [e]$
k	$\begin{Bmatrix} [\cos \Psi_0 \sin \Theta_0 \cos \Phi_0 + \sin \Psi_0 \sin \Phi_0] \\ \phi(-\sin \Psi_0 \sin \Theta_0 \cos \Phi_0 + \cos \Psi_0 \sin \Phi_0) \\ +\theta(\cos \Psi_0 \cos \Theta_0 \cos \Phi_0) \\ +\phi(-\cos \Psi_0 \sin \Theta_0 \sin \Phi_0 + \sin \Psi_0 \cos \Phi_0) \end{Bmatrix}$	$\begin{Bmatrix} [\sin \Psi_0 \sin \Theta_0 \cos \Phi_0 - \cos \Psi_0 \sin \Phi_0] \\ \phi(\cos \Psi_0 \sin \Theta_0 \cos \Phi_0 + \sin \Psi_0 \sin \Phi_0) \\ +\theta(\sin \Psi_0 \cos \Theta_0 \cos \Phi_0) \\ -\phi(\sin \Psi_0 \sin \Theta_0 \sin \Phi_0 + \cos \Psi_0 \cos \Phi_0) \end{Bmatrix}$	$\begin{Bmatrix} [\cos \Theta_0 \cos \Phi_0] \\ -\theta(\sin \Theta_0 \cos \Phi_0) \\ -\phi(\cos \Theta_0 \sin \Phi_0) \end{Bmatrix}$	

(4-61)

Here $[E_0]$ is the matrix made up of the operating point quantities alone (underlined, square-bracketed terms) and $[e]$ is the matrix made up of the perturbation quantities alone.

Assumption 5 limits the applicability of these equations to what are called "small perturbations." In return for these restrictions, the nonlinearities are removed and sets of linear equations result. This permits an important simplification in the mathematical methods necessary to analyze aircraft motions. Also, while the linearizations are applicable in theory only to infinitesimal disturbances from trim, experience has shown that quite accurate results can be obtained for disturbances of much larger magnitude.

Although the equations are linear, they are also formidably complex because of the high degree of generality presumed for the trim conditions. Because of this complexity the equations are seldom used in this "complete" form. Instead, simpler cases which nevertheless reveal fundamental control and operating problems are more commonly used. For instance, a situation of great interest is that for steady, straight ($\dot{\psi}_0 = \dot{\theta}_0 = 0$), symmetric ($\psi_0 = V_0 = 0$), wings-level ($\phi_0 = 0$) flight. Under these circumstances, the trim, or operating point, conditions consist of U_0 , U_0 , W_0 , and θ_0 , as connected by

$$U = U \cos \theta + W \sin \theta$$

$$U_0 + u = U_0 \cos \theta_0 + W_0 \sin \theta_0 + u \cos \theta_0 + w \sin \theta_0 \quad (4-62)$$

$$- U_0(\sin \theta_0)\theta + W_0(\cos \theta_0)\theta$$

The stability characteristics with or without automatic control for such conditions are of major interest, because if they are unsatisfactory the vehicle is useless. Then neglecting changes in the distance to the geocenter, r , the perturbed angular velocities, including rotation of the vertical, become

$$\begin{array}{lcl}
p = \dot{\phi} - \dot{\psi} \sin \theta_0 & \left[\begin{array}{l} -\dot{\psi} \frac{U_0}{r} \cos \theta_0 \\ + \theta \left(\frac{U_0 \sin \theta_0 - W_0 \cos \theta_0}{r} \right) - u \frac{\cos \theta_0}{r} - w \frac{\sin \theta_0}{r} \end{array} \right. \\
q = \dot{\theta} & & \\
r = \dot{\psi} \cos \theta_0 & \left[\begin{array}{l} -\dot{\psi} \frac{U_0}{r} \sin \theta_0 + \dot{\phi} \frac{U_0}{r} \\ -\frac{U_0}{r} = -\frac{1}{r} (U_0 \cos \theta_0 + W_0 \sin \theta_0) \end{array} \right. \\
Q_0 = & & \\
P_0 = R_0 = & \left[\begin{array}{l} 0 \end{array} \right. & \text{Rotation of vertical relative to } xyz
\end{array}$$

(4-63)

In Laplace transform style, ϕ , ψ , and θ are given by

$$\phi = \frac{\left(s \cos \theta_0 - \frac{U_0}{r} \sin \theta_0 \right) p + \left(s \sin \theta_0 + \frac{U_0}{r} \cos \theta_0 \right) r}{\cos \theta_0 \left(s^2 + \frac{U_0^2}{r^2} \right)}$$

$$\psi = \frac{sr - \frac{U_0}{r} p}{\cos \theta_0 \left(s^2 + \frac{U_0^2}{r^2} \right)} \quad (4-64)$$

$$\theta = \frac{q + \frac{u \cos \theta_0}{r} + \frac{w \sin \theta_0}{r}}{s + \frac{U_0 \sin \theta_0 - W_0 \cos \theta_0}{r}}$$

Substituting the Eqs. 4-63 and 4-64 relations into the Laplace-transformed perturbed equations (4-59) specialized for straight symmetric, wings-level flight, we get Eqs. 4-65 and 4-66 (overleaf).

Besides being considerably simplified over the formidable complete linearized set, these equations are seen to be separated into two groups of three each. In the first, Eqs. 4-65, the dependent motion variables are u , w , and θ , and the motions described are thus confined to the XZ

$$\begin{aligned}
\left(s - \frac{W_0}{r} \cos \Theta_0\right)u &- \frac{U_0}{r} \left(1 + \frac{W_0 \sin \Theta_0}{U_0}\right)w &+ \left[W_0 s + g \cos \Theta_0 + \frac{W_0}{r} (U_0 \sin \Theta_0 - W_0 \cos \Theta_0)\right]\theta &= \frac{dX}{m} \\
\frac{U_0}{r} \left(1 + \frac{U_0 \cos \Theta_0}{U_0}\right)u &+ \left(s + \frac{U_0 \sin \Theta_0}{r}\right)w &- \left[U_0 s - \left(g - \frac{U_0^2}{r}\right) \sin \Theta_0 - \frac{U_0 W_0}{r} \cos \Theta_0\right]\theta &= \frac{dZ}{m} \quad (4-65) \\
-\frac{\cos \Theta_0}{r} su &- \frac{\sin \Theta_0}{r} sw &+ \left(s + \frac{U_0 \sin \Theta_0 - W_0 \cos \Theta_0}{r}\right)\theta &= \frac{dM}{I_y}
\end{aligned}$$

4-40

$$\begin{aligned}
\left[\begin{array}{c} W_0 + \frac{g(s \cos \Theta_0 - \frac{U_0}{r} \sin \Theta_0)}{s^2 + \frac{U_0^2}{r^2}} \end{array} \right] p &+ \left[\begin{array}{c} U_0 - \frac{g(s \sin \Theta_0 + \frac{U_0}{r} \cos \Theta_0)}{s^2 + \frac{U_0^2}{r^2}} \end{array} \right] r &= \frac{dY}{m} \\
0 &+ \left(s + \frac{I_{xz}}{I_x} \frac{U_0}{r}\right) p &- \left[\frac{I_{xz}}{I_x} s + \left(\frac{I_z - I_y}{I_x}\right) \frac{U_0}{r} \right] r &= \frac{dL}{I_x} \quad (4-66) \\
0 &- \left[\frac{I_{xz}}{I_z} s + \left(\frac{I_y - I_x}{I_z}\right) \frac{U_0}{r} \right] p &+ \left(s - \frac{I_{xz}}{I_z} \frac{U_0}{r}\right) r &= \frac{dN}{I_z}
\end{aligned}$$

plane. These are generally referred to as the "longitudinal motions." The other set, Eqs. 4-66, are lateral/directional and consist of side-slipping, rolling, and yawing. Actually, as shown in Eq. 4-66, the rolling and yawing acceleration equations are not explicitly coupled with the sideslip equation, although implicitly, and in practice, a great deal of coupling can exist through the medium of the aerodynamic forces presently contained on the right side. In fact, the lateral and longitudinal separation indicated above is, at this point, only a separation of the gravitational and inertial forces, and the six degrees of freedom may actually be coupled through propulsive or aerodynamic forces and moments. The separation occurs largely because of the assumed trim conditions and is equally true whether or not effects due to rotation of the vertical are included.

In passing we should note, in connection with Eqs. 4-65 and 4-66, that whereas pitch displacement, θ , is the angular motion quantity used in the longitudinal equations, the lateral equations utilize the angular velocities p and r . This is only a matter of convenience and simplification; substituting for p and r (Eq. 4-63) would greatly expand Eqs. 4-66, and Eqs. 4-65 would suffer similarly if expressed in terms of q rather than θ . However, the choice of motion variables purely as a matter of simplifying the resulting equations can mask important physical effects and, further, may not be consistent with the sensory equipment commonly used to exercise feedback control.

To illustrate, consider the side acceleration equation in Eq. 4-66. It is apparent from the expression for ϕ (Eq. 4-64) that an alternate form is

$$sv - W_0 p + U_0 r - g \cos \theta_0 \phi = \frac{dy}{dt} \quad (4-67)$$

and that an added contribution to the ϕ term arises when the Eq. 4-63 expression for r is substituted. That is, doing so results in

$$sv - W_0 p + U_0 \left(s\psi \cos \theta_0 - \psi \frac{U_0}{r} \sin \theta_0 \right) - \left(g \cos \theta_0 - U_0 \frac{U_0}{r} \right) \phi = \frac{dy}{dt} \quad (4-68)$$

We see now that the net side acceleration due to ϕ perturbations is proportional to the difference between the gravitational attraction, $g \cos \theta_0$, and the centrifugal forces due to high speed flight at a nearly constant

value of r , $U_0(U_0/r)$. Physically, what happens is that a constant value of ϕ , which is a gravity-directed angle, produces a body axis turn rate, r , proportional to $\phi(U_0/r)$ as illustrated in Fig. 4-16 for the simply visualized case of $\phi = +90^\circ$. Note that the positive direction of r is reversed (counterclockwise rather than clockwise) because we are viewing the underside of the vehicle.

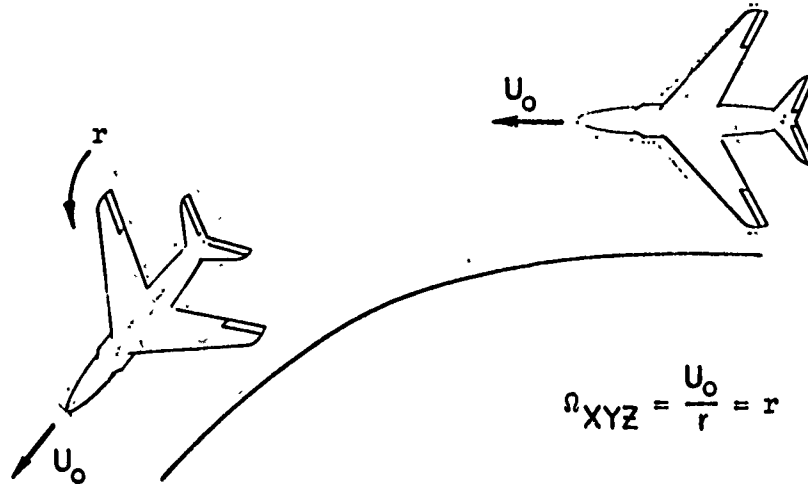


Fig. 4-16. Illustration of Physical Origins of Body Axis Turn Rate

The similar-appearing "weightlessness" term, $\theta(g - U_0^2/r) \sin \Theta_0$, in the Z acceleration equation of Eqs. 4-63 is, correspondingly, eliminated by using body axis pitch rate, q , rather than θ . That is, from the perturbed equations (4-59) specialized for the initial conditions of interest and the relations in Eqs. 4-63 and 4-64,

$$\frac{U_0}{r} u + sw - U_0 q + g \sin \Theta_0 \left\{ \frac{q + \frac{u \cos \Theta_0}{r} + \frac{w \sin \Theta_0}{r}}{s + \frac{U_0 \sin \Theta_0 - W_0 \cos \Theta_0}{r}} \right\} = \frac{dz}{dt} \quad (4-69)$$

where the bracketed term is just the expression for θ (Eq. 4-64).

Considering now the appropriateness of Eqs. 4-65 and 4-66 for feedback control application, it is immediately clear that Eqs. 4-66 are directly usable in conjunction with body-oriented rate gyro sensors.

Conversely, Eq. 4-65 is most appropriate for a gravity-erected gyro or platform. One final point worth mentioning is the appearance of the second-order denominator in the side force expression of Eq. 4-66. This oscillation, with a period $(2\pi r/U_0)$ equal to the time to circle the earth, is of special importance for inertial guidance and navigation systems.

4.6 EXPANSION OF THE AERODYNAMIC FORCES AND MOMENTS

The aerodynamic forces are exerted on the vehicle by the surrounding atmosphere; they are present whenever there are any reactive forces between the air mass and the vehicle. In steady flight they may be due to relative motion between the vehicle and the air mass or to accelerated flows produced by the propulsion system. Although the specific forces depend on their peculiar origins, the form of the expressions which describe perturbations in these forces is not so particularly dependent on origin. For instance, while on vehicles designed to fly at very low speeds (e.g., helicopters and VTOL aircraft) the dominant forces and moments are produced by the accelerated flows surrounding the propulsion-lift system, the distortions of the accelerated flows (produced by motion disturbances from the trim condition) result in force and moment changes of similar character to those associated with "pure" aerodynamic flight. Consequently, the end results of the treatment here are pertinent to most kinds of air vehicles. However, whenever details of specific forces are needed in the ensuing discussion we will consider "pure" aerodynamic flight of fixed-wing craft for simplicity.

It can be shown by dimensional analysis* that the forces acting on solids moving through fluids can be expressed in the form

$$F = C_F \frac{1}{2} \rho V_a^2 S \quad (4-70)$$

where C_F = a dimensionless coefficient
 ρ = density of fluid
 V_a = velocity of the solid relative to the fluid
 S = characteristic area of the solid

Since a moment is the product of a force by a moment arm, the expression for a moment can also be written in a form similar to that of Eq. 4-70. The aerodynamic moments and forces acting on an airplane in flight (see Fig. 4-17) may then be written as

$$\begin{aligned} X_a &= C_x(1/2) \rho V_a^2 S &= \text{aerodynamic force along X axis} \\ Y_a &= C_y(1/2) \rho V_a^2 S &= \text{aerodynamic force along Y axis} \quad (4-71) \\ Z_a &= C_z(1/2) \rho V_a^2 S &= \text{aerodynamic force along Z axis} \\ I_a &= C_l(1/2) \rho V_a^2 S b &= \text{rolling moment} \\ M_a &= C_m(1/2) \rho V_a^2 S c &= \text{pitching moment} \\ N_a &= C_n(1/2) \rho V_a^2 S b &= \text{yawing moment} \end{aligned}$$

where S = wing area
 c = mean aerodynamic chord;* the wing chord which has the average characteristics of all chords in the wing
 b = wing span

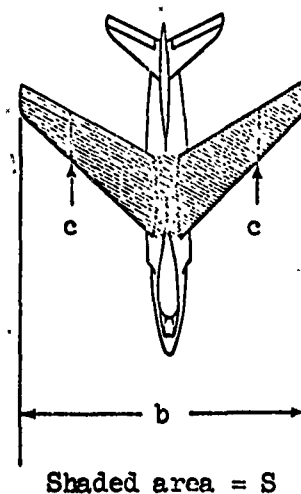


Fig. 4-17. S , b , and c of Wing

*C. B. Millikan, Aerodynamics of the Airplane, John Wiley and Sons, New York, 1941.

The total steady aerodynamic force on an aircraft is conventionally decomposed into lift and drag components. As shown in Fig. 4-18, the lift acts normal to the flight path (i.e., to the relative wind), and the drag acts parallel to the flight path:

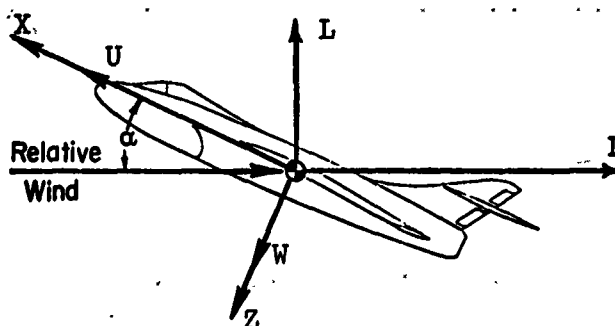


Fig. 4-18. Lift and Drag Acting on an Airplane

Akin to Eq. 4-71, the lift and drag are

$$\begin{aligned} L &= C_L \frac{1}{2} \rho V_a^2 S = \text{Lift} \\ D &= C_D \frac{1}{2} \rho V_a^2 S = \text{Drag} \end{aligned} \quad (4-72)$$

Note that, to avoid confusion, the dimensionless coefficient in the lift equation is written with a capital "L," while a lower case "l" is used in the rolling moment coefficient. When resolved into body-fixed axes, the lift and drag become the X, Y, and Z aerodynamic forces of Eq. 4-71.

The angles orienting lift and drag forces relative to the body-fixed axes are the angles of attack, α , and of sideslip, β . These are shown in Fig. 4-19. Here, as previously, the subscript "a" is used to indicate that the velocity and its components are relative, i.e., air-frame relative to air mass. If the air mass velocity relative to inertial space is assumed to be constant, then the subscript can be removed. The velocity components of V_a along the body axes are

$$\begin{aligned} U_a &= V_a \cos \beta \cos \alpha \\ V_a &= V_a \sin \beta \\ W_a &= V_a \cos \beta \sin \alpha \end{aligned} \quad (4-73)$$

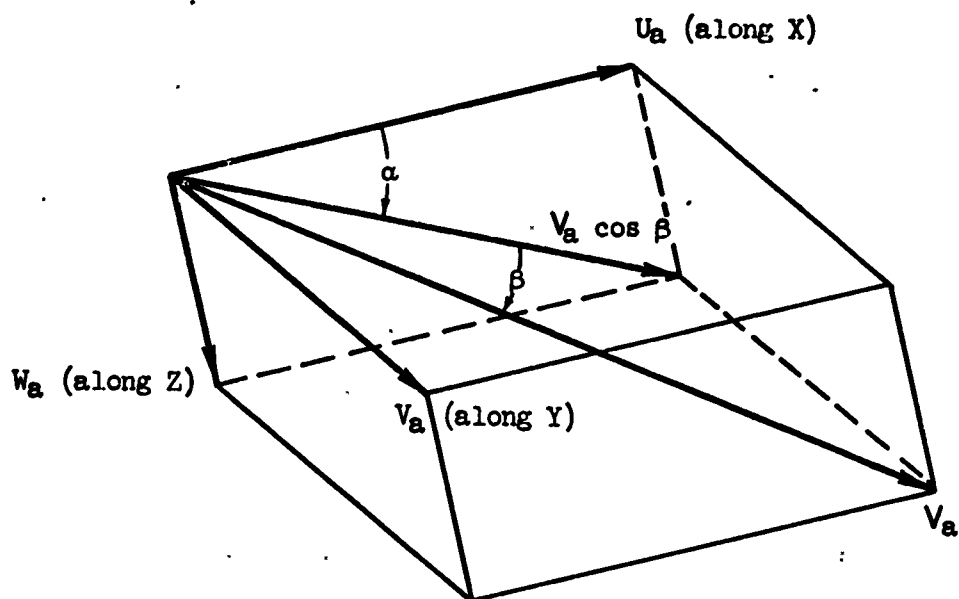


Fig. 4-19. Orientation of Relative Wind
With Body-Fixed XYZ Axes

The angles of attack and sideslip are

$$\alpha = \tan^{-1} \frac{W_a}{U_a} \quad (4-74)$$

$$\beta = \sin^{-1} \frac{V_a}{V_a}$$

and, as required by physical considerations, the latter is independent of the orientation of the X axis in the plane of symmetry. Finally, the aerodynamic lift and drag force components along X, Y, and Z are

$$\begin{aligned} X_a &= L \sin \alpha - D \cos \beta \cos \alpha \\ Y_a &= D \sin \beta \\ Z_a &= -L \cos \alpha - D \cos \beta \sin \alpha \end{aligned} \quad (4-75)$$

As indicated explicitly by the form of Eq. 4-70, the aerodynamic forces and moments are functions of air density and the relative velocity, and are therefore implicitly dependent on the altitude and the linear velocity components. Also, the dimensional coefficients C_F are themselves dependent on Reynolds' and Mach number, angles of attack and sideslip,

and linear and angular velocity components and their derivatives. If the aerodynamic forces are considered to be continuous functions of all these variables, each of the forces (X_a , Y_a , and Z_a) and the moments (L_a , M_a , and N_a) can be expressed in terms of the variables by expanding the forces in a Taylor series. These series have the form

$$F = F_0 + \left(\frac{\partial F}{\partial \Lambda_1} \right)_0 \lambda_1 + \left(\frac{\partial F}{\partial \Lambda_2} \right)_0 \lambda_2 + \left(\frac{\partial F}{\partial \Lambda_3} \right)_0 \lambda_3 + \dots \quad (4-76)$$

where Λ and λ represent the variables, including their derivatives, and perturbations thereof, respectively, and the subscript zero indicates the quantities are evaluated at the operating point or trim condition. In Eq. 4-76, terms of the order $(\partial^2 F / \partial \Lambda^2)_0 (\lambda^2 / 2!)$ and all higher order terms have been omitted in accordance with Assumption 5. In spite of this, the number of potential contributing aerodynamic derivatives, $\partial F / \partial \Lambda_1$, is dishearteningly large; and one way of eliminating some of them is to specialize the trim conditions as we have already done for the inertial and gravitational components.

Steady-State Trim Specialization

To see how the trim situation can affect the aerodynamic derivatives, consider, as a pertinent example, the X and Z forces due to lift and drag as shown in Fig. 4-18. For an angle of sideslip, β , equal to zero, Eq. 4-75 becomes

$$X_a = -D \cos \alpha + L \sin \alpha$$

$$Z_a = -L \cos \alpha - D \sin \alpha$$

or, in terms of the dimensionless coefficients of Eq. 4-71,

$$\begin{aligned} X_a &= \frac{1}{2} \rho V_a^2 S (-C_D \cos \alpha + C_L \sin \alpha) \\ Z_a &= \frac{1}{2} \rho V_a^2 S (-C_L \cos \alpha - C_D \sin \alpha) \end{aligned} \quad (4-77)$$

To simplify the example, both C_L and C_D are considered to be functions only of the angle of attack, α , and the Mach number, M . Accordingly the

appropriate expansions of the perturbed forces, at constant density, involve derivatives with respect to M , α , and V_a , as follows:

$$\begin{aligned} \frac{\partial x_a}{\partial \Lambda} = & \rho V_a S \left\{ \frac{\partial V_a}{\partial \Lambda} (-C_D \cos \alpha_0 + C_L \sin \alpha_0) + \frac{V_a}{2} \frac{\partial M}{\partial \Lambda} \left(\frac{-\partial C_D}{\partial M} \cos \alpha_0 + \frac{\partial C_L}{\partial M} \sin \alpha_0 \right) \right. \\ & \left. + \frac{V_a}{2} \frac{\partial \alpha}{\partial \Lambda} \left(\frac{-\partial C_D}{\partial \alpha} \cos \alpha_0 + \frac{\partial C_L}{\partial \alpha} \sin \alpha_0 + C_D \sin \alpha_0 + C_L \cos \alpha_0 \right) \right\} \end{aligned} \quad (4-78)$$

$$\begin{aligned} \frac{\partial z_a}{\partial \Lambda} = & \rho V_a S \left\{ \frac{\partial V_a}{\partial \Lambda} (-C_L \cos \alpha_0 - C_D \sin \alpha_0) + \frac{V_a}{2} \frac{\partial M}{\partial \Lambda} \left(\frac{-\partial C_L}{\partial M} \cos \alpha_0 - \frac{\partial C_D}{\partial M} \sin \alpha_0 \right) \right. \\ & \left. + \frac{V_a}{2} \frac{\partial \alpha}{\partial \Lambda} \left(\frac{-\partial C_L}{\partial \alpha} \cos \alpha_0 - \frac{\partial C_D}{\partial \alpha} \sin \alpha_0 + C_L \sin \alpha_0 - C_D \cos \alpha_0 \right) \right\} \end{aligned}$$

The various partial derivatives with respect to Λ are to be taken holding the remaining primary motion variables constant. In this limited case the primary variables are simply U_a and W_a , and from Eq. 4-73, for $\beta = 0$,

$$dU_a = dV_a \cos \alpha_0 - V_a \sin \alpha_0 d\alpha$$

$$dW_a = dV_a \sin \alpha_0 + V_a \cos \alpha_0 d\alpha$$

These can be solved to yield for $\Lambda = U_a$, $dW_a = 0$,

$$\frac{\partial V_a}{\partial U_a} = \left(\frac{dV_a}{dU_a} \right)_{W_a = \text{const}} = \cos \alpha_0$$

$$\frac{\partial \alpha}{\partial U_a} = \frac{-\sin \alpha_0}{V_a}$$

and, recognizing $M = V_a/a$, where a is the speed of sound

$$\frac{\partial M}{\partial U_a} = \frac{\cos \alpha_0}{a} \quad (4-79)$$

(Continued on next page)

Similarly, for $\Lambda = W_a$, $dU_a = 0$,

$$\begin{aligned}
 \frac{\partial V_a}{\partial W_a} &= \sin \alpha_0 \\
 \frac{\partial \alpha}{\partial W_a} &= \frac{\cos \alpha_0}{V_a} \\
 \frac{\partial M}{\partial W_a} &= \frac{\sin \alpha_0}{a}
 \end{aligned}
 \tag{4-79}$$

(Concluded)

Applying these values to Eq. 4-78, collecting terms, and simplifying the notation in the usual way, i.e., $\partial C_D / \partial \alpha \equiv C_{D\alpha}$, etc., $(M/2)(\partial C_L / \partial M) \equiv C_{L_M}$, etc., yields

$$\begin{aligned}
 \frac{\partial X_a}{\partial U_a} &= \rho V_a S \left\{ (-C_D - C_{D_u}) \cos^2 \alpha_0 + \left[\frac{1}{2}(C_{D\alpha} - C_L) + C_L + C_{L_u} \right] \sin \alpha_0 \cos \alpha_0 \right. \\
 &\quad \left. - \frac{1}{2}(C_{L\alpha} + C_D) \sin^2 \alpha_0 \right\}
 \end{aligned}
 \tag{4-80}$$

$$\begin{aligned}
 \frac{\partial X_a}{\partial W_a} &= \rho V_a S \left\{ \frac{1}{2}(C_L - C_{D\alpha}) \cos^2 \alpha_0 + \left[\frac{1}{2}(C_{L\alpha} + C_D) - C_D - C_{D_u} \right] \sin \alpha_0 \cos \alpha_0 \right. \\
 &\quad \left. + (C_L + C_{L_u}) \sin^2 \alpha_0 \right\}
 \end{aligned}$$

$$\begin{aligned}
 \frac{\partial Z_a}{\partial U_a} &= \rho V_a S \left\{ (-C_L - C_{L_u}) \cos^2 \alpha_0 + \left[\frac{1}{2}(C_{L\alpha} + C_D) - C_D - C_{D_u} \right] \sin \alpha_0 \cos \alpha_0 \right. \\
 &\quad \left. - \frac{1}{2}(C_L - C_{D\alpha}) \sin^2 \alpha_0 \right\}
 \end{aligned}$$

$$\begin{aligned}
 \frac{\partial Z_a}{\partial W_a} &= \rho V_a S \left\{ \frac{1}{2}(C_{L\alpha} - C_D) \cos^2 \alpha_0 - \left[\frac{1}{2}(C_{D\alpha} - C_L) + C_L + C_{L_u} \right] \sin \alpha_0 \cos \alpha_0 \right. \\
 &\quad \left. - (C_D + C_{D_u}) \sin^2 \alpha_0 \right\}
 \end{aligned}$$

The recurring trigonometric terms are typical of the usual axis transformation relations (see Eq. 4-99) which, in effect, we have derived by this process for the quantities of interest. That is, the $\alpha_0 = 0$ derivatives or groups of them comprise the coefficients of the general trigonometric expansion for $\alpha_0 \neq 0$. It is clear that the choice of trim α_0 cannot eliminate any of the derivatives, but can only influence their assigned values and for $\alpha_0 = 0$, considerably simplify their literal forms.

For the analogous situation in the XY plane as sketched in Fig. 4-20, there are similar (lateral) lift and drag forces acting, and expressions for X and Y corresponding to Eqs. 4-78 and 4-80 could easily be written.

There is an important difference, however, in the values to be assigned the dimensionless coefficients, C_L and $C_{D\alpha}$. In the vertical (XZ) plane, lift is necessary to sustain flight, and since $C_{D\alpha}$ is proportional to C_L both parameters are usually positive and set by the trim condition. In the lateral (XY) plane, side lift is undesirable and ordinarily avoided, and it is unusual to set up trim conditions involving steady sideslip, β_0 . Thus the value of $\partial X/\partial v_a$, which can be inferred by substituting β for α in the Eq. 4-80 expression for $\partial X/\partial w$, is

usually zero. That is, for $\beta_0 = 0$ and the corresponding $C_L = \partial C_D/\partial \beta = 0$, $\partial X/\partial v_a = 0$. This really results because the XZ plane is not only a plane of inertial and geometric symmetry, but usually also of aerodynamic trim symmetry. When this is true ($P_0 = R_0 = V_0 = 0$) then lateral perturbed motions, p , r , and v , do not produce X and Z forces or M moments as inferred by the foregoing discussion of v effects. Thus, we are led to Assumption 6.

Assumption 6

The steady lateral trim conditions are assumed to be $P_0 = R_0 = V_0 = \Phi_0 = 0$, and the longitudinal forces and moments due to lateral perturbations about such trim conditions are assumed negligible.

The assumed trim conditions are those prevailing for the great majority of all flying*, and are identical to those which lead to the "simplified" relationships of Eqs. 4-63 through 4-66. While complete

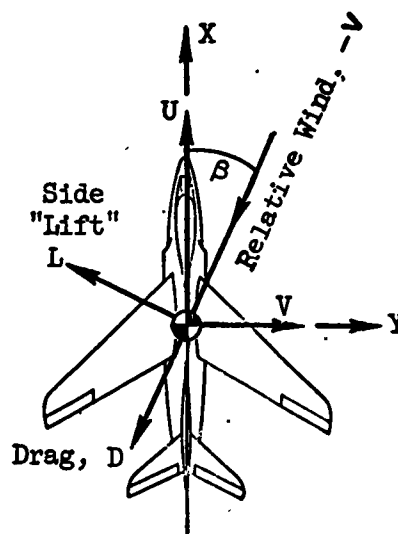


Fig. 4-20. Lateral Lift and Drag Acting on an Airplane

*Baird, Applied Aerodynamics, First Edition, Longmans Green and Co., London, 1920, considers turning and straight flight and shows minor differences for the example airplane considered.

aerodynamic symmetry is not necessarily guaranteed by these conditions (as, for example, for propellers rotating in the same direction), the independence of longitudinal forces and moments from lateral perturbed motions is still assumed to hold with negligible error.

Assumption 6 has a corollary. With the aerodynamic trim forces essentially symmetrical about the XZ plane, there can be no appreciable lateral forces or moments induced by longitudinal perturbed motions (u, w, q). The net result therefore is that the perturbed longitudinal and lateral forces and moments are in general influenced respectively only by longitudinal and lateral perturbed motions, and of course by control inputs. This separation of the longitudinal and lateral aerodynamic forces and moments is completely parallel and analogous to the separation of the inertial and gravity terms shown in the Eqs. 4-65 and 4-66 sets. Accordingly, the complete equations are now, by virtue of Assumption 6, separated into longitudinal and lateral sets.

Quasi-Steady Flow, Downwash and Sidewash

Unfortunately, the sets are still potentially overcomplicated because of the implied inclusion in Eq. 4-76 of higher order terms due to body accelerations. Such effects arise because when the vehicle is in accelerated motion the air mass in its immediate surroundings must also accelerate in order to establish the quasi-steady flow. The latter condition is one where the aerodynamic forces and moments are dependent only on the velocities of the vehicle relative to the air mass. Generally speaking, the quasi-steady forces and moments are of primary importance and the unsteady flow effects are usually secondary and negligible. However, the behavior of some modern high speed jet airplanes has exhibited marked discrepancies between the predicted damping and the observed flight test damping of high frequency oscillatory modes due, at least partly, to nonsteady flow effects. These effects become more important as the "natural" frequency is increased, as, for example, by a "tight" control system. Such possibilities should be kept in mind as perhaps requiring further investigation in specific cases. Nevertheless, we shall, because of its great applicability and essential simplification, resort to Assumption 7.

Assumption 7. The flow is assumed to be quasi-steady.

Because of Assumption 7 all derivatives with respect to the rates of change of velocities are omitted with the exception of those with respect to \dot{w} and \dot{v} , which are retained to account for the effect on the tail of the wing/body downwash and sidewash. This effect is present, as explained below, even when purely quasi-steady considerations apply.

As an airplane wing travels through the air it leaves behind it an emanating downwash pattern having a particular distribution and average value at the horizontal tail location. If the wing lift is suddenly increased by an abrupt change in w (quasi-steady assumption), the increased downwash at the horizontal tail (or at the sweptback wing-tip for a tailless airplane), proportion to Δw , does not change immediately. The tail must actually arrive at the point in space where the wing lift was changed before it experiences the resulting downwash change; and the time interval, Δt , for this to happen is just the tail length, l_t , divided by the forward speed, U_a . That is, for a given time history in w_a and a resulting angle of attack variation with time, $\alpha(t)$, the corresponding downwash time history is given by $(\partial \epsilon_t / \partial \alpha) \alpha(t - l_t / U_a)$, as depicted in Fig. 4-21.

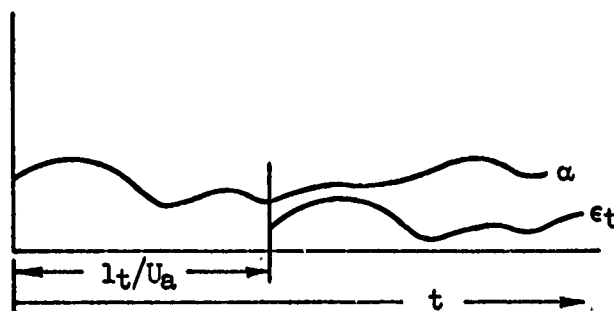


Fig. 4-21. Tail Downwash Delay
Following an Angle of Attack Input

Recognizing that the Laplace transform of $f(t - \tau)$ is simply $F(s)e^{-\tau s}$ allows us to write the Laplace-transformed net tail angle of attack, $\alpha_t = \alpha - \epsilon_t$, as

$$\alpha_t(s) = \alpha(s) \left[1 - \frac{\partial \epsilon}{\partial \alpha} e^{-(l_t/U_a)s} \right]$$

The corresponding pitching moment is given by

$$C_M(s) = C_{M\alpha t} \alpha(s) \left[1 - \frac{\partial \epsilon}{\partial \alpha} e^{-(l_t/U_a)s} \right] \quad (4-81)$$

This most general representation of downwash lag effects can become quite important at high frequencies.* On a less accurate basis it can be translated into an approximate $\dot{\alpha}$ derivative by noting that, for the usual small values of l_t/U_a , $e^{-(l_t/U_a)s} \doteq 1 - (l_t/U_a)s$. Then,

$$\begin{aligned} C_M(s) &\doteq C_{M\alpha t} \alpha(s) \left[1 - \frac{\partial \epsilon}{\partial \alpha} \left(1 - \frac{l_t}{U_a} s \right) \right] \\ &\doteq C_{M\alpha t} \left[\alpha(s) \left(1 - \frac{\partial \epsilon}{\partial \alpha} \right) + \dot{\alpha}(s) \frac{l_t}{U_a} \frac{\partial \epsilon}{\partial \alpha} \right] \end{aligned} \quad (4-82)$$

and

$$C_{M\dot{\alpha}} \equiv \frac{\partial C_M}{\partial \left(\frac{\dot{\alpha} c}{2U_a} \right)} \doteq \frac{2l_t}{c} \frac{\partial \epsilon}{\partial \alpha} C_{M\alpha t}$$

Thus we have shown that aerodynamic partial derivatives with respect to $\dot{w} = U_a \dot{\alpha}$ can be included in the equations of motion on the basis of purely quasi-steady considerations.

An analogous examination of the sidewash field due to a wing/body combination undergoing lateral velocity perturbations, and the resulting forces on the vertical fin, yields a similar conclusion with respect to \dot{v} derivatives. Such derivatives are not usually as important as those due to \dot{w} motions, and are sometimes neglected. For the time being we shall carry them along.

Effects Due to Nonuniform Atmosphere

While both the aerodynamic and inertial plus gravity terms have now been suitably reduced, they are not yet on common ground. That is, the aerodynamic forces and moments are dependent on perturbations in the

*I. C. Statler, "Dynamic Stability at High Speeds from Unsteady Flow Theory," J. Aeron. Sci., Vol. 17, No. 4, Apr. 1950.

motions relative to the atmosphere rather than to inertial space. To rectify this condition we need to recognize the existence of atmospheric winds or gusts, and to note that perturbed motions relative to the atmosphere are given by

$$\lambda_a = \lambda - \lambda_g \quad (4-83)$$

where now λ , being a general perturbed inertial motion quantity, is measurable in the body reference frame, and the subscript "g" identifies the wind or gust component of the atmosphere. Substituting this relationship into Eq. 4-76 and suitably specializing λ to those quantities of remaining interest in view of the simplifying results of Assumptions 6 and 7, the perturbed forces and moments can be written as

$$\begin{aligned} dX &= \frac{\partial X}{\partial U}(u-u_g) + \frac{\partial X}{\partial W}(w-w_g) + \frac{\partial X}{\partial \dot{W}}(\dot{w}-\dot{w}_g) + \frac{\partial X}{\partial Q}(q-q_g) + \sum \frac{\partial X}{\partial \delta} \delta \\ dZ &= \frac{\partial Z}{\partial U}(u-u_g) + \frac{\partial Z}{\partial W}(w-w_g) + \frac{\partial Z}{\partial \dot{W}}(\dot{w}-\dot{w}_g) + \frac{\partial Z}{\partial Q}(q-q_g) + \sum \frac{\partial Z}{\partial \delta} \delta \\ dM &= \frac{\partial M}{\partial U}(u-u_g) + \frac{\partial M}{\partial W}(w-w_g) + \frac{\partial M}{\partial \dot{W}}(\dot{w}-\dot{w}_g) + \frac{\partial M}{\partial Q}(q-q_g) + \sum \frac{\partial M}{\partial \delta} \delta \\ dY &= \frac{\partial Y}{\partial V}(v-v_g) + \frac{\partial Y}{\partial \dot{V}}(\dot{v}-\dot{v}_g) + \frac{\partial Y}{\partial P}(p-p_g) + \frac{\partial Y}{\partial R}(r-r_g) + \sum \frac{\partial Y}{\partial \delta} \delta \\ dL &= \frac{\partial L}{\partial V}(v-v_g) + \frac{\partial L}{\partial \dot{V}}(\dot{v}-\dot{v}_g) + \frac{\partial L}{\partial P}(p-p_g) + \frac{\partial L}{\partial R}(r-r_g) + \sum \frac{\partial L}{\partial \delta} \delta \\ dN &= \frac{\partial N}{\partial V}(v-v_g) + \frac{\partial N}{\partial \dot{V}}(\dot{v}-\dot{v}_g) + \frac{\partial N}{\partial P}(p-p_g) + \frac{\partial N}{\partial R}(r-r_g) + \sum \frac{\partial N}{\partial \delta} \delta \end{aligned} \quad (4-84)$$

where the summation of δ allows for more than one control input, e.g., elevator and/or throttle; aileron and/or rudder.

Motions of the atmosphere can be discrete or random; in any case they are usually characterized by only the three orthogonal components u_g , v_g , w_g . However, variations in space and time of these components can be considered to supply the additional gust gradient inputs shown in Eq. 4-84, \dot{v}_g , \dot{w}_g , p_g , q_g , r_g . Furthermore, for the long wave lengths characterizing atmospheric turbulence, the rotary gusts can be thought of as arising from the

spatial distributions of linear gust velocities. For example, a rolling gust, p_g , is the result of a spanwise distribution of w_g , as shown in Fig. 4-22. Here the aircraft is considered to be encountering an effective vertical gust at its centerline plus an average spanwise gradient, $\partial w_g / \partial y$, negative in sign. Since a rolling velocity imparts a spanwise

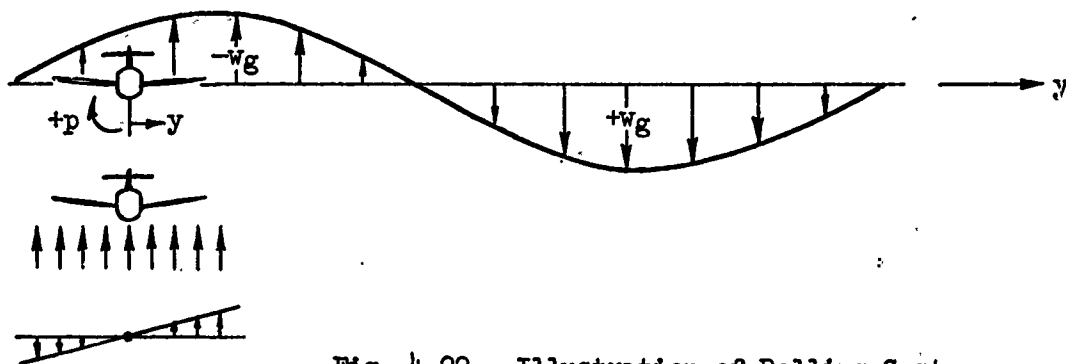


Fig. 4-22. Illustration of Rolling Gust, p_g

gradient in w given by py so that $\partial w / \partial y = p$, the effective p_g is simply $\partial w_g / \partial y$. For a fore and aft distribution of w_g as shown in Fig. 4-23,

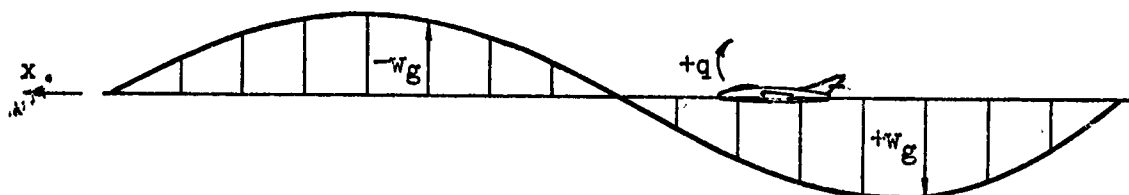


Fig. 4-23. Illustration of Pitching Gust, q_g

a similar decomposition of the gust produces $q_g = -\partial w_g / \partial x$; however this can be better expressed in terms of the gust time variations felt by the aircraft. That is, differentiating numerator and denominator,

$$q_g = \frac{-\partial w_g / \partial t}{\partial x / \partial t} = \frac{-\dot{w}_g}{U_0} = \frac{-s w_g^*}{U_0}$$

*W. H. Phillips and C. C. Kraft, Jr., Theoretical Study of Some Methods for Increasing the Smoothness of Flight Through Rough Air, NACA TN 2416, July 1951.

B. Etkin, A Theory of the Response of Airplanes to Random Atmospheric Turbulence, Univ. of Toronto, Inst. of Aerophysics, UTIA Tech. Note 54, Nov. 1960

Similarly, the yawing gust due to a fore and aft distribution of side gust velocity, v_g , is given by $r_g = sv_g/U_0$.

These last expressions cannot be substituted directly into all of Eqs. 4-84 because of the detailed way in which certain of the derivatives arise, as explained more fully later in this chapter. For instance, the rolling-moment derivative $\partial L/\partial R$ stems primarily from the spanwise distribution of forward velocity due to yaw rate, which produces an asymmetric wing lift distribution. An effective r_g due to fore and aft variations in the side gust velocity seen by an airplane traveling at speed U_0 would not produce a corresponding wing rolling moment. Similarly, the derivative $\partial X/\partial Q$, usually neglected, is theoretically the result of a vertical distribution of horizontal velocity due to pitch rate; therefore, an effective q_g due to a fore and aft distribution (as above) does not produce forces proportional to $\partial X/\partial Q$.

In addition to the possibilities noted above, there are higher order gust input terms and derivatives which are sometimes considered.* Generally speaking, however, such terms are most appropriate to the detailed computation of random gust response spectra and are seldom considered necessary for the engineering solution of flight control problems.

In addition to the small scale atmospheric nonuniformities which produce winds and gusts in a given layer of air, there are also large scale nonuniformities with altitude. The most obvious of these is the variation in density, ρ , which through the basic Eq. 4-71 relations produces changes in the forces and moments with change in altitude. The speed of sound, a , also varies in general, so that altitude displacement perturbations at a given speed can give rise to Mach number, $M \equiv V/a$, perturbations. If the dimensionless aerodynamic force and moment coefficients are Mach-number-dependent, as they are except for subsonic or hypersonic flight, then the resulting change in M gives an additional altitude-dependent set of force and moment perturbations. Finally, there can be

*B. Etkin, Theory of Flight of Airplanes in Isotropic Turbulence—Review and Extension, AGARD Rept. 372, 1961.

J. M. Eggleston and W. H. Phillips, The Lateral Response of Airplanes to Random Atmospheric Turbulence, NASA TR R-74, 1960.

large scale changes in steady wind speed and direction with altitude (so-called wind shear) which will produce force and moment perturbations on a diving or climbing airplane. Notice that all these effects are dependent, not on the vertical perturbed velocity measured along the body-fixed Z axis, but rather on the perturbed altitude displacement and rate measured in earth-fixed coordinates.

Detailed investigations of the influence of altitude gradients* and the exact conditions under which they may be ignored indicate that these effects are insignificant for most flight situations and flight control problems, and, consequently, that a good assumption is:

Assumption 8

Variations of atmospheric properties, such as density or speed of sound, are considered negligible for the small altitude perturbations of usual interest.

4.7 EXPANSION OF THE DIRECT THRUST FORCE

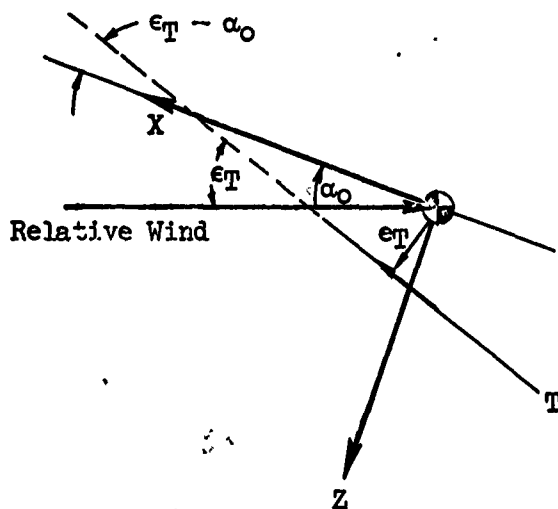
Many of the derivatives appearing in Eq. 4-84 will be the result not only of forces connected with the motion of the body through the atmosphere, but also of forces arising from flows induced by the propulsion system. When such flows pass near or over portions of the vehicle they can produce profound and difficult-to-predict effects on the derivatives, which usually must be evaluated in model tests employing properly scaled jets or slipstreams. For configurations which inherently eliminate such slipstream interference (e.g., a subsonic jet centrally exhausting aft of the tail), the forces and moments associated with the direct thrust can still contribute significantly to various derivatives. Among the contributions requiring general consideration are the forces produced on the inlet due to the changed

*I. L. Ashkenas, "Effects of Atmospheric Gradients on Longitudinal Control," Section I of Analysis of Several Handling Quality Topics Pertinent to Advanced Manned Aircraft, AFFDL-TR-67-2, 1967.

J. K. Zbrozek, Aircraft Behavior in a Vertical Gradient of Wind Velocity, RAE TN Aero 2810, 1962.

S. Neumark, Dynamic Longitudinal Stability in Level Flight, Including the Effects of Compressibility and Variations of Atmospheric Characteristics with Height, RAE Rept. Aero 2265, 1950.

direction of the entering air mass; the moments caused by the angular velocity of a tube (engine plus tailpipe) containing a moving air mass; and, finally, the forces and moments resulting from the thrust itself. All but the last of these contributions depend on detailed knowledge of the vehicle layout and powerplant performance characteristics, and further consideration here is not warranted. However, an exposure of the direct thrust effects is pertinent since it is simply accomplished and the effects are always present and sometimes important. Accordingly, consider Fig. 4-24, where the thrust line angle with the initial relative wind, ϵ_T , is set by the trim condition and airplane geometry, and its angle with respect to the X axis is fixed at $(\epsilon_T - \alpha_0) = \text{constant}$. Then by direct resolution,



$$\begin{aligned} X_T &= T \cos (\epsilon_T - \alpha_0) \\ Z_T &= -T \sin (\epsilon_T - \alpha_0) \quad (4-85) \\ M_T &= T e_T \end{aligned}$$

where e_T , the thrust eccentricity (positive downward), is not a function of the axis orientation. With thrust a function only of density, control setting, and airplane relative speed, (sometimes, but rarely, also of α_0) the resulting perturbed forces are

Fig. 4-24. Thrust Alignment Notation

$$\begin{aligned} dX_T &= \cos (\epsilon_T - \alpha_0) \left[\frac{\partial T}{\partial V} \left(\frac{\partial V}{\partial U} u + \frac{\partial V}{\partial W} w \right) + \frac{\partial T}{\partial \delta_T} \delta_T \right] \\ dZ_T &= -\sin (\epsilon_T - \alpha_0) \left[\frac{\partial T}{\partial V} \left(\frac{\partial V}{\partial U} u + \frac{\partial V}{\partial W} w \right) + \frac{\partial T}{\partial \delta_T} \delta_T \right] \end{aligned} \quad (4-86)$$

Applying Eq. 4-79 (dropping the "a" subscript for simplicity) and expanding the trigonometric functions, the partial derivatives are:

$$\begin{aligned}
\frac{\partial X_T}{\partial U} &= \frac{\partial T}{\partial V} (\cos \epsilon_T \cos^2 \alpha_0 + \sin \epsilon_T \sin \alpha_0 \cos \alpha_0) \\
\frac{\partial X_T}{\partial W} &= \frac{\partial T}{\partial V} (\cos \epsilon_T \sin \alpha_0 \cos \alpha_0 + \sin \epsilon_T \sin^2 \alpha_0) \\
\frac{\partial X_T}{\partial \delta_T} &= \frac{\partial T}{\partial \delta_T} (\cos \epsilon_T \cos \alpha_0 + \sin \epsilon_T \sin \alpha_0) \\
\frac{\partial Z_T}{\partial U} &= \frac{-\partial T}{\partial V} (\sin \epsilon_T \cos^2 \alpha_0 - \cos \epsilon_T \sin \alpha_0 \cos \alpha_0) \\
\frac{\partial Z_T}{\partial W} &= \frac{-\partial T}{\partial V} (\sin \epsilon_T \sin \alpha_0 \cos \alpha_0 - \cos \epsilon_T \sin^2 \alpha_0) \\
\frac{\partial Z_T}{\partial \delta_T} &= \frac{-\partial T}{\partial \delta_T} (\sin \epsilon_T \cos \alpha_0 - \cos \epsilon_T \sin \alpha_0)
\end{aligned} \tag{4-87}$$

When combined with Eqs. 4-80 these will provide composite derivatives, such as $\partial X/\partial U = \partial X_a/\partial U + \partial X_T/\partial U$, for the force equation.

Unlike the perturbed forces, the perturbed moment is not obtained by simple differentiation of the Eq. 4-85 expression because of the influence of balancing aerodynamic trim moments. To show this, consider that at trim the total moment must be zero by definition, i.e., no resulting rotary acceleration and $P_0 = R_0 = 0$ (see Eq. 4-58) according to Assumption 6. Therefore the thrust moment is balanced by an opposite and equal aerodynamic moment having the form of Eq. 4-71, i.e.,

$$M_0 = T\epsilon_T + \frac{\rho}{2} V^2 S c C_M = 0 \tag{4-88}$$

Neglecting aerodynamic C_M variations with Mach number as an additional effect to those of specific interest here, the moment change is

$$dM = \epsilon_T \left[\frac{\partial T}{\partial V} \left(\frac{\partial V}{\partial u} u + \frac{\partial V}{\partial w} w \right) + \frac{\partial T}{\partial \delta_T} \delta_T \right] + \rho V_0 S c C_M \left(\frac{\partial V}{\partial u} u + \frac{\partial V}{\partial w} w \right)$$

But by Eq. 4-88, $\rho V_0 S c C_M = \frac{-2T\epsilon_T}{V_0}$

so that applying Eqs. 4-79,

$$dM = e_T \left[\left(\frac{\partial T}{\partial V} - \frac{2T_0}{V_0} \right) (u \cos \alpha_0 + w \sin \alpha_0) + \frac{\partial T}{\partial \delta_T} \delta_T \right] \quad (4-89)$$

We see that proper inclusion of the trim conditions has led to the additional T_0/V_0 terms.

The foregoing is another good example of the importance of carefully considering the operating or trim point conditions when evaluating the force and moment derivatives. In the present case, neglecting such considerations would have led to possibly important errors in the moment perturbation.

4.8 COMPLETE LINEARIZED EQUATIONS OF MOTION

Now that the individual contributions have been evaluated, the remaining generally important terms can be assembled into complete sets of the linearized equations of motion. Before doing this, however, we will invoke

Assumption 9

Effects associated with rotation of the vertical relative to inertial space will be assumed negligible; furthermore, the trim body-axis pitching velocity, Q_0 , will be assumed zero.

The vertical rotation effects involve terms proportional to U_0/r , and W_0/r (see Eqs. 4-65 and 4-66) where r is approximately 2×10^7 ft. Even for orbital velocities, $U_0 \doteq \sqrt{gr}$, such terms are insignificant for the frequencies of usual concern in flight control problems. However, the weightlessness terms proportional to U_0^2/r (Eqs. 4-65 and 4-68) will not be negligible except for speeds less than about 5000 ft/sec. For speeds greater than this we will later show how the weightlessness terms can be reincluded in the stability axis set of equations (next article). In spite of this exception, the first part of Assumption 9 is generally valid for the great majority of airborne vehicular control situations of interest. The second part of Assumption 9, $Q_0 = 0$, is in keeping with the first part and the assumed $\dot{\Theta}_0 = 0$ corresponding to straight flight which leads to Eqs. 4-63; that is, for U_0/r negligible, Eq. 4-63 gives $Q_0 = 0$. In effect Assumption 9 confines our interest to operating points corresponding to straight flight over an effectively flat earth.

Turning now to the process of assembling the pertinent components of the perturbed equations of motion, we divide the force equations by m and the moment equations by the appropriate moment of inertia as in Eqs. 4-65, 4-66, yielding terms similar to:

$$\frac{1}{m} \frac{\partial X}{\partial U} u \quad \text{and} \quad \frac{1}{I_x} \frac{\partial L}{\partial R} r$$

Replacing these, respectively, by $X_u u$ and $L_r r$ and extending this convention to all the partial derivative terms considerably simplifies the notation. These quantities are called either "dimensional stability derivatives" or simply "stability derivatives"; they are understood to cover all effects due to relative motion between the vehicle and the atmosphere, i.e., basic aerodynamic as well as propulsion system effects, both induced and direct.

Using this notation, and limiting the gust inputs to those discussed in connection with, Eq. 4-84 (i.e., dropping $X_q q_g$ and $L_r r_g$ terms) directly yields the right side of the desired equations of motion. Since the Eqs. 4-5 and 4-66 results are no longer of interest in view of Assumption 9, the left side is obtained most directly by Laplace-transforming Eq. 4-59 for the trim conditions of Assumptions 6 and 9, $P_0 = Q_0 = R_0 = V_0 = \Phi_0 = 0$. This procedure yields:

Longitudinal perturbed equations

$$\begin{aligned} su + W_0 q + g \cos \Theta_0 \theta &= X_u(u-u_g) + X_w(w-w_g) + X_{\dot{w}}\dot{s}(w-w_g) + X_q q + \sum X_{\delta} \delta \\ sw - U_0 q + g \sin \Theta_0 \theta &= Z_u(u-u_g) + Z_w(w-w_g) + Z_{\dot{w}}\dot{s}(w-w_g) + Z_q \left(q + \frac{sw_g}{U_0} \right) + \sum Z_{\delta} \delta \\ sq &= M_u(u-u_g) + M_w(w-w_g) + M_{\dot{w}}\dot{s}(w-w_g) + M_q \left(q + \frac{sw_g}{U_0} \right) + \sum M_{\delta} \delta \end{aligned} \quad (4-90)$$

Lateral perturbed equations

$$\begin{aligned} sv + U_0 r - W_0 p - g \cos \Theta_0 \phi &= Y_v(v-v_g) + Y_{\dot{v}}\dot{s}(v-v_g) + Y_p(p-p_g) + Y_r \left(r - \frac{sv_g}{U_0} \right) + \sum Y_{\delta} \delta \\ sp - \frac{I_{xz}}{I_x} sr &= L_v(v-v_g) + L_{\dot{v}}\dot{s}(v-v_g) + L_p(p-p_g) + L_r r + \sum L_{\delta} \delta \\ sr - \frac{I_{xz}}{I_z} sp &= N_v(v-v_g) + N_{\dot{v}}\dot{s}(v-v_g) + N_p(p-p_g) + N_r \left(r - \frac{sv_g}{U_0} \right) + \sum N_{\delta} \delta \end{aligned} \quad (4-91)$$

The last two equations can be further simplified by substituting the expression for sr obtained from the yawing moment equation into the roll equation (considering a single control input for simplicity), and, similarly, substituting the roll equation expression for sp into the yawing equation, as follows:

$$sp = L_v(v-v_g) + L_v^*s(v-v_g) + L_p(p-p_g) + L_r r + L_\delta \delta + \frac{I_{xz}}{I_x} \left\{ \begin{aligned} &N_v(v-v_g) + N_v^*s(v-v_g) + N_p(p-p_g) \\ &+ N_r \left(r - \frac{sv_g}{U_0} \right) + N_\delta \delta + \frac{I_{xz}}{I_z} sp \end{aligned} \right\}$$

$$sr = N_v(v-v_g) + N_v^*s(v-v_g) + N_p(p-p_g) + N_r \left(r - \frac{sv_g}{U_0} \right) + N_\delta \delta + \frac{I_{xz}}{I_z} \left\{ \begin{aligned} &L_v(v-v_g) + L_v^*s(v-v_g) + L_r r \\ &+ L_p(p-p_g) + L_\delta \delta + \frac{I_{xz}}{I_x} sr \end{aligned} \right\}$$

Collecting like terms,* we define the "primed derivatives" for a general motion or input quantity designated by the subscript "i",

$$L_i' = \frac{L_i + \frac{I_{xz}}{I_x} N_i}{1 - \frac{I_{xz}^2}{I_x I_z}} \quad ; \quad N_i' = \frac{N_i + \frac{I_{xz}}{I_z} L_i}{1 - \frac{I_{xz}^2}{I_x I_z}}$$

which implies, also,

(4-92)

$$L_i = L_i' - \frac{I_{xz}}{I_x} N_i' \quad ; \quad N_i = N_i' - \frac{I_{xz}}{I_z} L_i'$$

Then the roll and yaw equations reduce to

$$sp = L_v'(v-v_g) + L_v^{*'}s(v-v_g) + L_p'(p-p_g) + L_r' r - (L_r')_g \frac{sv_g}{U_0} + \sum L_\delta' \delta$$

$$sr = N_v'(v-v_g) + N_v^{*'}s(v-v_g) + N_p'(p-p_g) + N_r' r - (N_r')_g \frac{sv_g}{U_0} + \sum N_\delta' \delta$$

(4-93)

*This procedure was apparently first reported by E. M. Frayn, "The Simplification of Lateral Response Calculations, When the Product of Inertia Is Not Negligible, by the Use of Modified Derivatives," Appendix D in K. Mitchell and E. M. Frayn, Lateral Response Theory, A.R.C. R&M 2297, 1952, pp. 35, 36. It was later rediscovered and emphasized in the United States by C. N. Tsu, "A Note About the Effects of Product of Inertia in Lateral Stability," J. Inst. Aeron. Sci., Vol. 21, No. 7, July 1954, p. 189.

and we see that the use of primed derivatives eliminates the direct appearance of the product of inertia terms. The use of the g subscript gust-gradient input term reflects the fact that there is no L_r gust gradient term in Eq. 4-91, i.e., $(N_r')_g \equiv N_r / (1 - I_{xz}^2 / I_x I_z)$, $(L_r')_g \equiv (I_{xz} / I_x) N_r / (1 - I_{xz}^2 / I_x I_z)$.

The relationships between the gravity angles, θ and ϕ , and the motion parameters, which are needed to complete the foregoing sets of equations, are obtained by substituting the trim conditions of Assumptions 6 and 9 into Eqs. 4-60; that is, for $\phi_0 = P_0 = Q_0 = R_0 = 0$, and the corresponding $\dot{\psi}_0 = \dot{\theta}_0 = \dot{\phi}_0 = 0$ (Eq. 4-41),

$$\begin{aligned} p &= \dot{\phi} - \dot{\psi} \sin \theta_0 \\ q &= \dot{\theta} \\ r &= \dot{\psi} \cos \theta_0 \end{aligned} \quad (4-94)$$

The associated trim equations, Eqs. 4-58, are

$$\begin{aligned} mg \sin \theta_0 &= X_0 \\ -mg \cos \theta_0 &= Z_0 \\ 0 &= M_0 \\ 0 &= Y_0 = L_0 = N_0 \end{aligned} \quad (4-95)$$

where X_0 and Z_0 are composed of the lift, drag, and thrust terms in Eqs. 4-77 and 4-85 and M_0 is given by Eq. 4-88.

The Stability Axis System

Thus far, considerable progress has been made in reducing the equations of motion to simple and analytically useful forms. A final simplification is immediately obtained by orienting the axis system to make $W_0 = 0$; that is so the X axis in the steady state is pointed into the relative wind. Such an alignment results in a stability axis system which is initially inclined to the horizon at the flight path angle, γ_0 (since $\theta_0 = \gamma_0 + \alpha_0$, and $\alpha_0 = \tan^{-1} W_0 / U_0 = 0$).

It is important to recognize that the initial alignment does not alter the body-fixed nature of the axis system. All perturbed motions

are still measured in a body-fixed frame; however the alignment of the frame with respect to the body changes as a function of the operating or trim point condition. When the airframe is disturbed from the trim condition, the axes rotate with the airframe and do not change direction with respect to the airplane; consequently, the perturbed X axis may or may not be parallel to the relative wind while the vehicle is in disturbed flight (see Fig. 4-25).

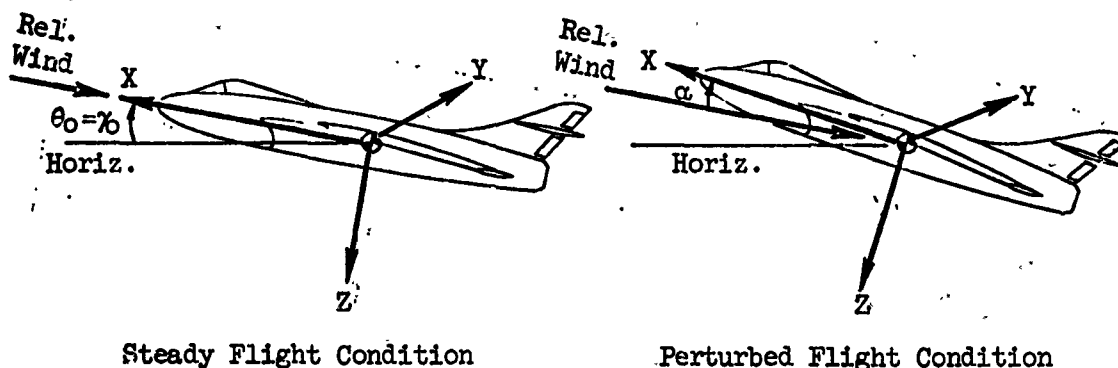


Fig. 4-25. Direction of Stability Axes with Respect to the Relative Wind During the Steady Flight and Disturbed Flight Conditions

Using this axis system ($W_0 = 0$, $\theta_0 = \gamma_0$) the Eq. 4-94 relationships, in Laplace transform notation, give

$$\begin{aligned} s\phi &= p + r \tan \gamma_0 \\ s\theta &= q \\ s\psi &= \frac{r}{\cos \gamma_0} \end{aligned} \quad (4-96)$$

Incorporating this result, setting $W_0 = 0$, $\theta_0 = \gamma_0$, considering one control input at a time (i.e., δ rather than $\sum \delta$), and collecting motion- and input-dependent terms on the left and right sides, respectively, the resulting equations are:

$$\text{Longitudinal set} \quad (4-97)$$

$$\begin{aligned} (s - X_u)u - (X_\phi s + X_w)v + (-X_q s + g \cos \gamma_0)\theta &= X_\delta \delta - [X_u u_E + (X_\phi s + X_w)v_E] \\ -Z_u u + (s - Z_\phi s - Z_w)v + [(-U_0 - Z_q)s + g \sin \gamma_0]\theta &= Z_\delta \delta - [Z_u u_E + (Z_\phi s + Z_w)v_E - Z_q \frac{sw_E}{U_0}] \\ -M_u u - (M_\phi s + M_r)v + s(s - M_q)\theta &= M_\delta \delta - [M_u u_E + (M_\phi s + M_r)v_E - M_q \frac{sw_E}{U_0}] \end{aligned}$$

$$[s(1-Y_V) - Y_V]v - (Y_Ps + g \cos \gamma_0) \frac{p}{s} + [(U_0 - Y_R)s - g \sin \gamma_0] \frac{r}{s} = Y_\delta \delta - [(Y_\phi s + Y_V)v_g + Y_P p_g - Y_R \frac{sv_g}{U_0}]$$

$$-(L_V^i s + L_V^i)v + (s - L_P^i)p - L_R^i r = L_\delta^i \delta - [(L_V^i s + L_V^i)v_g + L_P^i p_g]$$

$$-(N_V^i s + N_V^i)v - N_P^i p + (s - N_R^i)r = N_\delta^i \delta - [(N_V^i s + N_V^i)v_g + N_P^i p_g - (N_R^i) \frac{sv_g}{U_0}]$$

Inclusion of Weightlessness Terms in Stability Axis Equations of Motion

As mentioned earlier, the flat-earth assumption, No. 9, limits the applicability of either the stability axis or body axis sets of equations to speeds less than about 5000 ft/sec. However, for the stability axis set, the specific assumption of $W_0 = 0$ allows a significant simplification without neglecting the weightlessness terms appearing in Eqs. 4-65 through 4-68. We still omit the generally negligible terms proportional to U_0/r and U_0^2/r , but now we take note of $W_0 = 0$, $\Theta_0 = \gamma_0$ and the simple relationships of Eq. 4-96. Then, the only added (weightlessness) term in the Z equation (4-65) is simply $(-U_0^2/r) \sin \gamma_0 \theta$. For the side force equation we note that for $W_0 = 0$, $U_0 = U_0 \cos \gamma_0$ and, from Eq. 4-96, $s\psi \cos \Theta_0 = s\psi \cos \gamma_0 = r$; then Eq. 4-68 reduces to

$$sv + U_0 r - \left(g - \frac{U_0^2}{r}\right) \cos \gamma_0 \phi = \frac{dY}{m}$$

In effect, therefore, we simply replace g by $g - U_0^2/r$ to extend the applicability of Eqs. 4-97 and 4-98 to orbital speeds.

Further simplification of these equations is possible by dropping terms found to be negligible in specific instances, but, excepting this, these are the simplest of all generally applicable sets of the linearized equations of motion. They are especially convenient for computing and understanding the basic vehicle dynamic characteristics which are of course independent of the chosen axis system. However, as already mentioned, for situations where the measurement or sensing axes differ markedly from the stability axes, motions computed in the latter system must be transformed before they can be compared with flight test results

or used in closed-loop analyses. Under such circumstances the use of a body-fixed system aligned with the sensor axes may be preferable. The only difference in form between body axis and stability axis equations of motion for the same set of assumptions is the appearance in the former of the W_0 terms and the use of $\theta_0 = \gamma_0 + \tan^{-1} W_0/U_0$ rather than γ_0 to orient the g vector. However, the stability derivatives used in each generally differ because of the axis rotation through α_0 .

Stability Derivative Transformation Relationships

The complete transformation from stability axis to body axis derivatives must consider resolution not only of the forces and moments, but also of the perturbed motions and the changed inertias. Applying these considerations results in the following relationships between body axes, subscript "b", and stability axes, no subscript. Notice that for the lateral primed derivatives, the transformations are exactly the same as those for the basic (unprimed) dimensional derivatives $\partial L/\partial P$, $\partial N/\partial r$, etc.* For the unprimed derivatives, e.g., I_p , N_r , etc., the transformed values of $(\partial L/\partial P)_b$, $(\partial N/\partial r)_b$, etc., must be divided through by the transformed $(I_x)_b$, $(I_z)_b$ expressions, also given. This simplification accruing to the use of prime derivatives is due to the fact that they correctly account for all accelerations about a given axis due to a given perturbation and can, accordingly, be treated as simple vectors.

Longitudinal

$$\begin{pmatrix} X_u \end{pmatrix}_b = X_u \cos^2 \alpha_0 - (X_w + Z_u) \sin \alpha_0 \cos \alpha_0 + Z_w \sin^2 \alpha_0$$

$$\begin{pmatrix} X_w \end{pmatrix}_b = X_w \cos^2 \alpha_0 + (X_u - Z_w) \sin \alpha_0 \cos \alpha_0 - Z_u \sin^2 \alpha_0$$

$$\begin{pmatrix} X_{\dot{w}} \end{pmatrix}_b = X_{\dot{w}} \cos^2 \alpha_0 - Z_{\dot{w}} \sin \alpha_0 \cos \alpha_0$$

*Edward Seckel, Stability and Control of Helicopters, Academic Press, New York, 1964.

$$\begin{aligned}
(X_{q;\delta})_b &= X_{q;\delta} \cos \alpha_0 - Z_{q;\delta} \sin \alpha_0 \\
(Z_u)_b &= Z_u \cos^2 \alpha_0 - (Z_w - X_u) \sin \alpha_0 \cos \alpha_0 - X_w \sin^2 \alpha_0 \\
(Z_w)_b &= Z_w \cos^2 \alpha_0 + (Z_u + X_w) \sin \alpha_0 \cos \alpha_0 + X_u \sin^2 \alpha_0 \\
(\dot{Z}_w)_b &= \dot{Z}_w \cos^2 \alpha_0 + \dot{X}_w \sin \alpha_0 \cos \alpha_0 \\
(Z_{q;\delta})_b &= Z_{q;\delta} \cos \alpha_0 + X_{q;\delta} \sin \alpha_0 \\
(M_u)_b &= M_u \cos \alpha_0 - M_w \sin \alpha_0 \\
(M_w)_b &= M_w \cos \alpha_0 + M_u \sin \alpha_0 \\
(\dot{M}_w)_b &= \dot{M}_w \cos \alpha_0 \\
(M_{q;\delta})_b &= M_{q;\delta} \\
(I_y)_b &= I_y
\end{aligned} \tag{4-99}$$

Notice that the X_u , X_w , Z_u , and Z_w expressions are equivalent to those in Eqs. 4-80 and 4-87.

Lateral

$$\begin{aligned}
(Y_{v;\delta})_b &= Y_{v;\delta} \\
(\dot{Y}_v)_b &= \dot{Y}_v \\
(Y_p)_b &= Y_p \cos \alpha_0 - Y_r \sin \alpha_0 \\
(Y_r)_b &= Y_r \cos \alpha_0 + Y_p \sin \alpha_0 \\
(L'_{v;\delta})_b &= L'_{v;\delta} \cos \alpha_0 - N'_{v;\delta} \sin \alpha_0 \\
(\dot{L}'_v)_b &= \dot{L}'_v \cos \alpha_0 - \dot{N}'_v \sin \alpha_0
\end{aligned}$$

$$\begin{aligned}\left(L_p^i\right)_b &= L_p^i \cos^2 \alpha_0 - \left(L_r^i + N_p^i\right) \sin \alpha_0 \cos \alpha_0 + N_r^i \sin^2 \alpha_0 \\ \left(L_r^i\right)_b &= L_r^i \cos^2 \alpha_0 - \left(N_r^i - L_p^i\right) \sin \alpha_0 \cos \alpha_0 - N_p^i \sin^2 \alpha_0\end{aligned}\quad (4-100)$$

$$\left(N_{V;\delta}^i\right)_b = N_{V;\delta}^i \cos \alpha_0 + L_{V;\delta}^i \sin \alpha_0$$

$$\left(N_V^i\right)_b = N_V^i \cos \alpha_0 + L_V^i \sin \alpha_0$$

$$\left(N_p^i\right)_b = N_p^i \cos^2 \alpha_0 - \left(N_r^i - L_p^i\right) \sin \alpha_0 \cos \alpha_0 - L_r^i \sin^2 \alpha_0$$

$$\left(N_r^i\right)_b = N_r^i \cos^2 \alpha_0 + \left(L_r^i + N_p^i\right) \sin \alpha_0 \cos \alpha_0 + L_p^i \sin^2 \alpha_0$$

$$\left(I_x\right)_b = I_x \cos^2 \alpha_0 + 2I_{xz} \sin \alpha_0 \cos \alpha_0 + I_z \sin^2 \alpha_0$$

$$\left(I_z\right)_b = I_z \cos^2 \alpha_0 - 2I_{xz} \sin \alpha_0 \cos \alpha_0 + I_x \sin^2 \alpha_0$$

$$\left(I_{xz}\right)_b = \left(I_z - I_x\right) \sin \alpha_0 \cos \alpha_0 + I_{xz} \left(\cos^2 \alpha_0 - \sin^2 \alpha_0\right)$$

4.9 DESCRIPTION OF THE DIMENSIONAL AND NONDIMENSIONAL STABILITY AXIS DERIVATIVES

The adoption of Assumptions 6 and 7 has greatly reduced the number of stability derivatives appearing in the equations of motion. In this section each of the dimensional stability derivatives in Eqs. 4-90 and 4-91 is first given a brief physical interpretation, then expanded into a more basic form, and shown to be a function of what are called "basic nondimensional stability derivatives." Some discussion of these basic nondimensional stability derivatives is also given.* The longitudinal

*There is of course an extensive literature pertaining to the origin and estimation of nondimensional stability derivatives. Two compendia are of particular note;

USAF Stability and Control Datcom, Air Force Flight Dynamics Lab., Wright-Patterson AFB, Ohio, Oct. 1960 (Rev. Nov. 1965).

Royal Aeronautical Society Data Sheets, Royal Aeronautical Society, London.

and considerable bibliographic material is given in some of the texts, already referenced, e.g.,

Edward Seckel, op. cit.

stability derivatives are treated first, and the lateral stability derivatives are treated later. Equations 4-71, used in the discussion, are repeated here for reference; but the "a" subscript is dropped for simplicity, since the derivatives are not dependent on the specific origin of the relative motions between the vehicle and the atmosphere.

$$\begin{array}{ll}
 L = C_L(1/2)\rho V^2 S & Z = C_Z(1/2)\rho V^2 S \\
 D = C_D(1/2)\rho V^2 S & L = C_L(1/2)\rho V^2 S_b \\
 X = C_X(1/2)\rho V^2 S & M = C_M(1/2)\rho V^2 S_c \\
 Y = C_Y(1/2)\rho V^2 S & N = C_N(1/2)\rho V^2 S_b
 \end{array} \quad (4-101)$$

It can be readily appreciated that the direct conversion from the nondimensional aerodynamic coefficients to the corresponding forces and moments requires a common axis system for both. That is, in this instance, the coefficients must be obtained in, or reduced to, a set applicable to stability axes. When other than stability axis systems are used for the equations of motion, the coefficients or the dimensional derivatives must be converted to, or set up in, that axis system (e.g., Eqs. 4-99 and 4-100).

While none of the aerodynamic coefficients are guaranteed to behave linearly with any of the variables, in most cases, for small perturbations it is reasonably accurate to linearize the coefficients about the operating point as in Eq. 4-76. Some of the more significant nonlinearities are noted in the discussions to follow which are, at best, incomplete in this respect.

Dimensional and Nondimensional Forms

The stability derivatives, dimensional and nondimensional, as we shall develop and use them are of a particular, commonly-used form. Other forms appear in the literature relating to aircraft stability and control, but little or no distinction in terminology is made among them; all are referred to as "stability derivatives" regardless of the particular form. For purposes of discussion and clarification, it is convenient to illustrate the four forms most generally found before selecting those to be given detailed treatment.

Example-1. Basic dimensional stability derivatives:

$$\frac{\partial L}{\partial P} \quad \text{or} \quad \frac{\partial L}{\partial p}$$

Example 2. Dimensional stability derivative parameters:

$$I_p = \frac{1}{I_x} \frac{\partial L}{\partial P} = \left(\frac{1}{I_x} \right) \left(\frac{\partial L}{\partial p} \right)$$

Example 3. Basic nondimensional stability derivatives:

$$C_{l_p} = \frac{\partial C_l}{\partial (pb/2U)} = \left(\frac{1}{qSb} \right) \left(\frac{\partial L}{\partial (pb/2U)} \right)$$

Example 4. Nondimensional stability derivative parameters:

$$l_p = \left(\frac{1}{4} \right) \left(\frac{b}{k_x} \right)^2 C_{l_p} ; \quad \text{where } k_x^2 = \frac{I_x}{m}$$

The equivalence between forms like $\partial L/\partial P$ and $\partial L/\partial p$ shown above comes about because we are normally dealing with trim conditions which eliminate accelerated steady motions, thereby making $dP/dp = 1$. Accordingly we can, and will, express most derivatives in terms of either upper or lower case (perturbation) symbols to suit our convenience.

It may be seen from the examples that the dimensional forms (Examples 1 and 2) are concerned with direct forces and moments (or accelerations), and with motion velocities, whereas the nondimensional form (Examples 3 and 4) is concerned with force and moment coefficients and with nondimensional velocities (e.g., $pb/2U$ is the nondimensionalized form of the rolling velocity, p). It may also be seen that the basic stability derivatives (Examples 1 and 3) do not involve inertial quantities, whereas the stability derivative parameters (Examples 2 and 4) do. Conversion relations among these four general forms and also specific mathematical definitions of individual derivatives are given in Tables 4-1 and 4-4 at the end of this chapter.

It must be emphasized that the specific notation and the specific definitions used here are not necessarily employed by all writers on the subject. For example, Jones* in a basic aerodynamic reference work

*B. Melvill Jones, "Dynamics of the Aeroplane," in W. F. Durand, ed., Aerodynamic Theory, Div. N, Vol. V, Durand Reprinting Committee, Pasadena, Calif., 1943. Reprinted by Dover Publications (Vols. V and VI bound in one volume), New York, 1963.

uses the notation L_p to signify the partial derivative $\partial L/\partial p$, whereas most of the present-day writers use L_p (or L_p^*) to represent the stability derivative parameter $(1/I_x)(\partial L/\partial p)$. On the other hand, almost everyone uses the same notation for such basic nondimensional stability derivatives as C_{L_p} , $C_{L_{\dot{\alpha}}}$, and C_{M_q} .

Of the four forms listed above the two of most practical importance are the basic nondimensional stability derivative (e.g., C_{L_p}) and the dimensional stability derivative parameter (e.g., L_p). The basic nondimensional form (C_{L_p}) is important because correlation between the aerodynamic characteristics of different airframes or the same airframe at different flight conditions is most easily attained with these stability derivatives; as a result, aerodynamic stability derivative data from wind tunnel tests, flight tests, and theoretical analyses are usually presented in the basic nondimensional form.* The dimensional stability derivative parameter form (L_p) is important because it leads directly to the numerical coefficients in the sets of simultaneous differential equations describing the real time dynamics of the airframe. Thus, stability derivatives in this form are useful in determining the analytic transfer functions of the airframe and in setting up its mathematical model on an analog computer.

Accordingly the discussion dealing with the evaluation of stability derivatives makes use of the basic nondimensional stability derivative form (C_{L_p}), and that dealing with airframe transfer functions makes use of the dimensional stability derivative parameter form (L_p).

Perturbation Effects on the Total Velocity

It should be noted that the quantity V^2 , which appears in Eq. 4-101, is the square of the total linear velocity. In the stability axis system

*An important exception to this otherwise general state of affairs occurs for the low speed range of vehicles capable of hovering operation. For $V \rightarrow 0$, as in hover, dynamic pressure $= (\rho/2)V^2$ is a poor measure of the aerodynamic forces on the vehicle which are more appropriately related to parameters indicative of slipstream (or jet efflux) velocities, e.g., R. L. Stapleford, J. Wolkovitch, R. E. Magdaleno, C. P. Shortwell, and W. A. Johnson, An Analytical Study of V/STOL Handling Qualities in Hover and Transition, AFFDL-TR-65-73, May 1965.

the total linear velocity during the steady flight condition is equal to U_0 , which is the velocity in the direction of the X axis. When disturbed from steady flight, the airplane can have velocity components $U_0 + u$, v , and w directed along the X, Y, and Z axes, respectively. During disturbed flight the magnitude of the total linear velocity can be expressed as

$$V = \sqrt{(U_0 + u)^2 + v^2 + w^2}$$

$$\text{or } V = \sqrt{U_0^2 + 2U_0u + u^2 + v^2 + w^2} \quad (4-102)$$

In Assumption 5, u , v , and w were assumed to be very small so that their products and squares could be neglected. Thus,

$$\begin{aligned} V &= \sqrt{U_0^2 + 2U_0u} \\ &\doteq U_0 \left(1 + \frac{u}{U_0} \right) = U \end{aligned}$$

Also, when 1 is very much greater than u/U_0 , a very good approximation is $U \doteq U_0$. Therefore,

$$V \doteq U \doteq U_0 \quad (4-103)$$

Thus, V , U_0 , and U can be used somewhat interchangeably for stability axes and the conditions implicit in Assumption 5.

Longitudinal Stability Derivatives

The longitudinal force derivatives have already been treated for a general axis system (see Eq. 4-80); however, they are included and rederived in the present discussion for the sake of completeness.

Effect of u , the change in forward speed

As an airplane increases its forward speed, the lift, L , drag, D , and moment, M , change. Generally, but not always, each of these quantities increases. Also, the thrust component in the flight direction, T_x , changes.

X_u Since drag acts along the negative axis, an increase in drag contributes a negative X force; conversely an increase in T_x contributes a positive X force. The change in X force due to a change in forward speed can be expressed mathematically in the form

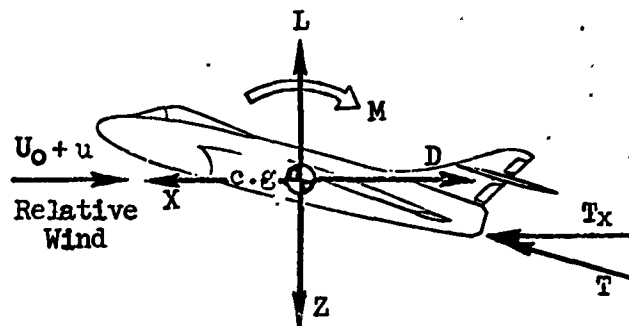


Fig. 4-26. Variation of Lift, Drag, and Pitching Moment with Change in Forward Velocity

$$\Delta X = \frac{\partial X}{\partial U} u = \frac{\partial D}{\partial U} u + \frac{\partial T_x}{\partial U} u$$

$$X_u = \frac{1}{m} \frac{\partial X}{\partial U} = \frac{1}{m} \left(\frac{\partial D}{\partial U} + \frac{\partial T_x}{\partial U} \right) \quad (4-104)$$

Using the drag equation from Eq. 4-101, substituting U for V in accordance with Eq. 4-103, and performing the indicated differentiation yields

$$X_u = \frac{-\rho S}{2m} \left[U^2 \frac{\partial C_D}{\partial U} + 2UC_D \right] + \frac{1}{m} \frac{\partial T_x}{\partial U}$$

and

$$X_u = \frac{-\rho S U}{m} \left[\frac{U}{2} \frac{\partial C_D}{\partial U} + C_D \right] + \frac{1}{m} \frac{\partial T_x}{\partial U} \quad (4-105)$$

The drag coefficient, C_D , is the equilibrium drag divided by $\rho U^2 S / 2$. By definition, it is always measured along the direction of the relative wind; hence the equilibrium drag coefficient is measured along the negative equilibrium X axis in the stability axis system (Fig. 4-26) and is always positive in sign. In contrast, it should be pointed out that the derivative X_u is at all times measured along the X axis and is always negative in sign.

The equation for thrust can be written in a form similar to that of the lift and drag equations in Eqs. 4-101:

$$T = \frac{\rho U^2 S}{2} C_T \quad (4-106)$$

However, this form is misleading since the coefficient C_T is basically not aerodynamic in nature. In fact, for jet engines the thrust, T , is more nearly constant than is C_T . Accordingly, the most generally applicable expression for the thrust contribution to X_u is that given in Eq. 4-105, above, where the partial derivative $\partial T/\partial U$ is obtainable from powerplant performance estimates.

The change in drag coefficient with varying forward velocity for constant angle of attack and altitude, $\partial C_D/\partial U$, can arise from two sources—Mach number effects and aeroelastic effects. In most cases the latter are small and can be neglected. Changes due to Mach number are also small and negligible for low subsonic and high supersonic Mach numbers, but become appreciable in the transonic region ($0.8 < M < 1.2$) where a large increase in drag occurs.

The appearance, in Eq. 4-105, of the nondimensional grouping $(U/2)(\partial C_D/\partial U)$ suggests a simplified notation, viz:

$$\frac{U}{2} \frac{\partial C_\lambda}{\partial U} = C_{\lambda u} \quad (4-107)$$

where C_λ is any basic nondimensional stability derivative. Accordingly,

$$X_u = \frac{-\rho S U}{m} (C_{D_u} + C_D) + \frac{1}{m} \frac{\partial T_x}{\partial U} \quad (4-108)$$

The direct thrust contributions to all other derivatives is generally negligible for conventional airplanes, except as it affects the equilibrium, operating point, conditions. Accordingly, its possible variation with other perturbations, and about or along other axes, is not considered in the formulation of the remaining derivative expressions.

Z_u Since lift acts along the negative Z axis, an increase in lift due to a change in forward speed contributes a negative Z force:

$$\begin{aligned} \Delta Z &= \frac{\partial Z}{\partial U} u = \frac{-\partial L}{\partial U} u \\ Z_u &= \frac{1}{m} \frac{\partial Z}{\partial U} = \frac{-1}{m} \frac{\partial L}{\partial U} \end{aligned} \quad (4-109)$$

By noting the similarity between Eqs. 4-109 and 4-104, and between the lift and drag equations of Eq. 4-101, we can immediately write

$$Z_u = \frac{-\rho S U}{m} [C_{L_u} + C_L] \quad (4-110)$$

The lift coefficient, C_L , is the equilibrium of trim lift divided by $\rho U^2 S/2$. For the trim conditions assumed (Assumptions 8 and 9) for the stability axis equations of motion, the trim lift is equal to the airplane weight times $\cos \gamma_0$ minus the upward thrust component normal to the flight path. By definition, lift coefficient is always measured perpendicular to the relative wind and is positive upward (Fig. 4-26), and so the equilibrium lift coefficient is measured along the negative equilibrium z axis of the stability axis system. On the other hand, Z_u is always measured along the positive Z axis and is positive downward. Low values of C_L are associated with low angles of attack and high speeds, whereas high values of C_L are associated with high angles of attack and low speeds.

The derivative C_{L_u} is the nondimensional change in lift coefficient with variations in forward velocity for constant angle of attack and altitude, $(U/2)(\partial C_L / \partial U)$. C_{L_u} arises from Mach number and aeroelastic effects. The magnitude of the total C_{L_u} can vary considerably and its sign can change, depending not only on the airframe geometry and its elastic properties, but also on the Mach number and dynamic pressure at which it is flying. The magnitude of C_{L_u} is negligibly small for low speed flight, but it may reach a considerable value near the critical Mach number of the airframe.

M_u The change in moment caused by a change in forward speed can be expressed as:

$$\begin{aligned} \Delta M &= \frac{\partial M}{\partial U} u \\ M_u &= \frac{1}{I_y} \frac{\partial M}{\partial U} \end{aligned} \quad (4-111)$$

The same mechanics used in the expansion of X_u can be used to derive M_u :

$$M_u = \frac{\rho S U c}{I_y} [C_{Mu} + C_M] \quad (4-112)$$

Here, we must remember that C_M represents only the aerodynamic portion of the total trimmed pitching moment, and that the latter is, by Assumptions 6 and 9, zero. Thus, in general there will be a nonzero C_M only in the presence of thrust asymmetry (Eq. 4-88).

The derivative C_{Mu} is the nondimensional change in pitching moment coefficient with variation in forward velocity for constant angle of attack and altitude, $(U/2)(\partial C_M / \partial U)$. The magnitude of C_{Mu} can vary considerably and the sign can change, depending on such factors as the airframe's geometry and its elastic properties, and the Mach number and dynamic pressure at which it is flying. This derivative can arise from three sources—thrust or power effects, Mach number effects, and aeroelastic effects. The early treatment of C_{Mu} was as a power effect arising from the propwash of propeller-driven aircraft. Today, because of the use of jet engines and the associated alleviation of power effects on dynamic stability, the C_{Mu} from slipstream effects is small except for "unconventional" VTOLs. (The direct thrust effects themselves were thoroughly discussed earlier in connection with Eq. 4-89.) On the other hand, the contributions to C_{Mu} due to Mach number and aeroelastic effects have become increasingly important.

Effect of w , the change in speed along the Z axis

In Fig. 4-27 the quantities L_0 and D_0 represent the lift and drag acting on the airplane during the steady flight condition. The lift and drag always act, respectively, normal and parallel to the relative wind. According to the definition of stability axes, the relative

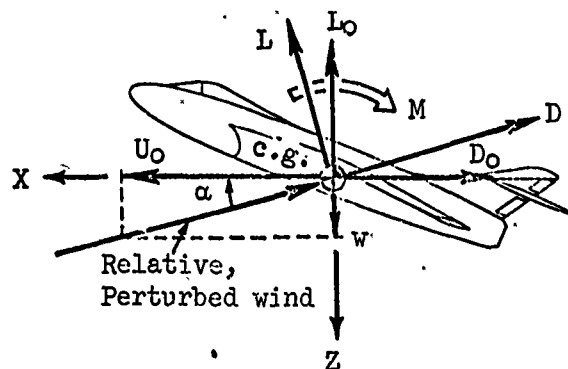


Fig. 4-27. Variation of Lift and Drag with Change in w

wind during the steady flight condition is parallel to the X axis. Therefore the only component of linear velocity during the steady flight condition is U_0 ; and L_0 and D_0 are, respectively, perpendicular and parallel to the X axis. When the airplane is disturbed from steady flight so that it has a component of velocity, w , along the Z axis as well as a forward velocity, U_0 , the relative wind shifts to a new position, as shown in Fig. 4-27. This shift results in an increase in angle of attack, denoted by the perturbed angle α . (The trim angle of attack, α_0 , is zero by definition.) The quantities L and D in Fig. 4-27 represent the lift and drag acting on the airplane during the disturbed flight condition, and they act normal and parallel to the relative wind. The relative wind acts in the direction opposite to the vector sum of U_0 and w .

X_w The perturbed X forces due to w are found by resolving L and D along the X axis and taking the partial derivative with respect to w ,

$$X = L \sin \alpha - D \cos \alpha$$

$$\frac{\partial X}{\partial w} = \frac{1}{U_0} \frac{\partial X}{\partial \alpha} = \frac{1}{U_0} \left(L \cos \alpha_0 + \frac{\partial L}{\partial \alpha} \sin \alpha_0 + D \sin \alpha_0 - \frac{\partial D}{\partial \alpha} \cos \alpha_0 \right)$$

Neglecting perturbation products (Assumption 5), and recognizing $\alpha_0 = 0$,

$$X_w = \frac{1}{m} \frac{\partial X}{\partial w} = \frac{1}{m U_0} \left(L - \frac{\partial D}{\partial \alpha} \right) \quad (4-113)$$

Substitution of the values of lift and drag from Eq. 4-101 into Eq. 4-113 yields

$$X_w = \frac{1}{m U_0} \left[\frac{\rho S U^2}{2} C_L - \frac{\partial}{\partial \alpha} \left(\frac{\rho S U^2}{2} C_D \right) \right]$$

$$X_w = \frac{\rho S U}{2m} (C_L - C_{D_\alpha}) \quad (4-114)$$

where $C_{D_\alpha} \equiv \partial C_D / \partial \alpha$.

The derivative $C_{D\alpha}$ is the change in drag coefficient with varying angle of attack. When the angle of attack of an airframe increases from the equilibrium condition, the total drag increases, hence $C_{D\alpha}$ is positive in sign. By far the largest contribution to $C_{D\alpha}$ comes from the wing, but there are small contributions from the horizontal tail and the fuselage. $C_{D\alpha}$ is generally a nonlinear function of α , but it can be considered piecewise linear for small perturbations.

Z_w The change in the Z force due to w can be found by resolving the forces in Fig. 4-27 along the z axis and performing operations similar to those used in the derivation of Eq. 4-114:

$$Z_w = \frac{-\rho S U^2}{2m} (C_{L\alpha} + C_D) \quad (4-115)$$

The derivative $C_{L\alpha}$ is the change in lift coefficient with varying angle of attack; it is commonly known as the "lift curve slope." When the angle of attack of the airframe is increased, the lift force will increase more or less linearly until the wing stalls. The derivative $C_{L\alpha}$ is therefore always positive in sign at angles of attack below the stall. The total airframe $C_{L\alpha}$ is made up of contributions from the wing, the fuselage, and the horizontal tail. Ordinarily the wing accounts for about 80 to 90 percent of the total $C_{L\alpha}$, although it may account for less if the size of the fuselage is large in comparison with the size of the wing.

Aeroelastic distortion of the wing, under the incremental loads due to an angle of attack change, can alter its geometric twist to either increase or decrease the net change in lift and therefore the value of $C_{L\alpha}$. Figure 4-28 illustrates how pure bending deflections of a sweptback wing cause a reduction in the local angle of attack (washout) of the tip region. Viewed along the flight direction, the trailing edge (2) moves up with respect to the leading edge (1), producing a negative increment in net angle of attack. On the other hand, airloads concentrated forward of the elastic axis tend to twist the wing sections to a positive increment in angle of attack.

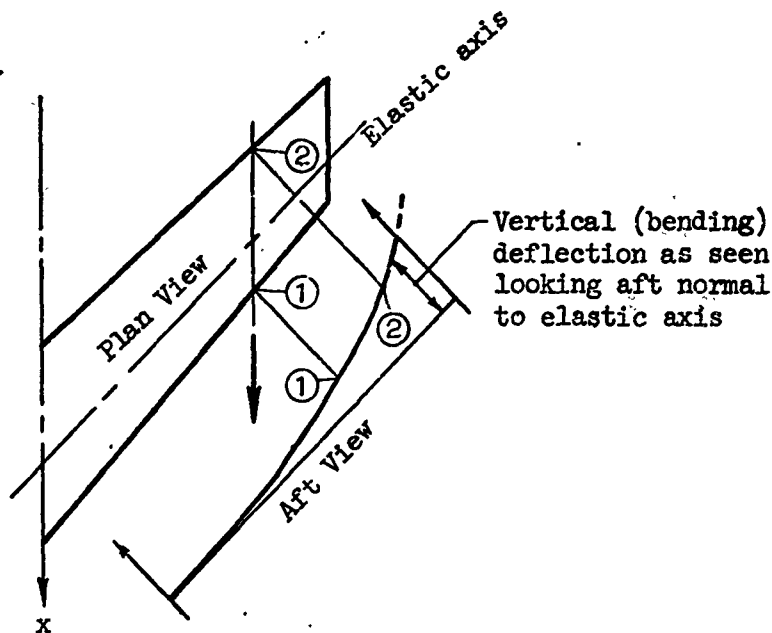


Fig. 4-28. Effect of Wing Bending on Local Angle of Attack

M_w The change in moment due to w is most easily visualized by observing the components of the total lift and drag that act on the wing and the horizontal tail. Figure 4-29 shows these components. The subscripts w and t refer to wing and tail. A vertical velocity, w , causes a change in angle of attack of both the wing and the horizontal tail, and consequently changes the lift and drag acting on these surfaces.

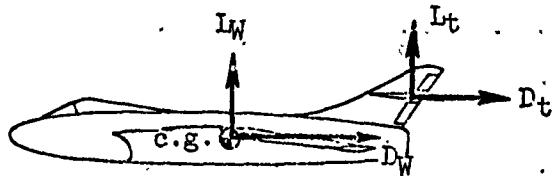


Fig. 4-29. Lift and Drag Acting on the Wing and the Horizontal Tail

The resulting moment can be found by summing the moments about the center of gravity caused by each of these forces to give the nondimensional coefficient C_M (Eq. 4-101) as a function of $\alpha \equiv w/U_0$. In terms of this coefficient

$$M = \frac{\rho U^2 S c}{2} C_M$$

$$\frac{\partial M}{\partial w} = \frac{1}{U_0} \frac{\partial M}{\partial \alpha} = \frac{\rho U S c}{2} \frac{\partial C_M}{\partial \alpha}$$

and

$$M_w \equiv \frac{1}{I_y} \frac{\partial M}{\partial w} = \frac{\rho S U c}{2 I_y} C_{M_\alpha} \quad (4-116)$$

where $C_{M_\alpha} \equiv \partial C_M / \partial \alpha$.

The derivative C_{M_α} is the change in pitching moment coefficient with varying angle of attack, and is commonly referred to as the "longitudinal static stability derivative." For a positive increment in angle of attack, the increased lift on the horizontal tail causes a negative pitching moment about the center of gravity of the airframe. Simultaneously, the increased lift of the wing causes a positive or negative pitching moment, depending on the fore and aft location of the lift vector with respect to the center of gravity. These contributions together with the pitching moment contribution of the fuselage are combined to establish the derivative C_{M_α} . Because of the distributed loads involved, C_{M_α} can be strongly influenced by aeroelastic distortions of the wing, tail, and fuselage. However, the major influence on the magnitude and sign of the total C_{M_α} for a particular airframe configuration is the center of gravity (c.g.) location. In fact, C_{M_α} is proportional to the distance between the c.g. and the aerodynamic center (a.c.), the latter being the point about which the increment of lift due to a change in angle of attack effectively acts. If the center of gravity is on the aerodynamic center C_{M_α} is zero; if ahead of the aerodynamic center C_{M_α} is negative, and the airframe is said to possess static longitudinal stability; if aft of the aerodynamic center C_{M_α} is positive, and the airframe is then statically unstable. C_{M_α} or the aerodynamic center, can have important configuration-dependent nonlinear variations with α , but can generally be considered piecewise linear over a limited range. Also the aerodynamic center generally moves aft in going from subsonic to supersonic flight.

Another way of expressing static stability is in terms of the derivative $-\partial C_M / \partial C_L = -C_{M_\alpha} / C_{L_\alpha}$. This quantity, called "static margin," is identically equal to the x-distance from the a.c. to the c.g. divided by the reference chord length,* i.e.,

$$\partial C_M / \partial C_L = C_{M_{C_L}} = -x_{a.c.} / c$$

where x is measured positive forward. A positive static margin corresponds to statically stable conditions, and a negative $\partial C_M / \partial C_L$ and C_{M_α} .

*e.g., Etkin, op. cit.

Static stability, characterized by either C_{M_α} or $\partial C_M / \partial C_L$, is perhaps the most important of the longitudinal derivatives, and is a major factor in determining the response of the airframe to elevator motions and to gusts.

Effect of \dot{w} , the rate of change of speed along the z axis

In the earlier discussion of unsteady and quasi-steady flows, the existence of a force due to \dot{w} was explained on the basis of quasi-steady flow considerations. It was pointed out that this rate of change of speed along the Z axis results in an effective change of the angle of attack

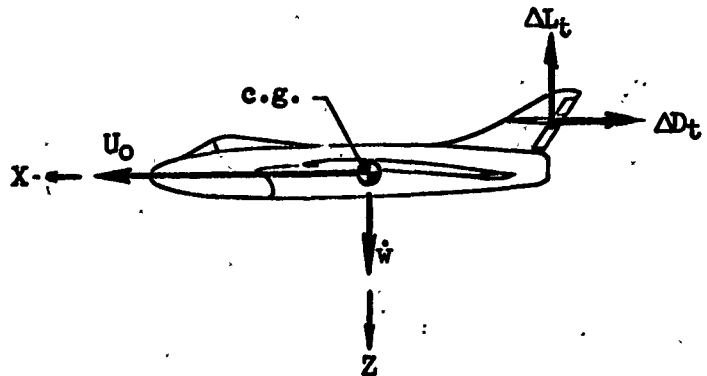


Fig. 4-30. Lift and Drag Changes on Horizontal Tail Due to Plunging Acceleration

of the horizontal tail. This change in angle of attack causes changes in the lift and drag acting on the horizontal tail. These are incremental forces and are represented by ΔL_t and ΔD_t in Fig. 4-30.

$X_{\dot{w}}$ The change in drag on the horizontal tail is the main contributor to the change in the X force. But the drag on the horizontal tail is generally small in comparison with the total drag, and the increment in the tail drag due to \dot{w} is even smaller. Therefore, $X_{\dot{w}}$ is considered zero in the first approximation.

$Z_{\dot{w}}$ The change in lift on the horizontal tail causes a sometimes important change in the total Z force which, in terms of the total lift coefficient, can be written

$$\begin{aligned} \frac{\partial Z}{\partial \dot{w}} &= \frac{1}{U} \frac{\partial Z}{\partial \alpha} = \frac{-1}{U} \frac{\partial L}{\partial \alpha} = \frac{-\rho S U}{2} \frac{\partial C_L}{\partial \alpha} \\ Z_{\dot{w}} &= \frac{1}{m} \frac{\partial Z}{\partial \dot{w}} = \frac{-\rho S U}{2m} \frac{\partial C_L}{\partial \alpha} \end{aligned} \quad (4-117)$$

To form a nondimensional coefficient, Eq. 4-117 is multiplied and divided by $c/2U$:

$$\begin{aligned} Z_{\dot{w}} &= \frac{-\rho S U}{2m} \frac{c}{2U} \frac{\partial C_L}{\partial (\dot{\alpha} c/2U)} \\ Z_{\dot{w}} &= \frac{-\rho S c}{4m} C_{L_{\dot{\alpha}}} \end{aligned} \quad (4-118)$$

where $C_{L_{\dot{\alpha}}} \equiv \partial C_L / \partial (\dot{\alpha} c/2U)$.

The derivative $C_{L\dot{\alpha}}$ arises essentially from two independent sources—an aerodynamic time lag effect, as explained in the discussion of quasi-steady flow, and various "deadweight" aeroelastic effects. For low speed flight, $C_{L\dot{\alpha}}$ arises mostly from the aerodynamic lag effect on the horizontal tail and its sign is positive. However, even tailless aircraft have $C_{L\dot{\alpha}}$'s due to the fact that the wing must accelerate the air mass in its path as it accelerates (apparent mass effect which goes beyond quasi-steady flow assumption). For high speed flight the sign of $C_{L\dot{\alpha}}$ can be positive or negative, depending on aeroelastic effects such as wing twisting due to the deadweight moments of projecting nacelles, and fuselage bending caused by the deadweight of the aft fuselage (see Fig. 4-31).

The effect of $C_{L\dot{\alpha}}$ on longitudinal dynamics is essentially the same as if the airframe's mass or inertia were changed in the equation relating the forces in the Z direction. This effect is very small, and for this reason $C_{L\dot{\alpha}}$ is often neglected in longitudinal dynamic analysis.

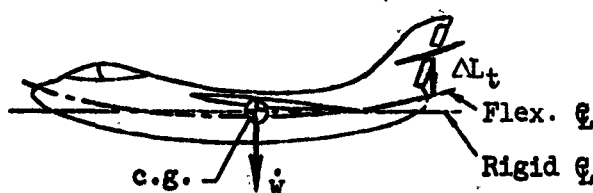


Fig. 4-31. \dot{w} Effect on Aeroelastic Distortion Due to Fuselage Flexibility

$M_{\dot{w}}$ This derivative can be expressed in terms of the total moment coefficient as:

$$\frac{\partial M}{\partial \dot{w}} = \frac{1}{U_0} \frac{\partial M}{\partial \dot{\alpha}} = \frac{\rho S U_0 c}{2} \frac{\partial C_M}{\partial \dot{\alpha}}$$

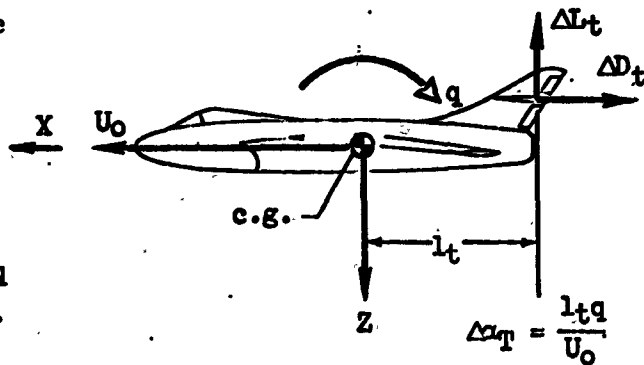
$$M_{\dot{w}} = \frac{1}{I_y} \frac{\partial M}{\partial \dot{w}} = \frac{\rho S c^2}{4 I_y} C_{M\dot{\alpha}} \quad (4-119)$$

where $C_{M\dot{\alpha}} = \partial C_M / \partial (\dot{\alpha} c / 2U)$.

The derivative $C_{M\dot{\alpha}}$ is produced by the same aerodynamic and aeroelastic effects that produce $C_{L\dot{\alpha}}$. However, whereas $C_{L\dot{\alpha}}$ is usually negligible, $C_{M\dot{\alpha}}$ is relatively important in longitudinal dynamics because it does have a significant, if not powerful, effect on the damping of the short-period mode. A negative value of $C_{M\dot{\alpha}}$, which is its normal sign, increases the short-period damping.

Effect of q , the pitching velocity

X_q In the light of the quasi-steady flow assumption (Assumption 7) the major effect of the airplane's pitching about its center of gravity is to cause an increase in the angle of attack of the horizontal tail. As in the case of the effect of \dot{w} , the resulting drag increase is neglected in the first approximation and X_q is normally set equal to zero.



Z_q, M_q The incremental lift produces a change both in the Z force and in pitching moment. The expressions for Z_q and M_q can be derived as follows:

Fig. 4-32. Lift and Drag Changes on Horizontal Tail Due to Pitching Velocity

$$\frac{\partial Z}{\partial q} = \frac{-\partial L}{\partial q} = \frac{-\rho S U^2}{2} \frac{\partial C_L}{\partial q} = \frac{-\rho S U^2}{2} \frac{c}{2U} \frac{\partial C_L}{\partial (qc/2U)}$$

$$Z_q = \frac{1}{m} \frac{\partial Z}{\partial q} = \frac{-\rho S U c}{4m} C_{Lq} \quad (4-120)$$

where $C_{Lq} = \partial C_L / \partial (qc/2U)$, and

$$\frac{\partial M}{\partial q} = \frac{\rho S U^2 c}{2} \frac{\partial C_M}{\partial q} = \frac{\rho S U^2 c}{2} \frac{c}{2U} \frac{\partial C_M}{\partial (qc/2U)}$$

$$M_q = \frac{1}{I_y} \frac{\partial M}{\partial q} = \frac{\rho S U c^2}{4I_y} C_{Mq} \quad (4-121)$$

where $C_{Mq} = \partial C_M / \partial (qc/2U)$.

The derivatives C_{Lq} and C_{Mq} are the change in lift and moment coefficients, respectively, with pitching velocity at a fixed angle of attack. As the airframe pitches about its center of gravity, the fore and aft angle of attack distribution changes, and lift forces develop primarily on the horizontal tail and wing (see Fig. 4-33). These produce contributions to both derivatives, positive in sign for C_{Lq} and negative for C_{Mq} .

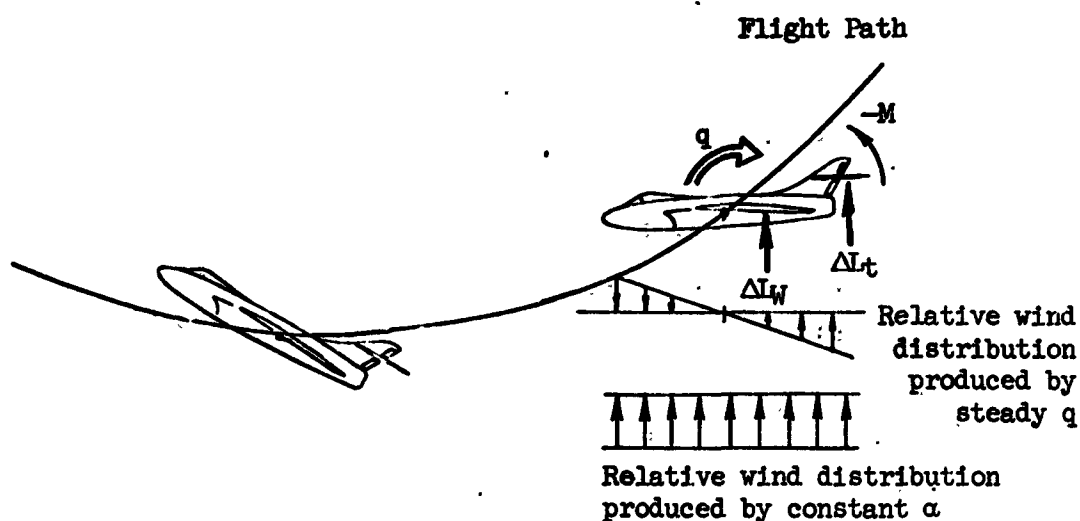


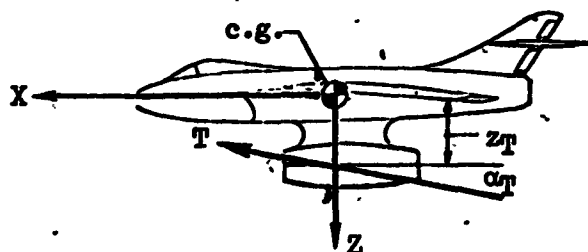
Fig. 4-33. Lift and Moment Coefficient Change
Due to Variation in Pitching Velocity

There are also contributions because of various "deadweight" aeroelastic effects. Since the airframe is moving in a curved flight path due to its pitching, a centrifugal force is developed on all the components of the airframe. This force can cause the wing to twist as a result of the deadweight moment of overhanging nacelles, and can cause the horizontal tail angle of attack to change as a result of fuselage bending due to the weight of the tail section. In low speed flight both C_{Lq} and C_{Mq} come mostly from the effect of the curved flight path on the horizontal tail, and their signs are positive and negative, respectively. In high speed flight the signs of either can be positive or negative, depending on the nature of the aeroelastic effects.

As with $C_{L\dot{\alpha}}$, the effect of C_{Lq} on longitudinal stability is usually very small and it is ordinarily neglected in dynamic analyses. On the other hand, C_{Mq} is very important in longitudinal dynamics because it contributes a large portion of the damping of the short-period mode for conventional aircraft. As pointed out, this damping effect comes mostly from angle of attack changes at the horizontal tail, which are proportional to the tail length, l_t (i.e., $\Delta\alpha_T = ql_t/U$). The tail length is also the lever arm converting tail lift into moment; therefore C_{Mq} is proportional to l_t^2 .

Effects of δ_T , the change of power plant control setting (throttle)

An increase in power plant control setting yields an increase in thrust having the general orientation shown in Fig. 4-34. By simple resolution,



$$X_{\delta_T} = (1/m)(\partial T / \partial \delta_T) \cos \alpha_T$$

$$Z_{\delta_T} = (-1/m)(\partial T / \partial \delta_T) \sin \alpha_T$$

$$M_{\delta_T} = (-z_T / I_y)(\partial T / \partial \delta_T) \cos \alpha_T$$

Fig. 4-34. Resolution of Thrust Into Forces and Moments

Further breakdown of these derivatives into conventional nondimensional coefficients is not warranted, as noted above in the discussion of X_u .

Effects of aerodynamic control surface deflections

Aerodynamic surfaces pertinent to longitudinal control include elevators, stabilizers, flaps, slats, dive brakes, etc. Where applicable the positive direction is taken as that giving positive lift, as in the definition of positive α (see Fig. 4-35). Usually, deflection of such

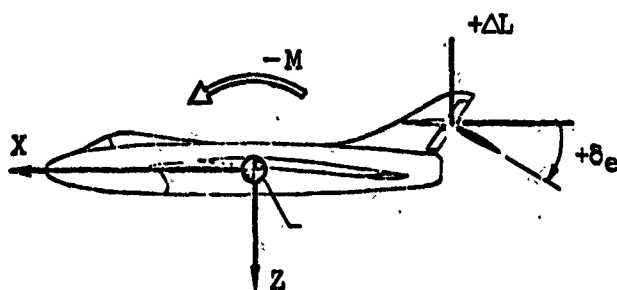


Fig. 4-35. Lift and Moment Changes Due to Surface Deflection

surfaces, in addition to producing the sought-for primary effect (e.g., tail lift to produce a pitching moment for an elevator, or drag to produce longitudinal deceleration for a dive brake), also produces secondary forces and moments.

Generally, therefore, we must consider contributions to the X and Z forces and to the pitching moment, M, as follows:

$$\begin{aligned} X_{\delta} &= \frac{1}{m} \frac{\partial X}{\partial \delta} = \frac{-\rho U^2 S}{2m} C_{D\delta} & \text{where} & \quad C_{D\delta} = \frac{\partial C_D}{\partial \delta} \\ Z_{\delta} &= \frac{1}{m} \frac{\partial Z}{\partial \delta} = \frac{-\rho U^2 S}{2m} C_{L\delta} & \text{where} & \quad C_{L\delta} = \frac{\partial C_L}{\partial \delta} \\ M_{\delta} &= \frac{1}{I_y} \frac{\partial M}{\partial \delta} = \frac{\rho U^2 S c}{2I_y} C_{M\delta} & \text{where} & \quad C_{M\delta} = \frac{\partial C_M}{\partial \delta} \end{aligned} \quad (4-122)$$

The general forms of Eqs. 4-122 are specialized by suitable subscripts for particular control surfaces, e.g., δ_e for elevator, δ_f for flap, δ_b for dive brakes, etc.

The elevator is, of course, the primary longitudinal control surface and its function is, through applied pitching moments, to control the angle of attack of the airframe in equilibrium and maneuvering flight. This function is usually considered to be the most important of all the control functions about the three axes, so the elevator control effectiveness, CM_{δ_e} is of great importance in airframe design. Its design value is determined by the anticipated fore and aft center of gravity travel, and the maximum C_L capability of the wing as influenced by high lift devices. In general, the larger the center of gravity range and the higher the maximum C_L , the larger the required value of CM_{δ_e} . Supersonic flight may impose additional requirements because of the attendant aft movement of the aerodynamic center. The sign of CM_{δ_e} depends on the location of the elevator, fore or aft of the c.g.; for aft locations (as in Fig. 4-35) and the elevator sign convention used here, CM_{δ_e} is negative.

CL_{δ_e} is always positive in accordance with the convention used here to define positive control deflection as a producer of positive lift (Fig. 4-35). On conventional aircraft with the horizontal tail mounted at an appreciable distance aft of the center of gravity, CL_{δ_e} is usually very small and its effect is relatively unimportant, except for automatic control involving vertical acceleration feedback. The value of CD_{δ_e} is invariably smaller than CL_{δ_e} because of the usual variation of drag with lift and it is normally negligible. However, on tailless aircraft having small effective elevator lever arms, the values of CL_{δ_e} and CD_{δ_e} are relatively large with respect to the required CM_{δ_e} and neither can be safely neglected. The sign of CD_{δ_e} can be positive or negative, depending on the trim position of the elevator and the trim angle of attack.

Lateral Stability Derivatives

Effect of v , the change in side velocity

When an airplane is disturbed from steady flight so that it has a side velocity, v , a force along the Y axis and moments about the X and Z axes are developed. The major forces caused by the side velocity are labeled F_1 , F_2 , F_3 , and F_4 in Fig. 4-36. F_1 arises from the change of the angle of attack of the vertical tail. F_2 is the side force acting on the fuselage, and F_3 and F_4 are differential lift forces acting on each semispan of the wing, due to its "effective dihedral."

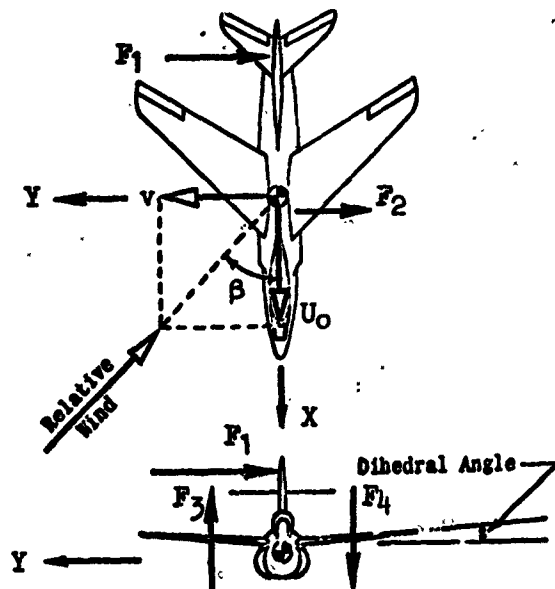


Fig. 4-36. Forces Accompanying Sideslipping Motions

From Eq. 4-101, the side force equation

has the form

$$Y = \frac{\rho U^2 S}{2} C_Y$$

so that

$$\frac{\partial Y}{\partial v} = \frac{\rho U^2 S}{2} \frac{\partial C_Y}{\partial v}$$

and, in terms of $\beta = \tan^{-1} v/U_0 \doteq v/U_0$,

$$Y_v = \frac{1}{m} \frac{\partial Y}{\partial v} = \frac{\rho U S}{2m} C_{Y\beta} \quad (4-123)$$

where $\partial C_Y / \partial \beta = C_{Y\beta}$.

The major portion of $C_{Y\beta}$ normally comes from the vertical tail, with small contributions from the fuselage and wing. It is usually negative in sign for practical airframe configurations; i.e., the side force opposes the sideward motion. However, the forces on a slender fuselage

can actually be in the aiding direction for high angles of attack.* These effects can apparently override the resisting tail forces to produce positive values of $C_{y\beta}$ for certain (as yet rare) configurations with low-aspect-ratio wings which operate at high angles of attack.

Small (or positive) values of $C_{y\beta}$ are undesirable because the resulting small (or reversed) side forces make the detection of sideslip difficult; accordingly, coordination of banked turns becomes a piloting problem. Also, such values of $C_{y\beta}$ contribute little to the damping of the dutch roll, whereas normal (negative) values of $C_{y\beta}$ can contribute substantially to the total damping.

L_v The rolling moment, L , about the X axis is caused mainly by the components F_z and F_4 which act normal to the wing and by F_1 at the fin center-of-pressure which can be either above or below the X axis. From Eq. 4-101,

$$L = \frac{\rho U^2 S b}{2} C_l$$

and
$$\frac{\partial L}{\partial v} = \frac{\rho U^2 S b}{2} \frac{\partial C_l}{\partial v} = \frac{\rho U S b}{2} \frac{\partial C_l}{\partial \beta}$$

$$L_v = \frac{1}{I_x} \frac{\partial L}{\partial v} = \frac{\rho U S b}{2 I_x} C_{l\beta} \quad (4-124)$$

where $C_{l\beta} = \partial C_l / \partial \beta$. Also,

$$I_\beta = U_o L_v = \frac{\rho U^2 S b}{2 I_x} C_{l\beta}$$

$C_{l\beta}$, the change in rolling moment coefficient with sideslip angle, is usually referred to as the "effective dihedral." This nomenclature is a holdover from earlier days when, in fact, the value of $C_{l\beta}$ was governed largely by the geometric dihedral built into the wing (Fig. 4-36). For positive geometric dihedral $C_{l\beta}$ is negative, and this leads to some confusion because negative values of $C_{l\beta}$ are referred to

*Bernard Spencer, Jr., and W. Pelham Phillips, Transonic Aerodynamic Characteristics of a Series of Bodies Having Variations in Fineness Ratio and Cross-Sectional Ellipticity, NASA TN D-2622, Feb. 1965.

as "positive dihedral." For modern configurations the wing contribution to $C_{l\beta}$ is a function not only of geometric dihedral but, more so, of sweep, aspect ratio, and angle of attack. In addition, the wing location on the fuselage, high or low, contributes negative or positive increments, respectively, to $C_{l\beta}$; and the direct forces on the vertical tail contribute decreasingly negative increments as the fin moves down with respect to the x axis with increasing trim angle of attack. While the general overriding importance of the wing contribution to $C_{l\beta}$ cannot be denied, there may be flight conditions where it is small relative to the vertical tail or wing/fuselage contribution.

$C_{l\beta}$ is very important in lateral stability and control, and it is therefore imperative to consider it in the preliminary design of an airframe. It is involved in damping both the dutch roll mode and the spiral mode, and also in the maneuvering characteristics of an airframe, especially with regard to lateral control with the rudder alone near stall. To improve the dutch roll damping characteristics of an airframe, small negative values of $C_{l\beta}$ are desired but difficult to obtain in general because of the influences noted above.

N_v The yawing moment, N , due to a side velocity, v , is caused mainly by the force on the vertical tail, F_1 . The forms of the stability derivatives N_v and N_β are similar to those of Eq. 4-124:

$$\begin{aligned} N_v &= \frac{\rho U S b}{2 I_z} C_{n\beta} \\ N_\beta &= \frac{\rho U^2 S b}{2 I_z} C_{n\beta} \end{aligned} \quad (4-125)$$

$C_{n\beta}$ is the change in yawing moment coefficient with variation in sideslip angle. It is usually referred to as the static directional, or "weathercock," stability. The major portion of $C_{n\beta}$ comes from the vertical tail area and lever arm, which stabilize the body of the airframe just as the tail feathers of an arrow stabilize the arrow shaft. The $C_{n\beta}$ contribution due to the vertical tail is positive, signifying static directional stability, whereas the $C_{n\beta}$ due to the body is negative, signifying static directional instability. There is also a

contribution to $C_{n\beta}$ from the wing, the value of which is usually positive but very small compared to the body and vertical tail contributions. Since both the major contributions depend essentially on the dimensions of the body, c.g. variations, which are limited by longitudinal considerations to a small fraction of the body length, have little effect on the value of $C_{n\beta}$. Increasing supersonic speeds generally have a deleterious effect on $C_{n\beta}$ because the fin lift curve slope decreases, whereas the body moments remain about constant. Also, for high angles of attack, the fin may be immersed in the wing-body wake with consequent drastic reductions in $C_{n\beta}$.

The derivative $C_{n\beta}$ is very important in determining dynamic lateral stability and control characteristics. It primarily establishes the natural frequency of the dutch roll oscillatory mode of the airframe, and is also a factor in determining the spiral stability characteristics. A high value of $C_{n\beta}$ aids the pilot in effecting coordinated turns and prevents excessive sideslip and yawing motions in extreme flight maneuvers; however, in rough air, excessive $C_{n\beta}$ magnifies the disturbances due to side gusts. There are cases on record where a reduction in the vertical tail resulted in improved over-all (rough and calm air) dynamic properties.

Effect of \dot{v} , the rate of change in side velocity

The existence of quasi-steady forces and moments due to \dot{v} was explained in the discussion of unsteady flow as arising from sidewash lags which produce angle of attack variations at the vertical tail.

$Y_{\dot{v}}$ The change in side force with \dot{v} in terms of the side force coefficient, C_y , is

$$\frac{\partial Y}{\partial \dot{v}} = \frac{1}{U} \frac{\partial Y}{\partial \dot{\beta}} = \frac{\rho S U_0}{2} \frac{\partial C_y}{\partial \dot{\beta}}$$

To nondimensionalize, multiply and divide by $b/2U$, whereby

$$Y_{\dot{v}} = \frac{1}{m} \frac{\partial Y}{\partial \dot{v}} = \frac{\rho S b}{4m} C_{y\dot{\beta}} \quad (4-126)$$

where $C_{y\dot{\beta}} \equiv \partial C_y / \partial (\dot{\beta} b / 2U)$.

1_y The change in rolling moment, L , in terms of the roll moment coefficient, C_L , is

$$\frac{\partial L}{\partial \dot{v}} = \frac{1}{U_0} \frac{\partial L}{\partial \dot{\beta}} = \frac{\rho S U_0 b}{2} \frac{\partial C_L}{\partial \dot{\beta}}$$

and nondimensionalizing, as above,

$$U_0 L_{\dot{v}} = L_{\dot{\beta}} = \frac{1}{I_x} \frac{\partial L}{\partial \dot{\beta}} = \frac{\rho S U_0 b^2}{4 I_x} C_{L_{\dot{\beta}}} \quad (4-127)$$

where $C_{L_{\dot{\beta}}} = \partial C_L / \partial (\dot{\beta} b / 2U)$.

1_y The corresponding yawing moment derivative is

$$U_0 N_{\dot{v}} = N_{\dot{\beta}} = \frac{1}{I_z} \frac{\partial N}{\partial \dot{\beta}} = \frac{\rho S U_0 b^2}{4 I_z} C_{N_{\dot{\beta}}} \quad (4-128)$$

where $C_{N_{\dot{\beta}}} = \partial C_N / \partial (\dot{\beta} b / 2U)$.

Generally speaking, not too much is known of the nondimensional aerodynamic derivatives appearing in the foregoing expressions. In fact, as concerns the usual formulation of the rigid-body equations of motion, all these derivatives are generally neglected. However, there are cases where the observed dutch roll damping can be accounted for only by including the significant $C_{N_{\dot{\beta}}}$ effects, when $C_{N_{\dot{\beta}}}$ is the same order of magnitude as C_{N_r} . The difficulty is that there is no good way of estimating $C_{N_{\dot{\beta}}}$ or of knowing a priori for which configurations it may be important.

Aside from aerodynamic lag effects, \dot{v} derivatives also arise due to aeroelastic effects. Fig. 4-37 shows how the aft fuselage distortion due to lateral acceleration of the distributed mass, produces a vertical tail angle of attack and a concomitant aerodynamic side force. This side force, proportional to \dot{v} , reduces the airplane's resistance to lateral motion (i.e., its effective mass), but only by a negligible amount; therefore, even considering such aeroelastic effects, $Y_{\dot{v}}$ is negligible. Usually the rolling moment contributed by the side force will also be negligible because of the small vertical moment arm involved. This leaves the yawing moment derivative, $N_{\dot{\beta}}$, as the most probable significant contribution of aeroelastic distortions and aerodynamic lag effects.

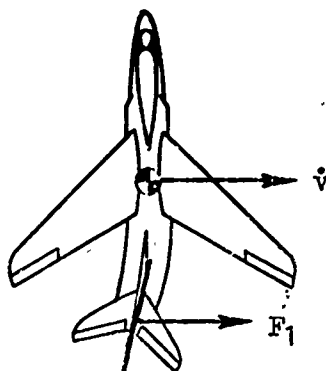


Fig. 4-37. Distortion Effects Due to \dot{v}

Effect of p , the change in rolling velocity

The rolling velocity, p , causes the various forces shown in Fig. 4-38.

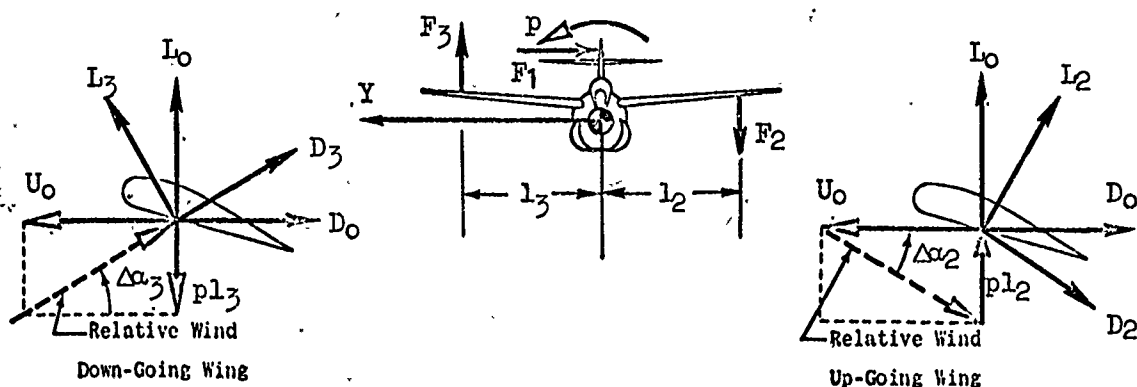


Fig. 4-38. Forces Arising from Roll Rate Perturbations, p

Y_p The change in the Y force with p , illustrated as F_1 acting on the vertical tail in Fig. 4-38, is expressed as:

$$\frac{\partial Y}{\partial p} = \frac{\rho U^2 S}{2} \frac{\partial C_y}{\partial p}$$

To form a nondimensional coefficient, multiply and divide by $b/2U$. Then,

$$Y_p = \frac{1}{m} \frac{\partial Y}{\partial p} = \frac{\rho U^2 S}{2m} \frac{b}{2U} \frac{\partial C_y}{\partial (pb/2U)}$$

$$Y_p = \frac{\rho U S b}{4m} C_{yp} \quad (4-129)$$

where $C_{yp} = \partial C_y / \partial (pb/2U)$.

The sign of C_{yp} can be positive or negative, depending on the vertical tail location with respect to the X axis, as a function of angle of attack; and also depending on the sidewash from the wing. Since C_{yp} is of very little importance in lateral dynamics, it is common practice to neglect this derivative in lateral dynamic calculations.

I_p There are also incremental forces acting on the wing, illustrated as F_2 and F_3 in Fig. 4-38. The vertical velocity of the down-going wing at any station a distance l_3 from the XZ plane is pl_3 . This vertical velocity increases the effective angle of attack at this station by an amount $\Delta\alpha_3$ (where $\Delta\alpha_3 = pl_3/U_0$). This increase in angle of attack increases the lift and drag acting on the wing. The effective angle of attack of the upgoing wing at a station a distance l_2 from the XZ plane is decreased by an amount $\Delta\alpha_2$ (where $\Delta\alpha_2 = pl_2/U_0$). This increase in effective angle of attack decreases the lift and drag acting on the wing at this station. Usually the change in drag force is a relatively negligible contribution to the change in rolling moment due to p , which can be expressed as:

$$\frac{\partial L}{\partial p} = \frac{\rho U^2 S b}{2} \frac{\partial C_l}{\partial p}$$

Multiplying and dividing by $b/2U$,

$$I_p = \frac{1}{I_x} \frac{\partial L}{\partial p} = \frac{\rho U S b^2}{4 I_x} C_{lp} \quad (4-130)$$

where $C_{lp} = \partial C_l / \partial (pb/2U)$.

The derivative C_{lp} is the change in rolling moment coefficient with change in rolling velocity and is usually known as the roll damping derivative. It is composed of contributions, negative in sign, from the wing and the horizontal and vertical tails. However, unless the size of the tails is unusually large in comparison with the size of the wing, the major portion of the total C_{lp} comes from the wing; and the variations in C_{lp} with Mach number and α closely follow the variations in wing lift-curve-slope, C_{l_α} .

C_{lp} is quite important in lateral dynamics because it, alone, essentially determines the damping in roll characteristics of the aircraft. Its value is more or less given by the wing planform geometry which is determined

by other more important design criteria. The value of C_{lp} does directly affect the design of the ailerons, however, since C_{lp} in conjunction with $C_{l\delta_a}$ establishes the airframe's maximum available rolling velocity; this is an important criterion of flying qualities.

Positive values of C_{lp} occur only when the wing, or portions thereof, are stalled. Flight situations involving stall or separated flow are generally avoided, except for demonstration purposes, and are seldom subjected to conventional dynamic analysis. Such situations usually lead to spinning motions which can only be successfully analyzed by including nonlinear terms and solving the equations of motion by numerical or analog methods.

N_p In addition to the change in magnitude of the lift forces acting on each semispan of the wing, it may be seen from Fig. 4-38 that the lift forces acting on the downgoing and upgoing semispans are rotated forward and backward, respectively. The change in direction of these forces results in a negative yawing moment about the Z axis.

Figure 4-38 represents the general case. However, for flight near the stall, the drag forces may become important and result in a yawing moment of opposite sign. The change in yawing moment due to p can be written immediately by analogy to the Eq. 4-130 result, viz:

$$N_p = \frac{\rho U S b^2}{4 I_z} C_{np} \quad (4-131)$$

where $C_{np} = \partial C_n / \partial (pb/2U)$.

The derivative C_{np} is the change in yawing moment coefficient with varying rolling velocity. While it arises mainly from the wing, as discussed above, the vertical tail can also contribute (see Fig. 4-38). The contribution from the vertical tail can be either positive or negative, depending on the vertical tail geometry, the sidewash from the wing, and the equilibrium angle of attack of the airframe.

C_{np} is fairly important in lateral dynamics because of its influence on dutch roll damping. It is usually negative in sign, and

for most airframe configurations, the larger its negative value, the greater the reduction in dutch roll damping. Also, the more negative its value, the higher the sideslipping (uncoordinated) motions accompanying turn entry or exit. Therefore, positive values of C_{np} are to be desired, although it is completely impractical to make this a design goal.

Effect of r , the change in yawing velocity

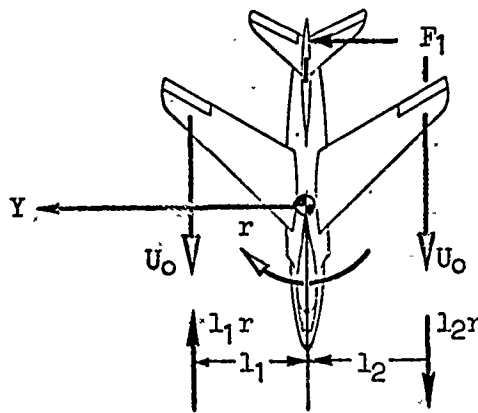


Fig. 4-39. Forces Due to Yaw Rate, r

Y_r A side force, F_1 , is caused by a yawing velocity, r , which is mainly due to the fact that the effective angle of attack of the vertical tail is increased. By analogy with Y_p , derived in Eq. 4-129, it is possible to write

$$Y_r \equiv \frac{1}{m} \frac{\partial Y}{\partial r} = \frac{\rho U S b}{4m} C_{Yr} \quad (4-132)$$

where $C_{Yr} = \partial C_Y / \partial (rb/2U)$.

The derivative C_{Yr} , the change in side force coefficient with yawing velocity, is of little importance in lateral dynamics; it is common practice to neglect this derivative in lateral calculations.

L_r As shown in Fig. 4-39, the forward speed of a station which is a distance l_1 from the XZ plane on the semispan of the wing is decreased an amount $l_1 r$, resulting in a decrease in lift at this station. Similarly, the forward speed of a station a distance l_2 normal to the XZ plane on the semispan of the wing is increased an amount $l_2 r$,

resulting in an increase in lift at this section. The result of the changes in lift acting on each semispan is then a rolling moment, usually positive, whose variation with r can be expressed by analogy with L_p (Eq. 4-130) as:

$$L_r \equiv \frac{1}{I_x} \frac{\partial L_r}{\partial r} = \frac{\rho U S b^2}{4 I_x} C_{l_r} \quad (4-133)$$

where $C_{l_r} = \partial C_l / \partial (rb/2U)$.

The derivative C_{l_r} is the change in rolling moment coefficient with change in yawing velocity. In addition to the major wing contribution, discussed above, the vertical tail will also contribute to C_{l_r} if it is located either above or below the X axis. Its contribution can therefore be positive or negative, depending on the vertical tail geometry and the equilibrium angle of attack of the airframe. The sign of C_{l_r} is usually dominated by the wing contribution, which is positive and proportional to the trimmed lift coefficient.

C_{l_r} is of secondary importance in lateral dynamics, but it should not be neglected in lateral dynamic calculations. For a conventional airframe configuration, changes in C_{l_r} of reasonable magnitude show only slight effects on the dutch roll damping characteristics. In the spiral mode, however, C_{l_r} has a considerable effect. For stability in this mode, it is desirable that the positive value of C_{l_r} be as small as possible.

N_r The side force, F_1 , in Fig. 4-39 also causes a moment about the Z axis since the vertical tail is some distance aft of the center of gravity. This moment is usually negative and its variation with r is, by analogy to L_r ,

$$N_r \equiv \frac{1}{I_z} \frac{\partial N}{\partial r} = \frac{\rho U S b^2}{4 I_z} C_{n_r} \quad (4-134)$$

where $C_{n_r} = \partial C_n / \partial (rb/2U)$.

The derivative C_{n_r} is the change in yawing moment coefficient with change of yawing velocity. It is known as the "yaw damping derivative" and is made up of contributions, all of negative sign, from the wing,

the fuselage, and, as discussed above, the vertical tail. The latter contribution is by far the largest, usually amounting to about 80 or 90 percent of the total C_{N_r} of the airframe. Like the horizontal tail contribution to C_{M_q} , it is proportional to the square of the tail lever arm.

The derivative C_{N_r} is very important in lateral dynamics because it is the main contributor to the damping of the dutch roll oscillatory mode and is important to the spiral mode. For each mode, large negative values of C_{N_r} are desired.

Effects of Control Surface Deflections

The conventional lateral control surfaces are rudder and aileron, depicted in Figs. 4-40 and 4-41, respectively. The primary rudder function is the provision of controllable yawing moments; the primary aileron function is the generation of rolling moments. Positive rudder deflection is defined to produce positive side force, as in Fig. 4-40, and positive aileron deflection produces positive rolling moment, as in Fig. 4-41.

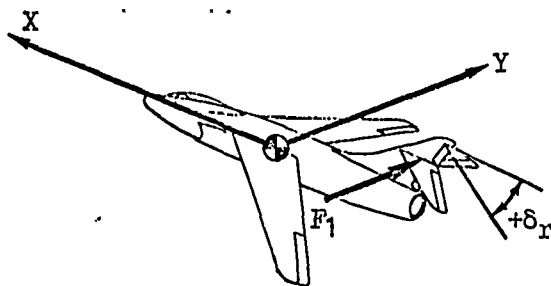


Fig. 4-40. Effect of the Rudder Deflection, δ_r

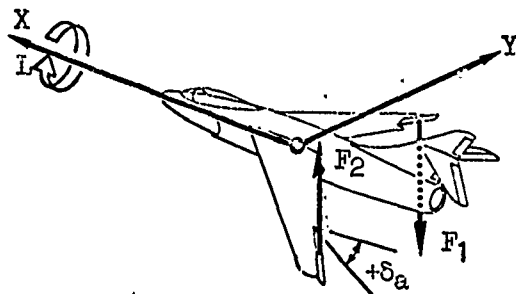


Fig. 4-41. Effect of the Aileron Deflection, δ_a

In addition to the direct (desired) moments, there are usually indirect (and undesirable) cross-moments and side forces so that in general either surface produces side forces and rolling and yawing moments. The lift, drag, and pitching moment effects of lateral/directional control deflections on longitudinal motion are generally ignored; however, there are special cases involving large differences between upgoing and downgoing ailerons (as e.g., in spoiler-type ailerons)

where significant changes in lift and pitching moment can occur. Even such situations do not usually strongly influence the lateral/directional motions, because the pilot, or autopilot, easily counters the effect with a small elevator deflection. Accordingly, for the general control surface deflection angle, δ , we limit ourselves to the following important lateral/directional derivatives:

$$Y_{\delta} = \frac{1}{m} \frac{\partial Y}{\partial \delta} = \frac{\rho U^2 S}{2m} C_{y\delta} \quad \text{where} \quad C_{y\delta} = \frac{\partial C_y}{\partial \delta}$$

$$L_{\delta} = \frac{1}{I_x} \frac{\partial L}{\partial \delta} = \frac{\rho U^2 S b}{2I_x} C_{l\delta} \quad \text{where} \quad C_{l\delta} = \frac{\partial C_l}{\partial \delta}$$

$$N_{\delta} = \frac{1}{I_z} \frac{\partial N}{\partial \delta} = \frac{\rho U^2 S b}{\delta I_z} C_{n\delta} \quad \text{where} \quad C_{n\delta} = \frac{\partial C_n}{\partial \delta}$$

These quantities are specialized for the particular control surface in question by the addition of a suitable subscript to δ , i.e., δ_r for rudder, δ_a for aileron.

$C_{y\delta_r}$ is the change in side force coefficient with variation in rudder deflection. According to the sign convention adopted here, a positive rudder deflection gives a positive side force; hence the derivative $C_{y\delta_r}$ is positive in sign. Its effects are relatively unimportant in lateral stability and control, except when considering lateral acceleration feedbacks to an autopilot.

$C_{y\delta_a}$ is the change in side force coefficient with aileron deflection. For most conventional airframe configurations, the magnitude of this derivative is essentially zero. However, for certain aircraft with highly swept wings of low aspect ratio or with inboard ailerons, the strong sidewash in the vicinity of the vertical tail caused by the asymmetrically deflected ailerons can produce finite values of either sign. Even then, however, the effects on lateral stability and control are usually negligibly small.

$C_{l\delta_r}$ is the change in rolling moment coefficient with variation in rudder deflection. Because the rudder is usually located above the X axis, a positive rudder deflection will create a positive rolling

moment. $C_{l\delta_r}$ is therefore usually positive in sign; however, it can be negative, depending on the particular airframe configuration and the angle of attack at which it is flying. The derivative $C_{l\delta_r}$ is usually of only minor importance in the dynamic lateral control of conventional aircraft, and it is sometimes neglected.

$C_{l\delta_a}$ is the change in rolling moment coefficient with change in aileron deflection. It is commonly referred to as the aileron effectiveness. According to the definition given above, left aileron down or right aileron up is a positive deflection. This produces a right-wing-down rolling moment which is positive; $C_{l\delta_a}$ is therefore positive. As far as lateral dynamics are concerned, the derivative $C_{l\delta_a}$ is most important of the control surface derivatives. The aileron effectiveness in conjunction with the damping in roll (C_{l_p}) establishes the maximum available rate of roll of an airframe, which is a very important consideration in fighter tactics at high speed. The aileron effectiveness is also very important in low speed flight during takeoffs and landings where adequate lateral control is necessary to counteract asymmetric gusts tending to roll the aircraft.

$C_{n\delta_r}$, the change in yawing moment coefficient with variation in rudder deflection, is commonly referred to as the "rudder effectiveness" (or rudder power). When the rudder is deflected positively, that is, to the left, a negative yawing moment is created on the airplane; hence the derivative $C_{n\delta_r}$ is negative. The design value of $C_{n\delta_r}$ is usually determined by considering such requirements as directional control for asymmetric power and crosswind takeoffs and landings, counteracting adverse yaw in rolling maneuvers, and spin recovery control.

$C_{n\delta_a}$ is the change in yawing moment coefficient with change of aileron deflection. This derivative arises in part from the difference in drag due to the down-aileron compared to the drag of the up-aileron. Where such effects predominate, the sign of $C_{n\delta_a}$ depends mainly on the rigging of the ailerons, their profile drag characteristics, and the angle of attack of the airframe. Aileron deflections can also produce side forces on the vertical tail, as discussed above in connection with $C_{y\delta_a}$, and these can become important contributors to $C_{n\delta_a}$. If negative,

$C_{n\delta_a}$ is called "adverse yaw" because it causes the airframe to yaw initially in a direction opposite to that desired by the pilot when he deflects the ailerons for a turn. If positive, it produces favorable or "proverse yaw" in the turning maneuver. Large values of either sign are undesirable for good lateral control qualities.

The longitudinal and lateral derivatives discussed above are listed in Tables 4-1 through 4-4 for easy reference. Appendix A contains dimensional derivative data for a variety of example vehicles.

TABLE 4-1

LONGITUDINAL NONDIMENSIONAL STABILITY DERIVATIVES
(STABILITY AXIS SYSTEM)

BASIC NONDIMENSIONAL STABILITY DERIVATIVES			NONDIMENSIONAL STABILITY DERIVATIVE PARAMETERS
TOTAL AIRFRAME		THEORETICAL AFT HORIZONTAL TAIL CONTRIBUTION	
DEFINITIONS	UNIT		
$C_D = \frac{\text{DRAG}}{qS}$	$\frac{1}{1}$		$x_u = (-C_D - C_{Du})$
$C_{Du} = \frac{U}{2} \frac{\partial C_D}{\partial U}$	$\frac{1}{1}$		
$C_{D\alpha} = \frac{\partial C_D}{\partial \alpha}$	$\frac{1}{\text{rad}}$		$x_w = \frac{1}{2}(C_L - C_{D\alpha})$
$C_{D\delta} = \frac{\partial C_D}{\partial \delta}$	$\frac{1}{\text{rad}}$		$x_\delta = \frac{-1}{2} C_{D\delta}$
$C_L = \frac{\text{LIFT}}{qS}$	$\frac{1}{1}$		
$C_{Lu} = \frac{U}{2} \frac{\partial C_L}{\partial U}$	$\frac{1}{1}$		$z_u = (-C_L - C_{Lu})$
$C_{L\alpha} = \frac{\partial C_L}{\partial \alpha}$	$\frac{1}{\text{rad}}$	$C_{L\alpha h} \frac{q_h}{q} \frac{S_h}{S} \left(1 - \frac{\partial \epsilon}{\partial \alpha}\right)$	$z_w = \frac{1}{2} (-C_{L\alpha} - C_D)$
$C_{L\dot{\alpha}} = \frac{\partial C_L}{\partial \left(\frac{d\alpha}{dt}\right)}$	$\frac{1}{\text{rad}}$	$2C_{L\dot{\alpha}h} \frac{q_h}{q} \frac{S_h}{S} \frac{l_h}{c} \frac{\partial \epsilon}{\partial \dot{\alpha}}$	$z_{\dot{w}} = \frac{-1}{4} C_{L\dot{\alpha}}$
$C_{Lq} = \frac{\partial C_L}{\partial \left(\frac{dq}{dt}\right)}$	$\frac{1}{\text{rad}}$	$2C_{Lqh} \frac{q_h}{q} \frac{S_h}{S} \frac{l_h}{c}$	$z_q = \frac{-1}{4} C_{Lq}$
$C_{L\delta} = \frac{\partial C_L}{\partial \delta}$	$\frac{1}{\text{rad}}$	$C_{L\delta h} \frac{q_h}{q} \frac{S_h}{S} \frac{\partial \epsilon_h}{\partial \delta}$	$z_\delta = -\frac{1}{2} C_{L\delta}$
$C_M = \frac{M}{qSc}$	$\frac{1}{1}$		
$C_{Mu} = \frac{U}{2} \frac{\partial C_M}{\partial U}$	$\frac{1}{1}$		$m_u = \frac{1}{2} \left(\frac{c}{k_y}\right)^2 (C_M + C_{Mu})$
$C_{M\alpha} = \frac{\partial C_M}{\partial \alpha}$	$\frac{1}{\text{rad}}$	$-\frac{l_h}{c} [C_{L\alpha}]_h$	$m_w = \frac{1}{2} \left(\frac{c}{k_y}\right)^2 C_{M\dot{\alpha}}$
$C_{M\dot{\alpha}} = \frac{\partial C_M}{\partial \left(\frac{d\alpha}{dt}\right)}$	$\frac{1}{\text{rad}}$	$-\frac{l_h}{c} [C_{L\dot{\alpha}}]_h$	$m_{\dot{w}} = \frac{1}{4} \left(\frac{c}{k_y}\right)^2 C_{M\dot{\alpha}}$
$C_{Mq} = \frac{\partial C_M}{\partial \left(\frac{dq}{dt}\right)}$	$\frac{1}{\text{rad}}$	$-\frac{l_h}{c} [C_{Lq}]_h$	$m_q = \frac{1}{4} \left(\frac{c}{k_y}\right)^2 C_{Mq}$
$C_{M\delta} = \frac{\partial C_M}{\partial \delta}$	$\frac{1}{\text{rad}}$	$-\frac{l_\delta}{c} C_{L\delta}$	$m_\delta = \frac{1}{2} \left(\frac{c}{k_y}\right)^2 C_{M\delta}$

*The symbol "q", in addition to its normal use to designate pitching velocity, is used in these tables to also denote the dynamic pressure, $\rho U^2/2$, in accordance with long-established aeronautical practice. When particularized by the subscript "h" (or "v") it signifies the local dynamic pressure at the horizontal (or vertical) tail. The local flow angles relative to free stream conditions are denoted by ϵ (xz plane) and ϵ_o (xy plane).

TABLE 4-2

LATERAL NONDIMENSIONAL STABILITY DERIVATIVES
(STABILITY OR BODY AXIS SYSTEMS)

BASIC NONDIMENSIONAL STABILITY DERIVATIVES			NONDIMENSIONAL STABILITY DERIVATIVE PARAMETERS
TOTAL AIRFRAME		THEORETICAL AFT VERTICAL	
DEFINITIONS	UNIT	TAIL CONTRIBUTION	
$C_{y\beta} = \frac{\partial C_y}{\partial \beta}$	$\frac{1}{\text{rad}}$	$-C_{l_{\alpha v}} \frac{q_v}{q} \frac{S_v}{S} \left(1 - \frac{\partial \sigma}{\partial \beta}\right)$	$y_v = \frac{1}{2} C_{y\beta}$
$C_{y\dot{\beta}} = \frac{\partial C_y}{\partial \left(\frac{\dot{\beta} b}{2U}\right)}$	$\frac{1}{\text{rad}}$	Unknown	$y_{\dot{v}} = \frac{1}{4} C_{y\dot{\beta}}$
$C_{y_r} = \frac{\partial C_y}{\partial \left(\frac{r b}{2U}\right)}$	$\frac{1}{\text{rad}}$	$2C_{l_{\alpha v}} \frac{q_v}{q} \frac{S_v}{S} \frac{I_v}{b} \left(1 - \frac{U}{I_v} \frac{\partial \sigma}{\partial r}\right)$	$y_r = \frac{1}{4} C_{y_r}$
$C_{y_p} = \frac{\partial C_y}{\partial \left(\frac{p b}{2U}\right)}$	$\frac{1}{\text{rad}}$	$2C_{l_{\alpha v}} \frac{q_v}{q} \frac{S_v}{S} \frac{h_v}{b} \left(1 - \frac{U}{h_v} \frac{\partial \sigma}{\partial p}\right)$	$y_p = \frac{1}{4} C_{y_p}$
$C_{y\delta} = \frac{\partial C_y}{\partial \delta}$	$\frac{1}{\text{rad}}$	$C_{l_{\alpha v}} \frac{q_v}{q} \frac{S_v}{S} \frac{\partial \alpha_v}{\partial \delta}$	$y_{\delta} = \frac{1}{2} C_{y\delta}$
$C_{n\beta} = \frac{\partial C_n}{\partial \beta}$	$\frac{1}{\text{rad}}$	$-\frac{I_v}{b} [C_{y\beta}]_v$	$n_v = \frac{1}{2} \left(\frac{b}{k_x}\right)^2 C_{n\beta}$
$C_{n\dot{\beta}} = \frac{\partial C_n}{\partial \left(\frac{\dot{\beta} b}{2U}\right)}$	$\frac{1}{\text{rad}}$	$-\frac{I_v}{b} [C_{y\dot{\beta}}]_v$	$n_{\dot{v}} = \frac{1}{4} \left(\frac{b}{k_x}\right)^2 C_{n\dot{\beta}}$
$C_{n_r} = \frac{\partial C_n}{\partial \left(\frac{r b}{2U}\right)}$	$\frac{1}{\text{rad}}$	$-\frac{I_v}{b} [C_{y_r}]_v$	$n_r = \frac{1}{4} \left(\frac{b}{k_x}\right)^2 C_{n_r}$
$C_{n_p} = \frac{\partial C_n}{\partial \left(\frac{p b}{2U}\right)}$	$\frac{1}{\text{rad}}$	$-\frac{I_v}{b} [C_{y_p}]_v$	$n_p = \frac{1}{4} \left(\frac{b}{k_x}\right)^2 C_{n_p}$
$C_{n\delta} = \frac{\partial C_n}{\partial \delta}$	$\frac{1}{\text{rad}}$	$-\frac{I_{\delta r}}{b} C_{y\delta}$	$n_{\delta} = \frac{1}{2} \left(\frac{b}{k_x}\right)^2 C_{n\delta}$
$C_{l\beta} = \frac{\partial C_l}{\partial \beta}$	$\frac{1}{\text{rad}}$	$\frac{h_v}{b} [C_{y\beta}]_v$	$l_v = \frac{1}{2} \left(\frac{b}{k_x}\right)^2 C_{l\beta}$
$C_{l\dot{\beta}} = \frac{\partial C_l}{\partial \left(\frac{\dot{\beta} b}{2U}\right)}$	$\frac{1}{\text{rad}}$	$\frac{h_v}{b} [C_{y\dot{\beta}}]_v$	$l_{\dot{v}} = \frac{1}{4} \left(\frac{b}{k_x}\right)^2 C_{l\dot{\beta}}$
$C_{l_r} = \frac{\partial C_l}{\partial \left(\frac{r b}{2U}\right)}$	$\frac{1}{\text{rad}}$	$\frac{h_v}{b} [C_{y_r}]_v$	$l_r = \frac{1}{4} \left(\frac{b}{k_x}\right)^2 C_{l_r}$
$C_{l_p} = \frac{\partial C_l}{\partial \left(\frac{p b}{2U}\right)}$	$\frac{1}{\text{rad}}$	$\frac{h_v}{b} [C_{y_p}]_v$	$l_p = \frac{1}{4} \left(\frac{b}{k_x}\right)^2 C_{l_p}$
$C_{l\delta} = \frac{\partial C_l}{\partial \delta}$	$\frac{1}{\text{rad}}$	$\frac{h_{\delta r}}{b} C_{y\delta}$	$l_{\delta} = \frac{1}{2} \left(\frac{b}{k_x}\right)^2 C_{l\delta}$

TABLE 4-3

LONGITUDINAL DIMENSIONAL STABILITY DERIVATIVE
(STABILITY AXIS SYSTEM)

QUANTITY	IN TERMS OF BASIC STABILITY DERIVATIVES			IN TERMS OF NONDIMENSIONAL STABILITY DERIVATIVE PARAMETERS
	DIMENSIONAL		NONDIMENSIONAL	
	DEFINITIONS	UNIT		
x_u	$\frac{1}{m} \frac{\partial \dot{x}}{\partial u}$	$\frac{1}{\text{sec}}$	$\frac{\rho S U}{m} (-C_D - C_{D_u})^\dagger$	$\frac{1}{\tau} x_u^\dagger$
x_w	$\frac{1}{m} \frac{\partial \dot{x}}{\partial w}$	$\frac{1}{\text{sec}}$	$\frac{\rho S U}{2m} (C_L - C_{D_\alpha})$	$\frac{1}{\tau} x_w$
x_δ	$\frac{1}{m} \frac{\partial \dot{x}}{\partial \delta}$	$\frac{\text{ft}}{\text{sec}^2 \text{rad}}$	$\frac{\rho S U^2}{2m} (-C_{D_\delta})$	$\frac{U}{\tau} x_\delta$
z_u	$\frac{1}{m} \frac{\partial \dot{z}}{\partial u}$	$\frac{1}{\text{sec}}$	$\frac{\rho S U}{m} (-C_L - C_{L_u})^*$	$\frac{1}{\tau} z_u$
z_w	$\frac{1}{m} \frac{\partial \dot{z}}{\partial w}$	$\frac{1}{\text{sec}}$	$\frac{\rho S U}{2m} (-C_{L_\alpha} - C_D)$	$\frac{1}{\tau} z_w$
$z_{\dot{w}}$	$\frac{1}{m} \frac{\partial \dot{z}}{\partial \dot{w}}$	$\frac{1}{\text{ft}}$	$\frac{\rho S c}{4m} (-C_{L_{\dot{\alpha}}})$	$\frac{c}{\tau U} z_{\dot{w}}$
z_q	$\frac{1}{m} \frac{\partial \dot{z}}{\partial q}$	$\frac{\text{ft}}{\text{sec-rad}}$	$\frac{\rho S U c}{4m} (-C_{L_q})$	$\frac{c}{\tau} z_q$
z_δ	$\frac{1}{m} \frac{\partial \dot{z}}{\partial \delta}$	$\frac{\text{ft}}{\text{sec}^2 \text{rad}}$	$\frac{\rho S U^2}{2m} (-C_{L_\delta})$	$\frac{U}{\tau} z_\delta$
M_u	$\frac{1}{I_y} \frac{\partial \dot{M}}{\partial u}$	$\frac{1}{\text{sec-ft}}$	$\frac{\rho S U c}{I_y} (C_M + C_{M_u})$	$\frac{2}{\tau c} m_u$
M_w	$\frac{1}{I_y} \frac{\partial \dot{M}}{\partial w}$	$\frac{1}{\text{sec-ft}}$	$\frac{\rho S U c}{2 I_y} C_{M_\alpha}$	$\frac{1}{\tau c} m_w$
$M_{\dot{w}}$	$\frac{1}{I_y} \frac{\partial \dot{M}}{\partial \dot{w}}$	$\frac{1}{\text{ft}}$	$\frac{\rho S c^2}{4 I_y} C_{M_{\dot{\alpha}}}$	$\frac{1}{\tau U} m_{\dot{w}}$
M_q	$\frac{1}{I_y} \frac{\partial \dot{M}}{\partial q}$	$\frac{1}{\text{sec}}$	$\frac{\rho S U c^2}{4 I_y} C_{M_q}$	$\frac{1}{\tau} m_q$
M_δ	$\frac{1}{I_y} \frac{\partial \dot{M}}{\partial \delta}$	$\frac{1}{\text{sec}^2 \text{rad}}$	$\frac{\rho S U^2 c}{2 I_y} C_{M_\delta}$	$\frac{U}{\tau c} m_\delta$

[†]The thrust-gradient terms are neglected here in the interests of symmetry and consistency.

[†] $\tau \equiv m/\rho U S$ in the dimensionless time first proposed by H. Glauert, A Nondimensional Form of the Stability Equations of an Aeroplane, Br ARC R and M 1093, 1927.

*For $C_{L_u} = 0$, as in subsonic flight, and $C_L = W/(\rho U^2 S/2)$, as in trimmed flight for $\gamma_0 = 0$, $z_u = -2g/U_0$.

TABLE 4-4

LATERAL DIMENSIONAL STABILITY DERIVATIVE PARAMETERS
(STABILITY OR BODY AXIS SYSTEMS)

QUANTITY	IN TERMS OF BASIC STABILITY DERIVATIVES			IN TERMS OF NONDIMENSIONAL STABILITY DERIVATIVE PARAMETERS
	DIMENSIONAL		NONDIMENSIONAL	
	DEFINITIONS	UNIT		
Y_v	$\frac{1}{mU} \frac{\partial Y}{\partial \beta}$	$\frac{1}{\text{sec}}$	$\frac{\rho SU}{2m} C_{y\beta}$	$\frac{1}{\tau} y_v$
$Y_{\dot{\beta}}$	$\frac{1}{mU} \frac{\partial Y}{\partial \dot{\beta}}$	$\frac{1}{\text{sec}}$	$\frac{\rho Sb}{4m} C_{y\dot{\beta}}$	$\frac{b}{\tau U} y_{\dot{\beta}}$
Y_r^*	$\frac{1}{mU} \frac{\partial Y}{\partial r}$	$\frac{1}{\text{rad}}$	$\frac{\rho Sb}{4m} C_{y_r}$	$\frac{b}{\tau U} y_r$
Y_p^*	$\frac{1}{mU} \frac{\partial Y}{\partial p}$	$\frac{1}{\text{rad}}$	$\frac{\rho Sb}{4m} C_{y_p}$	$\frac{b}{\tau U} y_p$
Y_{δ}^*	$\frac{1}{mU} \frac{\partial Y}{\partial \delta}$	$\frac{1}{\text{sec-rad}}$	$\frac{\rho SU}{2m} C_{y\delta}$	$\frac{1}{\tau} y_{\delta}$
N_{β}	$\frac{1}{I_z} \frac{\partial N}{\partial \beta}$	$\frac{1}{\text{sec}^2}$	$\frac{\rho SU^2 b}{2I_z} C_{n\beta}$	$\frac{U}{\tau b} n_v$
$N_{\dot{\beta}}$	$\frac{1}{I_z} \frac{\partial N}{\partial \dot{\beta}}$	$\frac{1}{\text{sec}}$	$\frac{\rho S U b^2}{4I_z} C_{n\dot{\beta}}$	$\frac{1}{\tau} n_{\dot{\beta}}$
N_r	$\frac{1}{I_z} \frac{\partial N}{\partial r}$	$\frac{1}{\text{sec}}$	$\frac{\rho S U b^2}{4I_z} C_{n_r}$	$\frac{1}{\tau} n_r$
N_p	$\frac{1}{I_z} \frac{\partial N}{\partial p}$	$\frac{1}{\text{sec}}$	$\frac{\rho S U b^2}{4I_z} C_{n_p}$	$\frac{1}{\tau} n_p$
N_{δ}	$\frac{1}{I_z} \frac{\partial N}{\partial \delta}$	$\frac{1}{\text{sec}^2 \text{rad}}$	$\frac{\rho SU^2 b}{2I_z} C_{n\delta}$	$\frac{U}{\tau b} n_{\delta}$
L_{β}	$\frac{1}{I_x} \frac{\partial L}{\partial \beta}$	$\frac{1}{\text{sec}^2}$	$\frac{\rho SU^2 b}{2I_x} C_{l\beta}$	$\frac{U}{\tau b} l_v$
$L_{\dot{\beta}}$	$\frac{1}{I_x} \frac{\partial L}{\partial \dot{\beta}}$	$\frac{1}{\text{sec}}$	$\frac{\rho S U b^2}{4I_x} C_{l\dot{\beta}}$	$\frac{1}{\tau} l_{\dot{\beta}}$
L_r	$\frac{1}{I_x} \frac{\partial L}{\partial r}$	$\frac{1}{\text{sec}}$	$\frac{\rho S U b^2}{4I_x} C_{l_r}$	$\frac{1}{\tau} l_r$
L_p	$\frac{1}{I_x} \frac{\partial L}{\partial p}$	$\frac{1}{\text{sec}}$	$\frac{\rho S U b^2}{4I_x} C_{l_p}$	$\frac{1}{\tau} l_p$
L_{δ}	$\frac{1}{I_x} \frac{\partial L}{\partial \delta}$	$\frac{1}{\text{sec}^2 \text{rad}}$	$\frac{\rho SU^2 b}{2I_x} C_{l\delta}$	$\frac{U}{\tau b} l_{\delta}$

The starred derivatives arise when β rather than v is used as the lateral motion parameter (see Chapter 6); in general, $Y_{\lambda}^ = Y_{\lambda}/U_0$.

CHAPTER 5

LONGITUDINAL DYNAMICS

5.1 INTRODUCTION

The vehicle dynamic properties, defined in general by the equations of motion derived in the last chapter, are best specified for use in control system analysis by a series of transfer functions which relate output quantities (various airframe motions) to input variables (usually control motions or external disturbances). These transfer functions are readily obtained from the linearized Laplace-transformed airframe equations of motion as sets of ratios between transformed airframe output and input quantities or initial conditions. The ratios comprise numerators and denominators expressed as rational polynomials in the Laplace transform variable, s . The various polynomial coefficients are composed of combinations of stability derivatives and inertial gravitational quantities.

For maximum utility it is desirable to have the numerator and denominator polynomials in factored form. Each transfer function is then made up of a ratio of first- and second-order polynomial products and a gain. The gains, poles, and zeros thus obtained define the fundamental properties of dynamic elements and are essential in most servoanalysis and synthesis methods and in response calculations. Even though most of the polynomials involved are of third-order or higher, numerical factorization is no problem, especially when digital computers are employed. However, unless a large number of cases are so computed, the specific connections between vehicle configuration (represented by stability derivatives, etc.) and transfer and response characteristics (represented by poles and zeros) are difficult to appreciate. Such an appreciation is important in:

- Developing the insight required for the determination of airframe/automatic-control combinations which offer possible improvements in over-all system complexity
- Assessing the effects of configuration changes on aircraft response and on airframe/autopilot/pilot system characteristics

- Showing the detailed effects of particular stability derivatives (and their estimated accuracies) on the poles and zeros, and hence on aircraft and airframe/autopilot/pilot characteristics
- Obtaining stability derivatives from flight test data

It is highly desirable, therefore, to express the locations of the poles and zeros directly in terms of the literal stability derivatives and inertial parameters. This can be accomplished directly by decomposing a fairly complete transfer function form, or indirectly by the use of fewer airframe degrees of freedom. In either case an approximation is required to arrive at reasonably compact and usable expressions which delineate dominant, as opposed to trivial, effects. Such effects can vary among vehicle types, so it is to be expected that literal approximate factors which apply to all vehicles for all flight conditions will be an exception rather than the rule.

With this background the immediately succeeding articles in this chapter will, first, recapitulate the longitudinal equations of motion as normally used; present the polynomial forms of the most significant control-input transfer functions; and develop some appreciation for the transfer functions and responses with two specific numerical examples. Based on the physical insights provided by the examples, further-simplified sets of the equations which apply to the individual modes of motion will be developed. Following this the complete gust-input transfer functions in polynomial form are presented and our numerical examples are extended to cover these transfer functions.

The basic understanding accruing from the above process is further developed by considering the approximate literal expressions for the various transfer function factors. These approximate factors are shown to be related to the simplified equations of motion appropriate for each mode, and their implications as regards the direct influence of the dominant stability derivatives on the important poles and zeros are discussed. In the final article a discussion of the modal response ratios in literal form is presented.

5.2 RECAPITULATION AND FURTHER SIMPLIFICATION OF THE LONGITUDINAL EQUATIONS OF MOTION

Equations 4-97 are somewhat more complicated than those generally used for transfer function computations; to simplify them further we make the following two assumptions:

Assumption 10. It is assumed that $X_{\dot{w}} = X_q = Z_{\dot{w}} = Z_q = 0$.

Perhaps the best general evidence in justification of Assumption 10 is that the derivatives named in it rarely appear in the technical literature concerned with aircraft dynamics. The inference here is that although individual investigators have evaluated the effects of these derivatives for a multitude of various airframe configurations, they have found them to be of only secondary importance. However, it must be remembered that if any of these derivatives are of actual importance for a particular airframe, this assumption may produce somewhat erroneous quantitative results for that airframe.

In general, any stability derivative may be neglected if it is first determined that the term containing the given derivative is small in comparison with other terms in the same equations. For the derivatives in question, comparing the term $X_{\dot{w}}s w$ with $X_w w$ shows that if the frequency range of interest extends as high as $|s| \doteq X_w/X_{\dot{w}}$, $X_{\dot{w}}$ can no longer be neglected a priori. Similarly, the upper frequency limit for the valid a priori neglect of X_q is $|s| \doteq |g/X_q|$. As Z_q occurs in the group $(Z_q + U_0)s w$, the appropriate criterion here is $|Z_q| \ll U_0$; and by grouping \dot{w} terms together as $(s - Z_{\dot{w}})w$ the criterion for neglecting $Z_{\dot{w}}$ is $|Z_{\dot{w}}| \ll 1$.

Assumption 11. In the steady flight condition, the flight path of the airplane is assumed to be horizontal, $\gamma_0 = 0$.

Assumption 11 is introduced solely to simplify the mechanics of the analysis. When the flight path of an airplane is initially inclined to the horizontal, γ_0 must of course be included in the transfer functions.

On the basis of these assumptions, the longitudinal equations of motion, referenced to stability axes, become:

$$\begin{aligned} (s - X_u)u - X_w w + g\theta &= X_{\delta}\delta - X_u u_g - X_w w_g \\ -Z_u u + (s - Z_w)w - U_0 s\theta &= Z_{\delta}\delta - Z_u u_g - Z_w w_g \quad (5-1) \\ -M_u u - (M_{\dot{w}}s + M_w)w + s(s - M_q)\theta &= M_{\delta}\delta - M_u u_g - [(M_{\dot{w}} - M_q/U_0)s + M_w]w_g \end{aligned}$$

$$\begin{aligned} \text{where (Eq. 4-96)} \quad s\theta &= q \\ \text{and (inertial terms of } Z \text{ equation of 5-1)} \quad a_z &= \dot{w} - U_0 s\theta = -U_0(\dot{\gamma}) = -\ddot{h} \quad (5-2) \end{aligned}$$

The auxiliary relationships of Eq. 5-2 are needed to convert the motion variables of Eq. 5-1 to the quantities sensed by flight instruments such as rate gyros, accelerometers, and altimeters.

5.3 CONTROL-INPUT TRANSFER FUNCTIONS

As fully discussed in Chapter 2, the transfer functions, for a given input, are obtained by simply solving the transformed simultaneous equations of motion for the output variable of interest with all other inputs considered to be zero. For example, using determinants we can directly write the attitude-to-control-input transfer function (i.e., neglecting gust inputs in Eq. 5-1) as:

$$\frac{\theta(s)}{\delta(s)} = \frac{\begin{vmatrix} s - X_u & -X_w & X_\delta \\ -Z_u & s - Z_w & Z_\delta \\ -M_u & -(M_w s + M_q) & M_\delta \end{vmatrix}}{\begin{vmatrix} s - X_u & -X_w & g \\ -Z_u & s - Z_w & -U_0 s \\ -M_u & -(M_w s + M_q) & s(s - M_q) \end{vmatrix}} = \frac{N_\theta^\delta(s)}{\Delta(s)} \quad (5-3)$$

By expanding the determinants, the transfer function can be expressed as the ratio of a numerator polynomial in s over a denominator polynomial. The denominator polynomial, $\Delta(s)$, is common to all the transfer functions and its factors determine the frequency and damping, or time constants, of the individual modes of motion. The numerator polynomials depend on the output quantity of interest. The general polynomial forms of the primary longitudinal transfer functions are given below, together with the most usual factored forms of the polynomial expressions.

$$\begin{aligned} \frac{\theta(s)}{\delta(s)} &= \frac{N_\theta^\delta(s)}{\Delta_{\text{long}}} = \frac{A_\theta s^2 + B_\theta s + C_\theta}{\Delta_{\text{long}}} \\ &= \frac{A_\theta (s + 1/T_{\theta_1})(s + 1/T_{\theta_2})}{\Delta_{\text{long}}} \end{aligned} \quad (5-4)$$

$$\frac{w(s)}{\delta(s)} = \frac{N_{\delta}^w(s)}{\Delta_{\text{long}}} = \frac{A_w s^3 + B_w s^2 + C_w s + D_w}{\Delta_{\text{long}}} \quad (5-5)$$

$$A_w \begin{cases} (s + 1/T_{w1})(s^2 + 2\zeta_w \omega_w s + \omega_w^2) \\ \text{or} \\ (s + 1/T_{w1})(s + 1/T_{w2})(s + 1/T_{w3}) \end{cases}$$

$$= \frac{\Delta_{\text{long}}}{\Delta_{\text{long}}}$$

$$\frac{u(s)}{\delta(s)} = \frac{N_{\delta}^u(s)}{\Delta_{\text{long}}} = \frac{A_u s^3 + B_u s^2 + C_u s + D_u}{\Delta_{\text{long}}} \quad (5-6)$$

$$A_u \begin{cases} (s + 1/T_{u1})(s + 1/T_{u2})(s + 1/T_{u3}) \\ \text{or} \\ (s + 1/T_{u1})(s^2 + 2\zeta_u \omega_u s + \omega_u^2) \end{cases}$$

$$= \frac{\Delta_{\text{long}}}{\Delta_{\text{long}}}$$

$$\frac{h(s)}{\delta(s)} = \frac{N_{\delta}^h(s)}{\Delta_{\text{long}}} = \frac{A_h s^3 + B_h s^2 + C_h s + D_h}{s \Delta_{\text{long}}} \quad (5-7)$$

$$A_h \begin{cases} (s + 1/T_{h1})(s + 1/T_{h2})(s + 1/T_{h3}) \\ \text{or} \\ (s + 1/T_{h1})(s^2 + 2\zeta_h \omega_h s + \omega_h^2) \end{cases}$$

$$= \frac{s \Delta_{\text{long}}}{s \Delta_{\text{long}}}$$

$$\frac{a_z(s)}{\delta(s)} = \frac{-s^2 N_{\delta}^h(s)}{\Delta_{\text{long}}} \quad (5-8)$$

where

$$\Delta_{\text{long}} = A s^4 + B s^3 + C s^2 + D s + E \quad (5-9)$$

$$= \frac{(s^2 + 2\zeta_p \omega_p s + \omega_p^2)}{\text{or}} \frac{(s^2 + 2\zeta_{sp} \omega_{sp} s + \omega_{sp}^2)}{\text{or}} \\ (s + 1/T_{p1})(s + 1/T_{p2}) \quad (s + 1/T_{sp1})(s + 1/T_{sp2})$$

The literal expressions for the various A, B, C., etc., coefficients of Eqs. 5-4 through 5-9 are given in Table 5-1 in terms of the stability derivatives. In many cases α derivatives (w derivatives multiplied by U_0) are used to achieve conciseness.

5.4 EXAMPLE TRANSFER FUNCTIONS, BODE FORMS, AND TIME RESPONSES FOR A CONVENTIONAL AIRPLANE

To develop an appreciation for the usual responses and transfer function forms we will study some numerical examples. Accordingly, we consider first a conventional airplane having the characteristics given below and the general arrangement shown in Fig. 5-1. Substituting these

Altitude (ft)	20,000
Weight (lb)	30,500
Mach number	0.638
True airspeed (ft/sec)	660
X_u	-0.0097
X_w	0.0016
X_{δ_e}	0.0
Z_u	-0.0955
Z_w	-1.430
Z_{δ_e}	-69.8
M_u	0.0
M_w	-0.0235
$M_{\dot{w}}$	-0.0013
M_q	-1.920
M_{δ_e}	-26.10

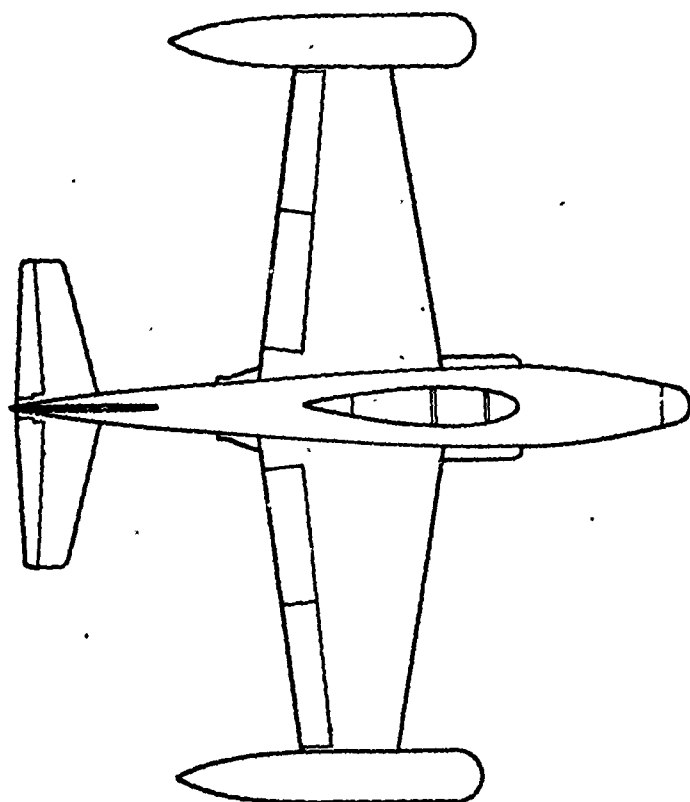
data into the Table 5-1 forms and routinely factoring the resulting polynomials yields the following transfer functions (the denominator, shown only for θ is common to all the transfer functions as indicated):

$$\frac{\theta(s)}{-\delta_e(s)} = 4.85 \frac{\left(\frac{s}{0.0098} + 1\right)\left(\frac{s}{1.371} + 1\right)}{\left[\frac{s^2}{(0.0630)^2} + \frac{2(0.0714)^2}{0.0630} + 1\right]\left[\frac{s^2}{(4.27)^2} + \frac{2(0.493)s}{4.27} + 1\right]}$$

(5-10)

TABLE 5-1
LONGITUDINAL CONTROL-INPUT TRANSFER FUNCTION COEFFICIENTS

	A	B	C	D	E
Δ	1	$-M_q - M_{\dot{q}} - Z_w - X_u$	$Z_w M_q - M_{\alpha} - X_w Z_u + X_u (M_q + M_{\dot{q}} + Z_w)$	$-X_u (Z_w M_q - M_{\alpha}) + Z_u (X_w M_q + g M_{\dot{w}}) - M_u (X_{\alpha} - g)$	$g (Z_u M_w - M_u Z_w)$
N_{δ}^{θ}	$M_{\delta} + Z_{\delta} M_{\dot{w}}$	$X_{\delta} (Z_u M_{\dot{w}} + M_u) + Z_{\delta} (M_w - X_u M_{\dot{w}}) - M_{\delta} (X_u + Z_w)$	$X_{\delta} (Z_u M_w - Z_w M_u) + Z_{\delta} (M_u X_w - M_w X_u) + M_{\delta} (Z_w X_u - X_w Z_u)$		
N_{δ}^w	Z_{δ}	$X_{\delta} Z_u - Z_{\delta} (X_u + M_q) + M_{\delta} U_0$	$X_{\delta} (U_0 M_u - Z_u M_q) + Z_{\delta} X_u M_q - U_0 M_{\delta} X_u$	$g (Z_{\delta} M_u - M_{\delta} Z_u)$	
N_{δ}^u	X_{δ}	$-X_{\delta} (Z_w + M_q + M_{\dot{q}}) + Z_{\delta} X_w$	$X_{\delta} (Z_w M_q - M_{\alpha}) - Z_{\delta} (X_w M_q + g M_{\dot{w}}) + M_{\delta} (X_{\alpha} - g)$	$g (M_{\delta} Z_w - Z_{\delta} M_w)$	
$s N_{\delta}^h$	$-Z_{\delta}$	$-X_{\delta} Z_u + Z_{\delta} (M_q + M_{\dot{q}} + X_u)$	$X_{\delta} Z_u (M_q + M_{\dot{q}}) - Z_{\delta} [X_u (M_q + M_{\dot{q}}) - M_{\alpha}] - M_{\delta} Z_{\alpha}$	$-X_{\delta} (Z_{\alpha} M_u - M_{\alpha} Z_u) + Z_{\delta} [M_u (X_{\alpha} - g) - M_{\alpha} X_u] + M_{\delta} [Z_{\alpha} X_u - Z_u (X_{\alpha} - g)]$	



(All dimensions in feet)

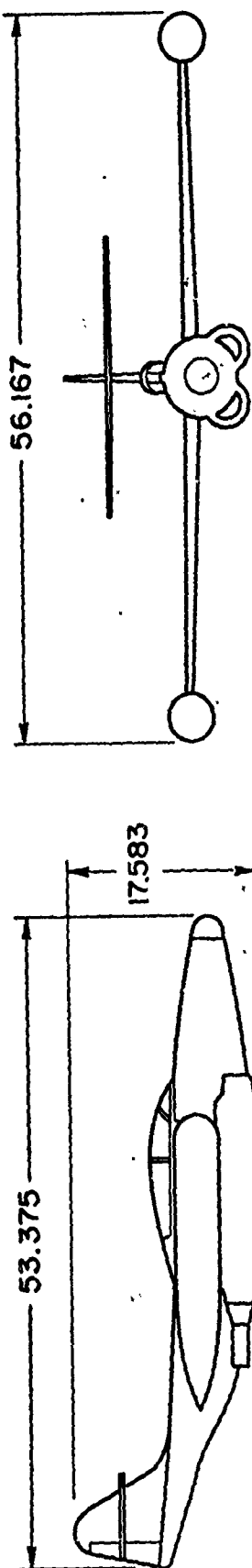


Figure 5-1. Three-View of Conventional Airplane Used for the Numerical Example

$$\frac{a_z(s)}{-\delta_e(s)} = \frac{-1}{U_0} \frac{w(s)}{\delta_e(s)} = \frac{1110}{660} \frac{\left(\frac{s}{248.5} + 1\right) \left[\frac{s^2}{(0.068)^2} + \frac{2(0.0713)s}{0.068} + 1\right]}{\left[\right] \left[\right]} \quad (5-11)$$

$$\frac{u(s)}{-\delta_e(s)} = -15920 \frac{\left(\frac{s}{1.44} + 1\right) \left(\frac{s}{-7251.4} + 1\right)}{\left[\right] \left[\right]} \quad (5-12)$$

$$\frac{a_z(s)}{-\delta_e(s)} = 2080 \frac{s \left(\frac{s}{0.0064} + 1\right) \left(\frac{s}{17.03} - 1\right) \left(\frac{s}{19.81} + 1\right)}{\left[\right] \left[\right]} \quad (5-13)$$

Inspection of the roots of the denominator which, set to zero, is the characteristic equation (commonly called the "longitudinal stability quartic") shows that the free longitudinal motions consist of two oscillatory modes. One of these is a relatively well damped high frequency oscillation called the "short period," and the other is a lightly damped relatively low frequency oscillation called the "phugoid." The subscript notation employed in Eq. 5-9 reflects this nomenclature.

Figure 5-2 contains $j\omega$ -Bode plots of the above transfer functions, including amplitude ratio and phase asymptotes. Among other things, the Bode diagrams are graphical representations of transforms of the weighting functions. In this view, they amount to response transforms for unit impulse inputs and can be used to draw conclusions concerning the appearance of the phugoid and short-period modes in the transient response of the airplane. For example, Part (c) of Fig. 5-2 shows that the amplitude ratio, $|u/\delta_e|$, is much smaller at the natural frequency of the short period than at that of the phugoid. This indicates that much smaller airspeed changes occur in the short-period transient mode than in the phugoid transient oscillation. Part (b) shows that the quadratic in the numerator of the a_z/δ_e transfer function very nearly cancels the denominator quadratic corresponding to the phugoid oscillation. Consequently, we expect almost

no change in angle of attack during the phugoid oscillation. A comparison between the Part (a) and Part (c) plots shows that the values of the amplitude ratio, $|\theta/\delta_e|$, at the short-period and phugoid frequencies are more nearly the same magnitude than those of $|u/\delta_e|$ at the same frequencies. This implies that, for the same inputs, the amplitudes of θ occurring in the characteristic modes are more similar than those of u . Finally, the Part (d) plot shows that the vertical acceleration amplitudes at phugoid are only somewhat higher than those at short period. However, considering the large differences in frequency, a given oscillatory vertical acceleration will involve much higher excursions in \dot{h} and \ddot{h} at phugoid than at short-period frequency. This can also be visualized on the Part (d) plot by considering that successive integrations of a_z to obtain \dot{h} and h involve successive clockwise rotations of the $|a_z/\delta_e|$ Bode, each of 20 db/decade. Such rotations progressively suppress the short-period hump relative to the phugoid peak.

In summary, it appears from our study of Fig. 5-2 that only relatively small amplitudes of u and h occur in the short-period mode and of α in the phugoid mode, whereas large amplitudes of θ can occur in both.

The response time history of the example airplane to an elevator pulse (the weighting functions themselves rather than their transforms), supports these conclusions. These are given in Fig. 5-3 using two time scales; that of Fig. 5-3a emphasizes short period, while that of Fig. 5-3b shows the phugoid best. Here we see that the maximum amplitudes of u and h are very much smaller in the short period than in the phugoid, and that the maximum amplitude of w ($\dot{h} = U_0 \alpha$) during the phugoid is very nearly zero. Further, the maximum amplitudes of θ in each mode are comparable in magnitude. All these facts are in agreement with what we inferred from the Bode plots.

Another way of studying the relative motions is to draw the time vectors and force and moment polygons (Chapter 2) as we have done in Fig. 5-4. Note the relative magnitudes and phases of the component motions for each mode as shown by the time vectors, and compare these with the appropriate time responses. The fore and aft perturbation from the undisturbed flight path ($\int u dt$) is negligible for the short-period mode, but for the phugoid it is of the same order as the height perturbation. The time

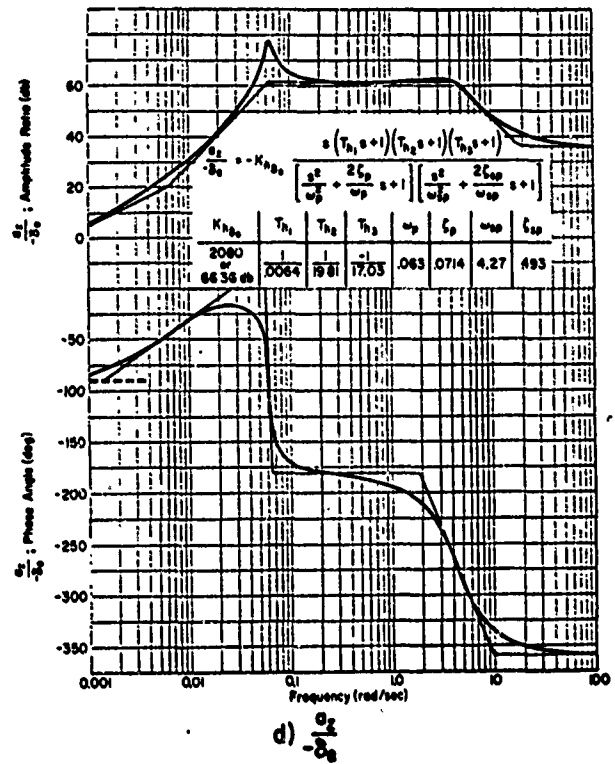
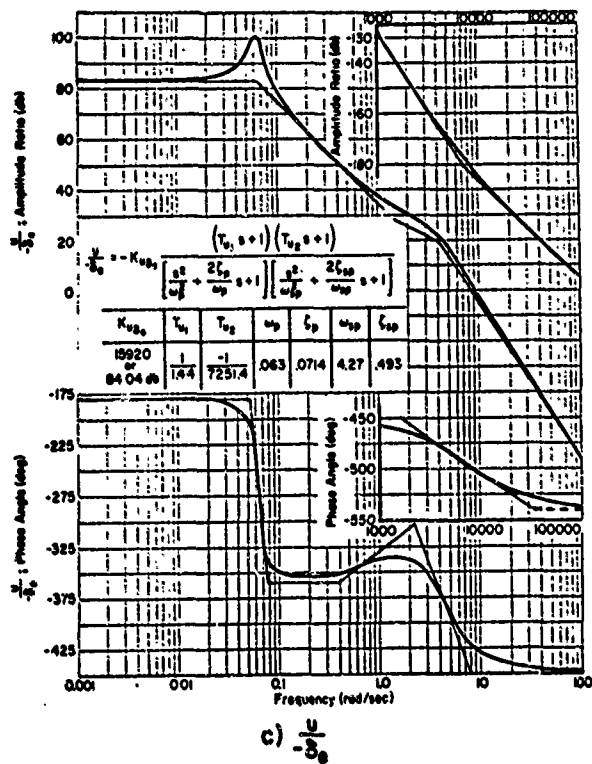
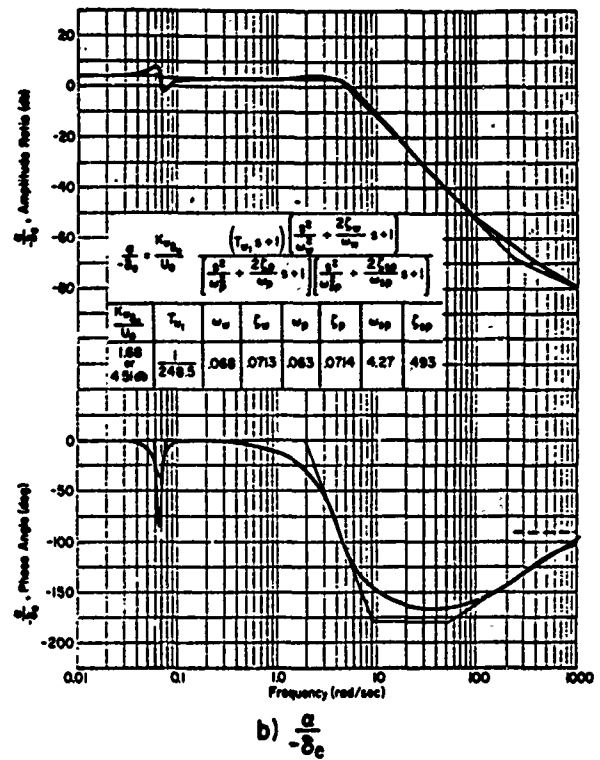
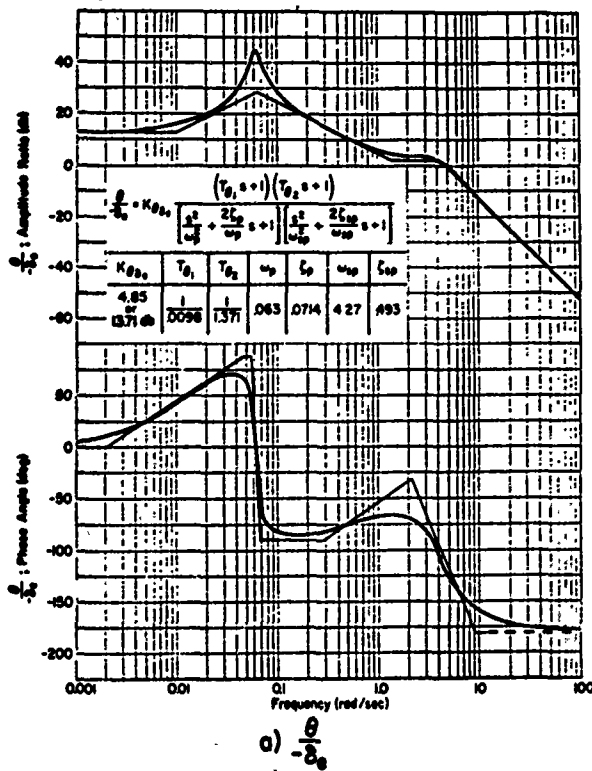
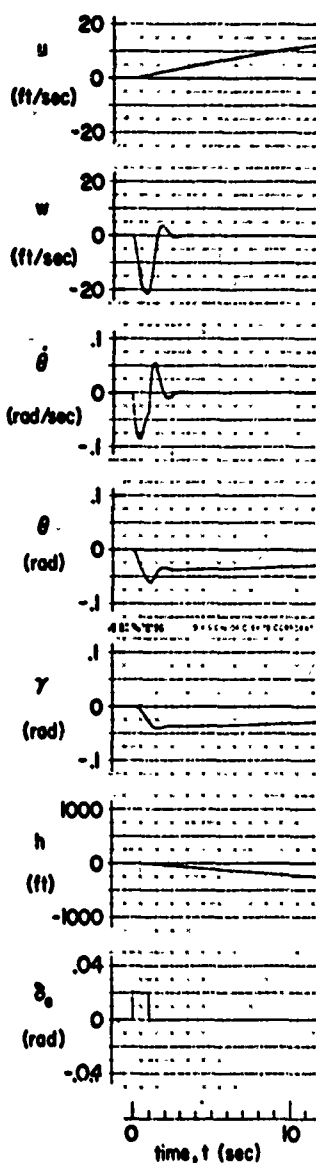
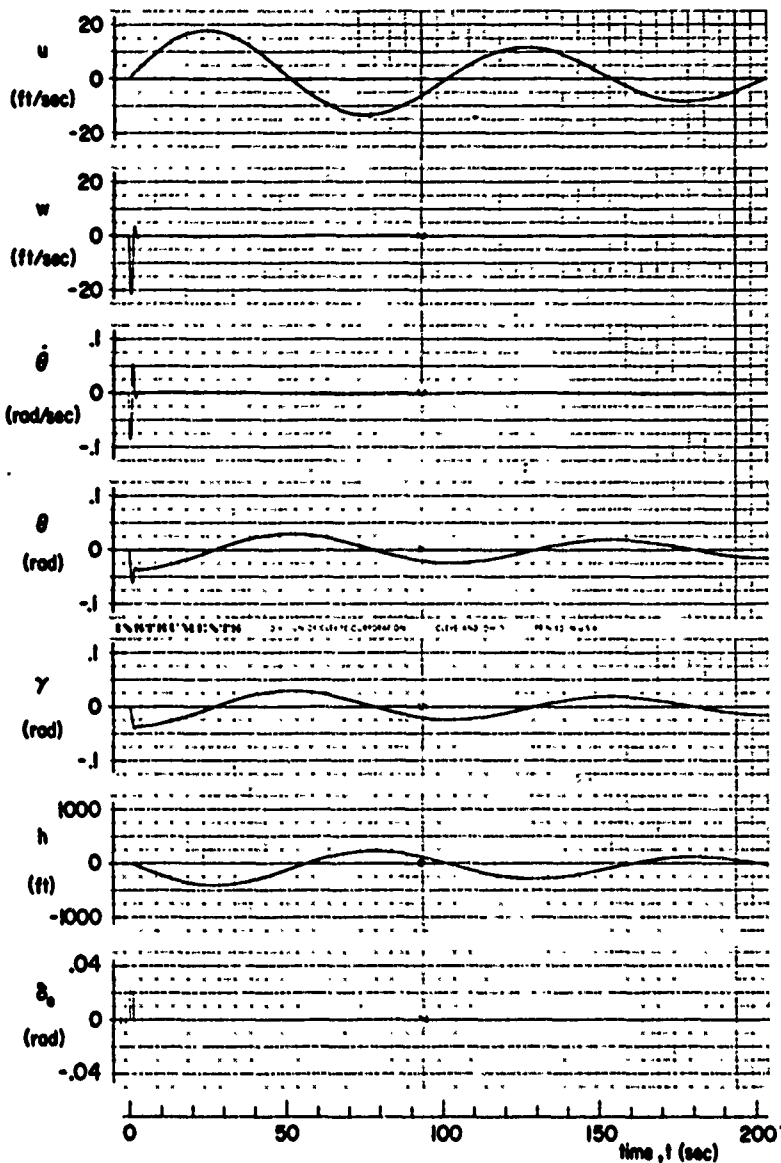


Figure 5-2. Example Control-Input Bode Plots for Conventional Airplane



a) Short Period



b) Phugoid

Figure 5-3. Analog Computer Record of Time History for Pulse Elevator Deflection. Conventional Airplane

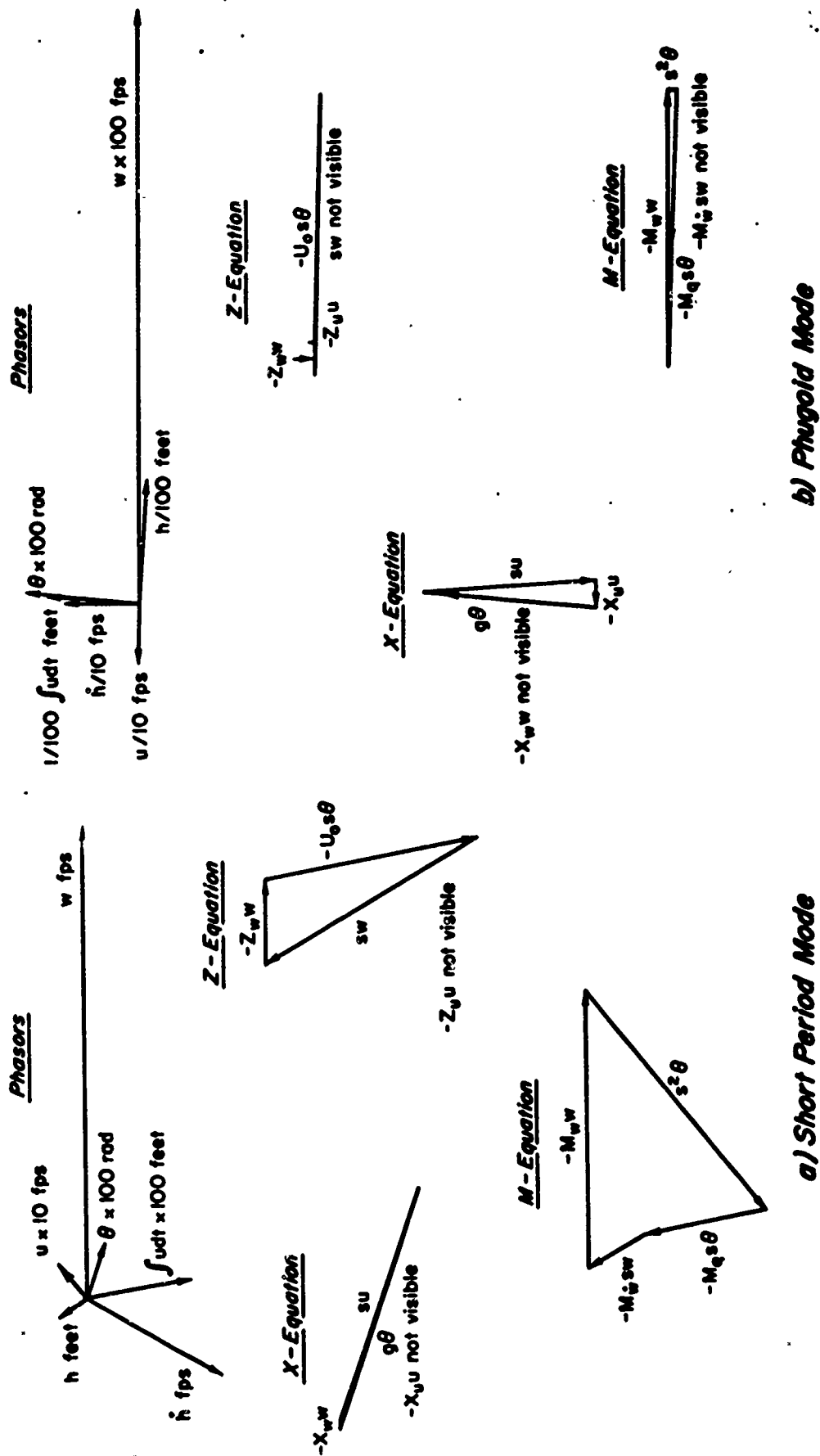


Figure 5-4. Time Vector Diagrams for the Example Airplane

vector polygons indicate the relative importance of each term in the equation of motion for each mode; e.g., compare the $s^2\theta$ inertial pitch acceleration time vector for the phugoid and short-period modes.

5.5 TWO-DEGREE-OF-FREEDOM SHORT-PERIOD APPROXIMATIONS

Using the foregoing observations of the detailed nature of the responses we can construct a simplified set of equations applicable specifically to short-period motions. This approximation involves setting the variation in forward velocity, u , equal to zero and deleting the first relation of Eq. 5-1. This reflects the previous statements that u is of relatively small amplitude in the short-period mode, and that the two degrees of freedom, α (i.e., w) and θ , are dominant; accordingly, with $u_g = 0$,

$$\begin{aligned} (s - Z_w)w - U_0 s \theta &= Z_\delta \delta - Z_w w_g \\ -(sM_w' + M_w)w + (s - M_q)s\theta &= M_\delta \delta - [(M_w' - M_q/U_0)s + M_w]w_g \end{aligned} \quad (5-14)$$

Solving this system of equations with $w_g = 0$ leads to the transfer functions

$$\begin{aligned} \frac{\alpha(s)}{\delta(s)} &= \frac{1}{U_0} \frac{w(s)}{\delta(s)} \\ &= \frac{1}{U_0} \frac{Z_\delta s + (U_0 M_\delta - Z_\delta M_q)}{[s^2 - (U_0 M_w' + Z_w + M_q)s + (M_q Z_w - U_0 M_w)]} \end{aligned} \quad (5-15)$$

$$\frac{\theta(s)}{\delta(s)} = \frac{(M_\delta + Z_\delta M_w')s + (Z_\delta M_w - M_\delta Z_w)}{s[s^2 - (U_0 M_w' + Z_w + M_q)s + (M_q Z_w - U_0 M_w)]} \quad (5-16)$$

The quadratic term in the denominator is of the form $s^2 + 2\zeta_{sp}\omega_{sp}s + \omega_{sp}^2$, with

$$\begin{aligned} \omega_{sp} &= \sqrt{M_q Z_w - M_\alpha} \\ 2\zeta_{sp}\omega_{sp} &= -(Z_w + M_q + M_\alpha') \end{aligned} \quad (5-17)$$

Evaluating Eqs. 5-15 and 5-16 for the example numerical values of the stability derivatives yields

$$\frac{\alpha(s)}{-\delta_e(s)} = 1.44 \frac{\frac{s}{248.5} + 1}{\left[\frac{s^2}{(4.27)^2} + \frac{2(0.493)s}{4.27} + 1 \right]} \quad (5-18)$$

and

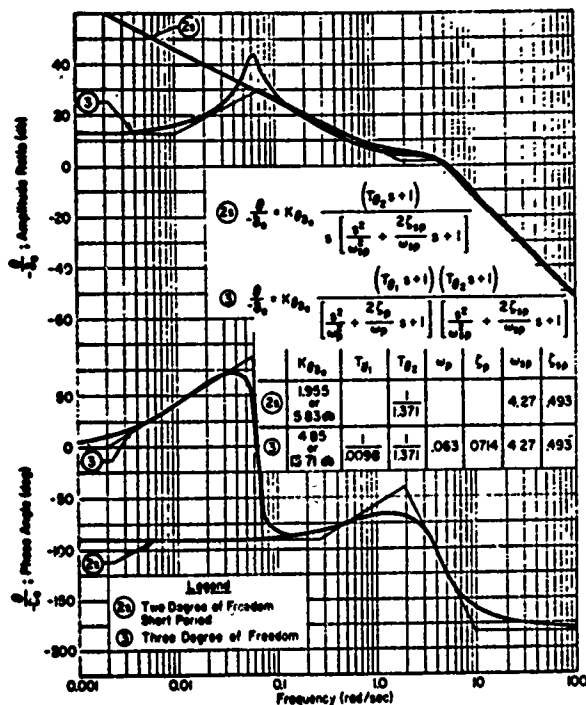
$$\frac{\theta(s)}{-\delta_e(s)} = 1.955 \frac{\frac{s}{1.371} + 1}{s \left[\right]} \quad (5-19)$$

These results are compared with those (Eqs. 5-10 and 5-11) obtained from the complete equations of motion in Fig. 5-5. We see that for frequencies above the phugoid the two-degree-of-freedom short-period transfer functions are very good approximations in both amplitude and phase. Furthermore, the two- and three-degree-of-freedom time responses in w and θ are in excellent agreement for times shorter than about 10 sec.

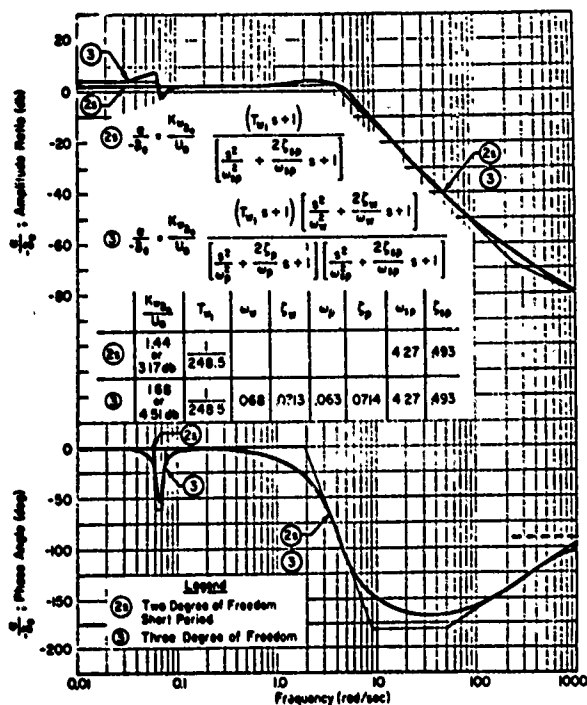
In summary, the two-degree of freedom solution of the pitching moment and vertical force equations of motion is a suitable approximation to the short-period mode. For typical flight conditions, the short-period mode can be considered to consist of changes only in angle of attack and in angle of pitch, and the short-period motion occurs before there is any appreciable change in forward speed. We shall later examine the limiting conditions for which this "typical" behavior is still reasonably accurate.

5.6 THREE-DEGREE-OF-FREEDOM PHUGOID APPROXIMATIONS

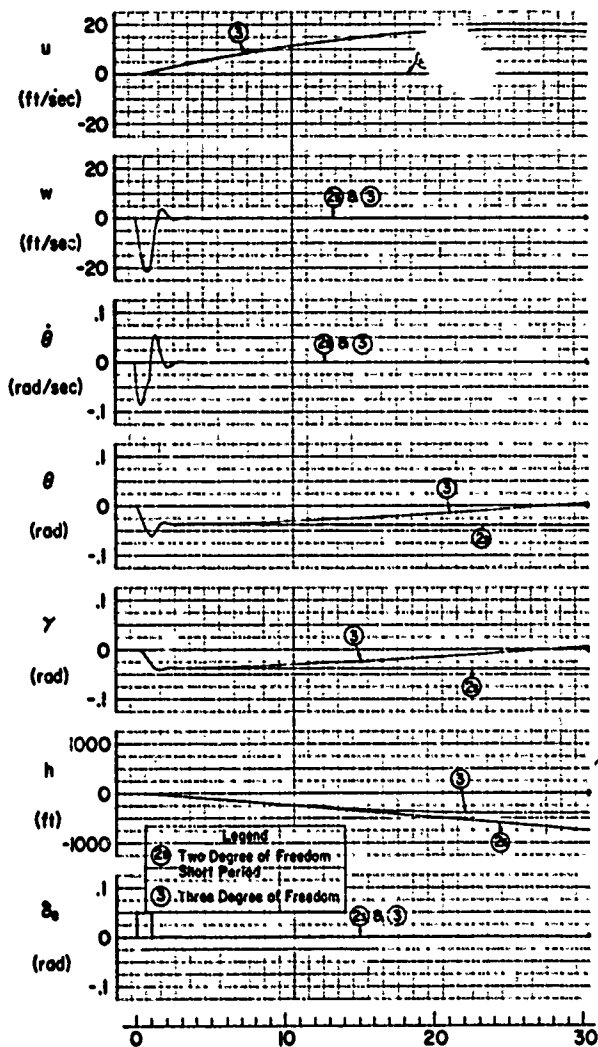
Characteristically, the phugoid components of vehicle motions are very slow compared to the short-period components. In an approximate sense the phugoid mode describes the long-term translatory motions of the vehicle center of mass, whereas the short-period describes rotations about the center of mass. For practical purposes in the phugoid motion, the "dynamic" pitching, inertial, and damping moments are small compared to the "static" pitching moment changes with speed and angle of attack. Classically, with $M_1 = 0$, the phugoid motion was conceived to involve fairly large oscillatory changes in forward speed, pitch attitude, and altitude, with approximately constant angle of attack; the static stability, M_{α} ,



a) $\frac{\theta}{\delta_e}$



b) $\frac{\alpha}{\delta_e}$



c) Time Responses to an Elevator Pulse (Weighting Function)

Figure 5-5. Comparisons of Complete Three Degree of Freedom and Short Period (Two Degree of Freedom) Control-Input Transfer Functions and Responses

being sufficiently large to decouple phugoid and short-period and to maintain α perturbations small. This is, of course, the case in the numerical example, where the w time vector is very small indeed (Fig. 5-4b).

On modern craft M_u is seldom zero, and the total static stability terms become $M_u u + M_w w$. When only these static moments are retained in the pitching moment equation, the three-degree-of-freedom phugoid equations of motion become

$$\begin{aligned} (s - X_u)u - X_w w + g\theta &= X_\delta \delta - X_u u_g - X_w w_g \\ -Z_u u + (s - Z_w)w - U_0 s\theta &= Z_\delta \delta - Z_u u_g - Z_w w_g \\ -M_u u - M_w w \quad 0 &= M_\delta \delta - M_u u_g - M_w w_g \end{aligned} \quad (5-20)$$

With $u_g = w_g = 0$, these lead to the transfer functions

$$\frac{\theta(s)}{\delta(s)} = \frac{M_\delta s^2 + [M_u X_\delta + M_w Z_\delta - (X_u + Z_w)M_\delta]s + [(Z_u M_w - Z_w M_u)X_\delta + (M_u X_w - M_w X_u)Z_\delta + (Z_w X_u - X_w Z_u)M_\delta]}{-M_\alpha \Delta_p} \quad (5-21)$$

$$\frac{u(s)}{\delta(s)} = \frac{[(X_\alpha - g)M_\delta - M_\alpha X_\delta]s + g(M_\delta Z_w - Z_\delta M_w)}{-M_\alpha \Delta_p} \quad (5-22)$$

$$\frac{w(s)}{\delta(s)} = \frac{U_0 M_\delta s^2 + (U_0 M_u X_\delta - U_0 X_u M_\delta)s + g(Z_\delta M_u - M_\delta Z_u)}{-M_\alpha \Delta_p} \quad (5-23)$$

where

$$\begin{aligned} \Delta_p &= s^2 + 2\zeta_p \omega_p s + \omega_p^2 \\ 2\zeta_p \omega_p &= -X_u + \frac{M_u(X_\alpha - g)}{M_\alpha} \quad ; \quad \omega_p^2 = \frac{-g}{U_0} \left(Z_u - \frac{M_u}{M_w} Z_w \right) \end{aligned} \quad (5-24)$$

Substituting the example numerical values, the resulting three-degree-of-freedom phugoid approximate transfer functions are

$$\frac{\theta(s)}{-\delta_e(s)} = 4.85 \frac{\left(\frac{s}{0.0098} + 1\right)\left(\frac{s}{1.363} + 1\right)}{\left[\frac{s^2}{(0.0683)^2} + \frac{2(0.0710)s}{0.0683} + 1\right]} \quad (5-25)$$

$$\frac{u(s)}{-\delta_e(s)} = -15920 \frac{\left(\frac{s}{1.415} + 1\right)}{\left[\frac{s^2}{(0.0683)^2} + \frac{2(0.0710)s}{0.0683} + 1\right]} \quad (5-26)$$

$$\frac{\alpha(s)}{-\delta_e(s)} = \frac{-1}{U_0} \frac{w(s)}{\delta_e(s)} = \frac{1110}{660} \frac{\left(\frac{s^2}{(0.0683)^2} + \frac{2(0.0710)s}{0.0683} + 1\right)}{\left[\frac{s^2}{(0.0683)^2} + \frac{2(0.0710)s}{0.0683} + 1\right]} \quad (5-27)$$

These transfer functions and the response to a pulse elevator input are compared with the complete three-degree-of-freedom results in Fig. 5-6. The correspondence is very good for frequencies below about 1 rad/sec, roughly one-quarter of ω_{sp} .

Because the example M_u is zero, we return to Eqs. 5-24 to obtain an appreciation for the general importance of M_u . We note that for the normally positive values of Z_w/M_w and $(X_\alpha - g)/M_\alpha$ the phugoid frequency and damping increase proportional to M_u . Conversely, for sufficiently negative values of M_u , ω_p^2 becomes negative and the phugoid mode is then characterized by two first orders, one convergent, the other a divergent "tuck," so called because as speed increases the airplane's nose has a tendency to "tuck under" (negative M_u).

When $M_u = 0$, the approximate factors for the classical case result. These are

$$2(\xi\omega)_p = -X_u \quad (5-28)$$

$$\omega_p^2 = \frac{-g}{U_0} Z_u \quad (5-29)$$

The undamped natural frequency result can be further simplified by considering $C_{L_u} \doteq 0$, as is generally true for subsonic flight, and taking the trimmed lift equal to the weight so that $Z_1 \doteq -2g/U_0$. Then,

$$\omega_p \doteq \sqrt{2} \frac{g}{U_0} \quad (5-30)$$

The period of this classical phugoid is $(\sqrt{2} \pi/g)U_0$, or about a fifth of the true airspeed in miles per hour. Based partly on these results, so-called two-degree-of-freedom phugoid approximate equations have been used from time to time. These are

$$(s - X_u)u + g\theta = 0 \quad (5-31)$$

$$-Z_u u - U_0 s\theta = Z_\delta \delta \quad (5-32)$$

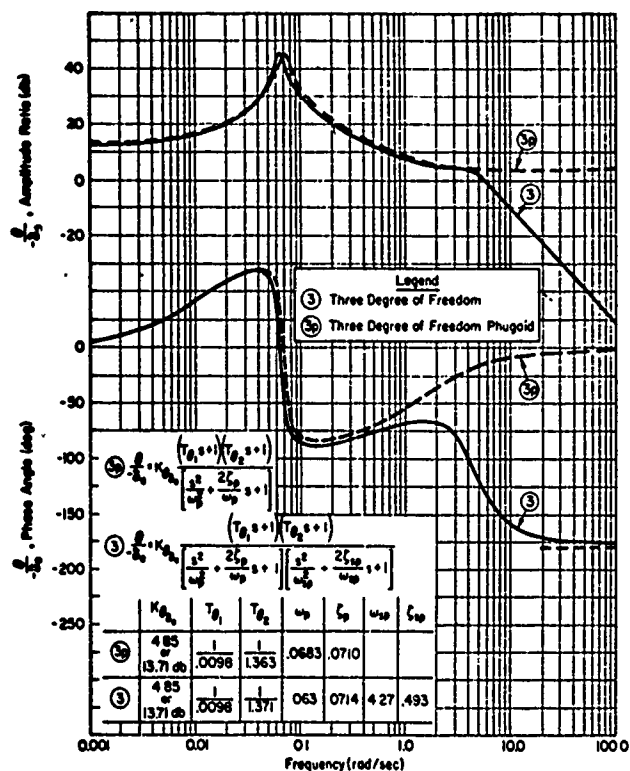
The characteristic equation of this set is

$$s^2 - X_u s - \frac{gZ_u}{U_0} = 0 \quad (5-33)$$

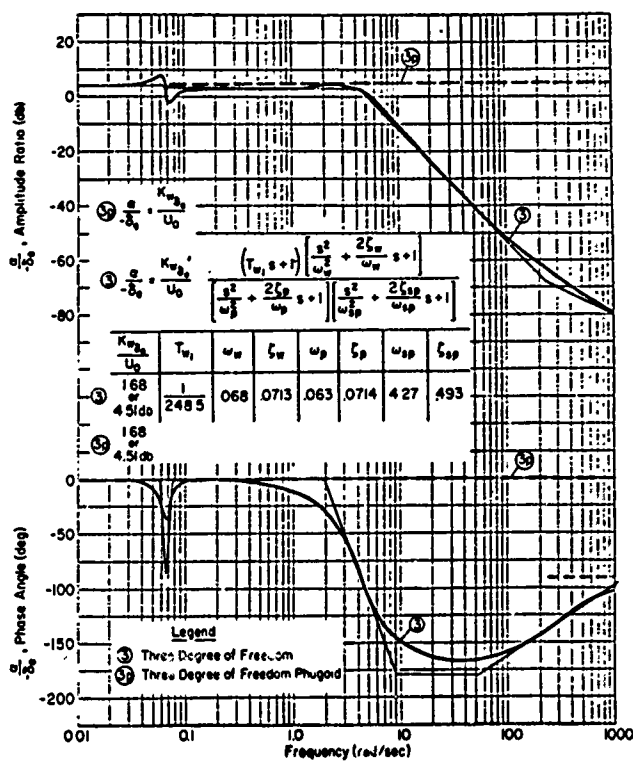
and the damping and undamped natural frequency are thereby the same as those given above (Eqs. 5-28, 5-29) for the classical ($M_u = 0$) case. Examination of the X and Z vector polygons in Fig. 5-4 indicates that the two-degree-of-freedom set is reasonably good for this example. Unfortunately, however, some of the transfer functions (and thus some time responses) derived from these equations are very poor approximations to the complete three-degree-of-freedom situation in the region of phugoid frequencies, and thus the two-degree-of-freedom set is oversimplified for most practical purposes.

5.7. HOVERING EQUATIONS OF MOTION, CONTROL-INPUT TRANSFER FUNCTIONS, AND MODAL RESPONSES

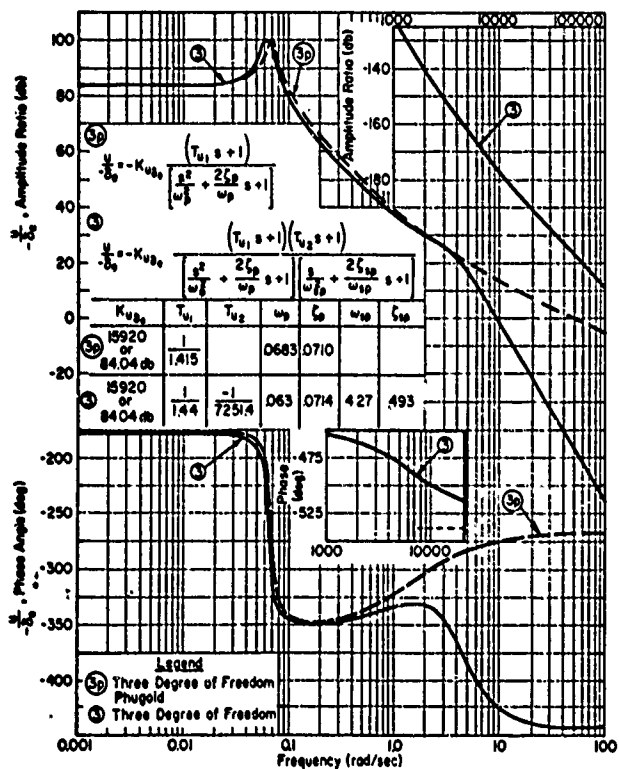
The preceding example has illustrated the phugoid and short-period modes which characterize the longitudinal motion of "conventional" aircraft, that is, aircraft supported principally by fixed wings, flying at the relatively high speeds demanded by this form of sustentation. For vehicles such as helicopters and VTOLs operating at zero and very



a) $\frac{\theta}{-\delta_e}$



b) $\frac{a}{-\delta_e}$



c) $\frac{u}{-\delta_e}$

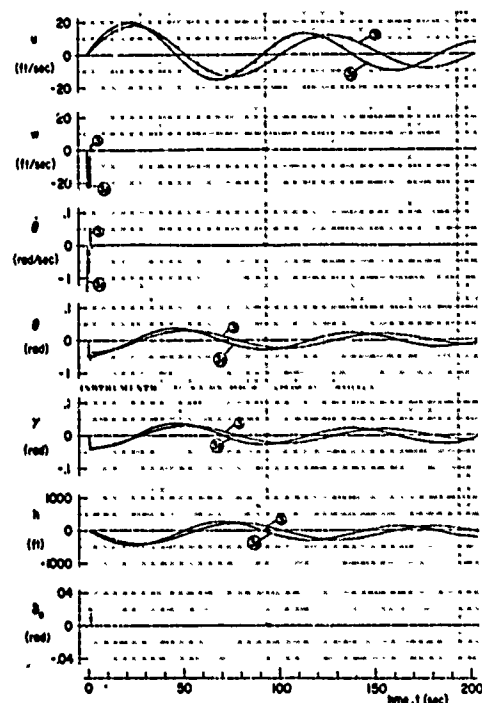


Figure 5-6. Comparison of Complete and Approximate Phugoid (Three Degree of Freedom) Control-Input Transfer Functions and Responses

low forward speeds, the longitudinal motions display modes very different from the phugoid and short-period. These differences arise because many of the usual derivatives disappear at hovering. It is pertinent, therefore, to delete such terms from the equations before considering a numerical example in detail.

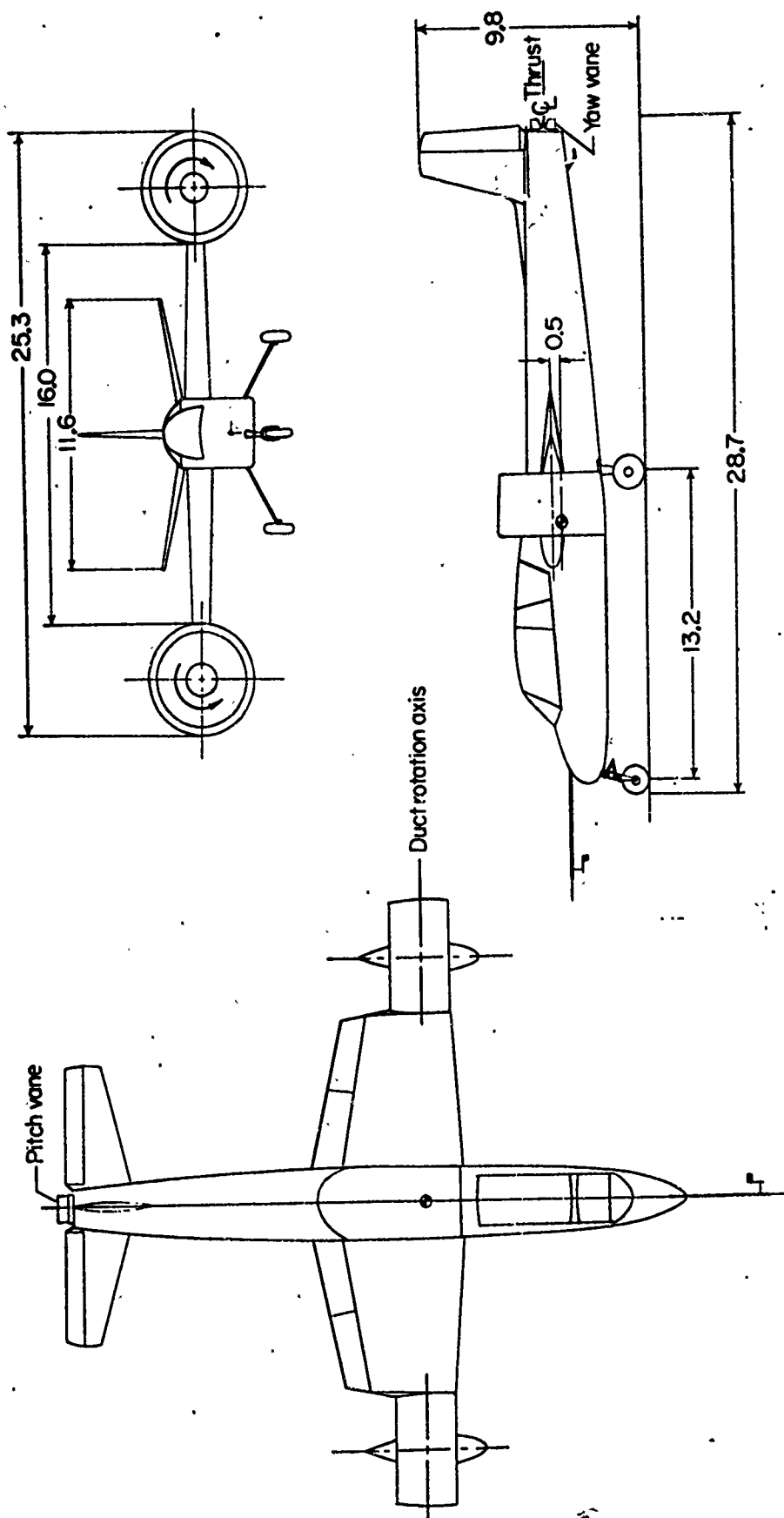
For hovering vehicles the derivatives M_w , M_w^* , and X_w are usually negligible due to considerations of symmetry. This can easily be seen for certain very simple VTOL aircraft, e.g., a "stand-on" ducted-fan.* With such vehicles perturbations in w can only produce Z forces because the configurations are symmetrical about the Z axis. For more complex VTOLs, such as the tilt-duct shown in Fig. 5-7, M_w arises principally through flat-plate drag on the horizontal tail and fuselage for the usual c.g. location near the duct axis, which is vertical in hover. The M_w resulting from these contributions is exceedingly small and may safely be neglected in calculating the frequencies, dampings, and time constants of the longitudinal modes. The contribution of the horizontal tail flat-plate drag to the M_w^* and X_w derivatives is totally negligible for this configuration; in fact, for any reasonable hover arrangement, nonzero X_w and/or M_w^* are very unlikely.

Significant M_w effects can occur in hover in the following cases:

1. When the tail jet (or rotor) is of high disk loading and contributes significant lift in the unperturbed trimmed condition. The thrust of a high-disk-loading tail jet (or rotor) is virtually unaffected by w perturbations and gives a negligible contribution to Z_w (and hence M_w). However, the main rotors now have a moment arm about the c.g. and thus induce some M_w .
2. When the tail disk loading (measured in the perturbed condition) is appreciably lower than the main disk loading. In this case the tail thrust is sensitive to perturbations in w and it may give a significant contribution to Z_w which induces some M_w due to the long moment arm about the c.g.

Even in these cases nonzero M_w usually does not change the character of the typical hovering modes. Their description can therefore proceed on the assumption that, for $U_0 = 0$, M_w^* , M_w , and X_w are negligible.

*J. P. Campbell, Vertical Takeoff and Landing Aircraft, Macmillan Co., New York, 1962.



(All dimensions in feet)

Figure 5-7. Example Tilt-Duct VTOL Aircraft

Deleting these and gust-input terms from the equations of motion (Eq. 5-2) gives

$$\begin{aligned}
 (s - X_u)u &+ g\theta &= X_\delta \delta \\
 -Z_u u &+ (s - Z_w)w &= Z_\delta \delta \\
 -M_u u &+ (s^2 - M_q s)\theta &= M_\delta \delta
 \end{aligned} \tag{5-34}$$

The corresponding control-input transfer functions in polynomial form are obtainable directly from Table 5-1 with M_w , M_q , and X_w terms deleted. Many of the numerator and denominator factors are directly separable, and canceling, because of the zero terms appearing in the left side of Eq. 5-34. For example, for $X_\delta \doteq 0$, a common occurrence, the w , θ , and u transfer functions are most directly obtained by expanding the determinant forms (Eq. 5-3) as follows:

$$\frac{w(s)}{\delta(s)} = \frac{\begin{vmatrix} s - X_u & 0 & g \\ -Z_u & Z_\delta & 0 \\ -M_u & M_\delta & s^2 - M_q s \end{vmatrix}}{\begin{vmatrix} s - X_u & 0 & g \\ -Z_u & s - Z_w & 0 \\ -M_u & 0 & s^2 - M_q s \end{vmatrix}} = \frac{Z_\delta \Delta_{\text{hover}}^*}{(s - Z_w) \Delta_{\text{hover}}} \tag{5-35}$$

$$\frac{\theta(s)}{\delta(s)} = \frac{\begin{vmatrix} s - X_u & 0 & 0 \\ -Z_u & s - Z_w & Z_\delta \\ -M_u & 0 & M_\delta \end{vmatrix}}{(s - Z_w) \Delta_{\text{hover}}} = \frac{M_\delta (s - X_u) (s - Z_w)}{(s - Z_w) \Delta_{\text{hover}}} \tag{5-36}$$

*Assuming that $|Z_u M_\delta| \ll |M_u Z_\delta|$ as usually appropriate to "throttle" (vertical thrust) control.

$$\frac{u(s)}{\delta(s)} = \frac{\begin{vmatrix} 0 & 0 & g \\ Z_0 & s-Z_w & 0 \\ M_0 & 0 & s^2-M_q s \end{vmatrix}}{(s-Z_w) \Delta_{\text{hover}}} = \frac{\cancel{gM_0(s-Z_w)}}{\cancel{(s-Z_w)} \Delta_{\text{hover}}} \quad (5-37)$$

$$\text{where} \quad \Delta_{\text{hover}} = (s-X_u)(s^2-M_q s) + gM_u \quad (5-38)$$

From these relationships we see that the $s-Z_w$ mode is associated only with w perturbations and does not appear in either θ or u motions. Since modal response ratios are independent of the input assumed (Chapter 2), this is a general conclusion which holds as well for $X_0 \neq 0$. Furthermore, since for $U_0=0$, $\dot{h}=-w$ (Eq. 5-2), the mode is characterized by pure vertical translatory motions in altitude (heaving motions) with an aperiodic time constant of $-1/Z_w$, invariably positive. Conversely, the modes associated with the longitudinal hovering cubic,

$$\Delta_{\text{hover}} = s^3 - (X_u + M_q)s^2 + X_u M_q s + gM_u \quad (5-39)$$

do not usually* involve w or h motions irrespective of whether there are three real or one real and two complex roots. That is, the longitudinal hovering cubic describes motions normally consisting of u and θ perturbations only. The relative u and θ motions can be most simply obtained from the X equation of Eq. 5-34 as a modal response ratio:

$$\frac{\theta}{u} = \left[\frac{s - X_u}{-g} \right]_{s=-q_{\text{hover}}} \quad (5-40)$$

where $-q_{\text{hover}}$ represents the roots of the hovering cubic. For real roots, and resulting aperiodic motions, the ratio is real; for complex roots, and

*The absence of h motions depends on Z_u being negligibly small, which is generally true in hover; however, the tilt-wing configuration examined in STI TR-128-1 (see footnote, p. 5-25, for complete reference) had Z_u almost equal to Z_w .

resulting oscillatory motions, the ratio is complex and must be characterized by an amplitude and phase.

5.8 EXAMPLE TRANSFER FUNCTIONS, BODE FORMS, AND TIME RESPONSES FOR A HOVERING VEHICLE

To illustrate the foregoing in more concrete terms, we now consider the example VTOL airplane of Fig. 5-7 which has the following characteristics under hovering conditions:*

Weight (lb)	3,100
Pitch inertia (slug-ft ²)	1,790
Groundspeed, U ₀ (ft/sec)	0
X _u	-0.137
X _w	0.0
X _{δ_e}	0.0
Z _u	0.0
Z _w	-0.137
Z _q	0.0
Z _{δ_e}	-1.08
M _u	0.0136
M _w	0.0
M _{q̇}	0.0
M _q	-0.0452
M _{δ_e}	-1.0

The resulting control-input transfer functions are

$$\frac{w}{-\delta_e} = \frac{\dot{h}}{s_e} = \frac{1.08}{(s + 0.137)} \quad (5-41)$$

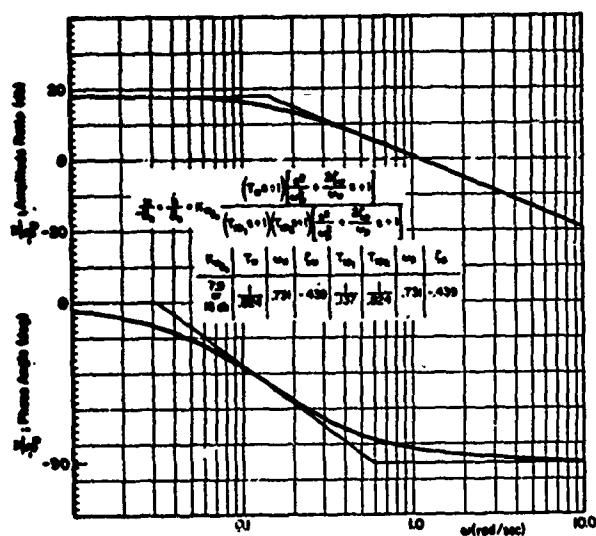
$$\frac{\theta}{-\delta_e} = \frac{(s + 0.137)}{\Delta_{\text{hover}}} \quad (5-42)$$

$$\frac{u}{-\delta_e} = \frac{-32.2}{\Delta_{\text{hover}}} \quad (5-43)$$

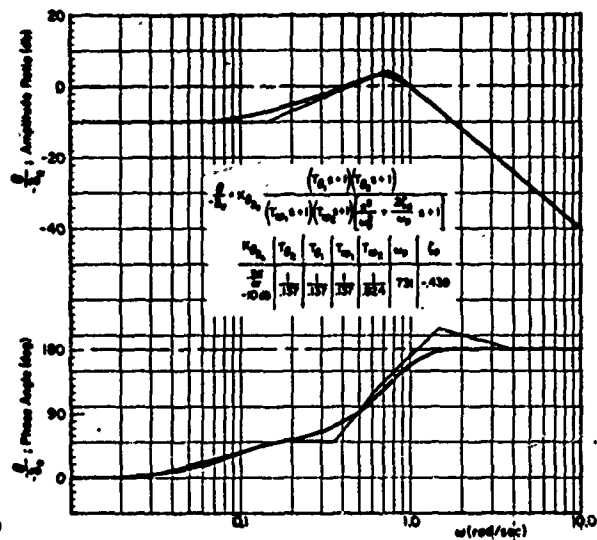
where

$$\begin{aligned} \Delta_{\text{hover}} &= \left(s + \frac{1}{T_{sp2}} \right) [s^2 + 2\zeta_p \omega_p s + \omega_p^2] \\ &= (s + 0.824) [s^2 - 2(0.439)(0.731)s + (0.731)^2] \end{aligned} \quad (5-44)$$

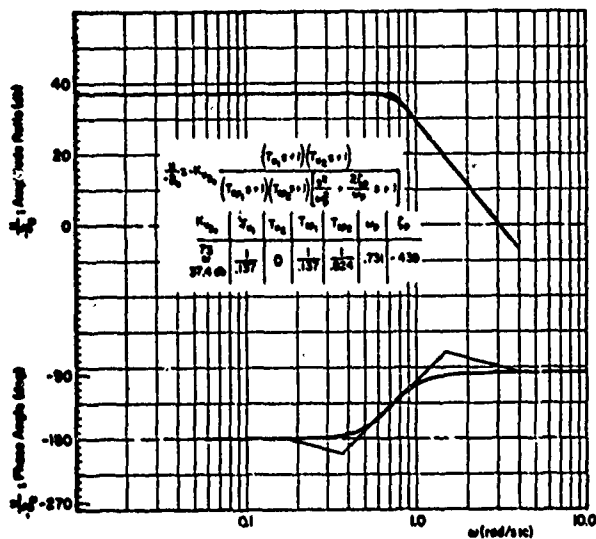
*J. Wolkovitch and R. P. Walton, VTOL and Helicopter Approximate Transfer Functions and Closed-Loop Handling Qualities, Systems Technology, Inc., Tech. Rept. 128-1, Sept. 1963.



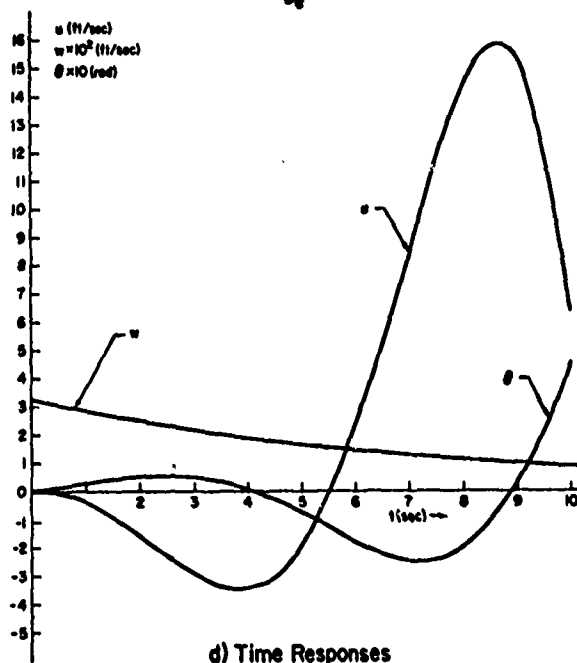
a) $\frac{u}{s_0} = \frac{1}{s_0}$



b) $\frac{\theta}{s_0}$



c) $\frac{u}{s_0}$



d) Time Responses

Figure 5-8. Example Control-Input Bode Plots and Time Responses for a Hovering Airplane

Figure 5-8 contains the corresponding Bode diagrams and time responses to an impulsive elevator input. The Bodes are much simpler than those given for the conventional airplane in Fig. 5-2. The leading phase shown for θ and u results from the negative damping of the hovering phugoid mode.*

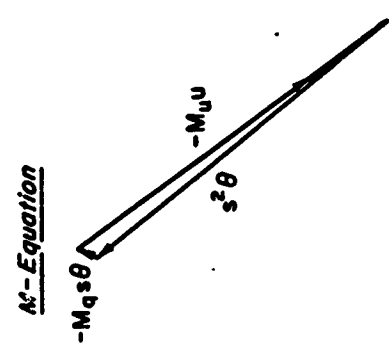
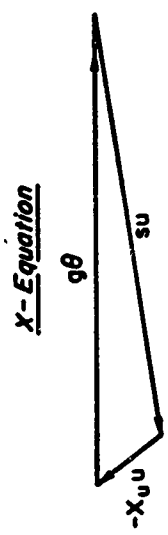
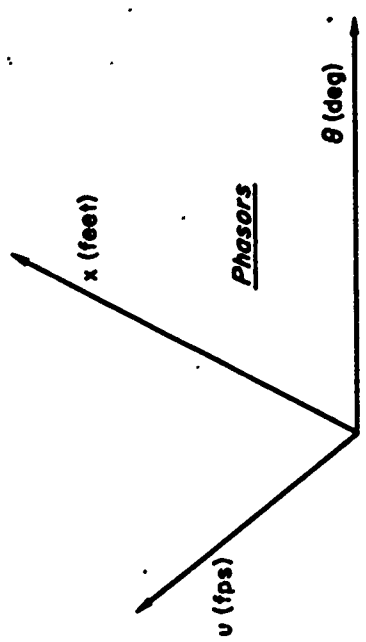
The time responses show the divergent oscillatory character of the u and θ motions and the first-order convergence of the w motions. The relative amplitudes of u and θ are clearly shown on the time vector diagrams of Fig. 5-9. Additionally, the time vectors for the phugoid mode, Fig. 5-9b, show that the instability is aggravated by a very small $|M_q|$ and a relatively large M_u . Such unstable oscillations are quite typical for hovering vehicles out of ground effect. The separate influences of these two derivatives can most easily be traced using the approximate literal transfer function factors considered subsequently.

5.9 GUST-INPUT TRANSFER FUNCTIONS

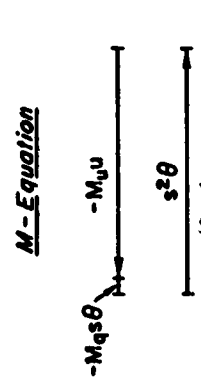
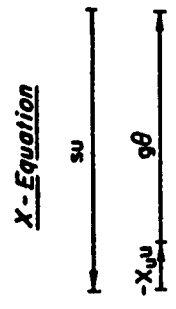
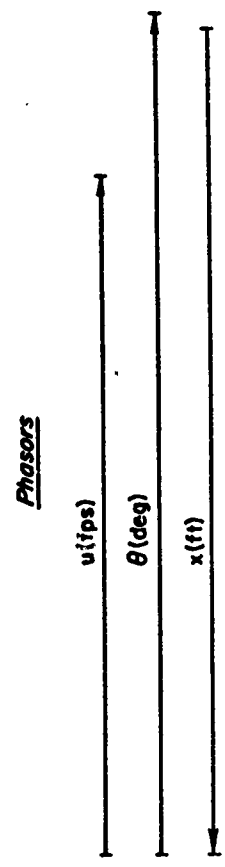
The gust-input transfer functions are obtained from the equations of motion (Eq. 5-1) using the same procedures as for control inputs. Because the denominator remains the same regardless of the type of input, we need consider only gust-input numerators. These are given in polynomial form in Table 5-2, which follows the format established in Table 5-1. In addition, Table 5-3 contains the gust transfer function numerators for the truncated short-period and phugoid equations of motion, Eqs. 5-14 and 5-20, respectively; the corresponding denominators are those given in Eqs. 5-16 and 5-23.

Figure 5-10 presents Bode plots of the u -gust transfer functions for the example conventional airplane. We see here that the primary response occurs at the phugoid frequency. Taking peak amplitudes as being approximately proportional to the magnitudes of the phugoid modal response coefficients in the several degrees of freedom, the magnitudes of the relative motions in decibels are given by

*For such nonminimum phase situations it must be remembered that the stability criterion for the closed-loop system is no longer simply that the open-loop amplitude ratio be less than one for phase lags greater than 180° (see Chapter 7 for example closures under such circumstances).



b) Phugoid Mode



a) Aperiodic Mode $(s + 1/I_{sp2})$

Figure 5-9. Time Vector Diagram for the Example Hovering Airplane

TABLE 5-2

LONGITUDINAL GUST-INPUT TRANSFER FUNCTION NUMERATOR COEFFICIENTS

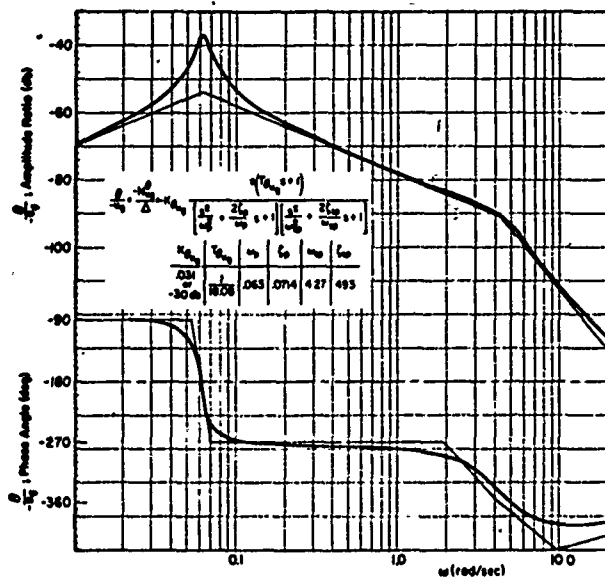
	A	B	C	D
$\frac{N_{u\dot{g}}^{\theta}}{s}$	$-(M_u + Z_u M_{\dot{w}})$	$Z_w M_u - M_w Z_u$		
$\frac{N_{u\dot{g}}^w}{s}$	$-Z_u$	$Z_u M_q - U_0 M_u$		
$N_{u\dot{g}}^u$	$-X_u$	$X_u(Z_w + M_q + M_{\dot{z}}) - Z_u X_w$	$-X_u(Z_w M_q - M_{\alpha}) + Z_u(X_w M_q + g M_{\dot{w}}) - M_u(X_{\alpha} - g)$	$g(Z_u M_w - M_u Z_w)$
$N_{u\dot{g}}^h$	Z_u	$-Z_u(M_q + M_{\dot{z}})$	$-(Z_u M_{\alpha} - M_u Z_{\alpha})$	
$\frac{U_0 N_{w\dot{g}}^{\theta}}{s}$	$M_q - M_{\dot{z}}$	$-M_{\alpha} - Z_w M_q - X_u(M_q - M_{\dot{z}})$	$X_u(M_{\alpha} + Z_w M_q) - X_w(U_0 M_u + Z_u M_q)$	
$N_{w\dot{g}}^w$	$-(Z_w - M_q + M_{\dot{z}})$	$X_u(Z_w - M_q + M_{\dot{z}}) - X_w Z_u - M_{\alpha} + Z_w M_q$	$X_u(M_{\alpha} - Z_w M_q) - X_w(U_0 M_u - Z_u M_q) + g Z_u(M_{\dot{w}} - \frac{M_q}{U_0})$	$g(Z_u M_w - M_u Z_w)$
$\frac{U_0 N_{w\dot{g}}^u}{s}$	$-X_{\alpha}$	$2X_{\alpha} M_q + g(M_{\dot{z}} - M_q)$	$g(M_{\alpha} + Z_w M_q)$	
$\frac{N_{w\dot{g}}^h}{s}$	Z_w	$-2Z_w M_q + X_w Z_u - Z_w X_u$	$-2M_q(X_w Z_u - Z_w X_u) - g Z_u(M_{\dot{w}} - \frac{M_q}{U_0})$	$-g(Z_u M_w - M_u Z_w)$

TABLE 5-3
LONGITUDINAL GUST-INPUT TRANSFER FUNCTION NUMERATOR COEFFICIENTS
FOR THE TRUNCATED SHORT-PERIOD AND PHUGOID EQUATIONS OF MOTION

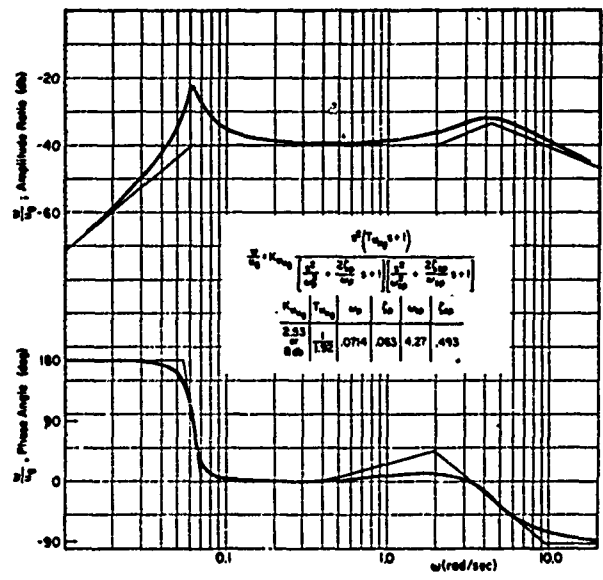
	PHUGOID		
	A	B	C
$\frac{N_{u1}^{\theta} g}{s}$	$-M_u$	$Z_w M_u - M_w Z_u$	
$\frac{N_{u1}^w g}{s^2}$	$-U_0 M_u$		
$N_{u1}^{u1} g$	$X_{u1} M_{\alpha} - M_{u1} (X_{\alpha} - g)$	$g (Z_{u1} M_w - M_{u1} Z_w)$	
$\frac{U_0 N_{w1}^{\theta} g}{s}$	$-M_{\alpha}$	$(X_{u1} M_{\alpha} - M_{u1} X_{\alpha})$	
$\frac{N_{w1}^w g}{s}$	$-M_{\alpha}$	$(X_{u1} M_{\alpha} - M_{u1} X_{\alpha})$	$g (Z_{u1} M_w - M_{u1} Z_w)$
$\frac{U_0 N_{w1}^{u1} g}{s}$	$g M_{\alpha}$		

SHORT-PERIOD

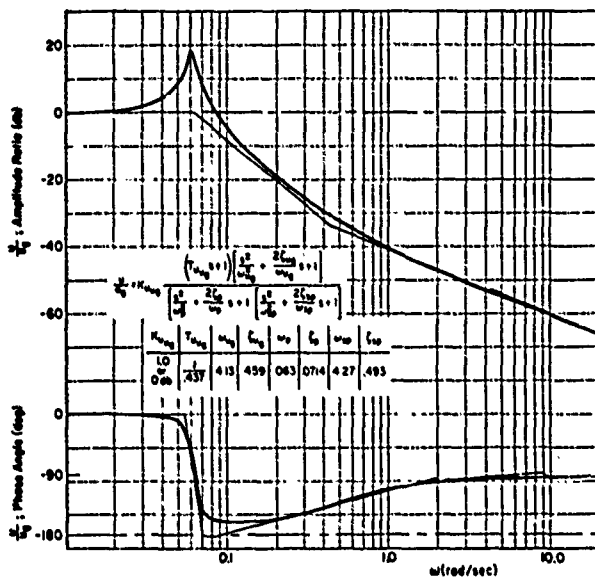
	SHORT-PERIOD		
	A	B	C
$\frac{U_0 N_{w1}^{\theta} g}{s}$	$(M_q - M_{\dot{\alpha}})$	$-M_{\alpha} - Z_w M_q$	
$\frac{N_{w1}^w g}{s}$	$-(Z_w - M_q + M_{\dot{\alpha}})$	$-M_{\alpha} + Z_w M_q$	



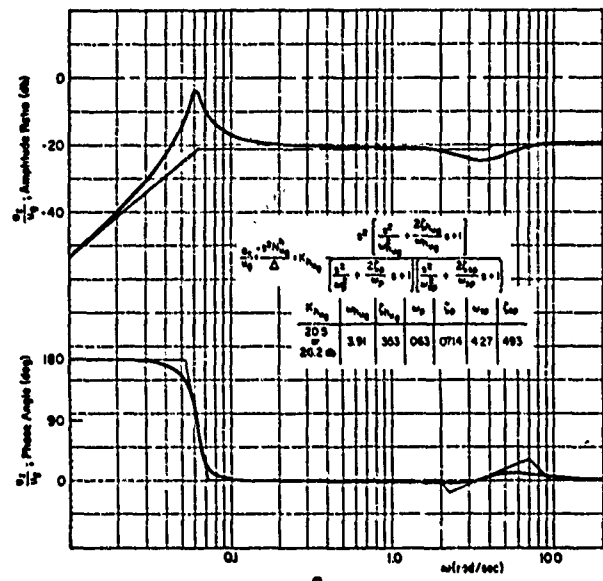
a) $\frac{\theta}{-u_g}$



b) $\frac{w}{u_g}$



c) $\frac{u}{u_g}$



d) $\frac{c_z}{u_g}$

Figure 5-10. Example u-Gust Bode Plots for Conventional Airplane

$$u : a_z : w : \theta = |18 : -5 : -23 : -37|_{\text{db}}$$

Converting a_z to \dot{h} (i.e., $|a_z(j\omega_p)/\omega_p| \doteq |\dot{h}(j\omega_p)|$) to correspond with the u and w velocities, θ to degrees as a more familiar measure, and, finally, considering linear amplitudes rather than db,

$$u : \dot{h} : w : \theta = (8 : 8.8 : 0.071)_{\text{fps}} : 0.8^\circ$$

These relative magnitudes are completely consistent with our already established picture of the phugoid motions. That is, they show that the phugoid responses to a u gust are predominantly in \dot{h} and u , secondarily in θ , and hardly at all in w . Note, however, that the u and θ responses drop off sharply with increasing frequency, whereas the w and a_z responses do not. Thus, in the short-period frequency region u and θ are essentially nonexistent, while w and a_z are about the same as in the phugoid region. Furthermore, the a_z response for frequencies beyond short-period remains constant, so that there is a distinct possibility of u gust excitation of lightly damped structural modes which may actually exist in this region, but which are eliminated by the rigid-body assumption. Finally, notice that the short period is almost exactly canceled by a corresponding numerator term in both the u and a_z transfer functions, indicating that the short-period mode itself will scarcely be present in u and a_z responses to u gusts.

The w gust transfer functions given in Fig. 5-11 show that low frequency responses progressively decrease in importance relative to high frequency responses as we consider, in turn, the u , θ , w , and a_z outputs. The u response is somewhat lower at phugoid and higher at short period than the corresponding u response to u_g (Fig. 5-10). Otherwise both plots are similar, the inference being that, regardless of input, u perturbations are always small except near phugoid frequency. The θ response at phugoid is about the same, but that at short period is considerably higher than the similar responses obtained for a u_g input. In this connection the similarity in form of the w/u_g (Fig. 5-10) and θ/w_g transfer functions should be noted, i.e., w responses to u_g are almost identical, except for a scale factor, to θ responses to w_g . This similarity also extends, but

not quite so markedly, to the w/w_g transfer function where, due to the near cancellation of the phugoid, the response is almost completely flat out to short period. The a_z response occurs predominantly at short period and beyond. Again the possibility of exciting structural a_z responses in this region must be considered for an elastic airplane.

5.10 COUPLING NUMERATORS

Multiloop situations in which more than a single input to the vehicle is involved require consideration of vehicle-introduced coupling effects between loops. Such consideration is based on the use of coupling numerators. These are defined in Chapter 3, where the notation established is a direct indication of the operations required to compute the coupling numerator. For example, the coupling numerator, $N_{\delta_e \delta_T}^{\theta u}$, appropriate for simultaneous $\theta \rightarrow \delta_e$ and $u \rightarrow \delta_T$ feedbacks is computed by substituting the δ_e and δ_T input coefficients for the terms normally appearing in the θ and u columns of the characteristic determinant. That is, from Eq. 5-1,

$$N_{\delta_e \delta_T}^{\theta u} = \begin{vmatrix} X_{\delta_T} & -X_w & X_{\delta_e} \\ Z_{\delta_T} & (s - Z_w) & Z_{\delta_e} \\ M_{\delta_T} & -(M_w s + M_{\dot{w}}) & M_{\delta_e} \end{vmatrix} \quad (5-45)$$

There can also be coupling effects between gust inputs and control inputs, and among more than two inputs, control, or disturbance (Chapter 3), so the possible variations are quite numerous. However, the coupling numerators are always easily computed and factored because replacement of at least two columns which are generally functions of s by two columns which are generally constants reduces the s polynomial to second-order or lower. Accordingly, it is unnecessary to catalogue all possible input combinations. Consequently only the more commonly used two-input control-coupling numerators are given in Table 5-4.

Table 5-4 contains the polynomial coefficients in literal form, the corresponding factored form, and literal approximations to the factors. Since the polynomials are either first- or second-order in s , factoring even in literal form is no problem and exact literal factors can easily

TABLE 5-4

LONGITUDINAL COUPLING NUMERATORS FOR ELEVATOR AND THROTTLE INPUTS

	A	B	C
δu $N_{\delta_e \delta_T}^{\theta u}$ or $-N_{\delta_e \delta_T}^{u \theta}$	$M_{\delta_e} X_{\delta_T} - M_{\delta_T} X_{\delta_e}$ $+ M_{\dot{w}} (Z_{\delta_e} X_{\delta_T} - Z_{\delta_T} X_{\delta_e})$	$M_w (Z_{\delta_e} X_{\delta_T} - Z_{\delta_T} X_{\delta_e})$ $+ Z_w (X_{\delta_e} M_{\delta_T} - X_{\delta_T} M_{\delta_e})$ $+ X_w (M_{\delta_e} Z_{\delta_T} - M_{\delta_T} Z_{\delta_e})$	
		$A_{\theta u} \left(s + \frac{1}{T_{\theta u}} \right)$ $A_{\theta u} \doteq X_{\delta_T} M_{\delta_e} ; \quad \frac{1}{T_{\theta u}} \doteq -Z_w + M_w \frac{Z_{\delta_e}}{M_{\delta_e}}$	
δh $sn_{\delta_e \delta_T}^{\theta h}$ or $-sn_{\delta_e \delta_T}^{h \theta}$ or $U_{\delta_e \delta_T}^{\alpha \theta}$ or $-U_{\delta_e \delta_T}^{\theta \alpha}$ or $sn_{\delta_e \delta_T}^{\alpha h}$ or $-sn_{\delta_e \delta_T}^{h \alpha}$	$Z_{\delta_e} M_{\delta_T} - Z_{\delta_T} M_{\delta_e}$	$X_u (M_{\delta_e} Z_{\delta_T} - M_{\delta_T} Z_{\delta_e})$ $+ Z_u (X_{\delta_e} M_{\delta_T} - X_{\delta_T} M_{\delta_e})$ $+ M_u (Z_{\delta_e} X_{\delta_T} - Z_{\delta_T} X_{\delta_e})$	
		$A_{\theta h} \left(s + \frac{1}{T_{\theta h}} \right)$ $A_{\theta h} \doteq -Z_{\delta_T} M_{\delta_e} ; \quad \frac{1}{T_{\theta h}} \doteq -X_u + \frac{X_{\delta_T}}{Z_{\delta_T}} \left(Z_u - M_u \frac{Z_{\delta_e}}{M_{\delta_e}} \right)$	
δu $sn_{\delta_e \delta_T}^{h u}$ or $-sn_{\delta_e \delta_T}^{u h}$	$X_{\delta_e} Z_{\delta_T} - X_{\delta_T} Z_{\delta_e}$	$(X_{\delta_T} Z_{\delta_e} - Z_{\delta_T} X_{\delta_e}) (M_q + M_{\dot{a}})$	$Z_{\alpha} (X_{\delta_e} M_{\delta_T} - X_{\delta_T} M_{\delta_e})$ $+ (X_{\alpha} - g) (Z_{\delta_T} M_{\delta_e} - M_{\delta_T} Z_{\delta_e})$ $+ M_{\alpha} (X_{\delta_T} Z_{\delta_e} - X_{\delta_e} Z_{\delta_T})$
		$A_{hu} [s^2 + 2(\zeta \omega)_{hu} s + \omega_{hu}^2]$ $A_{hu} \doteq -X_{\delta_T} Z_{\delta_e} ; \quad 2(\zeta \omega)_{hu} = -(M_q + M_{\dot{a}}) ; \quad \omega_{hu}^2 \doteq - \left(M_{\alpha} - \frac{X_{\delta_e}}{Z_{\delta_e}} Z_{\alpha} \right)$	
δu $U_{\delta_e \delta_T}^{\alpha u}$ or $-U_{\delta_e \delta_T}^{u \alpha}$	$X_{\delta_T} Z_{\delta_e} - Z_{\delta_T} X_{\delta_e}$	$U_o (X_{\delta_T} M_{\delta_e} - M_{\delta_T} X_{\delta_e})$ $- M_q (X_{\delta_T} Z_{\delta_e} - Z_{\delta_T} X_{\delta_e})$	$g (M_{\delta_e} Z_{\delta_T} - Z_{\delta_e} M_{\delta_T})$
		$A_{au} \left(s + \frac{1}{T_{au1}} \right) \left(s + \frac{1}{T_{au2}} \right)$ $A_{au} \doteq X_{\delta_T} Z_{\delta_e} ; \quad \frac{1}{T_{au1}} \doteq \frac{g}{U_o} \left(\frac{Z_{\delta_T}}{X_{\delta_T}} - \frac{Z_{\delta_e}}{M_{\delta_e}} \frac{M_{\delta_T}}{X_{\delta_T}} \right) ; \quad \frac{1}{T_{au2}} \doteq \frac{U_o M_{\delta_e}}{Z_{\delta_e}}$	

be written. However, the approximate factors shown are considerably more compact than exact literal factors because usually unimportant terms have been eliminated. The assumptions involved in obtaining the approximate factors are readily apparent, almost by inspection, and are not explicitly listed. They are however usually valid for conventional elevator and throttle controls (i.e., $|X_{\delta_e}| \ll |X_{\delta_T}|$; $|M_{\delta_T}| \ll |M_{\delta_e}|$). For unconventional controls, e.g., cyclic and collective pitch on a helicopter, the approximate factors shown may be inappropriate and, in such cases, the specifically important contributions to the exact polynomial coefficients should be used.

5.11 APPROXIMATE FACTORS

The literal approximate factors given in Table 5-4 for coupling numerators serve to reintroduce the subject of approximate factors in general. In addition to those given in Table 5-4 we have already implicitly derived some approximate factors in connection with the simplified short-period, phugoid, and hover equations of motion (i.e., Eqs. 5-17, 5-24, 5-35, 5-36). However, using such truncated equations does not always produce unambiguous and reasonably accurate approximate factors or adequately identify the conditions for which the approximations hold. A more direct attack, which meets these requirements, is simply to factor the literal polynomial expressions in Table 5-1 by first neglecting terms of minor significance, and then applying an approximate factorization technique such as that described in Section 3.4. Of course the relative importance of various derivatives or derivative groupings depends on the vehicle type and flight condition, so that there is no single set of literal approximate factors generally applicable to all situations. This is reflected in the profusion of approximate factors* given in Tables 5-5 and 5-8.

*Taken from:

I. L. Ashkenas and D. T. McRuer, Approximate Airframe Transfer Functions and Application to Single Sensor Control Systems, WADC-TR-58-82, June 1958.

J. Wolkovitch and R. P. Walton, VTOL and Helicopter Approximate Transfer Functions and Closed-Loop Handling Qualities, Systems Technology, Inc., Tech. Rept. 128-1, Sept. 1963.

R. L. Stapleford, J. Wolkovitch, R. E. Magdaleno, C. P. Shortwell, and W. A. Johnson, An Analytical Study of V/STOL Handling Qualities in Hover and Transition, AFFDL-TR-65-73, May 1965.

Table 5-5 presents the approximate factors for conventional airplanes, and these apply as well to VTOL machines and helicopters at cruise or high speed flight. Notice in particular that the approximate short-period frequency and damping are identical to those of Eqs. 5-17, and the phugoid frequency and damping are quite similar to those of Eq. 5-24 except for the appearance of the $Z_w M_q$ term in the Table 5-5 expressions. Similarly, the numerator factors implicit in Eqs. 5-15, 5-16, and 5-21 to -23 have their counterpart in Table 5-5. For example, the numerator time constants in Eqs. 5-15 and 5-16 reduce to the same expressions as those for $1/T_{w1}$ and $1/T_{\theta 2}$ in Table 5-5 when the Table 5-5 conditions of validity are invoked.

The various expressions in Table 5-5 tell us, almost at a glance, what derivatives are important for a given control situation. Furthermore, they also display the explicit connections between all the numerators and the denominators via the dominant derivatives. For example, changes in $1/T_{\theta 2}$ which involve changes in Z_w are also accompanied by important changes in $\xi_{sp} \omega_{sp}$, $1/T_{u1}$, and ω_h^2 (or $1/T_{h2} T_{h3}$).

The approximate factors can be simple and effective guides to the influences of speed, c.g., and configuration changes on the basic transfer functions and on the flight control system accommodations required for such changes. They are especially useful for the preliminary selection of appropriate flight control system feedbacks. For example, a very crude, albeit relatively accurate, way of considering the basic effects of a stability-augmenting flight control system is to regard its action primarily as one of directly augmenting various aerodynamic derivatives. From this point of view a pitch rate damper ($q \rightarrow \delta_e$) simply augments the derivatives M_q and Z_q (for X_{δ_e} negligible). Accordingly, the primary effect, related to the increased $-M_q$, is to improve the short-period damping. Table 5-6 delineates the important derivatives and the qualitative consequences of their augmentation for conventional aircraft.

The conditions for which the Table 5-5 approximate factors are valid do not extend to those appropriate for VTOL aircraft and helicopters in hovering and transition flight. Such situations are treated in Table 5-8 which, because of the different vehicle types considered, contains a variety of possibly applicable expressions. Table 5-7 serves as a guide

to Table 5-8 and contains additional information concerning the very simple transfer function forms appropriate for hover. Although the unconventional aircraft covered are all VTOL or helicopter types, we continue to call the primary control inputs "elevator" and "throttle." However, as noted in Table 5-7, "elevator" now means whatever device is used to produce a pitching moment (e.g., longitudinal cyclic pitch on a single-rotor helicopter) and "throttle" now means a thrust input regardless of direction (e.g., collective pitch on a helicopter which produces a vertical thrust).

The connections, established and apparent in Table 5-8, between the dominant derivatives and the resulting transfer function poles and zeros serve the general purpose, again, of delineating potentially important feedbacks and furnishing direct insight into the basic vehicle dynamics and the effects of changes in configuration, speed, etc. In this regard notice particularly the expression for the tilt-duct hovering oscillation given in Table 5-8a, and recall that the corresponding example time vectors (Fig. 5-9a) indicated strong M_q and M_u influences on the damping. We can examine such influences in detail by directly considering the approximate factor

$$2\zeta_p\omega_p \doteq -\sqrt[3]{gM_u} - \frac{2}{3}(X_u + M_q) \quad (5-46)$$

First we note that substituting the example values into Eq. 5-46 gives

$$\begin{aligned} 2\zeta_p\omega_p &\doteq -\sqrt[3]{32.2(0.0136)} + \frac{2}{3}(0.137 + 0.045) \\ &\doteq -0.759 + 0.121 \doteq -0.638 \end{aligned}$$

in good agreement with the exact value (Eq. 5-44) of -0.642 . With our confidence in the approximate expression thus established, we can now fix the relative effects of the dominant derivatives on the total damping. Applying Eq. 5-46, we see that for the example values the order of dominance is M_u , X_u , M_q ; and that a 100 percent increase in $-M_q$ can be counteracted by about a 12 percent decrease in M_u . For large changes in M_q Eq. 5-46 may not be appropriate because it requires as a condition of validity that $|gM_u| > |M_q^3|$. For example, if $-M_q$ is increased to 1.0 then $|gM_u| < |M_q^3|$ and the appropriate approximation (Table 5-8a) is

$$2\zeta_p\omega_p \doteq -X_u - \frac{M_q}{4} - \sqrt{\frac{M_q^2}{16} - \frac{gM_u}{2M_q}} \quad (5-47)$$

TABLE 5-5

SUMMARY OF CONVENTIONAL AIRPLANE LONGITUDINAL APPROXIMATE FACTORS

FACTORED FORMS	APPROXIMATE FACTORS	CONDITIONS OF VALIDITY
$\Delta(s) = \underbrace{\left(s^2 + 2\zeta_{sp}\omega_{sp}s + \omega_{sp}^2\right)}_{\text{or}} \left(s + \frac{1}{T_{P1}}\right)\left(s + \frac{1}{T_{P2}}\right)$	$\omega_{sp}^2 \doteq M_0 Z_0 - M_C$ $2\zeta_{sp}\omega_{sp} \doteq -(Z_0 + M_2 + M_3)$ $\omega_{sp}^2 \text{ or } \frac{1}{T_{P1}T_{P2}} \doteq \frac{g(M_2 Z_0 - M_3 Z_0)}{Z_0 M_0 - M_C}$ $2\zeta_{sp}\omega_{sp} \text{ or } \left(\frac{1}{T_{P1}} + \frac{1}{T_{P2}}\right) \doteq -X_1 - \frac{M_1(X_0 - g)}{Z_0 M_0 - M_C}$	$\left \frac{X_0 Z_0}{Z_0(X_1 + Z_0)}\right \ll 1$ $\left \frac{M_2(Z_0 - \frac{M_1}{M_0} Z_0)}{U_0}\right < \left(\frac{Z_0}{2}\right)^2 \text{ or } \left(\frac{M_2}{2}\right)^2$ $\left M_3\left(\omega_{sp}^2 + \frac{g}{U_0} Z_0\right) + M_0 X_0 Z_0\right \ll \left -M_1(X_0 - g)\right $
$N_{\delta_e}^{\delta}(s) = A_0\left(s + \frac{1}{T_{\theta 1}}\right)\left(s + \frac{1}{T_{\theta 2}}\right)$	$A_0 \doteq M_0$ $\frac{1}{T_{\theta 1}} \doteq -X_1 + \frac{X_0 Z_0}{Z_0}\left(\frac{1 - \frac{Z_0}{M_0} \frac{M_1}{Z_0}}{1 - \frac{Z_0}{M_0} \frac{M_2}{Z_0}}\right)$ $\frac{1}{T_{\theta 2}} \doteq -Z_0 + \frac{M_2}{M_0} Z_0$	$ Z_0 M_0 \ll M_0 $ $ X_1 \ll Z_0 $
$N_{\delta_e}^{\eta}(s) = A_{\eta}\left(s + \frac{1}{T_{\eta 1}}\right)\left(s^2 + 2\zeta_{\eta}\omega_{\eta}s + \omega_{\eta}^2\right)$	$A_{\eta} \doteq Z_0$ $\frac{1}{T_{\eta 1}} \doteq \frac{U_0 M_0}{Z_0}$ $\omega_{\eta}^2 \doteq \frac{g}{U_0}\left(-Z_0 + \frac{Z_0}{M_0} M_1\right)$ $2\zeta_{\eta}\omega_{\eta} \doteq -X_1$	$ Z_0(M_0 + X_1) \ll U_0 M_0 $
$N_{\delta_e}^{\eta}(s) = A_{\eta}\left(s + \frac{1}{T_{\eta 1}}\right)\left(s + \frac{1}{T_{\eta 2}}\right)$	$A_{\eta} \doteq Z_0 X_0$ $\frac{1}{T_{\eta 1}} \doteq \frac{-g}{X_0 - g}\left(-Z_0 + \frac{M_2}{M_0} Z_0\right)$ $\frac{1}{T_{\eta 2}} \doteq \frac{M_0(X_0 - g)}{Z_0 X_0}$	$ Z_0(g M_0 + M_0 X_0) \ll M_0(X_0 - g) $
$s N_{\delta_e}^h = A_h\left(s + \frac{1}{T_{h1}}\right)\left(s + \frac{1}{T_{h2}}\right)\left(s + \frac{1}{T_{h3}}\right)$ <p style="text-align: center;">or</p> $\left(s^2 + 2\zeta_{h}\omega_h s + \omega_h^2\right)$ <p style="text-align: center;">Forward Control</p>	$A_h \doteq -Z_0$ $\frac{1}{T_{h1}} \doteq -X_1 + (X_0 - g)\frac{Z_0}{Z_0}\left(\frac{1 - \frac{Z_0}{M_0} \frac{M_1}{Z_0}}{1 - \frac{Z_0}{M_0} \frac{M_2}{Z_0}}\right)$ $\frac{1}{T_{h2}} = \frac{-1}{T_{h3}} \doteq \left(M_0 - \frac{M_2}{Z_0} Z_0\right)^{1/2}$ $\omega_h^2 \doteq -X_0 + \frac{M_0}{Z_0} Z_0$ $2\zeta_h\omega_h \doteq -\left(M_0 + M_1 + X_1 + \frac{1}{T_{h1}}\right)$	$ X_1(M_0 + M_1) \ll \left M_0 - \frac{M_2}{Z_0} Z_0\right $

General assumption is $X_{\delta_e} = 0$.Applicable also to VTOL airplanes in cruise or high speed configuration (i.e., tilt-wing speeds for which wing incidence is δ_0° greater than that at hover; tilt-rotor speeds greater than 100 ft/sec; tilt-rotor at all speeds), and to single-rotor helicopters at speeds greater than 50 ft/sec. $\gamma/\delta = c N_h(s)/U_0 \Delta(s)$; $e_z = -g^2 N_h(s)/\Delta(s)$.

TABLE 5-6

QUALITATIVE IMPORTANCE OF NORMAL AIRFRAME STABILITY PARAMETERS
TO LONGITUDINAL ELEVATOR-INPUT TRANSFER FUNCTION QUANTITIES*

QUANTITIES AFFECTED	DERIVATIVE							CHANGE IN POINT OF CONTROL APPLICATION
	M_u	$M_{\dot{u}}$	M_q	Z_u	Z_q	X_u	$X_{\dot{u}}$	
Denominator, $\Delta(s)$								Δ
Short-period undamped frequency, ω_{sp}								
Short-period damping, $2\zeta_{sp}\omega_{sp}$	xxx		x		x			
Classical phugoid, $\omega_p = -\sqrt{2(g/U_0)}$, $2\zeta_{p\omega_p} \doteq -\lambda_u$		xx	xx		xx			
Normal phugoid undamped frequency, $\omega_p \doteq [g(M_q Z_u - M_u Z_q)/(Z_u M_q - M_u)]^{1/2}$	xxx		x	xx	x		xxx	
"Tuck" and longitudinal subsidence, $1/T_{p1}$ and $1/T_{p2}$	xxx		x	xx	x			
Normal or "tuck" damping, $2\zeta_{p\omega_p}$ or $(1/T_{p1} + 1/T_{p2})$	xx		x		x			
Pitch Numerator, $N_\theta(s)$								
Low frequency factor, $1/T_{\theta 1}$	x	x		x				
High frequency factor, $1/T_{\theta 2}$		xx			xxx			xx
Airspeed Numerator, $N_u(s)$								
Low frequency factor, $1/T_{u1}$								
High frequency factor, $1/T_{u2}$					xxx			x
Downward velocity numerator, $N_w(s)$								xxx
First-order factor, $1/T_{w1}$								
Quadratic factor undamped frequency, ω_w								xxx
Quadratic factor damping, $2\zeta_{w\omega_w}$	xx			x				xx
Altitude (Flight Path, Acceleration, Etc.) Numerator, $N_h(s)$								
First-order factor, $1/T_{h1}$	x	x		xx	xx			x
Aft control quadratic, $1/T_{h2}$ and $1/T_{h3}$		x			xxx			xxx
Forward control quadratic undamped frequency, ω_h					xxx			xxx
Forward control quadratic damping, $2\zeta_{h\omega_h}$	x	x	xx	x	x			x

CODE

Blank = little or no effect
 x = moderate effect
 xx = important effect
 xxx = predominant effect

*The only stability parameters considered in this table are those that
 1. Exist in the normal uncontrolled airframe
 2. Can be augmented by relatively simple automatic control systems
 Some of these (M_u , M_q , and the point of control application) are also
 modified by fairly simple airframe geometry changes.

TABLE 5-7
SUMMARY OF THE UNCONVENTIONAL AIRCRAFT LONGITUDINAL APPROXIMATE FACTORS GIVEN IN TABLE 5-8

		TILT-WING		HELICOPTER				TILT-DUCT			TILT-ROTOR	
				Single-Rotor		Tandem-Rotor						
				Low Speed	High Speed	1,3	2,3	Hover	High Speed	Hover		High Speed
						$U_0 \div 0$	$U_0 > 50$ fps	$U_0 \div 0$	$U_0 > 40$ fps $U_0 < 120$ fps	$U_0 \div 0$	$U_0 > 100$ fps	
	Denominator		Table 5-5	✓	Table 5-5	✓	Table 5-5	✓	✓	✓	Table 5-5	
NUMERATORS	Elevator	θ	✓	✓	✓	✓	✓	✓	✓	✓	✓	✓
	Pitching Moment Control	w	—	✓	Zero	✓	✓	Zero	✓	—	✓	/
		u	✓	✓	✓	✓	✓	✓	✓	✓	✓	✓
		\dot{h}	—	—	Zero	✓	Zero	✓	Zero	—	✓	—
	Throttle	θ	✓	✓	✓	Zero	✓	Zero	✓	Zero	✓	✓
		w	*	—	*	*	✓	*	✓	*	—	—
	Thrust Control	u	—	—	Zero	Zero	✓	Zero	✓	Zero	—	—
		\dot{h}	*	—	*	*	—	*	✓	*	—	—

¹ Including range of speed for which wing incidence is within 45° of wing incidence at hover.

² Wing incidence greater than 45° from incidence at hover.

³ The separation of high and low speed factors by wing incidence is empirical.

"Zero" indicates response is approximately zero.

Asterisk (*) indicates conditions for which numerator and denominator factors cancel to give, approximately, $\dot{h}/\delta\eta \div -w/\delta\eta \div -Z\delta\eta/(s-Z_w)$. In general, this requires close to zero response in θ and u , which can also occur for tilt-rotor and tilt-wing hover provided $M\delta\eta$ and $X\delta\eta$ are negligibly small.

TABLE 5-8
APPROXIMATE LONGITUDINAL FACTORS FOR UNCONVENTIONAL AIRCRAFT
(a) Denominator (Δ_{long}) Factors

FIRST COEFF.	APPROXIMATE FACTORS	CONDITIONS OF VALIDITY	APPLICABLE TO:
1	$\frac{1}{\pi_{sp1}} = -z_u$ $\frac{1}{\pi_{sp2}} = \frac{\partial x_u}{\partial x_u} + \frac{-x_u - M_q}{5}$ $2k_{sp} = -\frac{\partial x_u}{\partial x_u} + \frac{2}{5}(-x_u - M_q)$ $\omega_p^2 = \partial x_u \pi_{sp1}$	$ u_0 M_q \ll z_u M_q $ $\left \frac{\partial x_u}{M_q^2} \right > 1$ $\left \frac{\partial x_u}{x_u^2} \right > 1$	Tilt-wing Low speed ^{1,2} Tilt-duct Hover
	$\frac{1}{\pi_{sp1}} = -z_u$ $\frac{1}{\pi_{sp2}} = \frac{-x_u}{4} + \sqrt{\frac{M_q^2}{16} - \frac{\partial x_u}{2x_u}}$ $2k_{sp} = -x_u - \frac{x_u}{4} - \sqrt{\frac{M_q^2}{16} - \frac{\partial x_u}{2x_u}}$ $\omega_p^2 = \frac{\partial x_u}{-x_u/4 + \sqrt{\frac{M_q^2}{16} - \frac{\partial x_u}{2x_u}}}$	$ M_q \gg x_u $ $\left \frac{\partial x_u}{M_q^2} \right < 1$ If $ x_u \gg M_q $ and $\left \frac{\partial x_u}{x_u^2} \right < 1$ interchange x_u and M_q in equations	Helicopters: Hover
	$\frac{1}{\pi_{sp1}} = -\left(\frac{M_q + z_u + u_0 M_q}{2} \right) + \sqrt{\left(\frac{M_q + z_u + u_0 M_q}{2} \right)^2 + u_0 x_u - M_q z_u}$ $\frac{-1}{\pi_{sp2}} = \omega_p = -\left[\partial x_{sp1} (M_q z_u - x_u z_u) \right]^{1/3}$ $2k_{sp} = -x_u - \frac{1}{\pi_{sp2}}$	$\left \frac{1}{\pi_{sp1}} \right > 5 \left \frac{1}{\pi_{sp2}} \right $ $ \partial x_u \gg -x_u (M_q z_u - u_0 M_q) - M_q u_0 z_u + M_q x_u z_u + \partial x_u M_q $ If M_q is too small to satisfy this condition, use conventional airplane approximate factors (Table 5-5)	Helicopters 40 fps < U_0 < 120 fps

¹Including range of speed for which wing incidence is within 45° of wing incidence at hover.

²The separation of high and low speed factors by wing incidence is empirical.

Table 5-8 (Continued).
(b) θ Numerator (N_0^2) Factors

FIRST COEFF.	APPROXIMATE FACTORS	CONDITIONS OF VALIDITY	APPLICABLE TO:
	$\frac{1}{\pi_{\theta 1}} + \frac{1}{\pi_{\theta 2}} = \frac{X_0}{N_0} (Z_u M_0 + M_u) + \frac{Z_0}{N_0} (M_0 - Z_u M_0) - (X_u + Z_u)$ $\frac{1}{\pi_{\theta 1}} \frac{1}{\pi_{\theta 2}} = \frac{X_0}{N_0} (Z_u M_u - Z_u M_u) + \frac{Z_0}{N_0} (M_u Z_u - M_u X_u) + (Z_u Z_u - X_u Z_u)$	$ Z_0 M_0 \ll N_0 $	<p>Tilt-wing All speeds, elevator and throttle</p> <p>Tilt-duct All speeds, elevator $U_0 > 100$ fps, throttle</p> <p>Tilt-rotor All speeds, throttle</p>
M_0	$\frac{1}{\pi_{\theta 1}} = \frac{X_0(M_u Z_u - Z_u M_u) + Z_0(X_u M_u - M_u X_u) + M_0(Z_u Z_u - X_u Z_u)}{Z_u M_0}$ $\frac{1}{\pi_{\theta 2}} = -Z_u$	$\left \frac{1}{\pi_{\theta 1}} \right \ll \left \frac{1}{\pi_{\theta 2}} \right , \quad \left \frac{M_u Z_0}{N_0} \right \ll Z_u $	<p>Helicopters All speeds, elevator</p> <p>Tilt-rotor All speeds, elevator</p>
	$\frac{1}{\pi_{\theta 1}} = -X_u - \frac{M_u(Z_u Z_0 - X_u Z_0)}{M_u Z_0 - Z_u M_0}$ $\frac{1}{\pi_{\theta 2}} = -Z_u + \frac{M_u Z_0 + M_u X_0}{N_0} = -Z_u + \frac{M_u}{N_0} Z_0$	$\left \frac{1}{\pi_{\theta 1}} \right \ll Z_u $ $\left \frac{1}{\pi_{\theta 1}} \right \ll \left \frac{1}{\pi_{\theta 2}} \right $ $M_0 \neq 0$	Single-rotor helicopter $U_0 > 50$ fps, throttle
$Z_0 M_0$	$\frac{1}{\pi_{\theta 1}} = \frac{M_u}{N_u}$ $\frac{1}{\pi_{\theta 2}} = -X_u + M_u \frac{Z_u}{N_u}$	$M_0 \neq 0$ $ M_0 \ll Z_0 M_0 $ $ X_0 \ll Z_0 $ $U_0 \neq 0$	Tandem-rotor helicopter Throttle for $40 \text{ fps} < U_0 < 120 \text{ fps}$

Table 5-8 (Continued)
(c) w Numerator (M_0^w) Factors

FIRST COEFF.	APPROXIMATE FACTORS	CONDITIONS OF VALIDITY	APPLICABLE TO:
Z ₀	$\frac{1}{\pi_{w_1}} \doteq \frac{u_0 M_0}{Z_0}$ $\omega_0^2 \doteq \frac{g}{u_0} \left(\frac{M_0 Z_0}{M_0} - Z_u \right)$ $2\xi_{w_1} \doteq -\lambda_u$	$ Z_0(M_0 + x_u) - x_0 z_u \ll u_0 M_0 $ $ x_0(u_0 M_0 - z_u M_0) \ll x_u(z_0 M_0 - u_0 M_0) $	Tilt wing High speed, ¹ elevator Tilt duct U ₀ > 100 fps, elevator
	$\frac{1}{\pi_{w_1}} \doteq \frac{u_0 M_0}{Z_0}$ $\omega_0^2 \doteq \frac{g}{u_0} \left(\frac{M_0 Z_0}{M_0} - Z_u \right)$ $2\xi_{w_1} \doteq \frac{1}{u_0 M_0} [u_0(x_0 M_0 - x_u M_0) + M_0(x_u Z_0 - x_0 z_u) - Z_0 \omega_0^2]$	$\left \frac{1}{\pi_{w_1}} \right \gg M_0 $ $u_0 \neq 0 \text{ (at } u_0 = 0, Z_0 = 0)$ $\left \frac{1}{\pi_{w_1}} \right \gg \omega_0$ $ u_0 M_0 \gg x_u Z_0 $	Helicopters: Elevator Single-rotor, U ₀ > 50 fps Tandem-rotor, 40 fps < U ₀ < 120 fps Tilt-rotor All speeds, elevator
	$\frac{1}{\pi_{w_1}} \doteq -M_0$ $\frac{1}{\pi_{w_2}} \frac{1}{\pi_{w_3}} \text{ or } \omega_0^2 \doteq \frac{\partial M_0}{\partial M_0}$ $\frac{1}{\pi_{w_2}} + \frac{1}{\pi_{w_3}} \text{ or } 2\xi_{w_1} \doteq -\lambda_u - \frac{\partial M_0}{\partial M_0}$	$u_0 \neq 0 \left[\text{for } u_0 = 0, \frac{\partial M_0}{\partial M_0} = \frac{Z_0}{g - Z_u} \right]$ $ x_u \ll \left \frac{1}{\pi_{w_1}} \right $ $ x_u \ll \omega_0 $ $ x_0 \ll Z_0 $ $ u_0 M_0 \ll Z_0 M_0 $	Helicopters For above speeds, throttle

¹Wing incidence 45° greater than that at hover.

Table 5-8 (Continued)
(d) u Numerator (N_8^u) Factors

FIRST COEFF.	APPROXIMATE FACTORS	CONDITIONS OF VALIDITY	APPLICABLE TO:
$Z_6 X_4$	$\frac{1}{\pi_{u1}} \doteq \frac{N_8(u_0 X_4 - g)}{Z_6 X_4}$ $\frac{1}{\pi_{u2}} \doteq \frac{g \left(Z_4 - \frac{Z_6}{N_8} N_4 \right)}{(u_0 X_4 - g)}$	$\left \frac{Z_6 g N_4}{X_4 Z_6} \right \gg \left \frac{1}{\pi_{u2}} \right \gg \left \frac{1}{\pi_{u1}} \right $ $ Z_6(g N_4 + N_4 X_4) \ll N_8(u_0 X_4 - g) $ <p>For $u_0 \neq 0$, $\frac{1}{\pi_{u2}} = -Z_4$, $\frac{1}{\pi_{u1}} \rightarrow \infty$</p>	Tilt-wing All speeds, elevator Tilt-duct All speeds, elevator
X_8	$\frac{1}{\pi_{u1}} \doteq -Z_4$ $a_2^2 \doteq \frac{-g}{X_8} \left(N_8 - Z_6 \frac{N_4}{Z_4} \right)$ $2\zeta_{u1} \omega_1 \doteq -N_4$	$ X_8(N_4 + Z_4) \gg u_0 X_8 N_4 - Z_6 X_4 $ $ X_8 Z_4 N_4 - g N_8 \gg u_0(X_4 N_8 - X_8 N_4) - Z_6(g N_4 + X_4 N_8) $	Helicopters All speeds, elevator Tilt-rotor All speeds, elevator
	$\frac{1}{\pi_{u1}} \doteq -Z_4 + X_4 \frac{Z_6}{X_8}$ $a_2^2 \doteq \frac{-g N_8}{X_8}$ $2\zeta_{u1} \omega_1 \doteq -N_4$	$X_8 \neq 0 \text{ (Note: } X_8 = 0 \text{ at } u_0 = 0)$ $ X_4 Z_6 < Z_4 X_8 $	Single-rotor helicopter $U_0 > 50$ fps, throttle
$Z_6 X_4$	$\frac{1}{\pi_{u1}} \frac{1}{\pi_{u2}} \doteq \frac{-g N_4}{X_4}$ $\frac{1}{\pi_{u1}} + \frac{1}{\pi_{u2}} \doteq -N_4 - \frac{g N_4}{X_4}$	$X_8 = N_8 = 0$ $u_0 \neq 0$	Tandem-rotor helicopter Throttle for $40 \text{ fps} < U_0 < 120 \text{ fps}$

Table 5-8 (Concluded)
(e) \dot{h} Numerator (sn_0^2) Factors

FIRST COEFF.	APPROXIMATE FACTORS	CONDITIONS OF VALIDITY	APPLICABLE TO:
	$\frac{1}{\pi_{b1}} \doteq -x_u + (u_0 x_v - \varepsilon) \frac{x_u - \frac{x_0}{Z_0} z_u}{u_0 (x_v - \frac{x_0}{Z_0} z_v)}$ $-\frac{1}{\pi_{b2}} \doteq \frac{1}{\pi_{b3}} \doteq \sqrt{u_0 (x_v - \frac{x_0}{Z_0} z_v)}$	$\left(\frac{1}{\pi_{b2}}\right)^2 \gg \left \left(x_u - \frac{x_0 z_u}{Z_0}\right) (x_v + u_0 x_v) \right $ $\left \frac{1}{\pi_{b1}} \frac{1}{\pi_{b2}} \frac{1}{\pi_{b3}} \right \gg \left \frac{x_0}{Z_0} u_0 (z_v x_u - z_u x_v) \right $ <p>For $u_0 \doteq 0$, $\dot{h} \doteq -v$</p>	Tilt duct $U_0 > 100$ fps, elevator
$-Z_0$	$\frac{1}{\pi_{b1}} \doteq -\frac{\varepsilon z_u}{u_0 z_v} + \frac{z_0 \varepsilon x_u}{x_0 u_0 z_v} \doteq \frac{x_0}{x_0} \left(x_u - \frac{x_0 z_u}{Z_0}\right)$ $\omega_1^2 \doteq \frac{x_0 u_0 z_v}{Z_0}$ $2\xi_{b1}\omega_1 \doteq -x_v - u_0 x_v$	$\left \frac{1}{\pi_{b1}}\right \ll \omega_1$ $ x_v z_0 \ll z_v x_0 $ $\left \frac{1}{\pi_{b1}} \omega_1^2\right \gg u_0 x_v x_v - x_0 x_u + \frac{x_0}{Z_0} x_u z_v - x_v z_u $	Helicopters: Elevator Single-rotor, $U_0 > 50$ fps Tandem-rotor, 40 fps $< U_0 < 120$ fps
	$\frac{1}{\pi_{b1}} \doteq -x_u - (\varepsilon - u_0 x_v) \frac{x_u}{u_0 x_v}$ $\frac{1}{\pi_{b2}} + \frac{1}{\pi_{b3}} \text{ or } 2\xi_{b1}\omega_1 \doteq -x_v$ $\frac{1}{\pi_{b2}} \frac{1}{\pi_{b3}} \text{ or } \omega_1^2 \doteq -u_0 x_v$	$u_0 \neq 0, \left[\text{for } u_0 = 0, \frac{\dot{h}(s)}{s} = \frac{-z_0}{s - z_v} \right]$ $ z_u \ll u_0 z_v $ $ x_u \ll u_0 x_v $ $x_0 = x_0 = 0$	Tandem-rotor helicopter Throttle for 40 fps $< U_0 < 120$ fps

5.12 APPROXIMATE MODAL RESPONSE RATIOS

The ways in which the various degrees of freedom enter into the total motion corresponding to a given dynamic mode can most simply be studied by considering the modal response ratios. We have already used these in the time vector diagrams for the specific examples of this chapter, but now we generalize to obtain the more interesting approximate literal relationships for conventional airplanes. As noted in Chapter 2, the modal response ratios can be expressed using any one of the n cofactor sets (for n degrees of freedom) of the characteristic determinant, i.e., denoting two of the n degrees of freedom as α_i, α_j :

$$\left(\frac{\alpha_i}{\alpha_j} \right) = (-1)^{i-j} \left(\frac{\Delta_{ki}(s)}{\Delta_{kj}(s)} \right)_{s=-q_i} \quad (5-48)$$

where $k = 1, 2, \dots, n$

Short Period. Applying Eq. 5-48 to the short-period modal responses we first compute the ratio u/w from the selected cofactors of the Eq. 5-3 denominator:

$$\begin{aligned} \left(\frac{u}{w} \right)_{sp} &= \left(\frac{-\Delta_{11}}{\Delta_{12}} \right)_{s=-q_{sp}} \\ &= - \frac{\begin{vmatrix} s - Z_w & -U_0 s \\ -(M_w^* s + M_w) & s(s - M_q) \end{vmatrix}}{\begin{vmatrix} -Z_u & -U_0 s \\ -M_u & s(s - M_q) \end{vmatrix}}_{s=-q_{sp}} \\ &= \left(\frac{s^2 - s(Z_w + M_q + M_w^*) - M_w + M_q Z_w}{-Z_u(s - M_q) - U_0 M_u} \right)_{s=-\zeta_{sp}\omega_{sp} + j\omega_{sp}\sqrt{1-\zeta_{sp}^2}} \end{aligned} \quad (5-49)$$

For the approximate short-period frequency and damping given by (Eqs. 5-17)

$$\begin{aligned}\omega_{sp}^2 & \doteq -M_{\alpha} + M_Q Z_W \\ 2\zeta_{sp}\omega_{sp} & \doteq -(Z_W + M_Q + M_{\dot{\alpha}})\end{aligned}$$

it is obvious that the numerator of Eq. 5-49 is identically zero; i.e.,

$$\left(\frac{u}{w}\right)_{sp} = 0 \quad (5-50)$$

This is the classical statement of the conditions of validity for the short-period approximation. It is, in fact, taken as the starting point, based on flight test observations, for the development of the approximate two-degree-of-freedom short-period equations given previously (Eqs. 5-14).

From the characteristic determinant of the short-period equations we can now conveniently compute the ratio θ/w from either of the expressions:

$$\left(\frac{\theta}{w}\right)_{sp} \doteq \left(\frac{s - Z_W}{U_0 s}\right)_{s=-q_{sp}} \doteq \left[\frac{M_{\dot{W}}s + M_W}{s(s - M_Q)}\right]_{s=-q_{sp}}$$

Using the first, and converting to angle of attack, $\alpha \equiv w/U_0$,

$$\left(\frac{\theta}{\alpha}\right)_{sp} \doteq \left(\frac{s - Z_W}{s}\right)_{s=-q_{sp}} \doteq \frac{-(\zeta\omega)_{sp} - Z_W + j\omega_{sp}\sqrt{1-\zeta_{sp}^2}}{-(\zeta\omega)_{sp} + j\omega_{sp}\sqrt{1-\zeta_{sp}^2}} \quad (5-51)$$

The magnitude of the modal response ratio, which is the square root of the squared sums of the real and imaginary parts, can be simplified by substituting the approximate expressions for ω_{sp}^2 and $2(\zeta\omega)_{sp}$ (Eqs. 5-17) to yield

$$\left|\frac{\theta}{\alpha}\right|_{sp} \doteq \left[1 + \frac{Z_W(-M_{\dot{\alpha}} - M_Q)}{-M_{\alpha} + M_Q Z_W}\right]^{1/2} \doteq \left[\frac{-M_{\alpha} - M_{\dot{\alpha}} Z_W}{-M_{\alpha} + M_Q Z_W}\right]^{1/2} \quad (5-52)$$

The phase angle of the modal response ratio can be written as the difference between the numerator lead and the denominator lag contributions; and

these can be combined via the identity

$$\tan^{-1} x \pm \tan^{-1} y = \tan^{-1} \frac{(x \pm y)}{(1 \mp xy)}$$

to give

$$\angle \left(\frac{\theta}{\alpha} \right)_{sp} = \tan^{-1} \frac{\sqrt{1 - \zeta_{sp}^2}}{\zeta_{sp} + \frac{\omega_{sp}}{Z_w}} \quad (5-53)$$

For the usual $\zeta_{sp} \ll \omega_{sp}/Z_w$ this further reduces to

$$\angle \left(\frac{\theta}{\alpha} \right)_{sp} = \tan^{-1} \frac{Z_w}{\omega_{sp}} \sqrt{1 - \zeta_{sp}^2}$$

In terms of the flight path angle, $\gamma \equiv \theta - \alpha$, Eq. 5-51 can be expanded to

$$\left(\frac{\gamma}{\alpha} \right)_{sp} = \left(\frac{-Z_w}{s} \right)_{s=-q_{sp}} = \frac{-Z_w}{-\zeta_{sp}\omega_{sp} + j\omega_{sp}\sqrt{1 - \zeta_{sp}^2}} \quad (5-55)$$

whereby

$$\begin{aligned} \left| \frac{\gamma}{\alpha} \right|_{sp} &= \frac{-Z_w}{\omega_{sp}} \\ \angle \left(\frac{\gamma}{\alpha} \right)_{sp} &= -\tan^{-1} \frac{\omega_{sp}\sqrt{1 - \zeta_{sp}^2}}{-\zeta_{sp}\omega_{sp}} = \tan^{-1} \frac{\sqrt{1 - \zeta_{sp}^2}}{\zeta_{sp}} - 180^\circ \end{aligned} \quad (5-56)$$

Notice that for small ζ_{sp} , Eq. 5-55 becomes

$$\begin{aligned} -Z_w \alpha_{sp} &\doteq j\omega_{sp} \gamma_{sp} = \dot{\gamma}_{sp} \\ -Z_w \alpha_{sp} &\doteq U_0 \dot{\gamma}_{sp} = \dot{h}_{sp} \end{aligned} \quad (5-57)$$

This is simply the Z equation (5-1) with u perturbations neglected.

Accordingly, typical short-period motions for $-M_\alpha$ reasonably large involve $|\theta|$ approximately equal to but somewhat smaller than $|\alpha|$; θ lagging α (because Z_w is invariably negative) by an angle whose tangent is given by $-Z_w \sqrt{1 - \zeta_{sp}^2} / \omega_{sp}$; $|\gamma/\alpha|$ proportional to part of the same quantity, $-Z_w/\omega_{sp}$, and γ lagging α by somewhat more than 90° (the γ vector lies in the third quadrant).

Phugoid. From the complete denominator of Eq. 5-3 the phugoid modal response ratio, $(u/w)_p$, is most simply evaluated in literal terms using the expression

$$\begin{aligned} \left(\frac{u}{w}\right)_p &= \left(\frac{-\Delta_{31}}{\Delta_{32}}\right)_{s=-q_p} = - \frac{\begin{vmatrix} -X_w & g \\ s-Z_w & -U_0 s \end{vmatrix}_{s=-q_p}}{\begin{vmatrix} s-X_u & g \\ -Z_u & -U_0 s \end{vmatrix}_{s=-q_p}} \\ &= \left[\frac{s(X_\alpha - g) + gZ_w}{U_0 \left(s^2 - X_u s - \frac{g}{U_0} Z_u \right)} \right]_{s=-q_p} \end{aligned} \quad (5-58)$$

For $s = -\zeta_p \omega_p + j\omega_p \sqrt{1 - \zeta_p^2}$,

$$\left(\frac{u}{w}\right)_p = \frac{(X_\alpha - g)(-\zeta_p \omega_p + j\omega_p \sqrt{1 - \zeta_p^2}) + gZ_w}{U_0 \left[2\zeta_p^2 \omega_p^2 - \omega_p^2 - 2j\zeta_p \omega_p^2 \sqrt{1 - \zeta_p^2} - X_u(-\zeta_p \omega_p + j\omega_p \sqrt{1 - \zeta_p^2}) - \frac{g}{U_0} Z_u \right]} \quad (5-59)$$

where (Table 5-5)

$$\omega_p^2 \doteq \frac{g(M_w Z_u - M_u Z_w)}{M_q Z_w - M_\alpha} \quad ; \quad 2\zeta_p \omega_p \doteq -X_u - \frac{M_u(X_\alpha - g)}{M_q Z_w - M_\alpha}$$

Substituting these relationships into Eq. 5-59,

$$\left(\frac{u}{w}\right)_p \doteq \frac{(X_\alpha - g)(-\zeta_p \omega_p + j\omega_p \sqrt{1 - \zeta_p^2}) + gZ_w}{\frac{U_0}{M_q Z_w - M_\alpha} \left[M_u(X_\alpha - g)(-\zeta_p \omega_p + j\omega_p \sqrt{1 - \zeta_p^2}) + gZ_w \left(M_u - \frac{M_q Z_u}{U_0} \right) \right]} \quad (5-60)$$

Considering that the Z_w terms generally dominate both numerator and denominator,

$$\left(\frac{u}{w}\right)_p \doteq \frac{-U_0 M_w + M_q Z_w}{U_0 M_u - M_q Z_u} \quad (5-61)$$

However, assuming $|M_q Z_u| \ll |U_0 M_u|$ and $|M_q Z_w| \ll |U_0 M_w|$ produce the same result for either Eq. 5-60 or 5-61, namely,

$$\left(\frac{u}{w}\right)_p = \frac{-M_w}{M_u} \quad \text{or} \quad (M_u u + M_w w)_p = 0 \quad (5-62)$$

The last equation corresponds to that assumed for the three-degree-of-freedom phugoid equations of motion (Eqs. 5-20), i.e., a balance of only the static moments. Accordingly, we can now specify more precisely, via Eq. 5-60, the conditions under which these equations are valid. For $M_u = 0$, Eq. 5-62 shows the classical result, $w = 0$; i.e., constant angle of attack, α , for the phugoid. The $w = 0$ result is, in fact, given exactly by Eq. 5-58 when the classical results for the phugoid undamped natural frequency and damping (Eqs. 5-28, 5-29) are inserted.

Proceeding to another modal response ratio, using now the generally valid three-degree-of-freedom phugoid equations of motion (Eq. 5-20) we compute

$$\begin{aligned} \left(\frac{\theta}{u}\right)_p &= \left(\frac{\Delta_{23}}{\Delta_{21}}\right)_{s=-q_p} = \frac{\begin{vmatrix} s - X_u & -X_w \\ -M_u & -M_w \end{vmatrix}_{s=-q_p}}{\begin{vmatrix} -X_w & g \\ -M_w & 0 \end{vmatrix}_{s=-q_p}} \\ &= -\left[\frac{s - X_u + \frac{X_w M_u}{M_w}}{g}\right]_{s=-\zeta_p \omega_p + j\omega_p \sqrt{1-\zeta_p^2}} \end{aligned} \quad (5-63)$$

For the approximate factors of Eq. 5-24,

$$-X_u + \frac{X_w M_u}{M_w} = 2\zeta_p \omega_p + \frac{g M_u}{M_\alpha}$$

and

$$\left(\frac{-\theta}{u}\right)_p = \frac{\zeta_p \omega_p + \frac{g M_u}{M_\alpha} + j\omega_p \sqrt{1-\zeta_p^2}}{g} \quad (5-64)$$

The absolute magnitude, using the Eq. 5-24 approximations, is given by

$$\left| \frac{\theta}{u} \right|_p^2 = \frac{\frac{g}{U_0} \frac{M_u}{M_w} \left(-X_u + Z_w + \frac{X_w M_u}{M_w} \right) - \frac{g}{U_0} Z_u}{g^2} \quad (5-65)$$

Generally, Z_w will be the dominant term of those in the parentheses and for such circumstances

$$\left| \frac{\theta}{u} \right|_p^2 \doteq \frac{\frac{-g}{U_0} \left(Z_u - \frac{M_u Z_w}{M_w} \right)}{g^2} \doteq \frac{\omega_p^2}{g^2} \quad (5-66)$$

$$\left| \frac{\theta}{u} \right|_p \doteq \frac{\omega_p}{g} \quad \text{or} \quad |g\theta|_p \doteq |\dot{u}|_p$$

The phase angle from Eq. 5-64 is

$$\angle \left(\frac{-\theta}{u} \right)_p = \tan^{-1} \frac{\omega_p \sqrt{1 - \zeta_p^2}}{\zeta_p \omega_p + \frac{g M_u}{M_\alpha}} \quad (5-67)$$

and for the usual small values of ζ_p and $g M_u / \omega_p M_\alpha$ it approaches 90° . Because there is also roughly a 90° rotation between u and \dot{u} , θ is nearly aligned with $-u$, and in view of this and Eq. 5-66,

$$(\dot{u} + g\theta)_p \doteq 0 \quad (5-68)$$

This result is clearly evident from Eq. 5-63 by considering the s term to dominate the numerator.

For $M_u = 0$ we can multiply Eq. 5-68 by U and substitute \dot{h} for $U\dot{u}$ (since $w \doteq 0$), whereby

$$U\dot{u} + g\dot{h} \doteq 0 \quad (5-69)$$

Now, integrating, $\frac{U^2}{2} + gh \doteq \text{const}$

which shows us that, very roughly, the sum of kinetic plus potential

energies remains constant during the phugoid motion. This is again a "classical" result, first given by Lanchester. Another interesting result follows from Eq. 5-69 if we recognize (Eq. 5-30) that $\frac{g}{U_0} \doteq \frac{\omega_p}{\sqrt{2}}$ and that $\ddot{h}_p \doteq j\omega_p \dot{h}_p$; then

$$\text{or} \quad -\dot{u} \doteq \frac{g}{U_0} \dot{h} \doteq \frac{\ddot{h}}{j\sqrt{2}}$$

$$\ddot{h} + j\sqrt{2} \dot{u} \doteq 0$$

Integrating twice and neglecting the first constant of integration (it leads to a time variation inappropriate to the assumed trim conditions),

$$h + j\sqrt{2} x \doteq \text{const}$$

or, considering absolute values,

$$h^2 + 2x^2 \doteq \text{const} \quad (5-70)$$

Equation 5-70 shows that, as seen by an observer flying in steady formation with the airplane, the phugoid motions have an elliptical pattern with an amplitude in h about 1.4 times that in x . Furthermore, for positive climb rate, \dot{h} , \dot{u} is negative (Eq. 5-69) and x , 180° out of phase with \dot{u} , is positive; the motion around the ellipse is therefore counter-clockwise, with \dot{h} and x being in phase. Finally, for positive \dot{h} and negative \dot{u} , as above, θ is positive (Eq. 5-68), therefore in phase with \dot{h} and x , and also aligned with the path (since $w \doteq 0$). The complete picture sketched below (Fig. 5-12) is consistent with the time vectors shown in Fig. 5-4b.

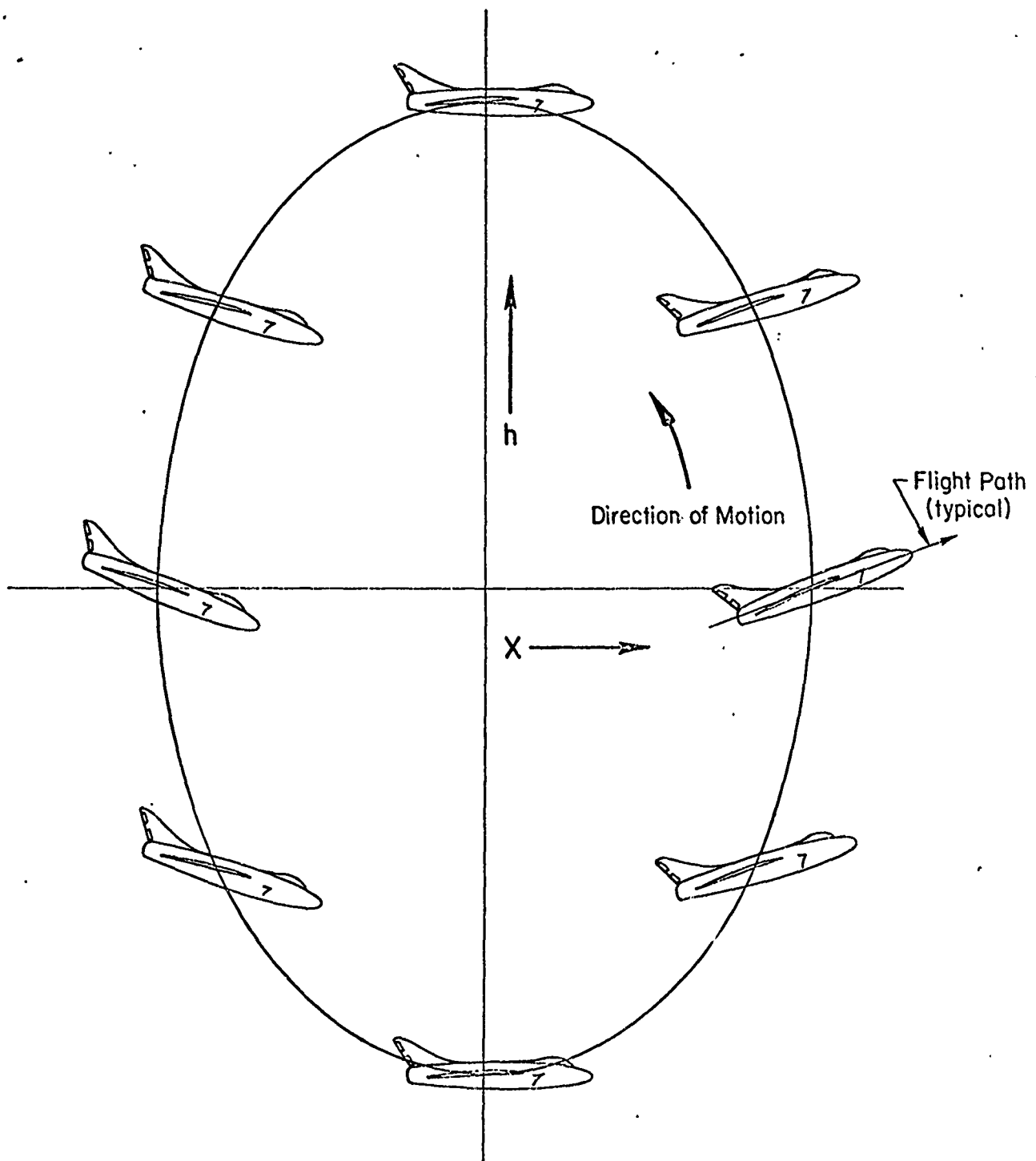


Fig. 5-12. Phugoid Perturbations in Space

CHAPTER 6

LATERAL DYNAMICS

6.1 INTRODUCTION

The treatment of the vehicle's lateral dynamic properties given in this chapter closely follows the form and content of the preceding chapter on longitudinal dynamics. The first of the succeeding articles in this chapter recapitulates the lateral equations of motion as commonly used; presents the polynomial forms of the more important control-input transfer functions; and develops an appreciation for the transfer functions and responses with numerical examples. Based on the physical insights thus afforded, we then develop further-simplified sets of equations which apply to the individual modes of motion appropriate for conventional aircraft; this is followed by similar considerations of VTOL aircraft in hover. Then we present the complete gust-input transfer functions in polynomial form and extend our numerical examples to cover these. Approximate literal expressions for the various transfer function factors are given next; their relation to the simplified equations are established and their implications as concerns the direct influence of the dominant stability derivatives on the important poles and zeros are drawn. Finally, we develop some important modal response ratios in literal form and discuss their implications.

6.2 RECAPITULATION AND FURTHER SIMPLIFICATION OF THE LATERAL EQUATIONS OF MOTION

Equations 4-98 are usually simplified according to the following assumptions:

Assumption 11. In the steady flight condition, the flight path of the airplane is assumed to be horizontal, $\gamma_0 = 0$.

This assumption has already been invoked in the simplification of the longitudinal equations (5-2) and is repeated here for convenience.

Assumption 12. It is assumed that $Y_v = Y_p = Y_r = L_v' = N_v' = 0$.

Generally speaking, this is a good assumption for most configurations, especially when only control inputs are being considered. Notice, however, that for gust inputs the assumption eliminates completely the p_g term in the Y equation, and requires $|Y_v s| \ll Y_v$ in addition to the more readily evaluated $|Y_v| \ll 1$. Also, in the N equation N_{r_g}'/U_0 is retained while N_v' is dropped, whereas they may both be of the same magnitude. In all cases the validity of the individual assumptions should be checked for the frequency range of interest, once the derivatives are known, by the process described on page 5-3 in connection with Assumption 10. Despite such reservations the approximations generally introduce only small errors, and are in accord with common flight control practice.

With these assumptions the lateral equations of motion, referenced to stability axes (Eq. 4-98) and conventionally written in terms of $\beta \equiv v/U_0$ rather than v ,[†] become:

$$\begin{aligned} (s - Y_v)\beta - \frac{g}{U_0} \frac{p}{s} + r &= Y_\delta^* \delta - Y_v \beta_g \\ -L_\beta' \beta + (s - L_p')p - L_r' r &= L_\delta' \delta - [L_\beta' + (L_r')_g s] \beta_g - L_p' p_g \quad (6-1) \\ -N_\beta' \beta - N_p' p + (s - N_r')r &= N_\delta' \delta - [N_\beta' + (N_r')_g s] \beta_g - N_p' p_g \end{aligned}$$

In terms of the unprimed derivatives, the equations (4-91) can also be written as:

$$\begin{aligned} (s - Y_v)\beta - \frac{g}{U_0} \frac{p}{s} + r &= Y_\delta^* \delta - Y_v \beta_g \\ -L_\beta \beta + (s - L_p)p - \left(\frac{I_{xz}}{I_x} s + L_r \right) r &= L_\delta \delta - L_\beta \beta_g - L_p p_g \quad (6-2) \\ -N_\beta \beta - \left(\frac{I_{xz}}{I_z} s + N_p \right) p + (s - N_r)r &= N_\delta \delta - (N_\beta + N_r s) \beta_g - N_p p_g \end{aligned}$$

The auxiliary relationships needed to convert the motion quantities to those usually sensed by flight instruments are (from Eq. 4-96 and the Y inertial terms of Eq. 6-1):

$$\begin{aligned} p &= s\phi \\ r &= s\psi \\ a_{y.c.g.} &= U_0 \dot{\beta} - g(p/s) + U_0 r = \dot{v} - g\phi + U_0 r \end{aligned} \quad (6-3)$$

[†]To do this we define $Y_\delta^* \equiv Y_\delta/U_0$ and note that $L_v' v = L_\beta' \beta$, $N_v' v = N_\beta' \beta$.

6.3 CONTROL-INPUT TRANSFER FUNCTIONS

The control-input transfer functions are easily obtained from the equations of motion as previously discussed and illustrated. For example, the β -output to δ -input transfer function can be written directly from Eq. 6-2 (i.e., assuming no gust inputs) as:

$$\frac{\beta(s)}{\delta(s)} = \frac{\begin{vmatrix} Y_{\delta}^* & \frac{-g}{U_0} & 1 \\ I_{\delta} & (s - I_p)s & -\left(\frac{I_{xz}}{I_x}s + L_r\right) \\ N_{\delta} & -\left(\frac{I_{xz}}{I_z}s + N_p\right)s & s - N_r \end{vmatrix}}{\begin{vmatrix} s - Y_v & \frac{-g}{U_0} & 1 \\ -Y_{\beta} & (s - I_p)s & -\left(\frac{I_{xz}}{I_x}s + L_r\right) \\ -N_{\beta} & -\left(\frac{I_{xz}}{I_z}s + N_p\right)s & s - N_r \end{vmatrix}} \quad (6-4)$$

Expanding the determinants gives the transfer function as a ratio of polynomials in s , where the denominator polynomial, $\Delta(s)$, is common to all transfer functions, and its factors determine the characteristic frequencies and dampings, or time constants, of the individual modes of motion. The numerator polynomials vary with the output quantity of interest. The polynomial forms of the primary lateral transfer functions are given below, together with their usual factored forms:

$$\begin{aligned} \frac{\beta(s)}{\delta(s)} &= \frac{N_{\delta}^{\beta}(s)}{\Delta_{lat}} = \frac{A_{\beta}s^3 + B_{\beta}s^2 + C_{\beta}s + D_{\beta}}{\Delta_{lat}} \\ &= \frac{A_{\beta}(s + 1/T_{\beta 1})(s + 1/T_{\beta 2})(s + 1/T_{\beta 3})}{\Delta_{lat}} \end{aligned} \quad (6-5)$$

$$\begin{aligned}\frac{\phi(s)}{\delta(s)} &= \frac{N_{\delta}^{\phi}(s)}{\Delta_{lat}} = \frac{A_{\phi}s^2 + B_{\phi}s + C_{\phi}}{\Delta_{lat}} \\ &= \frac{A_{\phi}(s^2 + 2\zeta_{\phi}\omega_{\phi}s + \omega_{\phi}^2)}{\Delta_{lat}}\end{aligned}\quad (6-6)$$

$$\begin{aligned}\frac{r(s)}{\delta(s)} &= \frac{N_{\delta}^r(s)}{\Delta_{lat}} = \frac{A_rs^3 + B_rs^2 + C_rs + D_r}{\Delta_{lat}} \\ &= \frac{A_r \begin{cases} (s + 1/T_{r1})(s^2 + 2\zeta_r\omega_rs + \omega_r^2) \\ \text{or} \\ (s + 1/T_{r1})(s + 1/T_{r2})(s + 1/T_{r3}) \end{cases}}{\Delta_{lat}}\end{aligned}\quad (6-7)$$

$$\begin{aligned}\frac{a_{y_{c.g.}}(s)}{\delta(s)} &= \frac{N_{\delta}^{a_{y_{c.g.}}}(s)}{\Delta_{lat}} = \frac{A_{ay}s^4 + B_{ay}s^3 + C_{ay}s^2 + D_{ay}s + E_{ay}}{\Delta_{lat}} \\ &= \frac{A_{ay}(s + 1/T_{ay1})(s + 1/T_{ay2})(s + 1/T_{ay3})(s + 1/T_{ay4})}{\Delta_{lat}}\end{aligned}\quad (6-8)$$

$$\text{where } \Delta_{lat} = As^4 + Bs^3 + Cs^2 + Ds + E$$

$$= A \begin{cases} (s + 1/T_s)(s + 1/T_r) \\ \text{or} \\ (s^2 + 2\zeta_1\omega_1s + \omega_1^2) \end{cases} (s^2 + 2\zeta_d\omega_d s + \omega_d^2) \quad (6-9)$$

An additional "a" or "r" subscript is often used on numerator quantities to specify aileron or rudder, respectively.

The literal expressions for the various A, B, C, etc., coefficients of Eqs. 6-5 through 6-9 are given in Table 6-1. There the coefficient expressions are in terms of unprimed derivatives, but can easily be

TABLE 6-1
LATERAL CONTROL-INPUT TRANSFER FUNCTION COEFFICIENTS

A	B	C	D	E
Δ	$1 - \frac{I_{xz}^2}{I_x I_z}$	$N_p + I_p (x_v + N_r)$ $+ N_p \left(\frac{I_{xz}}{I_x} x_v - I_r \right)$ $+ x_v \left(\frac{I_{xz}}{I_z} I_r + N_r \right) + \frac{I_{xz}}{I_z} I_p$	$-N_p I_p + x_v (N_p I_r - I_p N_r)$ $+ N_p I_p - \frac{I_{xz}}{U_0} \left(I_p + \frac{I_{xz}}{I_x} N_p \right)$	$\frac{I_{xz}}{U_0} (I_p N_r - N_p I_r)$
x_0^p	$-x_0^p \left[I_p + N_r + \frac{I_{xz}}{I_x} N_p + \frac{I_{xz}}{I_z} I_r \right]$ $- \frac{I_{xz}}{I_x} I_0 - N_0$	$y_0^p (I_p N_r - N_p I_r) + N_0 I_p$ $- I_0 N_p + \frac{I_{xz}}{U_0} \left(I_0 + \frac{I_{xz}}{I_x} N_0 \right)$	$\frac{I_{xz}}{U_0} (N_0 I_r - I_0 N_r)$	
N_0^p	$x_0^p \left(I_p + \frac{I_{xz}}{I_x} N_p \right) - I_0 (N_r + x_v)$ $+ N_0 \left(I_r - \frac{I_{xz}}{I_x} x_v \right)$	$y_0^p (I_p N_p - N_p I_p)$ $+ I_0 (x_v N_r + N_p)$ $- N_0 (I_p + x_v I_r)$		
N_0^r	$x_0^p \left(N_p + \frac{I_{xz}}{I_z} I_p \right)$ $+ I_0 \left(N_p - \frac{I_{xz}}{I_z} x_v \right)$ $- N_0 (x_v + I_p)$	$y_0^p (I_p N_p - N_p I_p)$ $- I_0 x_v N_p + N_0 x_v I_p$	$\frac{I_{xz}}{U_0} (I_0 N_p - N_0 I_p)$	
$N_0^{y/c.s.}$	$-x_0^p \left(I_p + N_r + \frac{I_{xz}}{I_x} N_p + \frac{I_{xz}}{I_z} I_r \right)$ $- \frac{I_{xz}}{I_x} I_0 - N_0$	$y_0^p \left(N_p + I_p N_r - N_p I_r + \frac{I_{xz}}{I_z} I_p \right)$ $- U_0 x_v \left(\frac{I_{xz}}{I_z} I_0 + N_0 \right)$	$x_0^p \left[N_p I_p - \frac{I_{xz}}{U_0} \right]$ $- N_p \left(I_p + \frac{I_{xz}}{U_0 I_x} \right)$ $+ U_0 x_v \left[I_0 \left(\frac{I_{xz}}{U_0} - N_p \right) + N_0 \left(\frac{I_{xz}}{I_x} + I_p \right) \right]$	$\frac{I_{xz}}{U_0} (I_p N_r - N_p I_r)$ $+ x_v (N_0 I_r - I_0 N_r)$

Note: To convert to primed derivatives, eliminate all I_{xz} terms and substitute L' and N' for L and N , respectively.

converted to prime derivatives by the simple expedient of eliminating all I_{xz} terms and priming the L and N derivatives; the compactness thus achieved is self-evident. While either the primed or unprimed form may be used, as convenient, to obtain the polynomial numerator and denominator expressions and eventually the factors, the transfer function gain is properly computed only when the same derivative forms are used in both numerator and denominator. This follows directly from a consideration of the A coefficients given in Table 6-1. For example, the high frequency gain of the β transfer function is given by:

$$\frac{\beta(s)}{\delta(s)} \rightarrow \frac{A_\beta s^3}{As^4} = \frac{A_\beta}{As} = \frac{Y_\delta^* \left[1 - \frac{I_{xz}^2}{I_x I_z} \right]}{\left[1 - \frac{I_{xz}^2}{I_x I_z} \right] s} = \frac{Y_\delta^*}{s} \quad (6-10)$$

If now the prime derivatives were used (i.e., $I_{xz} = 0$) for both numerator and denominator, the result would be the same. However, mixing the two forms would produce

or

$$\frac{\beta(s)}{\delta(s)} \rightarrow \frac{A_\beta}{A' s} = \frac{Y_\delta^* \left[1 - \frac{I_{xz}^2}{I_x I_z} \right]}{s}$$

$$\frac{\beta(s)}{\delta(s)} \rightarrow \frac{A'_\beta}{As} = \frac{Y_\delta^*}{\left[1 - \frac{I_{xz}^2}{I_x I_z} \right] s}$$

which are both incorrect.

6.4 EXAMPLE TRANSFER FUNCTIONS, BODE FORMS, AND TIME RESPONSES FOR A CONVENTIONAL AIRPLANE

For the example conventional airplane of Chapter 5 (see Fig. 5-1) the lateral characteristics are given by:

Altitude (ft).....	20,000
Weight (lb)	30,500
Mach number	0.638
True airspeed (ft/sec)	660

Y_V	-0.0829	N_β	3.55
Y_{δ_a}	0	N_p	-0.0025
$Y_{\delta_r}^*$	0.0116	N_r	-0.0957
L_p	-4.770	N_{δ_a}	-0.615
L_p	-1.695	N_{δ_r}	-1.383
L_r	0.1776	I_{xz}/I_x	0.0663
L_{δ_a}	27.25	I_{xz}/I_z	0.0370
L_{δ_r}	0.666		

The corresponding primed derivatives are:

L_p'	-4.546	N_β'	3.382
L_p'	-1.699	N_p'	-0.0654
L_r'	0.1717	N_r'	-0.0893
L_{δ_a}'	27.276	N_{δ_a}'	0.3952
L_{δ_r}'	0.5758	N_{δ_r}'	-1.362

Substituting these data into the Table 6-1 forms and factoring the resulting polynomials yields the following transfer functions ($a_{y,c.g.}/\delta_a$ is not given because of its minor importance):

For aileron inputs

$$\frac{\beta(s)}{\delta_a(s)} = -14.38 \cdot \frac{\left(\frac{s}{0.0495} + 1\right)\left(\frac{s}{-6.250} + 1\right)}{\left(\frac{s}{-0.001355} + 1\right)\left(\frac{s}{1.777} + 1\right)\left[\frac{s^2}{(1.8775)^2} + \frac{2(0.0243)}{1.8775}s + 1\right]} \quad (6-11)$$

$$\frac{n(s)}{\delta_a(s)} = -11070 \cdot \frac{\left[\frac{s^2}{(1.859)^2} + \frac{2(0.0047)}{1.859}s + 1\right]}{\left(\frac{s}{1.65} + 1\right)\left(\frac{s}{2.659} + 1\right)\left[\frac{s^2}{(2.659)^2} + \frac{2(-0.827)}{2.659}s + 1\right]} \quad (6-12)$$

$$\frac{r(s)}{\delta_a(s)} = -543.7 \cdot \frac{\left(\frac{s}{1.65} + 1\right)\left[\frac{s^2}{(2.659)^2} + \frac{2(-0.827)}{2.659}s + 1\right]}{\left(\frac{s}{-0.001355} + 1\right)\left(\frac{s}{1.777} + 1\right)\left[\frac{s^2}{(1.8775)^2} + \frac{2(0.0243)}{1.8775}s + 1\right]} \quad (6-13)$$

For rudder inputs

$$\frac{\beta(s)}{\delta_r(s)} = 1.049 \frac{\left(\frac{s}{-0.00374} + 1\right)\left(\frac{s}{1.75} + 1\right)\left(\frac{s}{117.25} + 1\right)}{\left(\frac{s}{-0.001355} + 1\right)\left(\frac{s}{1.777} + 1\right)\left[\frac{s^2}{(1.8775)^2} + \frac{2(0.0243)}{1.8775}s + 1\right]} \quad (6-14)$$

$$\frac{\varphi(s)}{\delta_r(s)} = 500 \frac{\left(\frac{s}{2.561} + 1\right)\left(\frac{s}{-2.885} + 1\right)}{\left(\frac{s}{1.7767} + 1\right)\left[\frac{s^2}{(0.293)^2} + \frac{2(0.00563)}{0.293}s + 1\right]} \quad (6-15)$$

$$\frac{r(s)}{\delta_r(s)} = 24.35 \frac{\left(\frac{s}{1.7767} + 1\right)\left[\frac{s^2}{(0.293)^2} + \frac{2(0.00563)}{0.293}s + 1\right]}{\left(\frac{s}{0.000725} + 1\right)\left(\frac{s}{1.705} + 1\right)\left(\frac{s}{2.551} + 1\right)\left(\frac{-s}{2.468} + 1\right)} \quad (6-16)$$

$$\frac{a_{y.c.g.}(s)}{\delta_r(s)} = 7.00 \frac{\left(\frac{s}{0.000725} + 1\right)\left(\frac{s}{1.705} + 1\right)\left(\frac{s}{2.551} + 1\right)\left(\frac{-s}{2.468} + 1\right)}{\left(\frac{s}{1.7767} + 1\right)\left[\frac{s^2}{(0.293)^2} + \frac{2(0.00563)}{0.293}s + 1\right]} \quad (6-17)$$

The roots of the denominator show that the lateral motions consist of three modes:

- A relatively lightly damped oscillatory mode called the "dutch roll"
- A first-order divergent mode of relatively long time constant called the "spiral" mode
- A first-order convergent mode of relatively short time constant called the "roll subsidence" mode

The subscript notation used in Eq. 6-9 and in subsequent tables and figures reflects the above nomenclature. The general aspects of these modes will be discussed in more detail later.

Figures 6-1 and 6-2 present the $j\omega$ -Bode plots of the transfer functions, including amplitude and phase asymptotes. Using these as representative of response transforms to unit impulse inputs, as in Chapter 5, we can draw certain conclusions concerning the appearance of the various modes in the airplane's transient response.

Consider first the dutch roll mode. For all transfer functions but ϕ/δ_a the dutch roll peak is a dominant characteristic, indicating that this oscillation will be a major component of the weighting function responses. For the exception, ϕ/δ_a , the quadratic numerator nearly cancels the dutch roll denominator. Because of this dipole effect, the modal response coefficient for the dutch roll mode in the ϕ weighting function for δ_a input will be small. If the cancellation were exact, the dutch roll would disappear entirely from this rolling response. Approximate values for the dutch roll modal response ratios can also be determined using the $j\omega$ -Bode plots because ζ_d is small; therefore, a typical amplitude ratio evaluated at the dutch roll root becomes

$$\left| G[-(\zeta\omega)_d + j\omega_d \sqrt{1 - \zeta_d^2}] \right| \doteq [G(j\omega_d)]$$

Just how well this works for the present example can be seen by comparing results read from Figs. 6-1 and 6-2 with the actual modal response ratios. Thus, for rudder inputs (Fig. 6-1),

$$\begin{aligned} \beta : \phi : r &\doteq [17 : 16 : 23]_{db} \\ &\doteq [0, -1, 6]_{db} \\ &\doteq 1 : 0.89 : 2.0 \end{aligned}$$

and for aileron inputs (Fig. 6-2),

$$\begin{aligned} \beta : \phi : r &\doteq [14 : 18 : 20]_{db} \\ &\doteq [0 : 4 : 6]_{db} \\ &\doteq 1 : 1.6 : 2.0 \end{aligned}$$

The exact model response ratio is

$$\beta : \phi : r = 1 : 0.99 : 1.87$$

Making the comparison, it is seen that all the plots but ϕ/δ_a yield values which are quite comparable to the exact set. The difficulty with ϕ/δ_a again stems from the presence of the numerator quadratic. The amplitude ratio of this transfer function evaluated at the exact dutch roll root, s_d , differs considerably from the approximation based on $s_d \doteq j\omega_d$. Except for

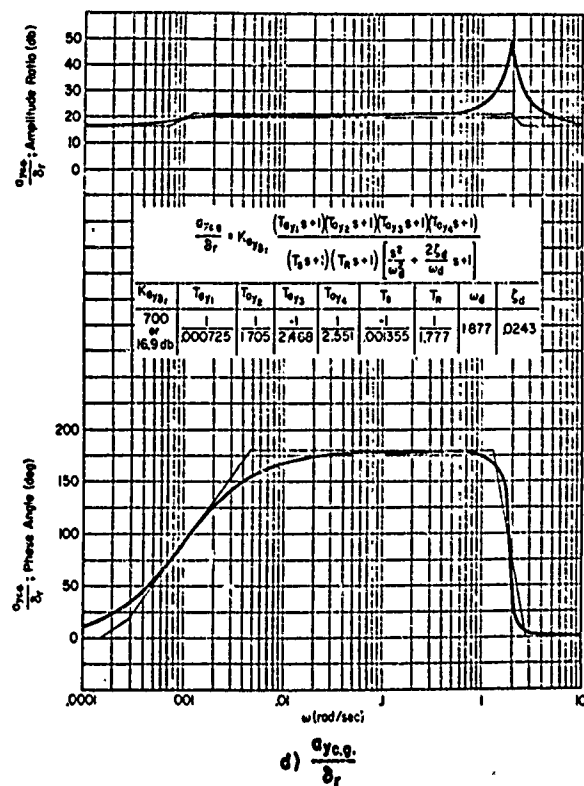
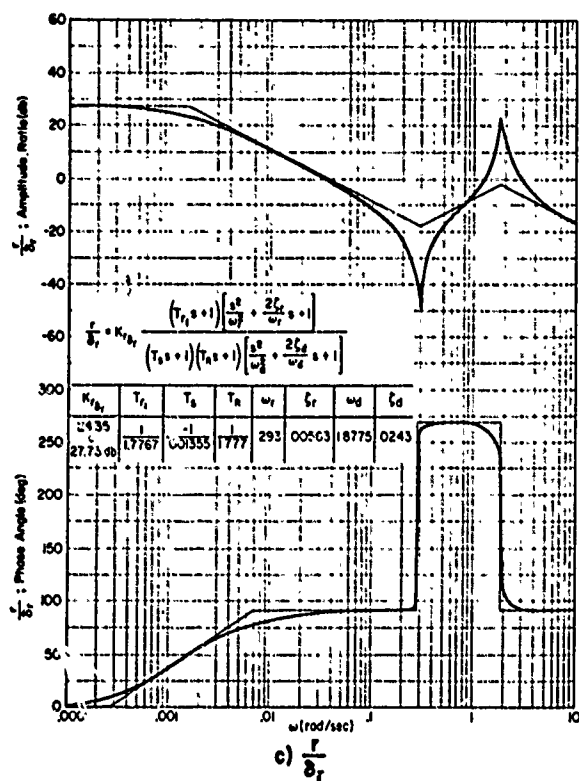
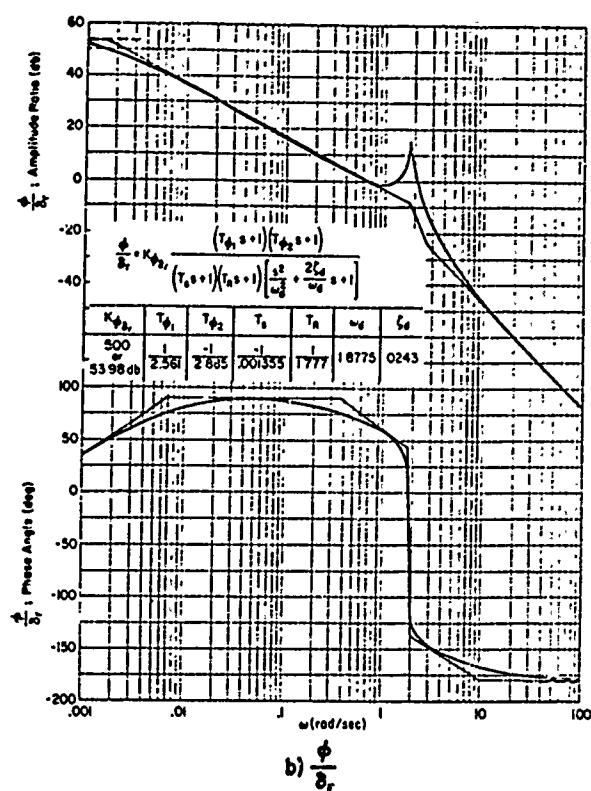
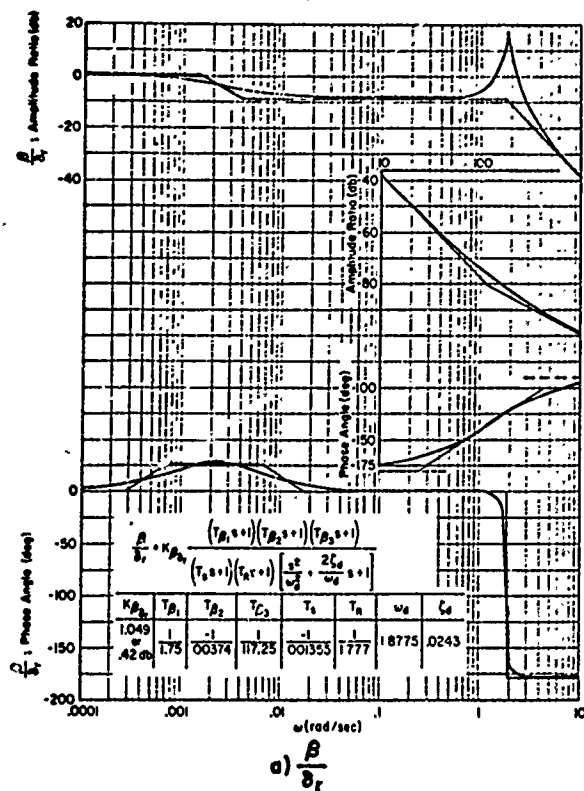
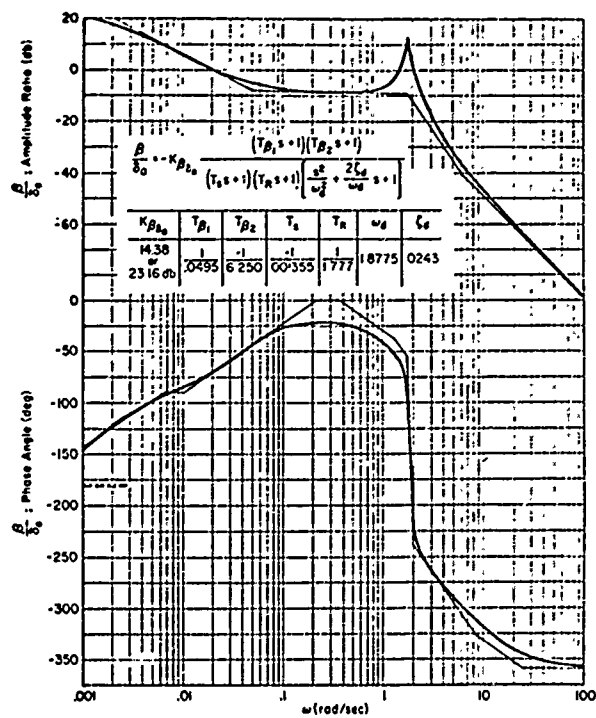
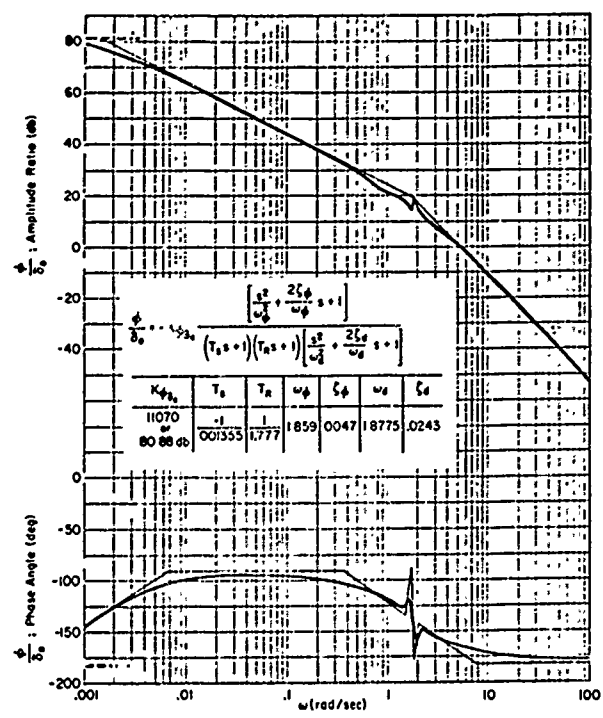


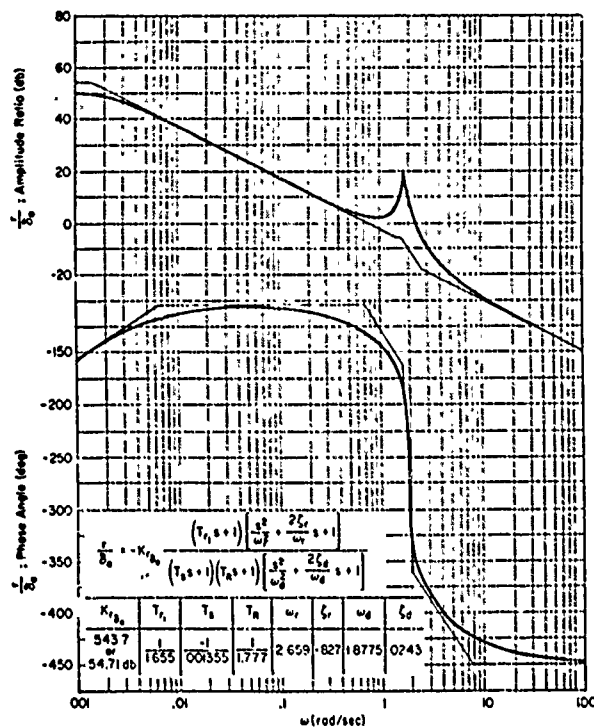
Fig. 6-1. Example Rudder-Input Bode Plots for a Conventional Airplane



a) $\frac{\beta}{\sigma_a}$



b) $\frac{\phi}{\sigma_a}$



c) $\frac{r}{\sigma_a}$

Fig. 6-2. Example Aileron-Input Bode Plots for a Conventional Airplane

this effect, the dutch roll modal response ratios computed from amplitude frequency response plots evaluated at ω_d are quite insensitive to the damping ratio, ζ_d , because its effect cancels when the response ratios are taken.

Turn now to the roll subsidence mode. For this, numerator terms in both β and r responses to rudder and r response to aileron essentially cancel the roll subsidence mode denominator. These dipole effects imply that the roll subsidence mode will be small in the β and r rudder-input and the r aileron-input weighting functions. The absence of a similar near-cancellation of the roll subsidence factor by a numerator term in the β/δ_a transfer function might, at first glance, be taken to imply that the roll subsidence mode component of the sideslip response to aileron would be substantial. Thus, we might be tempted to conclude that the relative magnitudes of the degrees of freedom occurring in a particular mode depend on whether the mode is excited by aileron or rudder. But we know from the modal response considerations presented in Section 2.5 that this cannot be so; that, in fact, the response ratios for a given mode are independent of the input. A second look at the β/δ_a and ϕ/δ_a transfer functions indicates a large difference in gains at $\omega = 1/T_R$ (when the dutch roll peaks are ignored) which results in a large $|\phi/\beta|$ computed for aileron inputs, just as the near-cancellation of β responses to rudder inputs also infers a large $|\phi/\beta|$. All of these considerations imply that the roll subsidence is small in r and β weighting functions, and that this mode is then characterized almost entirely by rolling motions. This is, of course, the origin of its name. The roll subsidence modal response ratios evaluated from the $j\omega$ -Bode plots will, in this case, be quite inaccurate if the plot itself is used because of the close proximity and dominance of the dutch roll peak. Good results can, however, be obtained if the asymptotic plot is used.

Finally, for the spiral mode the modal response ratios could be computed from the dc gains if all the other poles and zeros are far enough removed. For the aileron responses (Fig. 6-2) this condition obtains, and the modal response ratios approximated by the gain ratios,

$$\begin{aligned}\beta : \phi : r &\hat{=} (-14.38) : (-11,070) : (-543.7) \\ &\hat{=} 1 : 770 : 37.8\end{aligned}$$

correspond favorably to the exact ratios,

$$\beta : \phi : r = 1 : 756 : 36$$

The close proximity of a numerator factor to the spiral denominator term in the β/δ_r transfer functions makes the use of the gain ratios alone inaccurate for the rudder case; however, the $\phi : r$ modal response ratio computed using the rudder-input dc gains is satisfactory. The predominance of rolling and yawing in the spiral motion indicates that this mode, albeit unstable, is nonetheless nearly coordinated. Further, because of the relatively small sideslip, the $r : \phi$ ratio is approximately g/U_0 (e.g., Eq. 6-3).

Figure 6-3 presents time histories of the responses to an aileron pulse and a rudder step, which are in accord with the foregoing conclusions. Here we can see that the primary response to an aileron input is in roll angle; and that nearly constant angle is achieved in a short time, corresponding to a response time $3T_R$ of the roll subsidence mode. The spiral mode divergence is not discernible due to its extremely large time constant, 738 sec. The dutch roll excited by the aileron appears to be mostly in β and r , but the much larger scale used for the ϕ trace tends to mask its magnitude relative to β and r . The magnitudes of these three motions in the dutch roll mode are more easily seen in the time histories for a rudder step. These also show a relatively small average roll rate response, indicative of the reduced excitation of the roll subsidence mode by the rudder as compared to the aileron.

Figure 6-4 presents the time-vector diagrams, which directly indicate the relative magnitude and phasing of the free motions (phasors) and show the relative importance of each term in the equations of motion (polygons) for each mode. Again we see that β is almost nonexistent in the spiral mode, which consists therefore of coordinated banking and turning (i.e., no sideslipping) motions. For the roll subsidence, ϕ is the dominant motion parameter; and for the dutch roll, all motions are the same order of

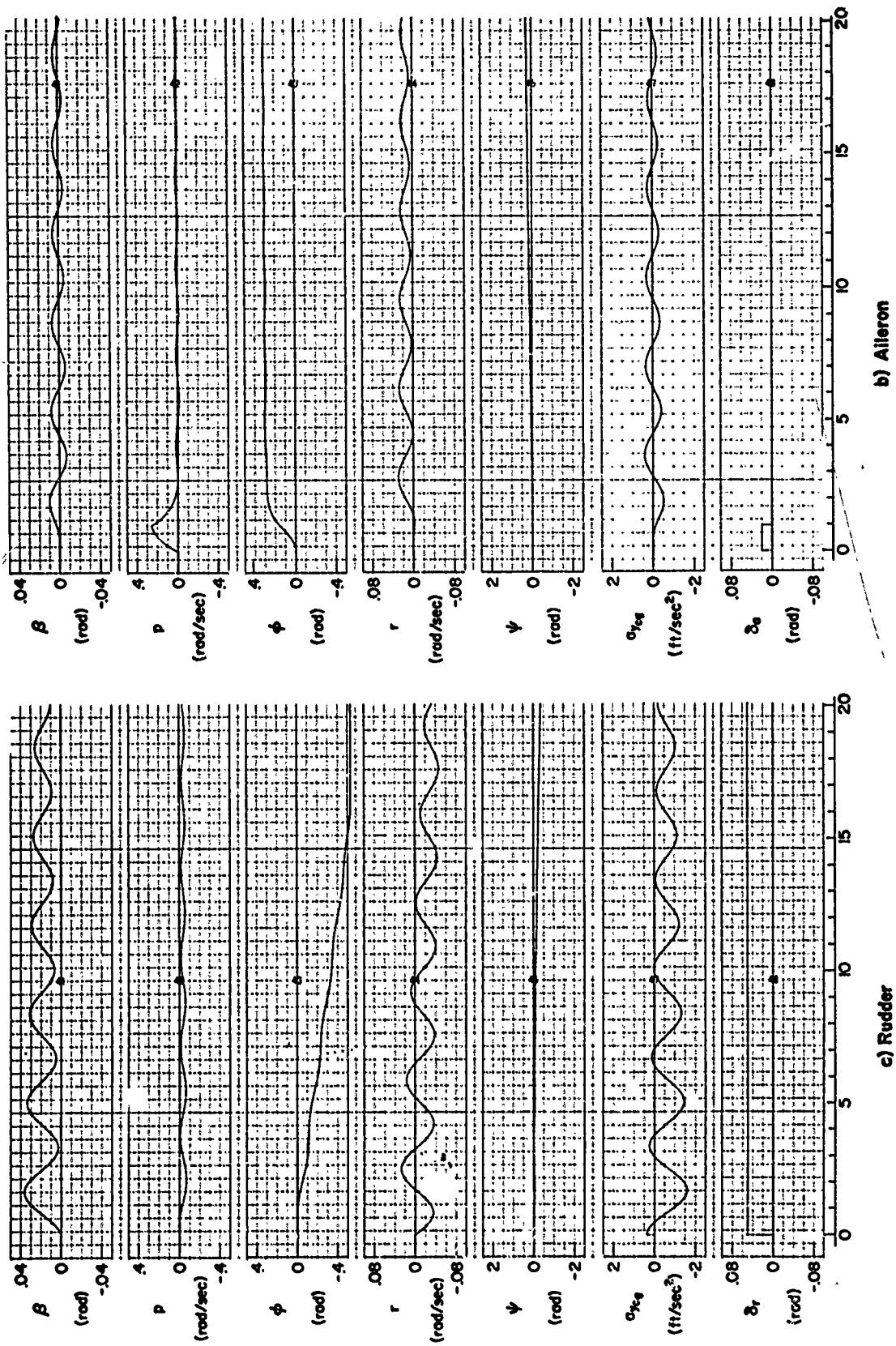


Figure 6-3. Time History of Lateral Motions to Rudder and Aileron Inputs

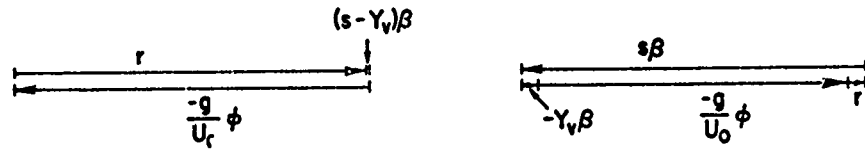
$$s = .001355$$

$$\beta : \phi : r = 1 : 756 : 36$$

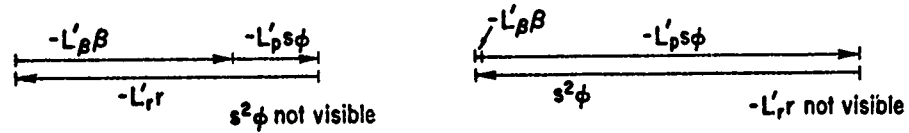
$$s = -1.777$$

$$\beta : \phi : r = 1 : -31.5 : .164$$

Side Force Equation



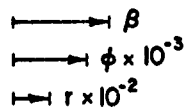
Rolling Moment Equation



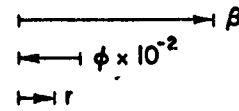
Yawing Moment Equation



Phasors



a) Spiral Mode



b) Roll Subsidence Mode

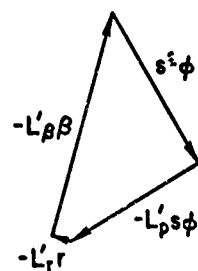
$$\zeta = .0243, \omega = 1.8775$$

$$\beta : \phi : r = 1 : .99 : 1.87$$

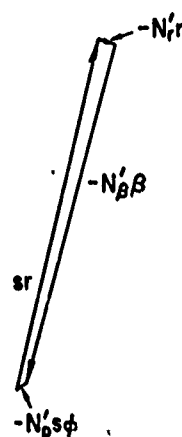
Side Force Equation



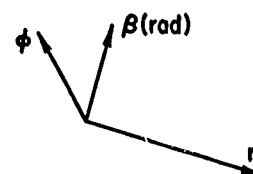
Rolling Moment Equation



Yawing Moment Equation



Phasors



c) Dutch Roll Mode

Figure 6-4. Time Vector Diagrams for the Example Conventional Airplane

magnitude. The small amount of lateral motion in the dutch roll is apparent in the approximate cancellation of the r and $s\beta$ side force components, i.e.,

$$y = \frac{U_0}{s} (\beta + \psi) = \frac{U_0}{s^2} (s\beta + r) \doteq 0$$

6.5 TWO-DEGREE-OF-FREEDOM DUTCH ROLL APPROXIMATIONS

Because the ϕ oscillations occurring in the dutch roll mode can be just as large as the β and ψ motions, it is clear that they cannot safely be neglected in formulating a generally applicable set of simplified dutch roll equations. Nevertheless, by analogy with the longitudinal short period, this is commonly done in the interests of obtaining simple physical insight. If we assume, therefore, that the ϕ motions are negligible, then the sum of the rolling moments must be zero at all times and the roll equation is eliminated along with ϕ perturbations. Thus the equations of motion (6-1), neglecting gust inputs, reduce to:

$$\begin{aligned} (s - Y_V)\beta + r &= Y_\delta^* \delta \\ -N_\beta' \beta + (s - N_r')r &= N_\delta' \delta \end{aligned} \quad (6-18)$$

The corresponding transfer functions are given by:

$$\begin{aligned} \frac{\beta(s)}{\delta(s)} &= \frac{Y_\delta^* \left(s - N_r' - \frac{N_\delta'}{Y_\delta^*} \right)}{\Delta_{d2}} \\ \frac{r(s)}{\delta(s)} &= \frac{N_\delta' \left(s - Y_V + \frac{Y_\delta^*}{N_\delta'} N_\beta' \right)}{\Delta_{d2}} \end{aligned} \quad (6-19)$$

where

$$\Delta_{d2} = s^2 + (-Y_V - N_r')s + N_\beta' + Y_V N_r'$$

There is, of course, no ϕ transfer function because of the assumptions made.

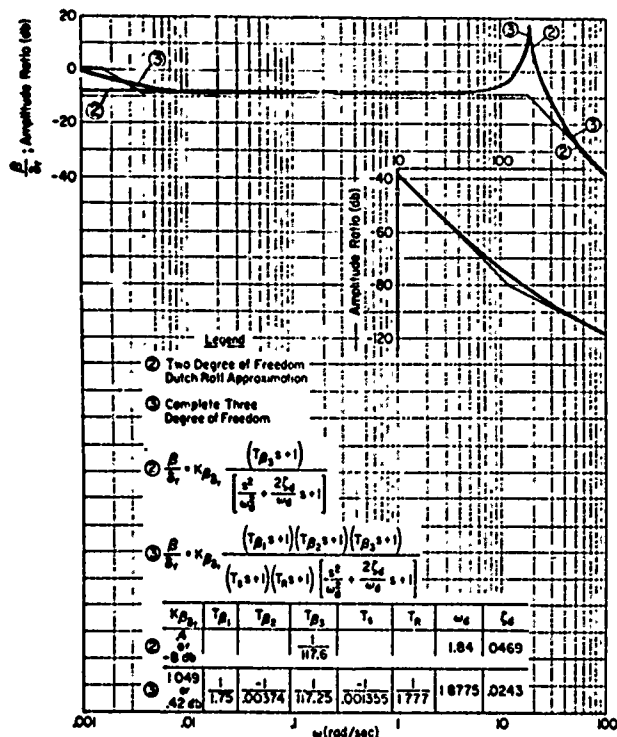
For the example airplane derivatives, the rudder and aileron numerical transfer functions are:

$$\begin{aligned}\frac{\beta(s)}{\delta_r(s)} &= 0.402 \cdot \frac{\left(\frac{s}{117.6} + 1\right)}{\left[\frac{s^2}{(1.84)^2} + \frac{2(0.0469)}{1.84}s + 1\right]} \\ \frac{r(s)}{\delta_r(s)} &= -0.0218 \frac{\left(\frac{s}{0.0541} + 1\right)}{\left[\right]} \\ \frac{\beta(s)}{\delta_a(s)} &= -0.1166 \frac{1}{\left[\right]} \\ \frac{r(s)}{\delta_a(s)} &= 0.00965 \frac{\left(\frac{s}{0.0829} + 1\right)}{\left[\right]}\end{aligned}\tag{6-20}$$

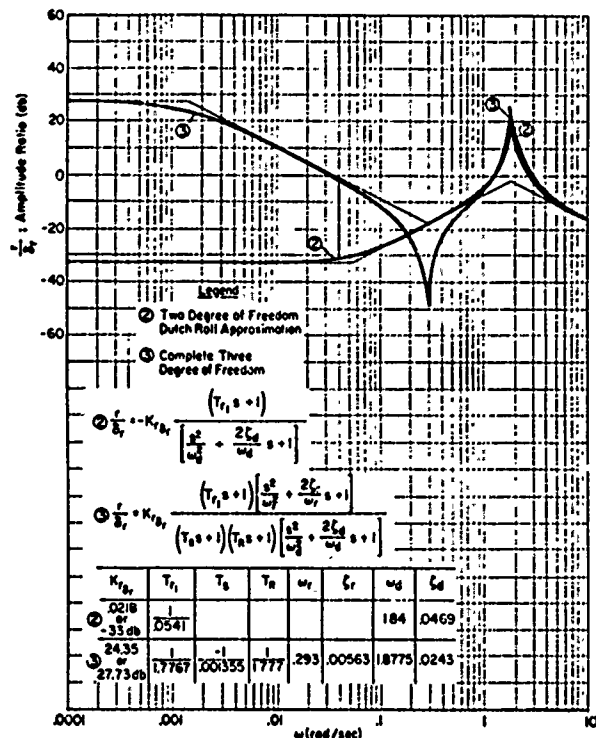
Comparing the dutch roll characteristics, we see that the frequency is fairly close to the exact value (1.8775), but that the damping is about twice as high (i.e., should be 0.0243). Also, the direct Bode amplitude comparisons given in Fig. 6-5 show that while the rudder transfer functions are fairly well matched, the two-degree-of-freedom aileron approximations depart considerably from the complete three-degree-of-freedom cases.

6.6 THREE-DEGREE-OF-FREEDOM DUTCH ROLL APPROXIMATIONS

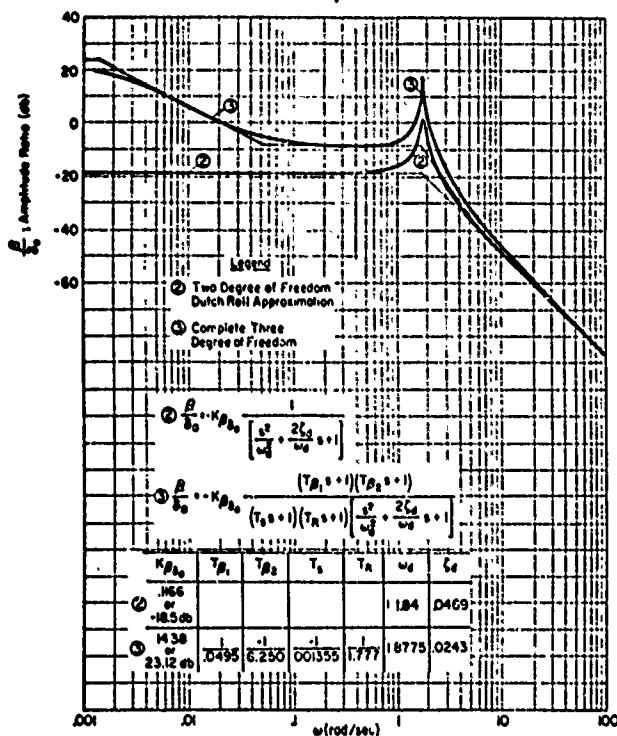
We can improve on our approximation to the dutch roll mode by considering that several of the smaller terms in the time vector diagrams of Fig. 6-4c are negligible. Prime candidates are the gravity terms, $g\phi/U_0$, the rolling acceleration due to rate of yaw, $L_r^1 r$, and the yawing acceleration due to rate of roll, $N_p^1 p$. With these simplifications the approximate three-degree-of-freedom set, considering only control inputs, becomes:



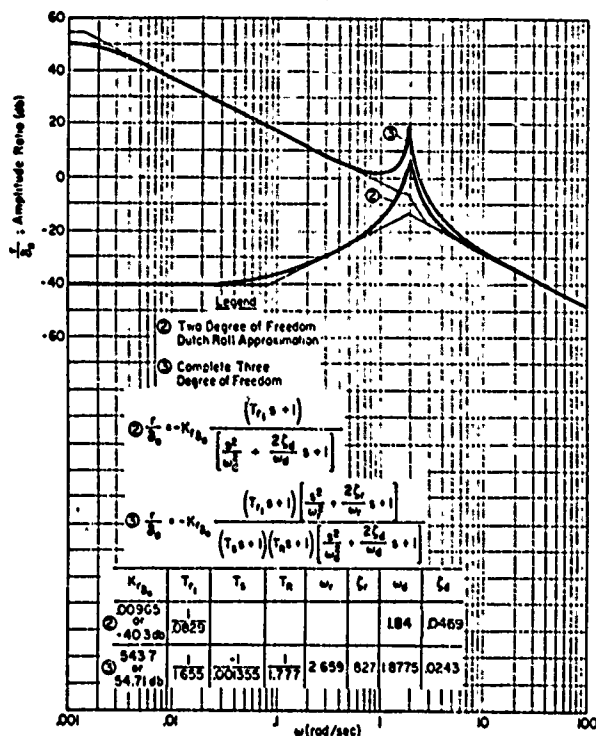
a) $\frac{\beta}{\delta_r}$



b) $\frac{r}{\delta_r}$



c) $\frac{\beta}{\delta_a}$



d) $\frac{r}{\delta_a}$

Fig. 6-5. Comparisons Between Complete Three- and Two-Degree-of-Freedom Dutch Roll Approximate Bode amplitudes

$$\begin{aligned}
(s - Y_V)\beta &+ r = Y_\delta^* \delta \\
-L_\beta' \beta + s(s - L_p') \phi &= L_\delta' \delta \\
-N_\beta' \beta + (s - N_r') r &= N_\delta' \delta
\end{aligned} \tag{6-21}$$

For this set of equations the denominator determinant is:

$$\Delta_{d3} = s(s - L_p') [s^2 + (-Y_V - N_r')s + (N_\beta' + Y_V N_r')] \tag{6-22}$$

Here the free s corresponds to the spiral mode, the $(s - L_p')$ factor to the roll subsidence, and the quadratic to the dutch roll. The dutch roll approximation is of course the same as that for the two-degree-of-freedom set. Likewise, the β and r transfer functions are unchanged. The advantage of the three-degree-of-freedom dutch roll approximation is to obtain ϕ transfer functions. Thus, Eqs. 6-21 yield the following ϕ numerator:

$$N_\delta^\phi = L_\delta' \left[s^2 + \left(-Y_V - N_r' + \frac{Y_\delta^*}{L_\delta'} L_p' \right) s + N_\beta' \left(1 - \frac{L_\beta' N_\delta'}{L_\delta' N_\beta'} \right) + Y_V N_r' - \frac{Y_\delta^*}{L_\delta'} L_\beta' N_r' \right] \tag{6-23}$$

The corresponding numerical transfer function for aileron-input to the example airplane is:

$$\frac{\phi(s)}{\delta_a(s)} = 15.71 \frac{\left[\frac{s^2}{(1.82)^2} + \frac{2(0.0474)}{1.82} s + 1 \right]}{s \left(\frac{s}{1.699} + 1 \right) \left[\right]} \tag{6-24}$$

Figure 6-6 compares the three-degree-of-freedom dutch roll approximation Bode plot with the complete set. This comparison shows that the ϕ/δ_a transfer function based on the approximate equations is quite close to that found using the complete three-degree-of-freedom set.

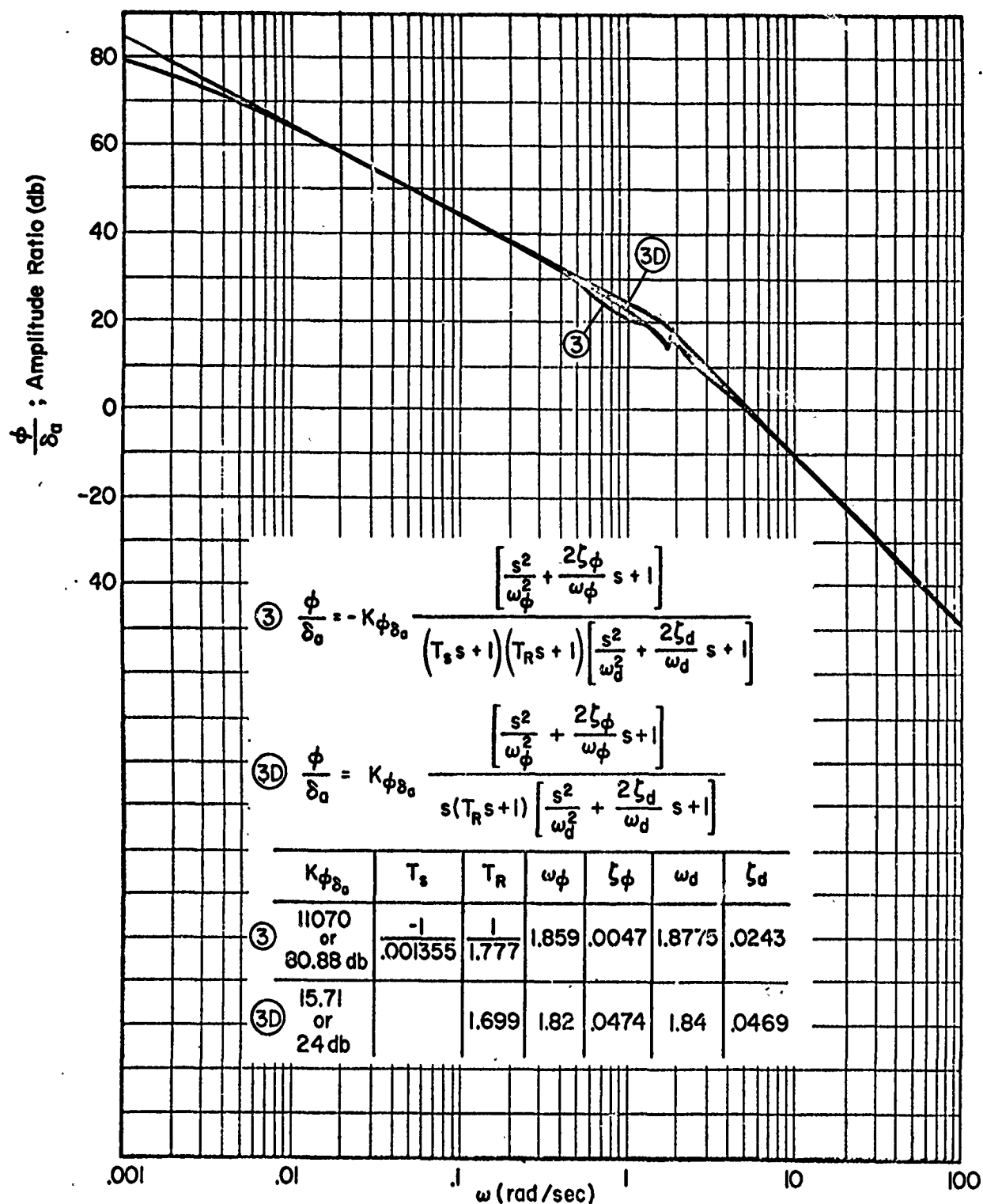


Fig. 6-6. Comparison Between Complete Three-Degree of Freedom and Dutch Roll Approximation Three-Degree-of Freedom Bode Amplitude Ratios for ϕ/δ_a

6.7 THREE-DEGREE-OF-FREEDOM SPIRAL AND ROLL SUBSIDENCE APPROXIMATIONS

Approximate equations of motion appropriate to the spiral and roll subsidence modes are obtained quite simply from the observation that for both modes the β motions are relatively small, as shown by the phasors of Fig. 6-4a and b; and that $(s - Y_V)\beta$ for the spiral mode is negligible with respect to the remaining side force terms (see Fig. 6-4a). Accordingly, we neglect this term to obtain the approximate equations of motion given by:

$$\begin{aligned} - (g/U_0)\varphi + r &= Y_\delta^* \delta \\ -L_p' \beta + s(s - L_p')\varphi - L_r' r &= L_\delta' \delta \\ -N_p' \beta - N_p' s\varphi + (s - N_r')r &= N_\delta' \delta \end{aligned} \quad (6-25)$$

These lead to the transfer functions:

$$\frac{\beta(s)}{\delta(s)} = \frac{N_\delta^\beta}{N_\beta' \Delta_{SR}} \quad \text{where } N_\delta^\beta \text{ is the complete form given in Table 6-1}$$

$$\frac{\varphi(s)}{\delta(s)} = \frac{Y_\delta^* L_p' \left[s - N_r' + \frac{N_\beta'}{L_p'} L_r' + \frac{1}{Y_\delta^*} \left(-N_\delta' + \frac{N_\beta'}{L_p'} L_\delta' \right) \right]}{N_\beta' \Delta_{SR}} \quad (6-26)$$

$$\frac{r(s)}{\delta(s)} = \frac{Y_\delta^* \left[s^2 + \left(-L_p' + \frac{L_p'}{N_\beta'} N_p' \right) s + \frac{g}{Y_\delta^*} \left(L_\delta' - \frac{L_p'}{N_\beta'} N_\delta' \right) \right]}{\Delta_{SR}}$$

where

$$\Delta_{SR} = s^2 + \left[-L_p' + \frac{L_p'}{N_\beta'} \left(N_p' - \frac{g}{U_0} \right) \right] s + \frac{g}{U_0} \left(\frac{L_p'}{N_\beta'} N_r' - L_r' \right)$$

For the example airplane, these transfer functions are:

$$\frac{\beta(s)}{\delta_r(s)} = 1.049 \frac{\left(\frac{s}{-0.00374} + 1\right)\left(\frac{s}{1.75} + 1\right)\left(\frac{s}{117.25} + 1\right)}{\left(\frac{s}{-0.00135} + 1\right)\left(\frac{s}{1.852} + 1\right)}$$

$$\frac{\phi(s)}{\delta_r(s)} = 498 \frac{\left(\frac{s}{80.4} + 1\right)}{\left(\frac{s}{-0.00135} + 1\right)\left(\frac{s}{1.852} + 1\right)}$$

$$\frac{r(s)}{\delta_r(s)} = 24.35 \frac{\left(\frac{s}{-1.57} + 1\right)\left(\frac{s}{3.36} + 1\right)}{\left(\frac{s}{-0.00135} + 1\right)\left(\frac{s}{1.852} + 1\right)}$$

$$\frac{\beta(s)}{\delta_a(s)} = -14.38 \frac{\left(\frac{s}{0.0495} + 1\right)\left(\frac{s}{-6.250} + 1\right)}{\left(\frac{s}{-0.00135} + 1\right)\left(\frac{s}{1.852} + 1\right)}$$

$$\frac{\phi(s)}{\delta_a(s)} = -11080 \frac{1}{\left(\frac{s}{-0.00135} + 1\right)\left(\frac{s}{1.852} + 1\right)}$$

$$\frac{r(s)}{\delta_a(s)} = -543.7 \frac{1}{\left(\frac{s}{-0.00135} + 1\right)\left(\frac{s}{1.852} + 1\right)}$$

(6-27)

Directly comparing these results with the complete transfer functions given in Eqs. 6-11 to 6-17 we see first that the approximate values of the spiral and roll subsidence inverse time constants are quite close to the exact values (i.e., -0.00135 and 1.852 versus -0.001355 and 1.777); that the low frequency gains for both sets are essentially the same, and that the β numerators for both sets are identical. However, the ϕ and r numerator

approximate factors are quite different from the exact factors. For the ϕ numerators these differences occur at frequencies greater than that corresponding to the roll subsidence mode, as might be expected. For the r numerators the breakpoint differences occur at frequencies below the roll subsidence, and it is quite clear that the approximate Bodes will not closely resemble the complete Bodes at the lower frequencies in the vicinity of the spiral root.

The spiral and roll subsidence approximations may often be further simplified by recognizing that for most conventional airplanes the value of $g/U_0[(L'_\beta/N'_\beta)N'_r - L'_r]$ is small relative to the other terms appearing in Δ_{SR} . Then, if $Y_{\delta_a}^* \doteq 0$,

$$\frac{\phi(s)}{\delta_a(s)} = \frac{L'_{\delta_a} \left(1 - \frac{N'_{\delta_a}}{L'_{\delta_a}} \frac{L'_\beta}{N'_\beta} \right)}{s \left[s - L'_p + \frac{L'_\beta}{N'_\beta} \left(N'_p - \frac{g}{U_0} \right) \right]} \quad (6-28)$$

This can be contrasted with the classical single-degree-of-freedom roll approximation obtained by considering only the rolling equation of motion, and neglecting β and r motions.

$$\frac{\phi(s)}{\delta_a(s)} = \frac{L'_{\delta_a}}{s(s - L'_p)} \quad (6-29)$$

We see that both the gain and the roll time constant are affected by three-degree-of-freedom considerations, but that the temporal nature of the motion is not, i.e., the response to a step aileron input is an exponential increase from zero to a steady rolling velocity in either case.

6.8 COMMENTARY ON APPROXIMATE EQUATIONS OF MOTION

In this article we will examine both the discrepant aspects of the approximations and their positive attributes. In this process we will take up the various approximations separately first and then consider them as a whole.

Two-Degree-of-Freedom Dutch Roll

Early versions of the simplified equations of motion for the dutch roll mode were very similar to Eq. 6-18, but used the unprimed derivatives in the yawing acceleration equation. A principal virtue of using the primed derivatives shows up in considering the denominator, Δ_{d2} , and its factors. The fact that $\omega_d^2 \doteq N'_\beta + Y_V N'_r$, as implied by Eq. 6-19, rather than $\omega_d^2 \doteq N_\beta + Y_V N_r$ is an important distinction. It shows that the effective directional stiffness is a function not only of the weathercock stability, N_β , but also of the dihedral, L_β , and the product of inertia, I_{xz} , i.e.,

$$N'_\beta \equiv \frac{N_\beta + (I_{xz}/I_z)L_\beta}{1 - (I_{xz}^2/I_x I_z)}$$

Thus, even though $N_\beta + Y_V N_r \rightarrow 0$ it is still possible to have positive stiffness and a finite dutch roll frequency if I_{xz} and L_β are of the same sign (i.e., for normally negative L_β and nose-up inclination of the principal axis of inertia to the direction of flight). Such situations are not uncommon for high angle of attack conditions where a negative N_β , e.g., due to fin immersion in the wing/body wake, can be stabilized by overriding negative values of I_{xz} and L_β . Of course unfavorable N_β characteristics can also occur, due to either Mach and/or aeroelastic effects, at low angles of attack corresponding to high speed operation. The possibility of $I_{xz}L_\beta$ overriding N_β in such situations is small because of the low angle of attack and correspondingly low I_{xz} and L_β generally involved.

The dutch roll damping implied by Eq. 6-19, $2\zeta_d \omega_d \doteq -Y_V - N'_r$, is almost always positive because usually both Y_V and N'_r are negative. There are rare cases, as noted in Chapter 4, where Y_V can become positive; and it is conceivable that the same high α conditions could "blanket" the fin and greatly reduce $-N'_r$. Except for such uncommon possibilities, the implication of the approximation is that dutch roll damping will always be positive. Divergent oscillations have been observed in practice, so these cannot be "explained" by this set of simplified equations.

The possible motions for the two-degree-of-freedom simplified equations must therefore be either a damped (or overdamped) oscillation

or a subsidence/divergence combination. Both forms have been observed, but the lightly damped oscillation is the more usual characteristic.

Three-Degree-of-Freedom Dutch Roll

This approximation is intended primarily to allow the computation of a bank angle transfer function or response to complement the two-degree-of-freedom approximation results for yawing velocity and sideslip. It satisfies this requirement, but is otherwise undistinguished.

Spiral and Roll Subsidence

Until recently the roll subsidence and spiral modes were usually thought of as unconnected and independent. Physically, the roll subsidence was associated primarily with the rolling behavior of the aircraft, which is described largely by the time lag in attaining a nearly steady-state rolling velocity after a step application of the ailerons. This lag is due principally to the combination of the roll rate damping moment and the roll moment of inertia, so the mode is conventionally considered to be essentially single-degree-of-freedom. On the other hand, the spiral mode has long been recognized generally as involving at least two degrees of freedom—yawing and rolling. Since the describing time constant for this mode involves a very small root of the lateral characteristic equation, the approximation for the root (i.e., E/D of Δ_{lat}) has been well known for many years.

As can be appreciated from these remarks, no particular reason existed for further exploration of the underlying physics of the roll subsidence and spiral modes at a time when most aircraft possessed three-degree-of-freedom rolling motions that approximated single-degree-of-freedom characteristics. However, modern craft with high effective dihedral, low roll damping, etc., occasionally exhibit a long period lateral oscillation, and rolling velocity calculations based on L_{δ_a} rather than $L_{\delta_a}' (\omega_p/\omega_d)^2$ have led to later surprises. Early contacts with these phenomena called attention to the problem of obtaining a more adequate physical understanding of the spiral and roll subsidence modes. Equation 6-25 brings the two modes into their present closely interconnected context.

The history related above has certain overtones of repetition because the earliest partially successful gliders and unmanned aircraft possessed considerable "lateral stability." In the terms used here, the roll subsidence and spiral were both stable modes and fairly close to or actually in the coupled state. Model aircraft also use the same principles to obtain as much over-all lateral dynamic stability as possible. It was not until the Wrights correctly deduced that a "neutral lateral stability" was desirable for lateral control that the roll subsidence became essentially single-degree-of-freedom and the spiral simply a minor headache to the pilot in IFR conditions.

Considering the terms combined in $\Delta_{GR}(s)$, it can be shown that the time-response characteristics for the lateral roll subsidence/spiral combination can take on almost any second-order form. The solitary exception on a normal winged aircraft is two divergent first-orders. All other forms, i.e., positively or negatively damped oscillation, two subsidences, or a subsidence/divergence pair, have actually occurred in practice.

Combined Considerations

Preferably we would like approximate relationships which could be connected together in some logical fashion to give a fairly accurate picture of the complete three-degree-of-freedom situation. As already noted, in terms of the denominator the two three-degree-of-freedom approximations to the dutch roll and spiral/roll-subsidence modes offer a combined set of denominator dynamic characteristics in general quite representative of the complete situation. The major denominator deficiency is the dutch roll damping. This can be alleviated by considering that the damping for the spiral/roll-subsidence mode is more correct than that for the two-degree-of-freedom dutch roll, and by recalling that the s^3 coefficient of the complete denominator is the sum of all the damping terms. Then a better estimate for the dutch roll damping will be

$$\begin{aligned} 2(\xi\omega)_d &\doteq (-Y_v - N_r' - L_p') - \left[-L_p' + \frac{L_{\beta}'}{N_{\beta}'} \left(N_p' - \frac{g}{U_0} \right) \right] \\ &\doteq (-Y_v - N_r') - \frac{L_{\beta}'}{N_{\beta}'} \left(N_p' - \frac{g}{U_0} \right) \end{aligned} \quad (6-30)$$

For normally negative L_p' and positive N_p' , negative values of N_p' and/or small values of U_0 will result in a negative damping contribution due to the added term. This can be large enough to overpower the "two-degree-of-freedom" damping provided by $(-Y_v - N_r')$ and thereby to produce a divergent oscillation.

Unfortunately, as observed earlier, the various example-case approximate numerators show a very spotty correspondence with the exact numerators. In all cases, however, we can say that for the spiral/roll-subsidence the asymptotic low frequency gain/dynamics closely approximate those for the complete transfer function; also, either of the dutch roll approximations approaches the correct asymptotic high frequency gain/dynamics. As for the numerator factors, those that are reasonably correct numerically for the example airplane are limited to:

Two-degree-of-freedom dutch roll

β/δ , r/δ --- Good agreement at high frequencies

Three-degree-of-freedom dutch roll

ϕ/δ_a --- Identical to exact complete numerator if $Y_{\delta_a} = 0$

β/δ , r/δ , ϕ/δ_r^* --- Good agreement at high frequencies

Three-degree-of-freedom spiral/roll-subsidence

ϕ/δ_a --- Good except in immediate region of dutch roll

β/δ_a , β/δ_r --- Identical to exact complete numerator

This picture contrasts somewhat to the situation for the longitudinal approximations where the numerator and denominator factors are in better agreement with the exact factors. It appears that the use of simplified modal equations of motion cannot in general yield good approximate numerator factors; and that another approach to approximate factors is required to supplement the approximate equation technique. Such an approach was outlined in Section 3.4, and has been applied extensively[†] to the problem of obtaining approximate factors.

*Not given in text; computed example-case factors are $\left(\frac{s}{-2.67} + 1\right)\left(\frac{s}{2.75} + 1\right)$.

†e.g., I. L. Ashkenas and D. T. McRuer, Approximate Airframe Transfer Functions and Application to Single Sensor Control Systems, WADC TR 58-82, June 1958, Appendix, pp. 191-210.

6.9 HOVERING EQUATIONS, CONTROL-INPUT TRANSFER FUNCTIONS, AND TIME RESPONSES

In their simplest practical form the lateral small-perturbation equations of motion in hover are:

$$\begin{aligned}(s - Y_V)v - g\phi &= Y_\delta \delta \\ -L_V v + s(s - L_P)\phi &= L_\delta \delta \\ (s - N_R)r &= N_\delta \delta\end{aligned}\tag{6-31}$$

Equation 6-31 assumes $U_0 = N_p = L_r = I_{xz} = N_v = Y_p = Y_r = 0$ and applies fairly well to any hovering vehicle without a tail rotor, or with a tail rotor of high disk loading. It is not completely valid for typical single-rotor helicopters because the tail rotor, being of low disk loading, is sensitive to local sideslip velocity perturbations and hence generates (for example) N_v and possibly L_r and N_p . Notice that it is completely analogous to the longitudinal hover equations (5-34) with ϕ replacing θ , v replacing u , and r replacing w ; the Y , N , L derivatives replace X , Z , and M derivatives, respectively. The resulting transfer functions and modal responses are correspondingly similar in form to those given previously for the longitudinal motions; that is:

$$\frac{r(s)}{\delta(s)} = \frac{N_\delta}{s - N_R}\tag{6-32}$$

$$\frac{\phi(s)}{\delta(s)} = \frac{L_\delta \left(s - Y_V + \frac{Y_\delta}{L_\delta} L_V \right)}{\Delta_{\text{hover}}}\tag{6-33}$$

$$\frac{v(s)}{\delta(s)} = \frac{Y_\delta \left(s^2 - L_P s + \frac{L_\delta}{Y_\delta} \right)}{\Delta_{\text{hover}}}\tag{6-34}$$

$$\text{where } \Delta_{\text{hover}} = s^3 + (-Y_V - L_P)s^2 + Y_V L_P s - g L_V\tag{6-35}$$

From these relationships we see that the $s - N_R$ mode is associated only

with yaw rate perturbations, r , and does not appear in either ϕ or v motions. Conversely, there are no r motions in the modes associated with the lateral hovering cubic (Eq. 6-35) which usually* factors into a negative real root describing a stable mode, plus a complex pair associated with a lightly damped, or unstable, oscillatory mode.

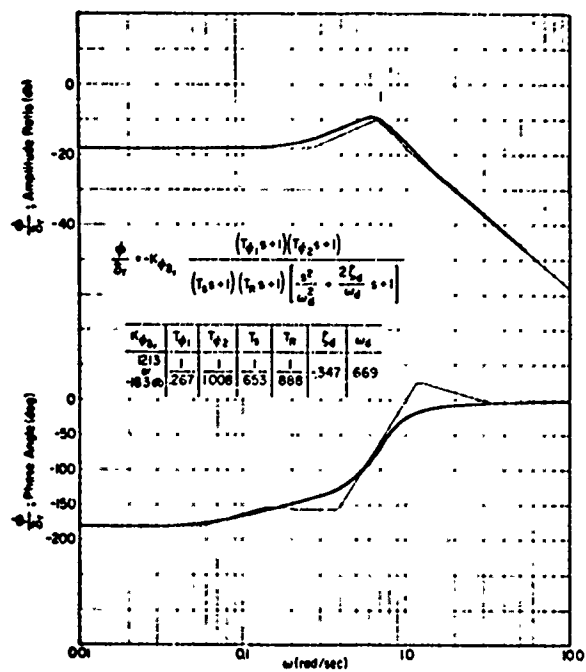
The similarity, in form, of these and the longitudinal equations is matched by similarities in the derivatives. For most hovering vehicles* $X_u = Y_v$ and $I_x L_v = -I_y M_u$; however, the equations of motion are not numerically identical because usually $I_x \neq I_y$, hence $L_v \neq -M_u$ even if $I_x L_v = -I_y M_u$. Similarly, $M_q \neq L_p$, although often $I_y M_q = I_x L_p$. Despite this, the analogy between longitudinal and lateral equations is sufficiently complete to suggest that the root locations and modal response coefficients may be very similar.

As an example which illustrates this we again choose the configuration shown in Fig. 5-7, and consider small perturbations from a near-hover condition ($U_0 = 1.0$ ft/sec) to detect any possibly significant effects of not being exactly at hover. As will be shown, the effects of small U_0 are trivial. $Y_p = Y_r = Y_{\delta_a} = L_r = N_v = N_p = N_{\delta_a}$ are zero, but $I_{xz} \neq 0$ and this produces some coupling of the yawing mode ($s - N_r$) with the roll and sideslip modes. Because the example configuration has no tail rotor, it has essentially zero N_v , L_r , and N_p . The assumed characteristics are:

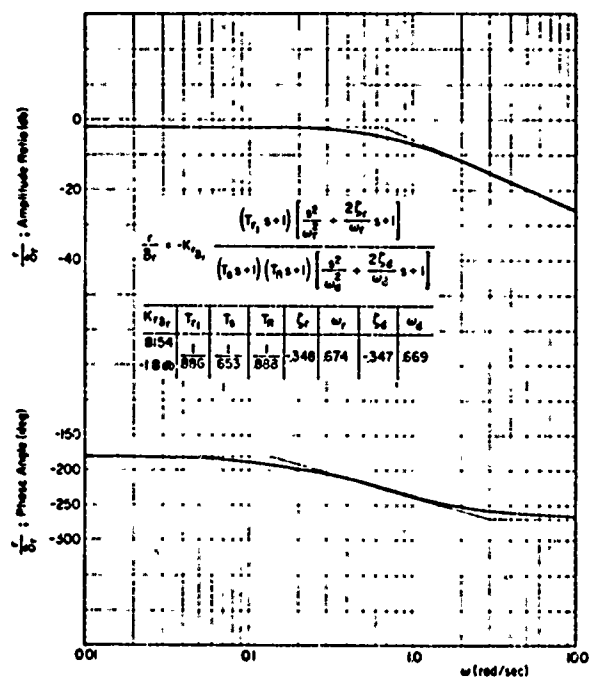
Weight (lb)	3,100
Roll inertia (slug-ft ²)	1,990
Yaw inertia (slug-ft ²)	3,450
Groundspeed, U_0 (ft/sec)	1

Y_p	0	L_p	-0.271
Y_r	0	L_r	0
Y_v	-0.14	L_v	-0.0122
Y_{δ_a}	0	L_{δ_a}	0.69
Y_{δ_r}	1.017	L_{δ_r}	-0.185

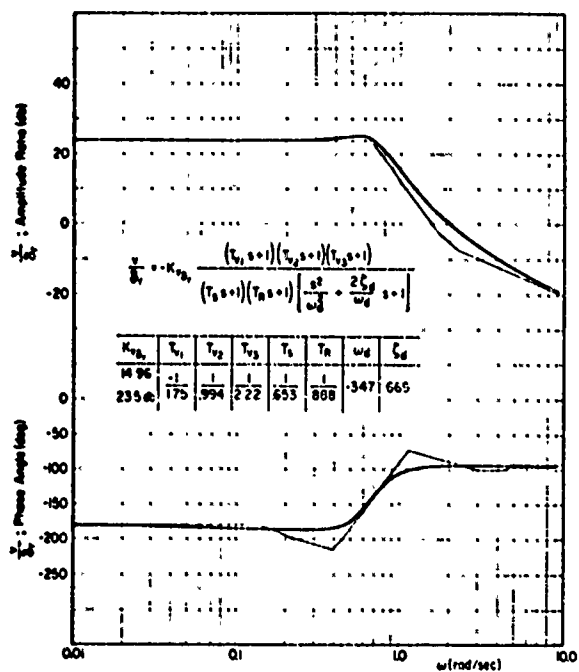
*J. Wolkovitch and R. P. Walton, VTOL and Helicopter Approximate Transfer Functions and Closed-Loop Handling Qualities, Systems Technology, Inc., Tech. Rept. 128-1, Sept. 1963.



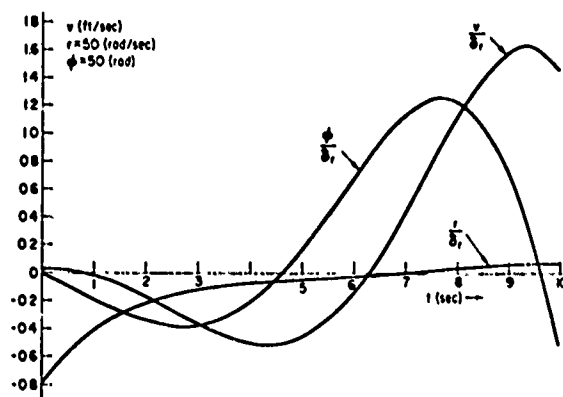
a) $\frac{\phi}{\sigma_r}$



b) $\frac{r}{\sigma_r}$



c) $\frac{v}{\sigma_r}$



d) Time Responses

Figure 6-7. Example Rudder Control—Input Bode Plots and Time Responses for a Hovering Airplane

N_p	0	I_{xz}/I_x	-0.1246
N_r	-0.656	I_{xz}/I_z	-0.07188
N_v	0		
N_{δ_a}	0		
N_{δ_r}	-0.539		

The corresponding primed derivatives are:

L_p'	-0.273	N_p'	0.0197
L_r'	0.0825	N_r'	-0.662
L_v'	-0.0123	N_v'	0.000885
L_{δ_a}'	0.696	N_{δ_a}'	-0.0500
L_{δ_r}'	-0.119	N_{δ_r}'	-0.531

For the above assumed characteristics, the control-input transfer functions are:

For yaw control, δ_r

$$\begin{aligned}\frac{\varphi}{\delta_r} &= \frac{-0.119(s + 0.267)(s + 1.008)}{\Delta_{lat}} \\ \frac{r}{\delta_r} &= \frac{-0.531(s + 0.886)[s^2 - 2(0.348)(0.674)s + (0.674)^2]}{\Delta_{lat}} \quad (6-35) \\ \frac{v}{\delta_r} &= \frac{1.017(s - 1.75)(s + 0.994)(s + 2.22)}{\Delta_{lat}}\end{aligned}$$

For roll control, δ_a

$$\begin{aligned}\frac{\varphi}{\delta_a} &= \frac{0.696(s + 0.14)(s + 0.6564)}{\Delta_{lat}} \\ \frac{r}{\delta_a} &= \frac{-0.0500s^2(s + 0.14)}{\Delta_{lat}} \quad (6-37) \\ \frac{v}{\delta_a} &= \frac{0.0500(s + 0.657)(s + 447.0)}{\Delta_{lat}}\end{aligned}$$

where

$$\Delta_{lat} = (s + 0.653)(s + 0.888)[s^2 - 2(0.347)(0.669)s + (0.669)^2]$$

Bode diagrams of these transfer functions and time responses for impulsive δ_a and δ_r inputs are given in Figs. 6-7 and 6-8. The Bodes, in general, show the approximate cancellations of the hovering cubic in the r transfer function and of the $(s - N_r)$ subsidence mode in the ϕ and v transfer functions, as anticipated by the approximate expressions 6-32 through 6-34. The one exception is the r/δ_a Bode which is radically different in appearance from r/δ_r . This difference is traceable to the product of inertia influence, which "recreates" many of the derivatives, e.g., L_r' , N_v' , N_p' , considered zero in their unprimed state, and to the size of these derivatives relative to N_{δ_a}' , the normally important yaw-rate-input excitation term.

The time responses are consistent with the foregoing differences and similarities. In particular, the yaw rate first-order subsidence can be clearly seen in the rudder-input response, and the negatively damped oscillation associated with the hovering cubic is clearly visible in the ϕ and v traces. However, the first-order portion of the cubic cannot easily be separated from the initial portions of these latter responses because its time constant is near the period of the second-order oscillation. This mode "subsides" almost completely in about 3 sec so that the residual trace thereafter is almost entirely due to the second-order.

The time vector diagrams of Fig. 6-9 enhance considerably our understanding of the physical nature of the modes of free motion and the significance of each derivative. For example, the yawing acceleration time vectors for the "spiral" mode, Fig. 6-9a, show that the approximation $s = N_r$ for the root is very accurate. The yawing moment induced by roll acceleration, $I_{xz}s^2\phi$, is not visible on the same scale, so for this mode the sideslip and roll equations of motion are superfluous.

The time vectors for the remaining modes present a quite different appearance. Considering both Fig. 6-9b and 6-9c, it is seen that the balance of yawing accelerations in free motion includes an appreciable contribution due to I_{xz} . However, the time vectors representing the rolling and side accelerations show negligible contributions due to yawing velocity or yawing acceleration. Hence these modes can be calculated using roll and side force equations of motion only.

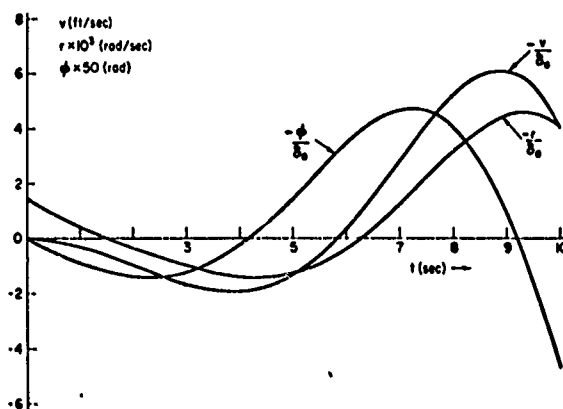
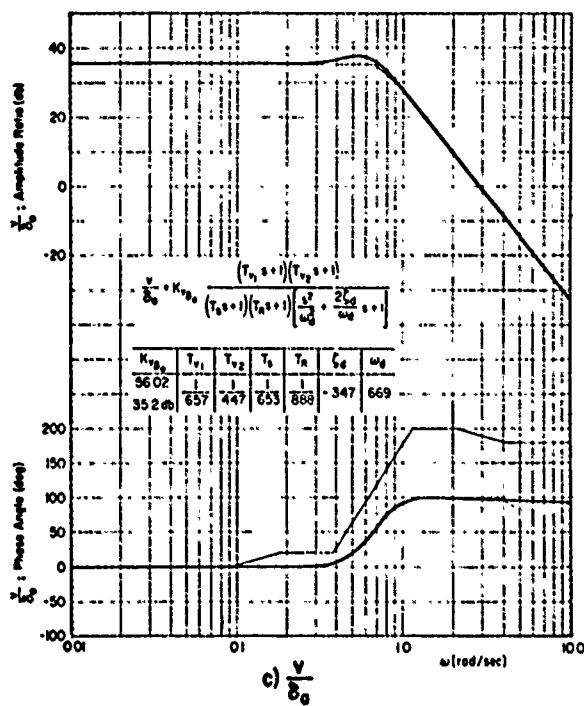
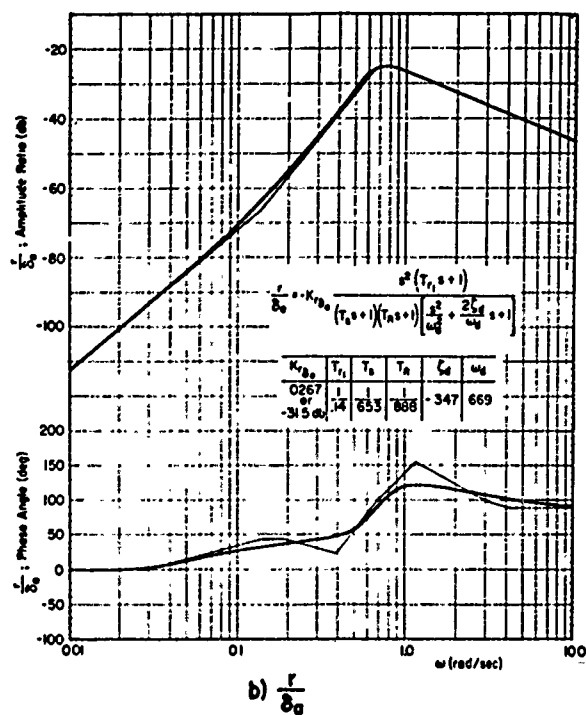
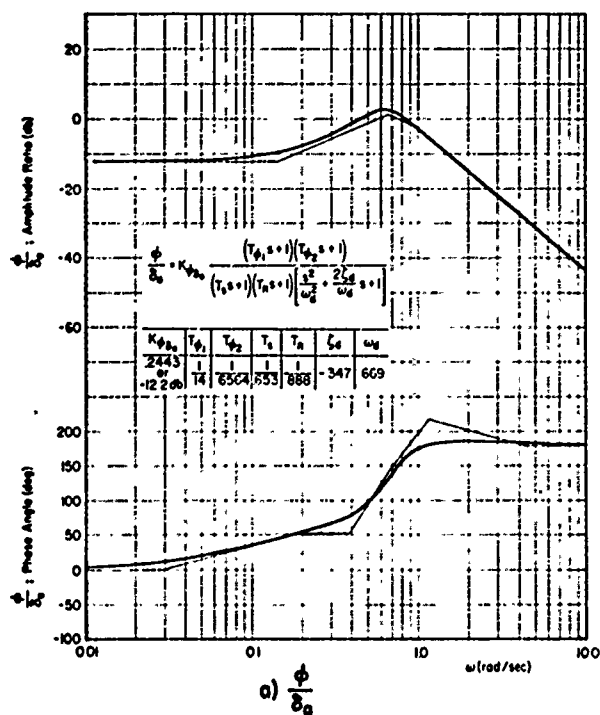
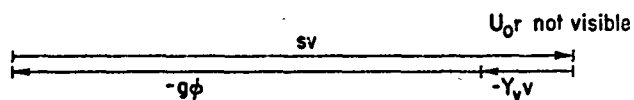
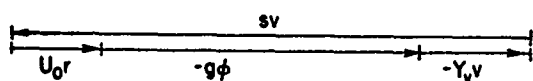


Figure 6-8. Example Aileron Control-Input Bode Plots and Time Responses for a Hovering Airplane

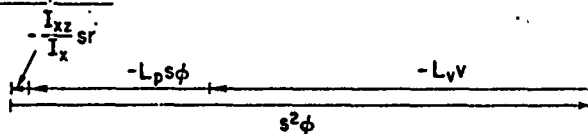
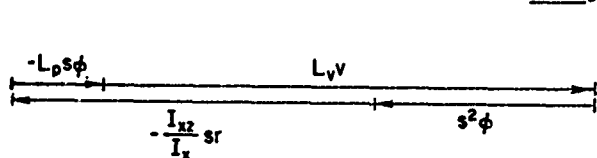
$$s = -.653$$

$$s = -.888$$

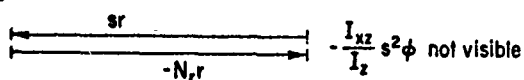
Side Force Equation



Rolling Moment Equation



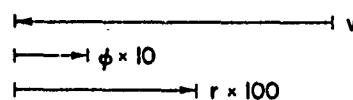
Yawing Moment Equation



Phasors



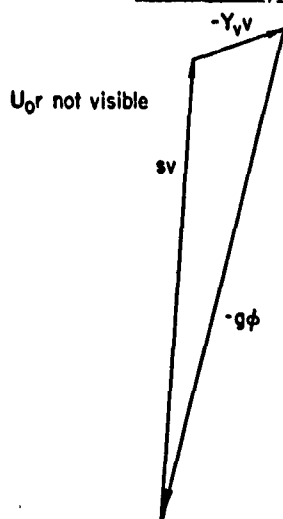
a) Spiral Mode



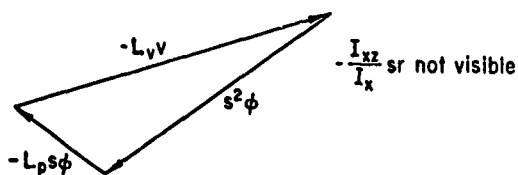
b) Roll Subsidence Mode

$$\omega_d = .669, \zeta_d = -.347$$

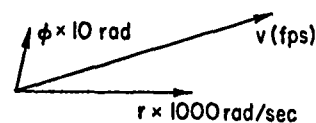
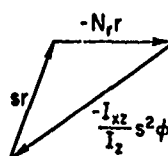
Side Force Equation



Rolling Moment Equation



Yawing Moment Equation



c) Dutch Roll Mode

Figure 6-9. Time-Vector Diagrams for the Example Hovering Vehicle

Thus, despite the nonzero I_{xz} , free yawing motions are essentially uncoupled, and the roll and sideslip motions are similar to the hovering forward displacement and pitching motions described in Chapter 5. In this regard, comparing the X force and pitching moment time vectors of Fig. 5-9 with the side force and rolling moment vectors of Fig. 6-9 shows that the principal difference between longitudinal and lateral motions is due to the greater damping in roll, $I_x L_p$, than that in pitch, $I_y M_q$. (The difference in the inertias is secondary, $I_x = 1,990$ versus $I_y = 1,790$ slug-ft².) The increased $L_p s\phi$ (compared to $M_q s\theta$) vector tends to distort the appropriate time vector polygon so as to make the damping angle, $\sin^{-1} \zeta_d$, less negative than its longitudinal counterpart, $\sin^{-1} \zeta_p$.

Criteria for the neglect of I_{xz} on the hovering modes can be found by substituting the missing I_{xz} terms into Eq. 6-31. The characteristic equation then becomes:

$$(s - N_r) \left[(s - Y_v)(s^2 - L_p s) - g L_v \right] - \left(\frac{I_{xz}^2}{I_x I_z} \right) s^4 + Y_v \left(\frac{I_{xz}^2}{I_x I_z} \right) s^3 = 0 \quad (6-38)$$

and the conditions for the hovering cubic roots to be hardly changed by I_{xz} are:

$$\frac{I_{xz}^2}{I_x I_z} \ll 1 \quad (6-39)$$

$$\left| \frac{Y_v I_{xz}^2}{I_x I_z} \right| \ll |Y_v + L_p + N_r|$$

The unimportance of a small nonzero forward speed on the dynamics is shown by the small size of the U_{or} time vector, which is invisible in the roll subsidence and dutch roll vector polygons; and, although visible in the spiral mode, it appears in the summation of side forces which are not needed to describe the mode, as noted earlier.

6.10 GUST-INPUT TRANSFER FUNCTIONS

The gust-input transfer function numerators (the denominator is independent of input and has already been fully considered) are obtained in their most general polynomial form from Eq. 6-2, and are given in

Table 6-2. Here, in order to allow direct conversion to the primed notation (Eq. 6-1) by conventional rules (i.e., $I_{xz} = 0$, $L \rightarrow L'$, $N \rightarrow N'$) we have included an $I_{rs}\beta_g$ input term not shown in Eq. 6-2; further, we have distinguished β -gust-gradient-input derivatives with a "g" subscript so that potential differences between response and input derivatives, e.g., as in $(N_r')_g$ of Eq. 6-1, can be identified.

Figure 6-10 presents Bode plots of the p gust transfer functions for the example conventional airplane; it shows quite clearly that the major response is in ϕ . In fact, considering the roll rate response, p (which corresponds to rotating the ϕ amplitude Bode plot counterclockwise 20 db/decade about the asymptotic zero db intersection, as indicated), we see that it is exactly equal to the p_g input for low frequencies and is sharply attenuated beyond frequencies corresponding to the roll subsidence mode. Because the dutch roll mode in ϕ almost cancels exactly, the dutch roll modal response coefficient for ϕ will be small, resulting in little ϕ dutch roll motion. For frequencies below dutch roll the β motions are quite small, and the r amplitudes are roughly g/U_0 times the ϕ amplitudes. All these observations are in agreement with our previous ideas regarding the relative motions appearing in the various modes.

The β gust Bode plots of Fig. 6-11 assume zero gust gradient terms [i.e., $(N_r)_g = (L_r)_g = 0$ (see Table 6-2)] because such terms are inconsistent with the step gusts assumed for the time histories to be subsequently considered (Fig. 6-12). At dutch roll frequencies the relative amplitudes between β , ϕ , and r are substantially the same as those for the rudder-input situations. If the peak amplitudes are used to estimate the modal response ratios, the result is

$$\begin{aligned}\beta : \phi : r &\doteq [26 : 26 : 31]_{db} \\ &\doteq 1 : 1 : 1.78\end{aligned}$$

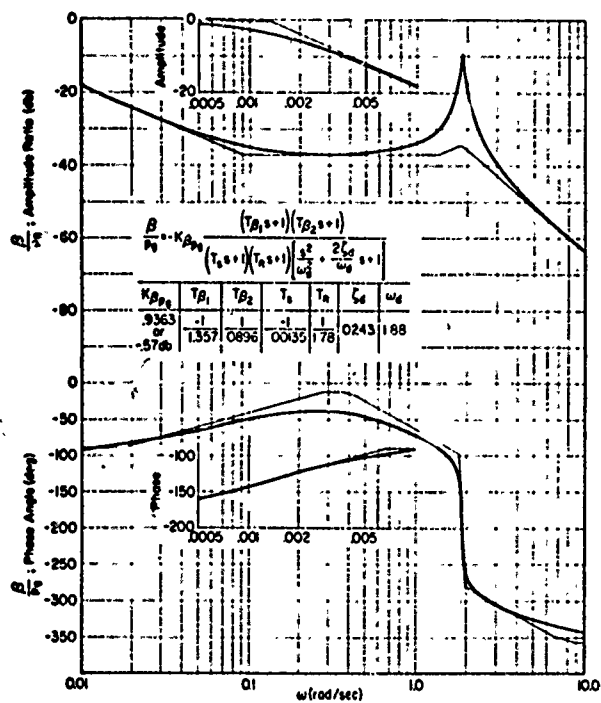
This is, of course, very close to the exact values, $1 : 0.99 : 1.87$.

For low frequencies, Fig. 6-11 shows that $\beta \doteq \beta_g$ so that $\beta - \beta_g \doteq 0$; this means that the sideslip relative to the air mass is zero (see Eq. 4-83). Thus the aerodynamic side forces are zero and the banking

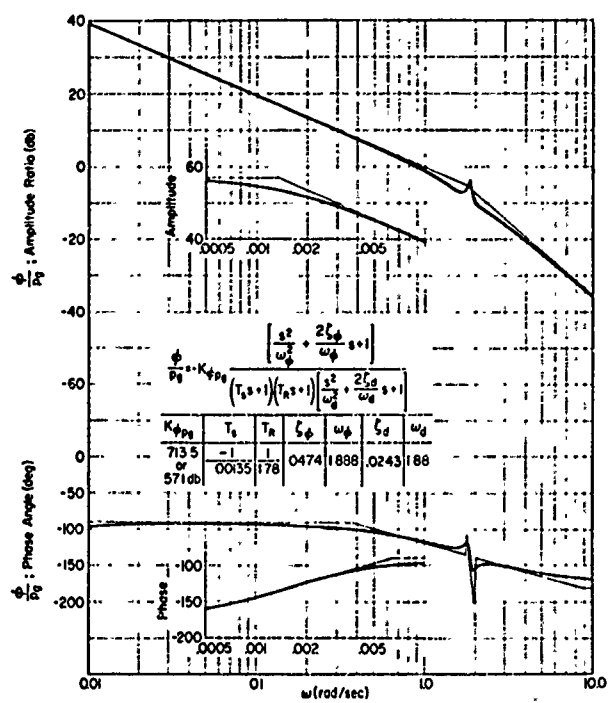
TABLE 6-2
LATERAL GUST-INPUT TRANSFER FUNCTION NUMERATORS

A	B	C	D
$N_p + \frac{I_{xz}}{I_z} I_p$	$\frac{g}{U_0} \left(-I_p - \frac{I_{xz}}{I_x} N_p \right)$	$\frac{g}{U_0} (I_p N_r - N_p I_r)$	
$-I_p - \frac{I_{xz}}{I_x} N_p$	$I_p N_r - N_p I_r + Y_v \left(I_p - \frac{I_{xz}}{I_x} N_p \right)$	$I_p N_p - N_p I_p + Y_v (N_p I_r - I_p N_r)$	
$-N_p - \frac{I_{xz}}{I_z} I_p$	$Y_v N_p + \frac{I_{xz}}{I_z} I_p$	0	$\frac{g}{U_0} (I_p N_r - N_p I_r)$
$-Y_v \left(-\frac{I_{xz}^2}{I_x^2} \right) + (N_r) g + \frac{I_{xz}}{I_z} (I_r) g$	$N_p + \frac{I_{xz}}{I_z} I_p - (N_r) g \left(I_p + \frac{I_{xz}}{I_x} \frac{g}{U_0} \right) + (I_r) g \left(N_p - \frac{g}{U_0} \right)$	$-Y_v (I_p N_r - I_r N_p) - \frac{g}{U_0} \left(I_r + \frac{I_{xz}}{I_x} N_p \right) + I_p N_p - N_p I_p - \frac{g}{U_0} (N_r) g I_r - (I_r) g N_r$	$\frac{g}{U_0} (I_p N_r - N_p I_r)$
$-(I_r) g - \frac{I_{xz}}{I_x} (N_r) g$	$Y_v \left[(I_r) g + \frac{I_{xz}}{I_x} (N_r) g \right] + N_r (I_r) g - I_r (N_r) g - \frac{I_{xz}}{I_x} N_p$	$Y_v \left[I_r (N_r) g - N_r (I_r) g \right] + I_p \left[N_r + (N_r) g \right] - N_p \left[I_r + (I_r) g \right]$	
$-(N_r) g - \frac{I_{xz}}{I_z} (I_r) g$	$Y_v \left[(N_r) g + \frac{I_{xz}}{I_z} (I_r) g \right] + I_p (N_r) g - N_p (I_r) g - \frac{I_{xz}}{I_z} I_p$	$N_p I_p - I_p N_p - Y_v \left[I_p (N_r) g - N_p (I_r) g \right]$	$\frac{g}{U_0} [I_p (N_r) g - N_p (I_r) g]$

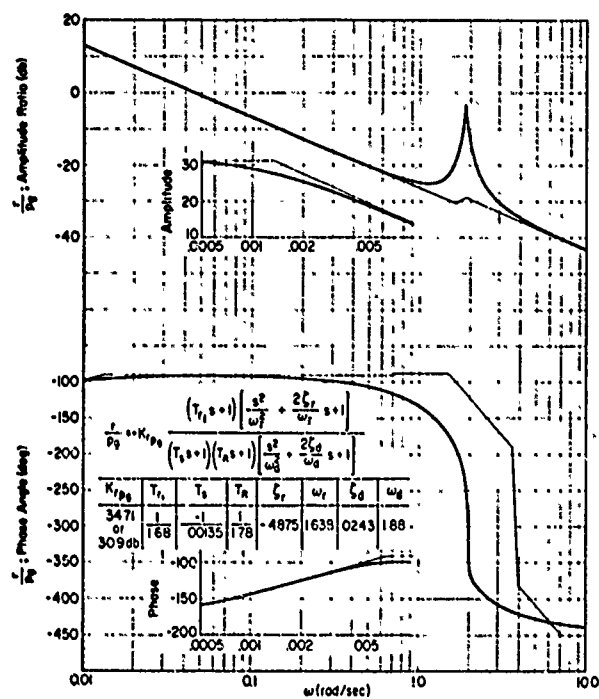
Note: To convert to primed derivatives, eliminate all I_{xz} terms and substitute L' and N' for L and N , respectively.



a) $\frac{B}{P_g}$

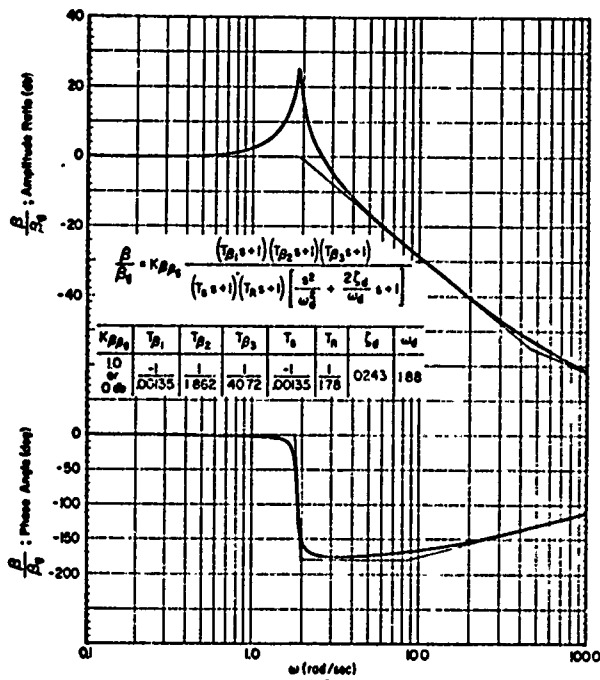


b) $\frac{\phi}{P_g}$

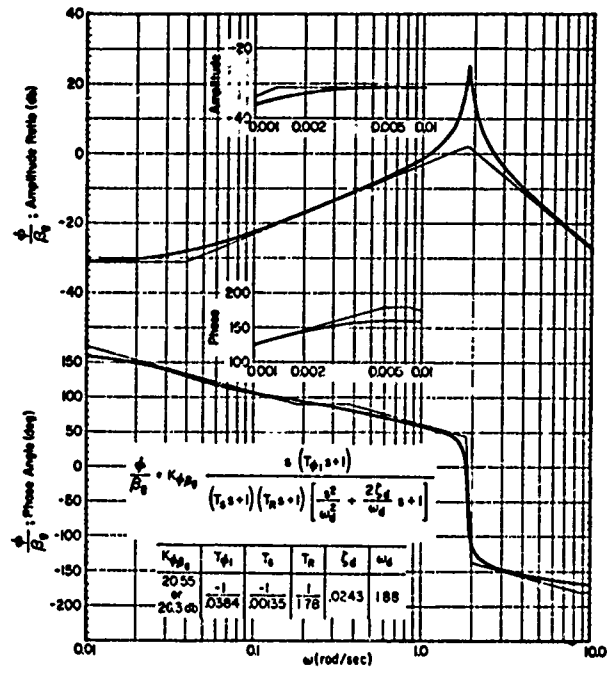


c) $\frac{r}{P_g}$

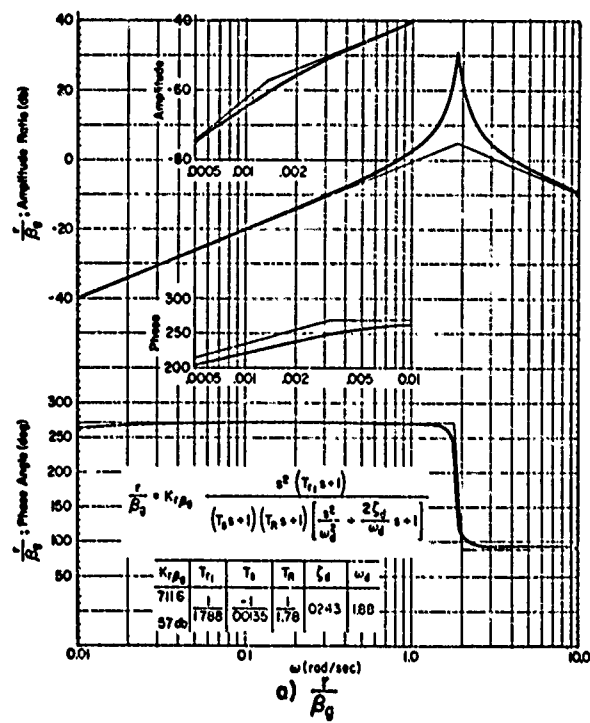
Figure 6-10. Bode Plots for Rolling Gust (p_g) Input



a) $\frac{\beta}{\beta_0}$



b) $\frac{\phi}{\phi_0}$



a) $\frac{r}{\beta_0}$

Figure 6-11. Bode Plots for Side Gust (β_g) Input

and turning motions for the spiral mode are coordinated, as we expect them to be, and as reflected in the g/U_0 (-26.3 db) relationship between ϕ and r at the spiral inverse time constant. However, whereas for other inputs (e.g., δ or p_g) the relationship $r \doteq (g/U_0)\phi$ holds as well for frequencies below the (open- or closed-loop) spiral mode, for β_g inputs it does not. For example, for a β_g ramp input, $\dot{\beta}_g = \text{constant}$, the resulting steady motions, applying the final value theorem, are $\dot{\beta} = \dot{\beta}_g$, $r = 0$, $\phi = (U_0/g)\dot{\beta}$.

Figures 6-10 and 6-11 show that for a given input all motions (except β/β_g discussed above) follow roughly the same pattern with frequency. That is, responses to p_g excitation are primarily low frequency in nature, whereas those due to β_g excitation occur primarily near dutch roll. Although not shown in Fig. 6-11, the lateral acceleration (a_y) response at high frequencies would be quite large. For example, using the basic Eq. 6-3 relationship,

$$a_{y_{c.g.}} = U_0(\dot{\beta} + r) - g\phi$$

The high frequency asymptote is given simply by

$$\left. \frac{a_{y_{c.g.}}}{\beta_g} \right]_{\text{hi freq}} \rightarrow \frac{U_0(A_\beta s^4 + A_r s^4) - gA_\phi s^3}{\left(1 - \frac{I_{xz}^2}{I_x I_z}\right) s^4}$$

where the A terms are those in Table 6-2. Accordingly,

$$\left. \frac{a_{y_{c.g.}}}{\beta_g} \right]_{\text{hi freq}} \rightarrow \frac{U_0(A_\beta + A_r)}{\left(1 - \frac{I_{xz}^2}{I_x I_z}\right)} = -U_0 Y_v \quad (6-40)$$

Notice that this asymptote is constant (i.e., not a function of s) and therefore does not attenuate with frequency. This situation is analogous to that noted with respect to the a_z high frequency asymptote in Chapter 5 and the same comment applies. That is, the possibility of exciting, and coupling with, high frequency structural responses must be considered in any system involving a_y feedbacks.

Figure 6-12 presents time histories of the response to a β_g step and to a p_g pulse (rather than a step to keep the bank angle trace within bounds). The motions shown are consistent with those deduced above from the Bode plots.

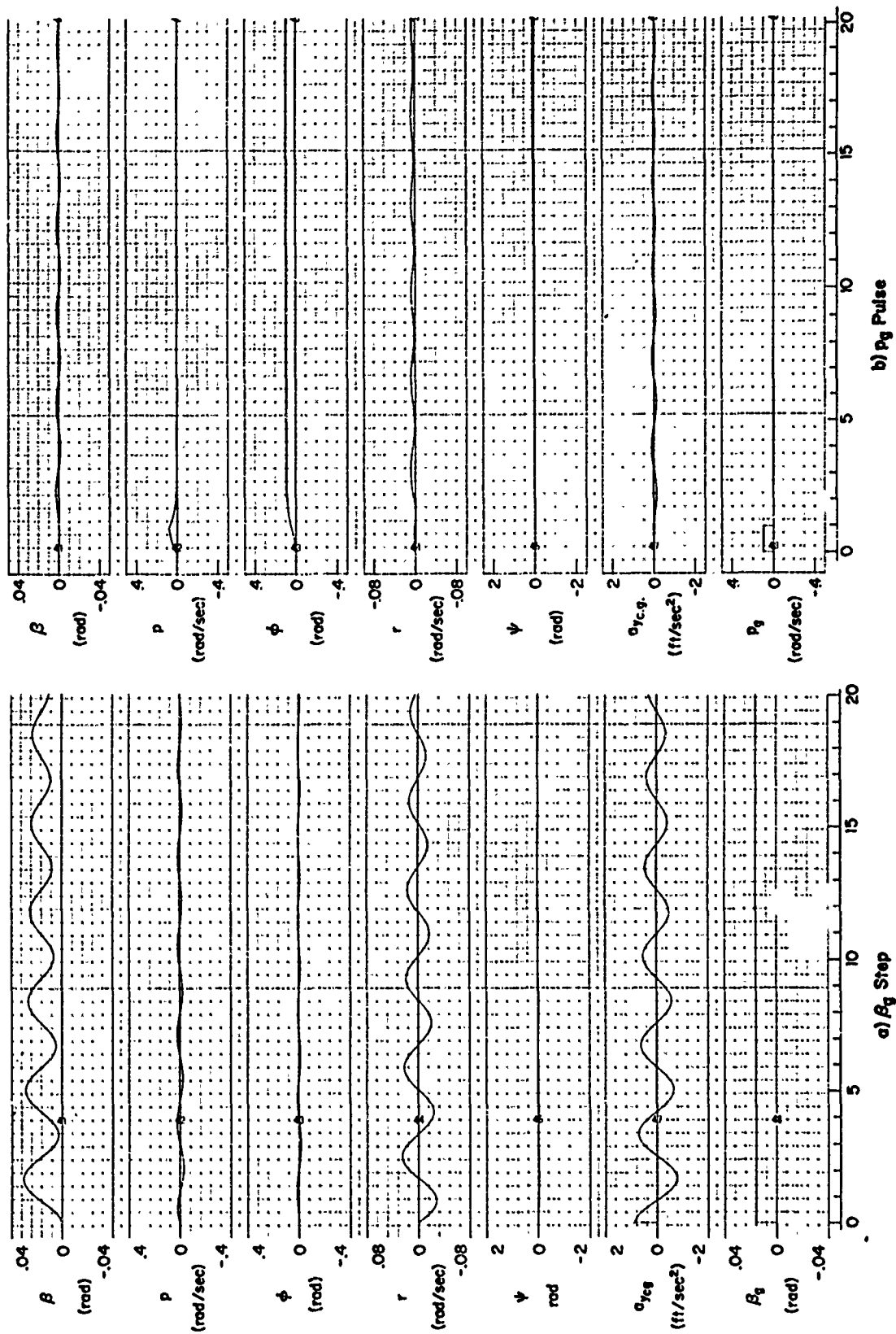


Figure 6-12. Responses of the Example Conventional Airplane to Gust Inputs

6.11 COUPLING NUMERATORS

The general uses of, comments on, and appreciation for the longitudinal coupling numerators given in Chapter 5 apply equally well to the lateral coupling numerators. In brief,

- They are required for analysis of multiloop situations involving more than a single input to the vehicle
- They are simply obtained by replacing motion derivatives in the characteristic determinant by the appropriate feedback control-input derivatives
- They can be due to coupling between gust- and control-inputs and among more than two inputs, control or disturbance
- They are always of order s^2 or lower, and are easily computed; therefore it is unnecessary to catalogue all possible combinations

The most commonly used aileron and rudder coupling numerators are given in Table 6-3, which contains the polynomial coefficients in literal primed-derivative terms, the corresponding factored forms, and literal approximations to the factors. The latter are based on neglecting terms usually unimportant for conventional airplanes (terms neglected are obvious by comparison with the complete polynomial coefficients). For unconventional configurations the approximate factors shown may not be appropriate, in which case the specifically important contributions to the exact polynomial coefficients can be used.

6.12 APPROXIMATE FACTORS

We have already derived some approximate factors in association with the various sets of simplified equations. However we have also noted that, in general, the numerator factors thus obtained are not necessarily good approximations to the complete situation. For these we can use a direct approach which involves factoring the literal polynomial expressions in Table 6-1 by partitioning the polynomial into a form $N(s) + KD(s)$ which can be factored by servo analysis methods (see Section 3.4). This approach yields relatively accurate factors for specific "conditions of validity."

Naturally, the relative significance of given derivatives or groups thereof depends on the vehicle configuration and/or flight condition; therefore,

TABLE 6-3
LATERAL COUPLING NUMERATORS FOR AILERON AND RUDDER INPUTS

	A	B	C
$N_{\delta_a \delta_r}^{\phi r}$ or $-N_{\delta_a \delta_r}^{r \phi}$	$L_{\delta_a}^i N_{\delta_r}^i - N_{\delta_a}^i L_{\delta_r}^i$	$-Y_v(L_{\delta_a}^i N_{\delta_r}^i - N_{\delta_a}^i L_{\delta_r}^i)$ $+ L_{\delta_a}^i (Y_{\delta_a}^* N_{\delta_r}^i - N_{\delta_a}^i Y_{\delta_r}^*)$ $- N_{\delta_a}^i (Y_{\delta_a}^* L_{\delta_r}^i - L_{\delta_a}^i Y_{\delta_r}^*)$ $A_{\phi r} \left(s + \frac{1}{T_{\phi r}} \right) \sim$ $A_{\phi r} \doteq L_{\delta_a}^i N_{\delta_r}^i ; \quad \frac{1}{T_{\phi r}} \doteq -Y_v + \frac{Y_{\delta_r}^*}{N_{\delta_r}^i} \left(N_{\beta}^i - \frac{N_{\delta_a}^i}{L_{\delta_a}^i} L_{\beta}^i \right)$	
$N_{\delta_a \delta_r}^{\phi \beta}$ or $-N_{\delta_a \delta_r}^{\beta \phi}$	$L_{\delta_a}^i Y_{\delta_r}^* - Y_{\delta_a}^* L_{\delta_r}^i$	$-N_r^i (L_{\delta_a}^i Y_{\delta_r}^* - Y_{\delta_a}^* L_{\delta_r}^i)$ $+ L_r^i (N_{\delta_a}^i Y_{\delta_r}^* - Y_{\delta_a}^* N_{\delta_r}^i)$ $+ (N_{\delta_a}^i L_{\delta_r}^i - L_{\delta_a}^i N_{\delta_r}^i)$ $A_{\phi \beta} \left(s + \frac{1}{T_{\phi \beta}} \right)$ $A_{\phi \beta} \doteq L_{\delta_a}^i Y_{\delta_r}^* ; \quad \frac{1}{T_{\phi \beta}} \doteq -N_r^i - \frac{N_{\delta_r}^i}{Y_{\delta_r}^*}$	
$N_{\delta_a \delta_r}^{\phi a y}$ or $-N_{\delta_a \delta_r}^{a y \phi}$	$U_0 (L_{\delta_a}^i Y_{\delta_r}^* - Y_{\delta_a}^* L_{\delta_r}^i)$ $+ x_a (L_{\delta_a}^i N_{\delta_r}^i - N_{\delta_a}^i L_{\delta_r}^i)$	$-U_0 N_r^i (L_{\delta_a}^i Y_{\delta_r}^* - Y_{\delta_a}^* L_{\delta_r}^i)$ $+ U_0 L_r^i (N_{\delta_a}^i Y_{\delta_r}^* - Y_{\delta_a}^* N_{\delta_r}^i)$ $+ x_a \left[-Y_v (L_{\delta_a}^i N_{\delta_r}^i - N_{\delta_a}^i L_{\delta_r}^i) \right.$ $\quad \left. + L_{\beta}^i (Y_{\delta_a}^* N_{\delta_r}^i - N_{\delta_a}^i Y_{\delta_r}^*) \right.$ $\quad \left. - N_{\beta}^i (Y_{\delta_a}^* L_{\delta_r}^i - L_{\delta_a}^i Y_{\delta_r}^*) \right]$	$U_0 \left[-Y_v (L_{\delta_a}^i N_{\delta_r}^i - N_{\delta_a}^i L_{\delta_r}^i) \right.$ $\quad \left. + L_{\beta}^i (Y_{\delta_a}^* N_{\delta_r}^i - N_{\delta_a}^i Y_{\delta_r}^*) \right.$ $\quad \left. - N_{\beta}^i (Y_{\delta_a}^* L_{\delta_r}^i - L_{\delta_a}^i Y_{\delta_r}^*) \right]$
	<p>where the a_y sensor is located x_a feet ahead of the c.g.</p> $A_{\phi y} \left[s^2 + 2(\zeta_{\phi y})_y s + (\omega_{\phi y})_y^2 \right]$ $x_{a_0} = -\frac{U_0 Y_{\delta_r}^*}{N_{\delta_r}^i} \sim \text{Center of rotation}$ $x_a = x_{a_0} + \Delta x_a$ $A_{\phi y} \doteq L_{\delta_a}^i (U_0 Y_{\delta_r}^* + x_a N_{\delta_r}^i) \doteq -L_{\delta_a}^i U_0 Y_{\delta_r}^* \frac{\Delta x_a}{x_{a_0}}$ $(\omega_{\phi y})_y^2 \doteq \frac{U_0}{\Delta x_a N_{\delta_r}^i} \left[Y_{\delta_r}^* \left(N_{\beta}^i - \frac{N_{\delta_a}^i}{L_{\delta_a}^i} L_{\beta}^i \right) - Y_v N_{\delta_r}^i \right] \doteq -\frac{U_0 Y_v}{\Delta x_a}$ $2(\zeta_{\phi y})_y \doteq \frac{x_a}{\Delta x_a N_{\delta_r}^i} \left[Y_{\delta_r}^* \left(N_{\beta}^i - \frac{N_{\delta_a}^i}{L_{\delta_a}^i} L_{\beta}^i \right) - Y_v N_{\delta_r}^i \right] - \frac{U_0 Y_{\delta_r}^*}{\Delta x_a N_{\delta_r}^i} \left(N_r^i - \frac{N_{\delta_a}^i}{L_{\delta_a}^i} L_r^i \right) \doteq -\frac{x_a}{\Delta x_a} Y_v$		

as in the longitudinal case, there is no single set of literal approximate factors which applies to all situations. This results in the large collection of approximate factors given in Tables 6-4 and 6-7, which are taken from the same references used for the corresponding longitudinal tables.

Table 6-4 contains the approximate factors for conventional airplanes, and these apply also to single-rotor helicopters at speeds over 50 ft/sec. Notice that the denominator factors are essentially identical to those obtainable (Eqs. 6-22, 6-26) from the three-degree-of-freedom dutch roll and spiral/roll-subsidence approximate equations of motion. Some of the numerator factors are expressed in terms of unprimed derivatives and some in terms of primed derivatives, depending on which results in the more compact form. As noted earlier, this may lead to confusion regarding the proper value of the transfer function gain; this is, however, easily resolvable according to the rules given on page 6-6.

The various expressions in Table 6-4 indicate directly the derivatives of primary importance for a given dynamic mode and the connections between denominator and numerator factors. These connections are specifically spelled out for conventional aircraft in Table 6-5, which can also be used to indicate the gross effects of artificial stability derivative augmentation via motion feedback to the control surfaces.

In general, the conditions for which the Table 6-4 approximate factors apply are inappropriate for hovering and transition flight of helicopters and VTOL aircraft. The latter situations are treated in Table 6-7, to which Table 6-6 serves as a guide. In Table 6-7 we continue to refer to aileron and rudder controls; as noted in Table 6-6, these are to be taken as whatever devices are used to produce rolling and yawing moments, respectively (e.g., main rotor lateral cyclic pitch and tail rotor collective pitch for a single-rotor helicopter).

We can check some of the VTOL approximate factors against our example hovering vehicle. Doing so, we find, for instance, from Table 6-7a and b that the approximate expressions yield

$$\frac{\phi(s)}{\delta_a(s)} = \frac{0.696(s+0.14)(s+0.662)}{(s+0.662)(s+0.873)[s^2 - 2(0.347)(0.662) + (0.662)^2]} \quad (6-41)$$

TABLE 6-4

SUMMARY OF CONVENTIONAL AIRPLANE LATERAL APPROXIMATE FACTORS

a) Denominator:

FACTORED FORMS	APPROXIMATE FACTORS	CONDITIONS OF VALIDITY
$\Delta(s) = \underbrace{\left(s + \frac{1}{T_S}\right) \left(s + \frac{1}{T_R}\right)}_{\text{or}} s^2 + 2\zeta\omega_d s + \omega_d^2$	$\omega_d^2 \doteq N_\beta^*$ $2(\zeta\omega)_d \doteq -(\gamma_V + N_T^*) - \frac{L_\beta^*}{N_\beta^*} \left(N_T^* - \frac{g}{U_0}\right)$ $\frac{1}{T_R} \doteq -L_\beta^* + \frac{L_\beta^*}{N_\beta^*} \left(N_T^* - \frac{g}{U_0}\right)$ $\frac{1}{T_S} \doteq T_R \frac{g}{U_0} \left(\frac{L_\beta^*}{N_\beta^*} N_T^* - L_\beta^*\right)$	$\left[\begin{aligned} &\gamma_T = \gamma_P = \gamma_Q = \gamma_V = L_V = N_T^* = 0 \\ & \gamma_V N_T^* - N_\beta^* L_T^* \ll N_\beta^* \\ &\left \frac{g}{U_0} \sin \gamma_0 \right \ll L_\beta^* \\ & \gamma_V L_T^* \ll L_\beta^* \\ &\left \frac{L_\beta^*}{N_\beta^*} (\gamma_V + N_T^*) \right < 0.3 \\ &\left \frac{L_\beta^*}{L_\beta^* N_\beta^*} \left(N_T^* - \frac{g}{U_0}\right) \right < 0.4 \end{aligned} \right]$ $\left \frac{L_\beta^* N_T^*}{L_\beta^* N_\beta^*} \right \ll 1, \quad \left \frac{1}{T_S} \right \ll \left \frac{1}{T_R} \right $
$(s^2 + 2\zeta_{SR}\omega_{SR}s + \omega_{SR}^2)$	$\omega_{SR}^2 \doteq \frac{\frac{g}{U_0} \left(\frac{L_\beta^* N_T^*}{N_\beta^*} - L_T^*\right)}{1 + \frac{L_\beta^*}{N_\beta^*} (\gamma_V + N_T^*)}$ $2(\zeta\omega)_{SR} \doteq \frac{L_\beta^* \left(N_T^* - \frac{g}{U_0}\right)}{1 + \frac{L_\beta^*}{N_\beta^*} (\gamma_V + N_T^*)}$ $2(\zeta\omega)_d \doteq -(\gamma_V + N_T^*) - \left\{ \frac{L_\beta^* (\gamma_V + N_T^*) + L_\beta^* (N_T^* - \frac{g}{U_0})}{N_\beta^* \left[1 + \frac{L_\beta^*}{N_\beta^*} (\gamma_V + N_T^*) \right]} \right\}$ $\omega_d^2 \doteq N_\beta^* \left[1 + \frac{L_\beta^*}{N_\beta^*} (\gamma_V + N_T^*) \right] - \omega_{SR}^2 - 4(\zeta\omega)_{SR}(\zeta\omega)_d$	<p>*Same conditions applicable</p> $\left \frac{\frac{g}{U_0} (L_\beta^* N_T^* - N_\beta^* L_T^*)}{N_\beta^* \left[1 + \frac{L_\beta^*}{N_\beta^*} (\gamma_V + N_T^*) \right]} \right \ll 1$ $\left \frac{-(\gamma_V + L_\beta^* + N_T^*) \left[-L_\beta^* N_\beta^* + L_\beta^* (N_T^* - \frac{g}{U_0}) \right]}{N_\beta^* \left[1 + \frac{L_\beta^*}{N_\beta^*} (\gamma_V + N_T^*) \right]^2} \right < 0.25$ $0.005 < \frac{\frac{g}{U_0} \left(\frac{L_\beta^* N_T^*}{N_\beta^*} - L_T^* \right)}{1 + \frac{L_\beta^*}{N_\beta^*} (\gamma_V + N_T^*)} < 1$

*Applicable also to single-rotor helicopters at high speed ($U_0 > 50$ fps).

TABLE 6-4 (Continued)
b) Alleron Numerators

FACTORED FORMS	APPROXIMATE FACTORS	CONDITIONS OF VALIDITY
$N_Q(s) = A_Q(s^2 + 2\xi_Q\omega_Q s + \omega_Q^2)$	$A_Q = L_{\delta_a}^i$ $\omega_Q^2 \doteq N_{\beta}^i \left(1 - \frac{N_{\delta_a}^i I_{\beta}^i}{L_{\delta_a}^i N_{\beta}^i} \right)$ $2\xi_Q\omega_Q \doteq - (Y_V + N_T^i) + \frac{N_{\delta_a}^i I_T^i}{L_{\delta_a}^i}$	$Y_{\delta_a} \doteq 0$ $ Y_V(L_{\delta_a}^i N_T^i - L_T^i N_{\delta_a}^i) \ll L_{\delta_a}^i N_{\beta}^i - L_{\beta}^i N_{\delta_a}^i $
$N_T(s) = A_T \left(s + \frac{1}{T_{T1}} \right) (s^2 + 2\xi_T\omega_T s + \omega_T^2)$	$A_T \doteq \frac{I_{xz}}{I_z} L_{\delta_a}$ $\frac{1}{T_{T1}} \doteq \omega_T \doteq \left(\frac{I_z}{I_{xz}} \frac{g}{U_0} N_{\beta} \right)^{1/3}$ $2\xi_T\omega_T \doteq \frac{I_z}{I_x} N_{\beta} - Y_V - \frac{1}{T_{T1}}$	$N_{\delta_a} = Y_{\delta_a} \doteq 0$ $B - AC^{1/3} \ll C^{2/3}$ $B = - \frac{I_z}{I_{xz}} Y_V N_{\beta}$ $A = \frac{I_z}{I_{xz}} N_{\beta} - Y_V$ $C = \frac{I_z}{I_{xz}} \frac{g}{U_0} N_{\beta}$
$N_{\beta}(s) = A_{\beta} \left(s + \frac{1}{T_{\beta1}} \right) \left(s + \frac{1}{T_{\beta2}} \right)$	$A_{\beta} \doteq N_{\delta_a}^i$ $\frac{1}{T_{\beta1}} \doteq \left(\frac{g}{U_0} \right) \frac{L_{\delta_a}^i N_T^i}{L_{\beta}^i - \frac{I_{\delta_a}^i}{N_{\delta_a}^i} (N_{\beta}^i - \frac{g}{U_0})}$ $\frac{1}{T_{\beta2}} \doteq - L_{\beta}^i + \frac{I_{\delta_a}^i}{N_{\delta_a}^i} (N_{\beta}^i - \frac{g}{U_0})$	$Y_{\delta_a}^* \doteq 0$ $\left \frac{g}{U_0} \left(L_T^i - \frac{L_{\delta_a}^i}{N_{\delta_a}^i} N_T^i \right) \right \ll \left[L_{\beta}^i - \frac{L_{\delta_a}^i}{N_{\delta_a}^i} (N_{\beta}^i - \frac{g}{U_0}) \right]^2$

TABLE 6-4 (Concluded)

c) Rudder Numerators

FACTORED FORMS	APPROXIMATE FACTORS	CONDITIONS OF VALIDITY
$N_D(s) = A_D \underbrace{(s^2 + 2\zeta_D \omega_D s + \omega_D^2)}_{\text{or}} \left(s + \frac{1}{T_{D1}}\right) \left(s + \frac{1}{T_{D2}}\right)$	$A_D = L_{D_r}^i$ $\omega_D^2 \text{ or } \frac{1}{T_{D1} T_{D2}} = N_D^i \left[1 - \frac{L_{D_r}^i N_{D_r}^i}{N_D^i L_{D_r}^i} + \frac{Y_{D_r}^i L_{D_r}^i}{L_{D_r}^i} \left(1 - \frac{L_{D_r}^i N_{D_r}^i}{N_D^i L_{D_r}^i} \right) \right]$ $2\zeta_D \omega_D \text{ or } \frac{1}{T_{D1}} + \frac{1}{T_{D2}} = - (Y_V + N_D^i) + \frac{Y_{D_r}^i L_{D_r}^i + N_{D_r}^i L_{D_r}^i}{L_{D_r}^i}$	$\left Y_V \left(N_D^i - \frac{Y_{D_r}^i N_{D_r}^i}{L_{D_r}^i} \right) \right \ll \omega_D^2$
$N_T(s) = A_T \underbrace{\left(s + \frac{1}{T_{T1}} \right) (s^2 + 2\zeta_T \omega_T s + \omega_T^2)}_{\text{or}} \left(s + \frac{1}{T_{T2}} \right) \left(s + \frac{1}{T_{T3}} \right)$	$A_T = N_{D_r}$ $\left. \begin{aligned} \frac{1}{T_{T1}} &= \left(-\frac{g}{U_0} L_p \right)^{1/2} \\ \omega_T &= \left \frac{1}{T_{T1}} \right \\ 2\zeta_T \omega_T &= -Y_V - L_p - \frac{1}{T_{T1}} \\ \frac{1}{T_{T2}} &= -L_p \\ \frac{1}{T_{T3}} &= - \left(Y_V - \frac{Y_{D_r}^i N_{D_r}^i}{N_{D_r}^i L_{D_r}^i} \right) \\ \frac{1}{T_{T3}} &= - \frac{g L_p}{U_0 L_p \left(Y_V - \frac{Y_{D_r}^i N_{D_r}^i}{N_{D_r}^i L_{D_r}^i} \right)} \\ \omega_T^2 &= \frac{g}{U_0} \frac{L_p}{L_p} \\ 2\zeta_T \omega_T &= - \left(Y_V - \frac{Y_{D_r}^i N_{D_r}^i}{N_{D_r}^i L_{D_r}^i} - \frac{g}{U_0} \frac{L_p}{L_p} \right) \end{aligned} \right\}$	$L_{D_r}^i \approx 0$ $\left \frac{g}{U_0} L_p \right \gg L_p^2 , \quad \left \frac{Y_{D_r}^i L_{D_r}^i}{N_{D_r}^i L_{D_r}^i} \right \ll 1$ $\left \frac{Y_{D_r}^i L_{D_r}^i N_{D_r}^i}{N_{D_r}^i L_{D_r}^i} \right \ll 1, \quad \left \frac{L_p N_{D_r}^i}{N_{D_r}^i L_{D_r}^i} \right \ll 1$ $\left \frac{g}{U_0} \frac{L_p}{L_p} \right < \left \frac{\left(Y_V - \frac{Y_{D_r}^i N_{D_r}^i}{N_{D_r}^i L_{D_r}^i} \right)^2}{4} \right $ $\left \frac{\left(Y_V - \frac{Y_{D_r}^i N_{D_r}^i}{N_{D_r}^i L_{D_r}^i} \right)^2}{4} \right < \left \frac{g}{U_0} \frac{L_p}{L_p} \right < \left \frac{L_p^2}{U_0} \right $
$N_D(s) = A_D \left(s + \frac{1}{T_{D1}} \right) \left(s + \frac{1}{T_{D2}} \right) \left(s + \frac{1}{T_{D3}} \right)$	$A_D = Y_{D_r}^i$ $\frac{1}{T_{D1}} = \left(\frac{g}{U_0} \right) \frac{L_p - \frac{L_{D_r}^i N_{D_r}^i}{N_{D_r}^i L_{D_r}^i}}{L_p - \frac{L_{D_r}^i N_{D_r}^i}{N_{D_r}^i L_{D_r}^i} \left(Y_V - \frac{g}{U_0} \right)}$ $\frac{1}{T_{D2}} = -L_p + \frac{Y_{D_r}^i N_{D_r}^i}{N_{D_r}^i L_{D_r}^i} \left(Y_V - \frac{g}{U_0} \right)$ $\frac{1}{T_{D3}} = -\frac{N_{D_r}^i}{Y_{D_r}^i}$	$ L_p + N_D^i \ll \left \frac{N_{D_r}^i}{Y_{D_r}^i} \right $ $ L_p N_D^i - N_{D_r}^i N_{D_r}^i \ll \left \frac{N_{D_r}^i}{Y_{D_r}^i} \left(L_p - \frac{L_{D_r}^i N_{D_r}^i}{N_{D_r}^i L_{D_r}^i} \left(Y_V - \frac{g}{U_0} \right) \right) \right $ $\left \frac{1}{T_{D1}} \left(\frac{1}{T_{D2}} + \frac{1}{T_{D3}} \right) \right \ll \left \frac{1}{T_{D2} T_{D3}} \right $
<p>General:</p> $N_{ay}(s) = A_{ay} \underbrace{\left(s + \frac{1}{T_{ay1}} \right) \left(s + \frac{1}{T_{ay2}} \right) (s^2 + 2\zeta_{ay} \omega_{ay} s + \omega_{ay}^2)}_{\text{or}} \left(s + \frac{1}{T_{ay3}} \right) \left(s + \frac{1}{T_{ay4}} \right)$ <p>where a_y sensor is located X_a feet ahead of the c.g.</p>	$A_{ay} = Y_{D_r} + X_a N_{D_r}^i$ $\frac{1}{T_{ay1}} = \frac{g}{U_0} \left[\frac{L_p}{L_p} - \frac{N_D (Y_V L_{D_r} - Y_{D_r}^i L_{D_r}^i)}{L_p (Y_V N_{D_r}^i - Y_{D_r}^i N_{D_r}^i)} \right]$ $\frac{1}{T_{ay2}} = -L_p$ $\omega_{ay}^2 \text{ or } \frac{1}{T_{ay3} T_{ay4}} = \frac{U_0}{\Delta X_a N_{D_r}^i} (Y_{D_r}^i N_{D_r}^i - Y_V N_{D_r}^i)$ $2\zeta_{ay} \omega_{ay} \text{ or } \frac{1}{T_{ay3}} + \frac{1}{T_{ay4}} = - \frac{Y_{D_r}}{\Delta X_a (N_{D_r}^i)^2} (Y_{D_r}^i N_{D_r}^i - Y_V N_{D_r}^i)$	$N_{D_r}^i L_{D_r}^i \approx N_{D_r}^i L_p$ $ L_{D_r}^i N_{D_r}^i < Y_{D_r}^i N_{D_r}^i $ $\left \frac{L_p N_{D_r}^i}{N_{D_r}^i L_{D_r}^i} \right \ll 1$ $ N_{D_r}^i L_p \gg Y_{D_r}^i N_{D_r}^i - Y_V N_{D_r}^i $ $\left \frac{L_p Y_{D_r}^i}{N_{D_r}^i} \right \ll 1$ $ L_{D_r}^i N_{D_r}^i \ll N_{D_r}^i L_p $
<p>At center of rotation:</p> $N_{ay}(s) = A_{ay} \left(s + \frac{1}{T_{ay1}} \right) \left(s + \frac{1}{T_{ay2}} \right) \left(s + \frac{1}{T_{ay3}} \right)$	$A_{ay} = Y_{D_r} \left(-N_D^i + Y_V - \frac{Y_{D_r}^i N_{D_r}^i}{N_{D_r}^i L_{D_r}^i} \right)$ $\frac{1}{T_{ay3}} = \frac{-U_0 (Y_V N_{D_r}^i - Y_{D_r}^i N_{D_r}^i)}{Y_{D_r} \left(-N_D^i + Y_V - \frac{Y_{D_r}^i N_{D_r}^i}{N_{D_r}^i L_{D_r}^i} \right)}$	$\frac{g}{U_0} \text{ and } N_D^i \ll L_p $ $Y_V N_{D_r}^i - Y_{D_r}^i N_{D_r}^i = Y_V N_{D_r}^i - Y_{D_r}^i N_{D_r}^i$

TABLE 6-5

QUALITATIVE IMPORTANCE OF NORMAL AIRFRAME STABILITY PARAMETERS
TO LATERAL, AILERON AND RUDDER INPUT, TRANSFER FUNCTION QUANTITIES*

DERIVATIVE	L_D	L_P	L_R	$N_{\dot{\phi}}$ and Y_V	N_P	N_R	CHANGE IN FORE AND AFT SENSOR LOCATION	CHANGE IN I_{xz}	CHANGE IN POINT OF CONTROL APPLICATION
1. Denominator, $\Delta(s)$									
a. Spiral Mode, $1/T_s$	xxx		xx	xx		xx			
b. Roll Subsidence Mode, $1/T_R$	x	xxx		x	x				
c. Dutch Roll Undamped Frequency, ω_d	xx			xxx				xx	
d. Dutch Roll Damping, $2\zeta_{d+d}$	xx			xx	x	xxx		xx	
e. Lateral Phugoid Undamped Frequency, ω_{SR}	xxx		x	xxx		xx			
f. Lateral Phugoid Damping, $2\zeta_{SR} \omega_{SR}$	xx	xxx		xx	x				
2. Roll (Aileron Input) Numerator, $N_{\phi_a}^D(s)$									
a. Undamped Frequency, ω_{ϕ_a}	xx			xxx					x to xxx (as re- flected in $C_{n\delta_a}/C_{l\delta_a}$)
b. Damping, $2\zeta_{\phi_a} \omega_{\phi_a}$			x	xx		xxx			x
3. Roll (Rudder Input) Numerator, $N_{\phi_r}^D(s)$									
a. Undamped Frequency, ω_{ϕ_r} or Product of First Orders, $1/T_{\phi_1} T_{\phi_2}$	x		x	xx		x			x to xxx
b. Damping, $2\zeta_{\phi_r} \omega_{\phi_r}$ or Sum of First Orders, $1/T_{\phi_1} + 1/T_{\phi_2}$	x		x			xx			x to xxx
4. Yawing Velocity (Aileron Input) Numerator, $N_{\dot{\phi}_a}^F(s)$									
a. First-Order Factor, $1/T_{ra}$ Undamped Frequency of Quadratic Factor, ω_{ra}				xx				xx	
b. Quadratic Factor Damping, $2\zeta_{ra} \omega_{ra}$				xx	xx			x	xx to xxx
5. Yawing Velocity (Rudder Input) Numerator, $N_{\dot{\phi}_r}^F(s)$									
a. First Factor, $1/T_{r1}$		xxx							
b. Second Factor, $1/T_{r2}$				xx					xx to xxx
c. Third Factor, $1/T_{r3}$	xx	xx		xx					x
d. Quadratic Factor Frequency, ω_r	xx	xx							
e. Quadratic Factor Damping, $2\zeta_r \omega_r$	x	x		x					x
6. Sideslip Numerator, N_{β}^D									
a. First Factor, $1/T_{p1}$		xx	xx		x	x			x
b. Second Factor, $1/T_{p2}$		xxx			x				x
c. Third Factor, $1/T_{p3}$ (Rudder Input)									xxx
7. Side Acceleration (Rudder Input) Numerator, $N_{\ddot{\phi}_r}^{AY}(s)$									
a. First Factor, $1/T_{ay1}$	x	x	x	x		x			x
b. Second Factor, $1/T_{ay2}$		xxx							
c. Third Factor, $1/T_{ay3}$				xx			xxx	x	xx
d. Fourth Factor, $1/T_{ay4}$				xx			xxx	x	xx
e. Quadratic Factor Frequency, ω_{ay}				xx			xxx	x	xx
f. Quadratic Factor Damping, $2\zeta_{ay} \omega_{ay}$				xx			xxx	x	xx

*The only stability parameters considered in this Table are those that
(1) Exist in the normal uncontrolled airframe, and
(2) Can be augmented by relatively simple automatic control systems.

CODE

Blank - Little or no effect
x - Moderate effect
xx - Important effect
xxx - Predominant effect

TABLE 5-6
SUMMARY OF THE UNCONVENTIONAL AIRCRAFT LATERAL APPROXIMATE FACTORS GIVEN IN TABLE 6-7

	TILT-WING	HELICOPTER						TILT-ROTOR	
		SINGLE-ROTOR			TANDEM-ROTOR			TILT-ROTOR	
		Low Speed ^{1,3}	High Speed ^{2,3}	Hover	High Speed	Hover	High Speed	Hover	High Speed
				(U ₀ ± 0)	(U ₀ > 50 ft/sec)	(U ₀ ± 0)	(U ₀ > 40 ft/sec)	(U ₀ ± 0)	(U ₀ > 100 ft/sec)
Denominator	—	—	—	Table 6-4	✓	✓	—	—	—
	✓	✓	✓	✓	✓	✓	✓	✓	✓
	—	—	✓	✓	✓	✓	—	—	—
	—	—	—	—	—	—	✓	✓	—
Aileron (Rolling Moment Control)	✓	✓	✓	✓	✓	✓	✓	✓	✓
	—	—	✓	✓	✓	✓	—	—	—
	—	—	—	—	—	—	✓	✓	—
	—	—	—	—	—	—	✓	✓	✓
Rudder (Yawing Moment Control)	—	—	✓	✓	✓	✓	✓	—	—
	—	—	—	—	—	—	—	—	—
	—	—	—	—	—	—	—	—	—
	—	—	—	—	—	—	—	—	—

Notes: ¹ Includes range of speed for which wing incidence is within 45° of wing incidence at hover.
² Wing incidence greater than 45° from incidence at lower.
³ The separation of high and low speed factors by wing incidence is empirical.
 Asterisk (*) indicates condition for which numerator and denominator factors cancel to give, approximately, $r/s_r \pm N_{6r}/(L - N_r)$.

TABLE 6-7
APPROXIMATE LATERAL FACTORS FOR UNCONVENTIONAL AIRCRAFT
(a) Denominator (Δ_{lat}) Factors

FIRST COEFF.	APPROXIMATE FACTORS	CONDITIONS OF VALIDITY	APPLICABLE TO:
1	$\frac{1}{T_6} = -N_1'$ $\frac{1}{T_R} = -\frac{2}{\sqrt{g L_V'}} + \left(\frac{L_P}{L_V} - \frac{Y_V}{L_P} \right)$ $2\xi_{d\omega} = \sqrt{\frac{g L_V'}{L_P}} + \frac{L_P}{2} \left(\frac{Y_V}{L_P} - \frac{Y_V}{L_P} \right)$ $P_{\omega}^2 = \left[\frac{\frac{Y_{13} A_5}{Y_{12} A_5} - \frac{Y_{12}}{Y_{13}}}{\frac{Y_{12}}{Y_{13}} - \frac{Y_{13}}{Y_{12}}} \right] \left[1 + \frac{L_P}{L_V} \right] \left[\frac{L_P}{L_V} \right]$	$ u_0 N_1' \ll N_1' L_P $ $ L_P > Y_V $ $\left \frac{g L_V'}{L_P} \right > 1$	Tilt-duct hover
1	$\frac{1}{T_6} = \left[\frac{L_P}{L_V} - \frac{Y_V}{L_P} \right] \left[1 + \frac{L_P}{L_V} \right] \left[\frac{L_P}{L_V} \right]$ $\frac{1}{T_R} = -\frac{2}{\sqrt{g L_V'}} + \frac{L_P}{2} \left(\frac{Y_V}{L_P} - \frac{Y_V}{L_P} \right)$ $2\xi_{d\omega} = -Y_V + \frac{g L_V'}{L_P}$ <p>In hover, a better approximation is</p> $2\xi_{d\omega} = -Y_V - \frac{L_P}{2} \sqrt{\frac{L_P}{L_V}} + \frac{g L_V'}{2 L_P}$ $P_{\omega}^2 = \frac{-g L_V' + u_0 (L_P N_1' - N_1' L_P)}{-L_P - \frac{g L_V'}{L_P} \left(\frac{L_P}{L_V} \right)}$		Tandem-rotor helicopters all speeds

Table 6-7 (Continued)

(b) Co-numerator (N_0^2) Factors

FIRST COEFF.	APPROXIMATE FACTORS	CONDITIONS OF VALIDITY	APPLICABLE TO:
L_0^1	$\frac{1}{T_{01}} + \frac{1}{T_{02}} = -\left(N_T^1 + Y_V\right) + \frac{N_0^1}{L_0^1} L_T^1 + \frac{Y_0^1}{L_0^1} L_V^1$ <p>or $2\xi_{00}$</p> $\frac{1}{T_{01}} \frac{1}{T_{02}} = \frac{-N_0^1}{L_0^1} \left(L_V^1 U_0 + Y_V L_T^1 \right) + \left(Y_V N_T^1 + U_0 N_V^1 \right) + \frac{Y_0^1}{L_0^1} \left(L_T^1 N_V^1 - L_V^1 N_T^1 \right)$ <p>or ξ_{01}^1</p>	None; this is <u>exact</u> expression	All configurations and speeds, and specifically to: Tilt-wing and tilt-rotor.....aileron and rudder Tilt-duct.....rudder Tandem-rotor helicopter.....rudder at hover
L_{0r}^1	$2\xi_{00} = -Y_V - N_T^1 + \frac{N_{0r}^1}{L_{0r}^1} L_T^1$ $\omega_0^2 = U_0 N_V^1 + \frac{Y_{0r}^1}{L_{0r}^1} L_V^1 N_T^1 - \frac{N_{0r}^1}{L_{0r}^1} U_0 L_V^1$	$ Y_{0r} L_T^1 \ll N_{0r} L_T^1 + L_{0r}^1 (Y_V + N_T^1) $ <p>$2\xi_{00}$ is given by small difference between $(-Y_V - N_T^1)$ and $(N_{0r}^1/L_{0r}^1) L_T^1$; hence, accuracy is low for small ξ</p>	Single-rotor helicopter.....rudder at all speeds Tandem-rotor helicopter.....rudder at high speed
L_{0a}^1	$2\xi_{00} = -N_T^1 - Y_V$ $\omega_0^2 = U_0 N_V^1 + Y_V N_T^1 - \frac{N_{0a}^1}{L_{0a}^1} L_V^1 U_0$	$Y_{0a} = 0$	Tilt-duct.....aileron
L_{0a}^1	$2\xi_{00} = -N_T^1 - Y_V$ $\omega_0^2 = U_0 N_V^1$	$ Y_{0a} L_T^1 \ll U_0^1 L_{0a}^1 $ $(-Y_V - N_T^1)^2 < U_0 N_V^1 $	Single-rotor helicopter.....aileron
L_{0a}^1	$\frac{1}{T_{01}} \frac{1}{T_{02}} = U_0 N_V^1 + Y_V N_T^1$ <p>or ω_0^2</p> $\frac{1}{T_{01}} + \frac{1}{T_{02}} = -Y_V - N_T^1$ <p>or $2\xi_{00}$</p>	$ N_{0a}^1 L_{VZ} \ll L_{0a}^1 L_T^1 $ $\left \frac{Y_{0a}^1}{L_{0a}^1} \left(L_V^1 + \frac{L_{VZ}^1}{L_X^1} N_V^1 \right) + \frac{N_{0a}^1}{L_{0a}^1} \left(\frac{L_T^1}{L_X^1} - \frac{L_{VZ}^1}{L_X^1} Y_V \right) \right \ll N_T^1 + Y_V $ $ Y_{0a}^1 (L_T^1 N_V^1 - L_V^1 N_T^1) - N_{0a}^1 (U_0 L_V^1 + Y_V L_T^1) \ll L_{0a}^1 (U_0 N_V^1 + Y_V N_T^1) $ <p>For $U_0 \approx 0$, use $\frac{1}{T_{01}} \approx -N_T^1$, $\frac{1}{T_{02}} \approx -Y_V + \left(\frac{Y_{0a}^1}{L_{0a}^1} \right) L_V^1$</p>	Tandem-rotor helicopter.....aileron

Table 6-7 (Continued)
(c) r-Numerator (N'_R) Factors

FIRST COEFF.	APPROXIMATE FACTORS	CONDITIONS OF VALIDITY	APPLICABLE TO:
N'_{Rr}	$\frac{1}{T_r} = -\frac{L'_V}{I_p}$ $\omega_r^2 = \frac{-L'_V}{I_p} \left(-L'_V + \frac{I'_{G_r}}{N'_{G_r}} N'_V \right)$ For single-rotor, $2\xi_r \omega_r = 0$ For tandem-rotor, $2\xi_r \omega_r = -Y_V + \frac{\omega_r^2}{I_p}$	$ L'_V \gg \left \frac{I'_{G_r}}{N'_{G_r}} N'_V + \frac{Y'_{G_r}}{N'_{G_r}} N'_V \right $ $Y'_{G_r} = 0$ $\left \frac{1}{T_r} \right \gg \omega_r$ $\left \frac{1}{T_r} \right \gg 2\xi_r \omega_r $	Single- and tandem-rotor helicopters.....rudder
$Y'_{G_a} N'_V + I'_{G_a} N'_p$	$2\xi_r \omega_r = \frac{Y'_{G_a} (L'_V N'_p - N'_V L'_p) - I'_{G_a} Y'_V N'_p}{I'_{G_a} N'_p + Y'_{G_a} N'_V}$ $\omega_r^2 = \frac{g I'_{G_a} N'_V}{I'_{G_a} N'_p + Y'_{G_a} N'_V}$	Expressions are exact for $N'_{G_a} = 0$ $N'_{G_a} \neq 0$ introduces third root and changes first coefficient to N'_{G_a}	Single-rotor helicopter.....aileron
N'_{G_a}	$\frac{1}{T_r} = \left[g \left(-L'_V + N'_V \frac{I'_{G_a}}{N'_{G_a}} \right) \right]^{1/3}$ $\omega_r = 1/T_r $ $\xi_r = 0.5$ for $1/T_r < 0$ $\xi_r = -0.5$ for $1/T_r > 0$	$\frac{I'_{G_a}}{N'_{G_a}} = \frac{I'_{G_a}}{N'_{G_a}}$	Tandem-rotor hel.copter.....aileron

Table 6-7 (Concluded)
(d) v-Numerator (N_s^v) Factors

FIRST COEFF.	APPROXIMATE FACTORS	CONDITIONS OF VALIDITY	APPLICABLE TO:
Y_{θ_r}	$\frac{1}{T_{v1}} \doteq 0$ $\frac{1}{T_{v2}} + \frac{1}{T_{v3}} \doteq -L_p^i - \frac{U_0 N_{\theta_r}^i}{Y_{\theta_r}}$ $\frac{1}{T_{v2}} + \frac{1}{T_{v3}} \doteq \left[L_p^i N_r^i - L_r^i N_p^i - \frac{I_{\theta_r}^i}{Y_{\theta_r}} (U_0 N_p^i - \epsilon) + \frac{N_{\theta_r}^i}{Y_{\theta_r}} U_0 N_p^i \right]$	$U_0 \neq 0$ $\left \frac{1}{T_{v1}} \right \ll \frac{1}{T_{v2}}$ $\left \frac{1}{T_{v1}} \right \ll \frac{1}{T_{v3}}$	Single-rotor helicopter.....rudder at high speed
$-U_0 N_{\theta_r}^i$	$\frac{1}{T_{v1}} + \frac{1}{T_{v2}} \doteq - \left[L_p^i + \frac{I_{\theta_r}^i}{N_{\theta_r}^i} \left(\frac{\epsilon}{U_0} - N_p^i \right) \right]$ $\frac{1}{T_{v1}} + \frac{1}{T_{v2}} \doteq - \left[\frac{\epsilon}{U_0} \left(L_p^i - \frac{I_{\theta_r}^i}{N_{\theta_r}^i} N_r^i \right) \right]$	$Y_{\theta_r} = 0, U_0 \neq 0 \text{ (but valid for } U_0 \doteq 0)$ <p>At $U_0 = 0$, numerator becomes first-order: $\epsilon \left[L_p^i (s - N_r) + L_r^i N_{\theta_r}^i \right]$</p>	Tandem-rotor helicopter.....rudder
Y_{θ_r}	$\frac{1}{T_{v3}} \doteq -L_p^i - N_r^i - \frac{U_0 N_{\theta_r}^i}{Y_{\theta_r}}$ $\frac{1}{T_{v1}} + \frac{1}{T_{v2}} \left\{ \begin{array}{l} \doteq \frac{2 T_{v3}}{Y_{\theta_r}} (-L_{\theta_r}^i N_r^i + L_r^i N_{\theta_r}^i) \\ \text{or } \omega_c^2 \end{array} \right\}$ $\frac{1}{T_{v1}} + \frac{1}{T_{v2}} \left\{ \begin{array}{l} \doteq T_{v3} \left[(L_p^i N_r^i - L_r^i N_p^i) + \frac{U_0}{Y_{\theta_r}} (L_r^i N_{\theta_r}^i - I_{\theta_r}^i N_p^i) - \omega_c^2 \right] \\ \text{or } 2 \xi_{v\omega} \end{array} \right\}$	$\left \frac{1}{T_{v3}} \right \gg \left \frac{1}{T_{v1}} \right $ $\left \frac{1}{T_{v3}} \right \gg \left \frac{1}{T_{v2}} \right $	Tilt-duct.....rudder at high speed
$-U_0 N_{\theta_a}^i$	$\frac{1}{T_{v1}} + \frac{1}{T_{v2}} \left\{ \begin{array}{l} \doteq \frac{I_{\theta_a}^i}{N_{\theta_a}^i} \left(N_p^i - \frac{\epsilon}{U_0} \right) \\ \text{or } 2 \xi_{v\omega} \end{array} \right\}$ $\frac{1}{T_{v1}} + \frac{1}{T_{v2}} \left\{ \begin{array}{l} \doteq \frac{\epsilon}{U_0} \left(\frac{I_{\theta_a}^i}{N_{\theta_a}^i} N_r^i - L_r^i \right) \\ \text{or } \omega_c^2 \end{array} \right\}$	$Y_{\theta_a} = 0 ; N_{\theta_a}^i \neq 0$ <p>For hover, if $N_{\theta_a}^i = 0$, first coefficient = $\epsilon I_{\theta_a}^i$, $1/T_{v1} = -N_r^i$</p>	Tilt-duct.....aileron

which is in excellent agreement with Eq. 6-37. Because of this correspondence, we can use the approximate factor expressions to answer a variety of questions. For example, to determine what changes will stabilize the negatively damped dutch roll mode in the above denominator, one should make

$$2\zeta_d \omega_d \doteq \sqrt[3]{g L_V'} + \frac{2}{3}(-L_p' - Y_V) \quad (6-42)$$

greater than zero. It takes about a 2.7-fold increase in $-L_p' - Y_V$ as opposed to a reduction by a factor of about 1/20 on $-L_V'$ to accomplish such a change; and these relative effects are consistent with the interpretation of the time vector polygons of Fig. 6-9c. For the stable system that results for such changes, the final value theorem applies (Chapter 2), but now a step aileron input, instead of producing a steady-state roll rate, as for a conventional airplane (with small $1/T_s$), results in a steady-state bank angle given approximately by (Eq. 6-33):

$$\lim_{t \rightarrow \infty} \phi(t) \doteq \frac{L_{\delta_a} \delta_a(-Y_V)}{-g L_V'} \quad (6-43)$$

6.13 APPROXIMATE MODAL RESPONSE RATIOS

We have already studied the modal responses of selected example configurations by means of the time vector diagrams. Now, on the basis of the approximate factors and equations of motion, we can generalize to show the most interesting literal relationships for conventional airplanes.

Spiral and Roll Subsidence

From the three-degree-of-freedom spiral and roll subsidence equations (6-25), and first considering the side forces, we can say that both spiral and roll subsidence (free) motions involve an approximate balance between gravitational forces ($g\phi$) and centripetal forces ($U_0 r$), and that side accelerations are produced only by sideslip, i.e., $(s - Y_V)\beta = 0$. Unfortunately, the latter condition tells us little about the values of β relative to the remaining motion quantities. To obtain information on

this point we can evaluate the modal response ratio β/r separately for the spiral and roll subsidence modes using the simplified equations.

We choose $\beta/r = \Delta_{21}/\Delta_{23}$ (see Eq. 5-48) for the spiral evaluation, whereby

$$\left(\frac{\beta}{r}\right)_S = \frac{\begin{vmatrix} \frac{-g}{U_0} & 1 \\ -N_p' s & s - N_r' \end{vmatrix}_{s=-1/T_S}}{\begin{vmatrix} 0 & \frac{-g}{U_0} \\ -N_\beta' & -N_p' s \end{vmatrix}_{s=-1/T_S}} \quad (6-44)$$

$$\left(\frac{\beta}{r}\right)_S = \frac{\left[s \left(N_p' - \frac{g}{U_0} \right) + \frac{g}{U_0} N_r' \right]}{\frac{-g}{U_0} N_\beta'}$$

for $s = \frac{-1}{T_S} = -T_R \frac{g}{U_0} \left(N_r' \frac{I_\beta'}{N_\beta'} - L_r' \right)$

Substituting the values of s , and collecting terms,

$$\begin{aligned} \left(\frac{\beta}{r}\right)_S &= \frac{-N_r'}{N_\beta'} \left[1 - T_R \frac{I_\beta'}{N_\beta'} \left(N_p' - \frac{g}{U_0} \right) \right] - \frac{L_r' T_R}{N_\beta'} \left(N_p' - \frac{g}{U_0} \right) \\ &= \frac{-N_r' T_R}{N_\beta'} \left[\frac{1}{T_R} - \frac{I_\beta'}{N_\beta'} \left(N_p' - \frac{g}{U_0} \right) + \frac{L_r'}{N_r'} \left(N_p' - \frac{g}{U_0} \right) \right] \end{aligned}$$

and now substituting for $1/T_R$ (from Table 6-4),

$$\left(\frac{\beta}{r}\right)_S = \frac{-N_r'}{N_\beta'} \frac{\left[-L_p' + \frac{L_r'}{N_r'} \left(N_p' - \frac{g}{U_0} \right) \right]}{\left[-L_p' + \frac{I_\beta'}{N_\beta'} \left(N_p' - \frac{g}{U_0} \right) \right]} = \frac{-N_r'}{N_\beta'} \quad (6-45)$$

The final approximation follows because of the usual magnitude of the $(N'_p - g/U_0)$ term relative to L'_p . Note that it accurately predicts the balance of yawing moment contribution shown in Fig. 6-4a.

For the values appropriate to conventional airplane flight, N'_r/N'_β is invariably small. The spiral mode is therefore usually characterized by banking and turning motions which produce little side acceleration and which, therefore, are approximately coordinated. In the case of an unstable spiral ($1/T_s < 0$) the uncontrolled bank angle and turn rate gradually increase (diverge); and as the bank angle increases, the vertical component of lift is reduced so the airplane's descent rate increases. Thus the motion through space consists of a tightening spiral dive, from which the mode takes its name.

For the roll subsidence mode, we evaluate $\beta/r = \Delta_{11}/\Delta_{13}$:

$$\left(\frac{\beta}{r}\right)_R = \frac{\begin{vmatrix} s(s-L'_p) & -L'_r \\ -N'_p s & s-N'_r \end{vmatrix}}{\begin{vmatrix} -L'_\beta & s(s-L'_p) \\ -N'_\beta & -N'_p s \end{vmatrix}} = \frac{(s-L'_p)(s-N'_r) - L'_r N'_p}{N'_\beta(s-L'_p) + L'_\beta N'_p} \Big|_{s=-1/T_R}$$

Recognizing that $|L'_r N'_p / L'_\beta N'_r| \ll 1$ and dividing through by $(s-L'_p)$,

$$\left(\frac{\beta}{r}\right)_R \doteq \frac{s - N'_r}{N'_\beta \left[1 + \frac{L'_\beta N'_p}{N'_\beta(s-L'_p)} \right]}$$

where

$$s = \frac{-1}{T_R} \doteq L'_p - \frac{L'_\beta}{N'_\beta} \left(N'_p - \frac{g}{U_0} \right)$$

$$\left(\frac{\beta}{r}\right)_R \doteq \frac{-\left(N'_p - \frac{g}{U_0}\right)}{\frac{g}{U_0} N'_\beta} \left[L'_p - N'_r - \frac{L'_\beta}{N'_\beta} \left(N'_p - \frac{g}{U_0} \right) \right] \quad (6-46)$$

When $(N_p' - g/U_0)$ is identically equal to zero, $(\beta/r)_R$ is also identically zero (Eq. 6-46). Then, to the extent that L_r' contributions are generally negligible, the single-degree-of-freedom dynamics apply regardless of the value of g/U_0 . This result is also indicated by the fact that for $(N_p' - g/U_0) = 0$ there is no difference between $-L_p'$ and $1/T_R$. Nevertheless, even for these ideally suitable circumstances the single-degree-of-freedom approximation is not adequate to accurately describe the magnitude of the rolling response which can be affected by β motions induced by aileron yaw (e.g., Eqs. 6-28 and 6-29).

Dutch Roll

The dutch roll motions, being oscillatory, are basically much more complex than the first-order spiral and roll subsidence modes. Nevertheless, as we shall see, there are pertinent generalizations which can be made. To derive these we examine the modal response ratios, ϕ/β and ψ/β , as obtained from the complete characteristic determinant of Eq. 6-1:

$$\begin{aligned} \left(\frac{\phi}{\beta}\right)_d &= \frac{-\Delta_{32}}{\Delta_{31}} = \frac{- \begin{vmatrix} s - Y_v & 1 \\ -L_p' & -L_r' \end{vmatrix}}{\begin{vmatrix} \frac{-g}{U_0} & 1 \\ s(s - L_p') & -L_r' \end{vmatrix}} \\ &= \frac{-L_r' \left[s - \left(Y_v + \frac{L_p'}{L_r'} \right) \right]}{s^2 - L_p' s - \frac{g}{U_0} L_r'} \end{aligned}$$

where

$$s = -\zeta_d \omega_d + j \omega_d \sqrt{1 - \zeta_d^2}$$

Noting that, usually, $|Y_v L_r'| \ll |L_p'|$ and $|(g/U_0) L_r'| \ll \omega_d^2$, and substituting the expression for s but dropping the subscript "d" for convenience,

$$\frac{\phi}{\beta} = \frac{L_p' + \zeta \omega L_r' - j \omega L_r' \sqrt{1 - \zeta^2}}{2\zeta^2 \omega^2 - \omega^2 + L_p' \zeta \omega - j \omega \sqrt{1 - \zeta^2} (L_p' + 2\zeta \omega)} \quad (6-47)$$

The magnitude is given by

$$\begin{aligned} \left| \frac{\Phi}{\beta} \right|^2 &= \frac{(L_p' + \zeta \omega L_R')^2 + \omega^2 L_R'^2 (1 - \zeta^2)}{\left[\omega^2 (1 - 2\zeta^2) - L_p' \zeta \omega \right]^2 + \omega^2 (1 - \zeta^2) (L_p' + 2\zeta \omega)^2} \\ &= \frac{L_p'^2 + \omega^2 L_R'^2 + 2\zeta \omega L_R' L_p'}{\omega^4 + \omega^2 L_p'^2 + 2\zeta \omega^3 L_p'} \end{aligned} \quad (6-48)$$

and for negligible L_R' terms, $\omega_d^2 \doteq N_p'$ and $-L_p' \doteq 1/T_R$.

$$\left| \frac{\Phi}{\beta} \right| \doteq \left| \frac{L_p'}{N_p'} \right| \frac{1}{\sqrt{1 + \frac{1}{\omega_d^2 T_R^2} (1 - 2\zeta_d \omega_d T_R)}} \quad (6-49)$$

The ζ_d term is usually negligible and is often discarded.

The phase angle (Eq. 6-47) is given by:

$$\angle \frac{\Phi}{\beta} = -\tan^{-1} \frac{\omega L_R' \sqrt{1 - \zeta^2}}{L_p' + \zeta \omega L_R'} + \tan^{-1} \frac{\omega \sqrt{1 - \zeta^2} (L_p' + 2\zeta \omega)}{\omega^2 (2\zeta^2 - 1) + L_p' \zeta \omega}$$

which, using the identity $\tan^{-1} x - \tan^{-1} y = \tan^{-1} \frac{x-y}{1+xy}$, reduces to:

$$\angle \frac{\Phi}{\beta} = \tan^{-1} \frac{\omega \sqrt{1 - \zeta^2} (L_p' L_p' + 2\zeta \omega L_p' + \omega^2 L_R')}{\omega^2 (2\zeta^2 - 1) L_p' + \zeta \omega^3 L_R' + \zeta \omega L_p' L_p' + \omega^2 L_R' L_p'} \quad (6-50)$$

For $\omega^2 \doteq N_p'$ and $\zeta \ll 1$, and dividing numerator and denominator by $\omega N_p' = \omega^3$,

$$\angle \frac{\Phi}{\beta} \doteq \tan^{-1} \frac{\frac{L_p'}{N_p'} (L_p' + 2\zeta_d \omega_d) + L_R'}{\frac{L_p'}{N_p'} (\zeta_d L_p' - \omega_d) + L_R' \left(\zeta_d + \frac{L_p'}{\omega_d} \right)} \quad (6-51)$$

Assuming L_R' terms are negligible and $2\zeta_d\omega_d \ll -L_p' \doteq 1/T_R$,

$$\angle \frac{\phi}{\beta} \doteq \tan^{-1} \frac{1}{\zeta_d + \omega_d T_R} \quad (6-52)$$

For $L_p'/N_\beta' \rightarrow 0$, so that only L_R' terms are left,

$$\angle \frac{\phi}{\beta} \doteq \tan^{-1} \frac{1}{\zeta_d - \frac{1}{\omega_d T_R}}$$

But, from Eq. 6-48 $|\phi/\beta|^2 = L_R'^2/(\omega_d^2 + L_p'^2)$ is very small, so that effectively $\phi \rightarrow 0$ and the phasing of ϕ/β is unimportant. In general, therefore, when significant ϕ motions do occur, Eqs. 6-49 and 6-52 are pertinent.

These relationships show that the predominant effect on the magnitude of the rolling motions is the ratio L_p'/N_β' , with the roll damping of increasing importance in reducing the motions as $1/\omega_d^2 T_R^2 \doteq L_p'^2/N_\beta'$ approaches and exceeds unity. The phasing between the ϕ and β motions is influenced primarily by the value of $\omega_d T_R$; i.e., from Eq. 6-52 for small ζ_d ,

$$\angle \frac{\phi}{\beta} \doteq \tan^{-1} \frac{1}{\omega_d T_R} \doteq \tan^{-1} \left(\frac{-L_p'}{\sqrt{N_\beta'}} \right)$$

and the bank angle therefore leads sideslip by less than 90° for $N_\beta' > 0$. The leading phase relationship is a result of the fact that in the dutch roll mode β is of opposite sign to the heading change, ψ , as we shall see below. Thus, referenced to the yawing oscillations, ϕ lags ψ by from approximately 90° to 180° as the roll damping decreases from large to small values.

To evaluate ψ/β as simply as possible, we express the side force equation (Eq. 6-1) as:

$$\frac{r}{\beta} - \frac{g}{U_0} \frac{\phi}{\beta} + (s - Y_V) = 0$$

so that

$$\left(\frac{r}{\beta}\right)_d = -s_d + Y_v + \frac{g}{U_0} \left(\frac{\varphi}{\beta}\right)_d \quad (6-53)$$

where

$$s_d = -\zeta_d \omega_d + j \omega_d \sqrt{1 - \zeta_d^2}$$

Generally, Y_v is very small with respect to ω_d , and for reasonable flight speeds, U_0 , so is $(g/U_0)(\varphi/\beta)$; accordingly,

$$\left(\frac{r}{\beta}\right)_d \doteq -s_d \quad \text{or} \quad \left(\frac{r}{s\beta}\right)_d = -1$$

Recognizing that (for $\gamma_0 = 0$) $\psi = r/s$, we get finally

$$\left(\frac{\psi}{\beta}\right)_d \doteq -1 \quad (6-54)$$

We see, therefore, that the usual heading and sideslip motions in dutch roll are consistent with those in relatively flat yawing oscillations. Implying from this that the rolling motions are not of primary importance leads to the two-degrees-of-freedom approximate dutch roll equations of motion (Eq. 6-18) presented earlier.

CHAPTER 7

ELEMENTARY LONGITUDINAL FEEDBACK CONTROL

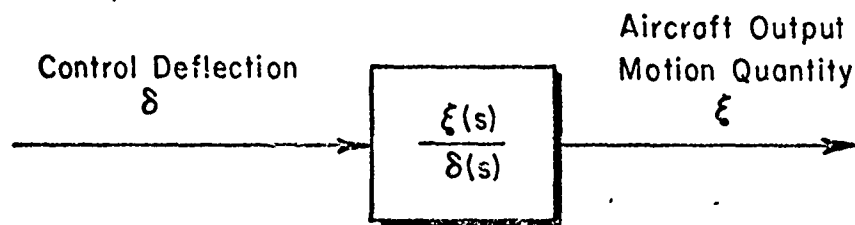
A most powerful approach to obtain an appreciation for the effects of automatic control on the motions of an aircraft is to consider closed-loop systems formed by direct feedback of aircraft motion quantities to the controls. Such systems are idealizations since, in fact, the controls cannot be moved without lag and instruments cannot sense and reproduce the motion quantities instantaneously and in a pure form. Nevertheless, consideration of these idealized systems shows the ultimate performance approachable by some practical system or, by way of contrast, reveals directions in which it would be unprofitable to proceed.

The prototype for all the systems to be discussed is the single-loop flight controller shown in Fig. 7-1. This illustrates the direct feedback of a generalized aircraft motion quantity, ξ , to a control deflection, δ . The reader will recognize that the transfer function which belongs in the controlled element block may be any one of the several developed in Chapters 5 or 6, which relate the aircraft motion quantities to control deflections. Table 7-1 lists the most promising possibilities in connection with longitudinal motions. Control using all of the output quantities listed will be discussed below using elevator as the actuation quantity.

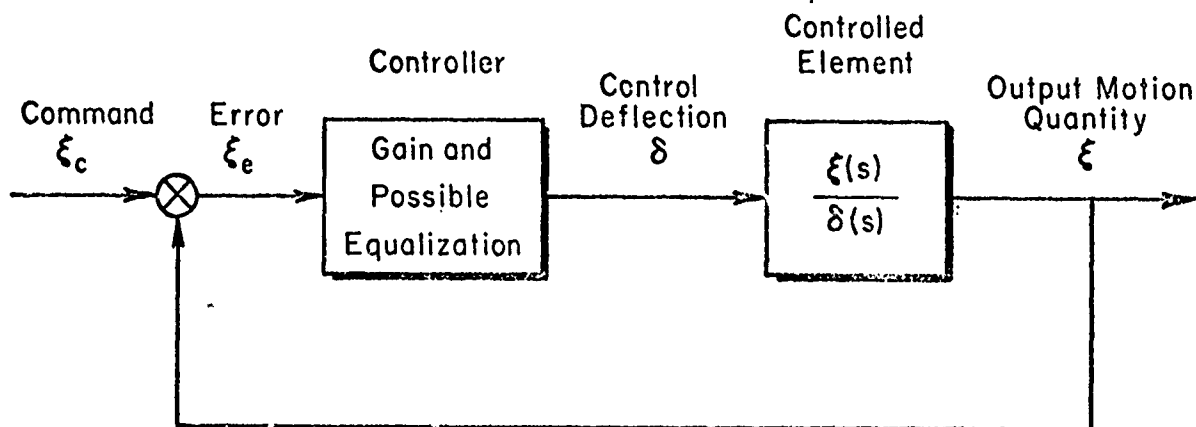
In many situations it will be instructive to consider that the controller is simply a gain, but in other cases it will be desirable to provide for lead, or lag and lead equalization. Yet in each instance only a single output motion variable will be of interest or concern.

7.1 FEEDBACK OF PITCH ANGLE AND PITCH RATE TO THE ELEVATOR

Historically, the earliest automatic pilots comprised a vertical gyroscope and an associated actuator which deflected the elevator in such a way as to oppose departures from the reference or commanded pitch attitude. In modern terms this would be described as negative feedback of the pitch attitude, θ , to the elevator control deflection, δ_e . The



a) The Open - Loop System (Controlled Element)



b) Elementary Single Sensor Control System

Fig. 7-1. Feedback of Aircraft Motion Quantities

TABLE 7-1
LONGITUDINAL MOTION AIRFRAME OUTPUT AND ACTUATING QUANTITIES

OUTPUT QUANTITIES	ACTUATING QUANTITIES
θ , pitch angle	δ_e , elevator deflection
q , pitch rate	δ_f , flap deflection
u , forward velocity	δ_T , engine power control deflection
α , angle of attack, w/U_0	
a_x , longitudinal acceleration	
a_z , normal acceleration, $a_{z.c.g.} - x_a \dot{q}$	
h , altitude	

appropriate controlled element transfer function is therefore $\theta(s)/\delta_e(s)$,

$$\frac{\theta(s)}{\delta_e(s)} = \frac{N_{\delta_e}^\theta}{\Delta_{\text{long}}} = \frac{A_\theta \left(s + \frac{1}{T_{\theta_1}}\right) \left(s + \frac{1}{T_{\theta_2}}\right)}{\left[s^2 + 2\zeta_p \omega_p s + \omega_p^2\right] \left[s^2 + 2\zeta_{sp} \omega_{sp} s + \omega_{sp}^2\right]} \quad (7-1)$$

In what follows several variants of this controlled element transfer function will be considered. First, we assume that the airplane pitch attitude characteristics are well behaved, with good short-period damping, large separation between short-period and phugoid frequencies, etc. Then we explore a variety of less favorable characteristics, including insufficient short-period damping, longitudinal divergences of one kind or another, non-zero position error, etc.

Conventional Pitch Attitude Control

Figure 7-2 shows the block diagram of the θ to δ_e ($\theta \rightarrow \delta_e$) feedback control system with a pure gain controller. The figure also contains a "system survey" using Bode and conventional root loci to show the location of the closed-loop roots as a function of the closed-loop system gain. The dynamics of the uncontrolled vehicle represented by the open-loop characteristics illustrated in Fig. 7-2 are typical of a well-behaved aircraft in cruising flight at moderate altitudes. The main features of these characteristics are the wide separation between the short-period and phugoid breakpoints, in both amplitude ratio and frequency, and the relatively heavy damping of the short-period mode.

From the system surveys it can be appreciated that, at moderate gain, the modified (closed-loop) phugoid roots are driven into close proximity to the zeros while the short-period roots move to a higher frequency and lower damping ratio. This is not undesirable provided the open-loop short-period damping is not initially already marginal. The key point is that the phugoid damping increase is obtained at the expense of the short period. In fact, the total system damping is unchanged by the feedback of terms which, when considered as creating or augmenting stability derivatives, do not affect the coefficient of the second term

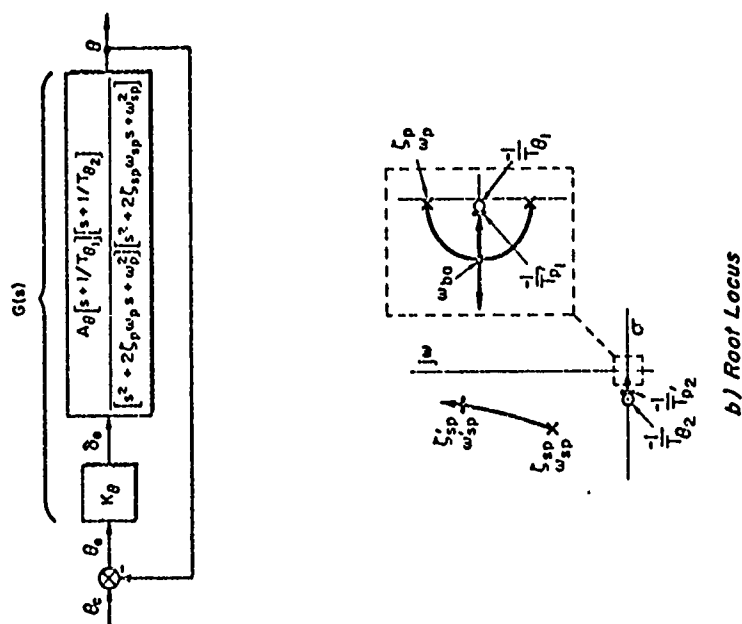
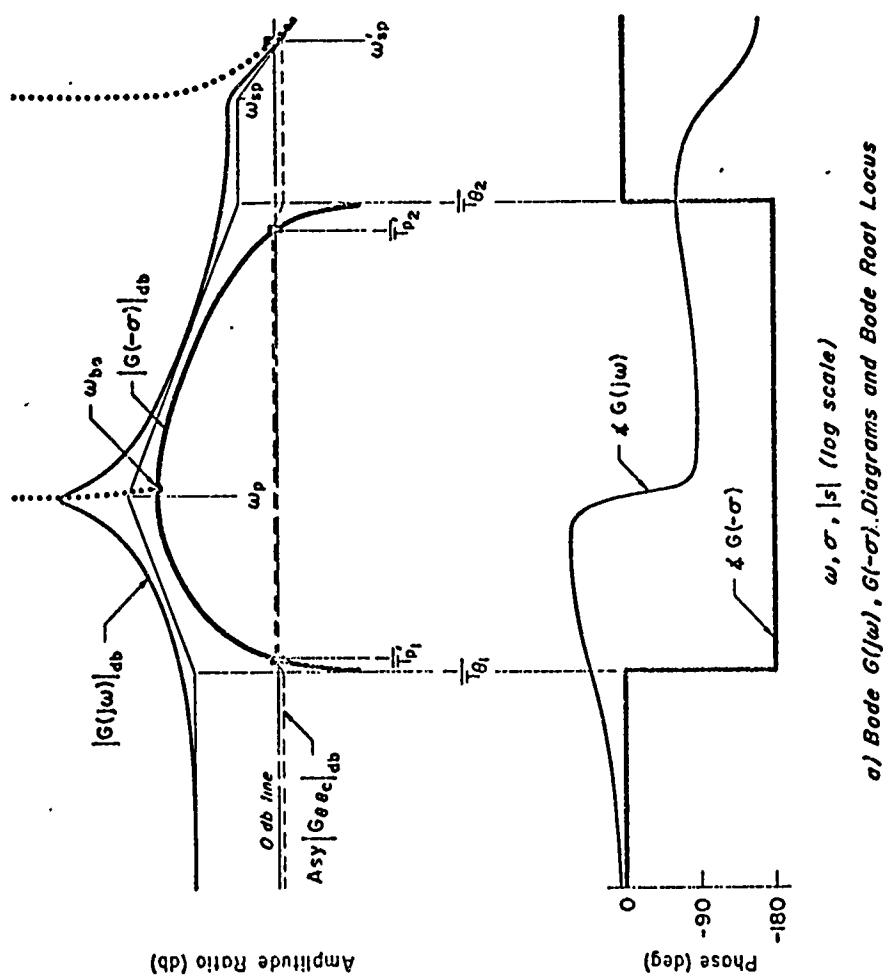


Fig. 7-2. System Survey of Pitch Attitude ($\theta \rightarrow \delta_e$) Control System for Well Behaved Aircraft.

in the characteristic equation. Such feedbacks, which do not augment X_u , Z_w , $M_{\dot{\alpha}}$, M_q , etc., can only redistribute the open-loop damping among the closed-loop modes. This is a specific example in somewhat different terms of a general algebraic rule previously given (in Chapter 3) as Rule 10 for the root locus method.

The closed-loop asymptotic amplitude Bode constructed for moderate gain shows, by its nearly flat properties in the vicinity of the modified phugoid, that this mode will be suppressed almost completely in the pitch attitude response to θ_c commands. Also, as a consequence of the heavily damped phugoid, any fluctuations of the other longitudinal degrees of freedom, such as speed and altitude, will exhibit well-damped long-period characteristics. This will be true even if the uncontrolled aircraft has negative phugoid damping. For these reasons the feedback of pitch angle alone to the elevator has been, and will continue to be, a successful control technique in many aircraft.

Attitude Control for Small Static/Short-Period Gain

In the feedback system described above the open-loop gain does not become infinite at zero frequency and, therefore, the closed-loop frequency response has an amplitude ratio slightly less than one at low frequencies. This corresponds to a small steady-state position error in response to step commands, which is not serious for the condition described in Fig. 7-2. However, the situation is likely to be aggravated at low speed, as in landing approach, or at very high altitude. Here the static-to-short-period-gain ratio, $1/u_p^2 T_{\theta_1} T_{\theta_2}$, is likely to be small and indeed may well be less than one. When this occurs the long-term response of the closed-loop system to commands is very poor. Figure 7-3 presents the $\theta \rightarrow \delta_c$ system survey plots for such an airplane in the approach configuration. The typical closed-loop zero db line shown is for a gain which is about as large as possible without seriously degrading the closed-loop short-period damping. Yet, as indicated graphically by the closed-loop asymptotes, there will be a very low frequency lead/lag and a DC gain less than unity in the closed-loop pitch attitude transfer function. In the indicial response of θ to a step θ_c these correspond to a very long time



Fig. 7-3. System Survey of Pitch Attitude ($\theta \rightarrow \delta_e$) Control System Illustrating a Low Frequency "Droop".

constant mode and to a steady-state position error. The closed-loop asymptotic plot, when considered as a frequency response, also exhibits this low frequency "droop" as a region, indicated by the cross-hatched area, where the output/input amplitude ratio is less than unity.

To define more precisely the aircraft characteristics which govern the static-to-short-period-gain ratio, $1/\omega_p^2 T_{\theta_1} T_{\theta_2}$, we can express it in terms of the approximate factors

$$\frac{1}{\omega_p^2 T_{\theta_1} T_{\theta_2}} = \frac{\left(1 - \frac{Z_w M_q}{M_\alpha}\right) \left[Z_w X_u - X_w Z_u + \frac{Z_{\delta_e}}{M_{\delta_e}} (X_w M_u - X_u M_w) \right]}{-\frac{g}{U_0} \left(Z_u - \frac{M_u Z_w}{M_w} \right)} \quad (7-2)$$

For the simplified but quite normal conditions where $|Z_w M_q / M_\alpha| \ll 1$, $|Z_{\delta_e} M_w / Z_w M_{\delta_e}| \ll 1$, and the M_u terms are negligibly small, the static-to-short-period-gain ratio becomes

$$\begin{aligned} \frac{1}{\omega_p^2 T_{\theta_1} T_{\theta_2}} &= \frac{Z_w X_u - X_w Z_u}{-\frac{g}{U_0} Z_u} \\ &= \frac{U_0 Z_w}{g Z_u} \left[-X_u + \left(X_w - \frac{g}{U_0} \right) \frac{Z_u}{Z_w} + \frac{g}{U_0} \frac{Z_u}{Z_w} \right] \\ &= \left[1 + \frac{U_0 Z_w}{g Z_u} \left(\frac{1}{T_{h_1}} \right) \right] \end{aligned} \quad (7-3)$$

The magnitude of $1/\omega_p^2 T_{\theta_1} T_{\theta_2}$ will be unity when $1/T_{h_1} = 0$ and less than unity as $1/T_{h_1}$ decreases to negative values. As developed in Chapter 5, $1/T_{h_1}$ is given by

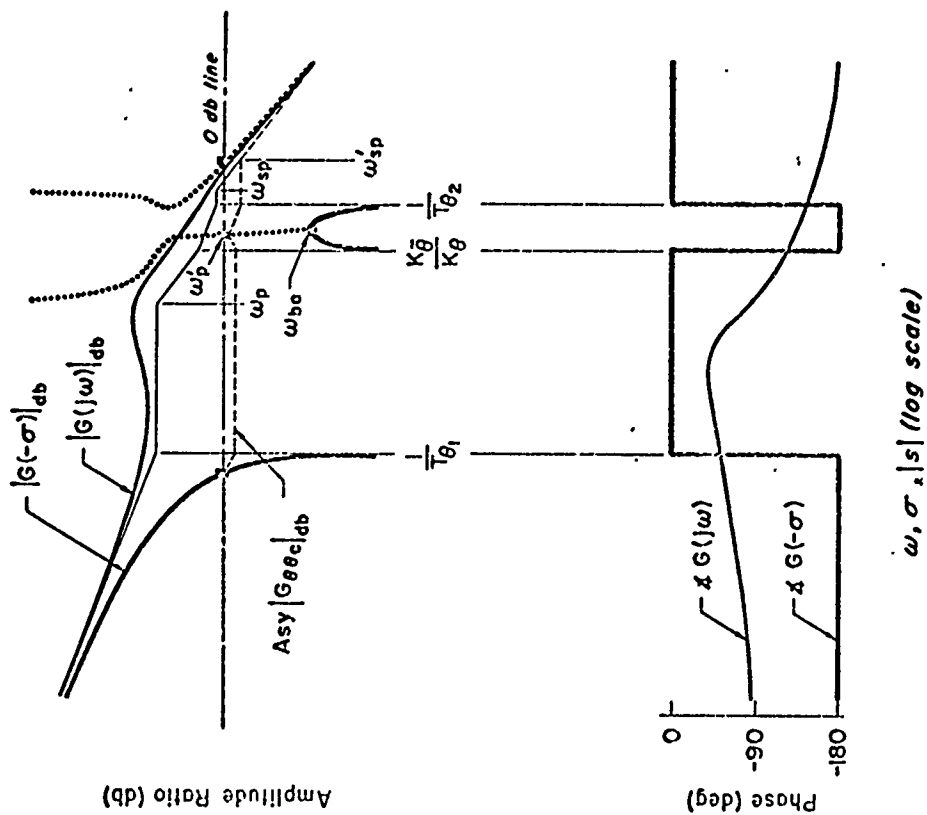
$$\frac{1}{T_{h_1}} = \frac{1}{m} \left(\frac{\partial D}{\partial U} - \frac{\partial T}{\partial U} \right) \quad (7-4)$$

Thus, a static-to-short-period gain of 1.0 occurs approximately at performance reversal, $m/Th_1 \doteq dD/dU - \partial T/\partial U = 0$. This is also usually close to the condition for minimum drag, i.e., $dD/dU = 0$. Because near-minimum-drag flight is sometimes desirable from a performance standpoint, flight conditions near the performance reversal are not uncommon.

For automatic pilot systems which are intended to follow commands, such as systems with attitude-hold features, the deficiency in low frequency gain can be made up with a form of integral control. A "pitch integrator" is added in parallel to the straight-through gain of the controller. This configuration is shown in Fig. 7-4. The transfer function of the controller is now $K_\theta + K_{\dot{\theta}}/s$ and an integration and higher frequency lead, $(K_\theta/s)(s + K_{\dot{\theta}}/K_\theta)$, are cascaded with the open-loop function representing the dynamics of the airplane. As indicated by the amplitude ratio asymptotes for the compensated system, the lead time constant represented by the ratio $K_\theta/K_{\dot{\theta}}$ is chosen so that its breakpoint, $K_{\dot{\theta}}/K_\theta$, is greater than ω_p , thus making the low frequency amplitude ratio in the region of ω_p as large as feasible. This effectively eliminates the "droop" shown in Fig. 7-3. The addition of the $K_{\dot{\theta}}$ feedback introduces a fifth root to the characteristic equation without changing the sum of the roots. The total system damping therefore remains constant and, since the added root is a low frequency subsidence, the effect of the integral feedback is to detract from the phugoid damping. This is, of course, offset by the K_θ feedback which damps the phugoid by taking damping away from the short period.

Attitude Control with Deficient Short-Period Damping

Somewhat by contradistinction to the two cases just considered, Fig. 7-5 is a system survey of $\theta \rightarrow \delta_e$ feedback for open-loop dynamics appropriate to an interceptor at supersonic speed and high altitude. Here the damping of the longitudinal short-period motion is weak, and the feedback causes it to deteriorate rapidly with increases in the controller gain. The desirable suppression of the phugoid, therefore, may be considered to exact too high a price with regard to the short period. To alleviate the short-period damping deficiency a pitch rate



a) Bode $G(j\omega)$, $G(-\sigma)$ Diagrams and Bode Root Locus

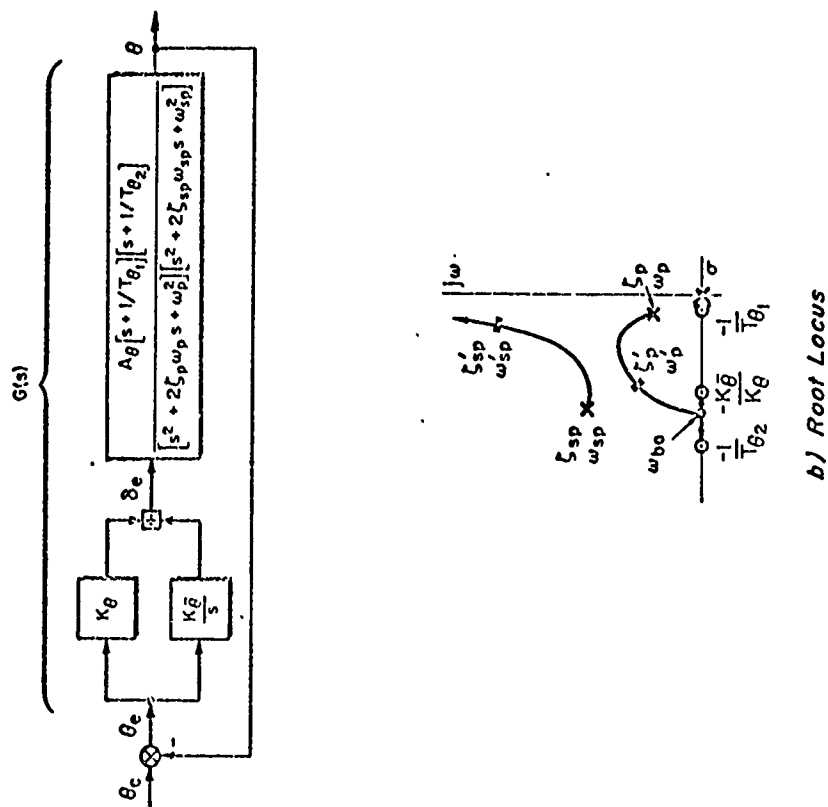


Fig. 7-4. System Survey of Pitch Attitude ($\theta \rightarrow \varepsilon_e$) Control System with Integrator.

signal can be fed back, as in a pitch damper, to produce an elevator deflection and a corresponding pitching moment proportional to pitching velocity, q , i.e.,

$$\delta_e = -K_q q \quad (7-5)$$

or

$$M_{\delta_e} \delta_e = -K_q M_{\delta_e} q$$

This feedback then has the same effect as an increase in magnitude of the stability derivative M_q . As seen from the short-period approximate factor

$$2(\zeta\omega)_{sp} \doteq -(Z_w + M_q + M_{\dot{\alpha}}) \quad (7-6)$$

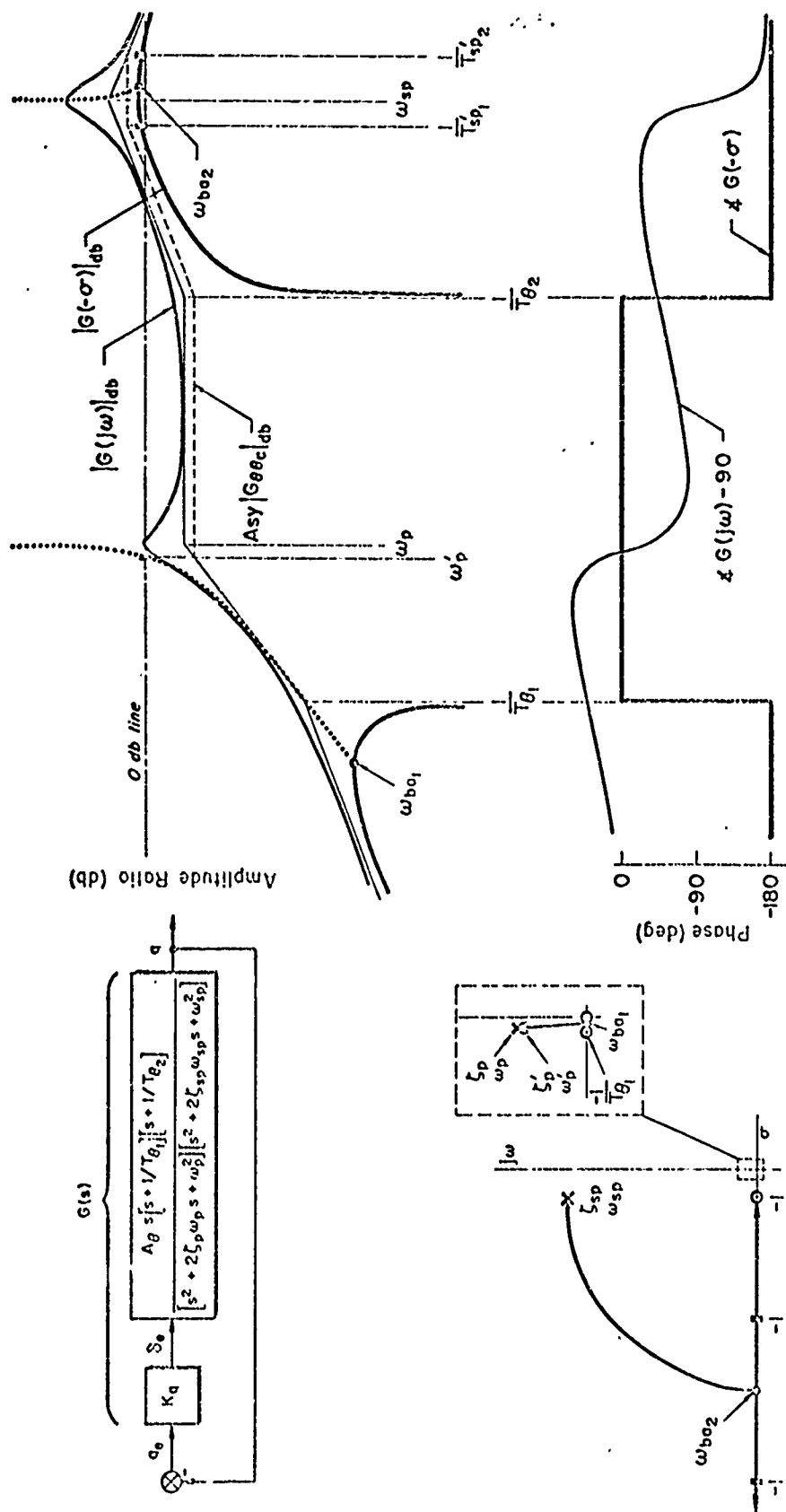
an increase in $-M_q$ directly increases the short-period damping.

This same effect is illustrated in the system survey in Fig. 7-6. These plots show that at a comparatively low value of the loop gain the short-period motion can easily be overdamped. The phugoid motion is hardly altered by the action of this relatively low gain feedback, although it can eventually be overdamped, with an attendant reduction in frequency, for sufficiently high gain.

Figure 7-7 illustrates the combined effect of pitch rate and pitch angle feedback for the preceding high speed, high altitude case. Now, at only moderately high controller gains, the phugoid is heavily damped and suppressed for attitude commands and the short-period motion is also heavily damped. This technique is so efficacious that it has become nearly universal, and most modern automatic pilots feed back pitch angle and pitch rate signals to the elevator. The technique is applicable not only to aircraft with typical dynamics, such as the ones which have been illustrated, but also in cases where the longitudinal motions of the vehicle alone (open-loop) are unstable.

Pitch Attitude Control of Longitudinal Divergences

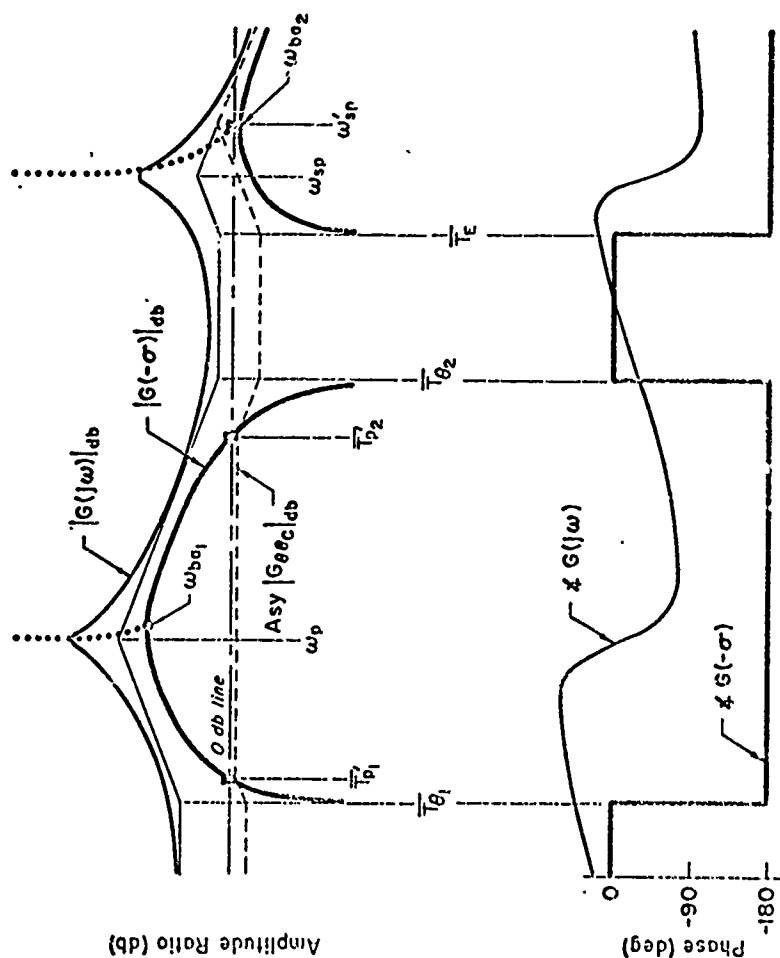
As we have seen in Chapter 5, the phugoid oscillation may become a convergence and a divergence, especially in the high subsonic flight regime. The unstable divergence is sometimes called the "tuck" mode because it usually manifests itself as a slow increase in speed and



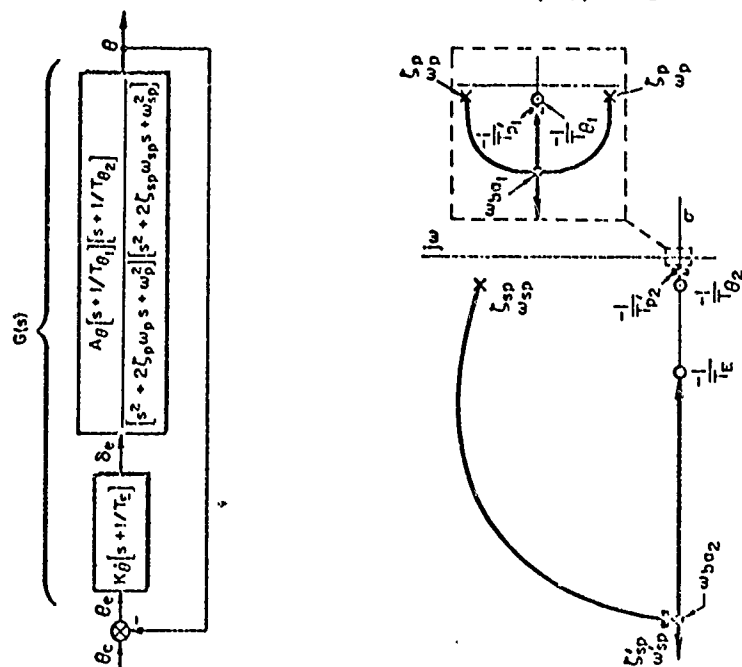
a) Bode $G(j\omega)$, $G(-\sigma)$ Diagrams and Bode Root Locus

b) Root Locus

Fig. 7-6. System Survey of Pitching Velocity ($\delta_e \rightarrow \delta_e$) Control System for Low Short-Period Damping Case.



$\omega, \sigma, |s|$ (log scale)
a) Bode $G(j\omega), G(-\sigma)$ Diagrams and Bode Root Locus



b) Root Locus

Fig. 7-7. System Survey of Pitch Attitude and Rate ($\theta, \dot{\theta} \rightarrow \delta_e$) Control System for Low Short-Period Damping Case.

nose-down pitch attitude. "Tuck" is, in essence, a static instability due to an M_u which is sufficiently negative to make

$$M_w Z_u - M_u \dot{w} < 0 \quad (7-7)$$

The result is a pole on the positive real axis.

Figure 7-8 presents a system survey for the feedback of pitch angle to elevator when the aircraft exhibits a tuck mode. The σ -Bode diagram shows that at a very moderate gain, corresponding to an open-loop DC gain of 1.0 (zero db), the closed-loop root crosses from the right half to the left half plane, and the closed-loop system becomes stabilized. The value of pitch angle feedback is evident here. Pitch rate feedback would serve, as before, to damp the short-period mode.

Figure 7-9 shows the effect of pitch angle feedback to the elevator in connection with another form of longitudinal instability. In this case the short-period oscillation has become a convergence and divergence associated with the inequality

$$M_q Z_w - M_{\alpha} < 0 \quad (7-8)$$

due to a sufficiently positive value of M_{α} . In all practical cases of this kind the inequality of Eq. 7-7 also applies. One possible fix for this condition is a pitch attitude control system. It may be seen in Fig. 7-9 that the feedback of pitch angle and pitch angle rate can stabilize the violent instability and that, here again, the value of this particular feedback is strikingly illustrated.

Still in connection with pitch angle feedback, consider the case of a hovering VTOL aircraft or helicopter. The transfer function relating pitch angle to longitudinal control is given by

$$\frac{\theta(s)}{\delta_e(s)} = \frac{M_{\delta_e} \left(s + \frac{1}{T_{\theta}} \right)}{\left(s + \frac{1}{T_{sp}} \right) \left[s^2 + 2\zeta_p \omega_p s + \omega_p^2 \right]} \quad (7-9)$$

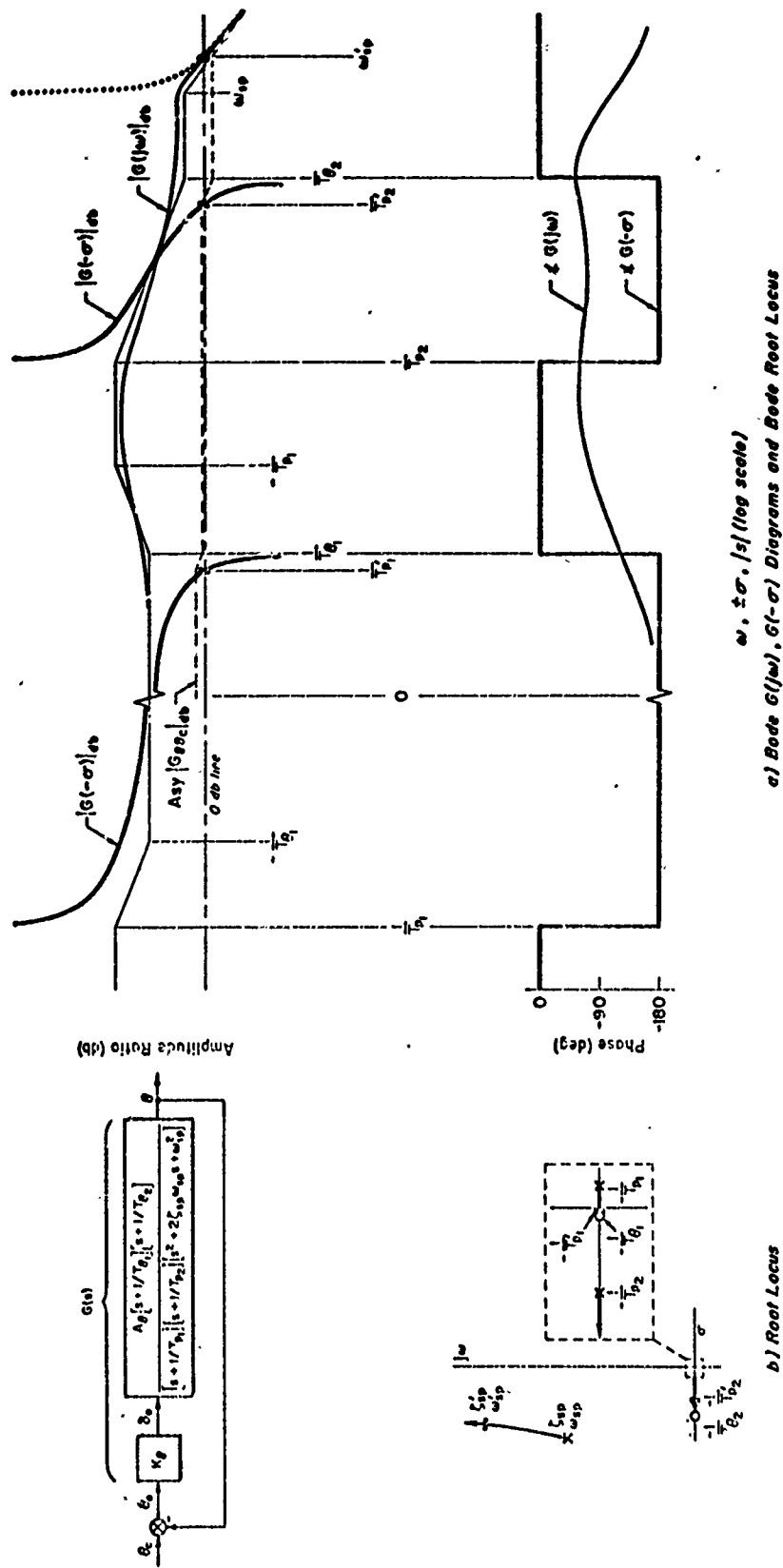


Fig. 7-8. System Survey of Pitch Attitude ($\theta \rightarrow \delta_e$) Control System for Aircraft with "Tuck" Mode.

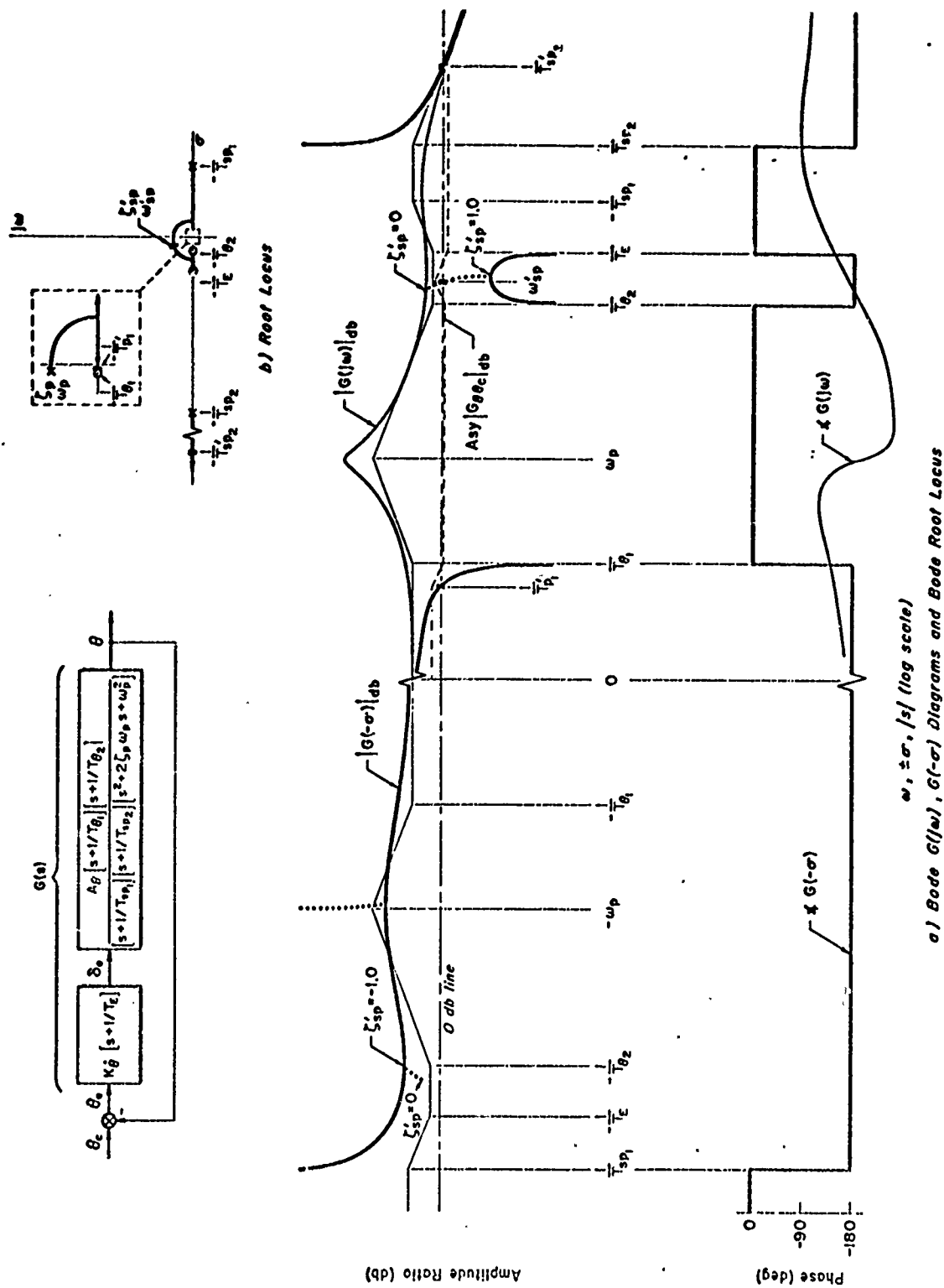


Fig. 7-9. System Survey of Pitch Attitude and Rate ($\theta, \dot{\theta} \rightarrow \delta_e$) Control System for Aircraft with Short Period Instability.

This is quite different, in both form and kind, from the corresponding θ/δ for a typical aircraft in forward flight. Not only does the transfer function have a third-order denominator, but typically the low frequency oscillation is unstable ($\xi_p < 0$). The system survey of Fig. 7-10 shows that when the feedback loop is closed at moderate gain, the divergent oscillation is made stable. Of course this possibility depends on $1/T_{sp}$ being sufficiently large. If it is not, pitch rate feedback should also be employed. This necessity is real for the majority of helicopters and VTOL machines, and Fig. 7-11 shows the effect of both pitch angle and pitch rate feedback. For simplicity the lead is set equal to $1/T_{sp}$, although this will not be true in general. Once again the benefits of these feedbacks, in combination, are apparent.

All of the systems described in this article are conditionally stable. That is, they require a minimum value of gain for stability to be attained. In actual designs this property demands careful consideration of nonlinearities (such as limiting), which tend to reduce gain from the nominal, small perturbation, linearized values.

Generalized Pitch Attitude Control and Nature of Gain Adjustments

Accumulating the experience gained from all the cases treated above indicates that a general pitch control law with rate, proportional, and integral terms would be adequate for all conceivable pitch command control and attitude stabilization situations. This would have the form

$$\delta_e = K_{\dot{\theta}} \dot{\theta}_e + K_{\theta} \theta_e + K_{\bar{\theta}} \int \theta_e dt \quad (7-10)$$

or, in transform style,

$$\begin{aligned} \frac{\delta_e}{\theta_e} &= \frac{K_{\dot{\theta}}}{s} \left(s^2 + \frac{K_{\theta}}{K_{\dot{\theta}}} s + \frac{K_{\bar{\theta}}}{K_{\dot{\theta}}} \right) \\ &= \frac{K_{\dot{\theta}}}{s} \left(s + \frac{1}{T_{E1}} \right) \left(s + \frac{1}{T_{E2}} \right) \end{aligned}$$

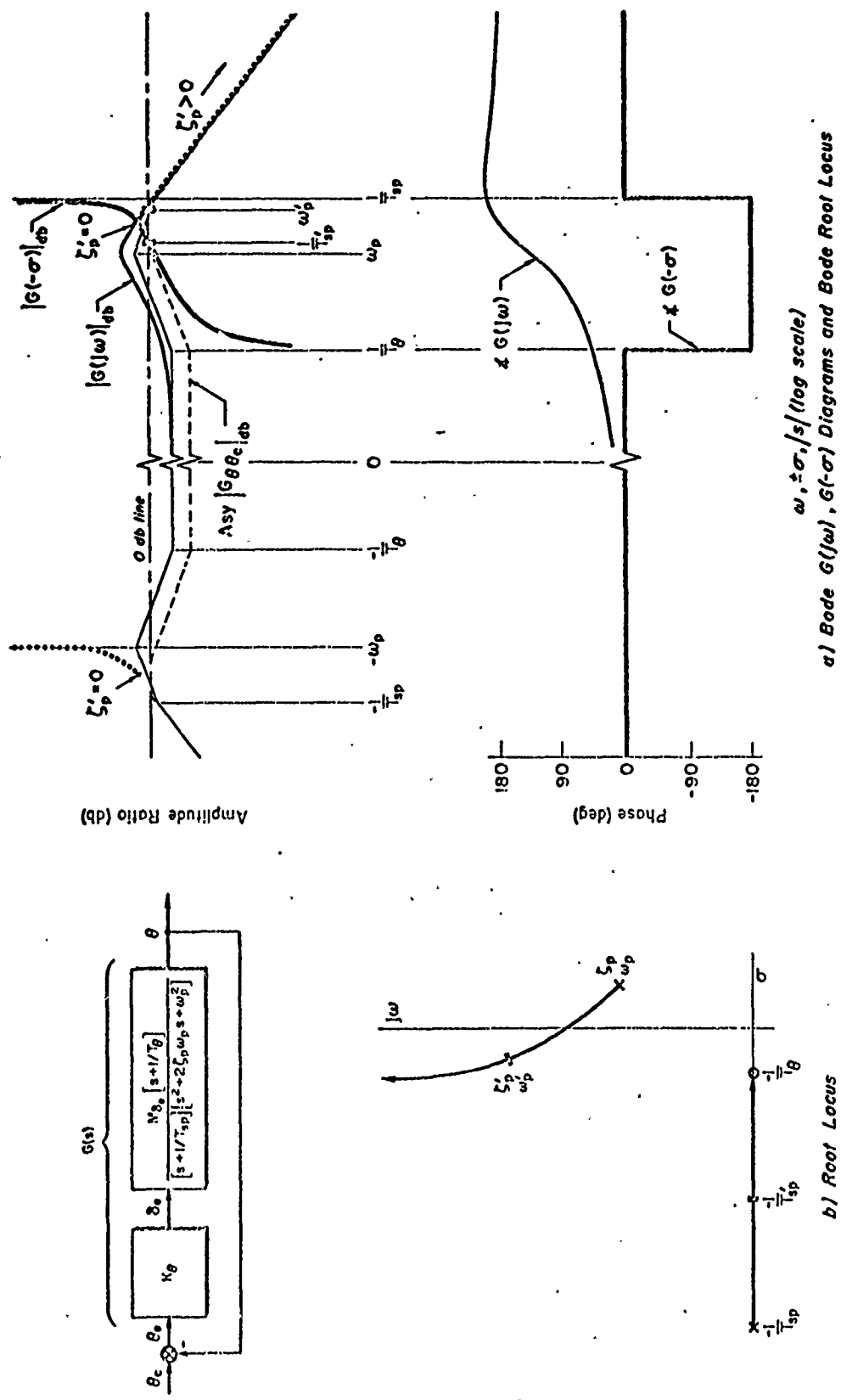


Fig. 7-10. System Survey of Pitch Attitude ($\theta \rightarrow \delta_e$) Control System for Hovering VTOL Aircraft or Helicopter.

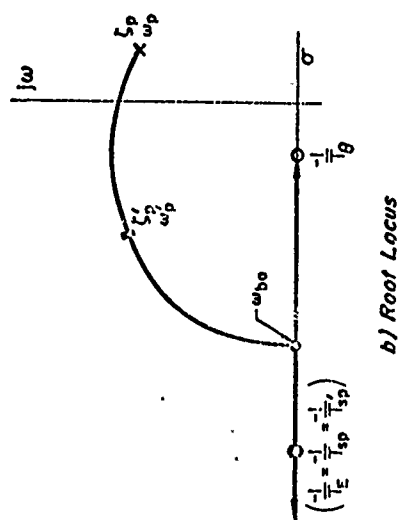
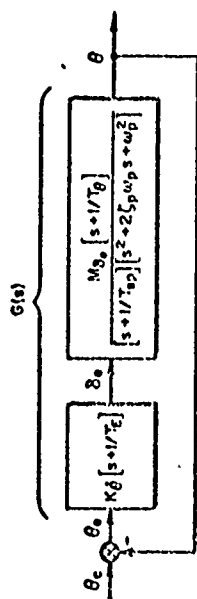
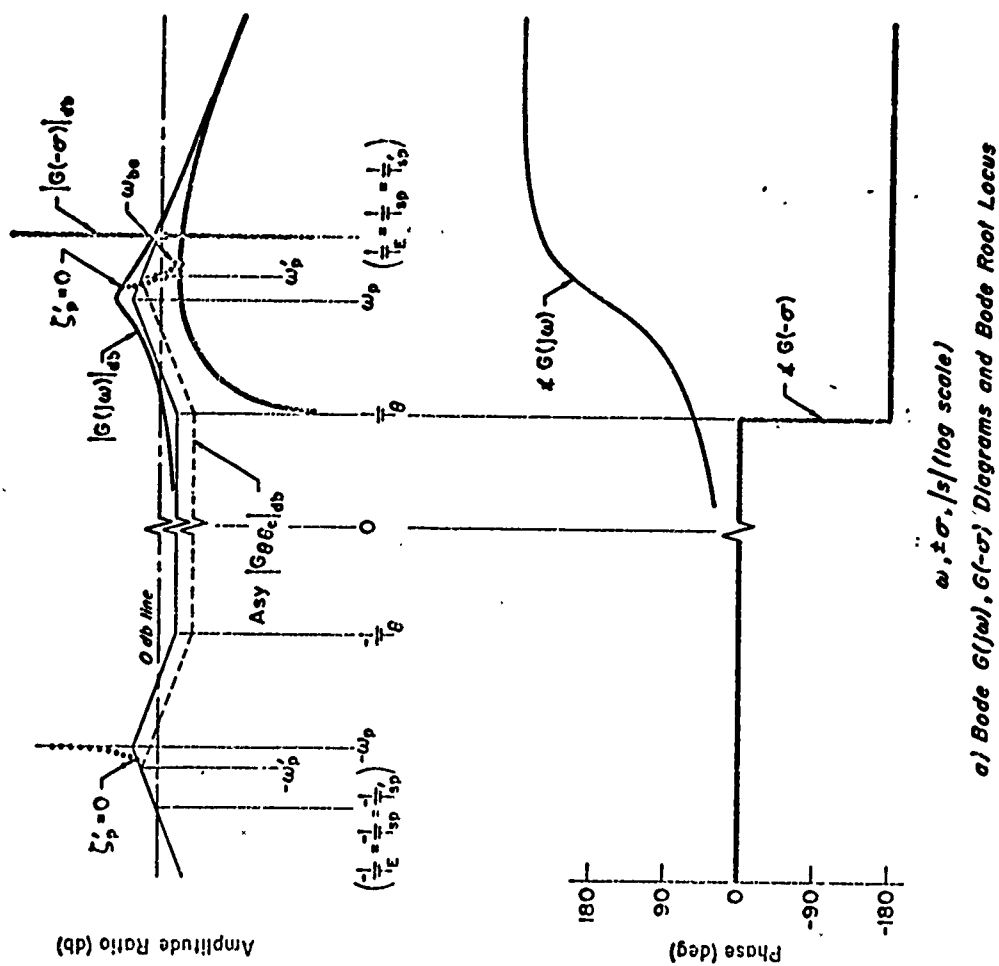


Fig. 7-11. System Survey of Pitch Attitude and Rate ($\theta, \dot{\theta} \rightarrow \delta_e$) Control System for Hovering VTOL Aircraft or Helicopter.

In most systems where pitch command, θ_c , is often steplike in nature the rate term, shown here as $K_{\dot{\theta}} \dot{\theta}_e$, is actually mechanized as $K_{\dot{\theta}} \dot{\theta}$ to avoid bad effects due to a pulsed elevator signal at the initiation of the command. This is, however, a detail which need not concern us further. While the control law form of Eq. 7-10 is generally satisfactory, the gains must be made consonant with the control requirements imposed by the airplane characteristics. Since the latter vary with changes in the conditions of flight, the gains must sometimes also be modified to accommodate these changes. The characteristics of the variations actually employed depend on the specific variations of key stability derivatives, the functional mechanization of the gain-changing devices, and the specified closed-loop performance envelope. However, some insight into the nature of appropriate gain variations can be obtained on an elementary basis by considering the pitch attitude control system sketched in Fig. 7-12. This shows the controller time constants appropriately oriented relative to each other and to the aircraft breakpoints, and indicates a desirable zero-db line location.

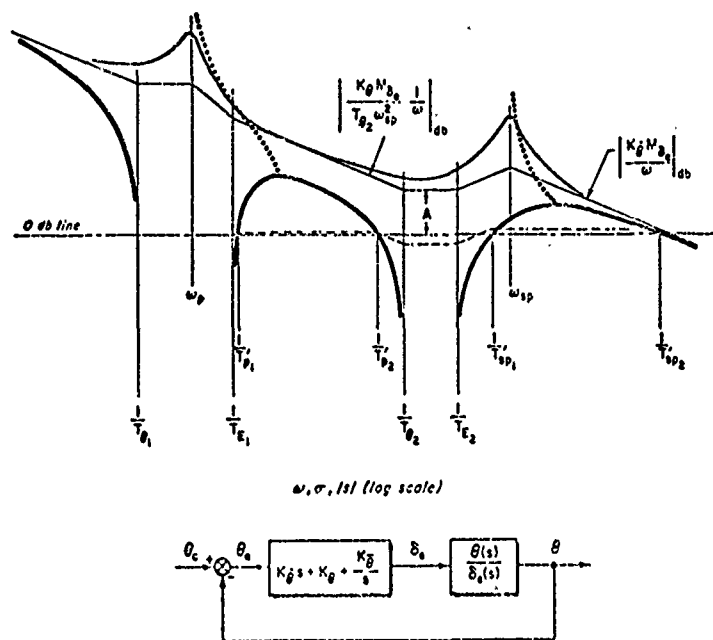


Fig. 7-12. Pitch Attitude Control with $\delta_e = K_{\theta} \theta_e + K_{\dot{\theta}} \dot{\theta}_e + K_{\ddot{\theta}} \ddot{\theta}_e$

When the controller time constants are well separated as shown, they may be expressed in terms of the controller gains as

$$\frac{1}{T_{E1}} \doteq \frac{K_{\theta}}{K_{\delta}} \quad , \quad \frac{1}{T_{E2}} \doteq \frac{K_{\theta}}{K_{\delta}} \quad (7-11)$$

If the relative locations illustrated can be maintained over the flight envelope, the pitch attitude control will generally be excellent, with both short period and phugoid extremely well damped and with good disturbance suppression.

The region where feedback is least effective occurs in the flat stretch between $1/T_{\theta 2}$ and $1/T_{E2}$. Ideally, the amplitude ratio in this region should be held at or above some minimum level to assure positive control and disturbance suppression, and to avoid dynamic "droops" due to the dipole pairs at $1/T_{p2}'$ and $1/T_{sp1}'$. The amplitude ratio of the asymptote here will be given approximately by*

$$A \doteq \frac{K_{\theta} M_{\delta e}}{\omega_{sp}^2} \quad (7-12)$$

$$\doteq K_{\theta} \left(\frac{C_{m\delta e}}{-C_{m\alpha}} \right)$$

"A" can be kept approximately constant by varying K_{θ} so as to offset the variations in $C_{m\delta e}/C_{m\alpha}$. With a fixed c.g. location this ratio varies only slightly with Mach number for subsonic and supersonic flight, although it is different in the two regimes. The ratio fluctuates in the transonic region and is, of course, in general a direct function of c.g. location. All of these factors enter into determining the required change in K_{θ} with flight condition to maintain A at or near a desired level.

*Notice that because of the negative sign on $M_{\delta e}$, K_{θ} must also be negative. In other words, a positive δ_c requires an up (negative) elevator deflection.

The equalization time constants should be kept approximately in the same positions relative to the key airplane breakpoints. For instance, $1/T_{E2}$ should remain somewhere between $1/T_{\theta 2}$ and ω_{sp} . Thus, as indicated below, its basic variation with flight environmental parameters should be proportional to a function intermediate between ρU_0 and $\rho^{1/2} U_0$, i.e.,

$$\frac{1}{T_{\theta 2}} \propto \rho U_0 C_{L\alpha} < \frac{1}{T_{E2}} < \omega_{sp} \propto \rho^{1/2} U_0 \sqrt{-C_{m\alpha}} \quad (7-13)$$

For the simplest condition where a fixed K_0 is feasible, appropriate adjustment of $1/T_{E2}$ could be obtained by varying K_0 inversely with $\rho^{1/2} U_0$; then the closed-loop short-period time constant, T'_{sp2} will vary as

$$\frac{1}{T'_{sp2}} \doteq K_0 M_{\phi e} \propto \rho^{1/2} U_0 \quad (7-14)$$

In theory, at least, a variation of $1/T_{E1}$ with ρU_0 or $\rho^{1/2} U_0$ can keep this breakpoint properly located relative to ω_p and $1/T_{\theta 2}$. It will be recalled, however, that the addition of integral control was only required at conditions near minimum drag. These are quite specific, so generally one or more fixed gain settings can be used instead of a continuous variation.

In concluding this discussion of single-loop attitude control, two further things should be mentioned. The first is a deficiency, one of the few associated with attitude as a feedback. The tight high-gain attitude control system described immediately above will tend to hold the pitch angle constant in the presence of disturbances. As a consequence, when the aircraft is subjected to gusts this rigidity in attitude prohibits any weathercocking tendency to nose into the wind and thereby reduce accelerations. It also tends to make the angle of attack change coincide with the gust, considered as an equivalent angle of attack. The net results are somewhat increased structural loads and linear accelerations due to gusts over those which would be present in the uncontrolled aircraft with the same short-period damping. The second point relates to the use of attitude as an inner loop for subsequent outer loop controls. Although multiloop systems are not discussed until Chapter 11, it is pertinent to

resulting in the phugoid mode being the dominant controlled element characteristic in such a system to achieve either loops involving either altitude or speed control operations.

7.2 FEEDBACK ON SPEED ERROR TO ELEVATOR DEFLECTION

Consider next the feedback of speed error to the elevator. The appropriate controlled element transfer function (with $X_{S_0} \neq 0$) is:

$$\frac{u(s)}{\delta_e(s)} = \frac{N_{\delta_e}^u}{A_{\text{long}}} = \frac{A_u \left(s + \frac{1}{T_{u1}} \right) \left(s + \frac{1}{T_{u2}} \right)}{\left[s^2 + 2\zeta_p \omega_p s + \omega_p^2 \right] \left[s^2 + 2\zeta_{sp} \omega_{sp} s + \omega_{sp}^2 \right]} \quad (7-15)$$

The zero, $1/T_{u2}$, can be in either the right or left half plane, depending on elevator location aft or forward and $C_{L_u}/C_{D_{\alpha}}$ larger or smaller than one.* In any event it is typically very remote from the origin, so that for most practical purposes it can be neglected.

Figure 7-13 presents the system survey for negative feedback of a speed error. This control may be seen to have a powerful effect on the phugoid undamped natural frequency, and also to increase the phugoid damping. The modified phugoid roots rapidly move up and deeper into the left half plane, and comparatively large damping ratios for the phugoid mode can be achieved before the short-period mode has been much altered.

The changes to both the phugoid frequency and damping illustrated in Fig. 7-13 are in accord with the approximate factors, i.e.,

$$\omega_p^2 \doteq \frac{g \left[M_w Z_u - Z_w M_{u\text{augmented}} \right]}{\omega_{sp}^2} \quad (7-16)$$

$$2(\zeta\omega)_p \doteq -X_u - \frac{(X_{\alpha} - g)}{\omega_{sp}^2} M_{u\text{augmented}}$$

*Ashkenas, Irving L., and Duane T. McRuer, Approximate Transfer Functions and Application to Single Sensor Control Systems, WADC-TR-58-82, June 1958.

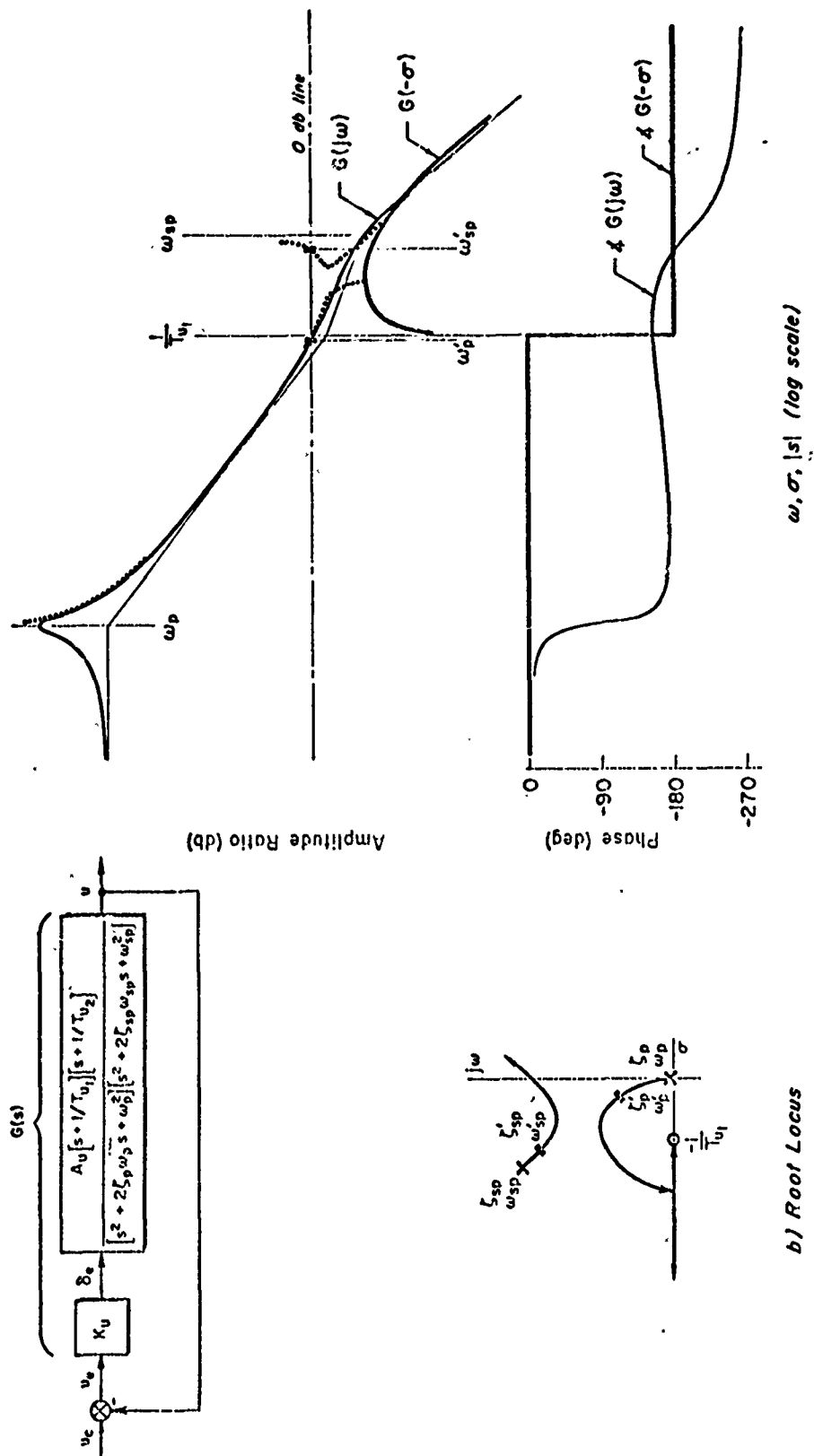


Fig. 7-13. System Survey of Airspeed ($u \rightarrow \delta_e$) Control System for Well Behaved Aircraft.

where $M_{u\text{augmented}} = M_u - K_u M_{\delta_e}$.^{*} The same beneficial effects on the phugoid occur when a tuck is present, and M_u augmentation is often used to counter such tendencies.

Although the closed-loop phugoid damping is somewhat improved by the feedback of speed error alone, it is materially increased if \dot{u} as well is fed back. This action creates a new stability derivative, $M_{\dot{u}}$; its effect on phugoid characteristics can be examined with the aid of the phugoid approximation equations. When an $M_{\dot{u}s}$ pitching acceleration is added to these (Eq. 5-), the characteristic equation becomes

$$\Delta_p = \begin{vmatrix} (s - X_u) & -X_w & g \\ -Z_u & (s - Z_w) & -U_0 s \\ -(M_{\dot{u}} s + M_u) & -M_w & 0 \end{vmatrix} = 0 \quad (7-17)$$

Using the primed notation to indicate that a loop has been closed, the characteristic equation for the modified phugoid becomes

$$s^2 + 2\zeta_p' \omega_p' s + \omega_p'^2 = s^2 - \frac{X_u - \frac{M_u(X_\alpha - g)}{M_u} - \frac{g M_{\dot{u}} Z_w}{M_\alpha}}{1 + \frac{M_{\dot{u}}(X_\alpha - g)}{M_\alpha}} s - \frac{\frac{g}{U_0} \left[Z_u - \frac{M_u Z_w}{M_w} \right]}{1 + \frac{M_{\dot{u}}(X_\alpha - g)}{M_\alpha}} \quad (7-18)$$

While $M_{\dot{u}}$ is present in the denominator for both the damping and the undamped natural frequency, the quantity in which it appears is generally small relative to one. On the other hand, the $g M_{\dot{u}} Z_w / M_\alpha$ addition to the s term in Eq. 7-18 can constitute a major modification to the damping. These conclusions hold, of course, only for the relatively small values of gain for which the approximate equations of motion are still applicable.

^{*}Notice that because of the negative sign on M_{δ_e} , K_u must be positive to augment M_u . In other words, a positive speed error (speed less than the set speed) requires a down (positive) elevator, which tends to restore the command speed.

The system survey of Fig. 7-14 shows that substantially the same effects are present for much larger values of gain.

To increase damping, $M_{\dot{u}}$ should be positive, as should M_u to increase the undamped natural frequency. The effect of the control is thus to apply a positive pitching moment whenever the speed is greater than the set speed and increasing. Speed is thus controlled at the expense of attitude changes. This property can cause difficulties if the pitching moments used to control speed are too great. The British experience cited in Chapter 1 is just such a case where the atmospheric turbulence components in the direction of flight were sensed by the speed error instrument, which actuated the elevator in such a way that large and disconcerting changes in the pitch angle of the aircraft occurred.

An explanation of this phenomenon was discovered by computing transient responses,* but it can likewise be appreciated by considering the ratio of the airspeed to attitude numerators for gust excitation. These are readily computed from the simplified phugoid equations with $M_{\dot{u}}$ added:

$$\begin{array}{rclcl} (s - X_u)u & -X_w w & +g\theta & = & -X_u u_g \\ -Z_u u & +(s - Z_w)w & -U_0 s \theta & = & -Z_u u_g \\ -(M_{\dot{u}} s + M_u)u & -M_w & & = & -(M_{\dot{u}} s + M_u)u_g \end{array} \quad (7-19)$$

The appropriate numerator ratio is

$$\frac{N_{u_g}^u}{N_{u_g}^\theta} = \frac{-g}{s} + \frac{X_u(M_{\dot{u}} s + M_u) - M_u X_u}{(M_{\dot{u}} s + M_u)(s - Z_w) + Z_u M_w} \quad (7-20)$$

At frequencies in the neighborhood of either the open- or closed-loop phugoid, i.e., either M_u and $M_{\dot{u}}$ approximately zero or M_u and $M_{\dot{u}}$ dominant,

*S. Neumark, The Disturbed Longitudinal Motion of an Uncontrolled Aircraft and of an Aircraft with Automatic Control, ARC R and M No. 2078, His Majesty's Stationary Office, London, Jan. 1943.

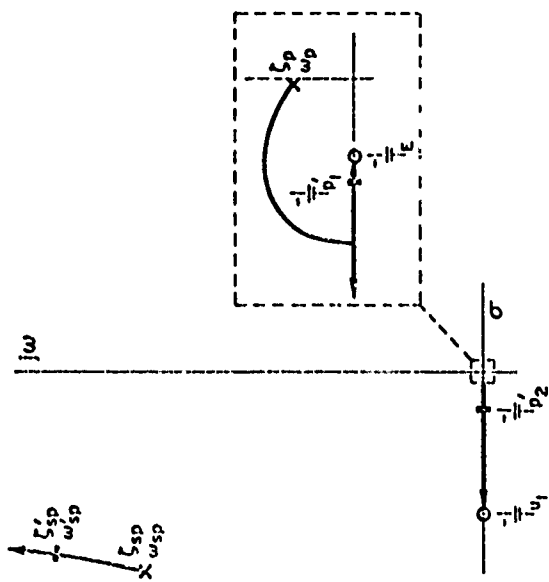
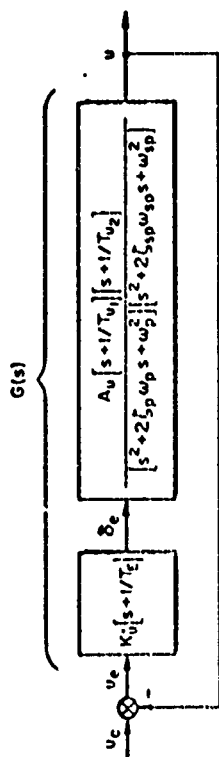
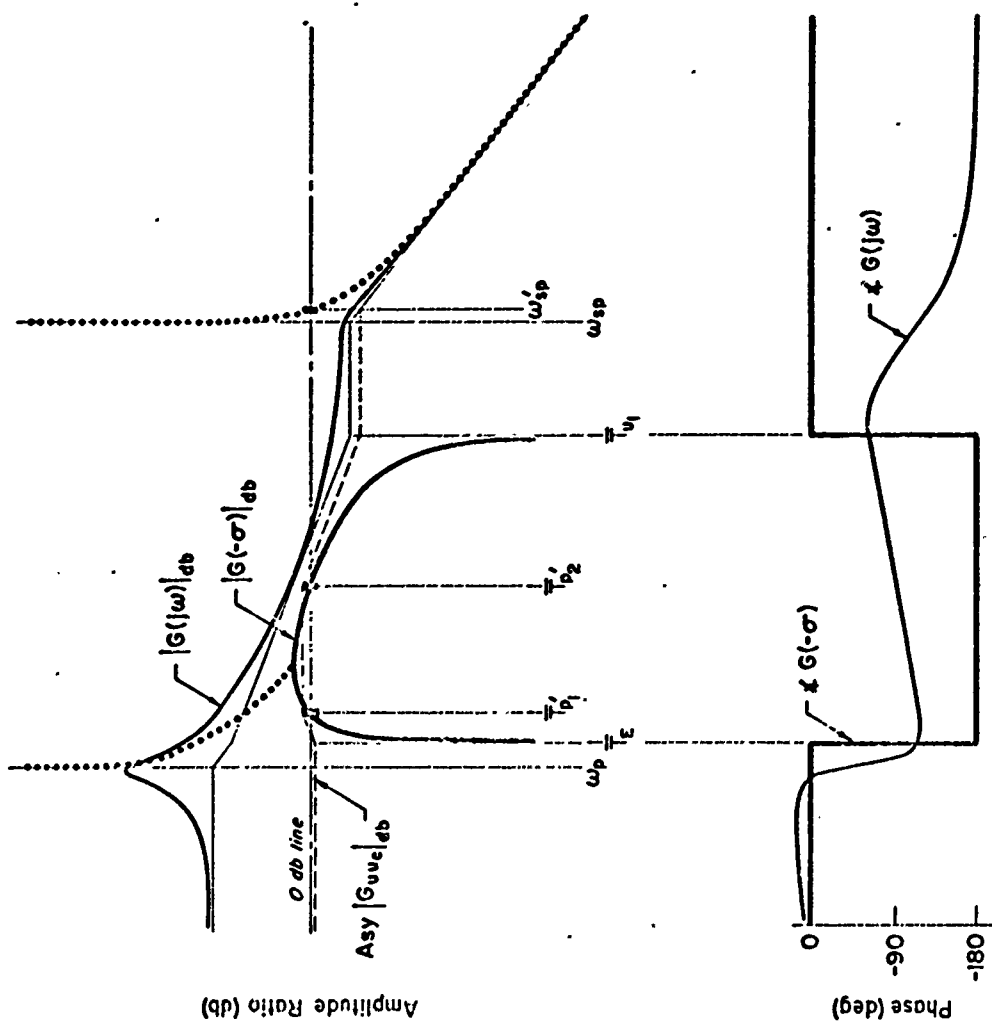


Fig. 7-14. System Survey of Airspeed and Airspeed Rate ($u, \dot{u} \rightarrow \delta_e$) Control System.

respectively, this ratio of numerators is very nearly the first term in Eq. 7-20 alone. That is,

$$\frac{N_{ug}^u}{N_{ug}^\theta} \doteq \frac{-g}{s} \quad (7-21)$$

or

$$su \doteq -g\theta, \text{ implying } du/dt \doteq -g\theta \quad (7-22)$$

as far as the phugoid motion components are concerned. (Note that this result is consistent with the phugoid approximate modal response ratios developed in Chapter 5.) The increase in phugoid undamped natural frequency and damping brought about by the $u, \dot{u} \rightarrow \delta_e$ feedbacks causes a corresponding increase in the du/dt and attitude responses to gusts. That is, Eq. 7-22 indicates that making the speed response more rapid must incidentally result in larger values of θ .

To avoid the phenomenon described here, an attitude loop is also ordinarily used when speed control is desired. This loop has, among other things, the effect of favorably modifying the ratio of closed-loop u and θ gust numerators.

7.3 FEEDBACK OF ANGLE OF ATTACK TO THE ELEVATOR

Angle of attack and its derivative are, in principle, very desirable feedbacks to the elevator. Considered as stability derivative augmentation, $\dot{\alpha} \rightarrow \delta_e$ and $\alpha \rightarrow \delta_e$ increase the magnitude of $M_{\dot{\alpha}}$ and $M_{\alpha} = U_0 M_w$ directly, which will increase the damping ratio and undamped natural frequency, respectively. These features are indicated by the short-period approximate factors

$$\begin{aligned} 2(\xi\omega)_{sp} &= -(Z_w + M_q + M_{\alpha_{augmented}}) \\ \omega_{sp}^2 &= Z_w M_q - M_{\alpha_{augmented}} \end{aligned} \quad (7-23)$$

The phugoid approximate factors do not contain an $M_{\dot{\alpha}}$ term, and M_{α} enters

only in conjunction with M_u , so there will be little effect of these feedbacks on the phugoid when $M_u \approx 0$.

The appropriate transfer function for the controlled element is

$$\frac{\alpha(s)}{\delta_e(s)} = \frac{N_{\delta_e}^w}{U_0 \Delta_{\text{long}}} = \frac{A_w \left(s + \frac{1}{T_{w1}} \right) [s^2 + 2\zeta_w \omega_w s + \omega_w^2]}{U_0 [s^2 + 2\zeta_p \omega_p s + \omega_p^2] [s^2 + 2\zeta_{sp} \omega_{sp} s + \omega_{sp}^2]} \quad (7-24)$$

and Fig. 7-15 illustrates the system survey for the feedback of angle of attack alone to the elevator. The close proximity of the complex zeros to the phugoid poles implies very little angle of attack change in the phugoid mode. This, of course, is an inference already well established above and in Chapter 5. Under the condition of closed-loop operation, the angle of attack motion in the phugoid mode will be suppressed to an even greater extent than in the open-loop case, but otherwise this feedback does not appreciably alter the phugoid characteristics. The short-period roots, on the other hand, are greatly affected by the feedback. They are seen to move rapidly to a very large frequency, just as would be expected from the approximate factors. In the idealized case extremely high gains can give very heavy damping of the modified short period. However, this is difficult to achieve in the practical case because of servo and sensor lag effects at the modified short-period frequencies, and because the high gains would tend to drive the servo to its limits for all but the smallest inputs or disturbance.

To improve the short-period damping in practice lead equalization is added, with the result shown by the system survey in Fig. 7-16. Here again the effect of the lead at moderate gains is just as would be predicted by the approximate factors.

The angle of attack system, when tightly closed, is similar to the pitch attitude plus rate systems described in Section 7.1. Thus, both systems stabilize attitude and damp short period, and the nature of gain compensation requirements is similar. However, the reference for orientation stabilization is quite different, being the g vector (or horizon)

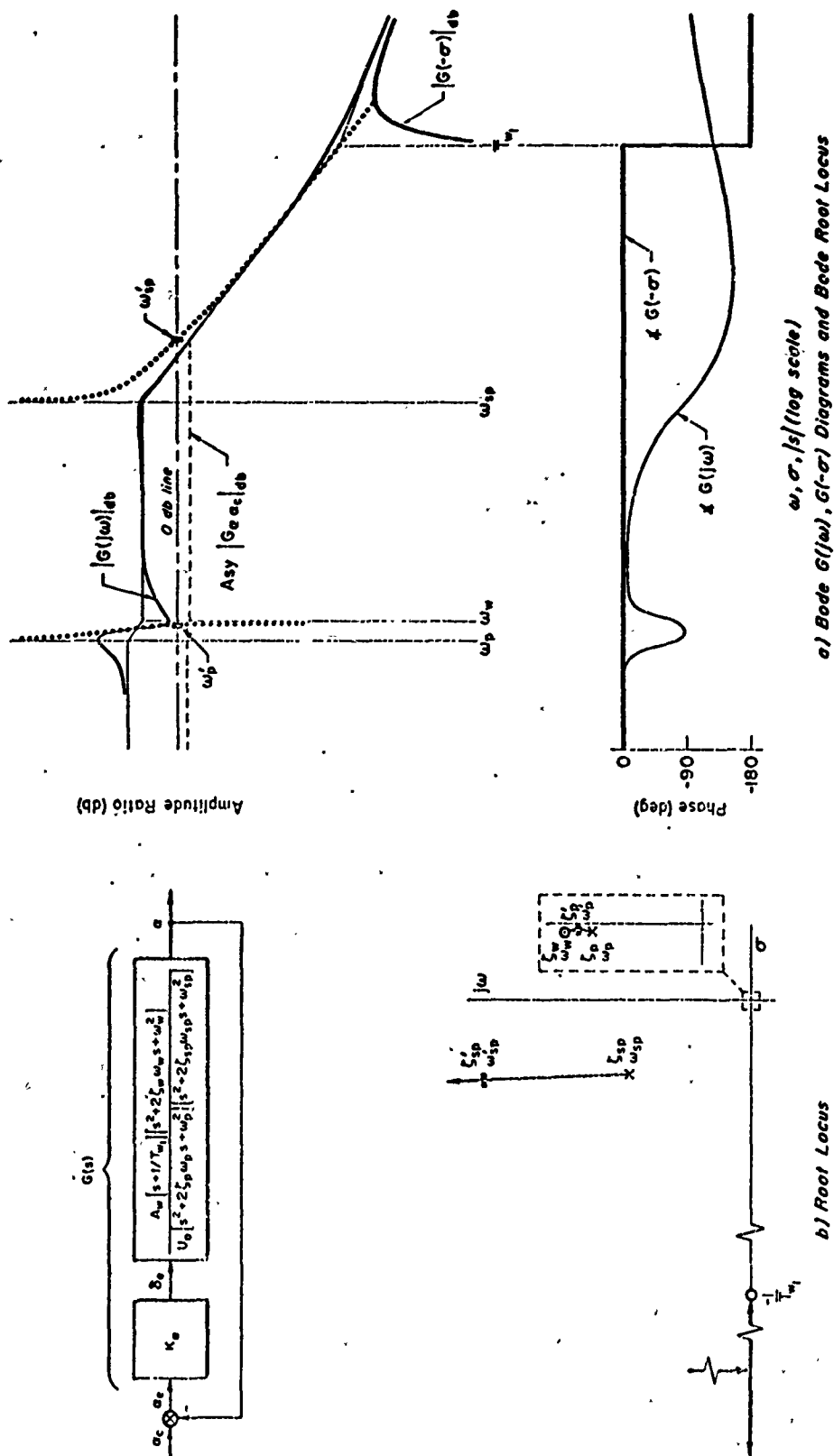


Fig. 7-15. System Survey of Angle of Attack ($\alpha \rightarrow \delta_e$) Control System

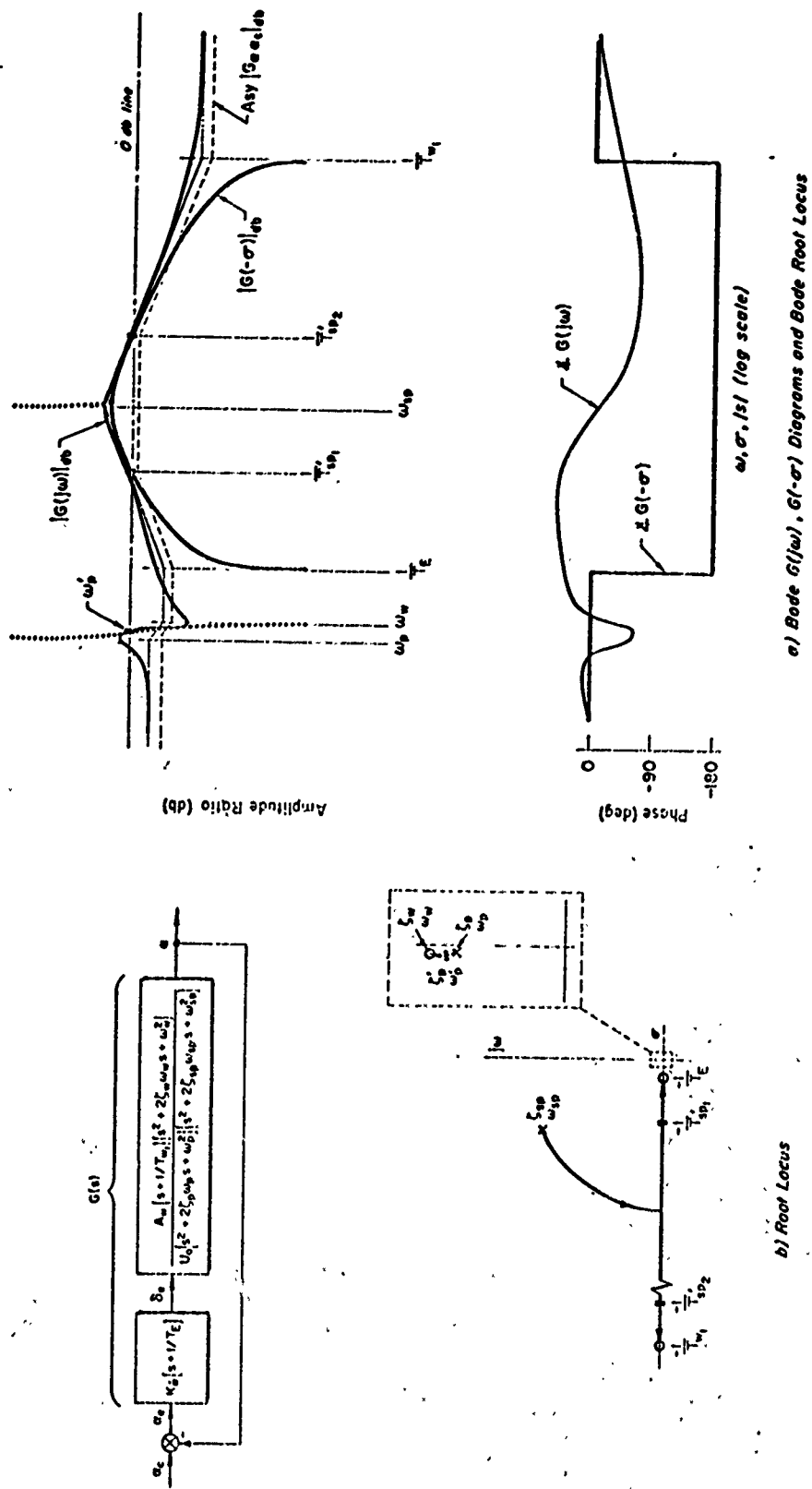


Fig. 7-16. System Survey of Angle of Attack Attitude and Rate (α , $\dot{\alpha} \rightarrow \delta_e$) Control System

for pitch attitude and the relative wind for angle of attack. Consequently, a substantial difference occurs when vertical gust disturbances are encountered. The angle of attack system rotates the craft into the new relative wind direction, thereby tending to maintain the angle of attack and load factor constant. In these same circumstances pitch attitude control, as already mentioned, will resist any tendencies to rotate the craft relative to inertial space. Also, the pitch attitude system has a very beneficial effect on phugoid stability, whereas the angle of attack system, as noted above, has essentially none.

7.4 FEEDBACK OF NORMAL ACCELERATION TO THE ELEVATOR

The favorable effects on the short-period characteristics of $\alpha, \dot{\alpha} \rightarrow \delta_e$ are often difficult to achieve with practical controls because of sensing problems. However, an alternative control system using a normal accelerometer as the basic sensor has many similar features. A major component in the normal acceleration signal is proportional to angle of attack. For instance, for $\gamma_0 = 0$, and considering only short-period characteristics, the acceleration at the c.g. is

$$a_{z_{c.g.}} = \dot{w} - U_0 q \doteq Z_\alpha \alpha + Z_{\delta_e} \delta_e \quad (7-25)$$

Actually, it is seldom possible, even if desirable, to measure normal acceleration at the aircraft's center of gravity under all operational loading distributions. A case of more interest is the feedback of normal acceleration measured in the plane of symmetry at some distance, x_a , from the center of gravity (x_a is positive forward). The normal acceleration at this point is

$$a_z = a_{z_{c.g.}} - x_a \dot{q} \doteq Z_\alpha \alpha + Z_{\delta_e} \delta_e - x_a \dot{q} \quad (7-26)$$

The frequency range over which the normal acceleration and angle of attack transfer functions are similar can be compared directly using the short-period approximations. The three transfer functions of interest are $a_{z_{c.g.}}/\delta_c$, a_z/δ_e , and α/δ_e . These are

$$\begin{aligned}
\frac{a_{z_{c.g.}}}{\delta_e} &= \frac{N_{\delta_e}^{a_{z_{c.g.}}}}{\Delta_{sp}} = \frac{Z_{\delta_e} \left[s^2 - (M_{\alpha}^* + M_q) s - \left(M_{\alpha} - \frac{M_{\delta_e}}{Z_{\delta_e}} Z_{\alpha} \right) \right]}{\Delta_{sp}} \\
&= \frac{\underbrace{\left(s^2 + 2\zeta_h \omega_h s + \omega_h^2 \right)}_{Z_{\delta_e} \left(s + \frac{1}{T_{h2}} \right) \left(s + \frac{1}{T_{h3}} \right)}}{s^2 + 2\zeta_{sp} \omega_{sp} s + \omega_{sp}^2} \quad (7-27)
\end{aligned}$$

$$\begin{aligned}
\frac{a_z}{\delta_e} &= \frac{N_{\delta_e}^{a_z}}{\Delta_{sp}} = \frac{\left[Z_{\delta_e} - x_a (M_{\delta_e} + Z_{\delta_e} M_w^*) \right] s^2 - \left[Z_{\delta_e} (M_{\alpha}^* + M_q) + x_a (Z_{\delta_e} M_w - M_{\delta_e} Z_w) \right] s + M_{\delta_e} \left(Z_{\alpha} - \frac{Z_{\delta_e} M_{\alpha}}{M_{\delta_e}} \right)}{\Delta_{sp}} \\
&= \frac{\underbrace{\left(s^2 + 2\zeta_{a_z} \omega_{a_z} s + \omega_{a_z}^2 \right)}_{\left[Z_{\delta_e} - x_a (M_{\delta_e} + Z_{\delta_e} M_w^*) \right] \left(s + \frac{1}{T_{a_z2}} \right) \left(s + \frac{1}{T_{a_z3}} \right)}}{s^2 + 2\zeta_{sp} \omega_{sp} s + \omega_{sp}^2} \quad (7-28)
\end{aligned}$$

$$\begin{aligned}
\frac{\alpha}{\delta_e} &= \frac{N_{\delta_e}^{\alpha}}{\Delta_{sp}} = \frac{\frac{Z_{\delta_e}}{U_o} \left[s + \left(\frac{U_o M_{\delta_e}}{Z_{\delta_e}} - M_q \right) \right]}{\Delta_{sp}} \\
&= \left(\frac{Z_{\delta_e}}{U_o} \right) \frac{\left(s + \frac{1}{T_{\alpha}} \right)}{s^2 + 2\zeta_{sp} \omega_{sp} s + \omega_{sp}^2} \quad (7-29)
\end{aligned}$$

The break frequencies corresponding to the numerators of Eqs. 7-27 and 7-29 ($a_{z_{c.g.}}/\delta_e$ and α/δ_e) are generally considerably greater than the

short-period undamped natural frequency. This will also be true for the a_z/δ_e numerator breakpoints for any accelerometer location suitable for control purposes. Below these breakpoints the acceleration transfer functions become

$$\frac{a_z}{\delta_e} \doteq \frac{M_{\delta_e} Z_\alpha - M_\alpha Z_{\delta_e}}{s^2 + 2\zeta_{sp}\omega_{sp}s + \omega_{sp}^2}, |s| < \left| \frac{1}{T_{h2}} \right|, \left| \frac{1}{T_{h3}} \right|; \left| \frac{1}{T_{az2}} \right|, \left| \frac{1}{T_{az3}} \right| \text{ or } \omega_{az} \quad (7-30)$$

Similarly, for frequencies less than $1/T_\alpha$ and the usual inequality,

$Z_{\delta_e} M_q / M_{\delta_e} U_0 \ll 1$, the angle of attack transfer function will be approximately

$$\frac{\alpha}{\delta_e} \doteq \frac{M_{\delta_e}}{s^2 + 2\zeta_{sp}\omega_{sp}s + \omega_{sp}^2}, |s| < \left| \frac{1}{T_\alpha} \right| \quad (7-31)$$

It is apparent, therefore, that for the frequency band defined by the minimum of the several numerator breakpoints the acceleration and angle of attack transfer functions are directly related by a proportionality factor, $a_z/\alpha \doteq Z_\alpha - (Z_{\delta_e}/M_{\delta_e})M_\alpha$; this can also be recognized from the approximate $0/\delta_e$ factors as equivalent to $-U_0(1/T_{\theta 2})$.

To determine the frequency range over which the above simple proportionality applies, and to consider means to make and keep this frequency range reasonably large (and thereby retain the desirable features of α feedback), we must now consider the magnitude of the smallest numerator breakpoint. Of those that require consideration (Eqs. 7-30, 7-31), $1/T_\alpha$ is easily eliminated as being generally the largest. That is,

$$\frac{1}{T_\alpha} \doteq \frac{U_0 M_{\delta_e}}{Z_{\delta_e}} \doteq \frac{-cU_0}{k_y^2} \frac{C_{m\delta_e}}{C_{L\delta_e}} \doteq \frac{U_0 l_{\delta_e}}{k_y^2} \quad (7-32)$$

which is of the order of, and varies directly with, airspeed and takes the sign of l_{δ_e} (positive for aft control). Next, consider the numerator terms for the acceleration at the c.g. When the point of control application is aft ($M_{\delta_e} < 0$), the constant term in the quadratic is negative since in general $|M_{\delta_e} Z_\alpha / Z_{\delta_e}| > M_\alpha$. The numerator then consists of two

real roots which are nearly equal but of opposite sign (the negative root is somewhat smaller in magnitude than the positive one because their sum, which is $-M_\alpha - M_q$, is invariably positive). The magnitude of these breakpoints is approximately

$$\frac{1}{T_{h3}} \doteq \frac{-1}{T_{h2}} \doteq \sqrt{M_\alpha - \frac{M_{\delta e}}{Z_{\delta e}}} Z_\alpha \quad (7-33)$$

When the longitudinal control is forward, the quadratic form does not factor and its undamped natural frequency becomes

$$\omega_h \doteq \sqrt{-M_\alpha + \frac{M_{\delta e}}{Z_{\delta e}}} Z_\alpha \quad (7-34)$$

For either the forward or aft elevator the numerator breakpoint is greater than ω_{sp} , although seldom by a large factor. This relatively close proximity has a profound effect on control systems using the c.g.-mounted accelerometer. As illustrated in the system survey of Fig. 7-17, the a_z feedback increases the short-period undamped natural frequency, but the right-half-plane zero, $1/T_{h3}$, pulls the short-period roots into the right half plane. As is apparent from the Bode root locus, much of the movement of the short-period roots occurs with but a slight change in the gain. For instance, only a tiny increment in gain is needed to drive the short period from a value where ω'_{sp} is about equal to $1/T_{h3}$ to the negative real axis rendezvous and thence unstable.

To extend the frequency range over which the a_z/α correspondence holds and, specifically, to alleviate the deleterious effects associated with the nonminimum phase numerator of the c.g.-located accelerometer, other locations are desirable. From Eq. 7-28 it is apparent that, including location effects,

$$\frac{1}{T_{a_z3}} \doteq \frac{-1}{T_{a_z2}} \doteq \sqrt{\frac{M_\alpha - \frac{M_{\delta c}}{Z_{\delta e}}} {1 - x_a \left(\frac{M_{\delta e}}{Z_{\delta e}} + M_w' \right)}} Z_\alpha \quad (7-35)$$

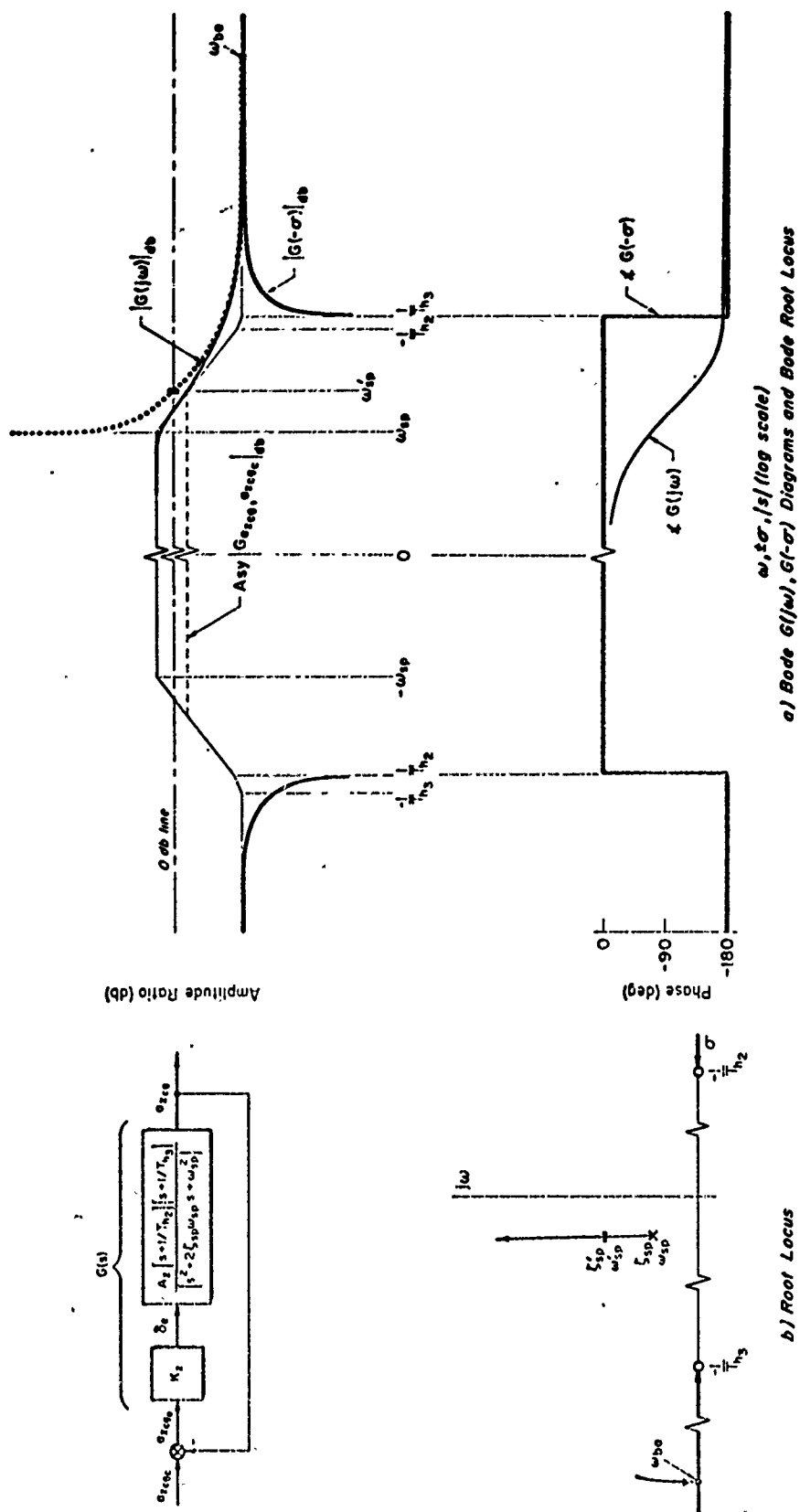


Fig. 7-17. System Survey of Normal Acceleration ($\delta_{acc} \rightarrow \delta_e$) Control System for Short-Period Approximation

We see now that the numerator roots can be increased in magnitude by locating the accelerometer so that the x_a term subtracts from one. For an aft elevator control ($M_{\delta e}/Z_{\delta e} > 0$) the appropriate x_a is positive, implying an accelerometer location ahead of the c.g. Up to a point the change in location simply moves the numerator breakpoints farther out and away from the short-period breakpoint, thereby permitting a higher gain without instability.

When the term involving x_a is greater than one, the numerator becomes a quadratic with an undamped natural frequency:

$$\omega_{az} = \sqrt{\frac{-M_\alpha + \frac{M_{\delta e}}{Z_{\delta e}} Z_\alpha}{1 - x_a \left(\frac{M_{\delta e}}{Z_{\delta e}} + M_w^* \right)}} \quad (7-36)$$

With further increase in x_a , ω_{az} is decreased and the numerator breakpoint starts back toward the short period.

The detailed nature of the numerator root variations with the accelerometer-position control-location parameter, $x_a M_{\delta e}/Z_{\delta e}$, can be explored by considering the general a_z numerator as an equivalent servo system which has $x_a M_{\delta e}/Z_{\delta e}$ as a gain. From Eqs. 7-27 and 7-28, the numerator is given by

$$\begin{aligned} N_{\delta e}^{a_z}(s) &= N_{\delta e}^{a_z c.g.}(s) - x_a M_{\delta e} s \left[\left(1 + \frac{Z_{\delta e} M_w^*}{M_{\delta e}} \right) s - Z_w + \frac{Z_{\delta e}}{M_{\delta e}} M_w \right] \\ &= N_{\delta e}^{a_z c.g.}(s) \left\{ 1 + \frac{-x_a M_{\delta e} s \left[\left(1 + \frac{Z_{\delta e} M_w^*}{M_{\delta e}} \right) s - Z_w + \frac{Z_{\delta e}}{M_{\delta e}} M_w \right]}{N_{\delta e}^{a_z c.g.}(s)} \right\} \quad (7-37) \end{aligned}$$

Considering that usually $|Z_{\delta e} M_w^*/M_{\delta e}| \ll 1$ and $|(Z_{\delta e}/M_{\delta e})(M_w/Z_w)| \ll 1$, then the zeros of $N_{\delta e}^{a_z}(s)$ will be the zeros of $(1+G)$, where G is given by

$$G \doteq \frac{-x_a M_{\delta_e}}{Z_{\delta_e}} \frac{s(s - Z_w)}{\left[s^2 - (M_{\delta_a} + M_{\delta_q})s + \frac{M_{\delta_e}}{Z_{\delta_e}} Z_a \right]} \quad (7-38)$$

or, with an aft control point,

$$G \doteq \left(\frac{-x_a M_{\delta_e}}{Z_{\delta_e}} \right) \frac{s(s - Z_w)}{\left(s + \frac{1}{T_{h2}} \right) \left(s + \frac{1}{T_{h3}} \right)} \quad (7-39)$$

Furthermore, $|1/T_{h2,3}|/|-Z_w| \doteq (M_{\delta_e}/Z_{\delta_e})(U_o/Z_w)$ will invariably be larger than one.

A survey of this equivalent servo system is shown in Fig. 7-18. At low gains the accelerometer zeros (the poles of the equivalent servo system) are near those for the c.g. location. As gain is increased, both the minimum and nonminimum phase zeros increase in magnitude until $|x_a M_{\delta_e}/Z_{\delta_e}| = 1$. At this point the minimum phase zero emanating from $-1/T_{h3}$ has gone to $-\infty$, but the nonminimum phase zero (from $-1/T_{h2}$) is still finite. For values of gain just slightly greater than one the minimum phase zero has gone through minus infinity and has become a very large positive number; and as gain is further slightly increased this zero and the nonminimum phase zero rendezvous to form a high frequency quadratic pair.* The undamped natural frequency of this pair initially decreases rapidly as gain is further increased, and then more gradually as the zeros proceed down the +40 db/decade Bode root locus asymptote between $-Z_w$ and $-1/T_{h2}$.

From the features just described, the most appropriate location for the accelerometer in the sense that the numerator breakpoints are as far removed from ω_{sp} as possible corresponds to locations where $|x_a M_{\delta_e}/Z_{\delta_e}|$ is near one. When this is exactly the case, the coefficient of the s^2

*This rendezvous point can occur in either the right half or left half plane, depending on the sign of $(M_{\delta_a} + M_{\delta_q} - Z_w)$. For an aft elevator and $(M_{\delta_a} + M_{\delta_q} - Z_w) > 0$ the rendezvous point is in the left half plane; for $(M_{\delta_a} + M_{\delta_q} - Z_w) < 0$ it is in the right half plane.

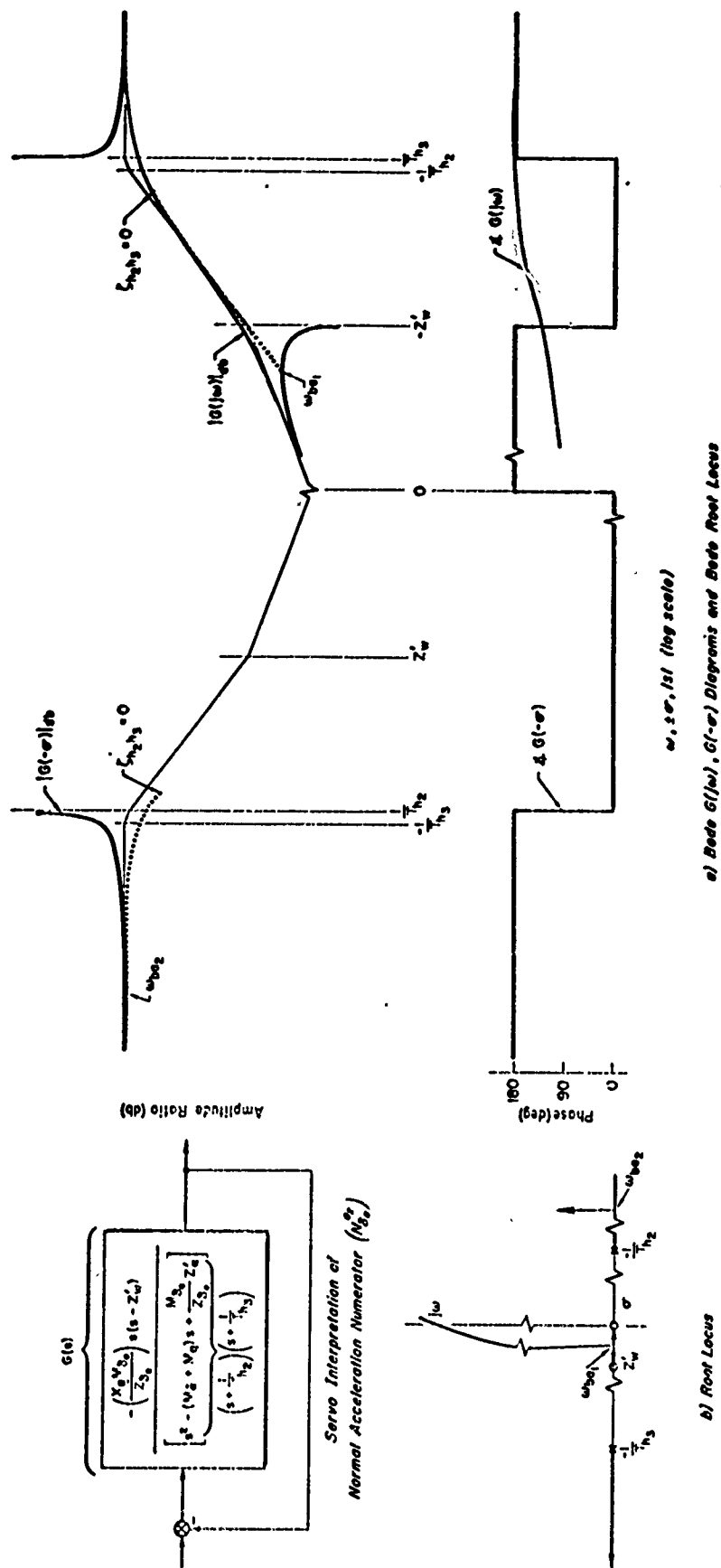


Fig. 7-18. System Survey Showing Accelerometer Location (x_a) Effects On Normal Acceleration Numerator (N_{a2})

term in the a_z/δ_e numerator is zero and the transfer function becomes

$$\frac{a_z}{\delta_e} = \frac{-Z_{\delta_e}(M_{\dot{\alpha}} + M_q - Z_w) \left[s - \frac{M_{\delta_e} Z_{\alpha}}{Z_{\delta_e}(M_{\dot{\alpha}} + M_q - Z_w)} \right]}{\Delta_{sp}} \quad (7-40)$$

The location $x_a = Z_{\delta_e}/M_{\delta_e}$ corresponds to an "instantaneous center of rotation" for which the center of pressure of the aerodynamic load due to deflecting the control surface is a "center of percussion." At the instantaneous center of rotation a step function elevator input will produce an initial vertical acceleration due to $Z_{\delta_e}\delta_e$ which is just balanced by that due to pitching acceleration, $x_a\dot{q}$. (Most readers will recall that the trademark on a baseball bat is at the center of percussion, and that the impulse on the bat when the ball is hit at this point does not result in translational forces on the batter's hands, i.e., the handle is the center of rotation.) This particular location is, of course, ideal for accelerometer control systems. In practice, however, the effective center of rotation shifts because of c.g. and effective control arm changes so that a location in its general neighborhood is the best that can normally be expected.

In all of the above discussion the accelerometer system has been considered as a replacement for systems involving angle of attack. The analogy can be carried further; for instance, an \dot{a}_z signal can be used to increase the short-period damping, effectively augmenting $M_{\dot{\alpha}}$. The major difference, then, between a good a_z system and an α system, other than those dwelt on at length above, is in the controller gain variation required for any reasonable control. This is generally quite extreme for accelerometer systems intended to perform angle of attack stabilization functions. More specifically, in an angle of attack controller for which a pure gain might be suitable, the a_z gain would have to vary inversely as ρU_0^2 .

For control in the range of phugoid frequencies, the properties of a normal acceleration control are considerably different from those of an angle of attack system. This can perhaps best be appreciated by

comparing the system survey of Fig. 7-19, which shows an $a_z \rightarrow \delta_e$ system, with the angle of attack control for the same airplane illustrated in Fig. 7-15. Unlike the angle of attack system, the normal acceleration control can have a significant effect on the phugoid. In this case the major effect is a reduction in the phugoid undamped natural frequency. However, for flight conditions which exhibit a performance reversal, i.e., $1/T_{h1}$ negative, this zero will appear in the right half plane and a normal acceleration system without washout will tend to drive the phugoid unstable.

7.5 FEEDBACK OF ALTITUDE TO THE ELEVATOR

The altitude is an important and very physical motion quantity which must often be controlled accurately. In the linearized equations for small perturbations from straight, level, and horizontal flight the altitude is proportional to the double integral of the normal acceleration at the c.g.,

$$h = U_0 \int \gamma dt = -U_0 \iint a_{z_{c.g.}} dt dt \quad (7-41)$$

and the altitude-to-elevator transfer function is given by

$$\frac{h(s)}{\delta_e(s)} = \frac{N_{\delta_e}^h}{\Delta_{\text{long}}} = \frac{\underbrace{s^2 + 2\zeta_h \omega_h s + \omega_h^2}_{\text{or}} A_h \left(s + \frac{1}{T_{h1}}\right) \left(s + \frac{1}{T_{h2}}\right) \left(s + \frac{1}{T_{h3}}\right)}{s \left(s^2 + 2\zeta_p \omega_p s + \omega_p^2\right) \left(s^2 + 2\zeta_{sp} \omega_{sp} s + \omega_{sp}^2\right)} \quad (7-42)$$

Just as in the $a_{z_{c.g.}}$ acceleration system discussed in the last article, the numerator quadratic or two first-orders correspond to forward and aft elevator control, respectively. Because of the free s , the feedback of altitude by itself drives the modified phugoid roots into the right half plane at very low values of gain (see Fig. 7-20). Consequently, some form of equalization is required to make an effective altitude

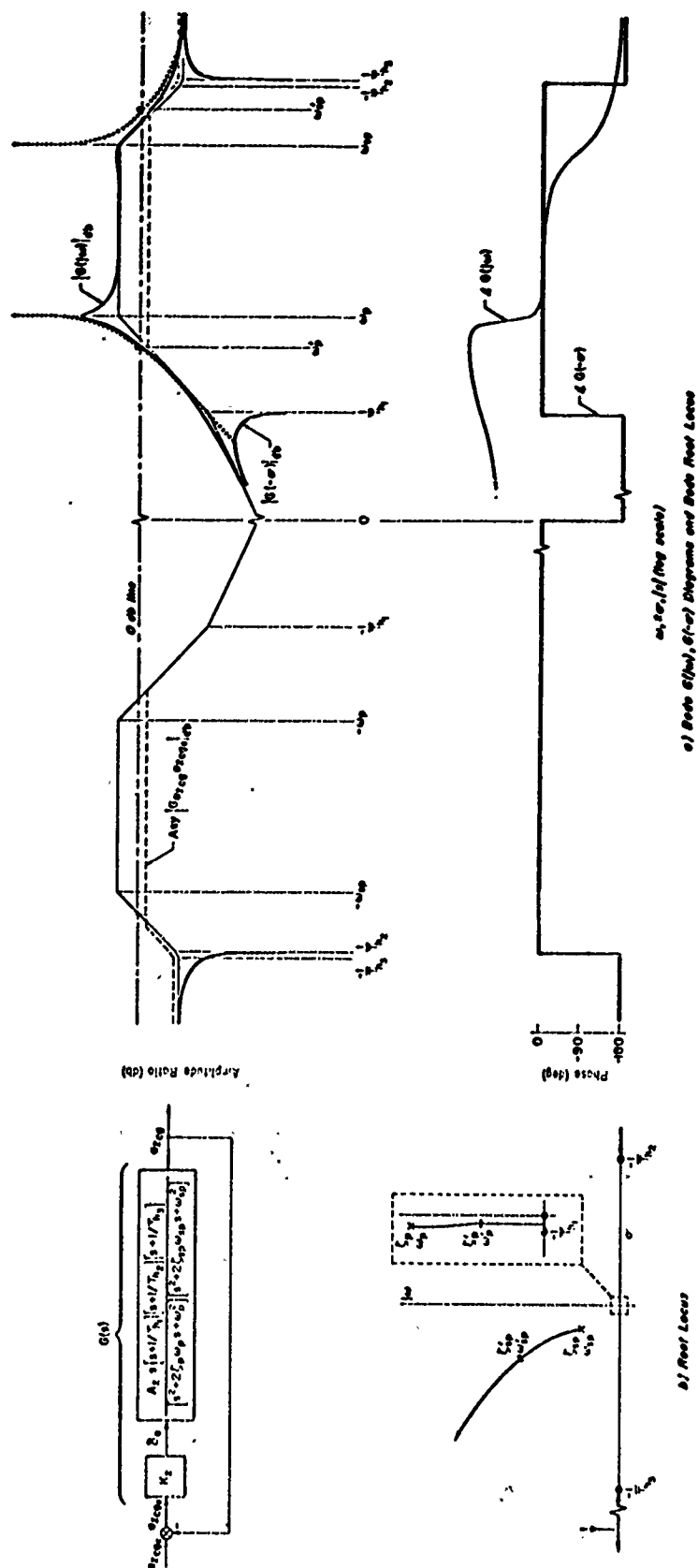
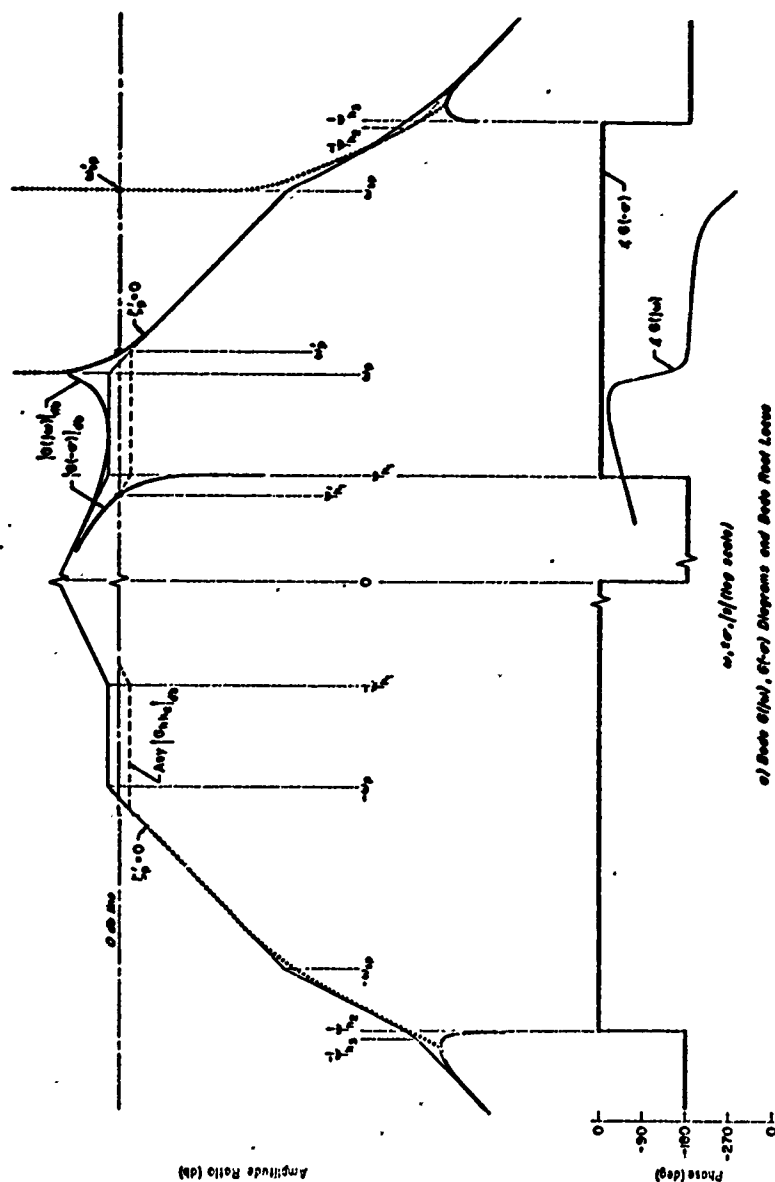
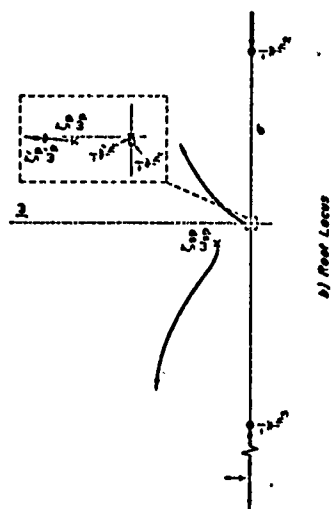
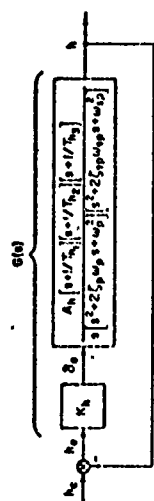


Fig. 7-19. System Survey of Normal Acceleration ($a_{zcg} \rightarrow \delta_e$) Control System



a) Bode $|G(j\omega)|$, $\angle G(j\omega)$ Diagrams and Root Locus



b) Root Locus

Fig. 7-20. System Survey of Altitude ($h \rightarrow \delta_e$) Control System

control. An inner attitude loop to damp the phugoid is one such possibility. Since this constitutes a multiloop system, its consideration is deferred until Chapter 11. Confining our attention here to single-loop or effective single-loop controllers, the appropriate equalization is a lead on the altitude error. Practically; this might be accomplished by rate equalization in series or by the use of an altitude rate or rate of climb signal. In any event, the inverse of the lead time constant, $1/T_E$, is adjusted to lie between the phugoid and short-period breakpoints. A system survey indicating the efficacy of this technique is shown in Fig. 7-21.

A major problem with altitude control is encountered for performance reversal situations where $1/T_{H1}$ becomes negative. As discussed at length in Chapter 5, $1/T_{H1}$ is approximated by

$$\frac{1}{T_{H1}} \doteq \frac{1}{m} \left(\frac{dD}{dU} - \frac{\partial T}{\partial U} \right) \quad (7-43)$$

It will change sign whenever the airplane is on the "backside" of the thrust-required versus speed curve. This is a common situation on very low speed approaches (e.g., carrier approaches), steep climbs, and other flight conditions where flight at near-minimum drag is desirable. When this performance reversal occurs, an altitude loop will drive the pole at the origin into the right half plane toward $1/T_{H1}$. The result is a divergent instability at any value of closed-loop gain. In principle, the performance reversal point could be detected and the sign of the gain changed to avoid divergence, but this would also change the root locus departure from the phugoid roots by 180° , thereby tending to drive the phugoid unstable at very low values of gain. Consequently, even in principle such a change is impractical. The conclusion to be drawn from these considerations is that altitude control using the elevator alone cannot be achieved for flight conditions in which the performance reversal exists. An additional control deflection (other than the elevator) must be added.

A similar conclusion on the same basis can be drawn for rate of climb systems. However, there are many situations in which a specific

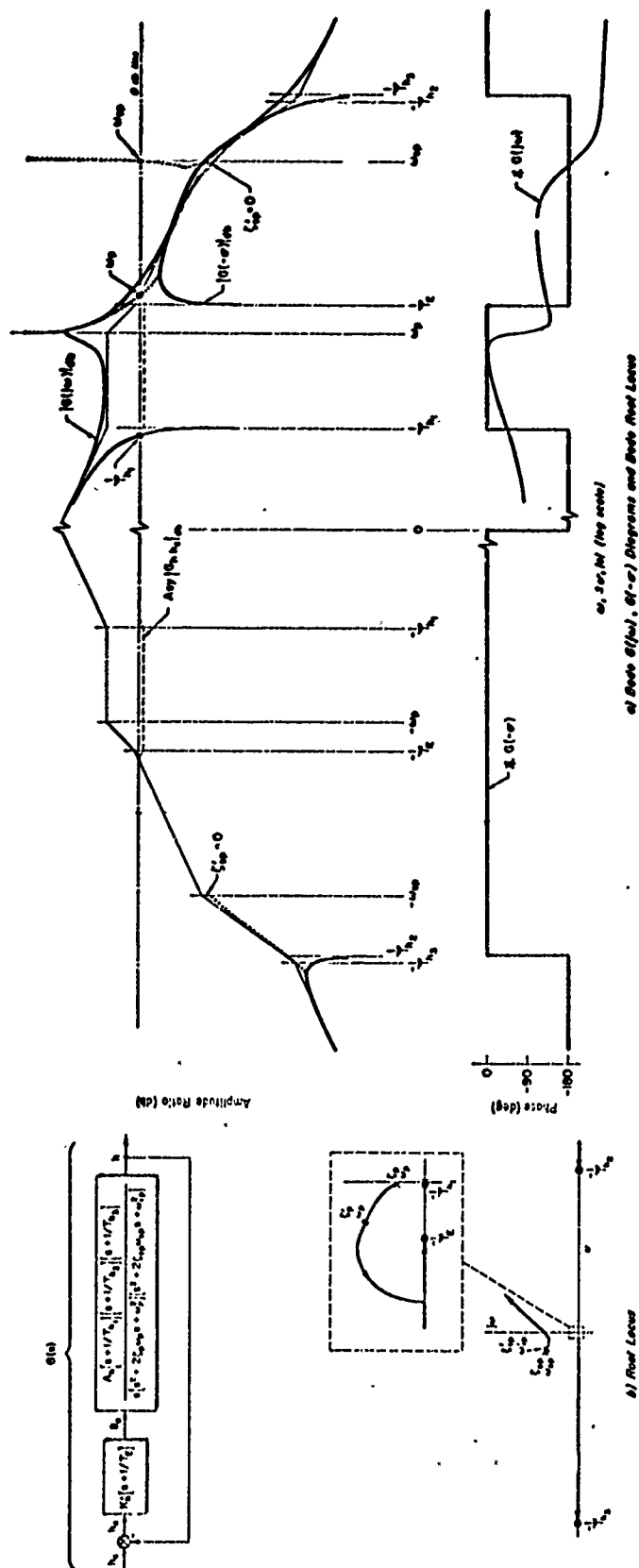


Fig. 7-21. System Survey of Altitude and Altitude Rate ($h, \dot{h} \rightarrow \delta_e$) Control System

value of rate of climb is not the basic requirement; rather, it is desired that nearly best rate of climb as a function of altitude be maintained. Under these conditions the use of airspeed-like feedbacks to control either indicated airspeed or Mach number to values approximating those for best-climb is most appropriate. Such feedback systems do not suffer from performance reversal problems and, further, they do not require command scheduling consistent with available flight performance as a function of altitude.

CHAPTER 8

ELEMENTARY LATERAL FEEDBACK CONTROL

The usefulness of studying feedback loops closed around the various transfer functions of aircraft is exactly the same in the case of lateral motions as it is for longitudinal. Idealized systems still serve to show the ultimate performance which practical systems can approach or, on the other hand, tend to show which feedbacks are unlikely to prove useful.

A general block diagram for the cases of lateral motion quantity feedback is identical to the one for longitudinal motion quantity feedback (see Fig. 7-1). Again it will be sufficient, in most instances, to consider that the controller is simply a gain, although in some cases simple forms of compensation or equalization may be provided to improve the performance of the feedback control loop.

The main lateral motion output quantities which have been controlled directly, and the actuating quantities for the lateral motions of aircraft, are summarized in Table 8-1. Because there are so many possible combinations, only the more useful and/or instructive of these will be described in this chapter.

8.1 FEEDBACK OF BANK ANGLE AND ROLLING VELOCITY TO THE AILERONS

The first successful aircraft automatic pilots employed the same vertical gyroscope which sensed the pitching motions to detect departures from a wings-level attitude and to cause the ailerons to move so as to oppose the bank angle. This action can be thought of as negative feedback of the bank angle motion variable to the aileron actuating quantity. The appropriate transfer function for the controlled element is

$$\frac{\varphi(s)}{\delta_a(s)} = \frac{N_{\delta_a}^{\varphi}}{\Delta_{lat}} = \frac{A_{\varphi} [s^2 + 2\zeta_{\varphi}\omega_{\varphi}s + \omega_{\varphi}^2]}{\left(s + \frac{1}{T_S}\right)\left(s + \frac{1}{T_R}\right)[s^2 + 2\zeta_d\omega_d s + \omega_d^2]} \quad (8-1)$$

TABLE 8-1

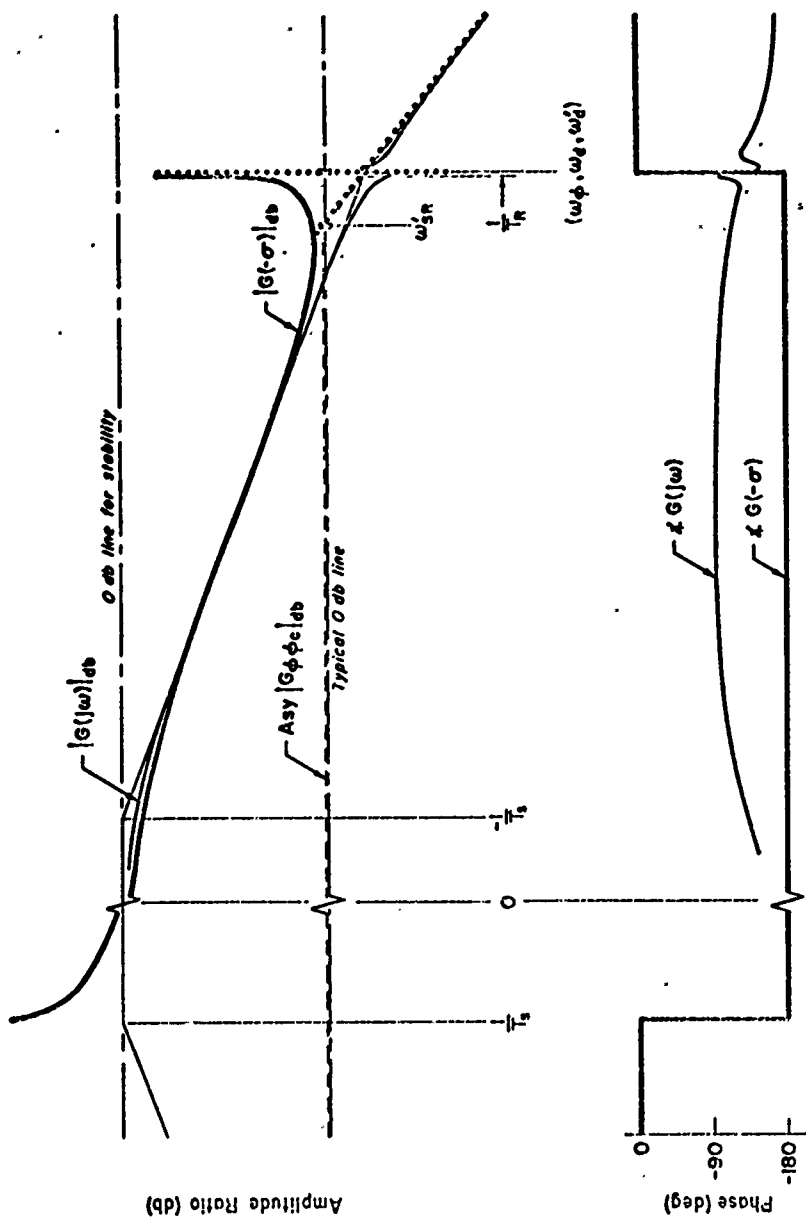
LATERAL MOTION AIRFRAME OUTPUT AND ACTUATING QUANTITIES

OUTPUT QUANTITIES	ACTUATING QUANTITIES
ϕ , bank angle	δ_a , aileron deflection
p , rolling velocity	δ_r , rudder deflection
r , yawing velocity	
ψ , heading angle	
β , sideslip angle, v/U_0	
a_y , side acceleration, $a_{y\text{c.g.}} + x_a \ddot{\phi}$	

Typically, in cruising flight the spiral time constant is very large and the mode itself can be either neutrally stable, or a slow convergence, or a slight divergence. Both the neutral and the unstable conditions are undesirable for unattended operation, and the slow convergence is little better. Consequently, one purpose of an automatic pilot is to impose a higher degree of spiral stability. With roll attitude control this is achieved by the creation of static stability in roll. Directly associated with the improvement in spiral mode stability with this kind of system is the provision of bank angle stability and a tendency to maintain roll attitude orientation in the presence of aircraft disturbances. Finally, the bank angle system permits the imposition of roll commands on the aircraft. In the discussion below several aspects of roll attitude and rolling velocity control will be considered for a variety of aircraft configurations which correspond to several degrees of control difficulty.

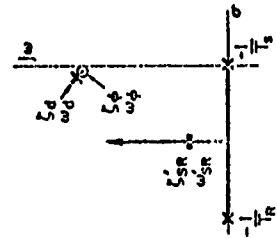
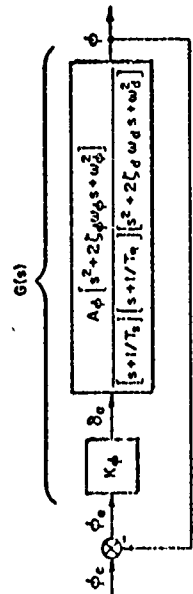
Conventional Roll Attitude Control

Figure 8-1 displays the feedback system analysis for the bank-angle-to-aileron closure ($\phi \rightarrow \delta_a$) for an aircraft with good rolling characteristics. The σ -Bode diagram (shown for both positive and negative values)



$\omega, \pm\sigma, |s|$ (log scale)

a) Bode $G(j\omega)$, $G(-\sigma)$ Diagrams and Bode Root Locus



b) Root Locus

Fig. 8-1. System Survey of Roll Attitude ($\phi \rightarrow \delta_a$) Control System for Aircraft with Good Rolling Characteristic

indicates that at a gain greater than $|K_\phi K_{\phi\delta_a}| = 1$ the spiral motion is made stable. For the vehicle dynamics presumed here this loop may, in fact, be closed with much higher gains without the danger of instability.

While the dutch roll mode in this airplane is weakly damped, the close proximity of the numerator zeros to the dutch roll poles implies that there will be very little excitation of this mode in response to aileron inputs. (However, the dutch roll mode will still be excited by rudder or gust inputs.) As far as the regulation of bank angle and the ability to follow bank angle commands are concerned, this system would be eminently satisfactory when the loop is closed with the typical zero db line location shown.

Control of the bank angle of a hovering VTOL aircraft, or helicopter, by means of feedback to the rolling moment control is the analog of pitch angle control for this type of vehicle (see Section 7.1, Eq. 7-8, and Fig. 7-10). The equations of motion and transfer functions have the same form and, except for changes in the numerical values of the stability derivatives or transfer function factors, they are appropriate for the description of either longitudinal or lateral motions at hover and at very low forward speeds. Figure 7-10 therefore can be considered to be equally as good an analysis of the bank-angle-to-rolling-moment control of a hovering helicopter as it is of pitch-angle-to-pitching-moment control.

Nature of Gain Adjustments for Conventional Roll Attitude Control

To maintain these satisfactory closed-loop characteristics over a broad regime of flight conditions may require changes in the controller gain to accommodate changes in the conditions of flight. Some appreciation for the nature of appropriate gain variations can be obtained by considering roll control of a much simplified airplane. If we assume that $1/T_R \gg 1/T_S$, and that the dutch roll mode is exactly canceled by the numerator quadratic, then the pure-gain roll control system has an open-loop transfer function given by

$$\frac{\phi}{\phi_e} = \frac{K_\phi I_{\phi\delta_a}}{s \left(s + \frac{1}{T_R} \right)} \quad (8-2)$$

The open- and closed-loop characteristics of this system are shown in Fig. 8-2.

The closed-loop roots for this system are defined by

$$2\zeta'_{SR}\omega'_{SR} = \frac{1}{T_R} \quad (8-3)$$

$$\omega'^2_{SR} = K_{\phi} L'_{\delta a} \quad (8-4)$$

The closed-loop damping ratio is therefore

$$\zeta'_{SR} = \frac{1}{2T_R \sqrt{K_{\phi} L'_{\delta a}}} \quad (8-5)$$

The controller gain required to obtain a specific closed-loop damping ratio (or, equivalently, a specific phase margin) is then

$$\begin{aligned} K_{\phi} &= \frac{1}{L'_{\delta a} (2\zeta'_{SR} T_R)^2} = \frac{L_p'^2}{4\zeta'^2_{SR} L'_{\delta a}} \\ &= \frac{\rho S b^3}{32\zeta'^2_{SR} I_x} \frac{(C_{l_p})^2}{C_{l_{\delta a}}} \end{aligned} \quad (8-6)$$

The ratio $(C_{l_p})^2/C_{l_{\delta a}}$ is reasonably constant at subsonic conditions, but is a function of Mach number in the transonic and supersonic regimes. To the extent that $(C_{l_p})^2/C_{l_{\delta a}}$ is approximately constant, an appropriate variation for K_{ϕ} to maintain constant closed-loop damping ratio and phase margin would be

$$K_{\phi} \propto \rho \quad (8-7)$$

With constant phase margin, it is clear from Fig. 8-2 that

$$\omega_c \propto \frac{1}{T_R} = -L_p' \quad (8-8)$$

or that the variation of the crossover frequency with flight environmental parameters will be

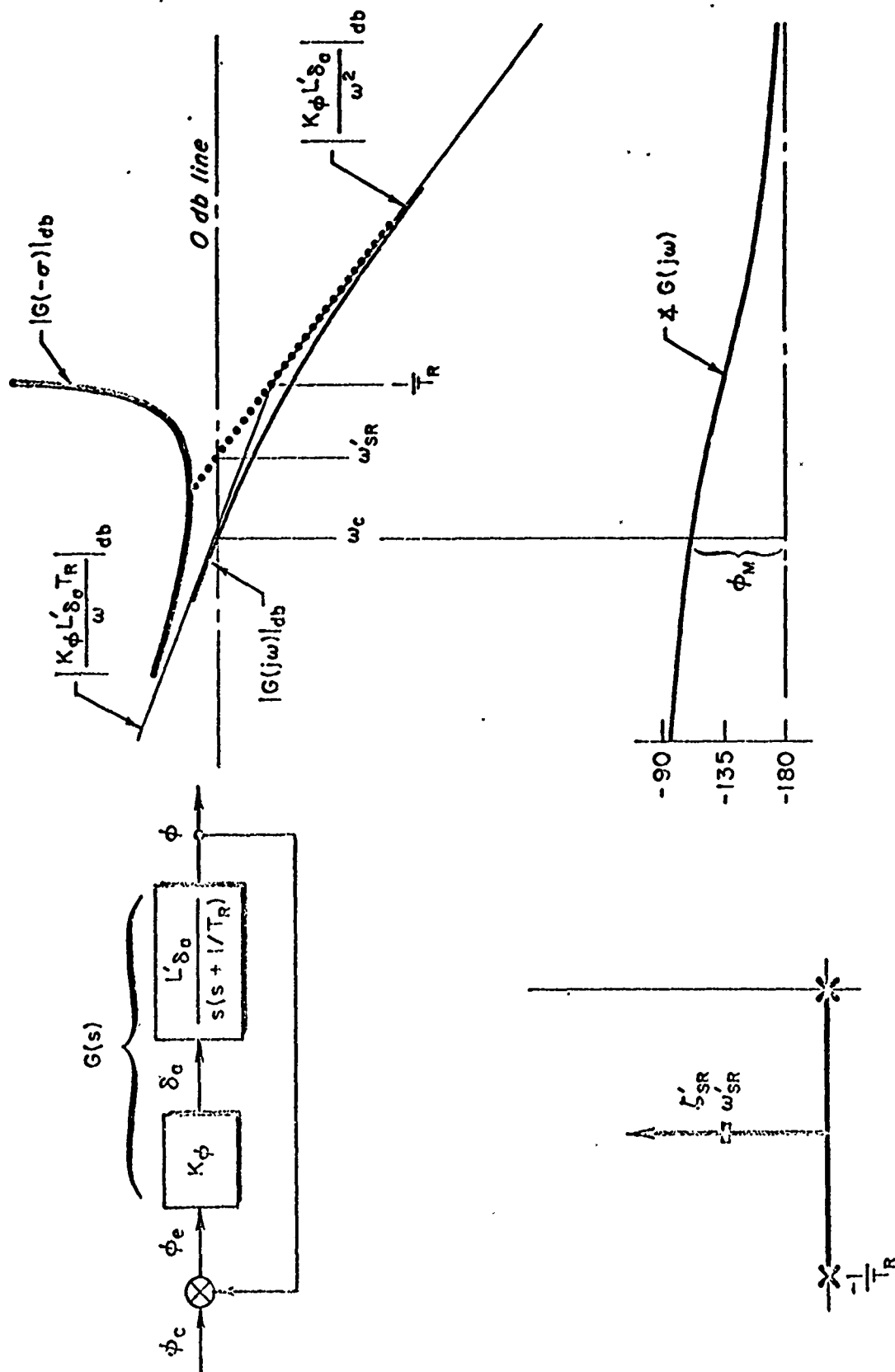


Fig. 8-2. Roll Attitude Control for Simplified Airframe ($1/T_R \gg 1/T_S$; $\omega_0 \approx \omega_d$)

$$\omega_c \propto \rho U_0 \quad (8-9)$$

If the desire is to keep the closed-loop undamped natural frequency, ω_{SR}^i , constant, a somewhat more drastic gain variation is required. From Eq. 8-4 it follows that K_ϕ must vary inversely with $I_{\delta_a}^i$, or in terms of flight environmental parameters

$$K_\phi \propto \frac{1}{\rho U_0^2} \quad (8-10)$$

Controller gain variation between the two extremes of Eqs. 8-7 and 8-10 results in a compromise between constant closed-loop damping ratio, ζ_{SR}^i , and constant undamped natural frequency, ω_{SR}^i .

Roll Attitude Control with Roll/Yaw Coupling

One facet of the good lateral control behavior exhibited by the aircraft considered above is the near absence of the dutch roll mode in rolling motions. In fact, the significant roll dynamics could have been treated almost as well using the three-degree-of-freedom spiral roll subsidence approximations in Chapter 6 in which neither numerator nor denominator quadratics appear. When the quadratic numerator in the ϕ/δ_a transfer function does not approximately cancel the dutch roll denominator, the magnitude of the dutch roll component in rolling motions becomes more significant and may in certain conditions lead to serious control problems. In the context of the simplified case this change amounts to the multiplication of the simplified transfer function by a ratio of quadratics.

The possible relative orientations of the quadratic pole/zero can best be developed by considering the simplified approximate factors

$$\begin{aligned} \frac{\omega_\phi}{\omega_d} &= \left(1 - \frac{N_{\delta_a}^i I_\beta^i}{I_{\delta_a}^i N_\beta^i} \right) \\ 2\zeta_{\phi\omega_\phi} &= -(Y_v + N_r^i) \\ 2\zeta_{d\omega_d} &= 2\zeta_{\phi\omega_\phi} - \frac{L_\beta^i}{N_\beta^i} \left(N_p^i - \frac{g}{U_0} \right) \end{aligned} \quad (8-11)$$

Great efforts are ordinarily made in the basic airframe design to keep I_{β}^i/N_{β}^i negative. To the extent that these succeed, $\omega_{\phi}/\omega_{\eta}$ will be less than one for adverse aileron yaw ($N_{\delta a}^i/L_{\delta a}^i < 0$) and greater than one for so-called favorable aileron yaw ($N_{\delta a}^i/L_{\delta a}^i > 0$). The difference in the damping terms depends mainly on the sign of $(N_p^i - g/U_0)$. On most aircraft each sign occurs somewhere in the flight regime, so the relative magnitudes of $\zeta_{\phi}\omega_{\phi}$ and $\zeta_{\eta}\omega_{\eta}$ alternate. In general, however, the magnitude of $\zeta_{\phi}\omega_{\phi}$ will be roughly that of $\zeta_{\eta}\omega_{\eta}$, except for those cases where ζ_{η} becomes negative since ζ_{ϕ} is invariably positive. Finally, the relative location of $1/T_R$ and ω_{η} affects the roll attitude system closure characteristics. Thus, the following matrix of possible conditions is of interest:

Case	$\omega_{\phi}/\omega_{\eta}$	$1/T_R\omega_{\eta}$
1	< 1	> 1
2	> 1	> 1
3	< 1	< 1
4	> 1	< 1

These various cases are illustrated in the $G(j\omega)$ Bode plots of Fig. 8-3. These plots are drawn with ζ_{ϕ} and ζ_{η} equal, and use phase asymptotes to emphasize the phase blip due to the quadratic pair.

Examination of Fig. 8-3 reveals that Cases 2 and 4 may become unstable for values of gain where the zero-db-line/amplitude-ratio intersection is in the region of the sharp dip in phase. The phase dip must, of course, take the phase angle to values greater than 180° for such an instability to occur. The magnitude of the dip depends on the values of ζ_{ϕ} , ζ_{η} , and the $\omega_{\phi}/\omega_{\eta}$ ratio; and in many circumstances the total maximum phase dip is not sufficient to reach -180° . For example, in aircraft with large values of dutch roll damping, both ζ_{ϕ} and ζ_{η} are fairly large and the phase dip is therefore small. Such craft are seldom affected by an unstable condition of this nature. The surest way to avoid the phase dip of Cases 2 and 4 is, of course, to have $\omega_{\phi} < \omega_{\eta}$, corresponding to Cases 1 and 3. These latter cases, for the minimum-phase airframe conditions shown in Fig. 8-3 and the ideal sensor and servo characteristics assumed here, cannot become unstable at any value of gain.

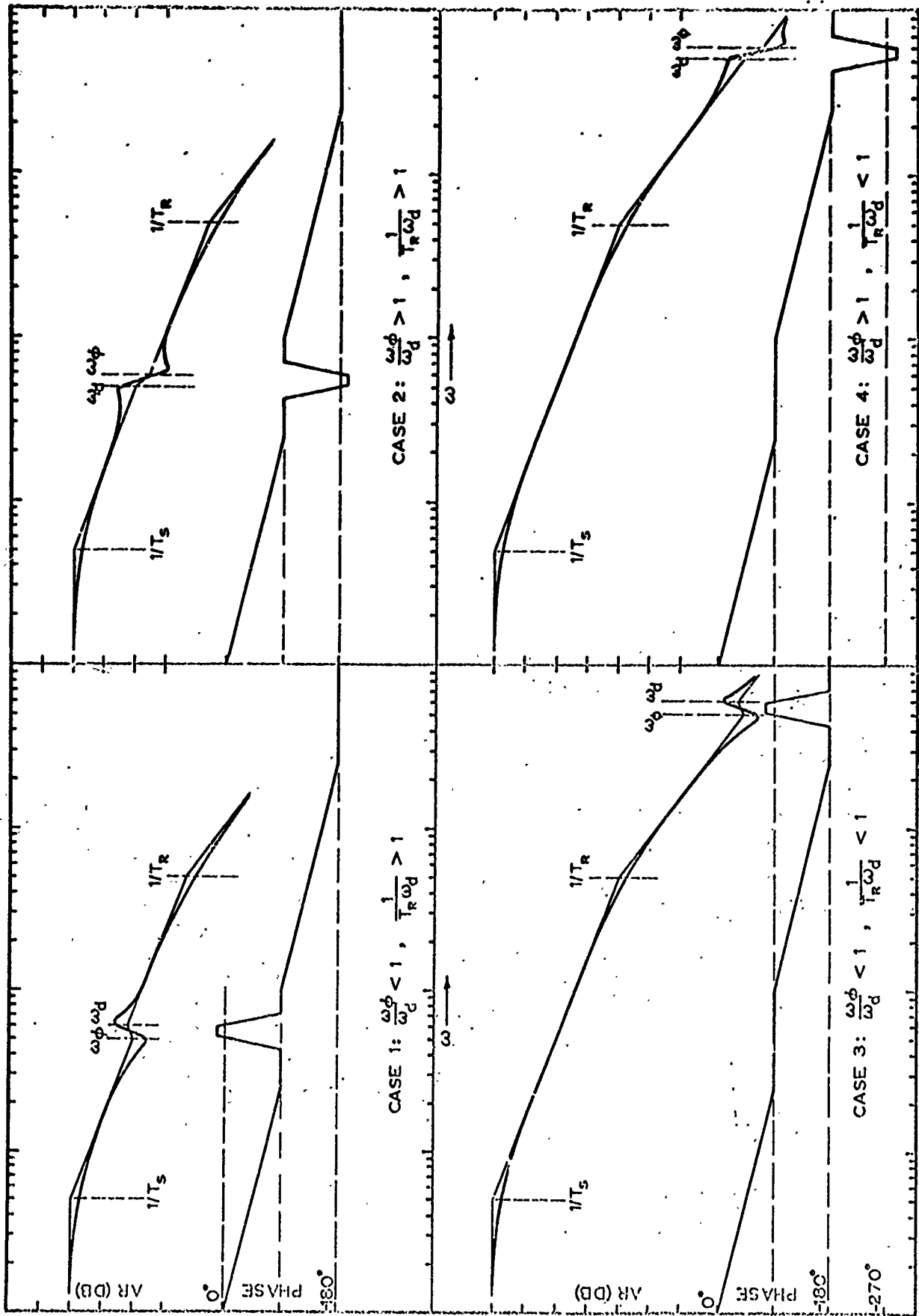


Fig. 8-3. Generic $G(j\omega)$ Bode Diagrams of $K_D \frac{\omega}{\delta_a}$ for Roll Control System Cases

Root locus diagrams for the four cases are shown in Fig. 8-4. In all cases the closed-loop spiral and roll subsidence roots proceed toward each other, couple, and break off from the real axis. This behavior is similar to that of the well-behaved aircraft situation, being precisely the same for low gains. A divergent spiral does not change this picture appreciably, although there is a minimum value of gain required for stability. Also, the direct correlation between the phase dip and the entry and subsequent exit of the closed-loop dutch roll mode from the right half plane is apparent.

The behavior of the spiral/roll-subsidence coupled pair after breakoff, and that of the modified dutch roll roots, is most interesting and varied. One of these pairs must go to the roll numerator at high gain, while the other proceeds toward the high gain asymptotes. Which pair goes where is the basis for further classification—in Subcase A the dutch roll poles go into the roll numerator pair, while the coupled spiral/roll-subsidence mode goes to the asymptote; Subcase B is the opposite of Subcase A. Whether a particular pole/zero configuration fits into a specific category depends primarily on the relative location of the root, especially that of the dutch roll and of the roll numerator. When $\zeta_{\phi\omega_{\phi}} = \zeta_{d\omega_d}$ and ω_{ϕ}/ω_d is near unity (Cases 1A and 4A), the infinite gain dutch roll characteristics are those of the roll numerator. As ω_{ϕ}/ω_d decreases (Cases 1B and 3) or $\zeta_{\phi\omega_{\phi}}$ and $\zeta_{d\omega_d}$ become separated in value (Cases 1B modified and 4B), the coupled spiral/roll-subsidence roots drive into the zeros. In either case the high gain characteristic of the closed-loop transfer function, ϕ/ϕ_c , is basically similar, since one or the other of the denominator pairs will approximately cancel the zeros. The net result for the high gain values of $G/(1+G)$ will then be

$$\left. \frac{G}{1+G} \right]_{K_{\phi\text{high}}} = \frac{\omega_{CL}^2}{s^2 + 2\zeta_{CL}\omega_{CL}s + \omega_{CL}^2} \quad (8-12)$$

The value of $\zeta_{CL}\omega_{CL}$ for high gain approaches the negative of the high gain root locus asymptote, i.e.,

$$\zeta_{CL}\omega_{CL} = -\sigma_{c.g.} = (\zeta_{d\omega_d} - \zeta_{\phi\omega_{\phi}}) + \frac{1}{2} \left(\frac{1}{T_R} + \frac{1}{T_S} \right) \quad (8-13)$$

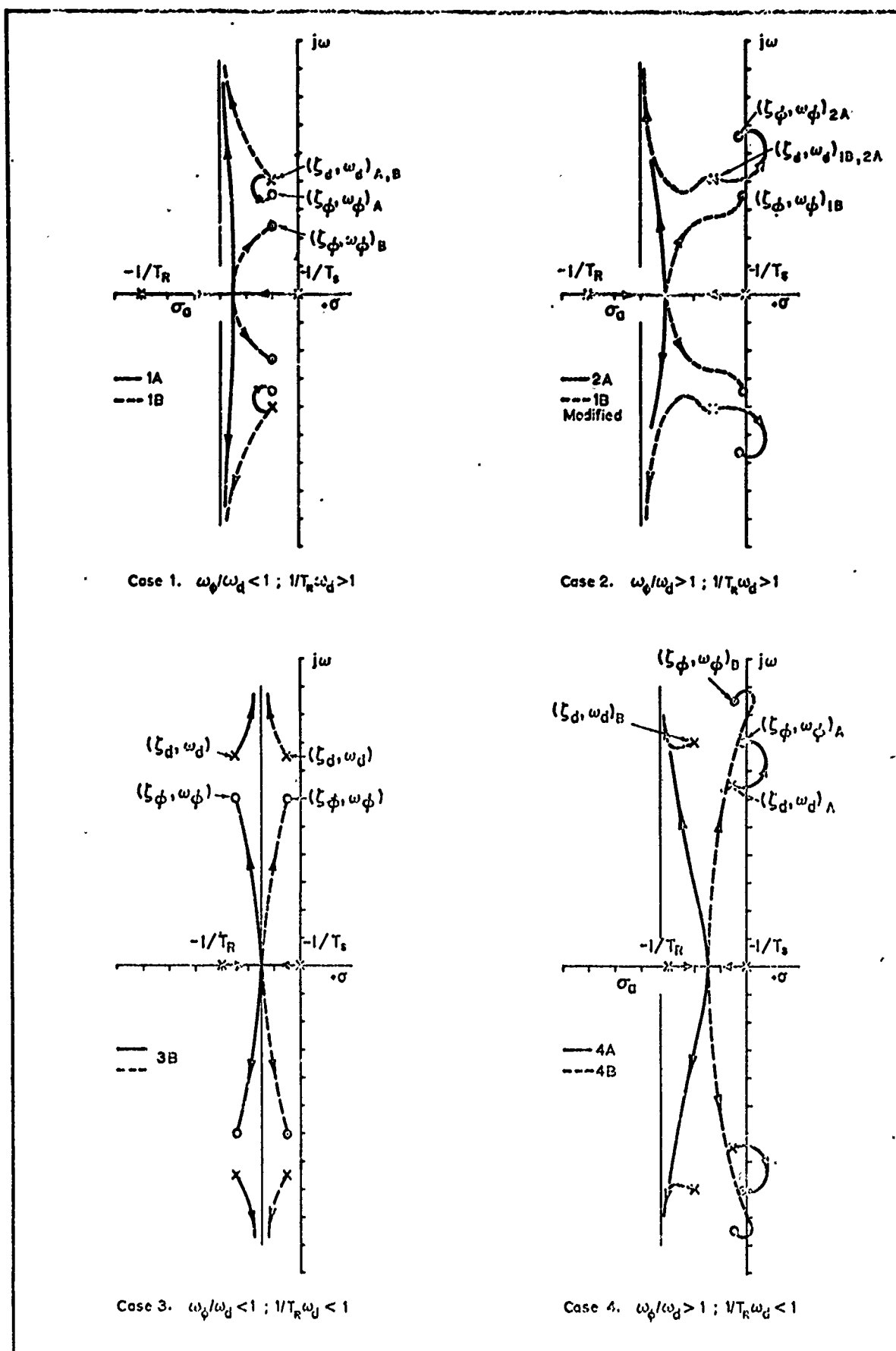


Fig. 8-4. Root Loci of $K_{\phi\psi}/\delta_a$ for Roll Control System Cases

Of all the varied airframe forms considered in Figs. 8-3 and 8-4, a "preferred," or most desirable, condition will usually be Case 1A. This would be nearly ideal when $\zeta_{\phi} \omega_{\phi}$ is large enough to satisfy dutch roll damping requirements—for then the roll loop can be made high gain, and will have a response to commands which is essentially second-order in character.

In a practical control with actuator and sensor lags, the unstable conditions due to the phase dip cannot ordinarily be overcome by raising the gain to force the dutch roll poles into the ω_{ϕ} zeros. Instead, more elaborate means of compensation must be sought. These typically involve the use of the rudder either to provide damping for the dutch roll, or the use of a crossfeed from the aileron to alter the apparent aileron yawing moment characteristics. The analysis of this important example of a separate loop closure as a means of compensation is deferred until Chapter 12.

Roll Attitude Control with Deficient Roll Damping

In many practical situations a roll control system based on only roll angle feedback is inadequate from the standpoint of tightness of control in response to disturbances and commands. This deficiency can be traced back, fundamentally, to the fact that with pure roll attitude feedback the open-loop and closed-loop total effective dampings are the same. To improve this situation the order of the open-loop transfer function numerator must be made no less than one below that of the denominator. Then, when the quantity $1+G$ is formed and divided through by the coefficient of the highest order s term, the second highest order s term (which represents the total system damping or the sum of all the roots) will be a function of open-loop gain. The damping factors of the various closed-loop modes can then be considerably increased, with attendant reduction in response time and increase in system tightness.

To accomplish this increase in relative numerator/denominator order in the $\phi \rightarrow \delta_a$ roll control system, the controller transfer function is changed from K_{ϕ} to $K_{\phi}(1+T_{\phi}s)$. From the mechanization standpoint this introduction of lead equalization can be obtained in several ways, all

adding lags at high frequency. These lags will be ignored here because they are no more important to the discussion at hand than sensor or servo lags. Also, the lead can be introduced in either the feedback or forward loops, although it is usually inserted in the feedback path. In this way the closed-loop system characteristics at high gain can be made to approach $\phi/\phi_c \doteq 1/(T_\phi s + 1)$. To the extent that high gain can be maintained throughout the flight regime, this provides constant closed-loop system dynamics in response to commands. Although such considerations are important in connection with ϕ_c inputs, the major interest in what follows is on the effective vehicle dynamics which are independent of input, i.e., on the closed-loop modes defined by $1 + G(s) = 0$.

In most respects the significant changes in lateral characteristics due to the addition of lead in the controller, i.e.,

$$\delta_a = (K_\phi s + K_\phi) \phi_c = K_\phi (s + 1/T_\phi) \phi_c$$

can be treated using the three-degree-of-freedom spiral/roll-subsidence approximation. The open-loop transfer function will then be

$$G = \frac{K_\phi L_{\phi a} \left(\frac{\omega_\phi}{\sigma_1} \right)^2 \left(s + \frac{1}{T_\phi} \right)}{\left(s + \frac{1}{T_s} \right) \left(s + \frac{1}{T_R} \right)} \quad (8-14)$$

Since the roll subsidence is always greater than the spiral root, the simplified system characteristics will be strongly dependent on the relative location of $1/T_\phi$ and $1/T_R$. The two possible cases (excluding the trivial one when $1/T_\phi = 1/T_R$) are shown in Figs. 8-5 and 8-6. When $1/T_\phi > 1/T_R$ (Fig. 8-5) the low gain closed-loop roots are similar to those for the simple roll case (which is a limiting condition corresponding to $1/T_\phi \rightarrow \infty$). With an increase in gain the modified spiral and roll subsidence approach one another until the zero db line reaches the break-away point, ω_{ba1} . At higher gains the roots become complex. At still higher gains the presence of $1/T_\phi$ becomes a more emphatic factor in the character of the system. For the zero db line at the rendezvous point, ω_{ba2} , or lower (higher gains), the two oscillatory roots have returned to

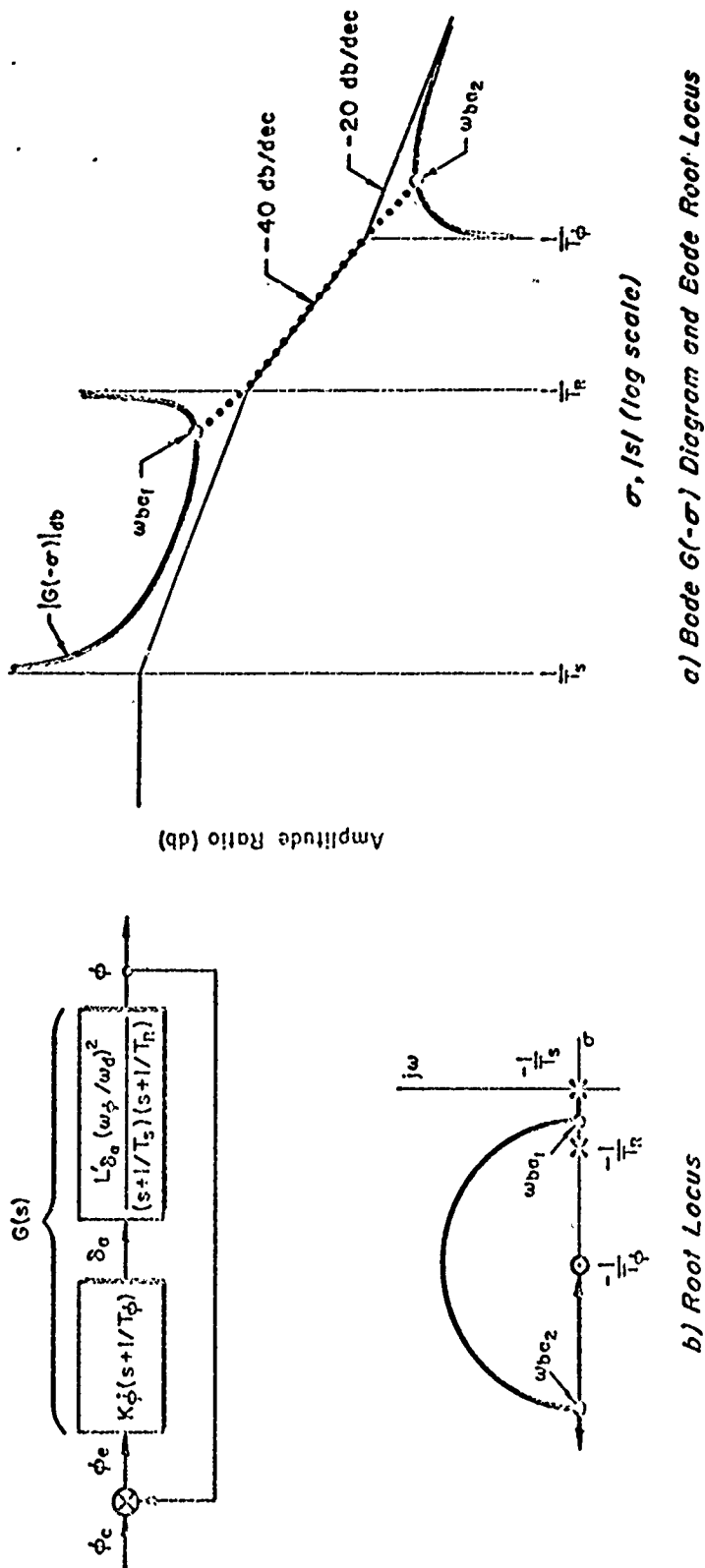


Fig. 8-5. System Survey of Roll Attitude and Roll Rate ($\phi, \dot{\phi} \rightarrow \delta_a$) Control System for $1/T_s < 1/T_R < 1/T_\phi$

the real axis—one goes into $(-1/T_\phi)$, while the other increases (negatively) with increased gain. The complex branch from ω_{ba1} to ω_{ba2} is, of course, a perfect circle centered at $-1/T_\phi$ on the conventional root locus.

In Fig. 8-6 the presence of the zero, $-1/T_\phi$, between the $-1/T_s$ and $-1/T_R$ poles leads to a system which exhibits considerable differences from the $\phi \rightarrow \delta_a$ case. The behavior of the closed-loop roots as gain is increased is straightforward—the modified spiral goes to the lead term, $1/T_\phi$, and the modified roll subsidence approaches the high frequency asymptote.

Different as the plots of Figs. 8-5 and 8-6 appear, they indicate very similar system behavior at low values of gain. At very high gains the results shown are also similar. Only at intermediate gains is the behavior of the two basically different.

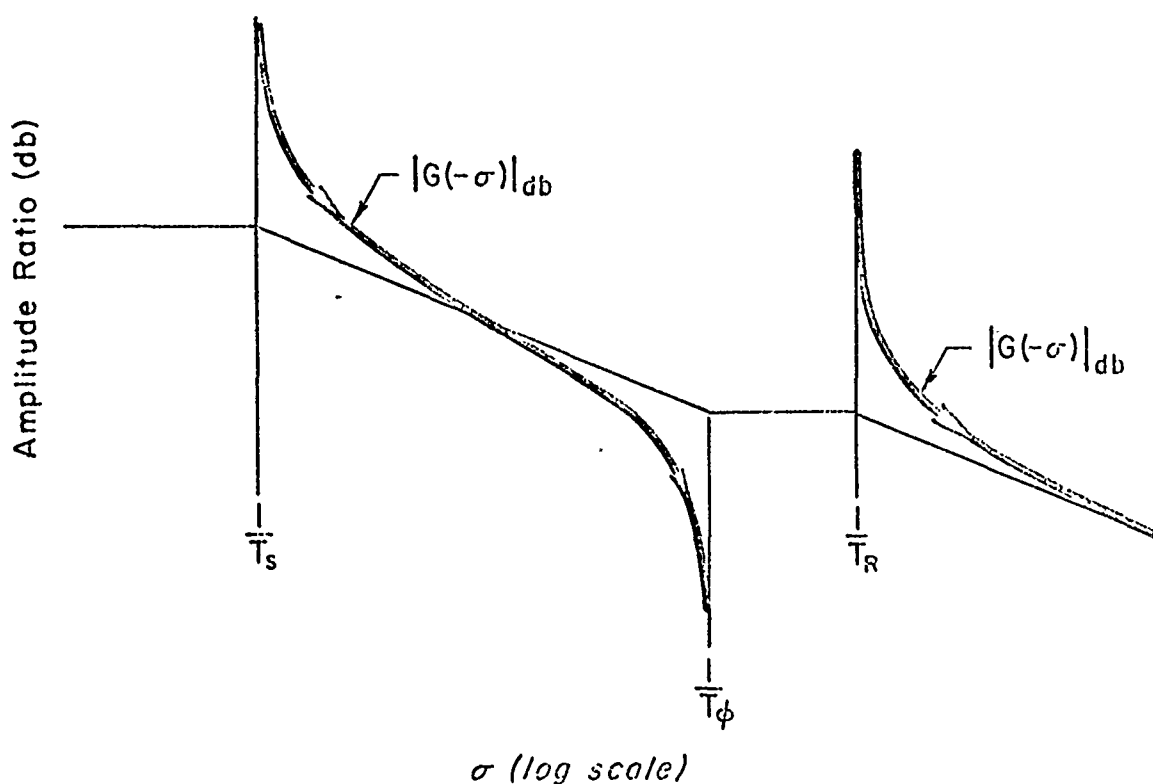


Fig. 8-6. Bode $G(-\sigma)$ Diagram of Roll Attitude and Roll Rate $(\phi, \dot{\phi} \rightarrow \delta_a)$ Control System for $1/T_s < 1/T_\phi < 1/T_R$

Roll Velocity Feedback (Roll Damper)

One of the simplest stability augmentation systems imaginable is the feedback of rolling velocity to aileron ($p \rightarrow \delta_a$). This system is seldom used as a command controller, i.e., there is no p_c command. Instead, its function is to augment the roll damping derivative L_p' . This may be desirable for one or more of several reasons. One was discussed in the last article, where the $\dot{\phi} \rightarrow \delta_a$ component of the $\phi, \dot{\phi} \rightarrow \delta_a$ system was used to improve the response of a roll command system. Other reasons will be described below, using the equivalent stability derivative approach and approximate factors.

When the aileron deflection is made proportional to rolling velocity, i.e.,

$$\delta_a = -K_p p \quad (8-15)$$

the effect on the roots of the closed-loop system is the same as those which would be caused by changing the stability derivative L_p' to $L_{p_{aug}}'$, where

$$L_{p_{aug}}' = L_p' - K_p L_{\delta_a}' \quad (8-16)$$

if $Y_{\delta_a}^*$ and N_{δ_a}' are neglected. The direct effect of this action is to increase the roll subsidence break frequency, expressed by the approximate factor

$$\frac{1}{T_R'} = -L_{p_{aug}}' + \frac{I_B'}{N_{\beta}'} \left(N_p' - \frac{g}{U_0} \right) \quad (8-17)$$

This may be desirable to improve the handling qualities in manual control or, as treated above, to allow a tighter roll attitude loop closure in automatic control.

An increase in $1/T_R'$ can also improve the aircraft response to rolling gusts. For instance, using the simplified airplane equations with $1/T_S = 0$, the rolling response to a rolling velocity gust, p_g , will be described approximately by the transfer function

$$\frac{\varphi}{p_g} \doteq \frac{-\left(I_p' - \frac{I_{\beta} N_p'}{N_{\beta}'}\right)}{s\left(s + \frac{1}{T_R}\right)} \quad (8-18)$$

In this relationship the low frequency gain is changed from approximately unity ($-I_p' T_R$) for the airplane-alone condition to $L_p'/L_{p_{aug}}'$ with augmentation.

Both the ratio of rolling and sideslipping amplitudes in the dutch roll mode and the roll response to a β_g gust input are measured by the ratio of φ and β modal response coefficients for the dutch roll mode. As developed in Chapter 6, this is given for the airplane-alone by the approximate expression

$$\left|\frac{\varphi}{\beta}\right|_d \doteq \left|\frac{L_{\beta}'}{N_{\beta}'}\right| \frac{1}{\sqrt{1 + I_p'^2/N_{\beta}'}} \quad (8-19)$$

if the dutch roll damping ratio is fairly small. Taking account of the augmentation by replacing L_p' with $L_{p_{aug}}'$ in Eq. 8-19 indicates that $|\varphi/\beta|_d$ can be reduced substantially by a roll damper if $|L_{p_{aug}}'|/\sqrt{N_{\beta}'} > 1$; otherwise the effect of augmentation on $|\varphi/\beta|_d$ will be minor.

Finally, the use of a roll damper to improve effective airframe numerator characteristics for outer loop equalization must not be overlooked, although it is beyond the scope of this chapter.

8.2 FEEDBACK OF OTHER QUANTITIES TO THE AILERONS

Bank angle and rolling velocity are the primary feedbacks in single-loop roll control systems. They are generally effective and are almost always present in automatic flight control systems. In addition to φ and/or p , other quantities have from time to time been used as feedbacks to the ailerons. The most common are lateral deviation and heading, as might be obtained from a localizer or other lateral guidance device and a directional gyro. Neither of these is generally suitable for direct feedback to the ailerons without extensive equalization. This is

normally supplied by virtue of inner attitude loops, so the feedback of these quantities, in practice, constitutes a multiple-loop situation and thus is a subject for Chapter 12.

Quantities other than bank angle and rolling velocity have been used occasionally in single-loop aileron control systems. These include feedbacks of yawing velocity ($r \rightarrow \delta_a$), sideslip ($\beta \rightarrow \delta_a$), and lateral acceleration ($a_y \rightarrow \delta_a$). On particular craft each of these has been made to serve some useful purpose, but their success has invariably been dependent on the existence of favorable vehicle characteristics which are by no means universally present. The favorable characteristics are exhibited in the transfer function numerators and, as already remarked in Chapter 6, such numerators as $N_{\delta_a}^r(s)$ are mavericks of the worse sort in that their basic characteristics differ not only between different aircraft, but even within a single vehicle at different flight regimes. Consequently, a thorough discussion of such single-loop feedbacks would have to cover a very large number of mostly unsuitable conditions. To avoid this we shall confine our attention here to the low gain behavior of such loops, thereby permitting us to use approximate factors and equivalent stability derivatives as the basis for the discussion. Most of the interesting features and deficiencies of β , r , and a_y feedbacks to aileron can be treated in this way in fairly general terms.

Feedback of Sideslip to the Ailerons

The feedback of sideslip angle to the ailerons modifies the stability derivatives L_β' and N_β' as follows:

$$\begin{aligned} L_{\beta_{aug}}' &= L_\beta' - K_\beta L_{\delta_a}' \\ N_{\beta_{aug}}' &= N_\beta' - K_\beta N_{\delta_a}' \end{aligned} \quad (8-20)$$

For most aircraft with reasonably large directional weathercock stability the principal effect will be on $L_{\beta_{aug}}'$, and in this sense the feedback of sideslip angle is analogous to changing the dihedral of the airplane. A very modest amount of this feedback is sufficient to stabilize an unstable spiral motion; that is, with K_β positive, the magnitude of $L_{\beta_{aug}}'$ can

easily be increased such that

$$I_{\beta_{avg}}' N_r' - I_x' N_{\beta}' > 0 \quad (8-21)$$

Unfortunately, at the same time this feedback may significantly decrease the damping of the dutch roll mode whenever $(N_p' - g/U_0)$ is negative, as shown by the approximate factor

$$2\zeta_d' \omega_d' \doteq -(\gamma_v + N_r') - \frac{I_{\beta_{avg}}'}{N_{\beta}'} \left(N_p' - \frac{g}{U_0} \right) \quad (8-22)$$

Sideslip-to-aileron feedbacks have also been proposed as a means to decrease the effective dihedral and thereby the dutch roll modal response ratio $|\psi/\beta|_d$. This requires a negative K_{β} , and all of the effects noted above are simply reversed. To achieve significant reduction in the effective $|I_{\beta}'|$ over a reasonable range of inputs, the gain, K_{β} , and the aileron authority must be fairly large. Further, the degree of spiral instability must be limited. This is automatically accomplished if the β/δ_a zeros are such that one of them is negative and slightly larger in magnitude than the spiral, thereby providing a zero for the spiral to approach. Unfortunately, this numerator has a basic dependence on such variable stability derivatives as N_{δ_a}' and $(N_p' - g/U_0)$, so the zero locations can shift drastically with flight condition. Other means to cope with the spiral exist, but most require additional feedbacks and so are beyond our present scope.

We can conclude from the above that $\beta \rightarrow \delta_a$ systems can provide some good features, but that these are usually accompanied by deleterious side effects. The disadvantages often outweigh the advantages, so such systems are seldom used except in the most special of circumstances.

Feedback of Side Acceleration to the Ailerons

The feedback of side acceleration, $a_{y_{c.g.}}$, to the ailerons is often practically equivalent to the feedback of side velocity. This follows from the relation

$$a_{y_{c.g.}} = Y_{\delta_a} \delta_a + Y_{\delta_r} \delta_r + Y_p p + Y_r r + Y_v v \quad (8-23)$$

where the terms Y_{δ_a} , Y_p , and Y_r are negligible so that

$$a_{y_{c.g.}} \doteq Y_{\delta_r} \delta_r + Y_v v \quad (8-24)$$

Then, overlooking for the moment the possible effect of rudder deflections, there remains only the very much simplified formula

$$v = \frac{a_{y_{c.g.}}}{Y_v} \quad (8-25)$$

Consequently, as a single-loop control the lateral accelerometer will share most of the characteristics of $\beta = v/U_0 \rightarrow \delta_a$ systems. (Similar to the correspondence between a_z and α in the longitudinal control.)

In some automatic pilots the connection between side acceleration and side velocity has been used as the basis for a coordination control in which the ailerons are driven so as to null a side acceleration signal. While this may seem contrary to the customary use of the rudder as the coordination control, it has been made to work as part of a multi-loop automatic flight control system on aircraft with characteristics favorable to this type of coordination device.

Feedback of Yawing Velocity to the Ailerons

An $r \rightarrow \delta_a$ feedback system corresponds to the alteration of the airplane stability derivative L_r' . This can be an effective means of stabilizing the spiral mode by making $L_{r_{aug}}'$ sufficiently negative (K_r positive) that

$$I_\beta N_{r_{aug}}' - L_{r_{aug}}' N_\beta' > 0 \quad (8-26)$$

If the aileron yaw is favorable (N_{δ_a}' positive), then this feedback will also tend to increase the magnitude of $N_{r_{aug}}'$. This will make the left side of the inequality still larger and will incidentally improve the dutch roll damping. On the other hand, for the more common adverse yaw (N_{δ_a}' negative) the $r \rightarrow \delta_a$ system gain cannot be made very large without making the modified dutch roll oscillation unstable.

There have been some proposed automatic pilot configurations which used the properties $r \rightarrow \delta_a$ feedback to advantage. These are especially effective when a tilted rate gyro can be satisfactorily employed. This will sense a combination of rolling and yawing velocity, and when this signal is used to actuate the ailerons the damping in roll and spiral stability are simultaneously improved. For more detailed studies of this type of system the airplane lateral-velocity-to-aileron transfer function, ω/δ_a , should be used. In fact, this is generally necessary in practice, for the angular velocity is sensed by a rate gyro which is fixed to the vehicle. Because the gyro input axis does not vary with flight condition, while the vehicle's stability axes do, the lateral angular velocity sensed will not always coincide with yawing velocity.

8.3 FEEDBACK OF HEADING ANGLE TO THE RUDDER

The earliest automatic pilots employed a feedback of heading angle to the rudder as a means of steering the airplane. For small perturbations about straight, level, and horizontal flight the appropriate transfer function for the study of this as an elementary feedback control system is

$$\frac{\psi(s)}{\delta_r(s)} = \frac{N_{\delta_r}^r}{s\Delta_{lat}} = \frac{A_r \left(s + \frac{1}{T_r} \right) \left[s^2 + 2\zeta_r \omega_r s + \omega_r^2 \right]}{s \left(s + \frac{1}{T_s} \right) \left(s + \frac{1}{T_R} \right) \left[s^2 + 2\zeta_d \omega_d s + \omega_d^2 \right]} \quad (8-27)$$

Figure 8-7 presents a system survey of this system for a typical case. This survey indicates that the feedback of heading to rudder stabilizes the divergent spiral motion by forcing it to combine with the pole at the origin. At a comparatively high value of the feedback gain the resulting low frequency oscillation is made stable, while at the same time the damping of the dutch roll mode is only slightly altered. Consequently, this type of system can be a very satisfactory directional stabilizer for aircraft with heavy dutch roll damping.

In the absence of actuator lags there is no danger of instability at high frequencies, although the dutch roll undamped natural frequency becomes much greater as the feedback gain is increased. However, for the

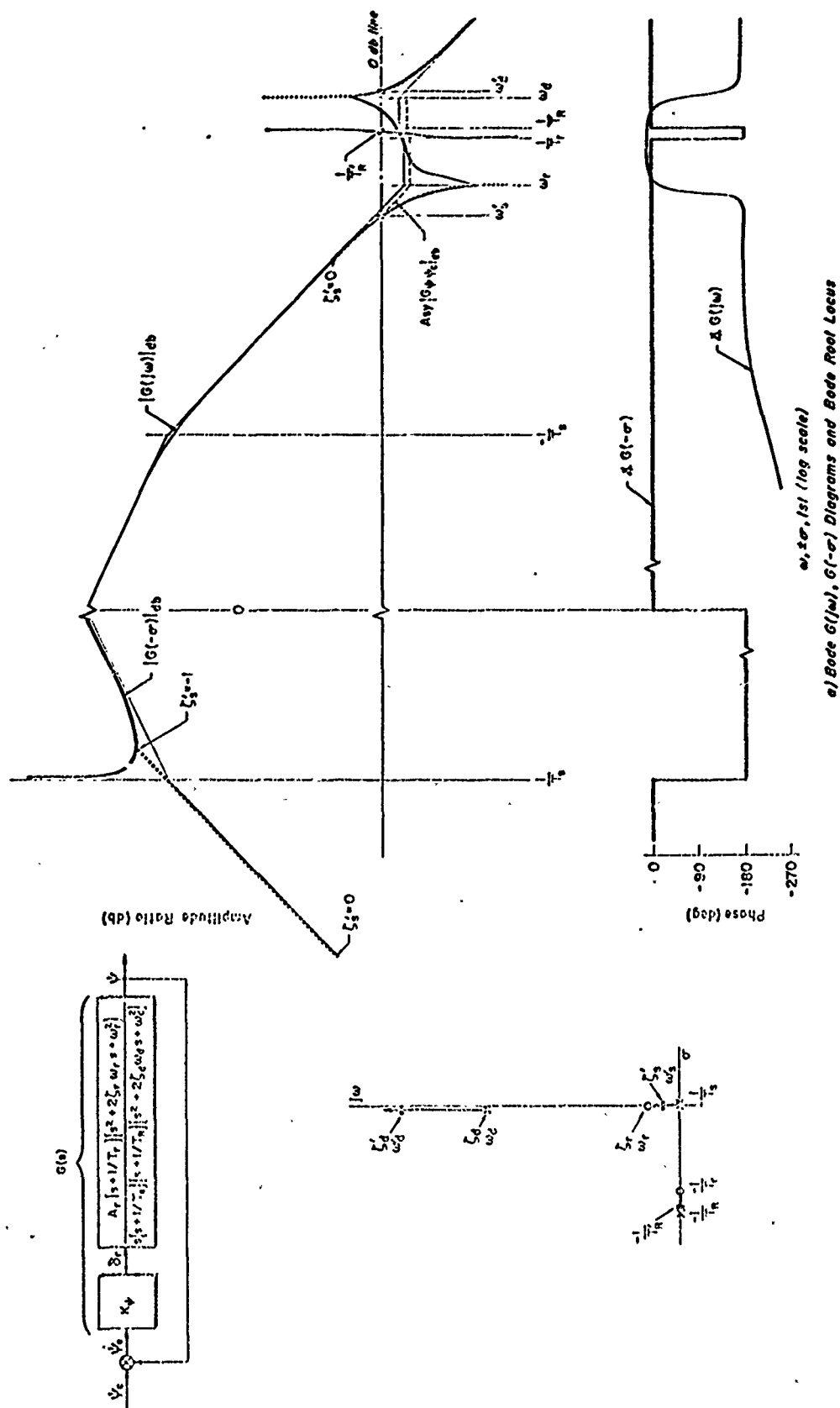


Fig. 8-7. System Survey of Yaw Attitude ($\psi \rightarrow \delta r$) Control System

typical location shown for the complex zeros of the transfer function, the dominant closed-loop heading mode (ζ'_s, ω'_s) can never become very satisfactorily damped because the ζ_r, ω_r zeros are themselves rather close to the imaginary axis. In fact, it is not at all uncommon for these zeros to be in the right half plane during some phase of flight. (This will be treated in more detail in the discussion of the $r \rightarrow \delta_r$ system given below.) To avoid the light or negative closed-loop damping accompanying a high gain closure, the gain is generally made fairly low. The closed-loop bandwidth of the system is, therefore, also bound to remain low. Some improvement in these deficiencies can be obtained by a combination of bank angle and heading angle feedback to the rudder, and a tilted directional gyroscope can provide a suitable signal. The first British automatic pilot was mechanized in this way.*

8.4 FEEDBACK OF YAWING VELOCITY TO THE RUDDER

In a number of modern airplane automatic pilots the rudder axis, instead of being slaved to a direction-sensing instrument, is actuated by a rate gyro which senses yawing velocity. This is particularly valuable in those aircraft which need dutch roll damping augmentation. Assuming that the yawing velocity sensor's input axis coincides approximately with the aircraft's stability axes,[†] the transfer function relating yaw rate to rudder has the same numerator and denominator factors as that given in Eq. 8-27 relating heading to rudder deflection, except for the free s , i.e.,

$$\frac{r(s)}{\delta_r(s)} = \frac{N_{\delta_r}^r}{\Delta_{lat}} = \frac{A_r \left(s + \frac{1}{T_r} \right) [s^2 + 2\zeta_r \omega_r s + \omega_r^2]}{\left(s + \frac{1}{T_s} \right) \left(s + \frac{1}{T_R} \right) [s^2 + 2\zeta_d \omega_d s + \omega_d^2]} \quad (8-28)$$

*F. W. Meredith and P. A. Cooke, "Aeroplane Stability and the Automatic Pilot," J. Royal Aeron. Society, Vol. XLI, No. 318, June 1937, pp. 415-436.

[†]In practice the ω/δ_r transfer function should be used to take into account sensor tilt angles which invariably exist. Alternatively, the transformation between instrument axes and body-fixed axes can be treated as a multiloop problem in which both r and p are fed back.

Spiral and Dutch Roll Stabilization with $\omega_r/\omega_\phi \ll 1$

Figure 8-8 presents the system analysis for an $r \rightarrow \delta_r$ feedback around the transfer function of Eq. 8-28. The aircraft characteristics are typical for a high-aspect-ratio straight wing aircraft at cruising speed and altitude.

The particular dynamics of this airplane and flight condition illustrate the powerful effect of yaw rate feedback on the lateral motions of the airplane. At a very low value of the feedback gain the spiral divergence is made stable, and at higher gains the very weakly damped dutch roll motion is made heavily damped. In fact, as the figure shows, in this idealized system it is not difficult to provide nearly critical damping for the closed-loop dutch roll roots. If $1/T_r$ and $1/T_R$ were somewhat closer together, as commonly occurs, all the roots could be made negative and real.

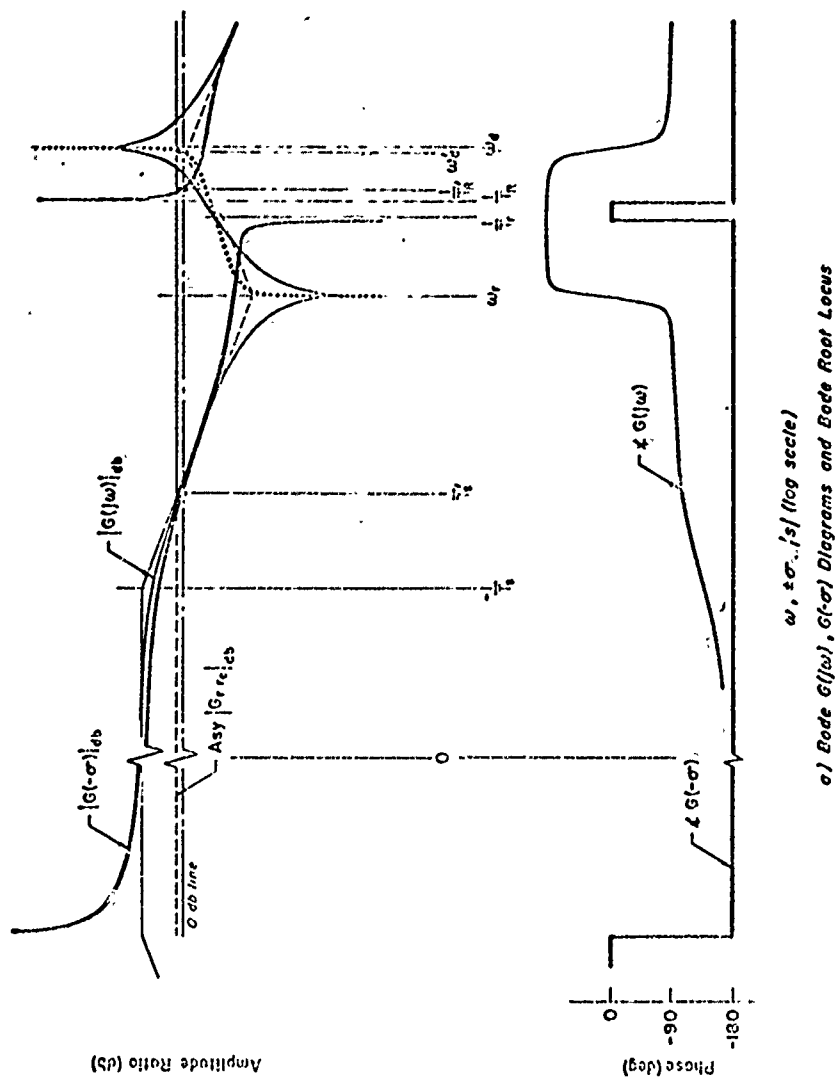
Washed-Out Yawing Velocity to the Rudder

In turning flight a straight-through feedback opposes the turn, requiring an increment of rudder or aileron into the turn to compensate for the action of the feedback system. Any necessity for supplying this increment of control has been found to be unacceptable on highly maneuverable craft. A "washout" is therefore usually installed in the feedback loop. This device has the property of having no output at d.c. so that the feedback no longer opposes a steady turn. (In some so-called single-axis automatic pilots which consist of a yaw rate feedback to the rudder, it is precisely the fact that they do oppose the almost steady turn of a developing spiral instability which is considered valuable. These devices are designed, therefore, without the washout feature.)

The transfer function of a washout has the form

$$\frac{e_o(s)}{e_i(s)} = \frac{s}{s + \frac{1}{T_{WO}}} \quad (8-29)$$

and the step function response of a washout is shown in Fig. 8-9. The



a) Bode $G(j\omega)$, $G(\sigma)$ Diagrams and Bode Root Locus

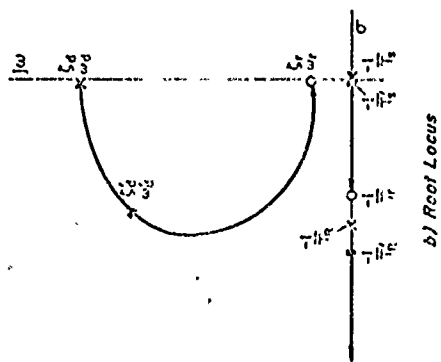
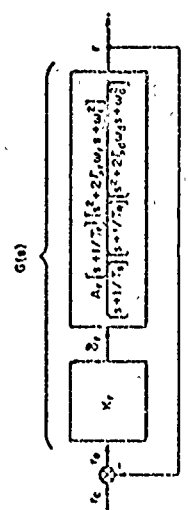


Fig. 8-8. System Survey of Van Rate ($r \rightarrow \delta_r$) Control System

device gets its name from the fact that the step function response decays or is washed out.

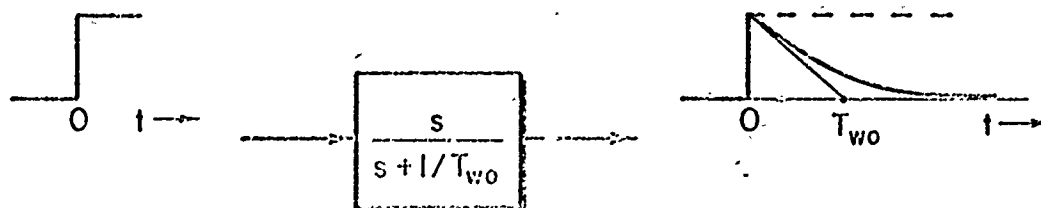


Fig. 8-9. Step Function Response of a Washout

A system survey of the washed-out yaw-rate-to-rudder system is shown in Fig. 8-10. To minimize the opposition of steady turns it is desirable to choose the inverse washout time constant, $1/T_{wo}$, as large as can be without detracting too much from the dutch roll damping. There is a direct tradeoff between these two desires in that the larger the inverse washout time constant becomes, the smaller will be the maximum obtainable value of the damping ratio of the modified dutch roll mode. This fact is illustrated by the sensitivity vectors on the root loci of the system survey shown in Fig. 8-11, which also serves as the basis of discussion in the next article.

Spiral and Dutch Roll Stabilization with Large ω_r

A less favorable configuration of the open-loop poles and zeros than those illustrated in Figs. 8-8 and 8-10 is easily possible. This is illustrated in Fig. 8-11, which is drawn for the dynamics of a jet interceptor operating at high lift coefficient. In this case the quadratic zeros (ζ_r , ω_r) are much closer to the dutch roll poles and the feedback of yaw rate to the rudder is of strictly limited effectiveness in damping the dutch roll. Further, the sensitivity vector S_{ω_r} clearly indicates that still closer ω_r , ω_1 spacings will be even more undesirable.

Although the $N_{\delta_r}^r$ numerator is another maverick, it is instructive to consider two limiting cases. These are:

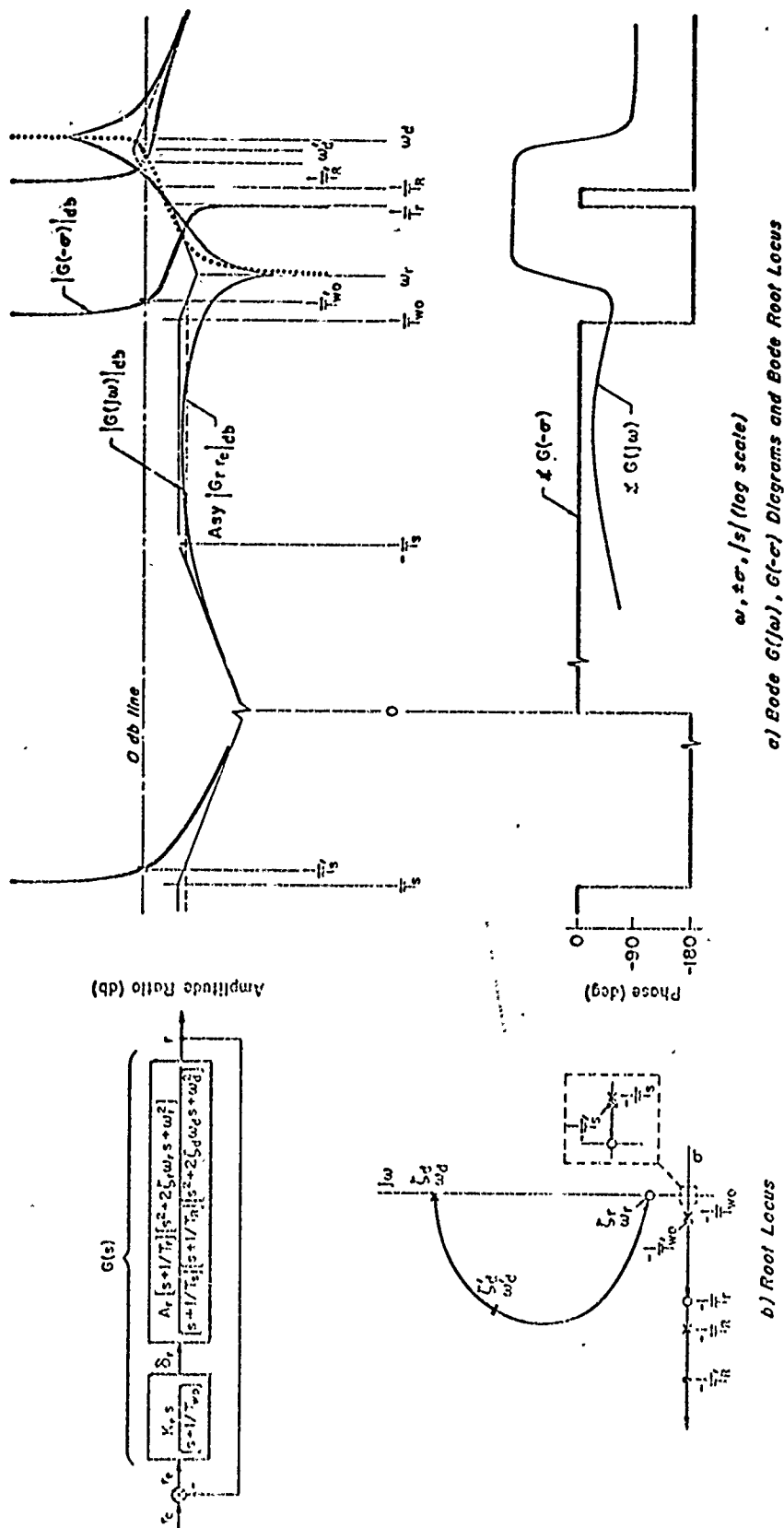


Fig. 8-10. System Survey of "Washed-Out" Yaw Rate ($r \rightarrow \delta_r$) Control System for Aircraft with Small ω_r/ω_d

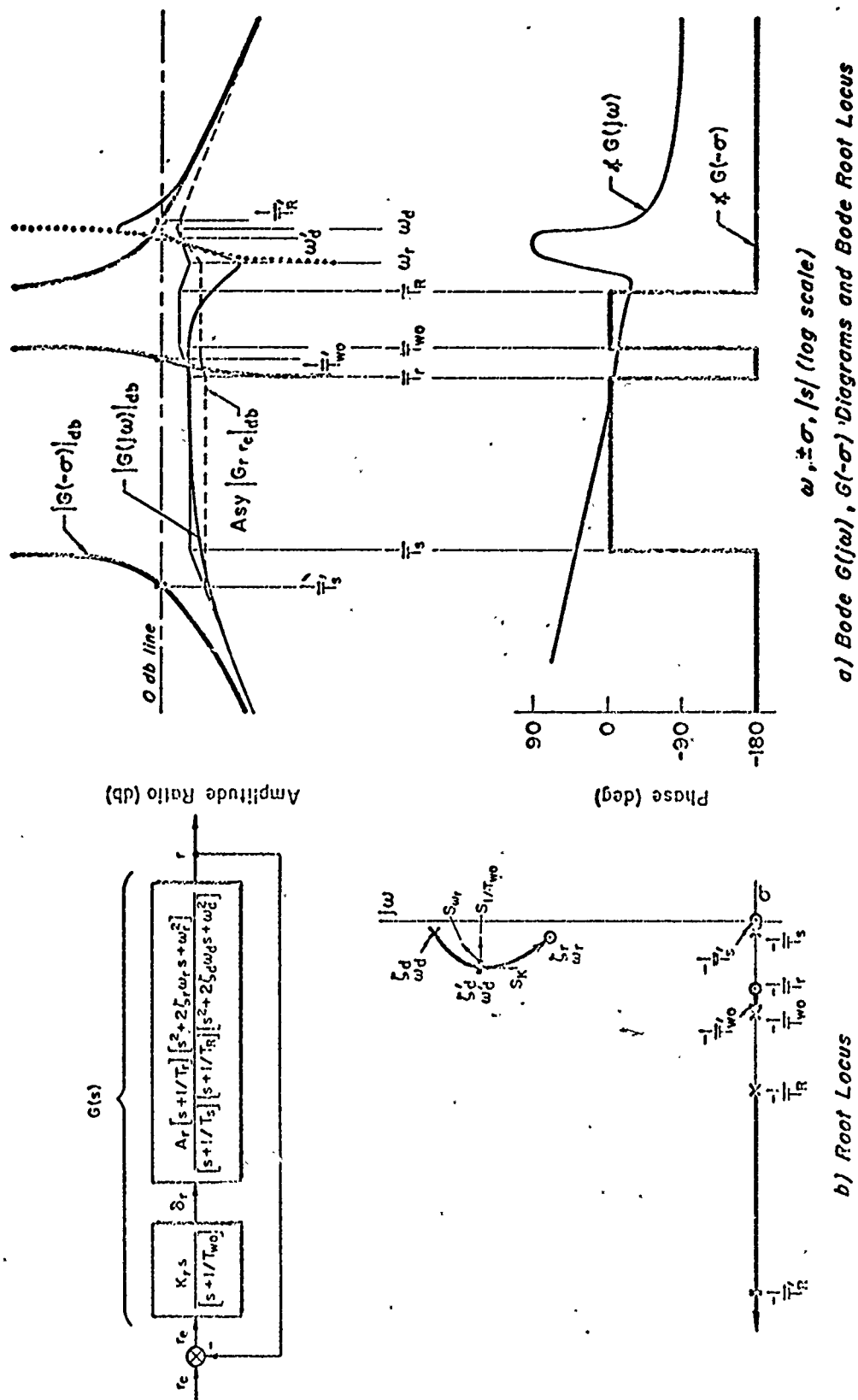


Fig. 8-11. System Survey of "Washed-Out" Yaw Rate ($r \rightarrow \delta_r$) Control System for Aircraft with Large ω_r/ω_d

Dihedral effect dominant $|(g/U_0)I_p'| \gg |L_p'^3|$

$$\frac{1}{T_r} \doteq \omega_r \doteq \left(-\frac{g}{U_0} I_p' \right)^{1/3} \quad (8-30)$$

$$2\zeta_r \omega_r \doteq -(Y_v + L_p') - \left(-\frac{g}{U_0} I_p' \right)^{1/3}$$

Roll damping dominant $\left| \frac{gI_p'}{U_0 L_p'^3} + \frac{Y_{\delta_r} N_{\beta}'}{U_0 N_{\delta_r}' L_p'} \right| \ll 1$

$$\frac{1}{T_r} \doteq -L_p'$$

$$\omega_r^2 \doteq \frac{g}{U_0} \frac{L_p'}{L_p'} \quad (8-31)$$

$$2\zeta_r \omega_r \doteq -\left(Y_v - \frac{Y_{\delta_r} N_{\beta}'}{U_0 N_{\delta_r}'} - \frac{g}{U_0} \frac{L_p'}{L_p'^2} \right)$$

Presuming that L_p' is negative, $2\zeta_r \omega_r$ can easily become negative for either case. Thus, the complex zeros are not only typically lightly damped, but are likely to be disadvantageously located in the right half plane. This can happen for all the systems illustrated in Figs. 8-8, 8-10, and 8-11.

The difficulties in improving the dutch roll damping occasioned by ω_r approaching ω_d can be alleviated by increasing L_p' . This is obvious in Eq. 8-31, but not at all apparent for Eq. 8-30. The secret there is that a sufficient increase in L_p causes the inequality $|(g/U_0)I_p'| \gg |L_p'^3|$ to be violated so that the approximate factors no longer apply and are replaced by the second set. The actual decrease of ω_r/ω_d is ordinarily accomplished with the aid of a roll damper.

Nature of Gain Adjustment for Dutch Roll Damping Augmentation

Just as with the other systems considered, the nature of appropriate gain adjustments with flight environmental parameters for the yaw damper depends on the desired closed-loop characteristics. If dutch roll damping is to be constant, then

$$K_R N'_{\delta_R} \doteq -N'_{r_{aug}} \doteq \text{constant} \quad (8-32)$$

or

$$K_R \propto \frac{1}{N'_{\delta_R}} \propto \frac{1}{\rho U_0^2} \quad (8-33)$$

On the other hand, if the closed-loop dutch roll damping ratio is to be nearly invariant, then the desired relationship will be

$$\zeta_d' \doteq \frac{-N'_{r_{aug}}}{2\sqrt{N'_\beta}} \doteq \frac{K_R N'_{\delta_R}}{2\sqrt{N'_\beta}} \doteq \text{constant} \quad (8-34)$$

This implies that the variation of gain with flight parameters should be

$$K_R \propto \frac{\sqrt{N'_\beta}}{N'_{\delta_R}} \propto \frac{1}{\rho^{1/2} U_0} \quad (8-35)$$

Again, as with all the gain compensation considerations discussed in this and the previous chapter, the actual nature of the compensation will depend on the specifics of vehicle dynamics, closed-loop dynamic performance envelope specifications, functional mechanization of the gain-changing devices, etc.

8.5 FEEDBACK OF SIDESLIP TO THE RUDDER

The feedback of sideslip angle or sideslipping velocity to the rudder is practically equivalent to the augmentation of the directional stability derivative N'_β (or N'_v). It serves in a very useful way to minimize the sideslip angle (uncoordination).

The transfer function which relates sideslip angle to rudder deflection has the form

$$\frac{\beta(s)}{\delta_R(s)} = \frac{N_{\delta_R}^v}{U_0 \Delta_{lat}} = \frac{A_\beta \left(s + \frac{1}{T_{\beta 1}}\right) \left(s + \frac{1}{T_{\beta 2}}\right) \left(s + \frac{1}{T_{\beta 3}}\right)}{\left(s + \frac{1}{T_s}\right) \left(s + \frac{1}{T_R}\right) [s^2 + 2\zeta_d \omega_d s + \omega_d^2]} \quad (8-36)$$

Figure 8-12 shows the system survey for negative feedback of the $\beta \rightarrow \delta_r$ system. This has the effect of destabilizing the aperiodic spiral motion and of moving the dutch roll roots to a higher frequency. This, of course, is the result expected of an increase in directional stability.

To improve the dutch roll damping, a $\dot{\beta}$ component can be added to the controller, i.e.,

$$\begin{aligned}\delta_r &= -(K_\beta \beta + K_{\dot{\beta}} s \beta) \\ &= -K_{\dot{\beta}} \left(s + \frac{1}{T_F} \right) \beta\end{aligned}\tag{8-37}$$

A survey of this system is given in Fig. 8-13. As indicated, this type of system has excellent characteristics as a single-loop control for the improvement of the dutch roll and the minimization of sideslip. Appropriate gain adjustments with flight environmental parameters are not extreme, being similar to those for $\alpha \rightarrow \delta_e$ systems. The system is also an excellent inner loop for roll attitude and other outer loop controllers. Its primary deficiency is a practical one in instrumenting an adequate sideslip sensor. This is, to some extent, alleviated by the possibility of a lateral acceleration system.

8.6 FEEDBACK OF LATERAL ACCELERATION TO THE RUDDER

Some of the favorable features of $\beta \rightarrow \delta_r$ or $\beta, \dot{\beta} \rightarrow \delta_r$ systems can be obtained by substituting a properly located lateral accelerometer for the sideslip sensor. The similarity between the two systems can be seen conceptually from the side acceleration equation and the expression for side acceleration at a general location, viz:

$$a_{y_{c.g.}} = Y_v v + Y_{\delta_r} \delta_r \tag{8-38}$$

$$\begin{aligned}a_y &= a_{y_{c.g.}} + x_a \dot{r} \\ &= Y_v v + Y_{\delta_r} \delta_r + x_a \dot{r}\end{aligned}\tag{8-39}$$

These equations are the lateral analogs to the longitudinal a_z discussed

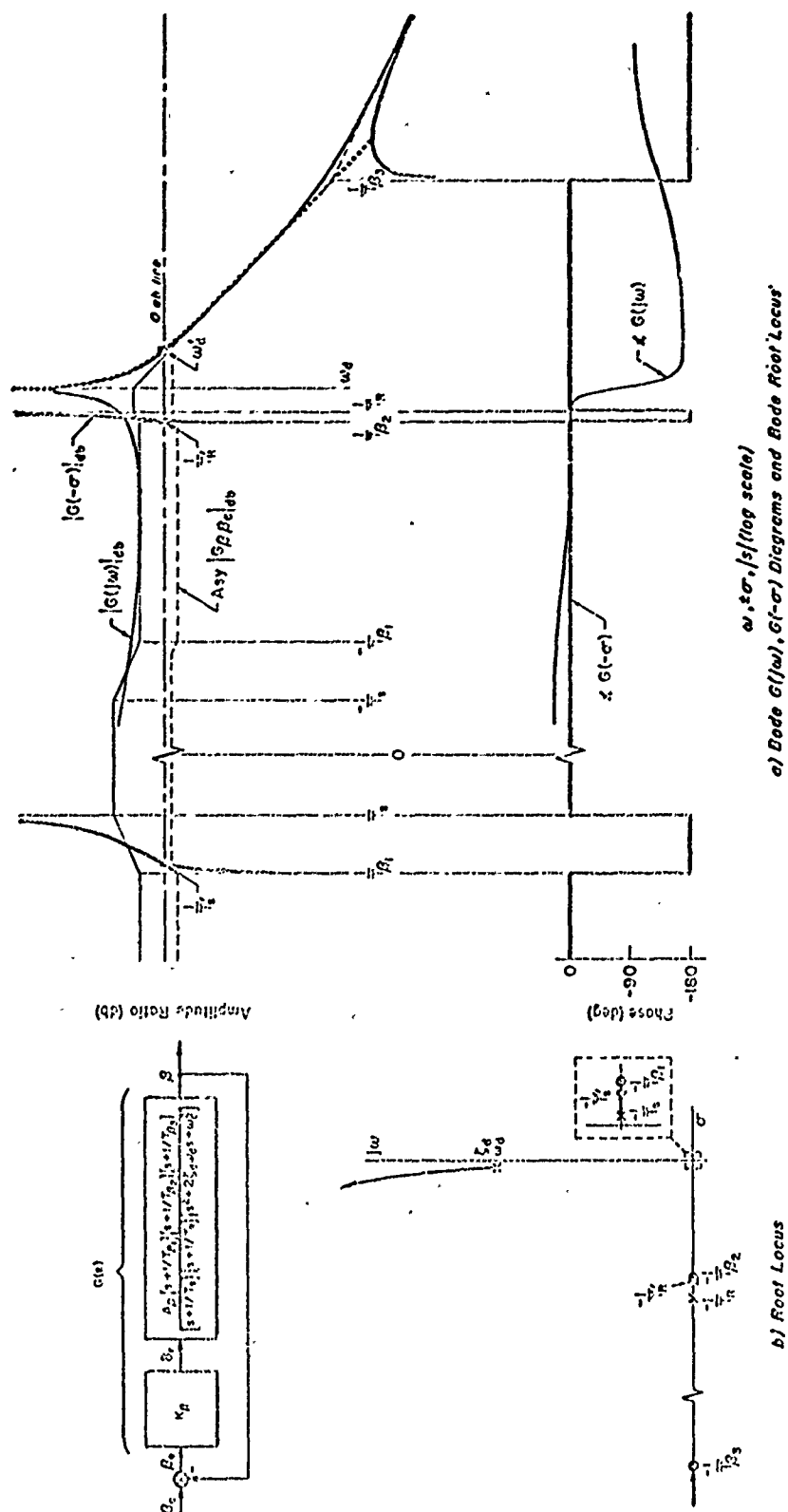
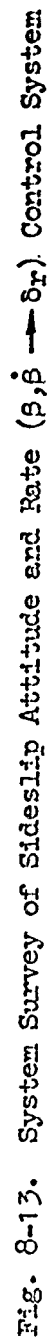


Fig. 8-12. System Survey of Sideslip Attitude ($\beta \rightarrow \delta_r$) Control System



at length in Chapter 7, and the same kind of center of rotation and center of percussion relationships apply. In this case the center of rotation corresponds to that accelerometer location distance, x_a , for which the $x_a \dot{r}$ component will tend to offset the $Y_{\delta_r} \delta_r$ component, thereby leaving Y_v (or Y_{β}) as the major part of the acceleration measured. The relationships can be developed in a fashion similar to the longitudinal case or, alternatively, directly by finding the instantaneous center of rotation. To do this, consider the initial yawing acceleration due to a rudder step input, δ_{r0}/s . This will be

$$\begin{aligned} \dot{r}(t) &= \lim_{t \rightarrow \infty} \left\{ s \left[\frac{r(s)}{\delta_r(s)} \right] \frac{\delta_{r0}}{s} \right\} \\ &= N'_{\delta_r} \delta_{r0} \end{aligned} \quad (8-40)$$

Consequently, if (Eq. 8-39)

$$Y_{\delta_r} \delta_{r0} + x_a N'_{\delta_r} \delta_{r0} = 0 \quad (8-41)$$

or

$$x_a = \frac{-Y_{\delta_r}}{N'_{\delta_r}}$$

the initial part of the lateral acceleration response to a step rudder input will be proportional to the sideslip response to the rudder deflection.

In terms of nondimensional derivatives the ideal x_a becomes

$$\begin{aligned} x_a &= \frac{-I_z}{mb} \frac{C_{y\delta_r}}{C_{n\delta_r}} \\ &= \frac{-k_z^2 C_{y\delta_r}}{b \left(\frac{-l\delta_r}{b} \right) C_{y\delta_r}} = \frac{k_z^2}{l\delta_r} \end{aligned} \quad (8-42)$$

The total acceleration numerator is given by

$$\begin{aligned}
 N_{\delta_r}^{ay} = & \left[Y_{\delta_r} + x_a \left(\frac{I_p^1}{I_p^1} \right) \right] s^4 + \left[-Y_{\delta_r} \left(\frac{I_p^1}{I_p^1} + \frac{I_p^1}{I_p^1} \right) + x_a \left(Y_{\delta_r} N_V^1 - N_{\delta_r}^1 Y_V + I_{\delta_r}^1 N_p^1 - N_{\delta_r}^1 I_p^1 \right) \right] s^3 \\
 & + \left[Y_{\delta_r} \left(\frac{I_p^1}{I_p^1} N_p^1 - \frac{I_p^1}{I_p^1} N_p^1 + I_p^1 \right) - N_{\delta_r}^1 Y_p + x_a \left(Y_{\delta_r} \frac{I_p^1}{I_p^1} N_p^1 - Y_{\delta_r} I_p^1 N_p^1 \right. \right. \\
 & \left. \left. - I_{\delta_r}^1 Y_V N_p^1 + N_{\delta_r}^1 Y_V I_p^1 \right) \right] s^2 \\
 & + \left[Y_{\delta_r} \left(\frac{I_p^1}{I_p^1} N_p^1 - \frac{I_p^1}{I_p^1} N_p^1 - I_V^1 \right) + N_{\delta_r}^1 Y_p I_p^1 - I_{\delta_r}^1 Y_p N_p^1 + I_{\delta_r}^1 Y_V \right. \\
 & \left. + x_a \left(I_{\delta_r}^1 N_V^1 - N_{\delta_r}^1 I_V^1 \right) \right] s \\
 & + g \left[Y_{\delta_r} \left(\frac{I_p^1}{I_p^1} N_p^1 - \frac{I_p^1}{I_p^1} N_p^1 \right) + N_{\delta_r}^1 Y_V I_p^1 - I_{\delta_r}^1 Y_V N_p^1 \right]
 \end{aligned}$$

From this it is seen that placing the accelerometer at the instantaneous center of rotation will make the leading coefficient zero, just as in the analogous longitudinal case. For the accelerometer at the instantaneous center of rotation, the numerator then becomes

$$N_{\delta_r}^{ay} = Y_{\delta_r} \left(-\frac{N_p^1}{I_p^1} + Y_V - \frac{Y_{\delta_r}}{N_{\delta_r}^1} \frac{N_V^1}{I_V^1} \right) \left(s + \frac{1}{T_{ay1}} \right) \left(s + \frac{1}{T_{ay2}} \right) \left(s + \frac{1}{T_{ay3}} \right) \quad (8-44)$$

The approximate factors for this numerator are (Table 6-4)

$$\frac{1}{T_{ay1}} = \frac{g}{U_0} \left[\frac{I_p^1}{I_p^1} - \frac{N_p^1}{I_p^1} \frac{\left(Y_V I_{\delta_r}^1 - Y_{\delta_r} I_V^1 \right)}{\left(Y_V N_{\delta_r}^1 - Y_{\delta_r} N_V^1 \right)} \right] \quad (8-45)$$

$$\frac{1}{T_{ay2}} = -I_p^1 \quad ; \quad \frac{1}{T_{ay3}} = \frac{-U_0 \left(Y_V N_{\delta_r}^1 - Y_{\delta_r} N_V^1 \right)}{Y_{\delta_r} \left(-\frac{N_p^1}{I_p^1} + Y_V - \frac{Y_{\delta_r}}{N_{\delta_r}^1} \frac{N_V^1}{I_V^1} \right)}$$

The sign of $1/T_{ayz}$ will generally depend only on the location of the rudder with respect to the c.g., and will be negative for aft and positive for forward locations. The breakpoint corresponding to $1/T_{ayz}$ provides a convenient upper limit of approximate correspondence between a_y and β . At frequencies below this the two are almost directly proportional, i.e.,

$$\frac{a_y}{\delta_r} \doteq Y_\beta \frac{\beta}{\delta_r} \quad , \quad |s| < \frac{1}{T_{ayz}} \quad (8-46)$$

Above this frequency the rudder deflection will destroy the correspondence between side acceleration and sideslip angle or sideslipping velocity.

Figures 8-14 and 8-15 show system surveys of $a_y \rightarrow \delta_r$ and $a_y, \dot{a}_y \rightarrow \delta_r$ control systems, respectively, for a situation where the accelerometer is near, but behind, the center of rotation. As expected, the dynamics of these systems are quite similar to those of the corresponding sideslip controllers illustrated in Figs. 8-12 and 8-13. A major difference, however, between these two general types of systems is not revealed explicitly in the system surveys. This is the matter of necessary gain variation to keep the closed-loop system dynamics within specified bounds. Again, the differences between the lateral a_y and β systems are similar to those between the longitudinal a_z and α controllers. In complete analogy to the latter systems, the controller gain, K_y , must vary as $1/\rho U_0^2$ if it is to simulate a constant-gain sideslip controller.

Although rudder control systems using $a_y, \dot{a}_y \rightarrow \delta_r$ are not as common as washed-out yaw dampers, they have been successful in past applications. This type of system is particularly advantageous for gun-firing aircraft where two-control (aileron and elevator) lead/pursuit maneuvers without sideslip are required, and on rocket-firing craft where sideslip minimization is desirable to simplify the fire control equipment design. It also shares the excellent properties of the $\beta, \dot{\beta} \rightarrow \delta_r$ system as an inner loop in more complex multiloop systems.

Early models of the B-52 bomber also depended on a side acceleration feedback to the rudder to damp the dutch roll, but the principle of operation of the damper was completely different from the one discussed

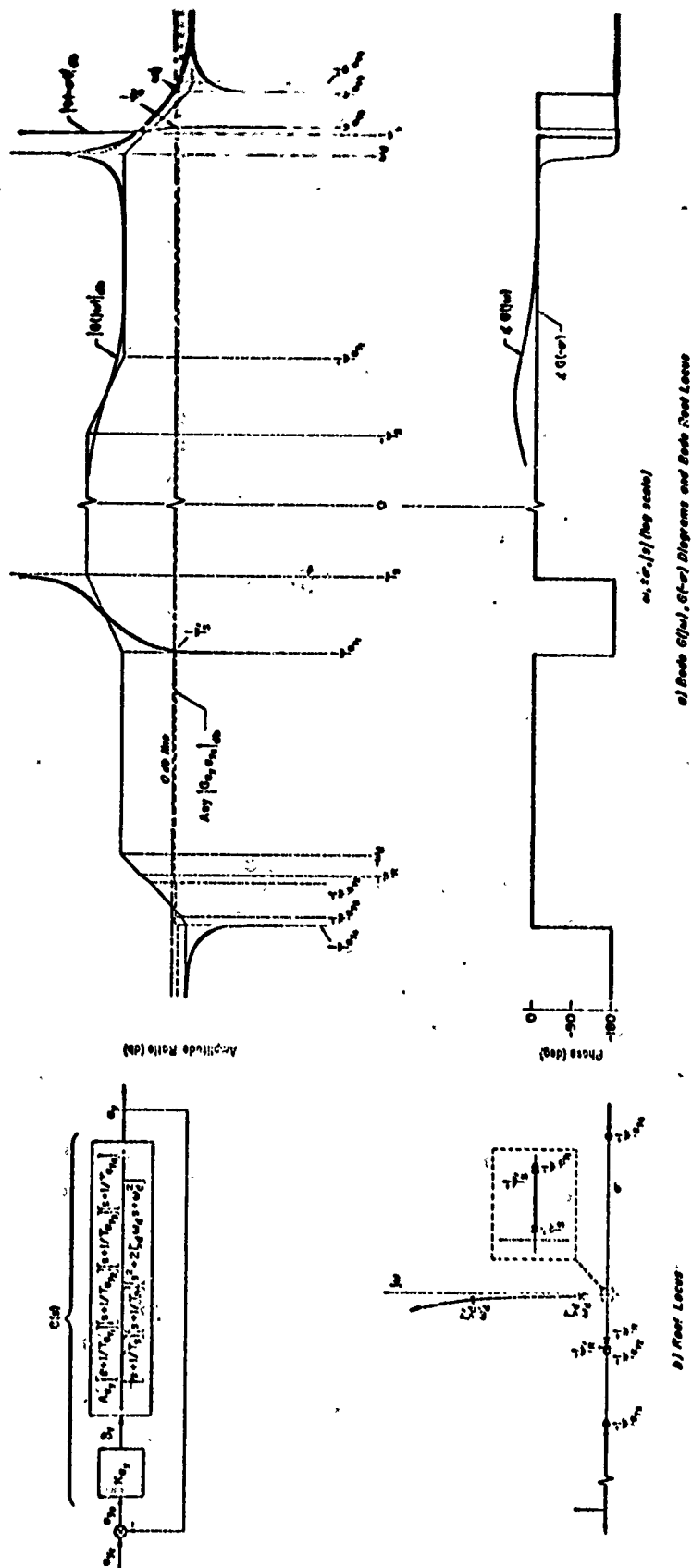


Fig. 8-14. System Survey of Side Acceleration ($a_y \rightarrow \delta r$) Control System

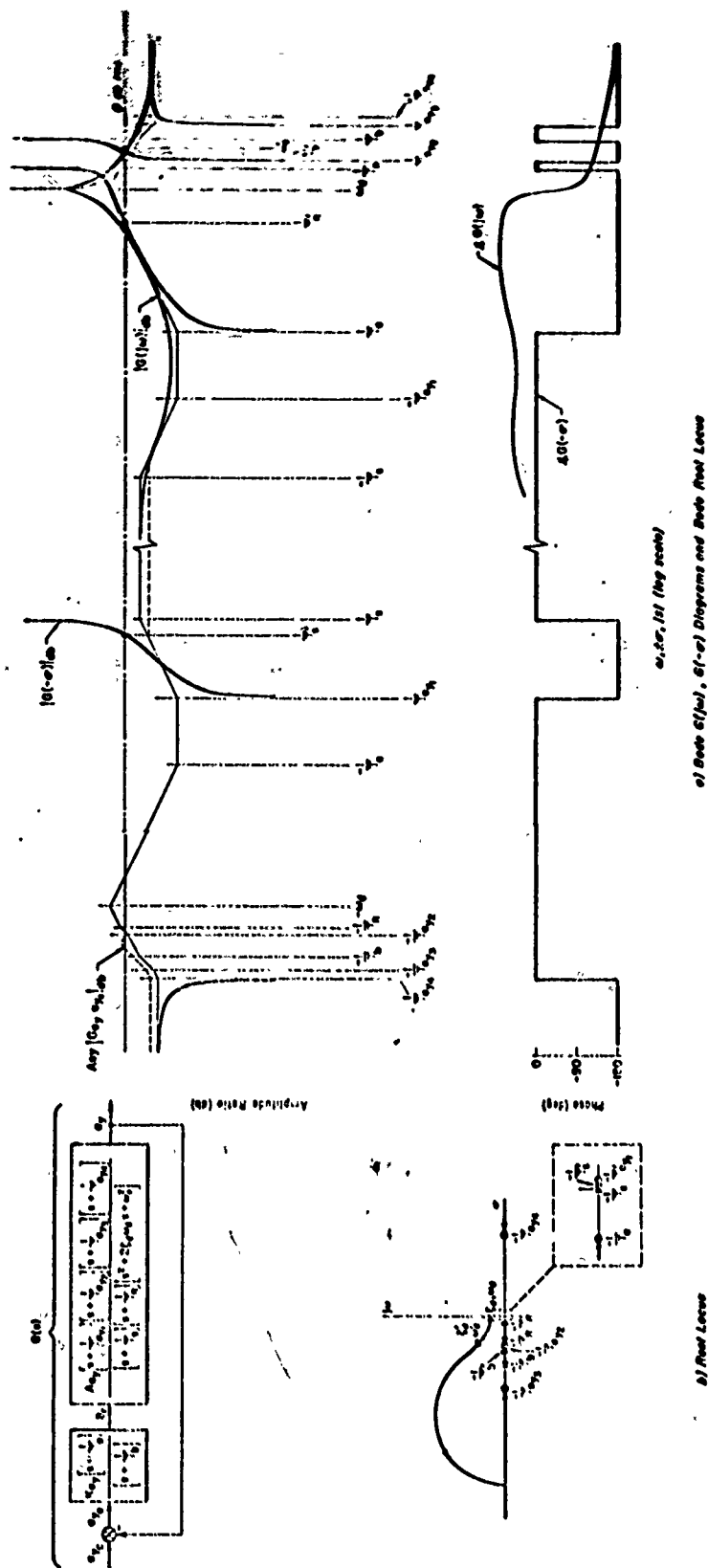


Fig. 8-15. System Survey of Side Acceleration ($\omega_r = 8\pi$) Control System with Lead/Lag Equalization

above. In the all-mechanical B-52 damper the side acceleration was sensed in the fin (where it consisted almost entirely of an $x_{\dot{y}} \dot{r}$ signal) and was pseudointegrated (lagged) so as to produce a signal roughly proportional to yawing velocity at the dutch roll frequency. This latter signal was then employed to deflect the rudder.

CHAPTER 9

REQUIREMENTS, SPECIFICATIONS, AND TESTING

9.1 INTRODUCTION: THE SYSTEM DESIGN PROCESS

In Chapter 1 there was occasion to suggest the importance of feedback to the solution of the problem of control and guidance of aeronautical vehicles. In particular, its roles in making the vehicle amenable to following guidance commands and in suppressing the effects of disturbances were emphasized. Since then the text has exposed the mathematical and physical principles necessary to the solution of the deterministic analysis problem, i.e., given the (deterministic) input and the mathematical description of the system, find the output or error. This, however, by no means represents a solution to the design or synthesis problem, i.e., given the input and the desired output or tolerable error, find the system.

As a general term, synthesis may be defined as the process of combining elements into a unified whole. A flight control system may be considered as the combination of two basic portions—a controlled element (vehicle) and a controller. The controlled element is characterized by output quantities to be controlled and input quantities to which control is applied. The controller has three functions, namely, sensing, actuation, and equalization. The first of these is performed by sensors, or elements capable of detecting the output quantities to be controlled. The second function requires actuators, or elements capable of applying control. The third function, equalization, includes all of the means required to connect or modify the performance of any of the system elements and of the overall system to achieve satisfactory system operation.

While, in principle, any of the components within the system are subject to modification to better the system as a whole, in practice some are more alterable than others. In many cases the controlled element is more or less predetermined by factors beyond the scope of the system designer. In other situations, it is assumed to be known

in order to facilitate the design process. Thus, while the controlled element is usually considered to be unalterable for the duration of a design calculation, this viewpoint should not be allowed to prohibit vehicle modifications which may improve the system. Sensing and actuating elements are only "quasi-alterable" in practice, because they can be changed only by selection of a different item of the same general class. Equalization elements are completely alterable within the realm of physical realizability and practicality. Following these remarks, system synthesis may be defined on a narrow basis as the process of determining the properties of a mechanism required to control an unalterable physical element in some desired fashion.

The final aim of system design is to integrate components into a functional system which performs its assigned tasks "satisfactorily." The design process leading to this end can be broken into several phases which are more or less chronological, yet which are extensively interrelated and interconnected. A typical set of such phases might include:

1. Specification of System Purpose and Overall System Requirements

At the design stage, system purpose can be equated with mission phase or task definitions. Requirements are partially derivable from the functions needed to be performed to accomplish these mission phases (operational requirements), and less directly from the characteristics of the interconnected components and the environment in which they operate (implied requirements).

2. Determination of Unalterable Element, Command, and Disturbance Environment Characteristics

Typically the characteristics of some component parts of the system are not subject to the choice of the system designer. In aeronautical control and guidance such "unalterable" elements often include the vehicle itself and possibly the control surface actuators and some of the motion quantity sensors. The "structure" of the commands and disturbances is likewise not subject to the choice of the designer but is instead a direct consequence of the mission or task and the environment.

3. Evolution of Competing Feasible Systems (Determination of Basic Functional Block Diagrams)

Usually the requirements can be met in more than one way, i.e., with different systems. Then it is possible to evolve competing systems which become candidates for selection on the basis of certain desirable properties.

4. Competing System Assessment, System Selection

The competing systems can be compared on a very large number of bases which can be divided into two categories: design quantities and design qualities. Design quantities include the dynamic performance (relative stability, accuracy, speed of response or bandwidth, etc.) and the physical characteristics (weight, volume, power or energy consumption, etc.). Design qualities include safety, operational capability, reliability, maintainability, cost and so forth. An "optimum" system is one which has some "best" combination of all these features.

5. Detailed Study of the Selected System

Once a "best" system has been selected, it is still necessary to wring it out for all nominal and abnormal operating conditions. The components which do not yet exist as hardware must be designed, fabricated and tested as components. As many of these as it is possible to include should be assembled in a simulation of the system, and finally the system needs to be tested in its actual operating environment, i.e., flight in our case. At each stage of the testing process the assumptions which were made in previous phases of the design should be checked for validity. If actual conditions violate the assumptions, a new iteration of the design should be begun at the point where the incorrect assumption was made.

It is in this, or a very similar way, that a functional system is synthesized, in practice, so as to satisfactorily meet all its performance objectives.

In the sections which follow, we present the concepts on which the requirements for automatic flight control systems are based. This process begins with a definition of the mission and becomes increasingly intricate and detailed as the flight control system is examined in its more intimate details. After the discussion of mission-centered and operational requirements, we turn to a consideration of the more obscure requirements implied by component or system design specifics. Flight

control systems are largely feedback controllers, so the subsequent article treats those flight control system requirements satisfied by the application of feedback principles. Finally, the bases for compromise in selecting system bandwidth are described.

After covering the first or requirements phase of design in the initial articles, the chapter concludes with a brief section on simulation and flight testing as the methods by which it is ultimately demonstrated that the automatic flight control system satisfies the requirements.

Important stages in the design process are not discussed in this chapter. For instance, the characteristics of the unalterable element, the aircraft itself, have been treated in Chapters 4-6, and the subjects of describing analytically the commands and disturbances, as well as an introduction to system dynamic performance assessment, are deferred to Chapter 10. This scrambling of the order of presentation is, in part, a reflection of the interrelationships between the subjects, and is done here partly to permit an orderly development of the mathematical background for the several topics.

9.2 MISSION PHASES AND OPERATIONAL REQUIREMENTS

In any aeronautical system design the requirements for subsystems evolve in a pyramidal fashion, and become more numerous and detailed as definition of the actual equipment is approached. The apex of the pyramid is the mission purpose and definition (see Fig. 9-1). Immediately below this central point are three blocks involving considerations which interact strongly in the earliest preliminary design stages: mission phases, vehicle operating point profile, and guidance possibilities. When the mission is feasible, one or more feasible vehicle operating-point profiles are joined with one or more guidance possibilities to enable the overall system to perform through the constituent phases of the mission.

Vehicle operating-point profiles and guidance possibilities can ordinarily be expressed in concrete numerical terms. The mission phase "structure," however, is basically open to choices. For flight control design purposes, the mission phase categories should be selected so that

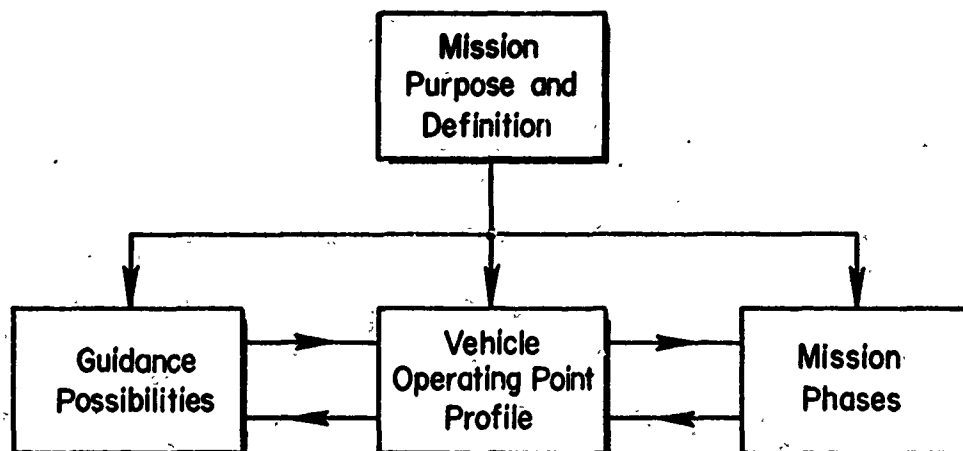


Figure 9-1. First Step in Flight Control Requirements Evolution

the quantities required to define flight control activities are determined once the phase is identified. A mission phase structure based on maneuvers is ideal for this purpose. In Table 9-1, for example, an aerospace mission is broken down into mission phases which serve to indicate the sequences required for its accomplishment.

At this point the flight control system commands and the basic flight control references are, in principle, determined since these must be such as to allow the vehicle to accomplish each mission phase. This usually amounts to the specification of the outer loops required.

Two other elements of the flight control problem also enter at this stage. These are those forcing functions and vehicle dynamic properties which depend on the environment (as defined by the various mission phases in a gross way) and on the operating-point profile. Such a dependence is illustrated in Fig. 9-2 and Table 9-2.

This brief discussion illustrates that decisions about guidance possibilities, operating-point profile, and mission phases have a direct influence on the flight control system design, since definition of the command structure, references, kinematics, and forcing functions is implied by the choices made.

TABLE 9-1

V/STOL AIRCRAFT MISSION-MISSION PHASE MATRIX

MISSION PHASE \ MISSION	TRANSPORT	RESCUE	ASW	CLOSE SUPPORT (ATTACK)	INTERDICTION (STRIKE)
Short field or vertical deck takeoff or launch	x	x	x	x	x
Ferry or cruise	x	x	x	x	x
Approach, transition, hover	*	*	*	*	*
Land at forward site	*	*		*	*
Takeoff, transition from hover		x	x		x
Takeoff from forward site	x	x		x	x
Loiter	(in traffic)	x	x	x	
Low altitude penetration					x
Weapon delivery			x	x	x
Approach transition and land at short field or recover on deck	*	*	*	*	*

Legend: x denotes applicable nonlanding segment.

* denotes approach transition, hover, and landing segments.

Thus far, two types of quantities about which information is needed prior to the evolution of flight control system requirements have been discussed. The first of these, the "mission-centered quantities" (i.e., vehicle operating-point profile and mission phases), result in "given" starting points for subsequent dynamic requirements evolution. The second kind of quantity, which might be called "system-interaction quantities," is implied, for example, by the block diagrams of Fig. 1-6. Considering Fig. 1-6 again, it is evident that dynamic requirements are imposed on the flight control system by virtue of its operation as an element of the overall system—specifically that it operate properly

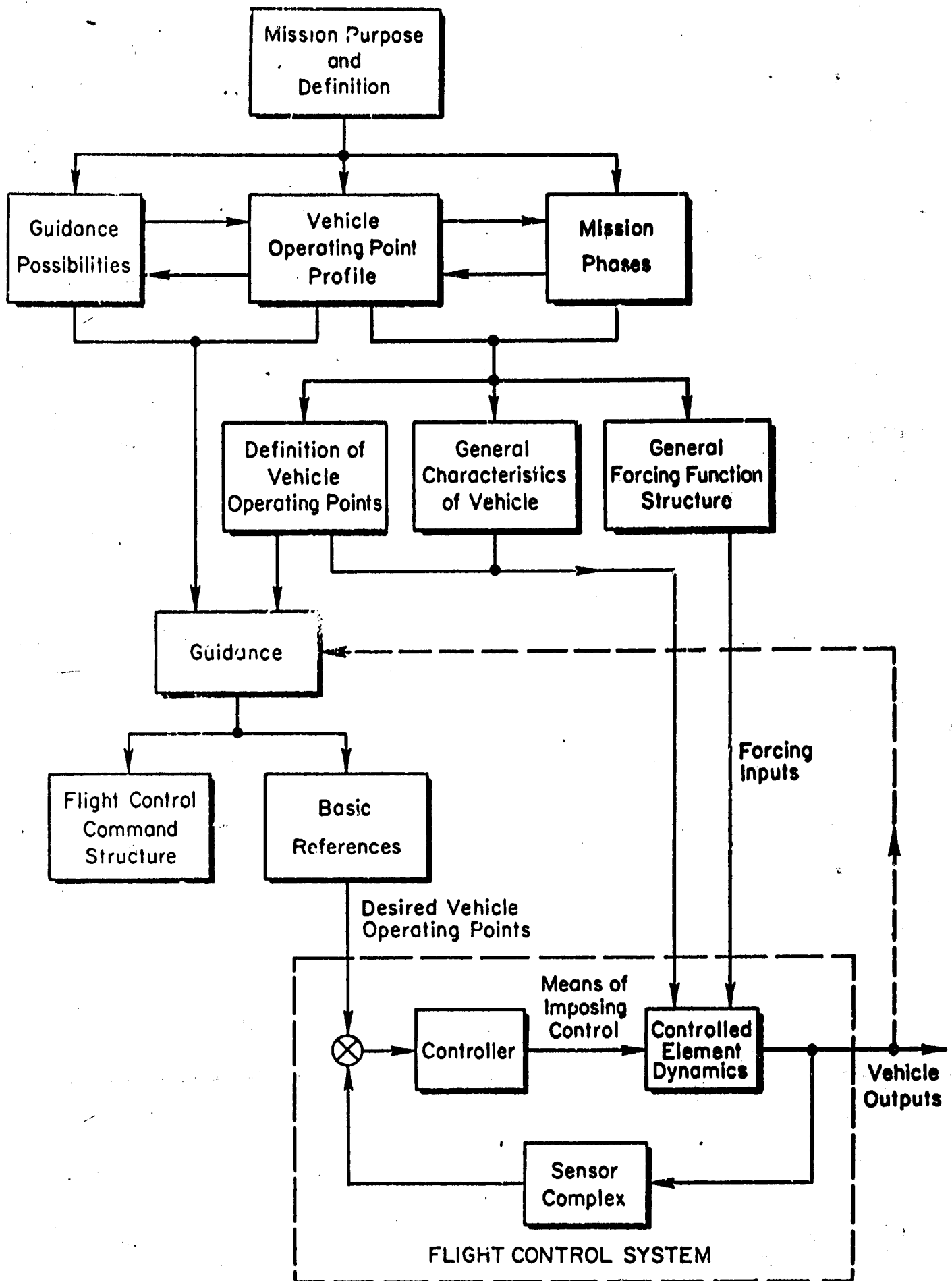


Figure 9-2. Family Tree for Evolution of Flight Control Requirements

TABLE 9-2

MISSION PHASE-FORCING FUNCTION STRUCTURE

MISSION PHASE	GUIDANCE		DISTURBANCE	
	EXTERNAL	INTERNAL	EXTERNAL	INTERNAL
Short field or vertical deck takeoff or launch	Radio, ground radar, and data link	Airborne radar, inertial, doppler	Turbulence, wind shear intrusions, traffic	
Ferry or cruise	Ground radar, loran or Decca, etc.	Airborne radar, inertial, dead reckoning	Turbulence	
Approach, transition, hover	Radio, ground radar, and data link			Configuration change, inadvertent stores release, crew motions
Land at forward site	Radio, ground radar, and data link	Doppler, inertial	Turbulence, wind shear intrusions, traffic	
Takeoff, transition from hover at forward site	Radio, ground radar, data link			
Loiter	Radio, ground radar, data link, loran, or Decca, etc.			
	Radio, ground radar, and data link	Radar, doppler, inertial	Turbulence, wind shear terrain, obstacles, intrusions	Stores release
Low altitude penetration	Radio, ground radar, and data link			
Weapon delivery	Radio, ground radar, and data link			
	Radio, ground radar, data link, laser	Doppler, inertial	Turbulence, intrusions, traffic, obstacles	Configuration change, inadvertent stores release
Approach, transition, and land at short field or recover on deck				

during phases of the mission in which a homing-type loop is closed. Based on this general requirement and the interaction defined by the block diagram, a series of possible specifications for desirable flight control system characteristics can be promulgated and expressed in servo terms, such as dominant features Bode or root plots. In the case illustrated in Chapter 1, the major interaction is due to the $(1-t/\tau)$ gain-changing term in the guidance loop (see Fig. 1-5). Recognition of this fact, and its implications on the overall system, provide the starting point for considering this particular system interaction.

9.3 AN APPROACH TO IMPLIED REQUIREMENTS FOR SYSTEM DESIGN

Unfortunately, any gross transfer function requirements derived from considerations of the mission-centered quantities and system interaction structure are not necessarily complete or even consistent with acceptable performance in other necessary phases of the mission, such as takeoff, response to nonguidance commands, etc. In many systems these other mission phases, in which the guidance loop is not "tightly" closed, impose stringent requirements on the flight control system over and above those required for proper operation of the overall flight control and guidance system. In such cases an appreciation of the interaction which exists between the vehicle and the controller requires a detailed examination of the flight control loop itself. Specifically, one must consider the requirements imposed on the flight control equipment by various types of controlled element (vehicle) characteristics, flight control system command inputs, and external disturbances; and conversely, requirements implied on the controlled element by various possible flight control equipments.

This leads us finally to the "component-centered quantities" which involve the primary elements of the flight control loop, the controller and the vehicle. Definition and thorough understanding of the general dynamic characteristics and operating features of the vehicle readily leads to identification of the physical quantities which might be controlled and to the means through which control can be readily imposed.

The following annotated outline summarizes the quantities required as a basis for flight control specification activities:

1. Mission-Centered Quantities (Mission Phase and Vehicle Operating-Point Profile)

Establish:

- a. Flight control system commands
- b. Basic flight control references
- c. Modal and command sequences

Define:

- a. Disturbance, or unwanted input, environment to be encountered throughout the operating-point profile
- b. General characteristics of the controlled element

2. Component-Centered Quantities

a. Vehicle-centered quantities, including

- Vehicle steady-state maneuvering characteristics
- Vehicle steady-state asymmetrical performance conditions
- Vehicle output quantities (vehicle motions)
- Vehicle input quantities (means of imposing control)
- Vehicle dynamic (transfer) characteristics
 - Linear, constant-coefficient
 - Nonlinear and/or time-varying linear

b. Controller-centered quantities, including

- Controller input possibilities (ability to sense vehicle output quantities)
- Controller output possibilities (actuation of vehicle input quantities)

3. System Interaction Quantities

a. Overall Flight Control and Guidance System

Interactions establish possible requirements imposed on the flight control system by operation within the overall system. Logically the guidance-control dichotomy has both static and dynamic interactions:

- Operating Point Control—The fundamental role of guidance is to indicate the desired vehicle operating-point profiles in some suitable physical form. Thus both the physical flight control command structure and basic references derive from guidance; and the role of operating-point control is to translate guidance desires into vehicle mass center motions.
- Limiting—Practical guidance equipment may impose limits upon allowable vehicle departures or rates thereof from operating-point conditions.
- Dynamic Interactions—In homing systems guidance and control are inseparable dynamically, so proper dynamic operation of the total overall system imposes demands upon the transfer characteristics of the flight control system.

b. Flight Control System

System interactions between vehicle and controller for various controller input and output possibilities establish bases for requirements selection and/or evolution. Interactions must consider:

- Sensing and equalization possibilities
- Relationships between loop dynamics, accuracy, stability, and response
- Partition of required system dynamic characteristics between vehicle and controller
 - Vehicle dynamic requirements
 - Controller dynamic requirements

When all of these quantities and possibilities are thoroughly understood, a detailed specification of functional requirements may be set up for the

flight control system. It is ordinarily possible at this stage to delineate functional requirements directly by assuming the vehicle characteristics to be unalterable and further assuming that "desirable" sensors fall into a relatively narrow class. With these assumptions the flight control system interactions for a specific case change from general to likely possibilities. The functional requirements may then be concretely established, and the choices of alternatives are limited largely to those possible at the detailed mechanization level. This procedure is the one most commonly adopted in flight control system design. On the other hand, if the vehicle characteristics are considered subject to modification, system interactions between vehicle and controller again assume the status of possibilities, and competition between alternatives can proceed on a somewhat broader level.

In either event, the process of evolving a final set of functional requirements which must be met by the system and its constituents is inevitably difficult. When properly performed it demands ruthless objectivity coupled with ingenuity and a flair for selecting among competing possibilities that one system configuration which is most favorably constituted to accomplish given purposes. In principle, a complete evolution of functional requirements is the result of an optimization process which, reduced to its logical constituents, requires

1. The establishment of an overall criterion which measures the degree to which systems accomplish their given purposes. The overall criterion depends upon a weighted intermix of subcriteria. Subcriteria are measures of those quantities contributing to system success (e.g., performance, pilot and/or vehicle safety, weight, energy, reliability, schedule, cost, etc.).
2. Establishment of competing configurations.
3. Assessment of the competing configurations in terms of the subcriteria and then the overall criterion.

The most fundamental element in the optimization procedure is, of course, the establishment of possible alternative configurations since criteria become academic and assessment meaningless unless there is a choice to

be made. It is at the configuration level that requirements implied by a particular system configuration meet in a contest with those which stem from physical limitations, the result being the functional requirements for that particular system. Assessment across competing systems then leads to a final system choice and a final set of requirements.

9.4 GENERAL FEEDBACK CONTROL SYSTEM CONSIDERATIONS IN FLIGHT CONTROL

The complete solution of flight control problems normally requires a suitable intermix of open- and closed-loop systems. By their very nature open-loop systems are calibrated, so their application is restricted largely to situations in which the acting inputs and desired control responses are fairly well known a priori. In flight control practice this required foreknowledge largely confines the role of open-loop elements to partial solution of operating-point control problems. Examples include throttle and flap setting, trim adjustment simultaneous with the release of stores, near-impulsive velocity corrections, etc. Even for these examples "loose," low response, feedback loops may exist or the open-loop elements may operate in conjunction with closed-loop vernierlike supplementary control systems. In any event, pure open-loop control actions depend only on the response characteristics of the controller and vehicle in series, so dynamic interactions are either practically nonexistent or relatively simple and straightforward. Consequently we shall here say no more about open-loop control serving by itself as a complete flight system.

The vast majority of flight control systems are multi-input, multi-output, multi-mode devices with many coupled degrees of freedom. Functionally and operationally they behave as multiloop feedback control mechanisms in which dynamic interaction between elements plays the central role in overall system dynamic performance. In this and other ways flight control systems share all the generic qualities of servomechanisms and regulators. Adopting a point of view in which flight control systems are considered as members of a broad class of feedback control systems is especially useful in the evolution of flight control system dynamic requirements, and this view is the basis for the remainder of the discussion of this chapter.

In order to provide concreteness in the subsequent development, we shall use the system shown in Fig. 9-3 as a prototype. Although some flight control systems may require a more complex block diagram representation, the system shown is suitable for a wide variety known as "single-sensor-loop" control systems. The system types classified under this title have the distinguishing characteristic that single-loop block diagrams composed of analytically simple transfer function blocks provide suitable descriptions of their functional operation. On the other hand, the forward-loop transfer function may actually include the closed-loop transfer functions of the inner loops in a multiloop structure. Specifically in Fig. 9-3 the actuator loop has not yet been replaced by its closed-loop equivalent, although this step shall be taken subsequently. Also, the feedback transfer function may be a combined representation of two or more sensors. As will be seen later, nearly every flight control system, including some with two different control inputs, can be represented by single-sensor-loop block diagrams.

A few remarks about the physical realities represented in Fig. 9-3 are now in order. Consider first the ideal system block, $H(s)$. This is, of course, not physical in that $H(s)$ represents the desired transfer function between output and command. [In subsequent developments $H(s)$ may represent: an ideal system between input, $R(s)$, and output, $C(s)$; input, $R(s)$, and indirectly controlled output, $Q(s)$; or command, $V(s)$, and indirectly controlled output, $Q(s)$; instead of between $C(s)$ and $V(s)$ as shown on the diagram. The distinction will always be clear from the context.] Turn now to the disturbances, which enter the system in four different locations. Disturbances may occur physically in yet other places, but essentially all of these can be lumped into those shown. Of the two internal disturbances, $\eta_e(s)$ and $\eta_a(s)$, the second is by far the more important. Normally the noise, or unwanted inputs, near the error point is minimized by using high quality sensing instruments and by careful design of signal circuits, so input signal-to-noise ratios are extremely high. Further, a large proportion of the error point disturbance is subsequently rejected in such elements as phase-sensitive

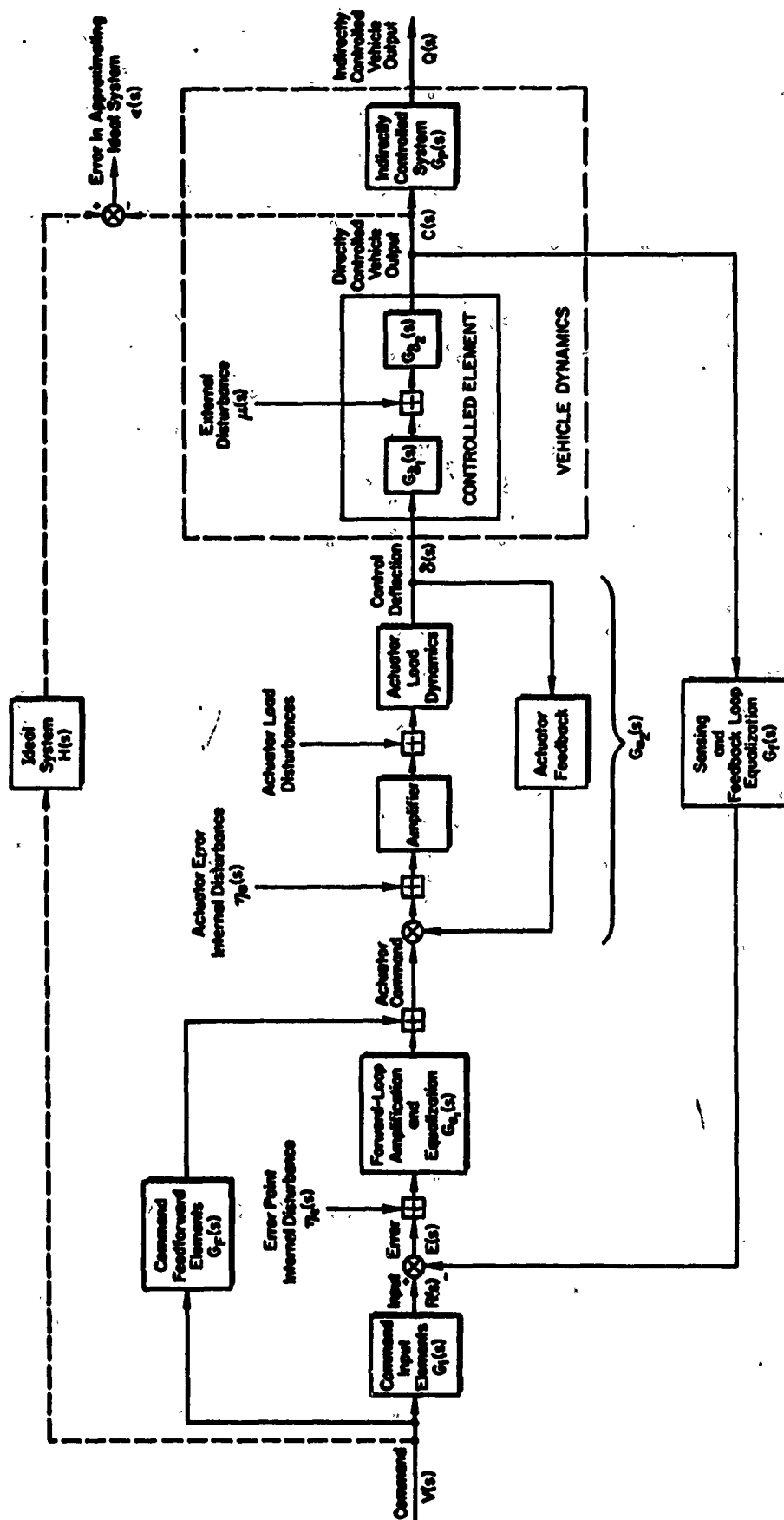


Figure 9-3. Prototype "Single-Sensor-Loop" Flight Control System

demodulators incorporated in the forward-loop amplification and equalization block. On the other hand, the actuator error disturbance, $\eta_a(s)$, while often small in absolute magnitude, is almost invariably followed by large amplification factors within the actuator loop. These are required in practice to minimize the effects of actuator load disturbances and closed-loop actuator dynamics on the overall system. These high gains coupled with the internal disturbance, $\eta_a(s)$, and limiting within the actuator loop can result in very deleterious consequences. The actuator load disturbances may arise physically from several sources inherent in the actual actuator installation; in addition they may include external disturbances imposed upon the control surfaces. With aerodynamic controls, a feedback path (not shown) also exists between the vehicle dynamics and the actuator load disturbance point.

As already mentioned, the actuator loop will ordinarily be closed with gains sufficiently high to eliminate the effects of actuator load disturbances on the control deflection. In these circumstances the block diagram of Fig. 9-3 reduces to the one shown in Fig. 9-4. Further, if the internal and external disturbances are neglected, the even simpler diagram of Fig. 9-5 appears. Finally, for those circumstances in which command feedforward and command input elements are not present, the overall block diagram takes on the especially simple form shown in Fig. 9-6. All of these block diagrams shall be used to illustrate particular points in the following discussion of flight control system functions.

The primary purposes of a flight control system are to impose control on the vehicle's flight path and attitude. In terms of the general definition of control given in Chapter 1, flight path and attitude control may be defined as:

Flight Path Control—The stabilization and operating-point control of the time history of a vehicle velocity vector.

Attitude Control—The stabilization and operating-point control of the orientation, aspect, or inclination of a vehicle or portions thereof.

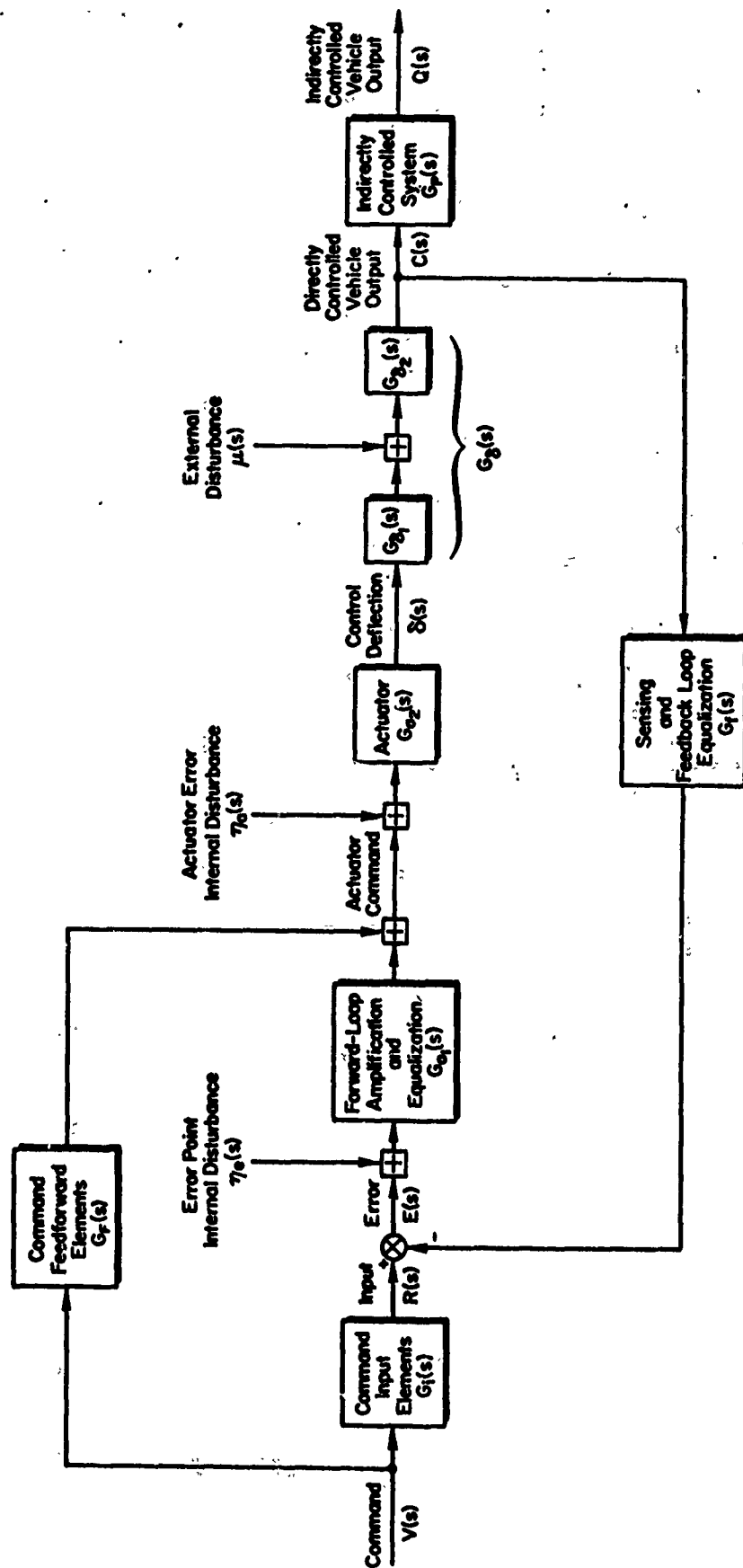


Figure 9-4. Simplification of "Single-Sensor-Loop" Flight Control System

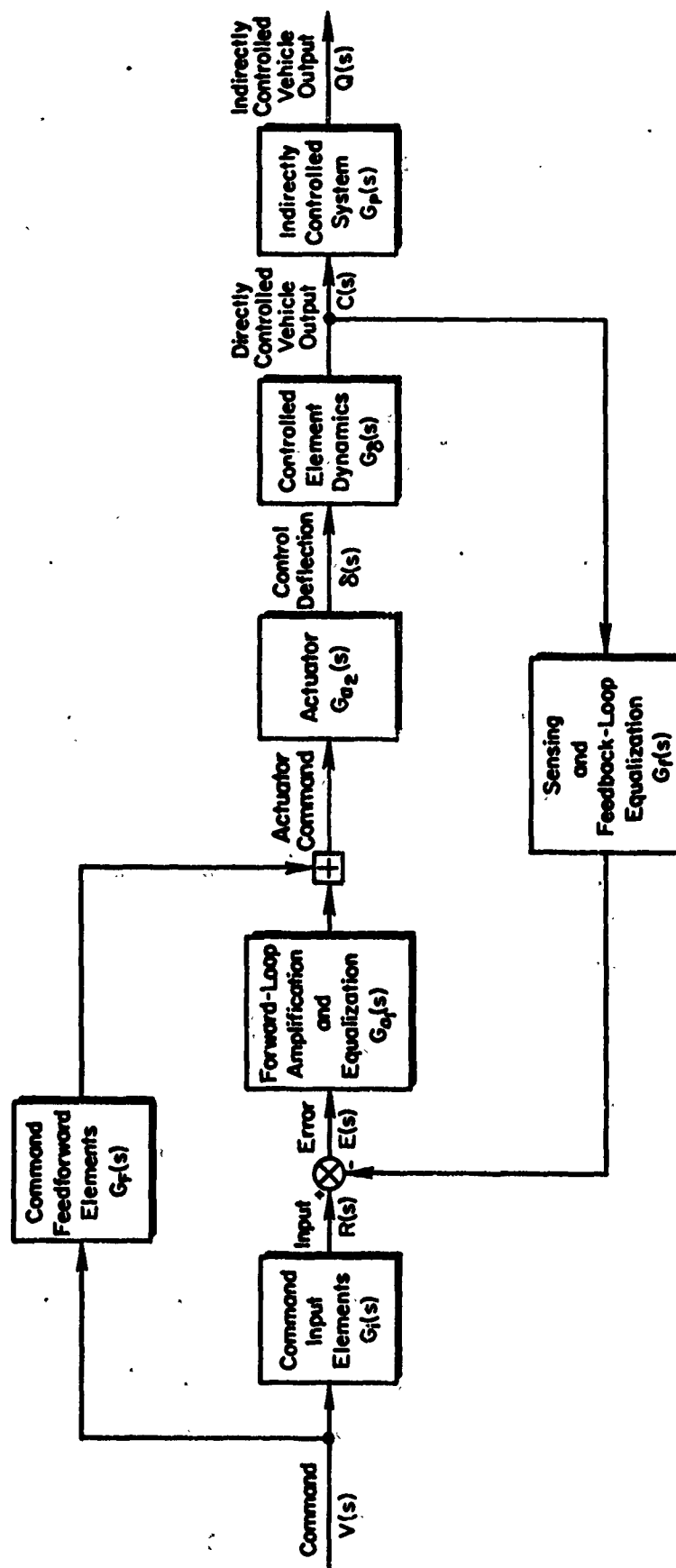
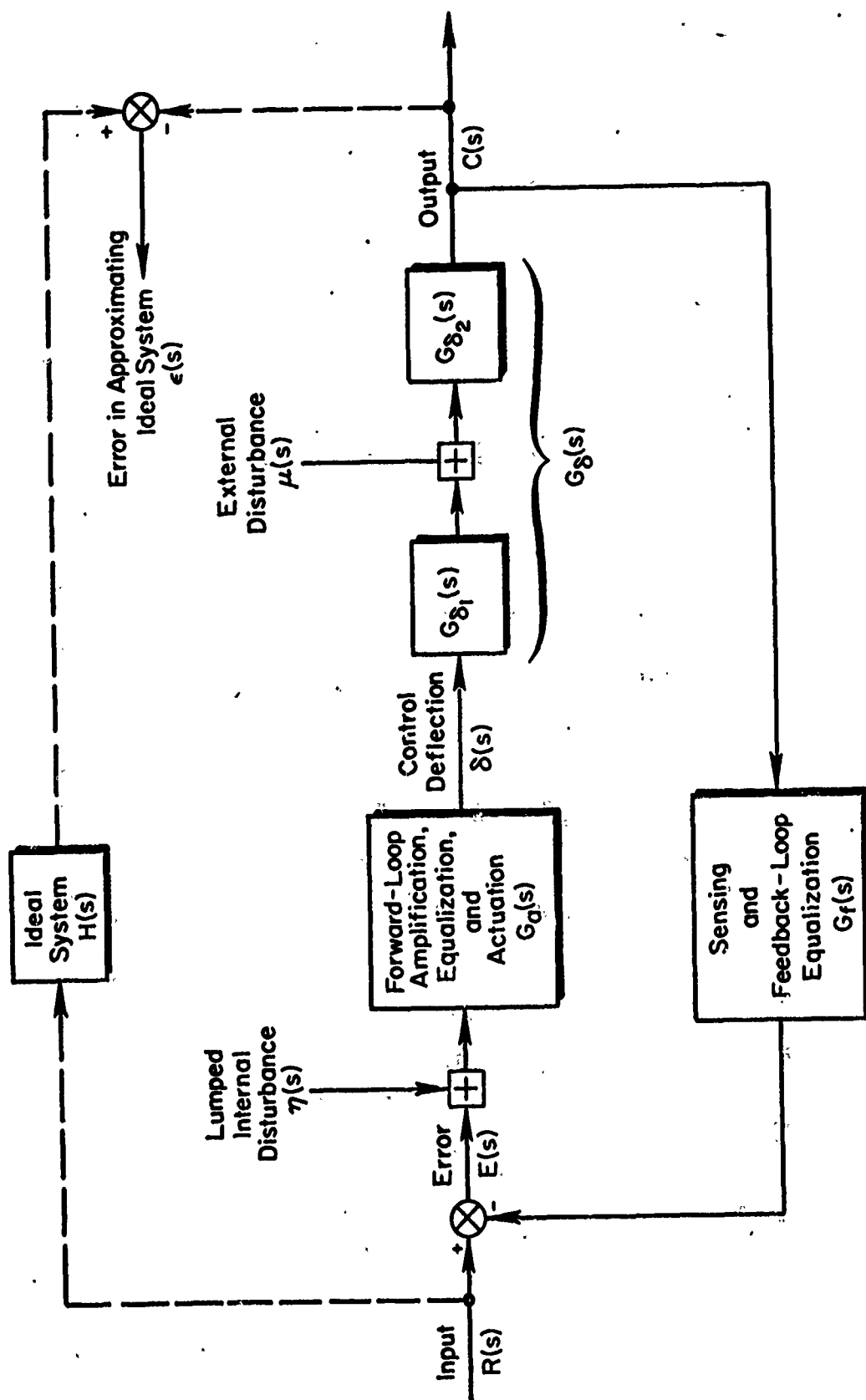


Figure 9-5. Prototype "Single-Sensor-Loop" Flight Control System Without External and Internal Disturbances



$$\text{Open-Loop Transfer Function } G(s) = G_a(s)G_g(s)G_f(s)$$

Figure 9-6. Prototype "Single-Sensor-Loop" Flight Control System Without Feedforward and Command Input Elements

Stabilization control often merges with operating-point control, especially when the system is in process of change from one operating-point to another. Still, the distinction between the two aspects of control is often helpful as a basis for establishing a dividing line between dynamic and steady-state operating requirements.

When broken down, the flight control system's basic overall function in accomplishing flight control purposes implies a control system which provides:

- Stability (either general or at specified times)
- Desired responses to specified inputs
- Suppressions of the effects of undesired inputs

To provide these features the flight control system is called upon to perform certain specific functions. The functions are interrelated, so lines of demarcation between them are difficult to draw distinctly. One breakdown of specific functions is given below.

- a. Provide Vehicle Stability. Most aeronautical and aerospace vehicles which operate over a wide range of flight conditions inevitably encounter stability difficulties in one or more flight regimes. Because of large variations in the types and magnitudes of the forces acting, sophisticated vehicle design measures alone are seldom sufficient to insure stability over the entire performance envelope. Consequently a prime flight control system function is ordinarily the augmentation or creation of vehicle dynamic stability. In terms of Fig. 9-6, a vehicle having unstable dynamic characteristics will possess a transfer function $G_\delta(s)$ containing poles in the right half of the s-plane (RHP). With a flight control system added, the "effective" vehicle characteristics are modified from

$$\frac{C(s)}{\delta(s)} = G_\delta(s) \text{ [unstable, i.e., poles in RHP]} \quad (9-1)$$

$$\text{to} \quad \frac{C(s)}{R(s)} = \frac{G_a(s)G_\delta(s)}{1 + G_a(s)G_f(s)G_\delta(s)}$$

$$= \frac{1}{G_f(s)} \left[\frac{G(s)}{1 + G(s)} \right] \quad (9-2)$$

With proper design, the poles of the "effective" vehicle transfer function (given by the zeros of $G_p(s)[1+G(s)]$) lie in the left half of the s -plane, thereby providing stability for the "effective" vehicle.

- b. Reduce "Effective Order" of Vehicle Dynamics. A consequence of feedback is effectively to reduce the order of the system transfer function within desired frequency regions. For instance, the denominator of the open-loop transfer function, $G(s)$, in Fig. 9-6 is ordinarily of high order; and the denominator of the closed-loop characteristics given by $G(s)/[1+G(s)]$ will be of this same order. However, the fact that $|G(j\omega)|$ can be made much greater than unity over wide frequency ranges sets up frequency regions in which either the closed-loop poles are nearly cancelled by zeros, or are otherwise removed from these regions to considerably higher or lower frequencies. So, while theoretically the denominators of $G(s)$ and $G(s)/[1+G(s)]$ are of the same order, practically the order of $G(s)/[1+G(s)]$, in a frequency range of interest, can be effectively lowered from that of $G(s)$. Expressed another way, the closed-loop transfer function

$$\left| \frac{G(j\omega)}{1 + G(j\omega)} \right| \doteq 1, \text{ when } |G(j\omega)| \gg 1 \quad (9-3)$$

so all the modes of $G(j\omega)$ in the frequency regions where $|G(j\omega)| \gg 1$ have been effectively removed. An example of the reduction of the effective order of vehicle dynamics has already been presented in Chapter 3 (see pp. 3-49 to 3-56).

This reduction in effective order is one of the most profound and significant features of feedback systems. One of its more important consequences is an improvement in performance potential. This is demonstrated in Fig. 9-7, which shows minimum values of two figures of merit versus system order, n . These results are obtained with unit numerator systems, i.e., systems having output/input transfer functions of the form

$$G_{cr}(s) = \frac{1}{s^n + a_1 s^{n-1} + \dots + a_{n-1} s + a_n} \quad (9-4)$$

subjected to unit step inputs. In each case, the system coefficients (the a_i 's) were adjusted to values for which

$$\frac{\partial(\text{Figure of merit})}{\partial a_1} = 0 \quad (9-5)$$

so the figures of merit shown are those for "optimum" systems, using a zero value of the total differential as the definition of optimum.* From Fig. 9-7 it is apparent that a high order system which is "reduced" to act like a second order system has the potential, if properly adjusted, to give lower (i.e., better) figures of merit than a similar system reduced only to the point where it acts like a fourth order system. Here the process of "reduction" requires the insertion of equalization, and the consequent addition of numerator terms to the unit numerator output/input transfer function, $G_{cr}(s)$.

- c. Adjust "Effective" Vehicle Dynamic Response. This function is related to the one directly above as the second step in a two-step process intended to improve the "effective" vehicle dynamic response for desired inputs. Reduction in effective system order stems directly from setting up the condition $|G(j\omega)| \gg 1$ over some desired frequency range; adjustment of effective vehicle dynamic response follows in the selection of the restricted frequency region where $|G(j\omega)| = O(1)$, and in the tailoring of $G(j\omega)$ in this region. Normally, the closed-loop system has three regions of interest, defined by

$$|G(j\omega)| \gg 1, \text{ over which } \left| \frac{G(j\omega)}{1 + G(j\omega)} \right| \doteq 1;$$

$$|G(j\omega)| \ll 1, \text{ over which } \left| \frac{G(j\omega)}{1 + G(j\omega)} \right| \doteq |G(j\omega)|; \quad (9-6)$$

$$\text{and } |G(j\omega)| = O(1)$$

The form of $|G(j\omega)/[1 + G(j\omega)]|$ in this last region defines the dominant modes of the closed-loop system dynamic response. In most cases, $G(j\omega)/[1 + G(j\omega)]$ in the region where $|G(j\omega)|$ is of the order of unity can be approximated by a first-, second-, or third-order system and one, two, or three modes will be "dominant" in the response.

*The validity of particular figures of merit is beside the point for the present discussion, although of extreme interest if a figure of merit is used as a performance criterion. For a detailed discussion of the latter point, see: Wolkovitch, J., R. Magdaleno, D. McRuer, D. Graham, and J. McDonnell, Performance Criteria for Linear Constant-Coefficient Systems with Deterministic Inputs, ASD-TR-61-501, Feb. 1962.

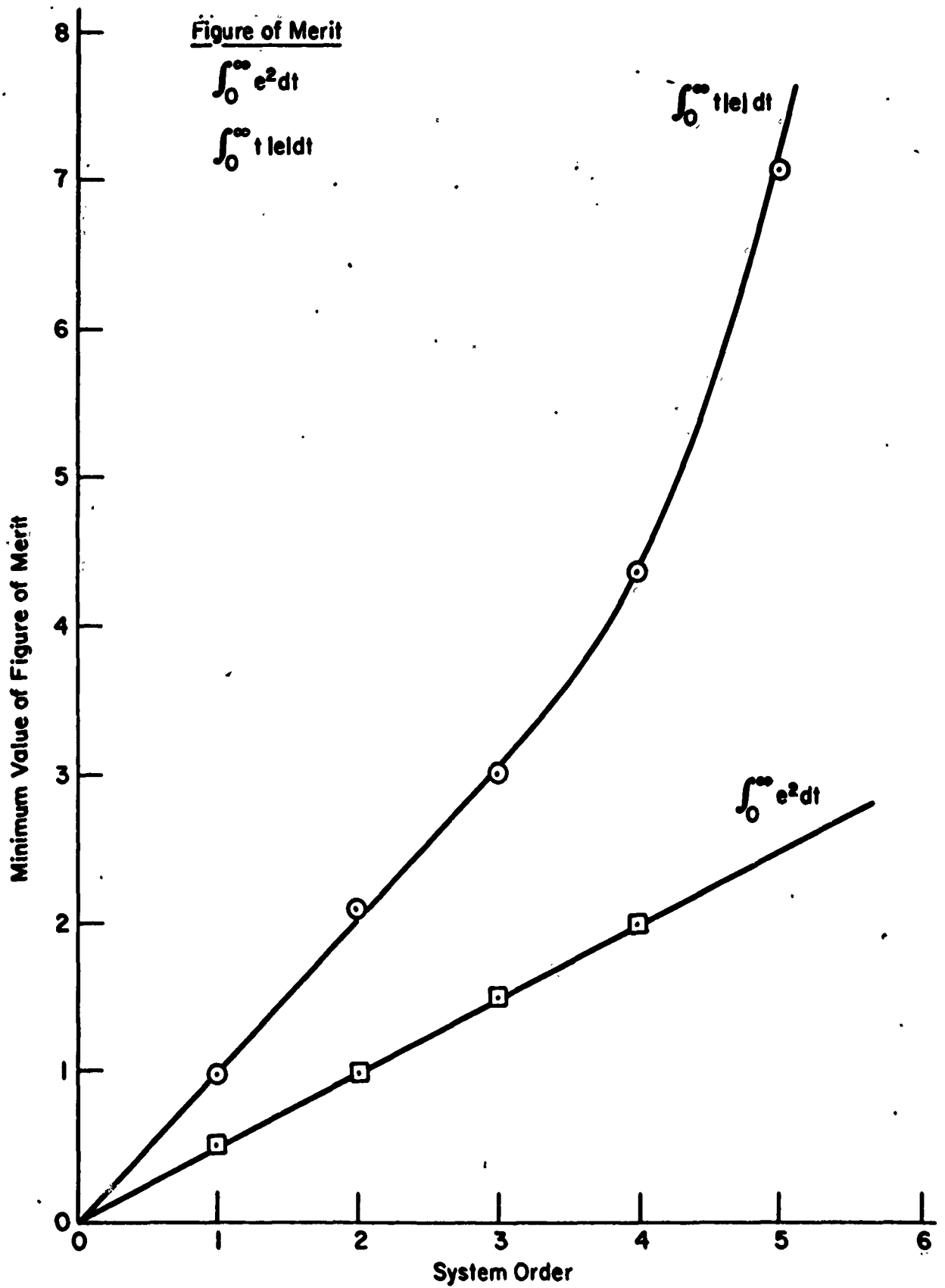


Figure 9-7. Variation of Minimum Value for Figure of Merit with System Order

- d. Provide Specified Command-Response Relationships. It is often desired that the flight control system provide some specified relationship between command and response. Referring to Fig. 9-5, it can be seen that the closed-loop transfer function in response to command inputs has the form:

$$G_{cv}(s) = \frac{G_b(s)[G_1(s)G_a(s) + G_F(s)]}{1 + G(s)} \quad (9-7)$$

When the magnitude of the open-loop transfer function, $|G(j\omega)|$, is much larger than unity, the relationship between the command and response reduces to

$$G_{cv}(j\omega) \doteq \frac{1}{G_F(j\omega)} \left[G_1(j\omega) + \frac{G_F(j\omega)}{G_a(j\omega)} \right] \quad (9-8)$$

The designer has complete control over the transfer functions $G_1(s)$ and $G_F(s)$ and some control over $G_F(s)$ and $G_a(s)$ [the latter two are, of course, involved in the open-loop transfer function, $G(s)$, so they cannot be arbitrarily adjusted without affecting the basic constraint $|G(j\omega)| \gg 1$]. By proper selection of the form of the transfer function combination shown in Eq. 9-8, the designer can provide almost any specified command response relationship, at least over the frequency regions where $|G(j\omega)| \gg 1$. For manual control purposes these transfer functions can be adjusted to provide a vehicle response to piloted command which approximates the best vehicle in the sense of pilot desires. Among other things, the effective vehicle dynamics as seen by the pilot can be made substantially invariant with flight conditions.

- e. Reduce Effects of Unwanted Input and Disturbance. The primary regulator function of a flight control system is to reduce the effects of external disturbances acting on the vehicle and internal disturbances acting on the flight controller itself. For all but those disturbances acting at the input, this function is again accomplished by virtue of the feedback aspects of the system. In Fig. 9-4, for example, the system output with no command input is given by

$$C(s) = \frac{1}{1 + G(s)} [G_{b2}(s)\mu(s) + G_{a2}(s)G_b(s)\eta_a(s) + G_a(s)G_b(s)\eta_e(s)] \quad (9-9)$$

Again, when $|G(j\omega)|$ is much greater than one, the output due to these disturbances is approximately

$$C(j\omega) = \frac{\mu(j\omega)}{G_a(j\omega)G_{\delta_1}(j\omega)G_f(j\omega)} + \frac{\eta_a(j\omega)}{G_{a_1}(j\omega)G_f(j\omega)} + \frac{\eta_e(j\omega)}{G_f(j\omega)} \quad (9-10)$$

Ordinarily the transfer functions $G_a(j\omega)G_{\delta_1}(j\omega)G_f(j\omega)$ and $G_{a_1}(j\omega)G_f(j\omega)$ can be made large compared with unity over the frequency regions for which the external disturbances, $\mu(j\omega)$, and the actuator error internal disturbances, $\eta_a(j\omega)$, are important. Unfortunately, it is seldom possible to specify independently the feedback transfer function, $G_f(j\omega)$, such that a similar reduction in output due to the internal disturbance, $\eta_e(j\omega)$, also occurs. Even if this could be done, the desired input, $R(j\omega)$, would have the same closed-loop transfer function as $\eta_e(j\omega)$, so no effective reduction in signal-to-noise would accrue by closing the loop. These facts are reflected in the emphasis placed on procuring high quality instruments for flight control systems.

- f. Suppress Effects of Vehicle and Component Variations and Uncertainties. One of the principal differences between flight control and other feedback systems is the enormous variation possible in the controlled-element (vehicle dynamics) over the entire operating-point profile. Consequently, an extremely important function of an adequate flight control system is to maintain the effective closed-loop dynamics more or less constant. Considering Fig. 9-6, a fractional change in $G_{cr}(s)$, denoted as $dG_{cr}(s)/G_{cr}(s)$, in terms of fractional changes in the elements within the loop, is given by

$$\frac{dG_{cr}(s)}{G_{cr}(s)} = \frac{1}{1+G(s)} \left[\frac{dG_a(s)}{G_a(s)} + \frac{dG_{\delta}(s)}{G_{\delta}(s)} - G(s) \frac{dG_f(s)}{G_f(s)} \right] \quad (9-11)$$

Again, when the open-loop transfer function magnitude $|G(j\omega)| \gg 1$, the fractional change in overall closed-loop characteristics reduces to

$$\frac{dG_{cr}(j\omega)}{G_{cr}(j\omega)} = \frac{1}{G(j\omega)} \left[\frac{dG_a(j\omega)}{G_a(j\omega)} + \frac{dG_{\delta}(j\omega)}{G_{\delta}(j\omega)} \right] - \frac{dG_f(j\omega)}{G_f(j\omega)} \quad (9-12)$$

The beneficial consequences of large values of open-loop transfer function in lowering the effects of forward-loop controller and vehicle variations on the overall transfer function are apparent from this equation. Another point worth noting is the complete absence of any beneficial effect on uncertainties in the feedback path. Again this is a reason for the necessity of very high quality instruments.

- g. **Improved Linearity.** The elements of flight control systems often contain nonlinearities either inadvertently or by design. With the exception of command and other limiting functions, it is ordinarily desirable to suppress the dynamic effects of these nonlinearities so that more or less proportional cause-effect relationships exist between the various system inputs and outputs. Although there are several ways of accomplishing this "approximate linearization," the most common method is also another attribute of feedback. In Fig. 9-8, for example, when the element containing nonlinearities is replaced by a describing function, $N(j\omega; \delta)$, and a remnant, $B(j\omega)$,* the system output becomes:

$$C(j\omega) = \frac{1}{G_f(j\omega)} \left[\frac{G_a(j\omega)G_f(j\omega)N(j\omega; \delta)}{1 + G_a(j\omega)G_f(j\omega)N(j\omega; \delta)} \right] R(j\omega) + \left[\frac{1}{1 + G_a(j\omega)G_f(j\omega)N(j\omega; \delta)} \right] B(j\omega)$$

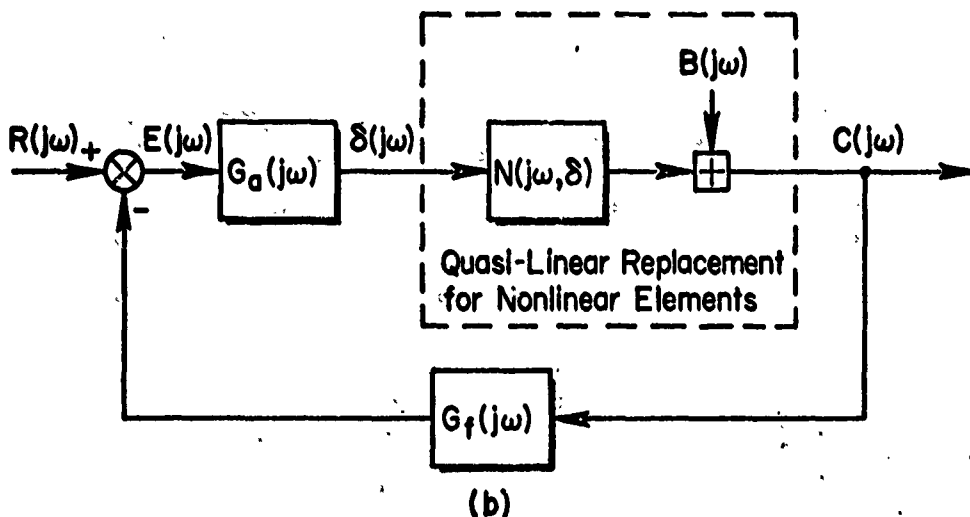
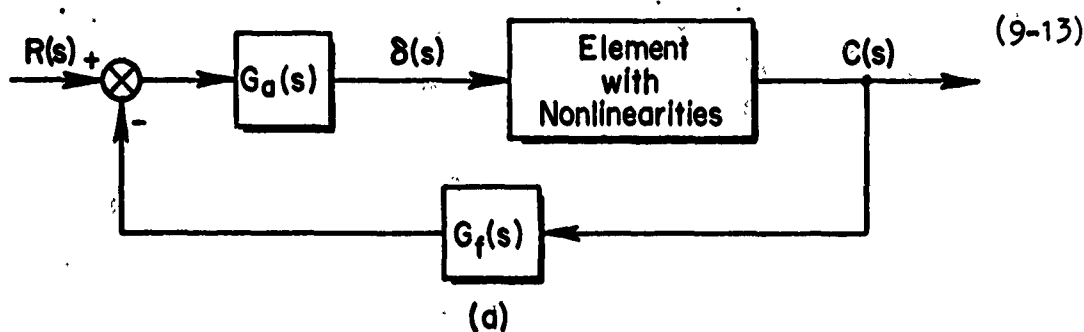


Figure 9-8. Replacement of Nonlinear Elements with Describing Function and Remnant

*See Graham, D., and D. McRuer, Analysis of Nonlinear Control Systems, John Wiley and Sons, Inc., New York, 1961.

This substitution of a quasi-linear representation for a nonlinear element can be accomplished precisely, in principle, when the input signal is a periodic or stationary-random function of time. For other inputs a quasi-linear representation is sometimes useful heuristically, although caution must be exercised to avoid carrying linear system notions too far.

When the input signal to the nonlinearity is confined within certain amplitude limits, the open-loop describing function can be made much larger than unity over some specified range of frequencies. Within these conditions the output reduces to:

$$C(j\omega) = \frac{1}{G_f(j\omega)} R(j\omega) + \frac{1}{G_a(j\omega)G_f(j\omega)N(j\omega;\delta)} B(j\omega)$$

Because the open-loop describing function, G_aG_fN , is so large over this frequency range, the remnant term will be much smaller than without feedback, and the output becomes approximately,

$$C(j\omega) = \frac{1}{G_f(j\omega)} R(j\omega) \quad (9-14)$$

To the extent that these concepts apply, the input and output bear an approximately linear relationship which is independent on the nonlinearity. Outside either the amplitude (of the nonlinearity's input) or frequency region where the open-loop describing function is much larger than unity, this relationship will, of course, no longer be valid.

Another illustrative analysis of the "linearizing" properties of feedback has been given by West* for the nondynamic case. Suppose, considering Fig. 9-8(a), that the element with nonlinearities is such that C is the function of δ illustrated in Fig. 9-9. Call this function $g(\delta)$. Then from the block diagram

$$\delta = G_a(R - G_f C) \quad (9-15)$$

$$C = g(\delta) = g(G_a R - G_a G_f C) \quad (9-16)$$

*West, J. C., Analytical Techniques for Nonlinear Control Systems, English Universities Press, London, 1960.

Now

$$\frac{dC}{dR} = \frac{dg}{d\delta} \frac{d\delta}{dR} = g'(\delta) \frac{d\delta}{dR} \quad (9-17)$$

Differentiating Eq. 9-15 and substituting,

$$\frac{dC}{dR} = g'(\delta) G_a \left[1 - G_f \frac{dC}{dR} \right] \quad (9-18)$$

or:

$$\frac{dC}{dR} = \frac{G_a g'(\delta)}{1 + G_a g'(\delta) G_f} \quad (9-19)$$

When the open-loop function $G_a G_f g'(\delta)$ is much larger than unity this becomes

$$\frac{dC}{dR} \doteq \frac{1}{G_f} ; \quad G_f G_a g'(\delta) \gg 1$$

Again this illustrates the fact that the action of the feedback is to linearize the nonlinearity as long as the loop gain is high.

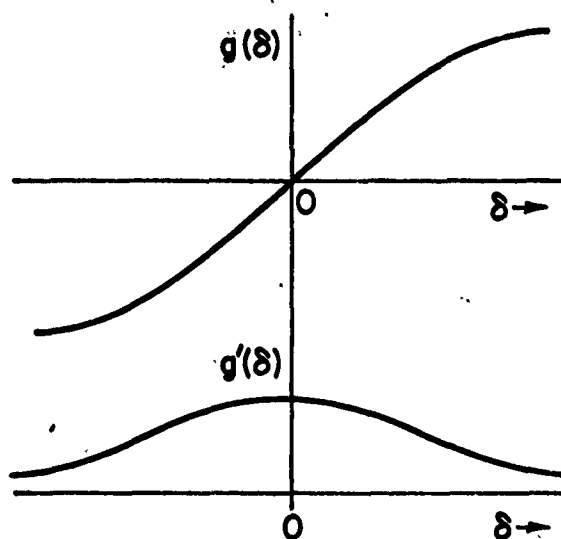


Figure 9-9. A Nonlinear Function and Its Derivative With Respect to the Input to the Nonlinearity

h. Modify or Eliminate Vehicle Cross-Coupling Forces.

Both aeronautical and aerospace vehicles often have several coupled degrees of freedom. Some of these couplings are desirable, while others can cause a great deal of grief. While high gain feedback loops are used to swamp many of these cross-couplings, it is occasionally desirable to cancel out cross-couplings by generating almost exactly opposing forces and moments via the flight control system. For instance, with vehicle equations of motion given by

$$\begin{bmatrix} a_{11}(s) & a_{12}(s) & a_{13}(s) \\ a_{21}(s) & a_{22}(s) & a_{23}(s) \\ a_{31}(s) & a_{32}(s) & a_{33}(s) \end{bmatrix} \begin{bmatrix} \beta \\ \phi \\ r \end{bmatrix} = \begin{bmatrix} 0 \\ 0 \\ N_\delta \delta \end{bmatrix} \quad (9-20)$$

the $a_{32}(s)$ off-diagonal term could be removed from the effective vehicle equations of motion by letting δ equal

$$\delta = \frac{a_{32}(s)\phi}{N_\delta} \quad (9-21)$$

Attempts to decouple vehicle modes of motion in this direct additive (or subtractive) fashion do not have as widespread application in flight control as one might expect because of the drastic variation of vehicle characteristics throughout the flight envelope. However, there are instances in which deliberate crossfeeds of the type illustrated above can be used with great success.

In feedback system terms the specification of desirable closed-loop characteristics requires the definition of several desired closed-loop transfer functions, $H_1(s)$. For the single-sensor-loop control system shown in Fig. 9-6 such a specification implies that the system output and command be related by

$$C(j\omega)_{\text{desired}} = H(j\omega)R(j\omega) \quad (9-22)$$

over a limited range of frequency.

The actual output for this system is

$$C(j\omega) = \frac{G(j\omega)}{G_F(j\omega)[1 + G(j\omega)]} R(j\omega) + \frac{G\delta_2(j\omega)}{1 + G(j\omega)} \mu(j\omega) + \frac{G(j\omega)}{G_F(j\omega)[1 + G(j\omega)]} \eta(j\omega) \quad (9-23)$$

where $G(j\omega)$ is the open-loop transfer function $G_a(j\omega)G_{\delta_1}(j\omega)G_{\delta_2}(j\omega)G_f(j\omega)$. An "error," ϵ , can be defined which measures the degree to which the actual system approximates the desired system.

$$\begin{aligned} \epsilon(j\omega) &= C(j\omega)_{\text{desired}} - C(j\omega) = H(j\omega)R(j\omega) - C(j\omega) \\ &= \left\{ H(j\omega) - \frac{G(j\omega)}{G_F(j\omega)[1 + G(j\omega)]} \right\} R(j\omega) - \frac{G\delta_2(j\omega)}{1 + G(j\omega)} \mu(j\omega) \\ &\quad - \frac{G(j\omega)}{G_F(j\omega)[1 + G(j\omega)]} \eta(j\omega) \end{aligned} \quad (9-24)$$

If no disturbances were acting ($\mu = \eta = 0$), the error in approximating the desired system by the actual system could be reduced to zero by designing the open-loop transfer function to be

$$G(j\omega) = \frac{G_F(j\omega)H(j\omega)}{1 - G_F(j\omega)H(j\omega)} \quad (9-25)$$

Tailoring the system to match this formula would, in principle, implicitly satisfy the flight control function of providing "good response to specified inputs." Unfortunately, Eq. 9-25 is only of qualitative value in flight control applications. This is due to the fact that disturbances are ignored in its formulation, and the equality is difficult to attain when $G_F(j\omega)$ and $H(j\omega)$ are only moderately variable while $G(j\omega)$ can vary between wide extremes.

In place of this direct, or "calibrated," approach most of the specific functions of flight control systems are accomplished by the "swamping"

action provided by feedback over limited regions of frequency by making $|G(j\omega)| \gg 1$. In addition, the specific flight control functions involving suppression of external disturbances, minimization of effects of system component variation, linearization, etc., are all obtained in an approximate way using the same conditions, i.e., $|G(j\omega)| \gg 1$ over the frequency ranges where these effects are important. Consequently, a set of limiting, ideal specifications on the overall flight control system would include:

1. $G(j\omega) \gg 1$
 2. $\frac{G(j\omega)}{G_f(j\omega)[1 + G(j\omega)]} \doteq H(j\omega)$
 3. $\frac{G(j\omega)}{G_f(j\omega)[1 + G(j\omega)]} \ll 1$
- $\left. \begin{array}{l} \text{Over the frequency range for which} \\ \text{the desired } H(j\omega) \text{ is to be closely} \\ \text{approximated and/or over the fre-} \\ \text{quencies at which } \mu(j\omega) \text{ and } R(j\omega) \\ \text{have substantial frequency components.} \end{array} \right\}$
 $\left. \begin{array}{l} \text{Outside the frequency region in which} \\ \text{the major frequency components of the} \\ \text{input and/or external disturbances} \\ \text{occur.} \end{array} \right\}$

The first and second conditions reflect the regulation (suppression of external disturbances) and servomechanism (development of an output which is a specified function of a command) aspects of the problem. The third condition minimizes the effects of internal disturbances to the extent possible without detracting seriously from the system's action as a servo or regulator. It is possible, depending upon the frequency content of the command signals and the external and internal disturbances, for the several conditions to be in conflict. In flight control systems, however, a reasonable compromise is ordinarily attainable.

The internal disturbances, $\eta(j\omega)$, lumped at the error point in Fig. 9-6 are not substantially reduced by feedback action (although the third condition above reduces their effect outside the frequency region where feedback operation is dominant). Therefore, these should be reduced to a minimum relative to the input, especially over the frequency range in which H is to be closely approximated. In practice, this reduction is accomplished primarily by detailed mechanizational considerations.

For control systems as a general class, techniques to synthesize mathematically an approximation to the conditions enumerated above range from elementary repetitive analyses to sophisticated exercises employing constraints and resulting in "optimal" systems (approximations to H) which meet specified criteria.* In general the more sophisticated synthesis techniques are best suited to problems where the characteristics (e.g., power spectral and cross spectral densities) of the commands and disturbances are known, where considerable latitude is allowable in the form of the open-loop transfer function, and where the controlled-element characteristics are no more than moderately variable. Unfortunately none of these conditions are present in most flight control problems to any appreciable extent. Instead, the many types of signals encountered are usually difficult to define in sufficiently general terms, and the dynamic dominance of the vehicle places severe restrictions on physically reasonable forms for the closed-loop transfer function. Consequently the emphasis in practical synthesis activities is heavily centered on an attempt to provide suitable control and stabilization for a wide range of vehicle dynamics in the presence of a large variety of command and disturbance signals. For this kind of problem intelligent repetitive analysis is usually the most suitable synthesis procedure. Regardless of the detailed procedure used, the basic question as to desirable forms for H and $G_f H$ must somehow be resolved. Certain very general aspects of this question deserve discussion here.

As noted, the functions of flight control systems involving regulation, or suppression of external disturbances, require an open-loop transfer function, G , which is large over the disturbance bandwidth. Similarly, the desire to cut off internal disturbances outside the command frequency band of interest requires G to be small at higher

*See, for example, Bryson, A., "Applications of Optimal Control Theory in Aerospace Engineering," J. Spacecraft and Rockets, May 1967, pp. 545-553, and Rynaski, E. G. and R. F. Whitbeck, The Theory and Application of Linear Optimal Control, AFFDL-TR-65-28, Jan. 1966.

frequencies. The desired closed-loop transfer function, $G_F H$, which is approximated by the actual closed-loop transfer function, $G/(1+G)$, can thus be seen to be basically that of a low pass filter.*

The three regions of interest, defined in terms of $|G(j\omega)|$, which shed light on the desired low pass form for $G_F H$ are:

$$\begin{aligned} |G(j\omega)| &>> 1 & , & \frac{G}{1+G} \doteq 1 \\ |G(j\omega)| &<< 1 & , & \frac{G}{1+G} \doteq G \\ |G(j\omega)| &= O(1) & , & \frac{G}{1+G} \end{aligned} \quad (9-26)$$

Since G itself is, in general, a low pass transfer function above some frequency, the first two relations satisfy the spirit of the desirable conditions enumerated above. The crux of the matter occurs, of course, in the crossover region about frequencies where $|G(j\omega)| \doteq 1$. The behavior of $G/(1+G)$ in this region defines the dominant modes of the closed-loop response, or their frequency domain correlates of bandwidth, peak magnification, etc. Consequently, the major part of the system closed-loop dynamic behavior is implicit in what goes on when $|G(j\omega)| = O(1)$. G and $G/(1+G)$ are so closely interconnected in this region that both ordinarily require consideration. At this point, gross general considerations must cease, and we must become more specific about system and element details.

9.5 BASES FOR COMPROMISE IN SELECTING CROSSOVER REGION

Considering Fig. 9-6, it is an easy task to find the closed-loop transfer function $G(s)/[1+G(s)]$ once $G(s)$ is given (the subject of

* $G/(1+G)$ does not necessarily possess a low pass nature all the way to zero frequency when only the vehicle short period modes are to be controlled. Even in these cases, however, the desire is still to have a low pass closed-loop system within and above the short period frequency regions.

Chapter 3). The dominant modes of the closed-loop system are also easy to find in these circumstances. On the other hand, it is often difficult to specify what the characteristic frequencies of the dominant modes should be. In terms of closed-loop frequency response, this last statement is equivalent to noting that the bandwidth is difficult to specify with any degree of precision. (Bandwidth is that frequency at which $|G(j\omega)/[1 + G(j\omega)]|_{dB}$ is down -3 dB from the low frequency value, usually zero dB when the closed-loop system is low pass.) Bandwidth is closely related to the crossover frequency (frequency at which $|G(j\omega)| = 1$) and is also a crude measure of the undamped natural frequencies and/or inverse time constants of the dominant modes. So, even though the latter quantities are actually of principal interest, the following discussion shall use all of these terms loosely as if they were more or less interchangeable.

The root of the difficulty in deciding upon a closed-loop bandwidth requirement stems from incomplete knowledge of the inputs and disturbances. Consequently, uncertainty exists about just how far in frequency the inequality $|G(j\omega)| \gg 1$ should hold in order to attain good performance in response to commands and suppression of disturbances. On the other hand, the total frequency range over which $|G(j\omega)|$ can, or should, be made large relative to unity is restricted by considerations of stability, equalization economy, actuator-loop characteristics, and suppression of internal disturbances appearing at the input. Each of these factors is discussed in relatively general terms below to indicate the broad bases for compromise involved in bandwidth selection.

Stability Considerations. Perhaps the biggest factor involved in bandwidth selection is the general form of the open-loop transfer function $G(s)$. For example in a single-sensor-loop system, $G(s)$ is made up of two primary components, the controlled-element transfer function, $G_b(s) = G_{b1}(s)G_{b2}(s)$, and the controller transfer function, $G_a(s)G_f(s)$. The product $G_a(s)G_f(s)G_b(s)$ must be such that a stable closed-loop system is possible. When the form of $G_a(s)G_f(s)$ is fairly limited for reasons of equalization economy (see below), and a relatively unalterable form exists for $G_b(s)$, crossover can occur only in particular

frequency regions if stability is to be assured. If "good" response to, say, a step or other input is also necessary these restricted frequency regions become even further limited.

The simplest limiting case in which a bandwidth specification and stability interact occurs when the vehicle transfer function is unstable. A single-sensor-loop control system is then conditionally stable, and some minimum gain (and hence some minimum bandwidth) is necessary if stability is to be achieved.

For systems containing a stable vehicle as an element, or for loops which do not require a stable closure (e.g., inner loop of a multi-axis flight control system), a theoretical minimum bandwidth does not exist. However, the regions in which gain crossovers consistent with stability and reasonable transient response can occur can be defined within narrow limits. For a system to be neutrally stable (i.e., have closed-loop poles on the imaginary axis of the s-plane), the open-loop transfer function must satisfy either

$$\left. \begin{array}{l} |G(j\omega)| = 1, \quad \angle G(j\omega) = -\pi \\ |G(j\omega)| = 1, \quad \angle G(-\sigma) = -\pi \end{array} \right\} \begin{array}{l} \text{for some value of } \omega, \text{ or} \\ G(0) \text{ positive} \end{array} \quad (9-27)$$

for $\sigma = 0$. Most of the transfer functions encountered in flight control applications can be adjusted to avoid either neutrally stable or unstable dominant modes simply by making

$$\begin{array}{ll} |G(j\omega)| < 1 & \text{when } \angle G(j\omega) = -\pi \\ \text{and } \angle G(j\omega) > -\pi & \text{when } |G(j\omega)| = 1 \end{array} \quad (9-28)$$

These are the common conditions of positive gain margin and phase margin, respectively. These simple statements always apply for minimum-phase transfer functions. Equivalent simplified conditions may be delineated for any given transfer function form by starting with the Nyquist

criterion, defining new gain and phase margins and modifying Eq. 9-28, etc., as appropriate for the particular system. For a given system the derived gain margin and phase margin conditions define a maximum bandwidth (crossover frequency).

Compatibility with requirements for stable closure can also be inferred from the general slope characteristics of the open-loop amplitude ratio, $|G(j\omega)|$, in the crossover region. This follows from the well-known relationships existing between amplitude ratio and phase. The phase angle of a minimum phase transfer function, at a frequency ω_c , in terms of the slope of the amplitude ratio is

$$\begin{aligned} \varphi(\omega_c) = & \frac{\pi}{40} \left[\frac{d|G(\omega)|}{d\left(\ln \frac{\omega}{\omega_c}\right)} \right]_{\omega=\omega_c} \\ & + \frac{1}{2\sigma\pi} \int_{-\infty}^{\infty} \left\{ \frac{d|G(\omega)|}{d\left(\ln \frac{\omega}{\omega_c}\right)} - \left[\frac{d|G(\omega)|}{d\ln \frac{\omega}{\omega_c}} \right]_{\omega=\omega_c} \right\} \ln \coth \frac{\left| \ln \frac{\omega}{\omega_c} \right|}{2} d\left(\ln \frac{\omega}{\omega_c}\right) \end{aligned} \quad (9-29)$$

where the slopes, $dG/d[\ln \omega/\omega_c]$ are expressed in dB/decade.* The $\ln \coth |\ln(\omega/\omega_c)|/2$ term in the integral, shown in Fig. 9-10, applies a large weighting to slope change in the immediate vicinity of ω_c . Consequently the phase at ω_c is affected primarily by the local dB amplitude ratio slope (the first term in the expression) and local changes in this slope (the integral term). If the dB amplitude ratio

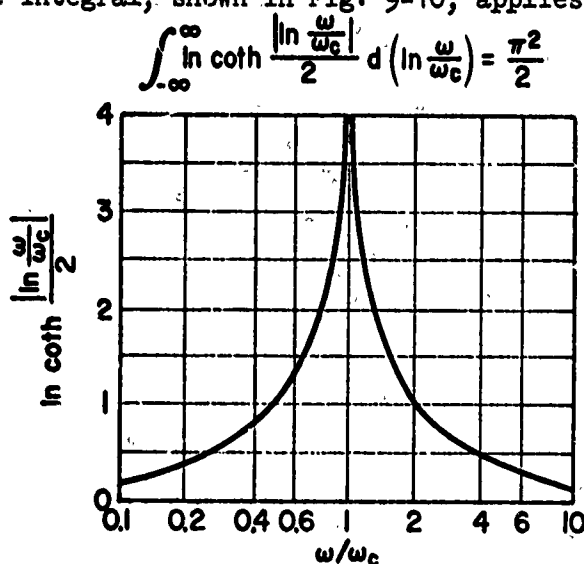


Figure 9-10. Weighting Function in Phase Integral

*Bode, H. W., Network Analysis and Feedback Amplifier Design, D. Van Nostrand Company, Inc., New York, 1945.

slope is essentially constant over a wide region about ω_c , the expression reduces to the first term only. For low pass open-loop transfer functions the amplitude ratio slope at gain crossover is negative, so a positive phase margin can exist only when $d|G(j\omega)|_{dB}/d(\ln \omega/\omega_c)$ in the immediate region is less (numerically) than -40 dB/decade, and the local changes in slope are moderate. Consequently, the available crossover regions for most transfer functions are confined to areas where the local amplitude ratio slope fulfills these conditions, and the possible bandwidths are restricted accordingly.

When a reasonable margin of stability and/or good transient response is to be provided, the frequencies of possible gain crossover are still more limited. For instance, when phase margin is viewed as a measure of stability margin alone (ignoring for the moment its interpretation as a measure of response and other qualities) a minimum phase margin specification of 35 deg to 40 deg results in both a maximum possible bandwidth specification (for a given system), and in relatively restricted regions of possible crossover. In terms of the implications of Eq. 9-29 such phase margins can be interpreted as limiting the crossover frequency to regions where the amplitude ratio slope is approximately -20 dB/decade. These limitations on crossover regions may be quite gross, but the main point of the present argument is that they do exist.

Equalization Economy. In its narrowest sense, series equalization is the process of modifying signals derived from sensors and presenting these modified signals to actuation devices. Physically the equalization elements form the connecting links between sensors and actuators; and they establish the form of the dominant low frequency cause/effect relationships between vehicle output motions sensed and control actions imposed upon the vehicle. Equalization thus reflects directly into the possible forms for $G_f(s)$ and $G_a(s)$, at least in the sense that the product $G_a G_f$ is the means by which a control action, proportional to some function of vehicle output quantities, is applied to the vehicle. Practical considerations impose limitations on the types of operational functions derivable from a given sensor. Examples are: equipment complexity; the ratio maximum-signal:minimum-increment-of-control

("dynamic range"); noise amplification, especially as it affects saturation in subsequent elements; etc. Ordinarily such factors restrict equalization generation (per sensor) to no more than integral, proportional, and rate signals. Thus, if the single-sensor-loop control system of Fig. 9-6 should contain only one sensor, the low frequency form of $G_a(s)G_f(s)$ is fairly well restricted to

$$G_a(s)G_f(s) \doteq \frac{K_C}{s} + K_C + K_C s \quad (9-30)$$

Sensor and actuator dynamics, as well as high frequency lags from the equalization elements, will be present in more precise mathematical descriptions of $G_a G_f$, but the above form serves to establish an upper limit on total equalization.

The primary role of equalization is to modify the transfer function $G(s)$ in a fashion calculated to provide "good" closed-loop dominant modes. As the means to this end, equalization elements may be employed to raise low frequency $|G(j\omega)|$ levels to approximate the conditions $|G(j\omega)| \gg 1$ over a desired frequency band, and also to modify the form of $G(s)$ in the crossover region such that "good" dominant closed-loop modes result. Therefore, equalization can be an important factor in the crossover and bandwidth limitations imposed by stability considerations.

None of these comments are news to anyone even remotely aware of elementary servo theory, but the point of the discussion—that total form of equalization available is often narrowly limited by practical considerations—still needs to be emphasized.

Actuator-Loop Characteristics. The actuation element, so blithely dismissed thus far as an inner loop, must often contend with a wide variety of nonlinearities and disturbances, as well as bewildering dynamic effects occasionally inherent in the elements themselves. Because of the difficulty encountered in coping with the physical realities imposed upon the actuation loop, many experienced flight control designers steadfastly believe that a sound solution of the

actuation problem is the real secret to an ultimately successful design.

In general terms, the suppression of load disturbances (Fig. 9-3) within the actuator loop demands that the open-loop amplitude ratio for this loop be large over a wide range of frequencies. Further, the closed-loop dynamics of the actuator loop are generally a predominant factor in setting the outer loop crossover to some value consistent with overall flight control system stability. On the basis of both these considerations, the bandwidth of the actuator loop should be as large as possible.

There is, of course, another side to the coin. Perhaps the easiest to see is the general effect of internal disturbances at the actuator loop input on practical elements contained within this loop. To illustrate this point, consider as a gross approximation that the closed-loop actuator dynamics have a form similar to that of the ideal low pass filter characteristics shown in Fig. 9-11. A system possessing these

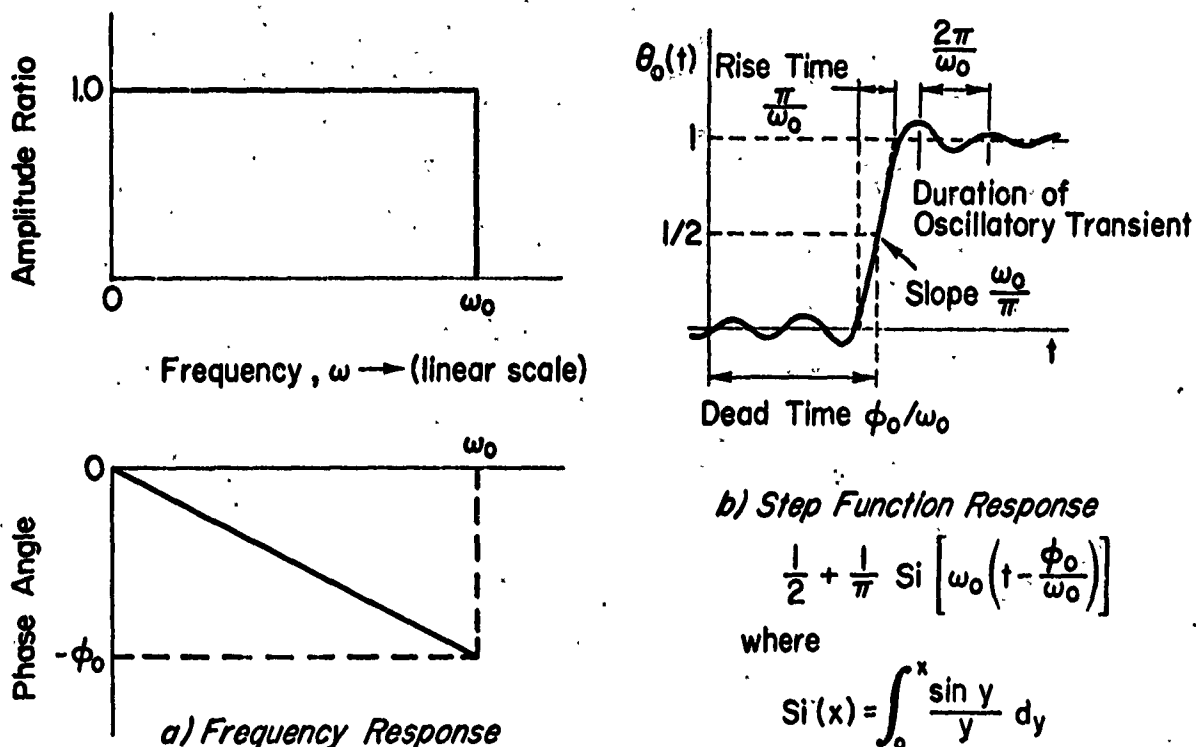


Figure 9-11. Response of the Ideal Low Pass Filter

characteristics would pass all signals without attenuation up to a frequency of ω_0 ; and the phase angle between an input sine wave and the steady-state sinusoidal output at the same frequency would vary linearly with frequency from zero to a maximum lag of ϕ_0 at ω_0 . These properties are, of course, unrealizable in a nonanticipatory device, as is made obvious by the initiation of the output response prior to the onset of the step input. Note, however, that neither the frequency response nor the transient step response is very far from approximating the characteristics of practical servomechanisms.

If the frequency response characteristic shown is obtained from a closed-loop control system, the simplification that the open-loop transfer function is very large for frequencies less than ω_0 and very small at higher frequencies is obvious. Thus, if the frequency content of actuator command and actuator load disturbance signals shown in Fig. 9-2 is largely composed of frequency components less than ω_0 , the system would be satisfactory in both its servo and regulator functions. In this sense the actuation system would have very high integrity indeed.

Now, assume that the flight control system internal disturbances presented at the input of the actuator loop, η_a , can be represented by a constant power spectral density, $\phi_{\eta\eta}$, over the actuator loop bandwidth. The mean-squared actuator output due to the internal disturbance input will then be given by*

$$\begin{aligned}\overline{\delta^2} &= \lim_{T \rightarrow \infty} \frac{1}{2T} \int_{-T}^{+T} \delta^2(t) dt \\ &= \frac{1}{2\pi} \int_0^{\infty} \phi_{\delta\delta}(\omega) d\omega \\ &= \frac{\phi_{\eta\eta}}{2\pi} \int_0^{\omega_0} d\omega = \frac{\phi_{\eta\eta}\omega_0}{2\pi}\end{aligned}\tag{9-31}$$

*See Chapter 10.

Eq. 9-31 indicates that this undesired mean-squared output increases directly with the bandwidth, ω_0 . Since the signals within the actuator loop are directly related to the output, these signals will also increase more or less proportionately to the actuator closed-loop bandwidth. Saturation, however, invariably occurs in one or more of the actuation loop elements, so an increase in the general signal levels within the loop will unavoidably result in more saturation occurrences per unit time. In the limit, of course, this can become bad enough to almost entirely remove any connection between the actuator output and its command input.

We have remarked previously that the effects of unwanted signals appearing at the input of the overall system are seldom deleterious in a good design, although the same effects mentioned here may exist in principle. The significant differences in this regard between the actuator and outer loops are that actuator loop bandwidth is an order of magnitude or more higher than those of the outer loops; and the relative magnitude of command and disturbance signals occurring at the actuator loop inputs are much more comparable.

Another physical effect directly related to that discussed above is the increase, with actuator bandwidth, in the power and energy required by the actuator to perform its totally useless task in following the unwanted disturbances.

Other practical points mitigating against indefinite extension of actuator loop bandwidth are the economic, weight, size, and reliability costs paid for extremely high dynamic performance devices operating at high power levels, and the almost inevitable troubles encountered due to higher order dynamic modes. The latter may stem from either the vehicle dynamics or the actuator load dynamics.

All of the above discussion is intended to lead to the conclusion that actuator loop bandwidth should be as low as possible, consistent with suppression of actuator loop disturbances, effective linearization of nonlinearities, and outer loop stability and dynamic performance.

Effects of Noise at the Input. As noted above, the argument for restricted actuator loop bandwidth can be made in principle for the outer loop. To the extent that this argument applies, one conceptual basis for bandwidth selection as a tradeoff is apparent. The competition involved would exist between command or input signals, $R(s)$, and internal disturbances, $\eta(s)$, (Fig. 9-6) and the tradeoff would be made between response to commands and suppression of external disturbances on the one hand, and the reduction of errors due to the internal disturbances on the other. This basis of compromise is seldom of much consequence in flight control systems since the scaling of desired signals relative to unwanted signals acting at the input can usually be made very large with careful design.

Summary of Compromises in Selecting Crossover Region. With equalization restricted to the reasonable forms noted, all of the discussion indicates that the bandwidth, ω_b , of the closed-loop transfer function, $G(s)/[1+G(s)]$, is often not a very independent parameter. Instead, it is ordinarily restricted in value by vehicle or actuator characteristics which may be relatively unalterable. This feature of flight control systems is quite different from many other servomechanism devices. It can possibly be avoided by the introduction of extensive equalization and by efforts to extend the bandwidth of sensors and actuators. But this can be accomplished only by some degradation in performance, an increase in overall cost and unreliability, and a liberal education in the almost inevitable troubles encountered with higher order modes. Thus the general conclusions of this section may be summarized as:

1. $|G(j\omega)/[1+G(j\omega)]| \doteq 1$ for $\omega < \omega_b$
2. $|G(j\omega)/[1+G(j\omega)]| \ll 1$ for $\omega \gg \omega_b$
3. ω_b must be great enough to control and/or stabilize the vehicle modes for which automatic control is desired; and, in any event, cannot be made significantly larger without exchanging the increased bandwidth for trouble.
4. Ranges of ω_b are essentially fixed by open-loop transfer function and stability considerations, at values which result in good closed-loop system stability.

9.6 SPECIFICATIONS AND TESTING

The reader will recall from the discussion at the beginning of this chapter that we proposed to defer consideration of the methods for determining the command and disturbance environment characteristics and the methods for assessing the dynamic performance until Chapter 10. We turn instead to a very brief description of the methods employed in the detailed study of a selected system.

Consider a case in which several competing flight control systems have been evolved on a block diagram basis and the performance and design qualities of these systems have been assessed. One of them is then selected as having the best combination of desirable qualities. It is subject to detailed study. Detailed study of the selected system, evolved from the preliminary design process, actually involves a series of increasingly realistic tests which attempt to thoroughly wring out the system in both normal and abnormal operating conditions. The purpose of all this testing is to insure, insofar as possible, that when the equipment is put into service, it will not have any surprises left for its designers and builders. Surprises occur when some mode or condition of operation has been overlooked or when the assumptions used in constructing the mathematical models of the system elements are invalid.

Very likely the first model of the system will have been based on linearized descriptions of the system elements including the perturbation equations of motion of the airframe written with respect to straight and level flight. Among the first checks to be made concern the effects of small parasitic nonlinearities in the elements of the system. This may be done on an individual and approximate basis by analytical means, but anything approaching a comprehensive study of the effect of multiple nonlinearities in the elements of the system is, of necessity, accomplished through simulation. Even before any hardware is built, estimates may be made of the characteristics of, for example, amplifier saturation, sensor thresholds, control system friction, and mechanical hysteresis, and these may be "mechanized" on a computer together with the other elements of the

system so as to permit the evaluation of performance in the presence of the system element nonlinearities.

It is next necessary to consider the performance of the system for motions which are no longer "small," and possibly also to relax the assumption of the airframe as a rigid body. Some facets of the subject of "large" motions and elastic modes are covered in the reports and papers listed in the bibliography at the end of this book. These references, however, may represent only an introduction to some of the difficulties of a specific system, and, again, the performance of the system in high climb or dive angles, at large bank angles, or in rapid rolls is usually studied by means of simulation. For this purpose the six degree of freedom equations with nonlinear aerodynamic terms, functions of several variables, are mechanized on a computer and often several elastic modes are also included in the simulation.

If, at this point, the system and its elements still show satisfactory performance, consideration may be given to the construction of prototype hardware. In general, the equipment may evolve through several stages, such as the breadboard model, the flight-worthy prototype, the preproduction model, and finally the production model. At each stage the equipments are subjected to tests as components and are assembled for tests as a system. It may very well happen, however, that not all the elements are in the same state of evolution during any particular system test. Thus, for example, a breadboard control amplifier might be combined with a preproduction actuator and so on.

Each component by itself, and the system as a whole, may be required to comply with general specifications or standards. The general specification governing automatic flight control systems for piloted, naval aircraft, is: Control and Stabilization Systems—Automatic, Piloted Aircraft, General Specification for; MIL-C-18244A(WEP), Bureau of Naval Weapons, Department of the Navy, 1 December 1962. This specification makes reference to 26 other specifications and 4 standards. These are listed by way of illustration in Table 9-3. The roughly corresponding specification for U. S. Air Force aircraft flight control systems is: Flight Control Systems—Design, Installation, and Test of, Piloted

Aircraft, General Specification for; MIL-F-9490C(USAF), Systems Engineering Group, Wright-Patterson Air Force Base, United States Air Force, 13 March 1964. This specification refers to 63 related specifications and 18 standards.

Many of the applicable specifications prescribe specific tests, such as the radio noise interference tests, the environmental tests, including vibration, altitude, sand and dust, humidity, high and low temperature and salt spray. Otherwise, each component and the system as a whole, insofar as is practical, is subjected to tests for the purpose of determining its frequency response, loading effects, linearity, effects of saturation and saturation levels, switching transients and noise characteristics. It is further usually the case that the automatic flight control system is tested in closed-loop operation in conjunction with an aircraft control system functional test stand and a computer simulation of the vehicle equations of motion. The ground equipment required for environmental tests and the closed-loop tests with the control system functional test stand is illustrated in Fig. 9-12.

A typical test stand comprises a steel frame on which are mounted all the important elements of the actual aircraft control system. It includes the complete control surface actuating system, pilot's seat, cockpit controls, and artificial feel devices. Stick forces which would appear in response to motion, such as those which might be produced by a bobweight, are applied by a force servo driven by the computer. Any automatic control equipment to be tested is installed on the control test stand in a manner representing, as closely as possible, the installation in the actual aircraft. Simulated aerodynamic loads are applied to the control surfaces by means of mechanical or hydraulic springs and dampers.

Some elements of the pilot's display are also often included to simulate the stimuli to which the pilot responds in flight. Cockpit instrument presentations which are commonly provided include the artificial horizon, altimeter, airspeed and Mach meters, the heading indicator, possibly the turn and slip indicator, and localizer and glide slope needles. In certain applications fire control or other weapon delivery displays may also be provided.

TABLE 9-3

SPECIFICATIONS AND STANDARDS APPLICABLE TO THE DESIGN,
INSTALLATION, AND OPERATION OF AUTOMATIC CONTROL
AND STABILIZATION SYSTEMS IN NAVAL AIRCRAFT

MIL-C-18244A(WEP)	Control and Stabilization Systems: Automatic, Piloted Aircraft, General Specification for
JAN-I-225	Interference Measurements, Radio, Methods of, 150 Kilocycles to 20 Megacycles (For Components and Complete Assemblies)
JAN-T-781	Terminal; Cable, Steel (For Swaging)
MIL-F-3541	Fittings, Lubrication
MIL-S-3950	Switches, Toggle
MIL-E-4682	Electron Tubes and Transistors, Choice and Application of
MIL-W-5088	Wiring, Aircraft, Installation of
MIL-E-5272	Environmental Testing, Aeronautical and Associated Equipment, General Specification for
MIL-E-5400	Electronic Equipment, Aircraft, General Specification for
MIL-H-5440	Hydraulic System; Aircraft Type I and II, Installation and Data Requirements for
MIL-I-6115	Instrument Systems, Pitot Tube and Flush Static Port Operated, Installation of
MIL-I-6181	Interference Control Requirements, Aircraft Equipment
MIL-L-6880	Lubrication of Aircraft, General Specification for
MIL-E-7080	Electrical Equipment, Piloted Aircraft Installation and Selection of, General Specification for
MIL-M-7969	Motors, Alternating Current, 400-Cycle, 115/200 Volt System, Aircraft, General Specification for
MIL-A-8064	Actuators and Actuating Systems, Aircraft, Class A and B, Electro-Mechanical, General Requirements for
MIL-M-7793	Meter, Time Totalizing
MIL-H-8501A	Helicopter Flying Qualities, Requirements for
MIL-S-8512	Support Equipment Aeronautical, Special, General, Specification for Design of
MIL-M-8609	Motors, Direct Current, 28-Volt System, Aircraft, General Specification for Class A and B
MIL-D-8706	Data, Design; Contract Requirement for Aircraft
MIL-F-8785	Flying Qualities of Piloted Airplanes
MIL-D-18300	Design Data Requirements for Contracts Covering Airborne Electronic Equipment
MIL-N-18307	Nomenclature and Nameplates for Aeronautical Electronic and Associated Equipment
MIL-E-19600	Electronic Modules, General Aircraft Requirements for
MIL-R-22256	Reliability Requirements for Design of Electronic Equipment or Systems
MIL-R-23094	Reliability Assurance for Production Acceptance of Avionic Equipment, General Specification for
MIL-STD-203	Cockpit Controls; Location and Actuation of For Fixed Wing Aircraft
MIL-STD-704	Electric Power, Aircraft, Characteristics and Utilization of
MS15001	Fittings, Lubrication (Hydraulic) Surface Check, 1/4-28 Taper Threads, Steel, Type I
MS15002	Fittings, Lubrication (Hydraulic) Surface Check, Straight Threads, Steel, Type II

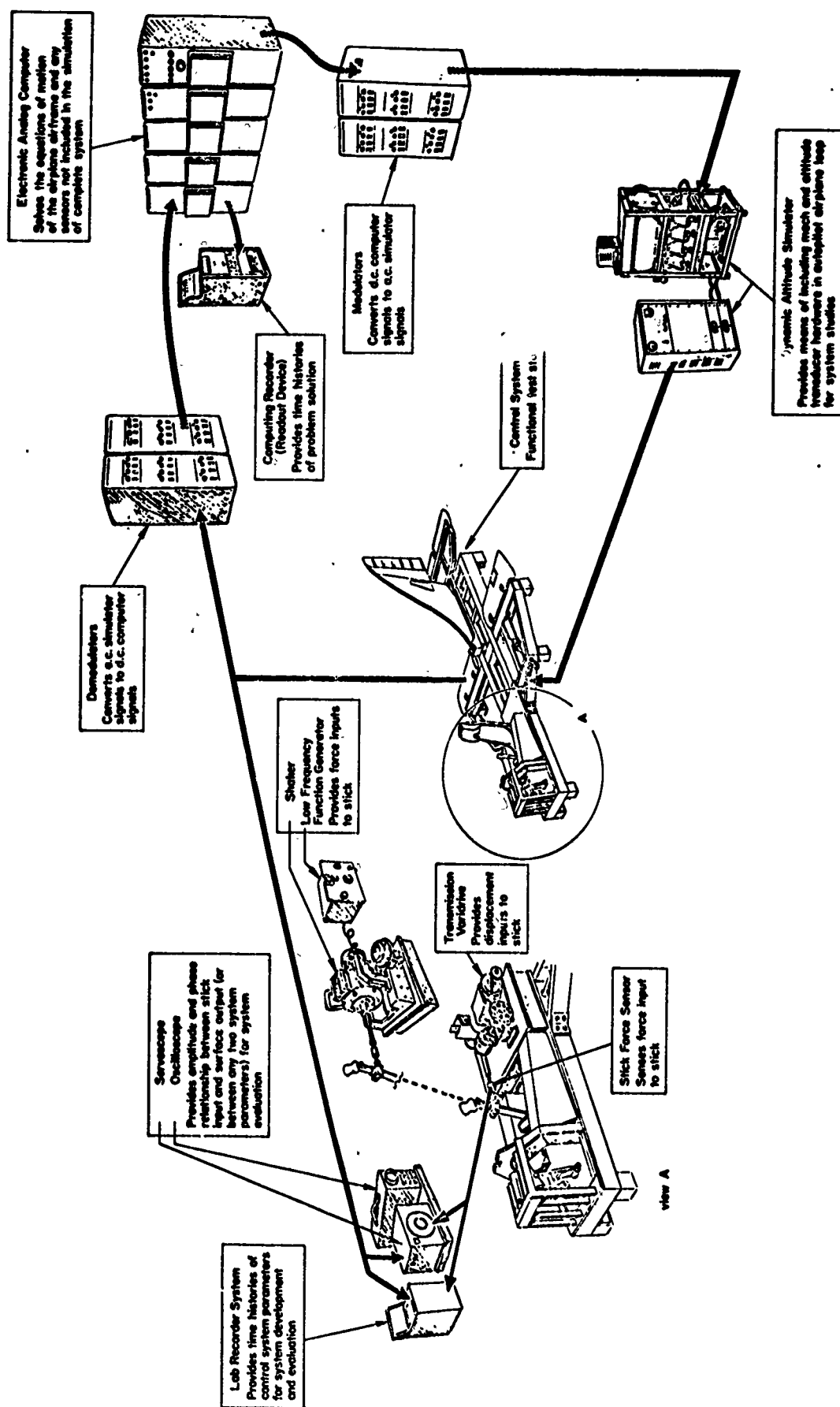


Figure 9-12. Flight Control Functional Test Stand Arrangement

Airframe dynamics are simulated on the computer. The computer inputs are voltages proportional to control surface deflections and its outputs can be voltages proportional to any or all of the airframe output quantities (motions). These voltages are then used to drive the pilot's displays, the simulated force producers, as simulated sensor inputs to the controller and for recording the responses on a recording oscillograph. Modulators, demodulators, and scale changing devices are used where necessary to change the form and level of electric signals.

The use of the test stand permits additional and more realistic tests to be conducted, especially for those modes of operation in which the human pilot plays an important role. Since the actual operating conditions of the equipment are also much more closely simulated than was the case when each component of the system was represented only by a mathematical model, the test stand provides information which might otherwise have to be obtained in flight. This serves the desirable purpose of cutting down the number of flight test hours required to tune up and wring out the automatic flight control equipment.

Another important application of the control test stand is in the investigation of the results of possible component failures. A systematic program of inducing specific failures such as mechanical malfunctions and open and shorted electrical circuits is conducted. These tests may be made both with and without the human pilot, since it is important to observe whether or not the pilot can detect the failure and can make a successful correction which does not result in dangerous motions of the airframe. In any cases in which there may be a question regarding the structural safety of the airplane, the tests on the test stand are mandatory because of the danger involved in determining the effects of component failures in flight.

Of course the test stand as it has been described above does not simulate the motion cues to which the pilot will be subject in flight. (Moving-base simulators are employed for research purposes, but they are not commonly used in flight control system development.) In fixed-base

simulation, the tests should be confined to cases in which the motion cues can be considered to be unimportant or for which fixed-base results are conservative:

At the conclusion of the test stand program the prototype equipment is installed in the airplane for ground tests. Some of the test stand tests may be repeated so as to provide assurance that the actual installation in the aircraft has not altered the nature of the test results to be obtained. It may even be desirable to perform some closed-loop tests with the computer representing the motion sensors and the dynamics of the vehicle, but with everything else being the actual equipment. An essential feature of the first tests of the flight control system in the actual vehicle, however, is the establishment of inspection test procedures for the production system. Inspection test procedures are required to insure that malfunctioning components are not installed in the airplane. In addition, many automatic flight control systems require individual adjustments after installation in the airplane to compensate for component and airplane tolerances. Procedures for accomplishing this must be developed and written in such a way as to be readily understandable by typical mechanics and technicians. Normally the procedure must be developed by cut and try and the occasion of the prototype installation is the first change to do this.

Final evaluation of the operating characteristics of an automatic flight control system is, of course, made by means of flight tests. The magnitude of the flight test program depends on the complexity of the system being tested and on the amount of ground testing which has preceded the flight tests. If a thorough flight simulation program has been carried out on the control test stand, the flight tests, with luck, may consist of very little more than verification of the results previously obtained on the ground. On the other hand it may be found that considerable development work has to be carried out during the flight test phase. This will be the case if, for example, the previously neglected motion cues for the pilot assume importance, or if previously neglected higher structural modes cause closed loop instability. It will almost certainly occur if great care is not

taken at all phases of the design to forecast and to take into account the unexpected and uncertain.

In any case many of the same aircraft input and output quantities which were recorded during the ground tests should be recorded in flight. In fact insofar as possible, some of the same tests should be repeated so as to reveal any discrepancies between the performance in the ground tests and the performance in flight. A number of additional quantities which may facilitate the analysis of system operation in the event of unexpected modes of operation should also be recorded.

It is then desirable to explore the conditions which may not have been examined in the ground tests. These might be simulated tactical situations, spins, or large scale maneuvers such as the Immelman turn sometimes used in bomb delivery. (It may have been difficult or impossible to simulate these.) Since these new test conditions may very well reveal new modes of automatic flight control system performance, some redesign or at least the adjustment of system parameters may well be called for at this juncture.

Following the successful completion of flight tests, the system design is frozen, the production design of the components is completed, detailed component test specifications are finished, and the system test specification (described above) is revised to accommodate the results of the flight test program. The design process is then, in principle, complete. Actually it will usually happen that the system design engineer may be called upon to resolve difficulties in manufacturing or in the in-service use of the automatic flight control system. The resolution of some of these difficulties may even involve new changes to component or system designs.

CHAPTER 10

INPUTS AND SYSTEM PERFORMANCE ASSESSMENT

10.1 INTRODUCTION

The elementary feedback control system concepts reviewed in the last chapter provide a basis for the view that flight control system performance "requirements," in the large, serve to define a system which will follow desired inputs, reject internal disturbances, and suppress external disturbances. There remain the inevitable questions of how well the "following," "rejecting," and "suppressing" needs to be done; and what the tradeoffs may be between the design qualities of reliability, weight, power demands, cost, etc., and the dynamic performance quantities of following, rejecting, and suppressing. Further, in flight control systems the controlled element (vehicle) is not entirely unalterable, so the consequences of possible interchanges of function between controller and vehicle are also subject to tradeoff considerations. In optimization efforts, interactions between all of these considerations occur, but only the dynamic performance quantities are at first involved in the satisfaction of dynamic requirements.

The three key dynamic performance attributes in any system are stability, response, and accuracy. There are many definitions of stability, most coined to satisfy requirements of generality and mathematical rigor. For our purposes a qualitative operational definition will suffice, i.e., "if a small temporary input applied to the system in equilibrium results only in a temporary change in the output or response, the system is stable." For constant-coefficient linear systems the stability according to this definition amounts to a specification on pole location; in particular, denying all of the left half plane and the axis of imaginaries, except the origin, to the poles of stable systems. Poles at the origin are permitted in principle by appropriately defining the output or response quantity. Because stability for constant-coefficient linear systems is specified by pole location, and because the methods of analysis given heretofore

give precise pole locations, we have bypassed discussion of conventional stability criteria in this book. Stability is, of course, readily determined by any and several analytical and graphical techniques without determining the precise location of the poles. These are fundamental and well known,* so no further mention is needed here.

Once stability, relative to some operating-point, is attained in a constant coefficient linear system, a unique stable equilibrium state exists insofar as the system dynamic excursions about that operating-point are concerned. The stable equilibrium state establishes a datum from which perturbed responses may be computed and accuracy assessed. Because the equilibrium is unique, accuracy and response are closely related, with accuracy being assessed by an "error" response related directly to the difference between input and output. If the equilibrium were not unique, as might occur in a nonlinear system, the accuracy might be completely independent of the input and output response. But, for linear systems, accuracy may be considered to be just another response quantity. In view of this, response considerations are central to flight control system performance assessment. Flight control systems are subjected to both deterministic and random inputs, so responses to both categories are of interest and will be considered. To make this possible, several simplified and idealized inputs will be introduced in the first part of this chapter. These can be used with the system mathematical model to determine the output responses which serve as the bases for system dynamic's assessments. In this connection we should remark that if all the details are considered, flight control systems are so complex and of such high order that the possibility of obtaining a simple and adequate system representation might seem remote. Yet a

*The more prominent are the Routh and Hurwitz tests and the Nyquist stability criterion. For the Routh-Hurwitz criteria see, for example, D. Graham and D. McRuer, Analysis of Nonlinear Control Systems, John Wiley and Sons, Inc., New York, 1961, pp. 457-460. For a comprehensive treatment of conventional and several generalized versions of the Nyquist criterion, see D. T. McRuer (ed.), Methods of Analysis and Synthesis of Piloted Aircraft Flight Control Systems, BuAer Rept. No. AE 61-41, Mar. 1952, pp. III-2 to III-10.

simple analytical form is almost an essential for preliminary design purposes if physical understanding is to be gained rapidly, and if repetitious, ad hoc, procedures are to be minimized. Fortunately the feedbacks inherent in flight control systems usually result in a large range of frequencies over which pertinent open-loop transfer functions have magnitudes much greater than unity. As a consequence simple systems can usually be derived which serve as close approximations to the actual systems. The development of simple low order systems to approximate complex high order systems has already been illustrated with an example in Chapter 3. (See pp. 3-49 to 3-56.)

In a fundamental sense a control system, to be useful, must contend successfully with all the inputs imposed upon it. A major step in the design process is, accordingly, the identification of the type, form and general character of the input environment—followed by a detailed assessment of the more critical input-system response combinations. The critical combinations are especially important in the selection of bandwidth (the general region of crossover) and the character of the response.

Because a flight control system has many different command tasks which must ordinarily be performed over a large range of environmental conditions and mission phases, a variety of inputs must be considered. These may be classified, according to their point of entry into the system block diagram, in three general categories—command point, internal, and external. The command point inputs comprise all the flight control system command signals generated by the guidance loop or otherwise inserted directly. Some of these inputs are desired instructions for control while others are unwanted consequences of nature or the result of simplifications in the guidance system mechanization. The internal inputs are, in general, all unwanted disturbances acting primarily on the controller. They arise either from design compromise or from the operation of nature's side-effects. The external inputs are forces or moments, induced by the vehicle or the external environment, which act as disturbances upon the vehicle. Suppression of the effects due to these forces and moments constitutes the action of the flight control system as a regulator.

A fair cross-section of flight control system inputs is presented in Table 10-1. Here another classification is introduced in tabulating the inputs as a function of their analytical form. The first five entries (steps, pulses, cut-off ramps; initial conditions or impulses; gust function; power series; and periodic or repetitive functions) are all members of the deterministic class. They can all be expressed as functions of time, and used to obtain system responses as functions of time under specific circumstances. The last entry, random or nondeterministic inputs, contains two somewhat different types within the random class. The first type are time functions which are either random by their nature or so complicated that a deterministic description is impractical. The second kind are generalizations of a wide range of inputs each of which, for a specific case, could be treated as deterministic. For some purposes it is more useful to consider these signals as an ensemble and to describe the whole class of inputs by a single random composite. Both types of random inputs have characteristics which can be expressed only in statistical terms, with probability distributions replacing a precise specification of the input as a function of time.

The "random" inputs based upon generalization of an ensemble of time functions which can also be treated as deterministic, in specific particular cases, might seem, at first glance, to be of little value since their use in response calculations can only give a smoothed-over, average view of "reality." Two important points in their favor should, therefore, be noted. The first advantage can be seen directly by taking a tack opposite to the one already mentioned. A smoothed-over, average answer can, itself, be significant, especially when classes of systems are being compared. The second advantage is less obvious. It derives from the fact that a statistical view, in practice, utilizes power spectra and correlation concepts. These, in turn, provide bases for the partition of the frequency domain into regions in which either the desired or the unwanted signals are dominant, and for system design procedures which make use of the distinction. No such basis exists for distinguishing between the two when the inputs are considered as deterministic, for then the desired signal and any errors (unwanted signal) are inseparable and indistinguishable. For these reasons, several deterministic input entries in Table 10-1 also have their random counterparts.

TABLE 10-1

FLIGHT CONTROL SYSTEM INPUTS; APPLICATION POINT AND SOURCE

INPUT FORM	COMMAND POINT INPUT		INTERNAL DISTURBANCES		EXTERNAL DISTURBANCES	
	DESIRED INPUT	UNWANTED INPUTS		VEHICLE INDUCED	ENVIRONMENT	
Steps, Pulses Cut-off Ramps	Operating Point Changes (Altitude, Speed, etc.)	Errors in Operating Point Changes	Mode Switching; Power Supply Variations with Load Switching	Thrust Eccentricities; c.g. Shifts; Vehicle Asymmetries; Stores Release	Wind; Wind Shear	
Initial Conditions or Impulses		Automatic Control Engagement		Tip-off; Mechanical Shocks	Non-simultaneous Release of Restraints; Particle Impact; Shock and Blast Waves; Exit-Entry (incl. water)	
Gust Function					Discrete Gust	
Power Series	Target Motion; Terrain Variation; Programmed Operating Point Changes	Higher Order Target Motions; Errors in Operating Point Changes; Reference Drifts	Unbalanced Component Drifts	Variable Burning Rate; c.g. Shift	Wind Shear; Wind Gradient	
Periodic or Repetitive	Some Terrain Variations			Dynamic Unbalance; Gun Firing; Vibration; Flutter; Reference Coordinate Rotation	Ambient Fields (orbital motion only)	
Random	Generalization of Target Motions; Generalization of Terrain Variations; Generalization of Step-pulse Sequences	Generalization of Higher order Target Maneuvers; Geometry-target Noise (Scintillation, Beam Reflection, etc.); Guidance System Internal Noise; Generalization of Errors in Step-pulse Sequences	Power-supply Fluctuations; Sensor Noise; Local Flow Changes on Control Surfaces; Electrical Noise	Vibration; Buffeting; Acoustic Noise; Random Variations in Burning Rates	Random Variations in Ambient Fields; Gusts and Turbulence	

In succeeding sections of this chapter the more critical input types given in Table 10-1 will be summarized and, in some cases, idealized into special "equivalent" forms which depend on only one or two parameters.

The initial discussion deals with the deterministic forms and with the response of linear systems to deterministic inputs. This proceeds quickly since no new mathematical techniques are required beyond those already exposed in Chapter 2.

The third section of this chapter is devoted to a presentation of the methods of describing random functions of time. This requires some new mathematics and the development of the connections between the statistical descriptors and behavior in the time domain. It is followed by the discussion, in detail, of the analytical description of some special random functions of time useful for the representation of flight control system inputs, and further by a discussion of the properties of the very practically important class of random processes with Gaussian amplitude distributions.

Methods for calculating the response of linear systems to random inputs are treated next, and the chapter concludes with two simple examples of the application of these methods.

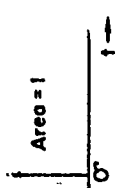
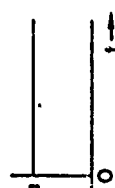
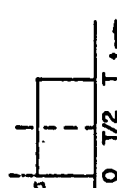


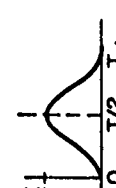
10.2 RESPONSE TO DETERMINISTIC INPUTS

Deterministic inputs listed in Table 10-1 include steps, pulses, impulses, cut-off ramps, power series, periodic functions, and a special function used to characterize a discrete gust. The type of time variation and the time domain and Laplace transform descriptions for the simpler of these functions are summarized in Table 10-2. Most of them are familiar.

The special function used to approximate a discrete gust, shown in Table 10-2, is made up of a step and a cosine wave, both cut off after one period of the cosine function (Fig. 10-1). The gust function is defined as:

$$x(t) = \begin{cases} \frac{k}{T} \left(1 - \cos \frac{2\pi t}{T} \right) ; & 0 \leq t \leq T \\ 0 ; & t > T \end{cases} \quad (10-1)$$

TABLE 10-2
SUMMARY OF SIMPLE TRANSIENT DETERMINISTIC INPUT CHARACTERISTICS

INPUT FORM	TIME CHARACTERISTICS	ANALYTICAL DESCRIPTIONS					
		Time Domain		Laplace Transform		Energy Spectrum	
		Exact	Approximate	Exact	Approximate	Exact	Approximate
Impulse		$\delta(t)$	—	1	—	1	—
Step		$au(t)$	—	$\frac{a}{s}$	—	$\frac{a^2}{\omega^2}$	—
Square pulse		$a[u(t) - u(t-T)]$ $u(t-T) = \begin{cases} 0, & t < T \\ 1, & t > T \end{cases}$	$au(t - \frac{T}{2})$	$\frac{a}{s}(1 - e^{-Ts})$	$aTe^{-Ts}/2$	$\frac{a^2}{\omega^2} 2(1 - \cos T\omega)$	$(aT)^2$
Cutoff ramp		$\frac{a}{T}[u(t) - (t-T)u(t-T)]$	$au(t - \frac{T}{2})$	$\frac{a}{Ts^2}(1 - e^{-Ts})$	$\frac{a}{s} e^{-Ts}/2$	$\frac{a^2}{T^2 \omega^4} 2(1 - \cos T\omega)$	$\frac{a^2}{\omega^2}$
Exponential		$au(t)e^{-t/T}$	—	$\frac{a}{s + 1/T}$	—	$\frac{(aT)^2}{1 + T^2 \omega^2}$	—
Gust function		$\frac{K}{T}(1 - \cos \frac{2\pi t}{T})$ $0 \leq t \leq T$	$K\delta(t - \frac{T}{2})$	$\frac{K(2\pi)^2}{T^3} \frac{(1 - e^{-Ts})}{s[s^2 + (\frac{2\pi}{T})^2]}$	$Ke^{-Ts}/2$	$\left(\frac{2\pi}{T}\right)^4 \left(\frac{K}{T}\right)^2 \left\{ \frac{2(1 - \cos T\omega)}{\omega^4} - 2\left(\frac{2\pi}{T}\right)^2 \omega^2 + \left(\frac{2\pi}{T}\right)^4 \right\}$	K^2

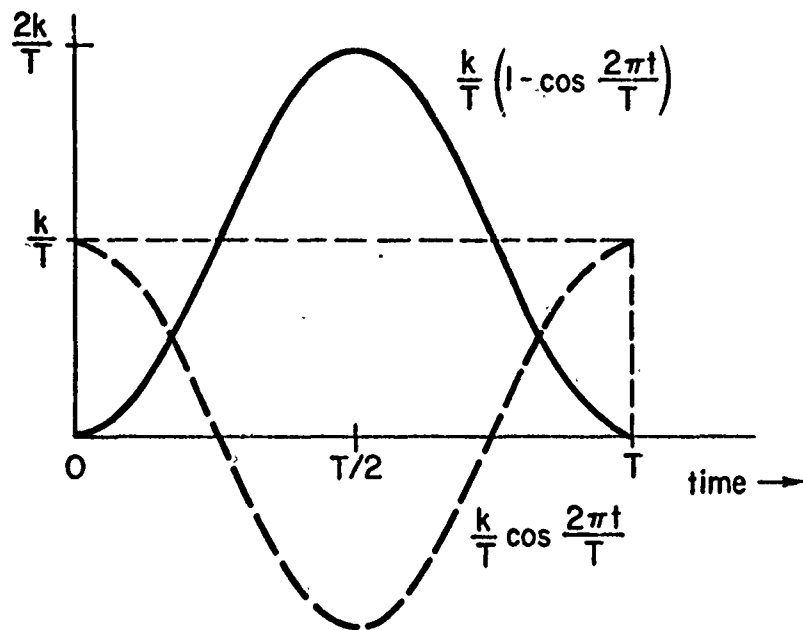


Fig. 10-1. Unit Area Gust Function

This form of gust description is intended to account for a gust gradient with a gradual buildup. The proportionality constant, k , can be selected to adjust the magnitude of the gust to any desired value. For aeronautical applications the gust length, T , is ordinarily taken to be equivalent to 25 chord lengths, so:

$$T = \frac{25c}{U_0} \quad (10-2)$$

As a Laplace transform, the discrete gust input becomes:

$$\begin{aligned} x(s) &= \frac{k}{T} \left[\frac{1}{s} - \frac{s}{s^2 + \left(\frac{2\pi}{T}\right)^2} \right] (1 - e^{-Ts}) \\ &= \frac{(2\pi)^2 k}{T^3} \frac{(1 - e^{-Ts})}{s \left[s^2 + \left(\frac{2\pi}{T}\right)^2 \right]} \end{aligned} \quad (10-3)$$

It will be noted that the table gives approximations for square pulses, cut-off ramps, and the gust function in terms of delayed impulses and steps. These approximations follow from reasoning which shall be illustrated for the pulse. The Laplace transform for the square pulse function is:

$$\begin{aligned}\mathcal{L}[\text{Square Pulse}] &= \frac{a}{s} (1 - e^{-Ts}) \\ &= \frac{a}{s} \left\{ 1 - \left[1 - Ts + \frac{(Ts)^2}{2} - \frac{(Ts)^3}{3!} + \dots \right] \right\} \quad (10-4)\end{aligned}$$

If the system's dominant modes are characterized by inverse time constants and undamped natural frequencies which are small when compared with $1/T$, then the higher order terms in the series for e^{-Ts} will make only minor contributions to all but the very first portion of the system's time response. So, carrying the exponential series only to terms in s^2 :

$$\begin{aligned}\mathcal{L}[\text{Square Pulse}] &\doteq \frac{a}{s} \left\{ Ts \left[1 - \frac{(Ts)}{2} \right] \right\} \\ &\doteq aTe^{-Ts/2} \quad (10-5)\end{aligned}$$

Thus the square pulse can, therefore, be replaced, under the conditions noted, by an impulse having strength equal to the area under the pulse and applied at a time $t = T/2$.* System response calculations for the square pulse, and cut-off ramp, and gust function inputs can thus be approximated simply by moving the time origin for impulse and step responses back from zero to $-T/2$ seconds. The approximations to output responses obtained in this way will range from very good when $t \gg T/2$, to very poor for $t < T/2$ (where the approximate responses are zero). The adequacy of the approximation for time values between $T/2$ and $t \gg T/2$ depends, as noted, upon the relative values of the system dominant mode characteristic and T . When the characteristic frequencies (inverse time constants and/or undamped natural frequencies) of the dominant modes are five or more times greater than $1/T$ the mid-range approximation ($t > T$) for the response is ordinarily quite satisfactory. The approximations improve as t becomes very large relative to $T/2$ regardless of the relationships between dominant mode characteristics frequencies and $1/T$. The fact that the initial parts of the responses to the

*For a more detailed justification of this approximation see, for example, J. L. Bower and P. M. Schultheiss, Introduction to the Design of Servomechanisms, John Wiley and Sons, Inc., New York, 1958.

approximating input forms are very poor approximations to actual system outputs is of no great consequence. Instead of using the approximating input forms, the responses in the time period from $t = 0$ to T can be found exactly by using a step for the square pulse, a ramp function for the cut-off ramp input, and the initial portion of a continuous $1 - \cos 2\pi t/T$ wave for the gust function.

To the extent that the approximations given above hold for the square pulse, cut-off ramp, and gust function inputs, systems subjected to the inputs given in Table 10-2 can be assessed by their step and impulse responses, i.e., by their indicial responses and weighting functions. Because the indicial response is the time integral of the weighting function these two responses are so closely related that only one need be used in most dynamic response assessment procedures. The weighting function is superior when emphasis is placed upon response to impulses, short pulses, and initial conditions. The indicial response is most suitable for response assessments for steps, cut-off ramps, and long pulses. When the short time ($0 < t < T$) response to cut-off ramps is also of interest, a pure ramp can be added to the test input inventory. However, because the ramp response is just the integral of the indicial response it is, again, seldom necessary to consider ramp responses in detail apart from the closely related weighting function or indicial response. The key inputs from Table 10-2 are, therefore, impulses and steps, sometimes delayed, with the ramp being useful occasionally. In terms of system response the corresponding quantities are related, for a general input-output set $x(t)$ and $y(t)$, by a transfer function W_{yx} , the weighting function (system response to unit impulse input) is,

$$w_{yx}(t) = \mathcal{L}^{-1} \left[W_{yx}(s) \right] = \mathcal{L}^{-1} \left[\frac{Y(s)}{X(s)} \right] \quad (10-6)$$

the indicial response or indicial admittance (system response to unit step input) is,

$$I_{yx}(t) = \int_0^t w_{yx}(\lambda) d\lambda = \mathcal{L}^{-1} \left[\frac{W_{yx}(s)}{s} \right] \quad (10-7)$$

and the ramp response (system response to unit ramp input) is:

$$V_{yx}(t) = \int_0^t I_{yx}(\lambda) d\lambda = \mathcal{L}^{-1} \left[\frac{W_{yx}(s)}{s^2} \right] \quad (10-8)$$

In the case of initial conditions or of impulse functions applied so as to represent portions of the initial conditions, it is impossible to distinguish these from inputs once the proper substitutions have been made.* For this reason it is unnecessary to discuss these "inputs" separately.

The next of the general deterministic inputs to be considered is the power series in time. As should be evident from Table 10-2, this type of input is a convenient catch-all for a wide variety of physical effects when it is desired to examine particular responses rather than an ensemble. Power series are also convenient for the description of the average effects of random input time functions which have stationary statistics about a time-varying mean. The random fluctuations about the mean can then be treated separately as a stationary process.

When represented as a power series in time, an input is described by a series:

$$x(t) = a_0 + a_1 t + a_2 t^2 + \dots + a_N t^N = \sum_{n=0}^N a_n t^n, \quad 0 \leq t \leq T \quad (10-9)$$

The derivatives of $x(t)$ are then,

$$\frac{dx}{dt} = a_1 + 2a_2 t + 3a_3 t^2 + \dots + N a_N t^{N-1} = \sum_{n=0}^N n a_n t^{n-1}$$

$$\frac{d^2 x}{dt^2} = 2a_2 + 6a_3 t + 12a_4 t^2 + \dots + N(N-1)a_N t^{N-2} = \sum_{n=0}^N n(n-1)a_n t^{n-2} \quad (10-10)$$

.

.

.

$$\frac{d^i x}{dt^i} = \sum_{n=0}^N n(n-1)(n-2) \dots [n - (i - 1)] a_n t^{n-i} = \sum_{n=i}^N \binom{n}{i} i! a_n t^{n-i}$$

The constants, a_n , may be derived from theoretical considerations or possibly from physical limits (e.g. target maneuvers with maximum load factors), or

*J. A. Aseltine, Transform Method in Linear System Analysis, McGraw-Hill Book Co., Inc., New York, 1958, pp. 29-30.

may simply be the results of curve fits to empirical data (e.g. a representation of a short segment of terrain). In this case a Maclaurin's series equivalent of Eq. 10-9 is useful:

$$x(t) = x(0) + t \left. \frac{dx}{dt} \right|_{t=0} + \frac{t^2}{2} \left. \frac{d^2x}{dt^2} \right|_{t=0} + \frac{t^3}{3!} \left. \frac{d^3x}{dt^3} \right|_{t=0} + \dots + \frac{t^N}{N!} \left. \frac{d^Nx}{dt^N} \right|_{t=0} + \dots \quad (10-11)$$

For most inputs represented as power series in time, this approximating series is valid only for very restricted intervals. For convenience, the interval can be taken to start at $t = 0$. Because the primary concern in response calculations for power series inputs centers on the system steady-state behavior, the system transient resulting from this selection of a distinct time origin is ordinarily of secondary interest compared with the steady-state response. When the transient is of significance, other input forms, such as steps and ramps, are still more convenient for assessment purposes. Consequently only the steady-state facet of the system response shall be discussed here.

When a generalized input, $x(t)$, is inserted into a linear system having a transfer function $W_{yx}(s)$, the output $y(t)$ will be given by the inverse transform of

$$Y(s) = W_{yx}(s)X(s) \quad (10-12)$$

As shown in Chapter 2 (pp. 2-21 to 2-22), the inverse transform of the steady-state response is:

$$y(t) = W_{yx}(0)x(t) + W'_{yx}(0)\dot{x}(t) + \frac{1}{2!} W''_{yx}(0)\ddot{x}(t) + \dots + \frac{1}{n!} W^{(n)}_{yx}(0) \frac{d^nx}{dt^n} + \dots$$

$$= C_0 x(t) + C_1 \dot{x}(t) + C_2 \ddot{x}(t) + \dots + C_n \frac{d^nx}{dt^n} + \dots \quad (10-13)$$

The primes denote differentiation with respect to s in the first expression; and the general output response coefficients C_n are used to replace

$\left. \frac{d^n W_{yx}(s)}{ds^n} \right|_{s=0}$ in the second expression. The discussion in Chapter 2 which

follows Eq. 2-42 is also applicable here. The reader will recall that a convenient method of calculating the C_n in terms of the polynomial coefficients of the system transfer function was presented there. It may also be recalled (from Section 2.6) that the output response coefficients, C_n , can be interpreted as time weighted moments of the weighting function, $w_{yx}(t) = \mathcal{L}^{-1}[W_{yx}(s)]$, i.e., that

$$C_n = \frac{1}{n!} \left. \frac{d^n W_{yx}(s)}{ds^n} \right|_{s=0} = \frac{(-1)^n}{n!} \int_0^{\infty} \tau^n w_{yx}(\tau) d\tau \quad (10-14)$$

The final category of deterministic inputs from Table 10-2 to be discussed is the periodic variety. Strictly speaking, a periodic function is one which recurs or repeats itself, with some period T , over all time, i.e.

$$x(t) = x(t \pm T), \quad -\infty < t < \infty \quad (10-15)$$

Because the time origin is indefinite and the time span infinite, such functions do not generate transient terms in the system output response. They are, however, suitable representations for a large class of flight control system inputs which are recurring in nature and can be thought of as having no distinct time origin. The natural way to describe such functions analytically is with the familiar Fourier series, which provides an expansion of $x(t)$ in terms of trigonometric functions. If a function $x(t)$ is periodic with period T , as in Eq. 10-15, then the Fourier series expansion will be:

$$x(t) = a_0 + \sum_{n=1}^{\infty} (a_n \cos \omega_n t + b_n \sin \omega_n t) \quad (10-16)$$

where $\omega_n = n\omega_0 = \frac{2\pi n}{T}$; $n = 1, 2, 3, \dots$

$$a_0 = \frac{1}{T} \int_{-T/2}^{T/2} x(t) dt$$

$$a_n = \frac{2}{T} \int_{-T/2}^{T/2} x(t) \cos \omega_n t dt$$

$$b_n = \frac{2}{T} \int_{-T/2}^{T/2} x(t) \sin \omega_n t dt$$

Alternative forms are:

$$x(t) = \sum_{n=0}^{\infty} c_n \cos(\omega_n t - \psi_n) \quad (10-17)$$

where

$$c_n = \sqrt{a_n^2 + b_n^2}, \quad \psi_n = \tan^{-1} \frac{b_n}{a_n}$$

or

$$a_n = c_n \cos \psi_n, \quad b_n = c_n \sin \psi_n, \quad a_0 = c_0, \quad \psi_0 = 0$$

and

$$x(t) = \sum_{n=-\infty}^{\infty} \alpha_n e^{j\omega_n t} \quad (10-18)$$

where

$$\alpha_n = \frac{a_n - jb_n}{2}, \quad \alpha_{-n} = \frac{a_n + jb_n}{2}, \quad \alpha_0 = a_0$$

The response to a periodic input involves the system frequency response transfer function, $W_{yx}(j\omega)$, where:

$$W_{yx}(j\omega) = \left[W_{yx}(s) \right]_{s=j\omega} = |W_{yx}(j\omega)| e^{j \angle W_{yx}(j\omega)} = \text{Re} \left[W_{yx}(j\omega) \right] + j \text{Im} \left[W_{yx}(j\omega) \right] \quad (10-19)$$

The system output $y(t)$ for an input $x(t)$ expressed as a Fourier series in terms of Eq. 10-16 is then:

$$y(t) = \sum_{n=0}^{\infty} \left[(a_n R_n + b_n I_n) \cos \omega_n t + (b_n R_n - a_n I_n) \sin \omega_n t \right] \quad (10-20)$$

where

$$R_n = \text{Re} \left[W_{yx}(jn\omega_0) \right] \quad \text{and} \quad I_n = \text{Im} \left[W_{yx}(jn\omega_0) \right]$$

When $x(t)$ is given by Eq 10-17, the corresponding output expression becomes:

$$y(t) = \sum_{n=0}^{\infty} \left| W_{yx}(jn\omega_0) \right| c_n \cos \left[\omega_n t - \psi_n + \angle W_{yx}(jn\omega_0) \right] \quad (10-21)$$

TABLE 10-3 (Concluded)

TIME FUNCTION	FOURIER SERIES	PROBABILITY DENSITY FUNCTION	AUTOCORRELATION FUNCTION	POWER SPECTRAL DENSITY
Sawtooth Wave 	$x(t) = \frac{2A}{\pi} \sum_{n=1,3,5,\dots}^{\infty} \left(\frac{-1}{n} \right)^n \sin(n\omega_0 t) ; \omega_0 = \frac{2\pi}{T}$ $= \frac{2A}{\pi} \left[\sin(\omega_0 t) - \frac{1}{3} \sin(3\omega_0 t) + \frac{1}{5} \sin(5\omega_0 t) - \dots \right]$	$p_1(x) = \begin{cases} \frac{1}{2A} ; -A < x < +A \\ 0 ; \text{elsewhere} \end{cases}$ 	$R_{xx}(\tau) = \frac{2A^2}{\pi^2} \sum_{n=1,3,5,\dots}^{\infty} \frac{1}{n^2} \cos(n\omega_0 \tau)$ 	$\Phi_{xx}(\omega) = \frac{1}{\omega^2} \sum_{n=1,3,5,\dots}^{\infty} \left[\delta(n\omega_0 - \omega) + \delta(n\omega_0 + \omega) \right]$
Triangular Wave 	$x(t) = \frac{2A}{\pi^2} \sum_{n=1,3,5,\dots}^{\infty} \left(\frac{-1}{n} \right)^n \left(\frac{n-1}{n} \right) \sin(n\omega_0 t) ; \omega_0 = \frac{2\pi}{T}$ $= \frac{2A}{\pi^2} \left[\sin(\omega_0 t) - \frac{4}{9} \sin(3\omega_0 t) + \frac{8}{25} \sin(5\omega_0 t) - \dots \right]$	$p_1(x) = \begin{cases} \frac{1}{2A} ; -A < x < A \\ 0 ; \text{elsewhere} \end{cases}$ 	$R_{xx}(\tau) = \frac{2A^2}{\pi^2} \sum_{n=1,3,5,\dots}^{\infty} \frac{1}{n^2} \cos(n\omega_0 \tau)$ 	$\Phi_{xx}(\omega) = \frac{1}{\omega^2} \sum_{n=1,3,5,\dots}^{\infty} \left[\delta(n\omega_0 - \omega) + \delta(n\omega_0 + \omega) \right]$
Pectified Triangular (or Sawtooth) Wave 	$x(t) = \frac{1A}{\pi} \left[\frac{2}{3} \sum_{n=1,3,5,\dots}^{\infty} \frac{1}{n^2} \cos(n\omega_0 t) \right] ; \omega_0 = \frac{2\pi}{T}$ $= \frac{1A}{\pi} \left[\frac{2}{3} \cos(\omega_0 t) - \frac{1}{9} \cos(3\omega_0 t) + \frac{1}{25} \cos(5\omega_0 t) - \dots \right]$	$p_1(x) = \begin{cases} \frac{1}{A} ; 0 < x < A \\ 0 ; \text{elsewhere} \end{cases}$ 	$R_{xx}(\tau) = \frac{A^2}{\pi^2} \left[\frac{1}{2} + \sum_{n=1,3,5,\dots}^{\infty} \frac{1}{n^2} \cos(n\omega_0 \tau) \right]$ 	$\Phi_{xx}(\omega) = \frac{A^2}{\omega^2} \sum_{n=1,3,5,\dots}^{\infty} \left[\delta(n\omega_0 - \omega) + \delta(n\omega_0 + \omega) \right]$
Sinusoid $x(t) = A \sin(\omega_0 t)$ 	$x(t) = A \sin(\omega_0 t) ; \omega_0 = \frac{2\pi}{T}$	$p_1(x) = \begin{cases} \frac{1}{\sqrt{A^2 - x^2}} ; -A < x < +A \\ 0 ; \text{elsewhere} \end{cases}$ 	$R_{xx}(\tau) = \frac{A^2}{2} \cos(\omega_0 \tau)$ 	$\Phi_{xx}(\omega) = \frac{A^2}{4} \left[\delta(\omega_0 - \omega) + \delta(\omega_0 + \omega) \right]$
Rectified Sinusoid $x(t) = A \left \sin\left(\frac{\omega_0}{2} t\right) \right $ 	$x(t) = \frac{1A}{\pi} \left[\frac{2}{3} \sum_{n=1,3,5,\dots}^{\infty} \frac{1}{n^2} \cos(n\omega_0 t) \right] ; \omega_0 = \frac{2\pi}{T}$ $= \frac{1A}{\pi} \left[\frac{2}{3} \cos(\omega_0 t) - \frac{1}{9} \cos(3\omega_0 t) + \frac{1}{25} \cos(5\omega_0 t) - \dots \right]$	$p_1(x) = \begin{cases} \frac{2}{\pi A \sqrt{1 - x^2}} ; 0 < x < +A \\ 0 ; \text{elsewhere} \end{cases}$ 	$R_{xx}(\tau) = \frac{A^2}{\pi^2} \left[\sum_{n=1,3,5,\dots}^{\infty} \frac{1}{n^2} \cos(n\omega_0 \tau) \right]$ 	$\Phi_{xx}(\omega) = \frac{1}{\omega^2} \sum_{n=1,3,5,\dots}^{\infty} \left[\delta(n\omega_0 - \omega) + \delta(n\omega_0 + \omega) \right]$

TABLE 10-3

DESCRIPTION OF SIMPLE PERIODIC FUNCTIONS


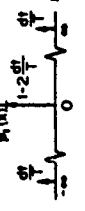
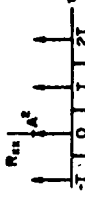
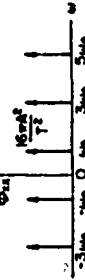
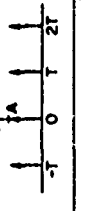
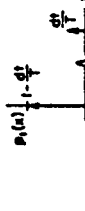
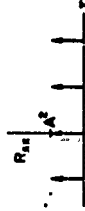
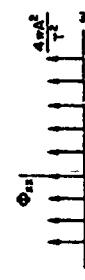
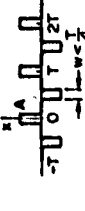

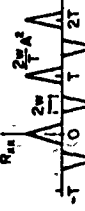
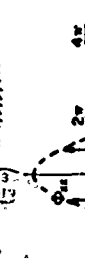
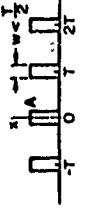
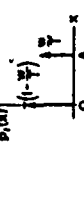

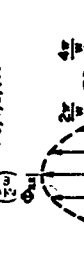
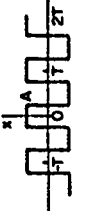
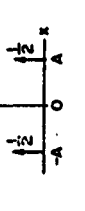

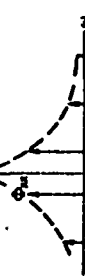
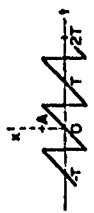
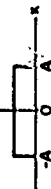

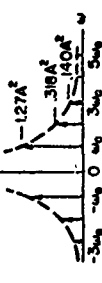



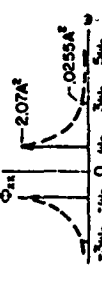
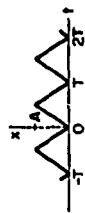
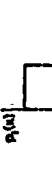

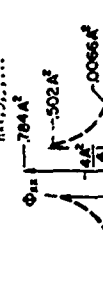

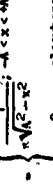
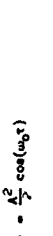
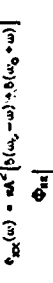

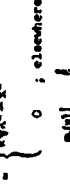
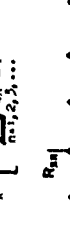

TIME FUNCTION	FOURIER SERIES	PROBABILITY DENSITY FUNCTION	AUTO-CORRELATION FUNCTION	POWER SPECTRAL DENSITY
<p>Alternating Impulses</p> 	$x(t) = \frac{A}{T} \sum_{n=1,3,5,\dots}^{\infty} \frac{\cos(n\omega_0 t)}{n} ; \omega_0 = \frac{2\pi}{T}$ $= \frac{A}{T} \left[\cos(\omega_0 t) + \cos(3\omega_0 t) + \cos(5\omega_0 t) + \dots \right]$ <p>Note: This series does not converge</p>			
<p>Impulses</p> 	$x(t) = \frac{A}{T} \left[\frac{1}{2} + \sum_{n=1,3,5,\dots}^{\infty} \frac{\cos(n\omega_0 t)}{n} \right] ; \omega_0 = \frac{2\pi}{T}$ $= \frac{A}{T} \left[\frac{1}{2} + \cos(\omega_0 t) + \cos(3\omega_0 t) + \dots \right]$ <p>Note: This series does not converge</p>			
<p>Alternating Pulses</p> 	$x(t) = \frac{A}{T} \sum_{n=1,3,5,\dots}^{\infty} \frac{1}{n} \sin\left(n\pi \frac{w}{T}\right) \cos(n\omega_0 t) ; \omega_0 = \frac{2\pi}{T}$ $= \frac{A}{T} \left[\sin\left(\pi \frac{w}{T}\right) \cos(\omega_0 t) + \frac{1}{3} \sin\left(3\pi \frac{w}{T}\right) \cos(3\omega_0 t) + \frac{1}{5} \sin\left(5\pi \frac{w}{T}\right) \cos(5\omega_0 t) + \dots \right]$			
<p>Pulses</p> 	$x(t) = \frac{A}{T} \left[\frac{1}{2} + \sum_{n=1,3,5,\dots}^{\infty} \frac{1}{n} \sin\left(n\pi \frac{w}{T}\right) \cos(n\omega_0 t) \right] ; \omega_0 = \frac{2\pi}{T}$ $= \frac{A}{T} \left[\frac{1}{2} + \sin\left(\pi \frac{w}{T}\right) \cos(\omega_0 t) + \frac{1}{3} \sin\left(3\pi \frac{w}{T}\right) \cos(3\omega_0 t) + \dots \right]$			
<p>Square Wave</p> 	$x(t) = \frac{A}{T} \sum_{n=1,3,5,\dots}^{\infty} \frac{(-1)^{(n-1)/2}}{n} \cos(n\omega_0 t) ; \omega_0 = \frac{2\pi}{T}$ $= \frac{A}{T} \left[\cos(\omega_0 t) - \frac{1}{3} \cos(3\omega_0 t) + \frac{1}{5} \cos(5\omega_0 t) + \dots \right]$			

TABLE 10-3 (Concluded.)

TIME FUNCTION	FOURIER SERIES	PROBABILITY DENSITY FUNCTION	AUTO-CORRELATION FUNCTION	POWER SPECTRAL DENSITY
Sawtooth Wave 	$x(t) = \frac{2A}{\pi} \sum_{n=1,2,3,\dots}^{\infty} \frac{(-1)^{n+1}}{n} \sin(n\omega_0 t) \neq \omega_0 = \frac{2\pi}{T}$ $= \frac{2A}{\pi} \left[\sin(\omega_0 t) - \frac{1}{2} \sin(2\omega_0 t) + \frac{1}{3} \sin(3\omega_0 t) - \dots \right]$	$p_1(x) = \begin{cases} \frac{1}{2A} & -A < x < +A \\ 0 & \text{elsewhere} \end{cases}$ 	$R_{xx}(\tau) = \frac{2A^2}{\pi^2} \sum_{n=1,2,3,\dots}^{\infty} \frac{1}{n^2} \cos(n\omega_0 \tau)$ 	$\Phi_{xx}(\omega) = \frac{1}{\omega^2} \sum_{n=1,2,3,\dots}^{\infty} \left[\delta(n\omega_0 - \omega) + \delta(n\omega_0 + \omega) \right]$ 
Triangular Wave 	$x(t) = \frac{8A}{\pi^2} \sum_{n=1,2,3,\dots}^{\infty} \frac{(-1)^{n+1}}{n^2} \sin(n\omega_0 t) \neq \omega_0 = \frac{2\pi}{T}$ $= \frac{8A}{\pi^2} \left[\sin(\omega_0 t) - \frac{1}{9} \sin(3\omega_0 t) + \frac{1}{25} \sin(5\omega_0 t) - \dots \right]$	$p_1(x) = \begin{cases} \frac{1}{2A} & -A < x < A \\ 0 & \text{elsewhere} \end{cases}$ 	$R_{xx}(\tau) = \frac{2A^2}{\pi^2} \sum_{n=1,2,3,\dots}^{\infty} \frac{1}{n^2} \cos(n\omega_0 \tau)$ 	$\Phi_{xx}(\omega) = \frac{1}{\omega^2} \sum_{n=1,2,3,\dots}^{\infty} \left[\delta(n\omega_0 - \omega) + \delta(n\omega_0 + \omega) \right]$ 
Rectified Triangular (or Sawtooth) Wave 	$x(t) = \frac{4A}{\pi^2} \sum_{n=1,2,3,\dots}^{\infty} \frac{1}{n^2} \cos(n\omega_0 t) \neq \omega_0 = \frac{2\pi}{T}$ $= \frac{4A}{\pi^2} \left[\cos(\omega_0 t) - \frac{1}{9} \cos(3\omega_0 t) + \frac{1}{25} \cos(5\omega_0 t) - \dots \right]$	$p_1(x) = \begin{cases} \frac{1}{A} & 0 < x < A \\ 0 & \text{elsewhere} \end{cases}$ 	$R_{xx}(\tau) = \frac{4A^2}{\pi^2} \sum_{n=1,2,3,\dots}^{\infty} \frac{1}{n^2} \cos(n\omega_0 \tau)$ 	$\Phi_{xx}(\omega) = \frac{1}{\omega^2} \sum_{n=1,2,3,\dots}^{\infty} \left[\delta(n\omega_0 - \omega) + \delta(n\omega_0 + \omega) \right]$ 
Sinusoid $x(t) = A \sin(\omega_0 t)$ 	$x(t) = A \sin(\omega_0 t) \neq \omega_0 = \frac{2\pi}{T}$	$p_1(x) = \begin{cases} \frac{1}{\sqrt{A^2 - x^2}} & -A < x < +A \\ 0 & \text{elsewhere} \end{cases}$ 	$R_{xx}(\tau) = \frac{A^2}{2} \cos(\omega_0 \tau)$ 	$\Phi_{xx}(\omega) = \pi A^2 \left[\delta(\omega - \omega_0) + \delta(\omega + \omega_0) \right]$ 
Rectified Sinusoid $x(t) = A \left \sin\left(\frac{\omega_0}{2} t\right) \right $ 	$x(t) = \frac{4A}{\pi} \sum_{n=1,2,3,\dots}^{\infty} \frac{1}{n} \cos(n\omega_0 t) \neq \omega_0 = \frac{2\pi}{T}$ $= \frac{4A}{\pi} \left[\cos(\omega_0 t) - \frac{1}{3} \cos(3\omega_0 t) + \frac{1}{5} \cos(5\omega_0 t) - \dots \right]$	$p_1(x) = \begin{cases} \frac{2}{\pi A} & 0 < x < A \\ 0 & \text{elsewhere} \end{cases}$ 	$R_{xx}(\tau) = \frac{2A^2}{\pi^2} \sum_{n=1,2,3,\dots}^{\infty} \frac{1}{n^2} \cos(n\omega_0 \tau)$ 	$\Phi_{xx}(\omega) = \frac{1}{\omega^2} \sum_{n=1,2,3,\dots}^{\infty} \left[\delta(n\omega_0 - \omega) + \delta(n\omega_0 + \omega) \right]$ 

functions of outcomes are called random variables, $X(\xi)$. (See Appendix E.) A real valued function of both the sample point, ξ , and time, t , is called a random, or stochastic, process.

$$X = X(\xi, t) \quad (10-22)$$

This definition is broad enough to include functions which we do not ordinarily think of as "random." Take, for example, a sine wave whose phase angle is determined by chance:

$$X(\varphi, t) = \sin(\omega t + \varphi) \quad (10-23)$$

This is, of course, a deterministic function of time once the phase angle is chosen. Actually, a random process may be one of four things:

1. a family of random time functions (ξ and t variable)
2. a single time function (ξ fixed, t variable)
3. a random variable (ξ variable, t fixed)
4. a constant number (ξ fixed, t fixed)

Ordinarily in considering random processes, the first of these numbered categories will be the one of the most interest, but functions from the other categories may well be used for illustrative purposes.

The members of a family of random processes which all arise in the same way are called an ensemble. If $X_n(t)$ is considered to be a typical member of such an ensemble, where we now omit to note the functional dependence on the sample point, then $X_n(t)$ itself could possibly be thought of as a deterministic function of time. An analytical expression, e.g. some series, could then be found which approximates $X_n(t)$ arbitrarily closely over a given time period, $-T \leq t \leq T$. For another random signal, $X_m(t)$, which arises from the same physical source, an analytical expression derived on the same basis as that used in characterizing $X_n(t)$ might be entirely different, even if $X_m(t)$ were simply a section of $X_n(t)$ taken for a time period other than $-T \leq t \leq T$. For this reason any attempt to describe a truly random input as a meaningful and typical function of time is doomed at the outset. Attention must therefore be given to the ensemble of functions, $X_1(t)$, $X_2(t)$, . . . , $X_n(t)$, . . . , which stem from common causes,

and where any one $X_i(t)$ is no more or less "typical" of the ensemble than any other member. The behavior of the ensemble, $X(t)$, must then be described in terms of averages of one sort or another. Average views are substituted for a precise knowledge of the nature of the signal variation with time. These remarks are the intuitive essence of what is meant by random signals and their analytical treatment.

The most fundamental averages are probability density functions. Consider Fig. 10-2. Illustrated there are a number of members of a family of random functions of time which comprise an ensemble of random processes.

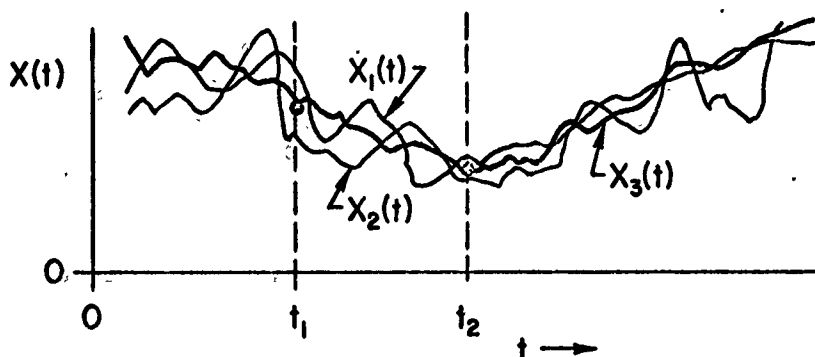


Fig. 10-2. An Ensemble of Random Processes

At any given time, t_1 , the probability that one of the functions $X(t)$ will be greater than x , and smaller than $x + \Delta x$, can be computed in a direct arithmetic fashion. For an ensemble with N members,

$$\Pr[x < X(t) < x + \Delta x \text{ at } t=t_1] = \frac{\left\{ \begin{array}{l} \text{No. of functions } X_1(t_1), X_2(t_1), \dots, X_N(t_1) \\ \text{which have values between } x \text{ and } x + \Delta x \end{array} \right\}}{N} \quad (10-24)$$

When the amplitude interval Δx is very small this probability will be roughly proportional to Δx , so:

$$\Pr[x < X(t) < x + \Delta x, t_1] \doteq p_1(x, t_1)_N \Delta x \quad (10-25)$$

$p_1(x, t_1)_N$ is the first probability density function for a finite ensemble. It will depend, in general, upon the total number of functions in the ensemble, the value of x , and the time t_1 at which the measurements are made.

To be of any practical use as a means to describe the average amplitude characteristic of a typical signal, the number of members in the ensemble must be sufficiently large so that $p_1(x, t_1)_N$ is not materially changed when the ensemble is made even larger. This factor can be taken into account, and the "roughly proportional" restriction can be removed if the first probability density function is defined as:

$$p_1(x, t_1) = \lim_{\substack{N \rightarrow \infty \\ \Delta x \rightarrow 0}} \frac{\text{Number of values lying between } x \text{ and } x + \Delta x}{N(\Delta x)} \quad (10-26)$$

When the probability that $X(t)$ lies within a range from x_1 to x_2 , at time t_1 , is desired, the density function is integrated over the range. In general:

$$\Pr[x_1 < X(t) < x_2, t_1] = \int_{x_1}^{x_2} p_1(x, t_1) dx \quad (10-27)$$

If the range from x_1 to x_2 is extended from $-\infty$ to $+\infty$, the probability that $X(t)$ lies within the range becomes a certainty.

$$\Pr[-\infty < X(t) < +\infty, t_1] = \int_{-\infty}^{+\infty} p_1(x, t_1) dx = 1 \quad (10-28)$$

When it is desired to find only the probability that $X(t)$ is less than x at time t_1 ,

$$\Pr[X(t) < x, t_1] = \int_{-\infty}^x p_1(x, t_1) dx = P_1(x, t_1) \quad (10-29)$$

where $P_1(x, t)$ is the first probability distribution function. It is an alternative measure of the amplitude characteristics of a typical signal $X(t)$, and has the properties:

$$P_1(-\infty, t_1) = 0$$

$$P_1(\infty, t_1) = 1 \quad (10-30)$$

$$\frac{dP_1(x, t_1)}{dx} = p_1(x, t_1)$$

To generalize the calculation of averages, suppose that the average value of some arbitrary function, $f[X(t_1)]$, of the random signal $X(t)$ is desired. The average of $f[X(t_1)]$ can be computed in the usual way by first finding the sum of a large number of observed values for $f[X(t_1)]$, and then dividing by the total number of values. The fraction of the values of $X(t_1)$ which lie between x and $x + dx$ is $p_1(x, t_1)dx$; and the value of $f[X(t_1)]$ when $X(t_1)$ lies in this range is just $f[x]$. Consequently, the fraction of values of $f[X(t_1)]$ which correspond to values of $X(t)$ falling between x and $x + dx$ is just $f[x]p_1(x, t_1)dx$. The average value of $f[X(t_1)]$ can then be found by summing these fractions over the entire range of values for X , or:

$$\text{Average of } f[X(t_1)] = E[f(X)] = \int_{-\infty}^{\infty} f(x)p_1(x, t_1)dx \quad (10-31)$$

The notation $E[\]$ means "expected value" or average. The averages where $f[X(t_1)]$ is $X^n(t_1)$ are particularly important. These are the moments of the distribution and have the form:

$$m_n(t_1) = E[X^n(t_1)] = \int_{-\infty}^{\infty} x^n p_1(x, t_1)dx \quad (10-32)$$

The three lowest order moments are:

$$\text{Zero-order moment: } m_0 = 1 \quad (10-33)$$

$$\text{First moment: } m_1(t_1) = \int_{-\infty}^{\infty} x p_1(x, t_1)dx = E[X(t_1)] \quad (10-34)$$

$$\text{Second moment: } m_2(t_1) = \int_{-\infty}^{\infty} x^2 p_1(x, t_1)dx = E[X^2(t_1)] \quad (10-35)$$

The first and second moments are interpreted as the arithmetic mean (usually called simply the mean) and the mean-square values of the typical random function $X(t)$ at time t_1 .

If the mean value is subtracted from all values of $X_1(t_1)$ in the ensemble, the moments derived from the results become central moments. Thus:

$$\mu_n(t_1) = E[X(t_1) - m_1(t_1)]^n = \int_{-\infty}^{\infty} [x - m_1(t_1)]^n p_1(x, t_1)dx \quad (10-36)$$

The first central moment, $\mu_1(t_1)$, is zero. The second central moment is:

$$\begin{aligned}\mu_2(t_1) &= \int_{-\infty}^{\infty} [x - m_1(t_1)]^2 p_1(x, t_1) dx \\ &= m_2(t_1) - [m_1(t_1)]^2 \\ &= E[X^2(t_1)] - \{E[X(t_1)]\}^2\end{aligned}\tag{10-37}$$

$\mu_2(t_1)$ is the variance, $[\sigma(t_1)]^2$. It is a measure of the average alternating fluctuating power in the signal. In terms of the density function, $\mu_2(t_1)$ is a measure of its width about the mean. Similarly the third moment, $\mu_3(t_1)$, gives an indication of the skew of the density function. The square root of the variance is the standard deviation, σ , of the distribution for the ensemble $X_1(t_1)$, $X_2(t_1)$, \dots , $X_n(t_1)$, \dots . When the mean is zero the variance and the mean-square are identical.

In general, not only the first probability density and the distribution function, but also the expected or mean value, the variance and other "statistics" of an ensemble of stochastic processes may depend on the time of observation. This is suggested in Fig. 10-2 where clearly both the average value and average fluctuating component of the signals are smaller at t_2 than at t_1 .

The first probability density function together with the moments and other averages derived from it provide information about the expected values of $X(t_1)$ that will occur on the average, and about the probability that various magnitudes may occur. However, these quantities give no information concerning the time scale in which the values might occur. To rectify this situation a second probability density function must be defined. The second probability density function, $p_2(x_1, t_1; x_2, t_2)$, when multiplied by $dx_1 dx_2$ is the probability that $X(t)$ will be within the bounds x_1 and $x_1 + dx_1$ at time t_1 , and that this same $X(t)$ will be between x_2 and $x_2 + dx_2$ at time t_2 , i.e.,:

$$\begin{aligned}\Pr[x_1 < X(t_1) < x_1 + dx_1; x_2 < X(t_2) < x_2 + dx_2] \\ &= p_2(x_1, t_1; x_2, t_2) dx_1 dx_2\end{aligned}\tag{10-38}$$

The concept is illustrated in Fig. 10-3. The second probability density function provides the means to find average values such as $\text{Average} [X(t_1)X(t_2)]$.

$$\text{Average} [X(t_1)X(t_2)] = E[X(t_1)X(t_2)] = \int_{-\infty}^{\infty} \int_{-\infty}^{\infty} x_1 x_2 p_2(x_1, t_1; x_2, t_2) dx_1 dx_2 \quad (10-39)$$

This average will be a function of t_1 and t_2 . When $t_1 = t_2$ the second probability density, $p_2(x_1, t_1; x_2, t_1)$, is just a product of the first probability density functions, $p_1(x_1, t_1)p_1(x_2, t_1)$. The expected value $E[X_1 X_2]$ then becomes simply the mean-square value or second moment, $m_2(t_1)$.

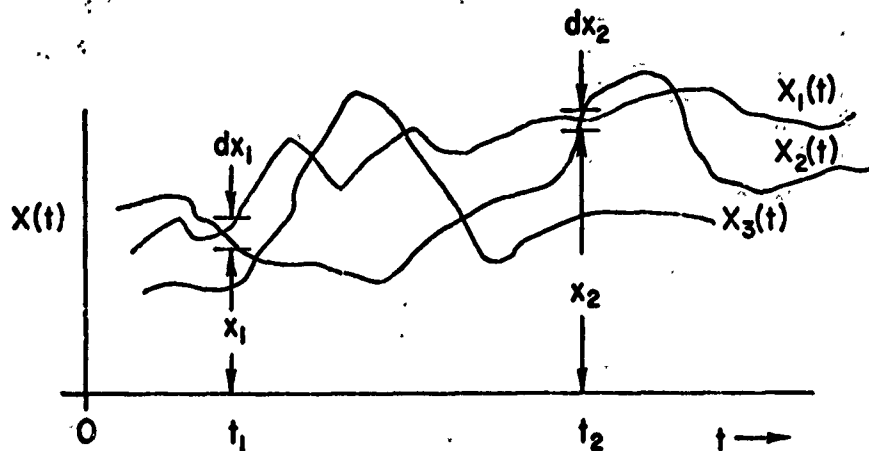


Fig. 10-3. Illustration for Second Probability Density Function

Higher order probability density functions are also defined, following the pattern established above, as the fraction of the ensemble members that have values which lie within given ranges at respectively given times. To completely describe the random process all of the probability density functions must be defined. Stated in another way, the process is defined in successively greater detail the higher the order of the known probability density functions. Each lower order density function can be derived from the highest order function by a succession of special cases, so the degree of

detailed knowledge about the complete process is incorporated in the highest order density function which is available.

In the above discussion, as we have noted, the density functions and averages derived therefrom all may be functions of the times of observation. However, in many applications the underlying mechanism which generates the random function does not vary with time, or can be considered to be time invariant for the time periods of interest in response calculations. The time signals actually measured as physical manifestations of the underlying process may not reflect this time invariance property directly because of the kinematics of the measurement situation, but transformations can often be made to find time signals (related to the actual signals measured) which do. When these circumstances apply, the probability density functions will not depend upon the observation times themselves, but rather only upon time differences. For the first probability density function, for example, the same function would be obtained regardless of the time when measurements were taken. $p_1(x, t_1)$ would then be equal to $p_1(x, t_2)$, so the time dependence would no longer be present. The first probability density function would then be simply $p_1(x)$, the second probability density function becomes $p_2(x_1, x_2, \tau)$, where $\tau = t_2 - t_1$, etc. When all the statistics describing the ensemble of time functions are not dependent upon the absolute times of observation, the random processes are strictly stationary. As a practical matter, however, it is usually impossible to determine if this is the case. If it can be shown, for example, that the first and second probability density functions are not dependent upon the time of observation, the random process is said to be stationary of order two. It often happens, that it is only shown that the process is stationary of order one and that the autocorrelation function (defined below) depends not on t_1 and t_2 but only on $\tau = t_2 - t_1$. We then say that the process is wide sense or weakly stationary.

When the statistics of the ensemble of functions, $X(t)$, are independent of the absolute time, an alternative possibility for finding averages exists. Instead of averaging in the conventional arithmetic way across an entire ensemble of functions at fixed times one could consider just one member of the ensemble and perform averages over all time. Such averages as

$$\overline{X(t)} = \lim_{T \rightarrow \infty} \frac{1}{2T} \int_{-T}^{+T} X(t) dt = \text{the mean value} \quad (10-40)$$

$$\overline{X^2(t)} = \lim_{T \rightarrow \infty} \frac{1}{2T} \int_{-T}^{+T} X^2(t) dt = \text{the mean square value} \quad (10-41)$$

$$R_{XX}(\tau) = \overline{X^*(t)X(t+\tau)} = \lim_{T \rightarrow \infty} \frac{1}{2T} \int_{-T}^{+T} X^*(t)X(t+\tau) dt \quad (10-42)$$

would then be the time-average equivalent of the ensemble averages $E[X(t)] = m_1$, $E[X^2(t)] = m_2$, and $E[X^*(t)X(t+\tau)]$, respectively. The last time average here is called the autocorrelation function.*

As a practical matter stationarity for the time averages requires only that averaging time be sufficiently long so that the results obtained would be substantially unchanged if it were made still longer. The practical equivalent to the averaging time for ensemble averages would be that the number of signals observed be sufficiently great so that the results are substantially unchanged when even more signals are added to the ensemble. (This, however, does not assure stationarity for the ensemble.)

The most extensive applications of the random input characteristics, discussed above, occur when time averages and ensemble averages are equal, i.e., when the random process is ergodic. Whether a given physical process is ergodic or not is very difficult to show, in general. Consequently, when processes are stationary (a necessary but not sufficient condition for ergodicity) and the lower averages (e.g. mean, mean-square, etc.) appear to be equal, ergodic properties are often assigned to the physical situation by hypothesis. Clearly, the process may be ergodic for some statistical

The asterisk notation in the autocorrelation function indicates that $X^(t)$ is the conjugate of $X(t)$. Since $X(t)$ is a real function this may seem superfluous. However, $X(t)$ might be expanded in the complex form of a Fourier series, and the conjugate would then be required when working with the series representation.

parameters and not for others.* With the hypothesis of ergodicity, time averages are used interchangeably with ensemble averages, and the statistical (probability density functions) and moment properties can be determined from either averages performed on an ensemble or time averages performed on a single member of the ensemble. This is an enormous practical advantage when data must be obtained from physical measurement. The assumption of ergodicity is also helpful from the theoretical standpoint since it tremendously simplifies analytical work. However, theoretical treatments of non-stationary random phenomena, while complicated, are now well advanced, so the major practical importance of ergodicity currently resides in the simplifications introduced in measurement. In any event, attention from this point on will be confined to random input descriptions which, as a practical matter, can be assumed to possess ergodic properties for the time periods of interest.

When the time functions are ergodic:

$$\overline{X(t)} = E[X(t)] = \int_{-\infty}^{\infty} x p_1(x) dx = m_1$$

$$\overline{X^2(t)} = E[X^2(t)] = \int_{-\infty}^{\infty} x^2 p_1(x) dx = m_2 \quad (10-43)$$

$$\overline{X^n(t)} = E[X^n(t)] = \int_{-\infty}^{\infty} x^n p_1(x) dx = m_n$$

and

$$\overline{X^*(t)X(t+\tau)} = E[X^*(t)X(t+\tau)] = \int_{-\infty}^{\infty} \int_{-\infty}^{\infty} x_1 x_2 p_2(x_1, x_2, \tau) dx_1 dx_2 = R_{XX}(\tau) \quad (10-44)$$

*Conditions for the ergodicity of the more commonly interesting statistical parameters are summarized in A. Papoulis, Probability, Random Variables, and Stochastic Processes, McGraw-Hill Book Co., Inc., New York, 1965.

Higher order averages could also be added to this list, but these are seldom used in practical calculations. With the functions defined thus far, it is possible to compute both mean and mean-square values and, for many cases of practical interest, the first probability density function may also be available. Thus a good indication of the response characteristics, on the average, can be found, and the probability that certain values of various signals will occur can be assessed.

From this point on we shall designate a function of time which may be either a random process or a deterministic periodic signal by a lower case letter.

For a stable, constant-coefficient, linear system with a weighting function $w(t)$ the autocorrelation function of the output response $y(t)$ to an input $x(t)$ having an autocorrelation function $R_{xx}(\tau)$ is:*

$$R_{yy}(\tau) = \int_{-\infty}^{\infty} \int_{-\infty}^{\infty} w(\lambda)w(\gamma)R_{xx}(\tau + \lambda - \gamma)d\gamma d\lambda \quad (10-45)$$

Thus the output signal autocorrelation can be computed from the input autocorrelation from what amounts to two convolutions with the system weighting function. Because the mean-square value of a stationary time function is given by its autocorrelation function at $\tau = 0$, the mean-square output will be:

$$\overline{y^2(t)} = R_{yy}(0) = \int_{-\infty}^{\infty} \int_{-\infty}^{\infty} w(\lambda)w(\gamma)R_{xx}(\lambda - \gamma)d\gamma d\lambda \quad (10-46)$$

Integrals of this nature are often awkward to work with, whereas their frequency domain equivalent is considerably simpler. To proceed into the frequency domain requires the definition of power spectral density functions. For either periodic or stationary random time functions this is here defined as four times the Fourier cosine transform of the autocorrelation function, viz.:

$$\Phi_{xx}(\omega) = 4 \int_0^{\infty} R_{xx}(\tau) \cos \omega \tau d\tau \quad (10-47)$$

*H. M. James, N. B. Nichols, and R. S. Phillips, Theory of Servomechanisms, McGraw-Hill Book Co., Inc., New York, 1947.

The autocorrelation function is also a Fourier cosine transform of the power spectral density, i.e.:

$$R_{xx}(\tau) = \int_0^{\infty} \phi_{xx}(f) \cos 2\pi f \tau df = \frac{1}{2\pi} \int_0^{\infty} \phi_{xx}(\omega) \cos \omega \tau d\omega \quad (10-48)$$

The mean-square value of $x(t)$ is given in terms of the power spectral density by:

$$\begin{aligned} \overline{x^2(t)} &= \frac{1}{2} \int_{-\infty}^{\infty} \phi_{xx}(f) df = \int_0^{\infty} \phi_{xx}(f) df \\ &= \frac{1}{2\pi} \int_0^{\infty} \phi_{xx}(\omega) d\omega = R_{xx}(0) \end{aligned} \quad (10-49)$$

The factor of four in Eq. 10-47 arises from the desire to have the mean-square value be the integral of the power spectral density over all positive frequencies. This usage agrees with James, Nichols, and Phillips and with Rice.* Others use a factor of two, which is compatible with having $\overline{x^2(t)}$ be the result of integrating $\phi_{xx}(f)$ over both positive and negative frequencies.

Analogously to Eq. 10-44 we can define a cross-correlation function, $R_{xy}(\tau)$, between two variables $x(t)$ and $y(t)$ as a species of average:

$$\begin{aligned} \overline{x^*(t)y(t+\tau)} &= E[x^*(t)y(t+\tau)] = R_{xy}(\tau) \\ &= \lim_{T \rightarrow \infty} \frac{1}{2T} \int_{-T}^T x^*(t)y(t+\tau) dt \end{aligned} \quad (10-50)$$

If $x(t)$ is the input and $y(t)$ is the output of a linear, constant coefficient device such that

$$y(t) = \int_{-\infty}^{\infty} w(\tau)x(t-\tau)d\tau = \int_{-\infty}^{\infty} w(t-\tau)x(\tau)d\tau \quad (10-51)$$

*S. O. Rice, "Mathematical Analysis of Random Noise," originally published in the Bell Systems Tech. J., Vols. 23 and 24, reprinted in N. Wax (ed.), Selected Papers on Noise and Stochastic Processes, Dover Publications, New York, 1954.

then

$$R_{xy}(\tau) = \int_{-\infty}^{\infty} w(u) R_{xx}(\tau - u) du = R_{yx}(-\tau) \quad (10-52)$$

The cross spectral density is again proportional to the Fourier transform of the cross-correlation function

$$\Phi_{xy}(j\omega) = 2 \int_{-\infty}^{\infty} R_{xy}(\tau) e^{-j\omega\tau} d\tau \quad (10-53)$$

and the cross-correlation function can be found by inverse Fourier transforming the cross spectral density.

$$R_{xy}(\tau) = \frac{1}{4\pi} \int_{-\infty}^{\infty} \Phi_{xy}(j\omega) e^{j\omega\tau} d\omega \quad (10-54)$$

Finally, if $W(j\omega)$ is the frequency response transfer function:

$$\Phi_{xy}(j\omega) = W(j\omega) \Phi_{xx}(\omega) \quad (10-55)$$

An instructive way in which to approximate a stationary random process is as a sum of a large number of sinusoids comprising the Fourier series approximation to an arbitrary function in the interval $-T/2$ to $T/2$. (See Eq. 10-18.)

$$x(t) = \sum_{n=-\infty}^{\infty} \alpha_n e^{j\omega_n t} \quad (10-56)$$

From Eq. 10-42 the autocorrelation function will be:

$$\begin{aligned} R_{xx}(\tau) &= \lim_{T \rightarrow \infty} \frac{1}{2T} \int_{-T}^T x^*(t) x(t + \tau) dt = \overline{x^*(t) x(t + \tau)} \\ &= \lim_{T \rightarrow \infty} \frac{1}{2T} \int_{-T}^T \left\{ \sum_{n=-\infty}^{\infty} \alpha_n^* e^{-j\omega_n t} \sum_{k=-\infty}^{\infty} \alpha_k e^{j\omega_k(t+\tau)} \right\} dt \quad (10-57) \\ &= \sum_{n=-\infty}^{\infty} \sum_{k=-\infty}^{\infty} \alpha_n^* \alpha_k e^{j\omega_k \tau} \left\{ \lim_{T \rightarrow \infty} \frac{1}{2T} \int_{-T}^T e^{j(\omega_k - \omega_n)t} dt \right\} \end{aligned}$$

The quantity in brackets:

$$= \lim_{T \rightarrow \infty} \frac{1}{2T} \left[\frac{e^{j(\omega_k - \omega_n)t}}{j(\omega_k - \omega_n)} \right]_{-T}^{+T} = 0 ; \omega_k \neq \omega_n \quad (10-58)$$

$$= \lim_{T \rightarrow \infty} \frac{1}{2T} \int_{-T}^T e^{j\omega_n t} e^{-j\omega_n t} dt = 1 ; \omega_k = \omega_n$$

Therefore:

$$R_{xx}(\tau) = \sum_{k=-\infty}^{\infty} |a_k|^2 e^{j\omega_k \tau} \quad (10-59)$$

But since $|a_n|^2 = \frac{a_n - jb_n}{2} \cdot \frac{a_n + jb_n}{2} = \frac{c_n^2}{4}$ and $\frac{e^{j\omega_k \tau} + e^{-j\omega_k \tau}}{2} = \cos \omega_k \tau$

$$R_{xx}(\tau) = c_0^2 + \sum_{n=1}^{\infty} \frac{c_n^2}{2} \cos \omega_n \tau \quad (10-60)$$

Consider now the power spectral density of the function $x(t)$. Substituting the expression on the right hand side of Eq. 10-60 in Eq. 10-47,

$$\phi_{xx}(\omega) = 4 c_0^2 \int_0^{\infty} \cos \omega \tau d\tau + 4 \sum_{n=1}^{\infty} \frac{c_n^2}{2} \int_0^{\infty} \cos \omega_n \tau \cos \omega \tau d\tau \quad (10-61)$$

The evaluation of this integral is somewhat circuitous. The Fourier transform of the delta function is identically unity, so that the inverse Fourier transform of unity must be the delta function, i.e.,

$$\int_{-\infty}^{\infty} \delta(t) e^{-j\omega t} dt = 1, \text{ then } \frac{1}{2\pi} \int_{-\infty}^{\infty} (1) e^{j\omega t} d\omega = \delta(t) \quad (10-62)$$

Consequently,

$$\int_{-\infty}^{\infty} (e^{j\omega_n t}) e^{-j\omega t} dt = \int_{-\infty}^{\infty} e^{-j(\omega - \omega_n)t} dt = 2\pi \delta(\omega - \omega_n) \quad (10-63)$$

From the trigonometric identity,

$$\cos \omega_n \tau \cos \omega \tau = \frac{1}{2} [\cos \tau(\omega_n - \omega) + \cos \tau(\omega_n + \omega)] \quad (10-64)$$

both the cosine and the delta function are even functions so,

$$\begin{aligned} \int_0^{\infty} \cos \omega_n \tau \cos \omega \tau d\tau &= \frac{1}{4} \int_{-\infty}^{\infty} \cos \tau(\omega_n - \omega) d\tau + \frac{1}{4} \int_{-\infty}^{\infty} \cos \tau(\omega_n + \omega) d\tau \\ &= \frac{1}{4} \int_{-\infty}^{\infty} \frac{e^{j(\omega_n - \omega)\tau} + e^{-j(\omega_n - \omega)\tau}}{2} d\tau + \frac{1}{4} \int_{-\infty}^{\infty} \frac{e^{j(\omega_n + \omega)\tau} + e^{-j(\omega_n + \omega)\tau}}{2} d\tau \\ &= \frac{\pi}{4} [\delta(\omega_n - \omega) + \delta(\omega - \omega_n) + \delta(\omega_n + \omega) + \delta(-\omega_n - \omega)] \\ &= \frac{\pi}{2} [\delta(\omega - \omega_n) + \delta(\omega + \omega_n)] \end{aligned} \quad (10-65)$$

Finally, therefore, the power spectral density of the function $x(t)$ is:

$$\Phi_{xx}(\omega) = 4\pi c_0^2 \delta(\omega) + \pi \sum_{n=1}^{\infty} c_n^2 [\delta(\omega - \omega_n) + \delta(\omega + \omega_n)] \quad (10-66)$$

This function may thus be seen to represent the distribution of the harmonic components in $x(t)$ with each component here proportional to the square of the amplitude coefficient in the original Fourier series.

If each wave in the original Fourier series were a voltage, the power, at that frequency, dissipated in a unit resistance would be proportional to the square of the voltage, hence the name power spectral density.

The first probability density functions, autocorrelation functions, and power spectral density functions for a number of periodic waveforms have already been presented in Table 10-3.

We next consider the probabilistic description of some particular random processes.

10.4 ANALYTICAL DESCRIPTION AND CATALOG OF SPECIAL RANDOM PROCESSES

From the discussion above it should be apparent that the random inputs listed in Table 10-1 must be characterized as autocorrelations or power spectral densities if even minimal information (mean-square values) is to be obtained about system response to these inputs. If more response information is required at least some of the lower order probability density functions are required. Even if these are known, however, the probability density functions for the system output are difficult to find unless the amplitudes of the random signals are characterized by a Gaussian or normal distribution. (See Appendix B.)

Table 10-4 shows a number of the more interesting random processes which may be used for describing automatic flight control commands and disturbances. In most cases a typical segment of the random process is shown together with its autocorrelation function and power spectral density.

A random binary transmission is the signal generated by abstracting the result of a coin tossing experiment whose outcome may change at intervals of T sec. Calling heads $+1$ and tails -1 , so that short sequences in which the signal is unchanged from toss to toss could occur, but that long ones are unlikely, and then shifting the signal along the time axis an amount, ϵ , where ϵ is equally likely to take any value in the interval $0, T$, the result would be as illustrated in item 1 in Table 10-4.

"Boxcar sequences" are generated by taking positive or negative steps whose size is determined in some random way at intervals whose statistics are also prescribed. There are at least three interesting cases.

There is a boxcar sequence, item 2 in the table, in which the axis crossings are always T sec apart, as in the random binary transmission, but in which the magnitude of the signal at any time is a random variable. If, however, the mean square value here were one, this signal would have an autocorrelation and power spectral density identical to the random binary transmission. This serves to emphasize the fact that the autocorrelation function and power spectral density are not specific to a particular time function.

TABLE 10-4

DESCRIPTION OF RANDOM SIGNALS

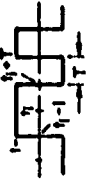
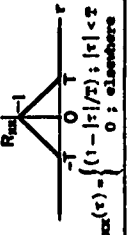
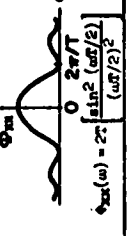
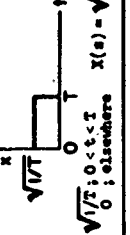

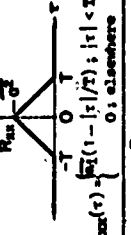
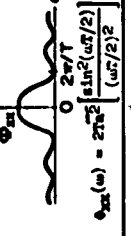
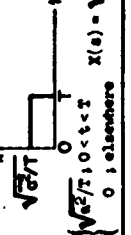

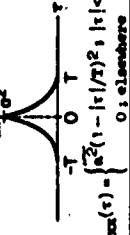
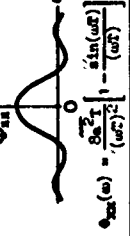
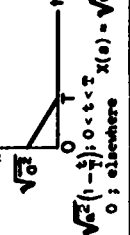
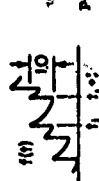
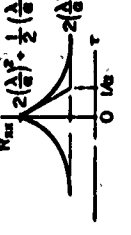
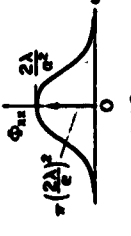
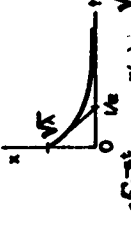
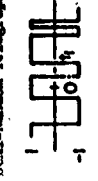
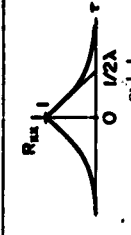
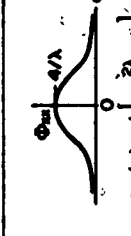
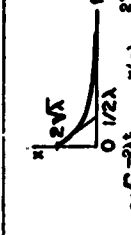
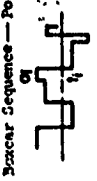
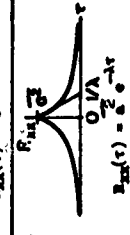
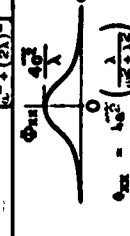
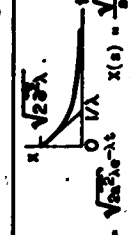

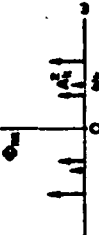

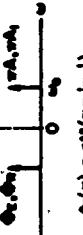

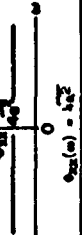




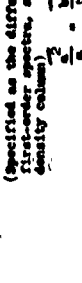

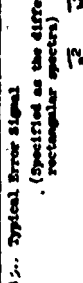
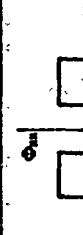
TYPICAL SIGNAL DEFINITION	EXPECTATIONS		AUTOCORRELATION FUNCTION	POWER SPECTRAL DENSITY	TRANSIENT ANALOG
	MEAN VALUE	PEAK-TO-PEAK VALUE			
1. Random Binary Transmission  $x(t) = \pm 1$, $t_1 < t < (t_1 + T)$ depending on the flip of a fair coin at t_1 . (Ensemble members randomly phased—uniform distribution in $0, T$)	0	1	 $R_{XX}(\tau) = \begin{cases} (1 - \tau /T) & \tau < T \\ 0 & \text{elsewhere} \end{cases}$	 $\Phi_{XX}(\omega) = \frac{2}{T} \left[\frac{\sin^2(\omega T/2)}{(\omega T/2)^2} \right]$	 $x(t) = \begin{cases} \sqrt{T/2} & 0 < t < T \\ 0 & \text{elsewhere} \end{cases}$ $X(s) = \sqrt{T/2} \frac{1 - e^{-sT}}{s}$
2. Semi-random Binary Sequence  $x(t) = \pm 1$, $t_1 < t < (t_1 + T)$ where the time characteristics are as in item 1; and a_1 is a random independent variable with zero mean-value.	0	$\frac{1}{\sqrt{2}}$	 $R_{XX}(\tau) = \begin{cases} \frac{1}{2} (1 - \tau /T) & \tau < T \\ 0 & \text{elsewhere} \end{cases}$	 $\Phi_{XX}(\omega) = \frac{1}{T} \left[\frac{\sin^2(\omega T/2)}{(\omega T/2)^2} \right]$	 $x(t) = \begin{cases} \sqrt{T/2} & 0 < t < T \\ 0 & \text{elsewhere} \end{cases}$ $X(s) = \sqrt{T/2} \frac{1 - e^{-sT}}{s}$
3. Boxcar Sequence—Uniform Distribution of Time Intervals  $x(t) = a_1$, $t_1 < t < (t_1 + T)$ where a_1 is defined as in item 2 and t_1 is a random uniformly distributed variable.	0	$\frac{1}{\sqrt{2}}$	 $R_{XX}(\tau) = \begin{cases} \frac{1}{2} (1 - \tau /T) & \tau < T \\ 0 & \text{elsewhere} \end{cases}$	 $\Phi_{XX}(\omega) = \frac{1}{T} \left[\frac{\sin^2(\omega T/2)}{(\omega T/2)^2} \right]$	 $x(t) = \begin{cases} \sqrt{T/2} & 0 < t < T \\ 0 & \text{elsewhere} \end{cases}$ $X(s) = \sqrt{T/2} \frac{1 - e^{-sT}}{s}$
4. Shot Noise (Special Case)  $x(t) = \sum_{i=1}^n a_i \delta(t - t_i)$, $N(t) = e^{-at}$ where t_1 is a poisson distributed points, that is $P_{t_1}(n, T) = \frac{(nT)^n e^{-nT}}{n!}$, $1/\lambda = \text{average interval between } t_1 \text{ and } t_{i+1}$ $T = \text{some time interval}$ $a = \text{the number of } t_1 \text{ in } T$	$\sqrt{2} \left(\frac{a}{T} \right)^2 + \frac{1}{2} \left(\frac{a}{T} \right)$		 $R_{XX}(\tau) = \begin{cases} \frac{1}{2} (1 - \tau /T) & \tau < T \\ 0 & \text{elsewhere} \end{cases}$	 $\Phi_{XX}(\omega) = \frac{2}{T} \left[\frac{\sin^2(\omega T/2)}{(\omega T/2)^2} \right]$	 $x(t) = \sqrt{T/2} \frac{1 - e^{-at}}{s}$ Note: The transient analog cannot and need not model impulsive features of the power spectral density
5. Semi-Random Telegraph Signal  $x(t) = \begin{cases} \pm 1, & t = 0 \\ \pm 1, & \text{depending on number of Poisson distributed zero crossings (see item 4)} \end{cases}$	e^{-2at} Not Stationary!	1	 $R_{XX}(\tau) = \begin{cases} \frac{1}{2} (1 - \tau /T) & \tau < T \\ 0 & \text{elsewhere} \end{cases}$	 $\Phi_{XX}(\omega) = \frac{2}{T} \left[\frac{\sin^2(\omega T/2)}{(\omega T/2)^2} \right]$	 $x(t) = \begin{cases} \sqrt{T/2} & 0 < t < T \\ 0 & \text{elsewhere} \end{cases}$ $X(s) = \sqrt{T/2} \frac{1 - e^{-sT}}{s}$
6. Boxcar Sequence—Poisson Time Intervals  $x(t) = a_1$, $t_1 < t < (t_1 + T)$ where t_1 is defined in item 4 and a_1 is a random independent variable with zero mean-value.	0	$\frac{1}{\sqrt{2}}$	 $R_{XX}(\tau) = \begin{cases} \frac{1}{2} (1 - \tau /T) & \tau < T \\ 0 & \text{elsewhere} \end{cases}$	 $\Phi_{XX}(\omega) = \frac{1}{T} \left[\frac{\sin^2(\omega T/2)}{(\omega T/2)^2} \right]$	 $x(t) = \begin{cases} \sqrt{T/2} & 0 < t < T \\ 0 & \text{elsewhere} \end{cases}$ $X(s) = \sqrt{T/2} \frac{1 - e^{-sT}}{s}$

TABLE 10-4 (Concluded)

TYPICAL SIGNALS AND THEIR DEFINITION	EXPECTATIONS		APPROXIMATIVE FUNCTION	POWER SPECTRAL DENSITY	TRANSIENT ANALOG
	MEAN VALUE	MEAN-SQUARE VALUE			
7. Sum of Random Sinus Waves $x(t) = A_0 + \sum_{k=1}^N A_k \cos(\omega_k t + \phi_k)$ A_k arbitrary ϕ_k uncorrelated ϕ_k random, independent and uniformly distributed in $0, 2\pi$	A_0	$A_0^2 + \sum_{k=1}^N \frac{A_k^2}{2}$		 $\Phi_{xx}(\omega) = \pi \sum_{k=1}^N A_k^2 \delta(\omega - \omega_k)$	See note for item 4
8. Sum of Sinus Waves of Equal Amplitude and Frequency $x(t) = \sum_{k=1}^N A \cos(\omega_k t + \phi_k)$, ϕ_k defined as in item 7 $A_1 = A \sqrt{2} \sum_{k=1}^N \cos(\phi_k - \phi_1)^{1/2}$ $\phi = \tan^{-1} \left(\frac{\sum_{k=1}^N \sin \phi_k}{\sum_{k=1}^N \cos \phi_k} \right)$	$x(t) = 0$ $\bar{x}(t) = 0$ Not Ergodic!	$x^2(t) = \frac{N^2 A^2}{2}$ $\bar{x}^2(t) = \frac{A^2}{2}$	 $x(t) = \sum_{k=1}^N A \cos(\omega_k t + \phi_k)$ $\bar{x} = \frac{A^2}{2} \cos(\omega_k t)$ $\bar{x}(t) = \frac{A^2}{2} \cos(\omega_k t)$	 $\Phi_{xx}(\omega) = \pi A^2 \delta(\omega - \omega_k)$	See note for item 4
9. Gaussian White Noise	0	Infinity	 $\bar{x}(t) = 0$ $\bar{x}^2(t) = \infty$	 $\Phi_{xx}(\omega) = \frac{N^2 A^2}{2}$	$x(t) = \sqrt{\frac{2}{\pi}} \delta(t)$ $\bar{x}(t) = \sqrt{\frac{2}{\pi}} \delta(t)$
10. Gaussian "Colored" Noise—First-Order Spectrum	0	$\frac{N^2 A^2}{2}$	 $\bar{x}(t) = 0$ $\bar{x}^2(t) = \frac{N^2 A^2}{2}$	 $\Phi_{xx}(\omega) = \frac{N^2 A^2}{2} \delta(\omega - \omega_k)$	$x(t) = \sqrt{\frac{2}{\pi}} \delta(t)$ $\bar{x}(t) = \sqrt{\frac{2}{\pi}} \delta(t)$
11. Gaussian "Colored" Noise—Second-Order Spectrum	0	$\frac{N^2 A^2}{2}$	 $\bar{x}(t) = 0$ $\bar{x}^2(t) = \frac{N^2 A^2}{2}$	 $\Phi_{xx}(\omega) = \frac{N^2 A^2}{2} \delta(\omega - \omega_k)$	$x(t) = \sqrt{\frac{2}{\pi}} \delta(t)$ $\bar{x}(t) = \sqrt{\frac{2}{\pi}} \delta(t)$
12. Typical Error Signal (Specified as the difference between two first-order spectra, see power spectral density column) $\frac{N^2 A^2}{2} = \frac{N^2 A^2}{2}$	0	$\frac{N^2 A^2}{2}$	 $\bar{x}(t) = 0$ $\bar{x}^2(t) = \frac{N^2 A^2}{2}$	 $\Phi_{xx}(\omega) = \frac{N^2 A^2}{2} \delta(\omega - \omega_k)$	—
13. Typical Error Signal (Specified as the difference between two rectangular spectra) $\frac{N^2 A^2}{2} = \frac{N^2 A^2}{2}$	0	$\frac{N^2 A^2}{2}$	 $\bar{x}(t) = 0$ $\bar{x}^2(t) = \frac{N^2 A^2}{2}$	 $\Phi_{xx}(\omega) = \frac{N^2 A^2}{2} \delta(\omega - \omega_k)$	—

Another type of boxcar sequence is one with random amplitudes and in which the intervals during which the signal is constant have a uniform distribution of lengths in the interval 0, T. See item 3 in the table.

The third boxcar sequence of interest, discussed below, depends for its description on a time function which comprises a sequence of impulses, each of weight (area), q_i , occurring randomly in time at a constant average rate. In Appendix B it is shown that the probability of finding a given number $s = 0, 1, 2, \dots, n$ impulses in a given interval of length, T, is then governed by the Poisson distribution. Such a sequence of impulses is, therefore, called a sequence of generalized Poisson impulses. It is also shown in Appendix B that the probability of finding an impulse in an interval more than t and less than $t + dt$ sec after its predecessor is governed by the exponential distribution. The mean interval between impulses, $T_{av} = 1/\beta$, where β is the "density" of the impulses along the time axis. The expression for the generalized Poisson impulse sequence is:

$$z(t) = \sum_i q_i \delta(t - t_i) \quad (10-66)$$

Here the t_i are understood to represent the (random) times of occurrence of the impulses. The manner of choosing the weights, q_i , remains to be specified. Figure 10-4 shows a typical generalized Poisson impulse sequence in which q_i is a random variable which may take either positive or negative values.

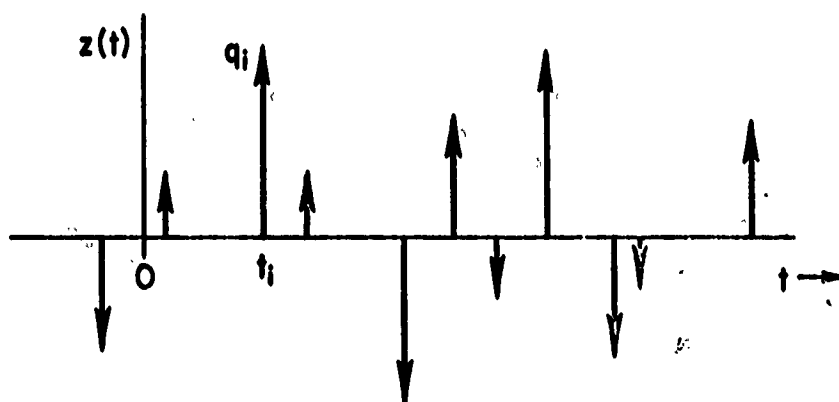


Fig. 10-4. Generalized Poisson Impulse Sequence

If the generalized Poisson impulse sequence is specialized in such a way that each $q_i = +1$, i.e. each impulse is a positive unit impulse occurring randomly in time at a constant average rate, and this signal is passed through a linear, constant coefficient filter with a weighting function, $h(t)$, the result is a random process known as "shot noise." Shot noise, from our point of view, is primarily of historical interest.* The shot noise process is illustrated as item 4 in Table 10-4 for the particular case in which $h(t) = e^{-\alpha t}$.

A time function called the semi-random telegraph signal is generated by switching from +1 to -1 at times t_i which are determined in the same way as the times of occurrence of the Poisson impulses. It is illustrated as item 5 in the table.

Next, item 6, take a boxcar sequence in which the occurrence of the steps in time is governed by the Poisson distribution. In fact the function we wish to consider is simply the integral of the generalized Poisson impulse sequence, Eq. 10-66. Note interestingly, that, except for constants, the autocorrelation function and power spectral density for this function are exactly the same as the ones for the quite different semi-random telegraph signal. In fact, the exponential autocorrelation function and the corresponding power spectral density are typical of many physical random processes. See also item 10 in the table. In this case, if the amplitudes of the steps in the boxcar sequence were chosen in such a way that the amplitude of the original function were normally (Gaussianly) distributed, it would be quite impossible to distinguish between this process and the one represented by item 10 on the basis of the first probability density function and the autocorrelation function or its transform, the power spectral density. Higher order density functions would be required to define each function in more detail in order to be able to tell the difference.

Sums of sine waves are very important special functions with random-like properties. This is because in computing and in experimental work

*S. O. Rice, "Mathematical Analysis of Random Noise," originally published in the Bell Systems Tech. J., Vols. 23 and 24, reprinted in N. Wax (ed.), Selected Papers on Noise and Stochastic Processes, Dover Publications, New York, 1954.

it is often convenient to have a segment of a "random process" which can be repeated and in which the mean-square value and power spectral density can easily be adjusted to meet particular requirements. The probability distribution for the amplitude of a sum of a comparatively small number of sine waves closely approaches a Gaussian distribution. Figure 10-5 shows the first probability density function for 1 sine wave and for sums of 3, 4, 8, and 12 sine waves of equal amplitude. In the case in which the sine waves have unequal amplitudes the density function does not approximate the density function of the Gaussian distribution as well for the same number of sine waves.* It is still amazing, however, how few sine waves need to be added together to yield a very good approximation to a random function of time with a Gaussian amplitude distribution. This is an illustration of the operation of the central limit theorem of statistics.

For analytical and experimental work, it is item 7 in Table 10-4 which is most important. Item 8 is interesting because of its statistical properties, but, of course, as a function of time it is merely a (periodic) sine wave with an initially randomly chosen phase angle.

The next five items in Table 10-4 are perhaps somewhat out of place since they are defined primarily in terms of the properties of the power spectral density function rather than as time functions.

"White" noise, item 9, is a signal whose power spectral density as a function of frequency is a constant. (The name is derived from the fact that white light is a composite of all the colors with their different wave lengths or frequencies.) Our principal interest in white noise is in connection with the signal at the output of a linear filter whose input may be an approximation to white noise. (The nature of the approximation lies in the fact that white noise, with a power spectral

*W. R. Bennett, "Distribution of the Sum of Randomly Phased Components," Quarterly of Applied Mathematics, Vol. V, no. 4, Jan. 1948.

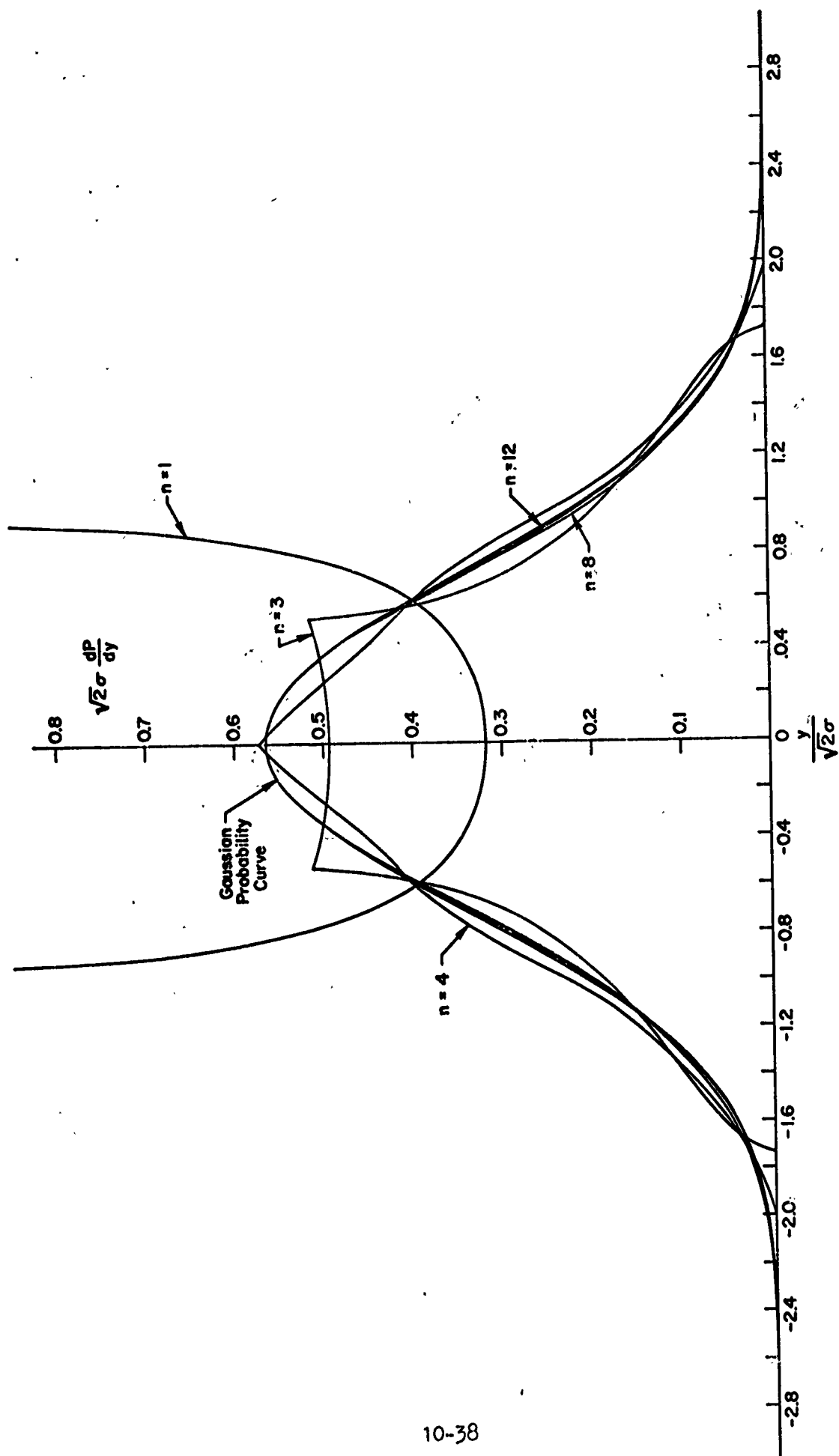


Fig. 10-5. Plot of the Probability Density Distributions of the Sum of n Sine Waves of Equal Amplitude

density flat to infinite frequency, is a physically unrealizable signal, but if the bandwidth of the noise is very large compared to the bandwidth of the filter, the approximation is accurate.)

When white noise is passed through a first order filter, i.e., one with a transfer function $1/(Ts+1)$, the result is a stochastic process which is typical of a very large number of physical phenomena (see item 10). Among other things, with a suitable choice of the time constant, T , it may be used as a model for atmospheric turbulence or as a model of terrain elevation as seen from an airplane in rectilinear flight. White noise through a first order filter is, therefore, a signal of particular interest and importance in flight control system engineering. This is especially true if the signal has a Gaussian amplitude distribution. (See the next section of this chapter.)

White noise through an underdamped second order filter, item 11, is a signal with a predominant band of frequencies which may give it some properties similar to a periodic signal. In this case, the filter has a transfer function $1/\left[\left(\frac{s}{\omega_n}\right)^2 + \frac{2\zeta}{\omega_n}s + 1\right]$. As the damping ratio, ζ , of the filter approaches zero, the output of the filter approaches a purely periodic sinusoidal wave with a noisy bias.

A typical error signal spectrum, item 12, may be simply the result of taking the difference between two spectra of the type illustrated as item 10.

Finally the rectangular spectrum, item 13, is of interest particularly in connection with experimental or computer work in which the signal is a sum of sine waves. Actually items 10 to 13 may be representative special cases of item 7 since the amplitudes of the constituent sine waves can be adjusted so as to produce any desired spectral shape. (See Eq. 10-61.)

10.5 PROPERTIES OF RANDOM PROCESSES WITH GAUSSIAN AMPLITUDE DISTRIBUTIONS

The most important stationary random functions, both theoretically and practically, are those which can be described in terms of Gaussian or normal amplitude distributions. Fortunately these are also among the simplest distributions to handle analytically.

Recall (or see Appendix B) that the first probability density and distribution functions for signals which have Gaussian statistics are

$$p_1(x) = \frac{1}{\sqrt{2\pi} \sigma} e^{-\frac{(x-m_1)^2}{2\sigma^2}} \quad (10-67)$$

and

$$P_1(x) = \frac{1}{2} \left[1 + \operatorname{erf} \frac{(x-m_1)}{\sqrt{2} \sigma} \right] \quad (10-68)$$

where

$$\operatorname{erf} z = \frac{2}{\sqrt{\pi}} \int_0^z e^{-\lambda^2} d\lambda$$

It may be noted that the distributions are specified completely when the mean, m_1 , and standard deviation, σ , are known. In linear systems, response calculations for the mean, or steady-state value can be separated from those for the fluctuating portions of the response, so it is possible to consider the fluctuations about m_1 alone. Under these circumstances the distributions about the mean are pertinent, m_1 can be taken equal to zero without loss of generality, and the variance, σ^2 , becomes simply the mean-square value of the signal.

When a signal within the system may be described by a Gaussian distribution, information about the probabilities of the signal having various values, being within certain ranges, etc., is readily obtained from Eqs. 10-27 and 10-67 and tables of the distribution* once the standard deviation, σ , is known. The simplest probabilities of all to obtain are those given by the first distribution function directly. These take on especially simple forms when low probability values are considered, since then the error function can be approximated by:

*See, for example, A. Hald, Statistical Tables and Formulas, John Wiley and Sons, Inc., New York, 1952, or M. M. Abramowitz and I. Stegun (eds.), Handbook of Mathematical Functions, National Bureau of Standards Applied Mathematics Series 55, U. S. Government Printing Office, Washington, D. C., 1964.

$$\operatorname{erf} z \doteq 1 - \frac{e^{-z^2}}{z\sqrt{\pi}}; z \gg 1$$

Thus, when it is desired to find the probability that a Gaussian distribution signal is a factor k times greater than the standard deviation,

$$\Pr[x(t) > k\sigma] = 1 - P_1(k\sigma) \doteq \frac{e^{-k^2/2}}{\sqrt{2\pi} k} \quad (10-69)$$

when $k \gg 1$. (See also Table B-4, Appendix B.)

One of the most interesting properties of time signals which have Gaussian distributions is the fact that for some purposes they can be thought of as a sum of sinusoids. The time signal $x(t)$, as expressed in a Fourier series with zero mean,

$$x(t) = \sum_{k=1}^N A_k \cos(\omega_k t + \phi_k) \quad (10-70)$$

will have a probability density function as $N \rightarrow \infty$ which approaches a Gaussian distribution function if the frequencies are given by $\omega_k = k\Delta\omega$, and the phase angles ϕ_k are random and distributed uniformly (i.e., as in the rectangular distribution of Table B-1, Appendix B) over the range from zero to 2π . (Recall Fig. 10-5.) The constants A_k must be fixed at values to match the power spectral density of the random process. The power spectral density of the function described by Eq. 10-70 is

$$\Phi_{xx}(\omega) = \pi \sum_{k=1}^N A_k^2 [\delta(\omega - \omega_k) + \delta(\omega + \omega_k)] \quad (10-71)$$

This expression represents a series of spectral lines at frequencies $\omega = \pm\omega_k$, and with weights πA_k^2 . In response calculations the same answers will be obtained using Eq. 10-71 and an ordinary, continuous power spectral density function $\Phi(\omega)$ if $\pi A_k^2 = \Phi(\omega_k)$, and if N is made sufficiently large.

A consequence of surpassing importance follows almost intuitively from the use of a sum of sinusoids to represent a Gaussian random signal.

In a stable, constant-coefficient, linear system the steady-state response to a sinusoidal input is itself sinusoidal, although the amplitude and phase are, in general, modified. When many sinusoids are used in the input, they all appear in the output, again with different amplitudes and phases. Now, if the input phases of the sinusoids are randomly distributed, the phases in the output waves will still be randomly distributed, even though phase shifts occur for each of the sinusoids. In the limit, then, as the number of sinusoids in the input is increased to come closer and closer to a normal distribution, the distribution of the output will also approach a normal distribution. The variance of the output will, in general, be different from that of the input because of the change in the amplitudes of the individual waves. Thus, in a time-invariant, linear system, Gaussian inputs will produce Gaussian outputs, and the computation of the mean-square output will give complete information about the first probability density and distribution functions of the output signal.

Besides the interesting and valuable characteristics noted above, Rice* has presented a number of additional properties of Gaussian random processes which are useful in obtaining a physical grasp of the time history characteristics of Gaussianly distributed time signals. These are summarized in Table 10-5.

A useful idealization of a Gaussian random signal has the bandlimited power spectral density shown in Fig. 10-6. This is, of course, a special case of item 13, Table 10-4. The corresponding autocorrelation function is also illustrated, along with a tabulation of the characteristics given in Table 10-5.

10.6 RESPONSE OF LINEAR SYSTEMS TO RANDOM INPUTS

The effect of a linear filter, or feedback system, operating on a particular power spectral density, $\Phi_{xx}(\omega)$, may be found as follows. Let the system have a weighting function, $w(t)$, such that the output, $y(t)$, in response to an input, $x(t)$, is given by the convolution integral:

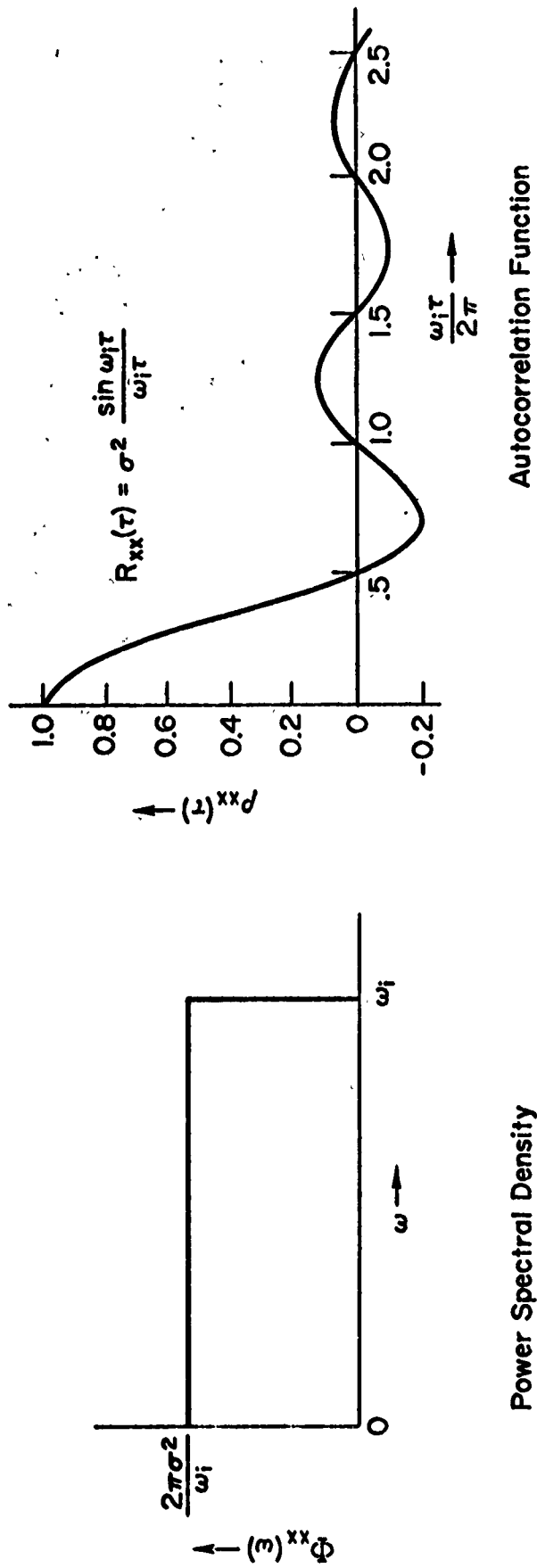
*S. O. Rice, "Mathematical Analysis of Random Noise," originally published in the Bell Systems Tech. J., Vols. 23 and 24, reprinted in N. Wax (ed.), Selected Papers on Noise and Stochastic Processes, Dover Publications, New York, 1954.

TABLE 10-5

SOME PROPERTIES OF A GAUSSIAN RANDOM PROCESS
COMPUTED FROM THE AUTOCORRELATION FUNCTION
OR THE POWER SPECTRAL DENSITY

PROPERTY	FROM THE AUTO-CORRELATION FUNCTION	FROM THE POWER SPECTRAL DENSITY
Mean Square	$\overline{x^2} = R_{xx}(0) = \sigma^2$	$\frac{1}{2\pi} \int_0^\infty \phi_{xx}(\omega) d\omega$
Axis Crossings per second	$N_0 = \frac{1}{\pi} \left[\frac{-R'_{xx}(0)}{R_{xx}(0)} \right]^{1/2}$ (see note below)	$\frac{1}{\pi} \left[\frac{\int_0^\infty \omega^2 \phi_{xx}(\omega) d\omega}{\int_0^\infty \phi_{xx}(\omega) d\omega} \right]^{1/2}$
Maxima per second	$N_m = \frac{1}{2\pi} \left[\frac{-R^{IV}(0)}{R''(0)} \right]^{1/2}$	$\frac{1}{2\pi} \left[\frac{\int_0^\infty \omega^4 \phi_{xx}(\omega) d\omega}{\int_0^\infty \omega^2 \phi_{xx}(\omega) d\omega} \right]^{1/2}$
Positive Crossings of level x , or number of maxima per second greater than x ; $x > 2\sigma$ (Exceedences)	$N_L(x) = \frac{N_0}{2} e^{-x^2/2\sigma^2}$ (See above for N_0 and σ)	$N_L(x) = \frac{N_0}{2} e^{-x^2/2\sigma^2}$ (See above for N_0 and σ)

Note: $R'_{xx}(0) = \left[\frac{d^2 R(\tau)}{d\tau^2} \right]_{\tau=0}$ etc.



Average Axis Crossing per second, $N_0 = \frac{\omega_i}{\sqrt{3}\pi} = 0.1837 \omega_i$

Average Number of Maxima per second, $N_m = \frac{1}{2\pi} \sqrt{\frac{3}{5}} \omega_i = 0.1232 \omega_i$

Average Number of Maxima $> x$, $N_L(x) = \frac{\sigma}{\sqrt{6\pi}} p_1(x) \omega_i = 0.230 \sigma p_1(x) \omega_i$

Fig. 10-6. Characteristics of Band-limited, Flat Spectrum, Gaussianly Distributed Signal

$$y(t) = \int_{-\infty}^{\infty} w(\tau_1) x(t - \tau_1) d\tau_1 = \int_{-\infty}^{\infty} w(t - \tau_1) x(\tau_1) d\tau_1 \quad (10-71)$$

Using Eq. 10-42 the autocorrelation function of the output can then be written in terms of the input as follows:

$$R_{yy}(\tau) = \lim_{T \rightarrow \infty} \frac{1}{2T} \int_{-T}^T dt \left[\underbrace{\int_{-\infty}^{\infty} w(\tau_1) x(t - \tau_1) d\tau_1}_{y(t)} \underbrace{\int_{-\infty}^{\infty} w(\tau_2) x(t + \tau - \tau_2) d\tau_2}_{y(t + \tau)} \right] \quad (10-72)$$

Interchanging the order of the integrations

$$R_{yy}(\tau) = \lim_{T \rightarrow \infty} \int_{-\infty}^{\infty} d\tau_1 \int_{-\infty}^{\infty} d\tau_2 w(\tau_1) w(\tau_2) \left[\frac{1}{2T} \int_{-T}^T dt x(t - \tau_1) x(t + \tau - \tau_2) \right] \quad (10-73)$$

but, in the limit, the quantity in square brackets may be seen to be the autocorrelation function, $R_{xx}(\tau_1 + \tau - \tau_2)$. Therefore, in the limit:

$$R_{yy}(\tau) = \int_{-\infty}^{\infty} d\tau_1 \int_{-\infty}^{\infty} d\tau_2 w(\tau_1) w(\tau_2) R_{xx}(\tau_1 + \tau - \tau_2) \quad (10-74)$$

Because the autocorrelation function is even, the Fourier transform of Eq. 10-74:

$$\begin{aligned} \Phi_{yy}(\omega) &= 2 \int_{-\infty}^{\infty} R_{yy}(\tau) e^{-j\omega\tau} d\tau = 4 \int_0^{\infty} R_{yy}(\tau) \cos \omega\tau d\tau \\ &= 2 \int_{-\infty}^{\infty} d\tau \int_{-\infty}^{\infty} d\tau_1 \int_{-\infty}^{\infty} d\tau_2 e^{-j\omega(\tau + \tau_1 - \tau_2)} \\ &\quad e^{j\omega\tau_1} e^{-j\omega\tau_2} R_{xx}(\tau + \tau_1 - \tau_2) w(\tau_1) w(\tau_2) \end{aligned} \quad (10-75)$$

Upon a change of the variable of integration τ to $(\tau + \tau_1 - \tau_2)$, the volume integral breaks up into the product of three independent integrals which may be recognized as representing the Fourier transforms of $w(t)$, its conjugate,

and the Fourier transform of $R_{xx}(\tau)$. Therefore, we have the important relationship in the transform domain:

$$\Phi_{yy}(\omega) = W(j\omega) W(-j\omega) \Phi_{xx}(\omega) = |W(j\omega)|^2 \Phi_{xx}(\omega) \quad (10-76)$$

where

$$W(j\omega) = \int_{-\infty}^{\infty} w(t) e^{-j\omega t} dt$$

and, of course, the mean-squared value of the signal of interest is found from the formula:

$$\overline{y^2} = \frac{1}{2\pi} \int_0^{\infty} \Phi_{yy}(\omega) d\omega = \frac{1}{2\pi} \int_0^{\infty} |W(j\omega)|^2 \Phi_{xx}(\omega) d\omega = R_{yy}(0) \quad (10-77)$$

Integrals of this type, evaluated for systems through seventh-order, appeared first in James, Nichols, and Phillips.* The tables have since† been modified in form and extended through tenth-order systems, with corrections found for the I_7 expression. These are duplicated in a condensed form in Table 10-6. The higher-order literal expressions are lengthy, and the integrals can be expressed more compactly in terms of Hurwitz determinants.† The actual tabulated forms are for the integral

$$\begin{aligned} I_n &= \int_0^{\infty} y^2(t) dt = \lim_{\sigma \rightarrow 0} \frac{1}{2\pi j} \int_{c-j\infty}^{c+j\infty} Y(s) Y(\sigma - s) ds \\ &= \frac{1}{2\pi j} \int_{-j\infty}^{j\infty} Y(s) Y(-s) ds \\ &= \frac{1}{2\pi j} \int_{-j\infty}^{j\infty} \frac{d(s)}{a(s)} \frac{d(-s)}{a(-s)} ds \end{aligned} \quad (10-78)$$

*H. M. James, N. B. Nichols, and R. S. Phillips, Theory of Servomechanisms, McGraw-Hill Book Co., New York, 1947, pp. 369-370.

†R. C. Booten, Jr., Max V. Mathews, and W. W. Seifert, Nonlinear Servomechanisms with Random Inputs, Rept. 70, Dynamic Analysis and Control Lab., MIT, Cambridge, Massachusetts, Aug. 20, 1953, pp. 38-42.

†G. C. Newton, Jr., L. A. Gould, and J. F. Kaiser, Analytical Design of Linear Feedback Controls, John Wiley and Sons, Inc., New York, 1957, pp. 366-381.

TABLE 10-6

ABBREVIATED TABLE OF INTEGRALS*

This is a table of integrals of the type

$$\overline{y^2} = \int_0^\infty y(t)^2 dt = \frac{1}{2\pi j} \int_{-j\infty}^{j\infty} Y(s)Y(-s) \quad \text{where} \quad Y(s) = \frac{d_0 s^{n-1} + d_1 s^{n-2} + \dots + d_{n-1}}{a_0 s^n + a_1 s^{n-1} + \dots + a_n}$$

and the roots of $a_0 s^n + a_1 s^{n-1} + \dots + a_n$ are all in the left-half plane.

$$I_1 = \frac{d_0^2}{2a_0 a_1}$$

$$I_2 = \frac{d_0^2 + \frac{a_0}{a_2} d_1^2}{2a_0 a_1}$$

$$I_3 = \frac{a_2 d_0^2 + a_0 (d_1^2 - 2d_0 d_2) + \frac{a_0 a_1}{a_3} d_2^2}{2a_0 (a_1 a_2 - a_0 a_3)}$$

$$I_4 = \frac{d_0 (a_2 a_3 - a_1 a_4) + a_0 a_3 (d_1^2 - 2d_0 d_2) + a_0 a_1 (d_2^2 - 2d_1 d_3) + \frac{a_0}{a_4} d_3^2 (a_1 a_2 - a_0 a_3)}{2a_0 (a_1 a_2 a_3 - a_0 a_3^2 - a_1^2 a_4)}$$

*Adopted from the table in Booten, Mathews, and Seifert, loc. cit.

This applies only for stable systems. Note in comparing Eq. 10-77 with Eq. 10-78 that

$$\begin{aligned}\overline{y^2} &= \frac{1}{2\pi} \int_0^\infty \phi_{yy}(\omega) d\omega = \frac{1}{2\pi} \int_{-\infty}^\infty \frac{\phi_{yy}(\omega)}{2} d\omega \\ &= \frac{1}{2\pi j} \int_{-j\infty}^{j\infty} Y(s)Y(-s)ds = \frac{1}{2\pi} \int_{-\infty}^\infty Y(j\omega)Y(-j\omega)d\omega\end{aligned}$$

or

$$Y(j\omega)Y(-j\omega) = \frac{\phi_{yy}}{2}$$

The factor of two is a consequence of the definition of the power spectral density such that $\overline{y^2}$ is given as an integral power density over only real frequencies. It is a point to be remembered when using Table 10-6.

An immediate application of Eq. 10-77 is the computation of mean-squared amplitude for an output quantity in response to an input spectrum, $\phi_{xx}(\omega)$. This is accomplished by evaluating Eq. 10-77 for $\phi_{yy}(\omega)$ to obtain $\overline{y^2}$, or the rms, σ . This technique allows computation of a variety of performance indices. Examples include flight path deviation about the ideal profile in terrain following, or the localizer course in an automatic approach. Design considerations such as rms control surface deflection and deflection rate can be studied as well.

Another application of Eq. 10-77 is in the modeling of a command input spectral density. If $\phi_{nn}(\omega)$ is a Gaussian white noise source, then a shaping filter, $G_f(j\omega)$, can be "fitted" to yield the input spectrum, $\phi_{xx}(\omega)$. The input spectrum is then given by:

$$\phi_{xx}(\omega) = |G_f(j\omega)|^2 \phi_{nn}(\omega) \quad (10-79)$$

Since $\phi_{nn}(\omega)$ is a constant, $|G_f(j\omega)|^2$ must have the shape of the desired input spectrum.*

*Actual disturbance and command data for automatic flight control system analyses are summarized in J. E. Hart, L. A. Adkins, and L. L. Lacau, Stochastic Disturbance Data for Flight Control System Analysis, ASD-TDR-62-347, Sept. 1962, and D. H. Weir, Compilation and Analysis of Flight Control System Command Inputs, AFFDL-TR-65-119, Nov. 1965.

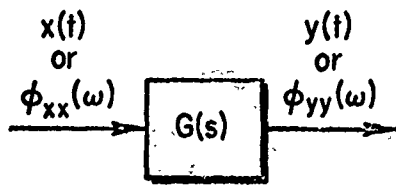


Fig. 10-7. A Simple Transfer Characteristic

A more general case is the one where the command input is the sum of several random signals. For N input components and one output, the transfer function characteristic of Fig. 10-7 becomes the one shown in Fig. 10-8. The inputs are assumed to have zero means,

but are not necessarily uncorrelated. Denote the cross-spectral density between the i th and k th inputs as $\phi_{ki}(\omega)$. Defining $G_k^*(j\omega)$ as the complex conjugate of $G_k(j\omega)$, yields the following equation for the spectrum of the sum:

$$\phi_{xx}(\omega) = \sum_{i=1}^N \sum_{k=1}^N G_i(j\omega) G_k^*(j\omega) \phi_{ki}(\omega) \quad (10-80)$$

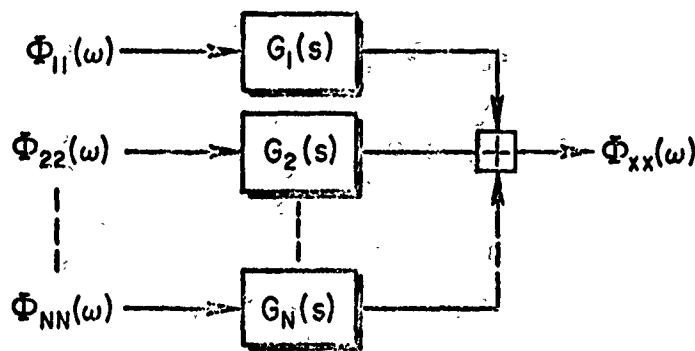


Fig. 10-8. A Multiple-Input System

When the N inputs are uncorrelated, Eq. 10-80 reduces to:

$$\phi_{xx}(\omega) = \sum_{k=1}^N |G_k(j\omega)|^2 \phi_{kk}(\omega) \quad (10-81)$$

If the inputs are summed prior to entering a single transfer block, the situation would be the one illustrated in Fig. 10-9. In this case Eq. 10-81 simplifies to:

$$\phi_{xx}(\omega) = |G_1(j\omega)|^2 \sum_{k=1}^N \phi_{kk}(\omega) \quad (10-82)$$

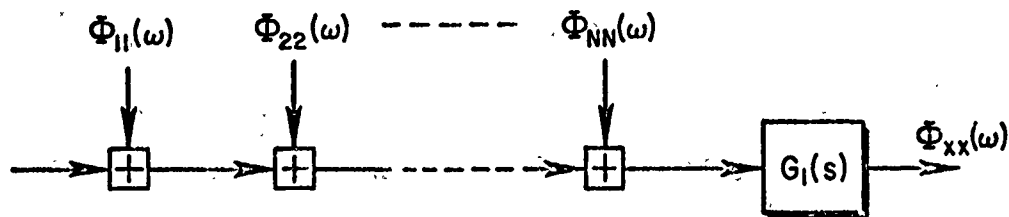
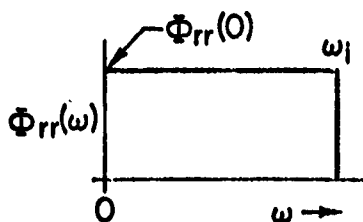


Fig. 10-9: Summation of Random Inputs

Many random disturbance and command input data are well approximated by the Gaussian probability density function.* With single or multiple Gaussian random inputs and a linear transfer characteristic (see Fig. 10-7), the output will also be Gaussianly distributed, so that evaluation of the mean-square value from the output power spectral density is only the beginning of the interesting calculations which can be made. Recall the previous section.

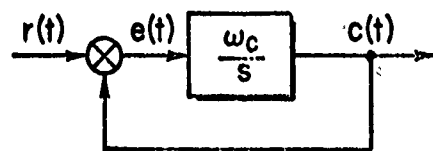
Example 1: Following error in a first-order servomechanism

Given a rectangular band limited input spectrum $\Phi_{rr}(\omega)$ as the input to a first-order servomechanism, find the dependence of the mean-square error in following this input on the cutoff frequency of the input, ω_i , and the inverse time constant (crossover frequency) of the closed-loop system, ω_c (Fig. 10-10).



$$\begin{aligned}\sigma_r^2 &= \frac{1}{2\pi} \int_0^{\infty} \Phi_{rr}(\omega) d\omega \\ &= \frac{\Phi_{rr}(0)\omega_i}{2\pi}\end{aligned}$$

(a) the input



$$\begin{aligned}\frac{E(s)}{R(s)} &= \frac{1}{1 + \frac{\omega_c}{s}} = \frac{s}{s + \omega_c} \\ &= \frac{s}{s + \frac{1}{T_{CL}}}\end{aligned}$$

(b) the system

Fig. 10-10. A Band Limited Input Spectrum and First Order Servomechanism

*J. E. Hart, I. A. Adkins, L. L. Lacau, loc. cit.
D. H. Weir, loc. cit.

From Eq. 10-77:

$$\begin{aligned}
 \overline{e^2} &= \frac{1}{2\pi} \int_0^\infty \left| \frac{E(j\omega)}{R(j\omega)} \right|^2 \Phi_{rr}(\omega) d\omega \\
 &= \frac{\Phi_{rr}(0)}{2\pi} \int_0^{\omega_i} \left(\frac{1}{1 + \frac{\omega_c}{j\omega}} \right) \left(\frac{1}{1 - \frac{\omega_c}{j\omega}} \right) d\omega \\
 &= \frac{\Phi_{rr}(0)}{2\pi} \int_0^{\omega_i} \frac{\omega^2}{\omega^2 + \omega_c^2} d\omega \\
 &= \frac{\Phi_{rr}(0)}{2\pi} \omega_i \left[1 - \frac{\omega_c}{\omega_i} \tan^{-1} \left(\frac{\omega_i}{\omega_c} \right) \right]
 \end{aligned}$$

The continued fraction* for the inverse tangent is:

$$\tan^{-1} x = \frac{x}{1 + \frac{x^2}{3 + \frac{4x^2}{5 + \frac{9x^2}{7 + \dots}}}}$$

Taking the third convergent as an approximation:

$$\begin{aligned}
 1 - \frac{1}{x} \tan^{-1} x &\doteq 1 - \frac{1}{x} \left[\frac{x}{1 + \frac{x^2}{3 + \frac{4x^2}{5}}} \right] \\
 &= \frac{x^2}{3 + \frac{9x^2}{5}}
 \end{aligned}$$

Finally:

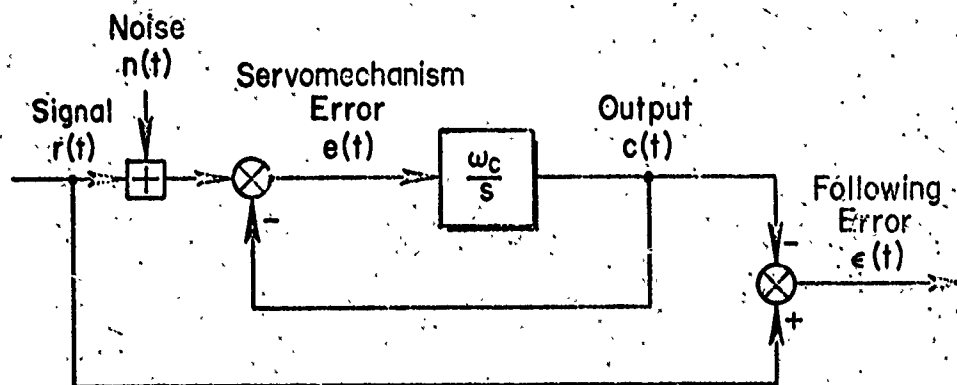
$$\frac{\overline{e^2}}{\sigma_r^2} \doteq \frac{(\omega_i/\omega_c)^2}{3 + \frac{9}{5} \left(\frac{\omega_i}{\omega_c} \right)^2} \doteq \frac{1}{3} \left(\frac{\omega_i}{\omega_c} \right)^2; \quad \omega_i \ll \omega_c$$

*C. D. Olds, Continued Fractions, Random House, Inc., New York, 1963.

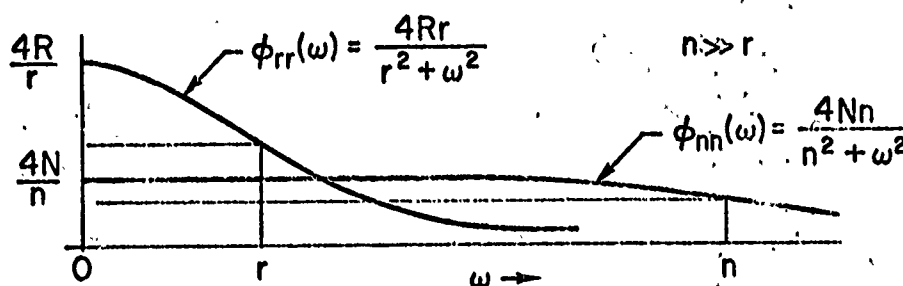
The mean-square error in following the input is roughly proportional to the mean-square input, σ_r^2 , to the square of the input bandwidth, ω_i^2 , and is inversely proportional to the square of the crossover frequency, ω_c^2 .

Example 2: The optimum fixed-form adjustment of a first-order servomechanism with signal and noise inputs

Given a first-order servomechanism with command signal and noise inputs, what is the best adjustment of the crossover frequency, ω_c , so as to minimize the error, $\epsilon(t)$, in following the desired signal $r(t)$ (see Fig. 10-11). Note that the injection of the noise signal might be in the feedback path (measurement noise) or at the servomechanism error point (amplifier noise) without altering this problem.



a) the system



b) the signal and noise inputs

Fig. 10-11. Minimizing the Following Error in the Presence of Noise

The error in following is given by the expression:

$$\epsilon = r - c$$

Then with a substitution for $C(s)$ the Laplace transform is

$$\epsilon(s) = R(s) - \left[R(s) + N(s) \right] \frac{\omega_c}{s + \omega_c}$$

or

$$\epsilon(s) = R(s) \frac{s}{s + \omega_c} - N(s) \frac{\omega_c}{s + \omega_c} = E_r + E_n$$

Assuming there is no correlation between signal and noise,

$$\begin{aligned} \Phi_{\epsilon\epsilon}(\omega) &= \frac{4Rr\omega^2}{\left| (r + \omega)(\omega_c + \omega) \right|^2} + \frac{4Nn\omega_c^2}{\left| (n + \omega)(\omega_c + \omega) \right|^2} \\ &= \Phi_{\epsilon\epsilon_r}(\omega) + \Phi_{\epsilon\epsilon_n}(\omega) \end{aligned}$$

Then the mean-squared error will be

$$\begin{aligned} \overline{\epsilon^2} &= \overline{\epsilon_r^2} + \overline{\epsilon_n^2} \\ &= \frac{1}{2\pi} \int_0^\infty \Phi_{\epsilon\epsilon_r}(\omega) d\omega + \frac{1}{2\pi} \int_0^\infty \Phi_{\epsilon\epsilon_n}(\omega) d\omega \\ &= \frac{1}{2\pi j} \int_{-j\infty}^{j\infty} E_r(s) E_r(-s) ds + \frac{1}{2\pi j} \int_{-j\infty}^{j\infty} E_n(s) E_n(-s) ds \end{aligned}$$

where

$$E_r(s) = \frac{\sqrt{2Rr}}{(s + r)} \frac{s}{(s + \omega_c)}$$

$$E_n(s) = \frac{\sqrt{2Rr}}{(s + n)} \frac{\omega_c}{(s + \omega_c)}$$

Both the following error components are given by a specialized form of the integral I_2 from Table 10-6, i.e.,

$$I_2 = \frac{d_0^2 + \frac{a_0}{a_2} d_1^2}{2a_0a_1}$$

For the following error in response to the signal,

$$d(s) = d_0s + d_1 = \sqrt{2Rr}$$

$$d_0 = \sqrt{2Rr}, \quad d_1 = 0$$

$$a(s) = a_0s^2 + a_1s + a_2 = s^2 + (r + \omega_c)s + r\omega_c$$

$$a_0 = 1, \quad a_1 = r + \omega_c, \quad a_2 = r\omega_c$$

$$\text{so } \overline{\epsilon_r^2} = \frac{Rr}{(r + \omega_c)}$$

Similarly, for the following error in response to the noise,

$$d_0 = 0, \quad d_1 = \sqrt{2Nn} \omega_c$$

$$a_0 = 1, \quad a_1 = n + \omega_c, \quad a_2 = n\omega_c$$

$$\begin{aligned} \text{and } \overline{\epsilon_n^2} &= \frac{\frac{1}{n\omega_c} (2Nn) \omega_c^2}{2(n + \omega_c)} \\ &= \frac{N\omega_c}{n + \omega_c} \end{aligned}$$

Combining the contributions to the mean-square following error:

$$\overline{\epsilon^2} = \overline{\epsilon_r^2} + \overline{\epsilon_n^2} = \frac{Rr}{r + \omega_c} + \frac{N\omega_c}{n + \omega_c}$$

To find the crossover frequency, ω_c , which minimizes the total mean-square error, we differentiate the expression for ϵ^2 with respect to ω_c , set the result equal to zero, and try to solve for ω_c .

$$\frac{d\epsilon^2}{d\omega_c} = -\frac{Rr}{(r + \omega_c)^2} + \frac{N}{(n + \omega_c)} - \frac{N\omega_c}{(n + \omega_c)^2} = 0$$

or

$$\frac{Nn}{(n + \omega_c)^2} = \frac{Rr}{(r + \omega_c)^2} = \frac{N/n}{\left(1 + \frac{\omega_c}{n}\right)^2} = \frac{R/r}{\left(1 + \frac{\omega_c}{r}\right)^2}$$

In the practical case in which $\omega_c \ll n$

$$\frac{N}{n} \doteq \frac{R}{r} \frac{1}{\left(1 + \frac{\omega_c}{r}\right)^2}$$

or

$$\left(\frac{\omega_c}{r}\right)^2 + \frac{2\omega_c}{r} + 1 \doteq \frac{R/r}{N/n}$$

Therefore:

$$\frac{\omega_c}{r} \doteq \sqrt{\frac{Rn}{Nr}} - 1$$

If, now, the "signal to noise" is large (i.e., $R/N \gg 1$) and the signal to noise bandwidth ratio is small (i.e., $n \gg r$), then

$$\frac{\omega_c}{r} \doteq \sqrt{\frac{Rn}{Nr}}$$

Back in 1951 J. R. Dutilh* conjectured that, in general, the half power frequency of the servomechanism (crossover frequency) should be adjusted to the frequency where the command signal power is equal to the noise power. In this problem, we could set the expressions for the two spectra equal and solve for the frequency, ω .

$$\frac{4Rr}{r^2 + \omega^2} = \frac{4Nn}{n^2 + \omega^2}$$

or

$$\frac{R/r}{1 + \frac{\omega^2}{r^2}} = \frac{N/n}{1 + \frac{\omega^2}{n^2}}$$

or again if $\omega \ll n$

$$1 + \frac{\omega^2}{r^2} = \frac{Rn}{Nr}$$

and

$$\frac{\omega}{r} = \sqrt{\frac{Rn}{Nr} - 1}$$

Under similar assumptions of signal to noise power and bandwidth ratios as above this will become

$$\frac{\omega}{r} = \sqrt{\frac{Rn}{Nr}}$$

*Comment in A. Tustin (ed.), Automatic and Manual Control, Butterworths Scientific Publications, London, 1951, p. 156.

10.7 COMPUTER METHODS

In many practical cases the response of vehicle control systems to random inputs and disturbances will be determined by automatic computation. If the calculations are to be performed on a computer anyway, there may be no advantage to working with the spectral descriptions. Computer methods of evaluating the mean square, and other statistics, of signals in control systems, including cases which often arise in guidance problems in which the system is time-varying, are discussed in Lanning and Battin.* Two particularly powerful and useful methods are the "transient analog,"† and the "adjoint system."‡ The methods are closely related, with the transient analog being a special feature of the adjoint technique. Here, however, they will be treated separately for simplicity.

For a system with transfer function, $W(s)$, excited by a random process $x(t)$, the mean-squared output is, of course,

$$\overline{y^2} = \lim_{T \rightarrow \infty} \frac{1}{2T} \int_{-T}^T y^2(t) dt = \frac{1}{2\pi} \int_0^\infty |W(j\omega)|^2 \Phi_{xx}(\omega) d\omega \quad (10-83)$$

The idea of the transient analog of a power spectral density, $\Phi_{xx}(\omega)$, is based on finding an input time function, $x_t(t)$, such that the system output response, y_t , has an integral square value which is the same as $\overline{y^2}$. That is,

$$\int_0^\infty y_t^2 dt = \overline{y^2} \quad (10-84)$$

* J. H. Lanning and R. H. Battin, Random Processes in Automatic Control, McGraw-Hill Book Co., New York, 1956.

† T. R. Benedict and V. C. Rideout, "Error Determination for Optimum Predicting Filters," Proc. National Electronics Conference, Vol. 13, 1957, pp. 875-887.

B. Etkin, "A Simple Method for the Analogue Computation of the Mean-Square Response of Airplanes to Atmospheric Turbulence," J. Aerospace Sciences, Vol. 28, No. 10, Oct. 1961, pp. 825-826.

R. Magdaleno and J. Wolkovitch, Performance Criteria for Linear Constant-Coefficient Systems with Random Inputs, ASD-TDR-62-170, Jan. 1963.

where the transient response y_t ,

$$y_t = \int_0^t w(\tau) x_t(t-\tau) d\tau = \int_0^t w(t-\tau) x_t(\tau) d\tau ; \quad t \geq 0 \quad (10-85)$$

To find the relationship between x_t and ϕ_{xx} required to make this so we shall resort to the real multiplication, real integration, and final value theorems of the Laplace transformation (see Table 2-1). Using the real multiplication theorem, the transform of y_t^2 will be

$$\begin{aligned} \mathcal{L}[y_t^2] &= \frac{1}{2\pi j} \int_{c-j\infty}^{c+j\infty} Y_t(s-\lambda) Y_t(\lambda) d\lambda \\ &= \frac{1}{2\pi j} \int_{c-j\infty}^{c+j\infty} W(s-\lambda) X_t(s-\lambda) W(\lambda) X_t(\lambda) d\lambda \quad (10-86) \end{aligned}$$

From the real integration theorem,

$$\begin{aligned} \mathcal{L}\left[\int_0^t y_t^2 dt\right] &= \frac{1}{s} \mathcal{L}[y_t^2] \\ &= \frac{1}{s} \frac{1}{2\pi j} \int_{c-j\infty}^{c+j\infty} W(s-\lambda) X_t(s-\lambda) W(\lambda) X_t(\lambda) d\lambda \quad (10-87) \end{aligned}$$

The final value theorem is subject to restrictions on $W(s)$ and $X_t(s)$ which insure that the integral square output has a finite value. As a practical matter this requires the system to be stable and $X_t(s)$ to be analytic on and to the right of the imaginary axis, thereby allowing c to be zero in the contour integral. The final value theorem can now be applied,

$$\begin{aligned}
\int_0^{\infty} y_t^2 dt &= \lim_{t \rightarrow \infty} \int_0^t y_t^2 dt = \lim_{s \rightarrow 0} s \mathcal{L} \left[\int_0^t y_t^2 dt \right] \\
&= \lim_{s \rightarrow 0} s \frac{1}{2\pi j s} \int_{-j\infty}^{j\infty} W(s-\lambda)W(\lambda)X_t(s-\lambda)X_t(\lambda)d\lambda \\
&= \frac{1}{2\pi j} \int_{-j\infty}^{j\infty} W(-\lambda)W(\lambda)X_t(-\lambda)X_t(\lambda)d\lambda \quad (10-88)
\end{aligned}$$

Changing the variable λ to $j\omega$,

$$\begin{aligned}
\int_0^{\infty} y_t^2 dt &= \frac{1}{2\pi} \int_{-\infty}^{\infty} W(-j\omega)W(j\omega)X_t(-j\omega)X_t(j\omega)d\omega \\
&= \frac{1}{2\pi} \int_{-\infty}^{\infty} |W(j\omega)|^2 |X_t(j\omega)|^2 d\omega \quad (10-89)
\end{aligned}$$

Comparison of Eqs. 10-83 and 10-89 reveals that the two integrals will be the same provided that the transient analog input, $x_t(t)$, is chosen so that

$$X_t(j\omega)X_t(-j\omega) = \frac{1}{2} \Phi_{xx}(\omega) \quad (10-90)$$

Thus, the transient analog, $x_t(t)$, appropriate to the power spectral density $\Phi_{xx}(\omega)$, must have an energy spectral density which is the same function of frequency (except for the units) as half the power spectral density of the random input.

The unit delta function is the transient analog of a white noise spectrum with 2 units of power per radian per second. If the random input of interest is considered to be the result of passing a unit white noise spectrum through a linear filter with a Fourier transfer function, $G_f(j\omega)$ (see Fig. 10-12 and recall Eq. 10-79), then the transient analog

of the random input of interest is the output of the same filter excited by an impulse with weight $1/\sqrt{2}$.

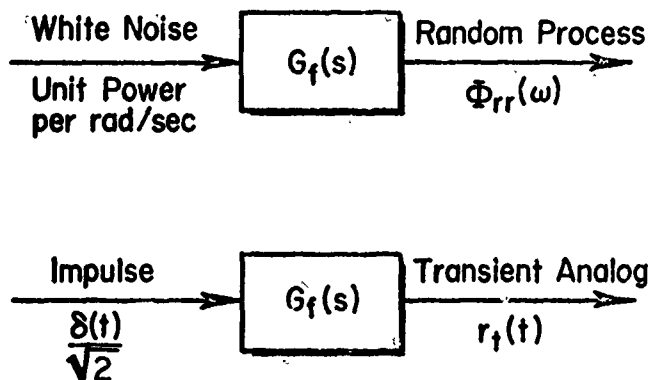


Fig. 10-12. The Transient Analog of a Random Process Formed by Passing White Noise Through a Filter

For constant coefficient situations the transient analog technique is all that is required for the computation of integral-square transient responses, and thus the analogous mean-square response. When time variations become important, however, we need a different approach. This is provided by the adjoint techniques described below.

To make the discussion concrete consider the problem of determining the effect of noise in the radar guidance system on the miss distance of a homing missile. A highly simplified block diagram of the automatic flight control and guidance system for control in a vertical plane is presented in Fig. 10-13. (Cf. Fig. 1-5 in Chapter 1.) The block diagram represents a system which is linear, but with time-varying coefficients. Even this very simple system is relatively intractable, and the usual recourse is to simulation. Figure 10-14 represents a simulation diagram* for the system, drawn in terms of components which

*C. L. Johnson, Analog Computer Techniques, McGraw-Hill Book Co., New York, 1956.

G. A. Korn and T. M. Korn, Electronic Analog and Hybrid Computers, McGraw-Hill Book Co., New York, 1964.

S. Fifer, Analogue Computation, McGraw-Hill Book Co., New York, 1961, 4 Vols.

A. E. Rogers and T. W. Connolly, Analog Computation in Engineering Design, McGraw-Hill Book Co., New York, 1960.

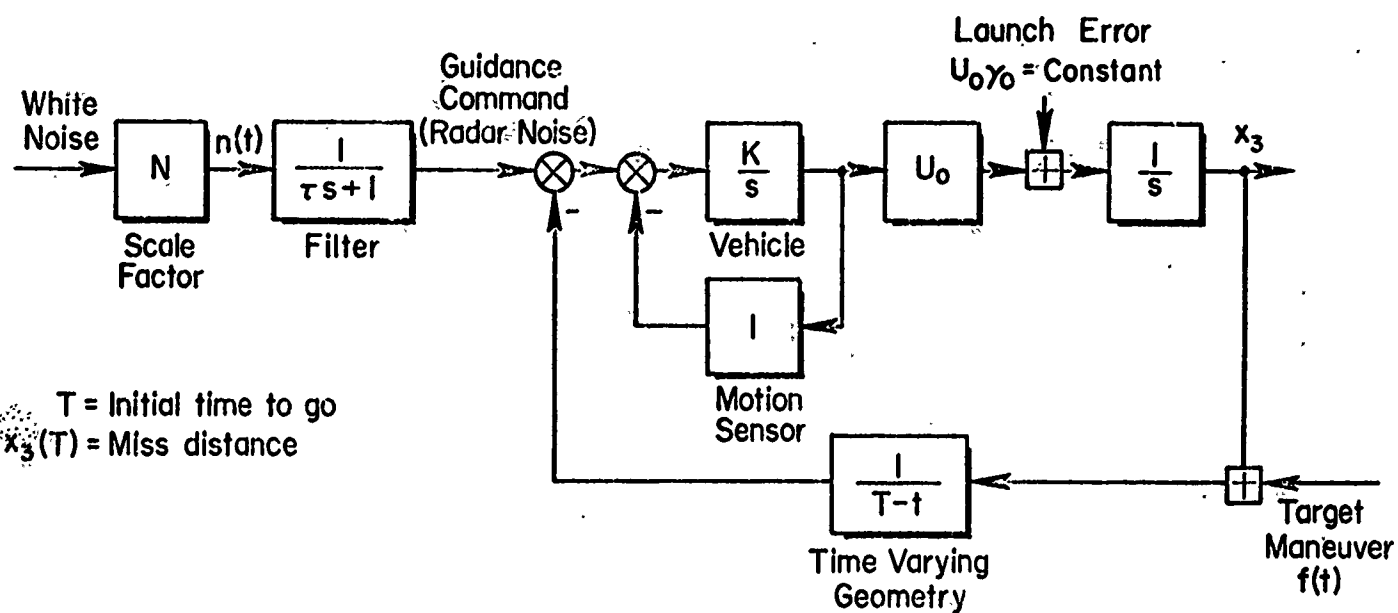


Fig. 10-13. Simplified Block Diagram for Guidance of a Homing Missile in the Vertical Plane

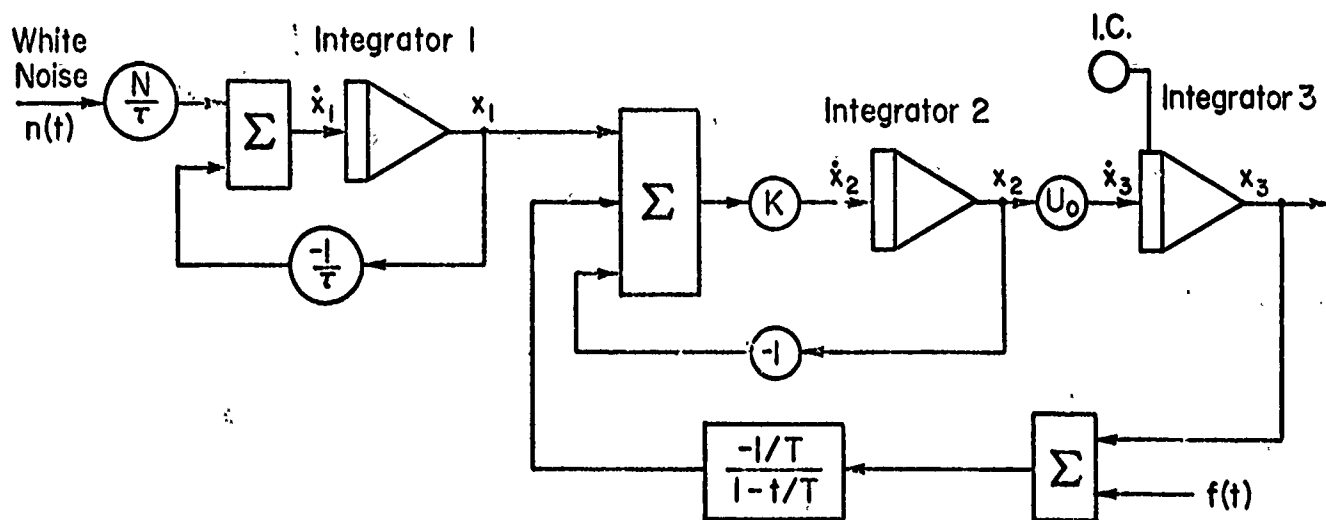


Fig. 10-14. Simulation Diagram; Homing Missile

are called "integrators," "summers," and "coefficient potentiometers." (We have neglected the usual sign change in integrators and summers.) From either the block diagram or the simulation diagram and the definitions of the operation of the several components, we may write the differential equations of the system. Considering only the noise input, $n(t)$ for the moment for simplicity,

$$\begin{aligned}\dot{x}_1 &= -\frac{1}{\tau} x_1 + \frac{N}{\tau} n(t) \\ \dot{x}_2 &= +Kx_1 - Kx_2 - \frac{K}{T} \left(\frac{1}{1 - \frac{t}{T}} \right) x_3 \\ \dot{x}_3 &= U_0 x_2\end{aligned}\quad (10-91)$$

The equations for x_1 , x_2 , and x_3 , sometimes called "state variables," may also be written in matrix form:

$$\begin{bmatrix} \dot{x}_1 \\ \dot{x}_2 \\ \dot{x}_3 \end{bmatrix} = \begin{bmatrix} -\frac{1}{\tau} & 0 & 0 \\ +K & -K & -\frac{K}{T} \left(\frac{1}{1 - \frac{t}{T}} \right) \\ 0 & +U_0 & 0 \end{bmatrix} \begin{bmatrix} x_1 \\ x_2 \\ x_3 \end{bmatrix} + \begin{bmatrix} \frac{N}{\tau} \\ 0 \\ 0 \end{bmatrix} n(t) \quad (10-92)$$

In general, equations such as Eq. 10-92 may be written in the form:

$$\dot{\mathbf{x}}(t) = \mathbf{A}(t)\mathbf{x}(t) + \mathbf{B}(t)\mathbf{u}(t) \quad (10-93)$$

$\mathbf{x}(t)$ is the $n \times 1$ matrix of system outputs, $\mathbf{u}(t)$ is the $m \times 1$ matrix of system inputs, $\mathbf{A}(t)$ is the square $n \times n$ matrix of system coefficients, and $\mathbf{B}(t)$ is the $n \times m$ matrix of input coefficients.

Note that in the concrete example of Fig. 10-14 and Eq. 10-91, the impulse responses of the system to a unit impulse $n(t) = \delta(t-z)$ applied at the first summer are the same things as the initial condition responses of the system if $x_1(z) = N/\tau$ and all other initial conditions (in this case

x_2 and x_3) are zero. This is, of course, because with no other inputs or initial conditions, the integration of the impulse by integrator 1 produces a step, or equivalently, an initial condition on the output when the problem begins to run at $t = z$. In general, the impulse responses of the system are the same as the initial condition responses for the initial condition on the same integrator to which the impulse would have been applied.

Consider next what it might take to give an answer to the original question, i.e., the effect of noise on the miss distance. Suppose that the guidance system noise could be represented by a white noise power spectral density so that a suitably scaled impulse would be its transient analog. The impulse response, $w(t, z)$ of a linear, time-varying system, however, is a function of two time variables:

1. The time, z , at which the impulse is applied
2. The time, t , at which the response is measured

By way of contrast, the impulse response of a linear, constant-coefficient system is a function only of the difference in time, $\tau = t - z$, between the application of the impulse and the time at which the response is measured.

Similar to the transient analog, the ensemble mean-square response* at a time t , $E[y^2(t)]$, of a time-varying system responding to a white noise input, x , with unit power per radian per second applied at input terminal 1 continuously from $-\infty$ to t , is derived below:

$$E[y^2(t)] = E \left[\int_{-\infty}^t x(z) w_{y1}(t, z) dz \right]^2 \quad (10-94)$$

where $w_{y1}(t, z)$ = the response in y at time, t , to a unit impulse applied at time, z , to input terminal (integrator) number 1.

*The ensemble average is the value of a statistical parameter at time, t , averaged over a large number of trials with random initial conditions and noise, but all having the same statistical properties. In time-varying problems, of course, ensemble averages are not equal to time averages.

Expanding Eq. 10-94 and moving the expected value operator inside the integrations gives

$$\begin{aligned}
 E[y^2(t)] &= E \left[\int_{-\infty}^t \int_{-\infty}^t w_{y1}(t,z) w_{y1}(t,\lambda) x(z) x(\lambda) dz d\lambda \right] \\
 &= \int_{-\infty}^t \int_{-\infty}^t w_{y1}(t,z) w_{y1}(t,\lambda) E[x(z)x(\lambda)] dz d\lambda \quad (10-95) \\
 &= \int_{-\infty}^t \int_{-\infty}^t w_{y1}(t,z) w_{y1}(t,\lambda) R_{xx}(z-\lambda) dz d\lambda
 \end{aligned}$$

Since x is unit white noise

$$R_{xx}(z-\lambda) = \frac{1}{2} \delta(z-\lambda) \quad (10-96)$$

Inserting Eq. 10-96 into 10-95 gives

$$E[y^2(t)] = \frac{1}{2} \int_{-\infty}^t [w_{y1}(t,z)]^2 dz \quad (10-97)$$

Suppose we wished to evaluate the ensemble mean-squared response using simulation and Eq. 10-94. $w_{y1}(t,z)$ might be obtained from direct measurements. If a unit impulse is applied at time, z , to input terminal 1, the simulation yields $w_{y1}(t,z)$ as a function of t . The variable of integration in Eq. 10-94, however, is z . It would, therefore, seem necessary to record a number of impulse responses for various values of z , cross plot the results, and integrate the kernel of the equation numerically or graphically. This procedure is illustrated in Fig. 10-15. In the example shown in the sketch, several simulator trials would be required in order to evaluate $E[y^2(t)]_{t=3}$, and the whole process would have to be repeated for any other values of t of interest. While it is entirely feasible

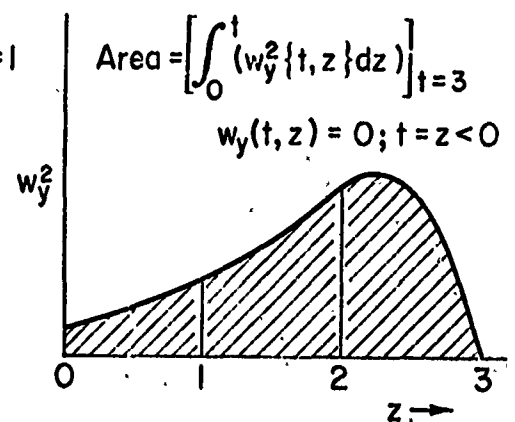
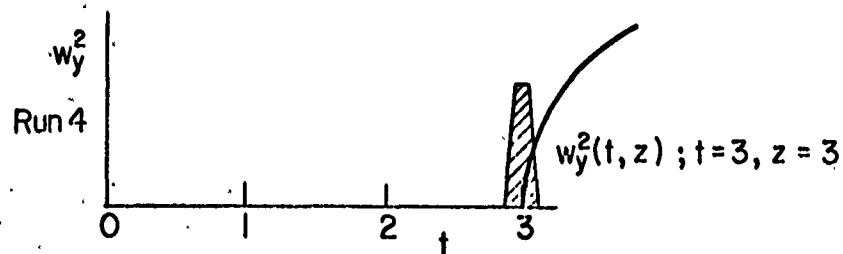
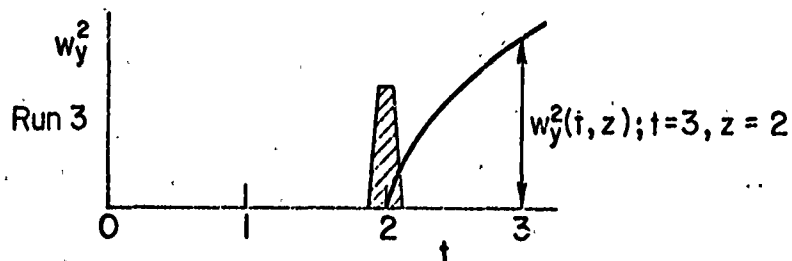
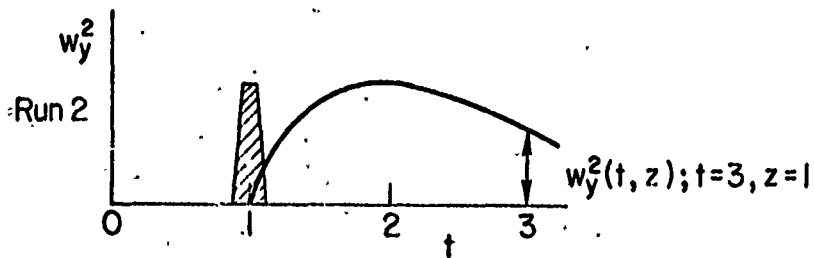
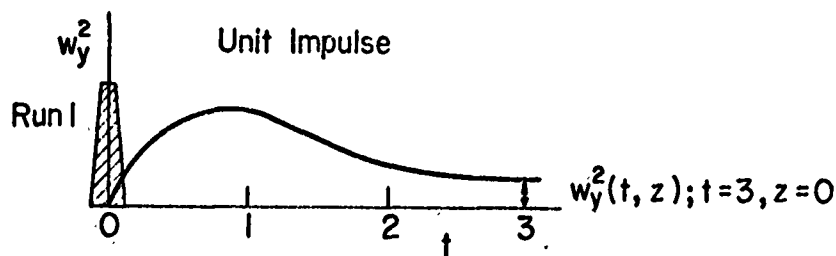
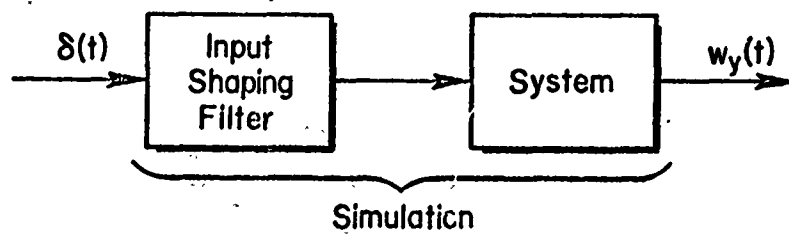


Fig. 10-15. Steps Required to Calculate Mean-Squared Response by the Direct (Non-Adjoint) Method

to do this it is tedious and uneconomical. Fortunately, it is also unnecessary.

The system simulation we should like to have would produce $w_{y1}(t, z)$ as a continuous function of z . The response would then be evaluated according to the formula (Eq. 10-94). The operations of squaring and integrating the impulse response could be mechanized in the simulation. Then only one run would be required for each value $t = T$ which might be of interest. Is there such a system? The answer is: yes. It is called the modified adjoint system.*

Heuristically the basic idea of the adjoint system can be introduced by considering the principle of reciprocity for linear systems. A familiar example of the reciprocity principle occurs in the theory of structures where a concentrated load applied at Point A produces a deflection at Point B equal to that which would be produced at Point A by the same load applied at Point B. The nature of the load influences are characterized by structural influence coefficients, analogous to weighting functions.

How does this apply to the present context, i.e., how do we obtain the same response, $w(t, z)$, in two different ways? One way we already know: a unit impulse applied to the system at time z produces an output at time t given by $w(t, z)$. Now how do we get an output $w(t, z)$ at time z by applying an input impulse at time t ? The direct answer is obvious enough: measure $w(t, z)$ at the original input terminal, apply the impulse

*J. H. Lanning and R. H. Battin, Random Processes in Automatic Control, McGraw-Hill Book Co., Inc., New York, 1956.

G. I. Teper and R. L. Stapleford, Adjoint Computer Techniques for a Homing Missile System, STI TM 241-5, Systems Technology, Inc., Hawthorne, Calif., Jan. 1963.

P. M. DeRusso, R. J. Roy, C. M. Close, State Variables for Engineers, John Wiley and Sons, Inc., New York, 1965, pp. 333-388.

S. Fifer, loc. cit., pp. 1052-1085.

A. E. Rogers and T. W. Connolly, loc. cit., pp. 233-246.

at the original output terminal, and run time backwards. This last requirement is awkward, to say the least, on analog computers! Consequently, to exploit the reciprocity idea it is necessary to develop a simulator diagram which is related to the original simulator circuit by a simple set of rules to be given below. This new simulator setup is that of the adjoint system. When it is achieved, then the adjoint output will produce a time history w_y versus z . When squared this produces w_y^2 versus z , identical to that illustrated in Fig. 10-15. Then, in terms of this example, integrating the squared time history from zero to 3 yields $[\int_0^t w^2(t,z)dz]_{t=3}$ in a single run.

In order to understand why the modified adjoint system may operate so as to produce the desired results, it is necessary to take a modest excursion via matrix calculus. The reader who may be less interested in the why than in the how to may skip the next four pages.

Take a system of linear, time-varying coefficient, differential equations of the form of Eq. 10-9 and a closely related system of equations:

$$\dot{\alpha}(t) = -A^T(t)\alpha(t) \quad (10-98)$$

Here to matrix $A^T(t)$ is the transpose of $A(t)$, formed by interchanging the rows and columns of $A(t)$. If Eq. 10-93 are the original equations, then the Eq. 10-98 homogeneous equations are said to be the adjoint equations. This simply means that they are formed from the original set of homogeneous equations $\dot{x} = A(t)x(t)$ according to the rule which specifies that the coefficient matrix of the adjoint equations, $-A^T$, is the negative transpose of the coefficient matrix of the original homogeneous equations, A .

Form the product $\alpha^T(t)x(t)$ and take the derivative with respect to time,

$$\frac{d}{dt}[\alpha^T(t)x(t)] = \dot{\alpha}^T(t)x(t) + \alpha^T(t)\dot{x}(t) \quad (10-99)$$

but from Eq. 10-98

$$\dot{\alpha}^T(t) = - [A^T(t)\alpha(t)]^T = -\alpha^T(t) [A^T(t)]^T = -\alpha^T(t)A(t) \quad (10-100)$$

Substituting this result and the expression on the right hand side of the first of Eq. 10-93 in Eq. 10-99

$$\begin{aligned} \frac{d}{dt} [\alpha^T(t)x(t)] &= -\alpha^T(t)A(t)x(t) + \alpha^T(t) [A(t)x(t) + B(t)u(t)] \\ &= \alpha^T(t)B(t)u(t) \end{aligned} \quad (10-101)$$

Integrating Eq. 10-101 from t_1 to t_2 ,

$$\alpha^T(t_2)x(t_2) = \alpha(t_1)x(t_1) + \int_{t_1}^{t_2} \alpha^T(t)B(t)u(t)dt \quad (10-102)$$

It is ordinarily possible to define the starting time t_1 such that $x(t_1) \equiv 0$, thereby simplifying Eq. 10-102 somewhat. Also, the boundary conditions on $\alpha(t)$ are arbitrary, so that when we are interested in one particular output, $x_1(t_2)$, all the components of $\alpha(t_2)$ except $\alpha_1(t_2)$ can be set equal to zero, i.e.,

$$\alpha_j(t_2) = \begin{cases} 0 & i \neq j \\ 1 & i = j \end{cases} \quad (10-103)$$

Eq. 10-102 can now be written as

$$x_1(t_2) = \int_{t_1}^{t_2} \alpha^T(t)B(t)u(t)dt \quad (10-104)$$

With $\alpha(t_2)$ fixed everything is known in Eq. 10-104 except $\alpha(t)$, which is the output of the adjoint system. To make the boundary conditions equal to initial conditions we substitute a new time variable $t^* = t_2 - t_1$ and

rewrite Eqs. 10-98 and 10-104 in terms of this new independent variable. Then they become,

$$\frac{d}{dt^*} [\alpha(t_2 - t^*)] = A^T(t_2 - t^*) \alpha(t_2 - t^*) \quad (10-105)$$

$$\begin{aligned} x_i(t_2) &= - \int_{t_2 - t_1}^0 \alpha^T(t_2 - t^*) B(t_2 - t^*) u(t_2 - t^*) dt^* \\ &= \int_0^{t_2 - t_1} \alpha^T(t_2 - t^*) B(t_2 - t^*) u(t_2 - t^*) dt^* \end{aligned} \quad (10-106)$$

where

$$(\alpha_j)_{t^*=0} = \begin{cases} 0 & i \neq j \\ 0 & i = j \end{cases} \quad (10-107)$$

Equations 10-105 and 10-106 are the equations of the modified adjoint system (modified by the change in the time variable). Their solution after the imposition of the initial conditions of Eq. 10-107 will yield $\alpha^T(t_2 - t^*)$. All of the rules for the formulation of the adjoint computer diagram can be derived from Eqs. 10-105 and 10-106.

The coefficient matrix, A^T , in the modified adjoint system is the transpose (rows and columns interchanged) of the coefficient matrix in the original system, Eq. 10-94, and with "time," t^* , in the modified adjoint system running "backwards," the coefficients are started at their values appropriate to $t = t_2$, i.e., $t^* = 0$. Thus if integrator, i , in the original system produces x_i from \dot{x}_i and feeds n integrators via coefficients $a_{ij}(t)$, $j = 1, 2, \dots, n$, in the modified adjoint system the inputs to integrator i come from $j = 1, 2, \dots, n$ integrators via coefficients $a_{ji}(t_2 - t^*)$. This is illustrated in Fig. 10-16. Similar considerations apply to summers when they are necessary and to the coefficient pots for the elements of the B matrix. (Actually summers become merely takeoff points and takeoff points become summers in the simulation of the modified adjoint system.)

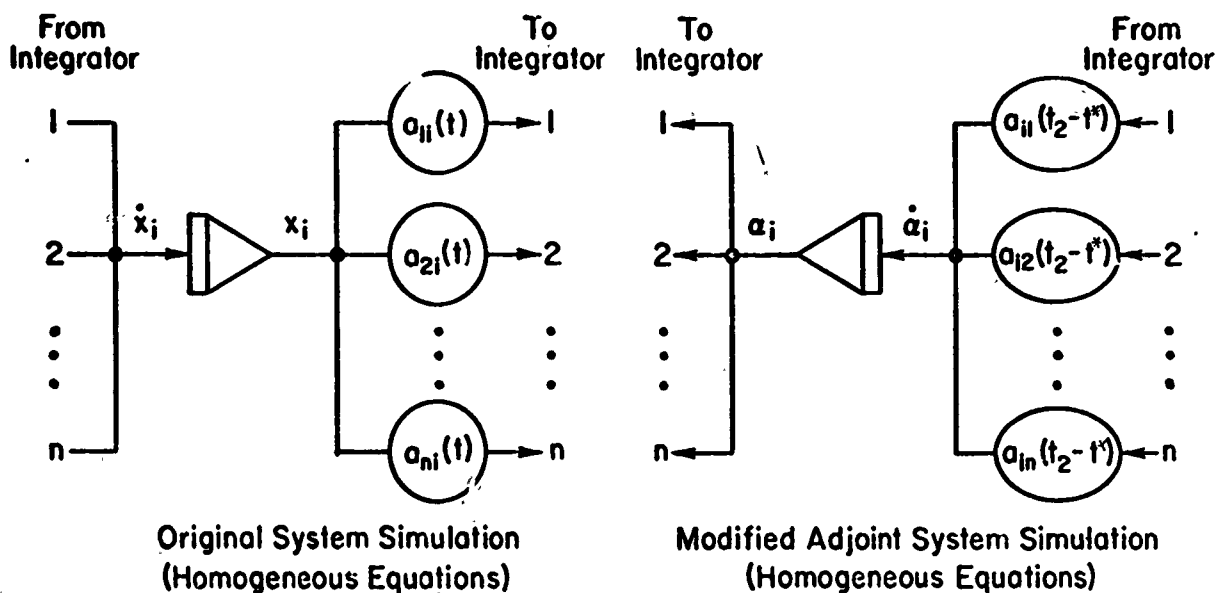


Fig. 10-16. The Interchange of Inputs and Outputs on Integrators and Coefficient Potentiometers

These facts lead to the following simple rules for simulating the modified adjoint system, starting with a simulation diagram of the original system.*

1. The outputs of each summer or integrator in the system analog become the inputs to that summer or integrator in the modified adjoint analog; the inputs in the system analog become the outputs in the modified adjoint analog.
2. The input and output are exchanged on all coefficient potentiometers.
3. Multipliers used to represent time-varying coefficients are replaced by multipliers representing the same coefficient as a function of the new variable $t^* = t_2 - t$, i.e., time-varying coefficients are started at their final values and run backward toward their initial values.

*T. S. Durand and G. L. Teper, An Analysis of Terminal Flight Path Control in Carrier Landings, TR 137-1, Systems Technology, Inc., Hawthorne, Calif., June 1964.

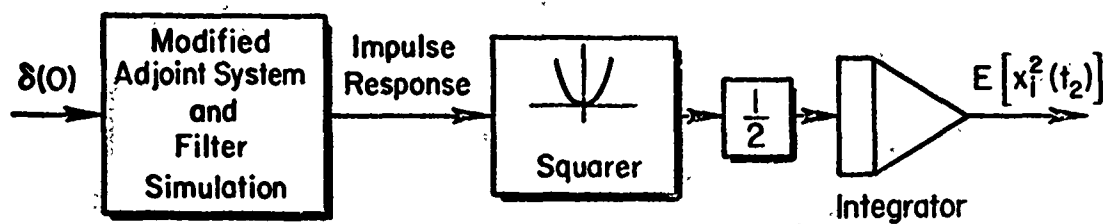
4. A unit impulse is put into the one integrator or summer from which the output of interest was taken in the system analog. Since, however, the integral of a unit impulse is a unit step, instead of attempting to generate an actual impulse, a step or initial condition can be put on the output of the integrator, or summer, but the step or initial condition should not exist at the output of the integrator until the problem begins to run.
5. The modified adjoint impulse response functions are then measured in the modified adjoint analog, at the points where the corresponding inputs in the system analog were introduced.
6. Components necessary to square, scale, and integrate the impulse response functions are added as needed. (See Fig. 10-17.)

Step (initial condition) or ramp responses of the original system may be obtained by once or twice integrating the impulse responses of the modified adjoint system at the terminals where the steps or ramps would have been introduced. Similarly the response to an arbitrary input may be obtained by multiplying the impulse response at the terminal in the modified adjoint system corresponding to the point of introduction of the arbitrary function in the original system, and integrating the result. This represents the computer mechanization of Eq. 10-106. The operations are shown symbolically in Fig. 10-17.

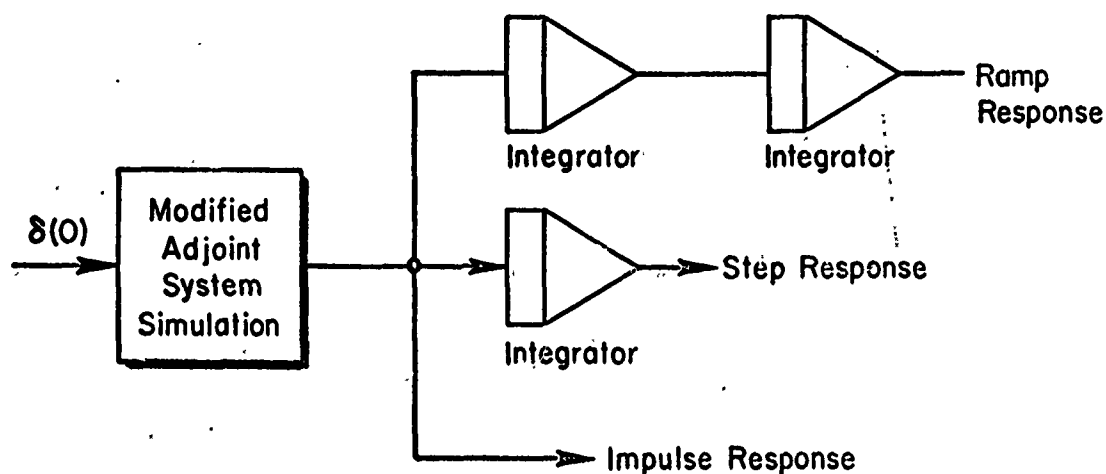
It is necessary to point out that it is not usually possible to associate physical quantities with all of the signals in the simulation of the modified adjoint system. This very likely leads to problems in the scaling of the simulation which are only overcome by trial and error.

Now, by way of illustration, the drawing of the simulation diagram shall be carried out explicitly in connection with the simple example of the guidance of a homing missile.

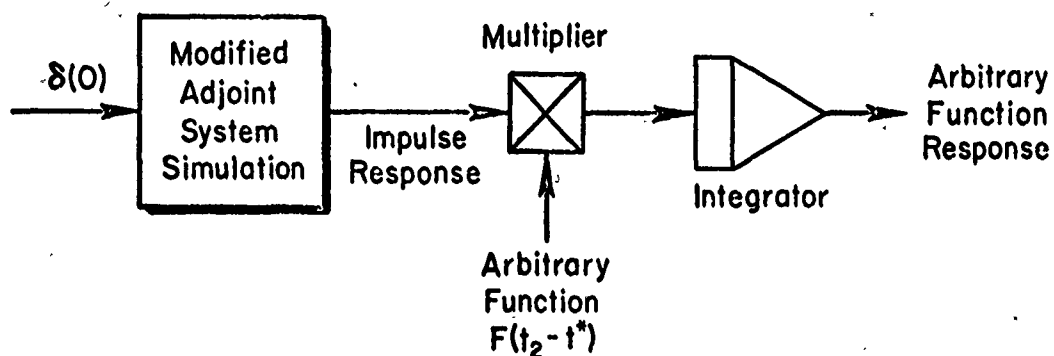
The simulation diagram of the original system has already been presented as Fig. 10-14. Identifying $t_2 = T$, and carrying out the instructions of the numbered rules above results in the simulation diagram of Fig. 10-18. Reversing the connections on the integrators and coefficient potentiometers is particularly straightforward, as is



a) Computing the Mean Square Response to a White Noise Input



b) Computing Step and Ramp Responses



c) Computing an Arbitrary Function Response

Fig. 10-17. The Responses of Interest Can be Generated from the Impulse Responses of the Modified Adjoint System Simulation

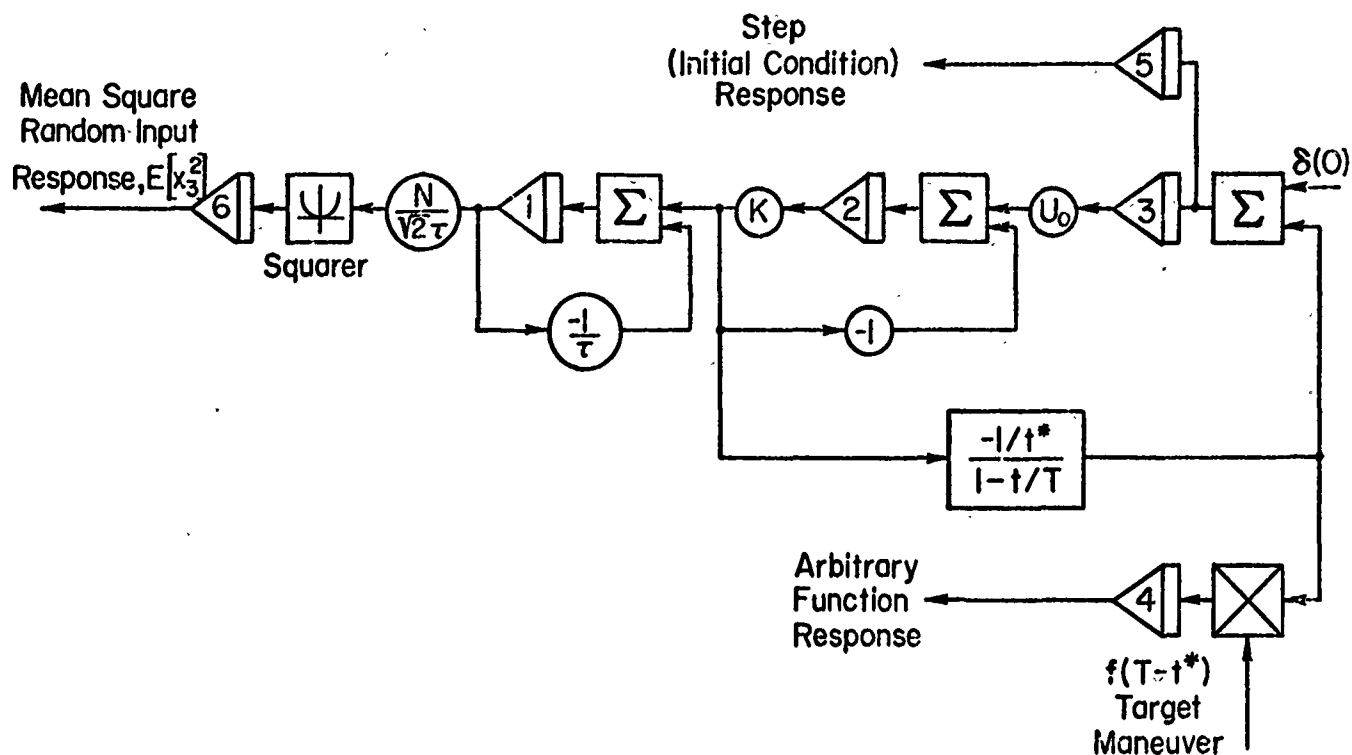


Fig. 10-18. The Modified Adjoint System Simulation
Derived from the Simulation Diagram of the Original System

making the summers takeoff points and the takeoff points summers. Taking the outputs from the points for the inputs in the original system and providing the impulse input at the original output point completes the diagram for the modified adjoint system. Notice that the factor of $\sqrt{2}$ is inserted as a modifier for N/τ . This permits the multiplier and Integrators 4 and 5 to be added to compute the miss distance responses to the target maneuver and launch error without any modifiers at all.

This concludes the discussion of the response of linear systems to deterministic and random inputs and of system performance assessment in terms of response quantities.

SUPPLEMENT

BIBLIOGRAPHY TO SUPPLEMENT AIRCRAFT DYNAMICS AND AUTOMATIC CONTROL

I. Additional Aspects of Aircraft Dynamics, including

- Steady rolling flight
 - Steady turning flight
 - Internal angular momenta effects
 - Structural flexibility
1. M. J. Abzug, "Effects of Certain Steady Motions on Small-Disturbance Airplane Dynamics," J. Aeron. Sci., Vol. 21, No. 11, Nov. 1954, pp. 749-752, 762.
 2. J. H. Blakelock, "Inertial Cross-Coupling," Chapt. 5 and "Structural Flexibility," Chapt. 8 in Automatic Control of Aircraft and Missiles, John Wiley and Sons, Inc., New York, 1965.
 3. B. Etkin, Dynamics of Flight, John Wiley and Sons, Inc., New York, 1959, pp. 304-307.
 4. W. R. Kolk, "Roll Coupling," Chapt. 7 and "Aero-Structure-Control Interactions," Chapt. 11 in Modern Flight Dynamics, Prentice-Hall, Inc., Englewood Cliffs, N. J., 1961.
 5. D. T. McRuer, "A Feedback-Theory Analysis of Airframe Cross-Coupling Dynamics," J. Aerosp. Sci., Vol. 29, No. 5, May 1962, pp. 525-533.
 6. B. H. Paiewonsky, The Effects of Engine Angular Momentum on an Airplane's Longitudinal and Lateral-Directional Dynamic Stability, WADC TR 56-225, June 1956.
 7. H. R. Pass, B. F. Pearce, R. K. Siskind, and J. Wolkovitch, Topics on Flexible Airplane Dynamics, ASD-TDR-63-334, Parts I through IV, July 1963.
 8. B. F. Pearce, W. A. Johnson, and R. K. Siskind, Analytical Study of Approximate Longitudinal Transfer Functions for a Flexible Airframe, ASD-TDR-62-279, Apr. 1962.
 9. W. H. Phillips, Effect of Steady Rolling on Longitudinal and Directional Stability, NACA TN-1627, 1948.

10. W. J. G. Pinsker, A Preliminary Note on the Effects of Inertia Cross-Coupling on Aircraft Response in Rolling Maneuvers, R.A.E. Tech. Note No. Aero 2419, 1955.
11. W. J. G. Pinsker, Critical Flight Conditions and Loads Resulting from Inertia Cross-Coupling and Aerodynamic Stability Deficiencies, R.A.E. Tech. Note No. Aero 2502, Mar. 1957; also AGARD Rept. 107.
12. W. J. G. Pinsker, Charts of Peak Amplitudes in Incidence and Sideslip in Rolling Maneuvers Due to Inertia Cross Coupling, R.A.E. Tech Note No. 2604, Apr. 1958.
13. D. W. Rhoads and J. M. Schuler, "A Theoretical and Experimental Study of Airplane Dynamics in Large-Disturbance Maneuvers," J. Aeron. Sci., Vol. 24, No. 7, July 1957, pp. 507-526, 532.
14. J. M. Schuler, Analytical Study of Airplane Dynamics and Tail Loads in Rolling Pull-Out Maneuvers, WADC TR 56-403, Sept. 1956.
15. J. M. Schuler, Flight Evaluation of an Automatic Control System for Stabilizing the Large Uncontrolled Motions of Airplanes in Stalled Flight, Cornell Aeronautical Lab., Inc., Rept. TB-1132-F-2, Oct. 1959.
16. R. C. Seamans, Jr., et al., "Recent Developments in Aircraft Control," J. Aeron. Sci., Vol. 22, No. 3, Mar. 1955, pp. 145-164.
17. R. L. Stapleford, L. G. Hofmann, J. J. Best, C. D. Wezeman, and W. A. Johnson, Transfer Function Approximations for Large Highly Coupled Elastic Boosters with Fuel Slosh, NASA CR-464, Apr. 1966.
18. H. H. B. M. Thomas and P. Price, A Contribution to the Theory of Aircraft Response in Rolling Manoeuvres Including Inertia Cross-Coupling Effects, R.A.E. Rept. No. Aero 2634, Apr. 1960; also A.R.C. R and M 3349.
19. W. K. Waymeyer and R. W. Sporing, An Industry Survey on Aeroelastic Control System Instabilities in Aerospace Vehicles, IAS Paper No. 62-47, Jan. 1962.
20. J. D. Welch and R. E. Wilson, "Cross-Coupling Dynamics and the Problems of Automatic Control in Rapid Rolls," J. Aeron. Sci., Vol. 24, No. 10, Oct. 1957, pp. 741-754.

II. Components

● Gyros and Accelerometers

1. Automatic Flight Control Systems for Piloted Aircraft, Northrop Aircraft, Inc., BuAer Rept. AE-61-4VI, Bureau of Aeronautics, Navy Dept., Apr. 1956, pp. II-93 thru II-113 and Appendix, "Equations of the Gyroscope."
2. W. R. Ahrendt and C. J. Savant, Servomechanism Practice, McGraw-Hill Book Co., Inc., New York, 1960.
3. J. S. Ausman, "Theory of Inertial Sensing Devices," in G. R. Pitman, Jr., ed., Inertial Guidance, John Wiley and Sons, Inc., New York, 1962, pp. 72-91.
4. L. Becker, "Gyro Pickoff Indications at Arbitrary Plane Attitudes," J. Aeron. Sci., Vol. 18, No. 11, Nov. 1951, pp. 718-724.
5. C. Broxmeyer, Inertial Navigation Systems, McGraw-Hill Book Co., Inc., New York, 1964.
6. J. G. R. Collette, Analysis and Design of Space Vehicle Flight Control Systems, Vol. XI - Component Dynamics, NASA CR-830, July 1967.
7. H. R. Hopkin and R. W. Dunn, Theory and Development of Automatic Pilots, 1937-1947, R.A.E. Rept. I.A.P. 1459, Aug. 1947.
8. B. Lichtenstein, B., Gyros, Platforms, Accelerometers, 5th ed., Kearfott Div., General Precision, Inc., Little Falls, N. J., June 1962.
9. W. R. MacDonald, "Acceleration Transducers of the Force Balance Type," Proc. International Flight Test Instrumentation Symposium (1960), Pergamon Press, New York, 1961, pp. 15-23.
10. K. I. T. Richardson, The Gyroscope Applied, Hutchinson and Company, Ltd., London, 1954.
11. C. J. Savant, Jr., R. C. Howard, C. B. Solloway, and C. A. Savant, Principles of Inertial Navigation, McGraw-Hill Book Co., Inc., New York, 1961.
12. P. H. Savet, ed., Gyroscopes: Theory and Design with Application to Instrumentation, Guidance and Control, McGraw-Hill Book Co., Inc., New York, 1961.
13. J. B. Scarborough, The Gyroscope, Theory and Application, Interscience Publishers, Inc., New York, 1958.

14. J. M. Slater, Inertial Guidance Sensors, Reinhold Publishing Corp., New York, 1964.

● Air Data Sensors

1. F. O. Smetana, Design and Tests of Aerodynamic Static Pressure Compensators for Four Service Aircraft, WADC TR 59-383, May 1959.
2. W. H. Coulthard, Aircraft Instrument Design, Pitman Publishing Corp., New York, 1952, Chapt. 1.
3. F. M. Emerson, F. H. Gardner, G. D. Gruenwald, R. Olshausen and L. V. Sloma, Study of Systems for True Angle of Attack Measurement, WADC TR 54-267, May 1955.
4. D. G. Goodman, C. Salter, and J. H. Warsap, A New Design of Pitot-Static Tube with a Discussion of Pitot-Static Tubes and Their Calibration Factors, National Physical Laboratory Aero Rept. 1013, 7 May 1962.
5. W. Gracey, "Recent Developments in Pressure Altimetry," J. Aircraft, Vol. 2, No. 3, May-June 1965, pp. 161-165.
6. E. E. Hilliard, Supersonic Wind Tunnel Tests of Several Pitot-Static Probes, AEDC TR 65-192, Aug. 1965.
7. S. R. Mallard, Calibration Tests of a Litton Conical Air Data Probe at Mach Numbers of 2 to 8, AEDC TDR 62-186, Oct. 1962.
8. J. F. Muller, "Systematic Determination of Simplified Gain Scheduling Programs, J. Aircraft, Vol. 4, No. 6, Nov.-Dec. 1967, pp. 529-534.
9. M. J. Teigen, Dimensional Variables Affecting Calibration Characteristics of Null-Seeking Differential-Pressure and Vane Angle of Attack Sensors, WADC TR 59-388, June 1959.
10. J. Chaffois, Pitot-Static Probes for Subsonic and Supersonic Aircraft, ("Sondes Anemo-Barometriques Pour Avions Subsoniques et Supersoniques," Techniques et Sciences Aeronautiques et Spatiales, [1962]1, pp. 7-17), R.A.E. Library Trans. No. 1032, Nov. 1963. Translated by L. H. Townend, edited by A. A. Woodfield.

● Actuators

1. Basic Research and Development in Fluid Power Control for the United States Air Force, ASD-TDR-62-3, Jan. 1962.
2. Bibliography on Servomechanisms. Bulletin of Automatic and Manual Control Abstracts, Ministry of Aviation TIL/BIB/52/37, Apr. 1964.
3. Report of the Second Piloted Aircraft Flight Control Symposium, BuAer Rept. AE-61-5, June 1952.
4. Proceedings of the First Piloted Aircraft Powered Surface Control System Symposium, Bureau of Aeronautics, Oct. 1949.
5. Electric Input Hydraulic Servovalve, SAE ARP 490, 15 July 1958.
6. The Hydraulic System, Northrop Aircraft, Inc., BuAer Rept. AE-61-4IV, Bureau of Aeronautics, Navy Dept., 1953.
7. W. H. Ahrendt and C. J. Savant, Jr., Servomechanism Practice, 2nd ed., McGraw-Hill Book Co., Inc., New York, 1960.
8. B. W. Anderson, The Analysis and Design of Pneumatic Systems, John Wiley and Sons, Inc., New York, 1967.
9. J. F. Blackburn, G. Reethof, and J. L. Shearer, Fluid Power Control, The Technology Press of M.I.T. jointly with John Wiley and Sons, Inc., New York, 1960.
10. R. S. Cataldo, Analysis of Electrohydraulic Valves and Systems, ISA Preprint ISA-11, presented at the Joint Automatic Control Conference, MIT, 7-9 Sept. 1960.
11. G. E. Click, A. P. Henry, and D. T. McRuer, Design Study of Multi-Function Hydraulic Actuating Devices, WADC TR 56-418, Aug. 1956.
12. J. G. R. Collette, Analysis and Design of Space Vehicle Flight Control Systems, Vol. XI - Component Dynamics, NASA CR-830, July 1967.
13. J. E. Gibson and F. B. Tuteur, Control System Components, McGraw-Hill Book Co., Inc., New York, 1958.
14. D. Graham, "Magnetic Clutches Add Muscle to Electronic Servos," Space/Aeronaut., Apr. 1959.
15. A. G. Kegel and G. S. Axelby, "Actuators," in E. M. Grabbe, S. Ramo, and D. E. Wooldridge, eds., Handbook of Automation Computation and Control, Vol. 3, Systems and Components, John Wiley and Sons, Inc., New York, 1961.

16. K. D. May, Advanced Valve Technology, NASA SP-5019, Feb. 1965.
17. J. M. Nightingale, "Hydraulic Servo-Valve Design," Machine Design, Vol. 27, No. 1, 1955, p. 191.
18. J. L. Shearer, "Dynamic Characteristics of Valve Controlled Hydraulic Servomotors," Trans. ASME, Aug. 1954.
19. J. L. Shearer, "Study of Pneumatic Processes," Trans. ASME, Vol. 78, 1956, p. 239.
20. R. K. Smyth, "Operation of Autopilot Servo Actuators," Applied Hydraulics and Pneumatics, Mar. 1959, pp. 110-113.
21. J. G. Truxal, ed., Control Engineer's Handbook, McGraw-Hill Book Co., Inc., New York, 1958, Sects. 12, 14, 15, and 16.
22. R. Walters, Hydraulic and Electro-Hydraulic Servo Systems, CRC Press, Cleveland, Ohio, 1967.
23. A. A. J. Willitt, "Developments in Aircraft Hydraulics Systems," The Aeroplane and Astronautics, Vol. 100, 17 Feb. 1961.

III. Descriptions of Complete Flight Control Systems and Related Documents

1. Automatic Flight Control Systems for Piloted Aircraft, Northrop Aircraft, Inc., BuAer Rept. AE-61-4VI, Bureau of Aeronautics, Navy Dept., Apr. 1956.
2. "P-3 Automatic Pilot—Attitude Control for Jet Aircraft," Digest (a publication of the U. S. Navy), Mar. 1951, pp. 9-17.
3. Current Autopilot Block Diagrams, prepared for SAE A-18 Committee, Oct. 1959.
4. Automatic Pilots, SAE AS 402A, Issued 1 Aug. 1947, revised 1 Feb. 1959.
5. Automatic Pilot Installations, SAE ARP 419, 15 Nov. 1957.
6. C. R. Abrams, Final Report on the General Electric Self-Adaptive Flight Control System, NADC-ED-6455, June 1964.
7. R. E. Andeen, "Self-Adaptive Autopilots," Space/Aeronaut., Vol. 43, No. 4, Apr. 1965, pp. 46-52.
8. H. E. Arnzen, "Flight Controls: A Look into the Future," Space/Aeronaut., Vol. 33, No. 2, Feb. 1960, pp. 46-49.

9. V. A. Bodner and M. S. Kozlov, Stabilization of Flying Craft and Autopilots, (Stabilizatsiya Letatel'nykh Apparatov i Autopiloty, Gosudarstvennoye Nauchno-Tekhnicheskoye Izdatel'stvo, Oborongiz, Moskva, 1961), Foreign Technology Div. Transl. FTD-TT-62-811, 31 July 1962.
10. B. Boskovich and R. E. Kaufmann, "Evolution of the Honeywell First-Generation Adaptive Autopilot and Its Applications to F-94, F-101, X-15, and X-20 Vehicles," J. Aircraft, Vol. 3, No. 4, July-Aug. 1966, pp. 296-304.
11. E. R. Buxton, "Smooth Automatic Flare Control," Space/Aeronaut., Nov. 1958.
12. C. H. Cannon, "Military and Civil All Weather Landing Systems for C-141," J. Aircraft, Vol. 3, No. 6, Nov.-Dec. 1966, pp. 529-534.
13. W. H. Coulthard, Aircraft Instrument Design, Pitman Publishing Corp., New York, 1952, Chapt. 18.
14. R. H. Cushman, "Vanguard Control Demonstrates Minimum Hardware Approach, Parts I and II," Automatic Control, June 1958, pp. 25-33, July 1958, pp. 16-20.
15. J. W. Dawson, L. P. Harris, and E. A. Swean, Dynamic Response of Two Aircraft-Autopilot Systems to Horizontal Turn Commands, M.I.T., Dynamic Analysis and Control Lab., Rept. No. 94, 31 Jan. 1955.
16. H. L. Ehlers, Technical Considerations in the Design of Gust Alleviation Control Systems, North American Aviation, Inc., Autonetics Div., Rept. X7-933/301, 17 Apr. 1967.
17. H. L. Ehlers, Helicopter Automatic Flight Control Systems, North American Rockwell Corp., Autonetics Div., Oct. 1967.
18. W. Eldridge, An Investigation of Ways of Improving the Coordinated Turn Maneuver of Jet Transport Aircraft, Boeing Airplane Co. Document No. D6-5998, 9 Dec. 1960.
19. D. Graham and R. C. Lathrop, "Automatic Feedback Control and All-Weather Flying," Aeronautical Eng. Rev., Vol. 14, No. 10, Oct. 1955, pp. 70-85.
20. J. Holahan, "Electronic Pilot Automates Fighter in Aerial Attack, Ground-Controlled Intercept, All-Weather Flight, Low Approach," Aviation Age, Dec. 1957, pp. 102-108.
21. H. R. Jex, I. L. Ashkenas, and R. A. Peters, "An Application of Airframe-Controller Optimization Techniques to a Supersonic Missile," Proc. IAS Symposium on Vehicle Systems Optimization, Garden City, N. Y., 28-29 Nov. 1961, pp. 115-126.

22. P. J. Klass, "Sperry Innovates Design in Autopilot for Jet Transport," Aviation Week, 26 Nov. 1956, pp. 76-86.
23. K. C. Kramer, "A-7A AFCS: A Flight-Proved High-Gain System," J. Aircraft, Vol. 3, No. 5, Sept.-Oct. 1966, pp. 454-461.
24. C. G. Mallery and F. C. Neebe, "Flight Test of General Electric Self-Adaptive Control," J. Aircraft, Vol. 3, No. 5, Sept.-Oct. 1966, pp. 449-453.
25. E. H. McDonald and J. A. Farris, The X-20 Flight Control System Development, Systems Engineering Group SEG-TDR-64-8, June 1964.
26. J. L. McKinley and R. D. Bent, "Electronic Navigation Equipment," Chapt. 20, "Autopilot for Light Aircraft," Chapt. 21, and "Autopilot for Jet Airliners," Chapt. 22 in Electricity and Electronics for Aerospace Vehicles, McGraw-Hill Book Co., Inc., New York, 1961.
27. W. R. Monroe, "Improving the Dynamic Response of Airplanes by Means of Electric Equipment," AIEE Trans., Vol. 72, Pt. II, Jan. 1953, pp. 441-447.
28. L. J. Mueller, "Problems Unique to VTOL Automatic Flight Control," J. Aircraft, Vol. 2, No. 5, Sept.-Oct. 1965, pp. 357-360.
29. K. I. T. Richardson, The Gyroscope Applied, Philosophical Library, Inc., New York, 1954, Sect. III, Chapt. 5 and Sect. IV, Chapt. 2.
30. C. L. Seacord, "Flight Control for Manned Spacecraft," Space/Aeronaut., Vol. 40, No. 6, Nov. 1963, pp. 72-80.
31. J. Stambler, "Boeing 707 Flight Control System Tailored for Safety," Aviation Age, May 1957, pp. 34-41.
32. C. A. Williams, Aircraft Instrument Control Systems, Odhams Press Ltd., New York, 1963.

APPENDIX I

STABILITY DERIVATIVES AND TRANSFER FUNCTION FACTORS FOR REPRESENTATIVE AIRCRAFT

To apply the methods and techniques described in the text to the design of automatic flight control systems for real aircraft it is necessary to have numerical data on the stability derivatives. In Chapters 5 and 6, for illustrative purposes, such data have been presented for a specific "conventional" straight-wing airplane and for a tilt-duct VTOL aircraft in hovering flight. Later, in Chapters 7 and 8 a wide variety of generic analyses of closed-loop dynamics were introduced to show how the open-loop dynamics of the vehicle may influence the choice of which loops should be closed or the compensation which may be required. While the characteristics illustrated there were not explicitly associated with particular aircraft, the reader can be assured that they were suggested by real features of the performance of actual vehicles.

Some readers of this volume may be engaged on projects in which stability and control aerodynamicists have made the necessary measurements or estimates, or they may themselves be stability and control aerodynamicists. If not, however, students of the subject will need a source of data in order to exercise the skills which they have acquired and to deepen their understanding. It is the purpose of this appendix to provide one such source.

Here the reader will find, conveniently arranged, stability derivatives and transfer function factors for nine aircraft. The notation which is employed has been defined in Chapters 4, 5, and 6. The choice of the aircraft has been somewhat arbitrary. It has been dictated primarily by the ready availability to the authors of unrestricted data. We have, however, attempted to provide a representative selection of both historical and modern aircraft of a very wide range of configurations. The reader will quickly note that in some cases the data are extensive, covering a large number of flight conditions. In other cases this is not so.

A caveat is in order here. The data presented in this appendix have been collected from very diverse sources over a long period of time. In a few cases the original source of the data is now unclear. Those familiar with the art will know the considerable difficulty which attends the attempt

to discover definitive data. In many cases we, our colleagues, and (we suspect) our predecessors have, according to the best judgment available, altered the data as may have been indicated by internal inconsistencies or physical improbabilities revealed by the attempt to use them. For these reasons we wish to make it clear that the data are only nominally representative of the several aircraft configurations. In particular, the manufacturers of the aircraft can not be held accountable for this information, nor would they be bound to concur in any conclusions with respect to their aircraft which might be derived from its use.

The data presented here may be made to serve at least two useful purposes. These are analysis and simulation. The stability derivative data are basic. They may be used to set up an analog or digital computer simulation of the linearized equations, or they may be used to compute, for example, the gust input numerators or some coupling numerators which are not tabulated here. On the other hand, most readers, for many purposes, will find it convenient to start with the tabulations of transfer function factors. These permit the methods and techniques, described in the text, to be quickly and relatively easily applied. The results are both interesting and informative.

The aircraft represented are:

Conventional Jet-Propelled

Straight Wing.....	F-89
Tailless Delta.....	F-106B
Delta.....	A-4D (A-4)

Transports

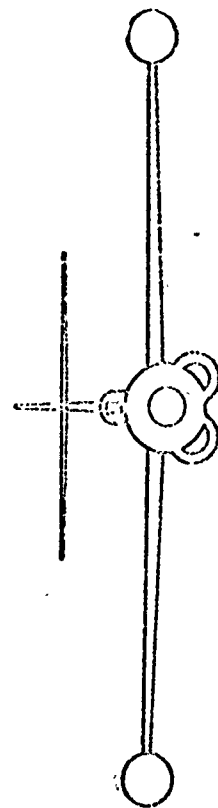
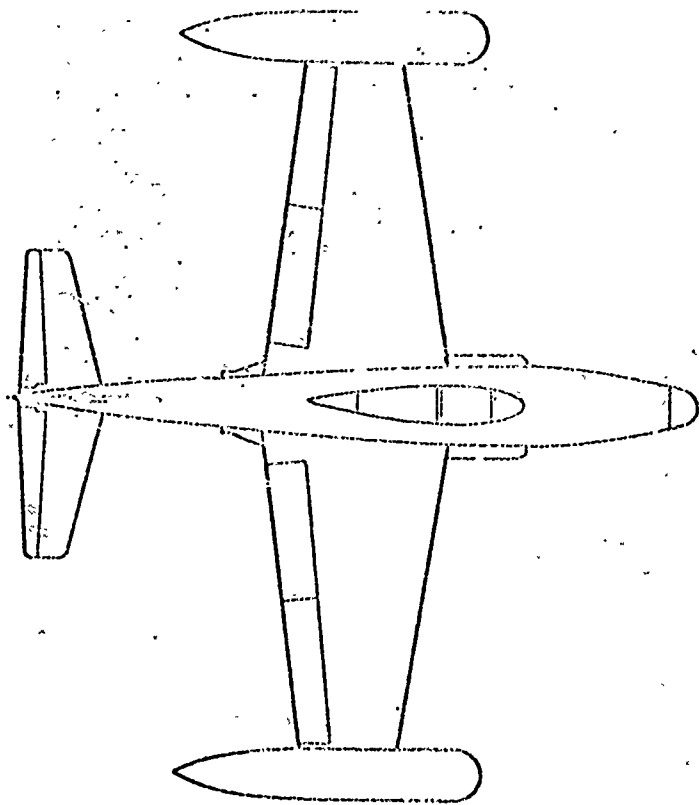
Propeller.....	C-47 (DC-3, R4D)
Jet.....	DC-8

VTOL

Tilt Wing.....	XC-142
Tilt Duct.....	VZ-4
Single-rotor Helicopter....	HH-19

Vintage Biplane

Bristol Fighter.....	F.2B
----------------------	------



F-89

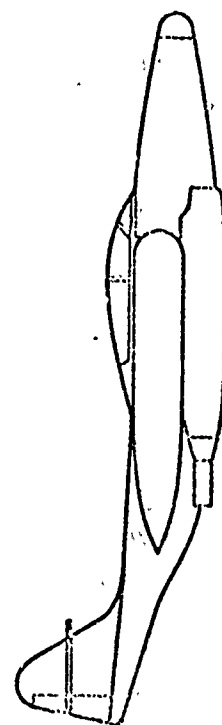
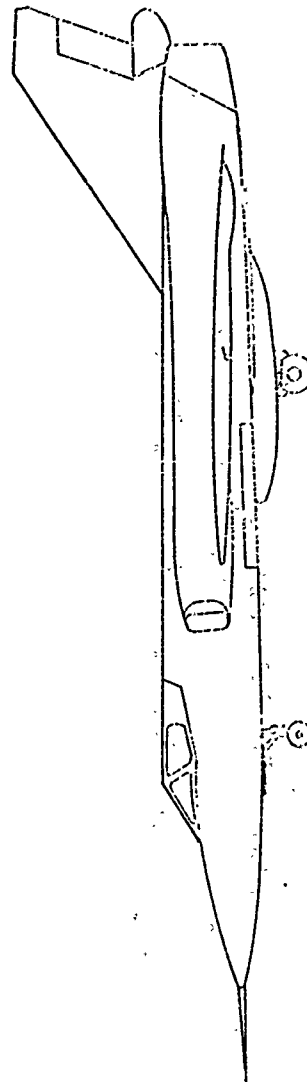
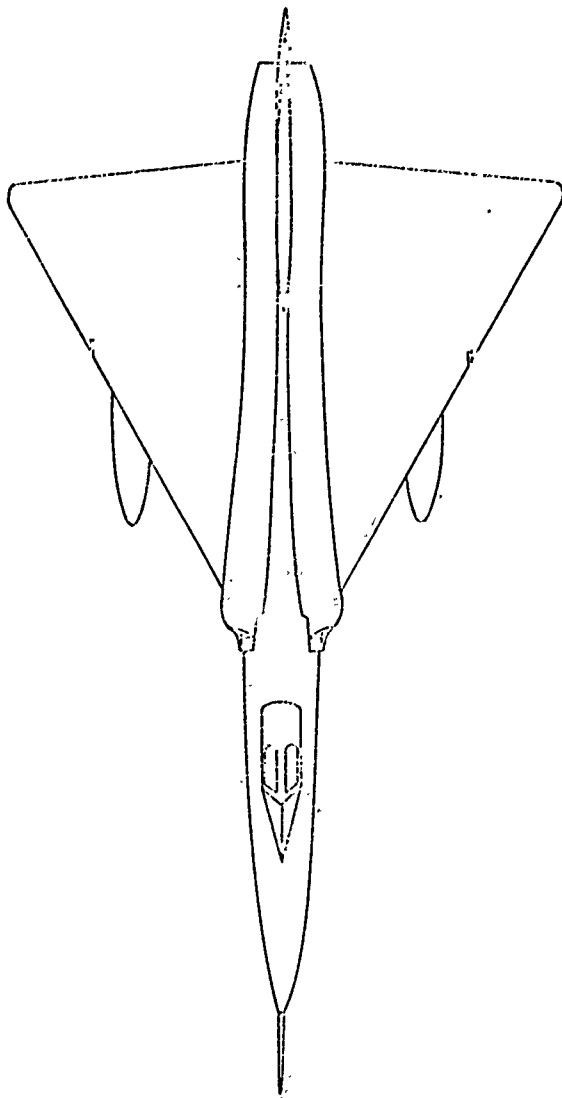


TABLE A-1

A		B		C	
GEOMETRICAL AND INERTIAL PARAMETERS FOR THE F-89		LONGITUDINAL DYNAMIC DERIVATIVES FOR THE F-89		LATERAL DIRECTIONAL DERIVATIVES FOR THE F-89	
Note: Data are for body-fixed stability axes		Note: Data are for body-fixed stability axes		Note: Data are for body-fixed stability axes	
	FLT. COND. 8901		FLT. COND. 8901		FLT. COND. 8901
h (ft)	20,000	h (ft)	20,000	h (ft)	20,000
k (—)	0.633	k (—)	0.633	k (—)	0.633
a (ft/sec)	1037	$\dot{\gamma}_u$ (1/sec) [*]	—	$\dot{\gamma}_v$ (1/sec)	-0.0029
c (slugs/ft ³)	0.00127	X_u (1/sec)	-0.0037	$\dot{\gamma}_r$ [(ft/sec ²)/rad]	-51.7
V_{T_0} (ft/sec)	660	X_w (1/sec)	0.0016	$\dot{\gamma}_{\dot{u}}$ [(ft/sec ²)/rad]	0
$\bar{q} = cV^2/2$ (lb/ft ²)	276	$X_{\dot{u}}$ [(ft/sec ²)/rad]	0	$\dot{\gamma}_{\dot{w}}$ [(1/sec)/rad]	0
W (lb)	30,500	Z_u (1/sec)	-0.0955	$\dot{\gamma}_{\dot{r}}$ [(ft/sec ²)/rad]	7.0
m (slugs)	947	Z_w (—)	—	$\dot{\gamma}_{\dot{r}}$ [(1/sec)/rad]	0.0116
		$Z_{\dot{u}}$ (1/sec)	-1.43	$I_{\dot{r}}$ (1/sec ²)	-1.77
		$Z_{\dot{w}}$ [(ft/sec ²)/rad]	-69.8	I_p (1/sec)	-1.70
		\dot{M}_u (1/sec-ft)	0	I_r (1/sec)	0.178
		\dot{M}_w (1/ft)	-0.0013	$I_{\dot{u}}$ (1/sec ²)	27.3
		$\dot{M}_{\dot{u}}$ (1/sec-ft)	-0.0235	$I_{\dot{w}}$ (1/sec ²)	0.666
		\dot{M}_q (1/sec)	-1.92	$I_{\dot{r}}$ (1/sec ²)	-1.55
		$\dot{M}_{\dot{u}}$ (1/sec ²)	-26.1	I_p^1 (1/sec)	-1.70
				I_r^1 (1/sec)	0.172
				$I_{\dot{u}}^1$ (1/sec ²)	27.3
				$I_{\dot{w}}^1$ (1/sec ²)	0.576
				$N_{\dot{u}}$ (1/sec ²)	3.52
				N_p (1/sec)	-0.0025
				N_r (1/sec)	-0.0927
				$N_{\dot{u}}$ (1/sec ²)	-0.615
				$N_{\dot{r}}$ (1/sec ²)	-1.38
				N_p^1 (1/sec ²)	3.38
				N_p^1 (1/sec)	-0.0021
				N_r^1 (1/sec)	-0.0893
				$N_{\dot{u}}^1$ (1/sec ²)	0.395
				$N_{\dot{r}}^1$ (1/sec ²)	-1.36

$$^* \dot{\gamma}_u = \frac{1}{a_m} \frac{\partial T}{\partial \dot{u}}$$

D			E			F			G		
PARAMETER VALUES FOR CASE 1			PARAMETER VALUES FOR CASE 2			PARAMETER VALUES FOR CASE 3			PARAMETER VALUES FOR CASE 4		
	PARAM. NO.	VALUE		PARAM. NO.	VALUE		PARAM. NO.	VALUE		PARAM. NO.	VALUE
Altitude, h (ft)	1	20,000	Altitude, h (ft)	1	20,000	Altitude, h (ft)	1	20,000	Altitude, h (ft)	1	20,000
Weight, W (lb)	2	30,000	Weight, W (lb)	2	30,000	Weight, W (lb)	2	30,000	Weight, W (lb)	2	30,000
Δ_{long}	ξ_{sp}	0.092	Δ_{lat}	$1/i_s$	-0.0013	Δ_{lat}	$1/i_s$	-0.0013	Δ_{lat}	A_{tr}	0.316
	ξ_{pr}	-0.27		$1/T_R$	1.78		$1/T_R$	1.78		$1/T_{R1}$	0
	ξ_p	0.0714		ξ_d	0.001		ξ_d	0.001		$1/T_{R2}$	118
	a_2	0.0030		a_d	1.86		a_d	1.86		A_{tr}	0.0000
H_{oc}	A_{tr}	-16.1	H_{oc}	ξ_p	27.3	H_{oc}	ξ_p	0.576	H_{oc}	ξ_{tr}	-0.0000
	$1/T_{R1}$	0.0025		$1/i_{p1}$	0		$1/i_{p1}$	0		a_{tr}	19.9
	$1/T_{R2}$	1.376		ξ_p	0.007		$1/i_{p2}$	2.56		A_{tr}	-37.1
	de gain	-1.85		a_p	1.86		$1/T_{R3}$	-2.89		$1/T_{R4}$	0.0000
H_{oc}	A_{tr}	-0.112	H_{oc}	de gain	0	H_{oc}	de gain	0	H_{oc}	A_{tr}	0.0000
	$1/T_{R1}$	1.376		ξ_{tr}	27.3		A_{tr}	0.576		A_{tr}	3.08
	$1/T_{R2}$	-72.1.4		ξ_{tr}	0.007		$1/T_{R1}$	2.56		$1/T_{R2}$	0.111
	de gain	159.0		a_{tr}	1.86		$1/T_{R2}$	-2.89		$1/T_{R3}$	2.40
H_{oc}	A_{tr}	-19.8	H_{oc}	de gain	-1107.5	H_{oc}	de gain	500	H_{oc}	A_{tr}	—
	$1/T_{R1}$	2.56		A_{tr}	0.392		A_{tr}	-1.36		A_{tr}	3.08
	ξ_{tr}	0.0013		$1/T_{R1}$	1.00		$1/T_{R1}$	1.78		$1/T_{R2}$	-1.00
	a_{tr}	0.003		ξ_{tr}	-0.003		ξ_{tr}	0.00096		ξ_{tr}	0.219
H_{oc}	de gain	-1110	H_{oc}	a_{tr}	2.89	H_{oc}	a_{tr}	0.292	H_{oc}	a_{tr}	2.89
	A_{tr}	0.8		de gain	-530		de gain	2.3		A_{tr}	209
	$1/T_{R1}$	0.0000		A_{tr}	-0.392		A_{tr}	0.0116		$1/T_{R2}$	0
	$1/T_{R2}$	19.8		$1/T_{R1}$	0.0096		$1/T_{R1}$	-0.00373		$1/T_{R3}$	2.47
H_{oc}	$1/T_{R3}$	-17.03	H_{oc}	$1/T_{R2}$	-6.23	H_{oc}	$1/T_{R2}$	1.72	H_{oc}	$1/T_{R4}$	-2.47
	de gain	-7020		$1/i_{s3}$	—		$1/T_{R3}$	118		A_{tr}	0.316
	A_{tr}	-69.8		de gain	-11.4		de gain	1.00		$1/T_{R1}$	118
	$1/T_{R1}$	0	H_{oc}	A_{tr}	27.6	H_{oc}	A_{tr}	7.65	H_{oc}	A_{tr}	209
H_{oc}	$1/T_{R2}$	0.0000		$1/T_{R1}$	0.0096		$1/T_{R1}$	-0.0011		$1/T_{R2}$	2.47
	$1/T_{R3}$	19.8		$1/T_{R2}$	-6.23		$1/T_{R2}$	1.70		$1/T_{R3}$	-2.47
	$1/T_{R4}$	-17.03		$1/T_{R3}$	—		$1/T_{R3}$	2.57		$1/T_{R4}$	—
	de gain	0		de gain	768		de gain	-49.5			



F-106B

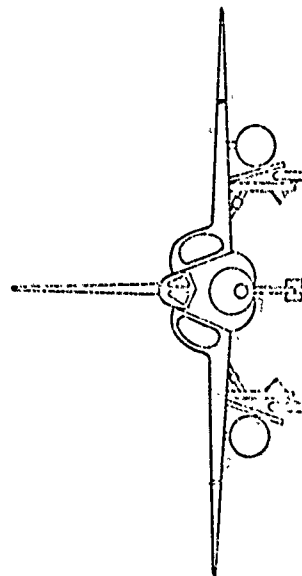


TABLE A-2

A. GEOMETRICAL PARAMETERS FOR THE F-106B

Note: Data are for body-fixed centerline axes

$$S = 695, \quad b = 38.13, \quad c = 23.755, \quad x_{\text{alat}} = 17.5, \quad z_{\text{alat}} = -3.35$$

	FLIGHT CONDITION											
	1	2*	3	4	5	6	7	8	9	10	11	12
h (ft)	20,000	20,000	20,000	S.L.	S.L.	20,000	S.L.	20,000	40,000	20,000	40,000	40,000
M (—)	0.755	0.755	0.755	0.4	0.4	0.4	0.9	0.9	0.9	1.4	1.4	2.0
α (°/sec)	1.037	1.037	1.037	1.116	1.116	1.037	1.116	1.037	0.63	1.037	0.63	0.63
ρ (slugs/ft ³)	0.001267	0.001267	0.001267	0.002377	0.002377	0.001267	0.002377	0.001267	0.000587	0.001267	0.000587	0.000587
$\dot{\psi}_{\text{to}}$ (°/sec)	785	785	785	446.4	446.4	444	1004.4	933	871	1,450	1,395	1,295
$\dot{\psi} = \dot{\psi}_{\text{to}}^2/2$ (11/ft ²)	302	392	392	59.3	237.2	108.6	1,199	551	223	1,332	549	1,100
$\dot{\psi}$ (1/s)	25,000	20,000	20,000	25,500	29,776	29,776	29,776	29,776	29,776	29,776	29,776	29,776
\dot{M}_{acc} (slugs)	1,050	931	870	791.9	924.7	924.7	924.7	924.7	924.7	924.7	924.7	924.7
\dot{I}_x (slug-ft ²)	25,490	18,744	15,809	15,800	18,634	18,634	18,634	18,634	18,634	18,634	18,634	18,634
\dot{I}_y (slug-ft ²)	155,156	185,300	177,615	160,783	177,858	177,858	177,858	177,858	177,858	177,858	177,858	177,858
\dot{I}_z (slug-ft ²)	215,262	198,797	187,115	170,201	191,236	191,236	191,236	191,236	191,236	191,236	191,236	191,236
\dot{I}_{xz} (slug-ft ²)	49,771	5310.9	5015.4	5,727	5,539	5,539	5,539	5,539	5,539	5,539	5,539	5,539
$\dot{x}_{c.g.}/\dot{c}$	0.29	0.305	0.26	0.305	0.305	0.305	0.305	0.305	0.305	0.305	0.305	0.305
$\dot{\sigma}_{\text{trim}}$ (deg)	4.42	4.04	3.83	18.0	4.9	11.0	2.0	2.7	5.4	1.2	2.70	1.2
\dot{C}_{L_0} (1/rad)	2.7	2.7	2.7	2.5	2.54	2.55	2.85	2.84	3.00	2.46	2.55	1.84
$\dot{\alpha}_0$ (deg)	4.42	4.04	3.88	18.0	4.9	11.0	2.0	2.7	5.4	1.2	2.7	1.2
$\dot{\psi}_0$ (°/sec)	784	784	784	212	445	405	1,004	933	868	1,450	1,395	1,295
$\dot{\psi}_0$ (°/sec)	60.6	55.4	53.1	73	40	80	36	44	82	30	51	40

B. LATERAL DIMENSIONAL DERIVATIVES FOR THE F-106B

Note: Data are for body-fixed centerline axes
 Static aeroelastic corrections are included
 δ_α and δ_r derivatives include effects of crossfeed shown

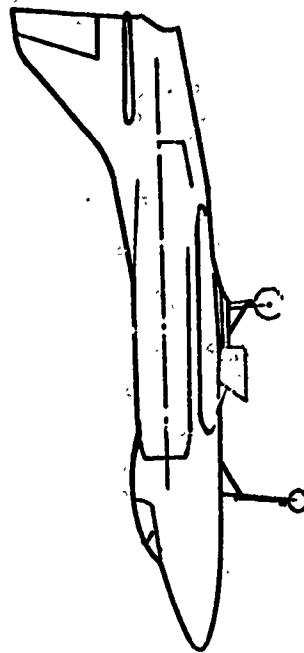
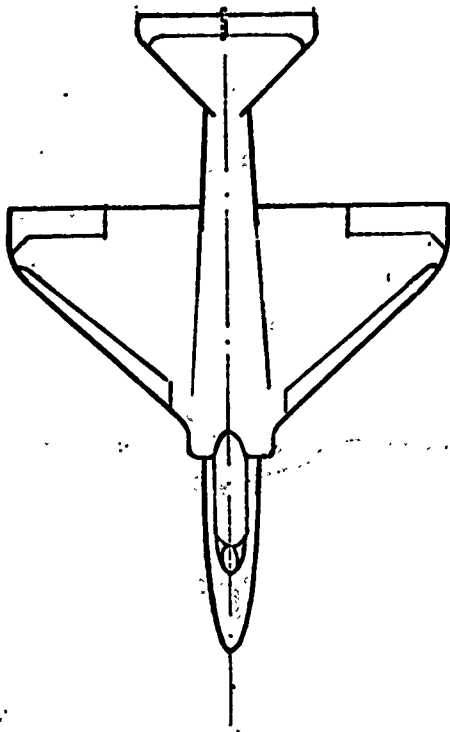
	FLIGHT CONDITION											
	1	2	3	4	5	6	7	8	9	10	11	12
$Y_{\dot{\alpha}}$	20,000	20,000	20,000	5.14	5.14	20,000	8.14	20,000	30,000	20,000	20,000	20,000
$Y_{\dot{\beta}}$	0.755	0.755	0.755	0.2	0.4	0.4	0.9	0.9	0.9	1.4	1.4	1.4
$Y_{\dot{\gamma}}$	-0.237	-0.239	-0.239	-0.126	-0.237	-0.109	-0.581	-0.277	-0.112	-0.423	-0.122	-0.217
$Y_{\dot{\delta}_a}$	-1.63	-1.68	-2.04	-29.6	-106	-16.1	-5.64	-259	-98.0	-615	-217	-129
$Y_{\dot{\delta}_r}$	0.0799	0.0326	0.100	0.042	0.059	0.043	0.179	0.160	0.0523	0.0470	0.0237	0.0122
$Y_{\dot{\delta}_\alpha}$ ($\delta_r = -1.584$)	0.0579	0.0393	0.0351	0.00720	0.0523	0.0109	0.0747	0.044	0.015	0.0110	0.0123	0.00423
$Y_{\dot{\delta}_r}$	0.0347	0.0402	0.0439	0.0230	0.0433	0.0225	0.0569	0.0382	0.0189	0.0239	0.00793	0.00346
$Y_{\dot{\delta}_\alpha}$ ($\delta_r = -0.1737$)	0.0433	0.0559	0.0606	0.0264	0.0569	0.0231	0.0797	0.0575	0.0374	0.0215	0.0129	0.0116
$Y_{\dot{\delta}_r}$	-5.61	-5.78	-10.1	-20.0	-22.3	-19.2	-31.2	-27.6	-18.9	-11.6	-25.1	-22.5
$Y_{\dot{\delta}_\alpha}$	-1.69	-2.30	-2.74	-1.22	-2.39	-1.08	-5.14	-1.87	-1.23	-1.25	-2.09	-2.09
$Y_{\dot{\delta}_r}$	1.22	1.64	1.91	3.51	2.65	2.12	4.56	2.59	1.60	2.53	1.35	2.09
$Y_{\dot{\delta}_\alpha}$ ($\delta_r = -0.1737$)	7.65	9.51	11.1	2.08	6.17	2.97	19.5	11.1	5.07	7.21	4.18	5.23
$Y_{\dot{\delta}_r}$	-0.550	-0.832	-1.30	-0.175	-0.475	-0.353	1.61	-0.975	-0.617	1.11	-0.271	0.724
$Y_{\dot{\delta}_\alpha}$	-14.7	-61.1	-73.0	-13.3	-39.1	-19.5	-109	-71.2	-34.7	-36.4	-26.2	-29.1
$Y_{\dot{\delta}_r}$ ($\delta_r = -1.584$)	-59.3	-79.4	-89.7	-16.4	-46.3	-29.9	-129	-87.9	-42.1	-47.4	-39.5	-34.0
$Y_{\dot{\delta}_\alpha}$	5.07	5.42	5.68	-2.152	2.17	0.596	16.0	7.50	2.79	10.9	7.70	11.1
$Y_{\dot{\delta}_r}$	-0.0307	-0.0227	-0.0187	-0.0251	-0.0522	-0.061	-0.133	-0.042	-0.021	-0.113	-0.0312	-0.0524
$Y_{\dot{\delta}_\alpha}$	-0.472	-0.463	-0.513	-0.199	-0.472	-0.210	-1.27	-0.237	-0.059	-0.633	-0.324	-0.375
$Y_{\dot{\delta}_r}$	-2.95	-2.68	-2.75	-0.595	-1.63	-0.722	-6.16	-3.28	-1.44	-2.90	-1.45	-1.61
$Y_{\dot{\delta}_\alpha}$ ($\delta_r = -0.1737$)	-3.41	-3.70	-3.95	-0.695	-2.23	-1.03	-2.77	-4.87	-2.09	-4.18	-2.23	-2.23
$Y_{\dot{\delta}_r}$	-5.09	-6.03	-7.01	-1.12	-3.91	-1.69	-15.4	-9.34	-3.85	-7.54	-4.59	-3.64
$Y_{\dot{\delta}_\alpha}$ ($\delta_r = -1.584$)	-1.28	-2.02	-2.29	-0.352	-1.07	-0.590	-6.13	-4.42	-1.69	-3.19	-2.41	-0.778

C. AILERON LATERAL TRANSFER FUNCTION FACTORS FOR BASIC F-106B

	Flight Condition											
	1	2	3	4	5	6	7	8	9	10	11	12
Wach No., X	0.755	0.755	0.755	0.2	0.4	0.4	0.9	0.9	0.9	1.4	1.4	1.4
Altitude, h	20,000	20,000	20,000	S.L.	20,000	20,000	S.L.	20,000	10,000	20,000	40,000	40,000
C.G.	29	20-5	26	20-5	20-5	20-5	20-5	20-5	20-5	20-5	20-5	20-5
Weight	35,000	30,000	28,000	25,500	29,776	29,776	29,776	29,776	29,776	29,776	29,776	29,776
Trim ϵ_p , deg	4.42	4.04	3.88	10.0	4.9	11.0	2.0	2.7	5.4	1.2	2.7	2.7
Δ_{int}	-0.0170	-0.0165	-0.0164	0.169	0.032	0.029	-0.004	-0.005	0.001	0.010	0.010	0.010
$1/\Delta_{int}$	1.60	2.19	2.02	0.592	2.67	0.578	5.03	1.04	1.05	4.59	1.77	1.77
ϵ_p	2.37	2.37	2.37	0.102	0.233	0.200	0.224	3.01	2.12	0.173	3.01	3.01
Δ_{int}	0.104	0.175	0.178	0.102	0.233	0.102	0.224	0.159	0.159	0.116	0.233	0.233
D.C. Gain	-5.35	-5.00	-4.25	1.43	3.71	2.32	-7.70	-13.2	117	0.794	2.57	2.57
$1/\Delta_{int}$	-11.7	-61.1	-73.0	-13.3	-29.1	-19.5	-105	-71.2	-31.7	-36.4	-26.2	-26.2
$1/\Delta_{int}$	-0.00310	-0.00282	-0.00270	-0.041	-0.005	-0.014	-0.001	-0.002	-0.003	-0.002	-0.001	-0.001
ϵ_p	2.31	2.53	2.51	1.24	2.03	1.38	4.05	3.27	2.22	0.456	5.12	5.12
Δ_{int}	0.171	0.121	0.135	0.208	0.205	0.152	0.200	0.191	0.152	0.157	0.171	0.171
D.C. Gain	1.727	1.722	1.805	-27.2	-633	-202	7.120	0.250	-31,300	-1,000	-2,450	-2,450
$1/\Delta_{int}$	-15.1	-61.5	-73.5	-13.3	-29.1	-19.5	-105	-71.2	-31.7	-36.4	-26.2	-26.2
$1/\Delta_{int}$	2.45	2.53	2.51	1.27	2.03	1.38	4.05	3.27	2.22	0.456	5.12	5.12
ϵ_p	0.172	0.122	0.188	0.277	0.205	0.159	0.232	0.191	0.152	0.157	0.172	0.172
D.C. Gain	69.2	70.8	71.7	-4.40	-13.3	-14.5	215	260	-1,240	-35.0	-53.0	-53.0
$1/\Delta_{int}$	-5.09	-6.23	-7.01	-1.12	-3.51	-1.69	-15.4	-9.31	-3.85	-7.24	-1.97	-1.97
$1/\Delta_{int}$	0.571	0.572	0.716	-0.420	0.019	0.065	-2.61	0.037	0.411	2.53	0.037	0.037
ϵ_p	1.80	1.97	1.99	2.32	1.87	2.15	1.40	1.87	1.20	1.31	2.03	2.03
Δ_{int}	0.254	0.318	0.318	0.110	0.250	0.109	0.700	0.282	0.157	0.505	0.254	0.254
D.C. Gain	7.31	7.57	7.65	-1.52	-7.70	-2.77	18.1	24.5	-114	-1.15	-1.51	-1.51
$1/\Delta_{int}$	0.0799	0.0926	0.100	0.019	0.025	0.014	0.175	0.108	0.022	0.017	0.039	0.039
$1/\Delta_{int}$	-0.259	-0.281	-0.271	-61.7	-1.57	-15.2	-0.116	-0.231	-0.045	-0.012	-0.003	-0.003
ϵ_p	2.35	3.55	3.53	(0.543)	(2.91)	(0.548)	4.78	1.70	2.25	3.03	2.03	2.03
Δ_{int}	20.6	18.0	20.3	(0.893)	(0.500)	(0.759)	67.9	56.5	10.3	185	117	117
D.C. Gain	-1,143	-1,254	-1,401	-35.6	635	147	-10,032	-6,250	11,200	763	361	361
$1/\Delta_{int}$	62.9	72.9	70.9	11.6	38.8	18.7	-1,176	101	45.8	63.3	37.0	37.0
$1/\Delta_{int}$	(1.79)	(2.19)	(2.10)	(3.23)	(1.59)	(2.97)	-2.23	-0.729	(1.64)	-0.278	-0.115	-0.115
$1/\Delta_{int}$	(0.753)	(0.619)	(0.608)	(0.073)	(0.553)	(0.077)	6.07	1.23	(0.601)	3.23	2.19	2.19
$1/\Delta_{int}$	(0.923)	(0.823)	(0.823)	(0.461)	(1.51)	(0.461)	-3.47	-1.63	(0.677)	-0.68	-2.07	-2.07
$1/\Delta_{int}$	(-0.353)	(-0.427)	(-0.511)	(0.559)	(0.002)	(0.510)	1.50	3.33	(0.677)	7.32	5.01	5.01
D.C. Gain	-1,143	-1,254	-1,401	-35.6	635	147	-10,032	-6,250	11,200	763	361	361
$1/\Delta_{int}$	62.9	72.9	70.9	11.6	38.8	18.7	-1,176	101	45.8	63.3	37.0	37.0
$1/\Delta_{int}$	(1.79)	(2.19)	(2.10)	(3.23)	(1.59)	(2.97)	-2.23	-0.729	(1.64)	-0.278	-0.115	-0.115
$1/\Delta_{int}$	(0.753)	(0.619)	(0.608)	(0.073)	(0.553)	(0.077)	6.07	1.23	(0.601)	3.23	2.19	2.19
$1/\Delta_{int}$	(0.923)	(0.823)	(0.823)	(0.461)	(1.51)	(0.461)	-3.47	-1.63	(0.677)	-0.68	-2.07	-2.07
$1/\Delta_{int}$	(-0.353)	(-0.427)	(-0.511)	(0.559)	(0.002)	(0.510)	1.50	3.33	(0.677)	7.32	5.01	5.01
D.C. Gain	-1,143	-1,254	-1,401	-35.6	635	147	-10,032	-6,250	11,200	763	361	361
$1/\Delta_{int}$	62.9	72.9	70.9	11.6	38.8	18.7	-1,176	101	45.8	63.3	37.0	37.0
$1/\Delta_{int}$	(1.79)	(2.19)	(2.10)	(3.23)	(1.59)	(2.97)	-2.23	-0.729	(1.64)	-0.278	-0.115	-0.115
$1/\Delta_{int}$	(0.753)	(0.619)	(0.608)	(0.073)	(0.553)	(0.077)	6.07	1.23	(0.601)	3.23	2.19	2.19
$1/\Delta_{int}$	(0.923)	(0.823)	(0.823)	(0.461)	(1.51)	(0.461)	-3.47	-1.63	(0.677)	-0.68	-2.07	-2.07
$1/\Delta_{int}$	(-0.353)	(-0.427)	(-0.511)	(0.559)	(0.002)	(0.510)	1.50	3.33	(0.677)	7.32	5.01	5.01
D.C. Gain	-1,143	-1,254	-1,401	-35.6	635	147	-10,032	-6,250	11,200	763	361	361
$1/\Delta_{int}$	62.9	72.9	70.9	11.6	38.8	18.7	-1,176	101	45.8	63.3	37.0	37.0
$1/\Delta_{int}$	(1.79)	(2.19)	(2.10)	(3.23)	(1.59)	(2.97)	-2.23	-0.729	(1.64)	-0.278	-0.115	-0.115
$1/\Delta_{int}$	(0.753)	(0.619)	(0.608)	(0.073)	(0.553)	(0.077)	6.07	1.23	(0.601)	3.23	2.19	2.19
$1/\Delta_{int}$	(0.923)	(0.823)	(0.823)	(0.461)	(1.51)	(0.461)	-3.47	-1.63	(0.677)	-0.68	-2.07	-2.07
$1/\Delta_{int}$	(-0.353)	(-0.427)	(-0.511)	(0.559)	(0.002)	(0.510)	1.50	3.33	(0.677)	7.32	5.01	5.01
D.C. Gain	-1,143	-1,254	-1,401	-35.6	635	147	-10,032	-6,250	11,200	763	361	361
$1/\Delta_{int}$	62.9	72.9	70.9	11.6	38.8	18.7	-1,176	101	45.8	63.3	37.0	37.0
$1/\Delta_{int}$	(1.79)	(2.19)	(2.10)	(3.23)	(1.59)	(2.97)	-2.23	-0.729	(1.64)	-0.278	-0.115	-0.115
$1/\Delta_{int}$	(0.753)	(0.619)	(0.608)	(0.073)	(0.553)	(0.077)	6.07	1.23	(0.601)	3.23	2.19	2.19
$1/\Delta_{int}$	(0.923)	(0.823)	(0.823)	(0.461)	(1.51)	(0.461)	-3.47	-1.63	(0.677)	-0.68	-2.07	-2.07
$1/\Delta_{int}$	(-0.353)	(-0.427)	(-0.511)	(0.559)	(0.002)	(0.510)	1.50	3.33	(0.677)	7.32	5.01	5.01
D.C. Gain	-1,143	-1,254	-1,401	-35.6	635	147	-10,032	-6,250	11,200	763	361	361
$1/\Delta_{int}$	62.9	72.9	70.9	11.6	38.8	18.7	-1,176	101	45.8	63.3	37.0	37.0
$1/\Delta_{int}$	(1.79)	(2.19)	(2.10)	(3.23)	(1.59)	(2.97)	-2.23	-0.729	(1.64)	-0.278	-0.115	-0.115
$1/\Delta_{int}$	(0.753)	(0.619)	(0.608)	(0.073)	(0.553)	(0.077)	6.07	1.23	(0.601)	3.23	2.19	2.19
$1/\Delta_{int}$	(0.923)	(0.823)	(0.823)	(0.461)	(1.51)	(0.461)	-3.47	-1.63	(0.677)	-0.68	-2.07	-2.07
$1/\Delta_{int}$	(-0.353)	(-0.427)	(-0.511)	(0.559)	(0.002)	(0.510)	1.50	3.33	(0.677)	7.32	5.01	5.01
D.C. Gain	-1,143	-1,254	-1,401	-35.6	635	147	-10,032	-6,250	11,200	763	361	361
$1/\Delta_{int}$	62.9	72.9	70.9	11.6	38.8	18.7	-1,176	101	45.8	63.3	37.0	37.0
$1/\Delta_{int}$	(1.79)	(2.19)	(2.10)	(3.23)	(1.59)	(2.97)	-2.23	-0.729	(1.64)	-0.278	-0.115	-0.115
$1/\Delta_{int}$	(0.753)	(0.619)	(0.608)	(0.073)	(0.553)	(0.077)	6.07	1.23	(0.601)	3.23	2.19	2.19
$1/\Delta_{int}$	(0.923)	(0.823)	(0.823)	(0.461)	(1.51)	(0.461)	-3.47	-1.63	(0.677)	-0.68	-2.07	-2.07
$1/\Delta_{int}$	(-0.353)	(-0.427)	(-0.511)	(0.559)	(0.002)	(0.510)	1.50	3.33	(0.677)	7.32	5.01	5.01
D.C. Gain	-1,143	-1,254	-1,401	-35.6	635	147	-10,032	-6,250	11,200	763	361	361
$1/\Delta_{int}$	62.9	72.9	70.9	11.6	38.8	18.7	-1,176	101	45.8	63.3	37.0	37.0
$1/\Delta_{int}$	(1.79)	(2.19)	(2.10)	(3.23)	(1.59)	(2.97)	-2.23	-0.729	(1.64)	-0.278	-0.115	-0.115
$1/\Delta_{int}$	(0.753)	(0.619)	(0.608)	(0.073)	(0.553)	(0.077)	6.07	1.23	(0.601)	3.23	2.19	2.19
$1/\Delta_{int}$	(0.923)	(0.823)	(0.823)	(0.461)	(1.51)	(0.461)	-3.47	-1.63	(0.677)	-0.68	-2.07	-2.07
$1/\Delta_{int}$	(-0.353)	(-0.427)	(-0.511)	(0.559)	(0.002)	(0.510)	1.50	3.33	(0.677)	7.32	5.01	5.01
D.C. Gain	-1,143	-1,254	-1,401	-35.6	635	147	-10,032	-6,250	11,200	763	361	361
$1/\Delta_{int}$	62.9	72.9	70.9	11.6	38.8	18.7	-1,176	101	45.8	63.3	37.0	37.0
$1/\Delta_{int}$	(1.79)	(2.19)	(2.10)	(3.23)	(1.59)	(2.97)	-2.23	-0.729	(1.64)	-0.278	-0.115	-0.115
$1/\Delta_{int}$	(0.753)	(0.619)	(0.608)	(0.073)	(0.553)	(0.077)	6.07	1.23	(0.601)	3.23	2.19	2.19
$1/\Delta_{int}$	(0.923)	(0.823)	(0.823)	(0.461)	(1.51)	(0.461)	-3.47	-1.63	(0.677)	-0.68	-2.07	-2.07
$1/\Delta_{int}$	(-0.353)	(-0.427)	(-0.511)	(0.559)	(0.002)	(0.510)	1.50	3.33	(0.677)	7.32	5.01	5.01
D.C. Gain	-1,143	-1,254	-1,401	-35.6	635	147	-10,032	-6,250	11,200	763	361	361
$1/\Delta_{int}$	62.9	72.9	70.9	11.6	38.8	18.7	-1,176	101	45.8	63.3	37.0	37.0
$1/\Delta_{int}$	(1.79)	(2.19)	(2.10)	(3.23)	(1.59)	(2.97)	-2.23	-0.729	(1.64)	-0.278	-0.115	-0.115
$1/\Delta_{int}$	(0.753)	(0.619)	(0.608)	(0.073)	(0.553)	(0.077)	6.07	1.23	(0.601)	3.23	2.19	2.19
$1/\Delta_{int}$	(0.923)	(0.823)	(0.823)	(0.461)	(1.51)	(0.461)	-3.47	-1.63	(0.677)	-0.68	-2.07	-2.07
$1/\Delta_{int}$	(-0.353)	(-0.427)	(-0.511)	(0.559)	(0.002)	(0.510)	1.50	3.33	(0.677)	7.32	5.01	5.01
D.C. Gain	-1,143	-1,254	-1,401	-35.6	635	147	-10,032	-6,250	11,200	763	361	361
$1/\Delta_{int}$	62.9	72.9	70.9	11.6	38.8	18.7	-1,176	101	45.8	63.3	37.0	37.0
$1/\Delta_{int}$	(1.79)	(2.19)	(2.10)	(3.23)	(1.59)	(2.97)	-2.23	-0.729	(1.64)	-0.278	-0.115	-0.115
$1/\Delta_{int}$	(0.753)	(0.619)	(0.608)	(0.073)	(0.553)	(0.077)	6.07	1.23	(0.601)	3.23		

D. RUDDER LATERAL TRANSFER FUNCTION FACTORS FOR BASIC F-106B

	Flight Condition											
	1	2	3	4	5	6	7	8	9	10	11	12
Mach No., M	0.755	0.755	0.755	0.2	0.4	0.4	0.9	0.9	0.9	1.4	1.4	1.4
Altitude, h	20,000	20,000	20,000	S.L.	S.L.	20,000	S.L.	20,000	20,000	20,000	20,000	20,000
C.G.	29	30.5	30.5	30.5	30.5	30.5	30.5	30.5	30.5	30.5	30.5	30.5
Weight	29,000	29,000	29,000	29,000	29,000	29,000	29,000	29,000	29,000	29,000	29,000	29,000
η_{12}/s^2	392	392	392	39	257	109	1,199	591	223	1,333	519	1,100
Δ_{lat}	-0.0170	-0.0166	-0.0164	0.169	0.032	0.000	-0.004	-0.006	0.001	0.010	0.010	-0.003
	1.60	2.19	2.62	0.592	2.09	0.676	5.03	1.04	1.09	4.39	1.97	2.15
η_D	2.37	2.47	2.54	2.42	2.01	2.00	4.34	3.01	2.12	4.73	3.22	3.37
ζ_D	0.164	0.173	0.176	0.162	0.233	0.162	0.224	0.159	0.129	0.116	0.093	0.074
D.C. gain	0.390	0.365	0.355	0.737	0.522	0.915	-72.1	-0.115	9.04	0.093	0.260	-0.163
A_{p_r}	7.06	9.51	11.1	2.08	6.17	2.97	19.5	11.1	5.07	7.31	4.18	5.23
$1/\tau_{p_{r1}}$	-0.00314	-0.00286	-0.00275	-0.013	-0.006	-0.015	-0.301	-0.702	-0.003	-0.0005	-0.001	-0.0002
$1/\tau_{p_{r2}}(\omega_{p_r})$	(1.64)	(1.72)	(1.79)	1.88	1.85	1.97	-0.001	-0.002	1.34	5.13	3.35	3.12
$1/\tau_{p_{r3}}(\zeta_{p_r})$	(0.0633)	(0.0701)	(0.0736)	-2.64	-2.05	-2.34	0.565	0.829	-1.69	-3.29	-3.40	-3.50
D.C. gain	-125	-128	-129	-19.3	-87.8	-65.0	11.9	74.9	-2,650	-207	-83	54
A_{p_r}	6.66	9.32	10.9	1.92	6.03	2.81	19.3	11.0	4.94	7.25	4.11	5.19
$1/\tau_{p_{r1}}(\omega_{p_r})$	(1.61)	(1.74)	(1.81)	-2.98	-2.12	-2.49	-0.406	-0.208	-1.74	-3.34	-3.45	-3.6
$1/\tau_{p_{r2}}(\zeta_{p_r})$	(0.0468)	(0.0545)	(0.0582)	1.99	1.85	2.02	0.553	0.823	1.55	5.13	3.37	3.40
D.C. gain	-5.04	-5.16	-5.23	-2.33	-6.09	-4.70	0.224	2.44	-99.7	-4.54	-3.31	7.0
A_{p_r}	-2.55	-2.68	-2.75	-0.505	-1.65	-0.792	-6.16	-3.28	-1.44	-2.90	-1.45	-1.91
$1/\tau_{p_{r1}}$	-0.436	-0.431	-0.427	0.442	2.18	0.430	5.37	2.00	0.735	4.28	1.43	2.71
$\omega_{p_r}(1/\tau_{p_{r2}})$	(0.349)	(0.366)	(0.375)	2.48	0.690	1.74	(0.353)	0.190	0.674	0.598	0.736	0.438
$\zeta_{p_r}(1/\tau_{p_{r3}})$	(2.00)	(2.71)	(3.28)	0.214	0.415	0.243	(0.0062)	0.582	0.502	0.435	0.610	0.394
D.C. gain	0.0251	0.0233	0.0172	-0.351	-0.560	-0.416	0.402	0.640	-8.39	-0.044	-0.070	0.336
A_{p_r}	0.0347	0.0402	0.0435	0.028	0.0438	0.023	0.067	0.039	0.019	0.024	0.009	0.009
$1/\tau_{p_{r1}}$	-0.00111	-0.000727	-0.000530	-0.259	-0.033	-0.086	-0.004	-0.009	-0.021	-0.003	-0.004	-0.010
$1/\tau_{p_{r2}}$	1.56	2.11	2.53	0.690	2.07	0.700	5.08	1.85	1.07	4.36	1.90	2.74
$1/\tau_{p_{r3}}$	89.5	83.8	81.1	41.3	50.4	64.0	104	97.8	103	130	184	215
D.C. gain	21.6	27.2	30.7	17.0	79.1	28.7	-159	-129	839	60.9	29.4	-16
A_{p_r}	27.3	31.6	34.2	6.57	19.6	9.52	67.2	36.6	16.2	34.1	12.2	18.2
$1/\tau_{p_{r1}}(\omega_{p_r})$	0.00614	0.00666	0.00679	(1.02)	-0.067	-0.333	-0.004	-0.010	-0.034	-0.012	-0.011	-0.018
$1/\tau_{p_{r2}}(\omega_{p_r})$	1.53	2.04	2.44	(0.995)	2.05	0.904	6.89	1.85	1.00	4.29	1.99	2.74
$1/\tau_{p_{r3}}(\omega_{p_r})$	-3.30	-3.41	-3.49	(1.21)	-2.42	-1.16	-5.65	-3.92	-2.44	-5.37	-4.59	-3.69
$1/\tau_{p_{r1}}(\zeta_{p_r})$	3.52	4.16	4.25	-(0.243)	3.25	1.88	5.17	4.29	2.85	6.16	3.02	3.99
D.C. gain	21.6	27.2	30.7	17.0	79.1	28.7	-159	-129	839	60.9	29.4	-16
A_{p_r}	6.40	16.6	23.3	4.71	11.8	5.60	24.9	16.5	8.03	7.89	0.764	2.39
$1/\tau_{p_{r1}}$	0.0046	0.00670	0.00693	-0.300	-0.061	-0.135	-0.004	-0.010	-0.031	-0.012	-0.010	-0.018
$1/\tau_{p_{r2}}$	-8.81	-6.05	-5.56	0.402	-6.36	0.428	-16.1	2.69	0.844	3.35	1.35	2.39
$(\omega_{p_r})/\tau_{p_{r3}}$	(3.05)	(2.99)	(3.08)	-5.38	(2.17)	-5.47	(5.81)	-8.13	-3.89	-21.5	-31.0	-34.4
$\zeta_{p_r})/\tau_{p_{r2}}$	(0.650)	(0.720)	(0.663)	3.26	(0.942)	3.55	(0.703)	3.39	3.35	8.69	10.9	8.34



A4D

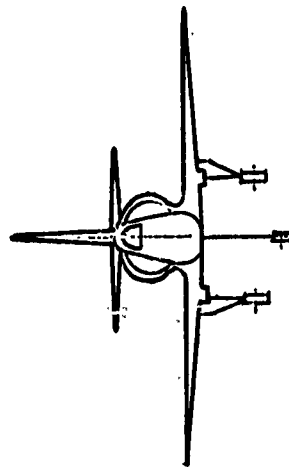


TABLE A-3

A. GEOMETRICAL AND INERTIAL PARAMETERS FOR THE A-4D

Note: Data are for body-fixed stability axes; $S = 260 \text{ ft}^2$, $b = 27.5 \text{ ft}$, $c = 10.8 \text{ ft}$

	FLIGHT CONDITION							
	1	2	3	4	5	6	7	8
h (ft)	0	0	0	15,000	15,000	15,000	35,000	35,000
M (-)	0.2	0.4	0.85	0.4	0.6	0.9	0.5	0.7
a (ft/sec)	1116	1116	1116	1057	1057	1057	973	973
ρ (slugs/ft ³)	0.00238	0.00238	0.00238	0.001496	0.001496	0.001496	0.000738	0.000738
V_{T_0} (ft/sec)	223	447	950	423	634	952	487	681
$\bar{q} = \rho V^2/2$ (lb/ft ²)	59.2	237	945	134	301	678	87	171
W (lb)	22,058	17,578	17,578	17,578	17,578	17,578	17,578	17,578
m (slugs)	658	546	546	546	546	546	546	546
I_x (slug-ft ²)	16,450	8,010	8,070	8,190	8,000	8,050	8,590	8,030
I_y (slug-ft ²)	29,300	25,900	25,900	25,900	25,900	25,900	25,900	25,900
I_z (slug-ft ²)	35,220	29,300	29,230	29,140	29,300	29,260	28,730	29,250
I_{xz} (slug-ft ²)	-5,850	-446	1,159	-1,994	37	1,040	-3,460	-891
$x_{c.g./\bar{c}}$	0.25	0.25	0.25	0.25	0.25	0.25	0.25	0.25
α_{trim} (deg)	19.5	4.7	0.4	8.9	3.4	0.7	13.0	5.9
γ_0 (deg)	0	0	0	0	0	0	0	0

B. LONGITUDINAL DIMENSIONAL DERIVATIVES FOR THE A-10

Note: Data are for body-fixed stability axes

	FLIGHT CONDITION							
	1	2	3	4	5	6	7	8
h (ft)	0	0	0	15,000	15,000	15,000	35,000	35,000
M (-)	0.2	0.4	0.85	0.4	0.6	0.9	0.5	0.7
\dot{T}_U (1/sec)	-0.001347	-0.000297	0	-0.000052	0.000225	0.00303	0.000489	0.000907
$X_{U_{\text{corr}}}$ (1/sec)	-0.0813	-0.0158	-0.0308	-0.01476	-0.01288	-0.0635	-0.01736	-0.01612
X_U (1/sec)	-0.0826	-0.01588	-0.0308	-0.01482	-0.01266	-0.0605	-0.01687	-0.01521
X_W (1/sec)	-0.0312	-0.00379	-0.0368	-0.0371	-0.00588	-0.034	-0.0338	-0.0245
$X_{\dot{e}}$ [(ft/sec ²)/rad]	—	—	—	—	—	—	—	—
$X_{\dot{T}}$ [(ft/sec ²)/rad]	0.00432	0.00582	0.00769	0.00374	0.00414	0.00707	0.00201	0.00238
$Z_{U_{\text{corr}}}$ (1/sec)	-0.26	-0.1442	-0.1134	-0.1518	-0.1012	-0.1346	-0.1291	-0.1013
Z_U (1/sec)	-0.26	-0.1442	-0.1134	-0.1518	-0.1012	-0.1346	-0.1291	-0.1013
Z_W (-)	-0.001681	-0.0022	-0.00382	-0.001385	-0.001616	-0.00265	-0.000797	-0.000902
$Z_{\dot{e}}$ (1/sec)	-0.307	-1.873	-2.23	-0.52	-0.818	-1.475	-0.211	-0.454
$Z_{\dot{T}}$ [(ft/sec ²)/rad]	-7.07	-40.71	-188.0	-22.93	-56.92	-101.3	-15.81	-33.3
$Z_{\dot{e}}$ [(ft/sec ²)/rad]	0	0	0	0	0	0	0	0
$M_{U_{\text{corr}}}$ (1/sec-ft)	-0.00285	-0.000433	0.001108	-0.000467	-0.000407	-0.01131	-0.000549	0.000513
M_U (1/sec-ft)	-0.0029	-0.000441	0.001108	-0.000468	-0.0004	-0.01122	-0.000533	0.000542
$M_{\dot{e}}$ (1/ft)	-0.000646	-0.000672	-0.001308	-0.000482	-0.000556	-0.000902	-0.000253	-0.000303
M_W (1/sec-ft)	-0.0102	-0.01972	-0.0502	-0.01338	-0.02	-0.0378	-0.00759	-0.0109
M_Q (1/sec)	-0.48	-0.988	-2.93	-0.67	-1.07	-1.934	-0.389	-0.592
$M_{\dot{e}}$ (1/sec ²)	-2.21	-11.53	-41	-7.4	-19.42	-33.8	-5.26	-11.33
$M_{\dot{T}}$ (1/sec ²)	0.000152	0.0001617	0.000243	0.0001181	0.0001309	0.000224	0.000637	0.000753

C. ELEVATOR LONGITUDINAL TRANSFER FUNCTION FACTORS FOR THE A-4D

		FLIGHT CONDITION							
		1	2	3	4	5	6	7	8
Mach No., M (-)		0.2	0.4	0.85	0.4	0.6	0.9	0.5	0.7
Altitude, h (ft)		0	0	0	15,000	15,000	15,000	35,000	35,000
c.g. (% c)		0.25	0.25	0.25	0.25	0.25	0.25	0.25	0.25
Weight, W (lb)		22,058	17,578	17,578	17,578	17,578	17,578	17,578	17,578
Δ_{long}	$\zeta_{sp} (1/T_{sp1})$	0.317	0.348	0.436	0.286	0.304	(-0.0783)	0.1883	0.225
	$\omega_{sp} (1/T_{sp2})$	1.358	3.11	7.35	2.45	3.69	(0.121)	1.941	2.77
	$\zeta_p (1/T_{p1})$	0.0371	0.0706	0.226	0.0439	0.0867	0.344	0.0488	0.1177
	$\omega_p (1/T_{p2})$	0.152	0.0905	0.0696	0.098	0.0635	6.23	0.0861	0.0752
$N_{\delta_e}^a$	A_θ	-2.21	-11.53	-64	-7.4	-19.42	-33.8	-5.26	-11.33
	$1/T_{\theta 1}$	0.0482	0.01519	0.0287	0.00308	0.01187	0.0578	-0.00544	0.00909
	$1/T_{\theta 2}$	0.309	0.804	2.08	0.49	0.76	1.365	0.21	0.428
	dc gain	-0.585	-1.779	-14.51	-0.194	-3.19	7.23	0.215	-1.014
$N_{\delta_e}^w$	A_w	-7.07	-40.7	-188	-22.9	-56.9	-101.3	-15.81	-33.3
	$1/T_{w1}$	70.2	127.6	326	137.1	218	319	162.2	232
	ζ_w	0.217	0.0782	0.245	0.069	0.0888	0.519	0.0917	0.1091
	ω_w	0.1394	0.101	0.0626	0.1067	0.0711	0.0583	0.0918	0.0696
	dc gain	-317	-669	-915	-622	-1140	298	-772	-863
$N_{\delta_e}^h$	A_h	7.07	40.7	188	22.9	56.9	101.3	15.81	33.3
	$1/T_{h1}$	-4.04	-9.58	-24.5	-7.72	-12.29	-19.84	-5.29	-9.59
	$1/T_{h2}$	-0.0777	0.00242	0.0268	-0.0208	0.00519	0.0554	-0.0511	-0.0023
	$1/T_{h3}$	4.71	10.61	27.4	8.44	13.37	21.8	5.74	10.2
	dc gain	10.45	10	-3380	31.1	-48.5	-2427	24.5	7.5
$N_{\delta_e}^{az}$ c.g.	A_{az}	12.81	63	388	43.6	117.9	203	31.5	68.7
	$1/T_{az1}$	0	0	0	0	0	0	0	0
	$1/T_{az2}$	-0.0772	0.00242	0.0268	-0.0208	0.00519	0.0554	-0.051	-0.0023
	ζ_{az}	0.0471	0.0422	0.0461	0.0346	0.0345	0.0365	0.0202	0.026
	ω_{az}	3.25	8.1	18.05	5.86	8.91	14.69	3.9	6.88
	dc gain	0	0	0	0	0	0	0	0

D. LATERAL DIMENSIONAL DERIVATIVES FOR THE A-4D

Note: Data are for body-fixed stability axes

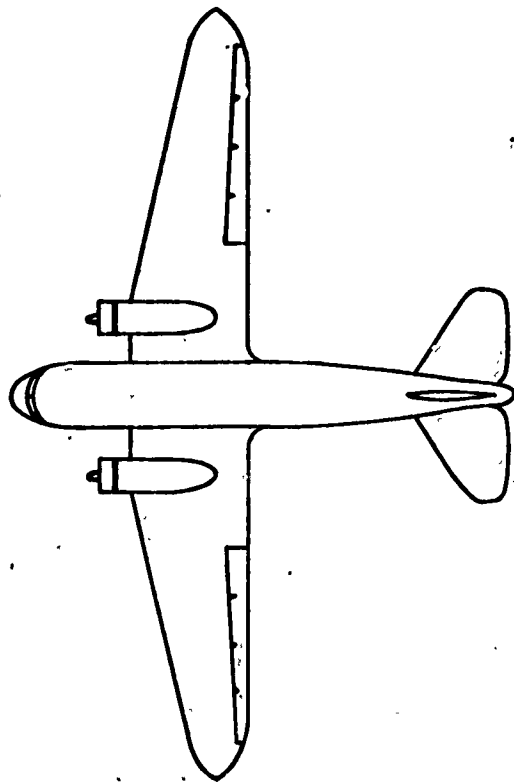
	FLIGHT CONDITION							
	1	2	3	4	5	6	7	8
h (ft)	0	0	0	15,000	15,000	15,000	35,000	35,000
M (-)	0.2	0.4	0.85	0.4	0.6	0.9	0.5	0.7
Y_V (1/sec)	-0.1026	-0.243	-0.575	-0.1476	-0.228	-0.363	-0.0864	-0.1221
Y_P (ft/sec ²)/rad	-22.9	-108.6	-547	-62.4	-144.8	-345	-42	-83.2
Y_{δ_a} (ft/sec ²)/rad	-0.606	-2.49	-7.41	-0.892	-2.37	-5	-0.416	-0.979
$Y_{\delta_a}^*$ (1/sec)/rad	-0.00272	-0.00557	-0.0078	-0.00211	-0.00373	-0.00525	-0.000855	-0.001437
Y_{δ_r} (ft/sec ²)/rad	3.70	15.83	85.3	8.92	25.1	52.3	7.28	14.11
$Y_{\delta_r}^*$ (1/sec)/rad	0.0166	0.0354	0.0898	0.0211	0.0395	0.0549	0.01497	0.0207
L_P (1/sec ²)	-3.21	-26.5	-127.3	-14.02	-35	-87.2	-6.4	-21.35
L_P (1/sec)	-0.412	-1.695	-3.84	-0.987	-1.516	-2.5	-0.534	-0.816
L_r (1/sec)	0.0317	0.913	2.13	0.608	0.875	1.391	0.288	0.523
L_{δ_a} (1/sec ²)	1.875	16.53	63.7	8.76	21.3	36.7	5.09	11.74
L_{δ_r} (1/sec ²)	0.1284	6.99	40.9	2.8	9.96	24.1	1.164	4.73
L_P^* (1/sec ²)	-4.47	-27.3	-117.6	-16.29	-34.9	-81.6	-9.03	-22.7
L_P^* (1/sec)	-0.396	-1.699	-3.83	-1.004	-1.516	-2.49	-0.562	-0.819
L_r^* (1/sec)	0.1455	0.948	1.93	0.717	0.872	1.273	0.404	0.56
$L_{\delta_a}^*$ (1/sec ²)	2.0	16.53	64.4	8.95	21.3	37.1	5.4	11.77
$L_{\delta_r}^*$ (1/sec ²)	0.617	7.36	37	3.75	9.92	21.9	2.25	5.27
N_P (1/sec ²)	2.8	14.49	72.7	8.21	18.73	46.4	5.44	11.3
N_P (1/sec)	-0.111	0.0392	0.1975	0	0.0398	0.1244	0	0.00845
N_r (1/sec)	-0.296	-0.624	-1.481	-0.4	-0.565	-0.957	-0.24	-0.321
N_{δ_a} (1/sec ²)	-0.024	0.319	2.49	-0.1641	0.478	1.49	-0.1087	0.0837
N_{δ_r} (1/sec ²)	-1.272	-6.43	-28.6	-3.64	-8.3	-17.38	-2.44	-4.69
N_P^* (1/sec ²)	3.54	14.9	68	9.32	18.69	43.4	6.52	11.99
N_P^* (1/sec)	-0.0452	0.0651	0.0456	0.0687	0.0379	0.0359	0.0676	0.0334
N_r^* (1/sec)	-0.32	-0.638	-1.404	-0.449	-0.564	-0.911	-0.288	-0.338
$N_{\delta_a}^*$ (1/sec ²)	-0.357	0.0671	5.05	-0.777	0.504	2.81	-0.759	-0.275
$N_{\delta_r}^*$ (1/sec ²)	-1.374	-6.54	-27.1	-3.9	-8.29	-16.6	-2.71	-4.85

E. AILERON LATERAL TRANSFER FUNCTION FACTORS FOR THE A-4D

		FLIGHT CONDITION							
		1	2	3	4	5	6	7	8
Mach No., M (-)		0.2	0.4	0.85	0.4	0.6	0.9	0.5	0.7
Altitude, h (ft)		0	0	0	15,000	15,000	15,000	35,000	35,000
c.g. (% c)		0.25	0.25	0.25	0.25	0.25	0.25	0.25	0.25
Weight, W (lb)		22,058	17,578	17,578	17,578	17,578	17,578	17,578	17,578
α_{trim} (deg)		19.5	4.7	0.4	8.9	3.4	-0.7	13.0	5.9
Δ_{lat}	$1/T_s$	0.0555	0.00931	0.00438	0.00509	0.00595	0.00595	-0.000577	0.00441
	$1/T_R$	0.553	1.707	3.81	1.016	1.535	2.48	0.562	0.842
	ζ_d	0.0502	0.1115	0.1203	0.0949	0.0885	0.0964	0.0734	0.0625
	ω_d	1.934	3.87	8.29	3.06	4.34	6.61	2.55	3.47
$N_{\delta_a}^p$	A_p	2.0	16.53	64.4	8.95	21.3	37.1	5.4	11.77
	$1/T_{p1}$	0	0	0	0	0	0	0	0
	ζ_p	0.1209	0.1148	0.1214	0.0954	0.0924	0.0977	0.0695	0.0663
	ω_p	1.665	3.89	8.84	2.82	4.43	7.07	2.3	3.39
	dc gain	0	0	0	0	0	0	0	0
$N_{\delta_a}^r$	A_r	-0.357	0.0671	5.05	-0.777	3.504	2.81	-0.759	-0.275
	$1/T_{r1}$	-1.074	17.47	5.57	-1.778	4.86	4.26	-1.294	-3.01
	ζ_r	0.644	-0.0945	-0.1411	0.548	-0.283	-0.223	0.531	0.464
	ω_r	1.439	3.90	2.45	1.975	2.93	2.28	1.382	2.78
	dc gain	5.92	75	146.9	111.6	122.6	96.4	-888	143
$N_{\delta_a}^b$	A_b	-0.00272	-0.00557	-0.0078	-0.00211	-0.00373	-0.00525	-0.000855	-0.001437
	$1/T_{b1}$	0.1874	-2.8	-0.1621	-368	-0.727	-0.1674	-887	-191.6
	$1/T_{b2} (\zeta_b)$	1.266	3.61	4.14	(0.935)	1.708	2.69	(0.835)	(0.871)
	$1/T_{b3} (\omega_b)$	-132	13.59	649	(0.583)	136.4	535	(0.33)	(0.811)
	dc gain								
$N_{\delta_a}^y$	A_{ay}	-0.606	-2.488	-7.406	-0.89	-2.365	-5.0	-0.416	-0.98
	$1/T_{ay1} (\zeta_{ay1})$	0.177	(-0.034)	-0.196	0.512	1.872	-0.214	(0.0163)	(-0.0056)
	$1/T_{ay2} (\omega_{ay1})$	1.07	(3.21)	4.227	0.57	4.191	2.747	(9.112)	(5.94)
	$1/T_{ay3} (\zeta_{ay3})$	(-0.064)	(0.706)	-16.82	(0.023)	(-0.896)	-11.81	(0.871)	(0.926)
	$1/T_{ay4} (\omega_{ay3})$	(4.198)	(1.81)	18.02	(7.96)	(2.223)	12.68	(0.317)	(0.661)
c.g.									

F. RUDDER LATERAL TRANSFER FUNCTION FACTORS FOR THE A-4D

		FLIGHT CONDITION:							
		1	2	3	4	5	6	7	8
Mach No., M (-)		0.2	0.4	0.85	0.4	0.6	0.9	0.5	0.7
Altitude, h (ft)		0	0	0	15,000	15,000	15,000	35,000	35,000
c.g. (% c)		0.25	0.25	0.25	0.25	0.25	0.25	0.25	0.25
Weight, W (lb)		22,058	17,578	17,578	17,578	17,578	17,578	17,578	17,578
α_{trim} (deg)		19.5	4.7	0.4	8.9	3.4	0.7	13.0	5.9
Δ_{lat}	$1/T_s$	0.0355	0.00931	0.00438	0.00509	0.00595	0.00595	-0.000577	0.00441
	$1/T_R$	0.563	1.707	3.81	1.016	1.535	2.48	0.562	0.842
	ζ_d	0.0502	0.1115	0.1203	0.0949	0.0885	0.0964	0.0734	0.0625
	ω_d	1.394	3.87	8.29	3.06	4.34	6.61	2.55	3.47
$N_{\delta_r}^P$	A_p	0.617	7.36	37	3.75	9.92	21.9	2.25	5.27
	$1/T_{p1}$	0	0	0	0	0	0	0	0
	$1/T_{p2}$	-2.55	-3.12	-4.15	-2.89	-3.28	-4.24	-2.17	-3.06
	$1/T_{p3}$	2.53	3.03	4.43	2.65	3.21	4.35	1.999	2.91
	dc gain	0	0	0	0	0	0		0
$N_{\delta_r}^F$	A_r	-1.374	-6.54	-27.1	-3.9	-8.29	-16.6	-2.71	-4.85
	$1/T_{r1}$	0.931	1.864	3.83	1.295	1.707	2.58	0.852	1.15
	ζ_r	-0.34	-0.0592	0.307	-0.198	-0.0796	0.0754	-0.28	-0.235
	ω_r	0.568	0.639	0.469	0.656	0.610	0.564	0.528	0.63
	dc gain	-4.32	-20.9	-19.97	-45	-30.7	-21.1	305	-49.6
$N_{\delta_r}^B$	A_{δ}	0.0166	0.0354	0.0898	0.0211	0.0395	0.0549	0.01497	0.0207
	$1/T_{\delta 1}$	-0.000527	-0.00964	-0.0001478	-0.021	-0.00349	-0.00944	-0.01869	-0.01081
	$1/T_{\delta 2}$	0.482	1.716	3.81	1.032	1.538	2.49	0.579	0.845
	$1/T_{\delta 3}$	83.0	185.4	304	185.4	210	303	181.2	234
$N_{\delta_r}^{AY}$	A_{ay}	3.70	15.83	85.3	8.91	25.09	52.26	7.28	14.11
	$1/T_{ay1}$	-0.063	-0.019	-0.0031	-0.034	-0.0145	-0.0055	-0.031	-0.0218
	$1/T_{ay2}$	0.434	1.72	3.82	1.041	1.54	2.49	0.591	0.848
	$1/T_{ay3}$	-2.054	-5.17	-9.61	-4.025	-5.13	-7.69	-2.88	-3.911
	c.g. $1/T_{ay4}$	2.40	5.80	11.03	4.471	5.68	8.61	3.17	4.243



C-47

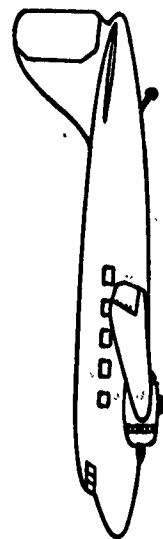
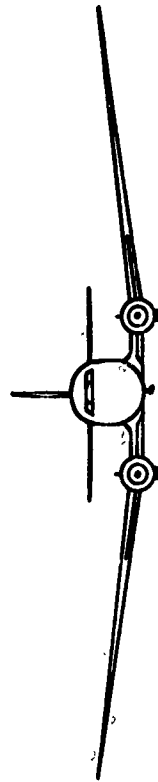
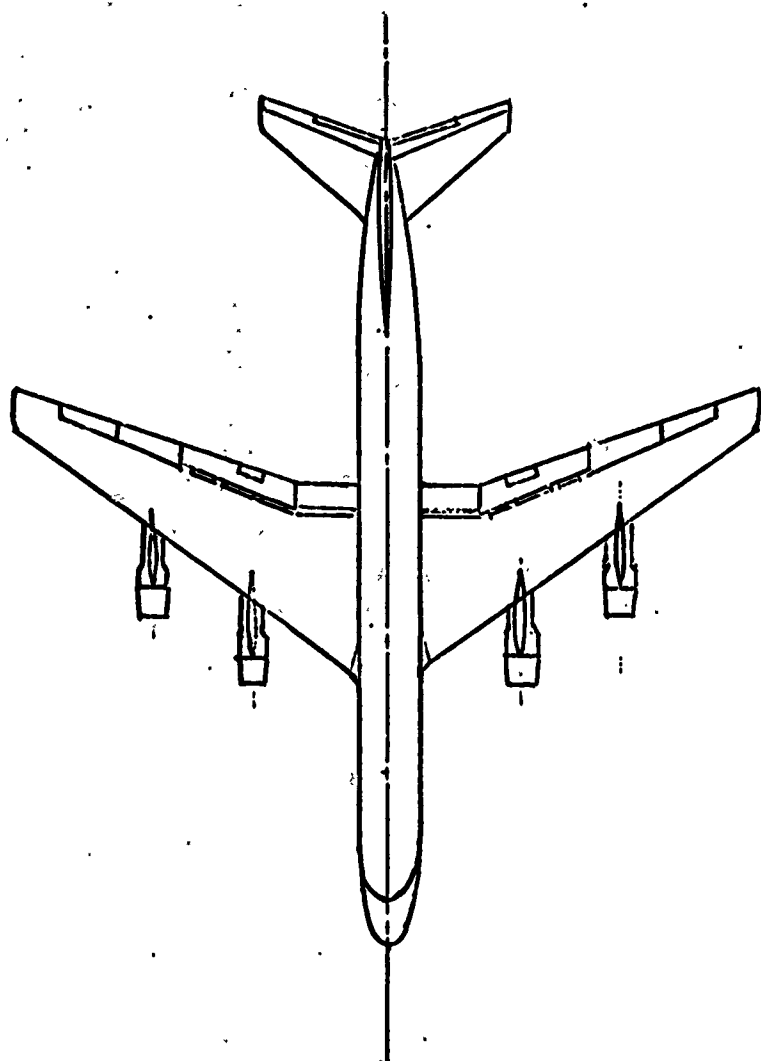


TABLE A-6

A		B		C	
GEOMETRICAL AND INERTIAL PARAMETERS FOR THE C-47		LONGITUDINAL DIMENSIONAL DERIVATIVES FOR THE C-47		LATERAL DIMENSIONAL DERIVATIVES FOR THE C-47	
Note: Data are for body fixed stability axes S = 987 ft ² , b = 95 ft, c = 11.5 ft, γ ₀ = 0 deg					
	FLT. COND. 4701 (APPROACH)		FLT. COND. 4701 (APPROACH)		FLT. COND. 4701 (APPROACH)
h (ft)	1,000	h (ft)	1,000	h (ft)	1,000
M (-)	0.122	M (-)	0.122	M (-)	0.122
a (ft/sec)	1113	T _u (1/sec)	—	Y _v (1/sec)	-0.0593
ρ (slugs/ft ³)	0.002309	X _{u_{zero}} (1/sec)	-0.0647	Y _p [(ft/sec ²)/rad]	-8.0548
V _{T0} (ft/sec)	136	X _u (1/sec)	-0.0647	Y _{p_a} [(ft/sec ²)/rad]	—
q̄ = ρV ² /2 (lb/ft ²)	21.3	X _w (1/sec)	0.115	Y _{p_a} [*] [(1/sec)/rad]	—
W (lb)	23,000	X _{p_e} [(ft/sec ²)/rad]	—	Y _{p_r} [(ft/sec ²)/rad]	5.488
m (slugs)	714			Y _{p_r} [*] [(1/sec)/rad]	0.0405
I _x (slug-ft ²)	61,887	Z _{u_{zero}} (1/sec)	-0.476	I _q (1/sec ²)	-2.05
I _y (slug-ft ²)	89,500	Z _u (1/sec)	-0.476	I _p (1/sec)	-6.65
I _z (slug-ft ²)	139,200	Z _w (-)	—	I _r (1/sec)	2.61
I _{xz} (slug-ft ²)	-4689	Z _w (1/sec)	-1.235	I _{p_a} (1/sec ²)	4.06
		Z _{p_e} [(ft/sec ²)/rad]	-0.712	I _{p_r} (1/sec ²)	—
				I _{p_a} [*] (1/sec ²)	-2.12
		M _{u_{zero}} (1/sec-ft)	—	I _{p_r} [*] (1/sec)	-6.63
		M _u (1/sec-ft)	—	I _r [*] (1/sec)	2.65
		M _w (1/ft)	-0.00845	I _{p_a} [*] (1/sec ²)	4.06
		M _w (1/sec-ft)	-0.011	I _{p_r} [*] (1/sec ²)	0.073
		M _{q̇} (1/sec)	-2.20	N _p (1/sec ²)	0.911
		M _{p_e} (1/sec ²)	-1.56	N _p (1/sec)	-0.423
		M _u (1/sec ²)	-1.496	N _r (1/sec)	-0.458
		M _{q̇} (1/sec)	-1.1492	N _{p_a} (1/sec ²)	0.184
				N _{p_r} (1/sec ²)	-0.956
				N _{p_a} [*] (1/sec ²)	0.983
				N _{p_r} [*] (1/sec)	-0.200
				N _r [*] (1/sec)	-0.547
				N _{p_a} [*] (1/sec ²)	0.047
				N _{p_r} [*] (1/sec ²)	-0.958

D			E			F			G		
ELEVATOR LONGITUDINAL TRANSFER FUNCTION FACTORS FOR THE C-47			AILERON LATERAL TRANSFER FUNCTION FACTORS FOR THE C-47			RUDDER LATERAL TRANSFER FUNCTION FACTORS FOR THE C-47			LATERAL COUPLING NUMERATORS FOR THE C-47		
	FLT. COND.			FLT. COND.			FLT. COND.			FLT. COND.	
	4701 (APPROACH)			4701 (APPROACH)			4701 (APPROACH)			4701 (APPROACH)	
Mach No., M (-)	0.122		Mach No., M (-)	0.122		Mach No., M (-)	0.122		Mach No., M (-)	0.122	
Altitude, h (ft)	1,000		Altitude, h (ft)	1,000		Altitude, h (ft)	1,000		Altitude, h (ft)	1,000	
ζ_{long}	$1/T_{sp1}$	1.25	Δ_{lat}	$1/T_s$	-0.043	Δ_{lat}	$1/T_s$	-0.043	$\frac{p}{s} \frac{r}{N_{\delta a} \delta_r}$	A_{p1}	0.164
	$1/T_{sp2}$	3.31		$1/T_R$	6.57		$1/T_R$	6.57		$1/T_{sp1}$	0
	ζ_p	0.201		ζ_d	0.323		ζ_d	0.323		$1/T_{sp2}$	24.4
	ω_p	0.201		ω_d	1.10		ω_d	1.10			
$\eta_{\zeta e}$	A_0	-4.55	$\eta_{\zeta a}^p$	A_p	4.06	$\eta_{\zeta r}^p$	A_p	0.0726	$\frac{p}{s} \frac{r}{N_{\delta a} \delta_r}$	A_{rp}	0.00191
	$1/T_{01}$	0.114		$1/T_{p1}$	0		$1/T_{p1}$	0		ζ_{rp}	-0.238
	$1/T_{02}$	1.19		ζ_p	0.312		$1/T_{p1}$	0.779		ω_{rp}	22.0
	dc gain	-3.54		ω_p	1.02		$1/T_{p2}$	-36.3			
$\eta_{\zeta e}$	A_u	-0.092	$\eta_{\zeta a}^u$	dc gain	0	$\eta_{\zeta r}^u$	dc gain	0	$\frac{p}{s} \frac{r}{N_{\delta a} \delta_r}$	A_{ru}	-3.89
	$1/T_{u1}$	2.40		A_p	4.06		A_p	0.0726		$1/T_{ru}$	0.0169
	$1/T_{u2}$	9.60		ζ_p	0.312		$1/T_{u1}$	0.779			
	dc gain	1074		ω_p	1.02		$1/T_{u2}$	-36.3			
$\eta_{\zeta e}$	A_w	-0.712	$\eta_{\zeta a}^w$	dc gain	-12.4	$\eta_{\zeta r}^w$	dc gain	6.02	$\frac{p}{s} \frac{r}{N_{\delta a} \delta_r}$	A_{pw}	-0.260
	$1/T_{w1}$	873		A_p	4.06		A_p	0.0726		$1/T_{pw1}$	0.377
	ζ_w	0.095		ζ_p	0.312		$1/T_{u1}$	0.779		$1/T_{pw2}$	-31.1
	ω_w	0.335		ω_p	1.02		$1/T_{u2}$	-36.3		$1/T_{pw3}$	-
$\eta_{\zeta e}$	dc gain	-4.15	$\eta_{\zeta a}^r$	dc gain	-12.4	$\eta_{\zeta r}^r$	dc gain	6.02	$\frac{p}{s} \frac{r}{N_{\delta a} \delta_r}$	c.g.	
				A_r	0.0474		A_r	-0.958		A_{rw}	0.260
				$1/T_{r1}$	1.35		$1/T_{r1}$	6.66		$1/T_{rw1}$	-10.5
				$1/T_{r2}$	-1.48		ζ_r	0.00311		ζ_{rw}	0.0418
$\eta_{\zeta e}$	A_h	0.712	$\eta_{\zeta a}^h$	dc gain	-2.83	$\eta_{\zeta r}^h$	dc gain	1.35	$\frac{p}{s} \frac{r}{N_{\delta a} \delta_r}$	c.g.	0.880
	$1/T_{h1}$	0.018		A_p	-0.0474		A_p	0.0404			
	$1/T_{h2}$	34.5		$1/T_{p1}$	0.377		$1/T_{p1}$	6.83		A_{py}	22.3
	$1/T_{h3}$	-31.1		$1/T_{p2}$	-31.1		$1/T_{p2}$	24.2		$1/T_{py1}$	0
$\eta_{\zeta e}$	dc gain	-20.3	$\eta_{\zeta a}^b$	$1/T_{p3}$	-	$\eta_{\zeta r}^b$	$1/T_{p3}$	-0.0888	$\frac{p}{s} \frac{r}{N_{\delta a} \delta_r}$	$1/T_{py2}$	-0.408
				dc gain	-1.53		dc gain	-1.73		$1/T_{py3}$	0.986
				A_{p1}	-0.0474		A_{p1}	0.0404			
				$1/T_{p1}$	0.377		$1/T_{p1}$	6.83			
$\eta_{\zeta e}$	A_{02}	-0.712	$\eta_{\zeta a}^{ay}$	$1/T_{p2}$	-31.1	$\eta_{\zeta r}^{ay}$	$1/T_{p2}$	24.2	$\frac{p}{s} \frac{r}{N_{\delta a} \delta_r}$		
	$1/T_{az1}$	0		$1/T_{p3}$	-		$1/T_{p3}$	-0.0888			
	$1/T_{az2}$	0.0177		dc gain	-1.53		dc gain	-1.73			
	$1/T_{az3}$	34.5		A_{ay}	0.302		A_{ay}	5.49			
$\eta_{\zeta e}$	$1/T_{az4}$	-31.1	$\eta_{\zeta a}^{ay}$	$1/T_{ay1}$	0.377	$\eta_{\zeta r}^{ay}$	$1/T_{ay1}$	1.00	$\frac{p}{s} \frac{r}{N_{\delta a} \delta_r}$		
	dc gain	0		$1/T_{ay2}$	-31.1		$1/T_{ay2}$	6.57			
				$1/T_{ay3}$	-		ζ_{ay}	-0.024			
				$1/T_{ay4}$	-		dc gain	0.283			
$\eta_{\zeta e}$			$\eta_{\zeta a}^{ay}$	dc gain	13.2	$\eta_{\zeta r}^{ay}$	dc gain	-8.50	$\frac{p}{s} \frac{r}{N_{\delta a} \delta_r}$		



DC-8

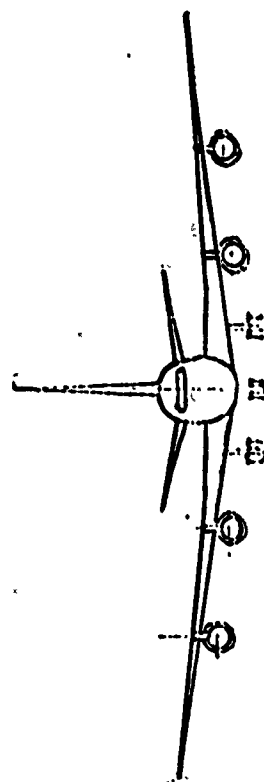
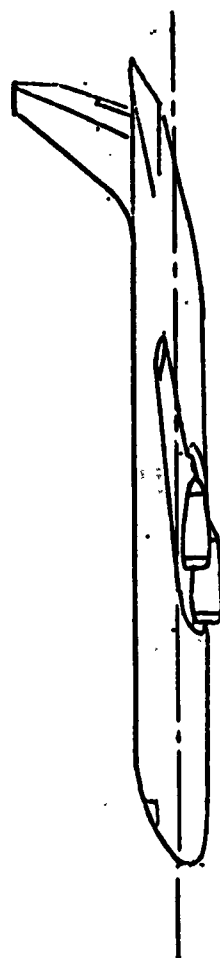


TABLE A-5

A. GEOMETRICAL AND INERTIAL PARAMETERS FOR THE DC-8

Note: Data are for body-fixed stability axes

$$S = 2600 \text{ ft}^2, \quad b = 142.3 \text{ ft}, \quad c = 23 \text{ ft}, \quad \gamma_0 = 0 \text{ deg.}$$

	FLIGHT CONDITION			
	8001 APPROACH	8002 HOLDING	8003 CRUISE	8004 V_{NE}
h (ft)	0	15,000	33,000	33,000
M (-)	0.219	0.443	0.84	0.88
a (ft/sec)	1117	1058	982	982
ρ (slugs/ft ³)	0.002378	0.001496	0.000795	0.000795
V_{T_0} (ft/sec)	243.5	468.2	824.2	863.46
$\bar{q} = \rho V^2/2$ (lb/ft ²)	71.02	163.97	270.0	296.36
W (lb)	190,000	190,000	230,000	230,000
m (slugs)	5900	5900	7143	7143
I_x (slug-ft ²)	3,090,000	3,110,000	3,770,000	3,770,000
I_y (slug-ft ²)	2,940,000	2,940,000	3,560,000	3,560,000
I_z (slug-ft ²)	5,580,000	5,880,000	7,130,000	7,130,000
I_{xz} (slug-ft ²)	28,000	-64,500	45,000	53,700
$x_{c.g.}/\bar{c}$	0.15	0.15	0.15	0.15
θ_0 (deg)	0	0	0	0
U_0 (ft/sec)	243.5	468.2	824.2	863.46
W_0 (ft/sec)	0	0	0	0
δ_F (deg)	35	0	0	0

B. LONGITUDINAL DIMENSIONAL DERIVATIVES FOR THE DC-8

Note: Data are for body-fixed stability axes

	FLIGHT CONDITION			
	8001	8002	8003	8004
h (ft)	0	15,000	33,000	33,000
M (-)	0.219	0.443	0.84	0.88
T_u (1/sec)	-0.000595	-0.0000846	0.000599	0.000733
$X_{u_{\text{ero}}}$ (1/sec)	-0.02851	-0.00707	-0.0145	-0.0471
X_u (1/sec)	-0.0291	-0.00714	-0.014	-0.0463
X_w (1/sec)	0.0629	0.0321	0.0043	-0.0259
X_{δ_e} [(ft/sec ²)/rad]	0	0	0	0
$Z_{u_{\text{ero}}}$ (1/sec)	-0.2506	-0.1329	-0.0735	0.0622
Z_u (1/sec)	-0.2506	-0.1329	-0.0735	0.0622
Z_w (-)	0	0	0	0
Z_w (1/sec)	-0.6277	-0.756	-0.806	-0.865
Z_{δ_e} [(ft/sec ²)/rad]	-10.19	-23.7	-34.6	-38.6
$M_{u_{\text{ero}}}$ (1/sec-ft)	-0.0000077	-0.000063	-0.000786	-0.00254
M_u (1/sec-ft)	-0.0000077	-0.000063	-0.000786	-0.00254
M_w (1/ft)	-0.001063	-0.00072	-0.00051	-0.00052
M_w (1/sec-ft)	-0.0087	-0.0107	-0.0111	-0.0139
M_q (1/sec)	-0.7924	-0.991	-0.924	-1.008
M_{δ_e} (1/sec ²)	-1.35	-3.24	-4.59	-5.12

C. ELEVATOR LONGITUDINAL TRANSFER FUNCTION FACTORS FOR THE DC-8

		FLIGHT CONDITION			
		8001	8002	8003	8004
Mach No., M (-)		0.219	0.443	0.84	0.88
Altitude, h (ft)		0	15,000	33,000	33,000
c.g. (% \bar{c})		15	15	15	15
Weight, W (lb)		190,000	190,000	230,000	230,000
Δ_{long}	ζ_{sp}	0.522	0.434	0.342	0.325
	ω_{sp}	1.619	2.40	3.15	3.59
	$\zeta_p (1/T_{p1})$	0.0606	0.0310	0.241	(-0.0708)
	$\omega_p (1/T_{p2})$	0.1635	0.0877	0.0243	(0.108)
$N_{\delta_e}^\theta$	A_θ	-1.338	-3.22	-4.57	-5.1
	$1/T_{\theta 1}$	0.0605	0.01354	0.01436	0.0493
	$1/T_{\theta 2}$	0.535	0.675	0.725	0.76
	dc gain	-0.618	-0.666	-8.14	1.939
$N_{\delta_e}^u$	A_u	-0.641	-0.761	-0.1489	1.00
	$1/T_{u1}$	1.08	1.279	0.816	0.449
	$1/T_{u2}$	-35.3	-72.7	-879	279
	dc gain	348	1598	18,257	-1272
$N_{\delta_e}^w$	A_w	-10.19	-23.7	-34.6	-38.6
	$1/T_{w1}$	33.0	65.0	110.2	-0.0364
	$\zeta_w (1/T_{w2})$	0.0781	0.037	0.1362	(0.0827)
	$\omega_w (1/T_{w3})$	0.1798	0.0947	0.0511	(115.5)
	dc gain	-155.3	-312	-1706	-136
$N_{\delta_e}^{\dot{h}}$	$A_{\dot{h}}$	10.19	23.7	34.6	38.6
	$1/T_{\dot{h}1}$	-3.75	-5.95	-8.24	-8.63
	$1/T_{\dot{h}2}$	-0.00182	-0.000026	0.0107	0.0531
	$1/T_{\dot{h}3}$	4.83	7.29	9.59	100.9
	dc gain	4.79	0.614	-5000	1811
$N_{\delta_e}^{a_z}$ c.g.	A_{a_z}	-10.19	-23.7	-34.6	-38.6
	$1/T_{a_z1}$	0	0	0	0
	$1/T_{a_z2}$	-3.75	-5.95	-8.24	-8.63
	$1/T_{a_z3}$	-0.00182	-0.000026	0.0107	0.0531
	$1/T_{a_z4}$	4.83	7.29	9.59	100.9
	dc gain	0	0	0	0

D. LATERAL DIMENSIONAL DERIVATIVES FOR THE DC-8

Note: Data are for body-fixed stability axes

	FLIGHT CONDITION			
	8001	8002	8003	8004
h (ft)	0	15,000	33,000	33,000
M (-)	0.219	0.443	0.84	0.88
Y_v (1/sec)	-0.1113	-0.1008	-0.0868	-0.0931
Y_β [(ft/sec ²)/rad]	-27.1	-47.2	-71.5	-80.4
Y_{δ_a} [(ft/sec ²)/rad]	0	0	0	0
$Y_{\delta_a}^*$ [(1/sec)/rad]	0	0	0	0
Y_{δ_r} [(ft/sec ²)/rad]	5.79	13.48	18.33	20.12
$Y_{\delta_r}^*$ [(1/sec)/rad]	0.0238	0.0288	0.0222	0.0233
L_β (1/sec ²)	-1.335	-2.68	-4.43	-5.05
L_p (1/sec)	-0.95	-1.233	-1.18	-1.289
L_r (1/sec)	0.612	0.391	0.336	0.35
L_{δ_a} (1/sec ²)	-0.726	-1.62	-2.11	-2.3
L_{δ_r} (1/sec ²)	0.1848	0.374	0.559	0.63
$L_{\dot{\beta}}$ (1/sec ²)	-1.328	-2.71	-4.41	-5.02
$L_{\dot{p}}$ (1/sec)	-0.951	-1.232	-1.181	-1.29
$L_{\dot{r}}$ (1/sec)	0.609	0.397	0.334	0.346
$L_{\delta_a}^*$ (1/sec ²)	-0.726	-1.62	-2.11	-2.3
$L_{\delta_r}^*$ (1/sec ²)	0.1813	0.392	0.549	0.612
N_β (1/sec ²)	0.763	1.271	2.17	2.47
N_p (1/sec)	-0.1192	-0.048	-0.01294	-0.00744
N_r (1/sec)	-0.268	-0.252	-0.23	-0.252
N_{δ_a} (1/sec ²)	-0.0496	-0.0365	-0.0519	-0.0615
N_{δ_r} (1/sec ²)	-0.39	-0.86	-1.168	-1.282
$N_{\dot{\beta}}$ (1/sec ²)	0.757	1.301	2.14	2.43
$N_{\dot{p}}$ (1/sec)	-0.124	-0.0346	-0.0204	-0.01715
$N_{\dot{r}}$ (1/sec)	-0.265	-0.257	-0.228	-0.25
$N_{\delta_a}^*$ (1/sec ²)	-0.0532	-0.01875	-0.0652	-0.0788
$N_{\delta_r}^*$ (1/sec ²)	-0.389	-0.864	-0.01164	-1.277

E. AILERON LATERAL TRANSFER FUNCTION FACTORS FOR THE DC-8

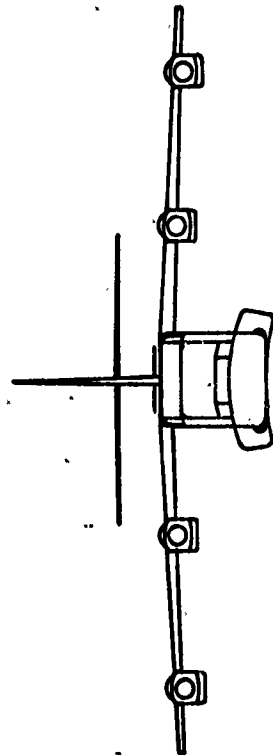
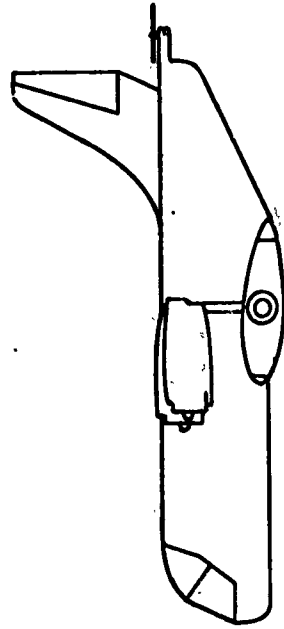
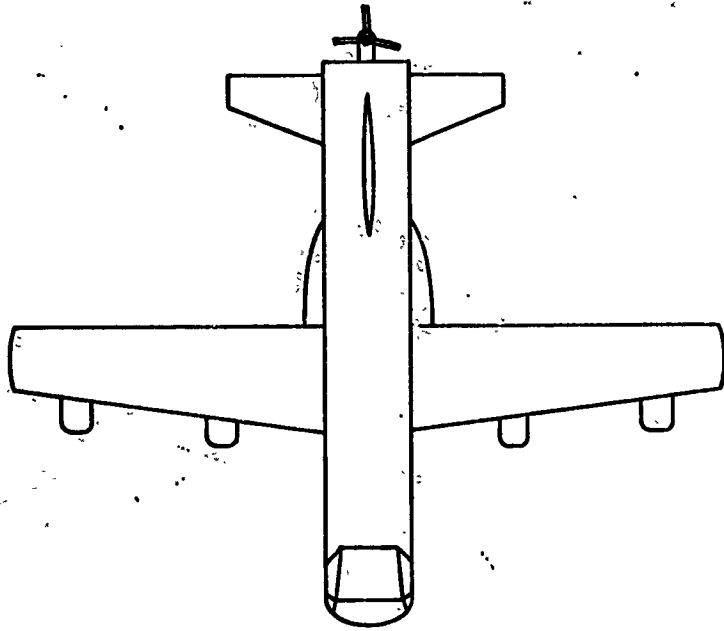
		FLIGHT CONDITION			
		8001	8002	8003	8004
Mach No., (-)		0.219	0.443	0.84	0.88
Altitude, h (ft)		0	15,000	33,000	33,000
c.g. (% \bar{c})		15	15	15	15
Weight, W (lb)		190,000	190,000	230,000	230,000
Δ_{lat}	$1/T_s$	-0.013	0.00649	0.00404	0.00447
	$1/T_R$	1.121	1.329	1.254	1.356
	ζ_d	0.1096	0.1061	0.0793	0.0855
	ω_d	0.996	1.197	1.495	1.589
$N_{\delta a}^p$	A_p	-0.726	-1.62	-2.11	-2.30
	$1/T_{p1}$	0	0	0	0
	ζ_p	0.223	0.1554	0.1072	0.1094
	ω_p	0.943	1.166	1.515	1.620
	dc gain	0	0	0	0
$\phi_{N_{\delta a}}$	A_ϕ	-0.726	-1.62	-2.11	-2.30
	ζ_ϕ	0.223	0.1554	0.1072	0.1094
	ω_ϕ	0.943	1.166	1.515	1.620
	dc gain	44.5	-177.9	-428	-395
$N_{\delta a}^r$	A_r	-0.0532	-0.01875	-0.0652	-0.0788
	$1/T_{r1}$	0.998	1.589	1.644	1.757
	ζ_r	-0.656	-0.727	-0.392	-0.345
	ω_r	1.242	2.23	1.323	1.269
	dc gain	5.66	-12.0	-16.57	-14.59
$N_{\delta a}^\beta$	A_β	0.0532	0.01875	0.0652	-0.0788
	$1/T_{\beta 1}$	-2.75	-7.9	-1.036	-0.704
	$1/T_{\beta 2}$	0.203	0.197	0.291	0.404
	$1/T_{\beta 3}$	—	—	—	—
	dc gain	2.05	-2.35	-1.733	-1.467
$N_{\delta a}^{ay}$ c.g.	A_{ay}	$-1.19 \cdot 10^{-7}$	-0.885	$-9.54 \cdot 10^{-7}$	-6.33
	$1/T_{ay1}$	-2.75	-7.9	-1.036	-0.704
	$1/T_{ay2}$	0.203	0.197	0.291	0.404
	$1/T_{ay3}$	—	—	—	—
	$1/T_{ay4}$	$1.21 \cdot 10^7$	—	$4.89 \cdot 10^6$	—
	dc gain	-55.6	111.1	123.9	117.9

F. RUDDER LATERAL TRANSFER FUNCTION FACTORS FOR THE DC-8

		FLIGHT CONDITION			
		8001	8002	8003	8004
Mach No., M (-)		0.219	0.443	0.84	0.88
Altitude, h (ft)		0	15,000	33,000	33,000
c.g. (% c)		15	15	15	15
Weight, W (lb)		190,000	190,000	230,000	230,000
Δ_{lat}	$1/T_s$	-0.013	0.00649	0.00404	0.00447
	$1/T_R$	1.121	1.329	1.254	1.356
	ζ_d	0.1096	0.1061	0.0793	0.0855
	ω_d	0.996	1.197	1.495	1.589
$N_{\delta_r}^p$	A_p	0.1813	0.392	0.545	0.612
	$1/T_{p1}$	0	0	0	0
	$1/T_{p2}$	1.028	1.85	2.43	2.57
	$1/T_{p3}$	-2.13	-2.56	-3.01	-3.15
	dc gain	0	0	0	0
$N_{\delta_r}^\phi$	A_ϕ	0.1813	0.392	0.545	0.612
	$1/T_{\phi 1}$	1.028	1.85	2.43	2.57
	$1/T_{\phi 2}$	-2.13	-2.56	-3.01	-3.15
	dc gain	27.5	-150.5	-353	-324
$N_{\delta_r}^r$	A_r	-0.389	-0.864	-1.165	-1.277
	$1/T_{r1}$	1.124	1.335	1.276	1.377
	ζ_r	-0.0743	-0.0451	-0.0619	-0.0475
	ω_r	0.339	0.330	0.323	0.323
	dc gain	3.46	-10.19	-13.68	-12.00
$N_{\delta_r}^\beta$	A_β	0.0238	0.0288	0.0222	0.0233
	$1/T_{\beta 1}$	-0.0559	-0.01475	-0.00726	-0.00637
	$1/T_{\beta 2}$	1.141	1.297	1.217	1.323
	$1/T_{\beta 3}$	16.47	30.2	52.6	55.0
	dc gain	1.725	-1.346	-0.912	-0.707
$N_{\delta_r}^{a_y}$ c.g.	A_{a_y}	5.79	13.48	18.33	20.1
	$1/T_{a_y 1}$	-0.819	-0.0347	-0.01883	-0.01746
	$1/T_{a_y 2}$	-0.1077	1.535	1.122	1.231
	$1/T_{a_y 3} (\zeta_{a_y})$	(0.994)	-1.157	-1.418	-1.494
	$1/T_{a_y 4} (\omega_{a_y})$	(1.078)	1.147	1.723	1.819
	dc gain	-41.0	77.0	83.5	76.9

G. LATERAL COUPLING NUMERATORS FOR THE DC-8

		FLIGHT CONDITION			
		8001	8002	8003	8004
Mach No., M (-)		0.219	0.443	0.84	0.88
Altitude, h (ft)		0	15,000	33,000	33,000
$\begin{matrix} p\beta \\ N_{\delta a \delta r} \end{matrix}$	$A_{p\beta}$	-0.01727	-0.0466	-0.0470	-0.0536
	$1/T_{p\beta 1}$	0	0	0	0
	$1/T_{p\beta 2}$	17.21	30.5	53.4	56.0
$\begin{matrix} r\beta \\ N_{\delta a \delta r} \end{matrix}$	$A_{r\beta}$	-0.00127	-0.00054	-0.00145	-0.001837
	$\zeta_{r\beta}$	-0.0672	-0.0656	0.0317	0.0507
	$\omega_{r\beta}$	5.52	13.39	8.2	7.79
$\begin{matrix} p/s\ r \\ N_{\delta a \delta r} \\ = N_{\delta a \delta r}^{\phi\ r} \end{matrix}$	$A_{\phi r}$	0.292	1.408	2.49	2.99
	$1/T_{\phi r}$	0.061	0.0567	0.0439	0.0464
$\begin{matrix} \beta a_y \\ N_{\delta a \delta r} \\ \text{c.g.} \end{matrix}$	$A_{\beta a_y}$	0.308	0.253	1.195	1.586
	$1/T_{\beta a_y 1}$	-2.75	-7.90	-1.036	-0.704
	$1/T_{\beta a_y 2}$	0.203	0.1967	0.291	0.404
	$1/T_{\beta a_y 3}$	—	—	—	—
$\begin{matrix} r a_y \\ N_{\delta a \delta r} \\ \text{c.g.} \end{matrix}$	$A_{r a_y}$	-0.308	-0.253	-1.195	-1.586
	$1/T_{r a_y 1}$	-1.532	-2.94	-1.281	-1.192
	$\zeta_{r a_y}$	0.359	0.317	0.593	0.645
	$\omega_{r a_y}$	1.1	1.86	1.519	1.536
$\begin{matrix} p a_y \\ N_{\delta a \delta r} \\ \text{c.g.} \end{matrix}$	$A_{p a_y}$	-4.21	-21.8	-38.7	-46.3
	$1/T_{p a_y 1}$	0	0	0	0
	$1/T_{p a_y 2}$	-0.871	-1.184	-1.413	-1.482
	$1/T_{p a_y 3}$	1.18	1.445	1.651	1.744
$\begin{matrix} \phi\beta \\ N_{\delta a \delta r} \end{matrix}$	$A_{\phi\beta}$	-0.01727	-0.0466	-0.0470	-0.0536
	$1/T_{\phi\beta}$	17.21	30.5	53.4	56.0
$\begin{matrix} \phi a_y \\ N_{\delta a \delta r} \\ \text{c.g.} \end{matrix}$	$A_{\phi a_y}$	-4.21	-21.8	-38.7	-46.3
	$1/T_{\phi a_y 1}$	-0.871	-1.184	-1.413	-1.482
	$1/T_{\phi a_y 2}$	1.18	1.445	1.651	1.744



XC-142

TABLE A-7

A. GEOMETRICAL AND INERTIAL PARAMETERS FOR THE XC-142

Note: Data are for body-fixed centerline axes

$$S = 534 \text{ ft}^2, \quad b = 67.5 \text{ ft}, \quad c = 8.07 \text{ ft}, \quad \gamma_0 = 0 \text{ deg}$$

	FLIGHT CONDITION		
	1420 HOVER	1421 60 KTS	1422 120 KTS
h (ft)	0	0	0
M (-)	0	0.0906	0.1812
a (ft/sec)	1,117	1,117	1,117
ρ (slugs/ft ³)	0.002378	0.002378	0.002378
V_{T_0} (ft/sec)	1.0	101.28	202.56
$\bar{q} = \rho V^2/2$ (lb/ft ²)	0	12.2	48.8
W (lb)	37,474	37,474	37,474
m (slugs)	1,163.8	1,163.8	1,163.8
I_x (slug-ft ²)	173,000	173,000	173,000
I_y (slug-ft ²)	122,000	122,000	122,000
I_z (slug-ft ²)	267,000	267,000	267,000
I_{xz} (slug-ft ²)	7,000	7,000	7,000
$x_{c.g./\bar{c}}$	0.20	0.20	0.20
i_w (deg)	90	14.5	1.25
θ_0 (deg)	0	0	0
U_0 (ft/sec)	1.0	101.28	202.56
W_0 (ft/sec)	0	0	0

B. LONGITUDINAL DIMENSIONAL DERIVATIVES FOR THE XC-142

Note: Data are for body-fixed centerline axes; thrust corrections are included.

	FLIGHT CONDITION		
	1420 HOVER	1421 60 KTS	1422 120 KTS
h (ft)	0	0	0
M (-)	0	0.0906	0.1812
X_u (1/sec)	-0.21	-0.196	-0.22
X_w (1/sec)	0	0.035	0.060
$^{\dagger}X_{\delta_e}$ [(ft/sec ²)/in.]	0	0.124	0.120
$^{\dagger}X_{\delta_T}$ [(ft/sec ²)/rad]	0	73	130.0
Z_u (1/sec)	0	-0.278	-0.15
Z_w (-)	0	0	0
$Z_{\dot{w}}$ (1/sec)	-0.065	-0.592	-0.85
$^{\dagger}Z_{\delta_e}$ [(ft/sec ²)/in.]	2.58	3.12	4.58
$^{\dagger}Z_{\delta_T}$ [(ft/sec ²)/rad]	-119.0	-130	-97
M_u (1/sec-ft)	0.0073	0.0045	0.01
$M_{\dot{w}}$ (1/ft)	-0.00127	-0.00127	-0.00127
M_w (1/sec-ft)	0.0003	-0.0002	-0.0095
M_q (1/sec)	-0.085	-0.486	-0.89
$^{\dagger}M_{\delta_e}$ [(1/sec ²)/in.]	0.765	0.87	1.195
$^{\dagger}M_{\delta_T}$ (1/sec ² -rad)	0.26	-3.71	-5.08

$^{\dagger}\delta_e$ —inches of scissors (horizontal tail and tail prop contributions included)

$^{\dagger}\delta_e$ —radius of main prop blade angle (includes static governor effects)

C. ELEVATOR LONGITUDINAL TRANSFER FUNCTION FACTORS FOR THE XC-142

δ_e inches of scissors (horizontal tail and tail prop contributions included)

		FLIGHT CONDITION		
		1420 HOVER	1421 60 KTS	1422 120 KTS
Mach No., M (-)		0	0.0906	0.1812
Altitude, h (ft)		0	0	0
c.g. (% \bar{c})		20	20	20
Weight, W (lb)		37,474	37,474	37,474
Δ_{long}	$\zeta_{sp} (1/T_{sp1})$	-0.373	-0.109	0.624
	$\omega_{sp} (1/T_{sp2})$	0.570	0.411	1.60
	$\zeta_p (1/T_{p1})$	(0.0650)	(0.552)	0.306
	$\omega_p (1/T_{p2})$	(0.722)	(.940)	0.352
$N_{\delta_e}^{\theta}$	A_{θ}	0.762	0.866	1.19
	$1/T_{\theta1}$	0.0663	0.225	0.241
	$1/T_{\theta2}$	0.210	0.566	0.798
	dc gain	0.694	1.26	0.715
$N_{\delta_e}^u$	A_u	-24.5	0.124	0.120
	$1/T_{u1}$	0.0663	0.667	1.32
	$1/T_{u2}$	—	-13.5	-12.6
	$1/T_{u3}$	—	14.9	15.6
	dc gain	-106	-189	-98.0
$N_{\delta_e}^w$	A_w	2.58	3.12	4.58
	$1/T_{w1}$	0.834	28.7	53.7
	ζ_w	-0.228	0.319	0.642
	ω_w	0.531	0.303	0.172
	dc gain	39.7	94.1	22.7
$N_{\delta_e}^h$	A_h	-2.58	-3.12	-4.58
	$1/T_{h1}$	0.731	0.0562	0.198
	$1/T_{h2} (\zeta_h)$	(-0.386)	-3.72	-6.00
	$1/T_{h3} (\omega_h)$	(0.562)	4.47	7.16
	dc gain	-39.0	-33.3	122
$N_{\delta_e}^{a_z}$ $x_a = 18$ ft pilot	A_{a_z}	-11.1	-12.5	-16.8
	$1/T_{a_z1}$	0	0	0
	$1/T_{a_z2}$	-0.293	0.0547	0.198
	ζ_{a_z}	0.660	0.178	0.110
	ω_{a_z}	0.428	2.07	3.42
	dc gain	0	0	0

D. THROTTLE LONGITUDINAL TRANSFER FUNCTION FACTORS FOR THE XC-142

δ_T —radians of main prop blade angle includes static governor effects

		FLIGHT CONDITION		
		1420 HOVER	1421 60 KTS	1422 120 KTS
Mach No., M (-)		0	0.0906	0.1812
Altitude, h (ft)		0	0	0
c.g. (% \bar{c})		20	20	20
Weight, W (lb)		37,474	37,474	37,474
Δ_{long}	ζ_{sp}	-0.373	-0.109	0.624
	ω_{sp}	0.570	0.411	1.60
	$\zeta_p (1/T_{p1})$	(0.0650)	(0.552)	0.306
	$\omega_p (1/T_{p2})$	(0.722)	(0.940)	0.352
$N_{\delta_T}^{\theta}$	A_{θ}	0.411	-3.54	-4.96
	$1/T_{\theta 1}$	-0.0457	0.1409	-0.1173
	$1/T_{\theta 2}$	0.210	0.567	0.755
	dc gain	-0.258	-3.24	1.374
$N_{\delta_T}^u$	A_u	-13.24	73.0	130
	$1/T_{u1}$	-0.0457	0.708	0.289
	ζ_u	—	0.1876	0.487
	ω_u	—	1.163	1.707
	dc gain	39.62	798	342
$N_{\delta_T}^W$	A_W	-119	-130	-97
	$1/T_{W1}$	0.721	3.63	11.92
	ζ_W	-0.375	0.1541	-0.0104
	ω_W	0.571	0.332	0.220
	dc gain	-1,831	-594	-175
$N_{\delta_T}^h$	A_h	119	130	97
	$1/T_{h1}$	0.722	-0.725	-1.739
	$1/T_{h2} (\zeta_h)$	(-0.373)	-0.1355	-0.242
	$1/T_{h3} (\omega_h)$	(0.570)	1.827	3.55
	dc gain	1,831	267	453
$N_{\delta_T}^{a_z}$ $x_a = 18$ ft Pilot	A_{a_z}	-126.4	-66.2	-7.78
	$1/T_{a_z1}$	0	0	0
	$1/T_{a_z2}$	0.707	-1.133	-4.60
	$1/T_{a_z3} (\zeta_{a_z})$	(-0.375)	-0.1258	-0.237
	$1/T_{a_z4} (\omega_{a_z})$	(0.555)	2.47	17.07
	dc gain	0	0	0

E. LATERAL DIMENSIONAL DERIVATIVES FOR THE XC-142

Note: Data are for body-fixed centerline axes

	FLIGHT CONDITION		
	1420 HOVER	1421 60 KTS	1422 120 KTS
h (ft)	0	0	0
M (-)	0	0.0906	0.1812
Y_v (1/sec)	-0.015	-0.0945	-0.175
Y_β [(ft/sec ²)/rad]	-0.015	-9.58	-35.5
$^{\dagger}Y_{\delta_a}$ [(ft/sec ²)/in.]	—	—	—
$^{\dagger}Y_{\delta_a}^*$ [(1/sec)/in.]	—	—	—
$^{\dagger}Y_{\delta_r}$ [(ft/sec ²)/in.]	0	0.248	0.94
$^{\dagger}Y_{\delta_r}^*$ [(1/sec)/in.]	0	0.00245	0.00464
L_β (1/sec ²)	-0.0006	-0.724	-1.93
L_p (1/sec)	-0.235	-0.533	-0.85
L_r (1/sec)	-0.025	0.395	0.582
$^{\dagger}L_{\delta_a}$ [(1/sec ²)/in.]	-0.285	-0.1663	-0.192
$^{\dagger}L_{\delta_r}$ [(1/sec ²)/in.]	0.0706	-0.081	0.0966
L_β' (1/sec ²)	-0.000616	-0.715	-1.91
L_p' (1/sec)	-0.235	-0.539	-0.855
L_r' (1/sec)	-0.0335	0.382	0.559
$^{\dagger}L_{\delta_a}'$ [(1/sec ²)/in.]	-0.285	-0.167	-0.193
$^{\dagger}L_{\delta_r}'$ [(1/sec ²)/in.]	0.0622	-0.0871	0.0913
N_β (1/sec ²)	-0.00037	0.237	0.630
N_p (1/sec)	0	-0.123	-0.094
N_r (1/sec)	-0.21	-0.342	-0.58
$^{\dagger}N_{\delta_a}$ [(1/sec ²)/in.]	0	-0.0085	-0.0215
$^{\dagger}N_{\delta_r}$ [(1/sec ²)/in.]	-0.21	-0.148	-0.134
N_β' (1/sec ²)	-0.000386	0.218	0.580
N_p' (1/sec)	-0.00617	-0.137	-0.116
N_r' (1/sec)	-0.211	-0.332	-0.565
$^{\dagger}N_{\delta_a}'$ [(1/sec ²)/in.]	-0.00748	-0.0129	-0.0266
$^{\dagger}N_{\delta_r}'$ [(1/sec ²)/in.]	-0.208	-0.150	-0.132

$^{\dagger}\delta_a$ —inches of lateral stick (includes aileron and differential main prop blade angle) positive δ_a gives negative \dot{p}

$^{\dagger}\delta_r$ —inches of pedal (includes rudder, aileron, and differential main prop blade angle) positive δ_r gives negative \dot{r}

F. AILERON LATERAL TRANSFER FUNCTION FACTORS FOR THE XC-142

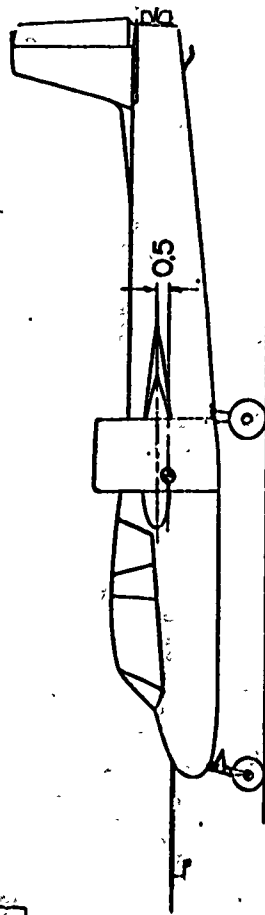
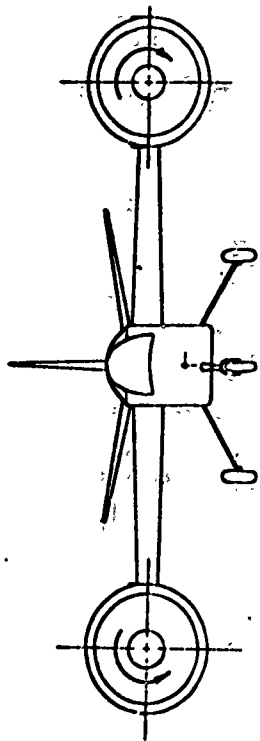
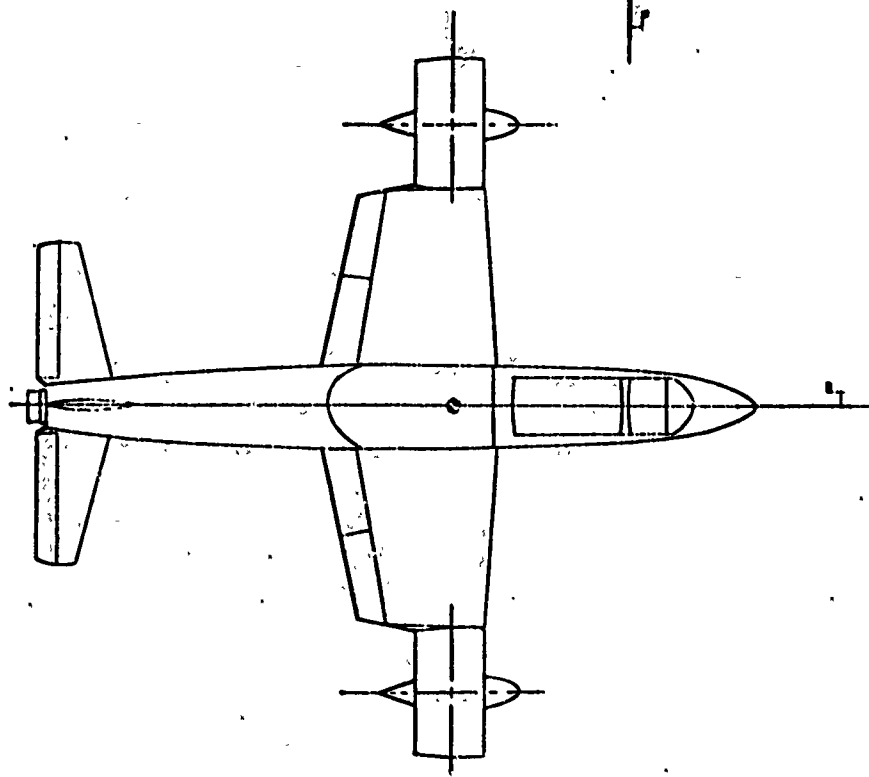
		FLIGHT CONDITION		
		1420 HOVER	1421 60 KTS	1422 120 KTS
Mach No., M (-)		0	0.0906	0.1812
Altitude, h (ft)		0	0	0
c.g. (% c)		20	20	20
Weight, W (lb)		37,474	37,474	37,474
Δ_{lat}	$1/T_s$	0.1911	0.1185	0.1236
	$1/T_R$	0.389	0.886	1.161
	ζ_d	-0.265	-0.0292	0.1699
	ω_d	0.225	0.683	0.914
$N_{\delta_a}^p$	A_p	-0.285	-0.1668	-0.1927
	$1/T_{p1}$	0	0	0
	$\zeta_p (1/T_{p2})$	(0.0131)	0.411	0.418
	$\omega_p (1/T_{p3})$	(0.212)	0.555	0.977
	dc gain	0	0	0
$N_{\delta_a}^\phi$	A_ϕ	-0.285	-0.1668	-0.1927
	$\zeta_\phi (1/T_{\phi1})$	(0.0131)	0.411	0.418
	$\omega_\phi (1/T_{\phi2})$	(0.212)	0.555	0.977
	dc gain	-0.211	-1.047	-1.536
$N_{\delta_a}^r$	A_r	-0.00748	-0.0129	-0.0266
	$1/T_{r1}$	-0.764	0.793	1.056
	ζ_r	0.505	-0.813	-0.454
	ω_r	0.771	1.19	0.960
	dc gain	0.903	-0.296	-0.215
$N_{\delta_a}^\beta$	A_β	0.00748	0.0129	0.0266
	$1/T_{\beta1}$	-1.228	-5.62	-1.605
	$1/T_{\beta2}$	0.210	0.265	0.462
	$1/T_{\beta3}$	—	—	—
	dc gain	-513	-0.391	-0.1643
$N_{\delta_a}^{ay}$ $x_a = 18$ ft $z_a = 1.0$ ft Pilot	A_{ay}	0.1507	-0.065	-0.285
	$1/T_{ay1}$	0.1449	-5.36	-1.152
	$1/T_{ay2}$	1.207	0.389	0.603
	ζ_{ay}	-0.448	-0.1224	0.0817
	ω_{ay}	1.048	1.165	1.876
	dc gain	7.69	3.74	5.82

G. RUDDER LATERAL TRANSFER FUNCTION FACTORS FOR THE XC-142

		1420 HOVER	1421 60 KTS	1422 120 KTS
Mach No., M (-)		0	0.0906	0.1812
Altitude, h (ft)		0	0	0
c.g. (% \bar{c})		20	20	20
Weight, W (lb)		37,474	37,474	37,474
Δ_{lat}	$1/T_s$	0.1911	0.1185	0.1236
	$1/T_R$	0.389	0.886	1.161
	ζ_d	-0.265	-0.0292	0.1699
	ω_d	0.225	0.683	0.914
$N_{\delta_r}^p$	A_p	0.0622	-0.087	0.0913
	$1/T_{p1}$	0	0	0
	$\zeta_p (1/T_{p2})$	(0.00725)	0.444	(-1.586)
	$\omega_p (1/T_{p3})$	(0.331)	1.245	(1.422)
	dc gain	0	0	0
$N_{\delta_r}^\phi$	A_ϕ	0.0622	-0.0871	0.0913
	$\zeta_\phi (1/T_{\phi1})$	(0.00725)	0.444	(-1.586)
	$\omega_\phi (1/T_{\phi2})$	(0.331)	1.245	(1.422)
	dc gain	0.0396	-2.76	-1.717
$N_{\delta_r}^r$	A_r	-0.208	-0.1504	-0.1318
	$1/T_{r1}$	0.394	0.863	1.15
	ζ_r	-0.291	-0.281	-0.0663
	ω_r	0.244	0.557	0.456
	dc gain	-1.303	-0.821	-0.263
$N_{\delta_r}^\beta$	A_β	0.208	0.00245	0.00464
	$1/T_{\beta1}$	0.326	-0.308	-0.0244
	$1/T_{\beta2}$	9.52	0.587	1.076
	$1/T_{\beta3}$	—	62.0	28.8
	dc gain	171.9	-0.560	-0.0293
$N_{\delta_r}^{a_y}$ $x_a = 18$ ft $z_a = 1.0$ ft Pilot	A_{a_y}	-3.81	-2.37	-1.524
	$1/T_{a_y1}$	0.0796	-0.204	-0.0506
	$1/T_{a_y2}$	0.399	0.765	1.110
	ζ_{a_y}	-0.397	-0.0377	-0.0746
	ω_{a_y}	0.283	0.861	1.664
	dc gain	-2.58	5.61	1.980

H. LATERAL COUPLING NUMERATORS FOR THE XC-142

		FLIGHT CONDITION		
		1420 HOVER	1421 60 KTS	1422 120 KTS
Mach No., M (-)		0	0.0906	0.1812
Altitude, h (ft)		0	0	0
$\begin{matrix} p \beta \\ N_{\delta_a \delta_r} \end{matrix}$	$A_{p\beta}$	-0.0599	-0.00041	-0.000894
	$1/T_{p\beta 1}$	0	0	0
	$1/T_{p\beta 2}$	—	59.0	31.8
$\begin{matrix} r \beta \\ N_{\delta_a \delta_r} \end{matrix}$	$A_{r\beta}$	-1.929	-0.000032	-0.000123
	$\zeta_{r\beta}$	—	-0.0398	0.000833
	$\omega_{r\beta}$	—	15.55	5.99
$\begin{matrix} p/s r \\ N_{\delta_a \delta_r} \\ = N_{\phi_a \delta_r} \end{matrix}$	$A_{\phi r}$	0.0599	0.0240	0.0278
	$1/T_{\phi r}$	0.015	0.0898	0.1479
$\begin{matrix} N_{\delta_a \delta_r}^{p a y} \\ x_a = 18 \text{ ft} \\ z_a = 1.0 \text{ ft} \\ \text{Pilot} \end{matrix}$	$A_{p a y}$	-0.0599	0.000159	0.00132
	$1/T_{p a y 1}$	0	-5.76	-0.37
	$1/T_{p a y 2}(\zeta_{p a y})$	-580	-0.0399	(-0.1797)
	$1/T_{p a y 3}(\omega_{p a y})$	—	-130.3	(6.14)
$\begin{matrix} N_{\delta_a \delta_r}^{r a y} \\ x_a = 18 \text{ ft} \\ z_a = 1.0 \text{ ft} \\ \text{Pilot} \end{matrix}$	$A_{r a y}$	0.0599	0.0208	0.00286
	$1/T_{r a y 1}$	0.790	1.599	4.10
	$\zeta_{r a y}$	-0.495	-0.452	-0.409
	$\omega_{r a y}$	0.782	1.445	3.36
$\begin{matrix} N_{\delta_a \delta_r}^{p a y} \\ x_a = 18 \text{ ft} \\ z_a = 1.0 \text{ ft} \\ \text{Pilot} \end{matrix}$	$A_{p a y}$	1.078	0.390	0.320
	$1/T_{p a y 1}$	0	0	0
	$\zeta_{p a y}$	0.26	0.0408	-0.041
	$\omega_{p a y}$	0.0289	0.748	1.615
$\begin{matrix} \phi \beta \\ N_{\delta_a \delta_r} \end{matrix}$	$A_{\phi \beta}$	-0.0599	-0.000408	-0.000894
	$1/T_{\phi \beta}$	—	59.0	31.8
$\begin{matrix} N_{\delta_a \delta_r}^{\phi a y} \\ x_a = 18 \text{ ft} \\ z_a = 1.0 \text{ ft} \\ \text{Pilot} \end{matrix}$	$A_{\phi a y}$	1.078	0.390	0.32
	$\zeta_{\phi a y}$	0.26	0.0408	-0.041
	$\omega_{\phi a y}$	0.0289	0.748	1.615



VZ-4

TABLE A-9

A. LONGITUDINAL DERIVATIVES FOR THE DOAK VZ-4

U_0 , ft/sec	0	58.8	73.0	126.6
X_u	-0.137	-0.130	-0.140	-0.210
X_w	0	-0.084	0.120	0.015
X_q	0	0	0	0
X_{δ_T}	0	0.342	0.442	0.914
X_{δ_e}	0	0	0	0
Z_u	0	-0.248	-0.285	-0.345
Z_w	-0.137	-0.526	-0.39	-0.718
Z_q	0	0	0	0
Z_{δ_T}	1.0	-0.940	-0.906	-0.406
Z_{δ_e}	1.08	1.00*	1.00*	1.00*
M_u	0.0136	0.0128	0.01205	0.0107
M_w	0	-0.032	-0.046	-0.082
M_q	0	0	0	0
M_{δ_T}	-0.0452	-0.858	-1.065	-1.839
M_{δ_e}	0	0	0	0
M_{δ_e}	1.0*	0.775	0.775	0.775
W , lb	3,100	3,100	3,100	3,100
I_y , slug-ft ²	1,790	1,790	1,790	1,790

*Normalized. (Note $M_{\delta_e}/Z_{\delta_e}$ changes with forward speed due to shift from jet to tail control. Values quoted are approximate.)

B. LONGITUDINAL EXACT AND APPROXIMATE FACTORS FOR THE DOAK VZ-4

		SPEED, U_0 (ft/sec)			
		0	58.8	73.0	126.6
DENOMINATOR	ω_{sp}	$1/T_{sp1} = 0.137$	1.40 (1.49)	1.90 (1.94)	3.404 (3.24)
	ζ_{sp}	$1/T_{sp2} = 0.824$	0.459 (0.464)	0.375 (0.374)	0.374 (0.406)
	ω_p	0.731	0.492 (0.457)	0.399 (0.395)	0.3161 (0.315)
	ζ_p	-0.439	0.234 (0.378)	0.216 (0.275)	0.346 (0.375)
STICK	$1/T_{\theta 1}$	0.137	0.0757	$\omega = 0.287$	0.224
	$1/T_{\theta 2}$	0.137	0.539	$\zeta = 0.820$	0.598
	$1/T_{u1}$	0.137 (0.137)	343.1 (325.0)	-150.8 (-151.5)	-1,564.0 (-1,570.0)
	$1/T_{u2}$	—	0.420 (0.441)	0.456 (0.434)	0.6510 (0.650)
	$1/T_v$	$= 1/T_{sp2}$	46.4 (45.8)	57.6 (56.5)	100.0 (97.5)
	ω_v	$= \omega_p$	0.377 (0.360)	0.361 (0.370)	0.299 (0.300)
	ζ_v	$= \zeta_p$	0.168 (0.181)	0.191 (0.189)	0.349 (0.350)
	$1/T_{h1}$	[at $U_0 = 0, v = -h]$	-4.095 (-4.71)	-3.66 (-4.32)	-6.81 (-7.71)
	$1/T_{h2}$		-0.218 (-0.215)	-0.1548 (-0.156)	0.0700 (0.060)
	$1/T_{h3}$		5.302 (4.71)	5.017 (4.32)	8.79 (7.71)
THROTTLE	$1/T_v$	[at $U_0 = 0, v = -h]$	1.36 (1.35)	1.58 (1.62)	3.24 (3.37)
	ω_v		0.550 (0.549)	0.495 (0.505)	0.326 (0.319)
	ζ_v		-0.258 (-0.239)	-0.241 (-0.276)	-0.634 (-0.648)
	$1/T_{\theta 1}$	—	0.288 (0.267)	0.264 (0.291)	0.0924 (0.930)
	$1/T_{\theta 2}$	—	—	—	—
	$1/T_u$	—	-0.688 (-0.712)	-0.645 (-0.878)	-0.0982 (-0.0914)
	ω_u	—	2.029 (1.98)	2.17 (1.84)	3.46 (3.60)
	ζ_u	—	0.5676 (0.594)	0.427 (0.567)	0.383 (0.360)
	$1/T_h$	$= 1/T_{sp2}$	0.580	0.425	1.25
	ω_h	$= \omega_p$	1.335	1.81	3.20
	ζ_h	$= \zeta_p$	0.104	0.254	0.247

() denotes approximate factors

C. LATERAL DERIVATIVES FOR THE DOAK VZ-4

(Primed derivatives shown in parentheses)

U _o , ft/sec	1.0	58.8	73.0	126.6
Y _v	-0.14	-0.2895	-0.2945	-0.333
Y _p	0	0	0	0
Y _r	0	0	0	0
Y _{8a}	0	-24.9	-26.8	-30.04
Y _{8r}	1.017	1.85	2.29	5.31
L _v	-0.0122 (-0.0123)	-0.0224 (-0.0236)	-0.0216 (-0.0241)	-0.0136 (-0.0158)
L _p	-0.271 (-0.273)	-0.455 (-0.467)	-0.497 (-0.508)	-0.67 (-0.677)
L _r	0 (0.0825)	1.75 (1.848)	0.911 (1.01)	0.659 (0.807)
L _{8a}	0.69 (0.696)	0.5013 (0.5055)	0.5208 (0.525)	0.972 (0.979)
L _{8r}	-0.185 (-0.119)	-0.141 (-0.0442)	-0.13 (-0.0102)	-0.15 (0.126)
N _v	0 (0.000885)	0.0081 (0.0098)	0.01 (0.0121)	0.0174 (0.0184)
N _p	0 (0.0197)	0.0605 (0.0940)	0.0535 (0.0900)	0.0109 (0.0596)
N _r	-0.656 (-0.662)	-0.655 (-0.788)	-0.723 (-0.796)	-1.13 (-1.19)
N _{8a}	0 (-0.0500)	0.003 (-0.0333)	0.0041 (-0.0336)	0.0133 (-0.0571)
N _{8r}	-0.539 (-0.531)	-0.78 (-0.777)	-0.962 (-0.961)	-2.204 (-2.213)
I _{xz} /I _x	-0.1246	-0.1246	-0.1246	-0.1246
I _{xz} /I _z	-0.07188	-0.07188	-0.07188	-0.07188
(W = 3,100 lb ; I _x = 1,990 slug-ft ² ; I _z = 3,450 slug-ft ² ; α _W = 12°)				

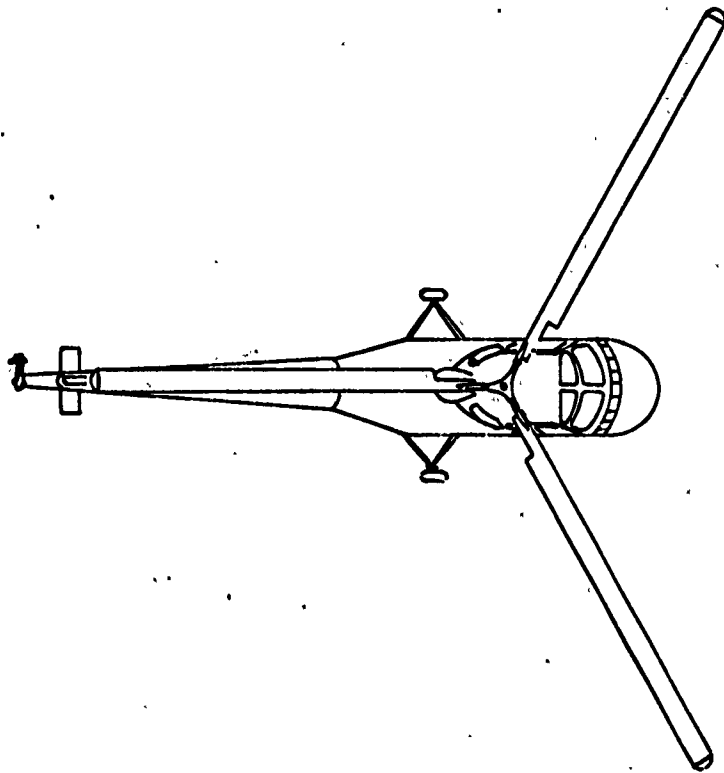
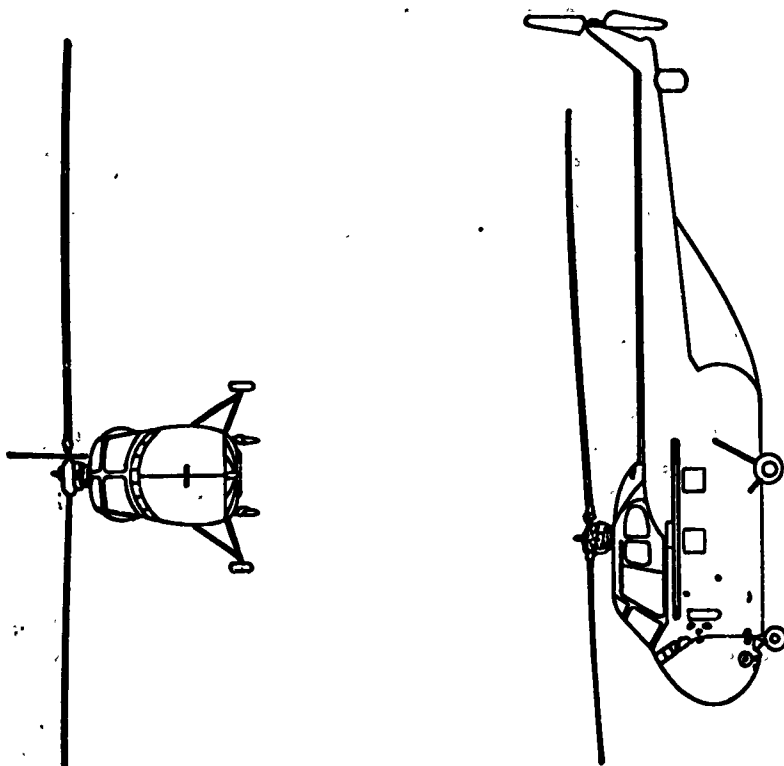
D. LATERAL EXACT AND APPROXIMATE FACTORS FOR THE DOAK VZ-4

		SPEED, U_0 (ft/sec)			
		1.0	56.8	73.0	126.0
DENOMINATOR	ω_d	0.669 (0.704)	0.866 (0.758)	0.914 (0.92)	1.59 (1.54)
	ζ_d	-0.347 (-0.355)	0.1655 (0.035)	0.205 (0.21)	0.421 (0.436)
	$1/T_R$	0.888 (0.914)	1.242 (1.477)	0.957 (1.023)	0.796 (0.804)
	$1/T_S$	0.653 (0.662)	0.0159 (0.0141)	0.265 (0.190)	0.0620 (0.0583)
AILERONS/DIFFERENTIAL THRUST	$1/T_{\phi 1}$	0.14 (0.14)	0.407 (0.464)	$\omega_{\phi} = 1.13 (1/T_{\phi 1} = 1.269)$	$\omega_{\phi} = 1.65 (1.70)$
	$1/T_{\phi 2}$	0.6564 (0.661)	1.712 (1.764)	$\zeta_{\phi} = 0.968 (1/T_{\phi 2} = 1.161)$	$\zeta_{\phi} = 0.595 (0.595)$
	$1/T_{r1}$	0 (0)	-0.646 (-0.671)	-0.606 (-0.614)	-0.7188 (-0.70)
	$1/T_{r2}$	0.140 (0.14)	0.382 (0.979)	1.02 (0.886)	1.51 (1.42)
RUDDER/TAIL JET	$1/T_{r3}$	0 (0)	6.329 (7.32)	8.24 (9.25)	9.01 (9.85)
	$1/T_{v1}$	0.657	-0.611	-0.577	-0.754
	$1/T_{v2}$	447.0	0.595	0.846	1.35
	$1/T_{v3}$		1.192	0.944	0.5911
	$1/T_{\phi 1}$	0.267 (0.368)*	1.03 (1.054)	1.90 (1.98)	2.39 (2.71)
	$1/T_{\phi 2}$	1.008 (0.775)*	33.5 (33.0)	99.5 (94.0)	-15.73 (-14.2)
	$1/T_{r1}$	0.886 (0.910)	1.17 (1.185)	1.188 (1.191)	1.15 (1.187)
	ω_r	0.674 (0.699)	0.802 (0.804)	0.793 (0.792)	0.642 (0.661)
	ζ_r	-0.348 (-0.352)	-0.274 (-0.303)	-0.259 (-0.252)	-0.147 (-0.1322)
	$1/T_{v1}$	-1.75	-0.793 (0.79)	-0.452 (-0.447)	-0.205 (-0.289)
	$1/T_{v2}$	0.994	1.27 (1.25)	0.968 (0.954)	0.896 (-0.979)
	$1/T_{v3}$	2.22	25.47 (25.96)	31.43 (31.9)	53.93 (53.97)

*Condition of validity not satisfied

() denotes approximate factors

H-19



A-43

TABLE A-8

A. GEOMETRICAL AND INERTIAL PARAMETERS FOR THE H-19

Note: Data are for body-fixed stability axes

	FLIGHT CONDITION			
	1901	1902	1903	1904
h (ft)	0	0	0	0
M (-)	0	0.0452	0.0643	0.104
a (ft/sec)	1,117	1,117	1,117	1,117
ρ (slugs/ft ³)	0.002378	0.002378	0.002378	0.002378
V_{T_0} (ft/sec)	1	50.4	71.8	116.4
$\bar{q} = \rho V^2/2$ (lb/ft ²)	0.00119	3.02	6.12	16.1
W (lb)	6,400	7,000	7,000	7,000
m (slugs)	198	217	217	217
I_x (slug-ft ²)	2,118	1,755	1,755	1,755
I_y (slug-ft ²)	9,640	9,430	9,430	9,430
I_z (slug-ft ²)	7,840	7,840	7,840	7,840
I_{xz} (slug-ft ²)	0	0	0	0
γ_0 (deg)	0	0	0	0

B. LONGITUDINAL DIMENSIONAL DERIVATIVES FOR THE H-19

Note: Data are for body-fixed stability axes

	FLIGHT CONDITION			
	1901	1902	1903	1904
h (ft)	0	0	0	0
V_{T_0} (ft/sec)	0	50.4	71.8	116.4
X_u (1/sec)	-0.0284	-0.0394	-0.0438	-0.0525
X_w (1/sec)	0	-0.00151	0.00513	0.0207
X_{δ_e} [(ft/sec ²)/rad]	32.2	33.0	32.0	30.6
X_{δ_T} [(ft/sec ²)/]	0	-4.02	-3.04	-0.88
Z_u (1/sec)	0	-0.141	-0.0638	0.0151
Z_w (-)	—	—	—	—
$Z_{\dot{w}}$ (1/sec)	-0.69	-0.79	-0.80	-0.81
Z_{δ_e} [(ft/sec ²)/rad]	0	39.4	56.6	92.0
Z_{δ_T} [(ft/sec ²)/]	-358	-284	-291	-304
M_u (1/sec-ft)	0.00609	0.00805	0.00654	0.00612
M_w (1/ft)	0	0	0	0
$M_{\dot{w}}$ (1/sec-ft)	0	-0.0011	-0.00171	-0.00231
M_q (1/sec)	-0.610	-0.944	-0.984	-1.004
M_{δ_e} (1/sec ²)	-6.65	-7.47	-7.35	-7.10
M_{δ_T} (1/sec ²)	0	1.26	0.902	0.425

C. ELEVATOR LONGITUDINAL TRANSFER FUNCTION FACTORS FOR THE H-19

		FLIGHT CONDITION			
		1901	1902	1903	1904
Altitude, h (ft)		0	0	0	0
V_{T_0} (ft/sec)		0	50.4	71.8	116.4
Weight, W (lb)		6,400	7,000	7,000	7,000
Δ_{long}	$\zeta_{sp} (1/T_{sp1})$	(0.69)	0.995	0.996	0.908
	$\omega_{sp} (1/T_{sp2})$	(0.874)	0.967	0.992	1.05
	ζ_p	-0.250	-0.159	-0.106	-0.0433
	ω_p	0.473	0.473	0.418	0.380
$N_{\delta e}^{\theta}$	A_{θ}	-6.65	-7.47	-7.35	-7.10
	$1/T_{\theta 1}$	-0.00109	0.00305	0.0153	0.0249
	$1/T_{\theta 2}$	0.69	0.797	0.813	0.843
$N_{\delta e}^u$	A_u	32.2	33.0	32.0	30.6
	$1/T_{u 1}$	0.69	0.788	0.809	0.874
	ζ_u	0.118	0.174	0.180	0.187
	ω_u	2.58	2.71	2.74	2.68
$N_{\delta e}^w$	A_w		39.4	56.6	92.0
	$1/T_{w 1}$		-8.71	-8.35	-7.94
	$\zeta_w (1/T_{w 2})$		0.0393	0.0922	(0.181)
	$\omega_w (1/T_{w 3})$		0.263	0.0955	(-0.163)
$N_{\delta e}^h$	A_h		-39.4	-56.6	-92.0
	$1/T_{h 1}$		-0.0761	0.00522	0.0560
	ζ_h		0.171	0.179	0.183
	ω_h		2.76	2.75	2.75
$N_{\delta e}^{a_z}$ c.g.	A_{a_z}		39.4	56.6	92.0
	$1/T_{a_z 1}$		0	0	0
	$1/T_{a_z 2}$		-0.0761	0.00522	0.0560
	ζ_{a_z}		0.171	0.179	0.183
	ω_{a_z}		2.76	2.75	2.75

D. THROTTLE LONGITUDINAL TRANSFER FUNCTION FACTORS FOR THE H-19

		FLIGHT CONDITION			
		1901	1902	1903	1904
Altitude, h (ft)		0	0	0	0
V_{T_0} (ft/sec)		0	50.4	71.8	116.4
Weight, W (lb)		6,400	7,000	7,000	7,000
Δ_{long}	$\zeta_{sp} (1/T_{sp1})$	(0.69)	0.995	0.996	0.908
	$\omega_{sp} (1/T_{sp2})$	(0.874)	0.967	0.992	1.05
	ζ_p	-0.250	-0.159	-0.106	-0.0433
	ω_p	0.473	0.473	0.418	0.380
$N_{\delta_T}^\theta$	A_θ		1.26	0.902	0.425
	$1/T_{\theta 1}$		0.0220	0.0227	0.0113
	$1/T_{\theta 2}$		1.03	1.35	2.49
$N_{\delta_T}^u$	A_u		-4.02	-3.04	-0.88
	$1/T_{u1}$		1.03	1.35	6.35
	ζ_u		0.094	0.149	0.533
	ω_u		3.19	3.09	2.45
$N_{\delta_T}^w$	A_w		-284	-291	-304
	$1/T_{w1}$		0.976	0.979	1.03
	ζ_w		-0.22	-0.191	-0.160
	ω_w		0.495	0.456	0.437
$N_{\delta_T}^h$	A_h		284	291	304
	$1/T_{h1}$		0.966	0.905	0.805
	ζ_h		0.503	0.483	0.501
	ω_h		0.0152	0.127	0.251
$N_{\delta_T}^{a_z}$ c.g.	A_{a_z}		-284	-291	-304
	$1/T_{a_z1}$		0	0	0
	$1/T_{a_z2}$		0.966	0.905	0.805
	ζ_{a_z}		0.503	0.483	0.501
	ω_{a_z}		0.0152	0.127	0.251

E. LATERAL DIMENSIONAL DERIVATIVES FOR THE H-19

Note: Data are for body-fixed stability axes

	FLIGHT CONDITION			
	1901	1902	1903	1904
h (ft)	0	0	0	0
V_{T_0} (ft/sec)	0	50.4	71.8	116.4
Y_V (1/sec)	-0.0731	-0.096	-0.1045	-0.122
Y_β [(ft/sec ²)/rad]	-0.0731	-4.85	-7.51	-14.2
Y_{δ_a} [(ft/sec ²)/rad]	32.2	21.3	24.8	27.9
$Y_{\delta_a}^*$ [(1/sec)/rad]	32.2	0.423	0.346	0.239
Y_{δ_r} [(ft/sec ²)/rad]	17.3	15.8	15.8	16.7
$Y_{\delta_r}^*$ [(1/sec)/rad]	17.3	0.314	0.220	0.143
L_β (1/sec ²)	-0.052	-3.65	-5.19	-8.43
L_p' (1/sec)	-3.18	-4.97	-5.01	-4.81
L_r' (1/sec)	0.804	1.00	1.00	1.00
L_{δ_a}' (1/sec ²)	29.2	31.7	34.7	36.8
L_{δ_r}' (1/sec ²)	9.78	12.3	12.3	13.0
N_β' (1/sec ²)	0.0352	1.71	2.42	3.79
N_p' (1/sec)	0.22	0.338	0.276	0.201
N_r' (1/sec)	-1.1	-1.1	-1.1	-1.1
N_{δ_a}' (1/sec ²)	0	0	0	0
N_{δ_r}' (1/sec ²)	-13.53	-13.80	-13.9	-14.4

F. AILERON LATERAL TRANSFER FUNCTION FACTORS FOR THE H-19

		FLIGHT CONDITION			
		1901	1902	1903	1904
Altitude, h (ft)		0	0	0	0
V_{T_0} (ft/sec)		0	50.4	71.8	116.4
Weight, W (lb)		6,400	7,000	7,000	7,000
Δ_{lat}	$1/T_s$	0.732	0.162	0.116	0.0821
	$1/T_R$	3.43	5.09	5.10	4.87
	ζ_d	0.155	0.344	0.317	0.276
	ω_d	0.609	1.33	1.58	1.96
$N_{\delta_a}^p$	A_p	29.2	31.7	34.7	36.8
	$1/T_{p1}$	0	0	0	0
	$\zeta_p (1/T_{p2})$	(0.081)	0.429	0.364	0.296
	$\omega_p (1/T_{p3})$	(1.04)	1.33	1.58	1.97
$N_{\delta_a}^\phi$	A_ϕ	29.2	31.7	34.7	36.8
	$\zeta_\phi (1/T_{\phi1})$	(0.081)	0.429	0.364	0.296
	$\omega_\phi (1/T_{\phi2})$	(1.04)	1.33	1.58	1.97
$N_{\delta_a}^r$	A_r	7.55	11.4	10.4	16.5
	$1/T_{r1}$	—	—	—	—
	ζ_r	0.117	0.103	0.119	0.136
	ω_r	2.09	1.74	1.90	2.15
$N_{\delta_a}^\beta$	A_β	32.2	0.423	0.346	0.239
	$1/T_{\beta1}$	1.11	2.85	3.65	4.50
	$1/T_{\beta2} (\zeta_\beta)$	0.295	0.375	0.334	0.218
	$1/T_{\beta3} (\omega_\beta)$	5.37	4.30	3.68	3.22

G. RUDDER LATERAL TRANSFER FUNCTION FACTORS FOR THE H-19

		FLIGHT CONDITION			
		1901	1902	1903	1904
Altitude, h (ft)		0	0	0	0
V_{T_0} (ft/sec)		0	50.4	71.8	116.4
Weight, W (lb)		6,400	7,000	7,000	7,000
Δ_{lat}	$1/T_s$	0.732	0.162	0.116	0.0821
	$1/T_R$	3.43	5.09	5.10	4.87
	ζ_d	0.155	0.344	0.317	0.276
	ω_d	0.609	1.33	1.58	1.96
$N_{\delta r}^p$	A_p	9.78	12.3	12.5	13.0
	$1/T_{p1}$	0	0	0	0
	$1/T_{p2}$	0.313	(1.58)	(1.85)	(2.39)
	$1/T_{p3}$	-0.283	(-1.55)	(-1.85)	(-2.37)
$N_{\delta r}^\phi$	A_ϕ	9.78	12.3	12.5	13.0
	$1/T_{\phi 1}$	0.313	1.58	1.85	2.39
	$1/T_{\phi 2}$	-0.283	-1.55	-1.85	-2.37
$N_{\delta r}^r$	A_r	-13.5	-13.8	-13.9	-14.4
	$1/T_{r1}$	3.11	4.73	4.82	4.69
	ζ_r	-0.0561	-0.000756	-0.00938	-0.0198
	ω_r	0.524	0.534	0.530	0.547
$N_{\delta r}^\beta$	A_β	17.3	0.314	0.220	0.143
	$1/T_{\beta 1}$	-0.00872	-0.00281	-0.000922	-0.000396
	$1/T_{\beta 2} (\zeta_\beta)$	(0.518)	5.26	5.17	4.88
	$1/T_{\beta 3} (\omega_\beta)$	(4.89)	44.8	64.1	101.4

F.2B
BRISTOL FIGHTER

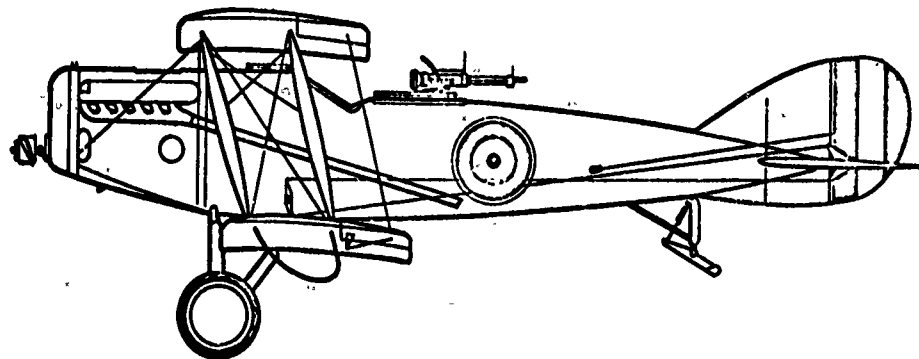
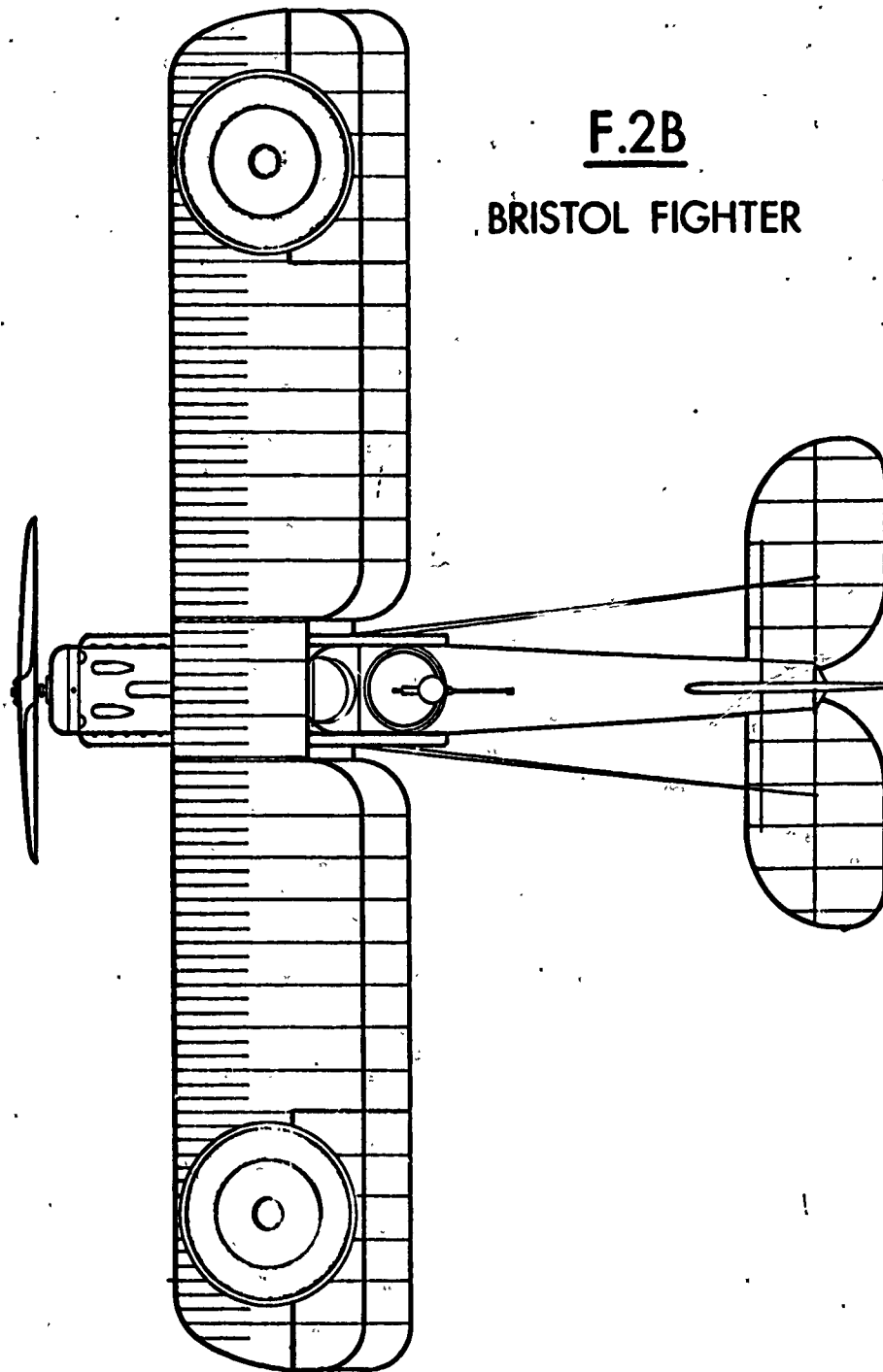


TABLE A-4

A			B			C		
GEOMETRICAL AND INERTIAL PARAMETERS FOR THE BRISTOL FIGHTER			LONGITUDINAL DIMENSIONAL DERIVATIVES FOR THE BRISTOL FIGHTER			LATERAL DIMENSIONAL DERIVATIVES FOR THE BRISTOL FIGHTER		
Note: Data are for body-fixed chord axes; engine off			Note: Data are for body-fixed chord axes; engine off			Note: Data are for body-fixed chord axes		
S = 405 ft ² , b = 40 ft, c = 5.17 ft								
	FLT. COND.			FLIGHT CONDITION			FLT. COND.	
	0001	0002		0001	0002		0001	0002
h (ft)	6,000	6,000	h (ft)	6,000	6,000	h (ft)	6,000	6,000
M (-)	0.126	0.0895	M (-)	0.126	0.0895	M (-)	0.126	0.0895
a (ft/sec)	1094	1094	X _u (1/sec)	-0.0471	-0.032	X _v (1/sec)	-0.176	-0.12
ρ (slugs/ft ³)	0.0020	0.0020	X _w (1/sec)	0.1765	0.248	X _p [(ft/sec ²)/rad]	-24.3	-11.8
V _{To} (ft/sec)	138	98	X _{δ_e} [(ft/sec ²)/rad]	0	0	X _{δ_a} [(ft/sec ²)/rad]	0	0
$\bar{q} = \rho V^2/2$ (lb/ft ²)	19.05	9.6	Z _u (1/sec)	-0.353	-0.400	X _{δ_a} [*] [(1/sec)/rad]	0	0
W (lb)	3090	3090	Z _δ (-)	0	0	X _{δ_r} [(ft/sec ²)/rad]	0	0
m (slugs)	96	96	Z _w (1/sec)	-2.06	-1.40	X _{δ_r} [*] [(1/sec)/rad]	0	0
I _x (slug-ft ²)	2600	2600	Z _{δ_e} [(ft/sec ²)/rad]	0	0	I _β [*] (1/sec ²)	-4.50	-4.11
I _y (slug-ft ²)	1925	1925	M _u (1/sec-ft)	+0.000684	+0.00186	I _β [*] (1/sec)	-7.17	-4.88
I _z (slug-ft ²)	4100	4100	M _δ (1/ft)	-0.00768	-0.00588	I _β [*] (1/sec)	2.06	2.36
I _{xz} (slug-ft ²)	0	0	M _w (1/sec-ft)	-0.016	-0.0108	I _{δ_a} [*] (1/sec ²)	26.1	12.7
x _{c.g./c}	0.33	0.33	M _q (1/sec)	-2.24	-1.28	I _{δ_r} [*] (1/sec ²)	0	0
α _{trim} (deg)	3	10	M _{δ_e} (1/sec ²)	-12	-5.8	N _β [*] (1/sec ²)	1.55	0
γ ₀ (deg)	-7	+1.5	M _δ (1/sec ²)	-2.21	-1.06	N _β [*] (1/sec)	-0.436	-0.52
U ₀ (ft/sec)	138	96.5	M _{δ_e} (1/sec)	-1.06	-0.576	N _β [*] (1/sec)	-0.341	-0.152
W ₀ (ft/sec)	7.24	17				N _{δ_a} [*] (1/sec ²)	-1.66	-0.805
γ ₀ (deg)	-10	-8.5				N _{δ_r} [*] (1/sec ²)	1.30	0.63

D. ELEVATOR LONGITUDINAL TRANSFER FUNCTION FACTORS FOR THE BRISTOL FIGHTER

		FLIGHT CONDITION	
		0001	0002
Mach No., M (-)		0.126	0.0895
Altitude, h (ft)		6,000	6,000
c.g. (% \bar{c})		33	33
Weight, W (lb)		3,090	3,090
Δ_{long}	$\zeta_{sp} (1/T_{sp1})$	(2.08)	0.956
	$\omega_{sp} (1/T_{sp2})$	(3.25)	1.69
	ζ_p	0.197	0.103
	ω_p	0.183	0.279
$N_{\delta e}^{\theta}$	A_{θ}	-12.0	-5.8
	$1/T_{\theta 1}$	0.0785	0.109
	$1/T_{\theta 2}$	2.03	1.32
	dc gain	-8.38	-3.75
$N_{\delta e}^u$	A_u	86.9	98.6
	ζ_u	0.518	0.571
	ω_u	3.00	1.63
	dc gain	3428	1178
$N_{\delta e}^w$	A_w	-1656	-568
	$1/T_{w1}$	—	—
	ζ_w	0.163	0.128
	ω_w	0.288	0.362
	dc gain	-603	-334

E. AILERON LATERAL TRANSFER FUNCTION FACTORS FOR THE BRISTOL FIGHTER

		FLIGHT CONDITION	
		0001	0002
Mach No., M (-)		0.126	0.0895
Altitude, h (ft)		6,000	6,000
c.g. (% \bar{c})		33	33
Weight, W (lb)		3,090	3,090
α_{trim} (deg)		3	10
Δ_{lat}	$1/T_s$	-0.000836	0.0508
	$1/T_R$	7.07	4.62
	ζ_d	0.215	0.273
	ω_d	1.44	0.886
$N_{\delta a}^p$	A_p	26.1	12.7
	$1/T_{p1}$	0.0278	-0.00865
	ζ_p	0.158	0.575
	ω_p	1.14	-0.444
	dc gain	-76.4	0.152
$N_{\delta a}^\phi$	A_ϕ	26.3	12.7
	$\zeta_\phi (1/T_{\phi 1})$	0.216	(0.563)
	$\omega_\phi (1/T_{\phi 2})$	1.14	(-0.463)
	dc gain	-2788	-18
$N_{\delta a}^r$	A_r	-1.66	-0.805
	$1/T_{r1}$	0.637	13.0
	$\zeta_r (1/T_{r2})$	(14.1)	0.261
	$\omega_r (1/T_{r3})$	(-0.512)	0.319
	dc gain	-622	-5.82
$N_{\delta a}^\beta$	A_β	3.03	2.96
	$1/T_{\beta 1}$	0.0656	-0.00547
	$1/T_{\beta 2}$	9.73	4.89
	$1/T_{\beta 3}$	—	—
	dc gain	-157	-0.431

F. RUDDER LATERAL TRANSFER FUNCTION FACTORS FOR THE BRISTOL FIGHTER

		FLIGHT CONDITION	
		0001	0002
Mach No., M (-)		0.126	0.0895
Altitude, h (ft)		6,000	6,000
c.g. (% \bar{c})		33	33
Weight, W (lb)		3,090	3,090
α_{trim} (deg)		3	10
Δ_{lat}	$1/T_s$	-0.000836	0.0508
	$1/T_R$	7.07	4.62
	ζ_d	0.215	0.273
	ω_d	1.44	0.886
$N_{\delta_r}^p$	A_p	2.67	1.49
	$1/T_{p1}$	0.0266	-0.00800
	$1/T_{p2}$	2.33	1.84
	$1/T_{p3}$	—	—
	dc gain	-13.5	-0.119
$N_{\delta_r}^\phi$	A_ϕ	-0.160	0.0165
	$1/T_{\phi 1}$	3.05	1.79
	$1/T_{\phi 2}$	-12.5	93.3
	dc gain	-495	14.9
$N_{\delta_r}^r$	A_r	1.30	0.630
	$1/T_{r1}$	7.16	4.79
	ζ_r	0.248	0.200
	ω_r	0.381	0.527
	dc gain	-110	4.55
$N_{\delta_r}^\beta$	A_β	-1.30	-0.621
	$1/T_{\beta 1}$	-0.0383	-0.176
	$1/T_{\beta 2}$	7.13	4.64
	$1/T_{\beta 3}$	—	—
	dc gain	-28.9	2.76

G. LATERAL COUPLING NUMERATORS FOR THE BRISTOL FIGHTER

		FLIGHT CONDITION	
		0001	0002
Mach No., M (-)		0.126	0.0895
Altitude, h (ft)		6,000	6,000
$N_{\delta_a \delta_r}^{p \beta}$	$A_{p\beta}$	-33.9	-7.88
	$1/T_{p\beta 1}$	0.0284	-0.00860
	$1/T_{p\beta 2}$	—	—
$N_{\delta_a \delta_r}^{r \beta}$	$A_{r\beta}$	-1.78	-1.37
	$\zeta_{r\beta}$	4.41	1.89
	$\omega_{r\beta}$	—	—
$N_{\delta_a \delta_r}^{p/s r}$ $= N_{\delta_a \delta_r}^{\phi r}$	$A_{\phi r}$	33.9	8.00
	$1/T_{\phi r}$	0.176	0.120
$N_{\delta_a \delta_r}^{\phi \beta}$	$A_{\phi \beta}$	-33.7	-7.92
	$1/T_{\phi \beta}$	—	—

APPENDIX B

ELEMENTS OF PROBABILITY

Because inputs to which automatic control systems for aircraft will be subjected are often either very complicated or are not known in detail, it may be necessary to consider performance of the system in response to commands and disturbances which are considered to be random variables. Other applications of the theory of random variables to the synthesis of automatic flight control systems have to do with the assessment of design qualities, in particular with the estimation of likelihood of failure of the system or its components.

The study of random variables, quantities which may take any values of a specified set with a specified probability, comprises the science of statistics. While it is not feasible here to give an account of more than a minute part of the subject, we can aspire to expose just those elements of the underlying theory which our examples in the main text require.*

Probability as a concept is treated first. This is immediately followed by a discussion of how certain probabilities may be computed if other probabilities are known, as in the addition and multiplication laws of probability. Random variables are then defined, and consideration of the

*Useful introductory references include:

A. C. Aitken, Statistical Mathematics, Oliver and Boyd, Edinburgh and London, 8th Edition, 1957.

M. J. Moroney, Facts from Figures, Penguin Books, 3rd Edition, 1956.

D. A. S. Frazer, Statistics, An Introduction, John Wiley and Sons, Inc., New York, 1958.

G. J. Hahn, "Probability and Statistics," Chapter 6 in H. Chestnut, Systems Engineering Tools, John Wiley and Sons, Inc., New York, 1965.

H. H. Goode, R. E. Machol, Systems Engineering, McGraw-Hill Book Co., Inc., New York, 1957.

W. R. Bennett, "Methods of Solving Noise Problems," Proceedings IRE, Vol. 44 (1956) pp. 609-638.

probability that a random variable will take certain values introduces the first probability distribution and density functions. Next the most important averages or "statistics" of random variables are defined. These include the mean, mean square, and the characteristic function. Finally the binomial, Poisson, uniform, exponential, and Gaussian distributions are described, derived, and put to use in elementary illustrative examples.

Although there is some inherent difficulty in defining probability in a completely satisfactory manner, for nearly every engineering use, empirical probability is a suitable interpretation of the concept.

Imagine or make a large number of experiments which may materialize, under what are taken to be identical conditions, in two or more outcomes or events. (An event is, generally, something concerning which it can be determined whether or not it occurred.) The set of all possible events comprises the sample space, \mathcal{S} , and, corresponding to each basic possible outcome of the experiment we associate a sample point, ξ_1 , in this space. An event may then correspond to a single sample point or to a set of such sample points. For example, the outcome "three spots showing" of the roll of a single die is an event and a sample point. On the other hand, the event "three or fewer spots showing" comprises three sample points since it corresponds to three basic possible outcomes of the experiment.

Now the results of certain experiments, repeated a large number of times, may show, or at least be believed to show, statistical regularity. If the outcome A occurs n_A times in N trials and the ratio $\text{Pr}(A) = n_A/N$ appears to approach a limit as the number of trials, N, becomes very large, $\text{Pr}(A)$ may be taken to be the probability of the event A.* (The simplest example is the flipping of a coin. We may take it that in each trial there are only two possible outcomes: heads or tails. The result of a large number of trials will be, for instance, that the number of heads divided by the number of trials is very close to $1/2$.) It follows directly from the

*The difficulty with empirical probability as a concept resides in the postulated limit. It is impossible to satisfactorily show that the limit should exist and be unique, and otherwise, the limiting process does not behave in the same way as the familiar mathematical limiting process for a sequence.

definition of probability that the probability has two properties, namely:

$$\begin{aligned} \Pr(A) &\geq 0 \\ \Pr(\mathcal{S}) &= 1 \end{aligned} \tag{B-1}$$

Consider further, and more generally, that there may be four identifiable outcomes of an experiment each one of which is a distinct possibility:

the event, A only, occurs n_A times in N trials
the event, B only, occurs n_B times in N trials
the events, A and B, occur together n_{AB} times in N trials
the event, neither A nor B, occurs $n_{\overline{(A+B)}}$ times in N trials

and that this takes care of all the possibilities. Then for a large number, of trials, N :

$$\begin{aligned} \text{the probability of the event A} &= \Pr(A) \doteq \frac{n_A + n_{AB}}{N} \\ \text{the probability of the event B} &= \Pr(B) \doteq \frac{n_B + n_{AB}}{N} \\ \text{the probability of the event A and B} &= \Pr(AB) \doteq \frac{n_{AB}}{N} \\ \text{the probability of the event A or B} &= \Pr(A+B) \doteq \frac{n_A + n_B + n_{AB}}{N} \\ \text{the probability of the event neither A nor B} &= \Pr(\overline{A+B}) \doteq \frac{n_{\overline{A+B}}}{N} \\ &= 1 - \Pr(A+B) \doteq 1 - \frac{n_A + n_B + n_{AB}}{N} \\ \text{the probability of the event A given that} &= \Pr(A/B) \doteq \frac{n_{AB}}{n_B + n_{AB}} \\ \text{event B has occurred} & \end{aligned} \tag{B-2}$$

Total probability is the probability of any one of several mutually exclusive outcomes, say, A, B, or C where each of the mutually exclusive events is a set of sample points or elements. The set of all possible outcomes (space) can be represented as the area inside a circle in an Euler or Venn diagram. Then the fractions of the area marked A, B, and C represent fractions of the total number of trials which resulted in the event A, B, or C. See Fig. B-1a.

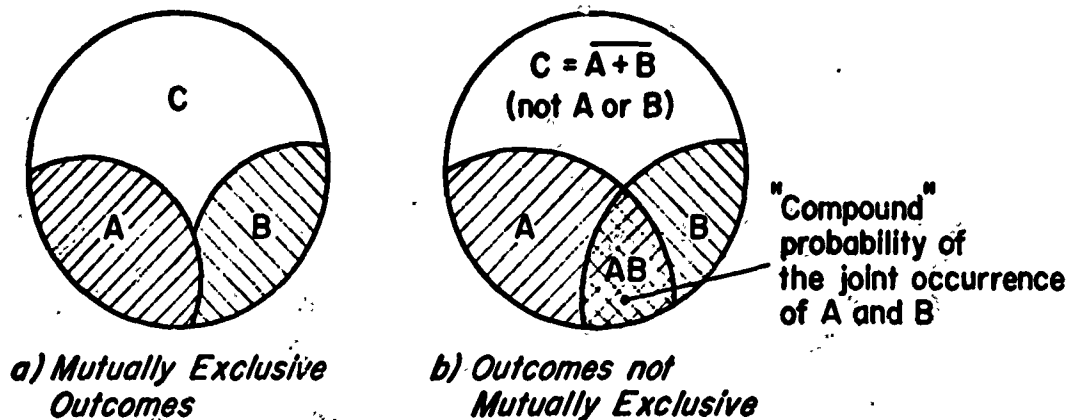


Fig. B-1. Euler Diagrams

On the other hand, if the outcomes are not mutually exclusive, areas on the Euler diagram may still represent the fractions of the area of the circle (sets of sample points) defined by Eq B-2.

Reasoning from either the algebraic expressions (Eq B-2) or the geometrical representation, (Fig. B-1).

$$\Pr(A + B) = \Pr(A) + \Pr(B) - \Pr(AB) \quad (B-3)$$

This is called the addition law of probabilities. If the event A and the event B are mutually exclusive, the compound or joint probability $\Pr(AB) = 0$, and the addition law is simply:

$$\Pr(A + B) = \Pr(A) + \Pr(B) \quad (B-4)$$

In the case in which the event A and the event B may occur together, the conditional probability, $\Pr(A/B)$, can be expressed in terms of the probability of the event B and the compound or joint probability, $\Pr(AB)$:

$$\Pr(A/B) \Pr(B) = \frac{n_{AB}}{n_B + n_{AB}} \cdot \frac{n_B + n_{AB}}{N} = \Pr(AB) \quad (B-5)$$

or

$$\Pr(A/B) = \frac{\Pr(AB)}{\Pr(B)}$$

It is not necessary for the events to be simultaneous in order to apply this definition of conditional probability. When the events A and B are independent,

$$\Pr(A/B) \equiv \Pr(A)$$

and $\Pr(AB) = \Pr(A/B) \Pr(B) = \Pr(A) \Pr(B)$ (B-6)

This is called the multiplication law.

The addition law and the multiplication law are easily generalized to cases of more than two independent events. Thus for three independent events, A, B, and C,

$$\begin{aligned} \Pr(A + B + C) &= \Pr(A) + \Pr(B) + \Pr(C) - \Pr(AB) - \Pr(AC) - \Pr(BC) + \Pr(ABC) \\ &= 1 - \Pr(\bar{A}) \Pr(\bar{B}) \Pr(\bar{C}) \\ &= 1 - [1 - \Pr(A)][1 - \Pr(B)][1 - \Pr(C)] \end{aligned} \quad (B-7)$$

$$\Pr(ABC) = \Pr(A) \Pr(B) \Pr(C) \quad (B-8)$$

and so forth. Equation B-6, or B-8 is the mathematical statement of the definition of independence, i.e. A and B are independent when Eq B-6 applies, or A, B, and C are independent when Eq B-8 applies.

An example of events which are not mutually exclusive but which are independent might be the drawing of an ace or a spade (on a single draw) from a standard deck of 52 playing cards.

$$\Pr(\text{Spade}) = \frac{13}{52} = \frac{1}{4}$$

$$\Pr(\text{Ace}) = \frac{4}{52} = \frac{1}{13}$$

The probability of drawing the card which is both a spade and an ace is

$$\Pr(\text{Space Ace}) = \Pr(\text{Spade}) \Pr(\text{Ace}) = \frac{1}{4} \times \frac{1}{13} = \frac{1}{52}$$

and this illustrates the multiplication law for independent events. Finally the probability of a spade or an ace is:

$$\begin{aligned}\Pr(\text{Spade} + \text{Ace}) &= \Pr(\text{Spade}) + \Pr(\text{Ace}) - \Pr(\text{Spade Ace}) \\ &= \frac{13}{52} + \frac{4}{52} - \frac{1}{52} \\ &= \frac{16}{52} = \frac{4}{13}\end{aligned}$$

This illustrates the operation of the addition law.

Consider next an example in which the events are neither mutually exclusive nor independent. Two coins are tossed simultaneously. There are four possible basic outcomes (sample points). They are head-head, head-tail, tail-head, and tail-tail. We ask first what is the probability that at least one head occurs. By counting the outcomes in which at least one head occurs:

$$\Pr(\text{Head}) = \frac{3}{4} = \Pr(\text{Tail})$$

Also the joint probability of a head and a tail is

$$\Pr(\text{Head Tail}) = \frac{1}{2}$$

and the conditional probability of a head, given that a tail has occurred, is:

$$\Pr(\text{Head/Tail}) = \frac{2}{3}$$

From the addition law, the probability of a head or a tail is:

$$\Pr(\text{Head} + \text{Tail}) = \frac{3}{4} + \frac{3}{4} - \frac{1}{2} = 1$$

and the relationship between the conditional and joint probabilities is illustrated by the calculation:

$$\Pr(\text{Head/Tail}) \Pr(\text{Tail}) = \Pr(\text{Head Tail})$$

$$\frac{2}{3} \times \frac{3}{4} = \frac{1}{2}$$

Note that here $\Pr(\text{Head Tail}) \neq \Pr(\text{Head}) \Pr(\text{Tail})$, i.e. the events, "at least one head" and "at least one tail," are not independent in simultaneous tosses of two coins.

RANDOM VARIABLES

It is often more interesting to consider some function of the outcomes of an experiment rather than the outcomes themselves. If then we assign to every sample point (element), ξ , of the sample space (set), \mathcal{S} , a number $X(\xi)$ according to some rule, the function $X(\xi)$, defined on the sample space, is a random variable* provided that $X(\xi) \leq x$ is an event and that $X(\xi) = \pm \infty$ are events but that the probability of their occurrence is zero. Note that the outcome itself falls under the definition of a random variable since the functional dependence may allowably comprise the identity function. Thus outcomes or functions of outcomes are random variables.

DISTRIBUTION AND DENSITY FUNCTIONS

Now define, for any number $-\infty < x < \infty$, the probability, that $X(\xi) \leq x$ as the real valued first probability distribution function of the random variable $X(\xi)$:

$$\Pr(X(\xi) \leq x) = P_1(x) \quad (\text{B-9})$$

The first probability distribution function has the properties:

$$\begin{aligned} P_1(-\infty) &= 0 \\ P_1(\infty) &= 1 \\ P_1(x_1) &\leq P_1(x_2); \quad x_1 < x_2 \end{aligned} \quad (\text{B-10})$$

If $n(x)$ is the number of times, in an experiment repeated N times, in which

*The use of the words "random variable" for a function is rooted in precedent.

$X(\zeta) \leq x$, then for a very large number of repetitions:

$$P_1(x) \doteq \frac{n(x)}{N} \quad (B-11)$$

The derivative of the first probability distribution function is called the first probability density function, $p_1(x)$.

$$\frac{dP(x)}{dx} = p_1(x) \quad (B-12)$$

Then the probability element $p_1(x)dx = \Pr[x < X(\zeta) < x + dx]$. As often happens, the distribution function may have step-form discontinuities, and there are delta functions in its derivative. For the case of so-called discrete random variables, the density functions actually consist of a sum of weighted delta functions:

$$p_1(x) = \sum_i p_i \delta(x - x_i) \quad (B-13)$$

The probability that a function $X(\zeta)$ lies between two values, say x_1 and x_2 , is obtained by integrating the density function between those limits.

$$\Pr[x_1 < X(\zeta) < x_2] = \int_{x_1}^{x_2} p_1(x) dx \quad (B-14)$$

and clearly, from the definition of a random variable,:

$$\Pr[-\infty < X(\zeta) < +\infty] = \int_{-\infty}^{\infty} p_1(x) dx = 1 \quad (B-15)$$

The names distribution function and density function come from the analogy to a unit mass distributed along the line which is the x-axis. The mass element in a small distance, dx , is $\frac{dM}{dx} dx$, where $\frac{dM}{dx}$ is the mass per unit length, or density. Then the total mass to the left of a given point x_1 is obtained by integrating the density function $\frac{dM}{dx}$, or:

$$M(x) = \int_{-\infty}^x \left(\frac{dM}{dx} \right) dx \quad (B-16)$$

Now $M(-\infty) = 0$ while $M(\infty) = 1$ as in the probability distribution function.

EXPECTATION, MEAN, AND VARIANCE

In the theory and application of probability, the average, mean, or mathematical expectation of a random variable has a surpassing importance. As every schoolboy knows, the way in which to find the average value of a random variable, X_1 , which takes a number of discrete values, is to multiply each value by the number of times, n_1 , it occurs, form the sum and divide by the total number of observations, N .

$$\text{Average of } X = E[X] = \frac{X_1 n_1 + X_2 n_2 + \dots + X_n n_n}{N} \quad (\text{B-17})$$

According to our interpretation of probability, however, a fraction such as n_1/N is simply the probability, p_1 , of the event x_1 so that Eq B-17 could be rewritten:

$$E[X] = X_1 p_1 + X_2 p_2 + \dots + X_n p_n = \sum_{i=1}^n X_i p_i \quad (\text{B-18})$$

In the case of a continuous random variable the probability that the variable lies in the narrow range between x and $x + dx$ is the probability element $p_1(x)dx$. Now considering the integral as the limit of a sum:

$$E[X] = \int_{-\infty}^{\infty} x p_1(x) dx \quad (\text{B-19})$$

When the expected value of some function of x , say $g(x)$, is wanted:

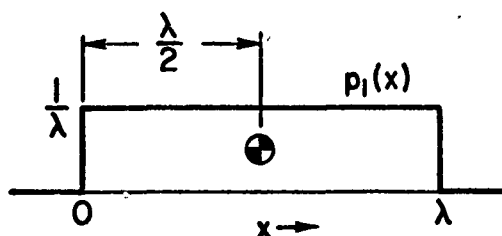
$$E[g(X)] = \int_{-\infty}^{\infty} g(x) p_1(x) dx \quad (\text{B-20})$$

Those averages in which $g(X) = X^n$ are of particular importance. They are called the moments of the distribution, and have the form:

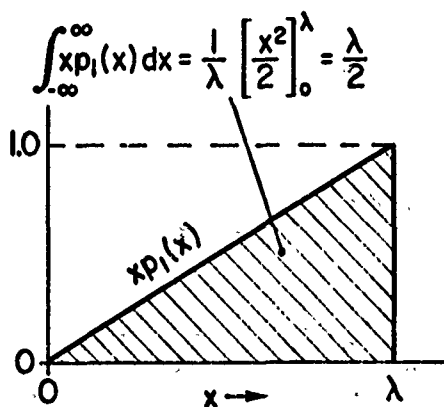
$$m_n = E[X^n] = \int_{-\infty}^{\infty} x^n p_1(x) dx \quad (\text{B-21})$$

From the defining properties of an allowable distribution function, the zero order moment, m_0 , always equals 1. The first moment, m_1 , is the arithmetic mean, the second moment, m_2 , is the mean-square, and so forth.

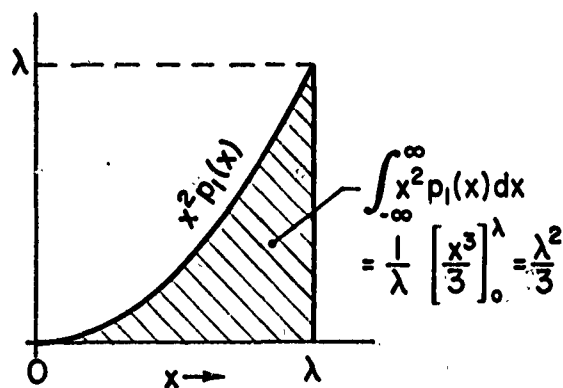
In terms of physical analogies, the mean is simply the centroid of the density function, while the mean-square value is the radius of gyration of the density function. These two moments are illustrated for a rectangular density function in Fig. B-2.



a) A Rectangular Density Function



b) Calculation of the Mean Value



c) Calculation of the Mean-Square Value

Fig. B-2. Mean and Mean-Square Values for the Rectangular Density Function

If the mean value is subtracted from all values of X , the moments derived from the results become central moments. Thus,

$$\mu_n = E[(X - m_1)^n] = \int_{-\infty}^{\infty} [x - m_1]^n p_1(x) dx \quad (\text{B-22})$$

The first central moment, μ_1 , is zero. The second central moment is

$$\begin{aligned}
\mu_2 &= \int_{-\infty}^{\infty} [x - m_1]^2 p_1(x) dx \\
&= \mu_2 - [m_1]^2 \\
&= E[X^2] - \{E[X]\}^2 = \sigma^2
\end{aligned}
\tag{B-23}$$

$\mu_2 = \sigma^2$ is the variance. The square root of the variance is the standard deviation of the distribution for the ensemble X_1, \dots, X_n, \dots .

When the mean is zero the variance and the mean-square are identical.

The mean and the variance (or standard deviation) are often the most significant quantities which may characterize a distribution.

CHARACTERISTIC FUNCTION

The characteristic function is the expected value of the complex conjugate Fourier transform of a random variable X .

$$\phi(\omega) = E[e^{j\omega X}] = \int_{-\infty}^{\infty} e^{j\omega x} p_1(x) dx \tag{B-24}$$

By expanding the exponential function in a series:

$$\begin{aligned}
\phi(\omega) &= \int_{-\infty}^{\infty} p_1(x) \left[1 + j\omega x + \frac{(j\omega x)^2}{2!} + \dots + \frac{(j\omega x)^n}{n!} + \dots \right] dx \\
&= \int_{-\infty}^{\infty} p_1(x) dx + j\omega \int_{-\infty}^{\infty} x p_1(x) dx + \frac{(j\omega)^2}{2!} \int_{-\infty}^{\infty} x^2 p_1(x) dx \\
&\quad + \frac{(j\omega)^3}{3!} \int_{-\infty}^{\infty} x^3 p_1(x) dx + \frac{(j\omega)^4}{4!} \int_{-\infty}^{\infty} x^4 p_1(x) dx + \dots
\end{aligned}
\tag{B-25}$$

The integrals of this last expression may be recognized as the central moments of the distribution defined by the density function $p_1(x)$. The characteristic function, therefore, contains information reflecting the character of all the central moments of the distribution. In fact, if the expression on the right hand side of Eq B-25 is compared to the Maclaurin series expansion for the characteristic function

$$\varphi(\omega) = \varphi(0) + \varphi'(0)\omega + \frac{\varphi''(0)}{2!}\omega^2 + \dots + \frac{\varphi^{(n)}(0)}{n!}\omega^n + \dots \quad (\text{B-26})$$

it may be seen that the central moments of the distribution can be computed from derivatives of the characteristic function evaluated at $\omega = 0$.

$$E(X^n) = \int_{-\infty}^{\infty} x^n p_1(x) dx = (j)^{-n} \left. \frac{d^n}{d\omega^n} \varphi(\omega) \right|_{\omega=0} \quad (\text{B-27})$$

Another use of the characteristic function is in the computation of the first probability density function of the sum of two random variables. The characteristic function of the sum of two independent random variables is the product of the characteristic functions of the individual variables.

$$\varphi(\omega) = \varphi_1(\omega) \varphi_2(\omega) \quad (\text{B-28})$$

Then the first probability density function for the sum is the inverse complex conjugate Fourier transform:

$$\begin{aligned} p_1(x_1 + x_2) &= \mathcal{F}^{-1}[\varphi(-\omega)] = \mathcal{F}^{-1}[\varphi_1(-\omega) \varphi_2(-\omega)] \\ &= \frac{1}{2\pi} \int_{-\infty}^{\infty} e^{-j\omega x} \varphi(\omega) d\omega \end{aligned} \quad (\text{B-29})$$

This inverse transform may be written as a convolution integral

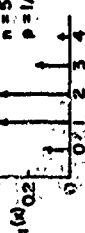
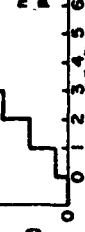


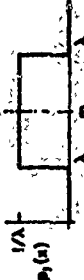
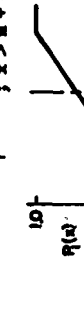


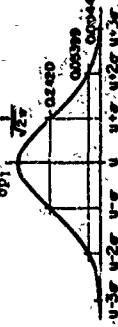
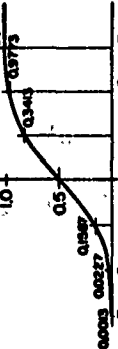
$$p_1(x_1 + x_2) = \int_{-\infty}^{\infty} p_{11}(t_1) p_{12}(x - t_1) dt_1 \quad (\text{B-30})$$

EXAMPLES OF DISTRIBUTION FUNCTIONS

While the conditions on the first probability distribution function are so broad as to admit of a very large number of interesting possibilities, the number of different distribution functions often encountered in engineering design work is quite small. It includes the binomial (or Bernoulli), Poisson, uniform, exponential, and Gaussian (or normal) distributions. The first two of these are discrete distributions in which the density function is a sum of delta functions. The next three are continuous distributions. Some of the characteristics of these one dimensional distributions are summarized in Table B-1.

TABLE B-1

PROPERTIES OF SOME PROBABILITY DISTRIBUTION FUNCTIONS

NAME	DOMAIN	PROBABILITY DENSITY FUNCTION	PROBABILITY DISTRIBUTION FUNCTION	RESTRICTIONS ON PARAMETERS	MEAN	VARIANCE	CHARACTERISTIC FUNCTION
Binomial or Bernoulli	$x = 0, 1, 2, \dots, n$	$p_1(x) = \binom{n}{x} p^x q^{n-x} \delta(x-s)$ 	$\int_{-\infty}^{\infty} p_1(x) dx$ 	$0 < p < 1$ $q = 1 - p$	np	npq	$(q + pe^{j\omega})^n$
Poisson	$x = 0, 1, 2, \dots, \infty$	$p_1(x) = e^{-m} \sum_{n=0}^{\infty} \frac{m^n}{n!} \delta(x-s)$ 	$\int_{-\infty}^{\infty} p_1(x) dx$ 	$0 < m < \infty$	m	m	$e^{m(e^{j\omega} - 1)}$
Uniform	$x = -\frac{\lambda}{2} \leq x \leq \frac{\lambda}{2}$	$p_1(x) = 1/\lambda$ 	$\int_{-\infty}^{\infty} p_1(x) dx = x - m + \lambda/2$ 	$-\infty < m < \infty$ $0 < \lambda < \infty$	m	$\frac{\lambda^2}{12}$	$\frac{2}{\lambda^2} \sin^2\left(\frac{\lambda \omega}{2}\right) e^{j\omega m}$
Exponential	$0 \leq t < \infty$	$p_1(x) = e^{-ct}$ 	$p_1(x) = \int_{-\infty}^{\infty} p_1(x) dx = 1 - e^{-ct}$ 	$0 < \frac{1}{c} < \infty$	$\frac{1}{c}$	$\frac{1}{c^2}$	$\frac{1}{(1 - je^{j\omega/c})}$
Gaussian or Normal	$-\infty < x < \infty$	$p_1(x) = \frac{1}{\sqrt{2\pi}\sigma} \exp\left[-\frac{(x-m)^2}{2\sigma^2}\right]$ 	$p_1(x) = \frac{1}{2} + \text{erf}\left(\frac{x-m}{\sigma}\right)$ 	$-\infty < m < \infty$ $0 < \sigma < \infty$	m	σ^2	$\exp(j\omega m - \frac{\sigma^2 \omega^2}{2})$

In order to illustrate the types of random variables to which each of these distributions is appropriate, we shall discuss each of them in turn.

The Binomial Distribution

The binomial distribution was discovered by Jakob Bernoulli and was published posthumously on his behalf in 1713. It was the first probability distribution to be discovered. It is useful for the description of the number of times a given event, say A, will occur in a given number of trials, say n, when the probability of success on each trial is the same and the trials are independent of one another. It may, for example, be used to find the number of ground to air missiles required, on the average, to score at least one hit on an airplane, or, alternatively, it may be used to describe the probability that an item of equipment will satisfactorily complete a mission. It is of surpassing importance in the theory of sampling inspection.

Consider a random experiment with two possible outcomes, A (success) and \bar{A} (failure). Define $\Pr(A) = p$ and $\Pr(\bar{A}) = q = 1 - p$. Then consider the experiment repeated 1, 2, . . . n times with the outcome on each trial independent of previous results.

On the first trial the result may be a failure or a success and their respective probabilities are q and p. After the second trial, we may have observed two failures (probability = q^2 , from the multiplication law), a failure and a success (probability = qp), a success and a failure (probability = pq), or two successes (probability = p^2). Similarly we could count the outcomes after three trials. We could then describe the results after the third trial. The results might be arranged as shown in Table B-2.

TABLE B-2

SEQUENCES OF FAILURES AND SUCCESSES

1st Trial	\bar{A} or A
2nd Trial	$\bar{A}\bar{A}$ or $\bar{A}A$ or $A\bar{A}$ or AA
3rd Trial	$\bar{A}\bar{A}\bar{A}$ or $\bar{A}\bar{A}A$ or $\bar{A}A\bar{A}$ or $A\bar{A}\bar{A}$ or $\bar{A}AA$ or $A\bar{A}A$ or $AA\bar{A}$ or AAA

Considering the probabilities of these occurrences, and now disregarding the precise sequence in which successes and failures might occur, the probabilities can also be arranged in a table. Once the pattern is clear (Pascal's triangle), the table can be extended very easily.

TABLE B-3

PASCAL'S TRIANGLE

0 Trials	1				
1 Trial		q		p	
2 Trials		q ²	2qp	p ²	
3 Trials		q ³	3q ² p	3qp ²	p ³
4 Trials	q ⁴	4q ³ p	6q ² p ²	4qp ³	p ⁴

Of course, terms on any given line represent the terms in the expansion of the binomial $(q + p)^n$. (Hence the name of the distribution.)

More generally, the number of equally likely sequences of s successes and $n - s$ failures in n trials is $\binom{n}{s} = n! / [s!(n - s)!]$, and the probability that the number $x = s$ (a specified number of successes):

$$\Pr(x = s) = \binom{n}{s} q^{n-s} p^s \quad (\text{B-31})$$

(This formula is only valid for integer values, $s = 0, 1, 2, \dots, n$.) Then a partial table of the distribution of the probabilities for any choice of a number of successes, s , and number of trials, n , might appear as follows:

Number of Successes, s	0	1	2	3	n
$\Pr(x=s)$	q^n	$n q^{n-1} p$	$\binom{n}{2} q^{n-2} p^2$	$\binom{n}{3} q^{n-3} p^3$	p^n

This is just one row in the triangle table.

Since $(q + p)^n = 1$, the sum of all the probabilities is one as it should be.

The density function of the binomial distribution may be written:

$$p_1(x) = \sum_{s=0}^n \binom{n}{s} p^s q^{n-s} \delta(x - s) \quad (B-32)$$

There is a binomial distribution for each value of n and p . These are known as the parameters of the distribution. Extensive tables of the distribution have been calculated.* This, however, is very tedious when the number of trials, n , is large. For many practical purposes, the binomial distribution can be successfully approximated. When the probability of either success or failure is small, the binomial distribution can be approximated by the Poisson distribution. (See below.) On the other hand if $p \approx q$, the continuous Gaussian distribution may be used as an approximation to the discrete binomial distribution, by fitting the mean and variance, provided only that the number of trials, n , is reasonably large.

As an example of the application of the binomial distribution to problems in aircraft subsystem reliability, consider the question of the relative reliability of single and twin engined airplanes. Suppose the probability that an engine will complete a four hour mission is $p = 0.9900$ and further that engine failures are independent events even in multi-engined airplanes. Then from Eq B-16, for a single engined airplane, during a single mission (trial):

$$\begin{aligned} \text{Pr}(\text{Success}) &= \binom{n}{s} p^s q^{n-s} = \binom{1}{1} p^1 q^0 \\ &= 0.9900 \end{aligned}$$

Similarly for a twin engined airplane which requires both engines to complete its flight (two successes in two trials):

$$\begin{aligned} \text{Pr}(\text{Success}) &= \binom{n}{s} p^s q^{n-s} = \binom{2}{2} p^2 q^0 \\ &= 0.9801 \end{aligned}$$

*Tables of the Binomial Probability Distribution, National Bureau of Standards, Applied Mathematics Series 6, U.S. Government Printing Office, Washington, D. C., 1950.

On the other hand, if a twin engined airplane can complete its flight on only one engine (at least one success in two trials), using the addition law for mutually exclusive events:

$$\begin{aligned}
 \Pr(\text{Success}) &= \Pr(\text{One Success}) + \Pr(\text{Two Successes}) \\
 &= \binom{2}{1} p^1 q^{2-1} + \binom{2}{2} p^2 q^0 \\
 &= 2pq + p^2 = 1 - q^2 = 1 - (1 - p)^2 \\
 &= 1 - 0.0001 = 0.9999
 \end{aligned}$$

This shows the powerful advantage of redundancy.

The Poisson Distribution

For the purpose of estimating the number, s , of independent events, A , which will occur when the average rate per unit time, length, area, or volume at which they occur is known, we use the Poisson distribution, named after Simeon Denis Poisson, the French mathematician. The events are isolated events in a continuum. Thus, for example, the Poisson distribution may characterize the number of cars arriving at an intersection in one minute, the number of bacteria on a slide, or the number of flaws in a casting.

If β is the "density" of the event, A , (the average rate per unit time, for example) then the probability that the event occurs in the interval between T and $T + \Delta T$ is proportional to ΔT , and the constant of proportionality is β . $\Pr[\text{event occurs between } T \text{ and } T + \Delta T] = \beta \Delta T$. Now from the multiplication law, Eq. B-6,

$$\begin{aligned}
 \Pr[\text{no event between } 0 \text{ and } T + \Delta T] &= P_0(T + \Delta T) \\
 &= \Pr[\text{no event between } 0 \text{ and } T] \Pr[\text{no event between } T \text{ and } T + \Delta T]
 \end{aligned}$$

or

$$P_0(T + \Delta T) = P_0(T) [1 - \beta \Delta T] \quad (\text{B-33})$$

On rearranging

$$\frac{P_0(T + \Delta T) - P_0(T)}{\Delta T} = -\beta P_0(T) \quad (B-34)$$

in the limit, or, as $\Delta T \rightarrow 0$:

$$\frac{d P_0(T)}{dT} + \beta P_0(T) = 0 \quad (B-35)$$

The initial condition is $P_0(0) = 1.0$ (the probability that no event occurs in zero time) and the solution is:

$$P_0(T) = e^{-\beta T} \quad (B-36)$$

Similarly $\Pr[1 \text{ event between } 0 \text{ and } T + \Delta T] = P_1(T + \Delta T)$. This probability is the sum of the probability that there is one event in the interval, 0 to T, and none in ΔT , together with the probability that there is no event in the interval, 0 to T, and that there is one in ΔT .

$$P_1(T + \Delta T) = P_1(T) [1 - \beta \Delta T] + P_0(T) \beta \Delta T \quad (B-37)$$

$$\frac{P_1(T + \Delta T) - P_1(T)}{\Delta T} = -P_1(T) \beta + P_0(T) \beta \quad (B-38)$$

Dividing by β , letting $\Delta T \rightarrow 0$, rearranging and substituting for P_0 ,

$$\frac{1}{\beta} \frac{d P_1(T)}{dT} + P_1(T) = e^{-\beta T} \quad (B-39)$$

which has the solution,

$$P_1(T) = \beta T e^{-\beta T} \quad (B-40)$$

By successively considering the probability that 2, 3, . . . n events will occur

in the interval $T + \Delta T$ we would find that $P_2(T) = \frac{(\beta T)^2}{2} e^{-\beta T}$, $P_3(T) = \frac{(\beta T)^3}{6} e^{-\beta T}$,
 $P_n(T) = \frac{(\beta T)^n}{n!} e^{-\beta T}$. These may be recognized as successive terms in the expansion

$$e^{-m} e^m = e^0 = 1 = e^{-m} \left[1 + \frac{m}{1!} + \frac{m^2}{2!} + \cdots + \frac{m^n}{n!} \right] \quad (B-41)$$

where $m = \beta T$. Notice that the sum of all the probabilities is one. For the Poisson distribution then

$$\Pr(x = s) = \frac{e^{-m} m^s}{s!} \quad (B-42)$$

and the density function is given by the expression:

$$p_1(x) = e^{-m} \sum_{s=0}^{\infty} \frac{m^s}{s!} \delta(x - s) \quad (B-43)$$

Again s takes only integer values. m is the "frequency parameter" of the Poisson distribution which represents the number of events in a typical finite interval, i.e. $m = \beta T$, for example, where β is the "density" of the events, and T is a convenient interval, say 1 sec or 1 year.

A quaint example of the application of the Poisson distribution is to the prediction of the number of cavalymen likely to be killed by horse kicks in the course of a year. Assuming that each such event is independent and occurs randomly in time, but with a constant overall frequency, suggests that the Poisson distribution may be appropriate. Data collected by von Bortkiewicz* for 10 Army Corps for 20 years (200 readings) shows a total of 122 deaths from horse kicks. There are, therefore, $122/200 = 0.61$ deaths per corps in a typical year. This is the "frequency parameter", m , of the distribution. Considering the probability of $s = 0, 1, 2, 3$, and 4 deaths occurring in any one corps in any one year we can construct a table of probabilities of the event, $\Pr(s = x) = e^{-0.61} (0.61)^s / s!$

*L. von Bortkiewicz, Das Gesetz der kleinen Zahlen, B. G. Teubner, Leipzig, 1898.

Number of deaths in one year per corps, s	0	1	2	3	4
Probability, $\Pr(x = s)$	0.543	0.331	0.101	0.021	0.003
Frequency expected in 200 readings	109	66.3	20.2	4.1	0.6
Actual number of corps-years the number s deaths occurred	109	65	22	3	1

It may be observed that the Poisson distribution gives a good fit to the actual data and might be used to extrapolate the experience.

We have had occasion to mention that the calculation of the binomial distribution is tedious when the number of trials, n , becomes large. In some cases, the Poisson distribution is a suitable approximation. Recall that the binomial distribution is characterized by the expression

$$\Pr(x = s) = \binom{n}{s} p^s q^{n-s} = \frac{n!}{s!(n-s)!} p^s (1-p)^{n-s} \quad (\text{B-44})$$

In the Poisson distribution the parameter, m , is the average number of occurrences (successes) in a typical finite interval of interest. Take the interval to extend over the number of independent "trials" in the case of the binomial distribution and therefore let $m = np$ the average number of successes in n trials. Substituting $p = m/n$ and rewriting Eq B-39:

$$\begin{aligned}
 \Pr(x = s) &= \binom{n}{s} \left(\frac{m}{n}\right)^s \left(1 - \frac{m}{n}\right)^{n-s} \\
 &= \frac{n!}{s!(n-s)!} \frac{m^s}{n^s} \left(1 - \frac{m}{n}\right)^{n-s} \\
 &= \underbrace{\frac{n(n-1) \cdots (n-s+1)(n-s)!}{n \cdots n \cdots n (n-s)!}}_{\substack{\text{there are } s \text{ of these} \\ \text{factors}}} \frac{m^s}{s!} \left(1 - \frac{m}{n}\right)^{n-s} \quad (\text{B-45}) \\
 &= 1 \left(1 - \frac{1}{n}\right) \cdots \left(1 - \frac{s-1}{n}\right) \frac{m^s}{s!} \left(1 - \frac{m}{n}\right)^{n-s}
 \end{aligned}$$

If we let n become very large while s remains small so that $n - s \approx n$ and further recognize that $\lim_{n \rightarrow \infty} \left(1 - \frac{n}{n}\right)^n = e^{-n}$:

$$\lim_{n \rightarrow \infty} 1 \left(1 - \frac{1}{n}\right) \cdots \left(1 - \frac{s-1}{n}\right) \frac{n^s}{s!} \left(1 - \frac{n}{n}\right)^{n-s} = (1) \frac{n^s}{s!} e^{-n} \quad (\text{B-46})$$

or finally

$$\Pr(x = s) = \binom{n}{s} \left(\frac{n}{n}\right)^s \left(1 - \frac{n}{n}\right)^{n-s} = \frac{n^s}{s!} e^{-n} \quad (\text{B-47})$$

This last expression, of course, is the one which defines the Poisson distribution. The approximation is useful when n is as small as 20 provided $m = np \leq 5$. For larger values of $m = np$ the approximation will only be useful for still larger values of n .

Consider now some continuous one-dimensional distributions.

The Uniform Distribution

A uniform distribution is appropriate to the description of a continuum of events which are equally likely in a given interval, say from $m - \frac{\lambda}{2}$ to $m + \frac{\lambda}{2}$. By equally likely we mean that the probability element

$p_1(x)dx = \Pr[x_1 < X < x_1 + dx_1]$ is a constant. The first probability density function itself is, therefore, a constant over the interval, and zero elsewhere. Since we have to arrange that

$$\Pr[-\infty < X < \infty] = \int_{-\infty}^{\infty} p_1(x)dx = 1 \quad (\text{B-48})$$

$p_1(x) = 1/\lambda$. Then the distribution function $P_1(x)$, is a cut-off ramp function rising from 0 to one while $(m - \frac{\lambda}{2}) < x < (m + \frac{\lambda}{2})$.

An example of the application of the uniform distribution would be to the calculation of the probability, disregarding the actually discrete nature of the problem, that a wheel of fortune would stop on any particular number.

The Exponential Distribution

Another important continuous distribution is the exponential distribution. It is often used in estimating the reliability of systems or components which are subject to a constant hazard.

Consider a component which has survived to the time, t . Letting F symbolize the event failure and S the event survival, the conditional probability of failure in a time, Δt , given that the component has survived up to time, t , from Eq B-5, is:

$$\Pr(F/S) = \frac{\Pr(FS)}{\Pr(S)} \quad (B-49)$$

The conditional probability of failure is proportional to the hazard, c , and the interval, Δt .

$$\Pr(F/S) = c(\Delta t) \quad (B-50)$$

Suppose that the cumulative probability distribution for failure as a function of time were known. Call it $P_1(t)$. Then the probability of the component's surviving to the time, t , is

$$\Pr(S) = \Pr(\bar{F}) = [1 - P_1(t)] \quad (B-51)$$

and the derivative $\frac{dP_1(t)}{dt} = p_1(t)$ times Δt is the probability element which defines the probability that the component will fail in the time, Δt . This is the same thing as surviving up to time, t , and then failing.

$$\Pr(FS) = \frac{dP_1}{dt} (\Delta t) \quad (B-52)$$

Substituting in Eq B-35:

$$c(\Delta t) = \frac{dP_1}{dt} (\Delta t) / [1 - P_1(t)] \quad (B-53)$$

or

$$\frac{1}{c} \frac{dP_1}{dt} + P_1(t) = 1 = u(t) ; t \geq 0$$

We may now solve this equation for the unknown distribution function

$$P_1(t) = [1 - e^{-ct}] ; t \geq 0 \quad (B-54)$$

and the corresponding density function is:

$$p_1(t) = \frac{dP_1}{dt} = ce^{-ct} ; t \geq 0 \quad (B-55)$$

The exponential functions which appear here give the distribution its name.

In applications to reliability calculations, the inverse of the parameter, c , which has the dimensions of time often goes by the name: mean time before failure or MTBF. This is its physical significance in such applications. Note from Table B-1 that the mean of the exponential distribution is $1/c$.

More generally the exponential distribution governs the time between occurrences of independent random events which occur at a constant average rate. In this respect the exponential distribution bears a close relationship to the Poisson distribution. Recall from Eq B-31, used in deriving the Poisson distribution, that for independent events occurring randomly in time at a constant average rate:

$$\text{Pr}[\text{no event between } 0 \text{ and } t] = P_0(t) = e^{-\beta t} \quad (B-56)$$

Similarly:

$$\text{Pr}[\text{no event between } t \text{ and } t + \Delta t] = e^{-\beta \Delta t} \quad (B-57)$$

and therefore:

$$\text{Pr}[\text{at least one event between } t \text{ and } t + \Delta t] = 1 - e^{-\beta \Delta t} \quad (B-58)$$

Since, for a very small Δt (approaching dt),

$$e^{-\beta \Delta t} \doteq 1 - \beta \Delta t$$

therefore,

$$1 - e^{-\beta dt} = \beta dt \quad (B-59)$$

and this is the probability of exactly one event in the interval between t and $t + dt$. Finally the product of the probabilities of no events in the interval between 0 and t and exactly one event in the interval between t and $t + dt$ yields the probability element $(e^{-\beta t})\beta dt$, which integrated from 0 to T , shows the probability of exactly one event occurring more than T seconds after its predecessor and less than $T + dt$ seconds afterward.

$$\begin{aligned}\Pr[\text{one event between } T \text{ and } T + dt] &= \int_0^T \beta e^{-\beta t} dt \\ &= 1 - e^{-\beta T}\end{aligned}\quad (\text{B-60})$$

Thus the intervals, T_1 , between the events in a Poisson process are seen to be governed by the exponential distribution. The mean time between the events $T_{av} = \frac{1}{\beta}$, the inverse of the "density" of the events.

To return briefly to the question of engine reliability used to illustrate the binomial distribution, one might have asked: "How was it determined that the probability of the engine's surviving a four hour flight, $p = 0.9900$?" Under conditions approximating a constant hazard, it means that, on the average, there are four-hundred engine operating hours (during short missions) between random failures. Alternatively the mean time between failures $\frac{1}{c} = 400$ hours. The cumulative probability of failure during the mission is governed by the exponential distribution. From Eq B-37 and B-40 the probability that the engine will survive (not fail) up to a time, $t = \text{mission time} = 4$ hours, is:

$$\begin{aligned}\Pr(S) = \Pr(\bar{F}) &= 1 - [1 - e^{-ct}] = e^{-ct} \\ &\approx 1 - ct = 1 - \frac{4}{400} = 0.9900\end{aligned}\quad (\text{B-61})$$

The Gaussian Distribution

By far the most important probability distribution in science and engineering is the normal or so-called Gaussian distribution. (It was actually discovered by Abraham De Moivre as an approximation to the binomial distribution and was published by him in 1733, 60 years before

Carl Friedrich Gauss used it in his astronomical calculations.) It can be derived very simply.*

The reader may recall that following some formulations of statistical mechanics, in the theory of communication, the entropy or information, H , of a discrete set of probabilities, p_1, p_2, \dots, p_n is defined in such a way that

$$H = - \sum_{i=1}^n p_i \log p_i \quad (\text{B-62})$$

Furthermore, the entropy is a measure of disorder or information (choice). For a continuous (single dimensional) probability distribution, the analogous expression is:

$$H = - \int_{-\infty}^{\infty} p_1(x) \log p_1(x) dx \quad (\text{B-63})$$

We may inquire as to the first probability density function which makes the entropy (disorder, randomness) a maximum, subject to the condition that the standard deviation of the variable x be a constant, σ . The square of the standard deviation or "variance" has been defined in terms of the density function in Eq B-23, repeated here,

$$\sigma^2 = \int_{-\infty}^{\infty} x^2 p_1(x) dx \quad (\text{B-64})$$

and from Eq B-15:

$$\int_{-\infty}^{\infty} p_1(x) dx = 1 \quad (\text{B-65})$$

Finding the maximum value of the integral function H , subject to the constraints (Eq B-48 and B-49) is a standard problem in the calculus of variations.[†]

*C. E. Shannon and W. Weaver, The Mathematical Theory of Communication, University of Illinois Press, Urbana, Illinois, 1949, pp. 54-56.

[†]L. E. Elsgolc, Calculus of Variations, Addison-Wesley Publishing Co., Inc. Reading, Mass., 1962.

It is done by adjoining the constraints (each multiplied by a Lagrange multiplier) to the payoff function and maximizing the sum. The problem then becomes to find:

$$\text{Max}_{p(x)} \int_{-\infty}^{\infty} [-p(x) \log p(x) + \lambda x^2 p(x) + \nu p(x)] dx \quad (\text{B-66})$$

A necessary condition for the maximum is that the Euler equation be satisfied. The Euler equation is: $\frac{\partial F}{\partial y} - \frac{d}{dx} \frac{\partial F}{\partial y'} = 0$ where $F(x, y, y')$ is the integrand.

In this case, where there are no derivatives of $p(x)$ in the integrand, the Euler equation is simply:

$$\frac{\partial}{\partial [p(x)]} [-p(x) \log p(x) + \lambda x^2 p(x) + \nu p(x)] = 0$$

$$-1 - \log p(x) + \lambda x^2 + \nu = 0 \quad (\text{B-67})$$

or

$$p(x) = e^{\nu-1} e^{\lambda x^2}$$

The constants ν and λ are then chosen so as to satisfy the equations of constraint. An appropriate choice yields

$$p_1(x) = \frac{1}{\sqrt{2\pi}\sigma} e^{-(x^2/2\sigma^2)} \quad (\text{B-68})$$

which is the first probability density function for the Gaussian distribution with a zero mean value. Its integral is the first distribution function

$$P_1(x) = \frac{1}{2} + \text{erf}\left(\frac{x}{\sigma}\right) \quad (\text{B-69})$$

where

$$\text{erf}\left(\frac{x}{\sigma}\right) = \frac{2}{\sqrt{\pi}} \int_0^{x/\sigma} e^{-u^2} du \quad (\text{B-70})$$

is the so-called error function.*

*I. N. Sneddon, Special Functions of Mathematical Physics and Chemistry, Oliver and Boyd, Edinburgh and London, 1961, p. 13, for example.

More generally the Gaussian distribution is defined by

$$p_1(x) = \frac{1}{\sqrt{2\pi} \sigma} \exp - \left[\frac{(x - m_1)^2}{2\sigma^2} \right] \quad (\text{B-71})$$

$$P_1(x) = \frac{1}{2} + \operatorname{erf} \left(\frac{x - m_1}{\sigma} \right) \quad (\text{B-72})$$

which allows for the case in which the mean value of x is not necessarily zero.

We have seen that, in a sense, the Gaussian distribution is the one associated with the maximum degree of randomness. Otherwise, subject to fairly general conditions, it can be shown that the first probability density function, $p_1(x)$, of the sum of a large number, N , of independent random variables tends to the probability density function of the normal (Gaussian) distribution. For this reason, if we are observing a random variable whose fluctuations are due to a large number of independent causes, and this is indeed often the case, the Gaussian distribution is likely to be the appropriate one characterizing the variable of interest.

For essentially the same reason, the Gaussian distribution is also an approximation to the discrete binomial and Poisson distributions if the mean np or m is large.

To fit a Gaussian distribution to a discrete one derived from plotting numbers of cases in given categories; so as to keep the total probability equal to one, the ordinates of the normal probability density curve are multiplied by the total number of observations, N .

$$y = \frac{N}{\sqrt{2\pi} s} e^{-\left(\frac{x - \bar{x}}{2s}\right)^2} \quad (\text{B-73})$$

where the standard deviation is

$$s = \left(\frac{\sum x_i^2}{N} - \bar{x}^2 \right)^{1/2} = \sigma \quad (\text{B-74})$$

and where \bar{x} is the mean of all the observations, $\bar{x} \doteq m_1$. In the cases of the binomial and Poisson distributions, the standard deviation, of course, is the square root of the known variance. See Table B-1.

Figure B-3 shows several normal density functions with different means and standard deviations. Since the area under each curve must be one, they are higher at the mean value if the standard deviation is small. The points of inflection on each curve are located one standard deviation from the mean.

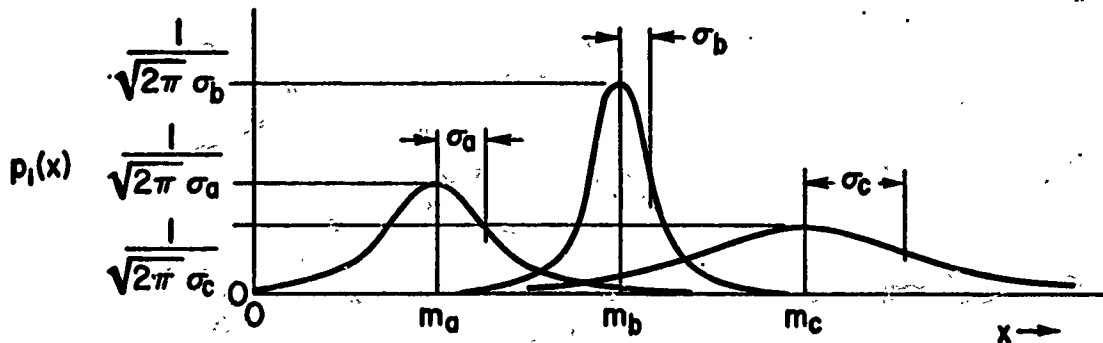


Fig. B-3. Normal Density Functions

In order to make numerical calculations, the normal density function is usually cast into the standard form in which the mean is zero and the standard deviation is unity. Deviations from the mean are then measured in units of standard deviations, $t = \frac{x - m_1}{\sigma} = [\text{standard deviations}]$. The standard form is:

$$z(t) = \frac{1}{\sqrt{2\pi}} e^{-t^2/2}$$

This function is found tabulated in a number of places.*

One very useful configuration of tabulated values is in terms of

$$\Pr [(x - m_1) > t] = 1 - \int_{-\infty}^t z(t) dt$$

*See, for example, A. Hald, Statistical Tables and Formulas, John Wiley and Sons, Inc., New York, 1952, p. 33 where it is designated $\phi(u)$; or M. M. Abramowitz and I. Stegun (eds.), Handbook of Mathematical Functions, National Bureau of Standards Applied Mathematics Series 55, U.S. Government Printing Office, Washington, D. C., 1964, pp. 666-972, where it is designated $Z(x)$.

which represents the probability of a random variable, known to be governed by the normal distribution, exceeding a given positive value, greater than the mean, by an amount expressed as a number of standard deviations, t . This probability is the hatched area under the curve in Fig. B-4. A very short table of such probabilities is presented in Table B-4.

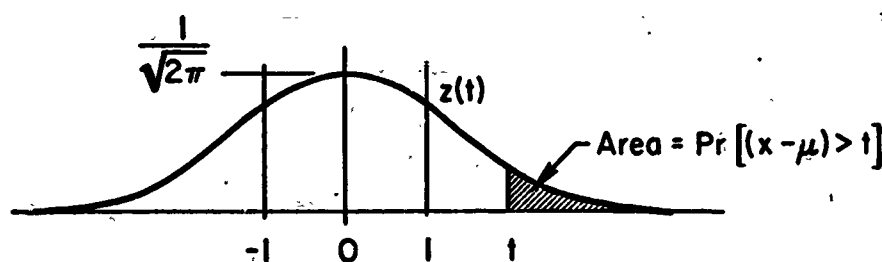


Fig. B-4. The Standard Form of the Normal Probability Density Function and $\Pr[(x - \mu) > t]$

TABLE B-4

PROBABILITY OF A VARIABLE EXCEEDING A VALUE t STANDARD DEVIATIONS GREATER THAN THE MEAN

t Standard Deviations	$\Pr[(x - m_1) > t]$	t Standard Deviations	$\Pr[(x - m_1) > t]$
0.00	0.50000	2.00	0.02275
0.50	0.30854	3.00	0.00135
1.00	0.15866	4.00	0.00003
1.50	0.06680	5.00	3×10^{-7}

Since the Gaussian curve is symmetrical, Table B-4 may also be used to calculate the probability that a variable will be less than the mean by an amount which exceeds t standard deviations; or, indeed, if the probability of a value either greater or less than the mean by the specified number of standard deviations is wanted, it is twice the values in the table. Thus the well remembered numbers

$$\Pr[x \approx \mu_1 \pm \sigma] \doteq \frac{1}{3}, \quad \Pr[x \approx \mu_1 \pm 2\sigma] \doteq \frac{1}{22}, \quad \text{and} \quad \Pr[x \approx \mu_1 \pm 3\sigma] \doteq \frac{1}{370}$$

As a simple example of the application of the normal distribution, consider that in typical aircraft carrier landing operations the mean sink rate of the airplanes at the instant of contact with the deck is $\bar{V}_I = 14.0$ ft/sec, that the standard deviation in the sink rate is 2.33 ft/sec, and that the sink rate is normally distributed about the mean value. If a sink rate of 21.0 ft/sec corresponds to the ultimate strength of the landing gear, in what fraction of all landings will the aircraft be damaged by a hard landing?

$$\Pr[V_I > 21] = \Pr[V_I > 14 + 3(2.33)]$$

From Table B-4, this is the probability that the sink rate will be more than the sum of the mean value and three standard deviations, i.e., $\Pr[V_I > 21] = 0.00135$, or the sink rate will be excessive once in 740 landings.

These few facts on the Gaussian and other distributions allow us to make a large number of interesting calculations concerning probabilities, but the material presented in this Appendix is only introductory, and it is no substitute for a more rigorous study of the subject.